



Functionalization of Strong Sigma Bonds by Nickel and Tungsten Catalysis

Raúl Martín Montero

ADVERTIMENT. L'accés als continguts d'aquesta tesi doctoral i la seva utilització ha de respectar els drets de la persona autora. Pot ser utilitzada per a consulta o estudi personal, així com en activitats o materials d'investigació i docència en els termes establerts a l'art. 32 del Text Refós de la Llei de Propietat Intel·lectual (RDL 1/1996). Per altres utilitzacions es requereix l'autorització prèvia i expressa de la persona autora. En qualsevol cas, en la utilització dels seus continguts caldrà indicar de forma clara el nom i cognoms de la persona autora i el títol de la tesi doctoral. No s'autoritza la seva reproducció o altres formes d'explotació efectuades amb finalitats de lucre ni la seva comunicació pública des d'un lloc aliè al servei TDX. Tampoc s'autoritza la presentació del seu contingut en una finestra o marc aliè a TDX (framing). Aquesta reserva de drets afecta tant als continguts de la tesi com als seus resums i índexs.

ADVERTENCIA. El acceso a los contenidos de esta tesis doctoral y su utilización debe respetar los derechos de la persona autora. Puede ser utilizada para consulta o estudio personal, así como en actividades o materiales de investigación y docencia en los términos establecidos en el art. 32 del Texto Refundido de la Ley de Propiedad Intelectual (RDL 1/1996). Para otros usos se requiere la autorización previa y expresa de la persona autora. En cualquier caso, en la utilización de sus contenidos se deberá indicar de forma clara el nombre y apellidos de la persona autora y el título de la tesis doctoral. No se autoriza su reproducción u otras formas de explotación efectuadas con fines lucrativos ni su comunicación pública desde un sitio ajeno al servicio TDR. Tampoco se autoriza la presentación de su contenido en una ventana o marco ajeno a TDR (framing). Esta reserva de derechos afecta tanto al contenido de la tesis como a sus resúmenes e índices.

WARNING. Access to the contents of this doctoral thesis and its use must respect the rights of the author. It can be used for reference or private study, as well as research and learning activities or materials in the terms established by the 32nd article of the Spanish Consolidated Copyright Act (RDL 1/1996). Express and previous authorization of the author is required for any other uses. In any case, when using its content, full name of the author and title of the thesis must be clearly indicated. Reproduction or other forms of for profit use or public communication from outside TDX service is not allowed. Presentation of its content in a window or frame external to TDX (framing) is not authorized either. These rights affect both the content of the thesis and its abstracts and indexes.



UNIVERSITAT
ROVIRA I VIRGILI

Functionalization of Strong Sigma Bonds by Nickel and Tungsten Catalysis

Raúl Martín Montero



DOCTORAL THESIS
2021

Functionalization of Strong Sigma Bonds by Nickel and Tungsten Catalysis

Raúl Martín Montero

DOCTORAL THESIS

Supervised by Prof. Rubén F. Martín Romo

Institut Català d'Investigació Química (ICIQ)

Universitat Rovira i Virgili (URV)

Department of Analytical Chemistry & Organic Chemistry



UNIVERSITAT ROVIRA i VIRGILI



Tarragona 2020



UNIVERSITAT ROVIRA I VIRGILI



Prof. Rubén Martín Romo, Group Leader at the Institute of Chemical Research of Catalonia (ICIQ) and Research Professor of the Catalan Institution for Research and Advanced Studies (ICREA),

STATES that the present study, entitled “Functionalization of Strong Sigma Bonds by Nickel and Tungsten Catalysis”, presented by Raúl Martín Montero for the award of the degree of Doctor, has been carried out under his supervision at the Institute of Chemical Research of Catalonia (ICIQ).

Tarragona, November 2020

Doctoral Thesis Supervisor

Prof. Rubén Martín Romo

List of Publications

At the time of printing, the results reported herein have been published as:

1. **Martin-Montero, R.**; Reddy V.; Yin, H.; Davies, J.; Martin, R. Ni-catalyzed Reductive Deaminative Arylation at sp^3 Carbon Centers. *Org. Lett.* **2019**, *21*, 2947-2951, DOI: 10.1021/acs.orglett.9b01016.
2. **Martin-Montero, R.**; Krolkowski, T.; Zarate, C.; Manzano R.; Martín R. Stereospecific Nickel-Catalyzed Borylation of Secondary Benzyl Pivalates. *Synlett*, **2017**, *28*, 2604-2608, DOI: 10.1055/s-0036-1590962.

The author has also contributed to the following:

3. Rand, A. W.; Yin, H.; Xu, L.; Giacoboni, J.; **Martin-Montero, R.**; Romano, C.; Montgomery, J.; Martin, R. Dual Catalytic Platform for Enabling sp^3 C–H Arylation & Alkylation of Benzamides *ACS Catal.* **2020**, *10*, 4671-4676. DOI: 10.1021/acscatal.0c01318.
4. Sun, S-Z.; Borjesson M.; **Martin-Montero R.**; Martin R. Site-Selective Ni-Catalyzed Reductive Coupling of alpha-Haloboranes with Unactivated Olefins. *J. Am. Chem. Soc.* **2018**, *140*, 12765–12769, DOI: 10.1021/jacs.8b09425.

Table of contents

List of Publications.....	iii
Abbreviations & Acronyms.....	xvi
Abstract.....	xix
Chapter 1. General Introduction.....	1
1.1 General introduction.....	2
1.2 Cleavage of strong sigma bonds.....	4
1.2.1 Nickel-Catalyzed C–Heteroatom bond formation via C–O bond cleavage.....	4
1.2.1.1 Introduction to nickel catalyzed C–O bond cleavage.....	4
1.2.1.2 C–N bond formation.....	6
1.2.1.3 C–Si bond formation.....	8
1.2.1.4 C–P bond formation.....	9
1.2.1.5 C–Sn bond formation.....	10
1.2.1.6 C–B bond formation.....	10
1.2.2 Nickel-catalyzed the cleavage of activated C(sp ³)–N bonds.....	12
1.2.2.1 Importance of alkyl C–N bond as electrophiles.....	12
1.2.2.2 Primary and secondary benzyl C(sp ³)–C bonds formation via boronic acids.....	13
1.2.2.3 Primary and secondary benzyl C(sp ³)–CO ₂ H bonds formation via CO ₂	15
1.2.2.4 C(sp ²)– and C(sp ³)–B bond formation of aromatic systems via B ₂ pin ₂ reagents.....	16
1.2.2.5 C(sp ³)–N scission of aziridines catalyzed by nickel.....	17
1.2.3 Remote functionalization of unactivated C–H bonds by walking metals.....	19
1.2.3.1 Introduction and mechanism of chain-walk events.....	19
1.2.3.2 Zirconium walking metal.....	21
1.2.3.3 Ruthenium, Rhodium, and Iridium walking metals.....	22
1.2.3.4 Iron walking metal.....	24
1.2.3.5 Cobalt walking metal.....	25
1.2.3.6 Palladium walking metal.....	27
1.2.3.7 Nickel walking metal.....	29
1.2.3.8 Tungsten as a promise chain-walk catalyst.....	32

1.3	General objectives of this Doctoral Thesis.....	34
1.4	References.....	35
Chapter 2.	<i>Stereospecific Nickel-Catalyzed Borylation of Secondary Benzyl Pivalates.....</i>	46
2.1	Introduction.....	47
2.2	Stereospecific cleavage of activated C(sp ³)-O bonds by nickel catalysis.....	47
2.2.1	Introduction.....	47
2.2.2	Ni-catalyzed stereospecific C-O cleavage of π -extended secondary benzyl ethers	48
2.2.3	Ni-catalyzed stereospecific reactions of benzyl C-O electrophiles by traceless directing groups.....	50
2.2.4	Nickel catalyzed stereospecific C-O cleavage of π -extended benzyl pivalates	51
2.2.5	Nickel catalyzed stereospecific C-O cleavage of allylic pivalates	52
2.3	Stereospecific Nickel-catalyzed borylation of secondary aryl benzyl pivalates.....	53
2.3.1	Aim of the project.....	53
2.3.2	Optimization of the reaction conditions.....	53
2.3.3	Substrate scope.....	60
2.3.4	Applications of benzyl boronates.....	63
2.3.5	Unsuccessful substrates.....	63
2.3.6	Mechanistic proposal.....	64
2.3.6.1	Ni/Cu mechanism.....	65
2.3.6.2	Nickel-fluoride activation picture.....	66
2.3.7	Future outlook	67
2.4	Conclusions.....	68
2.5	Experimental procedures.....	68
2.5.1	General considerations.....	68
2.5.2	Synthesis of starting material.....	69
2.5.3	Stereospecific borylation of benzyl pivalates.....	74
2.5.4	Synthetic applications.....	114
2.5.5	References of experimental procedures.....	118
2.5.6	¹ H-NMR, ¹³ C-NMR and ¹⁹ F-NMR spectra.....	119
2.5.7	HPLC.....	159
2.6	References.....	194

Chapter 3. Ni-catalyzed Reductive Deaminative Arylation at sp^3 Carbon Centers.....	197
3.1 Introduction.....	198
3.2 C–C and C–Heteroatom bond formation via $C(sp^3)$ –N bond cleavage of pyridinium salts.....	198
3.2.1 Introduction to the activation of unactivated alkyl amines by pyridinium salts.....	198
3.2.2 $C(sp^3)$ –C bond formation.....	199
3.2.2.1 $C(sp^3)$ – $C(sp^2)$ bond formation.....	199
3.2.2.2 $C(sp^3)$ – $C(sp)$ bond formation.....	201
3.2.2.3 Three-component C–C–C bond formation.....	202
3.2.2.4 $C(sp^3)$ – $C(sp^3)$ bond formation.....	203
3.2.3 C–Heteroatom bond formation.....	204
3.2.3.1 $C(sp^3)$ –N, $C(sp^2)$ –O, $C(sp^2)$ –S bond formation.....	204
3.2.3.2 $C(sp^3)$ –B bond formation.....	205
3.3 Ni-catalyzed Reductive Deaminative Arylation at sp^3 Carbon Centers.....	207
3.3.1 Aim of the project.....	207
3.3.2 Optimization of the reaction conditions.....	208
3.3.3 Substrate scope.....	217
3.3.4 Late-Stage Functionalization.....	220
3.3.5 Unsuccessful substrates.....	222
3.3.6 Mechanistic proposal.....	223
3.3.7 Future outlook.....	225
3.4 Conclusions.....	226
3.5 Experimental procedures.....	226
3.5.1 General considerations.....	226
3.5.2 Reaction conditions.....	227
3.5.3 Synthesis of Pyridinium salts.....	227
3.5.4 Ni-catalyzed reductive deaminative arylation with aryl halides.....	241
3.5.5 Photochemical conditions.....	256
3.5.6 Oxidative addition complex, Ni-1.....	256
3.5.7 Attempted reactions with sp^3 and sp -hybridized organic halides.....	257
3.5.8 Mechanistic studies.....	258

3.5.8.1	Electrochemical studies.....	258
3.5.8.2	Electrochemical potentials.....	262
3.5.8.3	Cyclic voltammograms.....	265
3.5.8.4	Radical trap experiments with TEMPO.....	271
3.5.8.5	Stoichiometric experiments with Ni(COD) ₂	272
3.5.8.6	Deaminative arylation of enantiopure secondary alkyl pyridinium salts.....	272
3.5.8.7	Radical clock experiments.....	273
3.5.9	References of experimental procedures.....	275
3.5.10	X-Ray Crystallography data for Ni(II) Complex Ni-1.....	276
3.5.11	¹ H NMR, ¹³ C NMR & ¹⁹ F NMR spectra.....	285
3.6	References.....	380
Chapter 4.	<i>Remote hydroboration of Alkenes Catalyzed by Tungsten</i>	384
4.1	Introduction.....	385
4.2	Hydroboration of alkenes.....	385
4.2.1	Uncatalyzed and catalyzed hydroboration of alkenes.....	385
4.2.2	Overview of metal-catalyzed hydroboration of alkenes.....	386
4.2.3	Metal-catalyzed remote hydroboration of alkenes.....	387
4.2.3.1	Co-catalyzed site-selective hydroboration of alkenes.....	387
4.2.3.2	Fe-catalyzed site-selective hydroboration of alkenes.....	389
4.2.4	Tungsten as unexpected catalyst.....	390
4.2.4.1	Hydrofunctionalization reactions using tungsten catalysis.....	390
4.2.4.2	Tungsten possibilities.....	392
4.3	Remote Hydroboration of Alkenes Catalyzed by Tungsten Complexes	392
4.3.1	Aim of the project.....	392
4.3.2	Optimization of the reaction conditions.....	392
4.3.3	Substrate scope.....	398
4.3.4	Applicability of W-catalysis.....	400
4.3.5	Mechanistic proposal.....	401
4.3.6	Future outlook.....	403
4.4	Conclusions.....	403

4.5	Experimental procedures.....	404
4.5.1	General considerations.....	404
4.5.2	Optimization of the reaction conditions.....	404
4.5.3	Synthesis of alkene amides.....	405
4.5.4	Remote alkene hydroboration of amides catalyzed by tungsten.....	413
4.5.5	Control reactions with α,β -unsaturated amides.....	424
4.5.6	Deuterium labeling experiments with DBpin.....	425
4.5.7	References of experimental procedures.....	426
4.5.8	X-Ray of compound 14.....	427
4.5.9	^1H NMR, ^{13}C NMR & ^{19}F NMR spectra.....	431
4.6	References.....	483
Chapter 5.	General conclusions.....	486

Acknowledgements

First of all, I would like to express my gratitude to my supervisor, **Rubén**. Without the opportunity that you gave me more than four years ago, all these pages would not be possible. You have taught me countless things about chemistry as a student in your group, and thanks to all this knowledge, I am right here, writing a Doctoral Thesis. I must admit that my scientific perspective has changed tremendously for the better, and is something that I am forever indebted to you. Moreover, and possibly more important to me, you taught about first principles and life values. Over this time, you showed me by your example how much one can take, and how to keep moving forward. Also, thanks for being always there, in the office or by email, 24/7, to listen my doubts and to talk about chemistry, the group or life. I want to end these lines by saying that you are one of the people I respect the most.

Second, I would like to thank the members of my committee, **Prof. Dr. Troels Skrydstrup**, **Dr. Martín Fañanás** and **Prof. Dr. Mariola Tortosa** for accepting our invitation to read and assess my work.

I would also like to acknowledge the collaborators that I have worked with during the projects summarized in this Thesis and in other publications not mentioned: **Tim Krolkowski**, **Dr. Cayetana Zarate** and **Dr. Ruben Manzano**, then **Dr. Shang-Zheng Sun** and **Dr. Marino Börjesson**. Also, **Dr. Reddy Yatham**, **Dr. Hongfei Yin** and **Dr. Jacob Davies**. Thanks to **Dr. Alexander Rand**, **Dr. Liang Xu**, **Dr. Jessica Giacobini**, **Dr. Ciro Romano** and **Prof. Dr. John Montgomery**. Finally, to **Tanner Jenkins**, **Dr. Phillippa Cooper** and **Prof. Dr. Keary Engle**.

Now, let's go to thank many many people, this is going to be long...

I want to thank all the past and present members of the Martin group, The Martinis, for all the help, discussions, lunches and good moments we had in the lab and also outside. Thanks **Ingrid**, **Miriam**, **Sope** and **David** for administrative support and your willingness to help in every moment. Thanks to my old generation of past members, **Toni**, **Morgane**, **Eloisa**, **Paco**, **Georgios**, **Alicia**, **Antonio**, **Marino**, **Rosie**. **Toni** and **Morgane**, I will always remember our volleyball matches at the beach and the beers and beers we drank, especially at the Chinese bar at Plaza de la Font. **Elo**, you supported me in many moments and you were always a chemist example in the lab. **Paco**, the smartest guy in the lab, ask anything and you will get an answer. Impossible to forget your discussions with Ruben in the group meetings about chemistry and looking at you with the most respect. **Georgios**, my bro, dude, yo, hermano, Zeus, what to say! You are very important to me as demonstrated every time you came by here. I am glad to say that you are my friend whatever the distance. But, you are a bastard that broke my heart when you decided not to continue with us. Thanks for all the good moments in the lab, kitchen, group meetings, and partying and drinking. **Alicia**, as everybody says, you came in the perfect moment. You brought to the group what we

needed, that team-atmosphere, organization, good vibes, energy. I remember that time as the happiest during my four years. **Antonio**, acho-pijo!!! What a natural man. I enjoyed every second at your side, sharing fumehood, projects, and parties. Please, do not change ever. Me emborracharée, me emborracharée por tu culpa, por tu culpa... **Marino**, best man with whom to get shitfaced. Above all, you are a fantastic person and a really good chemist. I have missed you in the lab and at home these last months. **Rosie**, My **RosaMaría**!!! Probably you are one of the persons with the biggest heart I have ever met. If I had to thank you for all the things you have helped me, the acknowledgments would be much longer. Please, do not change, and please, do not forget you will always have a friend in Spain.

Also thanks **Daniel**, **Tim**, **Yiting**, **YangYang**, **Reddy**, **Basudev**, **Liang** for helping me in every moment I needed and chatting and teaching about chemistry.

Now, I must thank the current members. **Andreu**, my brosito, what a person I met four years ago. Simply, you are an incredible friend. Thanks for helping me in the lab with tons of things. **Shang!** Sincerely, with Rosie you are one of the kindest person I have met in my life. I have shared with you many moments, especially stress moments that made me be your friend rapidly. Honestly, I wish you the best in your life, you deserve it. **Cris** (Maquilón), thanks for being almost part of our group all these years. We have talked and shared many things and moments and I will always remember you with a smile, Agnes. Do not forget your friend from Madrid because I will not forget mine from Elche. Te lo prometo, gracias. **Bradley**, what a smart and funny guy. Sometimes I believed we were brothers from another mother. **Carlota**, you are a wonderful person, and I have to say that I have a very good connection with you. Thanks for all the good moments, hopefully they will not be the last ones. **Laura**, lokita! Thanks for bringing to the lab all your character and positivism. Above all, you are a fantastic friend, and over this time you became important to me. **Hongfei**, my pretty friend. Thanks for helping me in the projects and being patient with me and the lab. **Jacob**, thanks for all your help in whatever thing I needed (chemistry, projects, organizing events, etc). Thanks again. **Ciro**, I do not have too much to say that you do not know. I am going to be simple, you got here a friend forever. I want to thank the rest of the group, **Yaya**, **Jessica**, **Fei**, **Craig**, **Victoria**, **Chris**, **Xinyang**, **Dmitry**, **Wen-Jun**, **Juzeng**, **Tiago**, **Mara**, **Ricardo**, **Jesus** for creating the atmosphere we have now in the group.

There have been many people at ICIQ important to me that I need to thank. Therefore this list is to remind me in the future that I consider all you as friends and an important part of this adventure: **Cris**, **Alba**, **Marghe**, **Ángel**, **Joan**, **Pablo**, **Bafa**, **Thomas**. THANKS.

I also thank **Prof. Keary Engle** for giving me the opportunity to join his group. Thanks to all the group, especially my lab-family there: **Van**, **Tanner**, **Joe**, **Omar**. You made my stay fantastic and now you are my dudes. **Patry**, you are incredible, I will never forget our moments there. **Fran**, I was so glad to see you again there, I wish you the best. Talking about the family, thanks to my other parents,

Connie, Mark, and Dee for welcoming me in the EEUU and treating me like one of your sons. I consider you my second family.

A los mastodontes, **Michelle, Edu, Javi, Dante, Alex**, gracias por tan largos y buenos momentos tanto en el OW como cuando os conocí. **Edu**, gracias por interesarte siempre por mí, te lo agradezco. **Michelle**, gracias por ser como eres, eres una maravilla de persona.

Tarragona's family time arrived. I am going to be simple because that is the way of real feelings. **Andreu**, gracias por ser el amigo que has sido y que eres. Tu corazón demuestra todo lo que vales y te considero una persona muy importante para mí, lo sabes. **Kike**, lo primero que me sale decirte es que te quiero mucho. Eres un jodido buen amigo, me alegro mucho haberte encontrado en este camino. **Nuria**, sabes que tenemos una conexión especial. Eres increíble, no cambies nunca porque te quiero mucho. Espero que sepas que aunque hayas cuidado de todos, yo también cuidaré que nuestra amistad continúe. **Alicia**, creo que mejor persona no puedes ser. Cariñosa, atenta y siempre cuidando de todos. Gracias por encontrarte de nuevo y disfrutar juntos de tantos momentos. **Jesús**, bro, gracias por todos esos inmensos momentos de reírnos hasta llorar y por aportar esa chispa. Espero que sigas teniendo siempre esa sonrisa y tan buenas vibraciones porque vales muchísimo, amigo. **Cris**, eres una bellísima persona y así ha salido **Victoria**. Me ha encantado compartir este tiempo contigo y gracias por enseñarnos como eres porque eres un ejemplo a seguir en muchas cosas. **Ester**, eres tan natural y tan como yo en muchas cosas que gracias por dejarme estar a tu lado este tiempo. Gracias por nuestras conversaciones y gracias por sacarme una sonrisa y un abrazo cada vez que te veo. Eres un 10. **Miguel**, no se puede ser tan grande y tener un corazón aún más grande. Tu naturalidad y sencillez simplemente enamoran y yo puedo decir que te quiero mucho, amigo. Gracias. **Alba**, ¡niña! Qué voy a decir de ti, si sabes que tengo debilidad contigo a pesar de que me cayeras mal al principio. Eres increíble, y doy gracias a que te conocí mejor para darme cuenta de ello. Te tengo mucho, mucho cariño y vales muchísimo. **Chuchi**, amigo mío, gracias por poner la serenidad en muchos momentos a este grupo de locura, y sobre todo gracias por seguir estando como un amigo aún con la distancia. **Alicia**, estás es todos lados. Gracias por aprovecharte de los recursos de mi casa incontables veces, porque entre eso y el lab hizo que te conociese mejor y mis ojos se tornasen a ti cada vez más. **Ana**, es increíble la de vueltas que da la vida. Has sido parte de esta familia pero tú ya llevabas en mi familia más tiempo. Sinceramente, os quiero mucho a todos. Ocurra lo que ocurra, estemos donde estemos, contad conmigo en lo que necesitéis, amigos.

A mis amigos/familia de toda la vida, GRACIAS. **Antonio**, no me cansaría de darte las gracias en esta vida y en la siguiente. Sabes todo lo que te aprecio, lo que te quiero y lo importante que eres. No hay líneas suficientes para rellenar por todo lo que hemos pasado y todo lo que nos queda. Eres una de esas personas que tengo a mi lado. FAE. **Sandra**, gracias por cuidar de Antonio y por ser como eres. He tardado en conocerte, pero eso no quita el cariño que te tengo. **Moreno**, quien diría que después de 24 años íbamos a estar tan unidos. Es para mí una de las mayores alegrías el poder seguir

teniéndote a mi lado después de tantas cosas. Es increíble todo lo que te quiero. Gracias por cuidarme una vida entera. **Cristina**, valenciana, sabes que te quiero mucho. Gracias por ofrecerme tu casa en mis primeros viajes a Valencia. **Chuky**, te daría las gracias por tantas cosas que elijo la mejor. Gracias por ser mi amigo. Ya sabes desde hace tiempo que te considero como parte de mi familia. Si ya tenía a estas dos personas a mi lado tú tienes otro hueco más. **Ana**, en el master ya apuntabas maneras para quedarte en mi vida y así ha sido. Gracias por acompañarme estos años, eres una bellísima persona y alguien a quien quiero tener al lado el resto de mi camino. **Vane**, la distancia ha hecho que nos hayamos separado un poco, pero tú sabes todo lo que te quiero y te quiero dar las gracias por todos los momentos que me has ayudado. **Natalia**, tan solo tú y yo sabemos por todo lo que hemos pasado. Gracias por mantenerte siempre como mi amiga y mi hermana pequeña. Eres maravillosa, Nat. **Kata**, guapa, eres un tío con un corazón inmenso y alguien que ha estado en mi vida desde pequeños. Gracias por estar ahí. **Melina**, debes de ocupar un lado especial aquí también. Gracias por darme tan buenos momentos en mi vida que nunca olvidaré. Una pequeña parte es gracias a ti. **Peri**, **Kiko**, **Jesús**, **Juan**, gracias por todos los buenos momentos, que no son pocos.

Alicia, quería darte las gracias de forma especial solo a ti. Es increíble como en esta etapa he podido conocerte de todas las maneras y me he llevado la mejor de ellas, ser tu pareja. Gracias por compartir momentos, gustos, aficiones, viajes conmigo, porque lo mejor de todo ello ha sido acompañarte. Eres una persona increíble con un corazón que se te sale del pecho y por ello estoy enamorado de ti. Por último, tengo que agradecer el inmenso esfuerzo que le has puesto a esta Tesis conmigo. Gracias por ayudarme a crecer y a hacerme mejorar en cada momento de mi vida. Te quiero.

Quiero dedicar esta tesis a las personas que más tengo que agradecer en mi vida y que me han dado todas las oportunidades para conseguirla, mis padres. **Papá**, eres la persona en la que pienso como ejemplo cuando me tengo que enfrentar a algo en la vida. Tu valentía, fuerza, y personalidad hace que hayas sido, seas y serás mi referente en la vida. Te quiero muchísimo. Gracias por todo. **Mamá**, eres la mejor persona que conozco, y siempre te tengo en mente para mejorar y ser como tú. Siempre me has apoyado y me has animado en cada momento. Cada vez que veo tu cara cuando vuelvo a casa hace que te quiera más y valore más todo lo que me has enseñado en la vida. Te estaré siempre agradecido por todo. Te quiero muchísimo. **Alberto**, eres lo más valioso que tengo en mi vida. Gracias por apoyarme siempre y recibir todo el cariño que me has dado estos años. Te quiero mucho, tate. **Abuela Amelia**, eres como mi segunda madre. Gracias por cuidarme toda mi vida y tratarme como a uno de tus hijos. Es inmenso el cariño que te tengo y lo que te quiero. **Abuelos Boni y Pepe**, os dedico esto junto a mis padres. Es una pena no poder compartirlo con vosotros. Al resto de la familia, entenderéis que sois muchos y no os puedo agradecer uno a uno esto, pero GRACIAS, GRACIAS y GRACIAS. Os quiero.

Abbreviations & Acronyms

acac = acetylacetonate
BDE = bond dissociation enthalpy
BINAP = Bis(diphenylphosphino)-1,1'-binaphthalene
COD = 1,5-cyclooctadiene
Cy = cyclohexyl
Conv = conversion
DMA = *N,N*-dimethylacetamide
DME = 1,2-dimethoxyethane
DMF = *N,N*-dimethylformamide
dcpe = 1,2-Bis(dicyclohexylphosphino)ethane
dppe = 1,2-bis(diphenylphosphino)ethane
ee = enantiomeric excess
equiv = equivalents
FID = Flame Ionization Detector
GC = gas chromatography
h = hour(s)
HPLC = High Pressure Liquid Chromatography
IPr = 1,3-Bis(2,6-diisopropylphenyl)imidazol-2-ylidene
L = ligand
Mes = mesityl
nep = neopentyl glycolate
NMP = *N*-methyl-2-pyrrolidone
NMR = Nuclear Magnetic Resonance
OA = oxidative addition
PDA = Photodiode Array Detector
phen = 1,10-phenanthroline
pin = pinacolate
piv = pivalate
PMT = Photomultiplier tube
ppm = parts per million
rac = racemic
rt = room temperature
SET = single-electron transfer
SM = starting material
S_N = nucleophilic substitution

T = temperature

TEMPO = 2,2,6,6-Tetramethyl-1-piperidinyloxy

THF = tetrahydrofuran

TMS = tetramethylsilane

Tol = tolyl

UPC2 = UltraPerformance Convergence Chromatography

UV = Ultraviolet

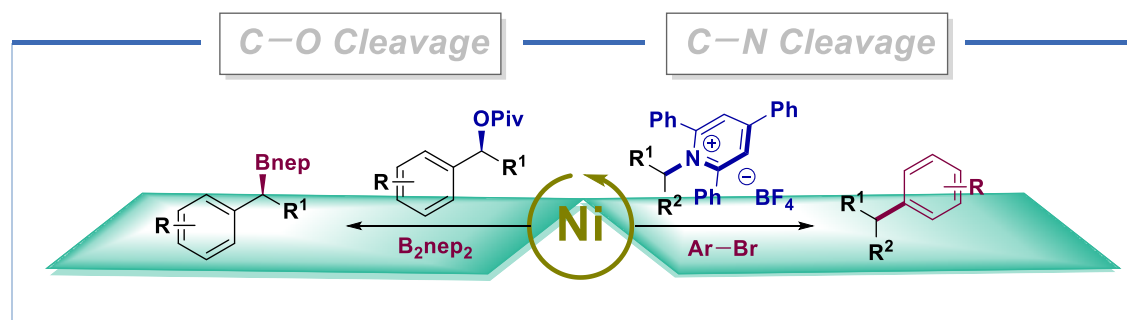
DAD = diode array detector

Abstract

In recent years, the functionalization of strong sigma bonds has received considerable attention as demonstrated by numerous investigations into the efficiency of transition metals in this process.^{1–3} Among them, nickel has been considered one of the leaders due to its earth-abundance, nucleophilicity, and capacity to participate in one- or two-electron redox pathways.^{4,5} On the other hand, the ability of tungsten to functionalize strong sigma bonds has only been hinted at by a small selection of promising W-catalysed reactions, which have opened the door for further studies.

In line with the Martin group's interest in developing catalytic methods for the activation of inert bonds, this Doctoral Thesis is focused on the nickel-catalyzed scission of C–O bonds to achieve the stereospecific formation of C–B bonds (*Chapter 2*), the cleavage of unactivated C–N bonds for the assembly of C–C bonds by nickel catalysis (*Chapter 3*), and the functionalization of strong sigma bonds by a site-selective C–H activation protocol utilizing tungsten catalysis (*Chapter 4*).

Despite all the advances recently performed in the scission of C–O bonds by the derivatization of unactivated phenol derivatives,⁶ such as benzyl esters or ethers, no stereospecific C–Heteroatom bond formations had been reported. In the *Chapter 2* of this dissertation, the first stereospecific borylation of secondary benzyl alcohol derivatives catalyzed by a cooperative Ni/Cu-catalysis is presented (Scheme 1, *left*). The final formation of an enantioenriched borylated product paves the way for further functionalizations.

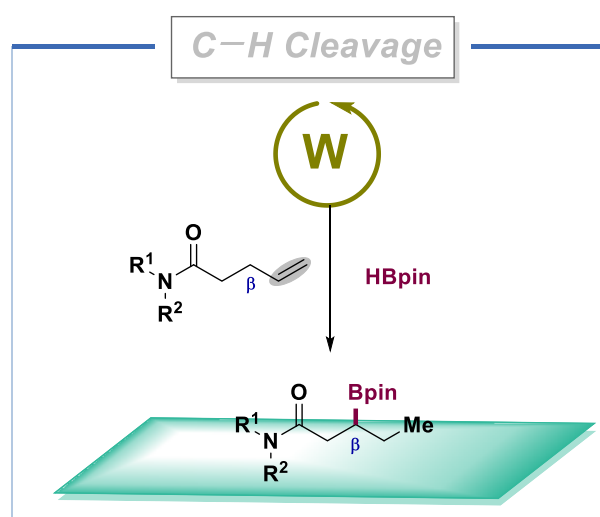


Scheme 1. Ni-Catalyzed C–O and C–N cleavages.

Subsequently, studies moved toward the functionalization of unactivated alkyl amines. In spite of the vast literature for the utilization of activated sp^3 C–N bonds in cross-coupling reactions,⁷ unactivated alkyl amine coupling partners did not initially attract the attention of chemists due to their high C–N bond dissociation energies. Nevertheless, the formation of C(sp^3)–C(sp^2) bonds was accomplished via the utilization of organometallic species or biased heteroarenes as coupling partners with pyridinium salts.^{8,9} In such a way, *Chapter 3* of this Thesis is based on a reductive deaminative arylation at sp^3 carbon centers catalyzed by nickel (Scheme 1, *right*). This strategy establishes a user-friendly and unbiased coupling partner that allows with the arylation of

unactivated alkyl amines. The work performed in this chapter also includes experimental results that clarify the mechanistic aspects of the transformation.

Driven by our interest in the functionalization of strong sigma bonds, remote C–H activation caught our attention. Despite the advances performed by many transition metals in this field,³ the final functionalized sites are commonly the terminal position of an alkyl chain or the α -carbon geminal to a functional group. Motivated by unique reactivity^{10–12} of tungsten and its abundance, *Chapter 4* reports a site-selective β -hydroboration of terminal alkenes catalyzed by tungsten complexes (Scheme 2). This protocol is complementary to that shown with Pd-, Ni- or Co-catalyzed chain-walking reactions offering a new strategy for promoting the functionalization at unactivated sp^3 C–H sites of alkyl chains. A series of applications have also been described, thus opening a gateway for investigations into further functionalizations that would otherwise be beyond reach.



Scheme 2. W-catalyzed remote functionalization of C–H bonds.

References:

- (1) Zarate, C.; van Gemmeren, M.; Somerville, R. J.; Martín, R. Phenol Derivatives: Modern Electrophiles in Cross-Coupling Reactions. *Adv. Organomet. Chem.* **2016**, *66*, 143–222. <https://doi.org/10.1016/bs.adomc.2016.07.001>.
- (2) Ouyang, K.; Hao, W.; Zhang, W. X.; Xi, Z. Transition-Metal-Catalyzed Cleavage of C–N Single Bonds. *Chem. Rev.* **2015**, *115* (21), 12045–12090. <https://doi.org/10.1021/acs.chemrev.5b00386>.
- (3) Sommer, H.; Juliá-Hernández, F.; Martín, R.; Marek, I. Walking Metals for Remote Functionalization. *ACS Cent. Sci.* **2018**, *4* (2), 153–165. <https://doi.org/10.1021/acscentsci.8b00005>.
- (4) Ananikov, V. P. Nickel: The “Spirited Horse” of Transition Metal Catalysis. *Acc. Chem. Res.* **2015**, *5*, 1964–1971. <https://doi.org/10.1021/acscatal.5b00072>.
- (5) Tasker, S. Z.; Standley, E. A.; Jamison, T. F. Recent Advances in Homogeneous Nickel Catalysis. *Nature* **2014**, *509* (7500), 299–309. <https://doi.org/10.1038/nature13274>.

- (6) Cornella, J.; Zarate, C.; Martin, R. Metal-Catalyzed Activation of Ethers via C-O Bond Cleavage: A New Strategy for Molecular Diversity. *Chem. Soc. Rev.* **2014**, *43* (23), 8081–8097. <https://doi.org/10.1039/c4cs00206g>.
- (7) Wang, Q.; Su, Y.; Li, L.; Huang, H. Transition-Metal Catalysed C-N Bond Activation. *Chem. Soc. Rev.* **2016**, *45* (5), 1257–1272. <https://doi.org/10.1039/c5cs00534e>.
- (8) Basch, C. H.; Liao, J.; Xu, J.; Piane, J. J.; Watson, M. P. Harnessing Alkyl Amines as Electrophiles for Nickel-Catalyzed Cross. *J. Am. Chem. Soc.* **2017**, *139*, 5313–5316. <https://doi.org/10.1021/jacs.7b02389>.
- (9) Klauck, F. J. R.; James, M. J.; Glorius, F. Deaminative Strategy for the Visible-Light-Mediated Generation of Alkyl Radicals. *Angew. Chemie. Int. Ed.* **2017**, *56* (40), 12336–12339. <https://doi.org/10.1002/anie.201706896>.
- (10) Kusama, H.; Yamabe, H.; Iwasawa, N. W(CO)5-Amine Catalyzed Exo- and Endo-Selective Cyclizations of ω -Alkynyl Silyl Enol Ethers: A Highly Useful Method for the Construction of Polycyclic Compounds. *Org. Lett.* **2002**, *4* (15), 2569–2571. <https://doi.org/10.1021/ol026202c>.
- (11) Lefebvre, F.; Bouhoute, Y.; Szeto, K. C.; Merle, N.; Mallmann, A. De; Gauvin, R.; Lefebvre, F.; Bouhoute, Y.; Szeto, K. C.; Merle, N.; Mallmann, A. De. Olefin Metathesis by Group VI (Mo, W) Metal Compounds. In *Alkenes*; IntechOpen, 2018. <https://doi.org/10.5772/intechopen.69320>.
- (12) Kocięcka, P.; Czeluśniak, I.; Szymańska-Buzar, T. Efficient and Selective Synthesis of E-Vinylamines via Tungsten(0)-Catalyzed Hydroamination of Terminal Alkynes. *Adv. Synth. Catal.* **2014**, *356* (16), 3319–3324. <https://doi.org/10.1002/adsc.201400568>.

Chapter 1.

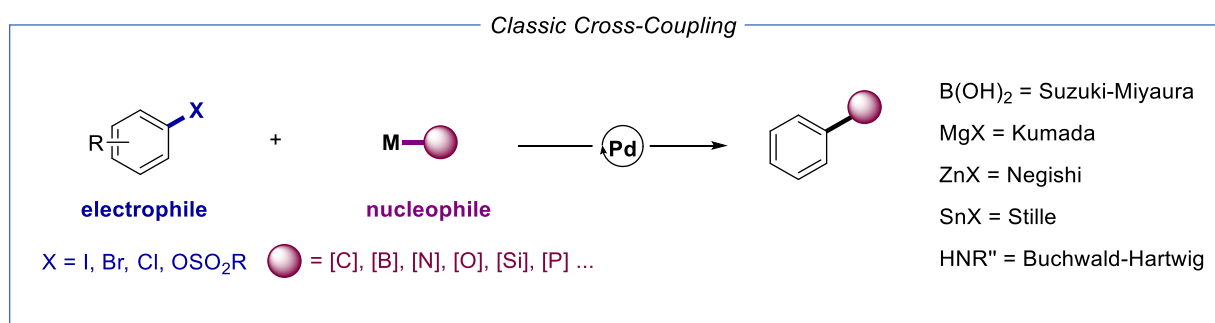
General Introduction

Chapter 1

1.1 General Introduction

Metal-catalyzed cross-coupling reactions have become one of the pillars of modern organic chemistry since their exponential growth 50 years ago.¹⁻³ These technologies have offered synthetic chemists in both academic and industrial laboratories a reliable new technique to rapidly build up molecular complexity when forging C–C and C–heteroatom bonds. Not surprisingly, the relevance of these technologies was recognized with the 2010 Noble Prize in Chemistry awarded to Heck, Negishi and Suzuki for their developments in Pd-catalyzed cross-coupling reactions.

Traditionally, C–C bond-formation by means of transition metal-catalyzed cross-coupling reactions rely on the combination of an organometallic nucleophile and an appropriately substituted electrophilic counterpart (Scheme 1.1). While a wide variety of transition metals can be employed for such purposes, Pd catalysts have been well-adopted by the Community due to their versatility, modularity and wide substrate scope across an array of differently substituted counterparts.



Scheme 1.1. Pd-catalyzed cross-coupling reactions.

Although organic halides are probably the most common electrophiles employed in metal-catalyzed cross-coupling reactions, their toxicity and difficult accessibility have prompted chemists to look for cheaper alternatives with improved flexibility, practicality and modularity. In recent years, particular attention has been devoted to the utilization of alcohols, amines, esters or carboxylic acid derivatives as surrogates of organic halides. In addition, the direct functionalization of alkanes and alkenes has also served as an alternative for forging C–C and C–heteroatom bonds without the need for prefunctionalization at the electrophilic site.^{3,4} Among different alternatives, the means to promote C–O and C–N cleavage in simple alcohols and amine as electrophilic partners have attracted considerable attention.⁵⁻¹⁰ These compounds are commonly found in nature, pharma, agrochemicals and material science, making them particularly useful for late-stage functionalization in densely functionalized substrates.

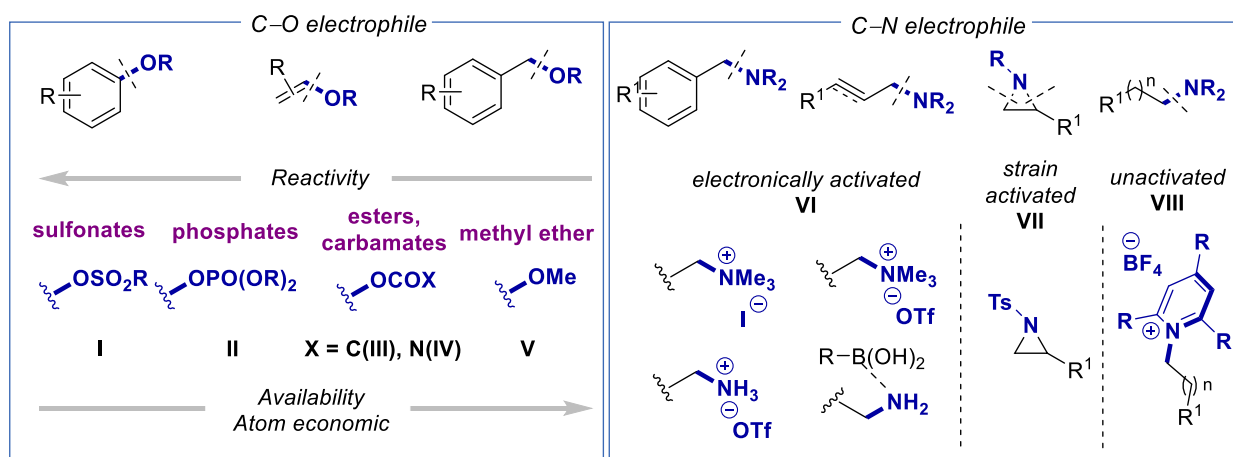


Figure 1.1. C–O and C–N electrophiles in metal-catalyzed cross-coupling reactions.

Despite the advances realized, the utilization of simple alcohols and amines in metal-catalyzed cross-coupling reactions is particularly challenging due to the high activation barrier required for effecting C–OH and C–NH₂ scissions. To this end, early research efforts have been devoted to the utilization of aryl triflates (Figure 1.1 I, R = CF₃) due to the low dissociation energy required for effecting C–O bond-cleavage in a canonical oxidative addition pathway. These conceptions served as a starting point for exploring less reactive aryl phenol derivatives such as aryl mesylates, (Figure 1.1, I, R = CH₃), tosylates, (I, R = *p*-C₆H₄CH₃), nonaflates (I, R = C₄F₉), and phosphates (II).¹¹ Although better alternatives than triflates, these derivatives do not represent an added value in terms of availability, stability and atom economy, thus limiting the potential application profile of these protocols. These challenges could partially be alleviated by the utilization of nickel catalysts and the employment of phenol derivatives possessing higher bond-dissociation energies such as aryl esters (III), carbamates (IV), or even aryl ethers (V), as nicely illustrated by the pioneering work of Dankwardt and Wenkert in 2004.^{12,13}

In 1988, Wenkert and co-workers reported that even trialkylammonium salts derived from aryl amines can be used as organic halide surrogates within the context of a Kumada-Corriu reaction, thus showing the viability of nickel complexes to promote a *sp*² C–N scission.^{14–16} It was not until 2003 when MacMillan demonstrated that these technologies could be applied with less basic organometallic reagents, resulting in the development of a Suzuki-Miyaura coupling of aryl trimethylammonium salts and Grignard reagents catalyzed by nickel complexes.¹⁷ These findings served as an entry point for extending the scope of these reactions beyond aryl amine electrophiles. Indeed, it was possible to promote similar cross-coupling reactions with activated benzyl alkyl ammonium salts (Figure 1.1, VI),⁹ propargylic ammonium salts,^{18,19} or strained aziridine counterparts.^{20–24} Few years later, the generality of these reactions was illustrated by the successful cross-coupling reactions of unactivated alkyl amine congeners (VIII) thus showing the potential that C–N electrophiles might offer within the context of metal-catalyzed cross-coupling reactions.^{25,26}

Chapter 1

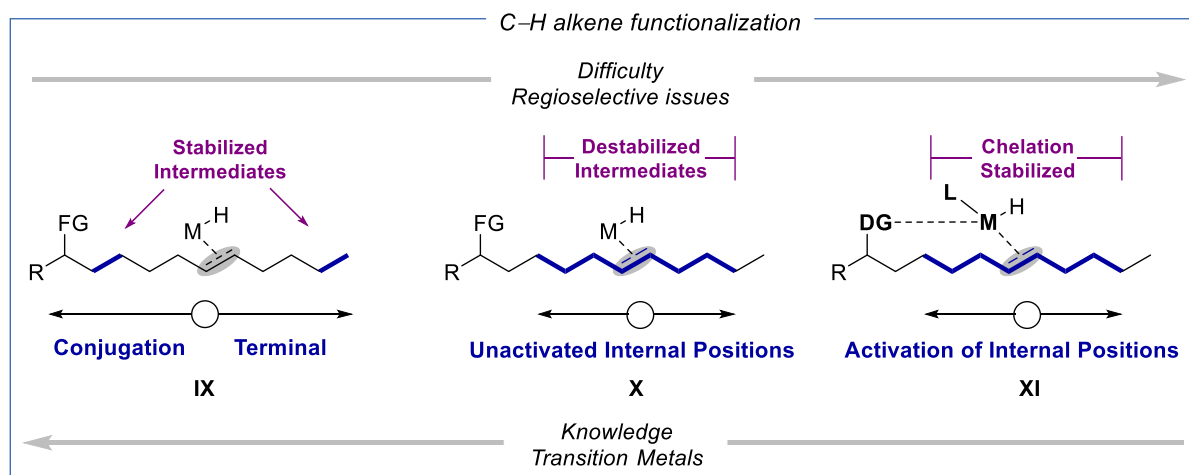


Figure 1.2. C–H alkene functionalization.

The desire to build complex architectures from simple, yet less-functionalized precursors, has turned the attention of chemists to alkenes, which rank amongst the most abundant building blocks in organic chemistry endeavors. Alkenes can be activated by some unique transition metal catalysts leading to elegant transformations²⁷ – some of these being particularly attractive in industrial settings – such as the Wacker process,²⁸ olefin metathesis,²⁹ olefin hydroformylation,³⁰ Heck reaction³¹ or hydroboration of olefins, undoubtedly one of the most important transformations in organic settings due to the versatility and applicability of organoboron compounds.^{32–35} While the vast majority of transformations of alkenes rely on the functionalization across the double C=C bond or at the allylic sp^3 C–H motif, the recent years have witnessed the development of catalytic techniques aimed at promoting the functionalization of alkenes at remote sp^3 C–H sites (Figure 1.2, **IX**).³⁶ However, site-selectivity has been a difficult challenge to tackle due to the intrinsic reactivity of non-partially stabilized alkyl-metal intermediates, thus leading to mixtures of different regioisomers (**X**). Despite these drawbacks, the development of new catalysts and ligands have allowed to tackle these challenges by promoting a wide variety of transformations that enable bond-formation at remote, yet previously unfunctionalized, sp^3 C–H sites (**XI**).^{37–44}

1.2 Cleavage of strong sigma bonds

1.2.1 Nickel-catalyzed C–Heteroatom bond formation via C–O bond cleavage

1.2.1.1 Introduction to nickel-catalyzed C–O bond cleavage

The inherent interest about the utilization of aryl C–O electrophiles in metal-catalyzed cross-coupling reactions arises from the abundance and ready availability of phenols compared to organic halides, and the prevalence of these motifs in a myriad of natural products, agrochemicals or pharmaceutically-relevant molecules.^{5,45} Not surprisingly, the higher bond-dissociation energy of sp^3

C–O bonds (BDE \sim 96 kcal/mol)⁴⁸ make them particularly problematic for the utilization of aliphatic alcohol derivatives in cross-coupling reactions (Figure 1.2.1, *bottom*).

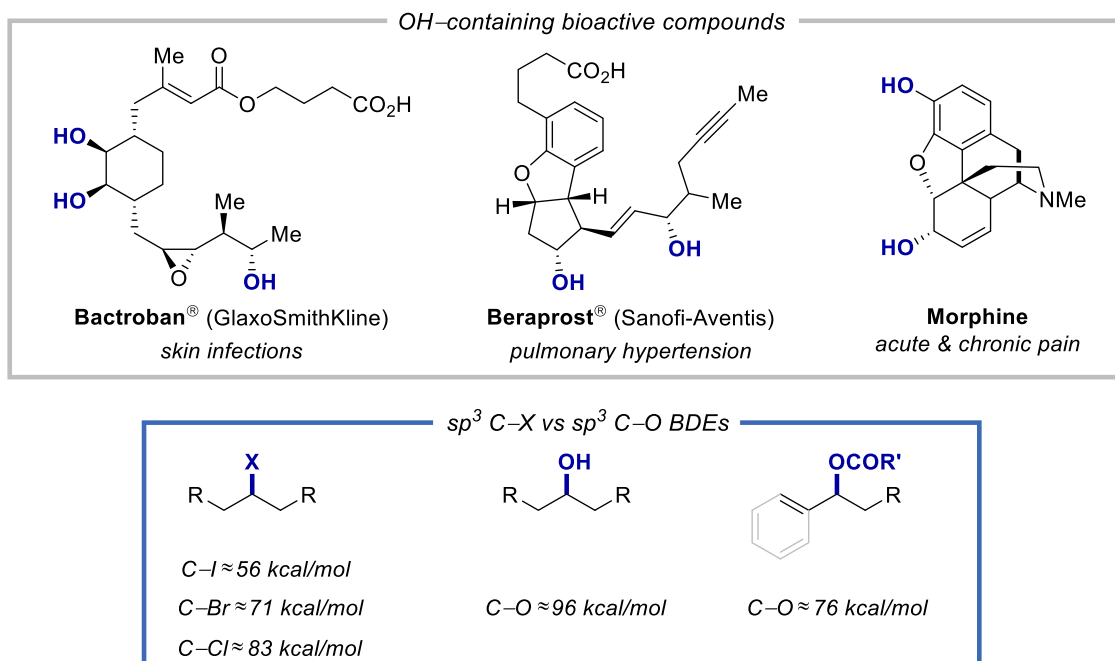


Figure 1.2.1. Importance and BDEs of alcohols.

Driven by these observations, chemists have devoted considerable attention to the development of Ni-catalyzed cross-coupling reactions of allylic C–O electrophiles due to the weak bond-dissociation energy of the corresponding sp^3 allylic C–O bond (Figure 1.2.2).^{49–52} Despite the advances realized in C–C bond forgings by C–O scission, C–Heteroatom bond formation protocols were not investigated only after the inspirational work of Shi in 2008 (Figure 1.2.2, *right*).⁵³

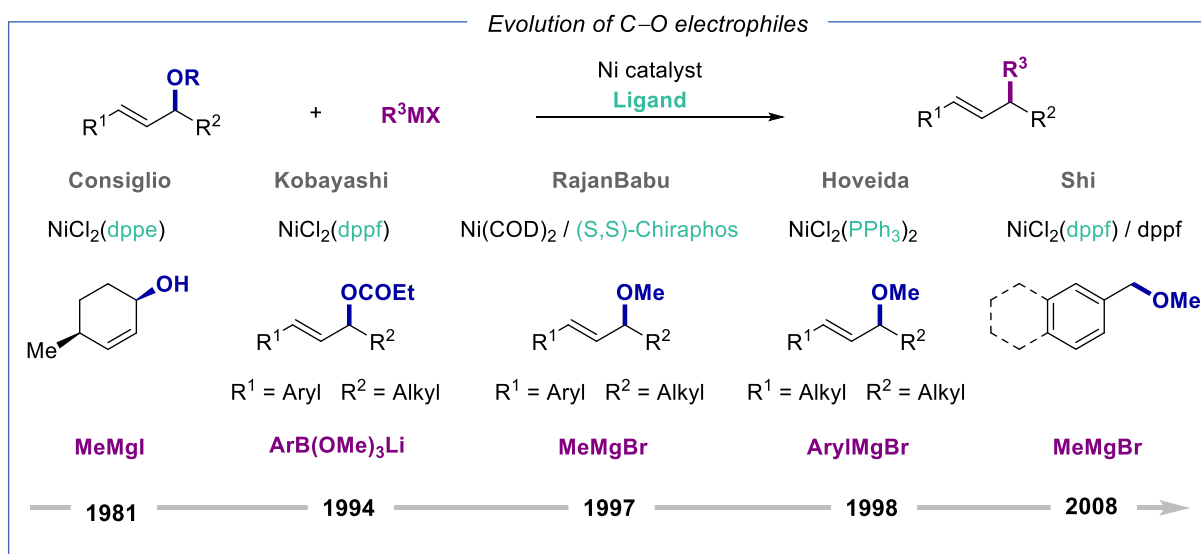
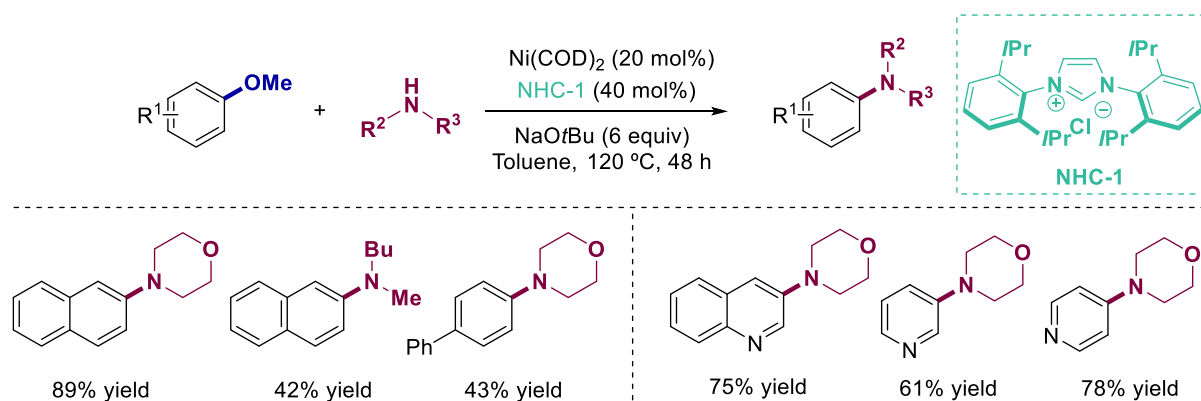


Figure 1.2.2. Evolution of C–O electrophiles in time.

Chapter 1

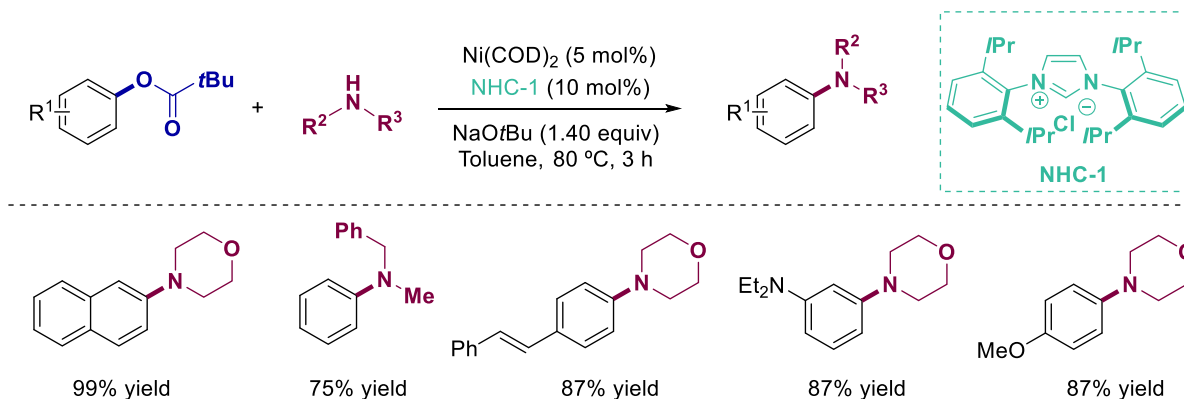
1.2.1.2 C–N bond formation

In 2009, Chatani and co-workers reported a direct amination of anisoles involving the cleavage of C(sp²)–OMe by means of nickel catalysis (Scheme 1.2.1, *left*).⁵⁴ This transformation is particularly interesting as it demonstrated, for the first time, the means to promote a C–N bond-formation at a particularly strong C(sp²)–OMe bond with simple Ni catalysts bearing NHC-carbene ligands. Unfortunately, however, this reaction was limited to π -extended anisoles, invariably requiring high temperatures and a limited set of amine counterparts. This reaction could subsequently be applied to the coupling of *N*-heteroaryl methyl ethers (Scheme 1.2.1, *right*).⁵⁵ While a step-forward, the functional group tolerance could not be fully demonstrated, and low yields were generally achieved when promoting the reaction with non- π -extended anisoles.



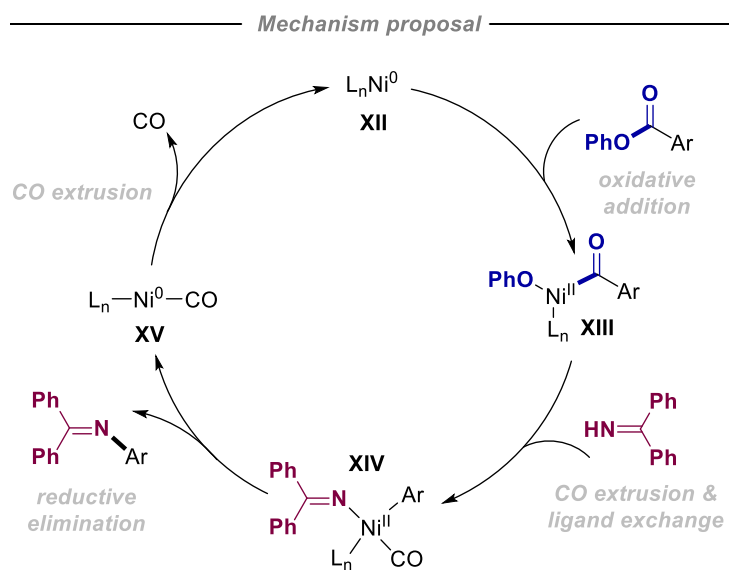
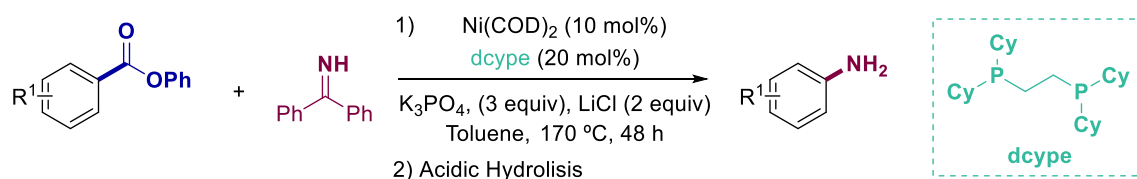
Scheme 1.2.1. Ni-catalyzed amination of anisoles derivatives *via* C–O cleavage.

In 2012, Garg and co-workers demonstrated that the combination of an air-stable NiCl₂·DME precatalyst with Ph–BPin as reducing agent could promote the amination of aryl carbamates and sulfonates.⁵⁶ Interestingly, the transformation tolerated a wide range of functionalities and sterically hindered *ortho*-substituted substrates, including non- π -extended systems and heteroaromatic rings. In 2010, Chatani’s group addressed the limitations of the amination of aryl methyl ethers beyond activated π -extended systems by using aryl esters as counterparts (Scheme 1.2.2).⁵⁷ These substrates still required the utilization of strong basic conditions, but offered a mild protocol for promoting C–N bond-formation *via* C–O scission.



Scheme 1.2.2. Ni-catalyzed amination of aryl pivalates *via* C–O cleavage.

In 2017, Rueping and co-workers reported a nickel-catalyzed decarbonylative amination of esters and amides by means of C–O and C–C bond functionalization (Scheme 1.2.3).⁵⁸ Unfortunately, the utilization of heteroaromatic substrates or non- π -extended systems resulted in lower yields of the targeted products. The mechanism of the reaction is proposed to start with an oxidative addition of the C(acyl)–O bond of the aryl ester to Ni(0) complex (**XII**). The corresponding acyl nickel(II) intermediate (**XIII**) triggers a CO extrusion and ligand exchange with the benzophenone imine (**XIV**). Reductive elimination delivers the targeted aminated product prior to acid hydrolysis and a Ni(0) bound to CO that ultimately recovers back the propagating **XII** by loss of CO.

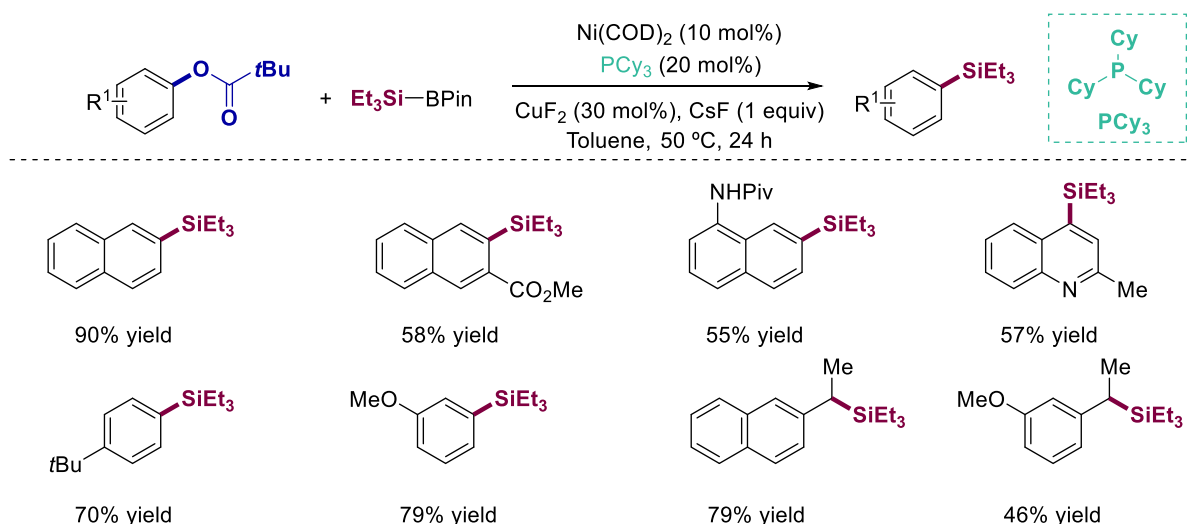


Scheme 1.2.3. Decarbonylative amination of esters and proposed mechanism.

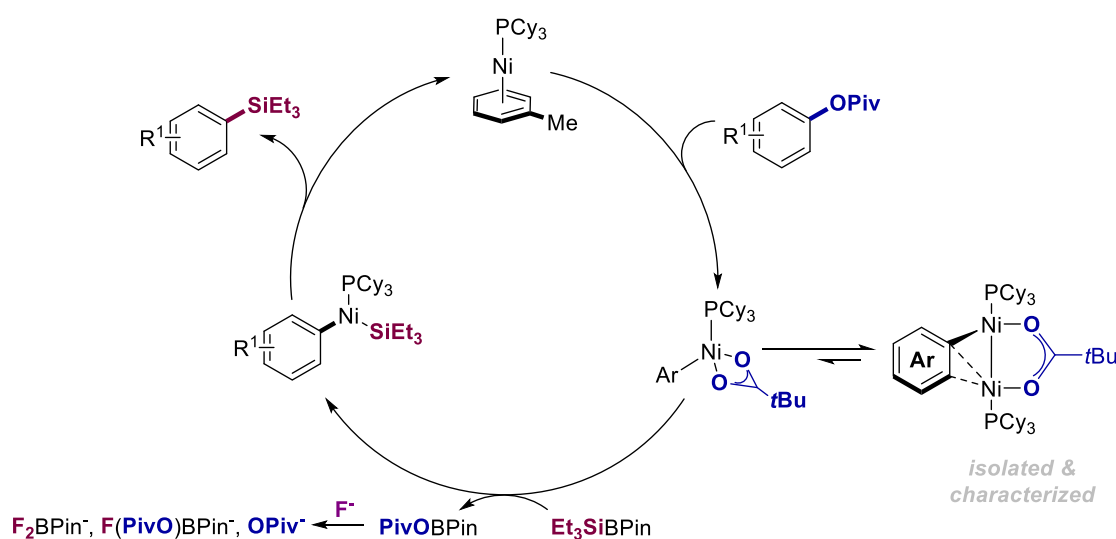
Chapter 1

1.2.1.3 C–Si bond formation

Prompted by the synthetic applicability of organosilanes in a myriad of different transformations, chemists have been challenged to come up with new catalytic technologies aimed at forging C–Si bonds.^{59–65} In 2014, our group reported the first C–O silylation of aryl esters with silylboronate reagents (Scheme 1.2.4).⁶⁶ This work could be executed with aryl esters possessing multiple functional groups, and the technology could be applied to both π -extended and non- π -extended systems. Moreover, benzylic substrates could be used, holding promise to design stereospecific or even enantioselective C–Si bond-forming reactions. Although initially a mechanism consisting of a Ni/Cu cooperative effect was proposed, later on the authors demonstrated that CuF₂ could be replaced by exogenous fluoride sources, an assumption that was corroborated by in depth mechanistic studies, DFT calculations and the isolation of some putative reaction intermediates that involved Ni(I) bimetallic intermediates as off-cycle reservoirs (Scheme 1.2.5).⁶⁷

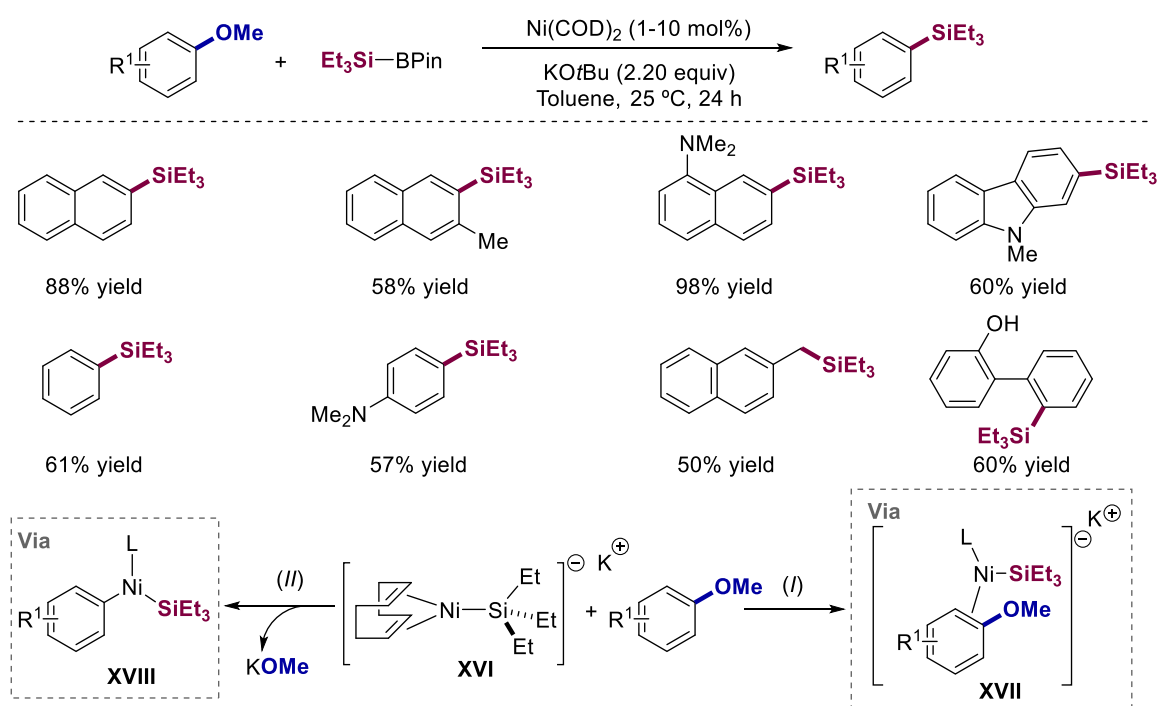


Scheme 1.2.4. Ni-catalyzed silylation of aryl- and benzyl pivalates.



Scheme 1.2.5. Mechanistic proposal for the nickel-catalyzed silylation of C–O bonds.

Subsequently, our group developed a new Ni-catalyzed protocol for the silylation of anisoles under remarkably mild reaction conditions and in the absence of external ancillary ligands (Scheme 1.2.6).⁶⁸ Importantly, the reaction could be extended to both π -extended and non- π -extended aryl methyl ethers. Among all different alternatives, it was proposed that the reaction might operate *via* $[\text{Ni}(\text{COD})\text{SiEt}_3]\text{K}$ complexes (**XVI**) that might trigger either an internal nucleophilic aromatic substitution assisted by complexation of the K^+ counterion with the lone pair of the etheral oxygen (Scheme 1.2.6, complex **XVII**) or a “non-classical” oxidative addition of the $\text{C}(\text{sp}^2)\text{--OMe}$ bond to $\text{Ni}(0)$ -ate complexes assisted by K^+ counterions (Scheme 1.2.6, complex **XVIII**).

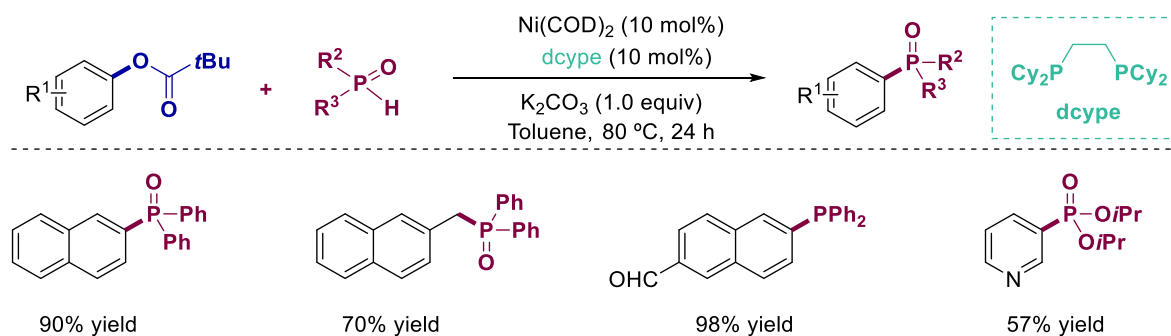


Scheme 1.2.6. Ni-catalyzed silylation *via* C–OMe cleavage and mechanistic proposal.

1.2.1.4 C–P bond formation

Usually, C–P bond-forming reactions are prepared *via* the reaction of Grignard reagents or organolithium species with the corresponding electrophilic phosphorous sources. However, these methods could not be applied in densely functionalized backbones due to chemoselectivity issues, lack of functional group tolerance or the need for special techniques due to the air-sensitivity of the corresponding organometallic reagents. Aimed at meeting these challenges, Chen and Han groups reported the first phosphoarylation of non- π -extended aryl and benzyl pivalates catalyzed by nickel complexes (Scheme 1.2.7).^{69,70} The reaction was proposed to operate *via* classical oxidative addition of the aryl ester to $\text{Ni}(0)$ followed by transmetalation and reduction elimination forming the C–P bond.

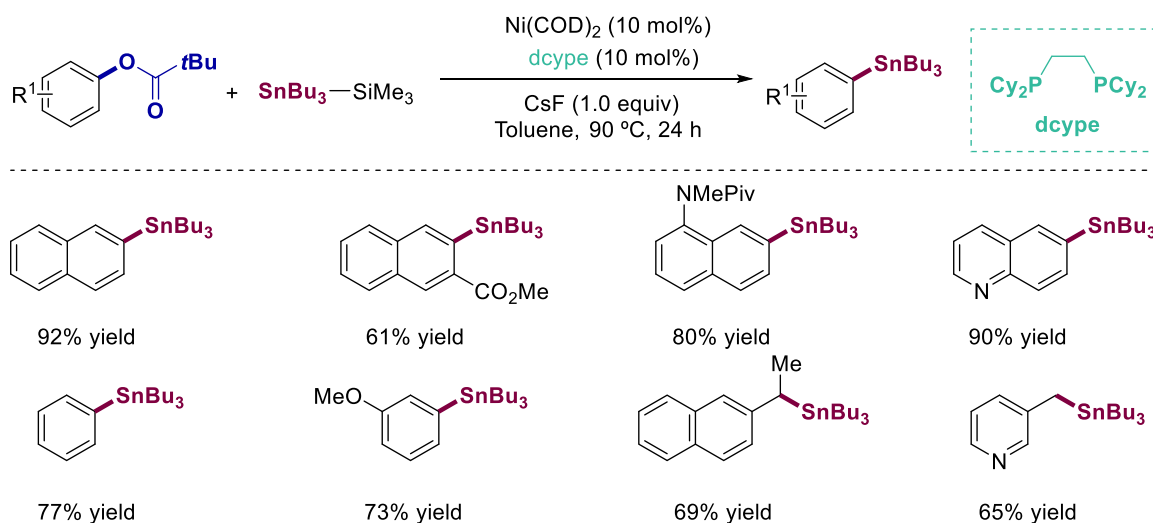
Chapter 1



Scheme 1.2.7. Ni-catalyzed phosphoarylation of aryl and benzyl pivalates.

1.2.1.5 C–Sn bond formation

Aiming at extending the generality of C–heteroatom bond-forming reactions *via* C–O bond-cleavage, our group reported a Ni-catalyzed stannylation of aryl esters en route to the corresponding organotin reagents (Scheme 1.2.8).⁷¹ Notably, even heterocyclic cores or non- π -extended arenes can be employed as substrates, thus allowing to access densely functionalized organotin reagents that can be used as linchpins for preparing a wide variety of compounds *via* C–Sn cleavage.^{72–74}



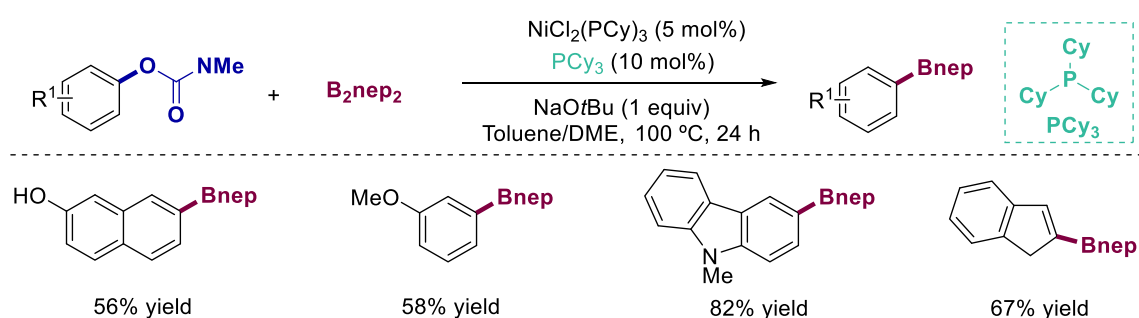
Scheme 1.2.8. Ni-catalyzed stannylation of aryl and benzyl esters.

1.2.1.6 C–B bond formation

Among all organometallic reagents, organoboron intermediates probably are the most versatile compounds to build up molecular complexity, allowing to enable a wide variety of C–C and C–heteroatom bond-forming reactions.⁷⁵ Traditionally, the preparation of aryl and benzoyl boronic acids involves the utilization of Grignard reagents or organolithium species.⁷⁶ Not surprisingly, chemists have been challenged to design catalytic C–H borylation techniques, thus avoiding the need for preformed organometallic reagents for the preparation of organoboron compounds.^{77–81} However, controlling the regioselectivity of these processes might not be particularly trivial in densely

functionalized backbones. Therefore, the catalytic borylation of organic (pseudo)halides still constitute a powerful and reliable technique for preparing organoboron compounds. Prompted by these limitations, the cleavage of sp^2 or sp^3 C–O bonds emerged over last years as an alternative method to forge C–B bonds.^{82,83}

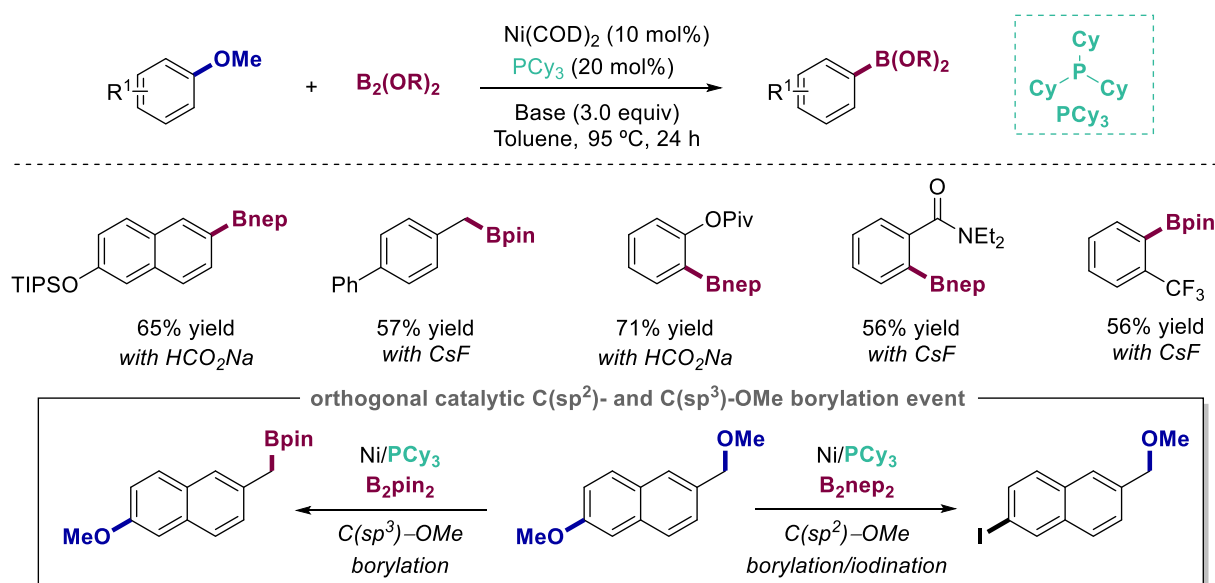
In 2011, Shi and co-workers published the first borylation of (hetero)aryl-carbamates *via* Ni-catalyzed C(sp^2)–O bond cleavage with B_2nep_2 as coupling partner (Scheme 1.2.9).⁸⁴ The scope included *N*-containing heterocycles and non- π -extended arenes, but the presence of electron-donating groups and *ortho*-substituents eroded the yield in a significant manner. Mechanistically, a canonical Ni(0)/Ni(II) pathway was proposed followed by a transmetalation and a final C–B bond reductive elimination.



Scheme 1.2.9. Ni-Catalyzed borylation of aryl carbamates.

In 2015, our group developed the first catalytic *ipso*-borylation of aryl methyl ethers *via* C–OMe bond cleavage using a Ni/ PCy_3 regime (Scheme 1.2.10).⁸⁵ As expected, π -extended arenes resulted in high yields, but the coupling of non- π -extended substrates required the presence of electron-withdrawing groups. Notably, two sets of conditions allowed the authors to promote a site-selective borylation of at either C(sp^3)–O or C(sp^2)–O linkages based on the *in situ* generation of nucleophilic boron reagents with different electronic and steric properties. Strategically, this protocol represented an alternative to conventional *ortho*-, *meta*-, and *para*-borylative protocols of anisole derivatives, where the methoxy entity is used as a mere regiocontrol element.^{86,87}

Chapter 1



Scheme 1.2.10. Ni-catalyzed borylation of aryl and benzyl methyl ethers *via* C–OMe cleavage.

In summary, the utilization of benzyl or phenyl C–O electrophiles has received considerable attention as alternatives to commonly employed organic halide counterparts in a myriad of cross-coupling reactions.⁴⁵ While not as well-adopted as the latter, C–O electrophiles offer new opportunities for synthetic design given the ready availability and lack of toxicity of the corresponding alcohol or phenol counterparts. In this line, such advances developed a series of stereospecific reactions opening a worthy gateway to obtain enantioenriched scaffolds (see *Chapter 2*).

1.2.2 Nickel-catalyzed the cleavage of activated C(sp³)–N bonds

1.2.2.1 Importance of alkyl C–N bond as electrophiles

Over the recent years, the prevalence of alkyl amines in a myriad of bioactive molecules, agrochemicals or natural products have prompted chemists to design catalytic cross-coupling reactions with the latter being electrophilic partners (Figure 1.2.3, *top*). However, the considerable high bond strength of the C(sp³)–NH₂ linkage (BDE ~88 kcal/mol,) makes alkyl amines not particularly suited as electrophiles in cross-coupling reactions unless these motifs are functionalized at the nitrogen terminus (Figure 1.2.3, *bottom*).⁴⁸

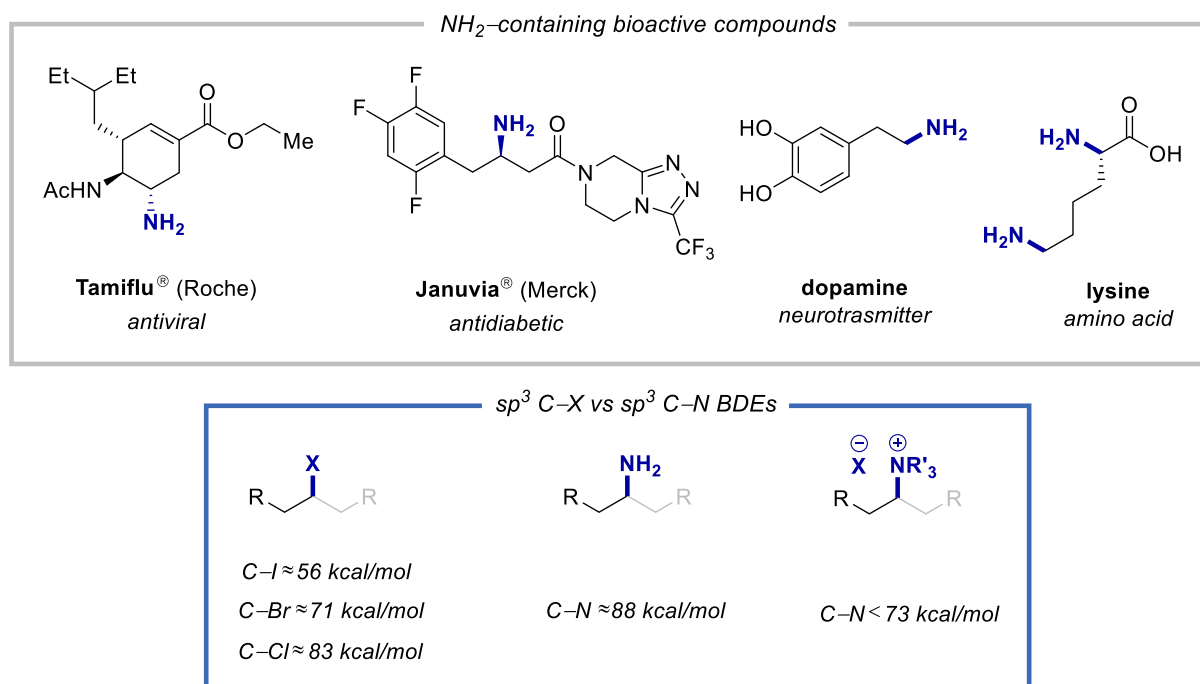


Figure 1.2.3. Importance and BDEs of alkyl amines.

In the early 80's, the first cleavage of $C(sp^3)-N$ bonds was reported by utilizing tetrahydropyridinium salts bearing β -silicon groups capable of inducing the fragmentation of the targeted alkyl $C-N$ bond by means of exogenous fluoride ions.⁸⁸ In 1987, Gumpton and co-workers derivatized allylic amines to more activated quaternary ammonium salts prior to coupling with Grignard reagents.⁸⁹ This publication paved the way for the future cross-coupling reactions using activated $C(sp^3)-N$ bonds as a means to promote derivatization of simple alkyl amines.

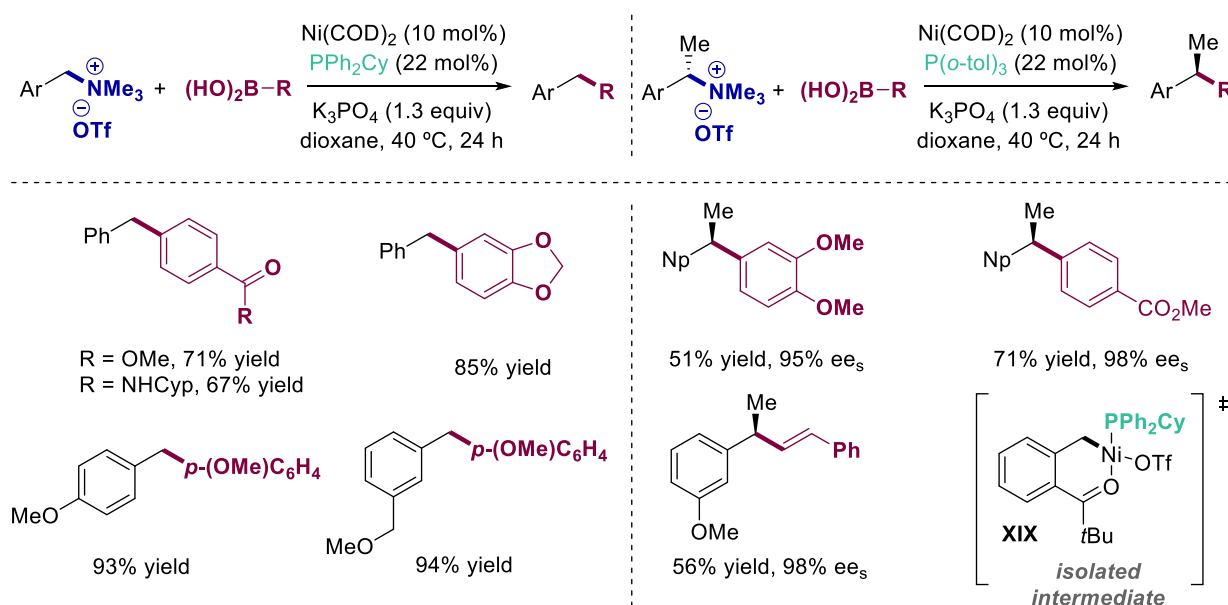
Some years later, Trost and co-workers disclosed a Ni-catalyzed cross-coupling of allylic amines with boronic acids obtaining the corresponding allylic products with moderate to good yields, with site-selectivity being dictated by the nature of the ligand backbone.¹⁵ In 1997, Mortreux and co-workers developed a Ni-catalyzed coupling reaction of allylic amines with soft nucleophiles instead.¹⁶ Despite these precedents, it is somewhat surprising that the attention of chemists was shifted to the activation of $C(sp^2)-N$ bonds instead of looking at the reactivity of simple unactivated alkyl amine congeners.¹⁷ It was not until recently that the potential of nickel catalysts was assessed in benzyl $C(sp^3)-N$ Et bonds and strained activated aziridines.

1.2.2.2 Primary and secondary benzyl $C(sp^3)-C$ bond formation *via* boronic acids

In 2013, Watson and co-workers reported the first nickel-catalyzed cross-coupling of benzylic ammonium triflate salts and boronic acids by the stereospecific formation of diarylethanes *via* $C-N$ bond activation (Scheme 1.2.11).⁹⁰ The choice of using ammonium triflates was not arbitrary: a) these compounds have shown their willingness to promote cross-coupling reactions with boronic acids,^{14,17} b) they offer an orthogonal method to both halides and ethers, c) also remained stable to long-term

Chapter 1

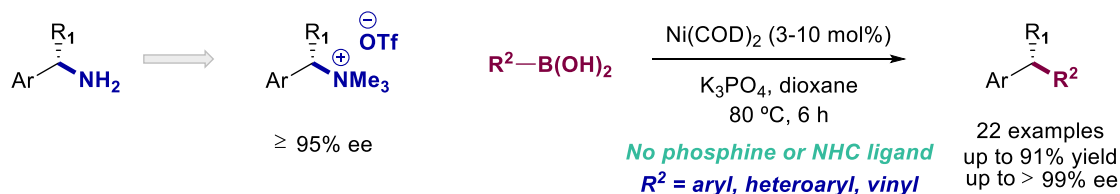
storage, d) highly enantioenriched benzylic amines are readily available *via* common asymmetric techniques, making them particularly attractive as coupling counterparts.⁹¹



Scheme 1.2.11. Nickel-catalyzed cross-coupling of benzylic ammonium salts and boronic acids.

The transformation could accommodate a wide variety of different benzylic ammonium salts bearing electron-rich and electron-poor substituents. Moreover, the transformation was suitable for a large variety of boronic acids bearing different functional groups such as ester, amides and acetals (Scheme 1.2.11, *left*). Remarkably, the C–N bond is selectively activated over the C–O bond under these conditions. The authors were able to develop a stereospecific version of the reaction by changing the ligand to a more electron-rich phosphine (Scheme 1.2.11, *right*). The scope showed a wide variety of boronic acids and enantioenriched secondary benzyl ammonium salts, allowing to extend the application of these methods to stereospecific C–N cleavage reports.^{92,93} Notably, the transformation operated with an inversion of stereochemistry *via* S_N2-type mechanisms.

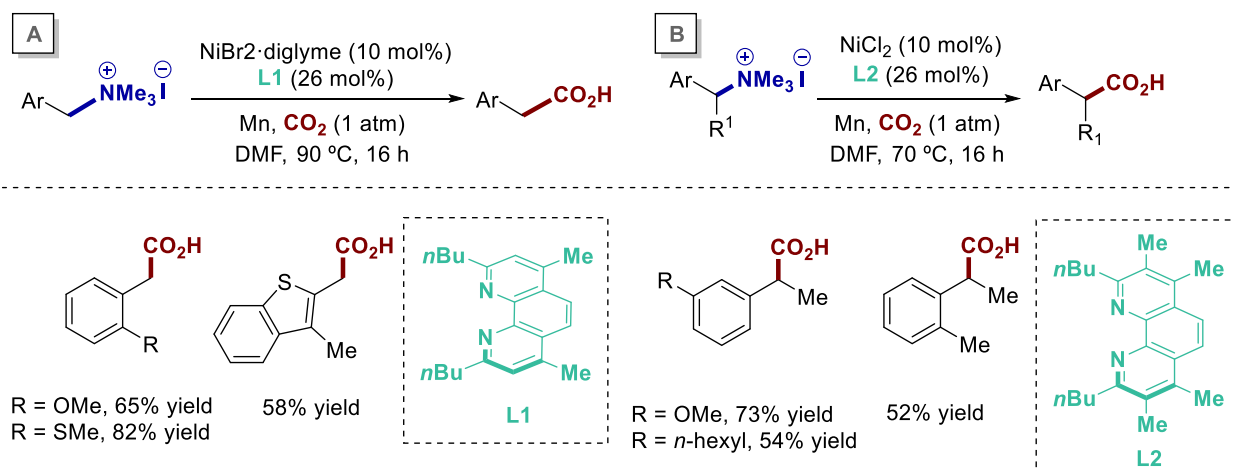
One year later, Watson and co-workers reported the same stereospecific cross-coupling protocol for benzylic ammonium triflates and boronic acids where no ligand was required (Scheme 1.2.12).⁹⁴ This permitted a vast improvement of the scope in heteroaromatic boronic acids with diverse electronics.



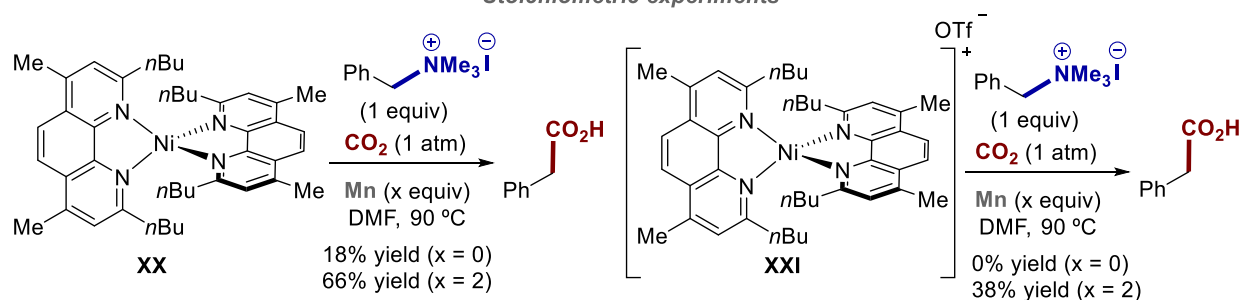
Scheme 1.2.12. Stereospecific cross-coupling of benzylic ammonium triflates and boronic acids: no phosphine ligand required.

1.2.2.3 Primary and secondary benzyl C(sp³)-CO₂H bond formation via CO₂

Traditionally, ammonium salts have been exclusively employed in nucleophile/electrophile regimes using well-defined stoichiometric organometallic reagents. As part of our investigations in nickel catalysis^{66,85,95} and cross-electrophile couplings with CO₂,⁹⁶⁻⁹⁹ our group reported the first cross-electrophile coupling of benzylic C–N bonds with CO₂ as electrophilic partners (Scheme 1.2.13).¹⁰⁰ This study comprised the utilization of primary and secondary benzyl ammonium salts with phenanthroline ligands (**L1-L2**) being particularly useful for success (Scheme 1.2.13, A and B). Although speculative, some stoichiometric experiments pointed out at the intermediacy of benzyl Ni(I) species *via* single-electron reduction of benzyl Ni(II) complexes mediated by Mn (Scheme 1.2.13, *bottom*). In line with this notion, **XXI** was found to be competent as reaction intermediate in the presence of Mn. The inhibition of the reaction in the presence of TEMPO suggested the involvement of radical intermediates in the reaction mixture. This proposal gains credence by the complete loss of optical purity by reacting enantioenriched ammonium salt under the optimized reaction conditions. However, care must be taken when generalizing this, as racemization might occur *via* bimolecular mechanisms in which an inversion occurs *via* reaction of a low-valent Ni(0) species to *in situ* generated Ni(II) intermediates *via* oxidative addition pathways.



Stoichiometric experiments

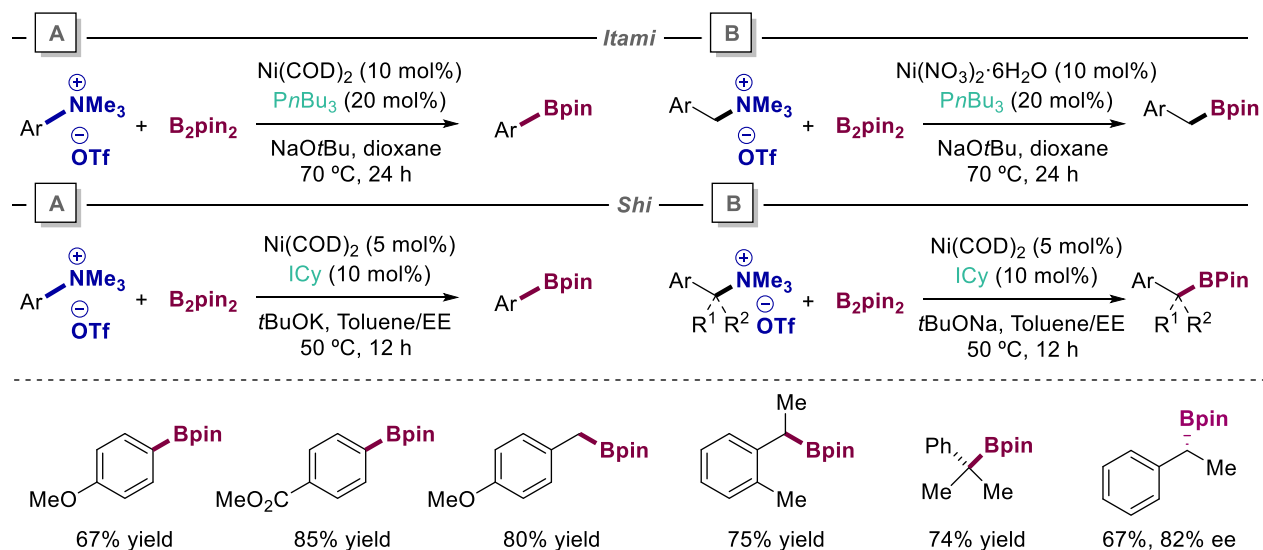


Scheme 1.2.13. Cross-electrophile coupling of benzylic C–N bonds with CO₂ catalyzed by nickel.

Chapter 1

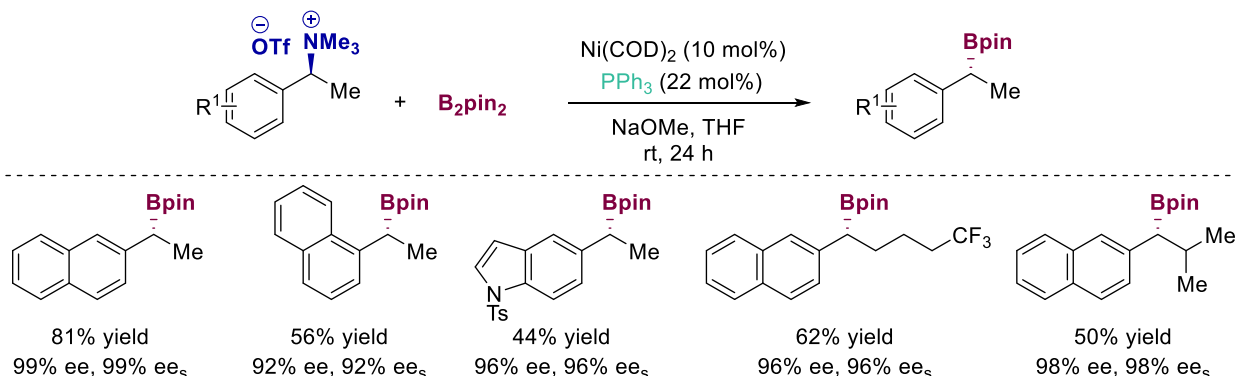
1.2.2.4 $C(sp^2)$ - and $C(sp^3)$ -B bond formation of aromatic systems via B_2pin_2 reagents

In 2015, Itami and Shi independently reported the first C–N borylation of phenyl and benzyl ammonium triflates with nickel catalysts supported by either $PnBu_3$ or ICy (1,3-dicyclohexyl-1H-imidazol-3-ium chloride) (Scheme 1.2.14, A and B).^{23,101} In both works, the borylation of phenyl and benzyl ammonium triflates was compatible with the presence of diverse electronic and steric substituents obtaining good yields.



Scheme 1.2.14. Nickel-catalyzed C–N borylation of phenyl and benzyl ammonium salts.

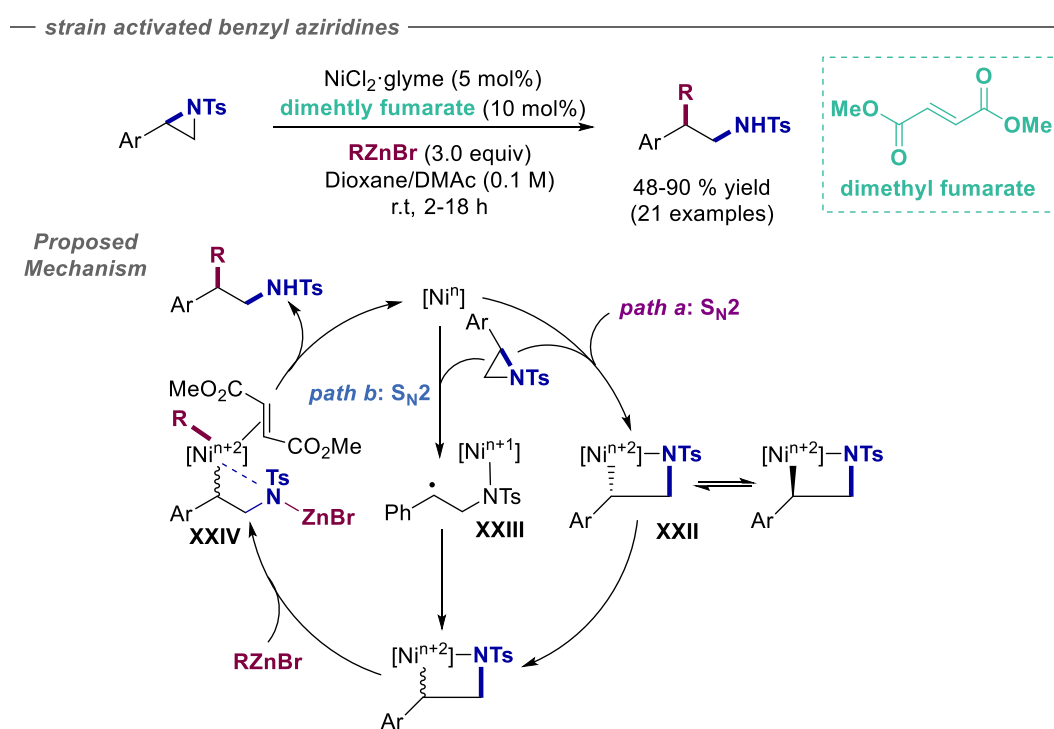
Watson reported the “first” stereospecific borylation of benzylic ammonium salts catalyzed by nickel complexes (Scheme 1.2.15).¹⁰² The procedure proved to be suited for the utilization of activated amines containing electron-rich, electron-poor and heteroaromatic rings in good yields and with an excellent chirality transfer. The attractiveness of this procedure relies on the formation of chiral benzylic boronic esters, useful intermediates for the construction of complex molecules in an enantioenriched fashion.



Scheme 1.2.15. Stereospecific borylation of benzylic ammonium salts catalyzed by nickel.

1.2.2.5 Nickel-catalyzed $C(sp^3)$ -N scission of aziridines

As part of a program aimed at the employment of aziridines in cross-coupling reactions, Doyle and co-workers reported the utilization of the latter as coupling partners for the formation of β -substituted amines *via* $C(sp^3)$ -N bond cleavage.¹⁰³ The inspiration for developing such a technique arose from the pioneering work reported by Hillhouse¹⁰⁴ and Wolfe,¹⁰⁵ where an oxidative addition of an aziridine to low-valent Ni(0) results in a four-membered azanickelacycle. In particular, Doyle reported a nickel-catalyzed Negishi alkylation of activated styrenyl aziridines in 2012 (Scheme 1.2.16, *top*).⁹³ Based on the available literature data,^{104,105} the author proposed two alternatives for the insertion of nickel catalyst into the C-N bond (Scheme 1.2.16, *bottom*). In *path a*, a S_N2 -type oxidative addition is accompanied by reversible homolysis at the benzylic Ni-C bond, thus furnishing **XXII**. In *path b*, an irreversible SET oxidative addition could afford the intermediate **XXIII**. Then, transmetalation with an alkylzinc reagent occurs (likely stabilized by the dimethyl fumarate ligand, **XXIV**) prior to reductive elimination en route to the targeted product.

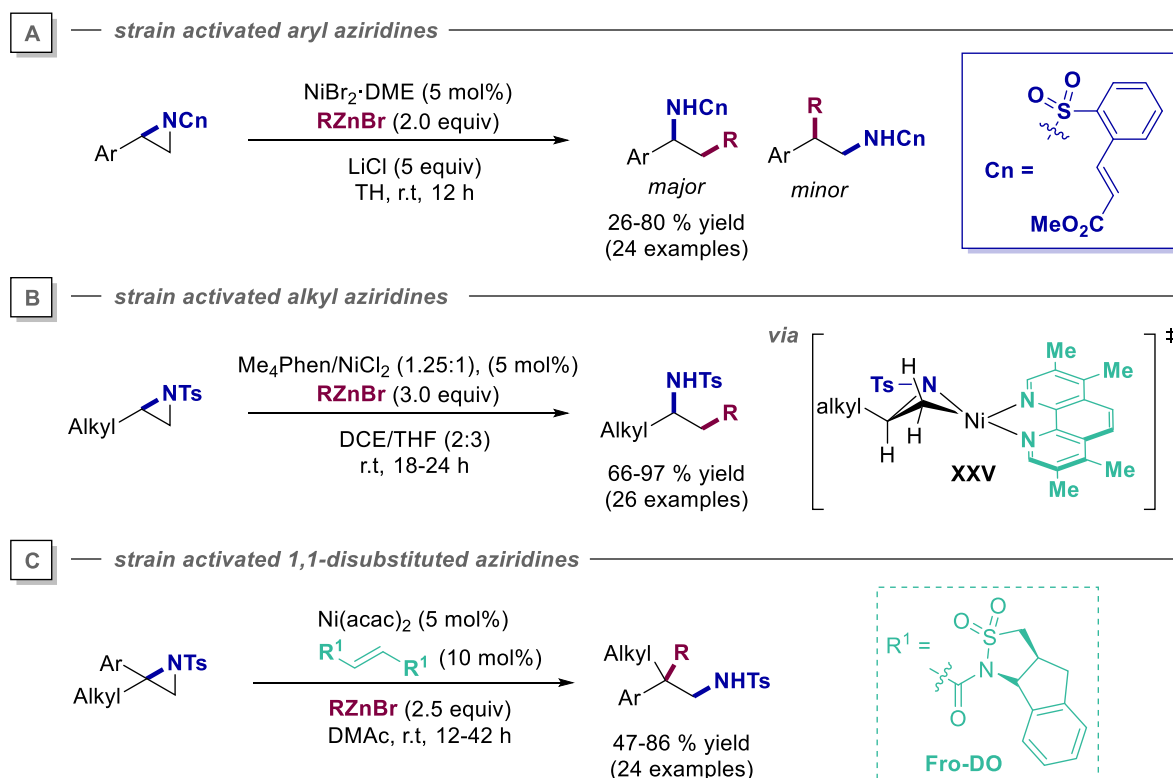


Scheme 1.2.16. Nickel-catalyzed Negishi alkylations of styrenyl aziridines & mechanism.

In 2013, the same authors reported a directed nickel-catalyzed Negishi cross-coupling of alkyl aziridines (Scheme 1.2.17, A)¹⁰⁶ possessing a protecting group that resembles a dimethyl fumarate ligand used before in the previous Negishi-type coupling reaction. The objective was to activate the C-N bond and stabilize the intermediates that are *a priori* prone to β -hydride elimination by facilitating the reductive elimination step. The methodology was applied to a wide number of aziridines bearing different functional groups and to diverse zinc reagents, albeit with low

Chapter 1

regioselectivities. Inspired by these results, Jamison and co-workers developed a highly regioselective nickel-catalyzed cross-coupling of *N*-tosylaziridines and alkylzinc reagents (Scheme 1.2.17, B).²⁴ This platform allowed the authors to furnish the linear amines by the utilization of nickel/phenanthroline regimes. The mechanism was believed to proceed *via* oxidative addition (**XXV**), followed by transmetalation and reductive elimination steps.



Scheme 1.2.17. Ni-catalyzed Negishi cross-coupling with aziridines.

In 2015, a Negishi cross-coupling of 1,1-disubstituted-aziridines catalyzed by nickel was reported by Doyle and co-workers (Scheme 1.2.17, C).¹⁰⁷ Interestingly, the protocol was based on the utilization of an electron-deficient olefin ligand (**Fro-DO**), likely allowing to adopt a U-shaped conformation with Ni, creating a sterically congested environment around the metal center. In this manner, reductive elimination is likely facilitated by bringing into close proximity the two fragments required for effecting C–C bond-formation. However, the substrate scope was limited to the presence of a pending aryl moiety, as the presence of a 1,1'-dialkyl motif was not tolerated.

A remarkable step-forward was reported in 2017 by Watson and co-workers, demonstrating the viability of promoting cross-coupling reactions with unactivated alkyl amines by using pyridinium salts as electrophilic partners.¹⁰⁸ This methodology paved the way for the discovery of deaminative cross-coupling reactions by employing pharmaceutically-important unactivated alkyl amine counterparts (see Chapter 3).

1.2.3 Remote functionalization of unactivated C–H bonds by walking metals

1.2.3.1 Introduction and mechanism of chain-walk events

In early 1970s,^{109–111} the concept of remote functionalization consisted of an indirect activation of a site distant from an initial functional group (Figure 1.2.4, A).³⁶ The control of such selectivity profile relies on the directionality of the substrate by directing groups, present or preinstalled or through an undirected activation of particularly reactive C–H bonds (Figure 1.2.4, B). Although directed activation of C–H bonds has been exploited over the last decades, this strategy is rather limited to the distance between the catalyst and the targeted C–H bond.¹¹²

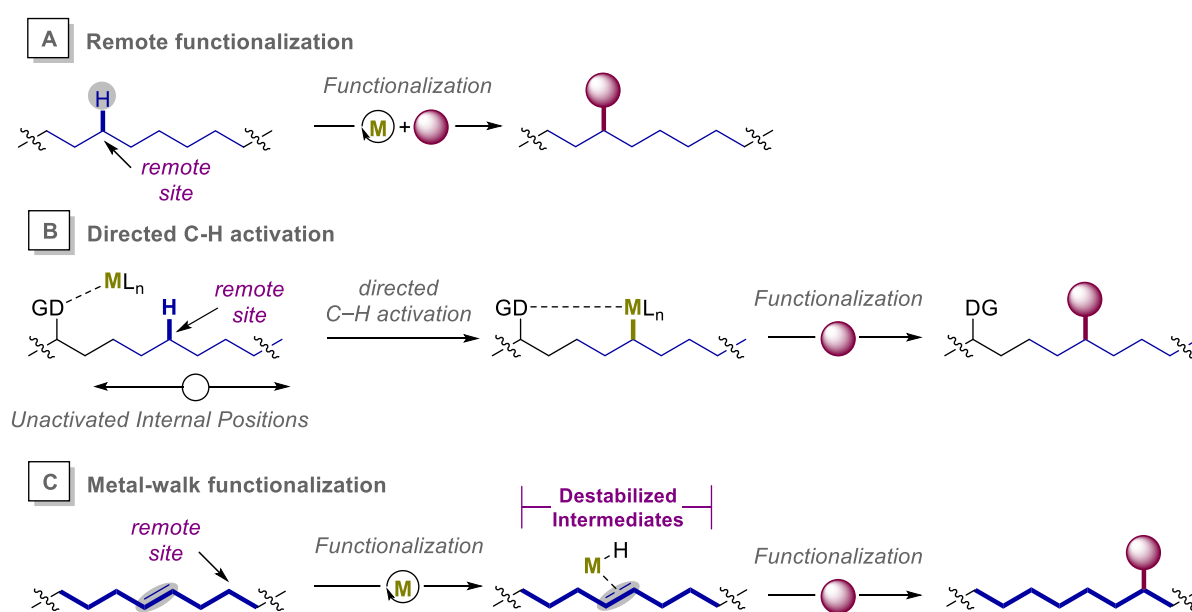


Figure 1.2.4. Metal-walk vs classical modes of activation.

In recent years, “metal-walking” or “chain-walking” processes have attracted the interest of chemists due to the possibility of performing undirected remote functionalization at distal sp^3 C–H bonds (Figure 1.2.4, C). This protocol consists of an iterative series of consecutive 1,2- or 1,3-hydride shifts of a metal complex along a hydrocarbon side-chain, allowing to formally translocate the metal at a different location within the hydrocarbon prior to C–C bond-forming reaction. One of the most important characteristics of the transition metal to carry out chain-walking processes is the ability to rapidly promote an insertion across the olefin followed by a β -hydride elimination in an iterative manner (Figure 1.2.5).

Chapter 1

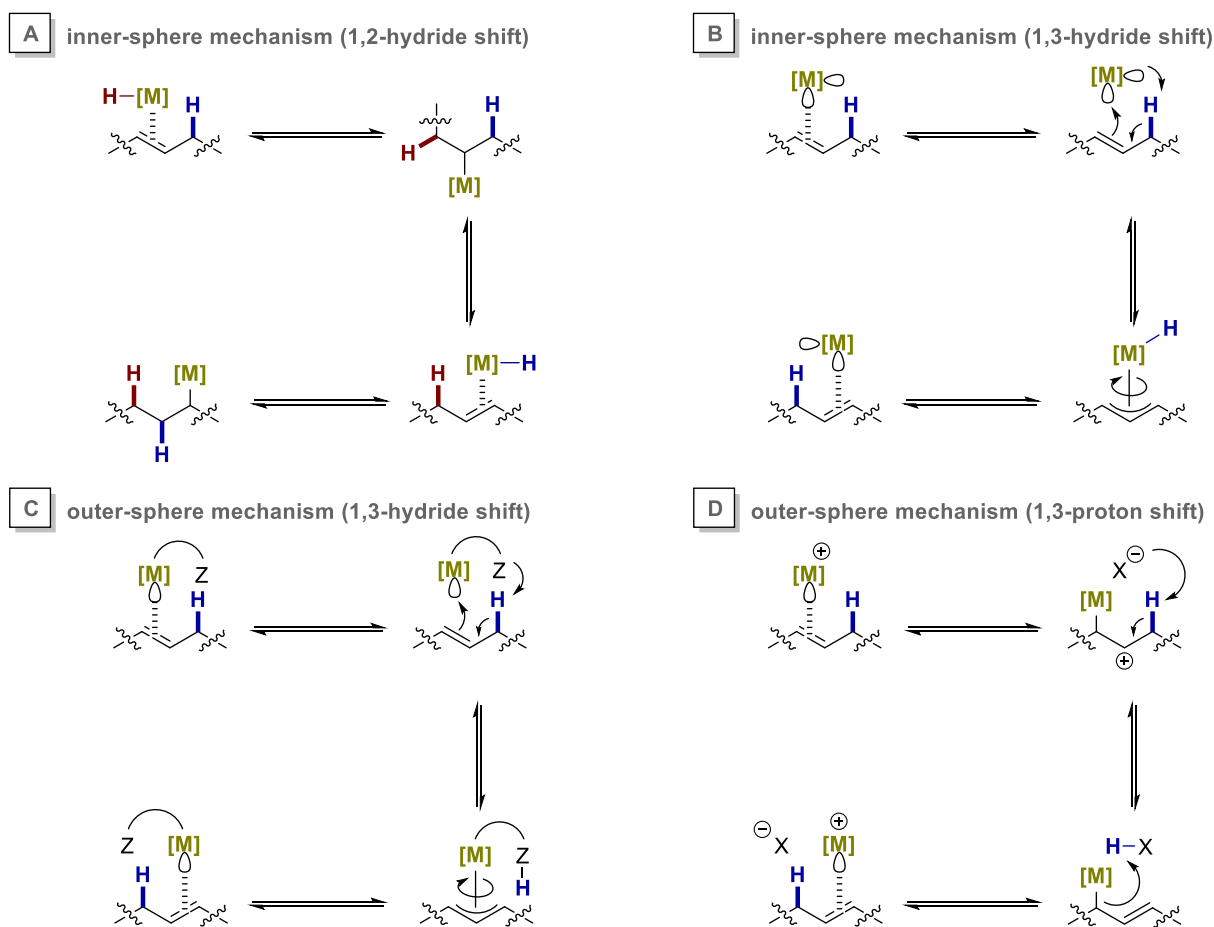


Figure 1.2.5. Mechanistic intricacies of olefin isomerization.

Four mechanistic scenarios can be envisioned for chain walking processes. Depending on the nature of the metal, olefin isomerization may occur *via* either 1,2- or 1,3-hydride shift (Figure 1.2.5):^{113,114} A) In a 1,2-hydride shift inner-sphere mechanism, the metal-hydride undergoes migratory insertion into an olefin, obtaining a well-defined alkyl-metal species. Subsequent β -hydride elimination furnishes the isomerized olefin π -complex, which undergoes rotation or hydrometalation (Figure 1.2.5, A). B) Alternatively, an olefin isomerization can take place *via* 1,3-hydride shift inner-sphere mechanism. In this context, the metal should possess two vacant orbitals, one for the olefin coordination and the other for the C–H allylic activation. Once the η^3 -allyl complex has been formed, a reductive elimination provides the isomerized olefin-metal complex (Figure 1.2.5, B). C) In an outer-sphere mechanism, one of the two vacant orbitals of the metal is filled by a base added to the system. Upon olefin coordination and allylic activation, the base can abstract the allylic proton generating an allylic metal-complex (Figure 1.2.5, C). Finally, an outer-sphere 1,3-proton shift mechanism can be proposed with π -acidic transition metals such as cationic silver and palladium complexes that can acidify the allylic position upon olefin coordination. Intermolecular deprotonation gives rise to the η^3 -allyl complex, obtaining rapidly the olefin isomerization by protodemetalation (Figure 1.2.5, D). A variety of metal-catalytic protocols have been developed depending on the final termination event (Figure 1.2.6).

Chain-walking Metals

Sc	Ti	V	Cr	Mn	Fe	Co	Ni	Cu	Zn
Y	Zr	Nb	Mo	Tc	Ru	Rh	Pd	Ag	Cd
La	Hf	Ta	W	Re	Os	Ir	Pt	Au	Hg

Figure 1.2.6. Metals capable of chain-walking events.

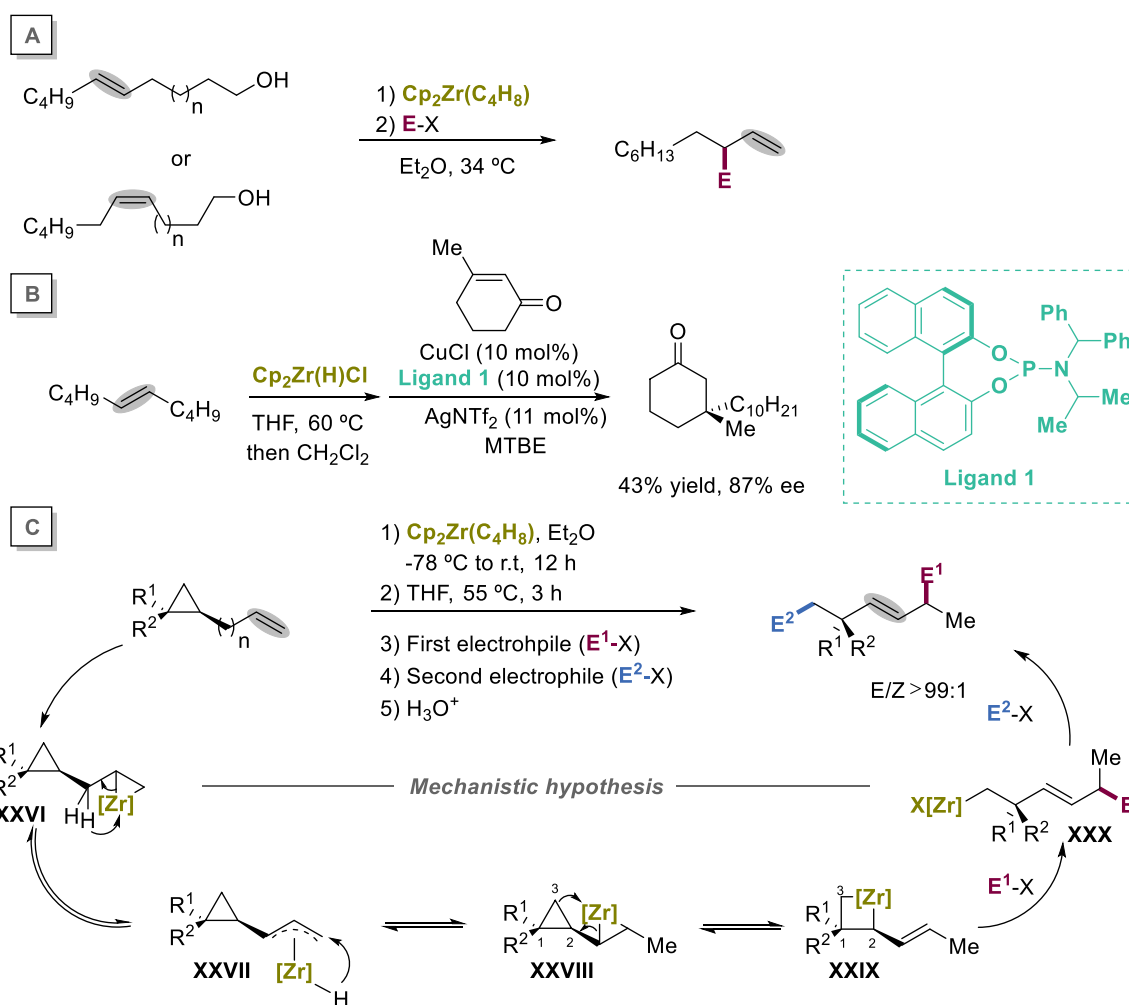
1.2.3.2 Zirconium walking metal

In 1961, Finkbeiner reported the first isomerization event where, under Ti or Zr catalysis, branched alkene Grignard reagents afforded linear compounds *via* olefin intermediates.^{115,116} It was not until 20 years later when Marek and co-workers made use of Schwartz's reagent ($\text{Cp}_2\text{Zr}(\text{H})\text{Cl}$)^{117,118} and Negishi reagent ($\text{Cp}_2\text{Zr}(\text{C}_4\text{H}_8)$)¹¹⁹ for the isomerization of fatty alcohols prior to electrophilic trapping in the presence of organozinc intermediates (scheme 1.2.18, A).¹²⁰

Subsequently, Fletcher showed that simple internal olefins served as vehicles to obtain terminal alkylzirconium species in the presence of Schwartz's reagent, setting the basis for promoting an asymmetric conjugate addition with α,β -unsaturated cyclic ketones catalyzed by copper (Scheme 1.2.18, B).¹²¹

More recently, Marek reported a bisfunctionalization of olefins by isomerization events with zirconium species. This protocol strategically positioned cyclopropanes along the chain, leading to double electrophilic coupling by C–C bond cleavage (Scheme 1.2.18, C).^{122,123} This methodology was based on the formation of an allyl zirconacyclobutane (**XXVII**) which react with carbonyl electrophiles at the allylic position (**XXIX**) followed by subsequent activation of the remaining zirconium species to promote a second electrophilic trapping (**XXX**). Although in all examples shown until today stoichiometric amounts of zirconium reagents are required, these transformations open a gateway to develop new catalytic methods by means of olefin isomerization.

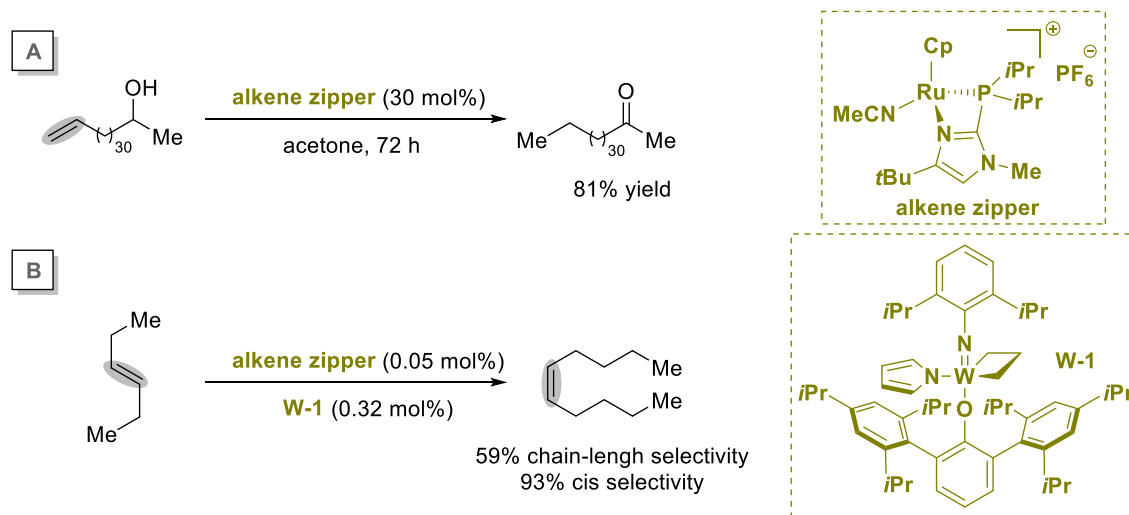
Chapter 1



Scheme 1.2.18. Zr complexes in chain-walking events.

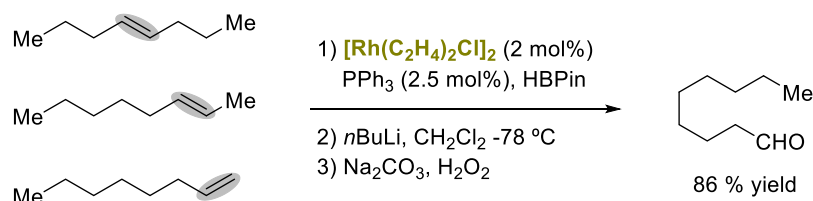
1.2.3.3 Ruthenium, Rhodium, and Iridium walking metals

In 1974, Wells and co-workers discovered the isomerization of 1-pentene to 2-pentene promoted by homogeneous ruthenium catalysis.¹²⁴ In 2007 Sharma and co-workers corroborated the robustness of olefin isomerization events by a ruthenium “alkene-zipper” catalyst. The protocol exhibited an olefin isomerization over more than 30 positions *via* an outer-sphere 1,3-hydride shift mechanism (Scheme 1.2.19, A).¹²⁵ One year later, Schrock published a combination of the “alkene-zipper” catalyst and an olefin metathesis catalyst (**W-1**) which were able to accomplish a tandem olefin isomerization/metathesis affording long-chain olefins (Scheme 1.2.19, B).¹²⁶



Scheme 1.2.19. Ru chain-walking reactions of olefins.

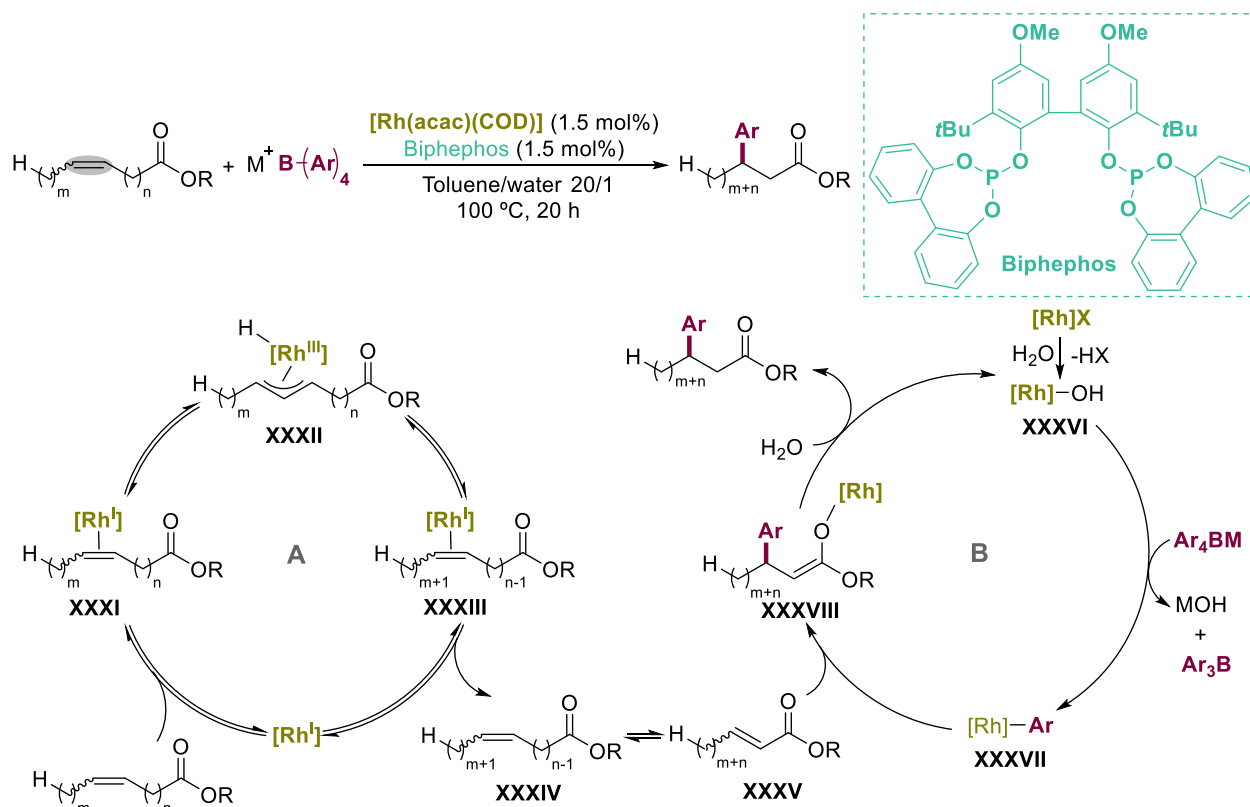
More than 50 years have passed since Wilkinson and Osborn discovered that PPh_3 ligands assist rhodium catalysts to perform hydroformylation reactions of terminal olefins.^{127,128} In the last 20 years novel rhodium catalytic systems have been discovered,¹²⁹ with the delivery of linear aldehydes or derivatives by isomerization of mixture of alkenes (Scheme 1.2.20).^{130–132}



Scheme 1.2.20. Rh chain-walking reactions of olefins.

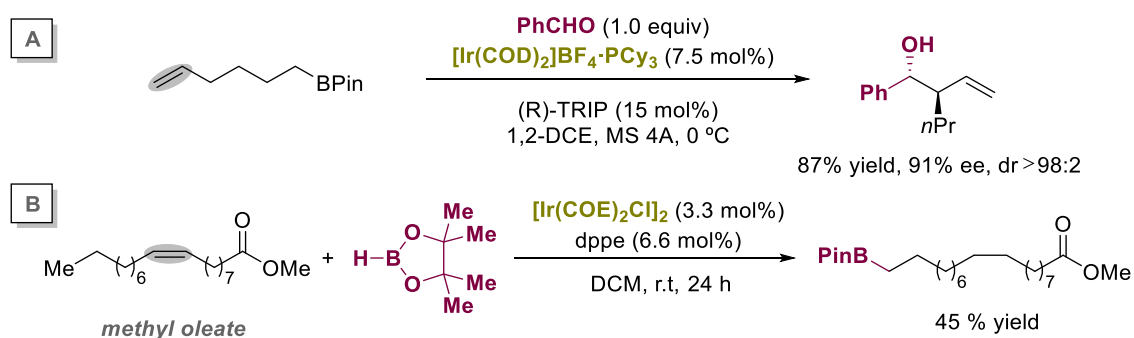
In 2011, a rhodium-catalyzed olefin isomerization/Michael addition sequence was achieved by Gooßen and co-workers (Scheme 1.2.21).¹³³ The authors proposed a combination of two cooperating catalytic cycles: one for the double-bond isomerization and the other one for the conjugative addition. Initiated by the isomerization cycle (Scheme 1.2.21, *cycle A*), the rhodium species sits on the olefin (**XXXI**) and undergoes a C–H insertion at the metal center to give π -allyl rhodium species (**XXXII**) that enable isomerization *via* migratory insertion/ β -hydride elimination (**XXXIII**) pathways. Although all the steps are *a priori* reversible, only the isomer at the α,β -position to the carboxy group can enter into the second catalytic cycle (Scheme 1.2.21, *cycle B*), thus ultimately leading to functionalization at this end.

Chapter 1



Scheme 1.2.21. Postulated mechanism of the isomerizing conjugate addition.

In the late 90's Miyaura and co-workers discovered that cationic iridium complexes in the presence of hydrogen readily promote olefin isomerization with exceptional ease.¹³⁴ By the utilization of similar cationic iridium complexes, Murakami developed a tandem isomerization/enantioselective allylation sequence in high yields and excellent enantioselectivities (Scheme 1.2.22, A).¹³⁵ Angelici and co-workers showed that terminal hydroboration of the fatty methyl oleate can be accomplished in the presence of an iridium catalyst (Scheme 1.2.22, B).¹³⁶

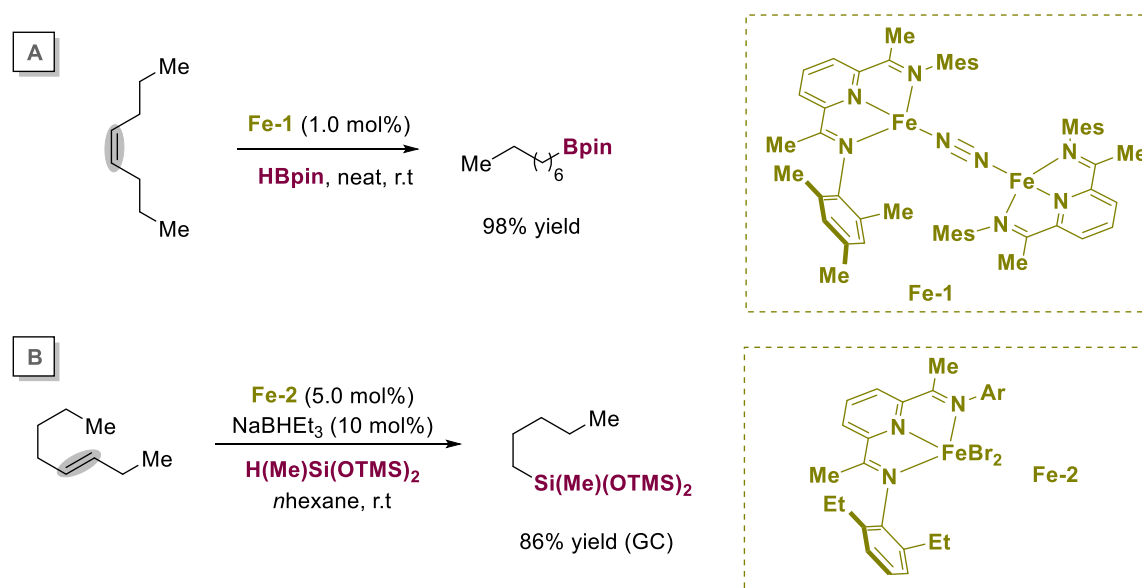


Scheme 1.2.22. Ir chain-walking reactions of olefins.

1.2.3.4 Iron walking metals

The ability of iron complexes to promote isomerization events was already discovered in the 60's.¹³⁷ However, it not was until the last decade that chemists revisited this concept as a means to

trigger C–C and C–heteroatom bond-forming reactions.^{138,139} Although only few examples of iron-catalyzed chain-walking processes have been reported so far, it is evident that the utilization of green metal catalysts will likely attract considerable interest in the next years to come. Particularly interesting is a methodology developed by Chirik that developed independently an iron-catalyzed isomerization/hydroboration sequence (Scheme 1.2.23, A).^{140,141} While a significant step forward, these reactions required the utilization of particularly air- and moisture-sensitive iron complexes. An interesting solution utilized by Huang and co-workers was the employment of iron (II) precursors that generated the active catalysts *in situ* via a tandem dehydrogenation/isomerization/hydrosilylation sequence (Scheme 1.2.23, B).¹⁴²



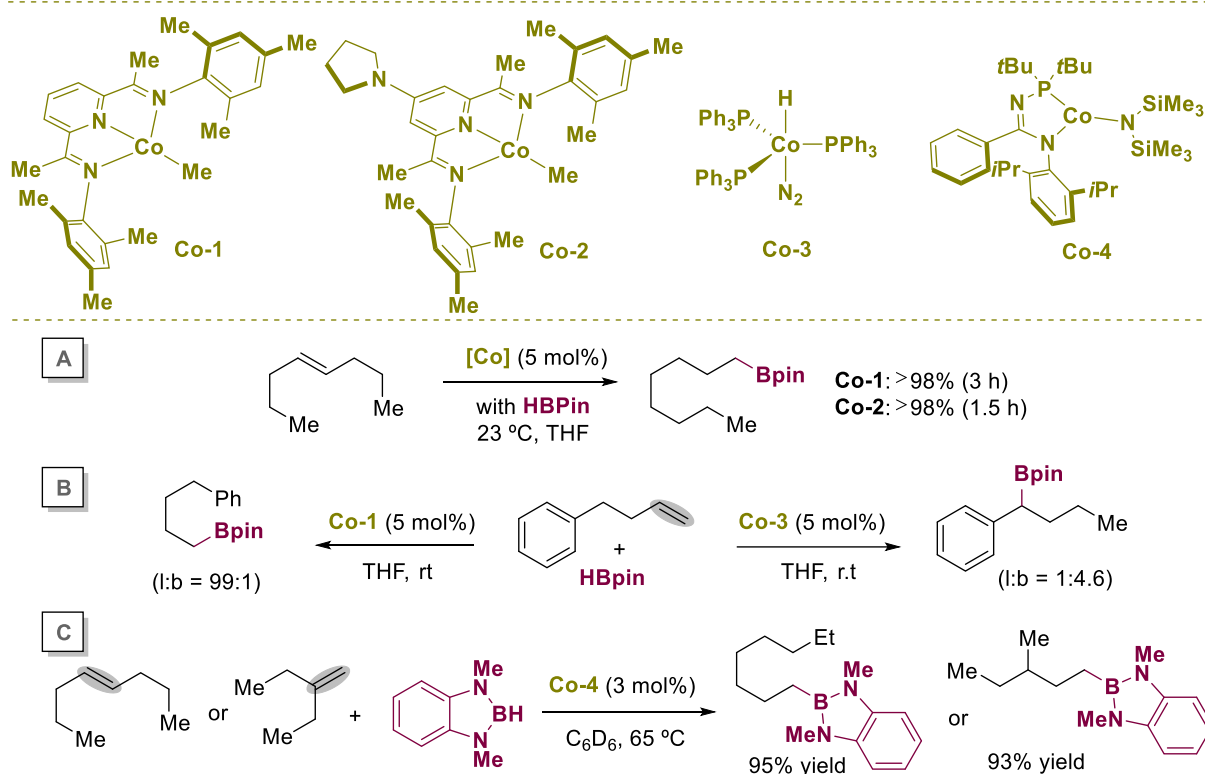
Scheme 1.2.23. Fe chain-walking hydroboration/hydrosilylation of internal olefins.

1.2.3.5 Cobalt walking metals

Since 2013, cobalt catalysts have been studied extensively for non-directed remote functionalization events *via* isomerization/hydroborations, hydrosilylations and C–C bond formations. For example, **Co-1** catalysts have been employed by Chirik in an isomerization/hydroboration of internal alkenes using pinacolborane (HBpin) with bis(imino)pyridine ligands, allowing to incorporate a Bpin residue at the terminal position (Scheme 1.2.24, A).¹⁴³ Subsequently, the same group discovered that the inclusion of electron-donating amino groups at *para* position of the pyridine moiety ligand afforded better reactivity (**Co-2**).¹⁴⁴ Some years later, Chirik reported a site-selective isomerization/hydroboration of terminal olefins decorated with pending arenes. The authors discovered that the reaction outcome can be controlled by tuning the ligand backbone obtaining either terminal or benzylic hydroboration products (Scheme 1.2.24, B).¹⁴⁵ The use of *N*-phosphinoamidinate ligands was shown to be crucial when expanding the source of boron utilized. In this line, Stradiotto and co-workers could extend the isomerization/hydroboration

Chapter 1

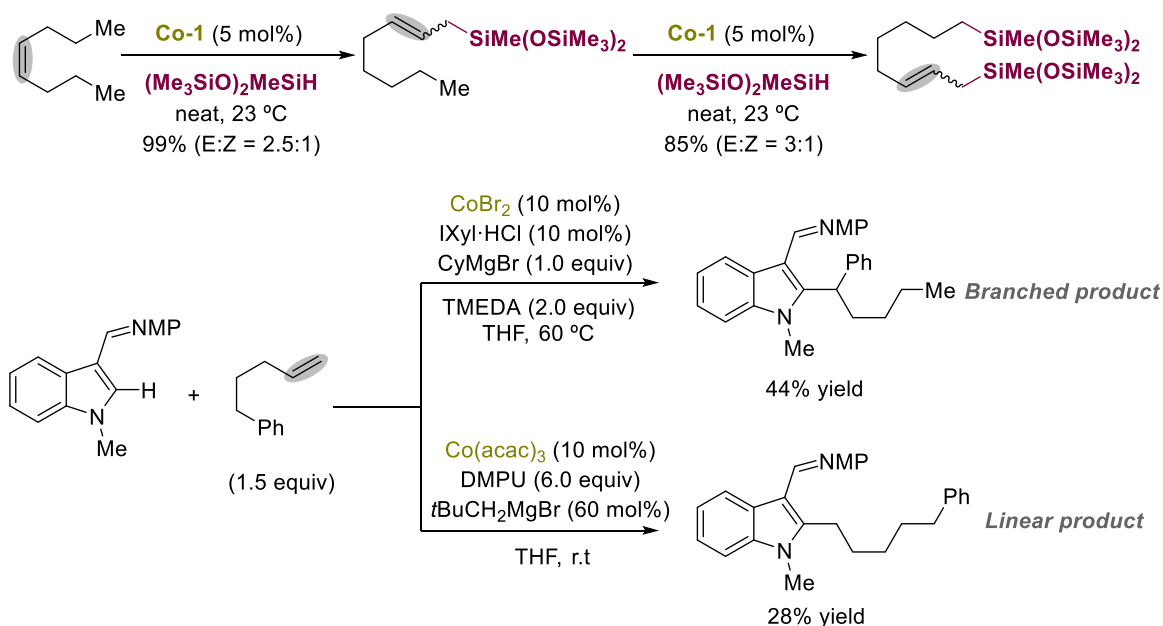
transformation to 1,3-dimethyl-1,3-diaza-2-boracyclopentane or benzo-1,3,2-diazaborolane with equal ease than HBpin (Scheme 1.2.24, C).^{146,147}



Scheme 1.2.24. Cobalt-catalyzed chain walking hydroboration events.

Superior performance has been found in cobalt complexes in terms of isomerization/hydrosilylation when compared to precious metals used for similar purposes.^{148,149} In 2014, Chirik presented a dehydrogenative silylation of internal alkenes promoted by **Co-1**, affording exclusively silylated products at the terminal position (Scheme 1.2.25, *top*). Indeed, this dehydrogenative event offers the opportunity to engage multiple C–Si bonds from simple precursors.¹⁵⁰

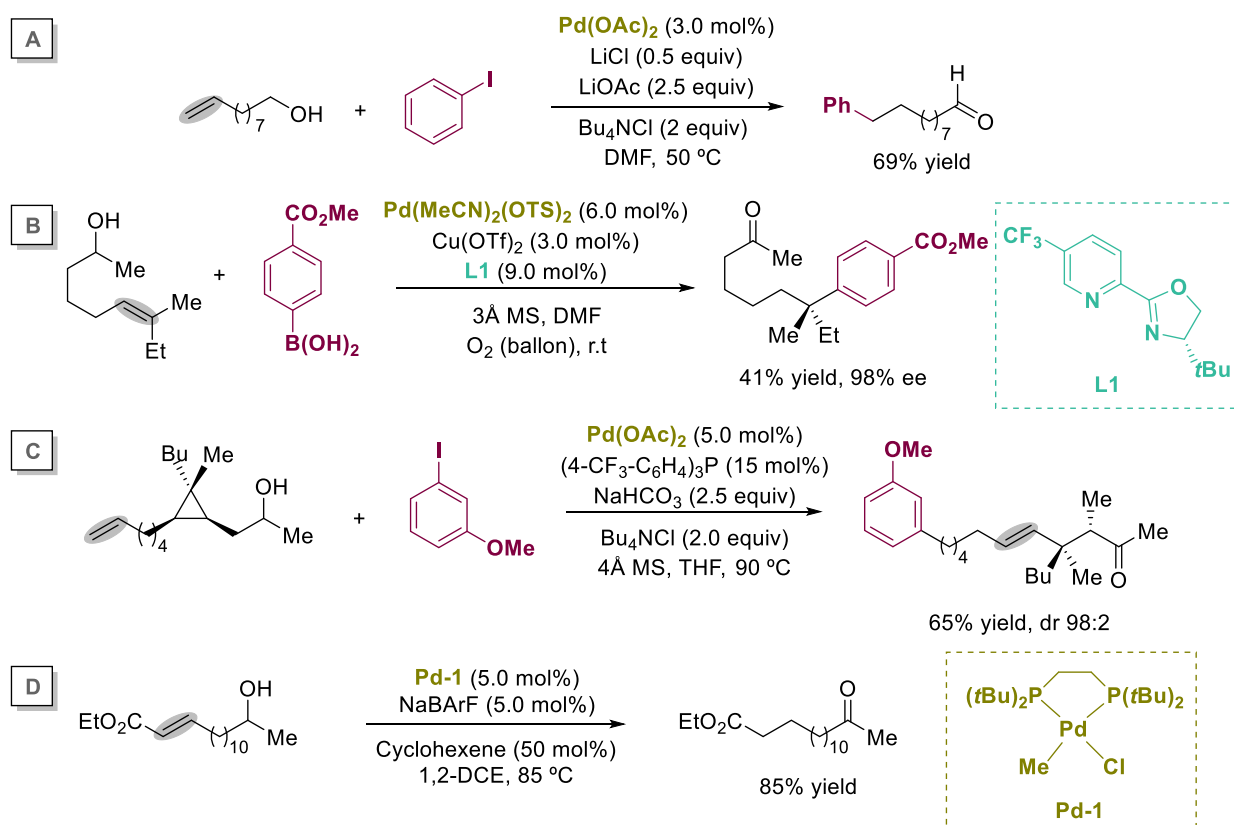
As indicated before, cobalt catalysts are able to forge C–C bonds through isomerization by remote C–H activation *via* cobalt hydride species.¹⁵¹ In 2014, Yoshikai and co-workers published a site-selective transformation involving unactivated olefins bearing pending arenes, with C–H acidic indoles (Scheme 1.2.25, *bottom*).¹⁵² On one hand, branched products were afforded with the use of *N*-heterocyclic carbenes at 60 °C and CyMgBr whereas linear products were assembled with the addition of *t*BuCH₂MgBr rather than the CyMgBr and in the absence of ligand. The latter selectivity is attributed to the formation of cobalt-hydride species by β-hydrogen elimination of the alkyl magnesium salt. Still, however, the role of the ligand is rather unclear and subject of considerable speculation.



1.2.3.6 Palladium walking metals

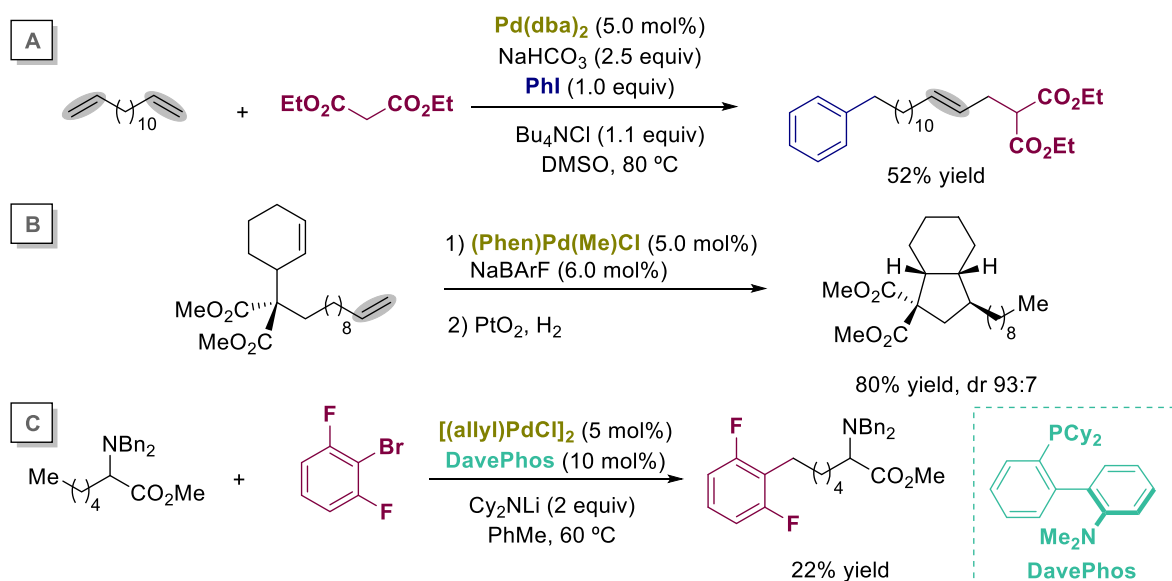
The utilization of Pd catalysts in chain-walking can be traced back from the work of Magennis and Heck by combining Heck reactions and chain-walking events, obtaining the corresponding products in low yields as mixtures.^{153–155} Subsequently, Larock reported that remote functionalization of aliphatic alcohols decorated with a pending alkene results in the corresponding carbonyl products by means of olefin isomerization (Scheme 1.2.26, A).¹⁵⁶ A considerable step forward was made by Sigman in 2012, describing an enantioselective remote functionalization of alcohols possessing a pending alkene with Pd catalysts bearing PyrOx ligands (Scheme 1.2.26, B).¹⁵⁷ Notably, the authors were able to achieve the formation of quaternary stereocenters in high enantioselectivity from trisubstituted olefins with a broad substrate scope.^{185–196} As for zirconium-catalyzed strategies, Marek demonstrated that the utilization of Pd catalysts can be employed with cyclopropanes decorated with pending olefins and appropriately substituted alcohol motifs, resulting in the corresponding carbonyl compound (Scheme 1.2.26, C).¹⁷⁰ Optionally, chain walking can be accomplished starting from α,β -unsaturated carbonyls *via in situ* formation of palladium hydride species that ultimately afford an isomerization event (Scheme 1.2.26, D).^{171,172}

Chapter 1



Scheme 1.2.26. Pd-catalyzed chain-walking events *via* C–C bond formations terminated by carbonyl formation.

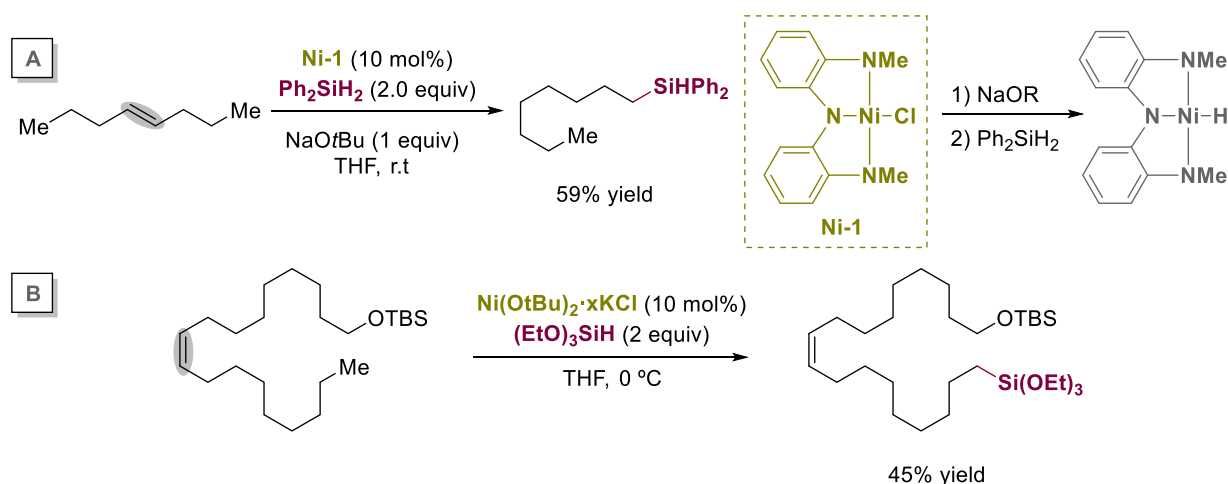
Although these reactions are terminated by the formation of a carbonyl group, these processes are by no means confined to these compounds. Indeed, Larock and Espinet reported a series of nucleophilic trapping processes with a variety of carbon and heteroatoms nucleophiles obtaining bisfunctionalized products (Scheme 1.2.27, A).^{173–176} In 2012, Kakiuchi and co-workers described a tandem sequence of chain-walking/cyclization with substrates possessing a strategically positioned olefin (Scheme 1.2.27, B).^{177,178} More recently, Baudoin and co-workers described that palladium-(II) species generated from oxidative addition can undergo chain-walking prior to reductive elimination. Therefore, this strategy was applied to the remote functionalization of amino acid derivatives (Scheme 1.2.27, C).¹⁷⁹ In 2016, the same group presented a selective linear Negishi type cross-coupling using mixtures of branched alkyl bromides.¹⁸⁰



Scheme 1.2.27. Pd-catalyzed chain-walking events *via* C–C bond formation by non-terminating carbonyl formation.

1.2.3.7 Nickel walking metals

The utilization of nickel catalysts in chain-walking reactions can be traced back from their use in polymerization events.^{181,182} Significant applications of this chemistry can be found in the Shell higher olefin process (SHOP) and Dupont process. More recently, Hu and co-workers established in 2015 a selective alkene isomerization/hydrosilylation by nickel pincer complexes, in which the nickel hydride was generated upon exposure to both metal alkoxides and silanes (Scheme 1.2.28, A).^{183,184} A significant improvement was obtained when nickel nanoparticles were utilized, extending the scope to tertiary silanes (Scheme 1.2.28, B).¹⁸⁵

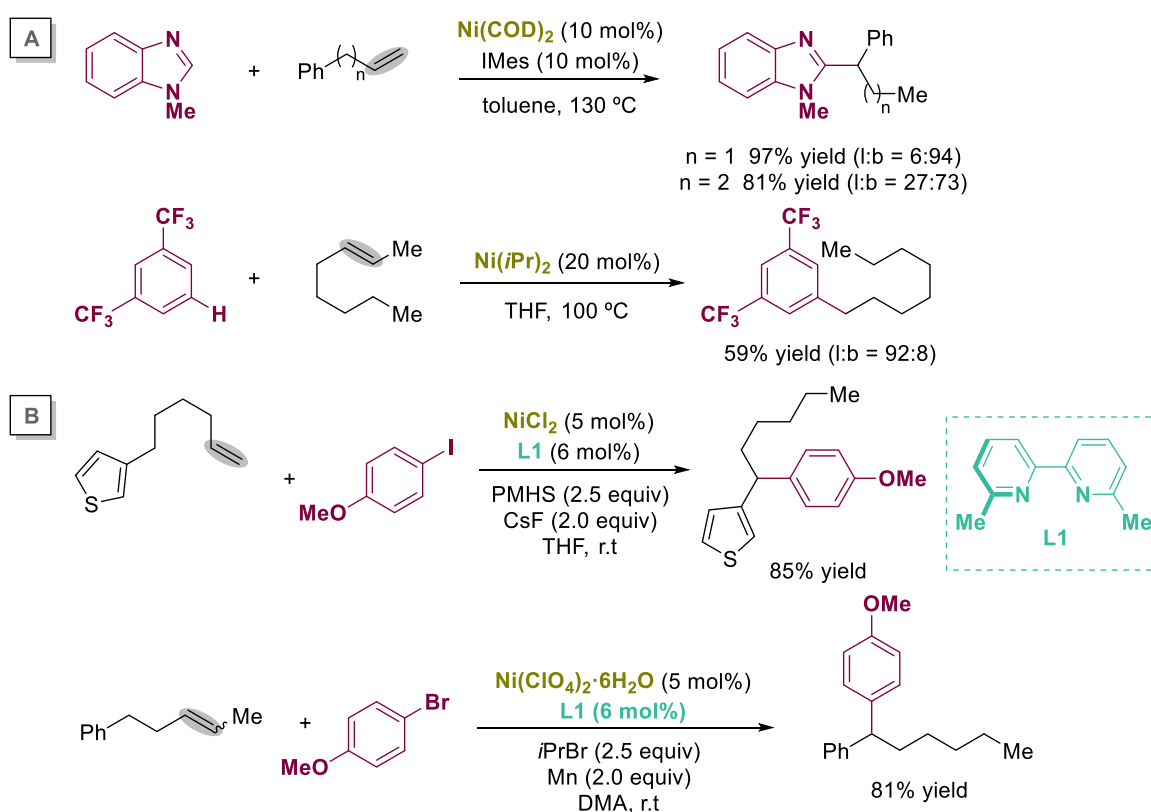


Scheme 1.2.28. Ni-catalyzed chain-walking hydrosilylations of internal olefins.

In 2013, Ong described a nickel-catalyzed olefin isomerization/hydroarylation of alkenes *via* initial C–H functionalization of (hetero)arenes with *N*-heterocyclic carbene ligand and Ni(COD)₂, enabling

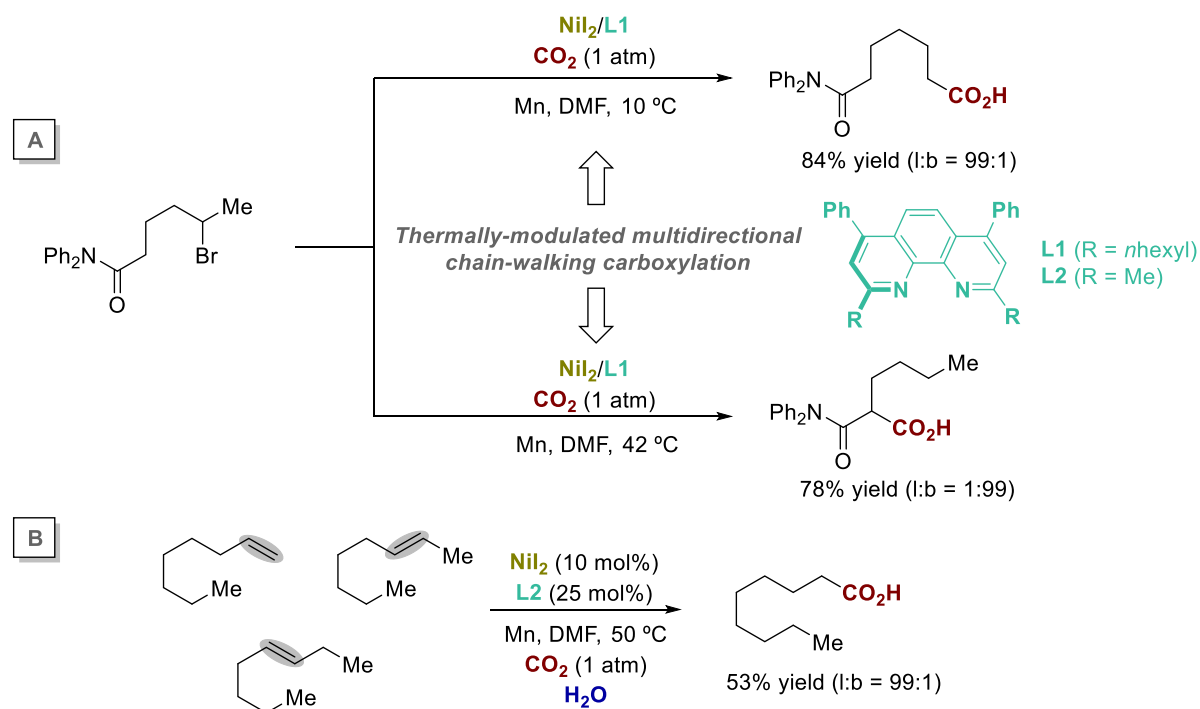
Chapter 1

bond-formation at the benzylic position. Interestingly, the presence of AlMe_3 inhibits olefin isomerization, resulting in the formation of linear products (Scheme 1.2.29, *A-top*).¹⁸⁵ Theoretical calculations supported an initial oxidative addition into the C–H bond (Scheme 1.2.29, *A-bottom*).¹⁸⁵ In 2017, Zhu and co-workers reported a site-selective catalytic hydroarylation of alkenes occurring exclusively at benzylic $\text{C}(\text{sp}^3)\text{--H}$ sites where the utilization of polymethylhydrosiloxane (PHMS) was crucial for success (Scheme 1.2.29, *B-top*).¹⁸⁶ Later, the same group described a follow-up where they were able to avoid the utilization of PHMS by utilizing light alkyl bromides as hydride sources¹⁸⁷ via β -hydride elimination (Scheme 1.2.29, *B-bottom*).^{188,189}



Scheme 1.2.29. Ni-catalyzed chain-walking hydroarylations.

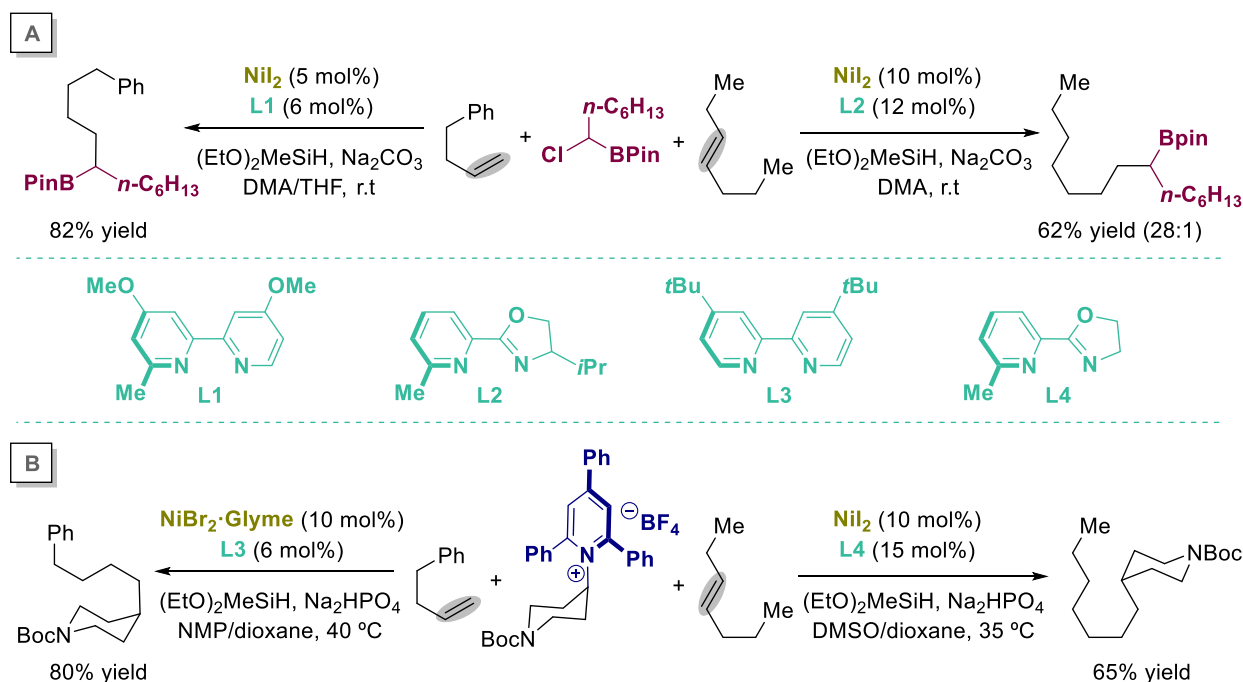
Driven by knowledge of our group in Ni catalysts, a remote and site-selective $\text{C}(\text{sp}^3)\text{--H}$ carboxylation of unactivated alkyl bromides with CO_2 (Scheme 1.2.30, *A*) was reported recently.¹⁹⁰ Importantly, this transformation occurs exclusively at the terminal $\text{C}(\text{sp}^3)\text{--H}$ bond, even with alkyl bromides possessing an arene on the side chain. In addition, this study showed the possibility of controlling site-selectivity by a subtle control of the temperature, allowing to trigger bond-formation at either branched or linear positions. In 2019, our group reported that a similar strategy can be implemented by means of photoredox catalysis in the absence of inorganic reductants.¹⁹¹ Moreover, Martín and co-workers demonstrated that a remote carboxylation of olefins can be implemented with water as formal hydride source (Scheme 1.2.30, *B*).¹⁹² Interestingly, statistical mixtures of olefins can promote a carboxylation even within the context of chain-walking reactions with an exquisite site-selectivity profile.



Scheme 1.2.30. Ni-catalyzed chain-walking for remote carboxylation.

Another example was reported by our group in 2018 when describing a Ni-catalyzed site-selective reductive coupling of α -haloboranes with unactivated olefins (Scheme 1.2.31, A),¹⁹³ thus resulting in the formation of densely functionalized organoboron reagents. More recently, Martín group described the development of a catalytic deaminative cross-electrophile coupling *via* remote functionalization of unactivated olefins (Scheme 1.2.31, B).¹⁹⁴ This method combined the $\text{C}(\text{sp}^3)\text{-N}$ cleavage with the remote functionalization of C-H bonds using unactivated olefins. Such protocol allowed us to promote this reaction within the context of late-stage functionalization of densely functionalized compounds possessing alkyl amines in their structures.

Chapter 1



Scheme 1.2.31. Ni-catalyzed chain-walking for remote C–C bond formation of olefins.

1.2.3.8 Tungsten as a promise chain-walking catalyst

The Szymańska-Buzar group reported the utilization of tungsten as catalyst for the hydroamination of terminal alkynes (Figure 1.2.7, *top right*).¹⁹⁵ In addition, tungsten catalysts have been employed within the context of olefin metathesis (*bottom right*),¹⁹⁶ hydrogenation/hydrodesulfurization processes (*top left*),¹⁹⁷ alkene(alkyne)-cyclizations, rearrangement processes (*bottom left*),¹⁹⁸ and in hydroisomerization/hydrocracking of alkanes for the production of high octane products in industry purposes.¹⁹⁹

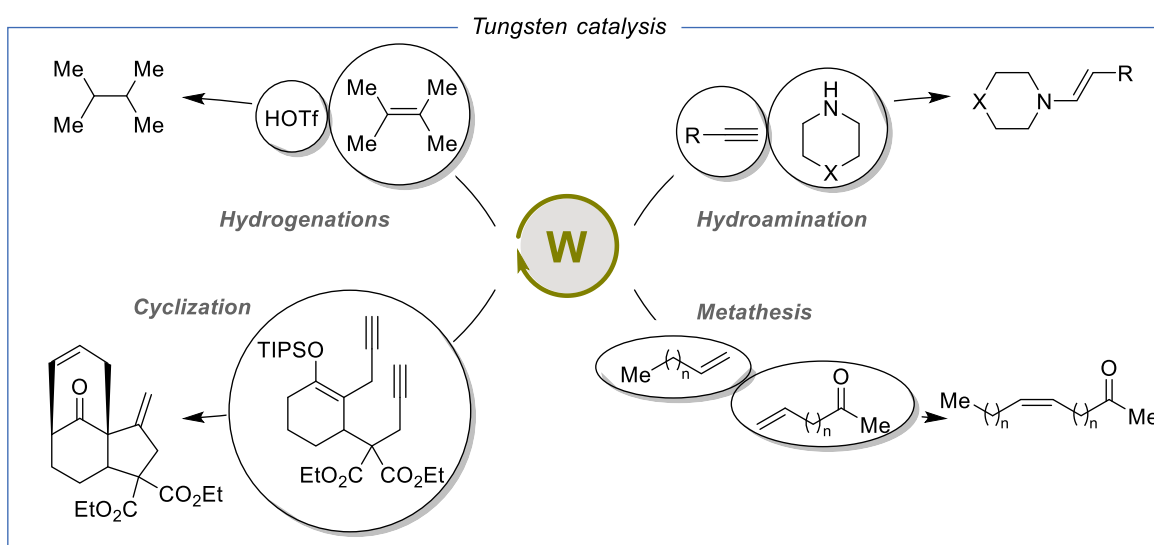
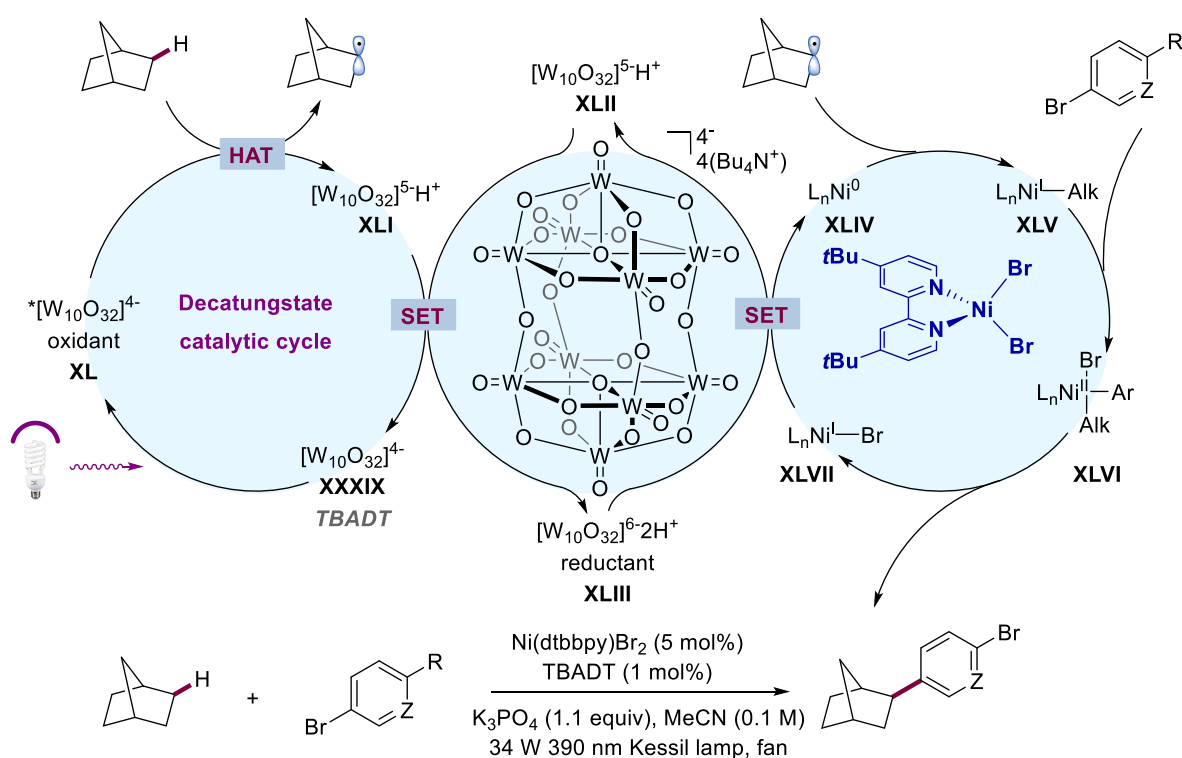


Figure 1.2.7. Basic lines of tungsten catalysis.

During last two years, Macmillan has discovered a new utility for tungsten metal using decatungstate complexes to perform the direct arylation of strong aliphatic C–H bonds (Scheme 1.2.32).²⁰⁰ Intriguingly, tungsten has a double role in this reaction acting first *via* a dual polyoxometalate HAT reagent and secondly as a reductant to recover the Ni(0) catalyst. The strongly photoactivated species formed after irradiation with blue Kessil lights can abstract protons of unactivated aliphatic C–H bonds with a high dissociation energy, thus resulting in a hydride species. Disproportionation of singly reduced decatungstate (XLI) regenerates the active HAT photocatalyst (XXXIX), concurrently forming a double reduced decatungstate (XLIII). Decatungstate was used later for the same group in order to afford trifluoromethylation of C(sp³)–H aliphatic bonds by merging this technology with copper catalysis.²⁰¹



Scheme 1.2.32. C(sp³)–H arylation *via* dual polyoxometalate HAT and nickel catalytic manifold.

Although not a single remote functionalization has been reported within the context of tungsten catalysis, the potential to carry out olefin isomerizations is known since 1974.²⁰² This premise will be tackled in *Chapter 4* where we tried to unravel the potential of tungsten catalysts in remote functionalization reactions.

Chapter 1

1.3 General objectives of this Doctoral Thesis

Despite the advances realized in nickel catalysis, C–O functionalization, C–N cleavage and remote functionalization, a number of challenges remain in these endeavors. In particular, we wondered whether it would be possible to enable stereospecific C–heteroatom bond-forming reactions by means of C–O cleavage, the ability to promote new deaminative technologies *via* C–N scission and the ability to promote remote functionalizations beyond the utilization of Pd, Rh, Fe or Ni catalysts. Specifically, the main objectives of this PhD thesis can be delineated in the following three objectives:

- To describe a stereospecific borylation by the utilization of π -extended secondary benzyl esters catalyzed by nickel complexes.
- To broaden the means to trigger deaminative C–C bond-forming reactions within the context of cross-electrophile coupling events.
- To discover new reactivity of tungsten catalysts for promoting the functionalization of remote sp^3 C–H sites.

1.4 References

- (1) Miyaura, N. *Cross-Coupling Reactions. A Practical Guide*; Springer-Verlag: Berlin, 2002.
- (2) de Mejeire, A.; Diedrich, F. *Metal-Catalyzed Cross-Coupling Reactions*, 2nd ed.; Wiley-VCH: Weinheim, Germany, 2004.
- (3) Campeau, L. C.; Hazari, N. Cross-Coupling and Related Reactions: Connecting Past Success to the Development of New Reactions for the Future. *Organometallics* **2019**, *38* (1), 3–35. <https://doi.org/10.1021/acs.organomet.8b00720>.
- (4) Henkel, T.; Brunne, R. M.; Müller, H.; Reichel, F. Statistical Investigation into the Structural Complementarity of Natural Products and Synthetic Compounds. *Angew. Chemie - Int. Ed.* **1999**, *38* (5), 643–647. [https://doi.org/10.1002/\(SICI\)1521-3773\(19990301\)38:5<643::AID-ANIE643>3.0.CO;2-G](https://doi.org/10.1002/(SICI)1521-3773(19990301)38:5<643::AID-ANIE643>3.0.CO;2-G).
- (5) Tollefson, E. J.; Hanna, L. E.; Jarvo, E. R. Stereospecific Nickel-Catalyzed Cross-Coupling Reactions of Benzylic Ethers and Esters. *Acc. Chem. Res.* **2015**, *48* (8), 2344–2353. <https://doi.org/10.1021/acs.accounts.5b00223>.
- (6) Blakemore, D. C.; Castro, L.; Churcher, I.; Rees, D. C.; Thomas, A. W.; Wilson, D. M.; Wood, A. Organic Synthesis Provides Opportunities to Transform Drug Discovery. *Nat. Chem.* **2018**, *10* (4), 383–394. <https://doi.org/10.1038/s41557-018-0021-z>.
- (7) Rosen, B. M.; Quasdorf, K. W.; Wilson, D. A.; Zhang, N.; Resmerita, A. M.; Garg, N. K.; Percec, V. Nickel-Catalyzed Cross-Couplings Involving Carbon-Oxygen Bonds. *Chem. Rev.* **2011**, *111* (3), 1346–1416. <https://doi.org/10.1021/cr100259t>.
- (8) Zarate, C.; van Gemmeren, M.; Somerville, R.; Martin, R. Phenol Derivatives: Moder Electrophiles in Cross-Coupling. *Adv. Organomet. Chem.* **2016**, *66*, 143.
- (9) Ouyang, K.; Hao, W.; Zhang, W. X.; Xi, Z. Transition-Metal-Catalyzed Cleavage of C-N Single Bonds. *Chem. Rev.* **2015**, *115* (21), 12045–12090. <https://doi.org/10.1021/acs.chemrev.5b00386>.
- (10) Wang, Q.; Su, Y.; Li, L.; Huang, H. Transition-Metal Catalysed C-N Bond Activation. *Chem. Soc. Rev.* **2016**, *45* (5), 1257–1272. <https://doi.org/10.1039/c5cs00534e>.
- (11) Martin, R.; Buchwald, S. L. Palladium-Catalyzed Suzuki-Miyaura Cross-Coupling Reactions Employing Dialkylbiaryl Phosphine Ligands. *Acc. Chem. Res.* **2008**, *41* (11), 1461–1473. <https://doi.org/10.1021/ar800036s>.
- (12) Dankwardt, J. W. Nickel-Catalyzed Cross-Coupling of Aryl Grignard Reagents with Aromatic Alkyl Ethers: An Efficient Synthesis of Unsymmetrical Biaryls. *Angew. Chemie - Int. Ed.* **2004**, *43* (18), 2428–2432. <https://doi.org/10.1002/anie.200453765>.
- (13) Wenkert, E.; Michelotti, E. L.; Swindell, C. S.; Tingoli, M. Transformation of Carbon-Oxygen into Carbon-Carbon Bonds Mediated by Low-Valent Nickel Species. *J. Org. Chem.* **1984**, *49* (25), 4894–4899. <https://doi.org/10.1021/j000199a030>.
- (14) Wenkert, E.; Han, A. L.; Jenny, C. J. Nickel-Induced Conversion of Carbon-Nitrogen into Carbon-Carbon Bonds. One-Step Transformations of Aryl, Quaternary Ammonium Salts into Alkylarenes and Biaryls. *J. Chem. Soc. Chem. Commun.* **1988**, No. 14, 975–976. <https://doi.org/10.1039/C39880000975>.
- (15) Trsots, B.; Spagnol, M. D. Nickel-Catalyzed Coupling of Allylamines and Boronic Acids. *J. Chem. Soc., Dalt. Trans. Chem.* **1995**, 2083–2096.
- (16) Bricout, H.; Carpentier, J.-F.; Mortreux, A. Efficient Coupling Reactions of Allylamines with Soft Nucleophiles Using Nickel-Based Catalysts. *Chem. Commun.* **1997**, 1393–1394.
- (17) Blakey, S. B.; MacMillan, D. W. C. The First Suzuki Cross-Couplings of Aryltrimethylammonium Salts. *J. Am. Chem. Soc.* **2003**, *125* (20), 6046–6047. <https://doi.org/10.1021/jao34908b>.
- (18) Guisán-Ceinos, M.; Martín-Heras, V.; Soler-Yanes, R.; Cárdenas, D. J.; Tortosa, M. Copper-Catalysed Cross-Coupling of Alkyl Grignard Reagents and Propargylic Ammonium Salts: Stereospecific Synthesis of Allenes. *Chem. Commun.* **2018**, *54* (60), 8343–8346. <https://doi.org/10.1039/c8cc03760d>.
- (19) Guisán-Ceinos, M.; Martín-Heras, V.; Tortosa, M. Regio- and Stereospecific Copper-Catalyzed Substitution Reaction of Propargylic Ammonium Salts with Aryl Grignard Reagents. *J. Am. Chem. Soc.* **2017**, *139* (25), 8448–8451. <https://doi.org/10.1021/jacs.7b05273>.

Chapter 1

- (20) Li, M. B.; Wang, Y.; Tian, S. K. Regioselective and Stereospecific Cross-Coupling of Primary Allylic Amines with Boronic Acids and Boronates through Palladium-Catalyzed C-N Bond Cleavage. *Angew. Chemie - Int. Ed.* **2012**, *51* (12), 2968–2971. <https://doi.org/10.1002/anie.201109171>.
- (21) Mary T. Didiuk, J. P. M. 1 and A. H. H. Phospine-Directed Stereo- & Regioselective Ni-Catalyzed Reactions of Grignard Reagents with Allylic Ethers. *Tetrahedron* **1998**, *54*, 1117–1130.
- (22) Moragas, T.; Gaydou, M.; Martin, R. Nickel-Catalyzed Carboxylation of Benzylic C-N Bonds with CO₂. *Angew. Chemie - Int. Ed.* **2016**, *55* (16), 5053–5057. <https://doi.org/10.1002/anie.201600697>.
- (23) Zhang, H.; Hagihara, S.; Itami, K. Making Dimethylamino a Transformable Directing Group by Nickel-Catalyzed C-N Borylation. *Chem. - A Eur. J.* **2015**, *21* (47), 16796–16800. <https://doi.org/10.1002/chem.201503596>.
- (24) Jensen, K. L.; Standley, E. A.; Jamison, T. F. Highly Regioselective Nickel-Catalyzed Cross-Coupling of N-Tosylaziridines and Alkylzinc Reagents. *J. Am. Chem. Soc.* **2014**, *136* (31), 11145–11152. <https://doi.org/10.1021/ja505823s>.
- (25) Plunkett, S.; Basch, C. H.; Santana, S. O.; Watson, M. P. Harnessing Alkylpyridinium Salts as Electrophiles in Deaminative Alkyl-Alkyl Cross-Couplings. *J. Am. Chem. Soc.* **2019**, *141* (6), 2257–2262. <https://doi.org/10.1021/jacs.9b00111>.
- (26) Basch, C. H.; Liao, J.; Xu, J.; Piane, J. J.; Watson, M. P. Harnessing Alkyl Amines as Electrophiles for Nickel-Catalyzed Cross Couplings via C-N Bond Activation. *J. Am. Chem. Soc.* **2017**, *139* (15), 5313–5316. <https://doi.org/10.1021/jacs.7b02389>.
- (27) Cristina Silva Costa, D. Additions to Non-Activated Alkenes: Recent Advances. *Arab. J. Chem.* **2020**, *13* (1), 799–834. <https://doi.org/10.1016/j.arabjc.2017.07.017>.
- (28) Takacs, J.; Jiang, X. The Wacker Reaction and Related Alkene Oxidation Reactions. *Curr. Org. Chem.* **2005**, *7* (4), 369–396. <https://doi.org/10.2174/1385272033372851>.
- (29) Hoveyda, A. H.; Zhugralin, A. R. The Remarkable Metal-Catalysed Olefin Metathesis Reaction. *Nature* **2007**, *450* (7167), 243–251. <https://doi.org/10.1038/nature06351>.
- (30) Chi, Y.; Tang, W.; Zhang, X. *Rhodium-Catalyzed Asymmetric Hydrogenation*; Wiley VCH: Weinheim, Germany, 2005. <https://doi.org/10.1002/3527604693.ch1>.
- (31) Corey, E. J.; Chelg, X. *Corey - The Logic of Chemical Synthesis*; Wiley VCH: New York, 1995.
- (32) Kerchner, H. A.; Montgomery, J. Synthesis of Secondary and Tertiary Alkylboranes via Formal Hydroboration of Terminal and 1,1-Disubstituted Alkenes. *Org. Lett.* **2016**, *18* (21), 5760–5763. <https://doi.org/10.1021/acs.orglett.6b03090>.
- (33) Smith, J. R.; Collins, B. S. L.; Hesse, M. J.; Graham, M. A.; Myers, E. L.; Aggarwal, V. K. Enantioselective Rhodium(III)-Catalyzed Markovnikov Hydroboration of Unactivated Terminal Alkenes. *J. Am. Chem. Soc.* **2017**, *139* (27), 9148–9151. <https://doi.org/10.1021/jacs.7b05149>.
- (34) Iwamoto, H.; Imamoto, T.; Ito, H. Computational Design of High-Performance Ligand for Enantioselective Markovnikov Hydroboration of Aliphatic Terminal Alkenes. *Nat. Commun.* **2018**, *9* (1), 1–10. <https://doi.org/10.1038/s41467-018-04693-9>.
- (35) Cai, Y.; Yang, X. T.; Zhang, S. Q.; Li, F.; Li, Y. Q.; Ruan, L. X.; Hong, X.; Shi, S. L. Copper-Catalyzed Enantioselective Markovnikov Hydroboration of α -Olefins Enabled by a Buttressed N-Heterocyclic Carbene Ligand. *Angew. Chemie - Int. Ed.* **2018**, *57* (5), 1376–1380. <https://doi.org/10.1002/anie.201711229>.
- (36) Sommer, H.; Juliá-Hernández, F.; Martin, R.; Marek, I. Walking Metals for Remote Functionalization. *ACS Cent. Sci.* **2018**, *4* (2), 153–165. <https://doi.org/10.1021/acscentsci.8b00005>.
- (37) Yang, K. S.; Gurak, J. A.; Liu, Z.; Engle, K. M. Catalytic, Regioselective Hydrocarbofunctionalization of Unactivated Alkenes with Diverse C-H Nucleophiles. *J. Am. Chem. Soc.* **2016**, *138* (44), 14705–14712. <https://doi.org/10.1021/jacs.6b08850>.
- (38) Chakrabarty, S.; Takacs, J. M. Synthesis of Chiral Tertiary Boronic Esters: Phosphonate-Directed Catalytic Asymmetric Hydroboration of Trisubstituted Alkenes. *J. Am. Chem. Soc.* **2017**, *139* (17), 6066–6069. <https://doi.org/10.1021/jacs.7b02324>.
- (39) Wang, H.; Bai, Z.; Jiao, T.; Deng, Z.; Tong, H.; He, G.; Peng, Q.; Chen, G. Palladium-Catalyzed Amide-Directed Enantioselective Hydrocarbofunctionalization of Unactivated Alkenes Using a Chiral Monodentate Oxazoline Ligand. *J. Am. Chem. Soc.* **2018**, *140* (10), 3542–

3546. <https://doi.org/10.1021/jacs.8b00641>.
- (40) Tran, V. T.; Gurak, J. A.; Yang, K. S.; Engle, K. M. Activation of Diverse Carbon–Heteroatom and Carbon–Carbon Bonds via Palladium(II)-Catalysed β -X Elimination. *Nat. Chem.* **2018**, *10* (11), 1126–1133. <https://doi.org/10.1038/s41557-018-0110-z>.
- (41) Coombs, J. R.; Morken, J. P. Catalytic Enantioselective Functionalization of Unactivated Terminal Alkenes. *Angew. Chemie - Int. Ed.* **2016**, *55* (8), 2636–2649. <https://doi.org/10.1002/anie.201507151>.
- (42) Margrey, K. A.; Nicewicz, D. A. A General Approach to Catalytic Alkene Anti-Markovnikov Hydrofunctionalization Reactions via Acridinium Photoredox Catalysis. *Acc. Chem. Res.* **2016**, *49* (9), 1997–2006. <https://doi.org/10.1021/acs.accounts.6b00304>.
- (43) Crossley, S. W. M.; Obradors, C.; Martinez, R. M.; Shenvi, R. A. Mn-, Fe-, and Co-Catalyzed Radical Hydrofunctionalizations of Olefins. *Chem. Rev.* **2016**, *116* (15), 8912–9000. <https://doi.org/10.1021/acs.chemrev.6b00334>.
- (44) Nguyen, K. D.; Park, B. Y.; Luong, T.; Sato, H.; Garza, V. J.; Krische, M. J. Metal-Catalyzed Reductive Coupling of Olefin-Derived Nucleophiles: Reinventing Carbonyl Addition. *Science*. **2016**, *354* (6310). <https://doi.org/10.1126/science.aah5133>.
- (45) Zarate, C.; van Gemmeren, M.; Somerville, R. J.; Martin, R. Phenol Derivatives: Modern Electrophiles in Cross-Coupling Reactions. *Adv. Organomet. Chem.* **2016**, *66*, 143–222. <https://doi.org/10.1016/bs.adomc.2016.07.001>.
- (46) Cornella, J.; Zarate, C.; Martin, R. Metal-Catalyzed Activation of Ethers via C–O Bond Cleavage: A New Strategy for Molecular Diversity. *Chem. Soc. Rev.* **2014**, *43* (23), 8081–8097. <https://doi.org/10.1039/c4cs00206g>.
- (47) Tobisu, M.; Chatani, N. Cross-Couplings Using Aryl Ethers via C–O Bond Activation Enabled by Nickel Catalysts. *Acc. Chem. Res.* **2015**, *48* (6), 1717–1726. <https://doi.org/10.1021/acs.accounts.5b00051>.
- (48) Luo, Y.-R. *Comprehensive Handbook of Chemical Bond Energies*. Taylor & Francis: New York 2002, pp 1–1687. <https://doi.org/10.2214/AJR.10.5057>.
- (49) Consiglio, G.; Morandini, F.; Piccolo, O. Stereochemical Aspects of the Nickel-Catalyzed Alkylation of Allylic Alcohols. *J. Am. Chem. Soc.* **1981**, *103* (7), 1846–1847. <https://doi.org/10.1021/ja00397a048>.
- (50) Mary T. Didiuk, J. P. M. 1 and A. H. H. Phosphine-Directed Stereo- & Regioselective Ni-Catalyzed Reactions of Grignards Reagents with Allylic Ethers. *Tetrahedron* **1998**, *54*, 1117–1130.
- (51) Nomura, N.; RajanBabu, T. V. Nickel-Catalyzed Asymmetric Allylation of Alkyl Grignard Reagents, Effect of Ligands, Leaving Groups and a Kinetic Resolution with a Hard Nucleophile. *Tetrahedron Lett.* **1997**, *38* (10), 1713–1716. [https://doi.org/10.1016/S0040-4039\(97\)00178-0](https://doi.org/10.1016/S0040-4039(97)00178-0).
- (52) Kobayashi, I. Ikeda, E. Nickel-Catalysed Substitution Reactions of Allylic Carbonates with Aryl- and Alkenyl-Borates. *J. Am. Chem. Soc.* **1994**, *116*, 1789–1790.
- (53) Guan, B. T.; Xiang, S. K.; Wang, B. Q.; Sun, Z. P.; Wang, Y.; Zhao, K. Q.; Shi, Z. J. Direct Benzylic Alkylation via Ni-Catalyzed Selective Benzylic sp^3 C–O Activation. *J. Am. Chem. Soc.* **2008**, *130* (11), 3268–3269. <https://doi.org/10.1021/ja710944j>.
- (54) Tobisu, M.; Shimasaki, T.; Chatani, N. Ni(0)-Catalyzed Direct Amination of Anisoles Involving the Cleavage of Carbon–Oxygen Bonds. *Chem. Lett.* **2009**, *38* (7), 710–711. <https://doi.org/10.1246/cl.2009.710>.
- (55) Tobisu, M.; Yasutome, A.; Yamakawa, K.; Shimasaki, T.; Chatani, N. Ni(0)/NHC-Catalyzed Amination of N-Heteroaryl Methyl Ethers through the Cleavage of Carbon–Oxygen Bonds. *Tetrahedron* **2012**, *68* (26), 5157–5161. <https://doi.org/10.1016/j.tet.2012.04.005>.
- (56) Hie, L.; Ramgren, S. D.; Mesganaw, T.; Garg, N. K. Nickel-Catalyzed Amination of Aryl Sulfamates and Carbamates Using an Air-Stable Precatalyst. *Org. Lett.* **2012**, *14*, 4682–4685. <https://doi.org/10.1021/ol301847m>.
- (57) Methods, A.; Shimasaki, T.; Tobisu, M.; Chatani, N. Nickel-Catalyzed Amination of Aryl Pivalates by the Cleavage of Aryl C–O Bonds. *Angew. Chem. Int. Ed.* **2010**, *49*, 2929–2932. <https://doi.org/10.1002/anie.200907287>.
- (58) Yue, H.; Guo, L.; Liao, H.; Cai, Y.; Zhu, C.; Rueping, M. Catalytic Ester and Amide to Amine Interconversion: Nickel-Catalyzed Decarbonylative Amination of Esters and Amides by C–O and C–C Bond Activation. *Angew. Chem. Int. Ed.* **2017**, *56*, 4282–4285. <https://doi.org/10.1002/anie.201611819>.

Chapter 1

- (59) Rappoport, Z.; Apeloig, Y. *The Chemistry of Organic Silicon Compounds*; John Wiley & Sons: Weinheim, Germany, 1998; Vol. 2.
- (60) Sun, D.; Ren, Z.; Bryce, R.; Yan, S. Materials for Organic Light-Emitting Diodes (OLEDs). *J. Mater. Chem.* **2015**, *3*, 9496–9508. <https://doi.org/10.1039/c5tc01638j>.
- (61) Cheng, C.; Hartwig, J. F. Iridium-Catalyzed Silylation of Aryl C – H Bonds. *J. Am. Chem. Soc.* **2015**, *137*, 592–595. <https://doi.org/10.1021/ja511352u>.
- (62) Cheng, C.; Hartwig, J. F. Mechanism of the Rhodium-Catalyzed Silylation of Arene C – H Bonds. *J. Am. Chem. Soc.* **2014**, *136*, 12064–12072. <https://doi.org/10.1021/ja505844k>.
- (63) Denmark, S. E.; Kallemeyn, J. M. Palladium-Catalyzed Silylation of Aryl Bromides Leading to Functionalized Aryldimethylsilanols. *Org. Lett.* **2003**, *5*, 2001–2004. <https://doi.org/10.1021/0l035288m>.
- (64) Cheng, C.; Hartwig, J. F. Rhodium-Catalyzed Intermolecular C – H Silylation of Arenes with High Steric Regiocontrol. *Science*. **2014**, *343*, 853–858.
- (65) Yamanoi, Y.; Nishihara, H. Direct and Selective Arylation of Tertiary Silanes with Rhodium Catalyst. *J. Org. Chem.* **2008**, *73*, 6671–6678. <https://doi.org/10.1021/jo8008148>.
- (66) Zarate, C.; Martín, R. A Mild Ni/Cu-Catalyzed Silylation via C-O Cleavage. *J. Am. Chem. Soc.* **2014**, *136* (6), 2236–2239. <https://doi.org/10.1021/ja412107b>.
- (67) Somerville, R. J.; Hale, L. V. A.; Gómez-Bengoá, E.; Burés, J.; Martín, R. Intermediacy of Ni-Ni Species in Sp² C-O Bond Cleavage of Aryl Esters: Relevance in Catalytic C-Si Bond Formation. *J. Am. Chem. Soc.* **2018**, *140* (28), 8771–8780. <https://doi.org/10.1021/jacs.8b04479>.
- (68) Zarate, C.; Nakajima, M.; Martín, R. A Mild and Ligand-Free Ni-Catalyzed Silylation via C-OME Cleavage. *J. Am. Chem. Soc.* **2017**, *139* (3), 1191–1197. <https://doi.org/10.1021/jacs.6b10998>.
- (69) Yang, J.; Chen, T.; Han, L. B. C-P Bond-Forming Reactions via C-O/P-H Cross-Coupling Catalyzed by Nickel. *J. Am. Chem. Soc.* **2015**, *137* (5), 1782–1785. <https://doi.org/10.1021/ja512498u>.
- (70) Yang, J.; Xiao, J.; Chen, T.; Han, L. B. Nickel-Catalyzed Phosphorylation of Phenol Derivatives via C-O/P-H Cross-Coupling. *J. Org. Chem.* **2016**, *81* (9), 3911–3916. <https://doi.org/10.1021/acs.joc.6b00289>.
- (71) Gu, Y.; Martín, R. Ni-Catalyzed Stannylation of Aryl Esters via C-O Bond Cleavage. *Angew. Chemie - Int. Ed.* **2017**, *56* (12), 3187–3190. <https://doi.org/10.1002/anie.201611720>.
- (72) Davies, A. G.; Gielen, M.; Pannell, K. H.; Tiekink, E. R. T. *Tin Chemistry: Fundamentals, Frontiers, and Applications*; Wiley VCH: Weinheim, Germany, 2008. <https://doi.org/10.1002/9780470758090>.
- (73) Furuya, T.; Strom, A. E.; Ritter, T. Silver-Mediated Fluorination of Functionalized Aryl Stannanes. *J. Am. Chem. Soc.* **2009**, *131* (5), 1662–1663. <https://doi.org/10.1021/ja8086664>.
- (74) Makaravage, K. J.; Brooks, A. F.; Mossine, A. V.; Sanford, M. S.; Scott, P. J. H. Copper-Mediated Radiofluorination of Arylstannanes with [18F]KF. *Org. Lett.* **2016**, *18* (20), 5440–5443. <https://doi.org/10.1021/acs.orglett.6b02911>.
- (75) Sandford, C.; Aggarwal, V. K. Stereospecific Functionalizations and Transformations of Secondary and Tertiary Boronic Esters. *Chem. Commun.* **2017**, *53*, 5471–5574. <https://doi.org/10.1039/c7cc01254c>.
- (76) Hall, D. . *Boronic Acids: Preparation and Applications in Organic Synthesis and Medicine*; Wiley VCH: Weinheim, Germany, 2005.
- (77) Hartwig, J. F. Borylation and Silylation of C-H Bonds: A Platform for Diverse C-H Bond Functionalizations. *Acc. Chem. Res.* **2012**, *45* (6), 864–873. <https://doi.org/10.1021/ar200206a>.
- (78) Molander, G. A.; Trice, S. L. J.; Dreher, S. D. Palladium-Catalyzed, Direct Boronic Acid Synthesis from Aryl Chlorides: A Simplified Route to Diverse Boronate Ester Derivatives. *J. Am. Chem. Soc.* **2010**, *132* (50), 17701–17703. <https://doi.org/10.1021/ja1089759>.
- (79) Yamamoto, E.; Izumi, K.; Horita, Y.; Ito, H. Anomalous Reactivity of Silylborane: Transition-Metal-Free Boryl Substitution of Aryl, Alkenyl, and Alkyl Halides with Silylborane/Alkoxy Base Systems. *J. Am. Chem. Soc.* **2012**, *134* (49), 19997–20000. <https://doi.org/10.1021/ja309578k>.
- (80) Uematsu, R.; Yamamoto, E.; Maeda, S.; Ito, H.; Taketsugu, T. Reaction Mechanism of the Anomalous Formal Nucleophilic Borylation of Organic

- Halides with Silylborane: Combined Theoretical and Experimental Studies. *J. Am. Chem. Soc.* **2015**, *137* (12), 4090–4099. <https://doi.org/10.1021/ja507675f>.
- (81) Hartwig, J. F. Regioselectivity of the Borylation of Alkanes and Arenes. *Chem. Soc. Rev.* **2011**, *40* (4), 1992–2002. <https://doi.org/10.1039/c0cs00156b>.
- (82) Chow, W. K.; So, C. M.; Lau, C. P.; Kwong, F. Y. Palladium-Catalyzed Borylation of Aryl Mesylates and Tosylates and Their Applications in One-Pot Sequential Suzuki-Miyaura Biaryl Synthesis. *Chem. - A Eur. J.* **2011**, *17* (25), 6913–6917. <https://doi.org/10.1002/chem.201100361>.
- (83) Wilson, D. A.; Wilson, C. J.; Moldoveanu, C.; Resmerita, A. M.; Corcoran, P.; Hoang, L. M.; Rosen, B. M.; Percec, V. Neopentylglycolborylation of Aryl Mesylates and Tosylates Catalyzed by Ni-Based Mixed-Ligand Systems Activated with Zn. *J. Am. Chem. Soc.* **2010**, *132* (6), 1800–1801. <https://doi.org/10.1021/ja910808x>.
- (84) Huang, K.; Yu, D. G.; Zheng, S. F.; Wu, Z. H.; Shi, Z. J. Borylation of Aryl and Alkenyl Carbamates through Ni-Catalyzed C-O Activation. *Chem. - A Eur. J.* **2011**, *17* (3), 786–791. <https://doi.org/10.1002/chem.201001943>.
- (85) Zarate, C.; Manzano, R.; Martín, R. Ipsi- Borylation of Aryl Ethers via Ni-Catalyzed C-OMe Cleavage. *J. Am. Chem. Soc.* **2015**, *137* (21), 6754–6757. <https://doi.org/10.1021/jacs.5b03955>.
- (86) Muetterties, E. L. Synthesis of Organoboranes. *J. Am. Chem. Soc.* **1960**, *82* (16), 4163–4166. <https://doi.org/10.1021/ja01501a010>.
- (87) Niu, L.; Yang, H.; Wang, R.; Fu, H. Metal-Free Ortho C-H Borylation of 2-Phenoxyppyridines under Mild Conditions. *Org. Lett.* **2012**, *14* (10), 2618–2621. <https://doi.org/10.1021/ol300950r>.
- (88) Bac, N. V.; Langlois, Y. Silicon-Induced Fragmentations: Stereoselective Preparation of (Z,E)- and (Z,Z)-1,4-Dienamine Derivatives. Synthesis of (9Z,12E)-Tetradecadien-1-yl Acetate, Pheromone of Various Lepidoptera. *J. Am. Chem. Soc.* **1982**, *104* (26), 7666–7667. <https://doi.org/10.1021/ja00390a051>.
- (89) Gupton, J. T.; Layman, W. J. Reaction of 2-Aryl-3-(N,N-Dimethylamino)-1-Propenes and Their Corresponding Quaternary Ammonium Salts with Organometallic Species and Reducing Agents. *J. Org. Chem.* **1987**, *52* (16), 3683–3686. <https://doi.org/10.1021/j000392a035>.
- (90) Maity, P.; Shacklady-mcatee, D. M.; Yap, G. P. A.; Sirianni, E. R.; Watson, M. P. Nickel-Catalyzed Cross Couplings of Benzylic Ammonium Salts and Boronic Acids: Stereospecific Formation of Diarylethanes via C-N Bond Activation. *J. Am. Chem. Soc.* **2013**, *135*, 280–285. <https://doi.org/10.1021/ja3089422>.
- (91) Nugent, T. C. *Chiral Amine Synthesis*, 1 st.; Wiley-VCH VerlagGmbH & Co. KGaA: Weinheim, Germany, 2010.
- (92) Weng, Z.; Li, Y.; Tian, S. Catalytic Asymmetric α -Alkylation of Ketones and Aldehydes with N-Benzylic Sulfonamides through Carbon-Nitrogen Bond Cleavage. *J. Org. Chem.* **2011**, *76*, 8095–8099. <https://doi.org/10.1021/jo2014142>.
- (93) Huang, C. D.; Doyle, A. G. Nickel-Catalyzed Negishi Alkylations of Styrenyl Aziridines. *J. Am. Chem. Soc.* **2012**, *134*, 9541–9545. <https://doi.org/10.1021/ja3013825>.
- (94) Shacklady-mcatee, D. M.; Roberts, K. M.; Basch, C. H.; Song, Y.; Watson, M. P. A General, Simple Catalyst for Enantiospecific Cross Couplings of Benzylic Ammonium Triflates and Boronic Acids: No Phosphine Ligand Required. *Tetrahedron* **2014**, *70* (27–28), 4257–4263. <https://doi.org/10.1016/j.tet.2014.03.039>.
- (95) Correa, A.; Martín, R. Ni-Catalyzed Direct Reductive Amidation via C-O Bond Cleavage. *J. Am. Chem. Soc.* **2014**, *136*, 7253–7256. <https://doi.org/10.1021/ja5029793>.
- (96) Leon, T.; Correa, A.; Martín, R. Ni-Catalyzed Direct Carboxylation of Benzyl Halides with CO 2. *J. Am. Chem. Soc.* **2013**, *135*, 1221–1225. <https://doi.org/10.1021/ja311045f>.
- (97) Leon, T.; Correa, A.; Martín, R. Ni-Catalyzed Carboxylation of C(Sp²) - and C(Sp³) - O Bonds with CO 2. *J. Am. Chem. Soc.* **2014**, *135*, 1062–1069. <https://doi.org/10.1021/ja410883p>.
- (98) Liu, Y.; Cornella, J.; Martín, R. Ni-Catalyzed Carboxylation of Unactivated Primary Alkyl Bromides and Sulfonates with CO 2. *J. Am. Chem. Soc.* **2014**, *135*, 11212–11215. <https://doi.org/10.1021/ja5064586>.

Chapter 1

- (99) Moragas, T.; Cornella, J.; Martín, R. Ligand-Controlled Regiodivergent Ni-Catalyzed Reductive Carboxylation of Allyl Esters with CO₂. *J. Am. Chem. Soc.* **2014**, *136*, 17702–17705. <https://doi.org/10.1021/ja509077a>.
- (100) Moragas, T.; Gaydou, M.; Martín, R. Nickel-Catalyzed Carboxylation of Benzylic C-N Bonds with CO₂. *Angew. Chem. Int. Ed.* **2016**, *55*, 5053–5057. <https://doi.org/10.1002/anie.201600697>.
- (101) Hu, J.; Sun, H.; Cai, W.; Pu, X.; Zhang, Y.; Shi, Z. Nickel-Catalyzed Borylation of Aryl- and Benzyltrimethylammonium Salts via C-N Bond Cleavage. *J. Org. Chem.* **2016**, *81* (1), 14–24. <https://doi.org/10.1021/acs.joc.5b02557>.
- (102) Basch, C. H.; Cobb, K. M.; Watson, M. P. Nickel-Catalyzed Borylation of Benzylic Ammonium Salts: Stereospecific Synthesis of Enantioenriched Benzylic Boronates. *Org. Lett.* **2016**, *18* (1), 136–139. <https://doi.org/10.1021/acs.orglett.5b03455>.
- (103) Lu, P. Recent Developments in Regioselective Ring Opening of Aziridines. *Tetrahedron* **2010**, *66* (14), 2549–2560. <https://doi.org/10.1016/j.tet.2010.01.077>.
- (104) Lin, B. L.; Clough, C. R.; Hillhouse, G. L. Interactions of Aziridines with Nickel Complexes: Oxidative-Addition and Reductive-Elimination Reactions That Break and Make C-N Bonds. *J. Am. Chem. Soc.* **2002**, *124* (12), 2890–2891. <https://doi.org/10.1021/ja017652n>.
- (105) Ney, J. E.; Wolfe, J. P. Synthesis and Reactivity of Azapalladacyclobutanes. *J. Am. Chem. Soc.* **2006**, *128* (48), 15415–15422. <https://doi.org/10.1021/jao660756>.
- (106) Nielsen, D. K.; Huang, C. Y.; Doyle, A. G. Directed Nickel-Catalyzed Negishi Cross Coupling of Alkyl Aziridines. *J. Am. Chem. Soc.* **2013**, *135* (36), 13605–13609. <https://doi.org/10.1021/ja4076716>.
- (107) Huang, C. Y.; Doyle, A. G. Electron-Deficient Olefin Ligands Enable Generation of Quaternary Carbons by Ni-Catalyzed Cross-Coupling. *J. Am. Chem. Soc.* **2015**, *137* (17), 5638–5641. <https://doi.org/10.1021/jacs.5b02503>.
- (108) Basch, C. H.; Liao, J.; Xu, J.; Piane, J. J.; Watson, M. P. Harnessing Alkyl Amines as Electrophiles for Nickel-Catalyzed Cross. *J. Am. Chem. Soc.* **2017**, *139*, 5313–5316. <https://doi.org/10.1021/jacs.7b02389>.
- (109) Breslow, B. R. Biomimetic Chemistry. *Chem. Soc. Rev.* **1972**, *1*, 553–580.
- (110) Schwarz, H. Remote Functionalization of C-H and C-C Bonds by “Naked” Transition-Metal Ions (Cosi Fan Tutte). *Acc. Chem. Res.* **1989**, *22* (8), 282–287. <https://doi.org/10.1021/ar00164a004>.
- (111) Breslow, R. Biomimetic Control of Chemical Selectivity. *Acc. Chem. Res.* **1980**, *13* (6), 170–177. <https://doi.org/10.1021/ar50150a002>.
- (112) Hartwig, J. F.; Larsen, M. A. Undirected, Homogeneous C-H Bond Functionalization: Challenges and Opportunities. *ACS Cent. Sci.* **2016**, *2* (5), 281–292. <https://doi.org/10.1021/acscentsci.6b00032>.
- (113) Crabtree, R. H. *The Organometallic Chemistry of the Transition Metals*; John Wiley & Sons, Inc.: New Haven, CT, 2014; Vol. 11. <https://doi.org/10.1259/jrs.1915.0040>.
- (114) Biswas, S. Mechanistic Understanding of Transition-Metal-Catalyzed Olefin Isomerization: Metal-Hydride Insertion-Elimination vs. π -Allyl Pathways. *Comments Inorg. Chem.* **2015**, *35* (6), 300–330. <https://doi.org/10.1080/02603594.2015.1059325>.
- (115) Finkbeiner, H. L.; Cooper, G. D. Titanium-Catalyzed Isomerization and Olefin-Exchange Reactions of Alkylmagnesium Halides: A Novel Method for Preparation of the Grignard Reagent. *J. Org. Chem.* **1961**, *26* (11), 4779–4780. <https://doi.org/10.1021/jo01069a607>.
- (116) Cooper, G. D.; Finkbeiner, H. L. Titanium-Catalyzed Rearrangement and Olefin-Exchange of Grignard Reagents. *J. Org. Chem.* **1962**, *27* (5), 1493–1497. <https://doi.org/10.1021/jo01052a001>.
- (117) Carr, D. B.; Schwartz, J. Preparation of Organoaluminum Compounds by Hydrozirconation-Transmetalation. *J. Am. Chem. Soc.* **1979**, *101* (13), 3521–3531. <https://doi.org/10.1021/ja00507a017>.
- (118) Buchwald, S. L.; LaMaire, S. J.; Nielsen, R. B.; Watson, B. T.; King, S. M. A Modified Procedure for the Preparation of Cp₂Zr(H)Cl (Schwartz's Reagent). *Tetrahedron Lett.* **1987**, *28* (34), 3895–3898. [https://doi.org/10.1016/S0040-4039\(00\)96413-X](https://doi.org/10.1016/S0040-4039(00)96413-X).
- (119) Negishi, E. Ichi; Takahashi, T. Patterns of Stoichiometric and Catalytic Reactions of Organozirconium and Related Complexes of Synthetic Interest. *Acc. Chem. Res.* **1994**, *27* (5), 124–130. <https://doi.org/10.1021/ar00041a002>.

- (120) Marek, I.; Chinkov, N.; Levin, A. A Zirconium Promenade - An Efficient Tool in Organic Synthesis. *Synlett* **2006**, No. 4, 501–514. <https://doi.org/10.1055/s-2006-932483>.
- (121) Mola, L.; Sidera, M.; Fletcher, S. P. Asymmetric Remote C-H Functionalization: Use of Internal Olefins in Tandem Hydrometallation-Isomerization-Asymmetric Conjugate Addition Sequences. *Aust. J. Chem.* **2015**, *68*(3), 401–403. <https://doi.org/10.1071/CH14556>.
- (122) Vasseur, A.; Perrin, L.; Eisenstein, O.; Marek, I. Remote Functionalization of Hydrocarbons with Reversibility Enhanced Stereocontrol. *Chem. Sci.* **2015**, *6*(5), 2770–2776. <https://doi.org/10.1039/c5sc00445d>.
- (123) Masarwa, A.; Didier, D.; Zabrodski, T.; Schinkel, M.; Ackermann, L.; Marek, I. Merging Allylic Carbon-Hydrogen and Selective Carbon-Carbon Bond Activation. *Nature* **2014**, *505*(7482), 199–203. <https://doi.org/10.1038/nature12761>.
- (124) Bingham, B. D.; Webster, D. E.; Wells, P. B. Homogeneous Catalysis of Olefin in Isomerisation. Part V. Pent-1-Ene Isomerisation Catalysed by Solutions of RuHCl(PPh₃), and of RuHCl(Co)-(PPh₃); Variation of the Isomeric Composition of Pent-2-Ene and Its Attribution to Steric Factors. *J. Chem. Soc., Dalt. Trans.* **1974**, *14*, 1519–1521.
- (125) Wakamatsu, H.; Nishida, M.; Adachi, N.; Mori, M. Isomerization Reaction of Olefin Using RuClH(CO)(PPh₃)₃. *J. Org. Chem.* **2000**, *65*(13), 3966–3970. <https://doi.org/10.1021/j09918753>.
- (126) Dobereiner, G. E.; Erdogan, G.; Larsen, C. R.; Grotjahn, D. B.; Schrock, R. R. A One-Pot Tandem Olefin Isomerization/Metathesis-Coupling (ISOMET) Reaction. *ACS Catal.* **2014**, *4*(9), 3069–3076. <https://doi.org/10.1021/cs500889x>.
- (127) Evans, B. D.; Osborn, A.; Wilkinson, G. Hydroformylation of Alkenes by Use of Rhodium Complex Catalysts. *J. Chem. Soc.* **1968**, *0*, 3133–3142.
- (128) Osborn, A.; Wilkinson, G.; Young, J. F. Mild Hydroformylation of Olefins Using Rhodium Catalysts. *Chem. Commun.* **1964**, *2*, 17.
- (129) Vilches-Herrera, M.; Domke, L.; Börner, A. Isomerization-Hydroformylation Tandem Reactions. *ACS Catal.* **2014**, *4*(6), 1706–1724. <https://doi.org/10.1021/cs500273d>.
- (130) Edwards, D. R.; Crudden, C. M.; Yam, K. One-Pot Carbon Monoxide-Free Hydroformylation of Internal Olefins to Terminal Aldehydes. *Adv. Synth. Catal.* **2005**, *347*(1), 50–54. <https://doi.org/10.1002/adsc.200404228>.
- (131) Seayad, A.; Ahmed, M.; Klein, H.; Jackstell, R.; Gross, T.; Beller, M. Internal Olefins to Linear Amines. *Science (80-.)*. **2002**, *297*(5587), 1676–1678. <https://doi.org/10.1126/science.1074801>.
- (132) Behr, A.; Obst, D.; Schulte, C.; Schosser, T. Highly Selective Tandem Isomerization-Hydroformylation Reaction of Trans-4-Octene to n-Nonanal with Rhodium-BIPHEPHOS Catalysis. *J. Mol. Catal. A Chem.* **2003**, *206*(1–2), 179–184. [https://doi.org/10.1016/S1381-1169\(03\)00461-8](https://doi.org/10.1016/S1381-1169(03)00461-8).
- (133) Ohlmann, D. M.; Gooßen, L. J.; Dierker, M. Regioselective Synthesis of β -Aryl- and β -Amino-Substituted Aliphatic Esters by Rhodium-Catalyzed Tandem Double-Bond Migration/Conjugate Addition. *Chem. - A Eur. J.* **2011**, *17*(34), 9508–9519. <https://doi.org/10.1002/chem.201100654>.
- (134) Ohmura, T.; Yamamoto, Y.; Miyaura, N. Stereoselective Synthesis of Silyl Enol Ethers via the Iridium-Catalyzed Isomerization of Allyl Silyl Ethers. *Organometallics* **1999**, *18*(3), 413–416. <https://doi.org/10.1021/om980794e>.
- (135) Miura, T.; Nishida, Y.; Morimoto, M.; Murakami, M. Enantioselective Synthesis of Anti Homoallylic Alcohols from Terminal Alkynes and Aldehydes Based on Concomitant Use of a Cationic Iridium Complex and a Chiral Phosphoric Acid. *J. Am. Chem. Soc.* **2013**, *135*(31), 11497–11500. <https://doi.org/10.1021/ja405790t>.
- (136) Ghebreyessus, K. Y.; Angelici, R. J. Isomerizing-Hydroboration of the Monounsaturated Fatty Acid Ester Methyl Oleate. *Organometallics* **2006**, *25*(12), 3040–3044. <https://doi.org/10.1021/om0600947>.
- (137) Manuel, T. . The Iron Carbonyl-Catalyzed Isomerization Of Olefins. *Trans. N. Y. Acad. Sci.* **1964**, *26*(4), 442–445.
- (138) Shang, R.; Ilic, L.; Nakamura, E. Iron-Catalyzed C-H Bond Activation. *Chem. Rev.* **2017**, *117*(13), 9086–9139. <https://doi.org/10.1021/acs.chemrev.6b00772>.
- (139) Sawyer, K. R.; Glascoe, E. A.; Cahoon, J. F.; Schlegel, J. P.; Harris, C. B. Mechanism for Iron-Catalyzed Alkene Isomerization in Solution. *Organometallics* **2008**, *27*(17), 4370–4379. <https://doi.org/10.1021/om800481r>.
- (140) Obligation, J. V.; Chirik, P. J. Highly Selective Bis(Imino)Pyridine Iron-Catalyzed Alkene Hydroboration. *Org. Lett.* **2013**, *15*(11), 2680–2683.

Chapter 1

- <https://doi.org/10.1021/ol40099ou>.
- (141) Zhang, L.; Peng, D.; Leng, X.; Huang, Z. Iron-Catalyzed, Atom-Economical, Chemo- and Regioselective Alkene Hydroboration with Pinacolborane. *Angew. Chemie - Int. Ed.* **2013**, *52* (13), 3676–3680. <https://doi.org/10.1002/anie.201210347>.
- (142) Jia, X.; Huang, Z. Conversion of Alkanes to Linear Alkylsilanes Using an Iridium-Iron-Catalysed Tandem Dehydrogenation-Isomerization-Hydrosilylation. *Nat. Chem.* **2016**, *8* (2), 157–161. <https://doi.org/10.1038/nchem.2417>.
- (143) Obligacion, J. V.; Chirik, P. J. Bis(Imino)Pyridine Cobalt-Catalyzed Alkene Isomerization-Hydroboration: A Strategy for Remote Hydrofunctionalization with Terminal Selectivity. *J. Am. Chem. Soc.* **2013**, *135* (51), 19107–19110. <https://doi.org/10.1021/ja4108148>.
- (144) Palmer, W. N.; Diao, T.; Pappas, I.; Chirik, P. J. High-Activity Cobalt Catalysts for Alkene Hydroboration with Electronically Responsive Terpyridine and α -Diimine Ligands. *ACS Catal.* **2015**, *5* (2), 622–626. <https://doi.org/10.1021/cs501639r>.
- (145) Scheuermann, M. L.; Johnson, E. J.; Chirik, P. J. Alkene Isomerization-Hydroboration Promoted by Phosphine-Ligated Cobalt Catalysts. *Org. Lett.* **2015**, *17* (11), 2716–2719. <https://doi.org/10.1021/acs.orglett.5b01135>.
- (146) Ruddy, A. J.; Sydora, O. L.; Small, B. L.; Stradiotto, M.; Turculet, L. (N-Phosphinoamidinate)Cobalt-Catalyzed Hydroboration: Alkene Isomerization Affords Terminal Selectivity. *Chem. - A Eur. J.* **2014**, *20* (43), 13918–13922. <https://doi.org/10.1002/chem.201403945>.
- (147) Ogawa, T.; Ruddy, A. J.; Sydora, O. L.; Stradiotto, M.; Turculet, L. Cobalt- and Iron-Catalyzed Isomerization-Hydroboration of Branched Alkenes: Terminal Hydroboration with Pinacolborane and 1,3,2-Diazaborolanes. *Organometallics* **2017**, *36* (2), 417–423. <https://doi.org/10.1021/acs.organomet.6b00823>.
- (148) Speier, J. L.; Webster, J. A.; Barnes, G. H. The Addition of Silicon Hydrides to Olefinic Double Bonds. Part II. The Use of Group VIII Metal Catalysts. *J. Am. Chem. Soc.* **1957**, *79* (4), 974–979. <https://doi.org/10.1021/ja01561a054>.
- (149) Karstedt, B. D. No Title. Patent 3715334A, 1973.
- (150) Atienza, C. C. H.; Diao, T.; Weller, K. J.; Nye, S. A.; Lewis, K. M.; Delis, J. G. P.; Boyer, J. L.; Roy, A. K.; Chirik, P. J. Bis(Imino)Pyridine Cobalt-Catalyzed Dehydrogenative Silylation of Alkenes: Scope, Mechanism, and Origins of Selective Allylsilane Formation. *J. Am. Chem. Soc.* **2014**, *136* (34), 12108–12118. <https://doi.org/10.1021/ja5060884>.
- (151) Ilies, L.; Chen, Q.; Zeng, X.; Nakamura, E. Cobalt-Catalyzed Chemoselective Insertion of Alkene into the Ortho C-H Bond of Benzamide. *J. Am. Chem. Soc.* **2011**, *133* (14), 5221–5223. <https://doi.org/10.1021/ja200645w>.
- (152) Yamakawa, T.; Yoshikai, N. Alkene Isomerization-Hydroarylation Tandem Catalysis: Indole C2-Alkylation with Aryl-Substituted Alkenes Leading to 1,1-Diaryllkanes. *Chem. - An Asian J.* **2014**, *9* (5), 1242–1246. <https://doi.org/10.1002/asia.201400135>.
- (153) Chalk, A. J.; Magennis, S. A. Palladium-Catalyzed Vinyl Substitution Reactions. II. Synthesis of Aryl Substituted Allylic Alcohols, Aldehydes, and Ketones from Aryl Halides and Unsaturated Alcohols. *J. Org. Chem.* **1976**, *41* (7), 1206–1209. <https://doi.org/10.1021/j000869a026>.
- (154) Chalk, A. J.; Magennis, S. A. Palladium-Catalyzed Vinyl Substitution Reactions. I. New Synthesis of 2- and 3-Phenyl-Substituted Allylic Alcohols, Aldehydes, and Ketones from Allylic Alcohols. *J. Org. Chem.* **1976**, *41* (2), 273–278. <https://doi.org/10.1021/j000864a018>.
- (155) Melpolder, J. B.; Heck, R. F. A Palladium-Catalyzed Arylation of Allylic Alcohols with Aryl Halides. *J. Org. Chem.* **1976**, *41* (2), 265–272. <https://doi.org/10.1021/j000864a017>.
- (156) Larock, R. C.; Leung, W. Y.; Stolz-Dunn, S. Synthesis of Aryl-Substituted Aldehydes and Ketones via Palladium-Catalyzed Coupling of Aryl Halides and Non-Allylic Unsaturated Alcohols. *Tetrahedron Lett.* **1989**, *30* (48), 6629–6632. [https://doi.org/10.1016/S0040-4039\(00\)70636-8](https://doi.org/10.1016/S0040-4039(00)70636-8).
- (157) Werner, E. W.; Mei, T.; Burckle, A. J.; Sigman, M. S. Enantioselective Heck Arylations of Acyclic Alkenyl Alcohols Using a Redox-Relay Strategy. *Science (80-.)* **2012**, No. December, 1455–1459.
- (158) Mei, T. S.; Werner, E. W.; Burckle, A. J.; Sigman, M. S. Enantioselective Redox-Relay Oxidative Heck Arylations of Acyclic Alkenyl Alcohols Using Boronic Acids. *J. Am. Chem. Soc.* **2013**, *135* (18), 6830–6833. <https://doi.org/10.1021/ja402916z>.
- (159) Mei, T. S.; Patel, H. H.; Sigman, M. S. Enantioselective Construction of Remote Quaternary Stereocentres. *Nature* **2014**, *508* (7496), 340–344. <https://doi.org/10.1038/nature13231>.

- (160) Prater, M. B.; Sigman, M. S. Enantioselective Synthesis of Alkyl Allyl Ethers via Palladium-Catalyzed Redox-Relay Heck Alkenylation of O-Alkyl Enol Ethers. *Isr. J. Chem.* **2019**, No. 801, 452–460. <https://doi.org/10.1002/ijch.201900077>.
- (161) Yuan, Q.; Sigman, M. S. Palladium-Catalyzed Enantioselective Alkenylation of Enelactams Using a Relay Heck Strategy. *Chem. - A Eur. J.* **2019**, *25* (46), 10823–10827. <https://doi.org/10.1002/chem.201902813>.
- (162) Xu, L.; Hilton, M. J.; Zhang, X.; Norrby, P. O.; Wu, Y. D.; Sigman, M. S.; Wiest, O. Mechanism, Reactivity, and Selectivity in Palladium-Catalyzed Redox-Relay Heck Arylations of Alkenyl Alcohols. *J. Am. Chem. Soc.* **2014**, *136* (5), 1960–1967. <https://doi.org/10.1021/ja4109616>.
- (163) Patel, H. H.; Sigman, M. S. Palladium-Catalyzed Enantioselective Heck Alkenylation of Acyclic Alkenols Using a Redox-Relay Strategy. *J. Am. Chem. Soc.* **2015**, *137* (10), 3462–3465. <https://doi.org/10.1021/ja5130836>.
- (164) Zhang, C.; Santiago, C. B.; Crawford, J. M.; Sigman, M. S. Enantioselective Dehydrogenative Heck Arylations of Trisubstituted Alkenes with Indoles to Construct Quaternary Stereocenters. *J. Am. Chem. Soc.* **2015**, *137* (50), 15668–15671. <https://doi.org/10.1021/jacs.5b11335>.
- (165) Zhang, C.; Santiago, C. B.; Kou, L.; Sigman, M. S. Alkenyl Carbonyl Derivatives in Enantioselective Redox Relay Heck Reactions: Accessing α,β -Unsaturated Systems. *J. Am. Chem. Soc.* **2015**, *137* (23), 7290–7293. <https://doi.org/10.1021/jacs.5b04289>.
- (166) Chen, Z. M.; Hilton, M. J.; Sigman, M. S. Palladium-Catalyzed Enantioselective Redox-Relay Heck Arylation of 1,1-Disubstituted Homoallylic Alcohols. *J. Am. Chem. Soc.* **2016**, *138* (36), 11461–11464. <https://doi.org/10.1021/jacs.6b06994>.
- (167) Patel, H. H.; Sigman, M. S. Enantioselective Palladium-Catalyzed Alkenylation of Trisubstituted Alkenols to Form Allylic Quaternary Centers. *J. Am. Chem. Soc.* **2016**, *138* (43), 14226–14229. <https://doi.org/10.1021/jacs.6b09649>.
- (168) Yuan, Q.; Sigman, M. S. Palladium-Catalyzed Enantioselective Relay Heck Arylation of Enelactams: Accessing α,β -Unsaturated δ -Lactams. *J. Am. Chem. Soc.* **2018**, *140* (21), 6527–6530. <https://doi.org/10.1021/jacs.8b02752>.
- (169) Patel, H. H.; Prater, M. B.; Squire, S. O.; Sigman, M. S. Formation of Chiral Allylic Ethers via an Enantioselective Palladium-Catalyzed Alkenylation of Acyclic Enol Ethers. *J. Am. Chem. Soc.* **2018**, *140* (18), 5895–5898. <https://doi.org/10.1021/jacs.8b02751>.
- (170) Singh, S.; Bruffaerts, J.; Vasseur, A.; Marek, I. A Unique Pd-Catalysed Heck Arylation as a Remote Trigger for Cyclopropane Selective Ring-Opening. *Nat. Commun.* **2017**, *8*, 1–10. <https://doi.org/10.1038/ncomms14200>.
- (171) Larionov, E.; Lin, L.; Guénee, L.; Mazet, C. Scope and Mechanism in Palladium-Catalyzed Isomerizations of Highly Substituted Allylic, Homoallylic, and Alkenyl Alcohols. *J. Am. Chem. Soc.* **2014**, *136* (48), 16882–16894. <https://doi.org/10.1021/ja508736u>.
- (172) Lin, L.; Romano, C.; Mazet, C. Palladium-Catalyzed Long-Range Deconjugative Isomerization of Highly Substituted α,β -Unsaturated Carbonyl Compounds. *J. Am. Chem. Soc.* **2016**, *138* (32), 10344–10350. <https://doi.org/10.1021/jacs.6b06390>.
- (173) Albéniz, A. C.; Espinet, P.; Lin, Y. S. Palladium Migration along Linear Carbon Chains: The Detection of H1-H2-Enyl Intermediates and the Study of Their Rearrangement. *Organometallics* **1997**, *16* (19), 4138–4144. <https://doi.org/10.1021/om9703907>.
- (174) Larock, R. C.; Wang, Y.; Lu, Y. de; Russell, C. E. Synthesis of Aryl-Substituted Allylic Amines via Palladium-Catalyzed Coupling of Aryl Iodides, Nonconjugated Dienes, and Amines. *J. Org. Chem.* **1994**, *59* (26), 8107–8114. <https://doi.org/10.1021/j000105a030>.
- (175) Larock, R. C.; Lu, Y. de; Bain, A. C.; Russell, C. E. Palladium-Catalyzed Coupling of Aryl Iodides, Nonconjugated Dienes, and Carbon Nucleophiles by Palladium Migration. *J. Org. Chem.* **1991**, *56* (15), 4589–4590. <https://doi.org/10.1021/j000015a002>.
- (176) Wang, Y.; Dong, X.; Larock, R. C. Synthesis of Naturally Occurring Pyridine Alkaloids via Palladium-Catalyzed Coupling/Migration Chemistry. *J. Org. Chem.* **2003**, *68* (8), 3090–3098. <https://doi.org/10.1021/j0026716p>.
- (177) Kochi, T.; Hamasaki, T.; Aoyama, Y.; Kawasaki, J.; Kakiuchi, F. Chain-Walking Strategy for Organic Synthesis: Catalytic Cycloisomerization of 1,*n*-Dienes. *J. Am. Chem. Soc.* **2012**, *134* (40), 16544–16547. <https://doi.org/10.1021/ja308377u>.
- (178) Hamasaki, T.; Aoyama, Y.; Kawasaki, J.; Kakiuchi, F.; Kochi, T. Chain Walking as a Strategy for Carbon-Carbon Bond Formation at Unreactive Sites in Organic Synthesis: Catalytic Cycloisomerization of Various 1,*n*-Dienes. *J. Am. Chem. Soc.* **2015**, *137* (51), 16163–16171. <https://doi.org/10.1021/jacs.5b10804>.
- (179) Aspin, S.; Goutierre, A. S.; Larini, P.; Jazzar, R.; Baudoin, O. Synthesis of Aromatic α -Aminoesters: Palladium-Catalyzed Long-Range Arylation

Chapter 1

- of Primary Csp³-H Bonds. *Angew. Chemie - Int. Ed.* **2012**, *51* (43), 10808–10811. <https://doi.org/10.1002/anie.201206237>.
- (180) Dupuy, S.; Zhang, K. F.; Goutierre, A. S.; Baudoin, O. Terminal-Selective Functionalization of Alkyl Chains by Regioconvergent Cross-Coupling. *Angew. Chemie - Int. Ed.* **2016**, *55* (47), 14793–14797. <https://doi.org/10.1002/anie.201608535>.
- (181) Möhring, V. M.; Fink, G. Novel Polymerization of α -Olefins with the Catalyst System Nickel/Aminobis(Imino)Phosphorane. *Angew. Chemie Int. Ed. English* **1985**, *24* (11), 1001–1003. <https://doi.org/10.1002/anie.198510011>.
- (182) Johnson, L. K.; Killian, C. M.; Brookhart, M. New Pd(II)- and Ni(II)-Based Catalysts for Polymerization of Ethylene and α -Olefins. *J. Am. Chem. Soc.* **1995**, *117* (23), 6414–6415. <https://doi.org/10.1021/ja00128a054>.
- (183) Buslov, I.; Becouse, J.; Mazza, S.; Montandon-Clerc, M.; Hu, X. Chemoselective Alkene Hydrosilylation Catalyzed by Nickel Pincer Complexes. *Angew. Chemie - Int. Ed.* **2015**, *54* (48), 14523–14526. <https://doi.org/10.1002/anie.201507829>.
- (184) Buslov, I.; Song, F.; Hu, X. An Easily Accessed Nickel Nanoparticle Catalyst for Alkene Hydrosilylation with Tertiary Silanes. *Angew. Chemie - Int. Ed.* **2016**, *55* (40), 12295–12299. <https://doi.org/10.1002/anie.201606832>.
- (185) Lee, W. C.; Wang, C. H.; Lin, Y. H.; Shih, W. C.; Ong, T. G. Tandem Isomerization and C-H Activation: Regioselective Hydroheteroarylation of Allylarenes. *Org. Lett.* **2013**, *15* (20), 5358–5361. <https://doi.org/10.1021/ol402644y>.
- (186) He, Y.; Cai, Y.; Zhu, S. Mild and Regioselective Benzylic C–H Functionalization: Ni-Catalyzed Reductive Arylation of Remote and Proximal Olefins. *J. Am. Chem. Soc.* **2017**, *139* (3), 1061–1064. <https://doi.org/10.1021/jacs.6b11962>.
- (187) Wang, X.; Nakajima, M.; Serrano, E.; Martin, R. Alkyl Bromides as Mild Hydride Sources in Ni-Catalyzed Hydroamidation of Alkynes with Isocyanates. *J. Am. Chem. Soc.* **2016**, *138* (48), 15531–15534. <https://doi.org/10.1021/jacs.6b10351>.
- (188) Chen, F.; Chen, K.; Zhang, Y.; He, Y.; Wang, Y. M.; Zhu, S. Remote Migratory Cross-Electrophile Coupling and Olefin Hydroarylation Reactions Enabled by in Situ Generation of Nih. *J. Am. Chem. Soc.* **2017**, *139* (39), 13929–13935. <https://doi.org/10.1021/jacs.7b08064>.
- (189) Peng, L.; Li, Y.; Li, Y.; Wang, W.; Pang, H.; Yin, G. Ligand-Controlled Nickel-Catalyzed Reductive Relay Cross-Coupling of Alkyl Bromides and Aryl Bromides. *ACS Catal.* **2018**, *8* (1), 310–313. <https://doi.org/10.1021/acscatal.7b03388>.
- (190) Juliá-Hernández, F.; Moragas, T.; Cornella, J.; Martin, R. Remote Carboxylation of Halogenated Aliphatic Hydrocarbons with Carbon Dioxide. *Nature* **2017**, *545* (7652), 84–88. <https://doi.org/10.1038/nature22316>.
- (191) Sahoo, B.; Bellotti, P.; Juliá-Hernández, F.; Meng, Q. Y.; Crespi, S.; König, B.; Martin, R. Site-Selective, Remote Sp³ C–H Carboxylation Enabled by the Merger of Photoredox and Nickel Catalysis. *Chem. Eur. J.* **2019**, *25* (38), 9001–9005. <https://doi.org/10.1002/chem.201902095>.
- (192) Gaydou, M.; Moragas, T.; Juliá-Hernández, F.; Martin, R. Site-Selective Catalytic Carboxylation of Unsaturated Hydrocarbons with CO₂ and Water. *J. Am. Chem. Soc.* **2017**, *139* (35), 12161–12164. <https://doi.org/10.1021/jacs.7b07637>.
- (193) Sun, S. Z.; Börjesson, M.; Martín-Montero, R.; Martín, R. Site-Selective Ni-Catalyzed Reductive Coupling of α -Haloboranes with Unactivated Olefins. *J. Am. Chem. Soc.* **2018**, *140* (40), 12765–12769. <https://doi.org/10.1021/jacs.8b09425>.
- (194) Sun, S. Z.; Romano, C.; Martín, R. Site-Selective Catalytic Deaminative Alkylation of Unactivated Olefins. *J. Am. Chem. Soc.* **2019**, *141* (41), 16197–16201. <https://doi.org/10.1021/jacs.9b07489>.
- (195) Kocięcka, P.; Czeliński, I.; Szymańska-Buzar, T. Efficient and Selective Synthesis of E-Vinylamines via Tungsten(o)-Catalyzed Hydroamination of Terminal Alkynes. *Adv. Synth. Catal.* **2014**, *356* (16), 3319–3324. <https://doi.org/10.1002/adsc.201400568>.
- (196) Lefebvre, F.; Bouhoute, Y.; Szeto, K. C.; Merle, N.; Mallmann, A. De; Gauvin, R.; Lefebvre, F.; Bouhoute, Y.; Szeto, K. C.; Merle, N.; Mallmann, A. De. Olefin Metathesis by Group VI (Mo, W) Metal Compounds. In *Alkenes*; IntechOpen, 2018. <https://doi.org/10.5772/intechopen.69320>.
- (197) Bullock, R. M. *Molybdenum and Tungsten Catalysts for Hydrogenation, Hydrosilylation and Hydrolysis*; 2010. <https://doi.org/10.1002/9783527631582.ch3>.
- (198) Kusama, H.; Yamabe, H.; Iwasawa, N. W(CO)₅-Amine Catalyzed Exo- and Endo-Selective Cyclizations of ω -Alkynyl Silyl Enol Ethers: A Highly Useful Method for the Construction of Polycyclic Compounds. *Org. Lett.* **2002**, *4* (15), 2569–2571. <https://doi.org/10.1021/ol026202c>.
- (199) Urzhuntsev, G. A.; Kodenev, E. G.; Echevskii, G. V. Prospects for Using Mo- and W-Containing Catalysts in Hydroisomerization: A Patent Review.

- II: Catalysts Based on Molybdenum and Tungsten Carbides. *Catal. Ind.* **2016**, *8* (3), 224–230. <https://doi.org/10.1134/S2070050416030120>.
- (200) Perry, I. B.; Brewer, T. F.; Sarver, P. J.; Schultz, D. M.; DiRocco, D. A.; MacMillan, D. W. C. Direct Arylation of Strong Aliphatic C–H Bonds. *Nature* **2018**, *560* (7716), 70–75. <https://doi.org/10.1038/s41586-018-0366-x>.
- (201) Sarver, P. J.; Bacauanu, V.; Schultz, D. M.; DiRocco, D. A.; Lam, Y. hong; Sherer, E. C.; MacMillan, D. W. C. The Merger of Decatungstate and Copper Catalysis to Enable Aliphatic C(Sp³)–H Trifluoromethylation. *Nat. Chem.* **2020**, *12* (5), 459–467. <https://doi.org/10.1038/s41557-020-0436-1>.
- (202) Wrighton, M.; Hammond, G.; Gray, H. Group VI Metal Carbonyl Photoassisted Isomerization of Olefins. *J. Org. Chem.* **1974**, *70*, 283–301.

Chapter 2.

Stereospecific Nickel-Catalyzed Borylation of Secondary Benzyl Pivalates

Research carried out in collaboration with

Tim Krolikowski, Cayetana Zarate, Rubén Manzano

Published in: *Synlett* **2017**, 28 (19), 2604-2608

Chapter 2

2.1 Introduction

Metal-catalyzed cross-coupling reactions have evolved as a mature discipline for building up molecular complexity. The vast majority of these reactions relies on the utilization of aryl and alkyl halides as coupling counterparts. Despite the advances realized, the toxicity of the latter and the difficulty of accessing advanced organic halides in densely functionalized backbones prompted the development of alternative coupling partners such as C–O electrophiles.^{1–3} The paucity of these processes relies on the inherent challenges posed by these electrophiles, such as the high activation barrier of the C–O cleavage and chemoselectivity profile, among others (Chapter 1.2.1). However, in recent years, numerous C–O bond-functionalization protocols have been reported, even within the context of stereospecific reactions.³

2.2 Stereospecific cleavage of activated C(sp³)–O bonds by nickel catalysis

2.2.1 Introduction

In recent years, the utilization of allyl and benzyl electrophiles have received significant attention in cross-coupling reactions due to the possibility of creating enantioenriched stereocenters *via* the formation of particularly stabilized organometallic intermediates, either in a stereoconvergent (catalyst-controlled) or stereospecific manner (substrate-controlled).^{4,5} Undoubtedly, the installation of a chiral stereogenic center by means of stereoconvergent reactions with an asymmetric catalyst is a particularly powerful tool, as the protocol makes use of achiral reagents. On the other hand, stereospecific reactions rely on enantioenriched precursors, and can *a priori* be triggered *via* inversion or retention of configuration, thus allowing to preserve the stereochemical information of the starting material without requiring chiral catalysts or chiral ligands.^{6–10}

Attention was initially focused on the utilization of nickel as catalyst due to its propensity to undergo oxidative addition and slow down β -hydride elimination.^{11–13} However, it is worth noting that nickel complexes often populate one-electron pathways instead of two-electron manifolds that operate within the realm of Pd catalysis,^{14,15} thus leaving a reasonable doubt on whether nickel catalysis might be suited within the context of stereospecific reactions due to the intermediacy of open-shell intermediates (Figure 2.2.1, *top*).^{16–20} In order to trigger a stereospecific reaction, the inherent radical reactivity of the nickel catalyst must be suppressed to favor a two-electron polar oxidative addition. In this line, the polar character of the electrophile is crucial for a two-electron oxidative addition reaction, and the combination of low-valent nickel complexes with benzyl ethers seemed to be particularly promising.^{1,21} In addition, highly enantioenriched starting materials can be easily synthesized from secondary aliphatic alcohols by many well-known reported enantioselective methods (Figure 2.2.1, *bottom*).²²

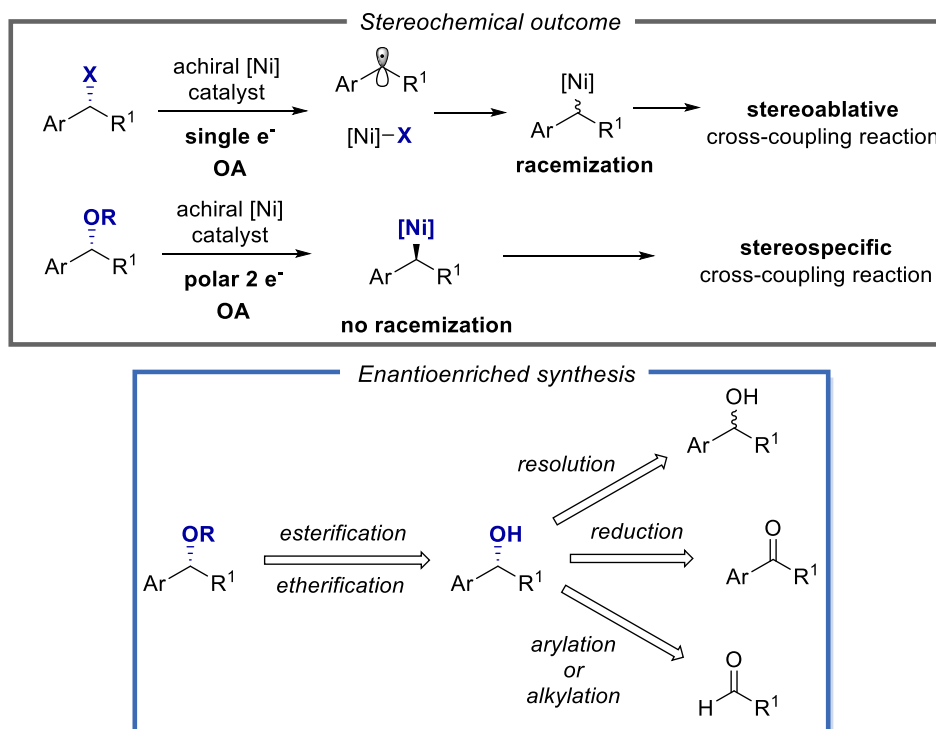
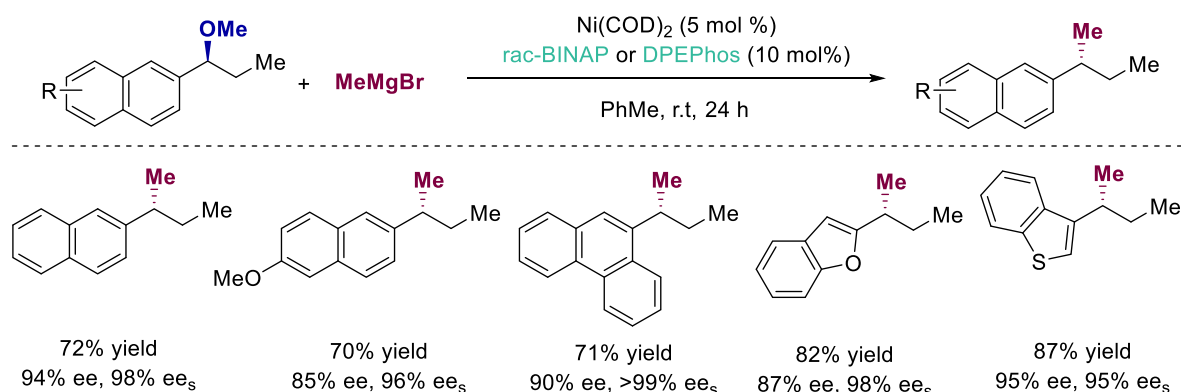


Figure 2.2.1. Stereospecific coupling and synthesis of benzyl esters or ethers.

2.2.2 Ni-catalyzed stereospecific C–O cleavage of π -extended secondary benzyl ethers

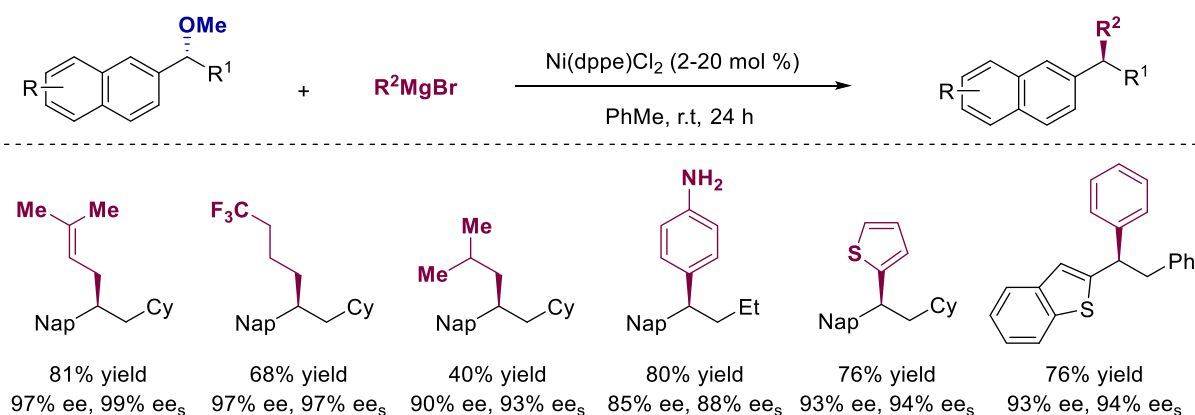
Jarvo and co-workers were able to develop Kumada-type cross-coupling reactions of enantioenriched secondary benzylic ethers with Grignard reagents as nucleophiles (Scheme 2.2.1).²³ One of the difficulties in developing the transformation was determining the optimal conditions to suppress undesired competing β -hydride elimination while accomplishing the formation of the desired product with an adequate transfer of the stereochemical information from the substrate to the product. The authors discovered that the combination of Ni(COD)₂ and rac-BINAP provided the final product in high yields and enantiospecificities. In this manner, a number of enantioenriched secondary benzyl ethers bearing π -extended arenes could be used as substrates, allowing to obtain the targeted products in good yields and excellent stereochemical fidelity. These results imply that the coordination of the nickel catalyst to the arene facilitates an oxidative addition, an assumption that was further corroborated in later a work by the authors.²⁴

Chapter 2



Scheme 2.2.1. Stereospecific Kumada cross-coupling of secondary benzylic ethers with alkyl Grignards.

Transmetalating agents with alkyl chains have shown to be more problematic due to their propensity to undergo competitive β -hydride elimination upon transmetalation to form alkylnickel intermediates. Therefore, a solution was required to expand the scope of the stereospecific Kumada coupling to these coupling partners. Jarvo and co-workers found that the use of dppe (1,2-bis(diphenylphosphino)ethane) ligand favored the formation of the product with the suppression of competing side reactions with alkyl Grignard reagents (Scheme 2.2.2).²⁵ The reaction conditions were able to accommodate a wide range of functional groups on the secondary benzyl substrate and most importantly, a diverse set of alkyl and even aryl Grignard reagents. Unfortunately, the utilization of secondary alkyl Grignard species resulted in lower yields as a result of the competitive β -hydride elimination. In general terms, the scope was broad, obtaining the targeted products with a neat inversion of configuration.



Scheme 2.2.2. Expanding the scope of C–O functionalization with Grignard reagents.

Interestingly, Jarvo and co-workers found an intriguing inverse correlation between the catalyst loading and enantioselectivity of the reaction. These findings could be interpreted on the basis of a nucleophilic attack of low-valent Ni(0) species to the *in situ* generated π -benzylnickel intermediate (I) under high catalyst loadings (Figure 2.2.2). To overcome the problem of low yields obtained for some

of the challenging substrates, a second portion of Ni(dppe)Cl₂ was added after 12 h to keep a low catalyst concentration at all time.

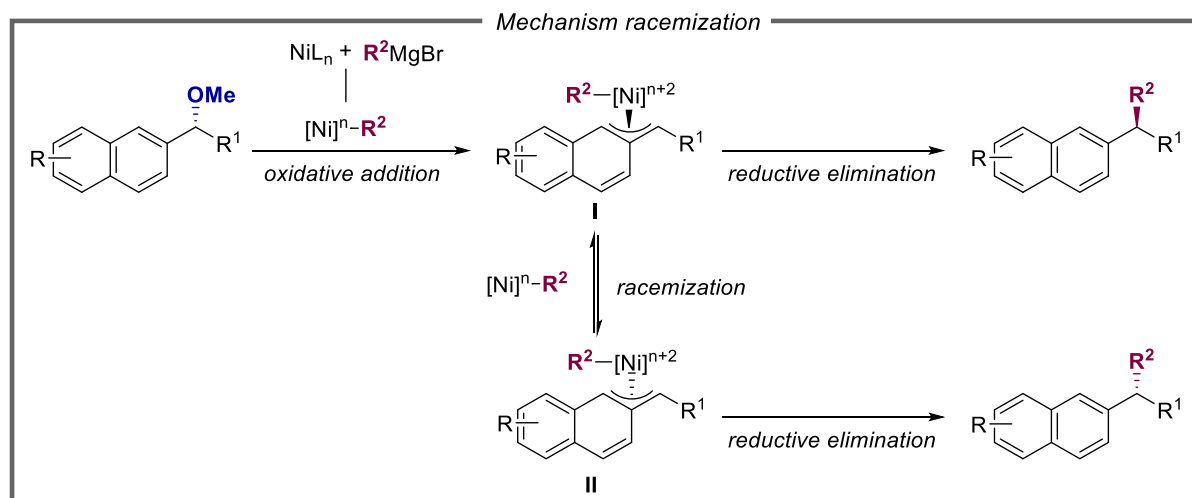


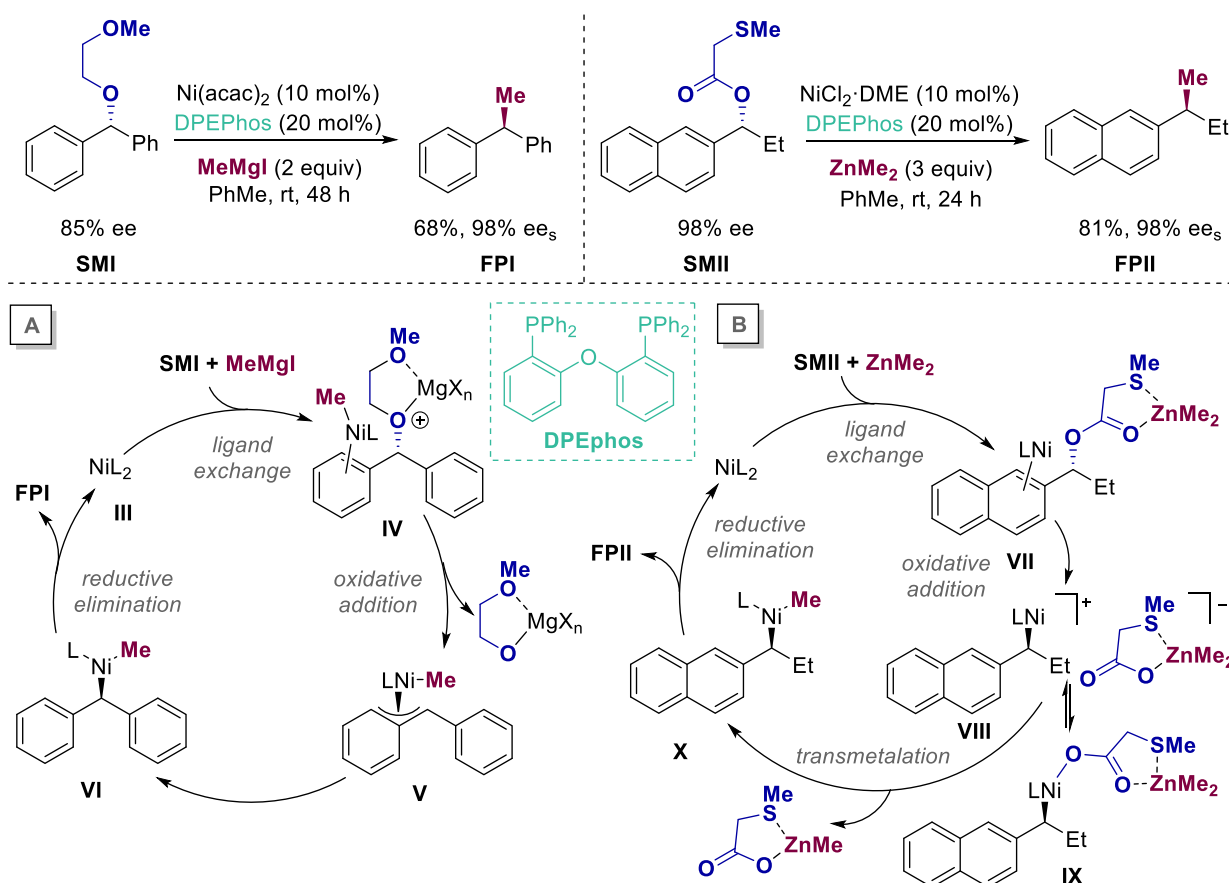
Figure 2.2.2. Rationalization for racemization at high catalyst loadings.

2.2.3 Ni-catalyzed stereospecific reactions of benzyl C–O electrophiles by traceless directing groups

Stereospecific nickel-catalyzed cross-coupling reactions of secondary benzylic ethers were achieved due to the inherent activation of the π -extended-systems such as naphthalene, benzothiophene or benzofuran to Ni(0). Unfortunately, regular arenes with lower aromatic stabilization energies reacted more smoothly, suggesting that the employment of non- π -extended systems might require a different strategy.^{26,27} To this end, Jarvo and co-workers developed a new approach by using benzyl-2-methoxyethyl ethers as traceless directing groups (Scheme 2.2.3, *left*).^{28,29} This approach likely forms five-membered ring chelates (**IV**) with the corresponding Mg salts, leading to the activation of the C–O bond towards S_N2-type oxidative addition with an overall inversion of configuration. This strategy employed benzhydryl alcohol derivatives that had previously resisted Kumada coupling reactions, thus expanding the scope of the electrophilic partner.

The chemoselectivity issues found by the utilization of Grignard reagents could be overcome by the use of organozinc reagents.³⁰ Inspired by the traceless directing group strategy used in Scheme 2.2.3 *left*, Jarvo found that similar chelates might be formed with Zn reagents, avoiding undesirable β -hydride elimination or isomerization pathways while ultimately leading to an excellent stereospecificity through a S_N2-type oxidative addition (Scheme 2.2.3, *right*).³¹ In this way, a large number of enantioenriched secondary benzyl alcohol derivatives bearing 2-naphthyl or benzo-fused heteroaryl substituents could be efficiently coupled with alkylzinc reagents.

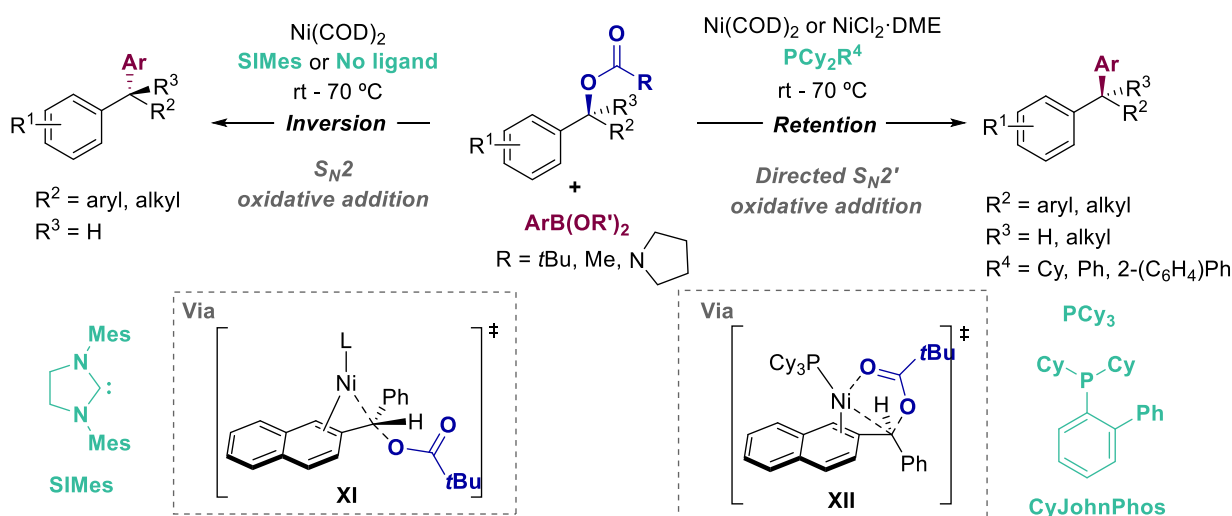
Chapter 2



2.2.4 Nickel catalyzed stereospecific C–O cleavage of π -extended benzyl pivalates

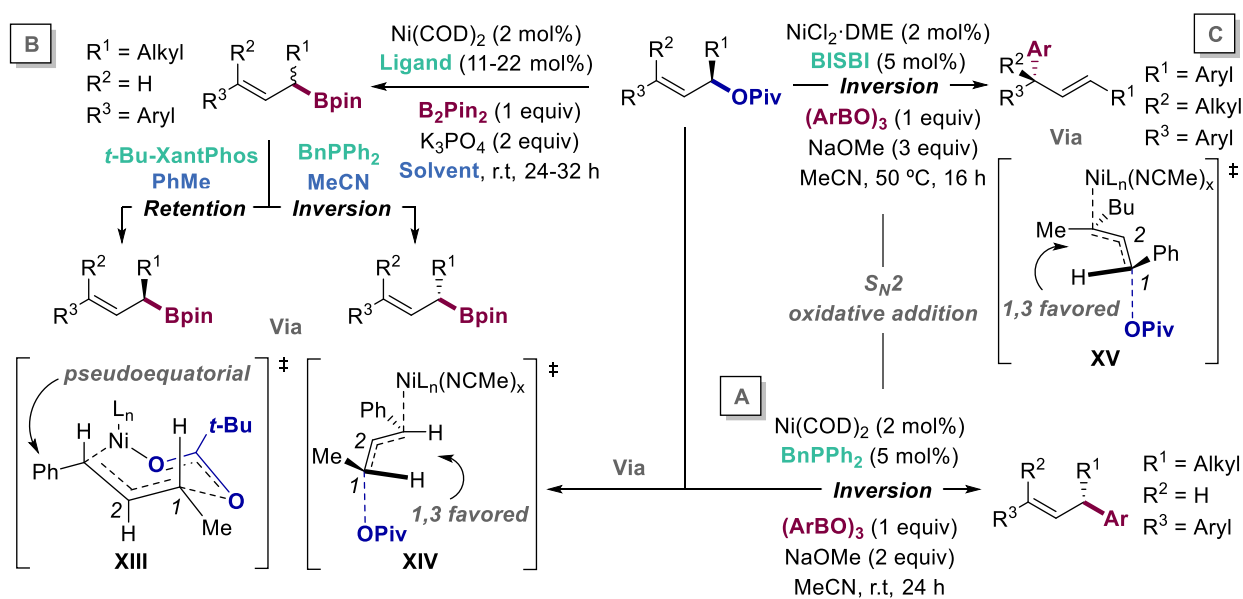
Prompted by the successful implementation of stereospecific reactions with both Grignard reagents and organozinc compounds, a significant attention was devoted to the utilization of less-basic organoboron reagents. Inspired by the first Suzuki-Miyaura cross-coupling reaction of achiral ester derivatives in 2005 by Kuwano and Yokogi using Pd(II) precatalysts,³² Jarvo and Watson independently developed a Suzuki-Miyaura-type coupling of secondary benzylic pivalates using aryl boronic esters or aryl boroxines (Scheme 2.2.4, *left*).^{33–35} Surprisingly, the use of different electron-rich ligands, such as SIMes (1,3-bis-(2,4,6-trimethylphenyl)-4,5-dihydroimidazol-2-ylidene) and PCy₂R (R = Ph, Cy) provided an opposite enantiomeric outcome with high stereochemical fidelity. In analogy to the previously described Negishi and Kumada-type coupling reactions,^{28,29,31} the utilization of *N*-heterocyclic carbene ligand (SIMes, **XI**) or a ligand-free catalytic system resulted in an inversion of the configuration. In contrast, Watson demonstrated that PCy₂R (R = Ph, Cy) ligands offered a retention of the configuration (Scheme 2.2.4, *right*, R³ = H). This phenomenon was also observed by Jarvo in the Ni(0)/PCy₃-catalyzed coupling of benzylic carbamates with aryl boronic esters.³⁴ In 2016, Watson was able to expand the scope of the reaction leading to the arylation of tertiary enantioenriched benzylic acetates with less sterically hindered CyJohnPhos ligand.³⁶ The authors

proposed a directed S_N2' oxidative addition *via* a seven-membered transition state in which the acetate binds to the Ni center (**XII**), an assumption further corroborated by theoretical calculations.²⁴



2.2.5 Nickel catalyzed stereospecific C–O cleavage of allylic pivalates

In 2014, the first report of stereospecific Ni-catalyzed cross-coupling of allylic pivalates and arylboroxines was published by Watson and co-workers (Scheme 2.2.5, A).³⁷ This protocol reunited the conditions commented above, avoiding the use of more expensive second row transition metal catalysts and the utilization of air sensitive coupling partners. The study produced enantioenriched 1,3-diaryl allyl products with an inversion of the stereochemical information *via* transition state **XIV**, thus avoiding the strain generated between the methyl and hydrogen at the 1,3-position.



Chapter 2

Later, the same group reported a successful stereospecific borylation of allylic pivalates to deliver highly enantioenriched α -stereogenic γ -aryl allylic boronates (Scheme 2.2.5, B).³⁸ The transformation proceeds either with inversion or retention of configuration, with selectivity arising by judicious choice of the ligand or the solvent. On one hand, stereochemical inversion was driven by strain release between the 1,3-positions of the transition state (**XIV**) and the use of MeCN as solvent. Given the ability of MeCN to act as a ligand for transition metals,³⁹ the authors claimed that MeCN coordinates to nickel, preventing the subsequent oxidative addition. On the other hand, retention of configuration was driven by the pivalate leaving group, which directs the nickel catalyst in non-polar solvents as PhMe. This observation indicates that although two 7-membered chair-like compounds could be formed, only the pseudoequatorial (**XIII**) is favored, leading to overall retention of configuration.

Watson and co-workers realized that a powerful approach for the synthesis of quaternary stereocenters may be performed by an allylic substitution reaction. In this endeavor, such a reaction does not only create a quaternary center, but also includes a versatile alkene substituent that provides multiple opportunities for further functionalization. Recognizing this potential, they reported a stereospecific nickel-catalyzed Suzuki-Miyaura cross-coupling of allylic pivalates to deliver quaternary stereocenters (Scheme 2.2.5, C).⁴⁰ The protocol proceeds with inversion of the stereochemical outcome, allowing to couple a variety of enantioenriched allylic pivalates with arylboroxine using a combination of NiCl₂·DME/BISBI.

2.3 Stereospecific Nickel-catalyzed borylation of secondary aryl benzyl pivalates

2.3.1 Aim of the project

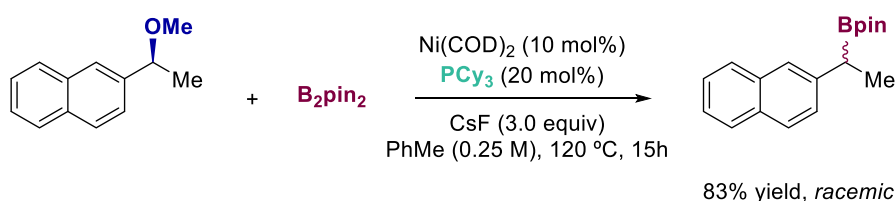
Despite the advances realized in catalytic stereospecific cross-coupling reactions *via* functionalization of benzylic and allylic C–O bonds, the majority of these processes are based on the formation of C–C bonds. In contrast, the ability to extend these processes to C–heteroatom bond-forming reactions has remained a much less-explored endeavor. Among the different scenarios, we anticipated that the possibility of triggering a stereospecific borylation *via* benzyl or allyl C–O cleavage would be a worthwhile endeavor given the versatility and modularity of the corresponding organoboranes. At the time that this PhD thesis was being developed, there were no examples of stereospecific borylations *via* sp^3 C–O bond-cleavage.

2.3.2 Optimization of the reaction conditions

We started our investigations by exposing enantioenriched 2-(1-methoxyethyl)naphthalene to our previously developed borylation of benzyl methyl ethers (Scheme 2.3.1). Unfortunately, no sign of stereospecificity was observed for this reaction, even by carefully tuning the experimental

Stereospecific Borylation of Benzyl C(sp³)-O Bonds

variables of the reaction (Ni(COD)₂/PCy₃ loadings, temperatures and reaction time), obtaining exclusively racemic mixtures.



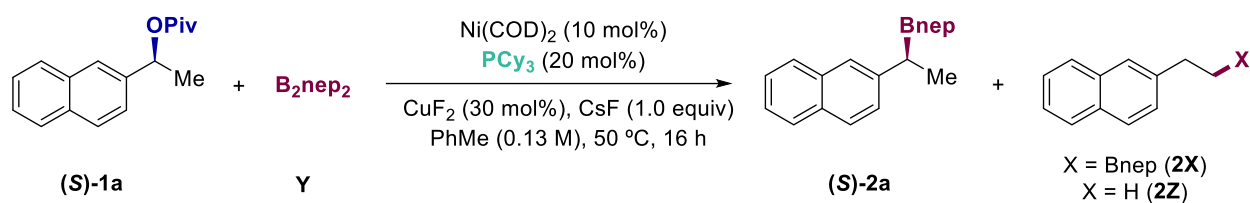
Scheme 2.3.1. Attempt of stereospecific borylation under previously optimized reaction conditions.

Despite these results, we turned our attention to study stereospecific borylations of benzyl pivalates, as these compounds have extensively been employed by both Jarvo and Watson in related cross-coupling reactions.^{33,34}

Prompted by previously developed silylation of aryl and benzyl pivalates by our group,⁴¹ we started the screening of our stereospecific borylation technique with B₂nep₂. An initial screening of the equivalents of the boron source revealed the potential of this system (Table 2.3.1). Gratefully, the desired product ((*S*)-**2a**) was obtained in moderate yields and promising stereospecificity. We observed a trend in the use of B₂nep₂ where the best results were achieved with 1.5 equivalents (entry **5**). The utilization of B₂pin₂ led to a much lower reactivity and a diminished stereospecificity, highlighting the influence of the stereoelectronic properties of the boron reagent. The conversion of the reaction was quantitative and GC analysis allowed the detection of two side-products: the linear borylated product **2X** and the reduced product **2Z**. For the former, an oxidative addition of Ni(0) species into the benzyl C(sp³)-O bond followed by a beta hydride elimination/nickel insertion might place the catalyst at the terminal position delivering the borylation. For the latter side-product, the benzyl radical – generated from the homolytic cleavage of the nickel oxidative addition species – abstracts a proton from the solvent delivering the reduced byproduct **2Z**.

It is remarkable that an overall retention of the configuration was observed, suggesting that the pivalate group coordinates to the nickel catalyst, thus setting the stage for a directed S_N2'-type oxidative addition. Due to the significant difficulties encountered in separating (*S*)-**1a** and (*S*)-**2a** by HPLC techniques and the low stability of the resulting products, the latter were transformed into the corresponding benzyl alcohol in order to measure the enantiomeric excess. While one might argue that the hydrolysis of (*S*)-**1a** might lead to wrong conclusions by forming the exact same benzyl alcohol, we corroborated that this was not the case, as the benzyl pivalate (*S*)-**1a** does not hydrolyze to the corresponding alcohol under the catalytic conditions.

Chapter 2



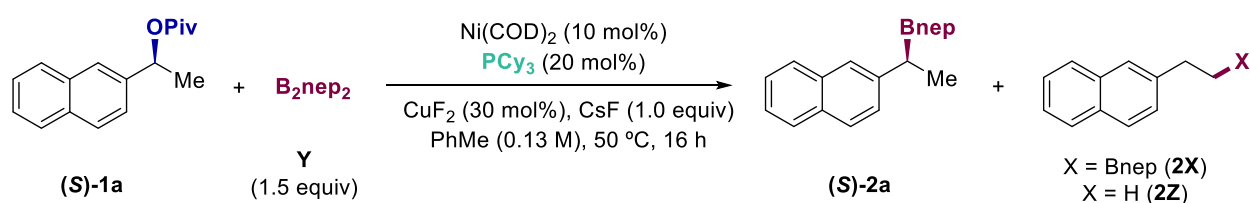
Entry	Deviation from standard conditions	Conv. (%)	2a (%)	(S)-2a ee (%)	2a/2X	2Z (%)
1	B ₂ nep ₂ (1.1 equiv.)	95	47	70	1.9	12
2	B ₂ nep ₂ (1.2 equiv.)	95	48	72	1.9	11
3	B ₂ nep ₂ (1.3 equiv.)	96	54	75	2.0	12
4	B ₂ nep ₂ (1.4 equiv.)	100	55	81	2.0	13
5	B ₂ nep ₂ (1.5 equiv.)	100	58	85	2.1	12
6	B ₂ nep ₂ (1.7 equiv.)	100	54	84	2.2	11
7	B ₂ nep ₂ (2.0 equiv.)	100	39	82	1.3	12
8	B ₂ pin ₂ (1.3 equiv.)	70	19	52	1.0	4

Reaction conditions: (S)-1a (0.2 mmol), Y (x mmol), Ni(COD)₂ (10 mol%), PCy₃ (20 mol%), CuF₂ (30 mol %), CsF (1.0 equiv.), PhMe (1.5 mL), 50 °C, 16 h. GC conversion and yields using decane as internal standard. ee calculated by HPLC analysis

Table 2.3.1. Screening of B₂nep₂ equivalents and B₂pin₂.

With a good result in hand (Table 2.3.1, entry 5), subsequent screening was carried out with different ligands, solvents, copper sources and fluoride derivatives (Table 2.3.2). Carbenes and acyclic phosphine ligands did not provide any reactivity (entries 1 & 4) whereas bidentate ligands and monodentate phosphines other than PCy₃ provided lower results in terms of both yields and enantioselectivities (entries 2 & 3). The utilization of THF or dioxane led to the products with similar *enantiomeric excess* (ee) albeit in lower yield (entries 5 & 6). As shown in entries 7-9, the utilization of different copper and fluoride sources did not result in better yields. Surprisingly, reducing the nickel and ligand loading while keeping constant the Ni/L ratio afforded a much better ee and a boost in the yield of 2a (entry 10). This avoid the formation of side-competitive reactions that might operates *via* bimolecular mechanism in which low-valent Ni(0) species react with the *in situ* generated Ni(II) intermediates losing chiral information and efficiency.

Stereospecific Borylation of Benzyl C(sp³)-O Bonds



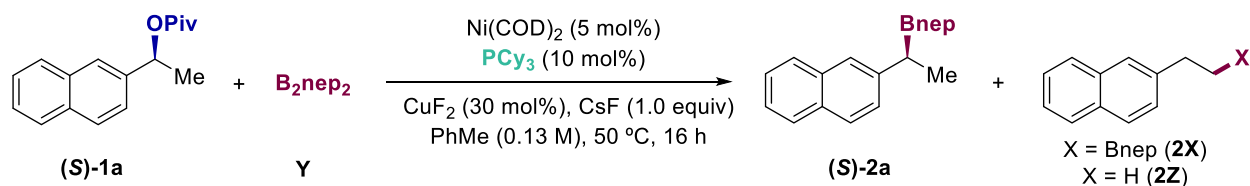
Entry	Deviation from standard conditions	Conv. (%)	2a (%)	(S)-2a ee (%)	2a/2X	2Z (%)
1	<i>i</i> Pr-HCl (20 mol%)	4	2	-	-	0
2	PCy ₂ Ph (20 mol%)	100	49	79	1.8	15
3	dcpe (20 mol%)	86	36	58	2	12
4	P/PR ₃ (20 mol%)	0	0	-	-	0
5	THF as solvent	61	29	81	2.6	9
6	Dioxane as solvent	49	28	82	4.5	8
7	AgF in lieu of CsF	25	13	81	3.3	7
8	CuBr ₂ in lieu of CuF ₂	0	0	-	-	0
9	Cu ₂ SO ₄	91	61	81	only 2a	10
10	Ni(COD) ₂ (5 mol%), PCy ₃ (10 mol%)	100	78	93	5.4	9

Reaction conditions: **(S)-1a** (0.2 mmol), **Y** (1.5 mmol), Ni(COD)₂ (10 mol%), PCy₃ (20 mol%), CuF₂ (30 mol %), CsF (1.0 equiv.), PhMe (1.5 mL), 50 °C, 16 h. GC conversion and yields using decane as internal standard. ee calculated by HPLC analysis

Table 2.3.2. Screening of ligands solvents and copper source.

Next, our attention turned to studying the loading of the fluoride base and the effect of the copper salt in the reaction outcome (Table 2.3.3). As shown in entries **1** and **2**, a lower loading of these parameters resulted in a slight increase in the branched/linear ratio, albeit in lower yields. In parallel with the development of this project, mechanistic studies on the silylation of aryl and benzyl pivalates were being performed in our group.⁴² These studies suggested that CuF₂ just served as a mere fluoride source, and that additional CsF could perform the same role as that of CuF₂. Interestingly, the addition of additional CsF improved the yield and the **2a/2X** ratio. However, these conditions led to substantial amounts of **2Z** and lower enantioselectivities (entries **3-6**). Similarly, low yields but high regioselectivities were found by conducting the reaction with CuF₂ in the absence of CsF, indicating that an optimal combination of these variables was essential for success (entry **7**).

Chapter 2

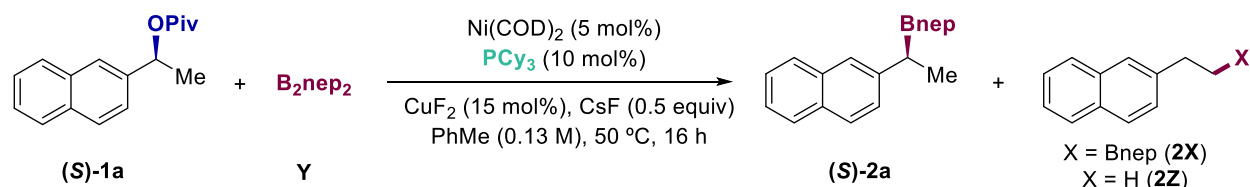


Entry	Deviation from standard conditions	Conv. (%)	2a (%)	(S)-2a ee (%)	2a/2X	2Z (%)
1	CuF ₂ (15 mol%), CsF (0.5 equiv)	72	48	94	6.5	5
2	CuF ₂ (7.5 mol%), CsF (0.25 equiv)	80	44	94	6.6	5
3	No CuF ₂ , CsF (0.5 equiv)	95	70	94	7.4	6
4	No CuF ₂ , CsF (2.0 equiv)	89	64	94	only 2a	9
5	No CuF ₂ , CsF (2.5 equiv)	89	64	94	32	8.8
6	No CuF ₂ , CsF (2.0 equiv), 24 h	87	66	94	62	12
7	CuF ₂ (15 mol%), no CsF	61	33	94	12.4	0

Reaction conditions: (S)-1a (0.2 mmol), Y (1.5 mmol), Ni(COD)₂ (5 mol%), PCy₃ (10 mol%), CuF₂ (30 mol %), CsF (1.0 equiv.), PhMe (1.5 mL), 50 °C, 16 h. GC conversion and yields using decane as internal standard. ee calculated by HPLC analysis

Table 2.3.3. Screening of CuF₂ and CsF equivalents.

Surprisingly, good regioselectivities were found upon using low amounts of CuF₂ but with substantial amounts of CsF (Table 2.3.4, entries 1-2). A subtle balance of these reagents gave rise to excellent yields and high 2a/2X ratio, with minimum amounts of reduced products (entry 4). Moreover, lower amounts of nickel/ligand improved the yield, but with considerable amounts of linear and reduced products (entry 3).



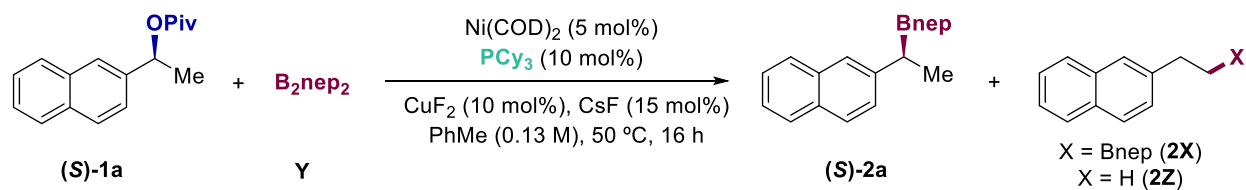
Entry	Deviation from standard conditions	Conv. (%)	2a (%)	(S)-2a ee (%)	2a/2X	2Z (%)	
Day 1	1	CuF ₂ (10 mol%), CsF (2.0 equiv)	74	51	94	18	9
	2	CuF ₂ (15 mol%), CsF (2.0 equiv)	75	51	94	17	10
	3	Ni(COD) ₂ (3.5 mol%), PCy ₃ (7 mol%)	100	83	94	9	9
Day 2	4	CuF ₂ (10 mol%), CsF (15% mol)	89	87	94	61	3
	5	Ni(COD) ₂ (3.5 mol%), PCy ₃ (7 mol%)	100	80	94	5.7	9
	6	Ni(COD) ₂ (3.5 mol%), PCy ₃ (7 mol%)	85	69	94	11	6
	7	CuF ₂ (10 mol%), CsF (15% mol)	96	71	93	6.9	9

Reaction conditions: (S)-1a (0.2 mmol), Y (1.5 mmol), Ni(COD)₂ (5 mol%), PCy₃ (10 mol%), CuF₂ (15 mol %), CsF (0.5 equiv.), PhMe (1.5 mL), 50 °C, 16 h. GC conversion and yields using decane as internal standard. ee calculated by HPLC analysis

Table 2.3.4. Demonstrating reproducibility issues.

Unfortunately, we faced notorious reproducibility issues by applying the optimized reaction conditions multiple times (entries **5** and **6**). Therefore, we invested a considerable amount of time to unravel the origin of such uncertainty.

A systematic analysis was performed by modifying all reaction parameters (Table 2.3.5). As shown in entry **11**, high yields and excellent stereospecificities were found by subjecting (**S**)-**1a** to a cocktail consisting of Ni(COD)₂/PCy₃ (7.50 mol%, 1:1 ratio) with minimum amounts of **2Z**. Unfortunately, variable results were found by repeating these reaction conditions (entries **12** and **13**).



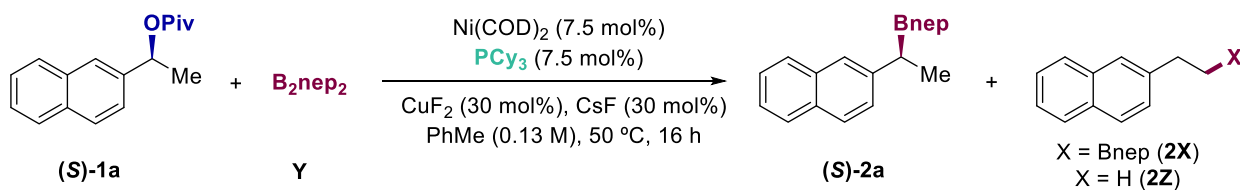
Entry	Deviation from standard conditions	Conv. (%)	2a (%)	(S)-2a ee (%)	2a/2X	2Z (%)
1	60 °C	92	65	94	9	7
2	0.4 mmol scale	97	67	94	6	10
3	0.4 mmol scale, CsF (20 mol%)	92	69	94	7	12
4	PCy ₃ (5 mol%)	66	63	94	32	3
5	PCy ₃ (7.5 mol%)	81	63	94	16	5
6	PCy ₃ (12 mol%)	100	59	94	4	10
7	PCy ₃ (15 mol%)	100	52	93	3	10
8	CuF ₂ (30 mol%)	92	73	94	11	7
9	CuF ₂ (40 mol%)	82	75	94	6.8	7
10	CuF ₂ (60 mol%)	88	67	94	6.7	7
11	Ni(COD) ₂ (7.5 mol%), PCy ₃ (7.5 mol%)	97	88	94	18	7
12	Ni/L (7.5 mol%), CuF ₂ /CsF (30 mol%)	96	91	94	20	7
13	Ni/L (7.5 mol%), CuF ₂ /CsF (30 mol%)	88	79	94	26	5

Reaction conditions: (**S**)-**1a** (0.2 mmol), **Y** (1.5 mmol), Ni(COD)₂ (5 mol%), PCy₃ (10 mol%), CuF₂ (15 mol%), CsF (15 mol%), PhMe (1.5 mL), 50 °C, 16 h. GC conversion and yields using decane as internal standard. ee calculated by HPLC analysis

Table 2.3.5. Screening of temperature, scale, ligand, copper and nickel parameters.

At this point we wondered whether the reproducibility issues might be solved by operating with stock solutions of Ni/L instead of weighing out both Ni and L. As shown in Table 2.3.6, this turned out to be the case obtaining same results by applying the same conditions in different days (entries **1-3**).

Chapter 2



Entry	Deviation from standard conditions	Conv. (%)	2a (%)	(S)-2a ee (%)	2a/2X	2Z (%)
1	Stock solution of Ni(COD) ₂ /PCy ₃	100	92	94	17	5
<i>Day 2</i>						
2	Stock solution of Ni(COD) ₂ /PCy ₃	100	92	94	17	6
<i>Day 3</i>						
3	Stock solution of Ni(COD) ₂ /PCy ₃	100	92	94	18	5

Reaction conditions: (S)-1a (0.2 mmol), Y (1.5 mmol), Ni(COD)₂ (7.5 mol%), PCy₃ (7.5 mol%), CuF₂ (30 mol%), CsF (30 mol%), PhMe (1.5 mL), 50 °C, 16 h. GC conversion and yields using decane as internal standard. ee calculated by HPLC analysis

Table 2.3.6. Screening of final conditions & influence of stock solutions.

Next, we turned our attention to the influence of the electrophile used in the targeted borylation event (Table 2.3.7). As shown, the utilization of benzyl esters, carbonates or amide derivatives provided lower reactivities and enantiomeric excesses (entries 2-9) whereas the employment of benzyl ethers did not undergo the desired C(sp³)-O borylation reaction (entries 10 & 11).

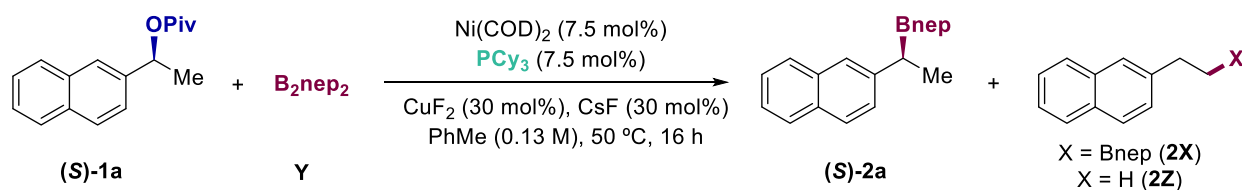


Entry	Deviation from standard conditions	Conv. (%)	2a (%)	(S)-2a ee (%)	2a/2X	2Z (%)
1	OPiv	100	93	94	18	5
2	OCOMe	65	39	64	3	10
3	OCOPh	89	51	68	2	16
4	OBoc	89	65	56	15	0
5	OCopy	4	3	94	only 2a	0
6	OCOCH ₂ OMe	98	35	59	0.5	24
7	OCOCH ₂ SMe	30	19	90	0.3	5
8	OCOCH ₂ SCOPh	0	0	-	-	0
9	OCNMe ₂	91	64	89	3	7
10	OMe	2	0	-	-	0
11	OCH ₂ CH ₂ OMe	10	0	-	-	8

Reaction conditions: (S)-Xa (0.2 mmol), Y (1.5 mmol), Ni(COD)₂ (5 mol%), PCy₃ (10 mol%), CuF₂ (15 mol%), CsF (15 mol%), PhMe (1.5 mL), 50 °C, 16 h. GC conversion and yields using decane as internal standard. ee calculated by HPLC analysis

Table 2.3.7. Stereospecific borylation with different secondary benzylic C-O electrophiles.

As expected, the reaction did not occur in the absence of Ni(COD)₂ or PCy₃ (Table 2.3.8, entries **2** & **3**). Surprisingly, the removal of CuF₂ and CsF resulted in 56% yield and 93% *ee* (entry **8**). Furthermore, the use of only one of these components still furnished the product in decent yields and good *ee* (entries **4-7**), indirectly suggesting that the presence of both CuF₂ and CsF avoids decomposition or deactivation of the catalyst. Lastly, we observed that an increase in the loading of PCy₃ had a deleterious effect (entry **9**).



Entry	Deviation from standard conditions	Conv. (%)	2a (%)	(S)-2a <i>ee</i> (%)	2a/2X	2Z (%)
1	None	100	95 (87) ^a	95	18	5
2	No Ni(COD) ₂	0	0	-	-	0
3	In the absence of PCy ₃	0	0	-	-	0
4	In the absence of CuF ₂	98	84	93	25	4
5	In the absence of CsF	94	75	92	16	6
6	No CsF, with CuF ₂ (1 equiv)	99	84	86	14	6
7	No CuF ₂ , with CsF (1 equiv)	90	73	85	11	7
8	No CuF ₂ , no CsF	82	56	93	3.5	8
9	Using PCy ₃ (20 mol%)	64	40	91	5	9

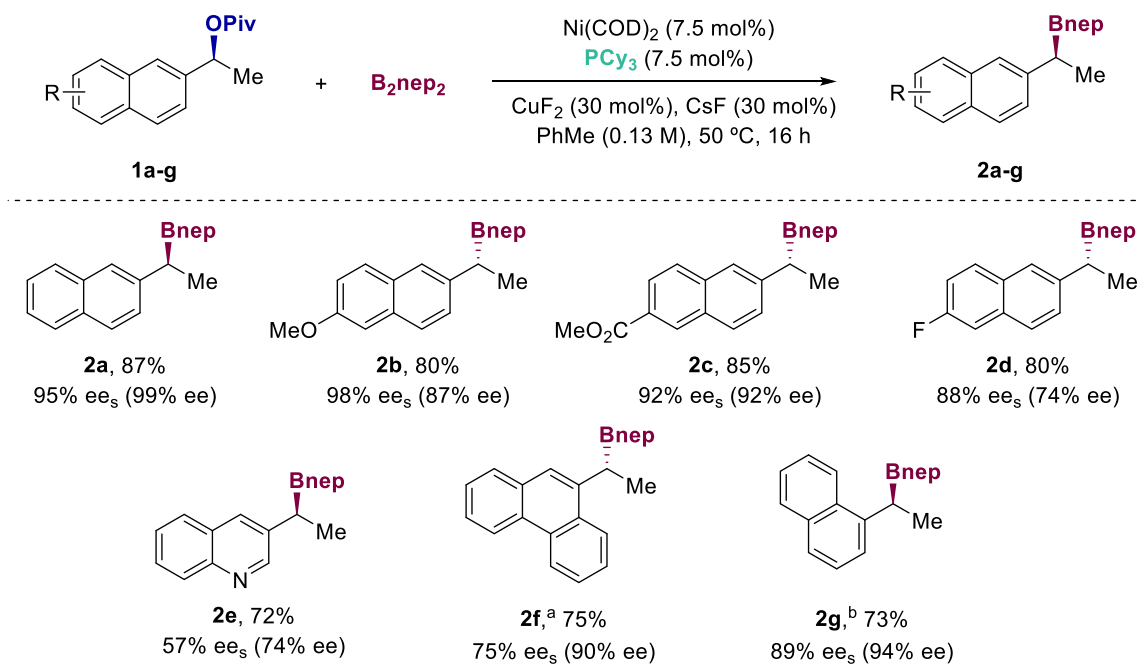
Reaction conditions: (S)-1a (0.2 mmol), Y (1.5 mmol), Ni(COD)₂ (7.5 mol%), PCy₃ (7.5 mol%), CuF₂ (30 mol%), CsF (30 mol%), PhMe (1.5 mL), 50 °C, 16 h. GC conversion and yields using decane as internal standard. *ee* calculated by HPLC analysis. ^aIsolated yield after oxidation of the Bnep to the alcohol.

Table 2.3.8. Screening of critical parameters for the stereospecific borylation.

2.3.3 Substrate scope

Subsequently, we focused on evaluating the generality of our stereospecific borylation. As shown in Scheme 2.3.2, a series of differently substituted enantioenriched benzyl pivalates – easily synthesized from the corresponding benzyl alcohol – delivered the targeted compounds in good yields and enantioselectivities. First, we analyzed the influence of the electronic nature of the substituents on the ring, demonstrating that electron-rich (**2b**) or electron poor (**2c** & **2d**) substituents worked equally well. Unfortunately, the employment of quinolone (**2e**) afforded low yields and low enantiomeric fidelity, probably due to competitive binding of the nitrogen atom to the metal center. In the case of phenanthrene analogues (**2f**), the drop in yield and *ee* might be ascribed to racemization of the enantioenriched oxidative addition species by a bimolecular mechanism with exogenous low-valent Ni(0)L_n. As shown for **2g**, excellent stereospecificities and yields were found when the benzyl pivalate is placed at C1.

Chapter 2

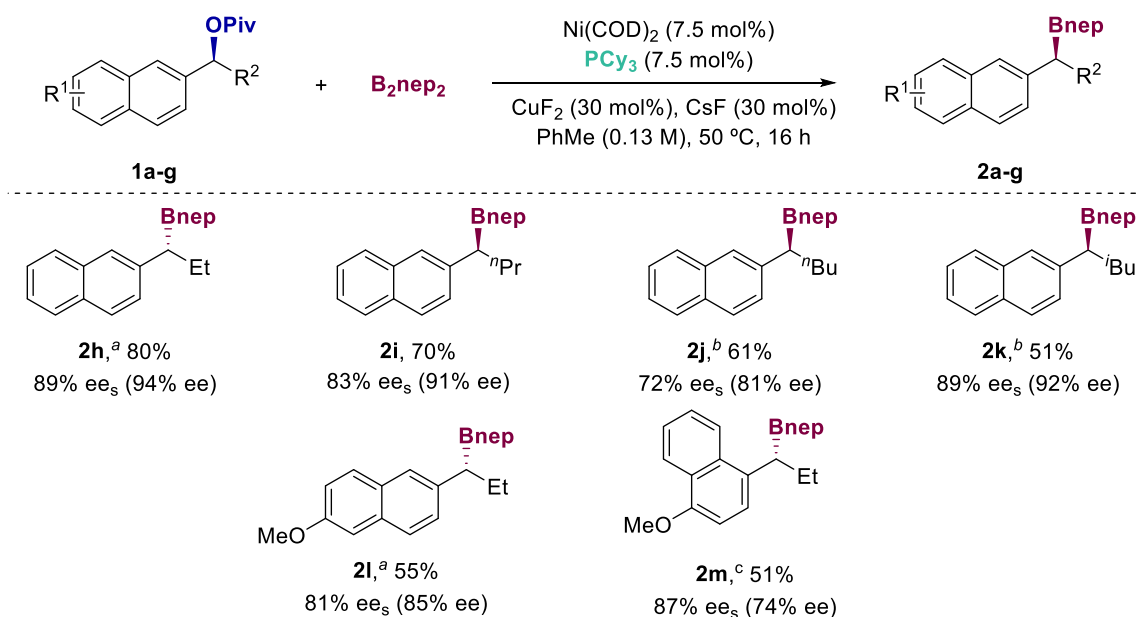


Reaction conditions: **1a-g** (0.2 mmol), B_2nep_2 (1.5 mmol), $\text{Ni}(\text{COD})_2$ (7.5 mol%), PCy_3 (7.5 mol%), CuF_2 (30 mol%), CsF (30 mol%), PhMe (1.5 mL), 50 °C, 16 h. Isolated yields, with enantiomeric excesses of starting precursors in parenthesis.
^a $\text{Ni}(\text{COD})_2$ (10 mol%), PCy_3 (20 mol%), CsF (1 equiv). ^b $\text{Ni}(\text{COD})_2$ (10 mol%), PCy_3 (10 mol%), CuF_2 (50 mol%), CsF (50 mol%), 55 °C.

Scheme 2.3.2. Scope of benzyl pivalates.

Substrates possessing aliphatic side chains other than methyl groups generally resulted in lower enantioselectivities (**2h-m**), suggesting that transmetalation or oxidative addition might be hampered by the presence of larger alkyl side chains that might trigger competitive β -hydride elimination pathways (Scheme 2.3.3). In line with this notion, non-negligible amounts of homobenzylic borylation were observed in the crude reaction mixtures. Electron-rich substituents containing methoxy groups can be tolerated, obtaining the products in good enantioselectivities albeit in lower yields (**2i**). Finally, a simple comparison can be made when a longer side chain is placed at C1 of the naphthalene ring, obtaining worse yields while maintaining good levels of *ee* (**2m**). Unfortunately, the extension of this reaction to non- π -extended aryl pivalates did not afford the desired borylation.

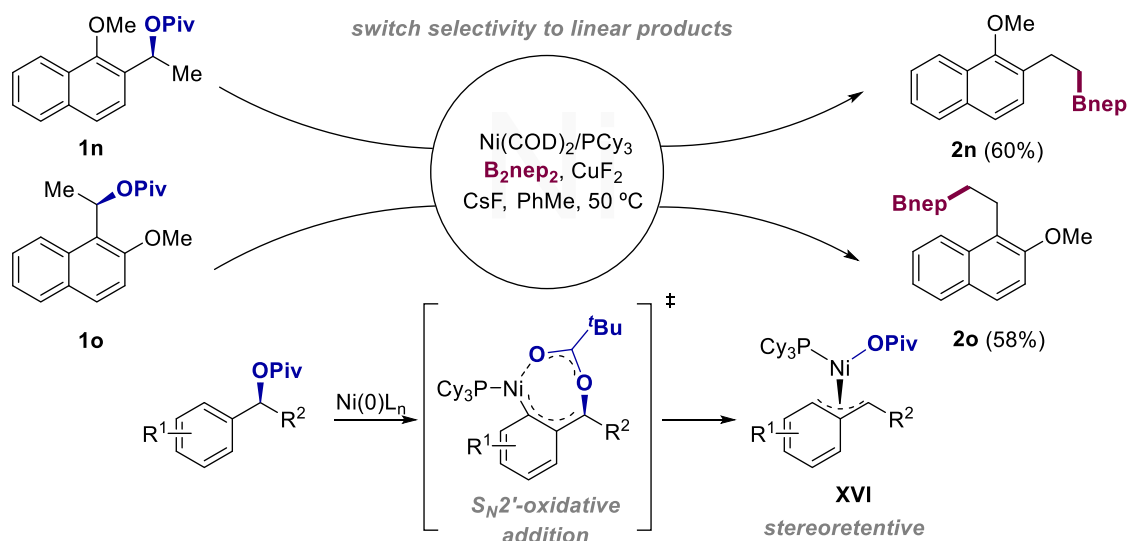
Stereospecific Borylation of Benzyl C(sp³)-O Bonds



Reaction conditions: **1a-g** (0.2 mmol), B₂nep₂ (1.5 mmol), Ni(COD)₂ (7.5 mol%), PCy₃ (7.5 mol%), CuF₂ (30 mol%), CsF (30 mol%), PhMe (1.5 mL), 50 °C, 16 h. Isolated yields, with enantiomeric excesses of starting precursors in parenthesis. ^aNi(COD)₂ (5 mol%), PCy₃ (5 mol%), no CuF₂, CsF (50 mol%). ^bNi(COD)₂ (10 mol%), PCy₃ (10 mol%). ^cNi(COD)₂ (10 mol%), PCy₃ (10 mol%), CuF₂ (50 mol%), CsF (50 mol%), 55 °C.

Scheme 2.3.3. Scope of benzyl pivalates with larger alkyl side chains.

Intriguingly, the presence of *ortho* substituents on the naphthyl ring resulted in a selectivity switch, obtaining the corresponding linear boronic esters instead (Scheme 2.3.4, **2n** & **2o**). This change in selectivity suggests that the inclusion of such substituents favour β-hydride elimination followed by a migratory insertion prior to a final C–B bond-forming reaction that avoids the clash with the proximal *ortho* group on the arene.

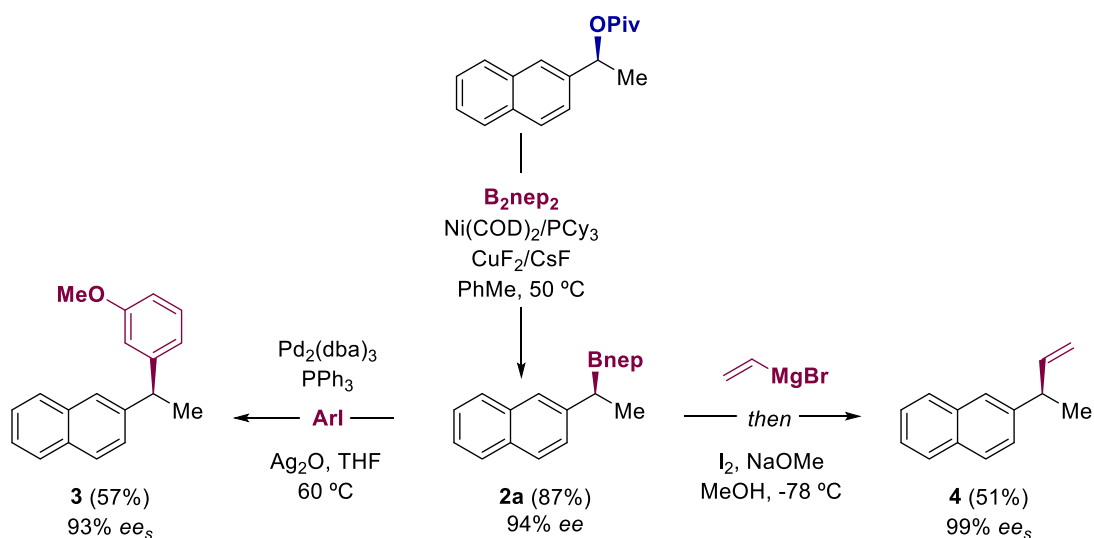


Scheme 2.3.4. Switch selectivity & stereoretentive approach.

Chapter 2

2.3.4 Applications of benzyl boronates.

Prompted by the pivotal role of the organoboron reagents as synthetic intermediates, we next explored the applicability of our protocol by utilizing the corresponding benzyl boronic ester in further synthetic applications. As shown in Scheme 2.3.5 *left*, the *in situ* generation of **2a** could be combined with a subsequent Suzuki-Miyaura reaction based on Pd₂(dba)₃/PPh₃, ending up in diarylethane **3** with an overall retention of configuration. In addition, exposure of **2a** to vinylmagnesium bromide followed by addition of I₂ and NaOMe/MeOH at -78 °C resulted in **4** with a good overall yield and excellent stereofidelity (Scheme 2.3.5, *right*).



Scheme 2.3.5. Synthetic applicability.

2.3.5 Unsuccessful substrates

During the course of our investigations, we found some substrates that failed to provide the targeted products (Figure 2.3.1). Specifically, the substitution of the methyl substituent by a phenyl ring on the benzylic position (**A**) led to the almost quantitative reduction of the pivalate group to the alcohol. The utilization of the anthracene-derived pivalate bearing the benzylic bond at C9 (**B**) resulted in hydrogenolysis side reaction, an observation ascribed to the electron-rich benzyl C–OPiv bond prone to undergo reductive transformations.⁴³ The electron-rich substrate **C** bearing an isobutyl group at the benzylic carbon resulted in negligible reactivity. The reaction did not occur with π -extended heteroaromatic rings (**D** & **E**) or non- π -extended rings (**F**, **G** and **H**), resulting in recovered starting material. As mentioned during the introduction, the lack of reactivity of non- π -extended arene systems might be due to the loss of aromaticity when the nickel species undergoes the oxidative addition, being this step the barrier to overcome.^{27,44}

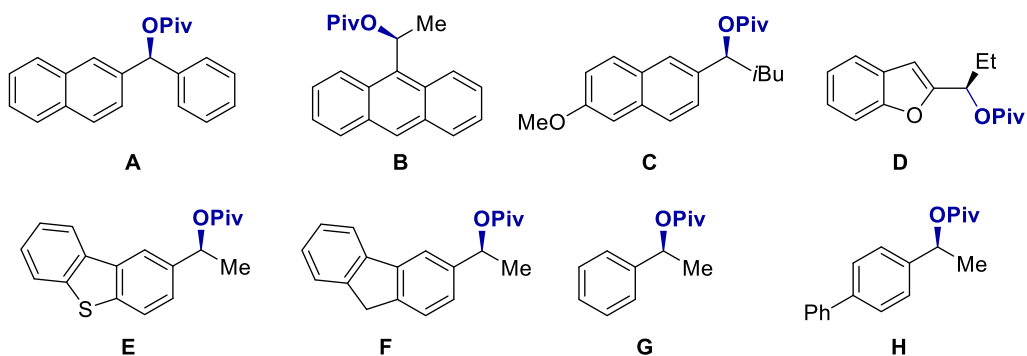
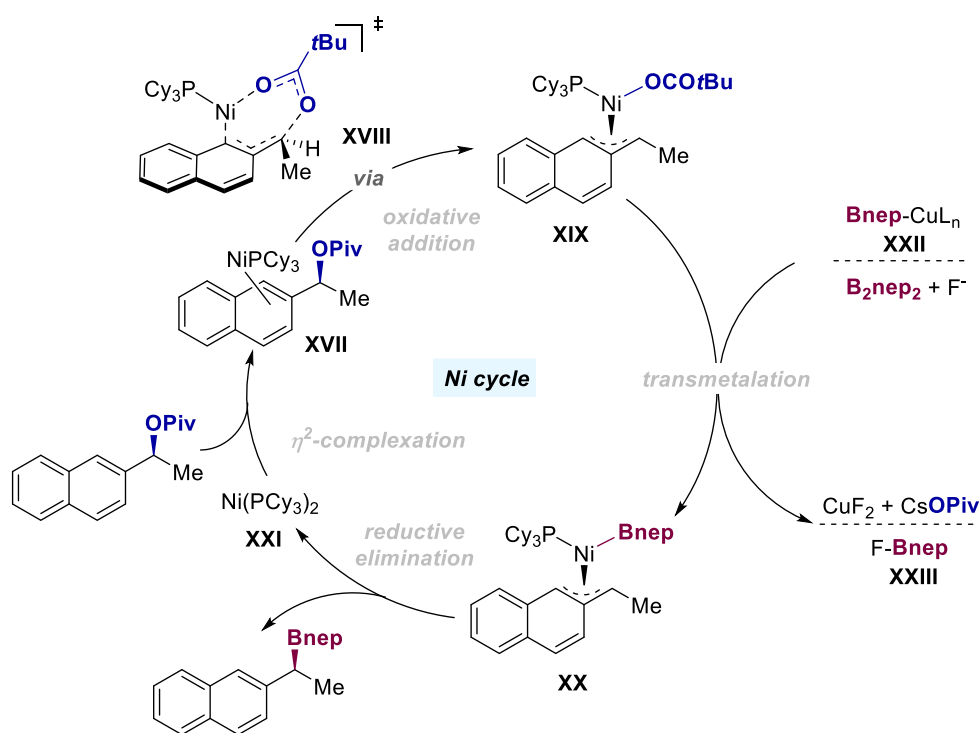


Figure 2.3.1. Unsuccessful stereospecific borylation of aryl pivalates.

2.3.6 Mechanistic proposal

At present, we believe that our reaction operates *via* a Ni(0)/Ni(II) regime consisting of oxidative addition, transmetalation and reductive elimination (Scheme 2.3.6, *Ni cycle*). Oxidative addition might be preceded by a η^2 -complexation between Ni(0) species and the aryl pivalate (**XVII**). The following transmetalation of the boron moiety might lead to a boron-containing intermediate (**XX**), that would reductively eliminate to deliver the desired borylated product while generating back the active Ni(0) species (**XXI**).



Scheme 2.3.6. Ni cycle mechanistic proposal.

After the publication of this work, Watson carried out a computational study to establish the differences of stereospecificity depending on the substrate, ligand and the conditions utilized.²⁴ As indicated before, a concerted oxidative addition through a cyclic transition state is likely operative

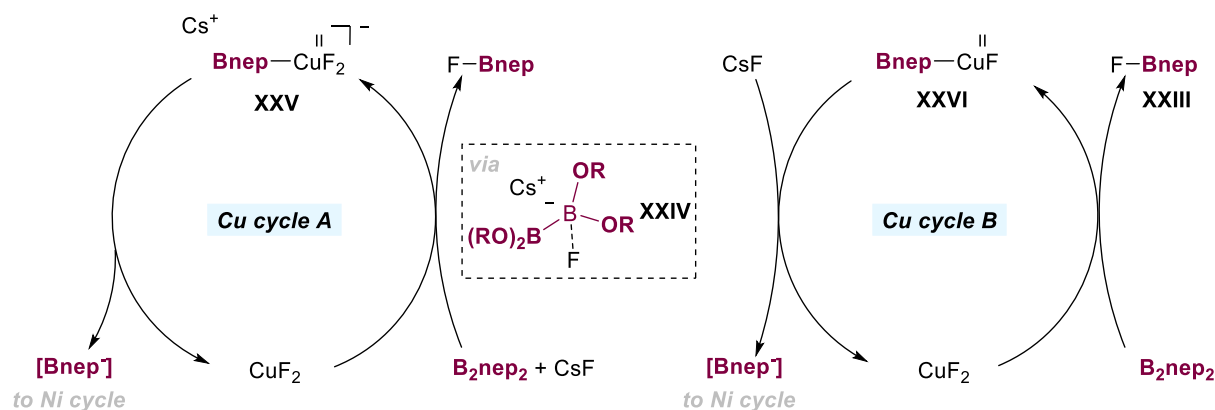
Chapter 2

where the nickel interacts with the pivalate carbonyl oxygen while cleaving the benzylic C(sp³)–O bond (**XVIII**), thus generating a benzylnickel complex with overall retention of configuration. The key difference between the retention or inversion stereoselectivity likely depends on the substrate–nickel–ligand angle. Although in depth experimental and computational studies are needed to unravel the intricacies of this reaction, two main transmetalation scenarios might come into play 1) a transmetalation consisting of a Cu–B intermediate with two intertwined catalytic cycles, and 2) a copper-free picture that may be aided by the presence of the fluoride salts.

2.3.6.1 Ni/Cu mechanism

In 2013, our group proposed that a related silylation event occurs by a transmetalation involving copper as catalyst.⁴¹ Therefore, it was somewhat tempted to invoke an otherwise similar pathway by activating the B–B bond by fluoride attack to generate Cu–B intermediates, which may favour the transmetalation of the boryl group to the oxidative addition complex (**XIX**) (Scheme 2.3.6).

Taking this into consideration, two plausible proposals have been suggested (Scheme 2.3.7).⁴¹ It has been demonstrated that fluoride anions can activate related (OR)₂B–B(OR)₂ bonds forming the corresponding B(sp³) adduct that serves as a boryl anion source (**XXIV**),⁴⁵ (Scheme 2.3.7, *Cu cycle A*). Such adduct can release the corresponding boryl anion, which in the presence of CuF₂ may generate a nucleophilic borylcopper species (**XXV**). This Cu–B complex should then transmetalate the boryl anion to the Ni cycle and recover the CuF₂.



Scheme 2.3.7. Plausible Cu catalytic cycles.

On the other hand, the B₂nep₂ unit might promote a transmetalation to form Cu(II)FBnep (**XXVI**) and FBnep (**XXIII**) (Scheme 2.3.7, *Cu cycle B*). **XXVI** would release the boryl anion to the Ni cycle while CsF would regenerate the active CuF₂ catalyst. This assumption is in line with previously proposed transmetalation of an aryl group from a B atom to Cu(OAc)₂,⁴⁶ and explains why Cu(II) sources may easily transmetalate with boron species *via* the formation of highly stable B–F or B–O bonds (Table 2.3.2). This mechanistic proposal has a number of flaws when examined more closely. First, sub-stoichiometric CsF is employed in contrast with the stoichiometric amounts required for this

mechanistic proposal to work. And more strikingly, a 60% yield of the desired product can be obtained in the absence of CuF₂ and CsF.

2.3.6.2 Nickel-fluoride activation picture

After the publication of the current project, our group investigated the mechanistic implications of the silylation of aryl pivalates.⁴² Such stoichiometric and kinetic experiments demonstrated that Cu-SiEt₃ intermediates are not necessary for the silylation reaction to occur, thus leaving a reasonable doubt on whether the reaction operated *via* Ni/Cu co-catalysis. Indeed, the inclusion of additional amounts of CsF resulted in similar results of the targeted product. Interestingly, the silylation reaction gave a 30% yield in the absence of fluoride sources. As mentioned above, we observed a 60% yield of the desired product in the absence of the CuF₂ and CsF. Both results pointed out that in the first hours of the reaction the transformation takes place through a fluoride-free mechanism. Our group carried out DFT studies for both systems in order to map out the energy profile of their proposed mechanism (Figure 2.3.2).

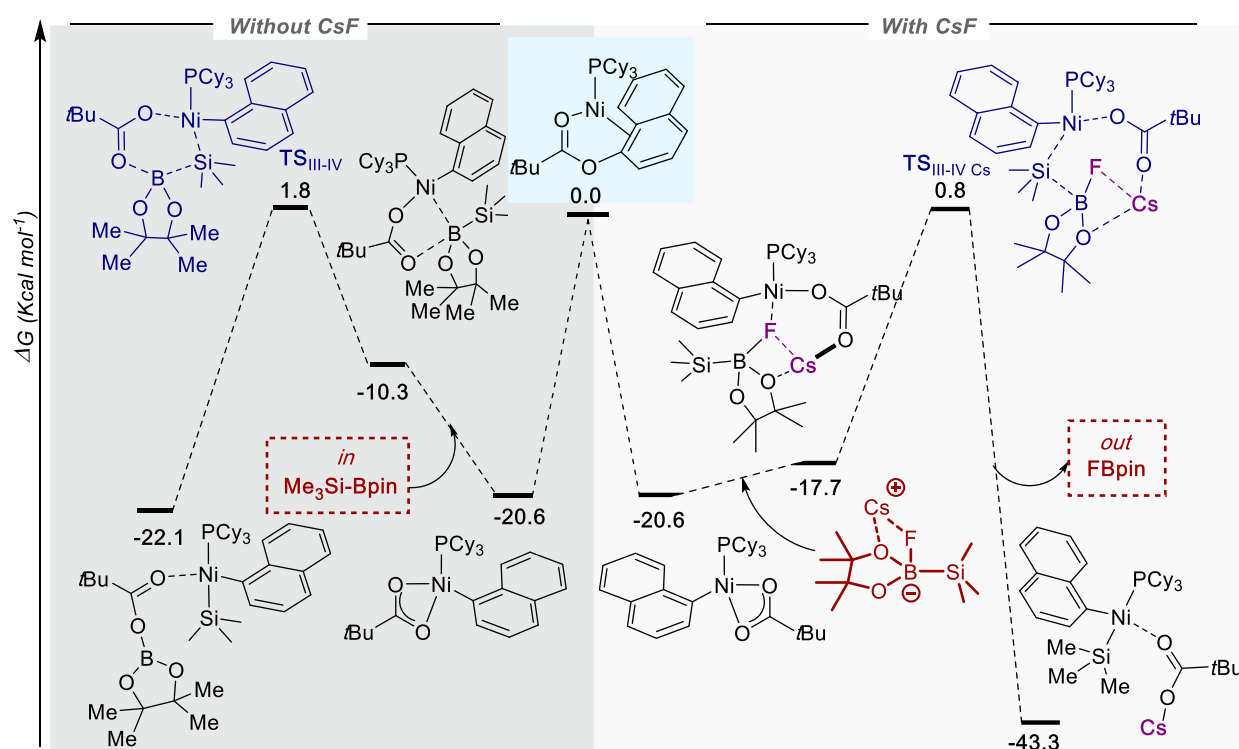
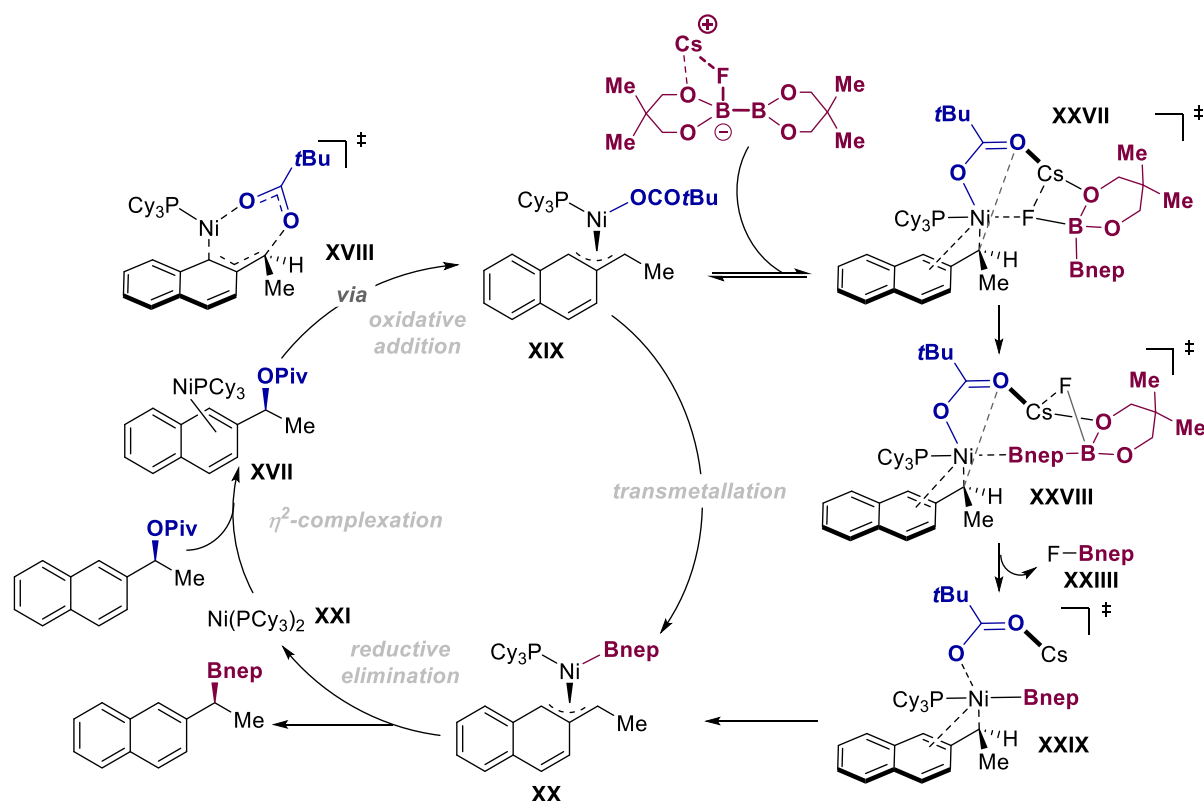


Figure 2.3.2. Free energy profile for the silylation reaction calculated in the absence and presence of fluoride sources. Energies are in kcal mol^{-1} .

Some conclusions were gathered from the DFT studies that shed some light in our borylation mechanism. First, we found a slightly lower energy pathway when CsF was involved in. Second, FBpin was released instead of PivOBpin. Third, the presence of CsF slightly lowers down the barrier of transmetalation slightly ($\Delta\Delta G^\ddagger = 1 \text{ kcal mol}^{-1}$). Finally, the loss of FBpin rather than PivOBpin also adds 20 kcal mol^{-1} to the barrier to the reverse reaction (figure 2.3.2, *with CsF*). Putting all these

Chapter 2

observations into perspective, we can speculate that our transformation might likely follow the reaction pathway of Figure 2.3.2, *right*, in which CuF_2 and CsF act as fluoride sources that help the activation of the B_2nep_2 while sequestering the Bnep byproduct. In such a way, we propose that the mechanism of our reaction operates *via* **XXVII**. Upon activation of B_2nep_2 by CsF and the nickel species (**XXVIII**), transmetalation occurs, driving the reaction forward by the formation of F-Bnep en route to intermediate **XXIX**.



Scheme 2.3.8. Ni/F activation mechanism proposal.

2.3.7 Future outlook

Despite the results presented in this chapter, there still exist a non-negligible number of limitations that could potentially be addressed in the future. Among these are the following:

- A. *Utilization of regular arenes.* As shown above, our reaction is inherently limited to π -extended systems due to the strong η^2 -binding of Ni centers to these polyarenes and to the electron-poor nature of these backbones. We hypothesize that the utilization of Cr or Rh complexes might be critical for extending the scope of these reactions beyond π -extended systems.^{47–49} As reported, the binding of these entities to regular arenes in a η^6 -fashion makes them particularly electron-poor and, therefore susceptible to nucleophilic attack at the benzylic position. In this manner, the BDE of the C–O bond will be considerably lower, making it particularly prone to promote oxidative addition with Ni complexes.

- B. *Enantioselective version.* A close look into the literature data reveals that while the development of enantioconvergent cross-coupling reactions of racemic benzyl halides or pseudohalides are known, the means to trigger a related process via C–O bond-cleavage is still not practiced as one might initially anticipate. Therefore, future efforts should be devoted to the implementation of an enantioconvergent cross-coupling of racemic benzyl pivalates with chiral ligands.
- C. *Different C–O derivatives.* The ultimate goal of the C–O bond-cleavage arena is the utilization of simple C–O electrophiles. That being set, future work should be devoted to the utilization of simple benzyl alcohols via C–OH cleavage, thus obviating the need for protecting group technologies to lower down the bond-dissociation energy of the targeted C–O linkage.

2.4 Conclusions

In summary, we have reported the first stereospecific borylation of benzyl pivalates catalyzed by nickel sources. The mild conditions of this reaction allow us to trigger a borylation event of a reasonable number of substrates with an excellent stereochemical fidelity by a mechanism consisting of a stereoretentive oxidative addition that results in an overall retention of configuration. This protocol can be used as a platform to build up enantioenriched benzyl boronates, important compounds that can be used as linchpins for further derivatization.

2.5 Experimental procedures

2.5.1 General considerations

Reagents. Commercially available materials were used without further purification. Ni(COD)₂ (stored at low temperature in the glovebox) and PCy₃ were purchased from Strem Chemicals. CuF₂ anhydrous (98% purity), CsF anhydrous, and B₂nep₂ (96% purity) were purchased from Aldrich. Anhydrous Toluene (99.8% purity) was purchased from Alfa Aesar. All other reagents were purchased from commercial sources and used as received.

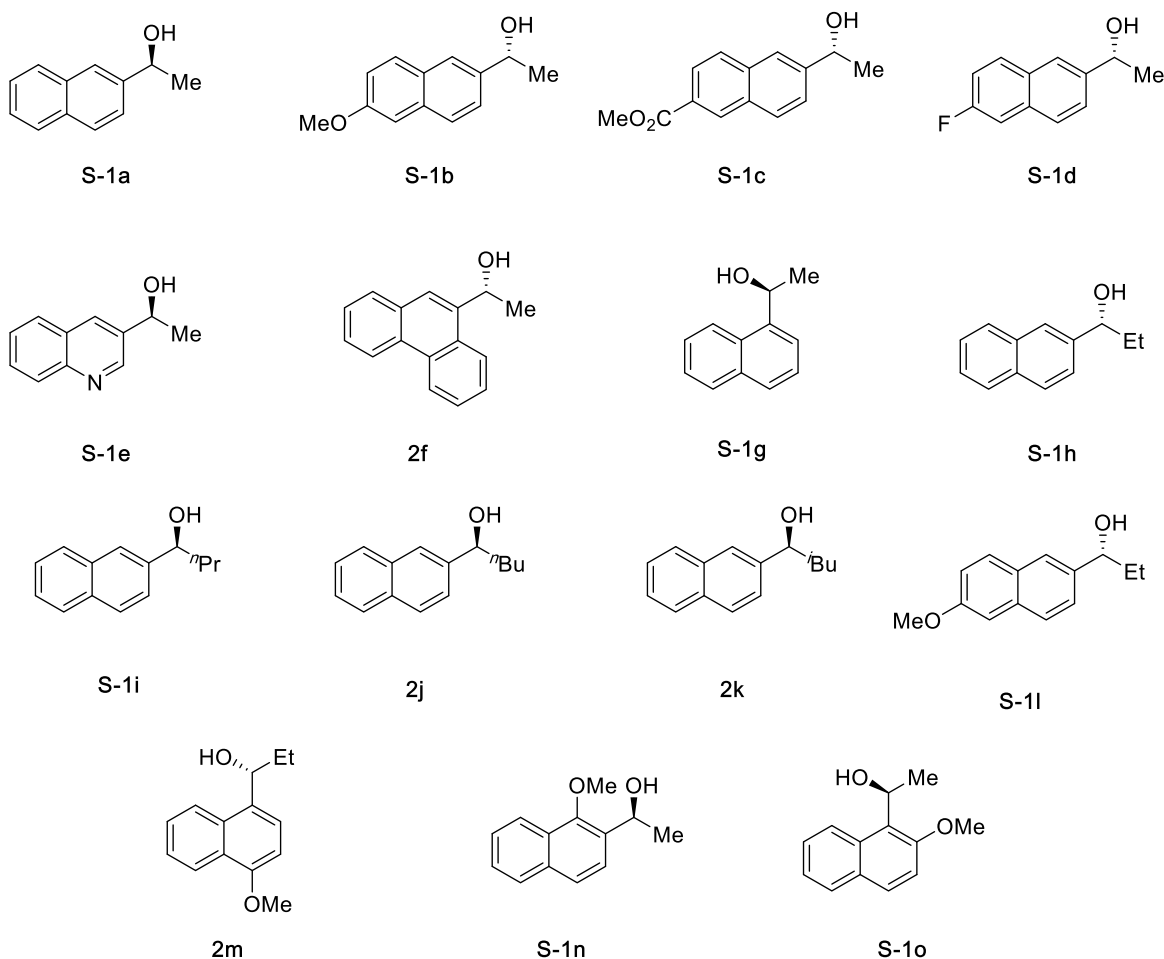
Analytical methods. ¹H, ¹³C NMR and ¹⁹F NMR spectra were recorded on a Bruker 300 MHz, 400 MHz and 500 MHz at 20 °C. All ¹H NMR spectra are reported in parts per million (ppm) downfield of TMS and were calibrated using the residual solvent peak of CHCl₃ (7.26 ppm), unless otherwise indicated. All ¹³C NMR spectra are reported in ppm relative to TMS, were calibrated using the signal of residual CHCl₃ (77.0 ppm), and were obtained with ¹H decoupling unless otherwise indicated. Coupling constants, *J*, are reported in Hertz. Melting points were measured using open glass capillaries in a Büchi B540 apparatus. Infrared spectra were recorded on a Bruker Tensor 27. Gas chromatographic analyses were performed on Hewlett-Packard 6890 gas chromatography instrument with a FID detector. Flash chromatography was performed with EM Science silica gel 60 (230- 400 mesh). Specific Optical Rotation was obtained using a Jasco P-1030 model polarimeter

Chapter 2

equipped with a PMT detector using the Sodium line at 589 nm. UltraPerformance Convergence Chromatography (UPC2) analysis was performed on Acquity UPC2 Waters instrument equipped with a Chiralpack IB/Chiralpack IC/Chiralpack IG column eluting *i*PrOH/CO₂, CO₂/MeOH, CO₂/MtBE-Hex at ambient temperature and monitored by Photodiode Array Detector (PDA). High Performance Liquid Chromatography (HPLC) analyses were performed on Agilent Technologies Model 1260 Infinity HPLC chromatography instrument equipped with Daicel Chiralpack IB column eluting Hexanes/EtOH supported with UV/Visible DAD detector.

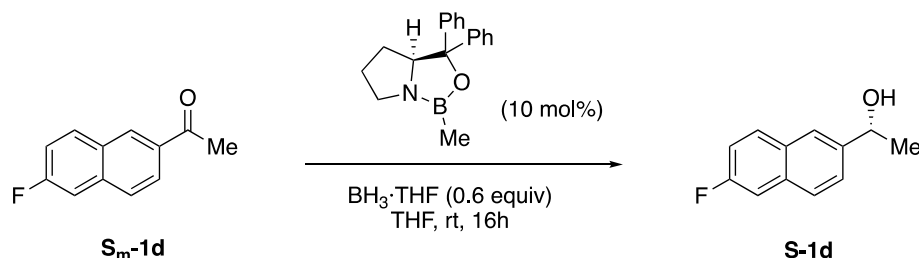
2.5.2 Synthesis of starting material

General procedure for the synthesis of enantiopure benzyl alcohols:

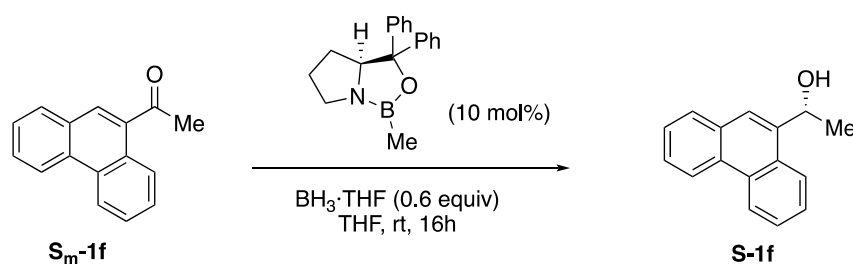


(S)-1-(Naphthalen-2-yl)ethanol (S-1a) and (S)-(-)-1-(1-Naphthyl)ethanol (S-1g) were purchased from Sigma Aldrich and Fluorochem respectively. Alcohols S-1b, S-1c, S-1d, and S-1fⁱ were prepared according to adapted literature procedures using Corey-Bakshi-Shibata reduction of ketones. Compounds S-1e, S-1j, S-1k, S-1l, S-1n, S-1o were prepared by asymmetric transfer hydrogenation of ketones.ⁱⁱ Alcohols S-1h, S-1i, S-1m were prepared according to literature procedures using asymmetric addition of diethyl zinc to the aldehydes.ⁱⁱⁱ All the enantiomeric excesses of crystalline

compounds were then increased via recrystallization from hexanes. Due to alcohols **S-1d**, **S-1f**, **S-1j**, **S-1k**, **S-1m**, **S-1n** and **S-1o** have not been prepared via these methods mentioned above, we have included the experimental routes for the procedures below.



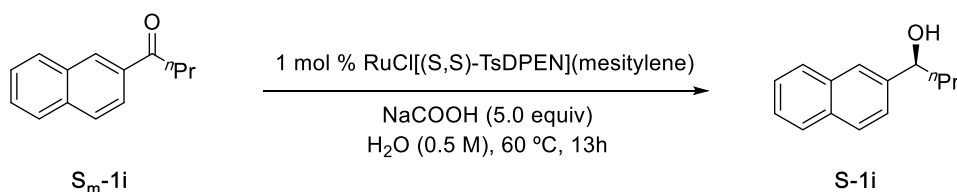
(R)-1-(6-fluoronaphthalen-2-yl)ethan-1-ol (S-1d). The following procedure is adapted from the literature.¹ A solution of CBS catalyst (1 M in THF, 0.19 mL, 0.19 mmol, 10 mol%) in THF (3 mL) was slowly added to a solution of ketone **S_m-1d** (356 mg, 1.89 mmol, 1.0 equiv), BH₃·THF (1 M, 1.1 mL, 1.1 mmol, 0.6 equiv.), and THF (35 mL). After stirring at room temperature for 16h, H₂O (25 mL) was added. The mixture was extracted with Et₂O. The combined organic layers were then dried (MgSO₄), filtered, concentrated. The resulting residue was purified by silica gel chromatography (Hexane/EtOAc 8/2) to give alcohol **S-1d** (93 mg, 26 %) as a white solid (m.p 84-86 °C). The enantiomeric excess was determined to be 74% ee by chiral HPLC analysis (CHIRALPAK IB, 1mL/min, 0.5% EtOH/Hexane, λ=220 nm); *t_R*(minor)= 12.3 min, *t_R*(major)= 13.6 min. ¹H-NMR (500 MHz, CDCl₃): δ 7.83-7.76 (m, 3H), 7.53 (d, *J* = 8.5 Hz, 1H), 7.44 (dd, *J* = 9.8, 2.6 Hz, 1H), 7.26 (t, *J* = 2.6 Hz, 1H), 5.06 (q, *J* = 6.4 Hz, 1H), 1.97 (s, 1H, OH), 1.58 (d, *J* = 6.4 Hz, 3H) ppm. ¹³C NMR (126 MHz, CDCl₃) δ 161.8, 159.4, 142.5, 133.6, 130.3, 127.7, 124.9, 123.8, 116.6, 110.7, 70.3, 25.2 ppm. ¹⁹F NMR (376 MHz, CDCl₃) δ -115.1 ppm. IR (neat, cm⁻¹): 3240, 2979, 1608, 1508, 1476, 1253, 1227, 1171, 1139, 1076, 873, 812, 479. HRMS calcd. for C₁₂H₁₀F (M-OH)⁺: 173.0761, found 173.0758.



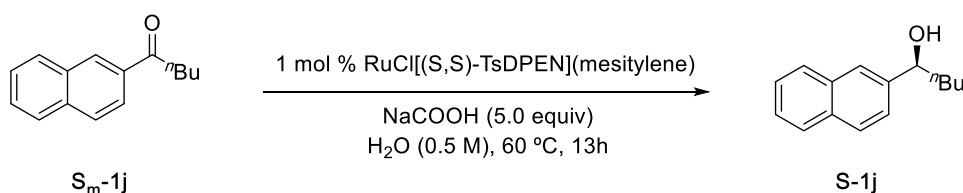
(R)-1-(phenanthren-9-yl)ethan-1-ol (S-1f). The following procedure is adapted from the literature.¹ A solution of CBS catalyst (1M in THF, 250 uL, 0.25 mmol, 0.1 equiv.) in THF (4 mL) was slowly added to a solution of ketone **S_m-1f** (541 mg, 2.46 mmol, 1.0 equiv.), BH₃·THF (1M, 1.5 mL, 1.48 mmol, 0.6 equiv.), and THF (40 mL). After stirring at room temperature for 16h, H₂O (20 mL) was added. The mixture was extracted with Et₂O. The combined organic layers were then dried (MgSO₄), filtered, concentrated. The resulting residue was purified by silica gel chromatography (hexanes/EtOAc 9/1) to give alcohol **S-1f** (330 mg, 61 %) as a white solid (m.p 102-104 °C). The enantiomeric excess was determined to be 89% ee. ¹H NMR (400 MHz, CDCl₃) δ 8.84 – 8.75 (m, 1H),

Chapter 2

8.67 (d, $J = 8.0$ Hz, 1H), 8.18 (dd, $J = 7.2, 2.3$ Hz, 1H), 7.96 (s, 1H), 7.93 – 7.88 (m, 1H), 7.75 – 7.56 (m, 4H), 5.71 (q, $J = 6.3$ Hz, 1H), 1.94 (s, 1H), 1.75 (d, $J = 6.4$ Hz, 3H) ppm. ^{13}C NMR (101 MHz, CDCl_3) δ 139.5, 131.5, 130.8, 130.0, 129.6, 128.8, 126.8, 126.7, 126.6, 126.3, 123.9, 123.3, 122.7, 122.4, 67.2, 24.1 ppm. The spectral data for this compound matches that reported in literature.^{IV}

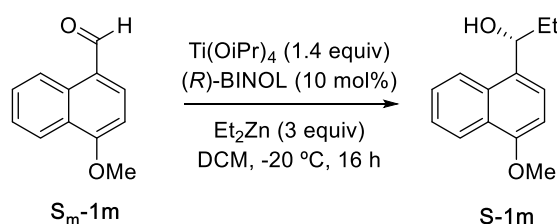


(S)-1-(naphthalen-2-yl)pentan-1-ol (S-1i). The following procedure is adapted from the literature.^{II} In a N_2 -atmosphere glovebox $\text{RuCl}[(S,S)\text{-TsDPEN}](\text{mesitylene})$ (13.3mg, 0.021 mmol, 1 mol%) was weighed out into a 25 mL flask. The flask was then capped and removed from glovebox. H_2O (degassed by sparging with N_2 , 5mL) was added, and the resulting mixture was stirred at 40 °C for 1h. The ketone **S_m-1i** (600 mg, 3.02 mmol, 1.0 equiv.) and NaCOOH (1.03 mg, 15.1 mmol, 5 equiv.) were added. The flask was evacuated and refilled with N_2 three times and then heated at 60 °C for 13h. The reaction mixture was diluted with Et_2O (10 mL), and filtered through silica gel, which was then rinsed with additional Et_2O (10 ml x2). The combined organic layers were concentrated. The resulting residue was purified by silica gel chromatography (hexanes/ EtOAc 9/1) and then recrystallized (hexanes) to give compound **S-1j** (480 mg, 80%, 94% ee) as a white solid (m.p 64-66 °C). ^1H NMR (400 MHz, CDCl_3) δ 7.88 – 7.70 (m, 4H), 7.57 – 7.41 (m, 3H), 4.86 (dd, $J = 7.4, 5.9$ Hz, 1H), 1.93 – 1.70 (m, 3H), 1.56 – 1.24 (m, 2H), 0.95 (t, $J = 7.4$ Hz, 3H) ppm. ^{13}C NMR (101 MHz, CDCl_3) δ 142.3, 133.3, 133.0, 128.2, 127.9, 127.7, 126.1, 125.8, 124.6, 124.1, 74.5, 41.1, 19.0, 14.0 ppm. IR (neat, cm^{-1}): 3240, 2952, 2868, 1311, 1097, 1035, 825. 746, 479. HRMS calcd. for $\text{C}_{14}\text{H}_{16}\text{O}$ ($\text{M}+\text{Na}$)⁺: 223.1093, found 223.1089

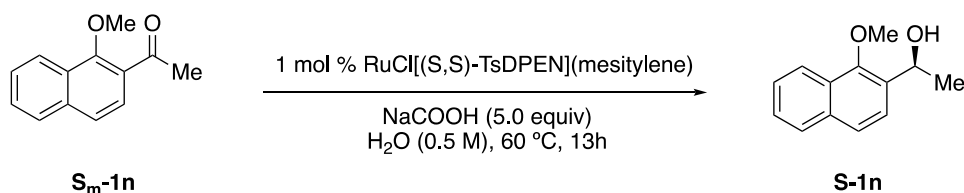


(S)-1-(naphthalen-2-yl)pentan-1-ol (S-1j). The following procedure is adapted from the literature.^{II} In a N_2 -atmosphere glovebox $\text{RuCl}[(S,S)\text{-TsDPEN}](\text{mesitylene})$ (13.3mg, 0.021 mmol, 1 mol%) was weighed out into a 25 mL flask. The flask was then capped and removed from glovebox. H_2O (degassed by sparging with N_2 , 5mL) was added, and the resulting mixture was stirred at 40 °C for 1h. The ketone **S_m-1j** (454 mg, 2.14 mmol, 1.0 equiv.) and NaCOOH (727 mg, 10.7 mmol, 5 equiv.) were added. The flask was evacuated and refilled with N_2 three times and then heated at 60 °C for 13h. The reaction mixture was diluted with Et_2O (10 mL), and filtered through silica gel, which was then rinsed with additional Et_2O (10 ml x2). The combined organic layers were concentrated. The

resulting residue was purified by silica gel chromatography (hexanes/EtOAc 9/1) and then recrystallized (hexanes) to give compound **S-1j** (260 mg, 57%, 99% ee) as a white solid (m.p 75-77 °C). ¹H NMR (400 MHz, CDCl₃) δ 8.00 – 7.81 (m, 3H), 7.78 (s, 1H), 7.72 – 7.33 (m, 3H), 4.85 (dd, *J* = 7.3, 6.0 Hz, 1H), 2.15 – 1.68 (m, 3H), 1.62 – 1.20 (m, 4H), 0.89 (t, *J* = 7.1 Hz, 3H) ppm. ¹³C NMR (101 MHz, CDCl₃) δ 142.4, 133.4, 133.1, 128.4, 128.1, 127.8, 126.3, 125.9, 124.8, 124.3, 75.0, 38.9, 28.1, 22.8, 14.2 ppm. The spectral data for this compound matches that reported in literature.^v



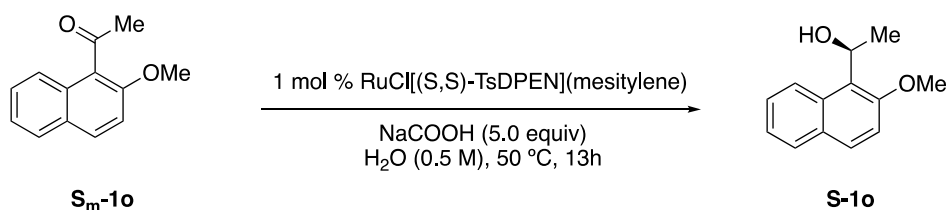
(R)-1-(4-methoxynaphthalen-1-yl)propan-1-ol (S-1m). The following procedure is adapted from the literature.ⁱⁱⁱ To a solution of (*R*)-binaphtol (155 mg, 0.54 mmol, 0.1 equiv.) in dichloromethane (40 mL) was added titanium tetraisopropoxide (2.2 mL, 7.46 mmol, 1.4 equiv.), and the solution was stirred 10 minutes. Diethylzinc (1 M, 16.2 mL, 16.2 mmol, 3.0 equiv.) was added and the mixture was stirred for an additional 10 minutes at room temperature. The solution was cooled to -25 °C and a solution of 4-methoxy-1-naphthaldehyde (1 g, 5.4 mmol, 1.0 equiv.) in dichloromethane (8 mL) was added. After stirring overnight at -25 °C, the reaction was quenched by the addition of 1 M hydrochloric acid (80 mL) and the product was extracted with CH₂Cl₂ (3 x 50 mL). The combined organics were washed with brine (50 mL), dried over MgSO₄, and concentrated in vacuo. The product was purified by flash chromatography (hexanes/EtOAc 9/1) to afford the title compound as colourless oil (647 mg, 56 %). The enantiomeric excess was determined to be 87% ee by chiral HPLC analysis. ¹H NMR (500 MHz, CDCl₃) δ 8.33 (dd, *J* = 8.2, 1.5 Hz, 1H), 8.11 (d, *J* = 8.4 Hz, 1H), 7.65 – 7.39 (m, 3H), 6.81 (d, *J* = 8.0 Hz, 1H), 5.30 (q, *J* = 5.5, 1H), 4.01 (s, 3H), 2.07 – 1.91 (m, 2H), 1.89 (s, 1H, OH), 1.02 (t, *J* = 7.4 Hz, 3H). ¹³C NMR (126 MHz, CDCl₃) δ 155.2, 132.2, 131.8, 126.7, 126.0, 125.1, 123.4, 123.3, 122.9, 103.3, 72.8, 55.7, 31.1, 10.8 ppm. IR (neat, cm⁻¹): 3379, 2961, 1585, 1462, 1392, 1269, 1158, 1089, 818, 762. HRMS calcd. for C₁₄H₁₆O₂ (M+Na)⁺: 239.1043, found 239.1045.



(S)-1-(1-methoxynaphthalen-2-yl)ethanol (S-1n). The following procedure is adapted from the literature.ⁱⁱ In a N₂-atmosphere glovebox RuCl[(*S,S*)-TsDPEN](mesitylene) (13.3mg, 0.021 mmol, 1 mol%) was weighed out into a 25 mL flask. The flask was then capped and removed from glovebox. H₂O (degassed by sparging with N₂, 5mL) was added, and the resulting mixture was stirred at 40 °C for 1h. The ketone **S_m-1n** (500 mg, 2.5 mmol) and NaCOOH (850 mg, 5 equiv.) were added. The flask

Chapter 2

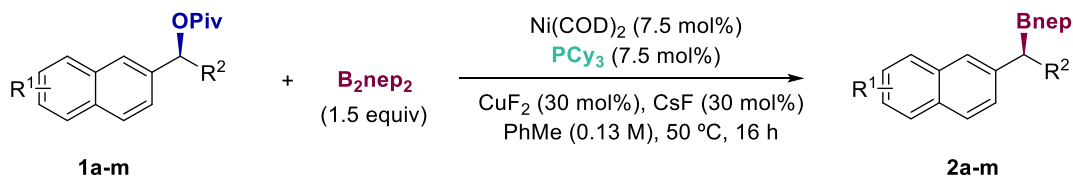
was evacuated and refilled with N₂ three times and then heated at 60 °C for 13h. The reaction mixture was diluted with Et₂O (10 mL), and filtered through silica gel, which was then rinsed with additional Et₂O (10 ml x2). The combined organic layers were concentrated. The resulting residue was purified by silica gel chromatography (hexanes/EtOAc 9/1) to give compound **S-1n** (390 mg, 77%, 95% ee) as colourless oil. $[\alpha]_D^{24} = -25.2^\circ$ (c 0.12, CHCl₃). ¹H NMR (400 MHz, CDCl₃) δ 8.12 – 7.99 (m, 1H), 7.88 – 7.78 (m, 1H), 7.65 (d, *J* = 8.6 Hz, 1H), 7.59 – 7.45 (m, 3H), 5.47 (d, *J* = 6.5 Hz, 1H), 3.98 (s, 3H), 2.25 (s, 1H, OH), 1.59 (d, *J* = 6.5 Hz, 3H). ¹³C NMR (101 MHz, CDCl₃) δ 152.3, 134.4, 133.4, 128.1, 127.7, 126.1, 126.0, 124.7, 123.8, 122.1, 64.7, 62.8, 24.2 ppm. IR (neat, cm⁻¹): 3249, 2960, 1369, 1066, 976, 747. HRMS calcd. for C₁₃H₁₄O₂ (M+Na)⁺: 225.0886, found 225.0896.



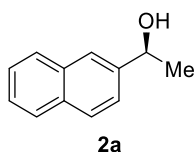
(S)-1-(2-methoxynaphthalen-1-yl)ethanol (S-1o). The following procedure is adapted from the literature.^{II} In a N₂-atmosphere glovebox RuCl[(S,S)-TsDPEN](mesitylene) (13.3mg, 0.021 mmol, 1 mol%) was weighed out into a 25 mL flask. The flask was then capped and removed from glovebox. H₂O (degassed by sparging with N₂, 5mL) was added, and the resulting mixture was stirred at 40 °C for 1h. The ketone **S_m-1o** (500 mg, 2.5 mmol) and NaCOOH (850 mg, 5 equiv.) were added. The flask was evacuated and refilled with N₂ three times and then heated at 50 °C for 13h. The reaction mixture was diluted with Et₂O (10 mL), and filtered through silica gel, which was then rinsed with additional Et₂O (10 ml x2). The combined organic layers were concentrated. The resulting residue was purified by silica gel chromatography (hexanes/EtOAc 9/1) to give compound **S-1o** (120 mg, 24%, 71% ee) as colourless oil. $[\alpha]_D^{24} = -19.4^\circ$ (c 0.51, CHCl₃): ¹H NMR (400 MHz, CDCl₃) δ 8.11 (dt, *J* = 8.4, 0.9 Hz, 1H), 7.87 – 7.68 (m, 2H), 7.49 (dd *J* = 8.6, 6.8 Hz, 1H), 7.36 (dd, *J* = 8.0, 6.7 Hz, 1H), 7.29 (d, *J* = 9.1 Hz, 1H), 5.75 (t, *J* = 7.0 Hz, 1H), 4.01 (s, 3H), 3.98 (s, 1H, OH), 1.68 (d, *J* = 6.8 Hz, 3H) ppm. ¹³C NMR (101 MHz, CDCl₃) δ 154.4, 131.4, 129.5, 129.2, 128.8, 126.8, 125.8, 123.8, 122.9, 113.5, 66.2, 56.5, 23.9 ppm. The spectral data for this compound matches that reported in literature.^{VI}

2.5.3 Stereospecific borylation of benzyl pivalates.

General procedure:



An oven-dried 5 mL screw-capped test tube containing a stirring bar was charged with the benzyl pivalate (51.2 mg, 0.2 mmol). The test tube was introduced in an argon-filled glovebox where $B_2(nep)_2$ (67.8 mg, 0.3 mmol, 1.5 equiv), CuF_2 (6 mg, 30 mol%), CsF (9.1 mg, 30 mol%), $Ni(COD)_2$ (304 μ L, 7.5 mol%, 0.05 M in toluene), PCy_3 (152 μ L, 7.5 mol%, 0.1 M) and toluene (1 mL) were then added sequentially. The tube with the mixture was taken out of the glovebox and stirred at 50 °C for 16 h. The mixture was then allowed to warm to room temperature, diluted with EtOAc (5 mL) and filtered through a Celite® plug, eluting with additional EtOAc (5 mL). The filtrate was concentrated removing the volatiles. Due to the instability of these products in silica gel, the borylated product was transformed into the corresponding benzyl alcohol in order to measure the enantiomeric excess.^{vii} The reaction was cooled to 0 °C (water/ice bath) and BHT (~1mg) was added followed by anhydrous THF (1 mL). An ice-cold degassed mixture of 3 M NaOH (1.2 mL) and 30% aqueous H_2O_2 (0.75 mL) was added all at once. The reaction mixture was stirred at room temperature for 2 h. Then, the reaction mixture was diluted with water (4 mL) and extracted with Et_2O (3 x 10 mL). The combined organic layers were washed with brine and dried over $MgSO_4$. The filtrate was concentrated and purified by silica gel chromatography to give the corresponding benzyl alcohol.



(S)-1-(naphthalen-2-yl)ethanol (2a). The targeted compound was prepared via the General Procedure using Pivalate **1a** (prepared in 99% ee). The crude material was purified by silica gel chromatography (hexanes/EtOAc 9/1) to give compound **2a** (30 mg, 87%) as a white solid (m.p 70-72 °C). The enantiomeric excess was determined to be 94% ee (95% ee_s) by chiral HPLC analysis (CHIRALPAK IB, 1 mL/min, 2% EtOH/Hexane, $\lambda=220$ nm); t_R (major)= 13.6 min, t_R (minor)= 14.8 min. ¹H NMR (500 MHz, $CDCl_3$) δ 7.90 – 7.77 (m, 4H), 7.57 – 7.41 (m, 3H), 5.07 (q, $J = 6.5$ Hz, 1H), 1.96 (s, 1H, OH), 1.59 (d, $J = 6.4$ Hz, 3H) ppm. ¹³C NMR (126 MHz, $CDCl_3$) δ 143.2, 133.3, 132.9, 128.3, 127.9, 127.7, 126.1, 125.8, 123.8, 123.7, 70.5, 25.1 ppm. The spectral data for this compound matches that reported in literature.ⁱⁱ

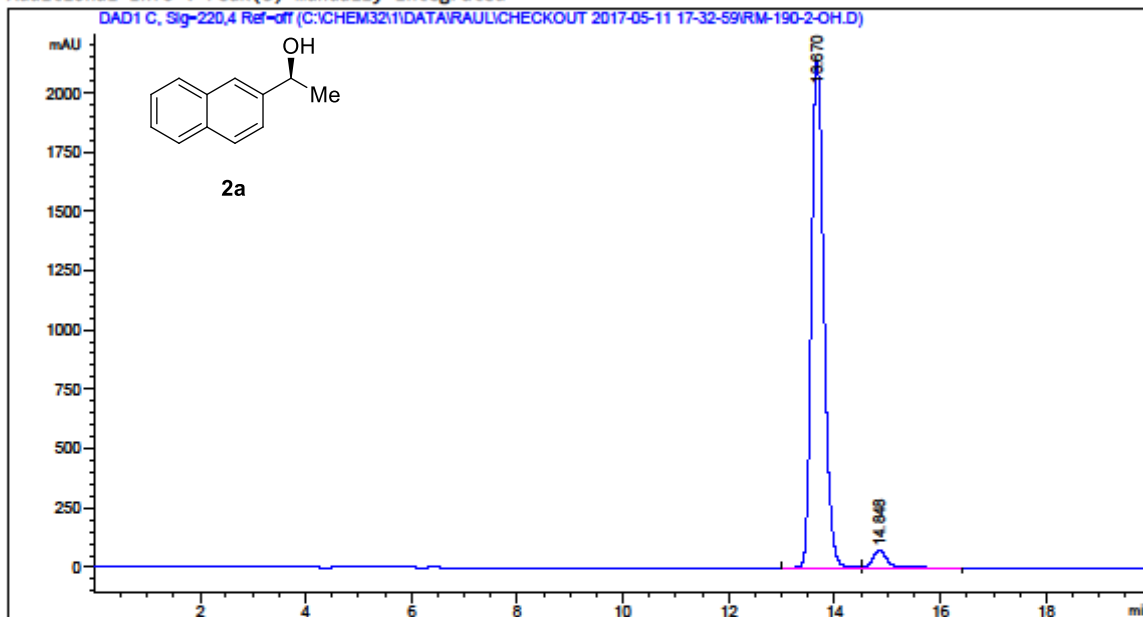
Chapter 2

Data File C:\CHEM32\1\DATA\RAUL\CHECKOUT 2017-05-11 17-32-59\RM-190-2-OH.D
Sample Name: RM-190-2-OH

=====

Acq. Operator	: SYSTEM	Seq. Line	: 2
Acq. Instrument	: HPLC 1260	Location	: 42
Injection Date	: 5/11/2017 5:54:41 PM	Inj	: 1
		Inj Volume	: 1.000 µl

Acq. Method : C:\Chem32\1\Data\Raul\checkout 2017-05-11 17-32-59\Chiral coloumn IB-Raul 98-2.M
Last changed : 5/11/2017 5:32:59 PM by SYSTEM
Analysis Method : C:\Chem32\1\Methods\Chiral coloumn IB-Raul 98-2.M
Last changed : 7/17/2017 5:48:55 PM by SYSTEM
Additional Info : Peak(s) manually integrated



=====
Area Percent Report
=====

Sorted By : Signal
Multiplier : 1.0000
Dilution : 1.0000
Use Multiplier & Dilution Factor with ISTDs

Signal 1: DAD1 C, Sig=220,4 Ref=off

Peak #	RetTime [min]	Type	Width [min]	Area [mAU*s]	Height [mAU]	Area %
1	13.670	BV	0.2534	3.46898e4	2137.00098	96.6129
2	14.848	VB	0.2563	1216.18481	72.28838	3.3871

Totals : 3.59060e4 2209.28935

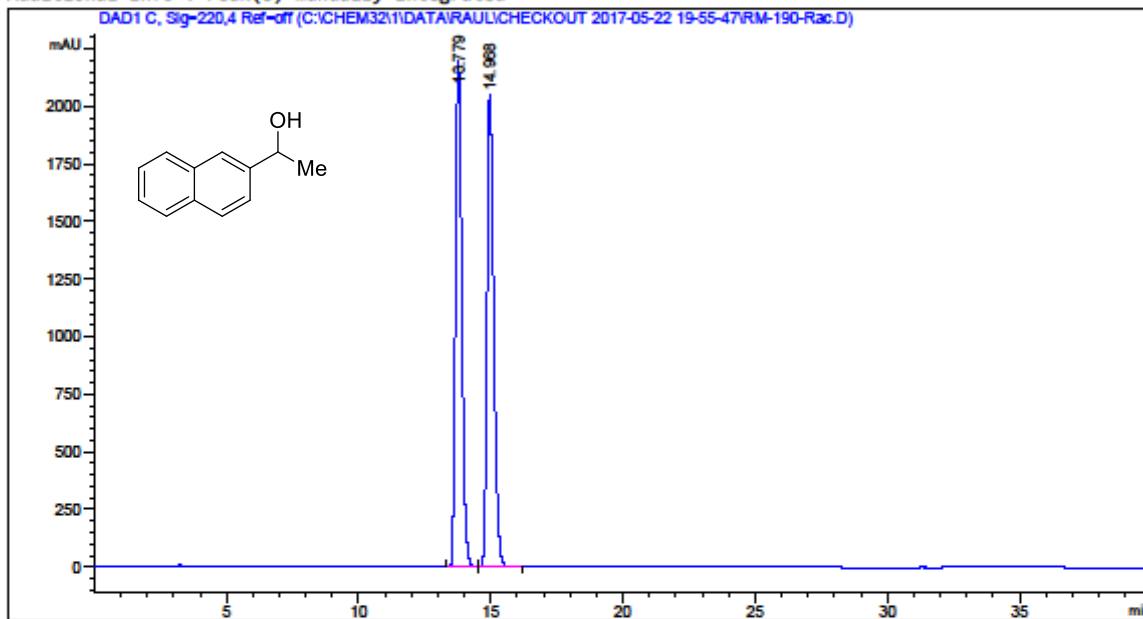
Stereospecific Borylation of Benzyl C(sp³)-O Bonds

Data File C:\CHEM32\1\DATA\RAUL\CHECKOUT 2017-05-22 19-55-47\RM-190-Rac.D
Sample Name: RM-190-Rac

=====

Acq. Operator	: SYSTEM	Seq. Line	: 2
Acq. Instrument	: HPLC 1260	Location	: 81
Injection Date	: 5/22/2017 8:38:13 PM	Inj	: 1
		Inj Volume	: 1.000 µl

Acq. Method : C:\Chem32\1\Data\Raul\checkout 2017-05-22 19-55-47\Chiral coloumn IB-Raul
98-2.M
Last changed : 5/22/2017 7:55:47 PM by SYSTEM
Analysis Method : C:\Chem32\1\Methods\Chiral coloumn IB-Raul 98-2.M
Last changed : 7/17/2017 5:48:55 PM by SYSTEM
Additional Info : Peak(s) manually integrated



=====
Area Percent Report
=====

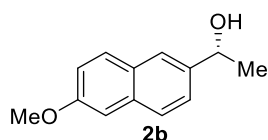
Sorted By : Signal
Multiplier : 1.0000
Dilution : 1.0000
Use Multiplier & Dilution Factor with ISTDs

Signal 1: DAD1 C, Sig=220,4 Ref=off

Peak #	RetTime [min]	Type	Width [min]	Area [mAU*s]	Height [mAU]	Area %
1	13.779	BB	0.2562	3.62079e4	2198.26904	49.6298
2	14.968	BB	0.2772	3.67481e4	2049.04468	50.3702

Totals : 7.29560e4 4247.31372

Chapter 2



(R)-1-(6-methoxynaphthalen-2-yl)ethanol (2b). The targeted compound was prepared via the General Procedure using Pivalate **1b** (prepared in 87% ee). The crude material was purified by silica gel chromatography (hexanes/EtOAc 9/1) to give compound **2b** (33 mg, 80%) as a white solid (m.p 110-112 °C). The enantiomeric excess was determined to be 85% ee (98% ee_s) by chiral HPLC analysis (CHIRALPAK IB, 1 mL/min, 2% EtOH/Hexane, λ=220 nm); *t*_R(minor)= 17.3 min, *t*_R(major)= 23.3 min. ¹H NMR (400 MHz, CDCl₃) δ 7.79 – 7.67 (m, 3H), 7.47 (dd, *J* = 8.6, 1.7 Hz, 1H), 7.22 – 7.10 (m, 2H), 5.03 (q, *J* = 6.5 Hz, 1H), 3.92 (s, 3H), 1.95 (s, 1H, OH), 1.57 (d, *J* = 6.5 Hz, 3H) ppm. ¹³C NMR (126 MHz, CDCl₃) δ 157.6, 140.9, 134.0, 129.4, 128.7, 127.1, 124.3, 123.7, 118.9, 105.7, 70.5, 55.3, 25.0 ppm. The spectral data for this compound matches that reported in literature.^{vii}

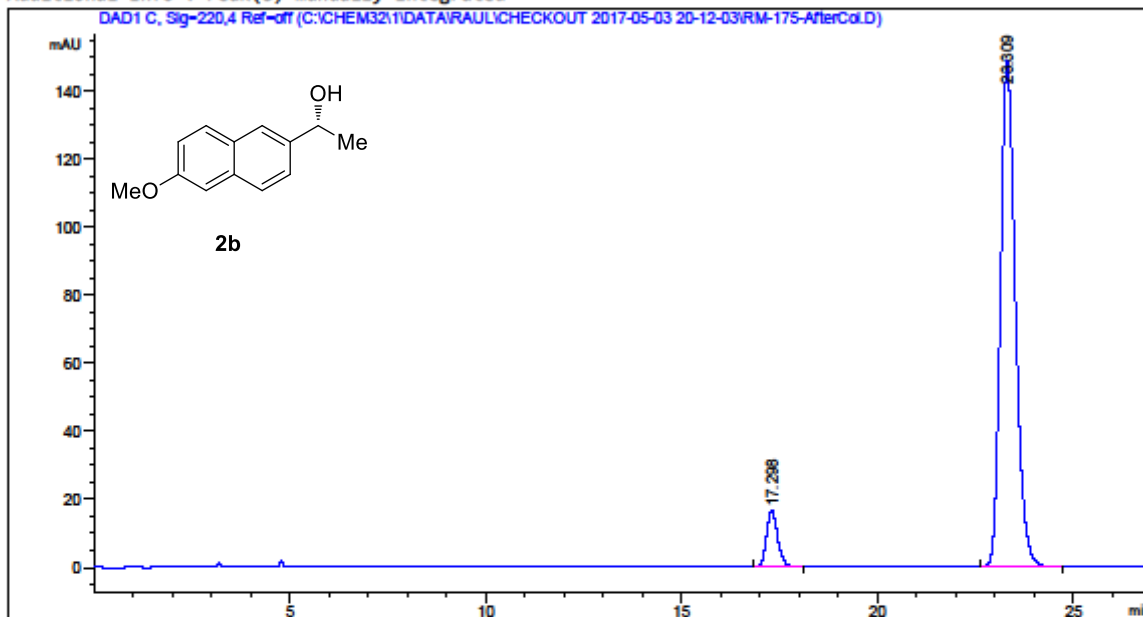
Stereospecific Borylation of Benzyl C(sp³)-O Bonds

Data File C:\CHEM32\1\DATA\RAUL\CHECKOUT 2017-05-03 20-12-03\RM-175-AfterCol.D
Sample Name: RM-175-AfterCol

=====

Acq. Operator	: SYSTEM	Seq. Line	: 1
Acq. Instrument	: HPLC 1260	Location	: 81
Injection Date	: 5/3/2017 8:13:17 PM	Inj	: 1
		Inj Volume	: 1.000 µl

Acq. Method : C:\Chem32\1\Data\Raul\checkout 2017-05-03 20-12-03\Chiral coloumn IB-Raul 98-2.M
Last changed : 5/3/2017 8:12:03 PM by SYSTEM
Analysis Method : C:\Chem32\1\Methods\Chiral coloumn IB-Raul 98-2.M
Last changed : 7/17/2017 5:48:55 PM by SYSTEM
Additional Info : Peak(s) manually integrated



=====
Area Percent Report
=====

Sorted By : Signal
Multiplier : 1.0000
Dilution : 1.0000
Use Multiplier & Dilution Factor with ISTDs

Signal 1: DAD1 C, Sig=220,4 Ref=off

Peak #	RetTime [min]	Type	Width [min]	Area [mAU*s]	Height [mAU]	Area %
1	17.298	BB	0.2964	321.62885	16.57477	7.6107
2	23.309	BB	0.4022	3904.40381	148.77463	92.3893

Totals : 4226.03265 165.34940

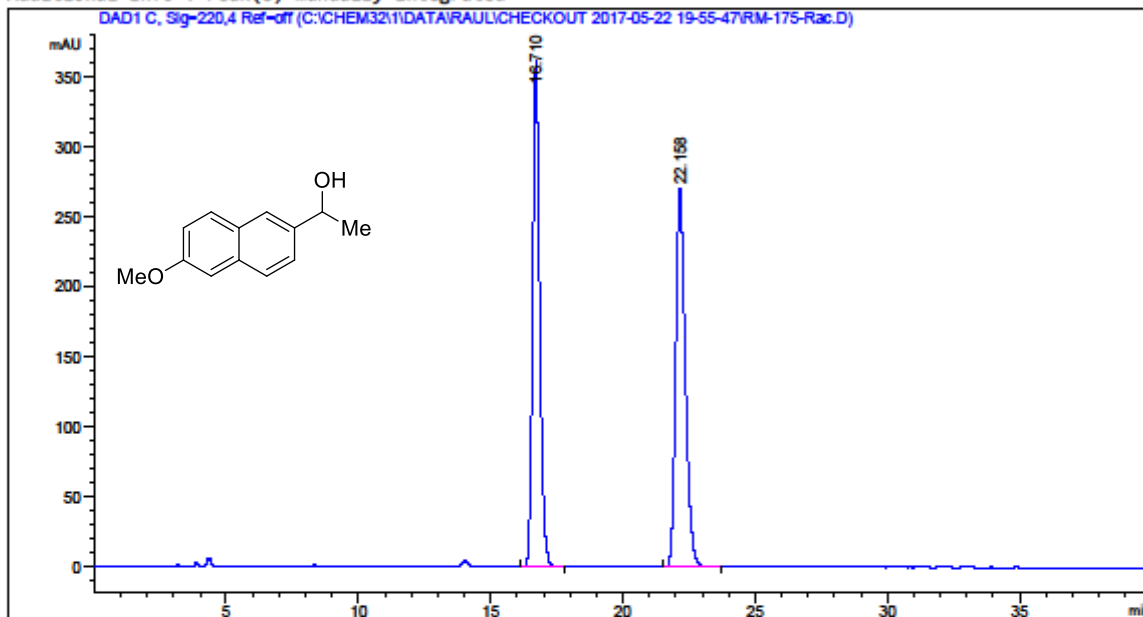
Chapter 2

Data File C:\CHEM32\1\DATA\RAUL\CHECKOUT 2017-05-22 19-55-47\RM-175-Rac.D
Sample Name: RM-175-Rac

=====

Acq. Operator	: SYSTEM	Seq. Line	: 8
Acq. Instrument	: HPLC 1260	Location	: 87
Injection Date	: 5/23/2017 12:43:23 AM	Inj	: 1
		Inj Volume	: 1.000 µl

Acq. Method : C:\Chem32\1\Data\Raul\checkout 2017-05-22 19-55-47\Chiral coloumn IB-Raul 98-2.M
Last changed : 5/22/2017 7:55:47 PM by SYSTEM
Analysis Method : C:\Chem32\1\Methods\Chiral coloumn IB-Raul 98-2.M
Last changed : 7/17/2017 5:48:55 PM by SYSTEM
Additional Info : Peak(s) manually integrated



=====
Area Percent Report
=====

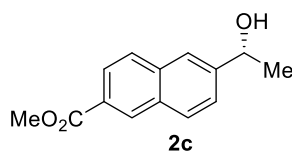
Sorted By : Signal
Multiplier : 1.0000
Dilution : 1.0000
Use Multiplier & Dilution Factor with ISTDs

Signal 1: DAD1 C, Sig=220,4 Ref=off

Peak #	RetTime [min]	Type	Width [min]	Area [mAU*s]	Height [mAU]	Area %
1	16.710	BB	0.2870	6796.98145	362.08362	49.9799
2	22.158	BB	0.3833	6802.45068	270.61493	50.0201

Totals : 1.35994e4 632.69855

Stereospecific Borylation of Benzyl C(sp³)-O Bonds



(R)-methyl 6-(1-hydroxyethyl)-2-naphthoate (2c). The targeted compound was prepared via the General Procedure using Pivalate **1c** (prepared in 92% ee). The crude material was purified by silica gel chromatography (hexanes/EtOAc 9/1) to give compound **2c** (39 mg, 85%) as a white solid (m.p 74-76 °C). The enantiomeric excess was determined to be 85% ee (92% ee_s) by chiral HPLC analysis (CHIRALPAK IB, 1 mL/min, 2% EtOH/Hexane, λ=220 nm); *t_R*(minor)= 22.9 min, *t_R*(major)= 28.7 min. ¹H NMR (400 MHz, CDCl₃) δ 8.58 (dd, *J* = 1.8, 0.9 Hz, 1H), 8.05 (dd, *J* = 8.6, 1.7 Hz, 1H), 7.94 (d, *J* = 8.5 Hz, 1H), 7.89 – 7.83 (m, 2H), 7.57 (dd, *J* = 8.5, 1.7 Hz, 1H), 5.09 (q, *J* = 6.5 Hz, 1H), 3.98 (s, 3H), 2.01 (s, 1H, OH), 1.59 (d, *J* = 6.5 Hz, 3H) ppm. ¹³C NMR (126 MHz, CDCl₃) δ 167.2, 145.8, 135.5, 131.9, 130.8, 129.7, 128.1, 127.3, 125.5, 124.7, 123.6, 70.4, 52.2, 25.2 ppm. The spectral data for this compound matches that reported in literature.^{vii}

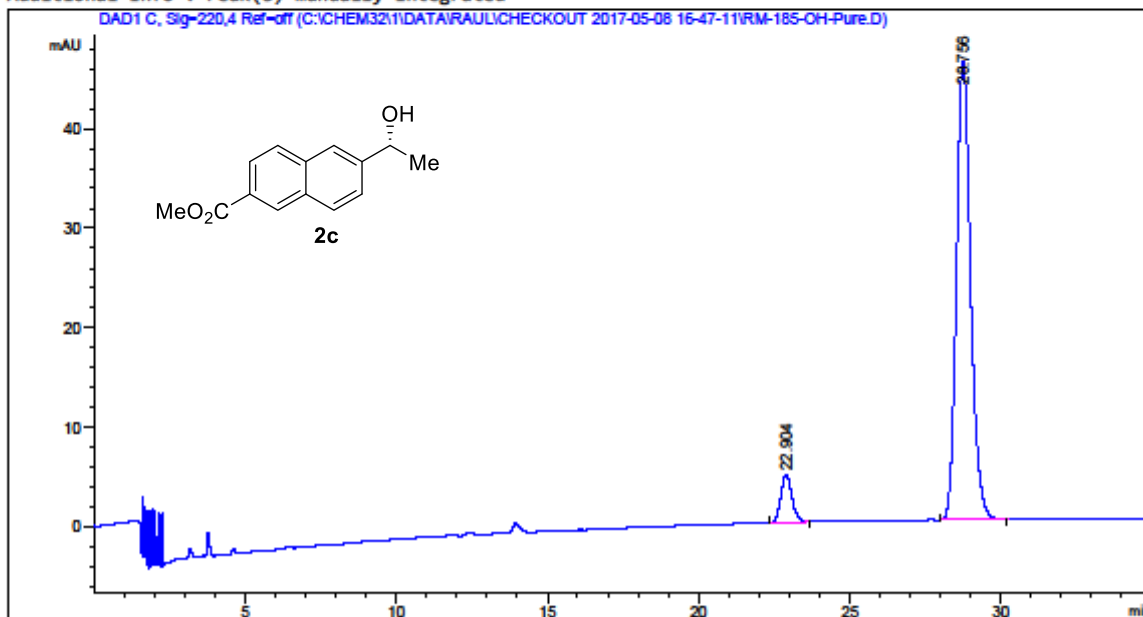
Chapter 2

Data File C:\CHEM32\1\DATA\RAUL\CHECKOUT 2017-05-08 16-47-11\RM-185-OH-Pure.D
Sample Name: RM-185-OH-Pure

=====

Acq. Operator	: SYSTEM	Seq. Line	: 1
Acq. Instrument	: HPLC 1260	Location	: 31
Injection Date	: 5/8/2017 4:49:04 PM	Inj	: 1
		Inj Volume	: 1.000 µl

Acq. Method : C:\Chem32\1\Data\Raul\checkout 2017-05-08 16-47-11\Chiral coloumn IB-Raul 98-2.M
Last changed : 5/8/2017 4:47:11 PM by SYSTEM
Analysis Method : C:\Chem32\1\Methods\Chiral coloumn IB-Raul 98-2.M
Last changed : 7/17/2017 5:48:55 PM by SYSTEM
Additional Info : Peak(s) manually integrated



=====
Area Percent Report
=====

Sorted By : Signal
Multiplier : 1.0000
Dilution : 1.0000
Use Multiplier & Dilution Factor with ISTDs

Signal 1: DAD1 C, Sig=220,4 Ref=off

Peak #	RetTime [min]	Type	Width [min]	Area [mAU*s]	Height [mAU]	Area %
1	22.904	BB	0.3908	123.06052	4.80450	7.6160
2	28.756	BB	0.4944	1492.75366	46.02183	92.3840

Totals : 1615.81418 50.82633

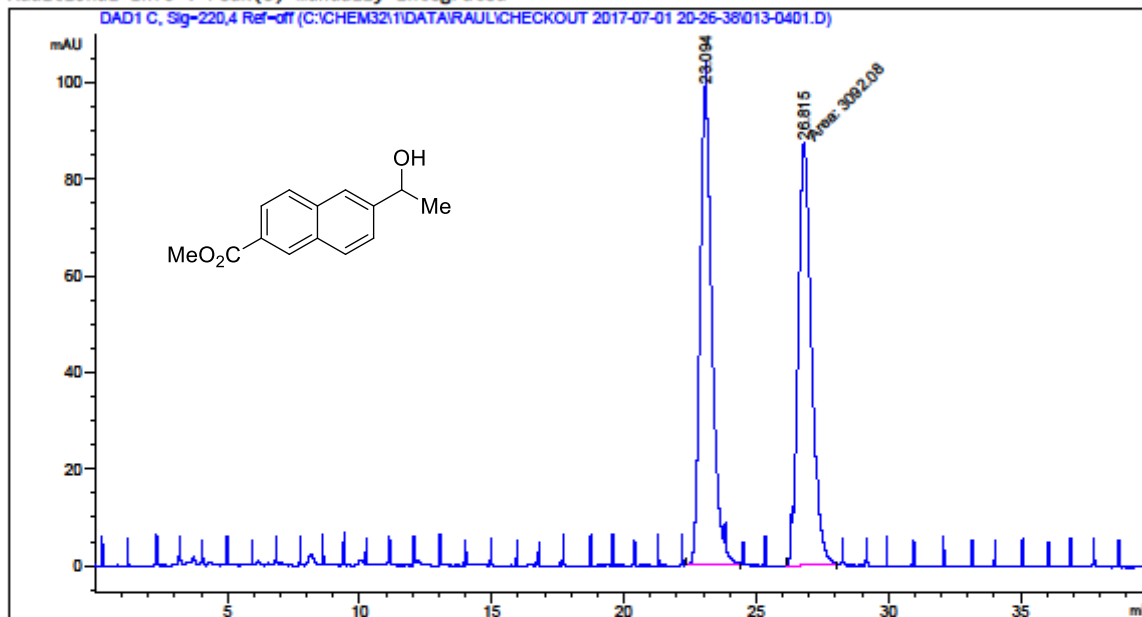
Stereospecific Borylation of Benzyl C(sp³)-O Bonds

Data File C:\CHEM32\1\DATA\RAUL\CHECKOUT 2017-07-01 20-26-38\013-0401.D
Sample Name: RT-3

=====

Acq. Operator	: SYSTEM	Seq. Line	: 4
Acq. Instrument	: HPLC 1260	Location	: 13
Injection Date	: 7/1/2017 10:29:31 PM	Inj	: 1
		Inj Volume	: 1.000 µl

Acq. Method : C:\Chem32\1\Data\Raul\checkout 2017-07-01 20-26-38\Chiral column IB-Raul 98-2.M
Last changed : 7/1/2017 8:26:38 PM by SYSTEM
Analysis Method : C:\Chem32\1\Methods\Chiral column IB-Raul 98-2.M
Last changed : 7/21/2017 9:40:12 AM by SYSTEM
Additional Info : Peak(s) manually integrated



=====
Area Percent Report
=====

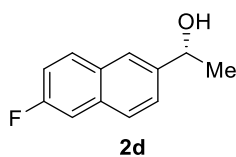
Sorted By : Signal
Multiplier : 1.0000
Dilution : 1.0000
Use Multiplier & Dilution Factor with ISTDs

Signal 1: DAD1 C, Sig=220,4 Ref=off

Peak #	RetTime [min]	Type	Width [min]	Area [mAU*s]	Height [mAU]	Area %
1	23.094	BV R	0.3590	3116.58447	104.40434	50.1973
2	26.815	MM	0.5895	3092.07983	87.41578	49.8027

Totals : 6208.66431 191.82011

Chapter 2



(R)-1-(6-fluoronaphthalen-2-yl)ethanol (2d). The targeted compound was prepared via the General Procedure using Pivalate **1d** (prepared in 74% ee). The crude material was purified by silica gel chromatography (hexanes/EtOAc 9/1) to give compound **2d** (30.5 mg, 80%) as a white solid (mp 84-86 °C). The enantiomeric excess was determined to be 65% ee (88% ee_s) by chiral HPLC analysis (CHIRALPAK IB, 1 mL/min, 2% EtOH/Hexane, λ=220 nm); *t_R*(minor)= 12.4 min, *t_R*(major)= 13.9 min. [α]_D²⁴ = 43.2° (c 0.06, CHCl₃); ¹H-NMR (500 MHz, CDCl₃): δ 7.83-7.76 (m, 3H), 7.53 (dd, *J* = 2.0 Hz, 1H), 7.44 (dd, *J* = 2.6 Hz, 1H), 7.26 (td, *J* = 2.6 Hz, 1H), 5.06 (q, *J* = 6.4 Hz, 1H), 1.97 (s, 1H, OH), 1.58 (d, *J* = 6.4 Hz, 3H) ppm. ¹³C NMR (126 MHz, CDCl₃) δ 161.8, 159.4, 142.5, 133.6, 130.3, 127.7, 124.9, 123.8, 116.6, 110.7, 70.3, 25.2 ppm. ¹⁹F NMR (376 MHz, CDCl₃) δ -115.1 ppm.

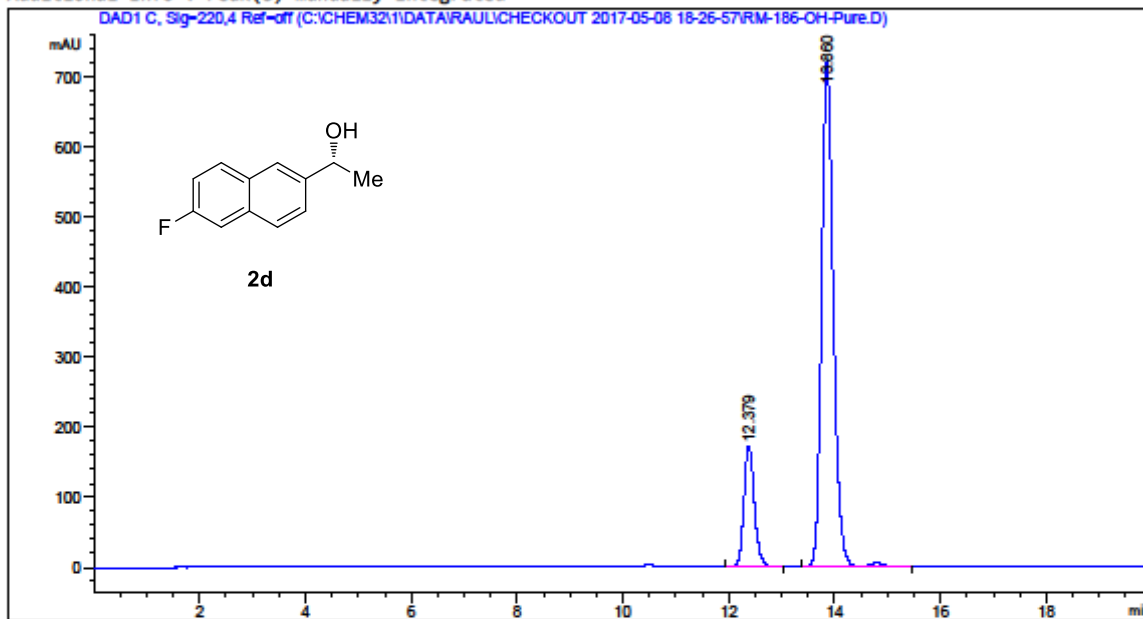
Stereospecific Borylation of Benzyl C(sp³)-O Bonds

Data File C:\CHEM32\1\DATA\RAUL\CHECKOUT 2017-05-08 18-26-57\RM-186-OH-Pure.D
Sample Name: RM-186-OH-Pure

=====

Acq. Operator	: SYSTEM	Seq. Line	: 2
Acq. Instrument	: HPLC 1260	Location	: 4
Injection Date	: 5/8/2017 6:49:51 PM	Inj	: 1
		Inj Volume	: 1.000 µl

Acq. Method : C:\Chem32\1\Data\Raul\checkout 2017-05-08 18-26-57\Chiral coloumn IB-Raul 98-2.M
Last changed : 5/8/2017 6:26:58 PM by SYSTEM
Analysis Method : C:\Chem32\1\Methods\Chiral coloumn IB-Raul 98-2.M
Last changed : 7/17/2017 5:48:55 PM by SYSTEM
Additional Info : Peak(s) manually integrated



=====
Area Percent Report
=====

Sorted By : Signal
Multiplier : 1.0000
Dilution : 1.0000
Use Multiplier & Dilution Factor with ISTDs

Signal 1: DAD1 C, Sig=220,4 Ref=off

Peak #	RetTime [min]	Type	Width [min]	Area [mAU*s]	Height [mAU]	Area %
1	12.379	BB	0.2094	2362.70264	172.94595	17.3299
2	13.860	BV R	0.2380	1.12710e4	723.37933	82.6701

Totals : 1.36337e4 896.32529

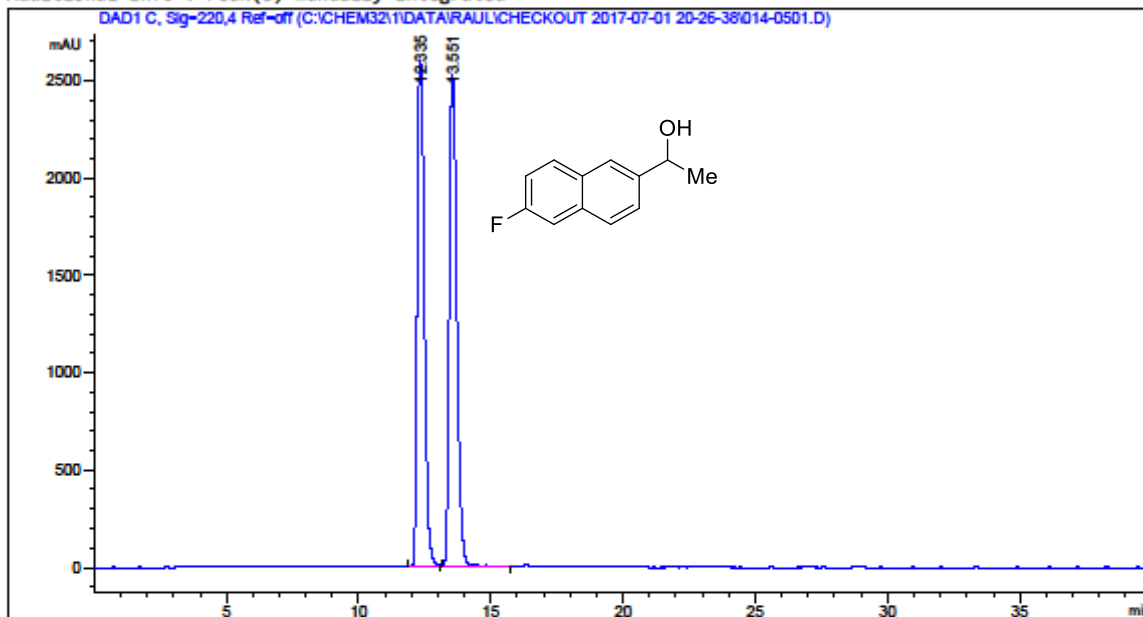
Chapter 2

Data File C:\CHEM32\1\DATA\RAUL\CHECKOUT 2017-07-01 20-26-38\014-0501.D
Sample Name: RT4

=====

Acq. Operator	: SYSTEM	Seq. Line	: 5
Acq. Instrument	: HPLC 1260	Location	: 14
Injection Date	: 7/1/2017 11:10:24 PM	Inj	: 1
		Inj Volume	: 1.000 µl

Acq. Method : C:\Chem32\1\Data\Raul\checkout 2017-07-01 20-26-38\Chiral coloumn IB-Raul 98-2.M
Last changed : 7/1/2017 8:26:38 PM by SYSTEM
Analysis Method : C:\Chem32\1\Methods\Chiral coloumn IB-Raul 98-2.M
Last changed : 7/21/2017 9:40:12 AM by SYSTEM
Additional Info : Peak(s) manually integrated



=====
Area Percent Report
=====

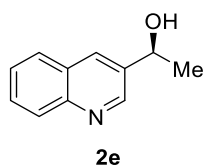
Sorted By : Signal
Multiplier : 1.0000
Dilution : 1.0000
Use Multiplier & Dilution Factor with ISTDs

Signal 1: DAD1 C, Sig=220,4 Ref=off

Peak #	RetTime [min]	Type	Width [min]	Area [mAU*s]	Height [mAU]	Area %
1	12.335	BV	0.2913	4.84631e4	2602.06543	48.9588
2	13.551	VV R	0.3125	5.05244e4	2533.07715	51.0412

Totals : 9.89875e4 5135.14258

Stereospecific Borylation of Benzyl C(sp³)-O Bonds



(S)-1-(quinolin-3-yl)ethanol (2e). The targeted compound was prepared via the General Procedure using Pivalate **1e** (prepared in 77% ee). The crude material was purified by silica gel chromatography (hexanes/EtOAc 1/1) to give compound **2e** (25 mg, 72%) as a light brown oil. The enantiomeric excess was determined to be 44% ee (57% ee_s) by chiral HPLC analysis (CHIRALPAK IB, 1 mL/min, 4% EtOH/Hexane, λ=220 nm); *t*_R(major)= 17.3 min, *t*_R(minor)= 19.3 min. ¹H NMR (400 MHz, CDCl₃) δ 8.91 (d, *J* = 2.2 Hz, 1H), 8.19 – 8.06 (m, 2H), 7.81 (dd, *J* = 8.1, 1.4 Hz, 1H), 7.69 (dd, *J* = 8.4, 6.9 Hz, 1H), 7.55 (dd, *J* = 8.1, 6.9 Hz, 1H), 5.14 (q, *J* = 6.3 Hz, 1H), 1.75 (s, 1H, OH), 1.62 (d, *J* = 6.5 Hz, 3H), ppm. ¹³C NMR (100 MHz, CDCl₃) δ 149.3, 147.6, 138.2, 131.9, 129.3, 129.1, 127.8, 127.8, 126.6, 68.4, 25.3 ppm. The spectral data for this compound matches that reported in literature.^{vii}

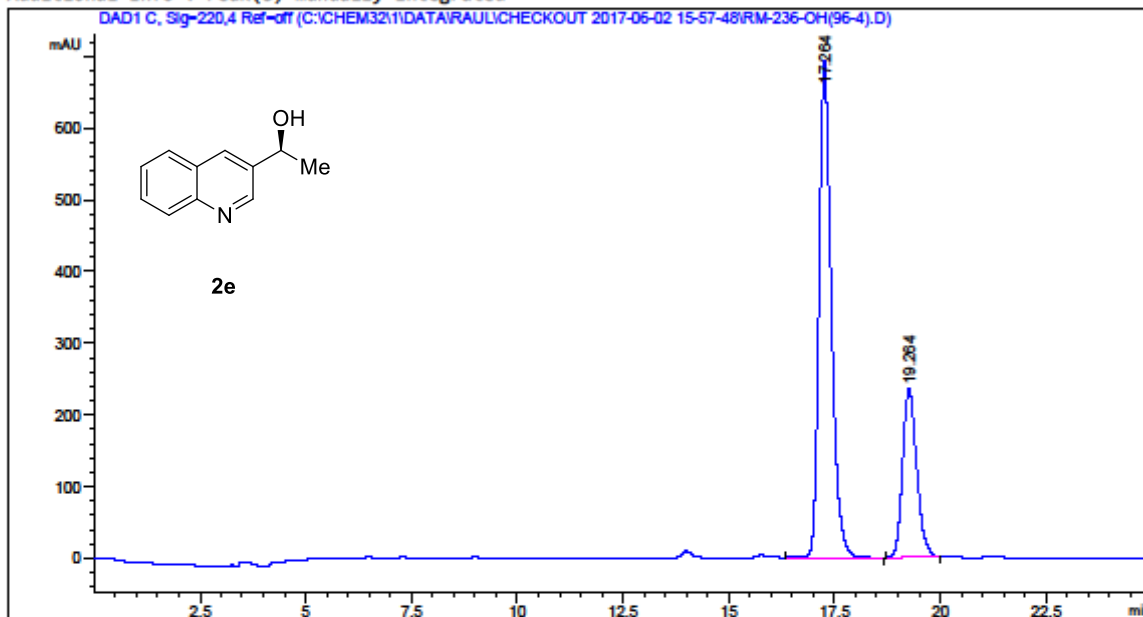
Chapter 2

Data File C:\CHEM32\1\DATA\RAUL\CHECKOUT 2017-06-02 15-57-48\RM-236-OH(96-4).D
Sample Name: RM-236-OH(96-4)

=====

Acq. Operator	: SYSTEM	Seq. Line	: 1
Acq. Instrument	: HPLC 1260	Location	: 3
Injection Date	: 6/2/2017 3:58:38 PM	Inj	: 1
		Inj Volume	: 1.000 µl

Acq. Method : C:\Chem32\1\Data\Raul\checkout 2017-06-02 15-57-48\Chiral coloumn IB-Raul 98-2.M
Last changed : 6/2/2017 3:57:48 PM by SYSTEM
Analysis Method : C:\Chem32\1\Methods\Chiral coloumn IB-Raul 98-2.M
Last changed : 7/17/2017 5:48:55 PM by SYSTEM
Additional Info : Peak(s) manually integrated



=====
Area Percent Report
=====

Sorted By : Signal
Multiplier : 1.0000
Dilution : 1.0000
Use Multiplier & Dilution Factor with ISTDs

Signal 1: DAD1 C, Sig=220,4 Ref=off

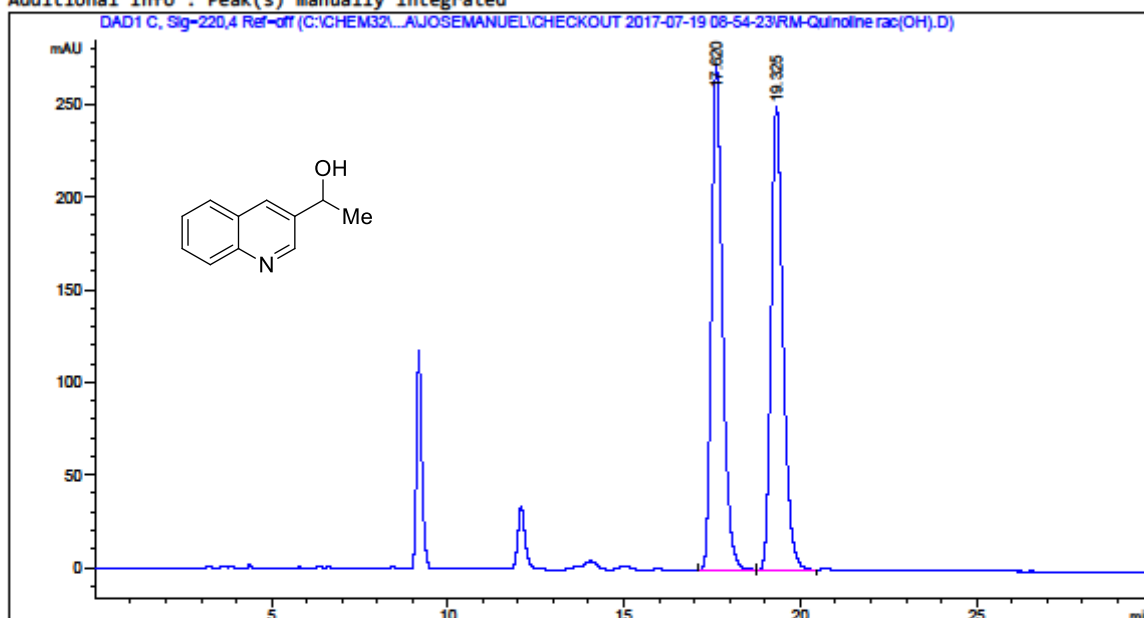
Peak #	RetTime [min]	Type	Width [min]	Area [mAU*s]	Height [mAU]	Area %
1	17.264	BB	0.3048	1.39578e4	693.39600	72.0017
2	19.264	BB	0.3515	5427.57178	236.69380	27.9983

Totals : 1.93854e4 930.08980

Stereospecific Borylation of Benzyl C(sp³)-O Bonds

Data File C:\CHEM32\1\DATA\JOSEMANUEL\CHECKOUT 2017-07-19 08-54-23\RM-Quinoline rac(OH).D
Sample Name: RM-Quinoline rac(OH)

```
=====
Acq. Operator   : SYSTEM                      Seq. Line :    2
Acq. Instrument : HPLC 1260                  Location  :   15
Injection Date  : 7/19/2017 9:26:02 AM      Inj       :    1
                                           Inj Volume: 1.000 µl
Acq. Method     : C:\Chem32\1\Data\JoseManuel\checkout 2017-07-19 08-54-23\Chiral coloumn IB-
                                           Raul 98-2.M
Last changed    : 7/19/2017 8:54:23 AM by SYSTEM
Analysis Method : C:\Chem32\1\Data\Raul\checkout 2017-07-25 09-32-31\Chiral coloumn IB-Raul
                                           99.5(1 BOTTLE).M (Sequence Method)
Last changed    : 7/25/2017 9:32:40 AM by SYSTEM
Additional Info  : Peak(s) manually integrated
=====
```



=====
Area Percent Report
=====

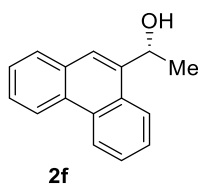
```
Sorted By      : Signal
Multiplier     : 1.0000
Dilution       : 1.0000
Use Multiplier & Dilution Factor with ISTDs
```

Signal 1: DAD1 C, Sig=220,4 Ref=off

Peak #	RetTime [min]	Type	Width [min]	Area [mAU*s]	Height [mAU]	Area %
1	17.620	BB	0.3296	5927.14404	272.65103	50.1211
2	19.325	BB	0.3613	5898.50293	249.97992	49.8789

Totals : 1.18256e4 522.63095

Chapter 2



(R)-1-(phenanthren-9-yl)ethanol (2f). The targeted compound was prepared via the General Procedure using Pivalate **1f** (prepared in 89% ee). The crude material was purified by silica gel chromatography (hexanes/EtOAc 9/1) to give compound **2f** (33.4 mg, 75%) as a white solid (m.p 101-103 °C). The enantiomeric excess was determined to be 68% ee (76% ee_s) by chiral HPLC analysis (CHIRALPAK IB, 1 mL/min, 2% EtOH/Hexane, λ=220 nm); *t*_R(minor)= 14.4 min, *t*_R(major)= 19.5 min. ¹H NMR (400 MHz, CDCl₃) δ 8.80 – 8.74 (m, 1H), 8.72 – 8.63 (m, 1H), 8.17 (dd, *J* = 7.5, 2.0 Hz, 1H), 7.98 – 7.87 (m, 2H), 7.75 – 7.55 (m, 4H), 5.69 (q, *J* = 6.5 Hz, 1H), 2.01 (s, 1H, OH), 1.74 (d, *J* = 6.4 Hz, 3H) ppm. ¹³C NMR (126 MHz, CDCl₃) δ 139.5, 131.5, 130.8, 130.0, 129.6, 128.8, 126.7, 126.6, 126.5, 126.3, 123.9, 123.3, 122.7, 122.4, 67.2 24.1 ppm. The spectral data for this compound matches that reported in literature.^{IV}

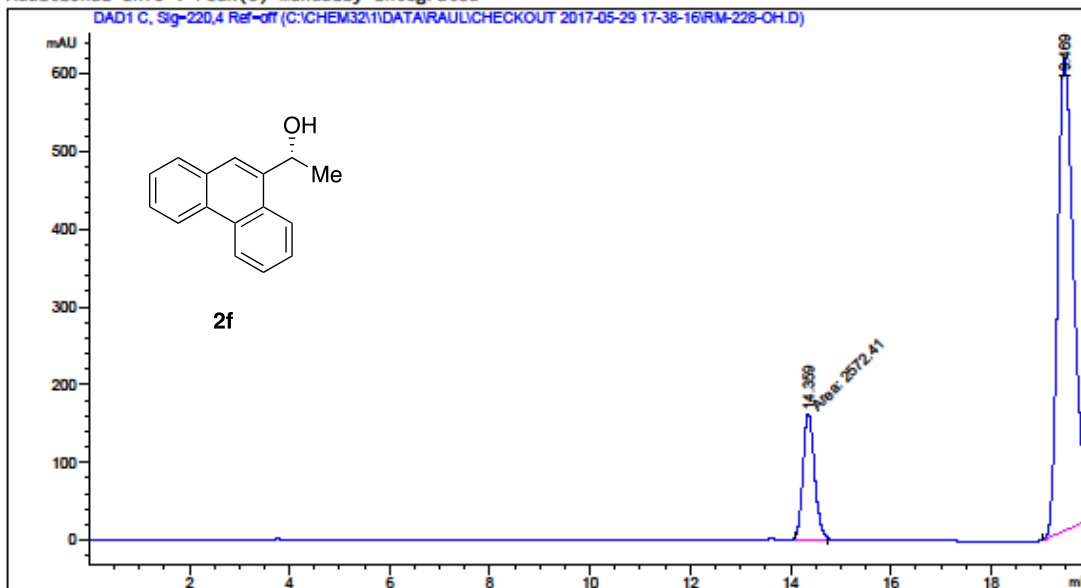
Stereospecific Borylation of Benzyl C(sp³)-O Bonds

Data File C:\CHEM32\1\DATA\RAUL\CHECKOUT 2017-05-29 17-38-16\RM-228-OH.D
Sample Name: RM-228-OH

=====

Acq. Operator	: SYSTEM	Seq. Line	: 3
Acq. Instrument	: HPLC 1260	Location	: 38
Injection Date	: 5/29/2017 6:20:48 PM	Inj	: 1
		Inj Volume	: 1.000 µl

Acq. Method : C:\Chem32\1\Data\Raul\checkout 2017-05-29 17-38-16\Chiral column IB-Raul 98-2.M
Last changed : 5/29/2017 5:38:16 PM by SYSTEM
Analysis Method : C:\Chem32\1\Methods\Chiral column IB-Raul 98-2.M
Last changed : 7/17/2017 5:48:55 PM by SYSTEM
Additional Info : Peak(s) manually integrated



=====
Area Percent Report
=====

Sorted By : Signal
Multiplier : 1.0000
Dilution : 1.0000
Use Multiplier & Dilution Factor with ISTDs

Signal 1: DAD1 C, Sig=220,4 Ref=off

Peak #	RetTime [min]	Type	Width [min]	Area [mAU*s]	Height [mAU]	Area %
1	14.359	MM	0.2659	2572.41187	161.25642	16.1864
2	19.469	BBA	0.3376	1.33200e4	607.94171	83.8136

Totals : 1.58924e4 769.19814

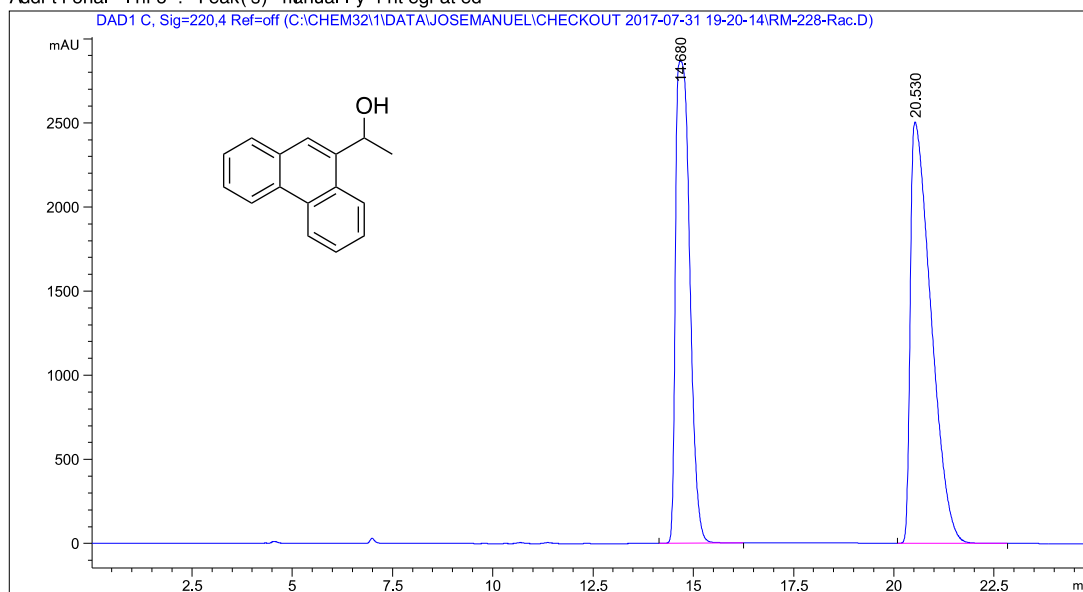
Chapter 2

Data File C:\CHEM82\1\DATA\JOSEMANUEL\CHECKOUT 2017-07-31 19-20-14\FM 228-Rac.D
 Sample Name: FM 228-Rac

```

=====
Acq. Operator   : SYSTEM                      Seq. Line :    2
Acq. Instrument : HPLC 1260                   Location  :   71
Injection Date  : 7/31/2017 7:46:25 PM       Inj       :    1
                                           Inj Volume: 1.000 µl

Method         : C:\Chem82\1\Dat a\JoseManuel\checkout 2017-07-31 19-20-14\Chiral column IB-
                Paul 98-2.M (Sequence Method)
Last changed   : 7/31/2017 7:20:14 PM by SYSTEM
Additional Info: Peak(s) manually integrated
  
```



Area Percent Report

```

Sorted By      : Signal
Multiplier     : 1.0000
Dilution       : 1.0000
Use Multiplier & Dilution Factor with ISTDs
  
```

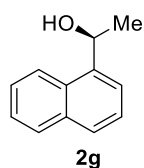
Signal 1: DAD1 C, Sig=220,4 Ref=off

Peak #	Ret Time [min]	Type	Width [min]	Area [mAU*s]	Height [mAU]	Area %
1	14.680	BB	0.3919	7.07513e4	2866.98315	44.0974
2	20.530	BB	0.5518	8.96920e4	2504.26343	55.9026

Totals : 1.60443e5 5371.24658

*** End of Report ***

Stereospecific Borylation of Benzyl C(sp³)-O Bonds



(S)-1-(naphthalen-1-yl)ethanol (2g). The targeted compound was prepared via the General Procedure using Pivalate **1g** (prepared in 98% ee). The crude material was purified by silica gel chromatography (hexanes/EtOAc 9/1) to give compound **2g** (25 mg, 73%) as a yellow oil. The enantiomeric excess was determined to be 87% ee (89% ee_s) by chiral HPLC analysis (CHIRALPAK IB, 1 mL/min, 2% EtOH/Hexane, λ=220 nm); *t*_R(major)= 14.3 min, *t*_R(minor)= 18.0 min. ¹H NMR (500 MHz, CDCl₃) δ 8.13 (dq, *J* = 8.7, 1.0 Hz, 1H), 7.92 – 7.84 (m, 1H), 7.79 (dt, *J* = 8.2, 1.0 Hz, 1H), 7.68 (dt, *J* = 7.1, 1.0 Hz, 1H), 7.58 – 7.43 (m, 3H), 5.68 (q, *J* = 6.5 Hz, 1H), 1.96 (s, 1H, OH), 1.68 (d, *J* = 6.5 Hz, 3H) ppm. ¹³C NMR (126 MHz, CDCl₃) δ 141.3, 133.8, 130.3, 128.9, 127.9, 126.0, 125.5, 125.5, 123.2, 122.0, 67.1, 24.3 ppm. The spectral data for this compound matches that reported in literature.^{viii}

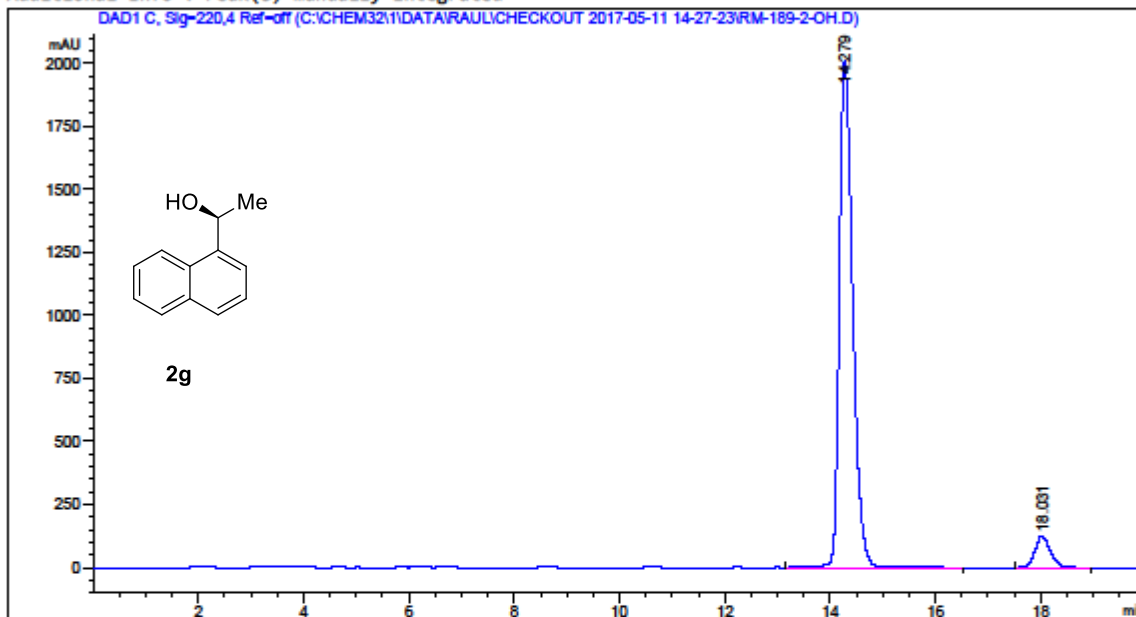
Chapter 2

Data File C:\CHEM32\1\DATA\RAUL\CHECKOUT 2017-05-11 14-27-23\RM-189-2-OH.D
Sample Name: RM-189-2-OH

=====

Acq. Operator	: SYSTEM	Seq. Line	: 2
Acq. Instrument	: HPLC 1260	Location	: 71
Injection Date	: 5/11/2017 2:48:30 PM	Inj	: 1
		Inj Volume	: 1.000 µl

Acq. Method : C:\Chem32\1\Data\Raul\checkout 2017-05-11 14-27-23\Chiral coloumn IB-Raul 98-2.M
Last changed : 5/11/2017 2:27:24 PM by SYSTEM
Analysis Method : C:\Chem32\1\Methods\Chiral coloumn IB-Raul 98-2.M
Last changed : 7/17/2017 5:48:55 PM by SYSTEM
Additional Info : Peak(s) manually integrated



=====
Area Percent Report
=====

Sorted By : Signal
Multiplier : 1.0000
Dilution : 1.0000
Use Multiplier & Dilution Factor with ISTDs

Signal 1: DAD1 C, Sig=220,4 Ref=off

Peak #	RetTime [min]	Type	Width [min]	Area [mAU*s]	Height [mAU]	Area %
1	14.279	VB R	0.2704	3.52513e4	2010.54358	93.4342
2	18.031	BB	0.3042	2477.17773	124.46545	6.5658

Totals : 3.77285e4 2135.00903

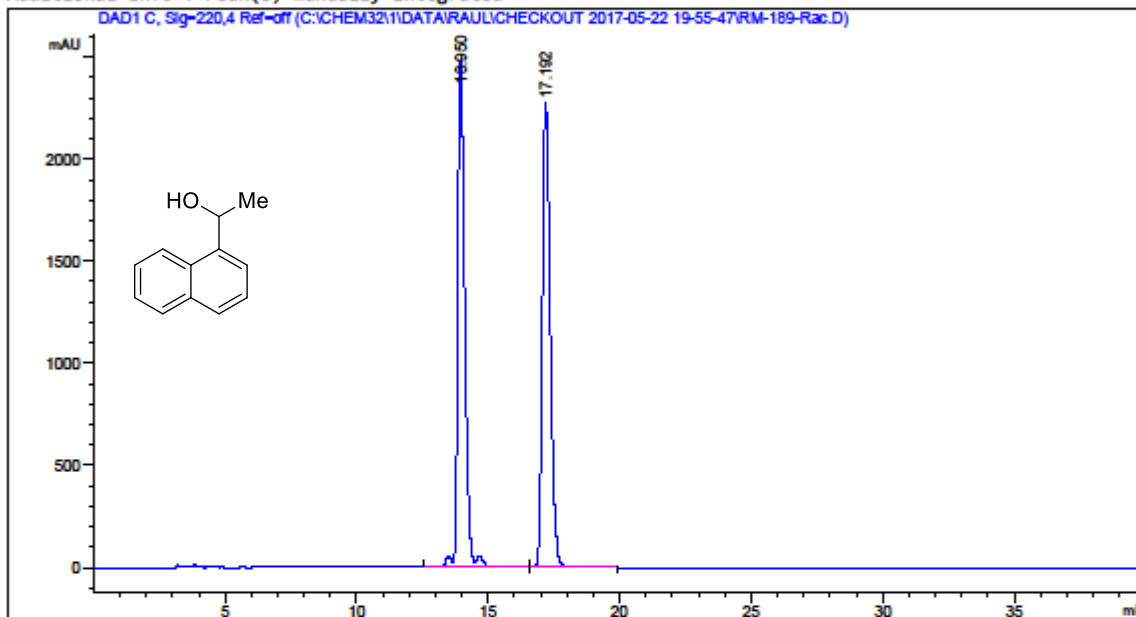
Stereospecific Borylation of Benzyl C(sp³)-O Bonds

Data File C:\CHEM32\1\DATA\RAUL\CHECKOUT 2017-05-22 19-55-47\RM-189-Rac.D
Sample Name: RM-189-Rac

=====

Acq. Operator	: SYSTEM	Seq. Line	: 10
Acq. Instrument	: HPLC 1260	Location	: 89
Injection Date	: 5/23/2017 2:05:09 AM	Inj	: 1
		Inj Volume	: 1.000 µl

Acq. Method : C:\Chem32\1\Data\Raul\checkout 2017-05-22 19-55-47\Chiral coloumn IB-Raul 98-2.M
Last changed : 5/22/2017 7:55:47 PM by SYSTEM
Analysis Method : C:\Chem32\1\Methods\Chiral coloumn IB-Raul 98-2.M
Last changed : 7/17/2017 5:48:55 PM by SYSTEM
Additional Info : Peak(s) manually integrated



=====
Area Percent Report
=====

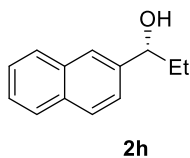
Sorted By : Signal
Multiplier : 1.0000
Dilution : 1.0000
Use Multiplier & Dilution Factor with ISTDs

Signal 1: DAD1 C, Sig=220,4 Ref=off

Peak #	RetTime [min]	Type	Width [min]	Area [mAU*s]	Height [mAU]	Area %
1	13.950	VV R	0.2865	4.73296e4	2483.45923	50.0385
2	17.192	BB	0.3219	4.72567e4	2279.12158	49.9615

Totals : 9.45862e4 4762.58081

Chapter 2



(R)-1-(naphthalen-2-yl)propan-1-ol (2h). The targeted compound was prepared via the General Procedure using Pivalate **1h** (prepared in 94% ee). The crude material was purified by silica gel chromatography (hexanes/EtOAc 1/1) to give compound **2h** (30 mg, 80%) as colourless oil. The enantiomeric excess was determined to be 84% ee (89% ee_s) by chiral HPLC analysis (CHIRALPAK IB, 1 mL/min, 2% EtOH/Hexane, $\lambda=220$ nm); $t_R(\text{minor})=11.6$ min, $t_R(\text{major})=12.9$ min. ^1H NMR (400 MHz, CDCl_3) δ 7.91 – 7.76 (m, 4H), 7.48 (m, 3H), 4.78 (t, $J = 6.6$ Hz, 1H), 2.02 – 1.79 (m, 3H), 0.95 (t, $J = 7.4$ Hz, 3H) ppm. ^{13}C NMR (100 MHz, CDCl_3) δ 141.9, 133.2, 133.0, 128.2, 127.9, 127.6, 126.1, 125.7, 124.7, 124.1, 76.1, 31.8, 10.1 ppm. The spectral data for this compound matches that reported in literature.¹¹¹

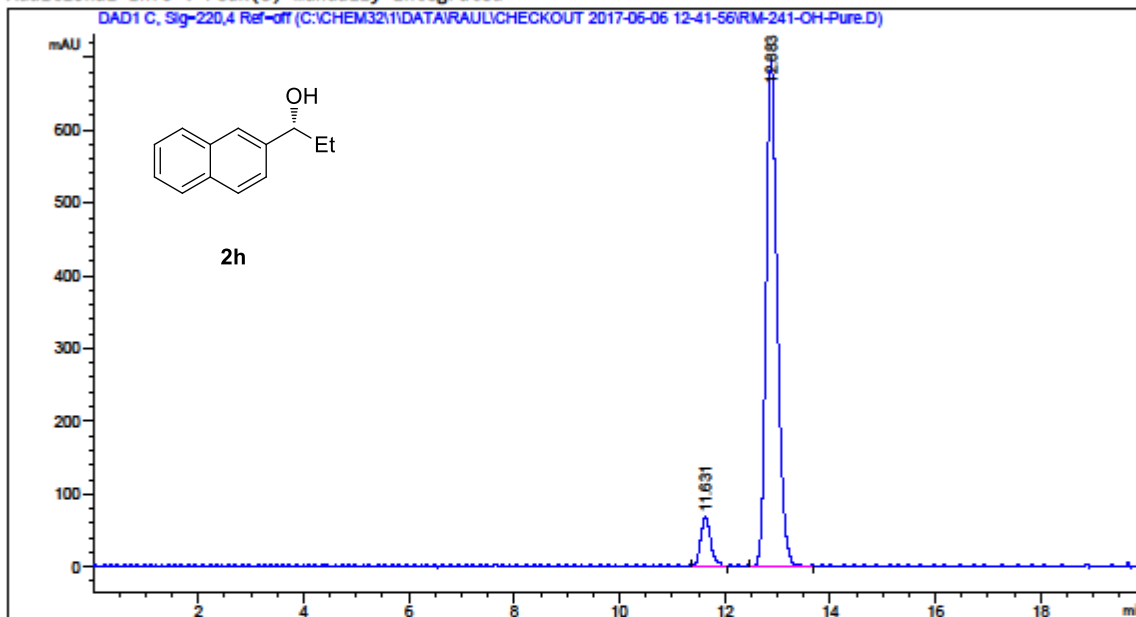
Stereospecific Borylation of Benzyl C(sp³)-O Bonds

Data File C:\CHEM32\1\DATA\RAUL\CHECKOUT 2017-06-06 12-41-56\RM-241-OH-Pure.D
Sample Name: RM-241-OH-Pure

=====

Acq. Operator	: SYSTEM	Seq. Line	: 2
Acq. Instrument	: HPLC 1260	Location	: 7
Injection Date	: 6/6/2017 1:03:04 PM	Inj	: 1
		Inj Volume	: 1.000 µl

Acq. Method : C:\Chem32\1\Data\Raul\checkout 2017-06-06 12-41-56\Chiral coloumn IB-Raul 98-2.M
Last changed : 6/6/2017 12:41:56 PM by SYSTEM
Analysis Method : C:\Chem32\1\Methods\Chiral coloumn IB-Raul 98-2.M
Last changed : 7/17/2017 5:48:55 PM by SYSTEM
Additional Info : Peak(s) manually integrated



=====
Area Percent Report
=====

Sorted By : Signal
Multiplier : 1.0000
Dilution : 1.0000
Use Multiplier & Dilution Factor with ISTDs

Signal 1: DAD1 C, Sig=220,4 Ref=off

Peak #	RetTime [min]	Type	Width [min]	Area [mAU*s]	Height [mAU]	Area %
1	11.631	BV R	0.1827	916.10138	68.59631	8.1921
2	12.883	BV R	0.2257	1.02666e4	696.09869	91.8079

Totals : 1.11827e4 764.69500

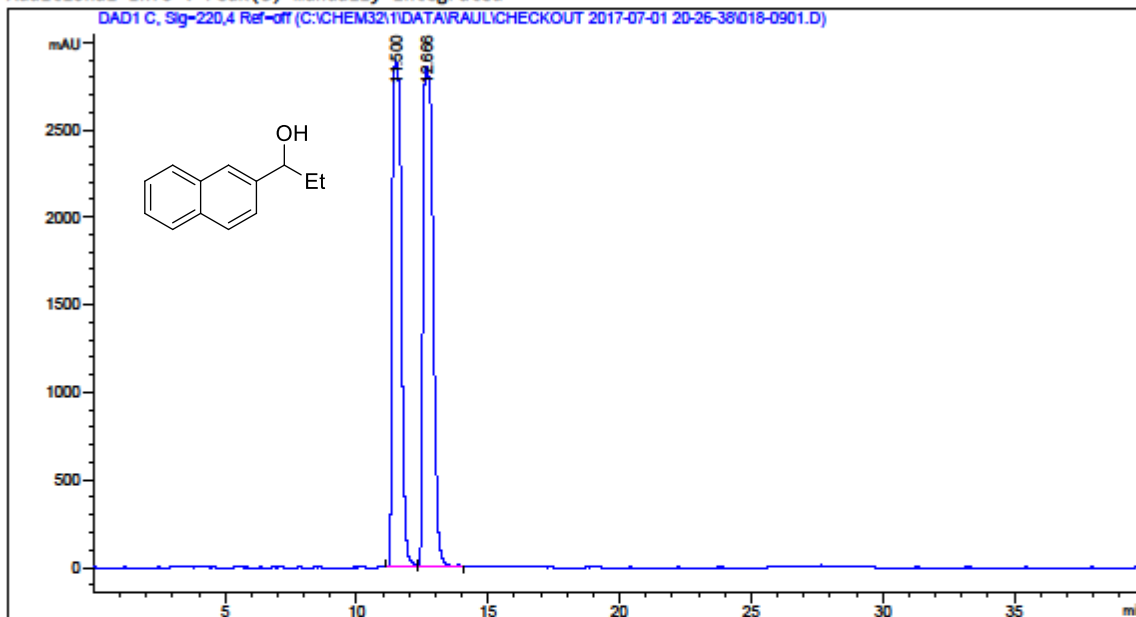
Chapter 2

Data File C:\CHEM32\1\DATA\RAUL\CHECKOUT 2017-07-01 20-26-38\018-0901.D
Sample Name: RT-8

=====

Acq. Operator	: SYSTEM	Seq. Line	: 9
Acq. Instrument	: HPLC 1260	Location	: 18
Injection Date	: 7/2/2017 1:53:49 AM	Inj	: 1
		Inj Volume	: 1.000 µl

Acq. Method : C:\Chem32\1\Data\Raul\checkout 2017-07-01 20-26-38\Chiral coloumn IB-Raul 98-2.M
Last changed : 7/1/2017 8:26:38 PM by SYSTEM
Analysis Method : C:\Chem32\1\Methods\Chiral coloumn IB-Raul 98-2.M
Last changed : 7/21/2017 9:40:12 AM by SYSTEM
Additional Info : Peak(s) manually integrated



=====
Area Percent Report
=====

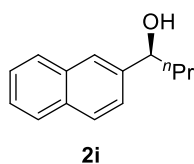
Sorted By : Signal
Multiplier : 1.0000
Dilution : 1.0000
Use Multiplier & Dilution Factor with ISTDs

Signal 1: DAD1 C, Sig=220,4 Ref=off

Peak #	RetTime [min]	Type	Width [min]	Area [mAU*s]	Height [mAU]	Area %
1	11.500	BV	0.3769	6.77066e4	2894.52515	47.3185
2	12.666	VV R	0.3613	7.53803e4	2861.42139	52.6815

Totals : 1.43087e5 5755.94653

Stereospecific Borylation of Benzyl C(sp³)-O Bonds



(S)-1-(naphthalen-2-yl)butan-1-ol (2i). The targeted compound was prepared via the General Procedure using Pivalate **1i** (prepared in 91% ee). The crude material was purified by silica gel chromatography (hexanes/EtOAc 9/1) to give compound **2i** (28 mg, 70%) as a white solid (85-87 °C). The enantiomeric excess was determined to be 76% ee (83% ee_s) by chiral HPLC analysis (CHIRALPAK IB, 1 mL/min, 1.5% EtOH/Hexane, λ=220 nm); *t*_R(major)= 12.4 min, *t*_R(minor)= 13.9 min. [α]_D²⁴ = -32.2° (0.05, CHCl₃): ¹H NMR (500 MHz, CDCl₃) δ 7.90 – 7.73 (m, 4H), 7.53 – 7.42 (m, 3H), 4.92 – 4.81 (m, 1H), 1.97 – 1.74 (m, 3H), 1.51 – 1.29 (m, 2H), 0.95 (t, *J* = 7.4 Hz, 3H) ppm. ¹³C NMR (126 MHz, CDCl₃) δ 142.3, 133.3, 133.0, 128.2, 127.9, 127.7, 126.1, 125.8, 124.6, 124.1, 74.5, 41.1, 19.1, 14.0 ppm.

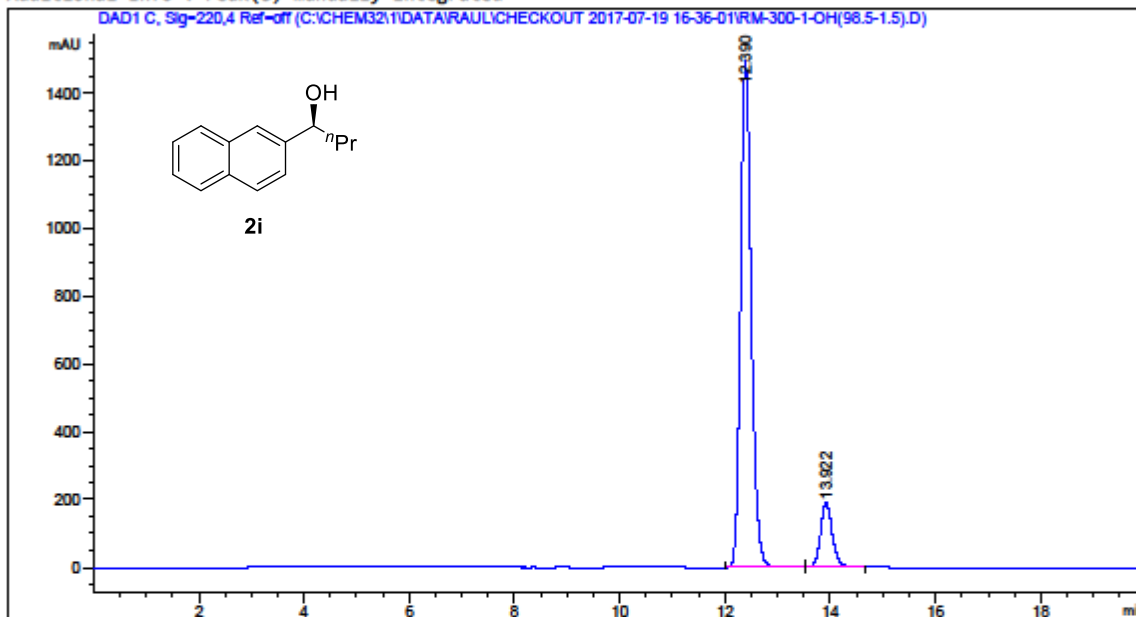
Chapter 2

Data File C:\CHEM32\1\DATA\RAUL\CHECKOUT 2017-07-19 16-36-01\RM-300-1-OH(98.5-1.5).D
Sample Name: RM-300-1-OH(98.5-1.5)

=====

Acq. Operator	: SYSTEM	Seq. Line	: 2
Acq. Instrument	: HPLC 1260	Location	: 82
Injection Date	: 7/19/2017 4:58:02 PM	Inj	: 1
		Inj Volume	: 1.000 µl

Acq. Method : C:\Chem32\1\Data\Raul\checkout 2017-07-19 16-36-01\Chiral coloumn IB-Raul 98-2.M
Last changed : 7/19/2017 4:36:01 PM by SYSTEM
Analysis Method : C:\Chem32\1\Methods\Chiral coloumn IB-Raul 98-2.M
Last changed : 7/21/2017 1:35:21 PM by SYSTEM
Additional Info : Peak(s) manually integrated



Area Percent Report

Sorted By : Signal
Multiplier : 1.0000
Dilution : 1.0000
Use Multiplier & Dilution Factor with ISTDs

Signal 1: DAD1 C, Sig=220,4 Ref=off

Peak #	RetTime [min]	Type	Width [min]	Area [mAU*s]	Height [mAU]	Area %
1	12.390	BB	0.2193	2.11825e4	1495.21533	87.7598
2	13.922	BB	0.2407	2954.42334	188.70074	12.2402

Totals : 2.41370e4 1683.91608

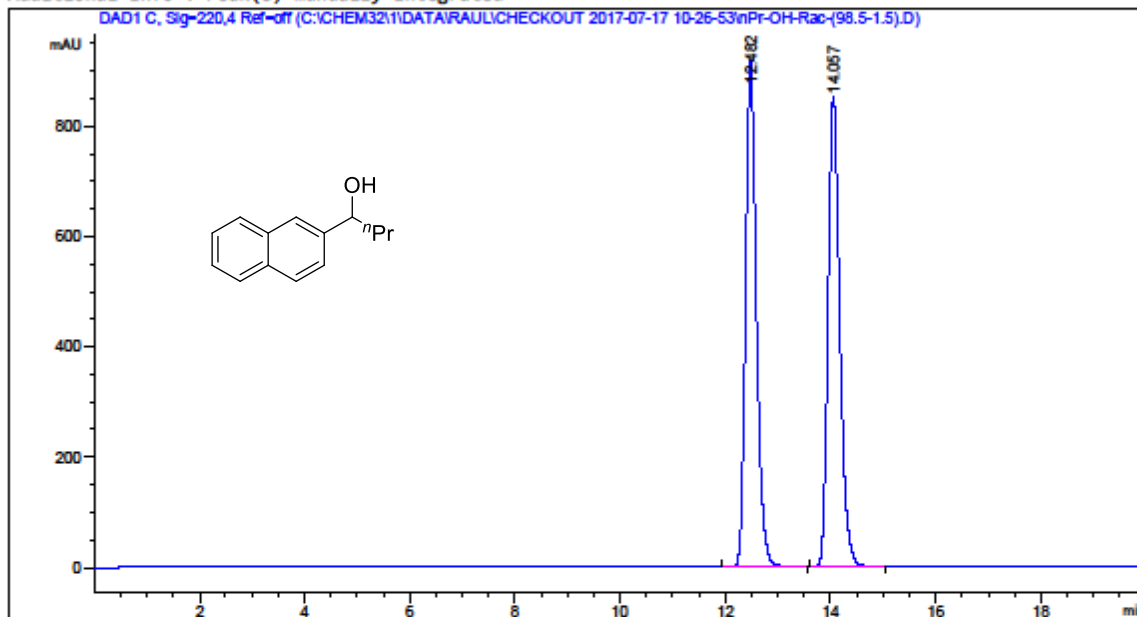
Stereospecific Borylation of Benzyl C(sp³)-O Bonds

Data File C:\CHEM32\1\DATA\RAUL\CHECKOUT 2017-07-17 10-26-53\nPr-OH-Rac-(98.5-1.5).D
Sample Name: nPr-OH-Rac-(98.5-1.5)

=====

Acq. Operator	: SYSTEM	Seq. Line	: 2
Acq. Instrument	: HPLC 1260	Location	: 81
Injection Date	: 7/17/2017 10:48:27 AM	Inj	: 1
		Inj Volume	: 1.000 µl

Acq. Method : C:\Chem32\1\Data\Raul\checkout 2017-07-17 10-26-53\Chiral column IB-Raul 98-2.M
Last changed : 7/17/2017 10:27:04 AM by SYSTEM
Analysis Method : C:\Chem32\1\Methods\Chiral column IB-Raul 98-2.M
Last changed : 7/21/2017 9:40:12 AM by SYSTEM
Additional Info : Peak(s) manually integrated



=====
Area Percent Report
=====

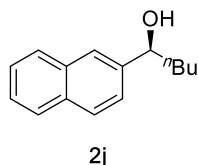
Sorted By : Signal
Multiplier : 1.0000
Dilution : 1.0000
Use Multiplier & Dilution Factor with ISTDs

Signal 1: DAD1 C, Sig=220,4 Ref=off

Peak #	RetTime [min]	Type	Width [min]	Area [mAU*s]	Height [mAU]	Area %
1	12.482	BB	0.2192	1.31570e4	917.97778	50.0446
2	14.057	BB	0.2361	1.31335e4	850.56329	49.9554

Totals : 2.62905e4 1768.54108

Chapter 2



(S)-1-(naphthalen-2-yl)pentan-1-ol (2j). The targeted compound was prepared via the General Procedure using Pivalate **1j** (prepared in 81% ee). The crude material was purified by silica gel chromatography (hexanes/EtOAc 9/1) to give compound **2j** (26 mg, 61%) as a white solid. The enantiomeric excess was determined to be 58% ee (72% ee_s) by chiral HPLC analysis (CHIRALPAK IB, 1 mL/min, 2% EtOH/Hexane, $\lambda=220$ nm); $t_R(\text{major})=10.7$ min, $t_R(\text{minor})=12.0$ min. ^1H NMR (500 MHz, CDCl_3) δ 7.89 – 7.74 (m, 4H), 7.54 – 7.44 (m, 3H), 4.92 – 4.77 (m, 1H), 1.98 – 1.76 (m, 3H), 1.47 – 1.23 (m, 4H), 0.89 (t, $J = 7.1$ Hz, 3H) ppm. ^{13}C NMR (126 MHz, CDCl_3) δ 142.3, 133.3, 133.0, 128.2, 127.9, 127.7, 126.0, 125.7, 124.6, 124.1, 74.8, 38.7, 28.0, 22.6, 14.0 ppm. The spectral data for this compound matches that reported in literature.^v

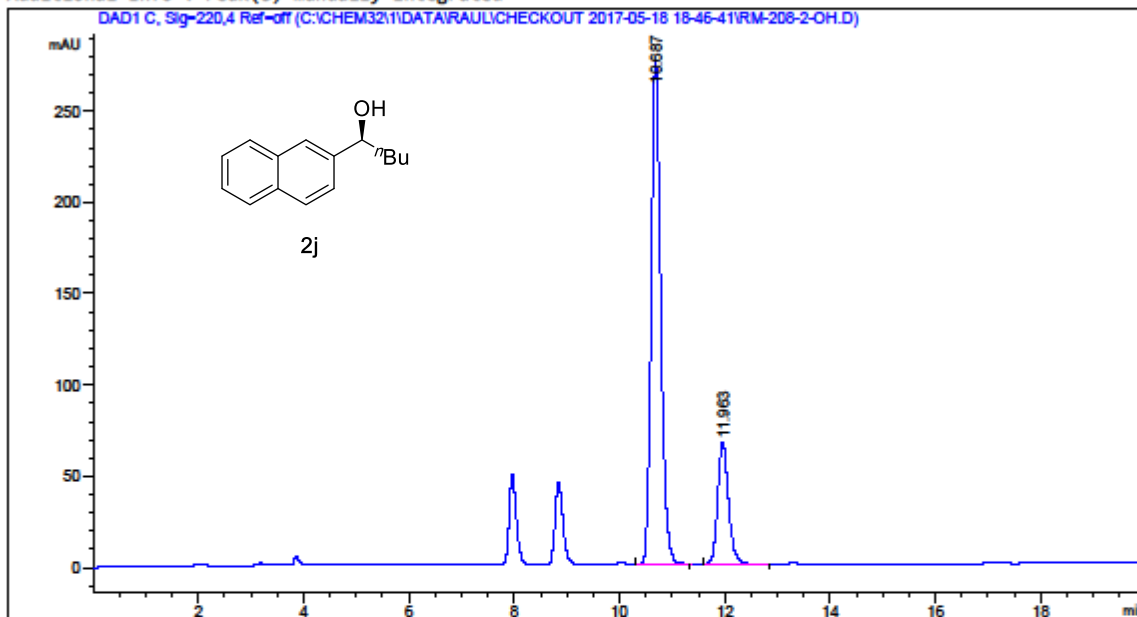
Stereospecific Borylation of Benzyl C(sp³)-O Bonds

Data File C:\CHEM32\1\DATA\RAUL\CHECKOUT 2017-05-18 18-46-41\RM-208-2-OH.D
Sample Name: RM-208-2-OH

=====

Acq. Operator	: SYSTEM	Seq. Line	: 1
Acq. Instrument	: HPLC 1260	Location	: 71
Injection Date	: 5/18/2017 6:47:35 PM	Inj	: 1
		Inj Volume	: 1.000 µl

Acq. Method : C:\Chem32\1\Data\Raul\checkout 2017-05-18 18-46-41\Chiral coloumn IB-Raul 98-2.M
Last changed : 5/18/2017 6:46:41 PM by SYSTEM
Analysis Method : C:\Chem32\1\Methods\Chiral coloumn IB-Raul 98-2.M
Last changed : 7/17/2017 5:48:55 PM by SYSTEM
Additional Info : Peak(s) manually integrated



=====
Area Percent Report
=====

Sorted By : Signal
Multiplier : 1.0000
Dilution : 1.0000
Use Multiplier & Dilution Factor with ISTDs

Signal 1: DAD1 C, Sig=220,4 Ref=off

Peak #	RetTime [min]	Type	Width [min]	Area [mAU*s]	Height [mAU]	Area %
1	10.687	BB	0.1932	3481.52026	275.97122	79.0434
2	11.963	BB	0.2148	923.04565	66.15916	20.9566

Totals : 4404.56592 342.13038

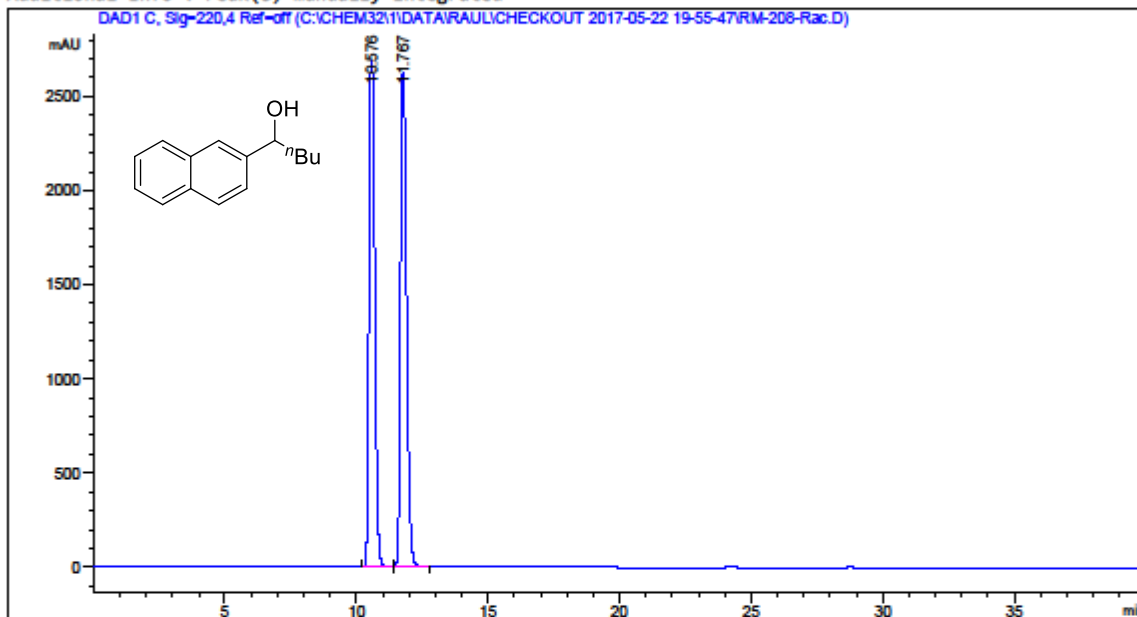
Chapter 2

Data File C:\CHEM32\1\DATA\RAUL\CHECKOUT 2017-05-22 19-55-47\RM-208-Rac.D
Sample Name: RM-208-Rac

=====

Acq. Operator	: SYSTEM	Seq. Line	: 4
Acq. Instrument	: HPLC 1260	Location	: 83
Injection Date	: 5/22/2017 9:59:55 PM	Inj	: 1
		Inj Volume	: 1.000 µl

Acq. Method : C:\Chem32\1\Data\Raul\checkout 2017-05-22 19-55-47\Chiral coloumn IB-Raul 98-2.M
Last changed : 5/22/2017 7:55:47 PM by SYSTEM
Analysis Method : C:\Chem32\1\Methods\Chiral coloumn IB-Raul 98-2.M
Last changed : 7/17/2017 5:48:55 PM by SYSTEM
Additional Info : Peak(s) manually integrated



=====
Area Percent Report
=====

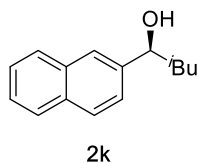
Sorted By : Signal
Multiplier : 1.0000
Dilution : 1.0000
Use Multiplier & Dilution Factor with ISTDs

Signal 1: DAD1 C, Sig=220,4 Ref=off

Peak #	RetTime [min]	Type	Width [min]	Area [mAU*s]	Height [mAU]	Area %
1	10.576	BB	0.2424	4.10936e4	2688.10132	48.6289
2	11.767	BB	0.2594	4.34108e4	2618.96216	51.3711

Totals : 8.45044e4 5307.06348

Stereospecific Borylation of Benzyl C(sp³)-O Bonds



(S)-3-methyl-1-(naphthalen-2-yl)butan-1-ol (2k). The targeted compound was prepared via the General Procedure using Pivalate **1k** (prepared in 92% ee). The crude material was purified by silica gel chromatography (hexanes/EtOAc 1/1) to give compound **2k** (22 mg, 51%) as a white solid (m.p 84-86 °C). The enantiomeric excess was determined to be 82% ee (89% ee_s) by chiral HPLC analysis (CHIRALPAK IB, 1 mL/min, 2% EtOH/Hexane, λ=220 nm); *t*_R(major)= 10.1 min, *t*_R(minor)= 10.8 min. ¹H NMR (500 MHz, CDCl₃) δ 7.90 – 7.76 (m, 4H), 7.56 – 7.42 (m, 3H), 4.93 (t, *J* = 6.4 Hz, 1H), 1.89 – 1.70 (m, 3H), 1.66 – 1.60 (m, 1H), 0.98 (dd, *J* = 6.6, 4.3 Hz, 6H) ppm. ¹³C NMR (126 MHz, CDCl₃) δ 142.6, 133.3, 133.0, 128.3, 127.9, 127.7, 126.1, 125.8, 124.5, 124.1, 73.0, 48.3, 24.9, 23.1, 22.3 ppm. The spectral data for this compound matches that reported in literature.^{VII}

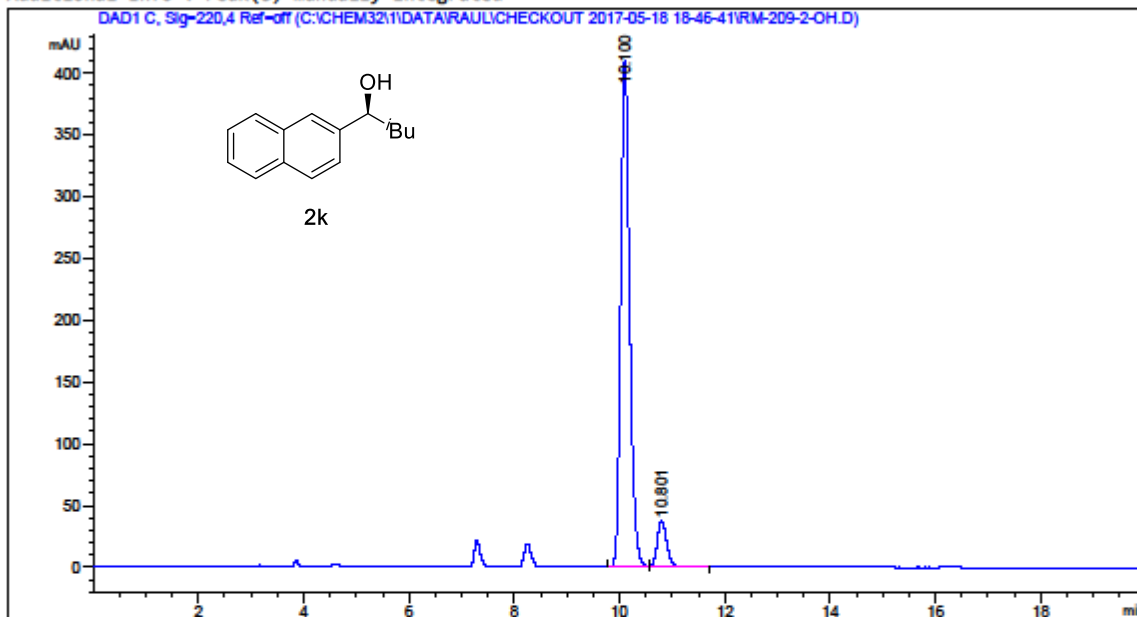
Chapter 2

Data File C:\CHEM32\1\DATA\RAUL\CHECKOUT 2017-05-18 18-46-41\RM-209-2-OH.D
Sample Name: RM-209-2-OH

=====

Acq. Operator	: SYSTEM	Seq. Line	: 2
Acq. Instrument	: HPLC 1260	Location	: 72
Injection Date	: 5/18/2017 7:08:26 PM	Inj	: 1
		Inj Volume	: 1.000 µl

Acq. Method : C:\Chem32\1\Data\Raul\checkout 2017-05-18 18-46-41\Chiral coloumn IB-Raul 98-2.M
Last changed : 5/18/2017 6:46:41 PM by SYSTEM
Analysis Method : C:\Chem32\1\Methods\Chiral coloumn IB-Raul 98-2.M
Last changed : 7/17/2017 5:48:55 PM by SYSTEM
Additional Info : Peak(s) manually integrated



=====
Area Percent Report
=====

Sorted By : Signal
Multiplier : 1.0000
Dilution : 1.0000
Use Multiplier & Dilution Factor with ISTDs

Signal 1: DAD1 C, Sig=220,4 Ref=off

Peak #	RetTime [min]	Type	Width [min]	Area [mAU*s]	Height [mAU]	Area %
1	10.100	BV	0.1790	4818.59717	410.39731	90.9179
2	10.801	VB	0.1957	481.34573	37.51536	9.0821

Totals : 5299.94290 447.91267

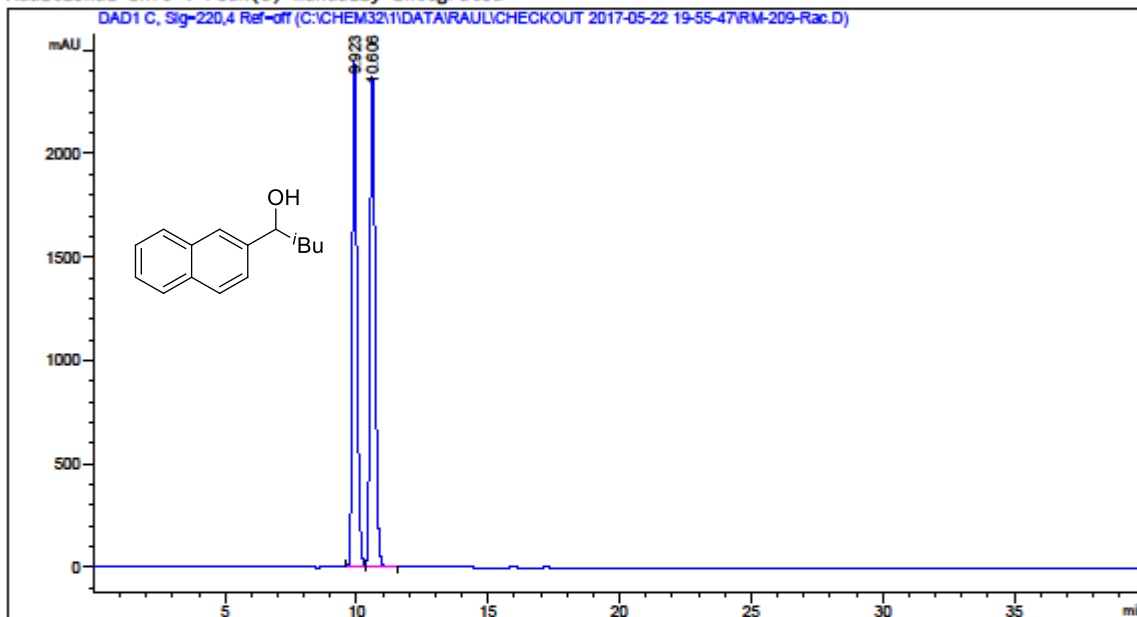
Stereospecific Borylation of Benzyl C(sp³)-O Bonds

Data File C:\CHEM32\1\DATA\RAUL\CHECKOUT 2017-05-22 19-55-47\RM-209-Rac.D
Sample Name: RM-209-Rac

=====

Acq. Operator : SYSTEM	Seq. Line : 6
Acq. Instrument : HPLC 1260	Location : 85
Injection Date : 5/22/2017 11:21:38 PM	Inj : 1
	Inj Volume : 1.000 µl

Acq. Method : C:\Chem32\1\Data\Raul\checkout 2017-05-22 19-55-47\Chiral coloumn IB-Raul 98-2.M
Last changed : 5/22/2017 7:55:47 PM by SYSTEM
Analysis Method : C:\Chem32\1\Methods\Chiral coloumn IB-Raul 98-2.M
Last changed : 7/17/2017 5:48:55 PM by SYSTEM
Additional Info : Peak(s) manually integrated



=====
Area Percent Report
=====

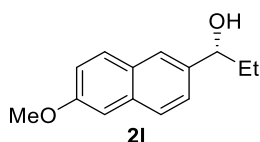
Sorted By : Signal
Multiplier : 1.0000
Dilution : 1.0000
Use Multiplier & Dilution Factor with ISTDs

Signal 1: DAD1 C, Sig=220,4 Ref=off

Peak #	RetTime [min]	Type	Width [min]	Area [mAU*s]	Height [mAU]	Area %
1	9.923	BV	0.1993	3.13576e4	2450.07251	49.4276
2	10.606	VB	0.2102	3.20839e4	2365.76758	50.5724

Totals : 6.34415e4 4815.84009

Chapter 2



(R)-1-(6-methoxynaphthalen-2-yl)propan-1-ol (2I). The targeted compound was prepared via the General Procedure using Pivalate **1I** (prepared in 85% ee). The crude material was purified by silica gel chromatography (hexanes/EtOAc 1/1) to give compound **2I** (29.4 mg, 55%) as colourless oil. The enantiomeric excess was determined to be 69% ee (81% ee_s) by chiral HPLC analysis (CHIRALPAK IB, 1 mL/min, 2% EtOH/Hexane, λ=220 nm); $t_{R}(\text{minor})= 14.3$ min, $t_{R}(\text{major})= 19.4$ min. ¹H NMR (500 MHz, CDCl₃) δ 7.77 – 7.66 (m, 3H), 7.45 (dd, $J = 8.4, 1.8$ Hz, 1H), 7.20 – 7.11 (m, 2H), 4.74 (t, $J = 6.6$ Hz, 1H), 3.92 (s, 3H), 1.96 – 1.77 (m, 3H), 0.94 (t, $J = 7.4$ Hz, 3H) ppm. ¹³C NMR (126 MHz, CDCl₃) δ 157.6, 139.7, 134.1, 129.4, 128.7, 127.1, 124.7, 124.6, 118.9, 105.7, 76.2, 55.6, 31.7, 10.2 ppm. The spectral data for this compound matches that reported in literature.ⁱⁱⁱ

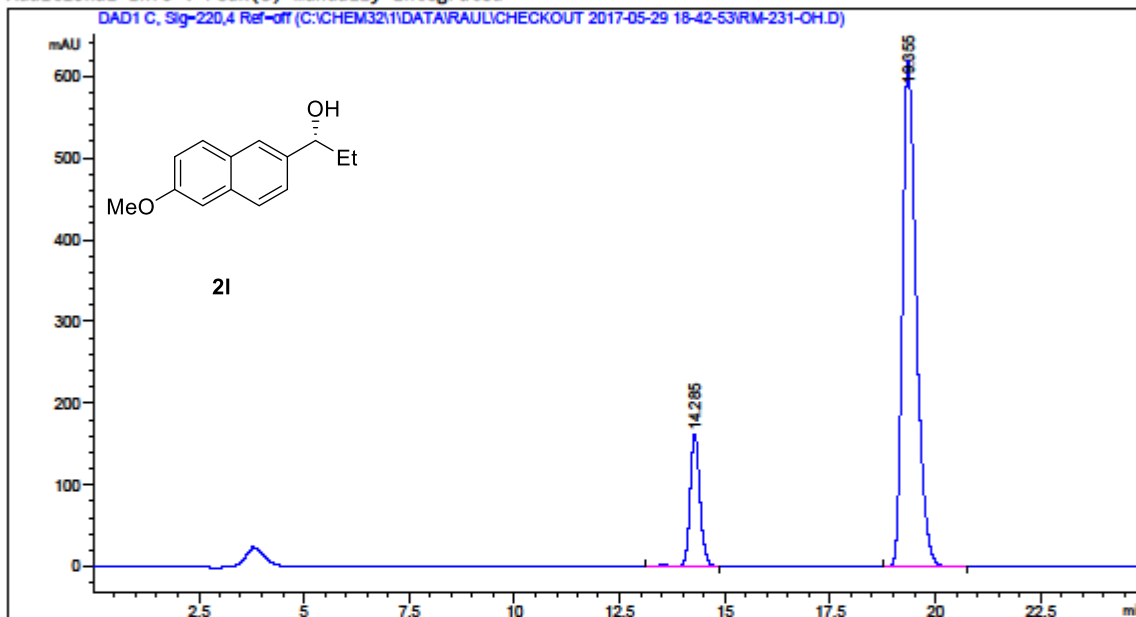
Stereospecific Borylation of Benzyl C(sp³)-O Bonds

Data File C:\CHEM32\1\DATA\RAUL\CHECKOUT 2017-05-29 18-42-53\RM-231-OH.D
Sample Name: RM-231-OH

=====

Acq. Operator	: SYSTEM	Seq. Line	: 1
Acq. Instrument	: HPLC 1260	Location	: 38
Injection Date	: 5/29/2017 6:43:43 PM	Inj	: 1
		Inj Volume	: 1.000 µl

Acq. Method : C:\Chem32\1\Data\Raul\checkout 2017-05-29 18-42-53\Chiral coloumn IB-Raul 98-2.M
Last changed : 5/29/2017 6:42:53 PM by SYSTEM
Analysis Method : C:\Chem32\1\Methods\Chiral coloumn IB-Raul 98-2.M
Last changed : 7/17/2017 5:48:55 PM by SYSTEM
Additional Info : Peak(s) manually integrated



=====
Area Percent Report
=====

Sorted By : Signal
Multiplier : 1.0000
Dilution : 1.0000
Use Multiplier & Dilution Factor with ISTDs

Signal 1: DAD1 C, Sig=220,4 Ref=off

Peak #	RetTime [min]	Type	Width [min]	Area [mAU*s]	Height [mAU]	Area %
1	14.285	VB R	0.2456	2635.91138	161.51656	15.7872
2	19.355	BB	0.3448	1.40606e4	619.52942	84.2128

Totals : 1.66966e4 781.04597

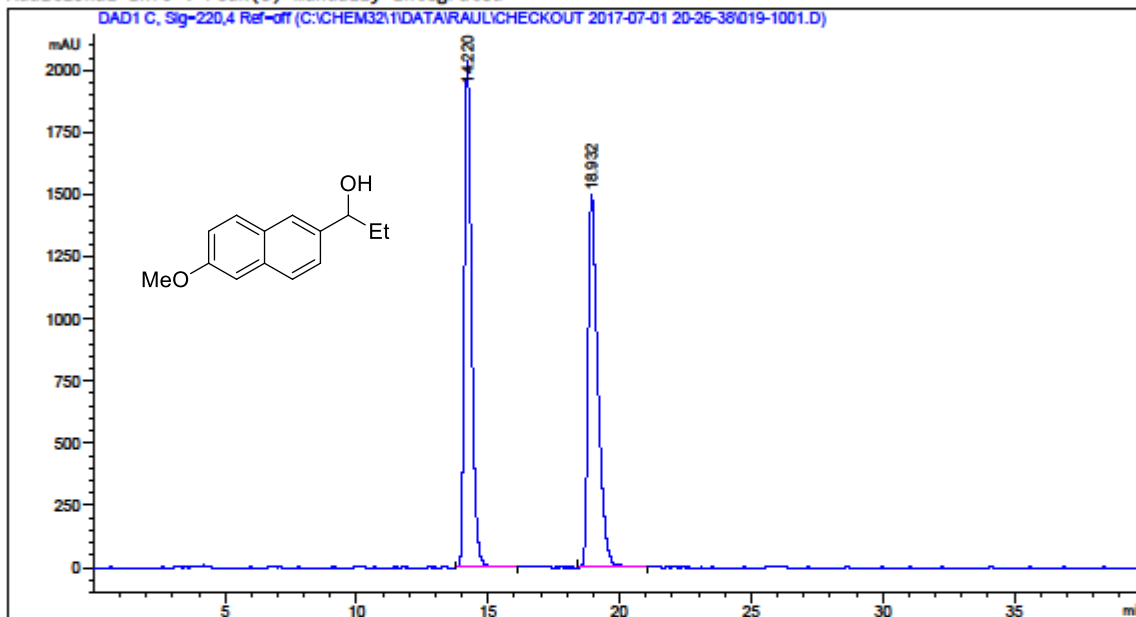
Chapter 2

Data File C:\CHEM32\1\DATA\RAUL\CHECKOUT 2017-07-01 20-26-38\019-1001.D
Sample Name: RT-9

=====

Acq. Operator	: SYSTEM	Seq. Line	: 10
Acq. Instrument	: HPLC 1260	Location	: 19
Injection Date	: 7/2/2017 2:34:41 AM	Inj	: 1
		Inj Volume	: 1.000 µl

Acq. Method : C:\Chem32\1\Data\Raul\checkout 2017-07-01 20-26-38\Chiral coloumn IB-Raul 98-2.M
Last changed : 7/1/2017 8:26:38 PM by SYSTEM
Analysis Method : C:\Chem32\1\Methods\Chiral coloumn IB-Raul 98-2.M
Last changed : 7/21/2017 9:40:12 AM by SYSTEM
Additional Info : Peak(s) manually integrated



=====
Area Percent Report
=====

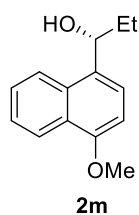
Sorted By : Signal
Multiplier : 1.0000
Dilution : 1.0000
Use Multiplier & Dilution Factor with ISTDs

Signal 1: DAD1 C, Sig=220,4 Ref=off

Peak #	RetTime [min]	Type	Width [min]	Area [mAU*s]	Height [mAU]	Area %
1	14.220	BV R	0.2872	3.83391e4	2040.33154	49.5938
2	18.932	BV R	0.3888	3.89671e4	1499.29529	50.4062

Totals : 7.73062e4 3539.62683

Stereospecific Borylation of Benzyl C(sp³)-O Bonds



(R)-1-(4-methoxynaphthalen-1-yl)propan-1-ol (2m). The targeted compound was prepared via the General Procedure using Pivalate **1m** (prepared in 78% ee). The crude material was purified by silica gel chromatography (hexanes/EtOAc 9/1) to give compound **2m** (22 mg, 51%) as colourless oil. The enantiomeric excess was determined to be 68% ee (87% ee_s) by chiral HPLC analysis (CHIRALPAK IB, 1 mL/min, 2% EtOH/Hexane, λ=220 nm); *t*_R(minor)= 16.4 min, *t*_R(major)= 25.0 min. [α]_D²⁴ = 43.7° (0.16, CHCl₃): ¹H NMR (400 MHz, CDCl₃) δ 8.34 (m, 1H), 8.13 (dd, *J* = 8.2, 1.3 Hz, 1H), 7.63 – 7.46 (m, 3H), 6.83 (d, *J* = 8.0 Hz, 1H), 5.33 (t, *J* = 6.5 Hz, 1H), 4.03 (s, 3H), 2.09 – 1.93 (m, 2H), 1.87 (s, 1H, OH), 1.04 (t, *J* = 7.4 Hz, 3H) ppm. ¹³C NMR (126 MHz, CDCl₃) δ 155.0, 132.0, 131.6, 126.5, 125.8, 124.9, 123.2, 123.1, 122.7, 103.1, 72.7, 55.5, 30.1, 10.6 ppm.

Chapter 2

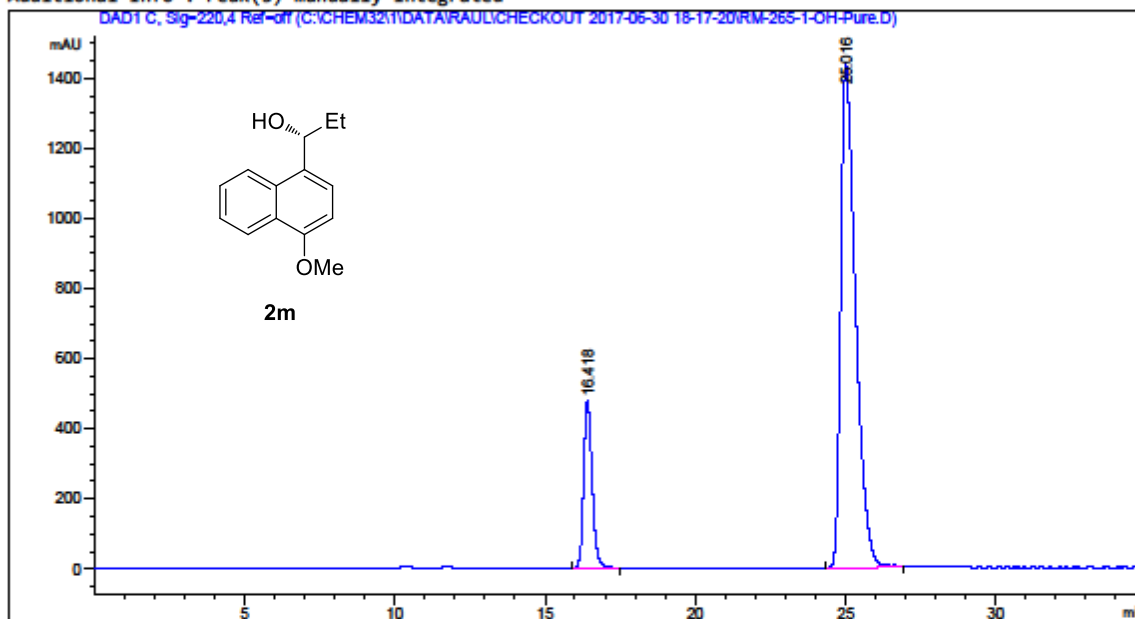
Data File C:\CHEM32\1\DATA\RAUL\CHECKOUT 2017-06-30 18-17-20\RM-265-1-OH-Pure.D
Sample Name: RM-265-1-OH-Pure

=====

Acq. Operator : SYSTEM	Seq. Line : 1
Acq. Instrument : HPLC 1260	Location : 44
Injection Date : 6/30/2017 6:18:12 PM	Inj : 1
	Inj Volume : 1.000 µl

Acq. Method : C:\Chem32\1\Data\Raul\checkout 2017-06-30 18-17-20\Chiral column IB-Raul 98-2.M
Last changed : 6/30/2017 6:17:20 PM by SYSTEM
Analysis Method : C:\Chem32\1\Data\Raul\checkout 2017-06-29 16-00-44\Chiral column IB-Raul 98-2.M (Sequence Method)
Last changed : 7/21/2017 10:07:18 AM by SYSTEM
(modified after loading)

Additional Info : Peak(s) manually integrated



=====
Area Percent Report
=====

Sorted By : Signal
Multiplier : 1.0000
Dilution : 1.0000
Use Multiplier & Dilution Factor with ISTDs

Signal 1: DAD1 C, Sig=220,4 Ref=off

Peak #	RetTime [min]	Type	Width [min]	Area [mAU*s]	Height [mAU]	Area %
1	16.418	BB	0.2978	9219.48340	476.30493	15.8345
2	25.016	BV R	0.4802	4.90044e4	1440.60901	84.1655

Totals : 5.82239e4 1916.91394

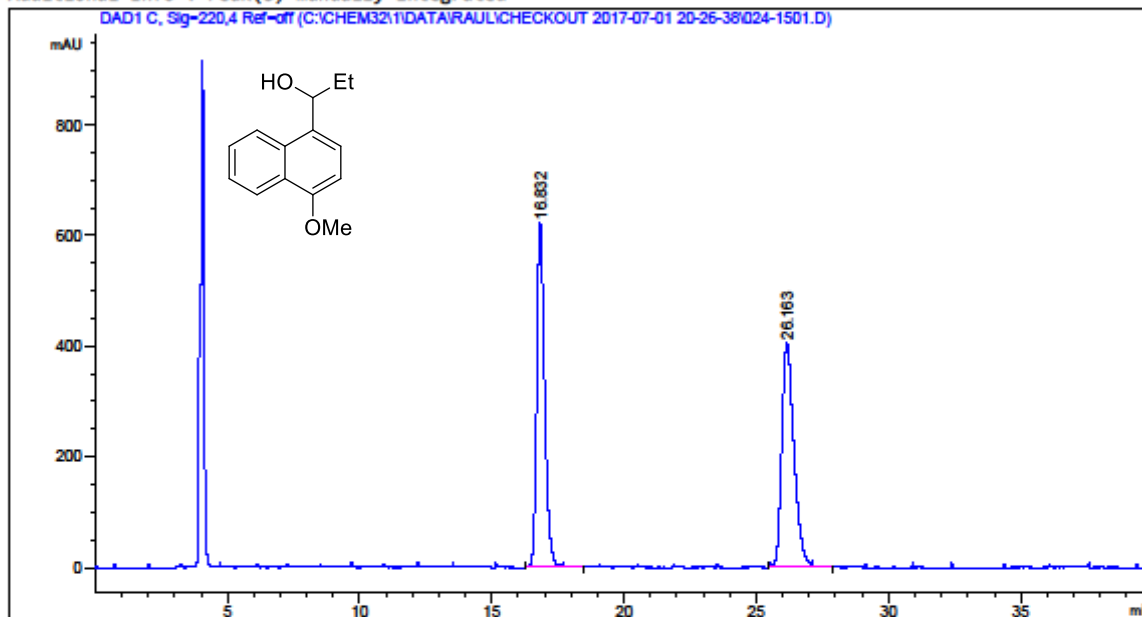
Stereospecific Borylation of Benzyl C(sp³)-O Bonds

Data File C:\CHEM32\1\DATA\RAUL\CHECKOUT 2017-07-01 20-26-38\024-1501.D
Sample Name: RT-14

=====

Acq. Operator	: SYSTEM	Seq. Line	: 15
Acq. Instrument	: HPLC 1260	Location	: 24
Injection Date	: 7/2/2017 5:59:01 AM	Inj	: 1
		Inj Volume	: 1.000 µl

Acq. Method : C:\Chem32\1\Data\Raul\checkout 2017-07-01 20-26-38\Chiral coloumn IB-Raul 98-2.M
Last changed : 7/1/2017 8:26:38 PM by SYSTEM
Analysis Method : C:\Chem32\1\Methods\Chiral coloumn IB-Raul 98-2.M
Last changed : 7/21/2017 9:40:12 AM by SYSTEM
Additional Info : Peak(s) manually integrated



=====
Area Percent Report
=====

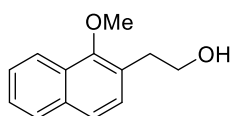
Sorted By : Signal
Multiplier : 1.0000
Dilution : 1.0000
Use Multiplier & Dilution Factor with ISTDs

Signal 1: DAD1 C, Sig=220,4 Ref=off

Peak #	RetTime [min]	Type	Width [min]	Area [mAU*s]	Height [mAU]	Area %
1	16.832	BV R	0.3170	1.29775e4	622.02307	49.9575
2	26.163	VV R	0.4873	1.29996e4	405.08572	50.0425

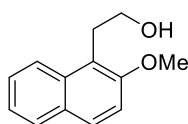
Totals : 2.59771e4 1027.10880

Chapter 2



2n

2-(1-methoxynaphthalen-2-yl)ethan-1-ol (2n). The targeted compound was prepared via the General Procedure using Pivalate **1n** (prepared in 95% ee). The crude material was purified by silica gel chromatography (hexanes/EtOAc 9/1) to give compound **2n** (24 mg, 60%) as colourless oil. ^1H NMR (500 MHz, CDCl_3) δ 8.09 (d, $J = 8.5$ Hz, 1H), 7.83 (d, $J = 8.1$ Hz, 1H), 7.60 (d, $J = 8.3$ Hz, 1H), 7.52 (dd, $J = 8.3, 6.8$ Hz, 1H), 7.46 (dd, $J = 8.1, 6.8$ Hz, 1H), 7.34 (d, $J = 8.4$ Hz, 1H), 3.96 (s, 3H), 3.95 (t, $J = 6.5$ Hz, 2H), 3.10 (t, $J = 6.5$ Hz, 2H), 1.87 (s, 1H, OH) ppm. ^{13}C NMR (126 MHz, CDCl_3) δ 154.0, 134.1, 128.4, 128.0, 127.9, 126.9, 126.0, 125.7, 124.3, 122.0, 63.3, 62.0, 35.6 ppm. IR (neat, cm^{-1}): 3413, 2932, 1661, 1369, 1240, 1085, 986, 814. HRMS calcd. for $\text{C}_{13}\text{H}_{14}\text{O}_2$ ($\text{M}+\text{Na}$) $^+$: 225.0886, found 225.0881.

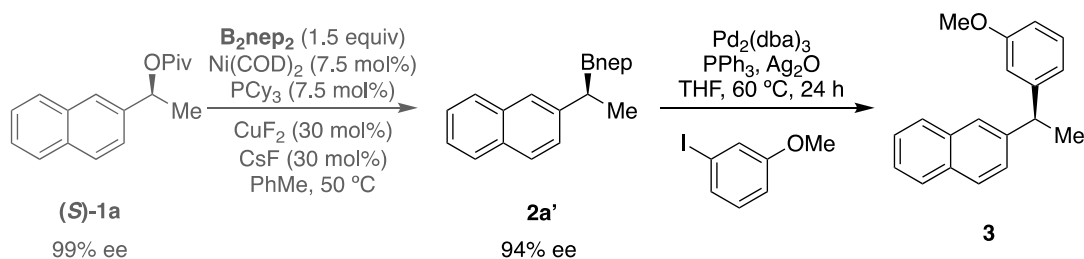


2o

2-(2-methoxynaphthalen-1-yl)ethan-1-ol (2o). The targeted compound was prepared via the General Procedure using Pivalate **1o** (prepared in 15% ee). The crude material was purified by silica gel chromatography (hexanes/EtOAc 9/1) to give compound **2o** (23 mg, 58%) as colourless oil. ^1H NMR (400 MHz, CDCl_3) δ 8.00 (dd, $J = 8.7, 1.0$ Hz, 1H), 7.85 – 7.73 (m, 2H), 7.49 (dd, $J = 8.4, 6.8$ Hz, 1H), 7.42 – 7.29 (m, 2H), 3.97 (s, 3H), 3.92 (t, $J = 6.8$ Hz, 2H), 3.42 (t, $J = 6.8$ Hz, 2H), 1.6 (s, 1H, OH) ppm. ^{13}C NMR (126 MHz, CDCl_3) δ 154.9, 133.3, 129.3, 128.6, 128.3, 126.5, 123.4, 123.0, 119.6, 113.1, 62.9, 56.5, 28.4 ppm. IR (neat, cm^{-1}): 2929, 1624, 1594, 1513, 1464, 1249, 1095, 1026, 806. HRMS calcd. for $\text{C}_{13}\text{H}_{14}\text{O}_2$ ($\text{M}+\text{Na}$) $^+$: 225.0886, found 225.0887.

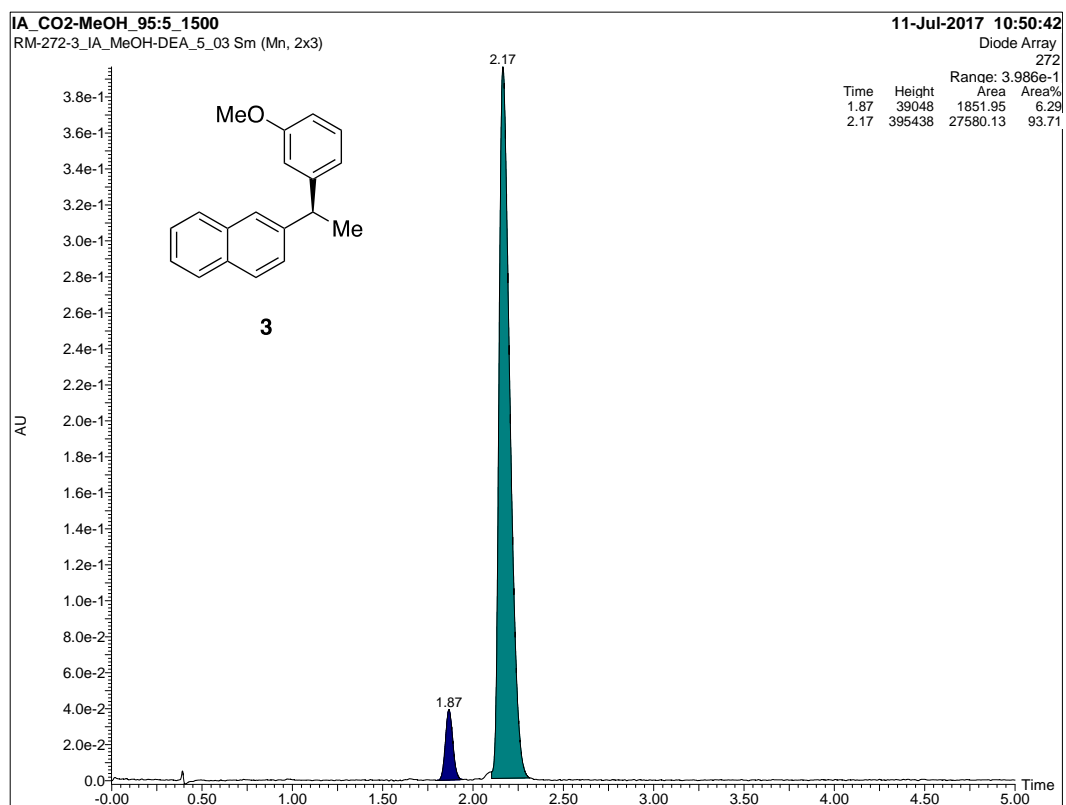
2.5.4 Synthetic applications.

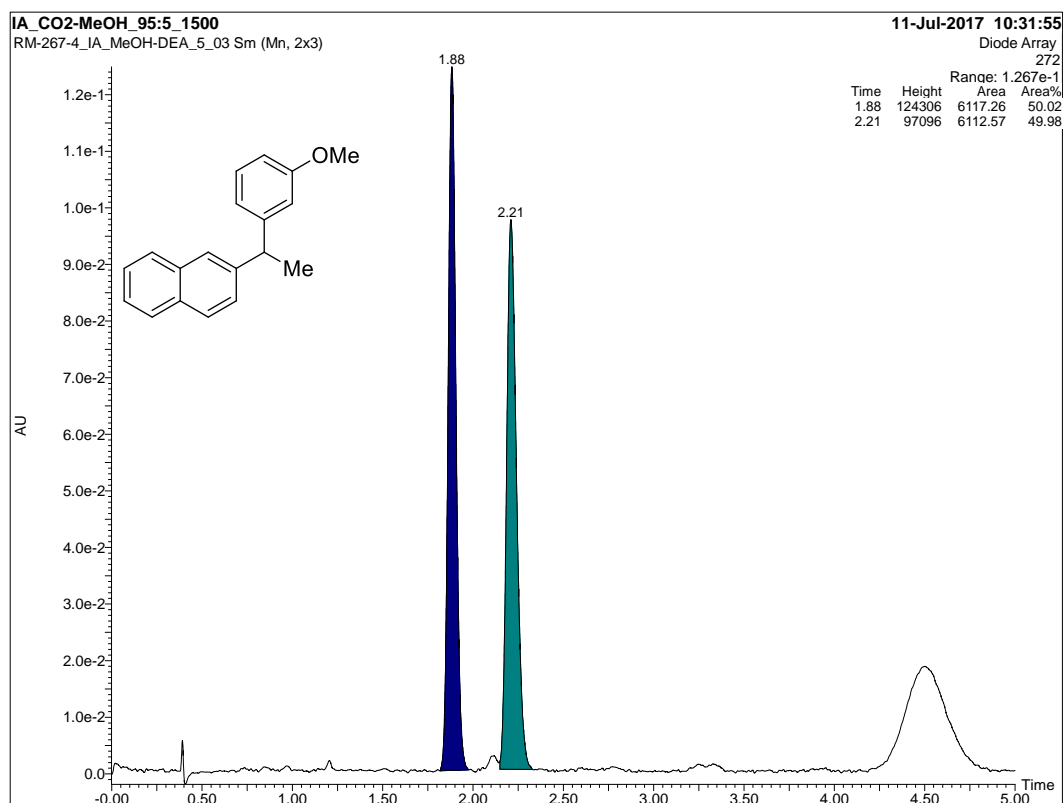
Suzuki-Miyaura Coupling reaction procedure.^{IX}



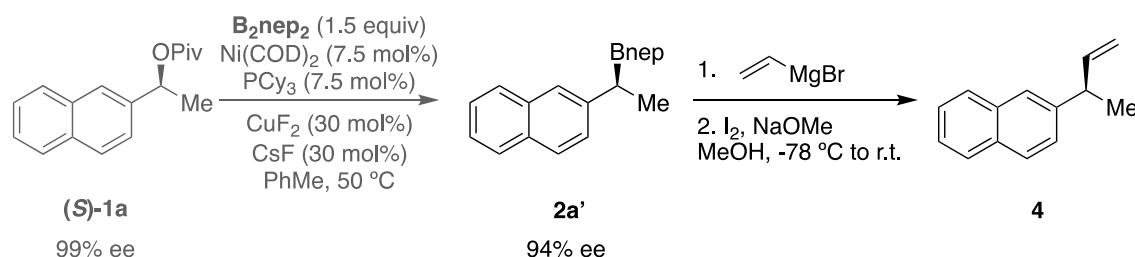
Prior **(S)-2a'** was prepared following the general procedure for the borylation of benzyl pivalates and was used without further purification step. Under inert atmosphere, 1-iodo-3-methoxybenzene (24 μL , 0.2 mmol), **(S)-2a'** (54 mg, 0.2 mmol), Ag_2O (48.9 mg, 0.21 mmol), $\text{Pd}_2(\text{dba})_3$ (9.1 mg, 0.01 mmol, 10 mol% Pd), PPh_3 (70.6, 0.2 mmol) were taken up in THF (2 mL). The reaction was sealed, and stirred at 60 °C for 24 h. The desired product was isolated by column chromatography (gradient hexanes/EtOAc 9/1) to yield the desired product **3** (29 mg, 57% yield based on **(S)-1a**) with 87% ee (93% ee_s) as a white solid (m.p 90-92 °C). Enantiomeric ratio was determined by SFC analysis (CHIRALPAK IA, 1 mL/min, 95% CO_2/MeOH , $\lambda=272$ nm); $t_{\text{R}}(\text{minor})= 1.87$ min, $t_{\text{R}}(\text{major})= 2.17$ min. $[\alpha]_{\text{D}}^{24} = -28.4^\circ$ (c 0.11, CHCl_3). ^1H NMR (400 MHz, CDCl_3) δ 7.85 – 7.68 (m, 4H), 7.51 – 7.40 (m, 2H), 7.33 (dd, $J = 8.5, 1.8$ Hz, 1H), 7.23 (dd, $J = 15.6, 7.7$ Hz, 1H), 6.88 – 6.80 (m, 2H), 6.75 (dd, $J = 8.2, 2.6$ Hz, 1H), 4.30 (q, $J = 7.2$ Hz, 1H), 3.77 (s, 3H), 1.74 (d, $J = 7.2$ Hz, 3H) ppm. ^{13}C NMR (101 MHz, CDCl_3) δ 159.6, 147.9, 143.6, 133.5, 132.1, 129.3, 127.9, 127.7, 127.5, 126.7, 125.9, 125.3, 125.2, 120.2, 113.9, 111.0, 55.1, 44.8, 21.7 ppm. The spectral data for compound **3** matches that reported in literature.^{VII}

Chapter 2





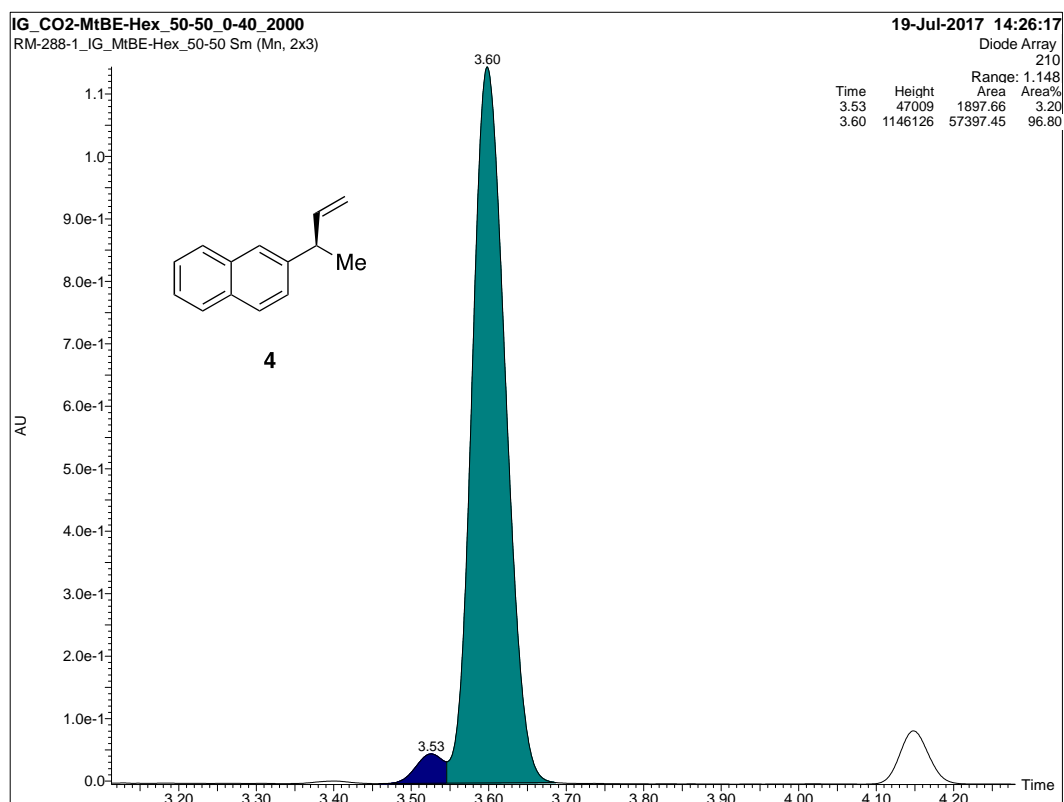
Procedure for the vinylation of benzylic boronic ester.^x

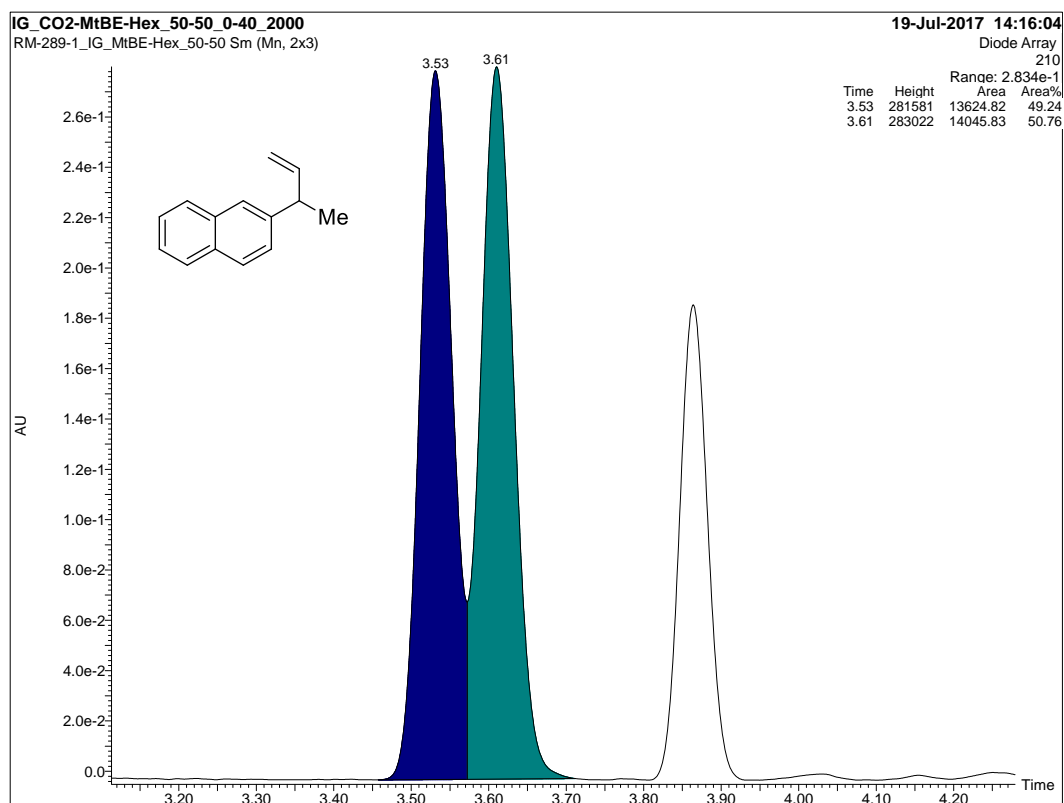


Prior **(S)-2a'** was prepared following the general procedure for the borylation of benzyl pivalates and was used further without purification step. To a solution of **2a** (0.2 mmol, 1.0 equiv.) in anhydrous THF (2 mL, 0.1 M) at room temperature was added vinylmagnesium bromide (1 M in THF, 0.8 mL, 0.8 mmol, 4.0 equiv.) dropwise. The resulting mixture was stirred for 30 min and then cooled down to -78 °C. A solution of iodine (203 mg, 0.8 mmol, 4 equiv.) in MeOH (3 mL) was added dropwise to the reaction mixture, followed 30 min later by a solution of MeONa in MeOH (25 w%, 370 mL, 1.6 mmol, 8.0 equiv.). The reaction mixture was then allowed to warm up to room temperature and stirred for an additional 1 hour, then diluted with pentane (30 mL) and washed with a 20% aq. Na₂O₃ solution (4 mL) and water (8 mL). The phases were separated, the aqueous layer was extracted with pentane (2 x 15 mL), and the combined organic layers were washed with brine (8 mL), dried (MgSO₄), filtered and concentrated *in vacuo*. The crude product was purified by flash chromatography (hexanes 100%) to yield the desired product **4** (18.6 mg, 51 % overall yield) with 94% ee (99% ee_s) as colourless oil.

Chapter 2

Enantiomeric ratio was determined by SFC analysis (CHIRALPAK IG, 1 mL/min, CO₂/MtBe-Hex 50-50, gradient 0-40, $\lambda=210$ nm); $t_R(\text{minor})=3.53$ min, $t_R(\text{major})=3.60$ min. $[\alpha]_D^{24} = -8.4^\circ$ (c 0.05, CHCl₃). ¹H NMR (400 MHz, CDCl₃) δ 7.79 (dd, $J = 8.2, 5.6$ Hz, 3H), 7.65 (s, 1H), 7.44 (dd, $J = 7.8, 5.7$ Hz, 2H), 7.36 (dd, $J = 8.5, 1.8$ Hz, 1H), 6.09 (dd, $J = 16.9, 10.3, 6.4$ Hz, 1H), 5.15 – 5.04 (m, 2H), 3.64 (t, $J = 6.9$ Hz, 1H), 1.46 (d, $J = 7.0$ Hz, 3H) ppm. ¹³C NMR (101 MHz, CDCl₃) δ 143.1, 143.0, 133.6, 132.2, 127.9, 127.7, 127.6, 126.2, 125.9, 125.3, 125.2, 113.4, 43.2, 20.7 ppm. The spectral data for compound **3** matches that reported in literature.^{XI}



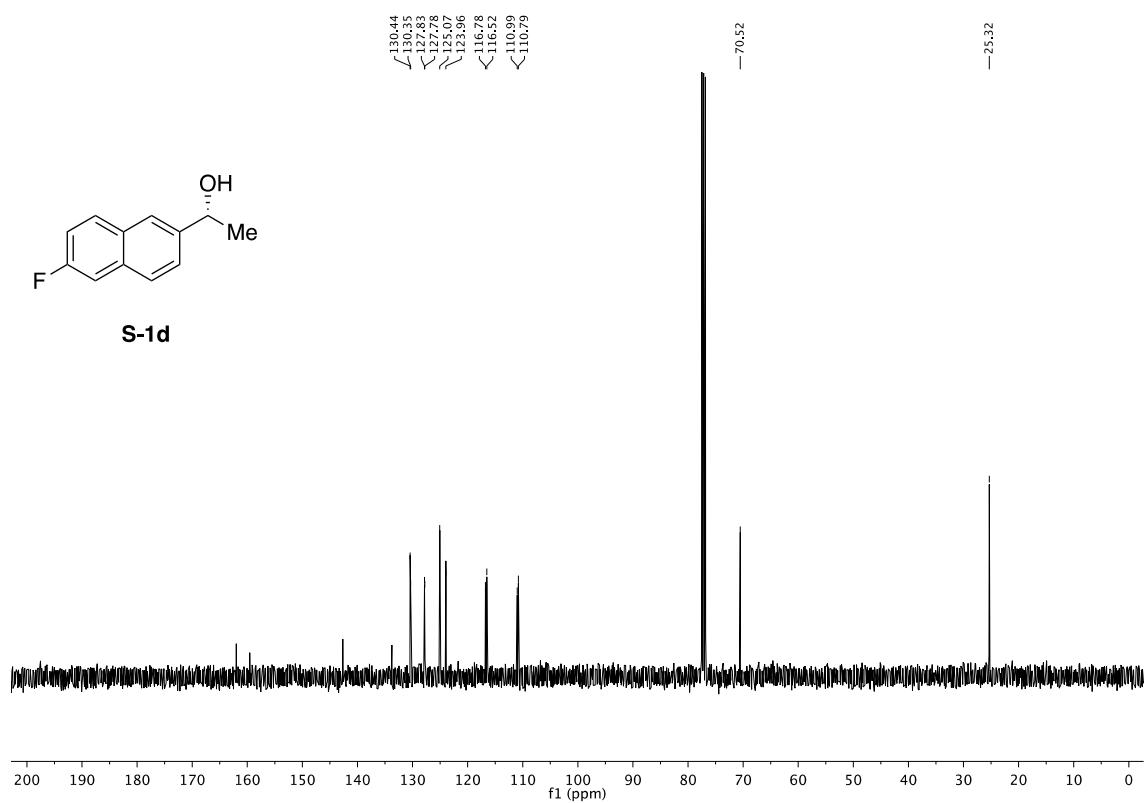
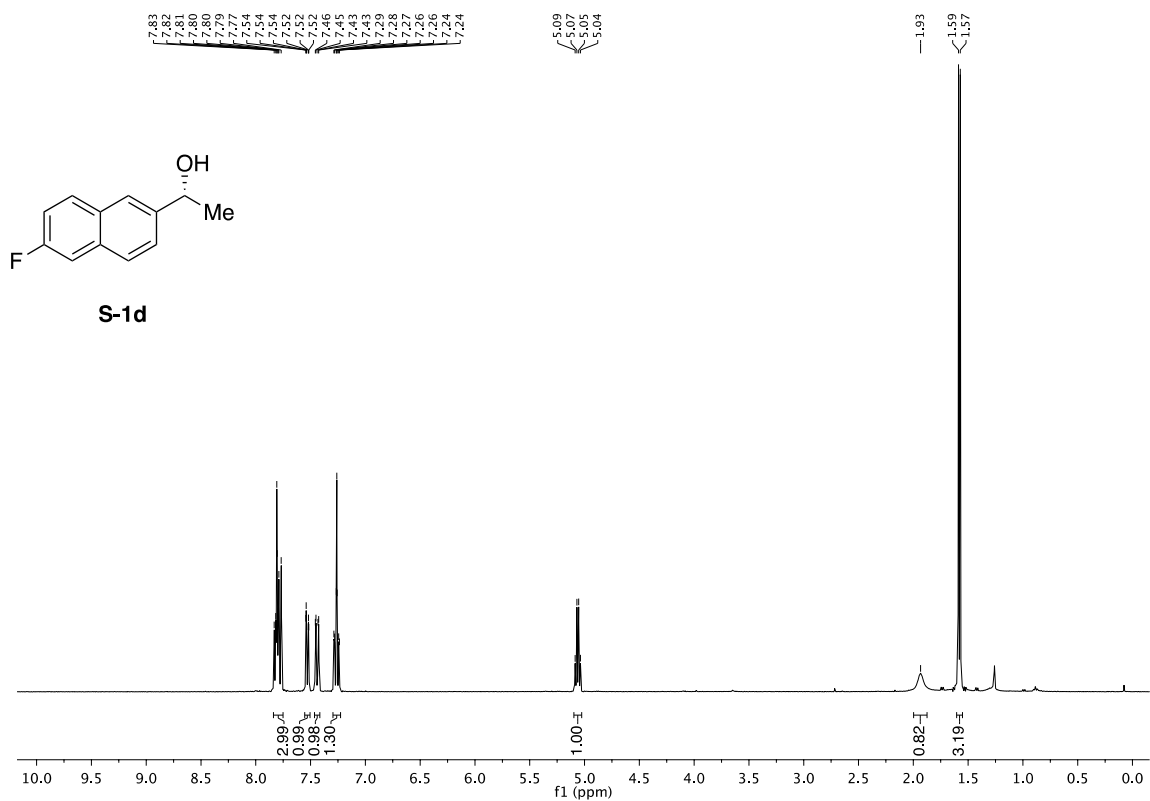


2.5.5 References of experimental procedures

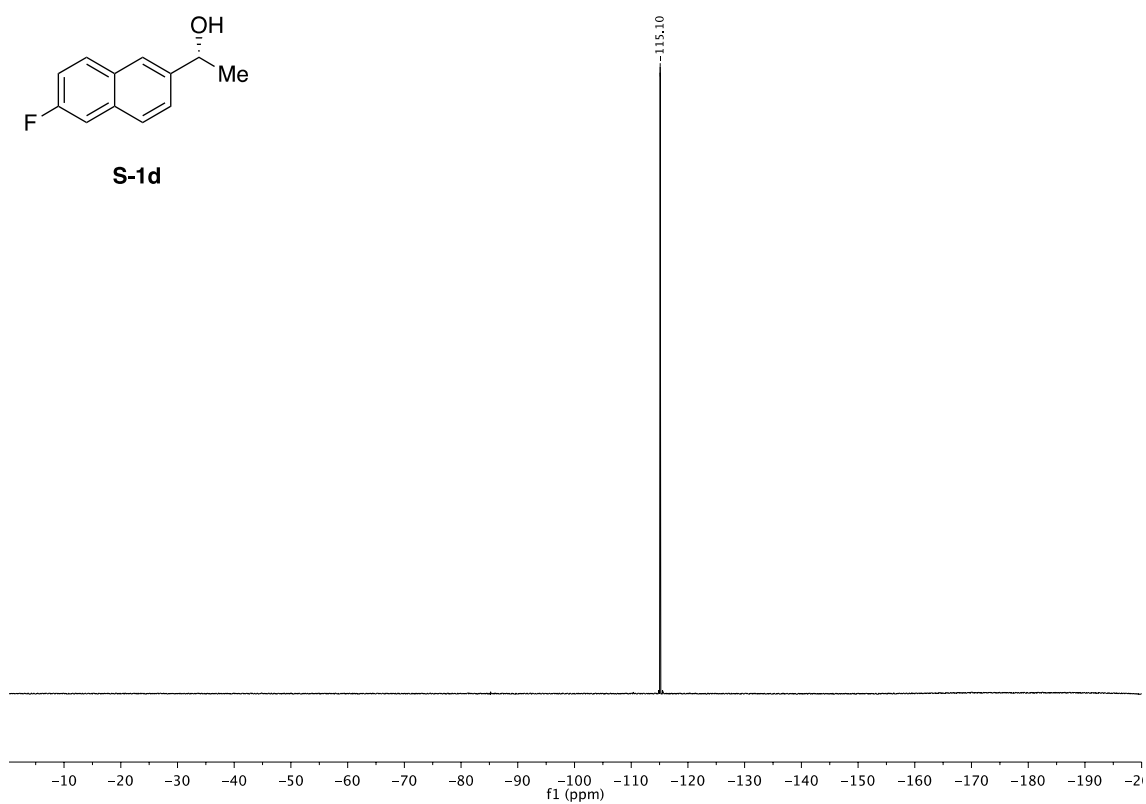
- I) Bakshi, R. K.; Shibata, S.; Chen, C.; Singh, V. K.; Corey, E. J. *J. Am. Chem. Soc.* **1987**, *109*, 7925.
- II) Wu, X.-F.; Li, X.-G.; Hems, W.; King, F.; Xiao, J.-L. *Org. Biomol. Chem.* **2004**, *2*, 1818.
- III) Taylor, B. L. H.; Swift, E. C.; Waetzig, J. D.; Jarvo, E. R. *J. Am. Chem. Soc.* **2011**, *133*, 389-391.
- IV) Kišić, A.; Stephan, M.; Mohar, B. *Org. Lett.* **2013**, *15*, 1614-1617.
- V) Zong, H.; Huang, H.; Song, L. *Tetrahedron: Asymmetry*. **2016**, *27*, 1069-1074.
- VI) Noji, M.; Ohno, T.; Futaba, N.; Tajima, H.; Ishii, K. *J. Org. Chem.* **2003**, *68*, 9340-9347.
- VII) Pulis, A. P.; Blair, D. J.; Torres, E.; Aggarwal, V. K. *J. Am. Chem. Soc.* **2013**, *135*, 16054.
- VIII) Zheng L.-S.; Llopis Q.; Echeverria P.-G.; Ferard C.; Guillamot G.; Phansavath P.; Ratovelomanana-Vidal V., *J. Org. Chem.*, **2017**, *82*, 5607-5615.
- IX) Imao, D.; Glasspole, B. W.; Laberge, V. S.; Crudden, C. M. *J. Am. Chem. Soc.* **1987**, *109*, 4756-4758.
- X) Sonawane, R. P.; Jheengut, V.; Rabalakos, C.; Larouche-Gauthier, R.; Scott, H. K.; Aggarwal, V. K. *Angew. Chem. Int. Ed.* **2011**, *50*, 3760-3763
- XI) Kiuchi H.; Takahashi D.; Funaki K.; Sato T.; Oi S., *Org. Lett.*, **2012**, *14*, 4502-4505.

Chapter 2

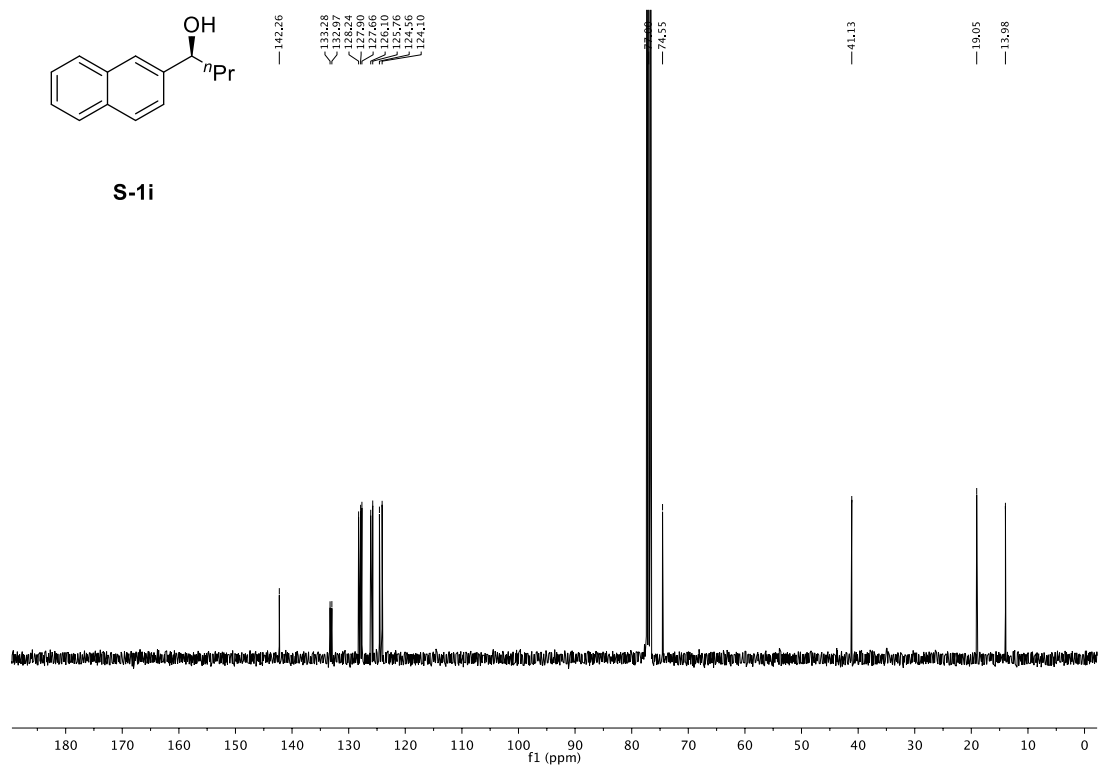
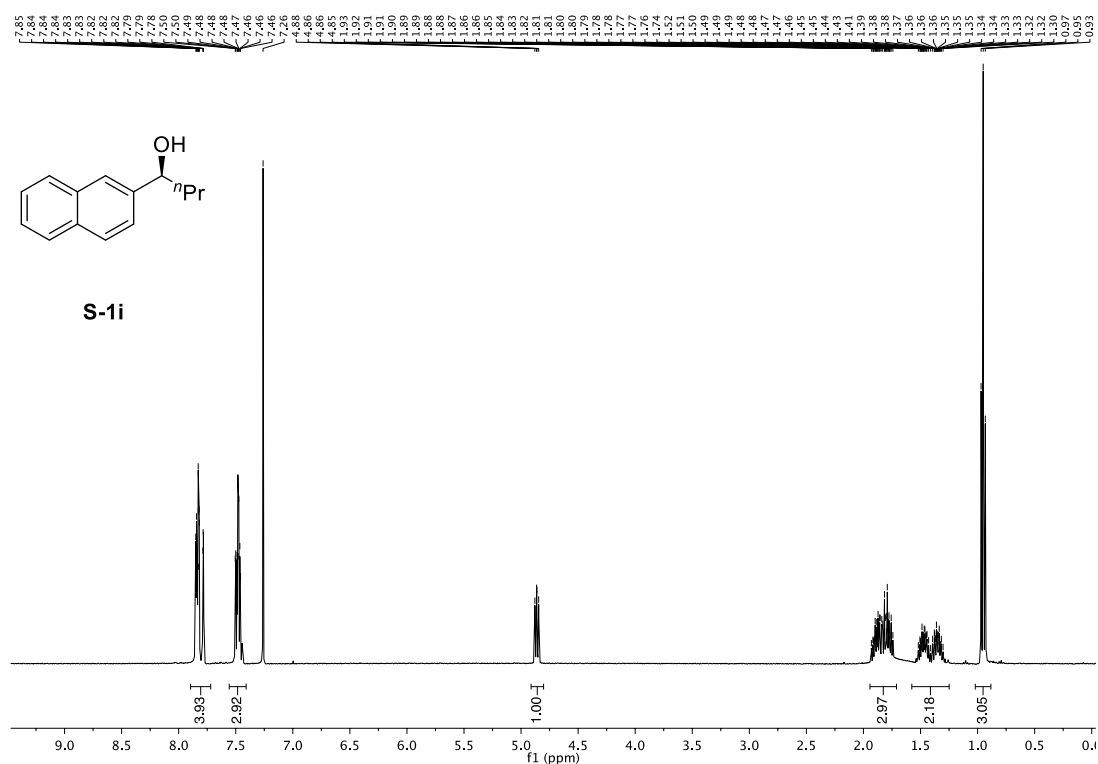
2.5.6 $^1\text{H-NMR}$, $^{13}\text{C-NMR}$ and $^{19}\text{F-NMR}$ spectra.



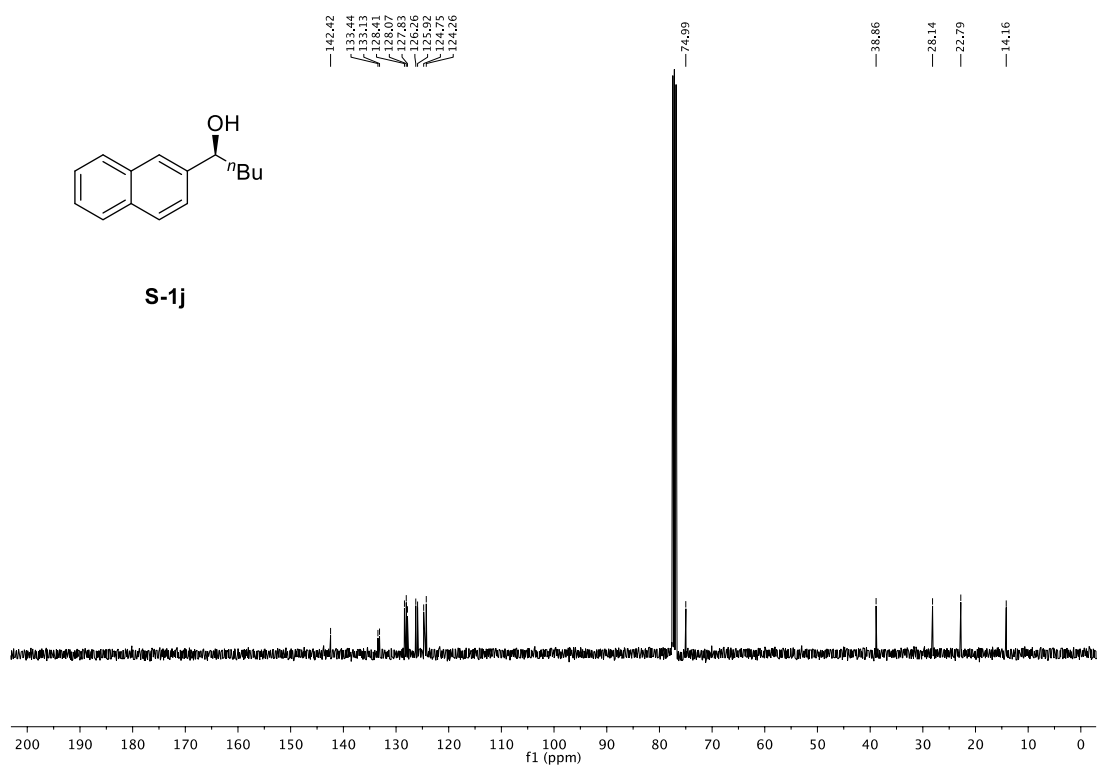
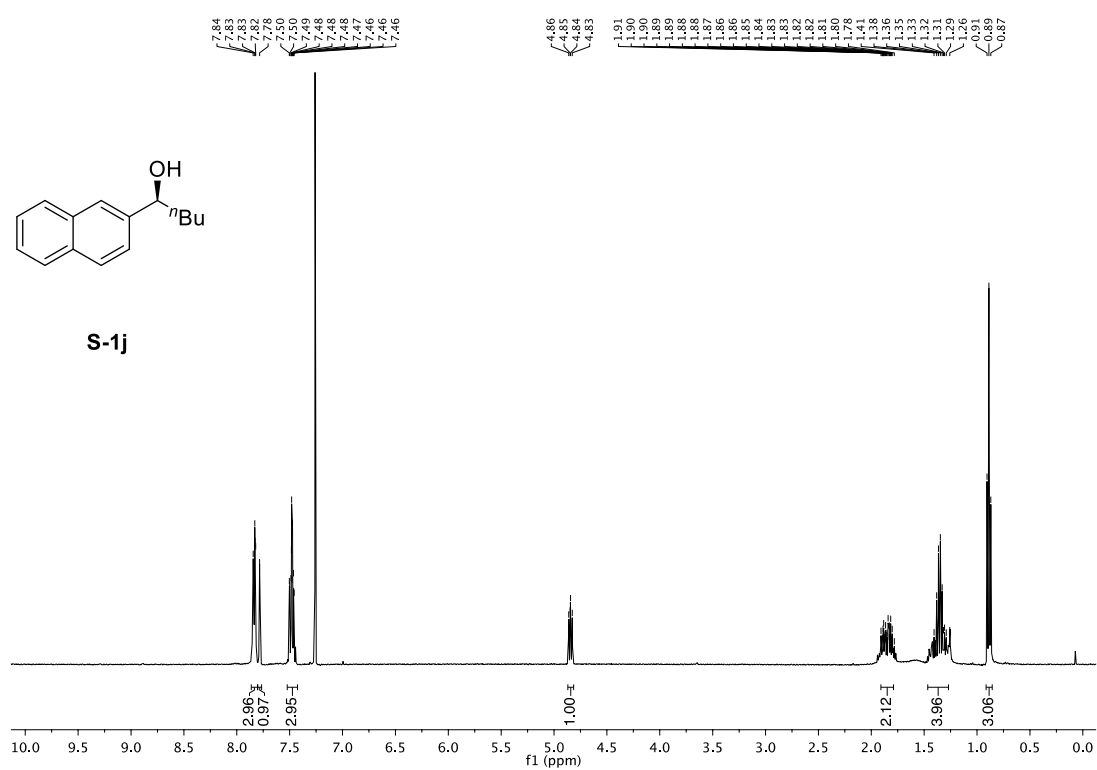
Stereospecific Borylation of Benzyl C(sp³)-O Bonds



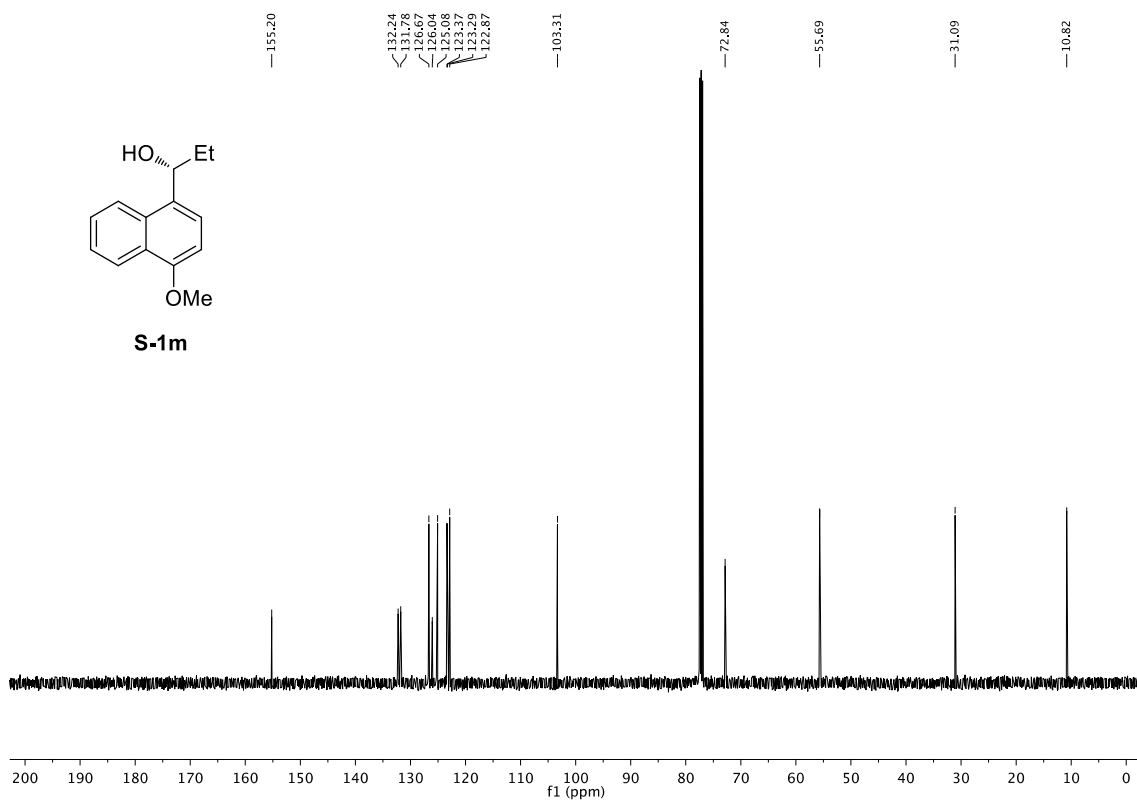
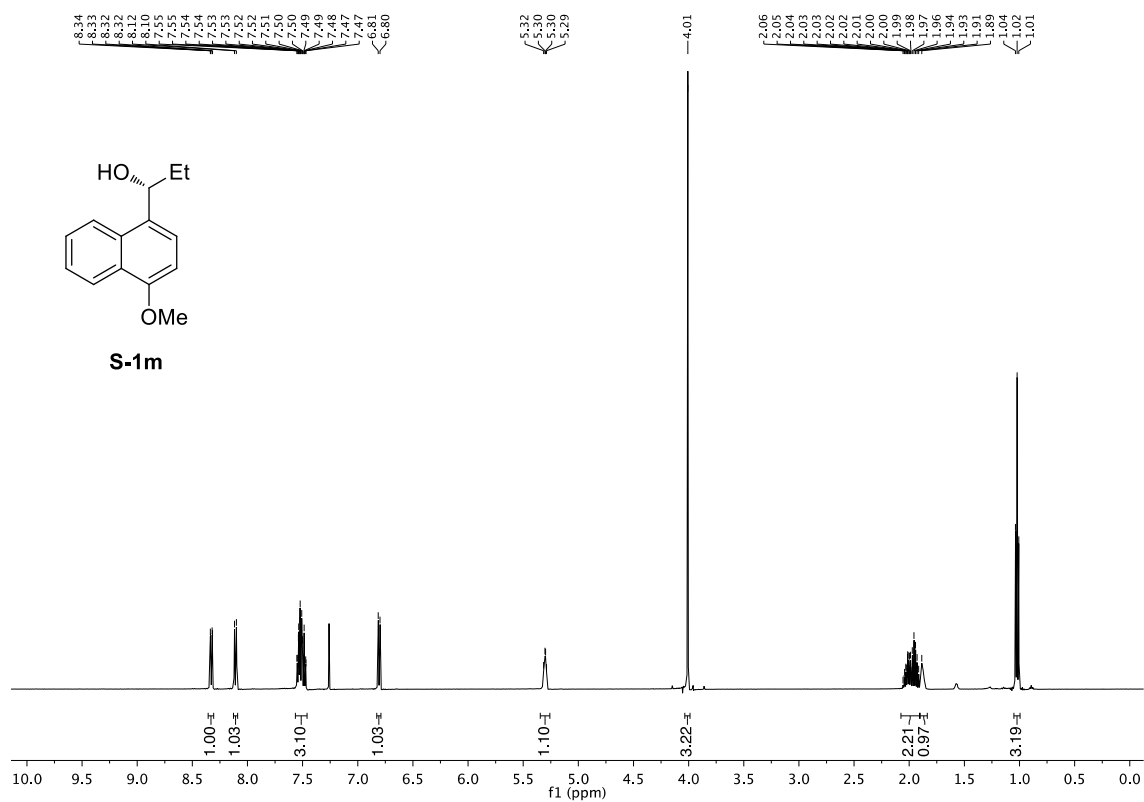
Chapter 2



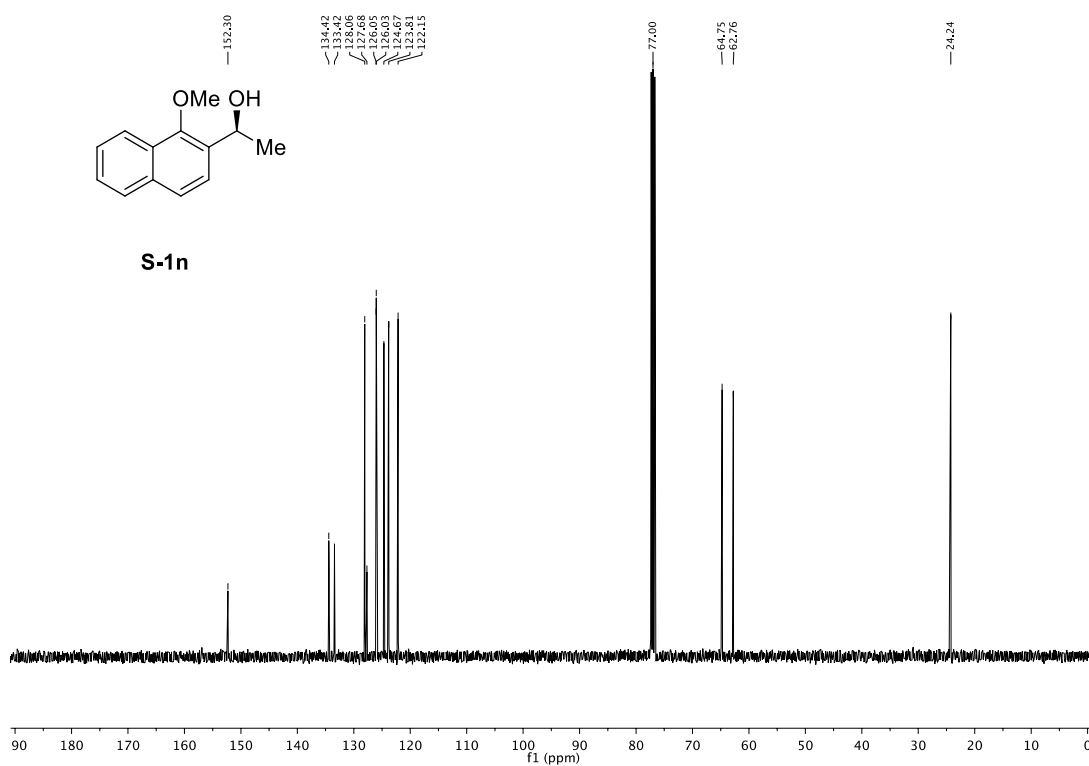
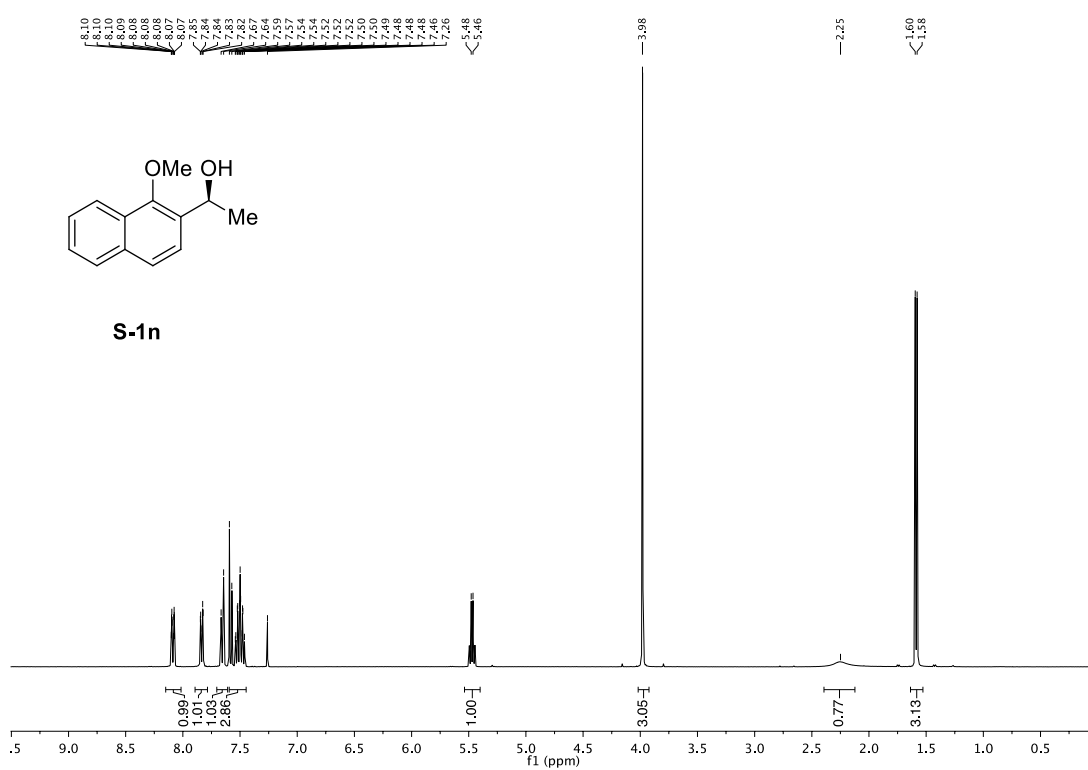
Stereospecific Borylation of Benzyl C(sp³)-O Bonds



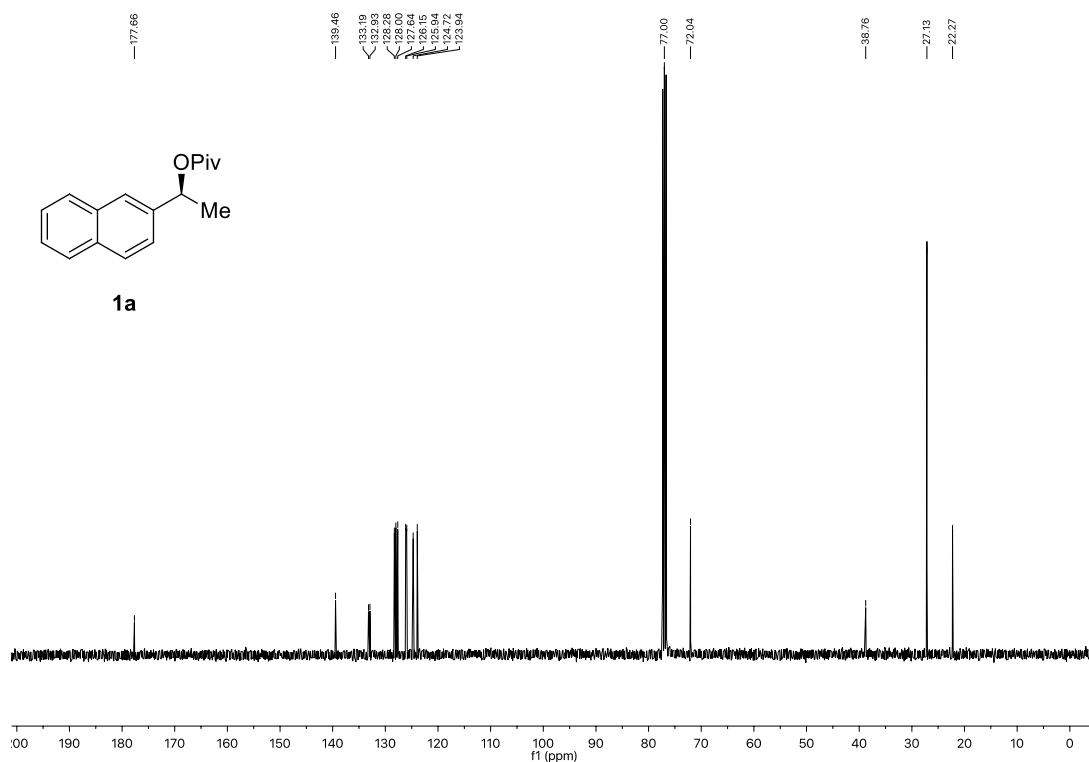
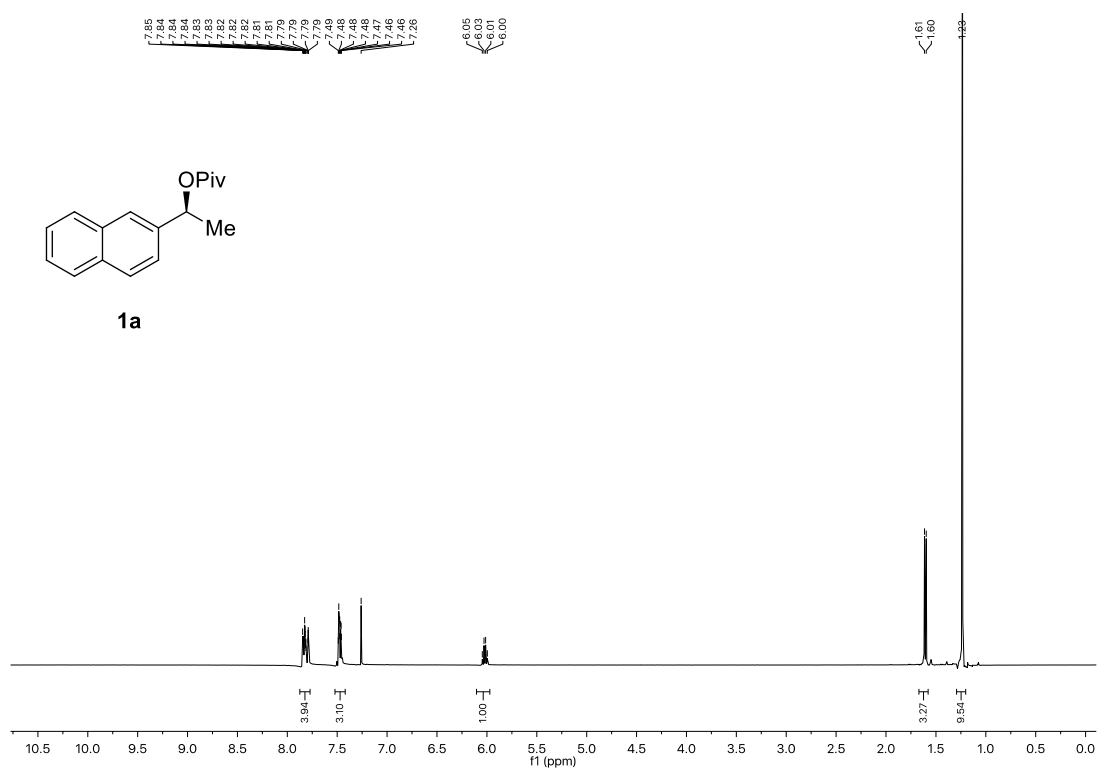
Chapter 2



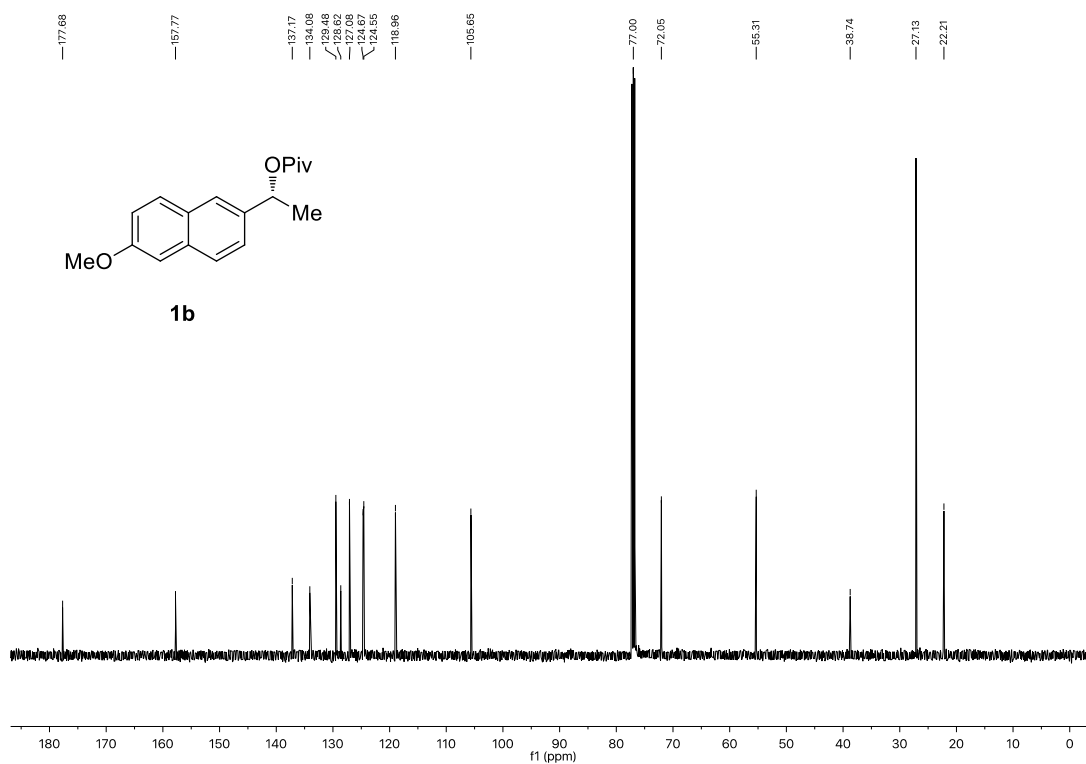
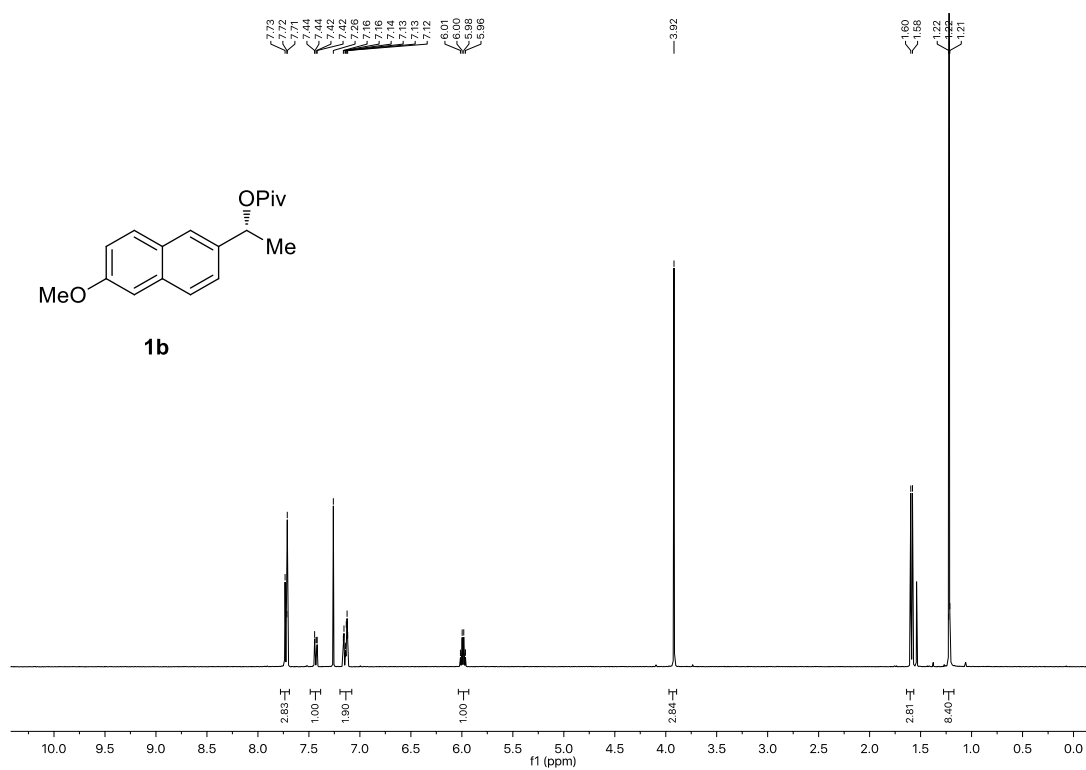
Stereospecific Borylation of Benzyl C(sp³)-O Bonds



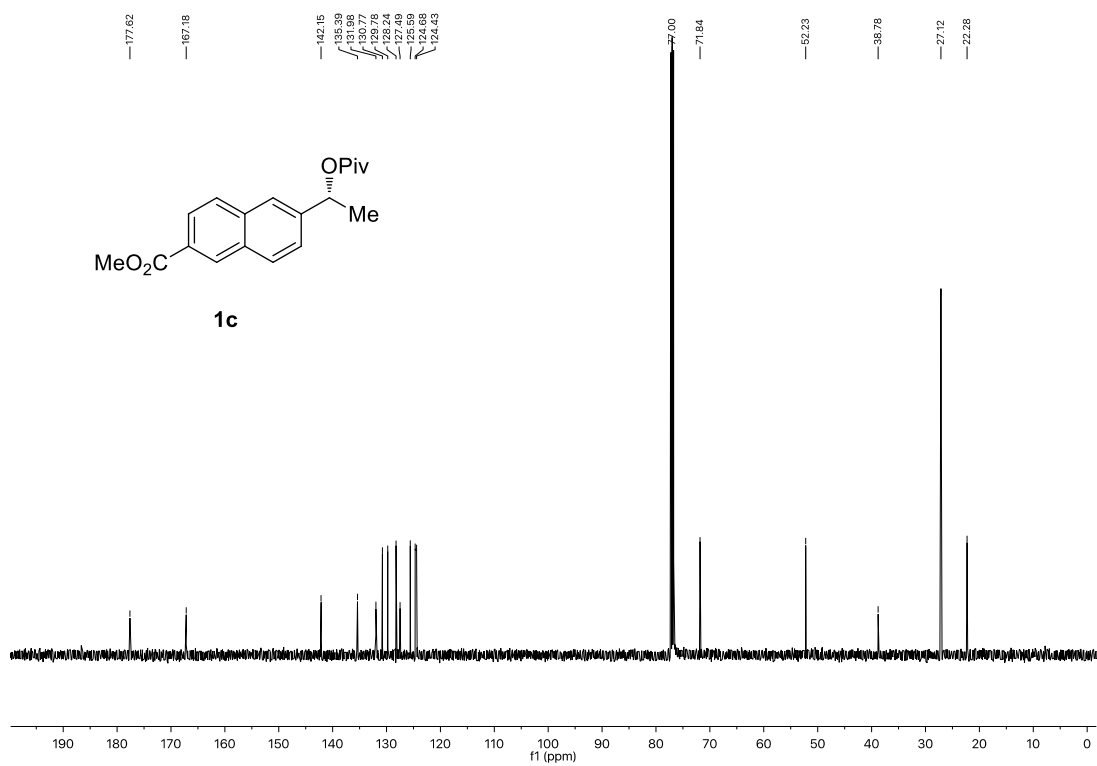
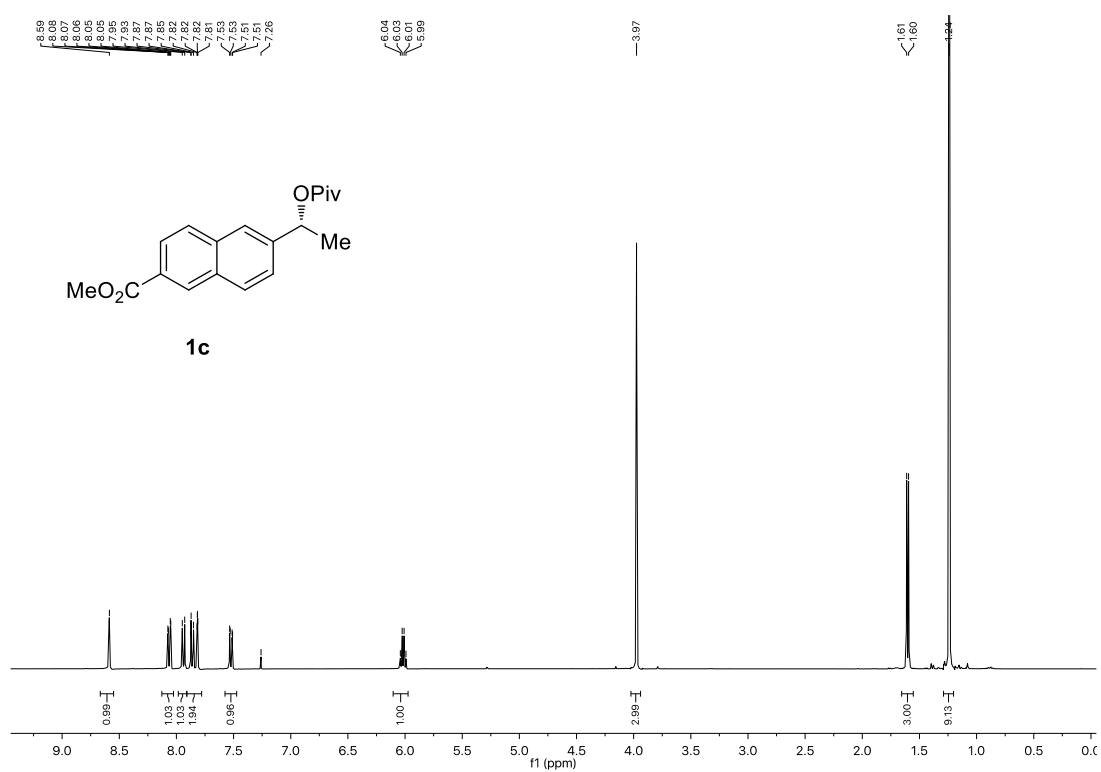
Chapter 2



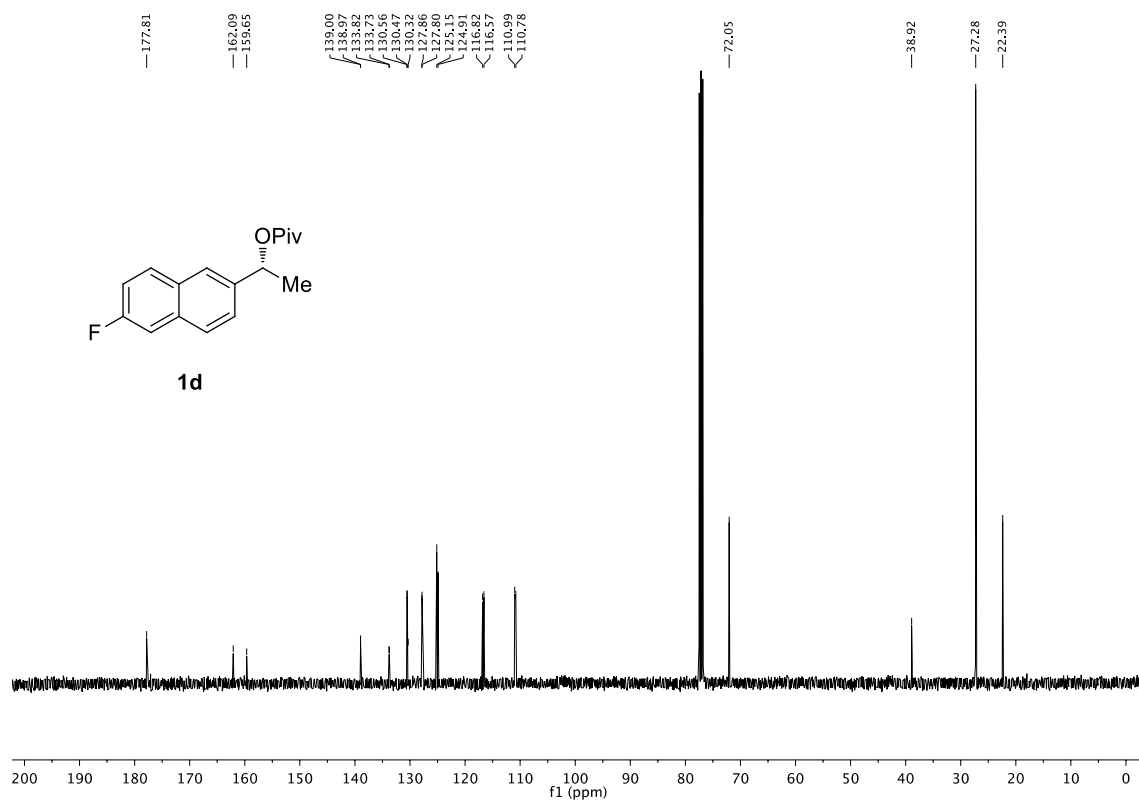
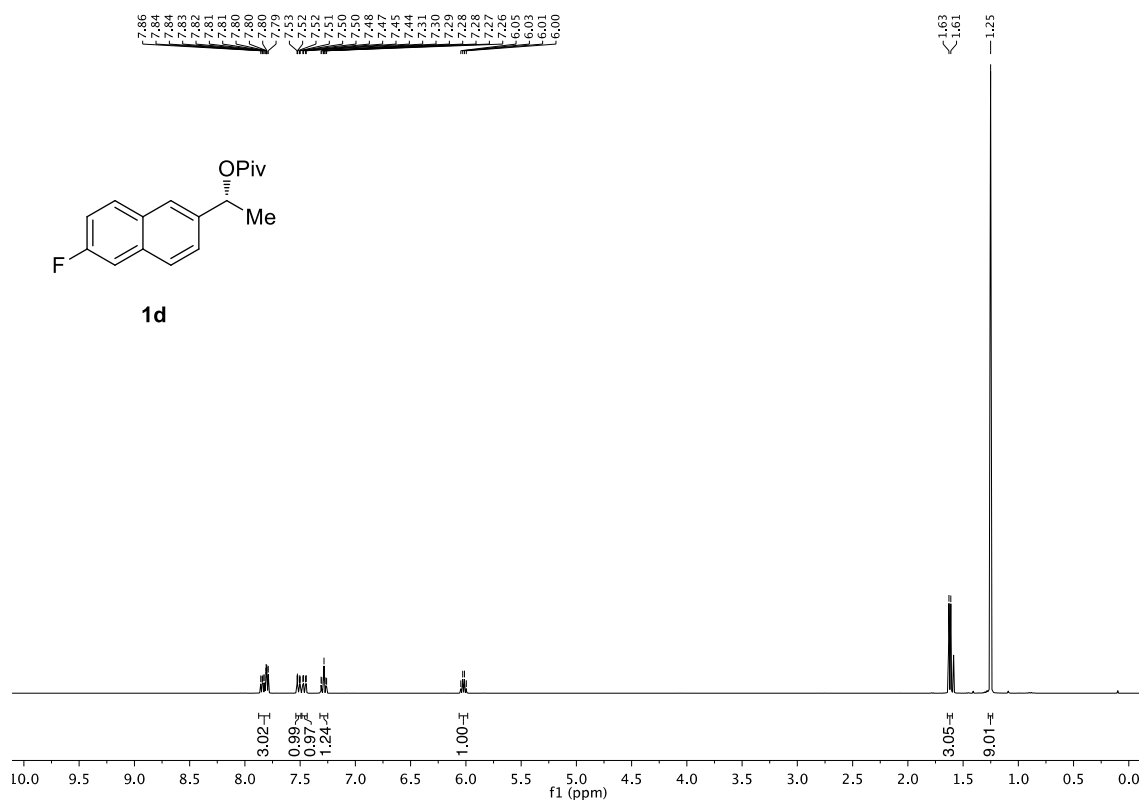
Stereospecific Borylation of Benzyl C(sp³)-O Bonds



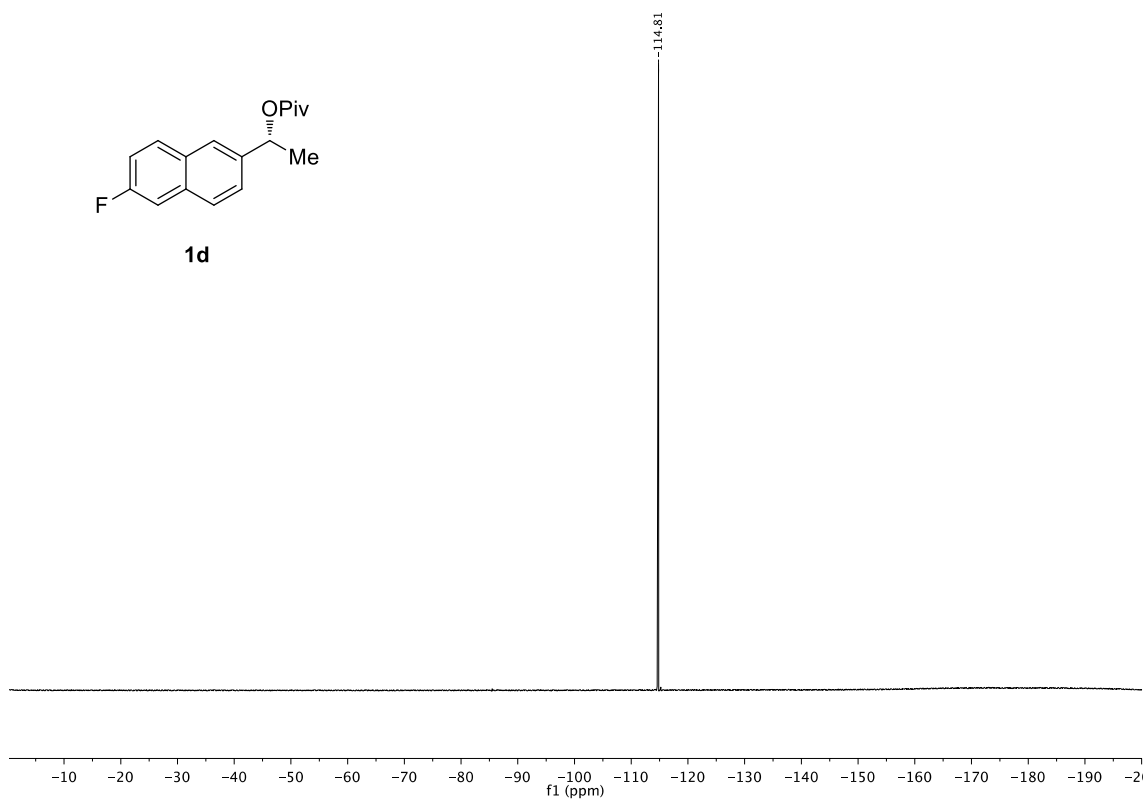
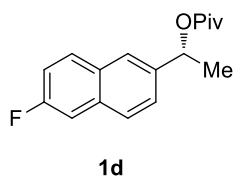
Chapter 2



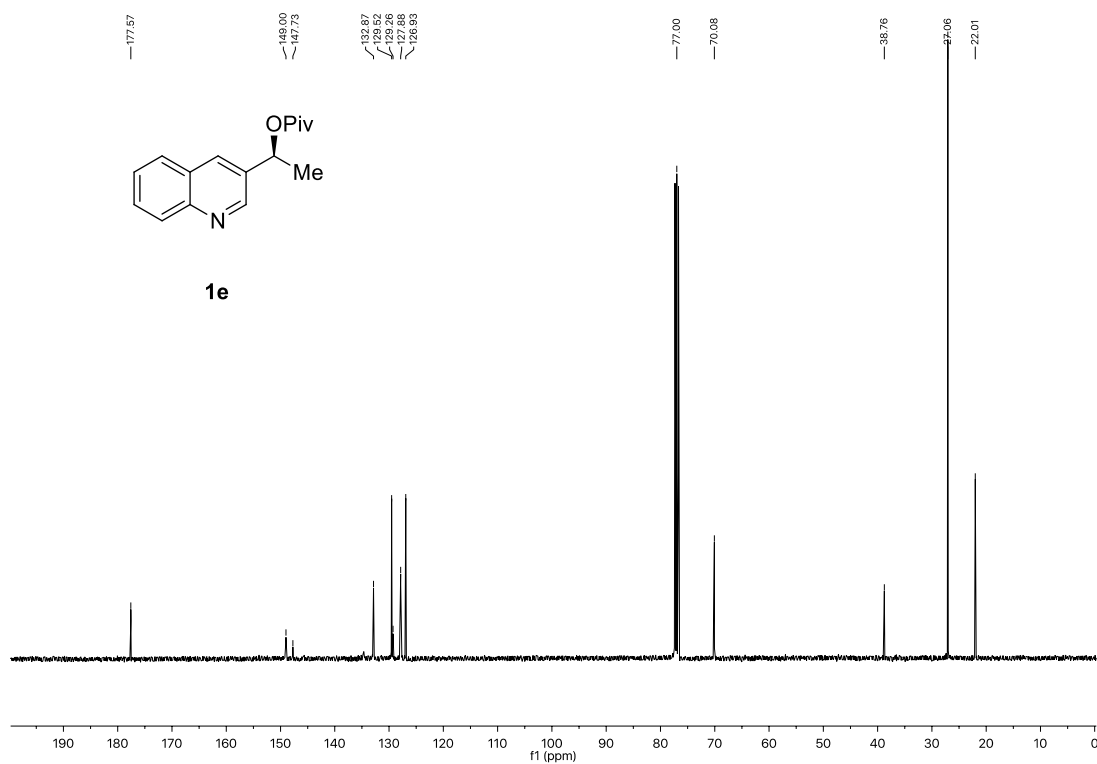
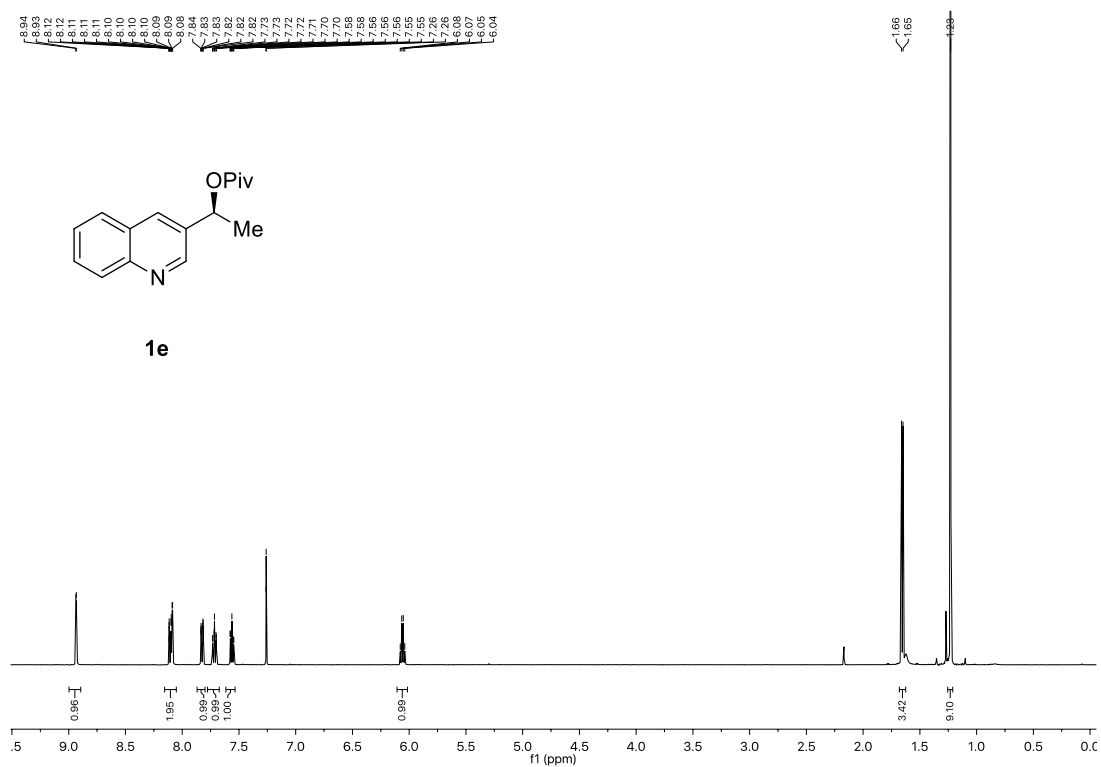
Stereospecific Borylation of Benzyl C(sp³)-O Bonds



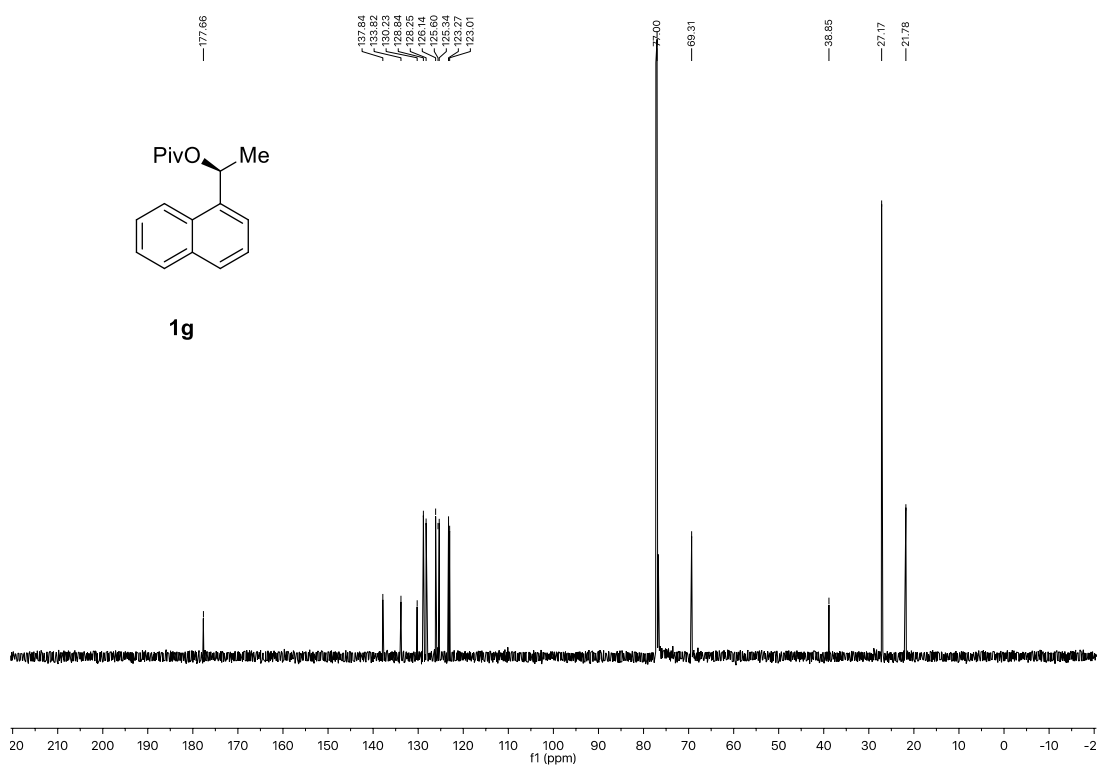
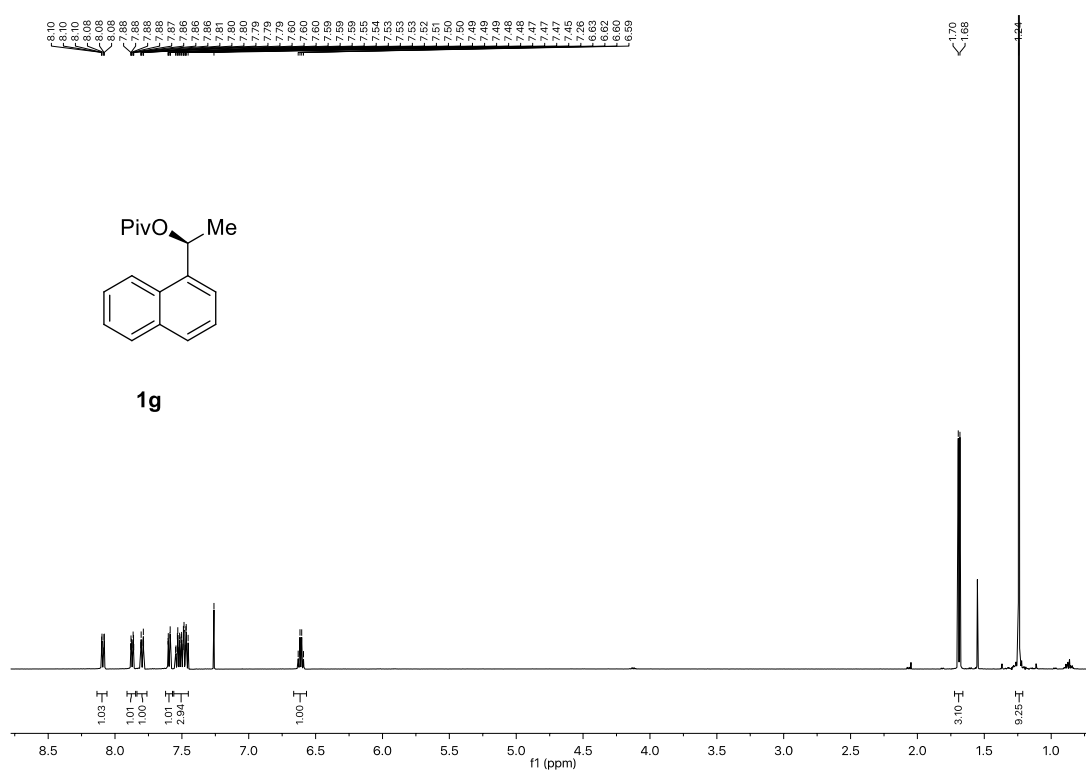
Chapter 2



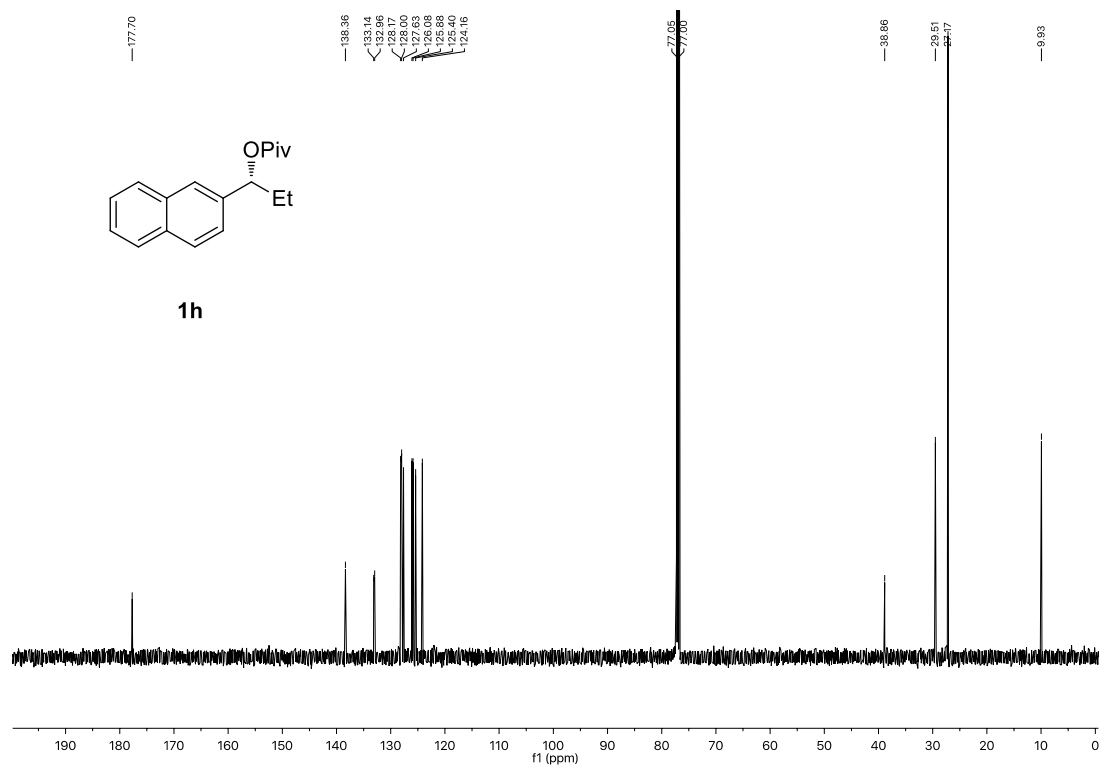
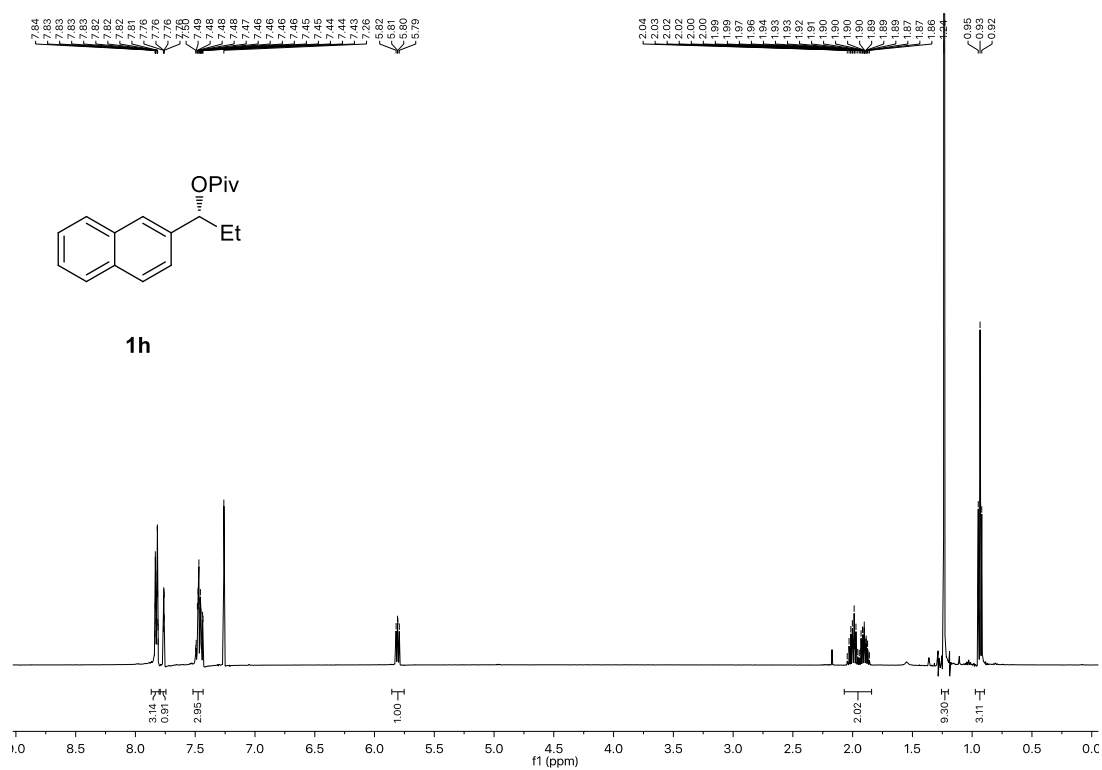
Stereospecific Borylation of Benzyl C(sp³)-O Bonds



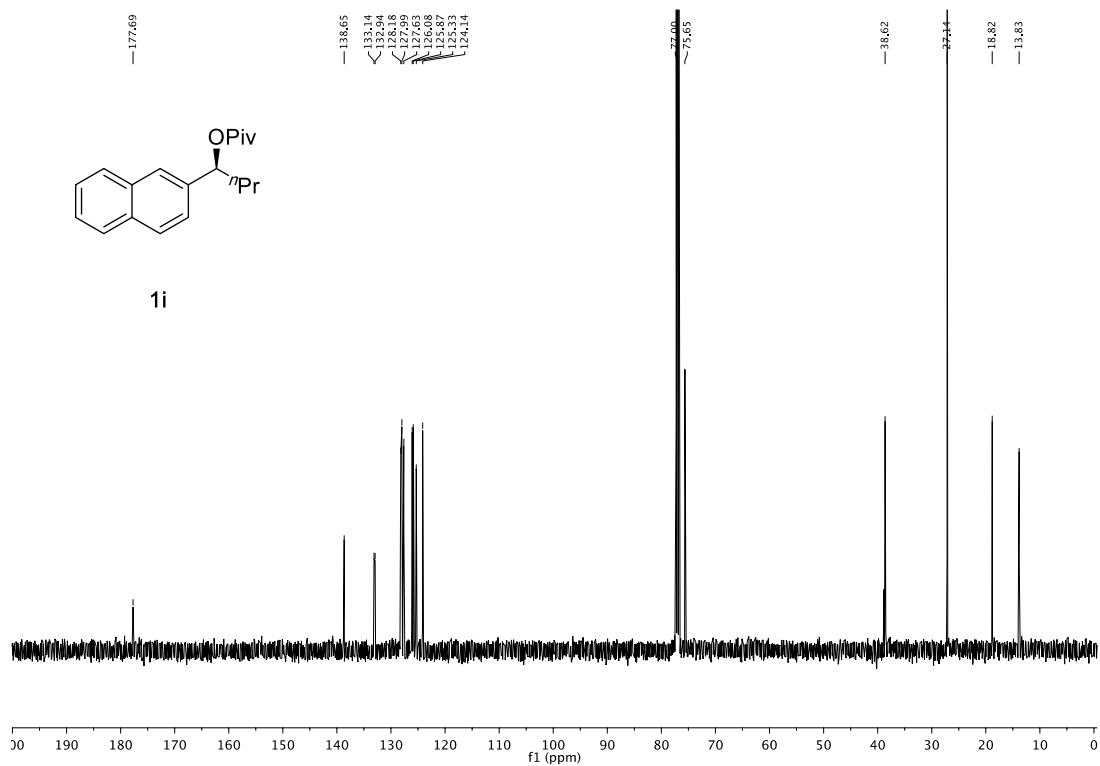
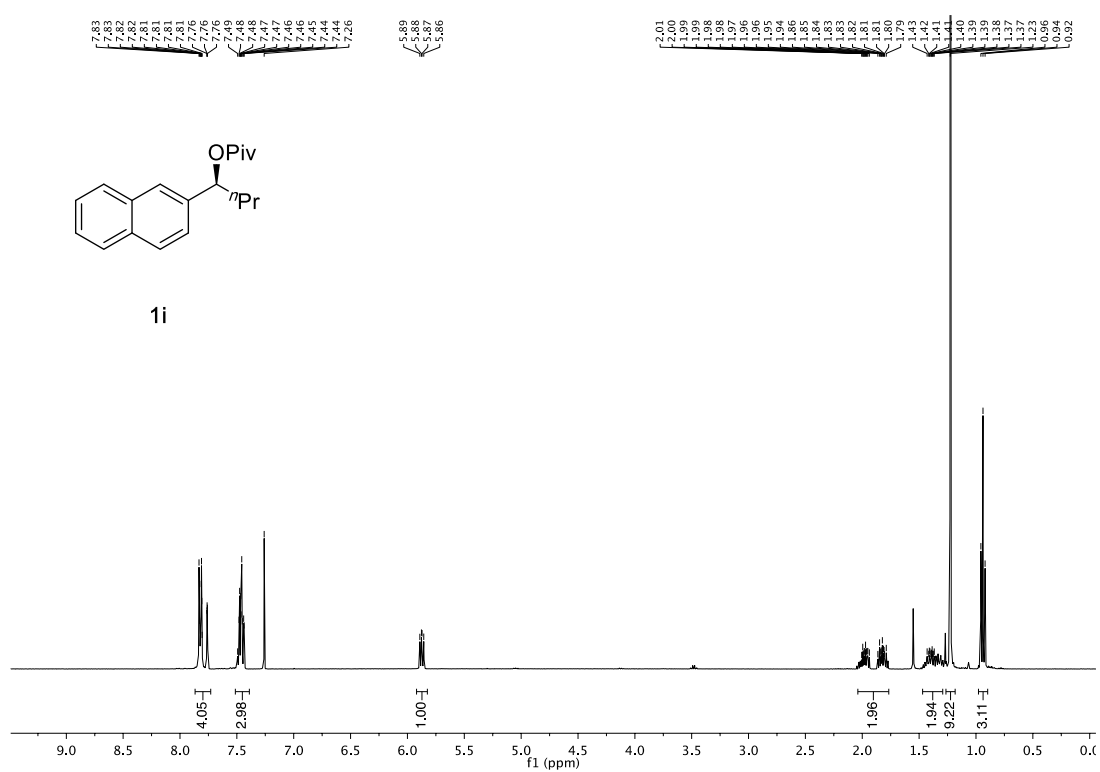
Stereospecific Borylation of Benzyl C(sp³)-O Bonds



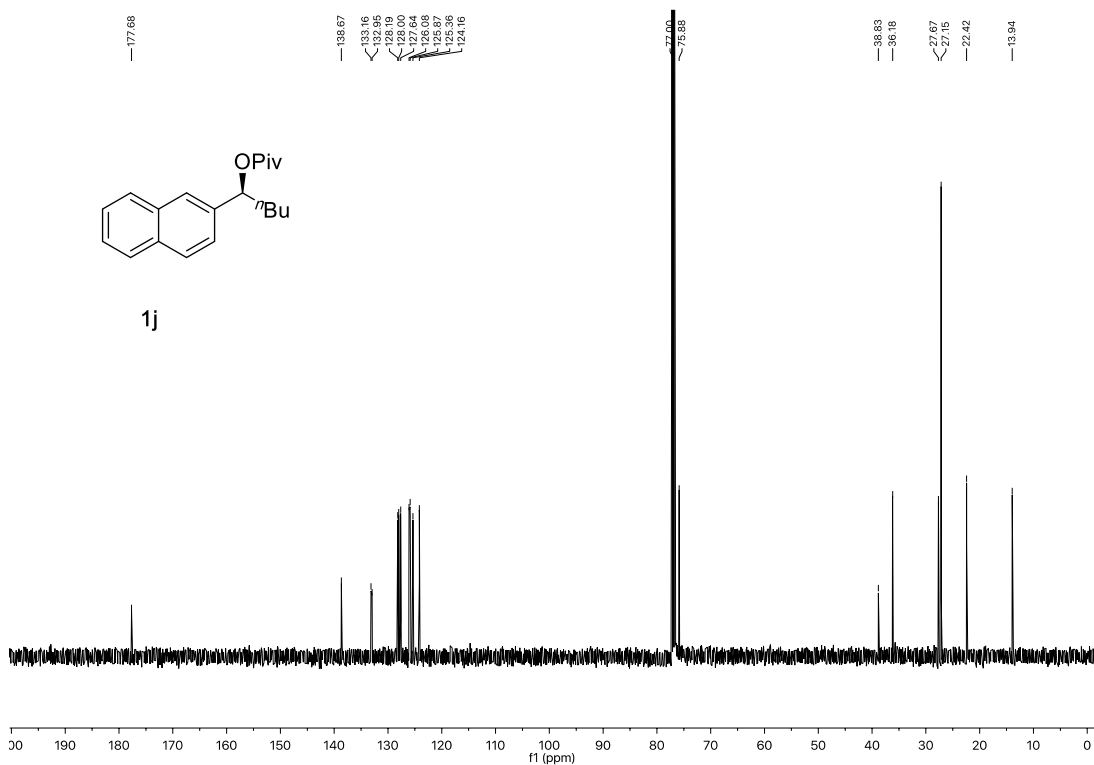
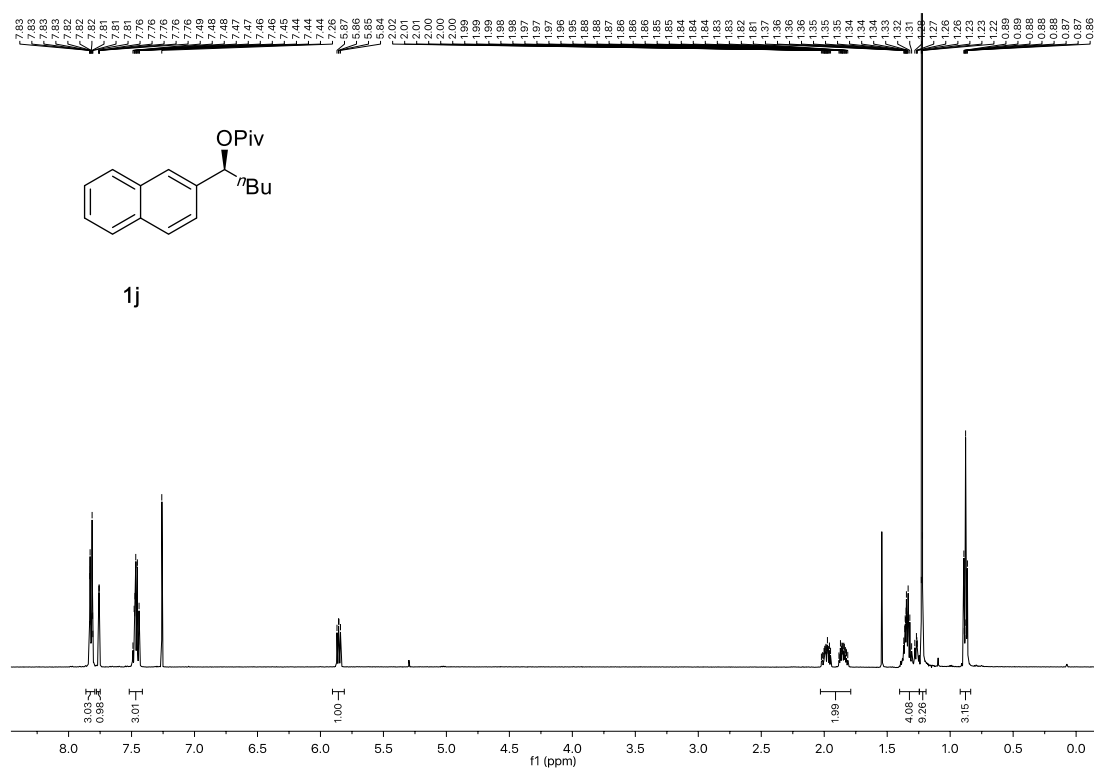
Chapter 2



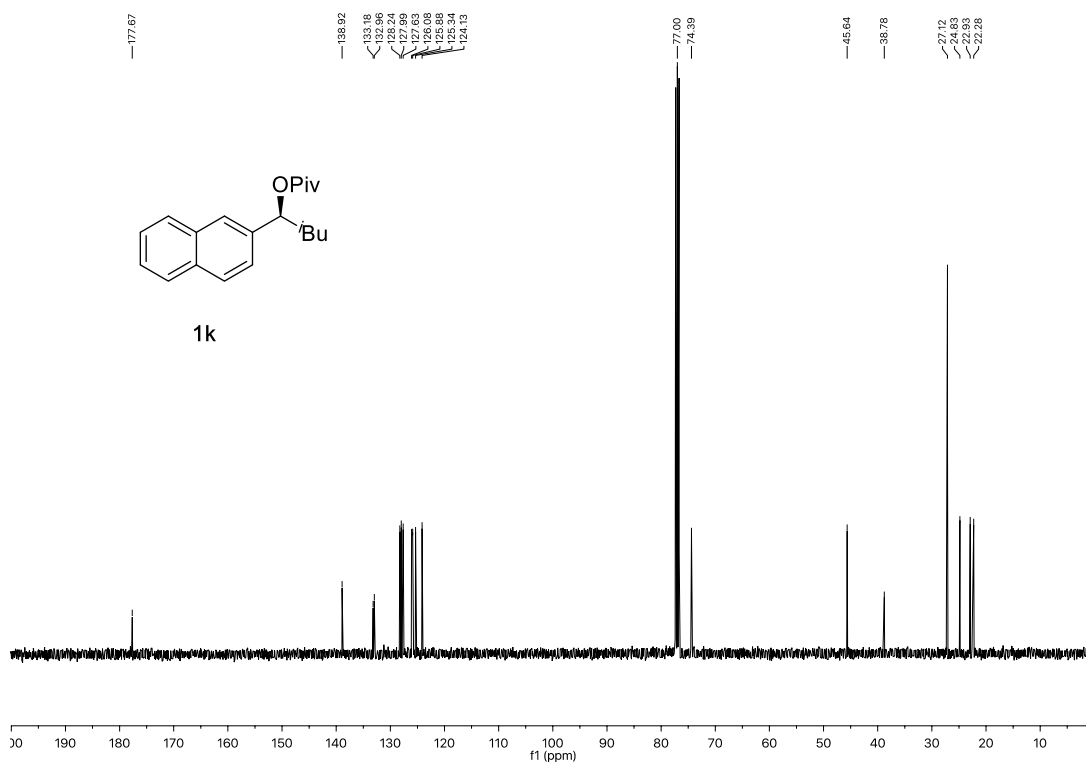
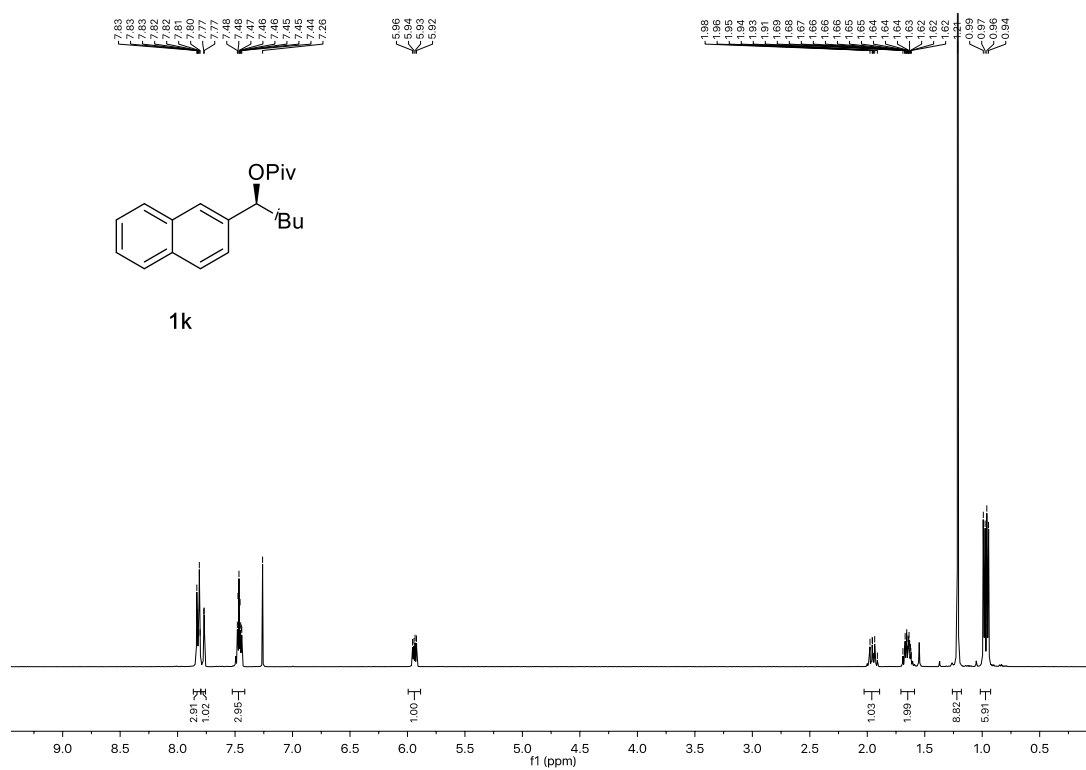
Stereospecific Borylation of Benzyl C(sp³)-O Bonds



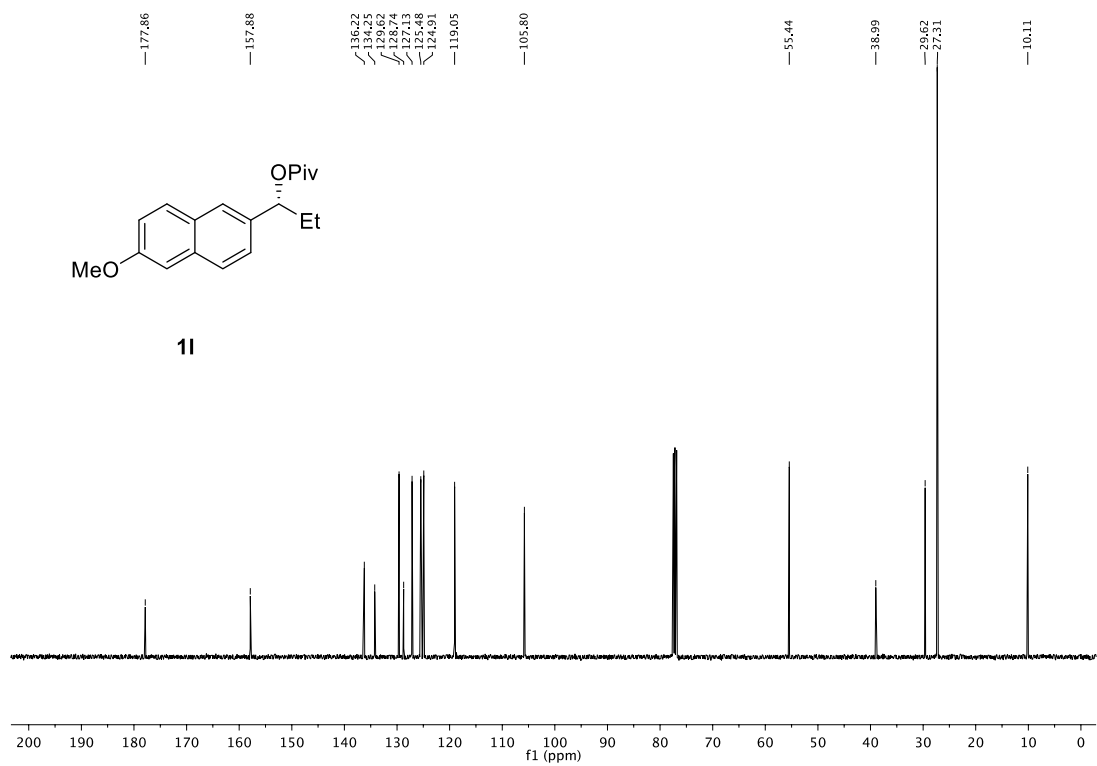
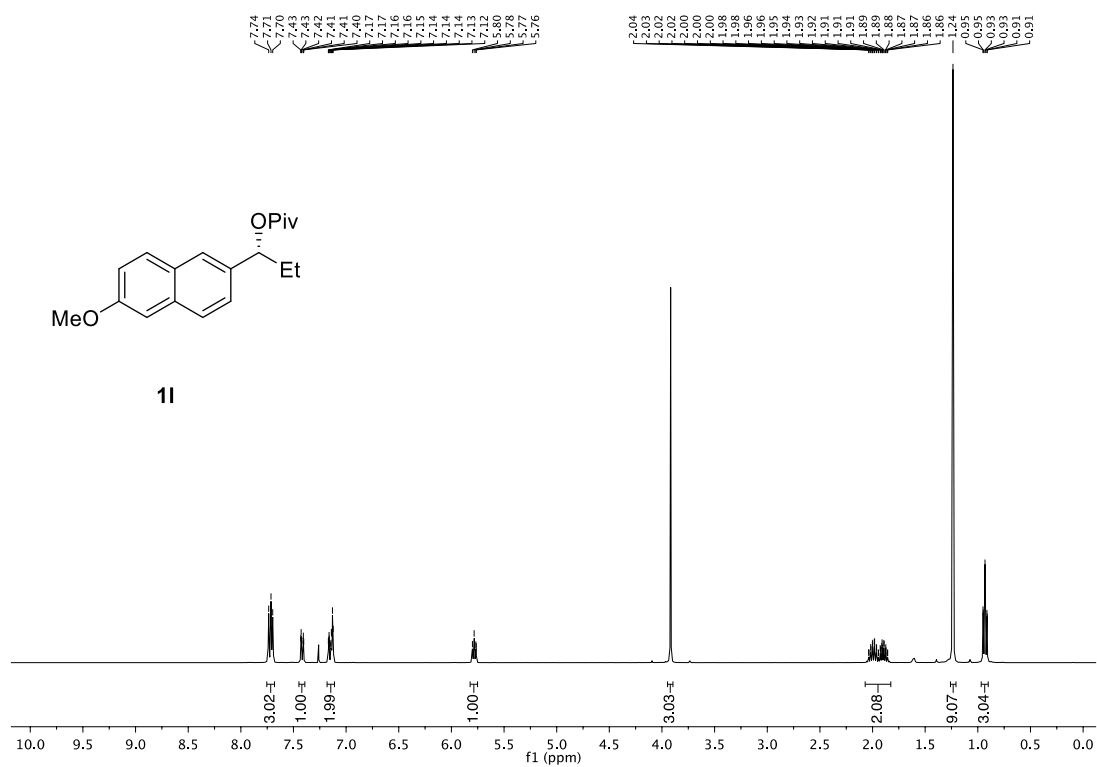
Chapter 2



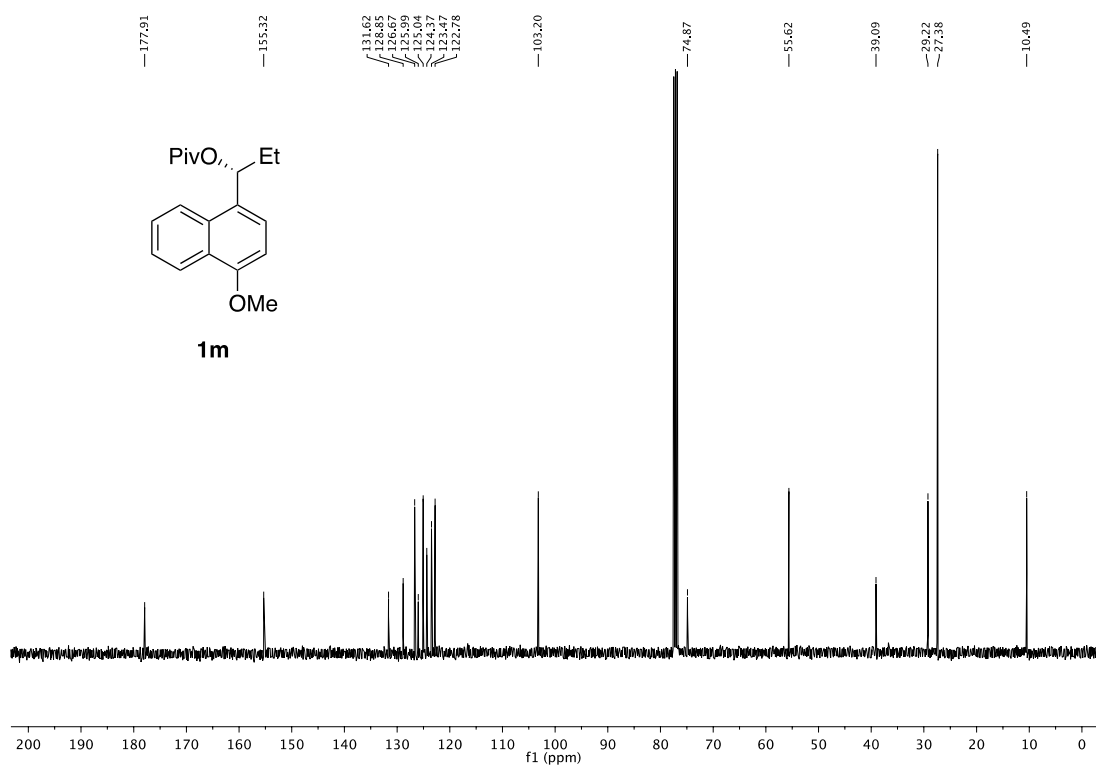
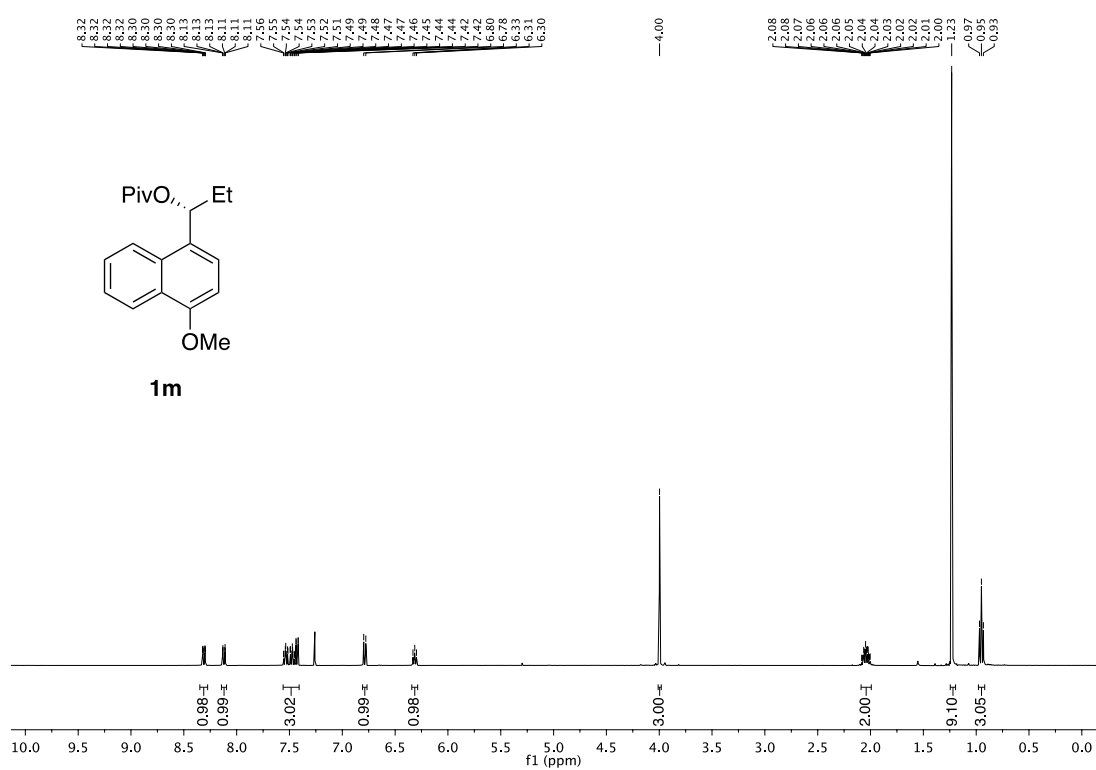
Stereospecific Borylation of Benzyl C(sp³)-O Bonds



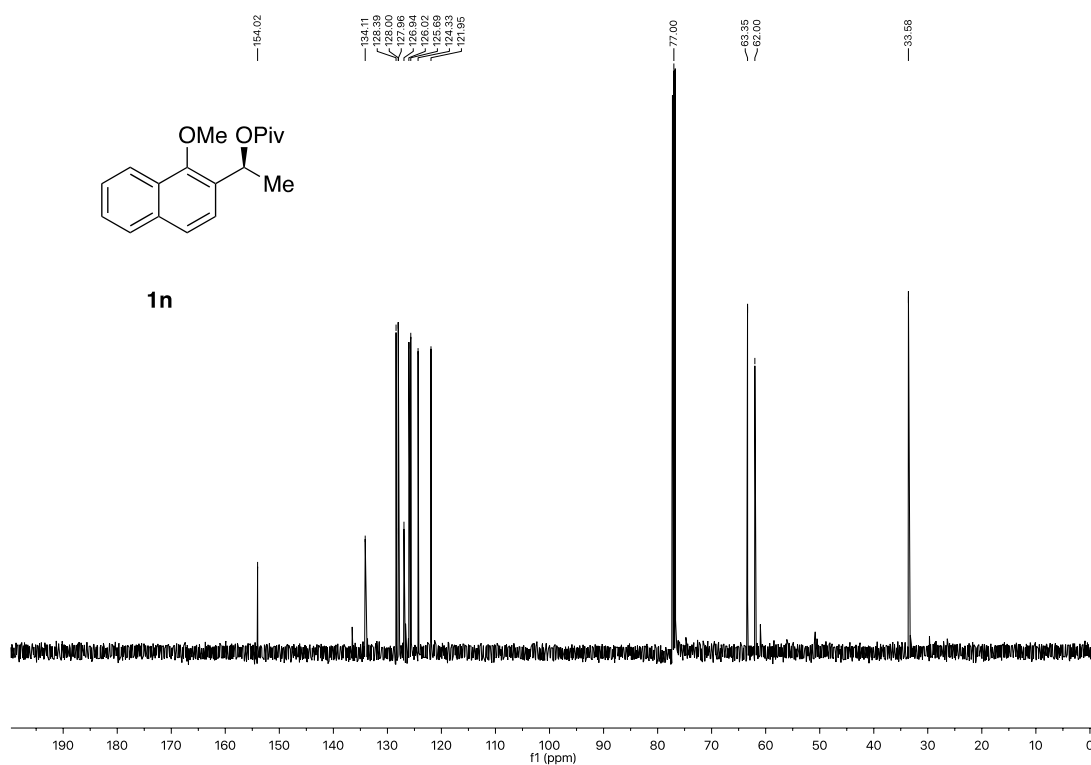
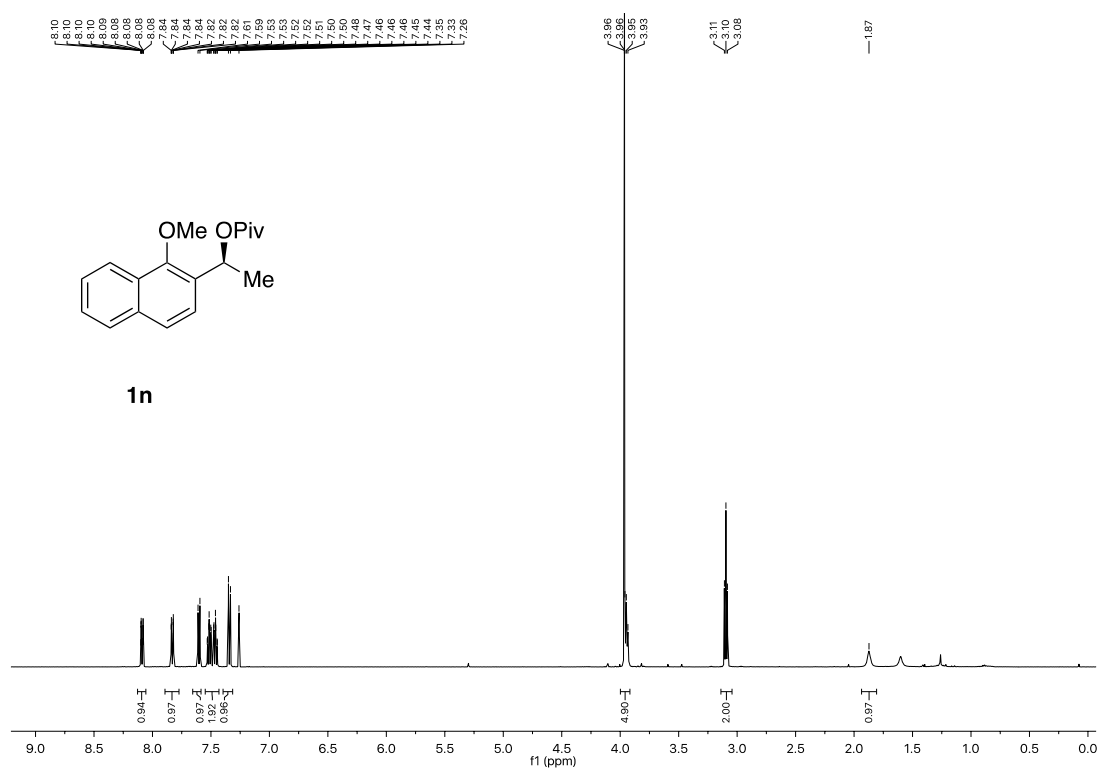
Chapter 2



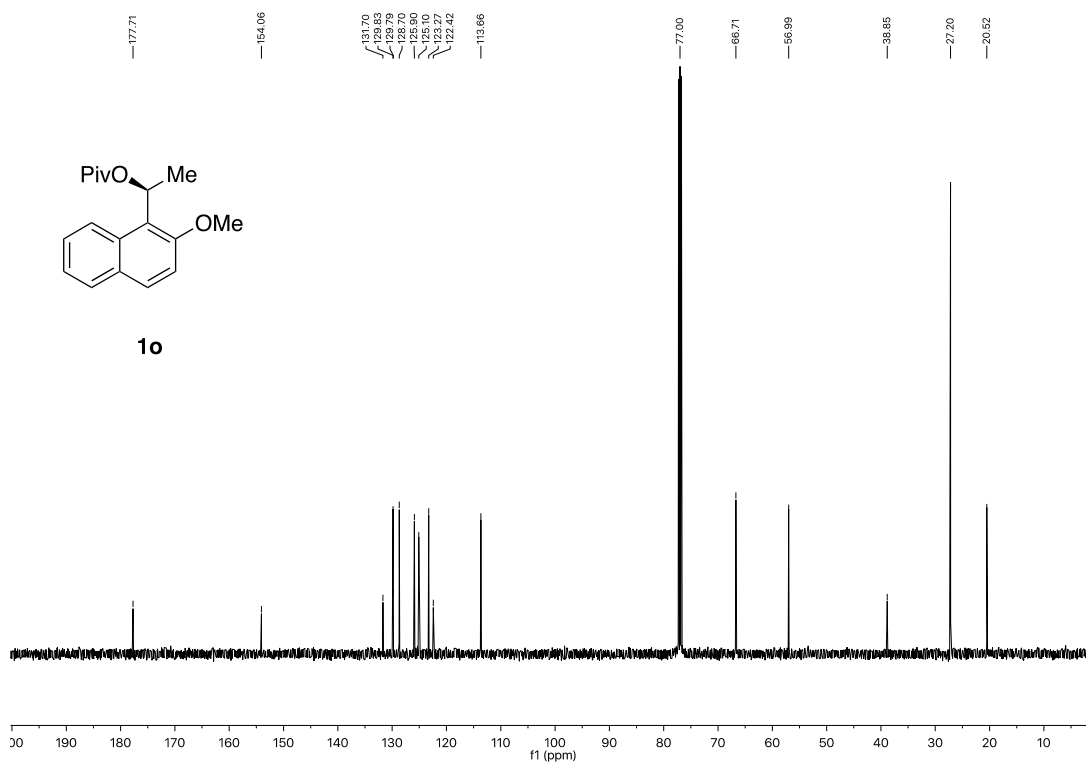
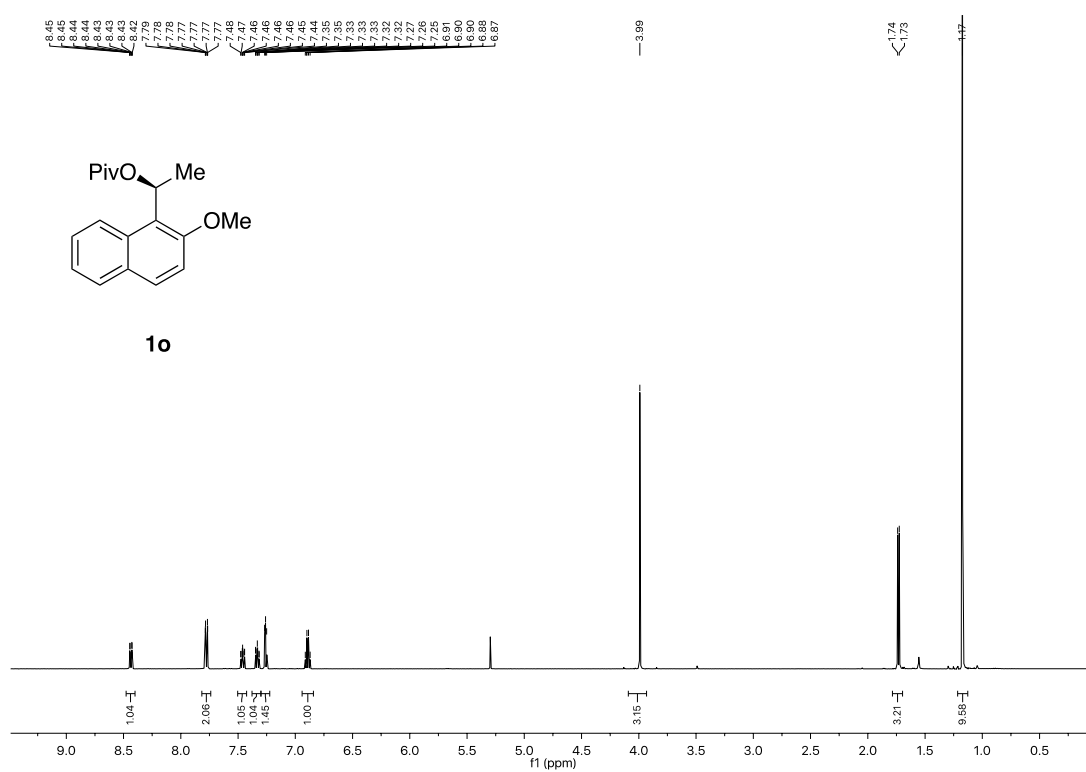
Stereospecific Borylation of Benzyl C(sp³)-O Bonds



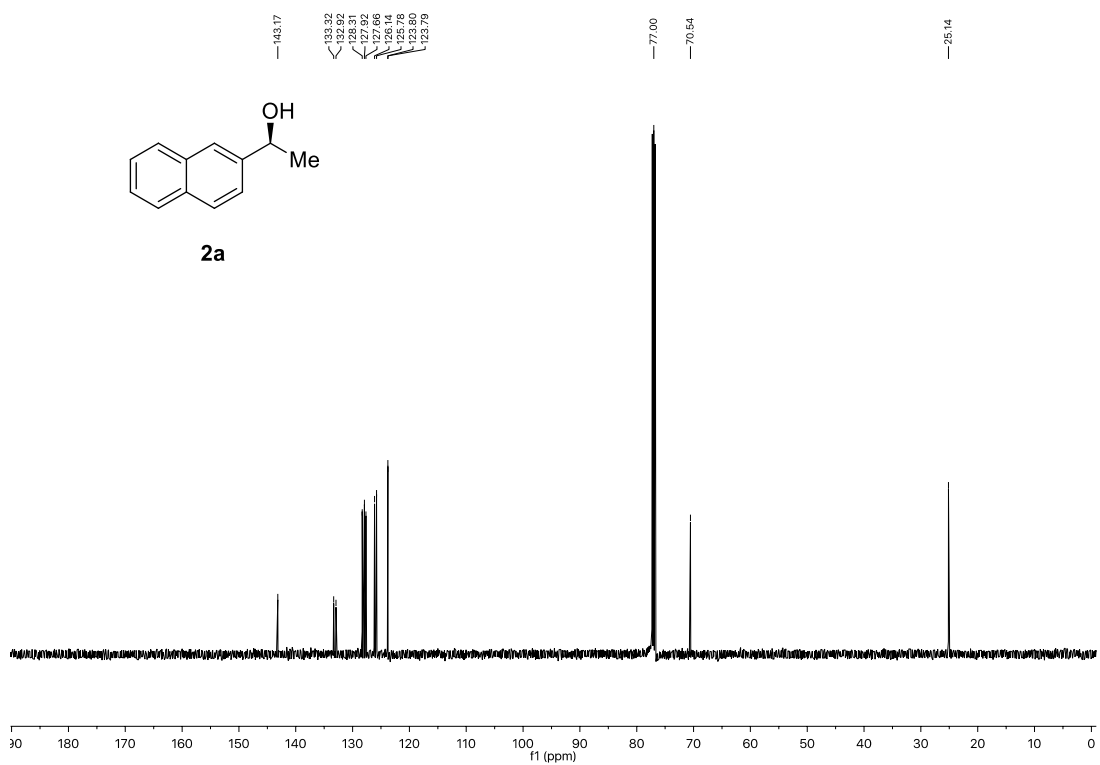
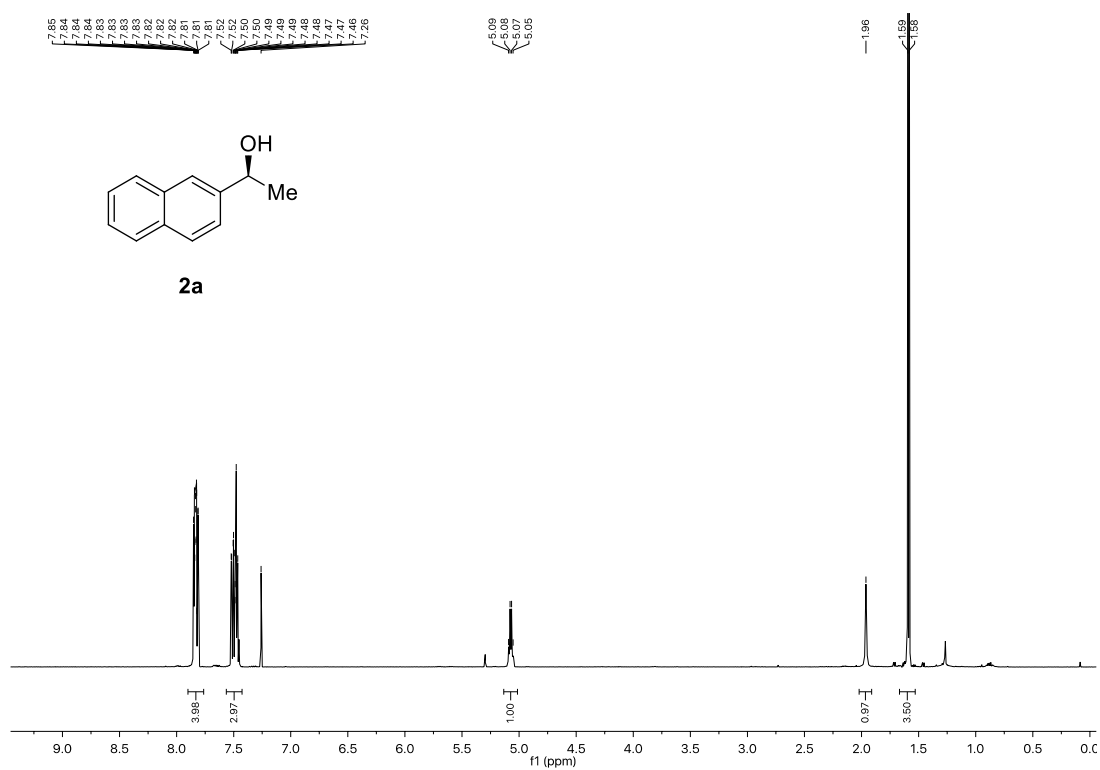
Chapter 2



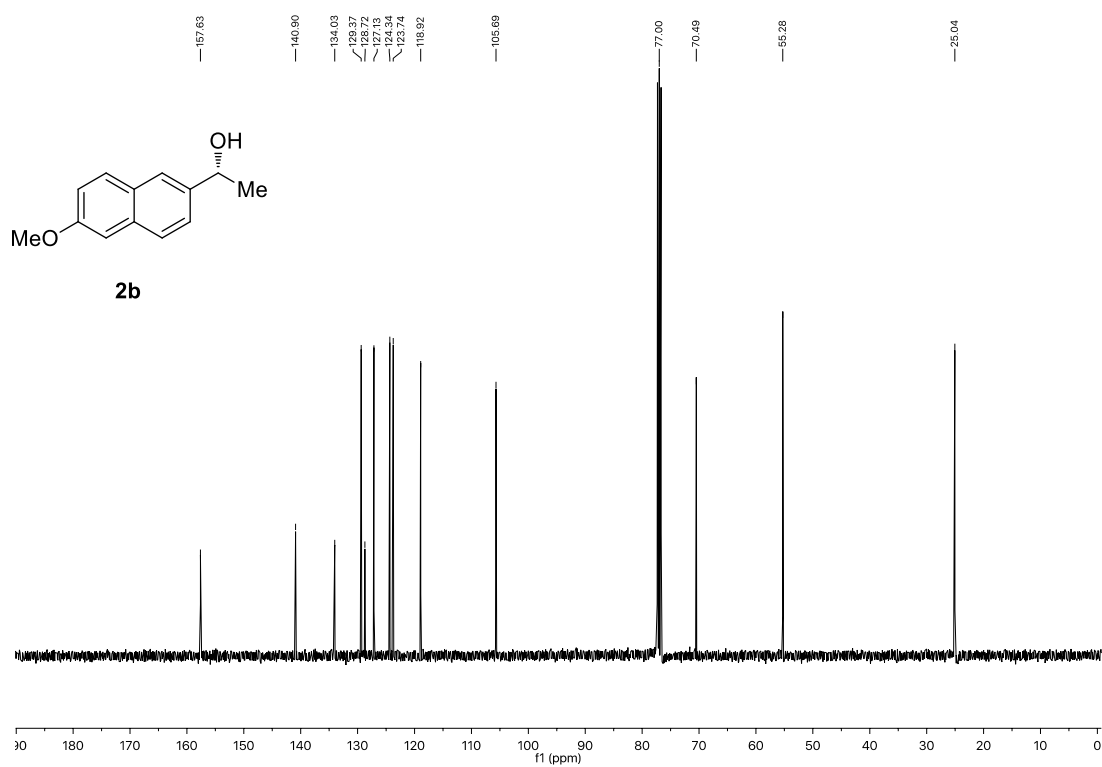
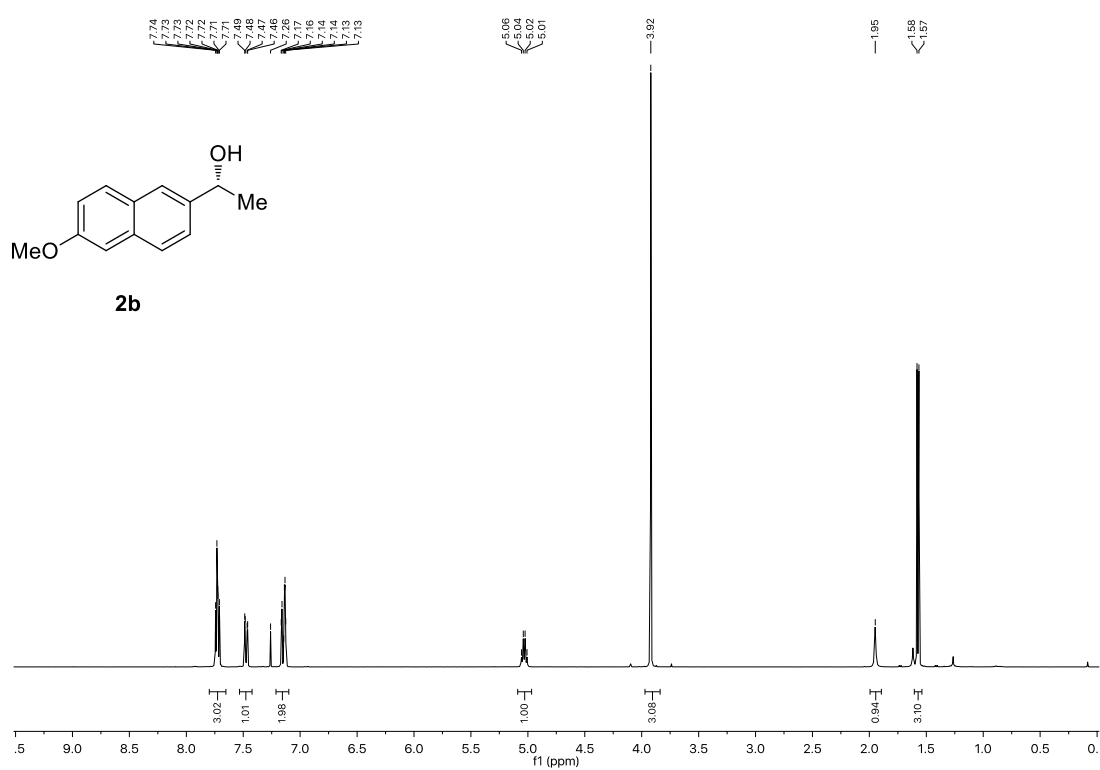
Stereospecific Borylation of Benzyl C(sp³)-O Bonds



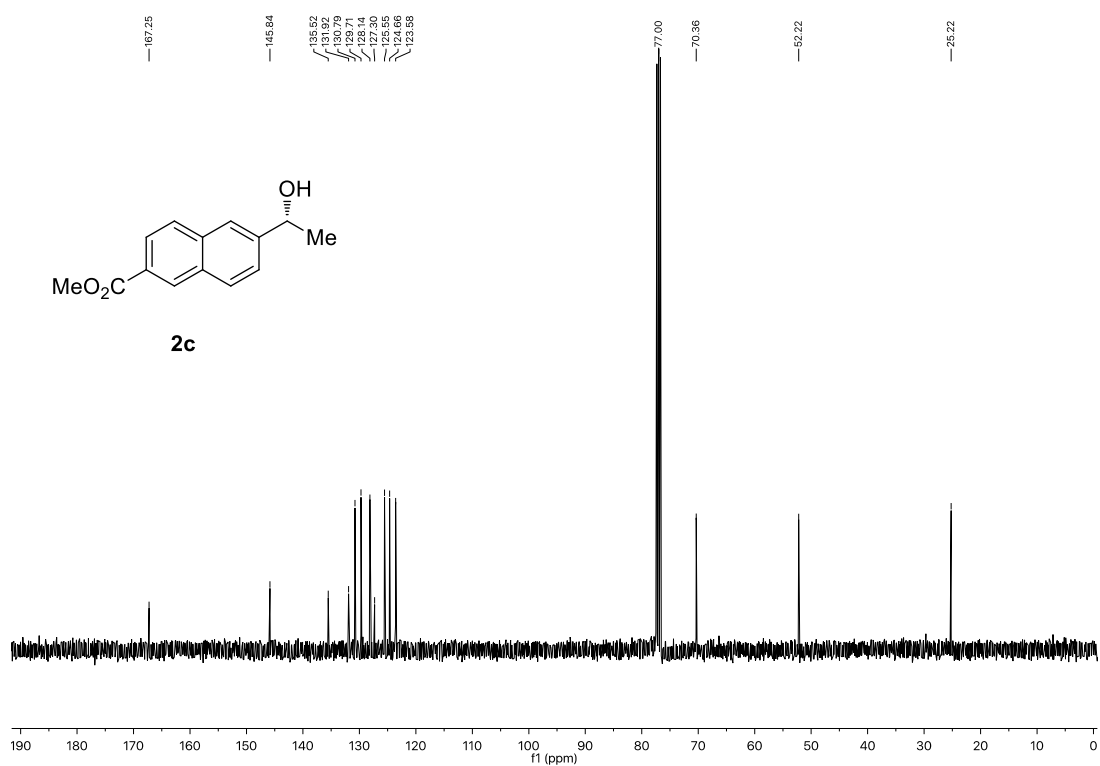
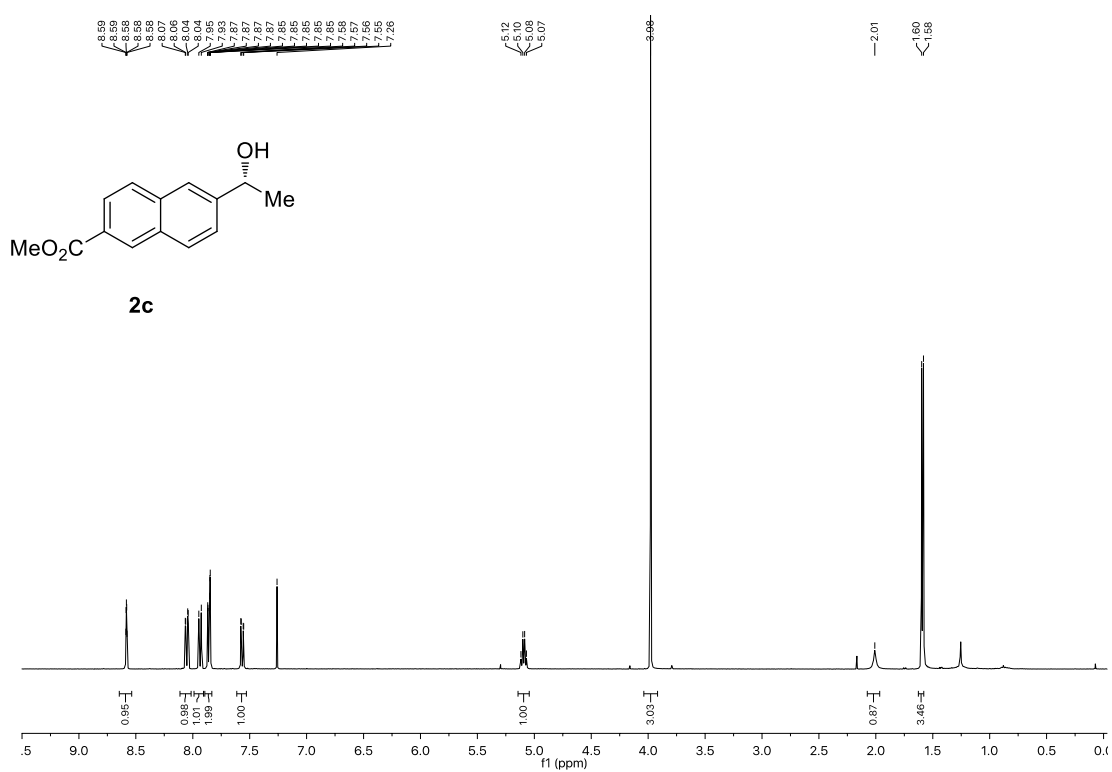
Chapter 2



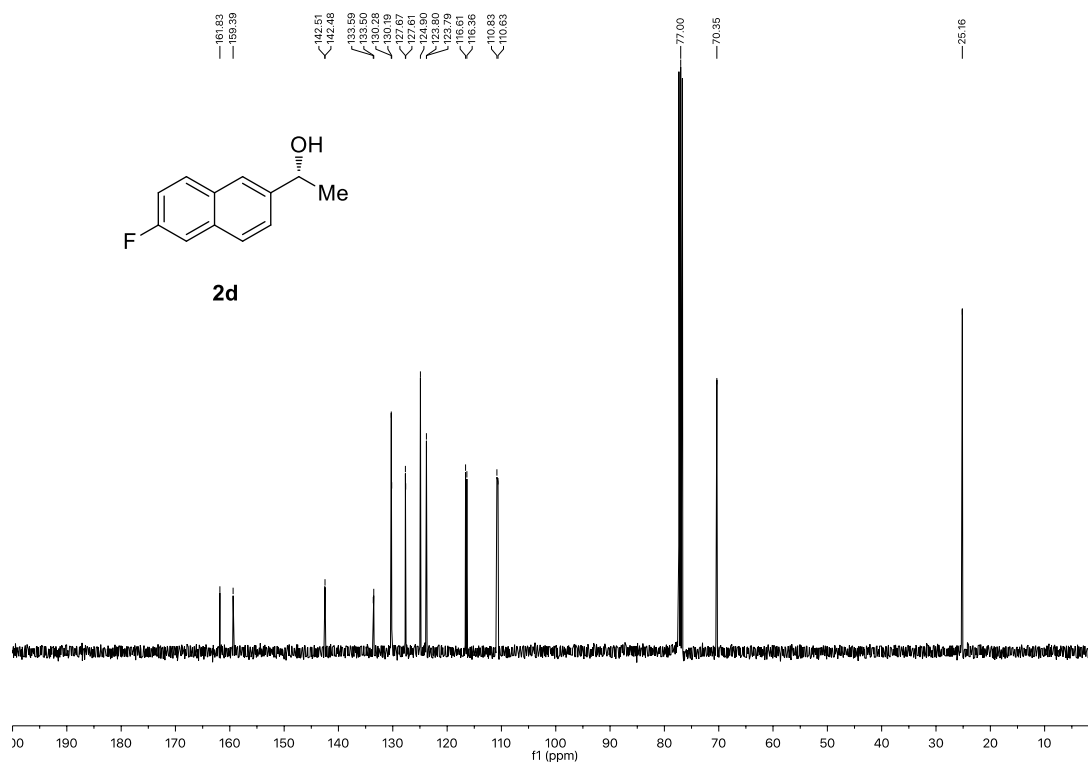
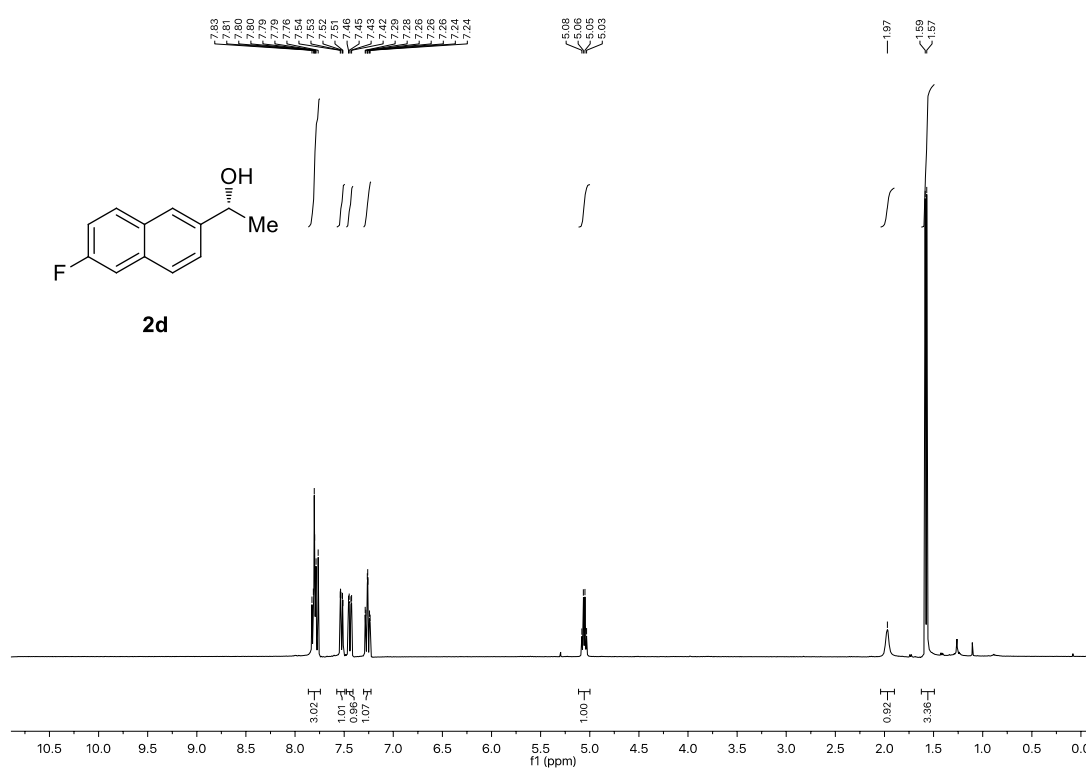
Stereospecific Borylation of Benzyl C(sp³)-O Bonds



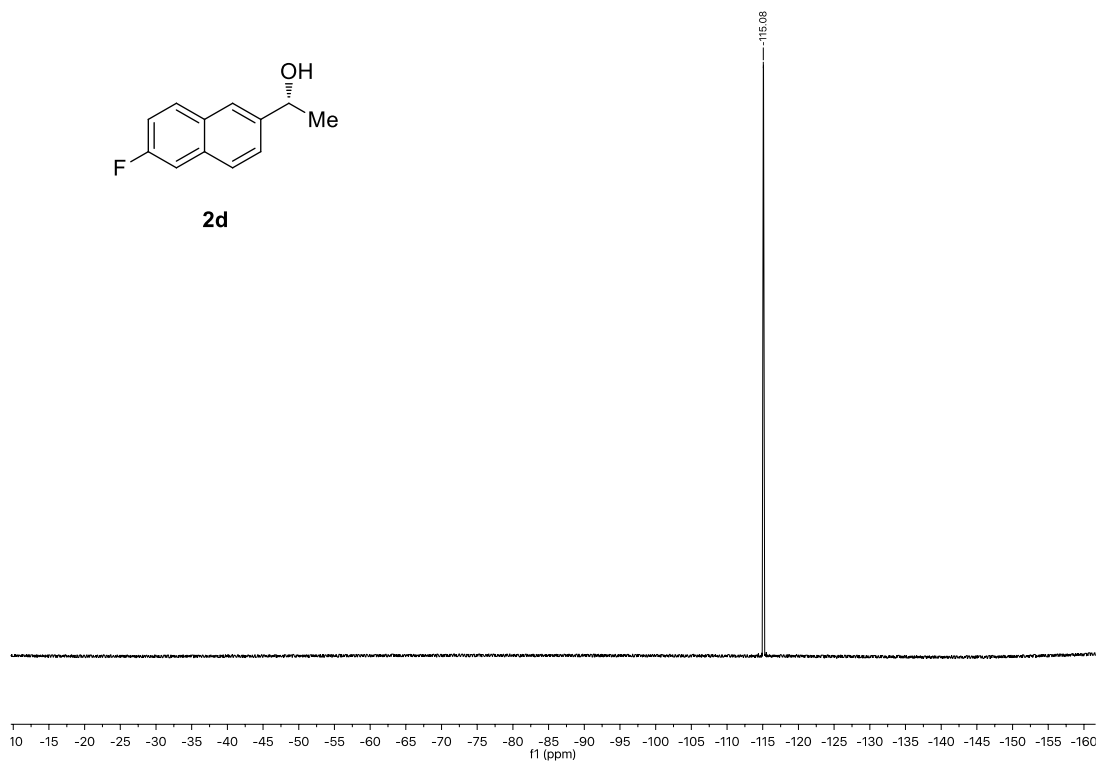
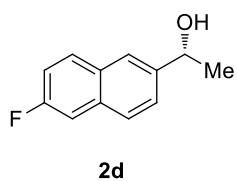
Chapter 2



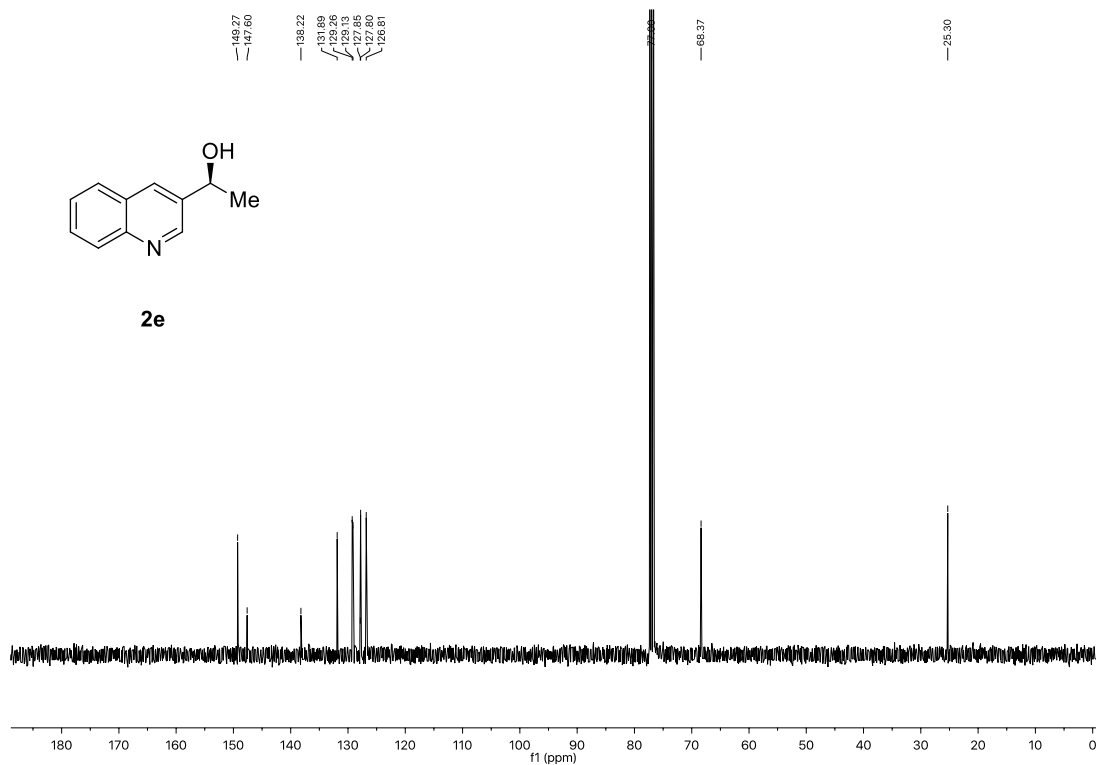
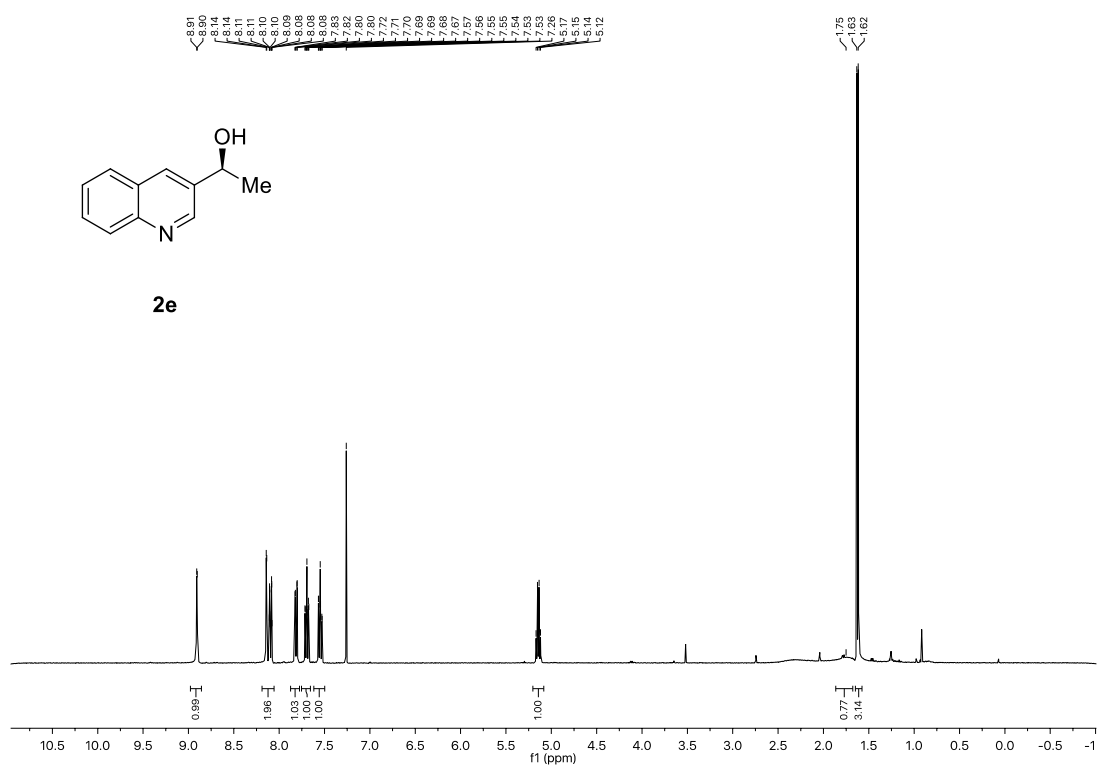
Stereospecific Borylation of Benzyl C(sp³)-O Bonds



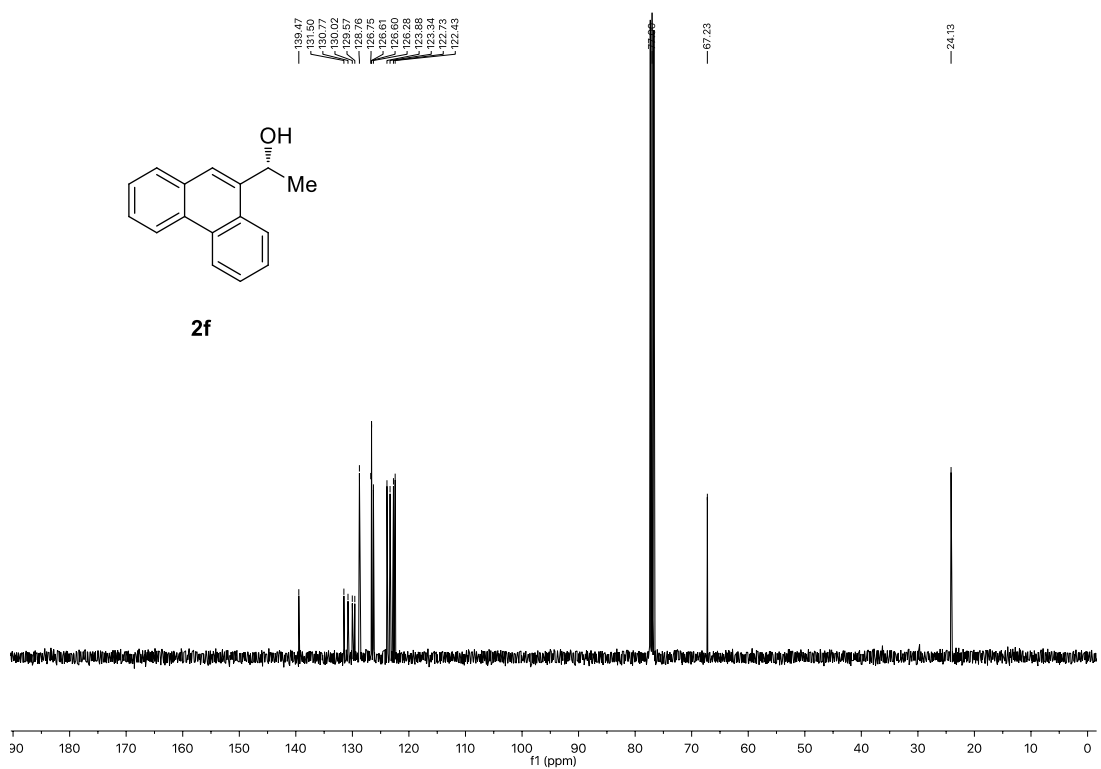
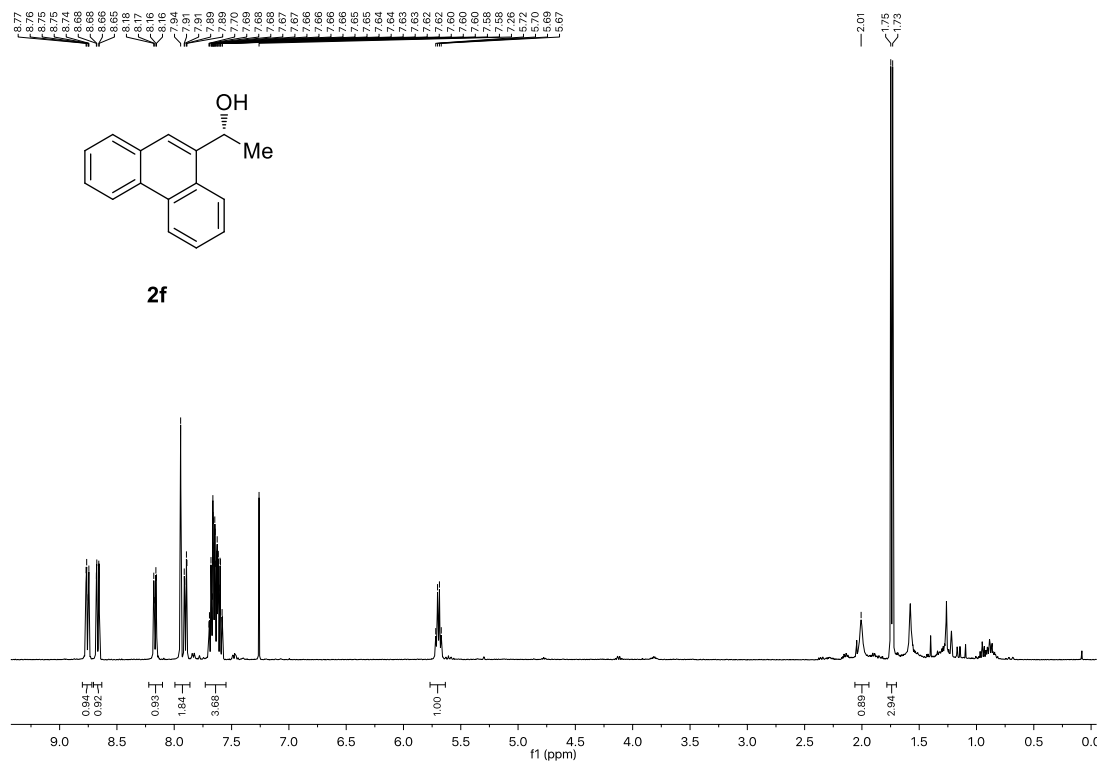
Chapter 2



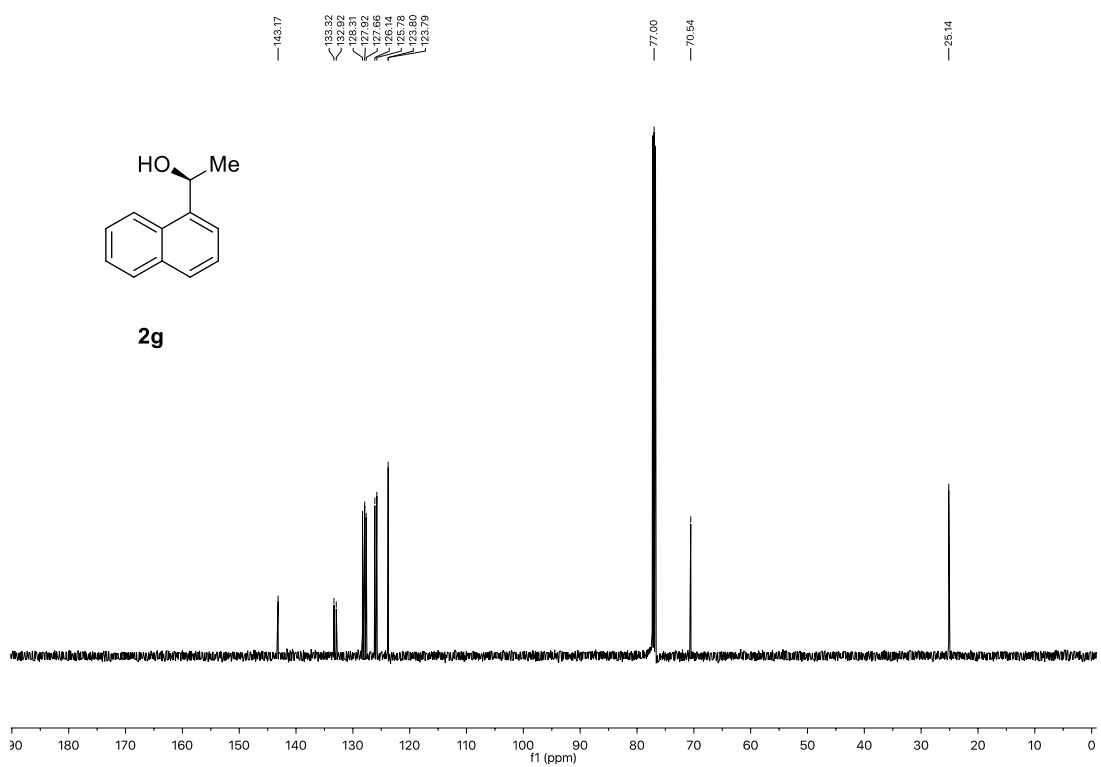
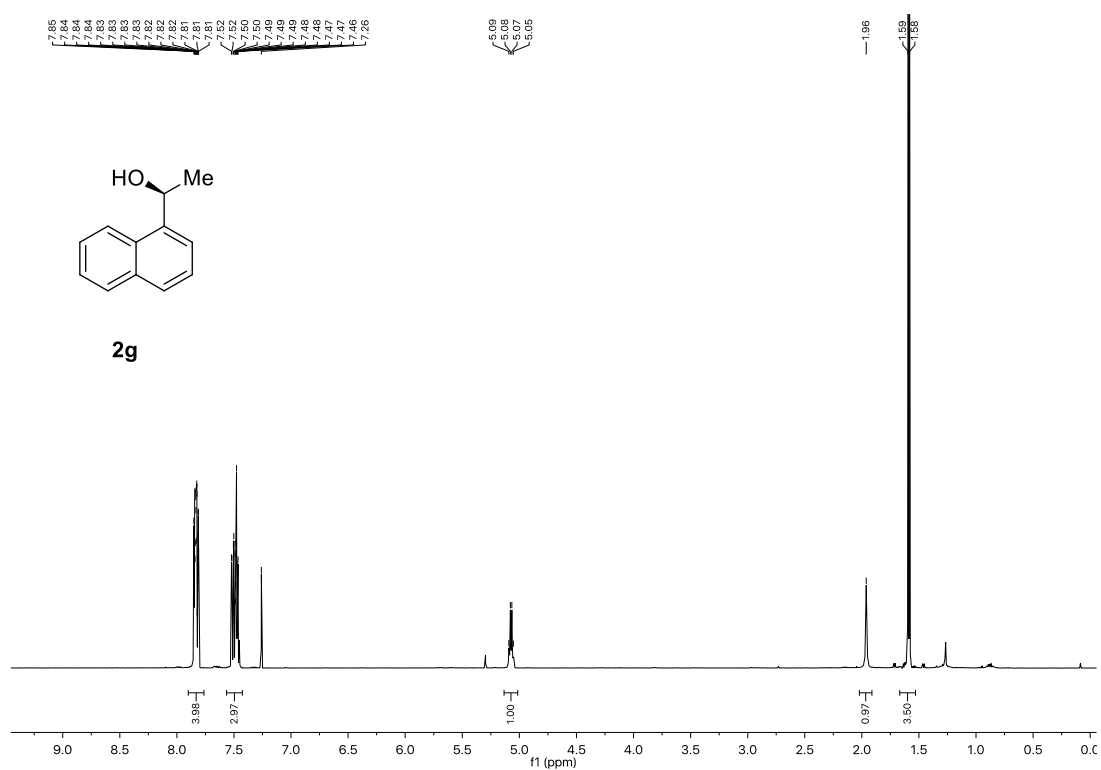
Stereospecific Borylation of Benzyl C(sp³)-O Bonds



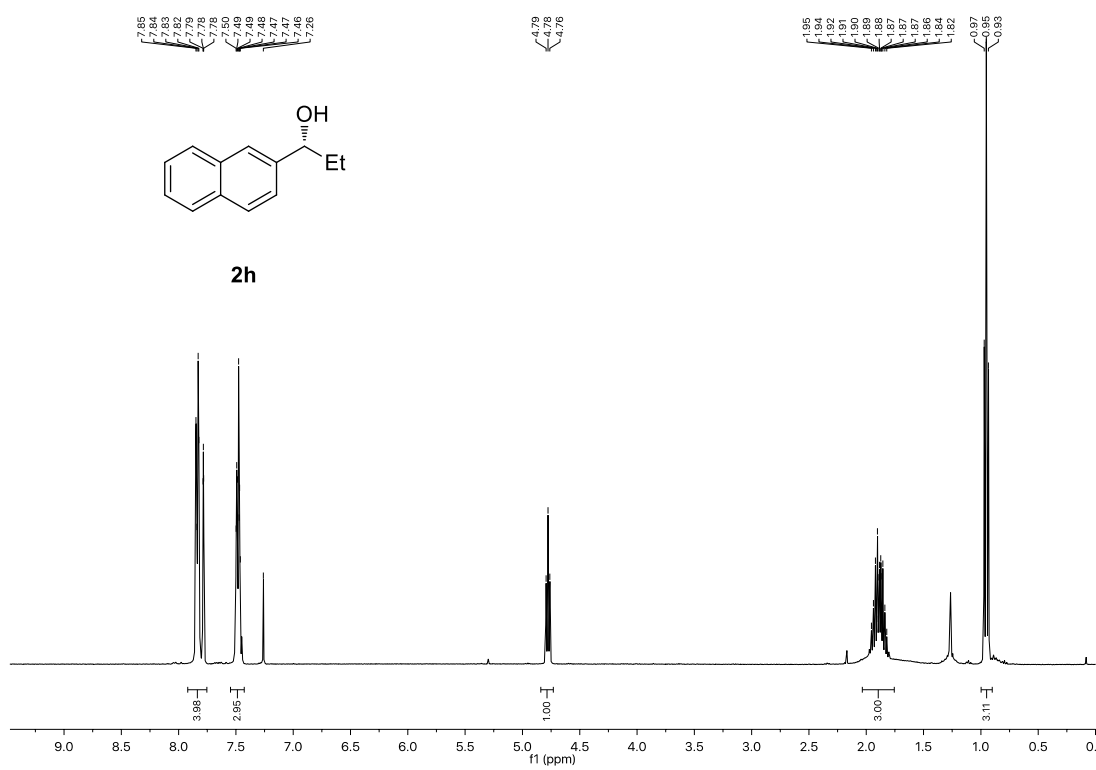
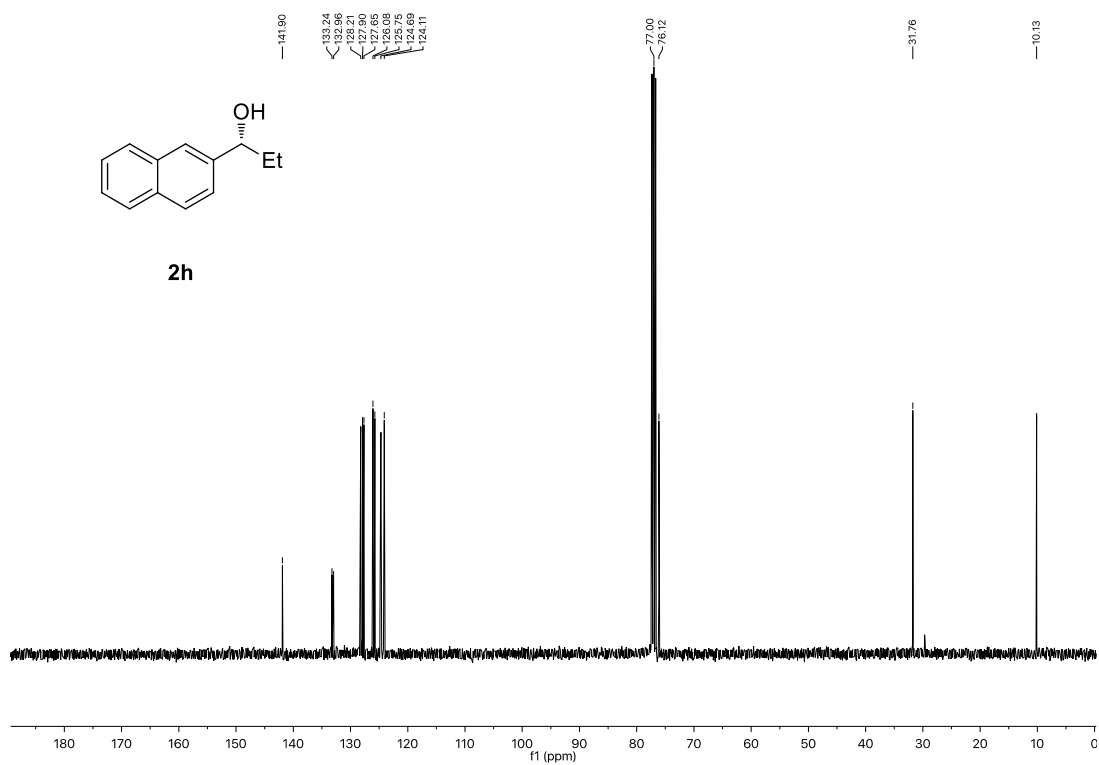
Chapter 2



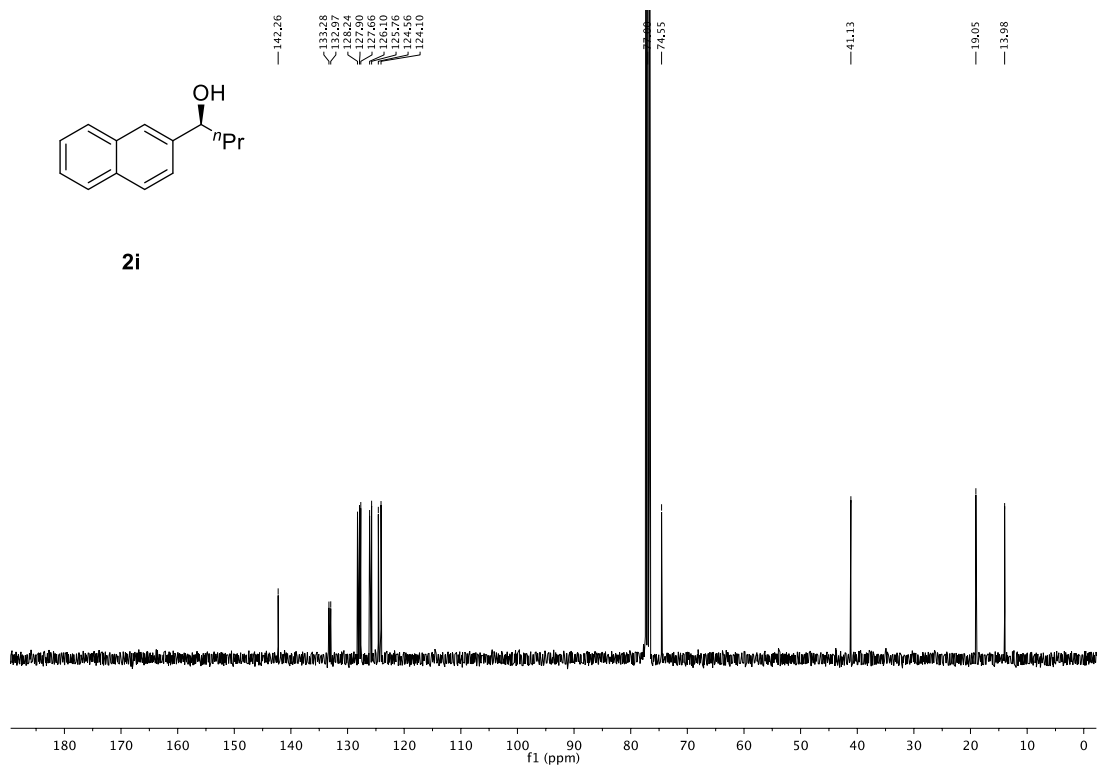
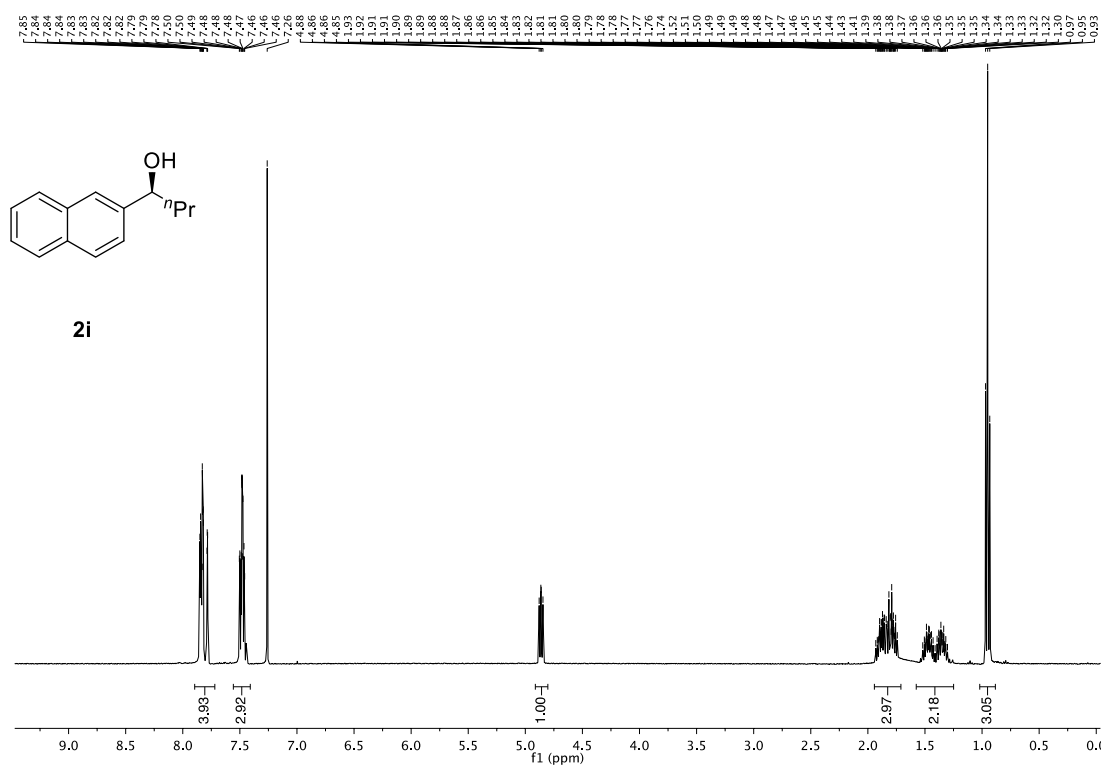
Stereospecific Borylation of Benzyl C(sp³)-O Bonds



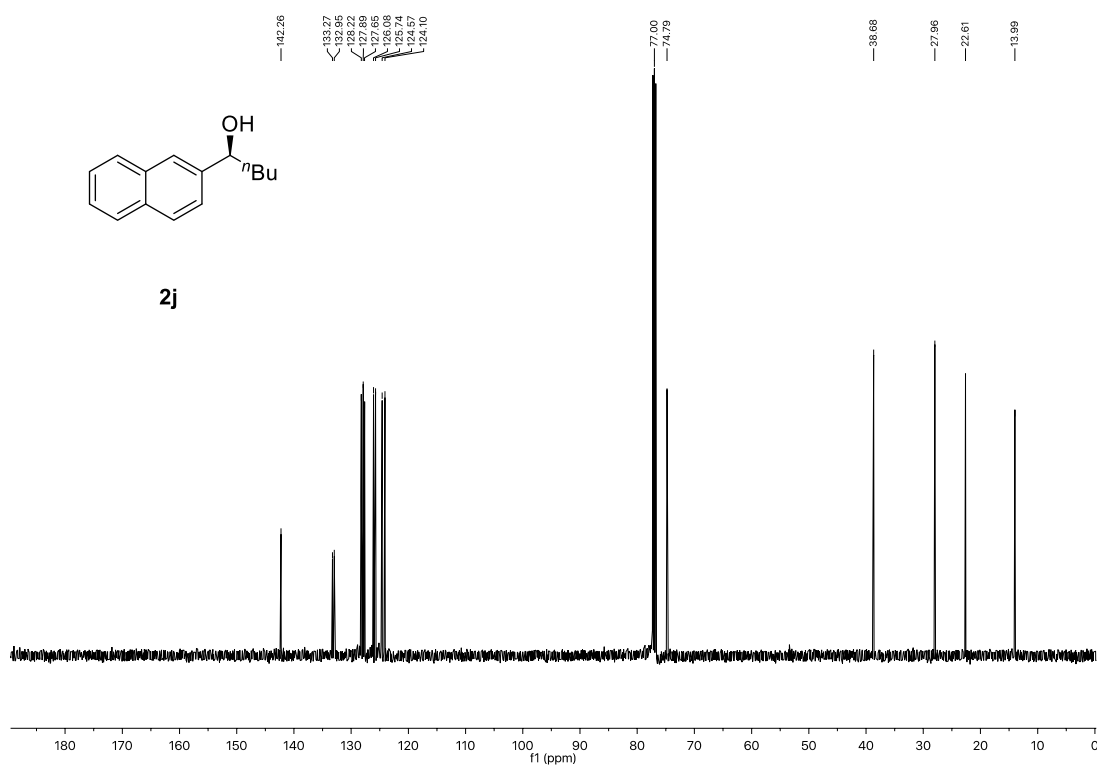
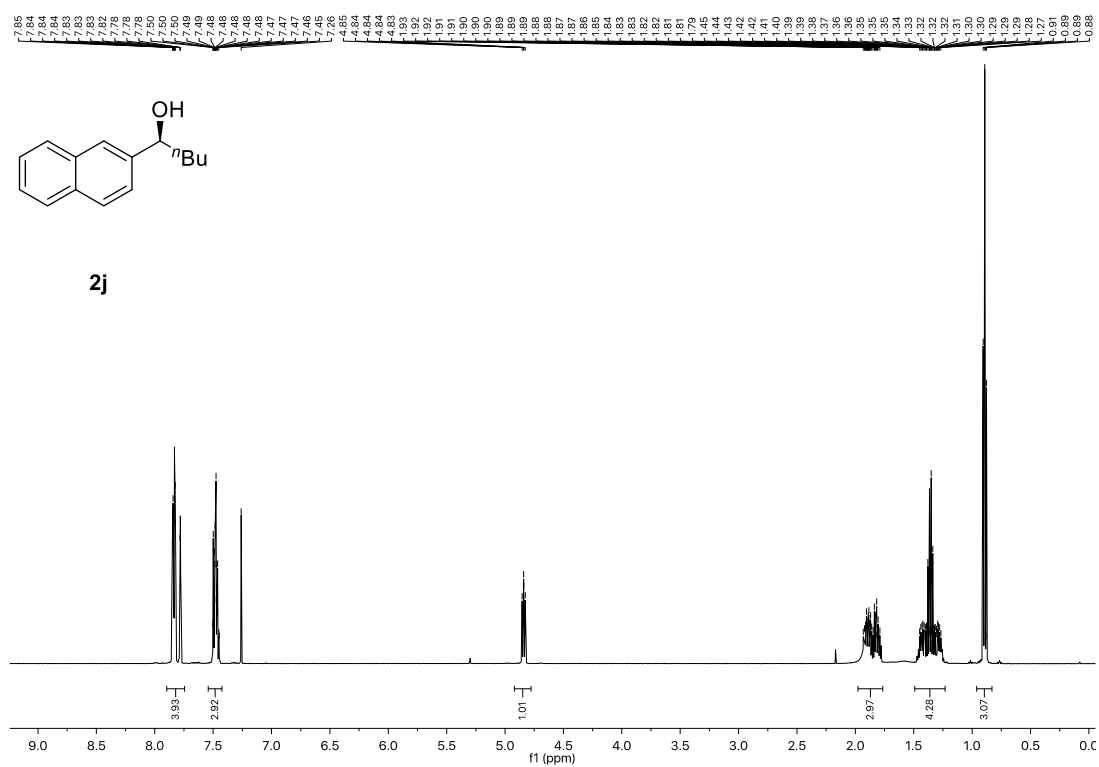
Chapter 2



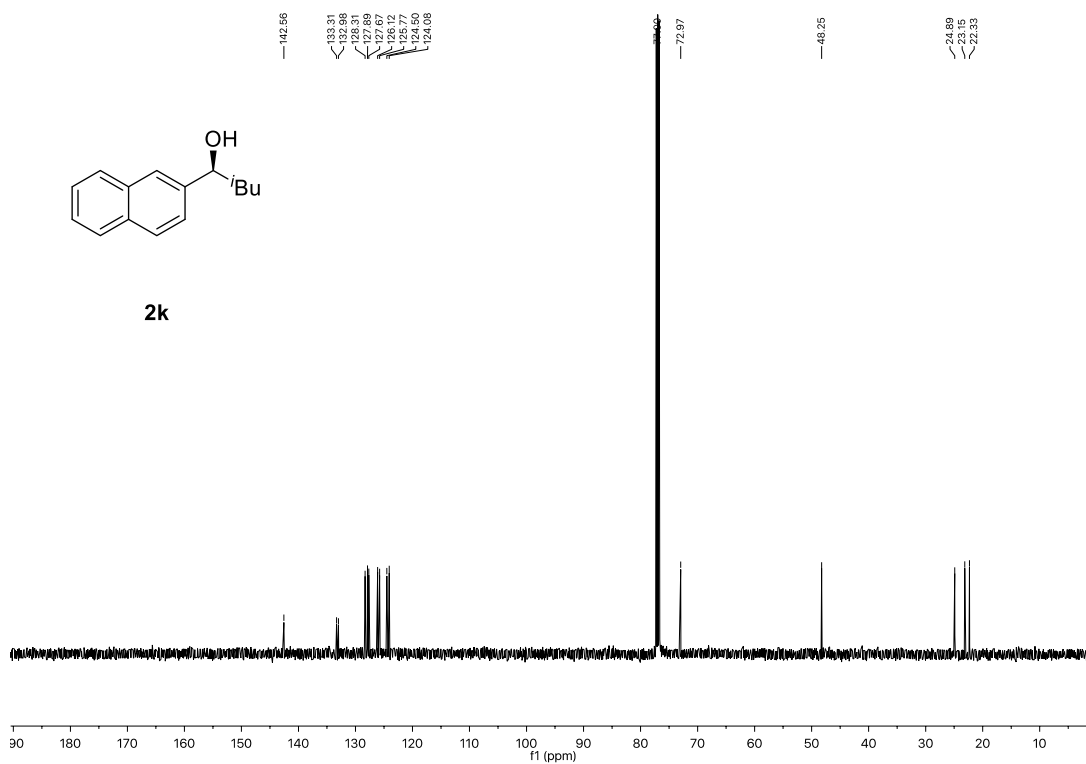
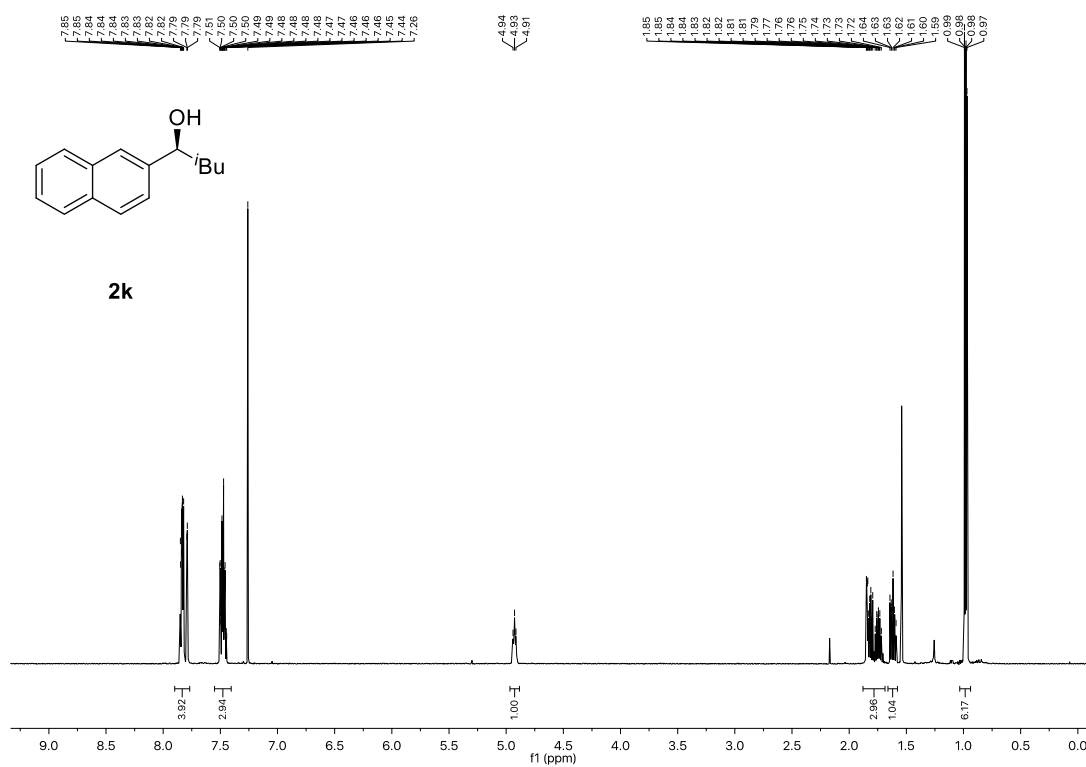
Stereospecific Borylation of Benzyl C(sp³)-O Bonds



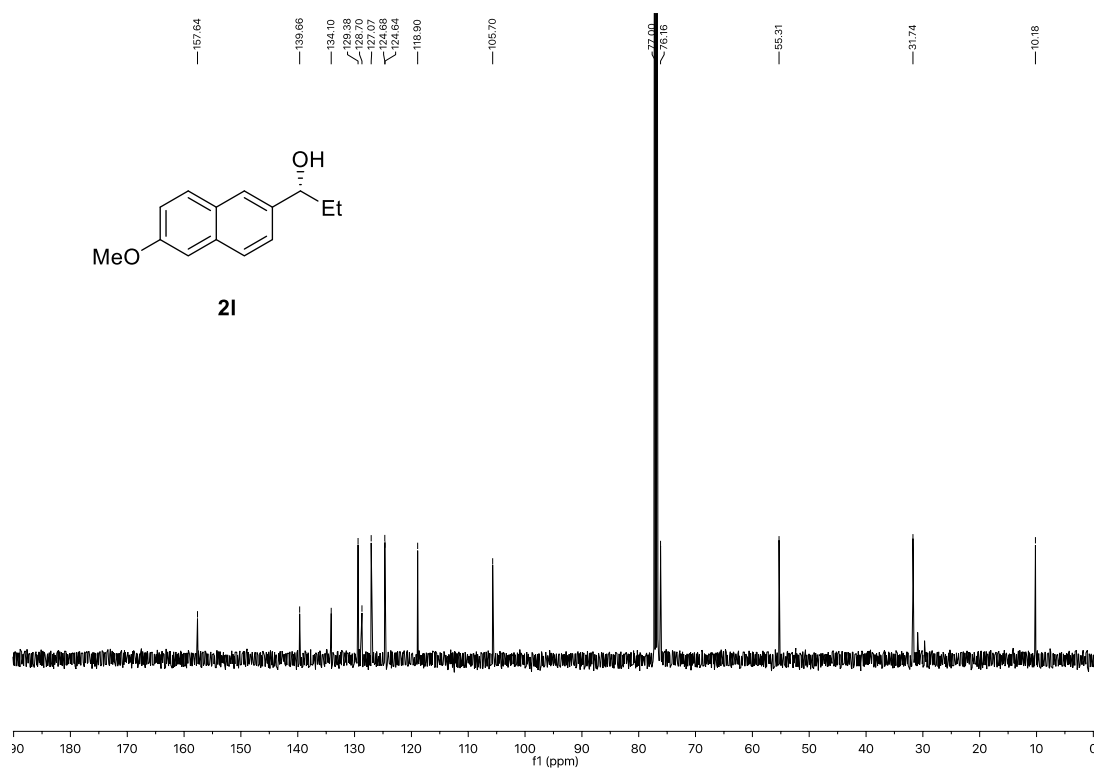
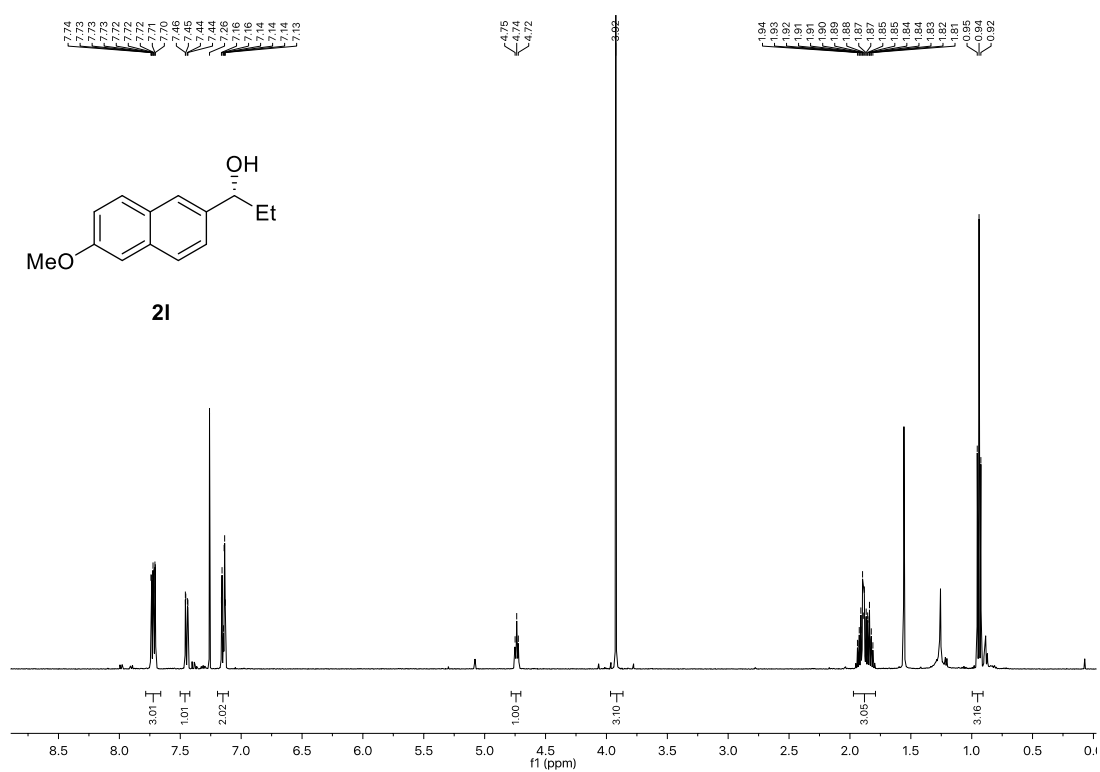
Chapter 2



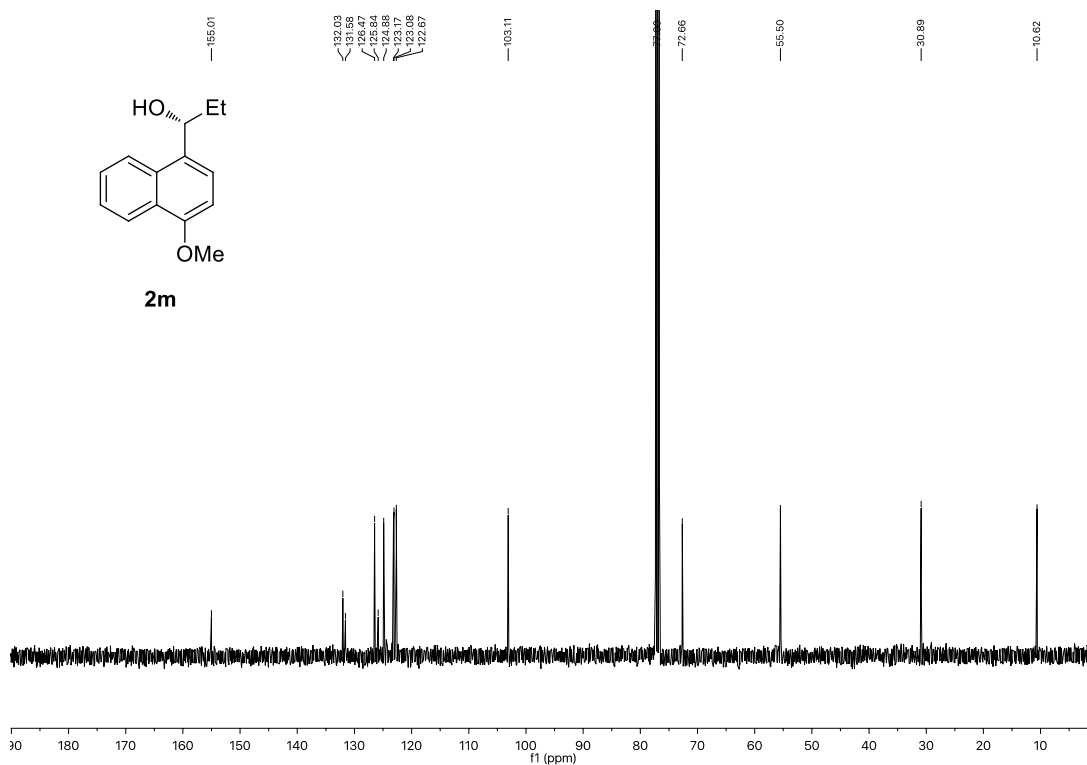
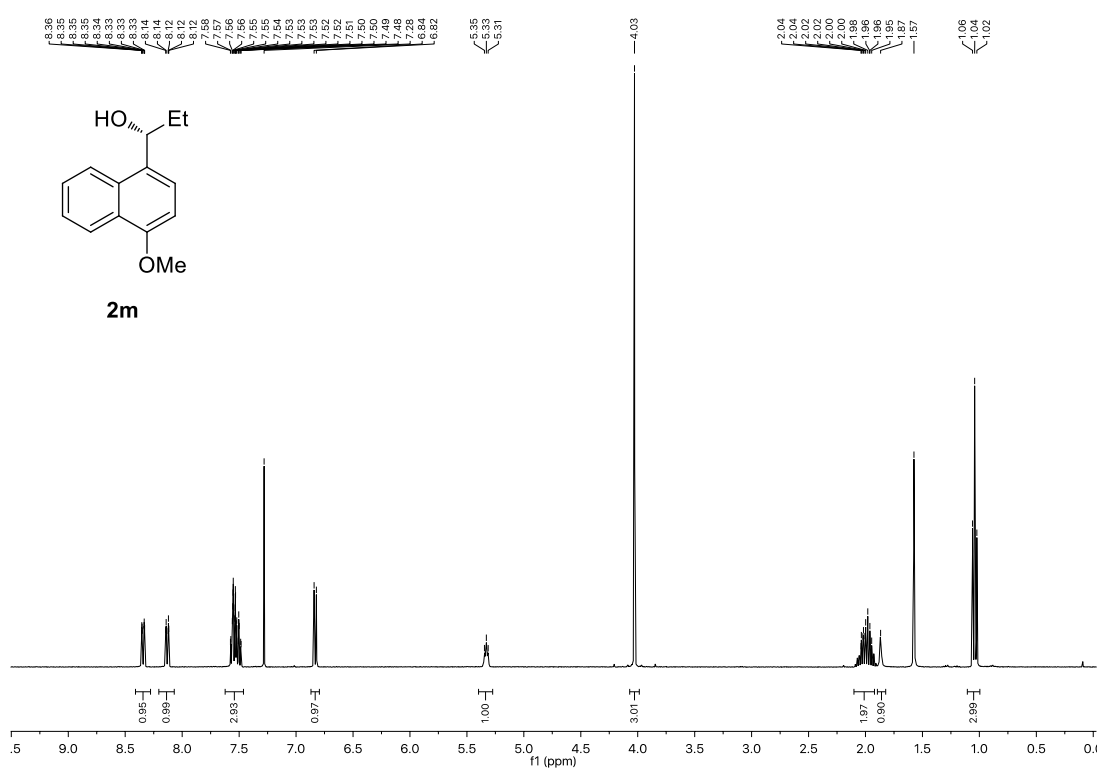
Stereospecific Borylation of Benzyl C(sp³)-O Bonds



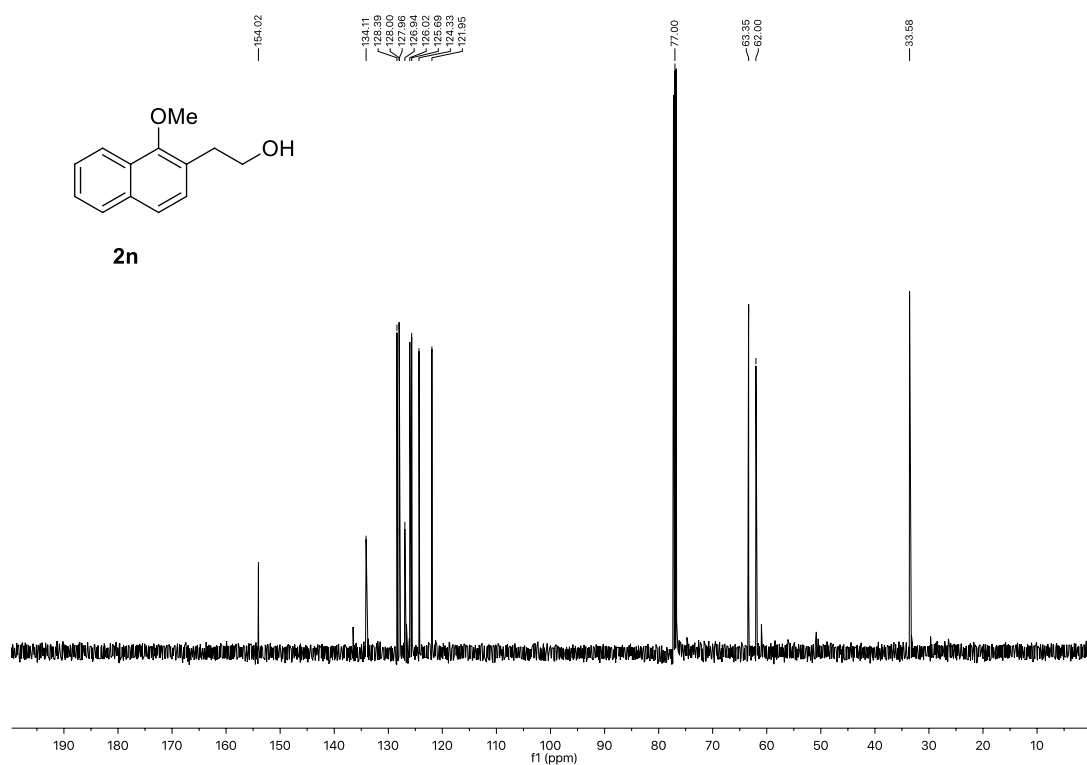
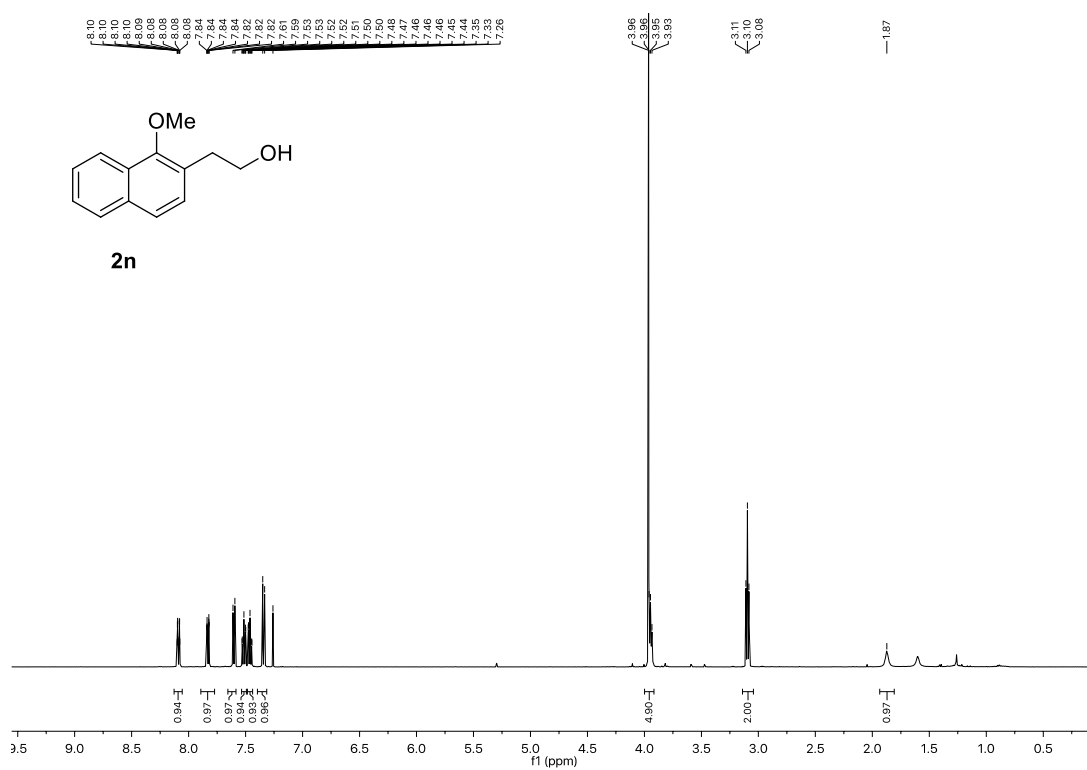
Chapter 2



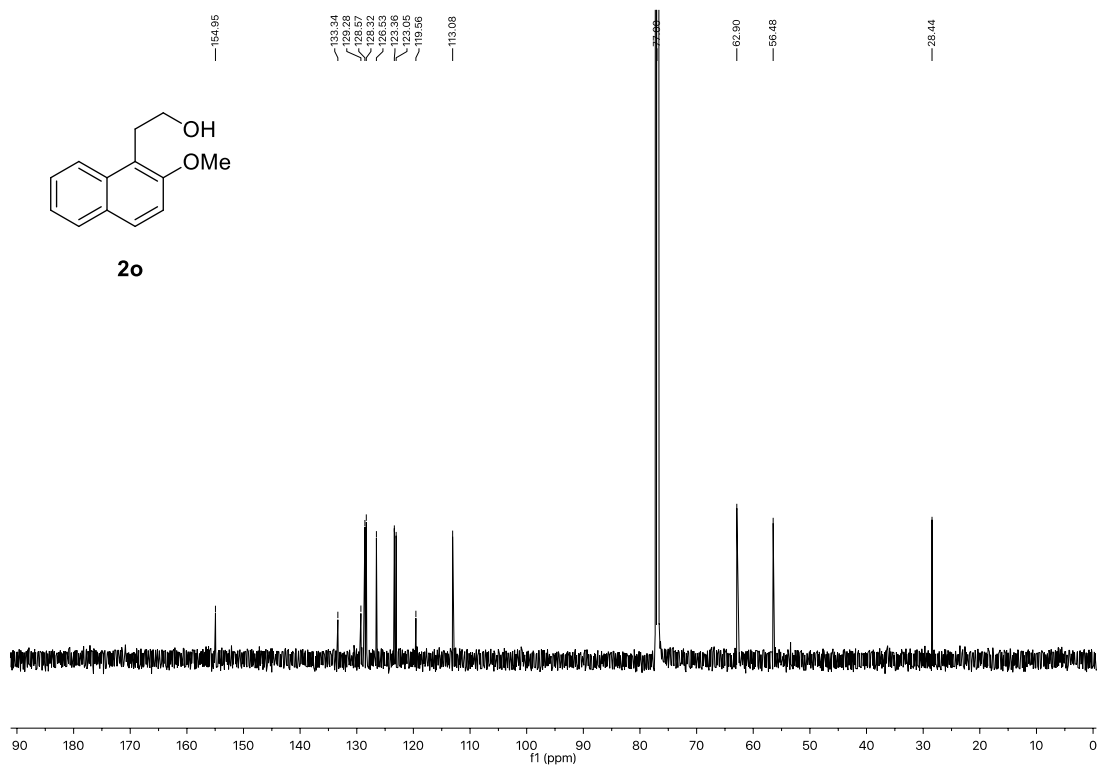
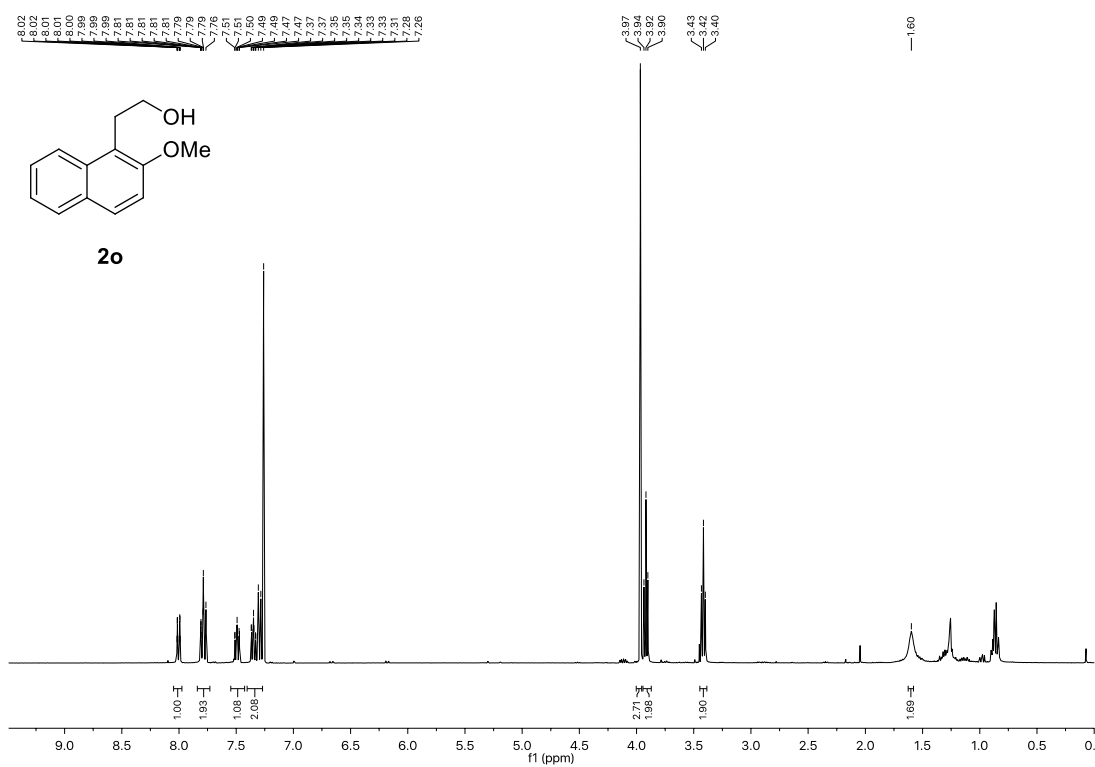
Stereospecific Borylation of Benzyl C(sp³)-O Bonds



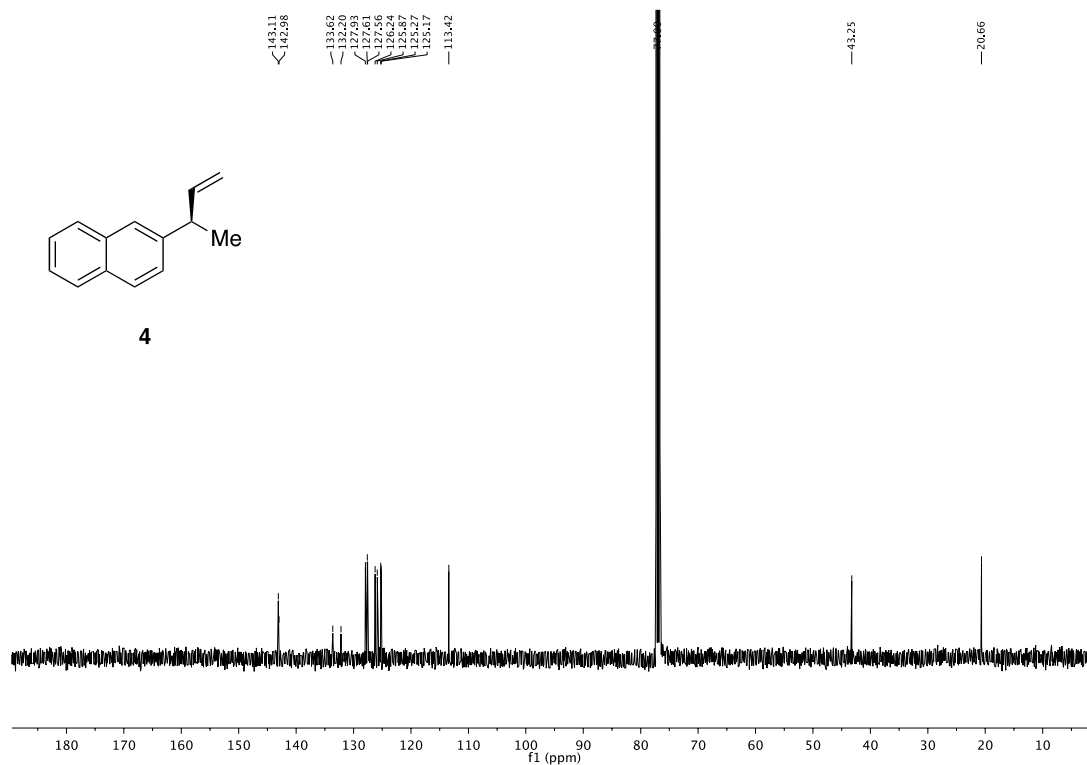
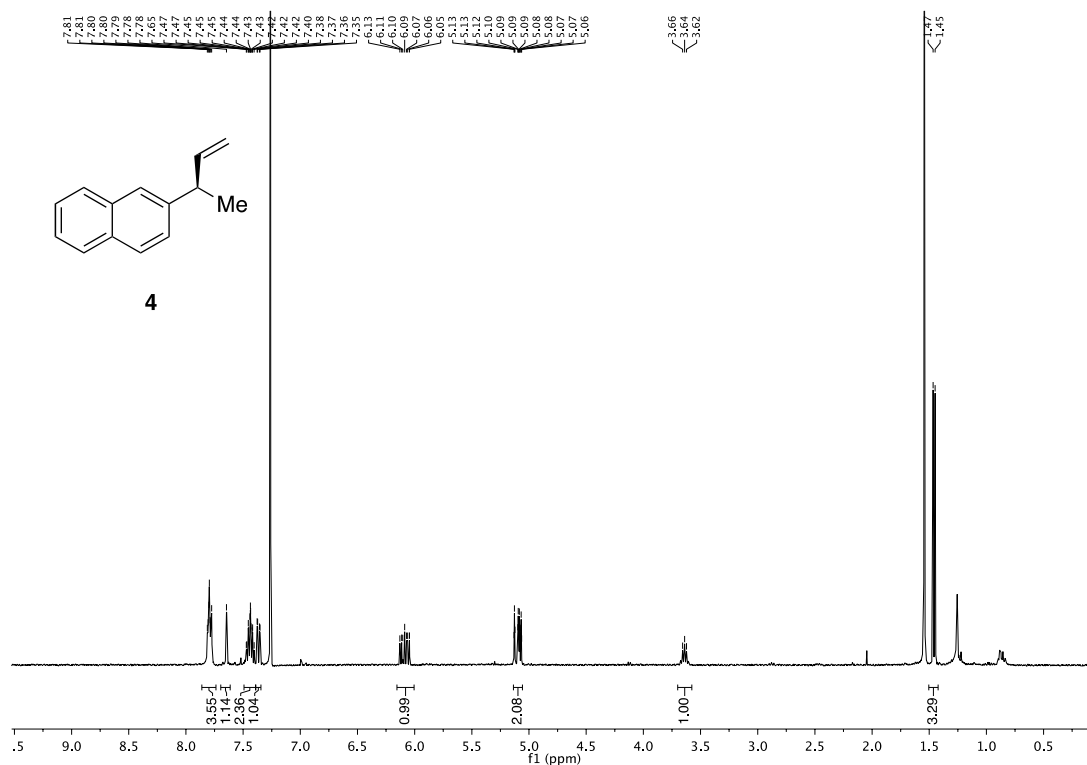
Chapter 2



Stereospecific Borylation of Benzyl C(sp³)-O Bonds



Stereospecific Borylation of Benzyl C(sp³)-O Bonds



Chapter 2

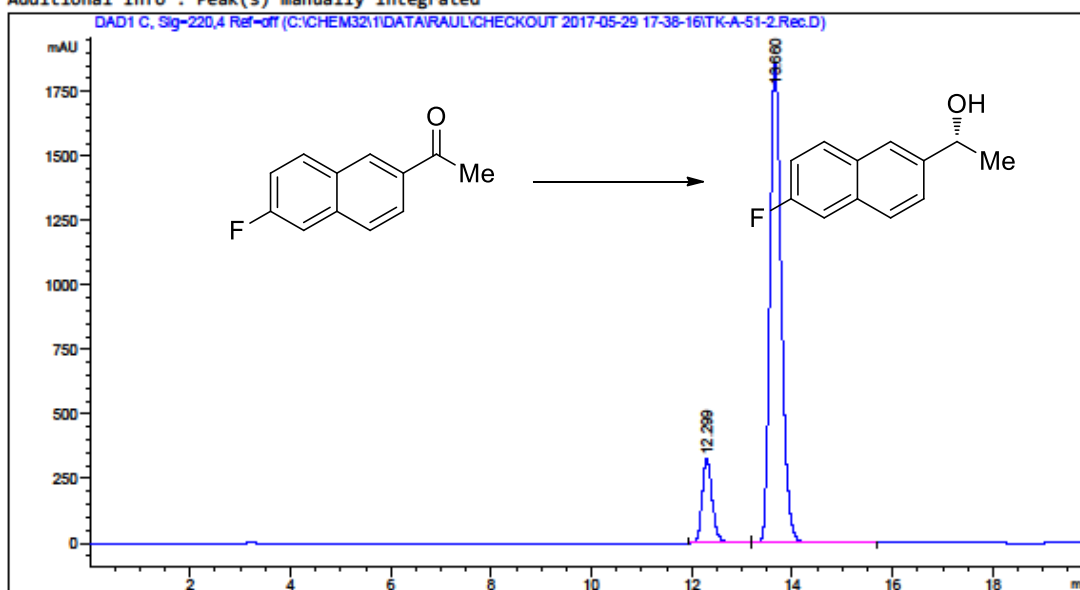
2.5.7 HPLC

Data File C:\CHEM32\1\DATA\RAUL\CHECKOUT 2017-05-29 17-38-16\TK-A-51-2.Rec.D
Sample Name: TK-A-51-2.Rec

=====

Acq. Operator	: SYSTEM	Seq. Line	: 1
Acq. Instrument	: HPLC 1260	Location	: 36
Injection Date	: 5/29/2017 5:39:07 PM	Inj	: 1
		Inj Volume	: 1.000 µl

Acq. Method : C:\Chem32\1\Data\Raul\checkout 2017-05-29 17-38-16\Chiral column IB-Raul 98-2.M
Last changed : 5/29/2017 5:38:16 PM by SYSTEM
Analysis Method : C:\Chem32\1\Methods\Chiral column IB-Raul 98-2.M
Last changed : 7/21/2017 1:35:21 PM by SYSTEM
Additional Info : Peak(s) manually integrated



Area Percent Report

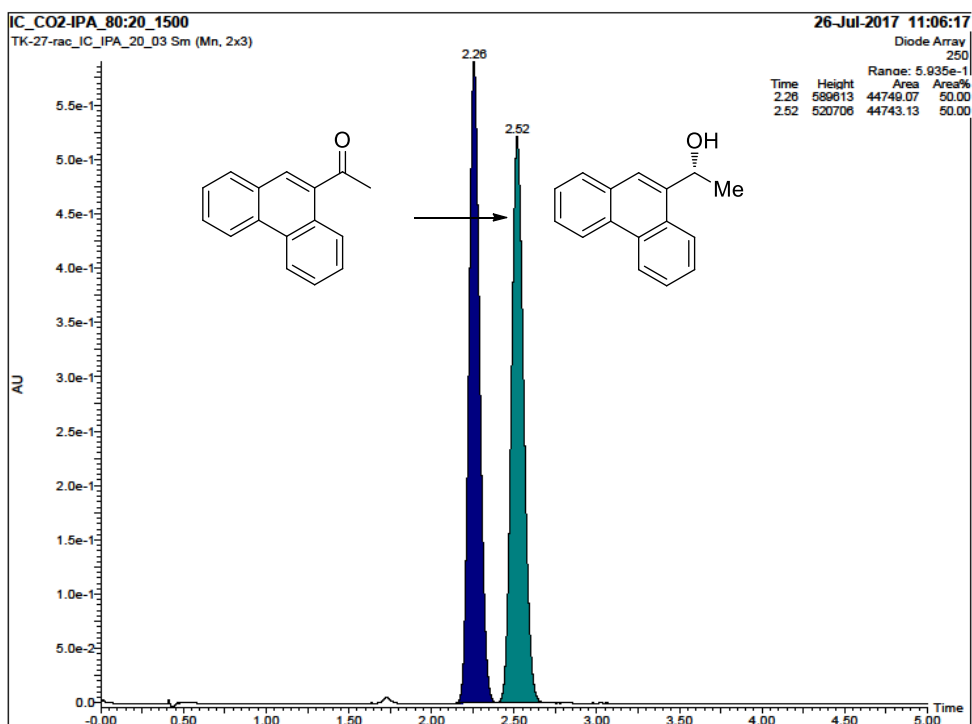
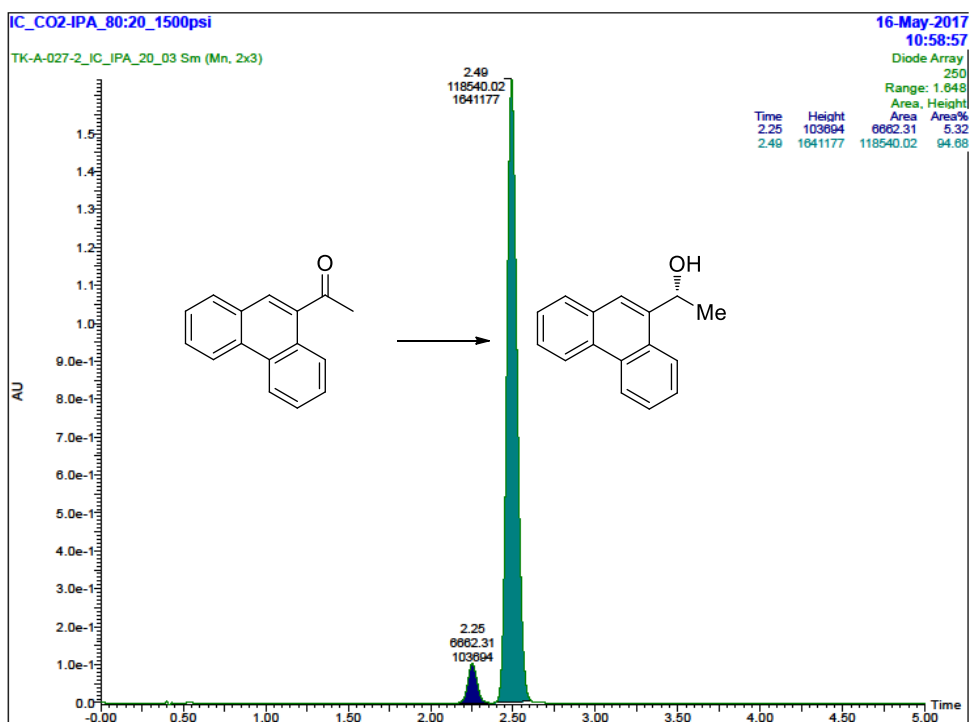
Sorted By : Signal
Multiplier : 1.0000
Dilution : 1.0000
Use Multiplier & Dilution Factor with ISTDs

Signal 1: DAD1 C, Sig=220,4 Ref=off

Peak #	RetTime [min]	Type	Width [min]	Area [mAU*s]	Height [mAU]	Area %
1	12.299	BB	0.2105	4531.68604	329.47348	13.2789
2	13.660	BB	0.2454	2.95954e4	1862.73413	86.7211

Totals : 3.41271e4 2192.20761

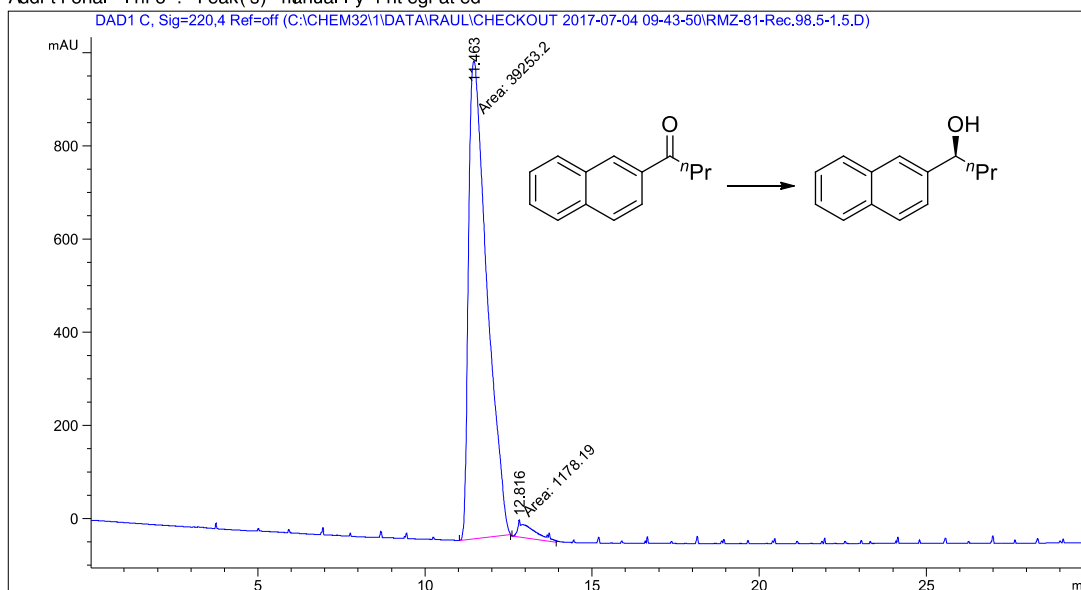
Stereospecific Borylation of Benzyl C(sp³)-O Bonds



Chapter 2

Data File C:\CHEM82\1\DATA\PAUL\CHECKOUT 2017-07-04 09-43-50\RMZ-81-Rec.98.5-1.5.D
 Sample Name: RMZ-81-Rec.98.5-1.5

```
=====
Acq. Operator   : SYSTEM                      Seq. Line :    1
Acq. Instrument : HPLC 1260                   Location  :   94
Injection Date  : 7/4/2017 9:44:49 AM        Inj       :    1
                                           Inj Volume: 1.000 µl
Acq. Method     : C:\Chem82\1\Dat a\Paul\checkout 2017-07-04 09-43-50\Chiral column IB-Paul
                                           98-2.M
Last changed    : 7/4/2017 9:43:51 AM by SYSTEM
Analysis Method : C:\Chem82\1\Met hods\Chiral column IB-Paul 98-2.M
Last changed    : 7/21/2017 9:40:12 AM by SYSTEM
Additional Info : Peak(s) manually integrated
=====
```



Area Percent Report

```
Sorted By      :      Signal
Multiplier     :      1.0000
Dilution       :      1.0000
Use Multiplier & Dilution Factor with ISTDs
```

Signal 1: DAD1 C, Sig=220.4 Ref=off

Peak #	Ret Time [min]	Type	Width [min]	Area [mAU*s]	Height [mAU]	Area %
1	11.463	MM	0.6375	3.92532e4	1026.26965	97.0859
2	12.816	MM	0.5366	1178.19458	36.59681	2.9141

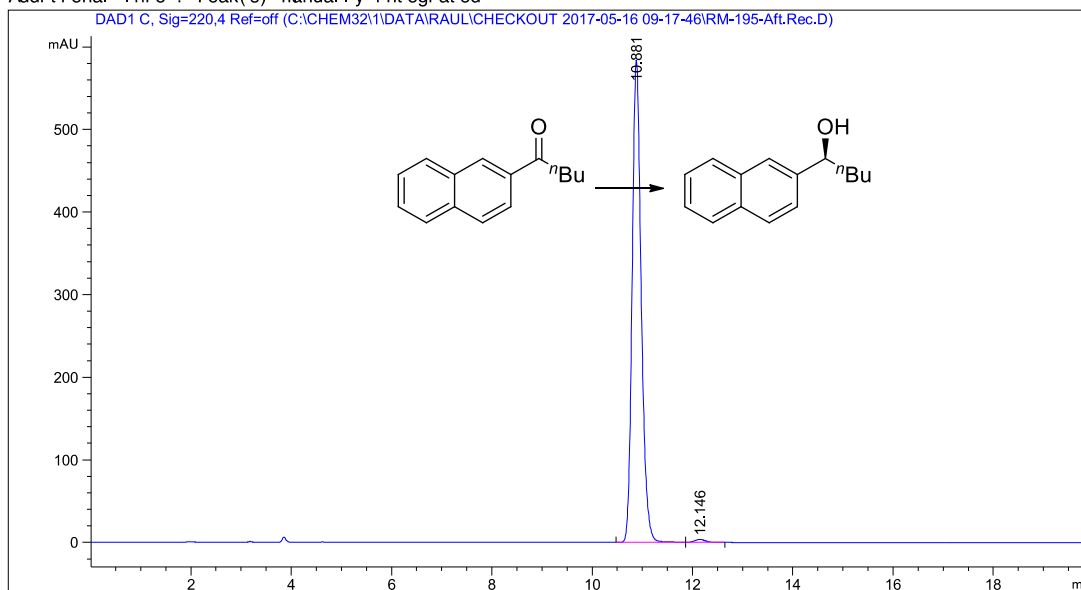
Totals : 4.04314e4 1062.86647

Stereospecific Borylation of Benzyl C(sp³)-O Bonds

Data File C:\CHEM82\1\DATA\RAUL\CHECKOUT 2017-05-16 09-17-46\RM 195-Aft. Rec. D
 Sample Name: RM 195-Aft. Rec

```
=====
Acq. Operator   : SYSTEM                      Seq. Line :    2
Acq. Instrument : HPLC 1260                   Location  :   21
Injection Date  : 5/16/2017 9:38:55 AM        Inj       :    1
                                           Inj Volume: 1.000 µl

Acq. Method     : C:\Chem82\1\Dat a\ Paul \checkout 2017-05-16 09-17-46\Chiral column IB-Paul
                  98-2, M
Last changed    : 5/16/2017 9:17:46 AM by SYSTEM
Analysis Method : C:\Chem82\1\Met hods\Chiral column IB-Paul 98-2, M
Last changed    : 7/17/2017 5:48:55 PM by SYSTEM
Additional Info : Peak(s) manually integrated
=====
```



Area Percent Report

```
Sorted By      :      Signal
Multiplier     :      1.0000
Dilution       :      1.0000
Use Multiplier & Dilution Factor with ISTDs
```

Signal 1: DAD1 C, Sig=220,4 Ref=off

Peak #	Ret Time [min]	Type	Width [min]	Area [mAU*s]	Height [mAU]	Area %
1	10.881	BB	0.1905	7331.90820	584.06335	99.3582
2	12.146	BB	0.2066	47.36023	3.48353	0.6418

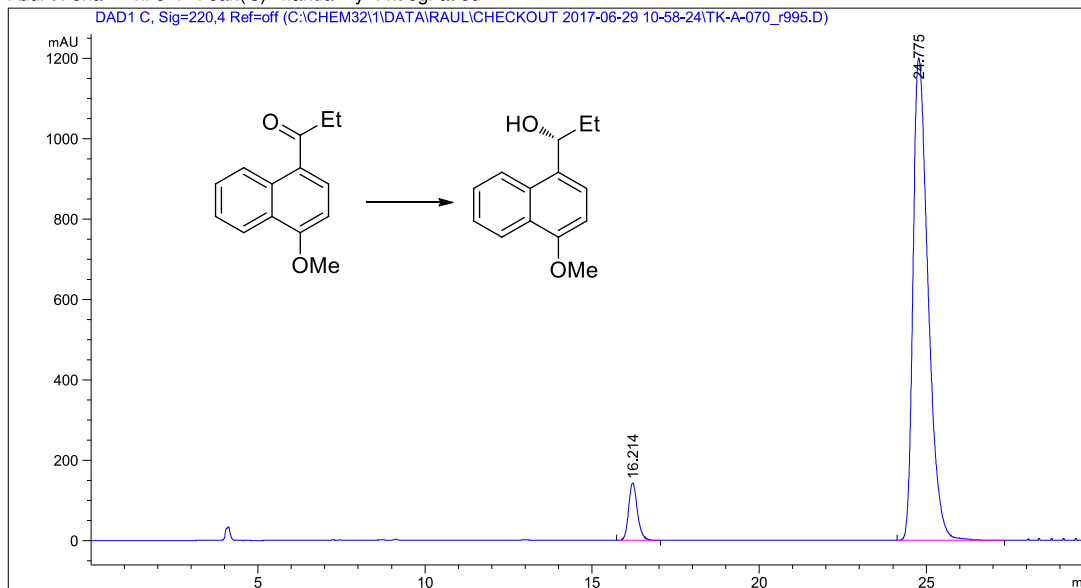
Totals : 7379.26843 587.54688

Chapter 2

Data File C:\CHEM82\1\DATA\RAUL\CHECKOUT 2017-06-29 10-58-24\TK-A-070_r995.D
 Sample Name: TK-A-070_r995

```
=====
Acq. Operator   : SYSTEM                      Seq. Line :    2
Acq. Instrument : HPLC 1260                   Location  :   61
Injection Date  : 6/29/2017 11:29:36 AM      Inj       :    1
                                           Inj Volume: 1.000 µl

Acq. Method     : C:\Chem82\1\Dat a\ Paul \checkout 2017-06-29 10-58-24\Chiral column IB-Paul
                  98-2, M
Last changed    : 6/29/2017 10:58:25 AM by SYSTEM
Analysis Method : C:\Chem82\1\Methods\Chiral column IB-Paul 98-2, M
Last changed    : 7/17/2017 5:48:55 PM by SYSTEM
Additional Info : Peak(s) manually integrated
=====
```



Area Percent Report

```
Sorted By      :      Signal
Multiplier     :      1.0000
Dilution       :      1.0000
Use Multiplier & Dilution Factor with ISTDs
```

Signal 1: DAD1 C, Sig=220,4 Ref=off

Peak #	Ret Time [min]	Type	Width [min]	Area [mAU*s]	Height [mAU]	Area %
1	16.214	BB	0.2786	2595.00635	142.40141	6.4533
2	24.775	BB	0.4795	3.76173e4	1200.79285	93.5467

Totals : 4.02123e4 1343.19426

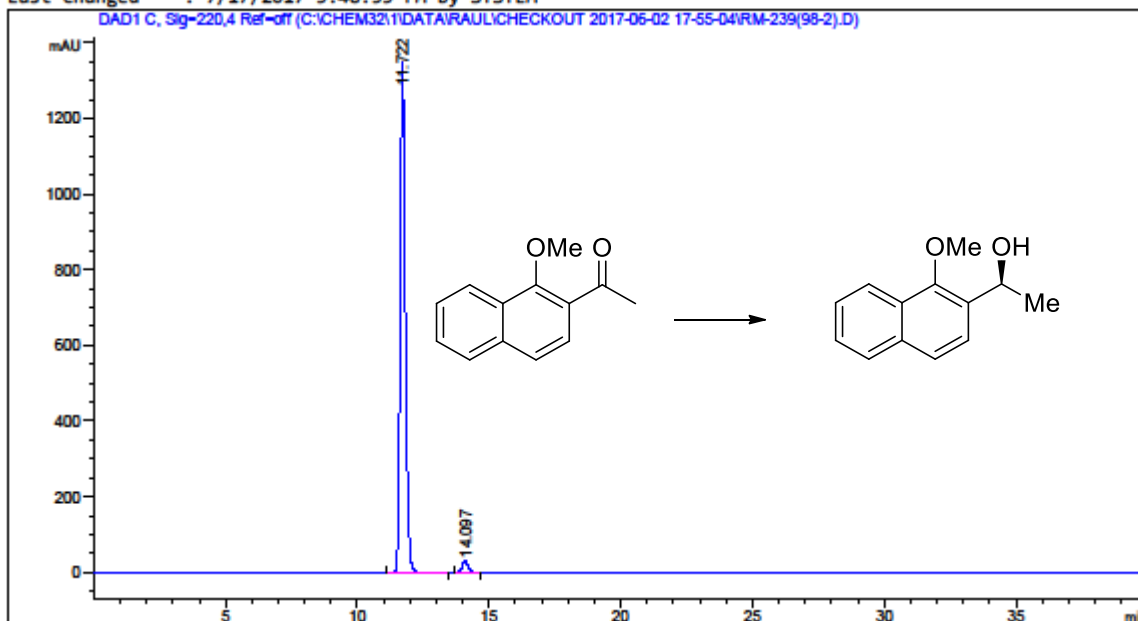
Stereospecific Borylation of Benzyl C(sp³)-O Bonds

Data File C:\CHEM32\1\DATA\RAUL\CHECKOUT 2017-06-02 17-55-04\RM-239(98-2).D
Sample Name: RM-239(98-2)

=====

Acq. Operator	: SYSTEM	Seq. Line	: 1
Acq. Instrument	: HPLC 1260	Location	: 4
Injection Date	: 6/2/2017 5:55:57 PM	Inj	: 1
		Inj Volume	: 1.000 µl

Acq. Method : C:\Chem32\1\Data\Raul\checkout 2017-06-02 17-55-04\Chiral coloumn IB-Raul 98-2.M
Last changed : 6/2/2017 5:55:05 PM by SYSTEM
Analysis Method : C:\Chem32\1\Methods\Chiral coloumn IB-Raul 98-2.M
Last changed : 7/17/2017 5:48:55 PM by SYSTEM



=====
Area Percent Report
=====

Sorted By : Signal
Multiplier : 1.0000
Dilution : 1.0000
Use Multiplier & Dilution Factor with ISTDs

Signal 1: DAD1 C, Sig=220,4 Ref=off

Peak #	RetTime [min]	Type	Width [min]	Area [mAU*s]	Height [mAU]	Area %
1	11.722	BB	0.2084	1.82860e4	1346.91638	97.4772
2	14.097	BB	0.2431	473.26337	29.83288	2.5228

Totals : 1.87592e4 1376.74927

=====
*** End of Report ***

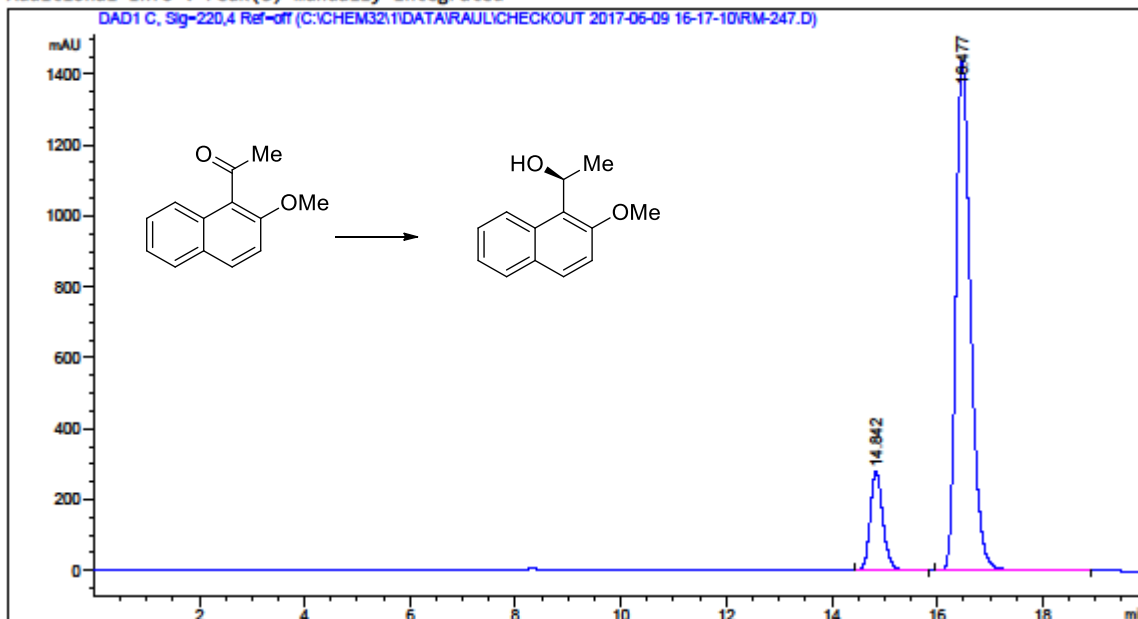
Chapter 2

Data File C:\CHEM32\1\DATA\RAUL\CHECKOUT 2017-06-09 16-17-10\RM-247.D
Sample Name: RM-247

=====

Acq. Operator	: SYSTEM	Seq. Line	: 1
Acq. Instrument	: HPLC 1260	Location	: 23
Injection Date	: 6/9/2017 4:18:00 PM	Inj	: 1
		Inj Volume	: 1.000 µl

Acq. Method : C:\Chem32\1\Data\Raul\checkout 2017-06-09 16-17-10\Chiral coloumn IB-Raul 98-2.M
Last changed : 6/9/2017 4:17:10 PM by SYSTEM
Analysis Method : C:\Chem32\1\Methods\Chiral coloumn IB-Raul 98-2.M
Last changed : 7/17/2017 5:48:55 PM by SYSTEM
Additional Info : Peak(s) manually integrated



=====
Area Percent Report
=====

Sorted By : Signal
Multiplier : 1.0000
Dilution : 1.0000
Use Multiplier & Dilution Factor with ISTDs

Signal 1: DAD1 C, Sig=220,4 Ref=off

Peak #	RetTime [min]	Type	Width [min]	Area [mAU*s]	Height [mAU]	Area %
1	14.842	BB	0.2540	4690.01709	281.98334	14.4222
2	16.477	BB	0.2979	2.78294e4	1437.17590	85.5778

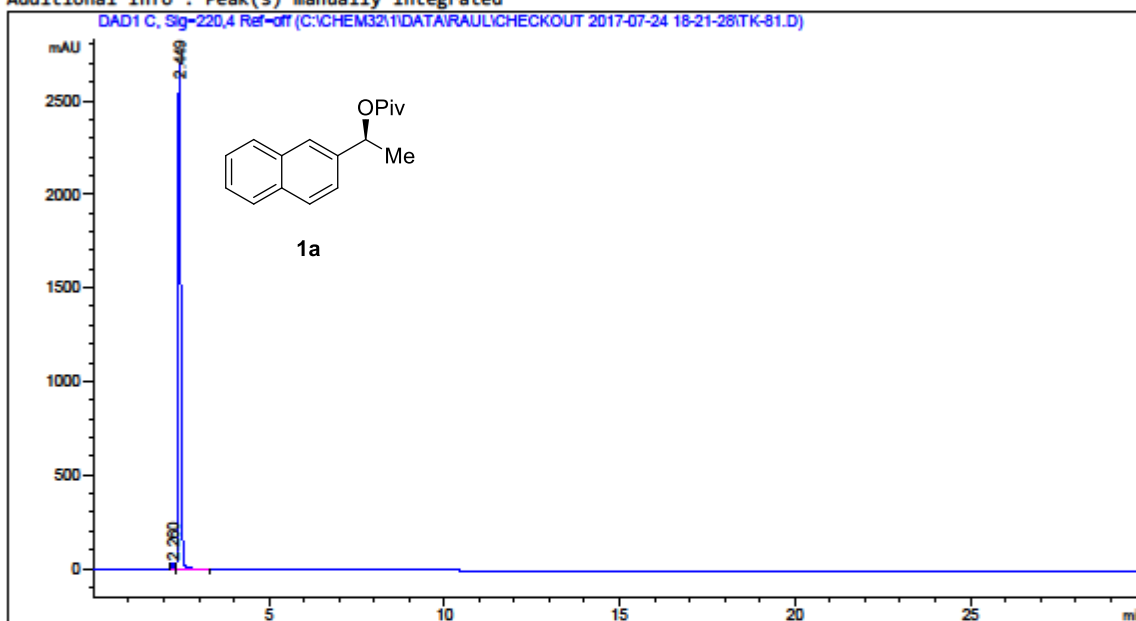
Totals : 3.25194e4 1719.15924

Stereospecific Borylation of Benzyl C(sp³)-O Bonds

Data File C:\CHEM32\1\DATA\RAUL\CHECKOUT 2017-07-24 18-21-28\TK-81.D
Sample Name: TK-81

```
=====
Acq. Operator   : SYSTEM                      Seq. Line :    3
Acq. Instrument : HPLC 1260                  Location  :   32
Injection Date  : 7/24/2017 7:24:03 PM      Inj       :    1
                                           Inj Volume: 1.000 µl

Acq. Method     : C:\Chem32\1\Data\Raul\checkout 2017-07-24 18-21-28\Chiral coloumn IB-Raul
99.5(1 BOTTLE).M
Last changed    : 7/24/2017 7:28:21 PM by SYSTEM
(modified after loading)
Analysis Method : C:\Chem32\1\Methods\Chiral coloumn IB-Raul 98-2.M
Last changed    : 7/21/2017 1:35:21 PM by SYSTEM
Additional Info  : Peak(s) manually integrated
=====
```



Area Percent Report

```
Sorted By      : Signal
Multiplier     : 1.0000
Dilution       : 1.0000
Use Multiplier & Dilution Factor with ISTDs
```

Signal 1: DAD1 C, Sig=220,4 Ref-off

Peak #	RetTime [min]	Type	Width [min]	Area [mAU*s]	Height [mAU]	Area %
1	2.260	BV	0.0576	86.42089	23.10045	0.6176
2	2.449	VV R	0.0841	1.39069e4	2694.85034	99.3824

Totals : 1.39933e4 2717.95079

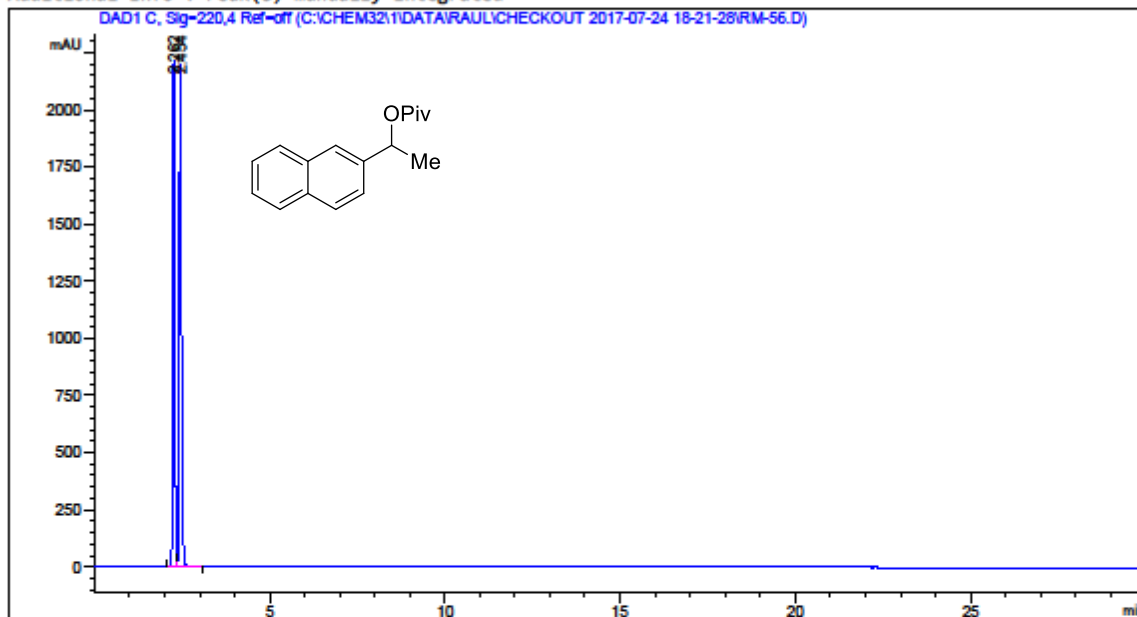
Chapter 2

Data File C:\CHEM32\1\DATA\RAUL\CHECKOUT 2017-07-24 18-21-28\RM-56.D
Sample Name: RM-56

=====

Acq. Operator	: SYSTEM	Seq. Line	: 2
Acq. Instrument	: HPLC 1260	Location	: 31
Injection Date	: 7/24/2017 6:53:12 PM	Inj	: 1
		Inj Volume	: 1.000 µl

Acq. Method : C:\Chem32\1\Data\Raul\checkout 2017-07-24 18-21-28\Chiral column IB-Raul 99.5(1 BOTTLE).M
Last changed : 7/24/2017 6:21:29 PM by SYSTEM
Analysis Method : C:\Chem32\1\Methods\Chiral column IB-Raul 98-2.M
Last changed : 7/21/2017 1:35:21 PM by SYSTEM
Additional Info : Peak(s) manually integrated



=====
Area Percent Report
=====

Sorted By : Signal
Multiplier : 1.0000
Dilution : 1.0000
Use Multiplier & Dilution Factor with ISTDs

Signal 1: DAD1 C, Sig=220,4 Ref=off

Peak #	RetTime [min]	Type	Width [min]	Area [mAU*s]	Height [mAU]	Area %
1	2.262	BV	0.0624	8834.95313	2219.48340	48.9156
2	2.454	VV R	0.0671	9226.69141	2193.05737	51.0844

Totals : 1.80616e4 4412.54077

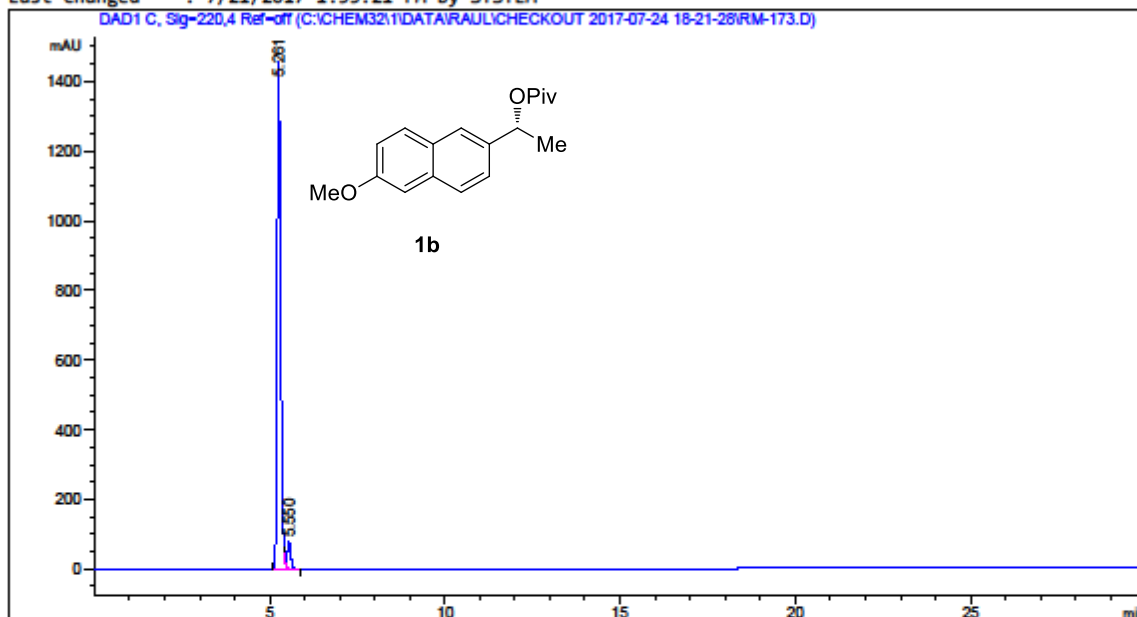
Stereospecific Borylation of Benzyl C(sp³)-O Bonds

Data File C:\CHEM32\1\DATA\RAUL\CHECKOUT 2017-07-24 18-21-28\RM-173.D
Sample Name: RM-173

=====

Acq. Operator	: SYSTEM	Seq. Line	: 4
Acq. Instrument	: HPLC 1260	Location	: 33
Injection Date	: 7/24/2017 7:54:55 PM	Inj	: 1
		Inj Volume	: 1.000 µl

Acq. Method : C:\Chem32\1\Data\Raul\checkout 2017-07-24 18-21-28\Chiral column IB-Raul
99.5(1 BOTTLE).M
Last changed : 7/24/2017 7:28:21 PM by SYSTEM
Analysis Method : C:\Chem32\1\Methods\Chiral column IB-Raul 98-2.M
Last changed : 7/21/2017 1:35:21 PM by SYSTEM



=====
Area Percent Report
=====

Sorted By : Signal
Multiplier : 1.0000
Dilution : 1.0000
Use Multiplier & Dilution Factor with ISTDs

Signal 1: DAD1 C, Sig=220,4 Ref=off

Peak #	RetTime [min]	Type	Width [min]	Area [mAU*s]	Height [mAU]	Area %
1	5.261	BV R	0.1023	9775.69922	1457.37537	94.8688
2	5.550	VB E	0.1022	528.74274	76.92770	5.1312

Totals : 1.03044e4 1534.30306

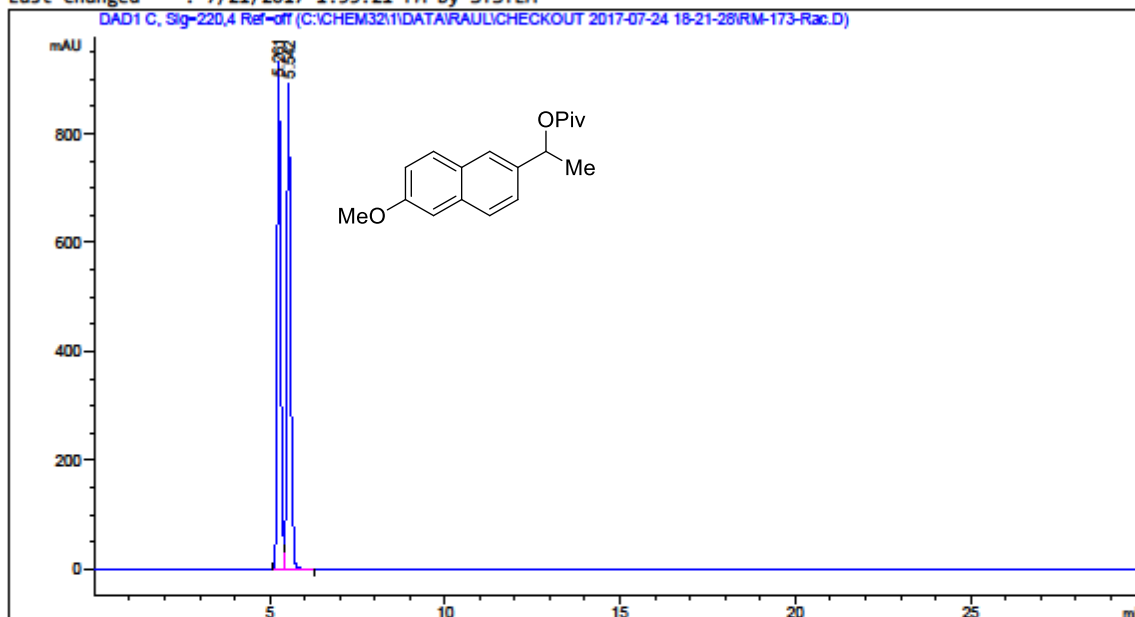
=====
*** End of Report ***

Chapter 2

Data File C:\CHEM32\1\DATA\RAUL\CHECKOUT 2017-07-24 18-21-28\RM-173-Rac.D
Sample Name: RM-173-Rac

```
=====
Acq. Operator   : SYSTEM                      Seq. Line :    5
Acq. Instrument : HPLC 1260                  Location  :   52
Injection Date  : 7/24/2017 8:25:46 PM      Inj       :    1
                                                Inj Volume: 1.000 µl

Acq. Method     : C:\Chem32\1\Data\Raul\checkout 2017-07-24 18-21-28\Chiral column IB-Raul
99.5(1 BOTTLE).M
Last changed    : 7/24/2017 7:28:21 PM by SYSTEM
Analysis Method : C:\Chem32\1\Methods\Chiral column IB-Raul 98-2.M
Last changed    : 7/21/2017 1:35:21 PM by SYSTEM
=====
```



Area Percent Report

```
Sorted By      : Signal
Multiplier     : 1.0000
Dilution       : 1.0000
Use Multiplier & Dilution Factor with ISTDs
```

Signal 1: DAD1 C, Sig=220,4 Ref=off

Peak #	RetTime [min]	Type	Width [min]	Area [mAU*s]	Height [mAU]	Area %
1	5.261	BV	0.1007	6139.77197	933.83826	49.5165
2	5.542	VB	0.1057	6259.68604	893.95709	50.4835

Totals : 1.23995e4 1827.79535

*** End of Report ***

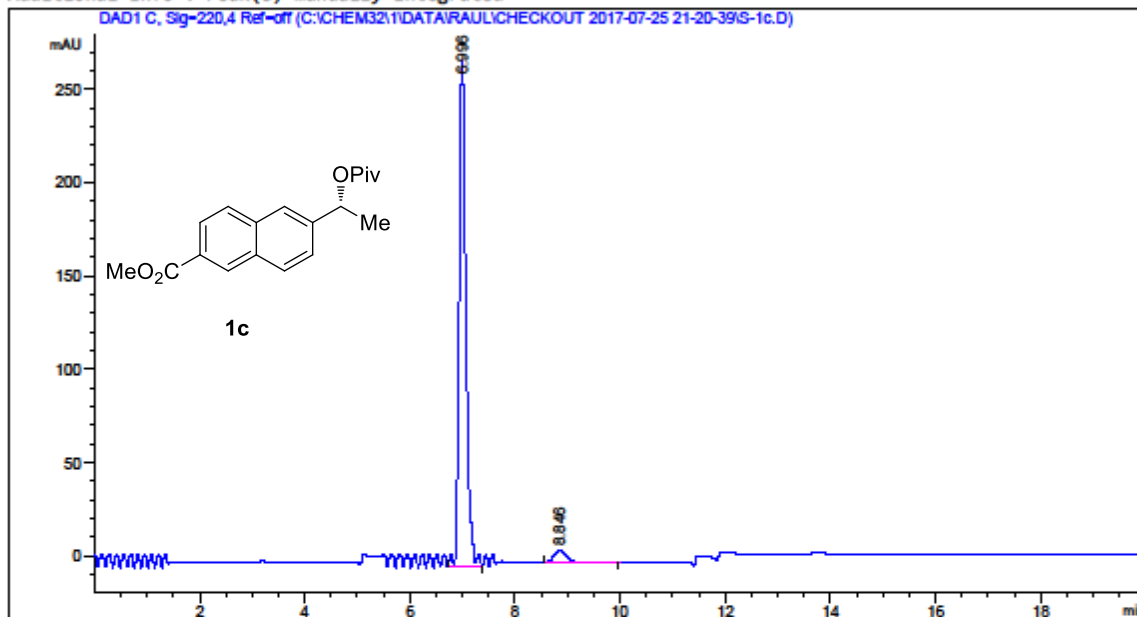
Stereospecific Borylation of Benzyl C(sp³)-O Bonds

Data File C:\CHEM32\1\DATA\RAUL\CHECKOUT 2017-07-25 21-20-39\S-1c.D
Sample Name: S-1c

=====

Acq. Operator	: SYSTEM	Seq. Line	: 13
Acq. Instrument	: HPLC 1260	Location	: 34
Injection Date	: 7/26/2017 1:31:29 AM	Inj	: 1
		Inj Volume	: 1.000 µl

Acq. Method : C:\Chem32\1\Data\Raul\checkout 2017-07-25 21-20-39\Chiral column IB-Raul 99.5(1 BOTTLE).M
Last changed : 7/25/2017 9:20:39 PM by SYSTEM
Analysis Method : C:\Chem32\1\Methods\Chiral column IB-Raul 98-2.M
Last changed : 7/21/2017 1:35:21 PM by SYSTEM
Additional Info : Peak(s) manually integrated



=====
Area Percent Report
=====

Sorted By : Signal
Multiplier : 1.0000
Dilution : 1.0000
Use Multiplier & Dilution Factor with ISTDs

Signal 1: DAD1 C, Sig=220,4 Ref=off

Peak #	RetTime [min]	Type	Width [min]	Area [mAU*s]	Height [mAU]	Area %
1	6.996	VV R	0.1323	2440.99951	271.42661	96.0486
2	8.846	BB	0.2420	100.42229	6.43872	3.9514

Totals : 2541.42180 277.86532

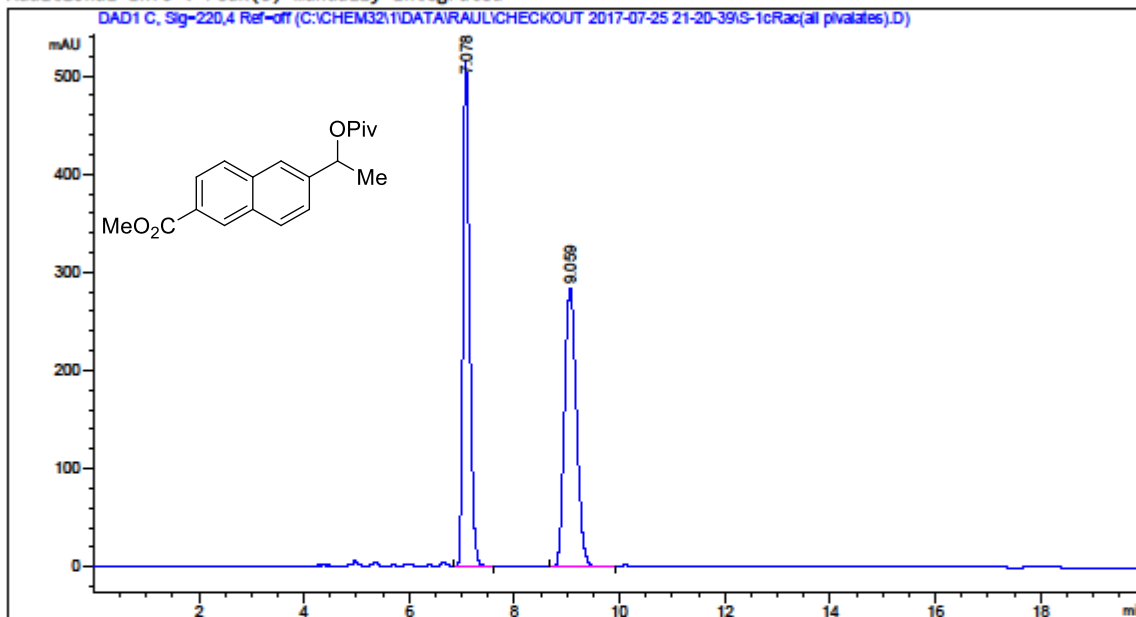
Chapter 2

Data File C:\CHEM32\1\DATA\RAUL\CHECKOUT 2017-07-25 21-20-39\S-1cRac(all pivalates).D
Sample Name: S-1cRac(all pivalates)

=====

Acq. Operator	: SYSTEM	Seq. Line	: 2
Acq. Instrument	: HPLC 1260	Location	: 53
Injection Date	: 7/25/2017 9:41:51 PM	Inj	: 1
		Inj Volume	: 1.000 µl

Acq. Method : C:\Chem32\1\Data\Raul\checkout 2017-07-25 21-20-39\Chiral coloumn IB-Raul
99.5(1 BOTTLE).M
Last changed : 7/25/2017 9:20:39 PM by SYSTEM
Analysis Method : C:\Chem32\1\Methods\Chiral coloumn IB-Raul 98-2.M
Last changed : 7/21/2017 1:35:21 PM by SYSTEM
Additional Info : Peak(s) manually integrated



=====
Area Percent Report
=====

Sorted By : Signal
Multiplier : 1.0000
Dilution : 1.0000
Use Multiplier & Dilution Factor with ISTDs

Signal 1: DAD1 C, Sig=220,4 Ref=off

Peak #	RetTime [min]	Type	Width [min]	Area [mAU*s]	Height [mAU]	Area %
1	7.078	BB	0.1324	4443.15039	516.21649	49.9286
2	9.059	BB	0.2471	4455.86475	283.84906	50.0714

Totals : 8899.01514 800.06555

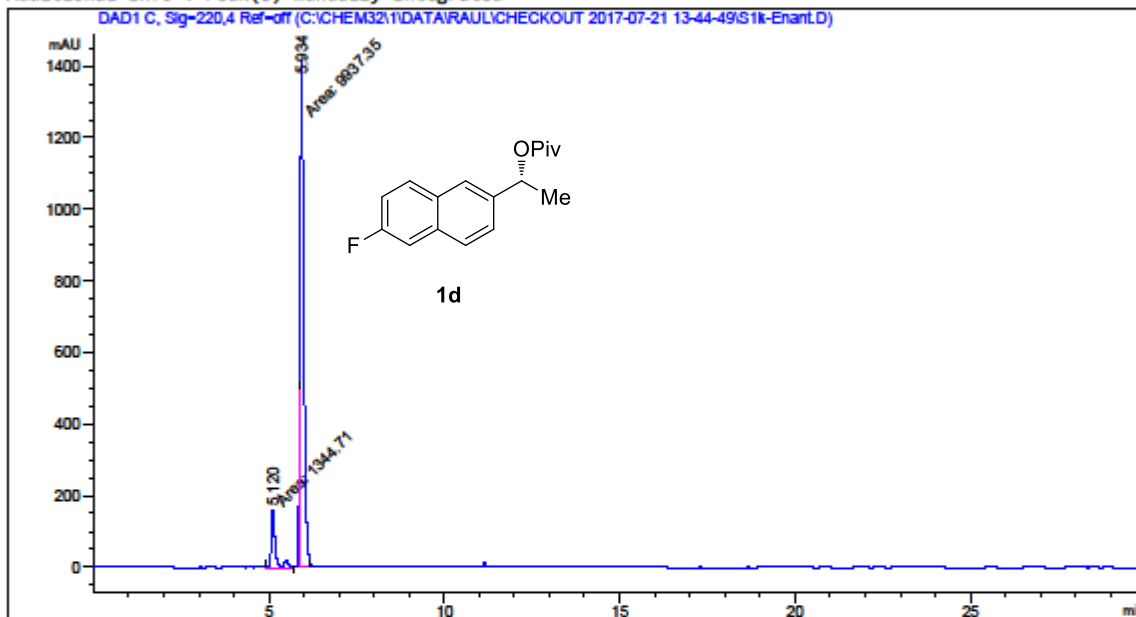
Stereospecific Borylation of Benzyl C(sp³)-O Bonds

Data File C:\CHEM32\1\DATA\RAUL\CHECKOUT 2017-07-21 13-44-49\S1k-Enant.D
Sample Name: S1k-Enant

=====

Acq. Operator	: SYSTEM	Seq. Line	: 23
Acq. Instrument	: HPLC 1260	Location	: 39
Injection Date	: 7/22/2017 1:04:47 AM	Inj	: 1
		Inj Volume	: 1.000 µl

Acq. Method : C:\Chem32\1\Data\Raul\checkout 2017-07-21 13-44-49\Chiral coloumn IB-Raul 98-2.M
Last changed : 7/21/2017 1:44:58 PM by SYSTEM
Analysis Method : C:\Chem32\1\Methods\Chiral coloumn IB-Raul 98-2.M
Last changed : 7/21/2017 1:35:21 PM by SYSTEM
Additional Info : Peak(s) manually integrated



=====
Area Percent Report
=====

Sorted By : Signal
Multiplier : 1.0000
Dilution : 1.0000
Use Multiplier & Dilution Factor with ISTDs

Signal 1: DAD1 C, Sig=220,4 Ref=off

Peak #	RetTime [min]	Type	Width [min]	Area [mAU*s]	Height [mAU]	Area %
1	5.120	MM	0.1362	1344.71411	164.49312	11.9190
2	5.934	MM	0.1171	9937.35254	1414.92688	88.0810

Totals : 1.12821e4 1579.42000

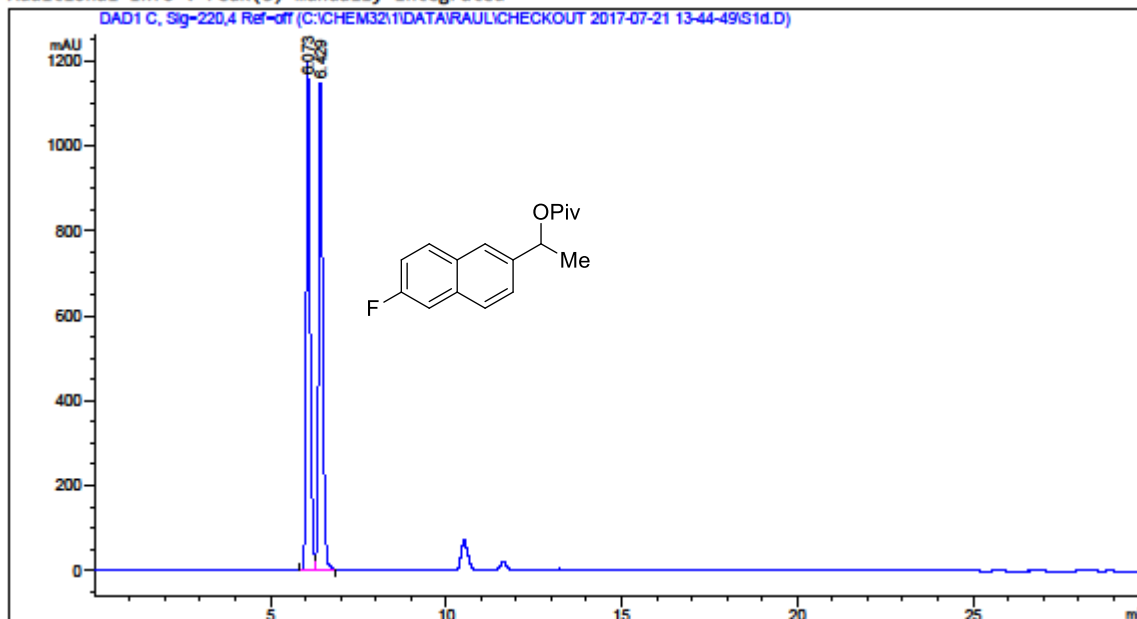
Chapter 2

Data File C:\CHEM32\1\DATA\RAUL\CHECKOUT 2017-07-21 13-44-49\S1d.D
Sample Name: S1d

=====

Acq. Operator	: SYSTEM	Seq. Line	: 5
Acq. Instrument	: HPLC 1260	Location	: 54
Injection Date	: 7/21/2017 3:49:14 PM	Inj	: 1
		Inj Volume	: 1.000 µl

Acq. Method : C:\Chem32\1\Data\Raul\checkout 2017-07-21 13-44-49\Chiral coloumn IB-Raul 98-2.M
Last changed : 7/21/2017 1:44:58 PM by SYSTEM
Analysis Method : C:\Chem32\1\Methods\Chiral coloumn IB-Raul 98-2.M
Last changed : 7/21/2017 1:35:21 PM by SYSTEM
Additional Info : Peak(s) manually integrated



=====
Area Percent Report
=====

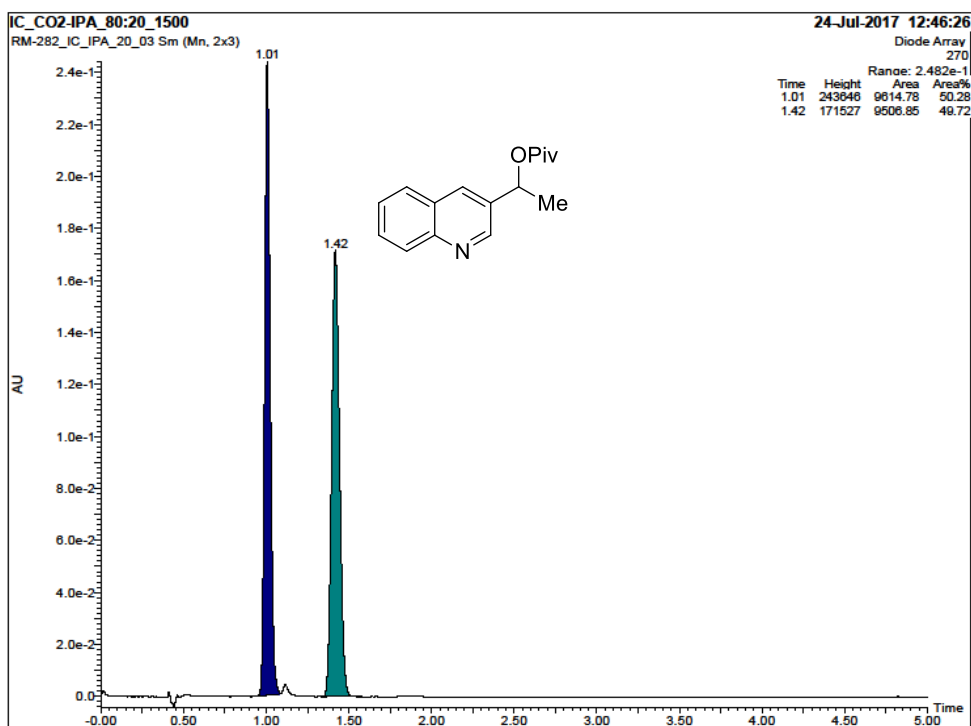
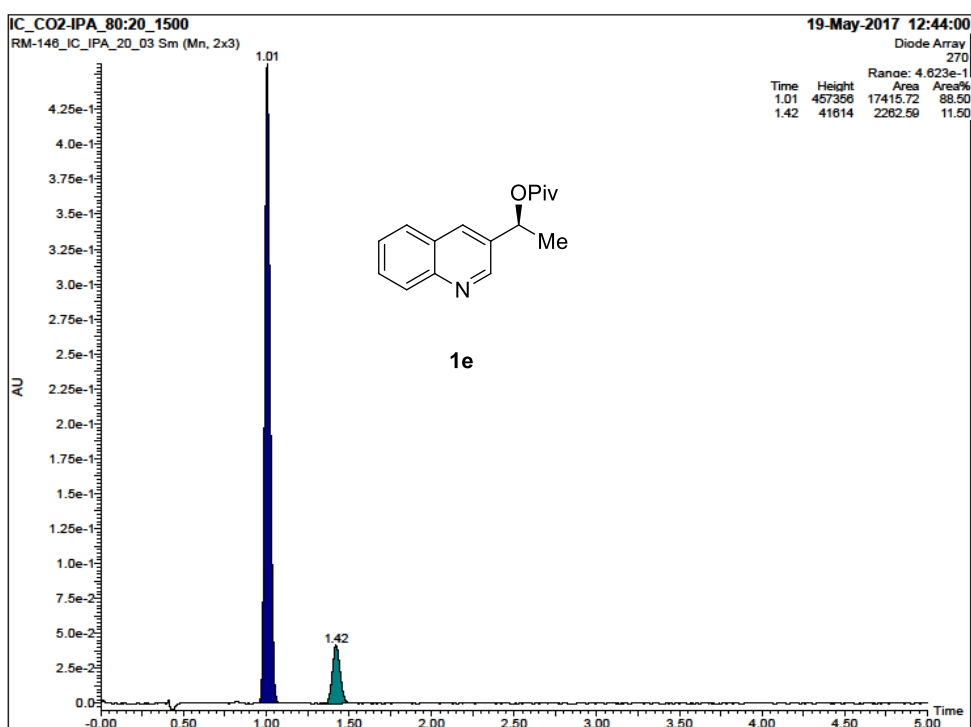
Sorted By : Signal
Multiplier : 1.0000
Dilution : 1.0000
Use Multiplier & Dilution Factor with ISTDs

Signal 1: DAD1 C, Sig=220,4 Ref=off

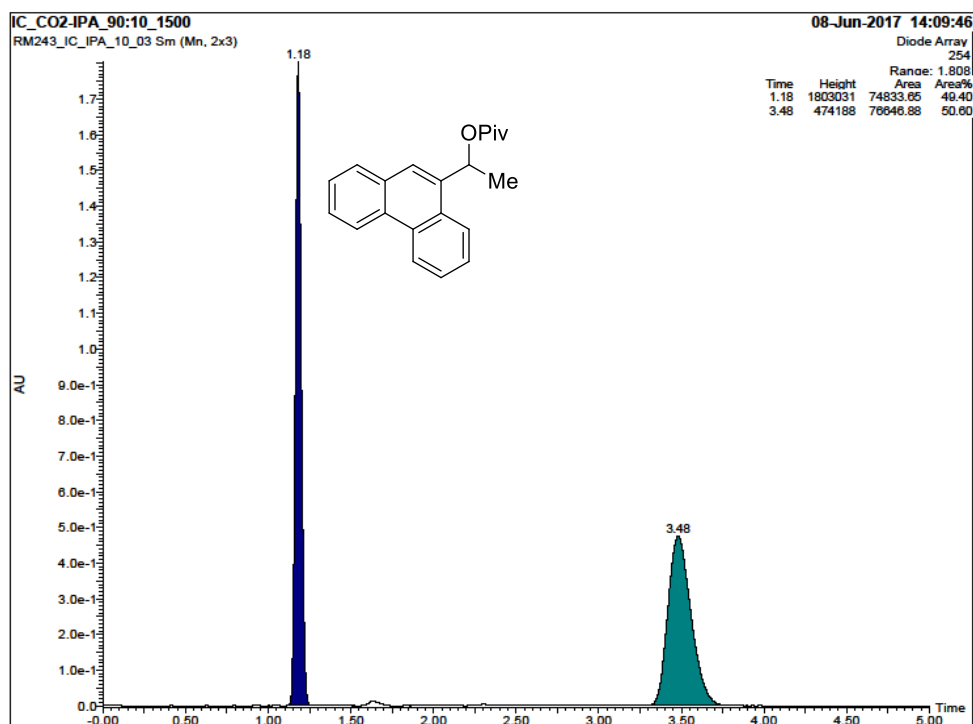
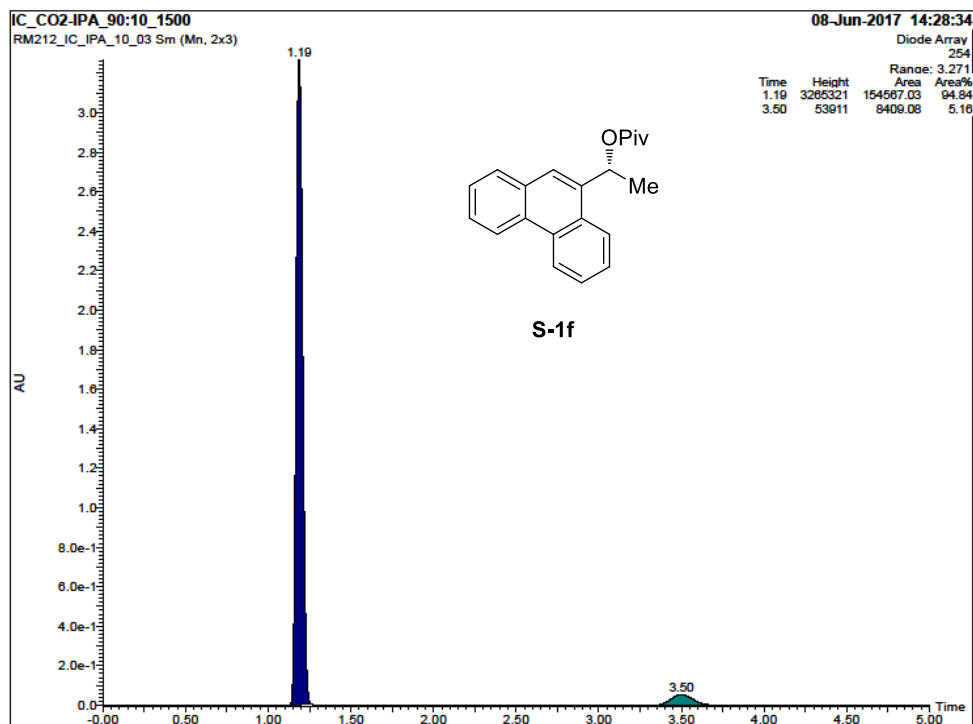
Peak #	RetTime [min]	Type	Width [min]	Area [mAU*s]	Height [mAU]	Area %
1	6.073	BV	0.1143	9078.61035	1199.21814	49.6243
2	6.429	VB	0.1217	9216.08691	1147.95068	50.3757

Totals : 1.82947e4 2347.16882

Stereospecific Borylation of Benzyl C(sp³)-O Bonds

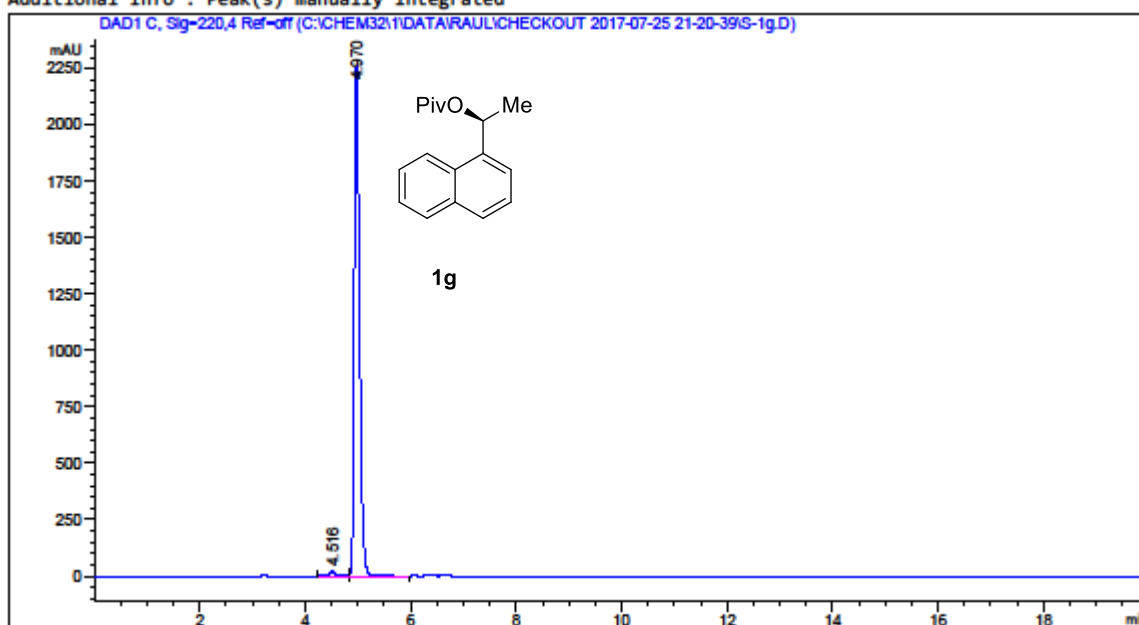


Chapter 2



Data File C:\CHEM32\1\DATA\RAUL\CHECKOUT 2017-07-25 21-20-39\S-1g.D
Sample Name: S-1g

```
=====
Acq. Operator   : SYSTEM                      Seq. Line : 14
Acq. Instrument : HPLC 1260                  Location  : 35
Injection Date  : 7/26/2017 1:52:20 AM       Inj       : 1
                                           Inj Volume: 1.000 µl
Acq. Method     : C:\Chem32\1\Data\Raul\checkout 2017-07-25 21-20-39\Chiral coloumn IB-Raul
                                           99.5(1 BOTTLE).M
Last changed    : 7/25/2017 9:20:39 PM by SYSTEM
Analysis Method : C:\Chem32\1\Methods\Chiral coloumn IB-Raul 98-2.M
Last changed    : 7/21/2017 1:35:21 PM by SYSTEM
Additional Info  : Peak(s) manually integrated
=====
```



Area Percent Report

```
Sorted By      : Signal
Multiplier     : 1.0000
Dilution       : 1.0000
Use Multiplier & Dilution Factor with ISTDs
```

Signal 1: DAD1 C, Sig=220,4 Ref=off

Peak #	RetTime [min]	Type	Width [min]	Area [mAU*s]	Height [mAU]	Area %
1	4.516	VV R	0.0894	177.19789	23.93011	1.1323
2	4.970	VB	0.1058	1.54719e4	2262.74805	98.8677

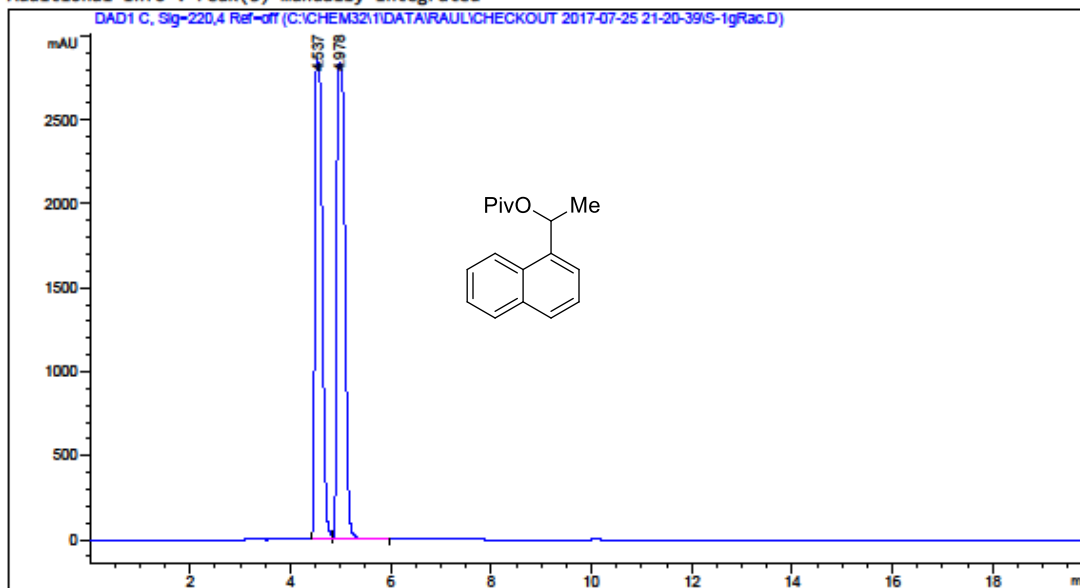
Totals : 1.56491e4 2286.67816

Chapter 2

Data File C:\CHEM32\1\DATA\RAUL\CHECKOUT 2017-07-25 21-20-39\S-1gRac.D
Sample Name: S-1gRac

```
=====
Acq. Operator   : SYSTEM                      Seq. Line :    4
Acq. Instrument : HPLC 1260                  Location  :   57
Injection Date  : 7/25/2017 10:23:37 PM      Inj       :    1
                                           Inj Volume: 1.000 µl

Acq. Method     : C:\Chem32\1\Data\Raul\checkout 2017-07-25 21-20-39\Chiral coloumn IB-Raul
                  99.5(1 BOTTLE).M
Last changed    : 7/25/2017 9:20:39 PM by SYSTEM
Analysis Method : C:\Chem32\1\Methods\Chiral coloumn IB-Raul 98-2.M
Last changed    : 7/21/2017 1:35:21 PM by SYSTEM
Additional Info  : Peak(s) manually integrated
=====
```



Area Percent Report

```
Sorted By      : Signal
Multiplier     : 1.0000
Dilution       : 1.0000
Use Multiplier & Dilution Factor with ISTDs
```

Signal 1: DAD1 C, Sig=220,4 Ref-off

Peak #	RetTime [min]	Type	Width [min]	Area [mAU*s]	Height [mAU]	Area %
1	4.537	BV	0.1701	2.94821e4	2864.07788	48.0662
2	4.978	VV R	0.1825	3.18543e4	2843.75659	51.9338

Totals : 6.13364e4 5707.83447

Stereospecific Borylation of Benzyl C(sp³)-O Bonds

Data File C:\CHEM32\1\DATA\RAUL\CHECKOUT 2017-07-25 21-20-39\S-1h.D
Sample Name: S-1h

=====

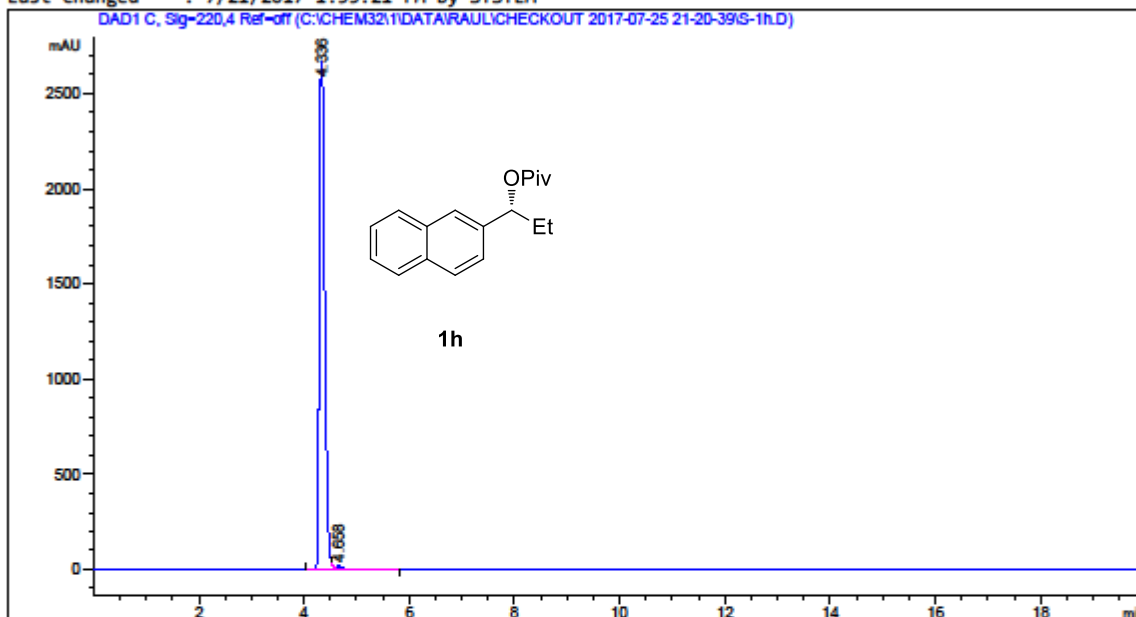
Acq. Operator : SYSTEM	Seq. Line : 15
Acq. Instrument : HPLC 1260	Location : 36
Injection Date : 7/26/2017 2:13:10 AM	Inj : 1
	Inj Volume : 1.000 µl

Acq. Method : C:\Chem32\1\Data\Raul\checkout 2017-07-25 21-20-39\Chiral coloumn IB-Raul
99.5(1 BOTTLE).M

Last changed : 7/25/2017 9:20:39 PM by SYSTEM

Analysis Method : C:\Chem32\1\Methods\Chiral coloumn IB-Raul 98-2.M

Last changed : 7/21/2017 1:35:21 PM by SYSTEM



=====
Area Percent Report
=====

Sorted By : Signal
Multiplier : 1.0000
Dilution : 1.0000
Use Multiplier & Dilution Factor with ISTDs

Signal 1: DAD1 C, Sig=220,4 Ref=off

Peak #	RetTime [min]	Type	Width [min]	Area [mAU*s]	Height [mAU]	Area %
1	4.336	BV R	0.1135	1.90674e4	2663.72827	99.3330
2	4.658	VB E	0.1168	128.03185	15.11627	0.6670

Totals : 1.91954e4 2678.84454

=====
*** End of Report ***

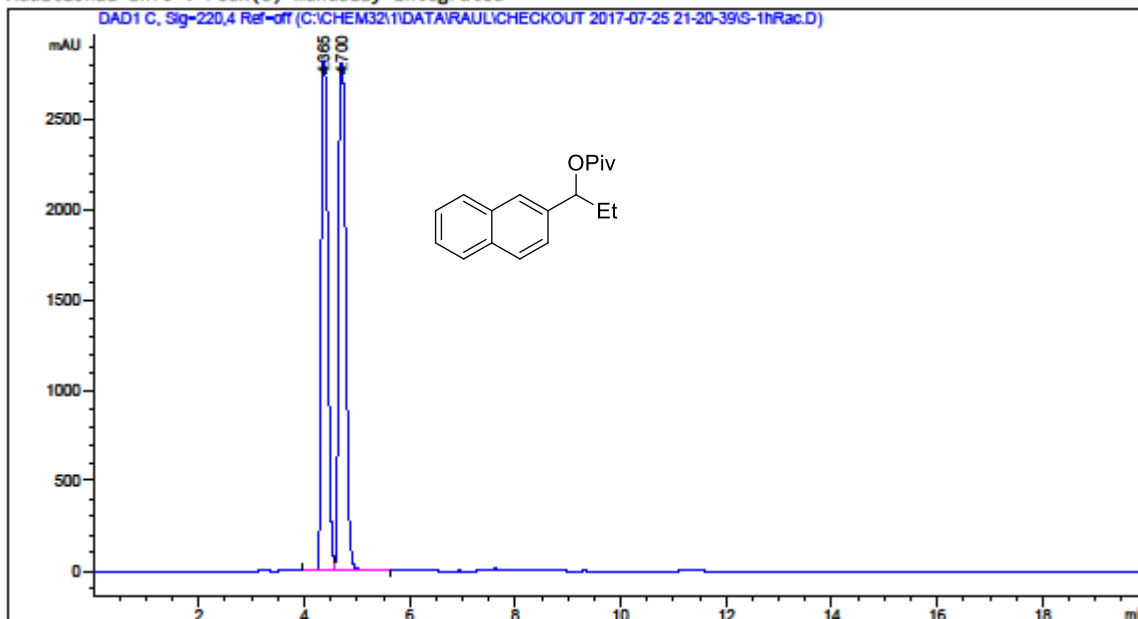
Chapter 2

Data File C:\CHEM32\1\DATA\RAUL\CHECKOUT 2017-07-25 21-20-39\S-1hRac.D
Sample Name: S-1hRac

=====

Acq. Operator	: SYSTEM	Seq. Line	: 5
Acq. Instrument	: HPLC 1260	Location	: 58
Injection Date	: 7/25/2017 10:44:28 PM	Inj	: 1
		Inj Volume	: 1.000 µl

Acq. Method : C:\Chem32\1\Data\Raul\checkout 2017-07-25 21-20-39\Chiral coloumn IB-Raul 99.5(1 BOTTLE).M
Last changed : 7/25/2017 9:20:39 PM by SYSTEM
Analysis Method : C:\Chem32\1\Methods\Chiral coloumn IB-Raul 98-2.M
Last changed : 7/21/2017 1:35:21 PM by SYSTEM
Additional Info : Peak(s) manually integrated



=====
Area Percent Report
=====

Sorted By : Signal
Multiplier : 1.0000
Dilution : 1.0000
Use Multiplier & Dilution Factor with ISTDs

Signal 1: DAD1 C, Sig=220,4 Ref-off

Peak #	RetTime [min]	Type	Width [min]	Area [mAU*s]	Height [mAU]	Area %
1	4.365	VV R	0.1428	2.48699e4	2822.26904	48.1945
2	4.700	VV R	0.1548	2.67332e4	2812.17358	51.8055

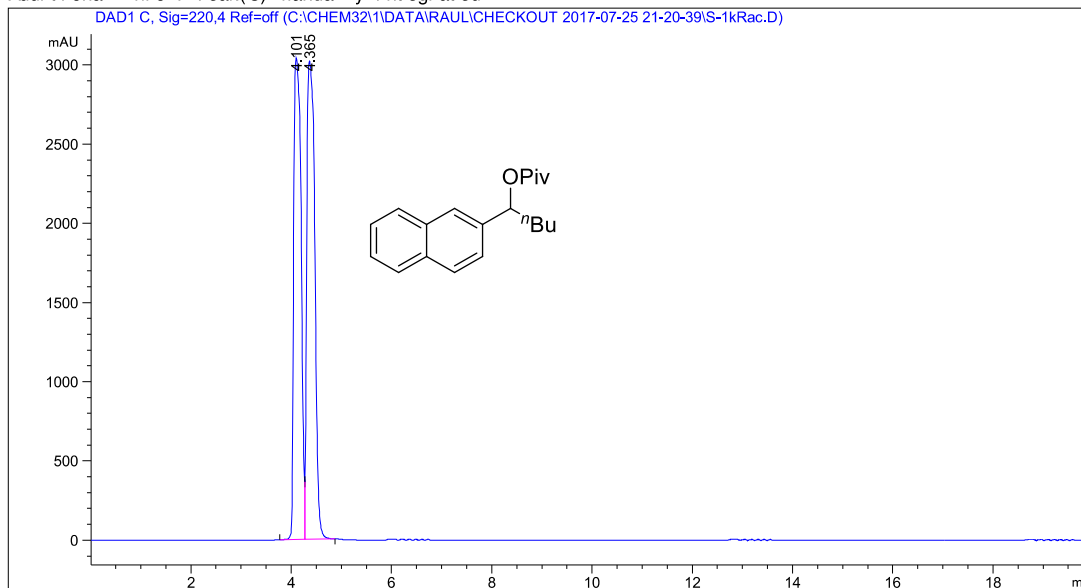
Totals : 5.16031e4 5634.44263

Chapter 2

Data File C:\CHEM82\1\DATA\RAUL\CHECKOUT 2017-07-25 21-20-39\S-1kRac.D
Sample Name: S-1kRac

```
=====
Acq. Operator   : SYSTEM                      Seq. Line :    8
Acq. Instrument : HPLC 1260                  Location  :   61
Injection Date  : 7/25/2017 11:47:08 PM      Inj       :    1
                                           Inj Volume: 1.000 µl

Acq. Method     : C:\Chem82\1\Dat a\ Paul \checkout 2017-07-25 21-20-39\Chiral column IB-Paul
                 99.5(1 BOTTLE), M
Last changed    : 7/25/2017 9:20:39 PM by SYSTEM
Analysis Method : C:\Chem82\1\Met hods\Chiral column IB-Paul 98-2.M
Last changed    : 7/21/2017 1:35:21 PM by SYSTEM
Additional Info : Peak(s) manually integrated
=====
```



Area Percent Report

```
Sorted By      : Signal
Multiplier     : 1.0000
Dilution      : 1.0000
Use Multiplier & Dilution Factor with ISTDs
```

Signal 1: DAD1 C, Sig=220,4 Ref=off

Peak #	Ret Time [min]	Type	Width [min]	Area [mAU*s]	Height [mAU]	Area %
1	4.101	W R	0.1680	3.07626e4	3040.91113	47.9695
2	4.365	VB	0.1809	3.33669e4	3020.03516	52.0305

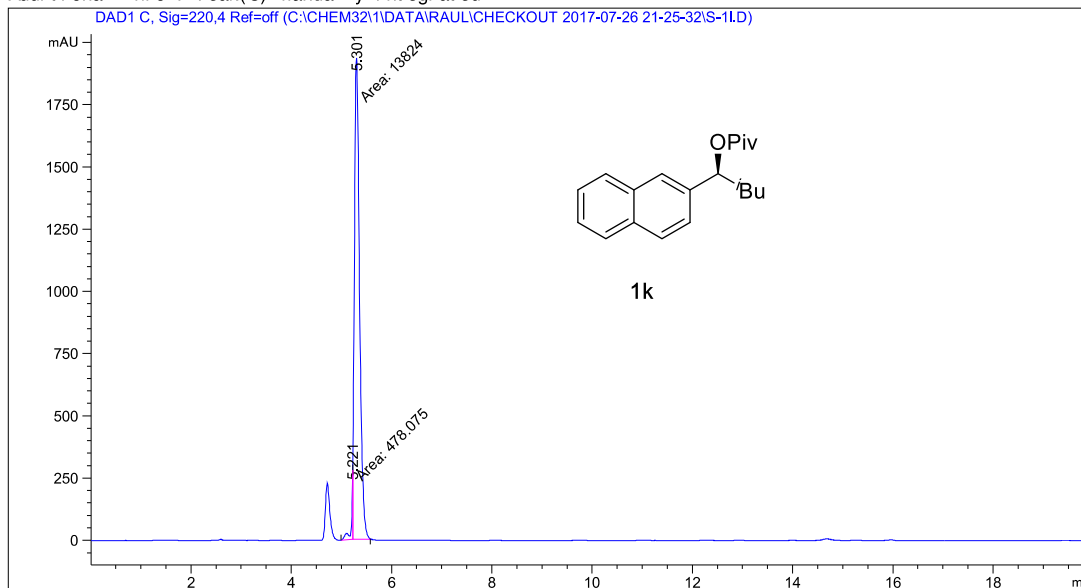
Totals : 6.41295e4 6060.94629

Stereospecific Borylation of Benzyl C(sp³)-O Bonds

Data File C:\CHEM82\1\DATA\RAUL\CHECKOUT 2017-07-26 21-25-32\S-11.D
 Sample Name: S-11

```
=====
Acq. Operator   : SYSTEM                      Seq. Line :    4
Acq. Instrument : HPLC 1260                  Location  :   39
Injection Date  : 7/26/2017 10:28:40 PM      Inj       :    1
                                           Inj Volume: 1.000 µl

Acq. Method     : C:\Chem82\1\Dat a\ Paul \checkout 2017-07-26 21-25-32\Chiral column IB-Paul
98-2, M
Last changed    : 7/26/2017 9:25:33 PM by SYSTEM
Analysis Method : C:\Chem82\1\Methods\Chiral column IB-Paul 98-2, M
Last changed    : 7/21/2017 1:35:21 PM by SYSTEM
Additional Info : Peak(s) manually integrated
=====
```



Area Percent Report

```
Sorted By      :      Signal
Multiplier     :      1.0000
Dilution       :      1.0000
Use Multiplier & Dilution Factor with ISTDs
```

Signal 1: DAD1 C, Sig=220,4 Ref=off

Peak #	Ret Time [min]	Type	Width [min]	Area [mAU*s]	Height [mAU]	Area %
1	5.221	MM	0.0359	478.07468	222.24596	3.3427
2	5.301	MM	0.1191	1.38240e4	1934.95618	96.6573

Totals : 1.43021e4 2157.20213

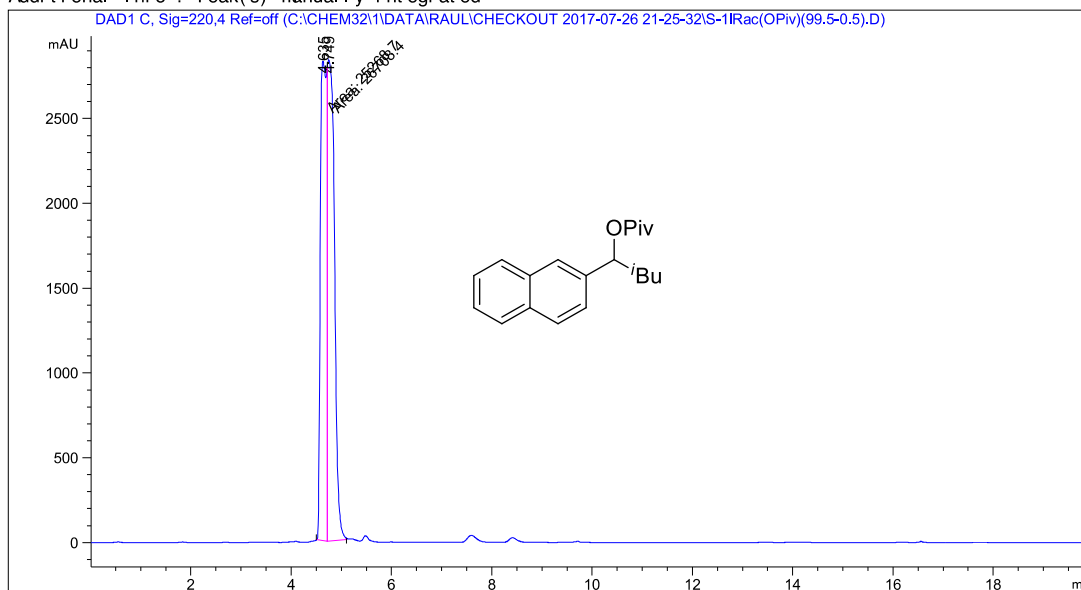
Chapter 2

Data File C:\CHEM82\1\DATA\PAUL\CHECKOUT 2017-07-26 21-25-32\5-1Rac(OPiv)(99.5-0.5).D
 Sample Name: 5-1Rac(OPiv)(99.5-0.5)

```

=====
Acq. Operator   : SYSTEM                               Seq. Line :    2
Acq. Instrument : HPLC 1260                             Location  :   62
Injection Date  : 7/26/2017 9:46:44 PM                 Inj       :    1
                                                    Inj Volume: 1.000 µl

Acq. Method     : C:\Chem82\1\Dat a\ Paul \ checkout 2017-07-26 21-25-32\ Chi r al coloum I B- Paul
                98-2, M
Last changed    : 7/26/2017 9:25:33 PM by SYSTEM
Analysis Method : C:\Chem82\1\Met hods\ Chi r al coloum I B- Paul 98-2, M
Last changed    : 7/21/2017 1:35:21 PM by SYSTEM
Additional Info : Peak(s) manually integrated
    
```



Area Percent Report

```

Sorted By      :      Signal
Multiplier     :      1.0000
Dilution       :      1.0000
Use Multiplier & Dilution Factor with ISTDs
    
```

Signal 1: DAD1 C, Sig=220,4 Ref=off

Peak #	Ret Time [min]	Type	Width [min]	Area [mAU*s]	Height [mAU]	Area %
1	4.635	MM	0.1490	2.52687e4	2826.07520	48.6150
2	4.749	MM	0.1569	2.67084e4	2836.55737	51.3850

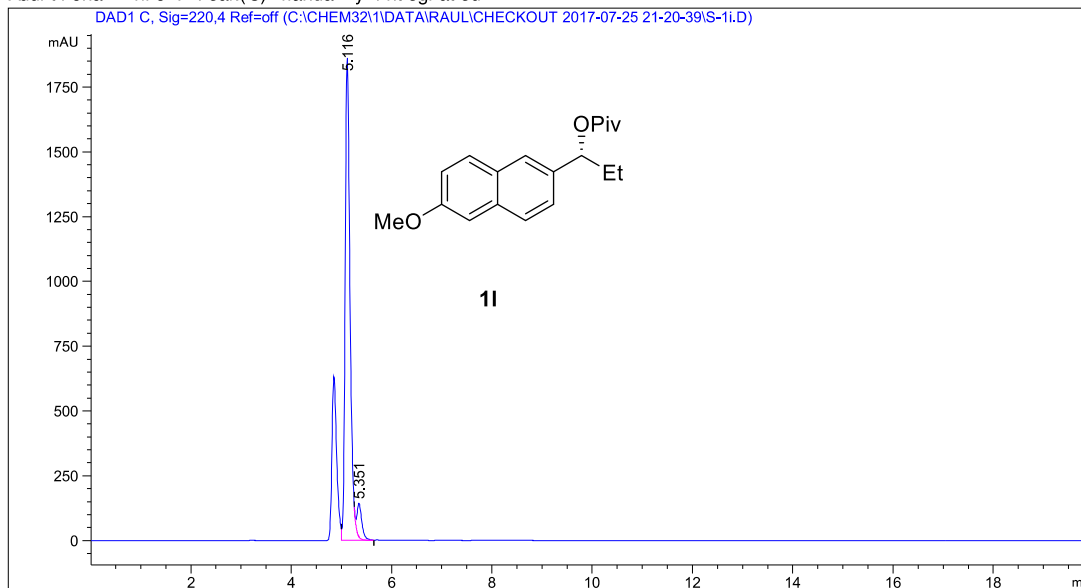
Totals : 5.19771e4 5662.63257

Stereospecific Borylation of Benzyl C(sp³)-O Bonds

Data File C:\CHEM82\1\DATA\RAUL\CHECKOUT 2017-07-25 21-20-39\S-1i.D
 Sample Name: S-1i

```
=====
Acq. Operator   : SYSTEM                      Seq. Line :   16
Acq. Instrument : HPLC 1260                  Location  :   37
Injection Date  : 7/26/2017 2:34:01 AM       Inj       :    1
                                           Inj Volume: 1.000 µl

Acq. Method     : C:\Chem82\1\Dat a\ Paul \checkout 2017-07-25 21-20-39\Chiral column IB-Paul
                 99.5(1 BOTTLE), M
Last changed    : 7/25/2017 9:20:39 PM by SYSTEM
Analysis Method : C:\Chem82\1\Met hods\Chiral column IB-Paul 98-2.M
Last changed    : 7/21/2017 1:35:21 PM by SYSTEM
Additional Info : Peak(s) manually integrated
=====
```



Area Percent Report

```
Sorted By      :      Signal
Multiplier     :      1.0000
Dilution       :      1.0000
Use Multiplier & Dilution Factor with ISTDs
```

Signal 1: DAD1 C, Sig=220,4 Ref=off

Peak #	Ret Time [min]	Type	Width [min]	Area [mAU*s]	Height [mAU]	Area %
1	5.116	W R	0.1008	1.25685e4	1861.41223	93.5896
2	5.351	VB E	0.0993	860.87994	129.90913	6.4104

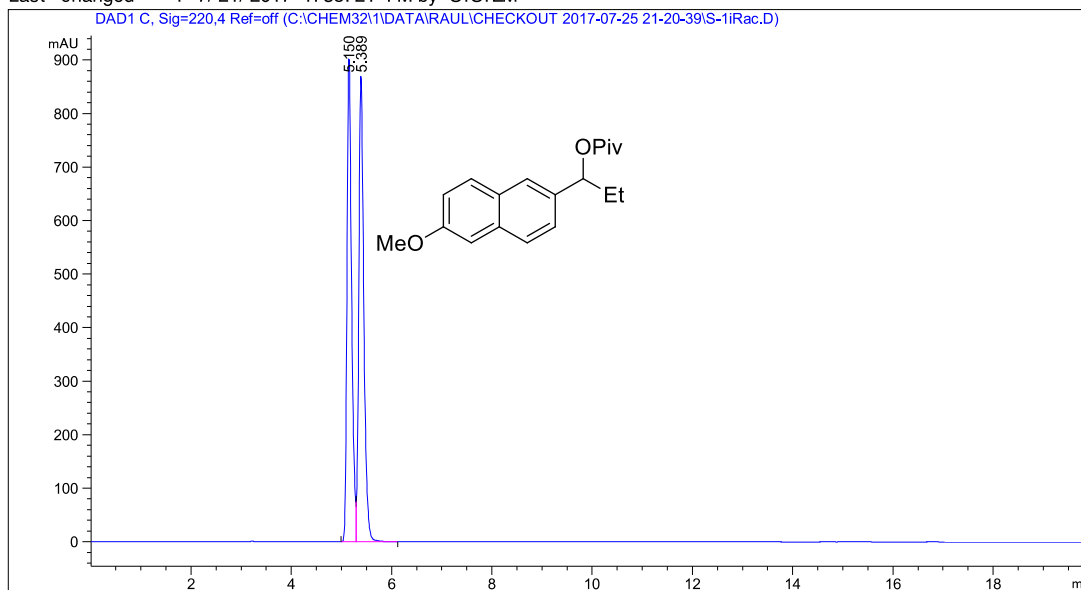
Totals : 1.34294e4 1991.32137

Chapter 2

Data File C:\CHEM82\1\DATA\RAUL\CHECKOUT 2017-07-25 21-20-39\S-1i Rac.D
 Sample Name: S-1i Rac

```
=====
Acq. Operator   : SYSTEM                      Seq. Line :    6
Acq. Instrument : HPLC 1260                  Location  :   59
Injection Date  : 7/25/2017 11:05:21 PM      Inj       :    1
                                           Inj Volume: 1.000 µl

Acq. Method     : C:\Chem82\1\Dat a\ Paul \checkout 2017-07-25 21-20-39\Chiral column IB-Paul
                 99.5(1 BOTTLE), M
Last changed    : 7/25/2017 9:20:39 PM by SYSTEM
Analysis Method : C:\Chem82\1\Met hods\Chiral column IB-Paul 98-2.M
Last changed    : 7/21/2017 1:35:21 PM by SYSTEM
=====
```



Area Percent Report

```
Sorted By      : Signal
Multiplier     : 1.0000
Dilution       : 1.0000
Use Multiplier & Dilution Factor with ISTDs
```

Signal 1: DAD1 C, Sig=220,4 Ref=off

Peak #	Ret Time [min]	Type	Width [min]	Area [mAU*s]	Height [mAU]	Area %
1	5.150	BV	0.0969	5801.21094	903.68774	48.9639
2	5.389	VB	0.1050	6046.73340	870.57117	51.0361

Totals : 1.18479e4 1774.25891

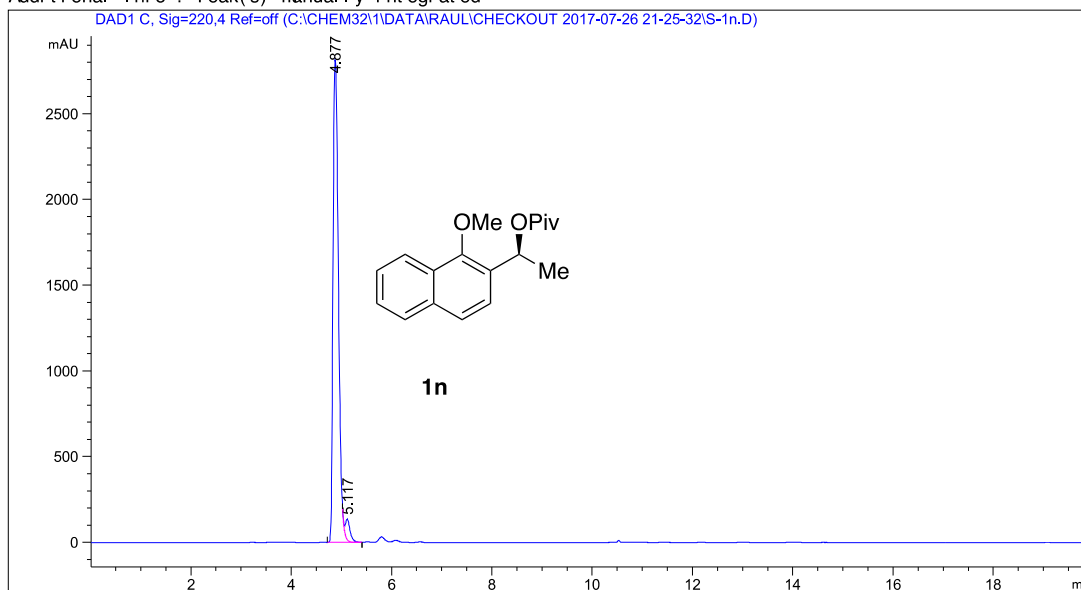
*** End of Report ***

Stereospecific Borylation of Benzyl C(sp³)-O Bonds

Data File C:\CHEM82\1\DATA\RAUL\CHECKOUT 2017-07-26 21-25-32\S-1n.D
 Sample Name: S-1n

```
=====
Acq. Operator   : SYSTEM                      Seq. Line :    5
Acq. Instrument : HPLC 1260                  Location  :   42
Injection Date  : 7/26/2017 10:49:32 PM      Inj       :    1
                                           Inj Volume: 1.000 µl

Acq. Method     : C:\Chem82\1\Dat a\ Paul \checkout 2017-07-26 21-25-32\Chi ral coloum IB-Paul
98-2, M
Last changed    : 7/26/2017 9:25:33 PM by SYSTEM
Analysis Method : C:\Chem82\1\Met hods\ Chi ral coloum IB-Paul 98-2, M
Last changed    : 7/21/2017 1:35:21 PM by SYSTEM
Additional Info : Peak(s) manually integrated
=====
```



Area Percent Report

```
Sorted By      :      Signal
Multiplier     :      1.0000
Dilution       :      1.0000
Use Multiplier & Dilution Factor with ISTDs
```

Signal 1: DAD1 C, Sig=220,4 Ref=off

Peak #	Ret Time [min]	Type	Width [min]	Area [mAU*s]	Height [mAU]	Area %
1	4.877	BV R	0.1176	2.11305e4	2813.50098	96.3800
2	5.117	VB E	0.0993	793.65070	119.85345	3.6200

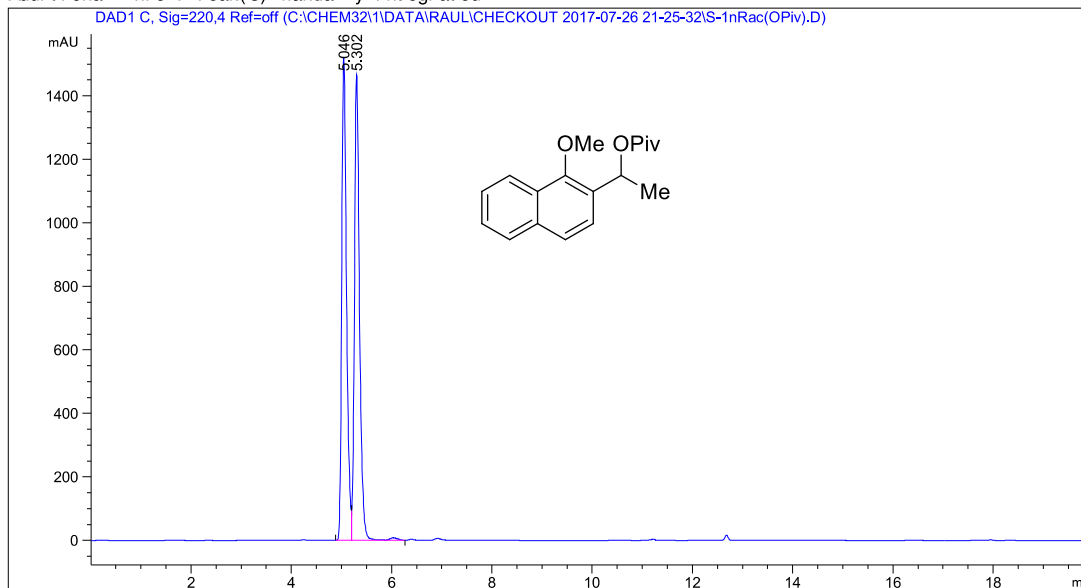
Totals : 2.19242e4 2933.35442

Chapter 2

Data File C:\CHEM82\1\DATA\RAUL\CHECKOUT 2017-07-26 21-25-32\S-1nFac(OPiv).D
 Sample Name: S-1nFac(OPiv)

```
=====
Acq. Operator   : SYSTEM                      Seq. Line :    3
Acq. Instrument : HPLC 1260                   Location  :   64
Injection Date  : 7/26/2017 10:07:36 PM      Inj       :    1
                                           Inj Volume: 1.000 µl

Acq. Method     : C:\Chem82\1\Dat a\ Paul \checkout 2017-07-26 21-25-32\Chiral column IB-Paul
                  98-2, M
Last changed    : 7/26/2017 9:25:33 PM by SYSTEM
Analysis Method : C:\Chem82\1\Met hods\Chiral column IB-Paul 98-2, M
Last changed    : 7/21/2017 1:35:21 PM by SYSTEM
Additional Info : Peak(s) manually integrated
=====
```



Area Percent Report

```
Sorted By      :      Signal
Multiplier     :      1.0000
Dilution       :      1.0000
Use Multiplier & Dilution Factor with ISTDs
```

Signal 1: DAD1 C, Sig=220,4 Ref=off

Peak #	Ret Time [min]	Type	Width [min]	Area [mAU*s]	Height [mAU]	Area %
1	5.046	BV	0.1006	9978.34375	1519.33752	49.0625
2	5.302	WV R	0.1057	1.03597e4	1468.33154	50.9375

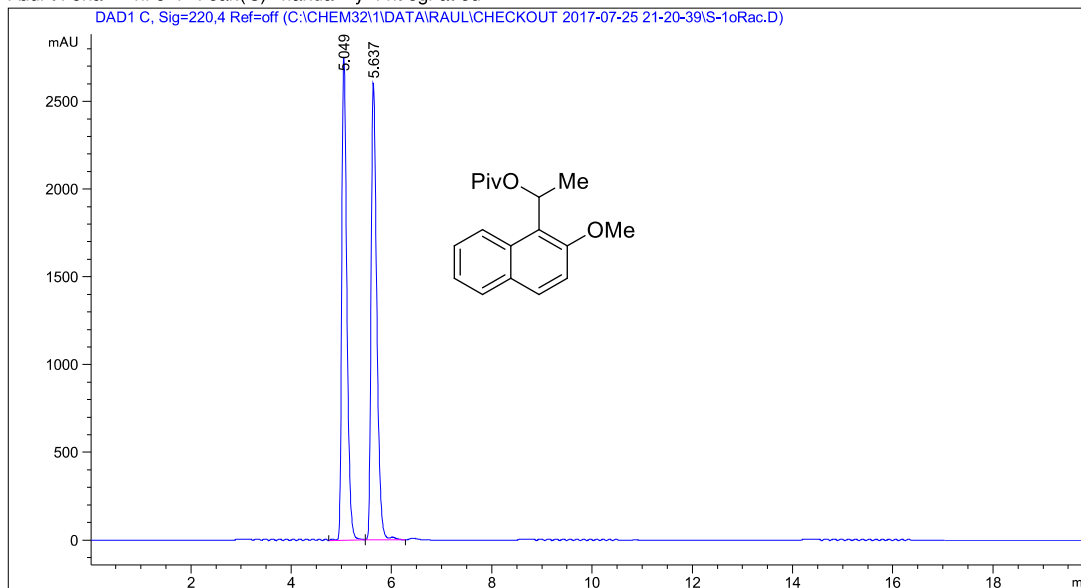
Totals : 2.03380e4 2987.66907

Chapter 2

Data File C:\CHEM82\1\DATA\RAUL\CHECKOUT 2017-07-25 21-20-39\S-1oFac.D
 Sample Name: S-1oFac

```
=====
Acq. Operator   : SYSTEM                      Seq. Line :   12
Acq. Instrument : HPLC 1260                  Location  :    65
Injection Date  : 7/26/2017 1:10:36 AM       Inj       :    1
                                           Inj Volume: 1.000 µl

Acq. Method     : C:\Chem82\1\Dat a\ Paul \checkout 2017-07-25 21-20-39\Chiral column IB-Paul
                  99.5(1 BOTTLE), M
Last changed    : 7/25/2017 9:20:39 PM by SYSTEM
Analysis Method : C:\Chem82\1\Met hods\Chiral column IB-Paul 98-2.M
Last changed    : 7/21/2017 1:35:21 PM by SYSTEM
Additional Info : Peak(s) manually integrated
=====
```



Area Percent Report

```
Sorted By      :      Signal
Multiplier     :      1.0000
Dilution       :      1.0000
Use Multiplier & Dilution Factor with ISTDs
```

Signal 1: DAD1 C, Sig=220,4 Ref=off

Peak #	Ret Time [min]	Type	Width [min]	Area [mAU*s]	Height [mAU]	Area %
1	5.049	VB R	0.1082	1.94062e4	2747.56250	48.7435
2	5.637	BV R	0.1187	2.04067e4	2606.21509	51.2565

Totals : 3.98129e4 5353.77759

2.6 References

- (1) Zarate, C.; van Gemmeren, M.; Somerville, R. J.; Martin, R. Phenol Derivatives: Modern Electrophiles in Cross-Coupling Reactions. *Adv. Organomet. Chem.* **2016**, *66*, 143–222. <https://doi.org/10.1016/bs.adomc.2016.07.001>.
- (2) Tobisu, M.; Chatani, N. Cross-Couplings Using Aryl Ethers via C-O Bond Activation Enabled by Nickel Catalysts. *Acc. Chem. Res.* **2015**, *48* (6), 1717–1726. <https://doi.org/10.1021/acs.accounts.5b00051>.
- (3) Tollefson, E. J.; Hanna, L. E.; Jarvo, E. R. Stereospecific Nickel-Catalyzed Cross-Coupling Reactions of Benzylic Ethers and Esters. *Acc. Chem. Res.* **2015**, *48* (8), 2344–2353. <https://doi.org/10.1021/acs.accounts.5b00223>.
- (4) Ernest Ludwig Eliel, Samuel H. Wilen, L. N. M. *Stereochemistry of Organic Compounds*; John Wiley & Sons: New York, 1994. [https://doi.org/10.1016/0016-7037\(95\)90151-5](https://doi.org/10.1016/0016-7037(95)90151-5).
- (5) Carreira, E. M.; Kvaerno, L. *Classics in Stereoselective Synthesis*; Wiley-VCH: Weinheim, Germany, 2009.
- (6) Li, L.; Zhao, S.; Joshi-Pangu, A.; Diane, M.; Biscoe, M. R. Stereospecific Pd-Catalyzed Cross-Coupling Reactions of Secondary Alkylboron Nucleophiles and Aryl Chlorides. *J. Am. Chem. Soc.* **2014**, *136* (40), 14027–14030. <https://doi.org/10.1021/ja508815w>.
- (7) Swift, E. C.; Jarvo, E. R. Asymmetric Transition Metal-Catalyzed Cross-Coupling Reactions for the Construction of Tertiary Stereocenters. *Tetrahedron* **2013**, *69* (29), 5799–5817. <https://doi.org/10.1016/j.tet.2013.05.001>.
- (8) Wilsily, A.; Tramutola, F.; Owston, N. A.; Fu, G. C. New Directing Groups for Metal-Catalyzed Asymmetric Carbon-Carbon Bond-Forming Processes: Stereoconvergent Alkyl-Alkyl Suzuki Cross-Couplings of Unactivated Electrophiles. *J. Am. Chem. Soc.* **2012**, *134* (13), 5794–5797. <https://doi.org/10.1021/ja301612y>.
- (9) Fischer, C.; Fu, G. C. Asymmetric Nickel-Catalyzed Negishi Cross-Couplings of Secondary α -Bromo Amides with Organozinc Reagents. *J. Am. Chem. Soc.* **2005**, *127* (13), 4594–4595. <https://doi.org/10.1021/ja0506509>.
- (10) Arp, F. O.; Fu, G. C. Catalytic Enantioselective Negishi Reactions of Racemic Secondary Benzylic Halides. *J. Am. Chem. Soc.* **2005**, *127* (30), 10482–10483. <https://doi.org/10.1021/ja053751f>.
- (11) Giovannini, R.; Stüdemann, T.; Knochel, P. An Efficient Nickel-Catalyzed Cross-Coupling Between Sp³ Carbon Centers. *Angew. Chem. Int. Ed.* **1998**, *28*, 2387–2390.
- (12) Tasker, S. Z.; Standley, E. A.; Jamison, T. F. Recent Advances in Homogeneous Nickel Catalysis. *Nature* **2014**, *509* (7500), 299–309. <https://doi.org/10.1038/nature13274>.
- (13) Rudolph, A.; Lautens, M. Secondary Alkyl Halides in Transition-Metal-Catalyzed Cross-Coupling Reactions. *Angew. Chemie - Int. Ed.* **2009**, *48* (15), 2656–2670. <https://doi.org/10.1002/anie.200803611>.
- (14) Legros, J. Y.; Toffano, M.; Fiaud, J. C. Palladium-Catalyzed Substitution of Esters of Naphthylmethanols, 1-Naphthylethanols, and Analogues by Sodium Dimethyl Malonate. Stereoselective Synthesis from Enantiomerically Pure Substrates. *Tetrahedron* **1995**, *51* (11), 3235–3246. [https://doi.org/10.1016/0040-4020\(95\)00061-C](https://doi.org/10.1016/0040-4020(95)00061-C).
- (15) Lau, K. S. Y.; Fries, R. W.; Stille, J. K. Stereochemistry of Oxidative Addition of Alkyl Halides to Palladium(0) Complexes. *J. Am. Chem. Soc.* **1974**, *96* (15), 4983–4986. <https://doi.org/10.1021/ja00822a044>.
- (16) Biswas, S.; Weix, D. J. Mechanism and Selectivity in Nickel-Catalyzed Cross-Electrophile Coupling of Aryl Halides with Alkyl Halides. *J. Am. Chem. Soc.* **2013**, *135* (43), 16192–16197. <https://doi.org/10.1021/ja407589e>.
- (17) Hegedus, L. S.; Miller, L. L. Reaction of π -Allylnickel Bromide Complexes with Organic Halides. Stereochemistry and Mechanism. *J. Am. Chem. Soc.* **1975**, *97* (2), 459–460. <https://doi.org/10.1021/ja00835a061>.
- (18) Lin, X.; Sun, J.; Xi, Y.; Lin, D. How Racemic Secondary Alkyl Electrophiles Proceed to Enantioselective Products in Negishi Cross-Coupling Reactions. *Organometallics* **2011**, *30* (12), 3284–3292. <https://doi.org/10.1021/om1012049>.
- (19) Choi, J.; Martín-Gago, P.; Fu, G. C. Stereoconvergent Arylations and Alkenylations of Unactivated Alkyl Electrophiles: Catalytic Enantioselective

Chapter 2

- Synthesis of Secondary Sulfonamides and Sulfones. *J. Am. Chem. Soc.* **2014**, *136* (34), 12161–12165. <https://doi.org/10.1021/ja506885s>.
- (20) Phapale, V. B.; Buñuel, E.; García-Iglesias, M.; Cárdenas, D. J. Ni-Catalyzed Cascade Formation of C(Sp³)-C(Sp³) Bonds by Cyclization and Cross-Coupling Reactions of Iodoalkanes with Alkyl Zinc Halides. *Angew. Chemie - Int. Ed.* **2007**, *46* (46), 8790–8795. <https://doi.org/10.1002/anie.200702528>.
- (21) Dankwardt, J. W. Nickel-Catalyzed Cross-Coupling of Aryl Grignard Reagents with Aromatic Alkyl Ethers: An Efficient Synthesis of Unsymmetrical Biaryls. *Angew. Chemie - Int. Ed.* **2004**, *43* (18), 2428–2432. <https://doi.org/10.1002/anie.200453765>.
- (22) Yamamoto, E. N. J. · A. P. · H. *Comprehensive Asymmetric Catalysis I-III*; Springer-Verlag: Berlin Heidelberg New York, 2000. [https://doi.org/10.1002/1615-4169\(20010129\)343:1<141::aid-adscl141>3.3.co;2-5](https://doi.org/10.1002/1615-4169(20010129)343:1<141::aid-adscl141>3.3.co;2-5).
- (23) Taylor, B. L. H.; Swift, E. C.; Waetzig, J. D.; Jarvo, E. R. Stereospecific Nickel-Catalyzed Cross-Coupling Reactions of Alkyl Ethers: Enantioselective Synthesis of Diarylethanes. *J. Am. Chem. Soc.* **2011**, *133* (3), 389–391. <https://doi.org/10.1021/ja108547u>.
- (24) Zhang, S. Q.; Taylor, B. L. H.; Ji, C. L.; Gao, Y.; Harris, M. R.; Hanna, L. E.; Jarvo, E. R.; Houk, K. N.; Hong, X. Mechanism and Origins of Ligand-Controlled Stereoselectivity of Ni-Catalyzed Suzuki-Miyaura Coupling with Benzylic Esters: A Computational Study. *J. Am. Chem. Soc.* **2017**, *139* (37), 12994–13005. <https://doi.org/10.1021/jacs.7b04973>.
- (25) Yonova, I. M.; Johnson, A. G.; Osborne, C. A.; Moore, C. E.; Morrisette, N. S.; Jarvo, E. R. Stereospecific Nickel-Catalyzed Cross-Coupling Reactions of Alkyl Grignard Reagents and Identification of Selective Anti-Breast-Cancer Agents. *Angew. Chemie - Int. Ed.* **2014**, *53* (9), 2422–2427. <https://doi.org/10.1002/anie.201308666>.
- (26) Hubig, S. M.; Lindeman, S. V.; Kochi, J. K. *Charge-Transfer Bonding in Metal-Arene Coordination*; 2000; Vol. 200–202. [https://doi.org/10.1016/S0010-8545\(00\)00322-2](https://doi.org/10.1016/S0010-8545(00)00322-2).
- (27) Brauer, D. J.; Krüger, C. Bonding of Aromatic Hydrocarbons to Ni(0). Structure of Bistricyclohexylphosphine (1,2-H₂-Anthracene) Nickel(0) - Toluene. *Inorg. Chem.* **1977**, *16* (4), 884–891. <https://doi.org/10.1021/ic50170a033>.
- (28) Greene, M. A.; Yonova, I. M.; Williams, F. J.; Jarvo, E. R. Traceless Directing Group for Stereospecific Nickel-Catalyzed Alkyl-Alkyl Cross-Coupling Reactions. *Org. Lett.* **2012**, *14* (16), 4293–4296. <https://doi.org/10.1021/ol300891k>.
- (29) Taylor, B. L. H.; Harris, M. R.; Jarvo, E. R. Synthesis of Enantioenriched Triarylmethanes by Stereospecific Cross-Coupling Reactions. *Angew. Chemie - Int. Ed.* **2012**, *51* (31), 7790–7793. <https://doi.org/10.1002/anie.201202527>.
- (30) Knochel, P.; Leuser, H.; Gong, L. Z.; Perrone, S.; Kneisel, F. F. *Polyfunctional Zinc Organometallics for Organic Synthesis*; 2008; Vol. 1. <https://doi.org/10.1002/9783527619467.ch7>.
- (31) Wisniewska, H. M.; Swift, E. C.; Jarvo, E. R. Functional-Group-Tolerant, Nickel-Catalyzed Cross-Coupling Reaction for Enantioselective Construction of Tertiary Methyl-Bearing Stereocenters. *J. Am. Chem. Soc.* **2013**, *135* (24), 9083–9090. <https://doi.org/10.1021/ja4034999>.
- (32) Kuwano, R.; Yokogi, M. Cross-Coupling of Benzylic Acetates with Arylboronic Acids: One-Pot Transformation of Benzylic Alcohols to Diarylmethanes. *Chem. Commun.* **2005**, No. 47, 5899–5901. <https://doi.org/10.1039/b513372f>.
- (33) Zhou, Q.; Srinivas, H. D.; Dasgupta, S.; Watson, M. P. Nickel-Catalyzed Cross-Couplings of Benzylic Pivalates with Arylboroxines: Stereospecific Formation of Diarylalkanes and Triarylmethanes. *J. Am. Chem. Soc.* **2013**, *135* (9), 3307–3310. <https://doi.org/10.1021/ja312087x>.
- (34) Harris, M. R.; Hanna, L. E.; Greene, M. A.; Moore, C. E.; Jarvo, E. R. Retention or Inversion in Stereospecific Nickel-Catalyzed Cross-Coupling of Benzylic Carbamates with Arylboronic Esters: Control of Absolute Stereochemistry with an Achiral Catalyst. *J. Am. Chem. Soc.* **2013**, *135* (9), 3303–3306. <https://doi.org/10.1021/ja311783k>.
- (35) Chen, Q.; Fan, X. H.; Zhang, L. P.; Yang, L. M. Ni(I) Source as a Pre-Catalyst for the Cross-Coupling of Benzylic Pivalates with Arylboronic Acids: Facile Access to Tri- and Diarylmethanes. *RSC Adv.* **2015**, *5* (20), 15338–15340. <https://doi.org/10.1039/c4ra16452k>.
- (36) Zhou, Q.; Cobb, K. M.; Tan, T.; Watson, M. P. Stereospecific Cross Couplings to Set Benzylic, All-Carbon Quaternary Stereocenters in High Enantiopurity. *J. Am. Chem. Soc.* **2016**, *138* (37), 12057–12060. <https://doi.org/10.1021/jacs.6b08075>.
- (37) Srinivas, H. D.; Zhou, Q.; Watson, M. P. Enantiospecific, Nickel-Catalyzed Cross-Couplings of Allylic Pivalates and Arylboroxines. *Org. Lett.*

- 2014, 16(13), 3596–3599. <https://doi.org/10.1021/ol5016724>.
- (38) Zhou, Q.; Srinivas, H. D.; Zhang, S.; Watson, M. P. Accessing Both Retention and Inversion Pathways in Stereospecific, Nickel-Catalyzed Miyaura Borylations of Allylic Pivalates. *J. Am. Chem. Soc.* **2016**, 138(36), 11989–11995. <https://doi.org/10.1021/jacs.6b07396>.
- (39) Rach, S. F.; Kuhn, F. E. Nitrile Ligated Transition Metal Complexes with Weakly Coordinating Counteranions and Their Catalytic Applications. *Chem. Rev.* **2009**, 109(5), 2061–2080. <https://doi.org/10.1021/cr800270h>.
- (40) Cobb, K. M.; Rabb-Lynch, J. M.; Hoermer, M. E.; Manders, A.; Zhou, Q.; Watson, M. P. Stereospecific, Nickel-Catalyzed Suzuki-Miyaura Cross-Coupling of Allylic Pivalates to Deliver Quaternary Stereocenters. *Org. Lett.* **2017**, 19(16), 4355–4358. <https://doi.org/10.1021/acs.orglett.7b02063>.
- (41) Zarate, C.; Martín, R. A Mild Ni/Cu-Catalyzed Silylation via C–O Cleavage. *J. Am. Chem. Soc.* **2014**, 136(6), 2236–2239. <https://doi.org/10.1021/ja412107b>.
- (42) Somerville, R. J.; Hale, L. V. A.; Gómez-Bengoa, E.; Burés, J.; Martín, R. Intermediacy of Ni-Ni Species in Sp² C–O Bond Cleavage of Aryl Esters: Relevance in Catalytic C–Si Bond Formation. *J. Am. Chem. Soc.* **2018**, 140(28), 8771–8780. <https://doi.org/10.1021/jacs.8b04479>.
- (43) Sergeev, A. G.; Webb, J. D.; Hartwig, J. F. A Heterogeneous Nickel Catalyst for the Hydrogenolysis of Aryl Ethers without Arene Hydrogenation. *J. Am. Chem. Soc.* **2012**, 134(50), 20226–20229. <https://doi.org/10.1021/ja3085912>.
- (44) Correa, A.; León, T.; Martín, R. Ni-Catalyzed Carboxylation of C(Sp²)- and C(Sp³)-O Bonds with CO₂. *J. Am. Chem. Soc.* **2014**, 136(3), 1062–1069. <https://doi.org/10.1021/ja410883p>.
- (45) Pietsch, S.; Neeve, E. C.; Apperley, D. C.; Bertermann, R.; Fanyang, M.; Di, Q.; Man Sing, C.; Li, D.; Jianbo, W.; Udo, R.; Zhenyang, L.; Christian, K.; Todd B, M. Synthesis, Structure, and Reactivity of Anionic Sp²–Sp³ Diboron Compounds: Readily Accessible Boryl Nucleophiles. *Chem. - A Eur. J.* **2015**, 21, 7082–7099. <https://doi.org/10.1002/chem.201500235>.
- (46) King, A. E.; Brunold, T. C.; Stahl, S. S. Mechanistic Study of Copper-Catalyzed Aerobic Oxidative Coupling of Arylboronic Esters and Methanol: Insights into an Organometallic Oxidase Reaction. *J. Am. Chem. Soc.* **2009**, 131, 5044–5045. <https://doi.org/10.1021/ja9006657>.
- (47) Ricci, P.; Krämer, K.; Cambeiro, X. C.; Larrosa, I. Arene-Metal π -Complexation as a Traceless Reactivity Enhancer for C–H Arylation. *J. Am. Chem. Soc.* **2013**, 135(36), 13258–13261. <https://doi.org/10.1021/ja405936s>.
- (48) Ricci, P.; Krämer, K.; Larrosa, I. Tuning Reactivity and Site Selectivity of Simple Arenes in C–H Activation: Ortho-Arylation of Anisoles via Arene-Metal π -Complexation. *J. Am. Chem. Soc.* **2014**, 136(52), 18082–18086. <https://doi.org/10.1021/ja510260j>.
- (49) Suga, T.; Mizuno, H.; Takaya, J.; Iwasawa, N. Direct Carboxylation of Simple Arenes with CO₂ through a Rhodium-Catalyzed C–H Bond Activation. *Chem. Commun.* **2014**, 50(92), 14360–14363. <https://doi.org/10.1039/c4cc06188h>.

Chapter 3.

Ni-catalyzed Reductive Deaminative Arylation at sp^3 Carbon Centers

Research carried out in collaboration with
Veera Reddy Yatham, Hongfei Yin, Jacob Davies
Published in: *Org. Lett.* **2019**, 21 (8), 2947-2951

Chapter 3

3.1 Introduction

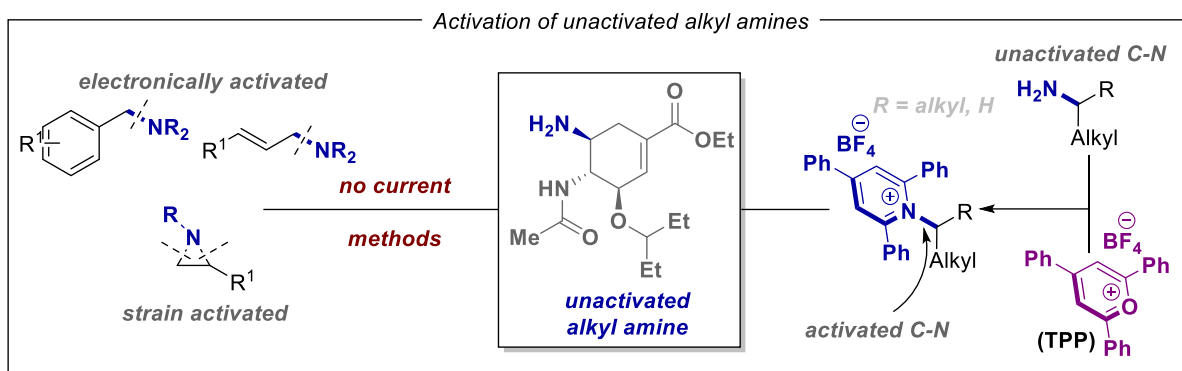
An increase of sp^3 character in drug candidates improves several molecular attributes that ultimately contribute to clinical success, including solubility, molecular shape (3D-structure) or substrate recognition, among others. In the last decades, transition metal-catalyzed coupling reactions of well-defined organometallic reagents (boronic acids, organozinc compounds, Grignard reagents, etc.) with electrophilic partners – typically organic (pseudo)halides – have offered new vistas for forging sp^3 – sp^3 linkages while providing revolutionary solutions for selectively functionalizing complex structures. These protocols operate with high regioselectivity, and have been widely utilized in both academic and industrial laboratories.^{1–5} However, practicality and cost-issues associated to these processes spurred the development of new sp^3 – sp^3 bond-forming strategies that rely on abundant, native (or naturally-occurring) functional groups, as these entities might offer innovative solutions for bond-construction at late-stages.

Alkyl amines are chemical feedstocks with a natural abundance slightly similar to that of carboxylic acids. Indeed, primary and secondary amines are one of the most prevalent motifs across a wide range of biologically-active molecules, pharmaceuticals and natural products.^{6–9} Specifically, 47000 primary alkyl amines vs about 28 000 primary and secondary alkyl halides can be found,¹⁰ reinforcing the need for designing catalytic protocols that utilize alkyl amines as functional handles for forging C–C bonds. Such a technology will be particularly relevant in the context of late-stage functionalization of drug intermediates possessing an aliphatic amine, a feature that will certainly be of utmost relevance in the drug discovery pipeline.^{11,12}

3.2 C–C and C–Heteroatom bond formation *via* C(sp^3)–N bond cleavage of pyridinium salts

3.2.1 Introduction to the activation of unactivated alkyl amines by pyridinium salts

In the last decade, many efforts have been done towards the development of catalytic technologies for the cleavage of C(sp^2)–N^{13–16} and particularly activated C(sp^3)–N bonds (Chapter 1.2.2). Unfortunately, the functionalization of unactivated alkyl amines *via* the activation of C(sp^3)–N bonds remain an unexplored endeavour (Figure 3.2.1, *left*). If successful, techniques aimed at such goal will open a new gateway to build up sp^3 architectures at late stages of advanced synthetic intermediates, and a powerful alternative to the utilization of alkyl halides,^{17–20} dual photoredox/nickel catalysis with oxalate counterparts,^{21,22} carboxylic acids,^{23,24} organoboronates^{25,26} or organosilicates^{27,28} among others.

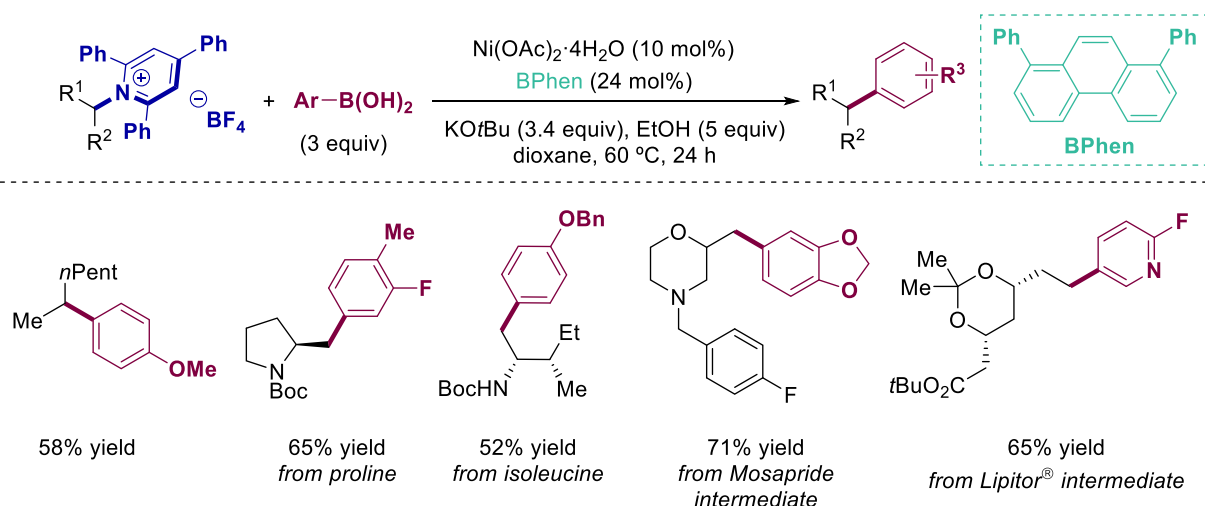


A considerable advance in the $C(sp^3)$ -N bond-cleavage arena was made by Watson and co-workers by the utilization of 2,4,6-triphenyl pyridinium salts – coined as Katritzky salts – as alkylating agents (Figure 3.2.1, *right*). These pyridinium cations have interesting features, such as being (a) air- and moisture-stable solids, crystalline and nonhygroscopic, (b) such compounds are easily prepared in one step *via* condensation of a primary or secondary alkyl amine with commercial available 2,4,6-triphenylpyridinium tetrafluoroborate (TPP),^{29,30} and (c) they have been employed as alkyl electrophiles in S_N2' reactions or radical-type mechanisms.^{31,32}

3.2.2 $C(sp^3)$ -C bond formation

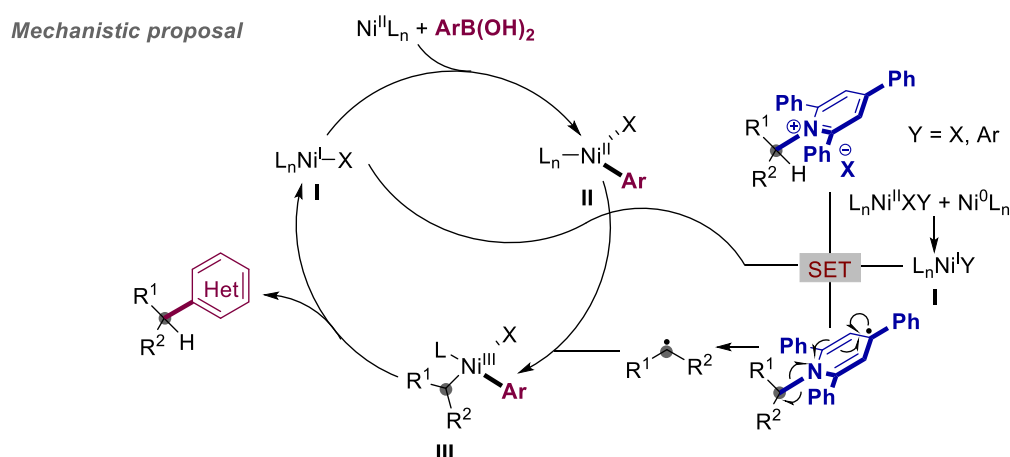
3.2.2.1 $C(sp^3)$ - $C(sp^2)$ bond formation

Despite Watson's protocol of harnessing unactivated alkyl amines as electrophiles represented a step forward (Scheme 3.2.1),³³ the protocol was not particularly suited for the coupling of unactivated secondary alkyl amines. Nevertheless, a wide variety of boronic acids bearing different functional groups were tolerated, and late-stage functionalization could be implemented with densely functionalized alkyl amine derivatives.



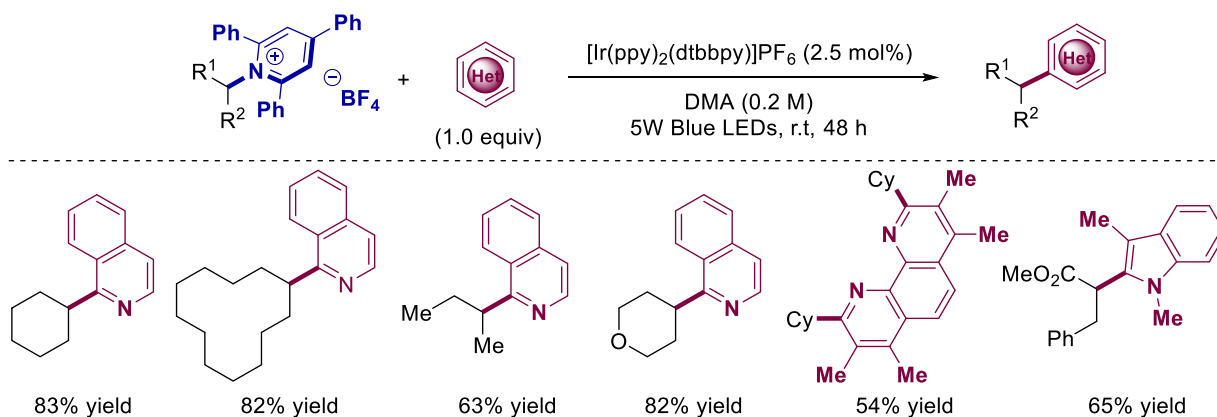
Chapter 3

The authors propose a catalytic manifold consisting of a Ni(I)/Ni(III) regime (Scheme 3.2.2), as racemic products were obtained by applying the methodology with enantioenriched alkyl pyridinium salts, and ring-opening products were observed with cyclopropyl-containing alkyl amines. Similarly to the utilization of redox-active esters,³⁴ pyridinium salts undergo single electron transfer (SET) with a Ni(I) intermediate (I), triggering an homolytic cleavage that recombines the resulting radical with an arynickel(II) intermediate (II) to form Ni(III) species (III) prior to reductive elimination. However, the authors did not provide any evidence on whether a canonical transmetalation or radical chain processes come into play.



Scheme 3.2.2. Ni(I)/Ni(III) mechanistic proposal.

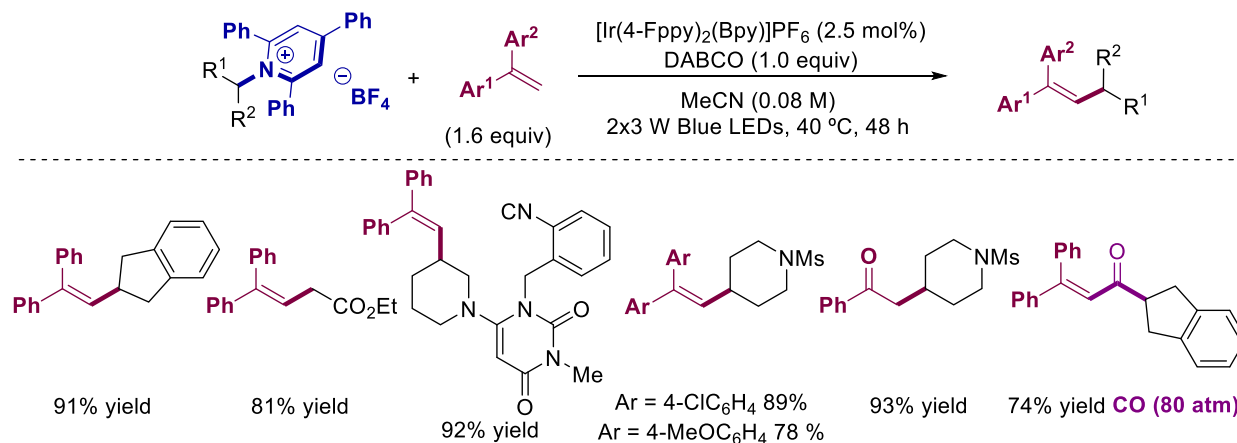
In 2017, Glorius and co-workers developed a photoredox process to activate pyridinium salts *via* SET en route to open-shell intermediates ($E_{1/2} = -0.93$ V vs SCE in DMF,³⁵ Scheme 3.2.3).³⁶ Such radical intermediates react with an electron-deficient heteroarene in a Minisci-type process that occurred with a wide substrate scope and a diverse set of different heterocycles. The protocol was amenable for the coupling of amino acids and electron-rich heteroarenes.



Scheme 3.2.3. Deaminative C-H alkylation of heteroarenes.

Subsequently, Lu and Xiao reported a deaminative alkyl-Heck-type reaction of alkyl amines through visible-light photoredox catalysis (Scheme 3.2.4).³⁷ This protocol represents a

complementary procedure to the work of Glorius, including the coupling of a wide variety of diaryl alkenes with different electronic properties. The authors also showed a representative set of examples for a catalytic deaminative carbonylative Heck-type reactions using CO at 80 atm. Lu and Xiao suggested a mechanism *via* Ni(I)/Ni(III) regimes that is based on a SET process of the photocatalyst to the pyridinium salt, generating an alkyl radical that is intercepted with an alkene to generate a new open-shell intermediate. A final single-electron oxidation by the oxidized photocatalyst and subsequent deprotonation affords the desired alkenylation product.

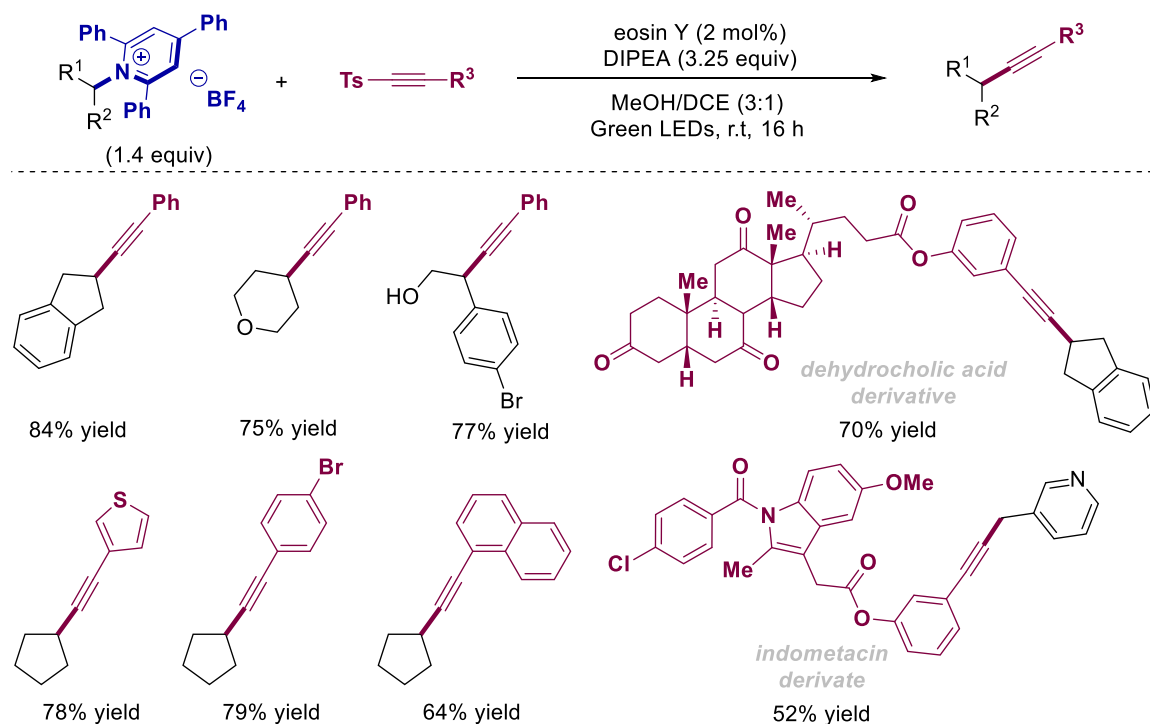


Scheme 3.2.4. Deaminative alkyl-Heck-type reaction of alkyl amines.

3.2.2.2 $C(sp^3)$ – $C(sp)$ bond formation

In 2018, Gryko and co-workers described a deaminative alkynylation process forming $C(sp^3)$ – $C(sp)$ and $C(sp^3)$ – $C(sp^2)$ bonds by metal free photoredox catalysis (Scheme 3.2.5).³⁸ In terms of scope, the methodology offered a wide tolerance to different functional groups, either for primary pyridinium salts or alkynyl precursors. However, the authors showed a limited number of examples when using secondary Katritzky salts or aromatic alkynyl substrates. It is worth noting that the technology could be applied to densely functionalized backbones. Experimental evidences collected through the work suggested the intervention of a mechanism similar to that proposed by Glorius in his photoredox scenario with pyridinium salts. In this case, single-electron transfer from the photoexcited eosin Y to the pyridinium salt released the alkyl radical, which is trapped by the alkynyl or alkenyl coupling partner, thus releasing the desired product.

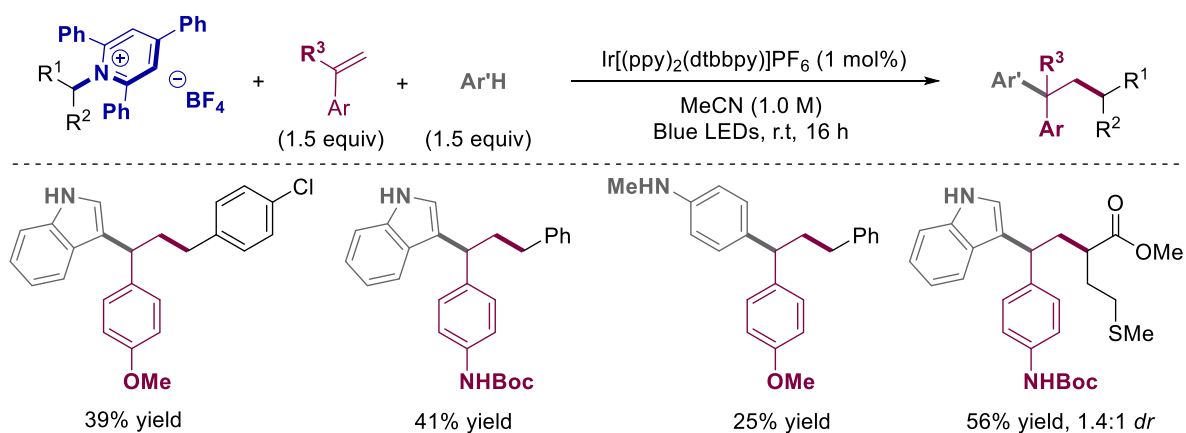
Chapter 3



Scheme 3.2.5. Deaminative alkynylation visible-light mediated.

3.2.2.3 Three-component C–C–C bond formation

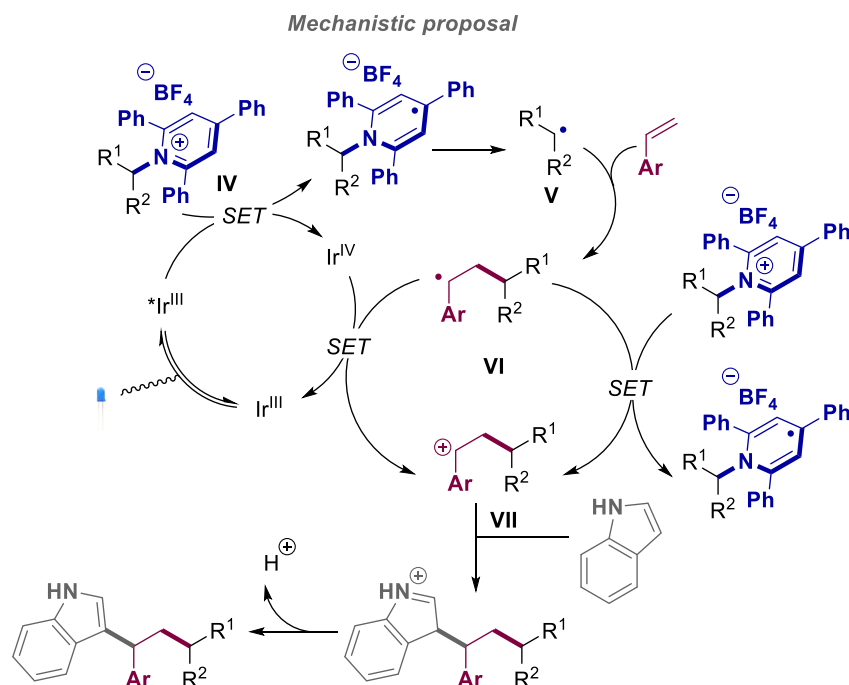
Dicarbonylation processes are well-established strategies in organic synthesis that employ abundant olefins to rapidly access complex architectures in one step.³⁹ Glorius and Lautens envisioned that the appropriate combination of an olefin, an arene and the alkyl radical generated by C(sp³)-N cleavage in pyridinium salts could engage an intermolecular three-component dicarbonylation. With this in mind, the authors developed an intriguing dicarbonylation of styrenes with *in situ* generated benzyl radicals (Scheme 3.2.6).⁴⁰ Unfortunately, the procedure was limited to benzyl amines.



Scheme 3.2.6. Deaminative dicarbonylation.

The authors proposed a mechanism based on a SET reduction of the Katritzky salt (**IV**), releasing the alkyl radical (**V**) which upon recombination with the styrene produces a new radical (**VI**) (Scheme

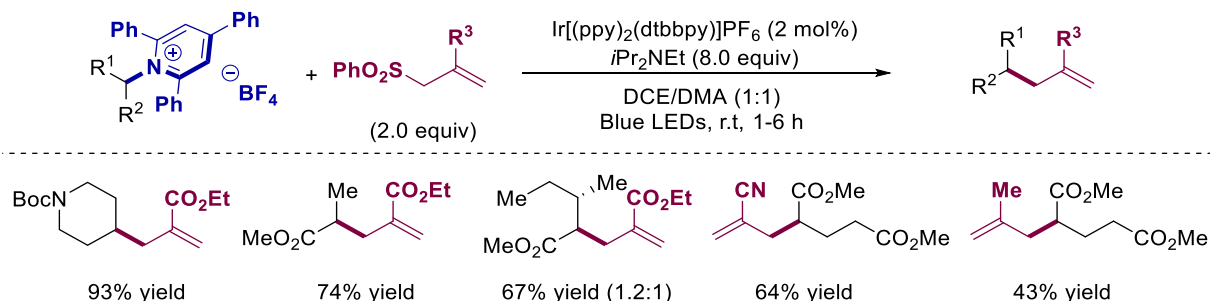
3.2.7). These species can reduce the oxidized photocatalyst or another molecule of pyridinium salt to maintain the chain reaction. The resulting cation (**VII**) is trapped by the nucleophilic attack of the arene to form the desired product.



Scheme 3.2.7. Mechanistic proposal of deaminative dicarbofunctionalization.

3.2.2.4 $C(sp^3)-C(sp^3)$ bond formation

Liu and co-workers reported a visible light-mediated protocol for the allylation of alkyl radicals generated by a reductive deaminative process of pyridinium salts (Scheme 3.2.8).⁴¹ Based on Glorius' discoveries about the formation of alkyl amine radicals promoted by a light-induced process, the authors combined an iridium photocatalyst and an organic base to promote the reaction between secondary alkyl amines and allylic sulfones.

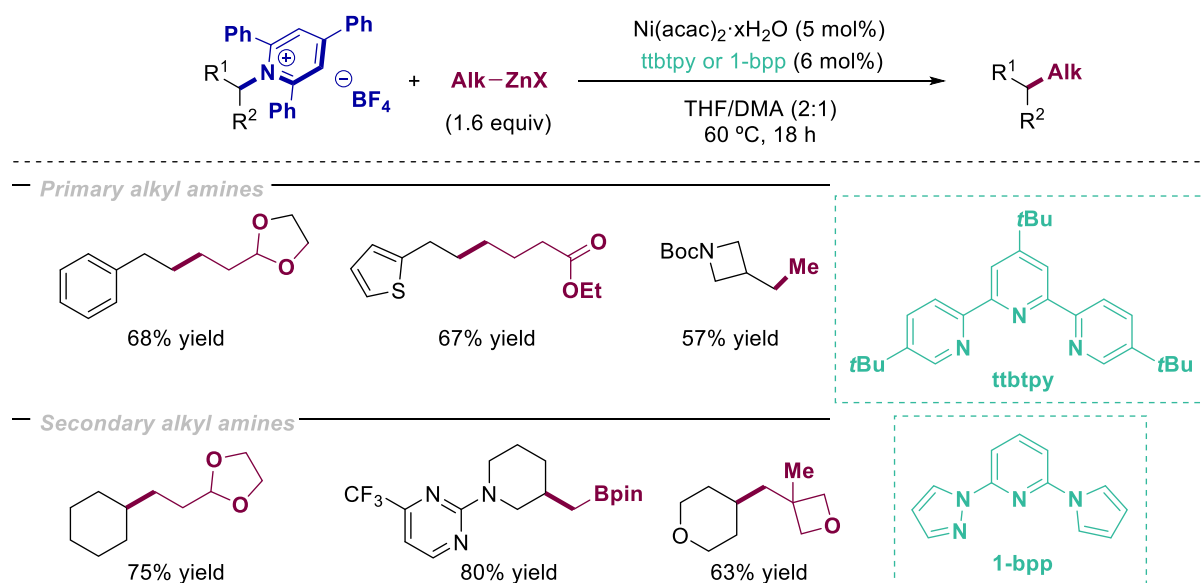


Scheme. 3.2.8. Deaminative visible-light-mediated allylation.

While the majority of the above-mentioned examples are based on the cross-coupling reaction of an *in situ* alkyl radical with an activated counterpart, Watson developed a deaminative $C(sp^3)-C(sp^3)$ cross-coupling catalyzed by nickel in 2019 within the context of a Negishi-type endeavour (Scheme 3.2.9).¹⁰ Interestingly, primary and secondary substituted alkyl amines behaved differently,

Chapter 3

and a different catalytic protocol had to be implemented for the successful coupling of these coupling partners. While primary alkyl amines were coupled by the utilization of tri(*tert*-butyl) terpyridine (ttbtpy) ligand, the utilization of secondary alkyl amines required 2,6-bis-(N-pyrazol)pyridine (1-bpp) ligand to deliver the targeted product in good yields. While tentative, the latter ligand is much smaller than the former, resulting in a better conformation to engage Ni(II) species with secondary alkyl radical intermediates.

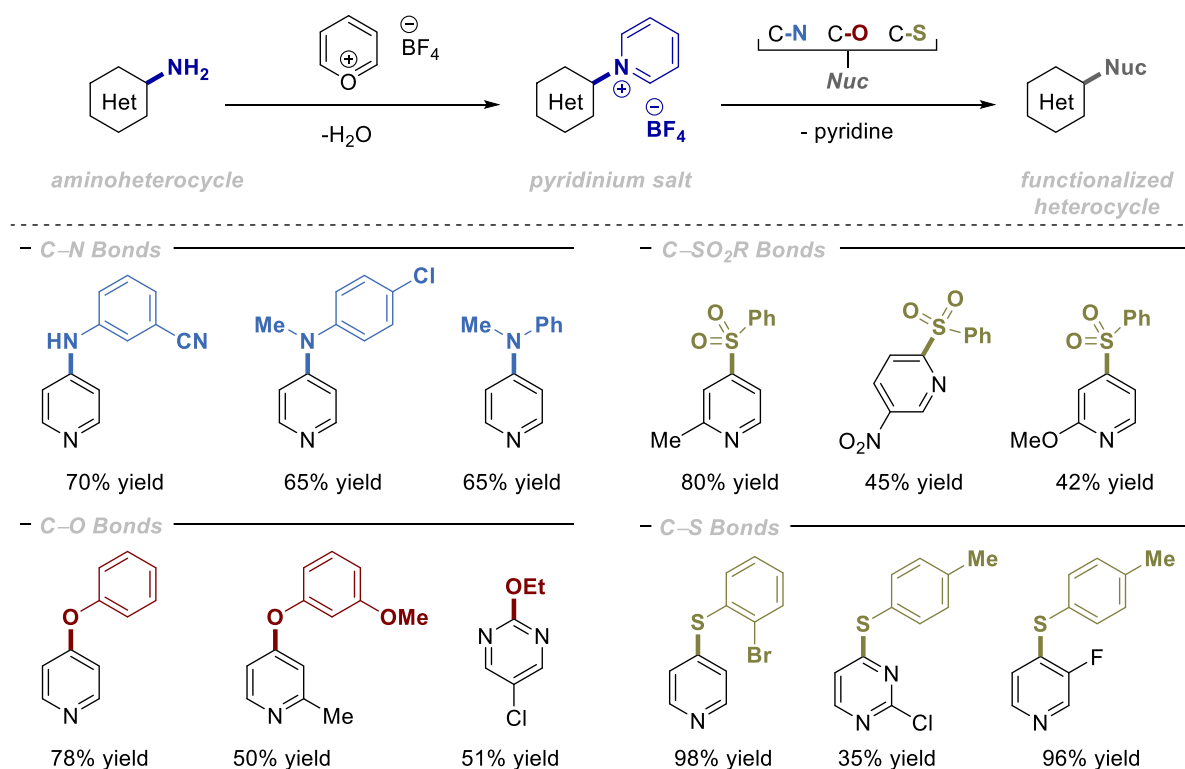


Scheme 3.2.9. Deaminative alkyl-alkyl cross-coupling reaction catalyzed by nickel.

3.2.3 C–Heteroatom bond formation

3.2.3.1 $\text{C}(\text{sp}^2)\text{--N}$, $\text{C}(\text{sp}^2)\text{--O}$, $\text{C}(\text{sp}^2)\text{--S}$ bond formation

In 2018, Cornella and co-workers reported a selective functionalization of aminoheterocycles bearing pyridinium salts, resulting in a *de novo* technique to forge C–Heteroatom skeletons (Scheme 3.2.10).⁴² While the low nucleophilicity of the NH_2 group in aminoheterocycles made the formation of the pyridinium salt problematic, the authors solved this limitation with the design of a pyrylium reagent capable to selectively activate the amino groups in heterocyclic motifs. Once the pyridinium salt was obtained, a subsequent nucleophilic attack was carried out forming different $\text{C}(\text{sp}^2)\text{--Heteroatom}$ bonds. Remarkably, Cornella and co-workers included more than 60 examples by forging a diverse set of C–N, C–O and C–S bonds with an excellent chemoselectivity profile.

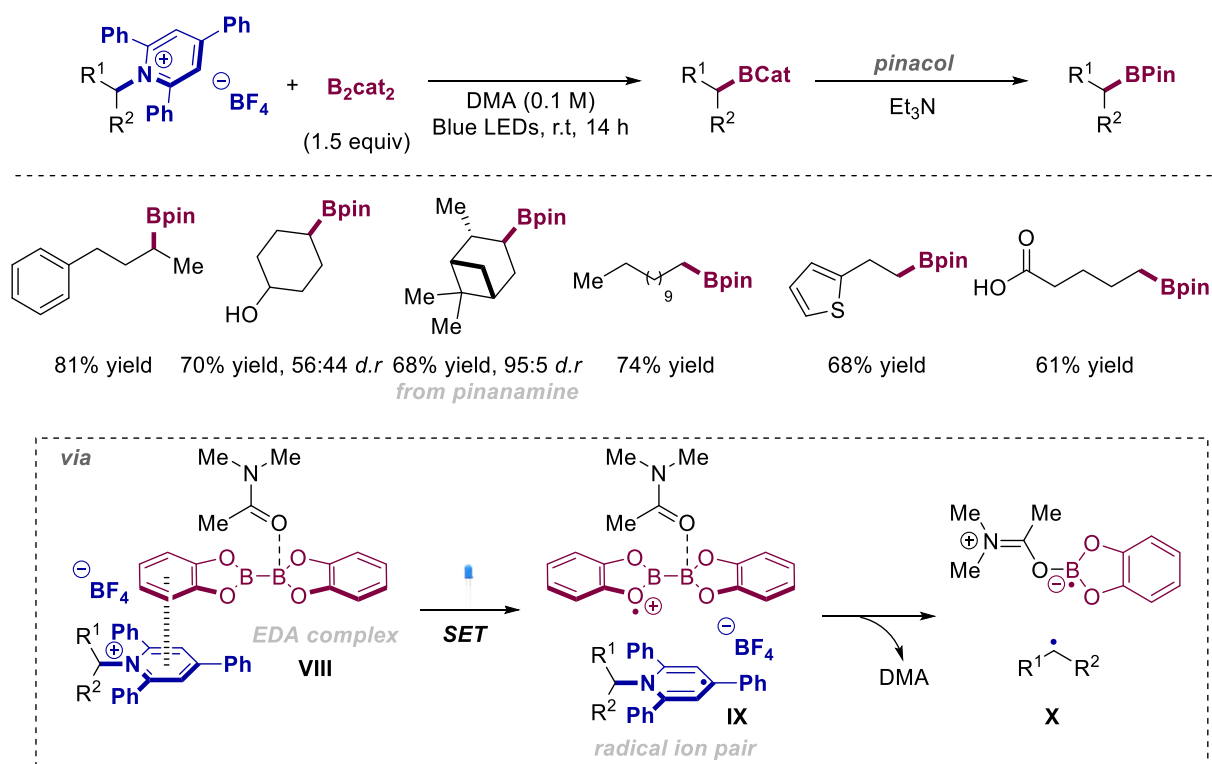


Scheme 3.2.10. Deaminative S_NAr mediated by Piry- BF_4 .

3.2.3.2 $C(sp^3)$ -B bond formation

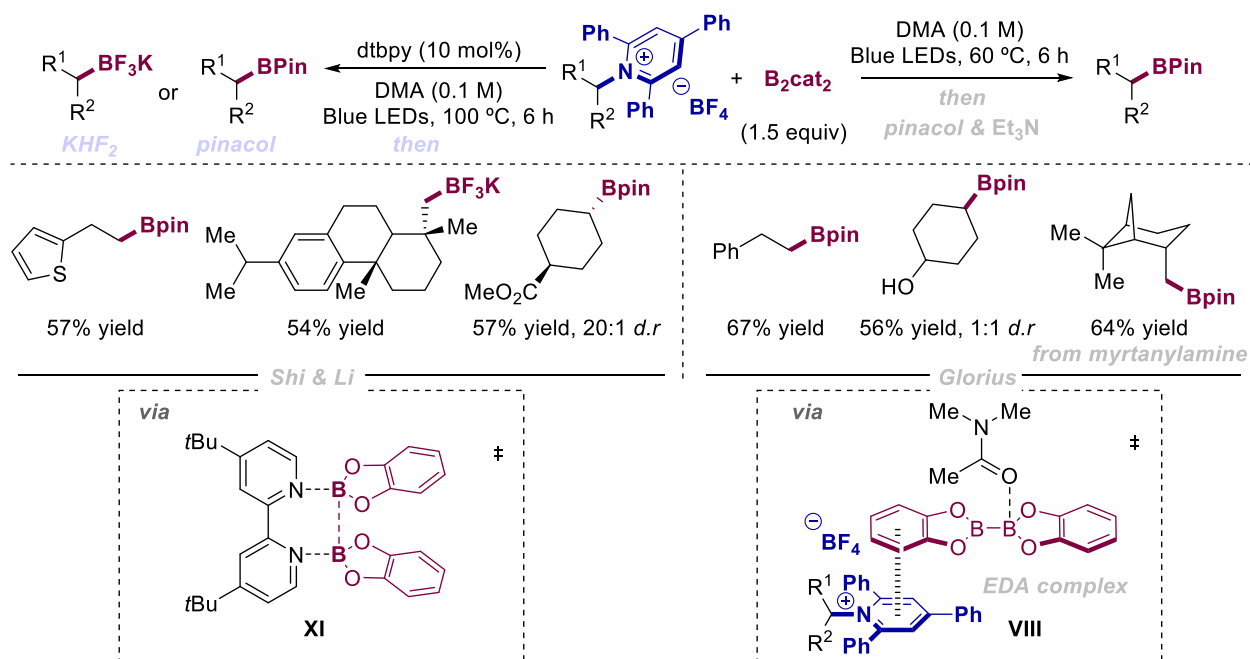
Aggarwal reported an interesting catalytic deaminative borylation of pyridinium salts without the need of photocatalyst *via* the *in situ* formation of alkyl radical intermediates generated by the intermediacy of electron-donor acceptor (EDA) complexes between the pyridinium salt and B_2cat_2 (Scheme 3.2.11).⁴³ The authors reported that this transformation could be applied to a wide number of primary and secondary unactivated alkylamines containing esters, free alcohols, amides, acids, cyclic and non-cyclic compounds, heteroarenes and sulfones. Moreover, they were able to obtain some natural product derivatives with moderate to good yields. From a mechanistic standpoint, the alkyl radical (**X**) generated by a photoinduced SET from the EDA complex (**VIII**) is trapped by B_2cat_2 , resulting in the targeted borylation product.

Chapter 3



Scheme 3.2.11. Photoinduced deaminative borylation of alkyl amines.

Subsequently, Shi and Glorius reported basically an identical deaminative borylation to that shown by Aggarwal for the borylative deaminative process (Scheme 3.2.12).^{44,45} Primary and secondary alkyl amines were perfectly tolerated, and the method could be applied to complex structures as well. Particularly, Shi showed that the corresponding catechol boronates can be transformed into the potassium trifluoroborate salts or to pinacol boronic esters, thus broadening the spectrum of the borylation products. While the strategy for activating B_2cat_2 in Glorius paper was the formation of an EDA complex (VIII), Shi proposed a Lewis acid activation pathway. The latter proposed that the dtbpy ligand facilitated the cleavage of the B_2cat_2 forming a Lewis acid adduct prior to the cleavage of the B–B bond (XI).



3.3 Ni-catalyzed Reductive Deaminative Arylation at sp^3 Carbon Centers

3.3.1 Aim of the project

Despite the advances realized in the general area of functionalization of $C(sp^3)-N$ bonds, the formation of $C(sp^3)-C(sp^2)$ bonds was accomplished *via* the utilization of organometallic species or biased heteroarenes as coupling partners (Scheme 3.2.1 & 3.2.3). Therefore, we recognized that the development of a new protocol that does not take recourse of neither organometallic reagents nor biased heteroarenes would be a worthwhile endeavour for chemical invention, particularly with easy-to-handle electrophilic counterparts, thus representing a valuable entry for enabling these methodologies within the context of late-stage functionalization of drug-type molecules (Figure 3.3.1).⁴⁶

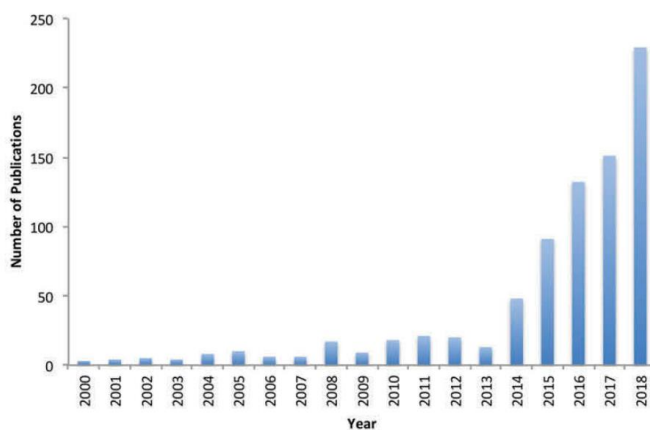


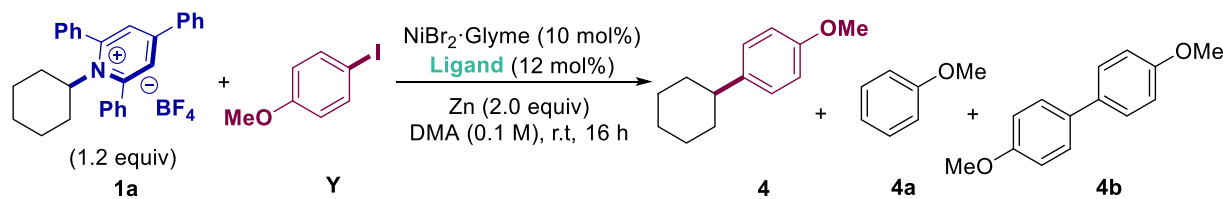
Figure 3.3.1. Publications including the concept of late-stage functionalization.

Chapter 3

3.3.2 Optimization of the reaction conditions

In view of the precedents highlighted above, we anticipated that the means to enable a catalytic deamination reaction of alkyl pyridinium salts with simple organic halides would be a particularly useful, yet practical, endeavour for building up sp^3 architectures. From a mechanistic standpoint, our strategy is based on a single electron transfer (SET) of a suitable reductant to an alkyl pyridinium salt, generating an alkyl radical that rapidly recombines with a Ni(II) oxidative addition complex generated by the reaction of an organic halide to Ni(0), allowing the formation of putative Ni(III) intermediates. The final product might be generated upon reductive elimination, and a final SET would recover back the propagating Ni(0) species within the catalytic cycle.

We began our investigations by reacting cyclohexyl pyridinium salt with *p*-methoxy iodobenzene with different Ni/ligand combinations and Zn as reducing agent in DMF (Table 3.3.1). As shown, non-negligible reactivity was observed for a different set of ligands, with better yields accomplished in the presence of electron-rich and less hindered backbones (entries **1-6**). In line with other catalytic reductive cross-coupling reactions,⁴⁷⁻⁴⁹ the utilization of phosphine ligands had a deleterious effect on reactivity (entries **7-9**). A close inspection into the crude mixtures revealed the formation of reduced arene (**4a**) and homocoupling side-reactions (**4b**). The former can be explained by the intermediacy of either aryl radicals formed upon homolytic cleavage of the putative oxidative addition Ni(II) species or organozinc intermediates arising from either Zn insertion into the sp^2 C-I bond or transmetalation pathways.⁵⁰ The formation of homocoupling products can be attributed to an initial ligand exchange between two oxidative addition complexes followed by reductive elimination.



Entry	Deviation from standard conditions	Conv. (%)	4 (%)	4a (%)	4b (%)
1	L1	99	28	43	9
2	L2	100	28	47	2
3	L3	98	24	50	7
4	L4	100	0	64	9
5	L5	96	14	47	10
6	L6	98	21	72	2
7	L7	84	0	35	11
8	L8	52	0	25	2
9	L9	46	0	10	0

Reaction conditions: **1a** (0.12 mmol), **Y** (0.1 mmol), $\text{NiBr}_2 \cdot \text{Glyme}$ (10 mol%), Ligand (12 mol%), Zn (2.0 equiv), DMA (1.0 mL), 25 °C, 16 h. GC conversion and yields using decane as internal standard.

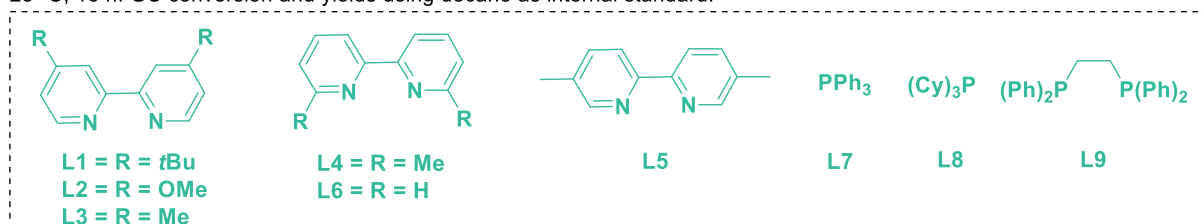
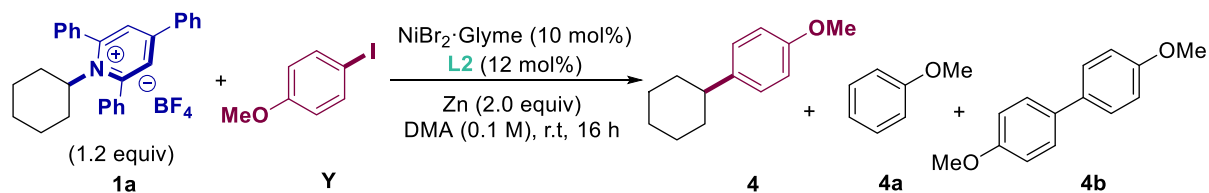


Table 3.3.1. Screening of ligands.

With these results in hand, we next focused our attention on the influence of several nickel sources and the nature of the reducing agent (Table 3.3.2). Although the yield was boosted into the 30% range when using $\text{NiCl}_2 \cdot \text{Glyme}$ and $\text{NiBr}_2 \cdot 3\text{H}_2\text{O}$ (entries **2** and **3**), substantial amounts of reduced byproducts were observed in these cases (**4a**). Importantly, the utilization of Mn as reducing agent allowed to improve the yields even further without observing even traces of **4a**, but with non-negligible amounts of **4b**. While tentative, these results suggest that a higher redox potential is beneficial for the reaction to occur ($E^0 [\text{Mn}^{\text{II}}/\text{Mn}^0] = -1.4 \text{ V vs Ag/AgCl}$) vs ($E^0 [\text{Zn}^{\text{II}}/\text{Zn}^0] = -0.96 \text{ V vs Ag/AgCl}$); a conversion factor of -0.2 V was used to convert the value from that vs normal hydrogen electrode (NHE) to Ag/AgCl reference electrode.⁵¹

Chapter 3

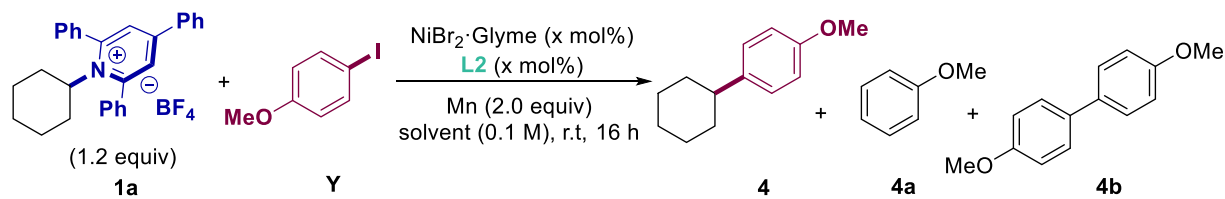


Entry	Deviation from standard conditions	Conv. (%)	4 (%)	4a (%)	4b (%)
1	Ni(COD) ₂	100	22	74	0
2	NiCl ₂ ·Glyme	100	34	60	4
3	NiBr ₂ ·3H ₂ O	100	38	58	2
4	NiCl ₂ ·6H ₂ O	100	24	70	4
5	NiBr ₂	100	23	71	3
6	Ni(II)ClO ₄ ·6H ₂ O	100	28	69	3
7	Ni(acac) ₂	0	0	0	0
8	L1 and Mn (2.0 equiv)	100	47	0	16
9	L2 and Mn (2.0 equiv)	100	50	0	16

Reaction conditions: **1a** (0.12 mmol), **Y** (0.1 mmol), NiBr₂·Glyme (10 mol%), L2 (12 mol%), Zn (2.0 equiv), DMA (1.0 mL), 25 °C, 16 h. GC conversion and yields using decane as internal standard.

Table 3.3.2. Screening of nickel catalysts and reducing agent.

Putting all these results into perspective, we concluded that the best results were accomplished with a regime based on NiBr₂·Glyme and **L2**. The next target was to explore the ratio between Ni/Ligand and the influence of different polar solvents on the reaction rate (Table 3.3.3). As shown, the utilization of NMP improved the yield (entries **6** and **8**), moreover when utilizing 6 mol% of NiBr₂·Glyme and 10 mol% of **L2** (entry **9**), the yield of **4** was increased to 76%.



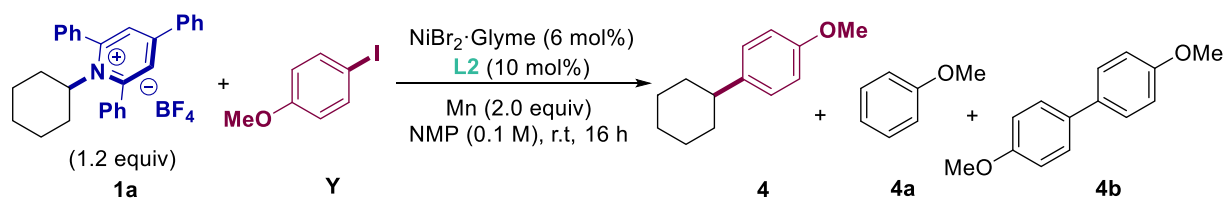
Entry	Deviation from standard conditions	Conv. (%)	4 (%)	4a (%)	4b (%)
1	Ni (5 mol%), L2 (20 mol%), DMA (0.1M)	0	0	0	0
2	Ni (5 mol%), L2 (10 mol%), DMA (0.1M)	88	43	3	13
3	Ni (5 mol%), L2 (10 mol%), DME (0.1M)	100	26	0	19
4	Ni (5 mol%), L2 (10 mol%), DMA/DME (0.1M)	100	54	0	15
5	Ni (5 mol%), L2 (10 mol%), DMF (0.1M)	38	0	0	0
6	Ni (5 mol%), L2 (10 mol%), DMA/NMP (0.1M)	100	63	0	10
7	Ni (5 mol%), L2 (10 mol%), DMA (0.06M)	100	63	0	10
8	Ni (5 mol%), L2 (10 mol%), NMP (0.1M)	100	70	0	7
9	Ni (6 mol%), L2 (10 mol%), NMP (0.1M)	100	76	0	8

Reaction conditions: **1a** (0.12 mmol), **Y** (0.1 mmol), $\text{NiBr}_2 \cdot \text{Glyme}$ ($x \text{ mol\%}$), **L2** ($x \text{ mol\%}$), Mn (2.0 equiv), solvent (1.0 mL), 25 °C, 16 h. GC conversion and yields using decane as internal standard.

Table 3.3.3. Nickel/ligand ratio screening & solvent.

Despite the good results accomplished, we decided to revisit the influence of other ligands. In line with our expectations, bipyridines and phenanthrolines possessing electron-rich and non-hindered *ortho*-substituents provided the best yields (entries **2-13**). Unfortunately, none of the ligands analyzed afforded better yields than **L2**. Only DMA (entry **15**) was comparable to NMP, thus highlighting the critical influence of polar aprotic solvents on the reaction outcome. Notably, lower amounts of Mn gave rise to **4** in slightly better yields (entries **17 & 18**).

Chapter 3



Entry	Deviation from standard conditions	Conv. (%)	4 (%)	4a (%)	4b (%)
1	None	100	75	0	8
2	L1	100	64	0	11
3	L3	35	30	0	2
4	L4	14	13	0	3
5	L5	100	14	37	15
6	L6	89	38	0	10
7	L7	100	11	13	22
8	L8	13	4	7	0
9	L9	100	20	4	20
10	L10	100	48	0	16
11	L11	100	59	0	16
12	L12	100	58	0	16
13	L13	39	18	12	3
14	DMF	13	11	3	0
15	DMA	79	67	0	6
16	DMSO	20	0	0	0
17	Mn (2.5 equiv)	100	58	0	14
18	Mn (1.5 equiv)	100	86	0	5

Reaction conditions: **1a** (0.12 mmol), **Y** (0.1 mmol), $\text{NiBr}_2 \cdot \text{Glyme}$ (6 mol%), **L2** (10 mol%), Mn (2.0 equiv), solvent (1.0 mL), 25 °C, 16 h. GC conversion and yields using decane as internal standard.

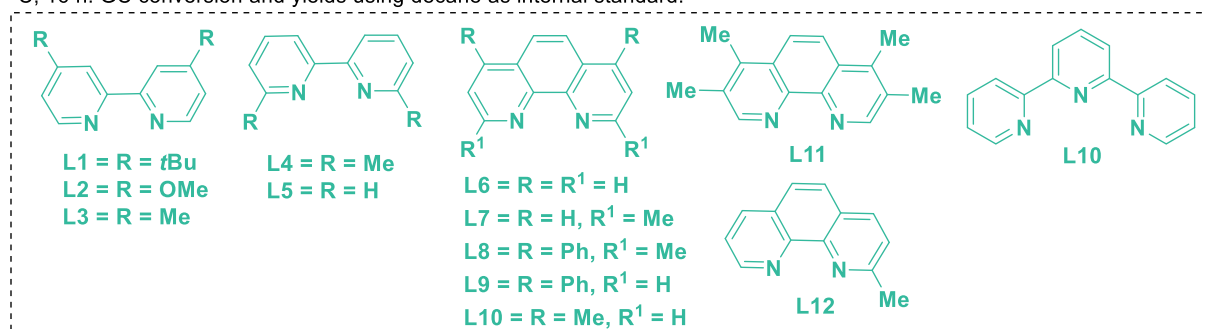
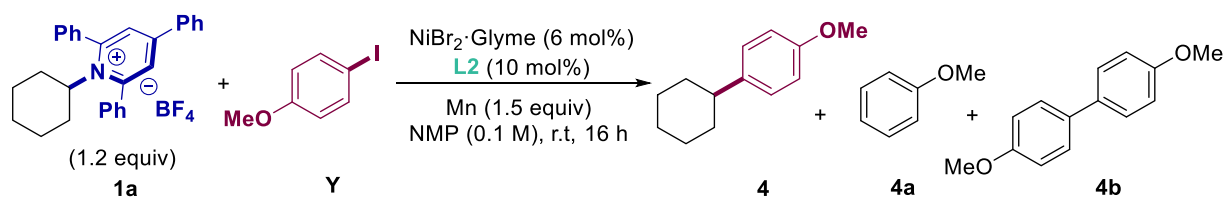


Table 3.3.4. Ligand, solvent and reducing agent screening.

Although we experienced reproducibility issues, these could be alleviated by the utilization of stock solutions of Ni/**L2** in NMP, resulting in excellent levels of reactivity while minimizing the side-reactions *en route* to both **4a** and **4b** (Table 3.3.5, entries **3** and **4**).

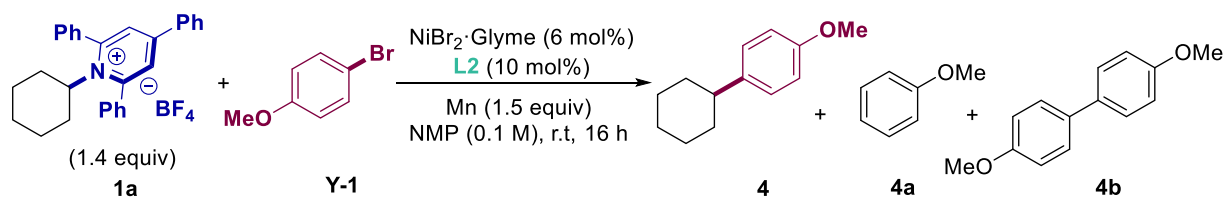


Entry	Deviation from standard conditions	Conv. (%)	4 (%)	4a (%)	4b (%)
1	no stock solution	100	61	0	12
2	no stock solution	100	72	0	8
3	stock solution	100	95	0	2
4	stock solution	100	94	0	2
5	stock solution with L1	100	89	0	2
6	stock solution with L1	100	90	0	3

Reaction conditions: **1a** (0.12 mmol), **Y** (0.1 mmol), NiBr₂·Glyme (6 mol%), L2 (10 mol%), Mn (1.5 equiv), NMP (1.0 mL), 25 °C, 16 h. GC conversion and yields using decane as internal standard.

Table 3.3.5. Stock solutions table.

Although we managed to optimize the targeted catalytic deaminative cross-coupling of alkyl pyridinium salts, our conditions required the utilization of rather expensive and non-particularly available aryl iodides. To this end, we wondered whether our conditions could be applied to the coupling of aryl bromides (Table 3.3.6). Unfortunately, low yields were obtained upon exposure of aryl bromide to the optimized conditions shown for aryl iodides (entry **1**). Interestingly, decent yields were obtained with 14 mol% **L2** (entry **5**), whereas lower results were obtained with lower or higher amounts of ligand (entries **4** and **6**).



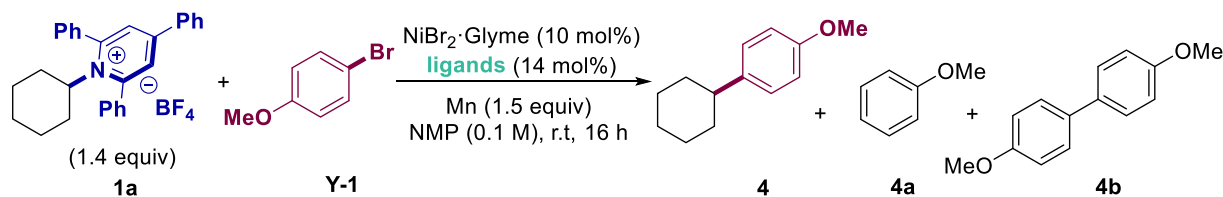
Entry	Deviation from standard conditions	Conv. (%)	4 (%)	4a (%)	4b (%)
1	1a (1.2 equiv)	28	6	6	6
2	none	36	12	3	5
3	Ni (8 mol%)/ L2 (12 mol%)	59	41	2	8
4	Ni (10 mol%)/ L2 (12 mol%)	79	40	4	7
5	Ni (10 mol%)/ L2 (14 mol%)	79	49	0	10
6	Ni (10 mol%)/ L2 (18 mol%)	25	17	0	1

Reaction conditions: **1a** (0.12 mmol), **Y-1** (0.1 mmol), NiBr₂·Glyme (6 mol%), L2 (10 mol%), Mn (1.5 equiv), NMP (1.0 mL), 25 °C, 16 h. GC conversion and yields using decane as internal standard.

Table 3.3.6. Nickel and ligand loading amount screening with aryl bromides.

Chapter 3

The low yielding achieved for aryl bromides might be due to the following: (a) the significantly higher BDE required for cleaving the C₆H₅-Br bond (80 ± 2 kcal/mol) vs the C₆H₅-I linkage (65 ± 2 kcal/mol),⁵² making oxidative addition particularly slow for aryl bromides, and (b) the utilization of particularly electron-rich aryl bromides possessing a *p*-methoxy unit makes oxidative addition, recombination events with electron-rich alkyl radicals and reductive elimination particularly uphill. Therefore, we decided to screen additional parameters for boosting the reactivity of aryl bromides. Unfortunately, none of the ligands analyzed afforded better yields than **L2** (Table 3.3.7).



Entry	Deviation from standard conditions	Conv. (%)	4 (%)	4a (%)	4b (%)
1	L2	88	51	0	10
2	L1	100	46	12	7
3	L3	100	48	15	6
4	L4	76	6	5	5
5	L5	83	5	59	2
6	L6	16	1	14	0
7	L7	77	45	0	6
8	L8	77	2	59	2
9	L9	71	39	0	4
10	L10	81	0	56	1
11	L11	52	9	8	3
12	L12	31	14	0	0
13	PPh ₃	23	7	9	5
14	PCy ₃	20	13	0	0
15	dcype	13	3	0	0

Reaction conditions: **1a** (0.14 mmol), **Y-1** (0.1 mmol), NiBr₂·Glyme (10 mol%), ligands (14 mol%), Mn (1.5 equiv), NMP (1.0 mL), 25 °C, 16 h. GC conversion and yields using decane as internal standard.

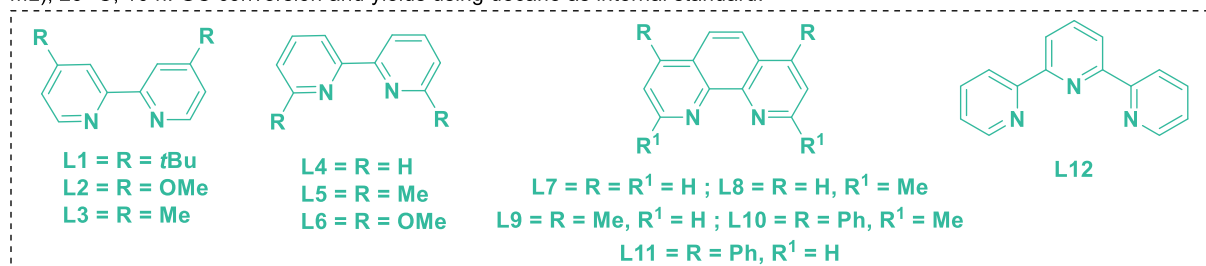
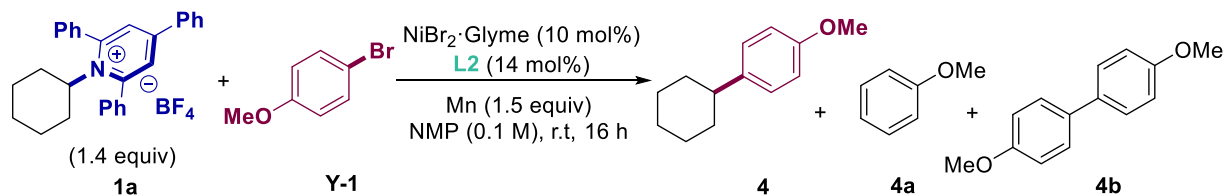


Table 3.3.7. Screening of ligands using aryl bromide.

We further investigated the nickel source effect however, as shown in Table 3.3.8, none of the entries provided better results than NiBr₂·Glyme (entries 1-6). Although replacing NMP by DMA (entry 7) afforded similar results, it is worth noting that the amount of homocoupling increased significantly in this case. Unfortunately, the reaction did not work when utilizing DMF likely to solubility issues (entry 8).



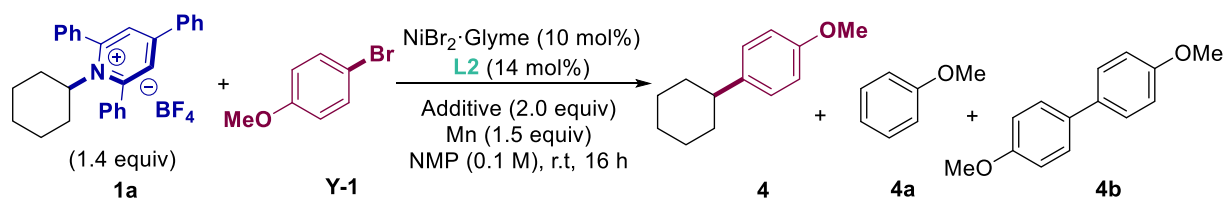
Entry	Deviation from standard conditions	Conv. (%)	4 (%)	4a (%)	4b (%)
1	NiCl ₂ ·6H ₂ O	24	5	0	0
2	NiBr ₂ ·3H ₂ O	99	42	0	10
3	NiI ₂	57	17	0	5
4	Ni(acac) ₂	0	0	0	0
5	NiCl ₂ ·Glyme	100	25	0	17
6	Ni(COD) ₂	86	10	0	18
7	DMA	80	46	0	13
8	DMF	5	0	0	0

Reaction conditions: **1a** (0.14 mmol), **Y-1** (0.1 mmol), NiBr₂·Glyme (10 mol%), L2 (14 mol%), Mn (1.5 equiv), solvent (1.0 mL), 25 °C, 16 h. GC conversion and yields using decane as internal standard.

Table 3.3.8. Nickel sources and solvent screening.

In light of these results, we hypothesized that the inclusion of iodide additives might form *in situ* oxidative addition species bearing an iodide anion *via* halide exchange, thus boosting the yield of the targeted product. As shown in Table 3.3.9, this turned out to be the case. In addition, the escorting cation had a non-negligible influence on the reaction (entries 2-7), with NaI providing the best results *en route* to **4**.

Chapter 3

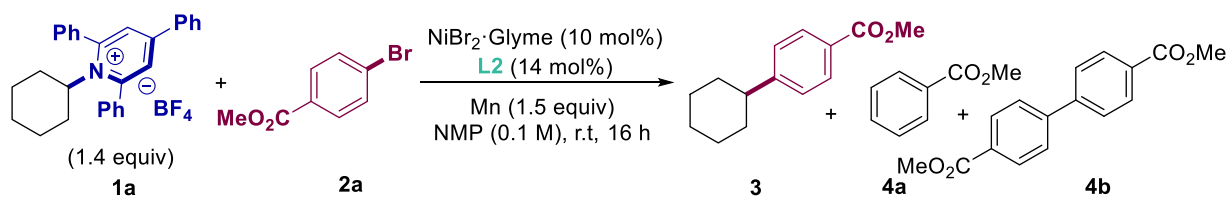


Entry	Deviation from standard conditions	Conv. (%)	4 (%)	4a (%)	4b (%)
1	none	59	41	2	8
2	KI	83	55	7	9
3	NaI	100	77	9	9
4	MgI ₂	92	44	0	11
5	ZnI ₂	74	41	2	0
6	CsI	75	57	7	9
7	Lil	88	61	9	10
8	(Bu) ₄ NI	90	58	8	6
9	Me ₄ NI	74	50	6	8
10	Et ₄ NI	78	55	5	8
11	EtMe ₃ NI	88	57	10	8
12	PhMe ₃ NI	92	66	7	6
13	Pr ₄ NI	67	65	8	9
14	(hep) ₄ NI	90	65	7	8
15	Ph ₄ NI	81	57	6	7

Reaction conditions: **1a** (0.14 mmol), **Y-1** (0.1 mmol), NiBr₂·Glyme (10 mol%), L2 (14 mol%), Additive (2.0 equiv), Mn (1.5 equiv), NMP (1.0 mL), 25 °C, 16 h. GC conversion and yields using decane as internal standard.

Table 3.3.9. Screening of iodide salts as additives.

Notably, the application of our optimized conditions to electron-poor aryl bromides resulted in nearly quantitative yields of **3** (Table 3.3.10, entry 1). Entry 2 shows that DMA could also be a valuable solvent for the reaction whereas the reduction of the nickel/ligand loading was detrimental for the reaction to occur (entry 3).

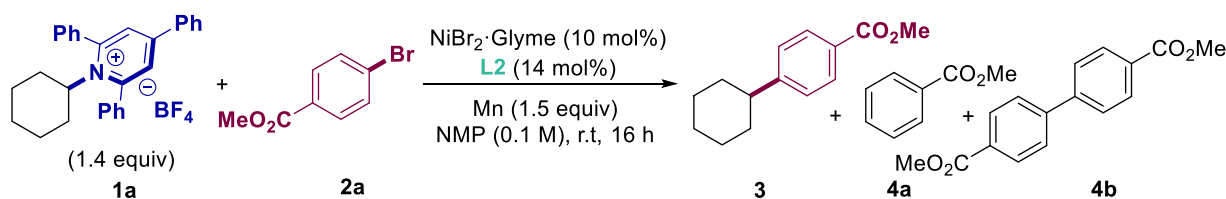


Entry	Deviation from standard conditions	Conv. (%)	3 (%)	4a (%)	4b (%)
1	none	100	98	0	0
2	DMA	100	96	0	0
3	Ni (6 mol%)/ L2 (10 mol%)	80	57	0	9

Reaction conditions: **1a** (0.14 mmol), **2a** (0.1 mmol), $\text{NiBr}_2 \cdot \text{Glyme}$ (10 mol%), **L2** (14 mol%), Mn (1.5 equiv), solvent (1.0 mL), 25 °C, 16 h. GC conversion and yields using decane as internal standard.

Table 3.3.10. Substrate changing; electron-poor substrate.

Finally, we decided to look at the influence of the metal reductant (Table 3.3.11). However, significantly lower results were accomplished in this case, probably due to the lower redox potential of Zn when compared to Mn (entry **2**). As expected, the utilization of aryl iodides provided access to **3** in comparable yields whereas an aryl chloride resulted in negligible conversion to products (entries **3** and **4**). Finally, control reactions under air or in absence of either Mn or Ni/**L2** resulted in traces, if any, of the corresponding cross-coupling product (entries **5** and **6**).



Entry	Deviation from standard conditions	Conv. (%)	3 (%)	4a (%)	4b (%)
1	none	100	98 (90) ^a	0	0
2	Zn (1.5 equiv)	27	12	5	3
3	using Ar-I	100	98	0	0
4	using Ar-Cl	5	2	0	0
5	under air	4	1	0	0
6	no Mn or no Ni/ L2	0	0	0	0

Reaction conditions: **1a** (0.14 mmol), **2a** (0.1 mmol), $\text{NiBr}_2 \cdot \text{Glyme}$ (10 mol%), **L2** (14 mol%), Mn (1.5 equiv), NMP (1.0 mL), 25 °C, 16 h. GC conversion and yields using decane as internal standard. ^aIsolated yield

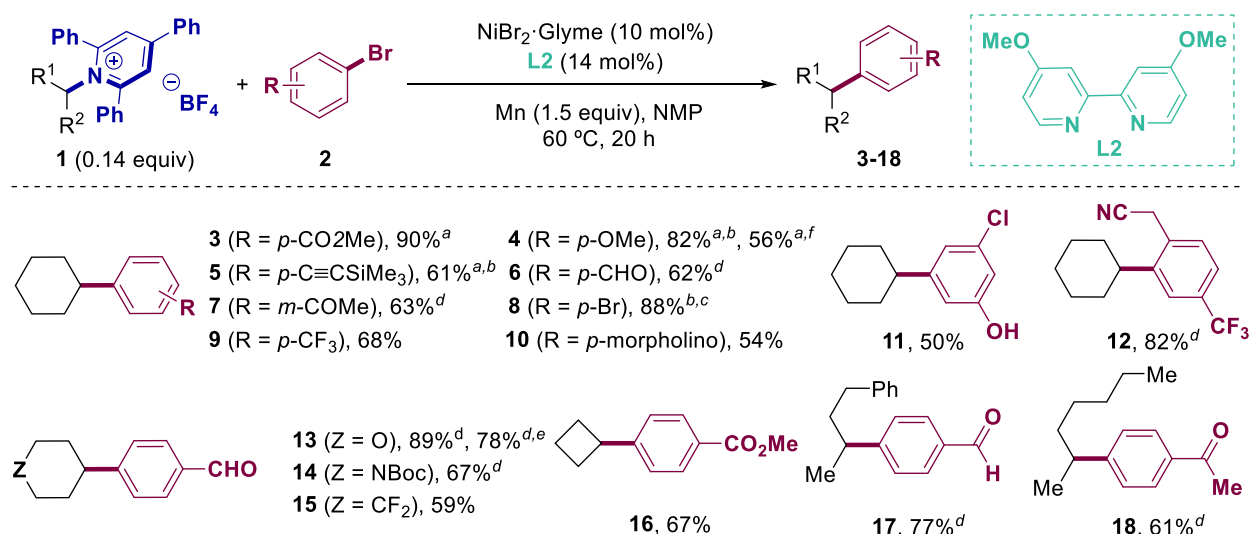
Table 3.3.11. Aryl halides and control screening.

3.3.3 Substrate scope

Encouraged by these results, we turned our attention to explore the generality of our reductive deamination methodology. To our surprise, we had to do initial readjustments in the set of conditions when we explored less activated aryl bromides. The lack of reactivity found in these substrates was

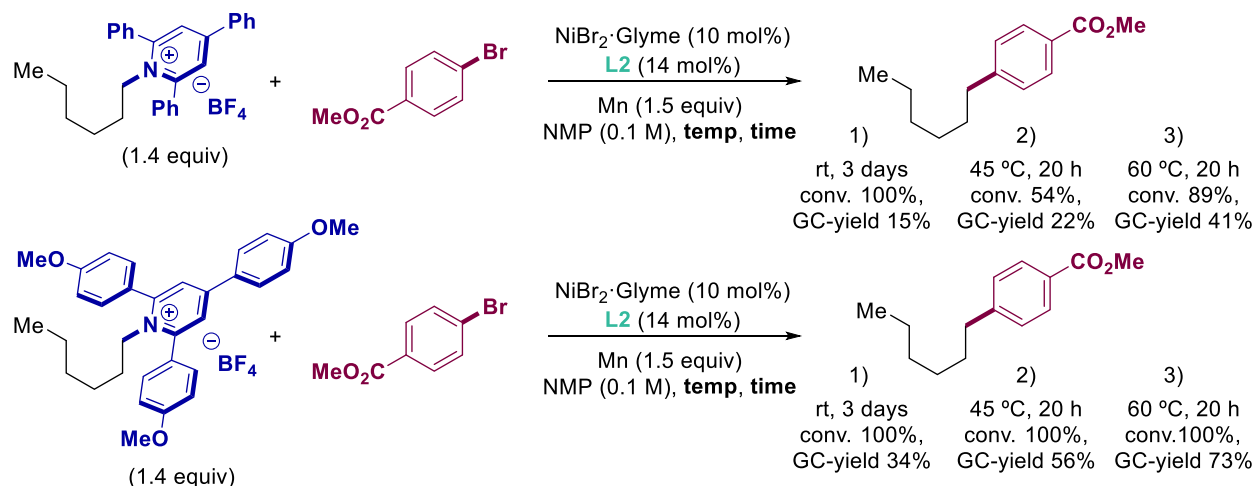
Chapter 3

compensated by conducting the reaction at 60 °C and stirred for 20 h. As shown in Scheme 3.3.1, we were able to accommodate arenes bearing esters (**3** & **16**), aldehydes (**6**, **13**, **14**, **15**, **17**), ketones (**7** & **18**), free alcohols (**11**), halides (**8** & **11**) and nitrile groups (**12**). The tolerance of our protocol with aldehydic counterparts is particularly important, as related approaches aimed at the same goal make use of organometallic reagents that would undergo a nucleophilic attack into the carbonyl moiety. Due to the lower reactivity of electron-rich aryl bromides, aryl iodides were used (**4** and **5**). In addition, we could trigger the reaction of an aryl iodide possessing a pending bromide at *para* position, providing a handle for further functionalization *via* cross-coupling reactions (**8**).



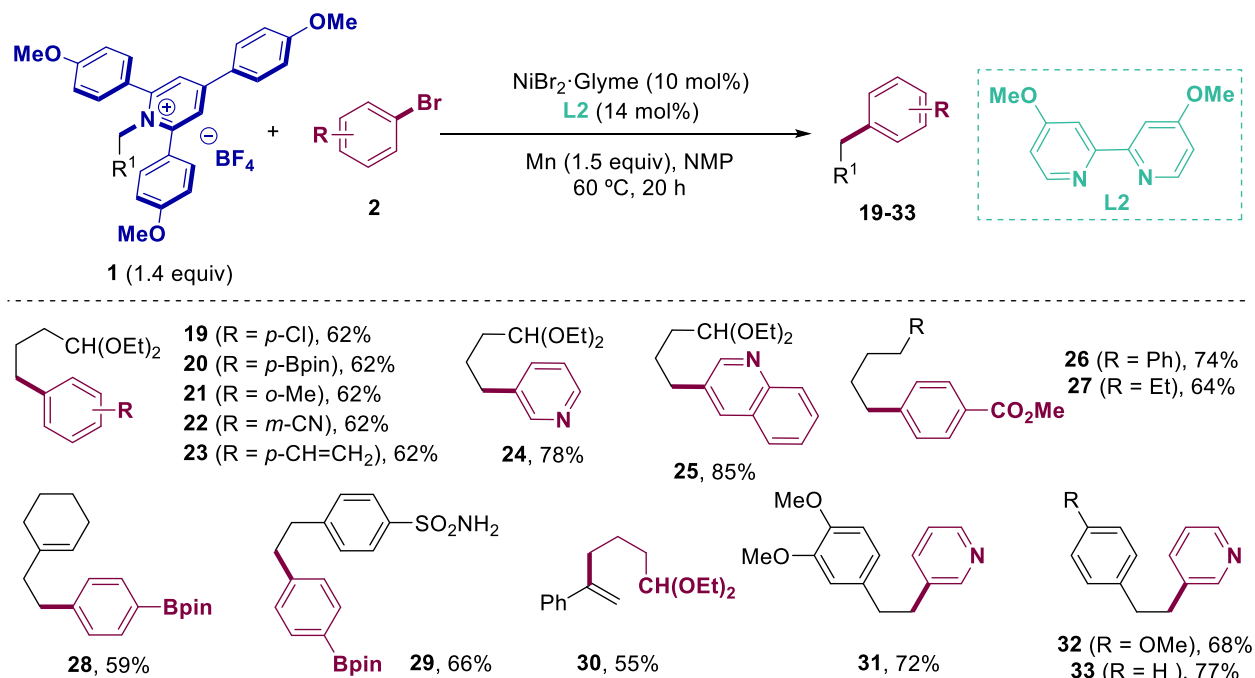
Scheme 3.3.1. Scope of unactivated secondary alkyl amines.

Next, we turned our attention to study the influence of the alkyl amine on the reaction. Cyclic substrates such as cyclobutane (**16**), cyclohexane (**3-15**) and acyclic alkyl amines (**17** & **18**) could be coupled without any problems. The ability to couple the latter is particularly important, as acyclic alkyl counterparts are commonly plagued by parasitic β -hydride elimination or homodimerization pathways. Importantly, this was not the case, and not even traces of alkene side-products were identified in the crude mixtures. Importantly for a synthetic and practical point of view, a gram scale reaction was performed giving rise to **13** in 78% isolated yield. Next, we turned our attention to study the reaction of unactivated primary amines that are particularly more difficult to employ due to their inherent reluctance to generate primary alkyl radicals *via* SET as compared to their secondary alkyl congeners. Indeed, lower yields were found for all primary alkyl pyridiniums tested (Scheme 3.3.2). To solve this problem, we hypothesized that the inclusion of electron-rich arenes at the pyridinium backbone would facilitate C–N scission albeit higher redox potentials to trigger the SET would be needed. As shown in Scheme 3.3.2, this was indeed the case. Notably, a subtle change in the reaction conditions allowed for triggering the reaction of primary alkyl pyridinium salts by adjusting the temperature of the reaction.



Scheme 3.3.2. Testing primary alkyl pyridinium salts.

With these results in hand, we then focused our attention to study the scope of the unactivated primary alkyl amines (Scheme 3.3.3). As shown, we were able to conduct the targeted cross-coupling reaction in the presence of esters (**26**), nitriles (**22**), alkenes (**23** & **28**), acetals (**19-25**, **30**), sulfonamides (**29**) and nitrogen containing heterocycles (**24**, **25**, **31-33**). This method could be even extended to vinyl bromides, albeit in lower yields (**30**). As for secondary alkyl pyridinium salts, the reaction could be applied to aryl bromides bearing organoboron groups (**20**, **28**, **29**) or aryl halides (**19**), thus opening a gateway to further functionalization *via* classical cross-coupling reactions.



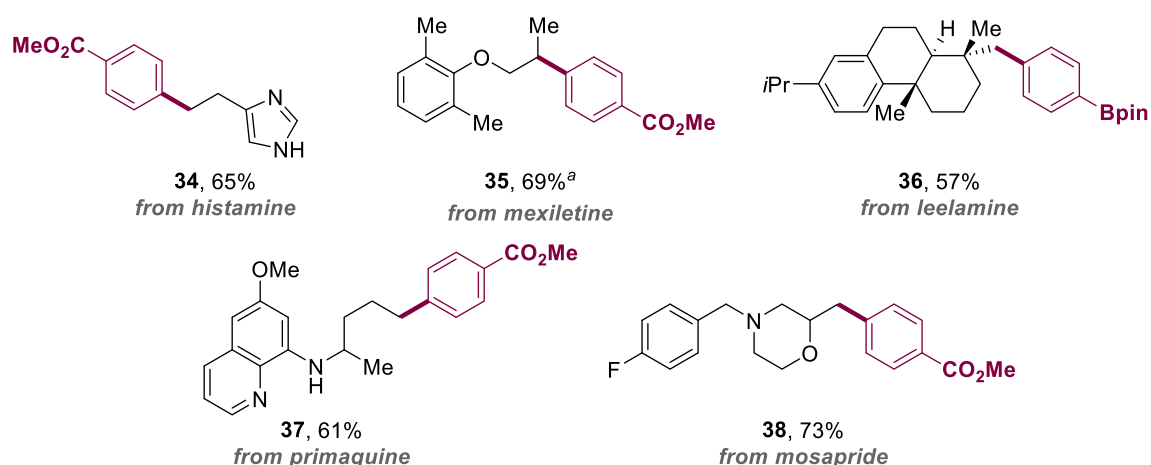
Reaction conditions: **1i-q** (0.28 mmol), aryl halide (0.2 mmol), NiBr₂·Glyme (10 mol%), L2 (14 mol%), Mn (1.5 equiv), NMP (0.1 M), 60 °C, 20 h. Isolated yields, average of two runs.

Scheme 3.3.3. Scope of unactivated primary alkyl amines.

Chapter 3

3.3.4 Late-Stage Functionalization

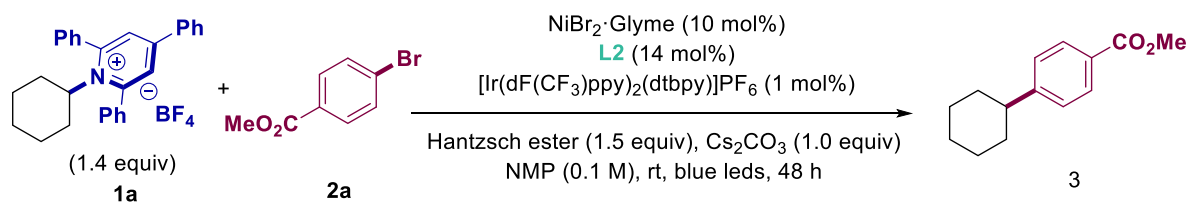
Prompted by our initial results, we then turned our attention to implement our deaminative cross-coupling protocol in advanced synthetic intermediates (Scheme 3.3.4). Indeed, a variety of biologically active compounds containing amine groups such as histamine, mexiletine, leelamine, primaquine, or mosapride could all be accommodated in our deaminative cross-electrophile coupling with aryl halides (**34–38**). Particularly interesting is the ability to tolerate the presence of an imidazole, ether, fused-rings, quinoline, free N–H bonds or aryl halides.



Reaction conditions: pyridinium salt (0.28 mmol), aryl halide (0.2 mmol), NiBr₂·Glyme (10 mol), L2 (14 mol%), Mn (1.5 equiv), NMP (0.1 M), 60 °C, 48 h. Isolated yields, average of two runs. ^aUsing ArI.

Scheme 3.3.4. Late-stage functionalization of alkyl amines.

Aimed at extending the versatility and practicality of our protocol, we hypothesized that we could trigger a non-invasive outer sphere SET mediated by a photocatalyst instead of using stoichiometric amounts of metal reductants (Table 3.3.12). Consequently, we tested a diverse set of iridium/ruthenium photocatalysts and organophotocatalysts (entries **2–8**), with the best results accomplished using [Ir(dF(CF₃)ppy)₂(dtbpy)]PF₆ and 4-CzIPN. The origin behind these results can be ascribed to the redox potential of the photocatalysts ($E_{1/2}$ [Ir^{III}*/Ir^{II}] = -1.33 V vs Ag/AgCl) ($E_{1/2}$ [P/P^{•-}] = -1.17 V vs Ag/AgCl) respectively, as these are capable of reducing either primary ($E_{1/2}$ = -0.74 vs Ag/AgCl) or secondary alkyl pyridinium salts ($E_{1/2}$ = ≈0.90 vs Ag/AgCl). It was found that Hantzsch esters performed better than other organic amines as sacrificial reducing agent (entry **11**) in combination with Cs₂CO₃ (entries **9** & **10**). Surprisingly, moderate yield was observed when performing the reaction without base, indicating that the pyridine generated might act as a base (entry **12**). As expected, no product was observed in the absence of light (entries **12–13**).

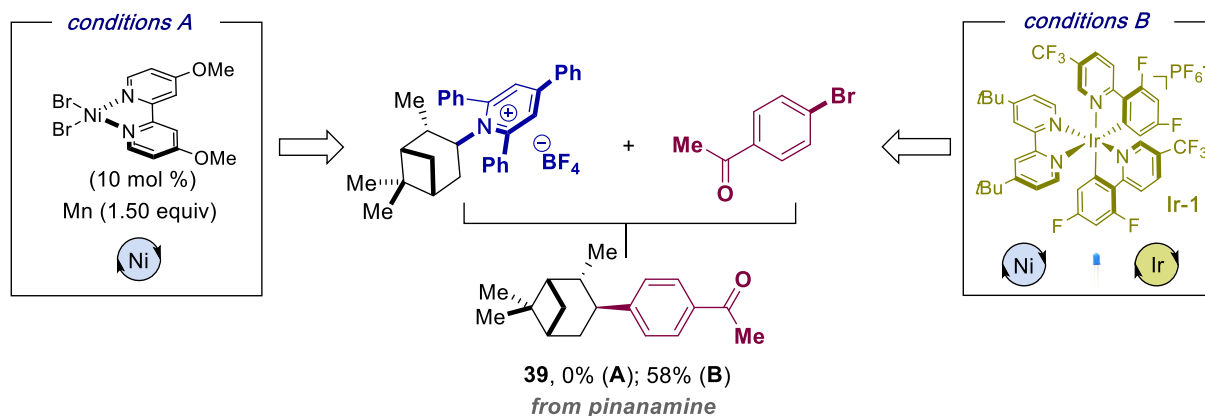


Entry	Deviation from standard conditions	Conversion of 1a (%)	3 (%)
1	None	100	95 (88) ^a
2	2 equivalents of Hantzsch ester	85	70
3	[Ru(bpy) ₃]Cl ₂ and 2 equiv. of Hantzsch ester	11	3
4	4-CzIPN and 2 equiv. of Hantzsch ester	100	75
5	MesAcrClO ₄ and 2 equiv. of Hantzsch ester	20	4
6	[Ir(ppy) ₂ (dtbbpy)]PF ₆ and 2 equiv. of Hantzsch ester	100	74
7	[Ir(dF(CF ₃)ppy) ₂ (ppy)]PF ₆ and 2 equiv. of Hantzsch ester	100	69
8	[Ir(ppy) ₃] and 2 equiv. of Hantzsch ester	51	32
9	K ₂ CO ₃ instead of Cs ₂ CO ₃	83	17
10	Rb ₂ CO ₃ instead of Cs ₂ CO ₃	4	0
11	DIPEA instead of Hantzsch ester	44	19
12	No base	100	39
13	No light	3	0

Reaction conditions: **1a** (0.14 mmol), **2a** (0.1 mmol), NiBr₂·Glyme (10 mol%), L2 (14 mol%), [Ir(dF(CF₃)ppy)₂(dtbbpy)]PF₆ (1 mol%), Hantzsch ester (1.5 equiv), NMP (1.0 mL), 25 °C, 48 h, blue LEDs. GC conversion and yields using decane as internal standard. ^aIsolated yield.

Table 3.3.12. Optimization of the photocatalytic conditions.

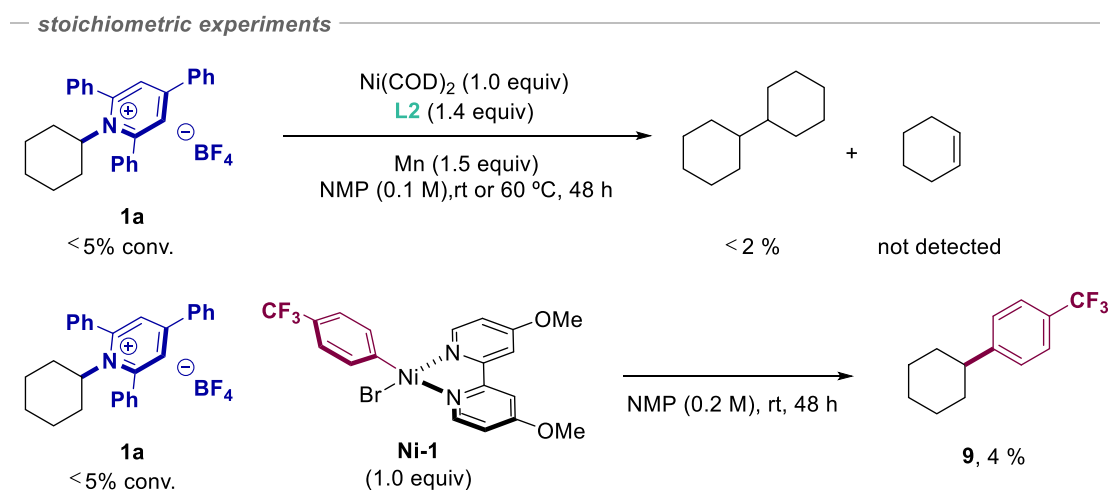
With these conditions in hand, we tested our hypothesis with a pinanamine derivative, as this compound could not be employed under Mn-mediated protocol (Scheme 3.3.5, *left*). Fortunately, a dual photoredox/Ni catalytic regime with Hantzsch ester as reductant cleanly furnished the desired product (**39**) in good yield. At present, we do not have any rationale behind these results.



Scheme 3.3.5. Dual photoredox/Ni catalyst regime for late-stage functionalization.

3.3.6 Mechanistic proposal

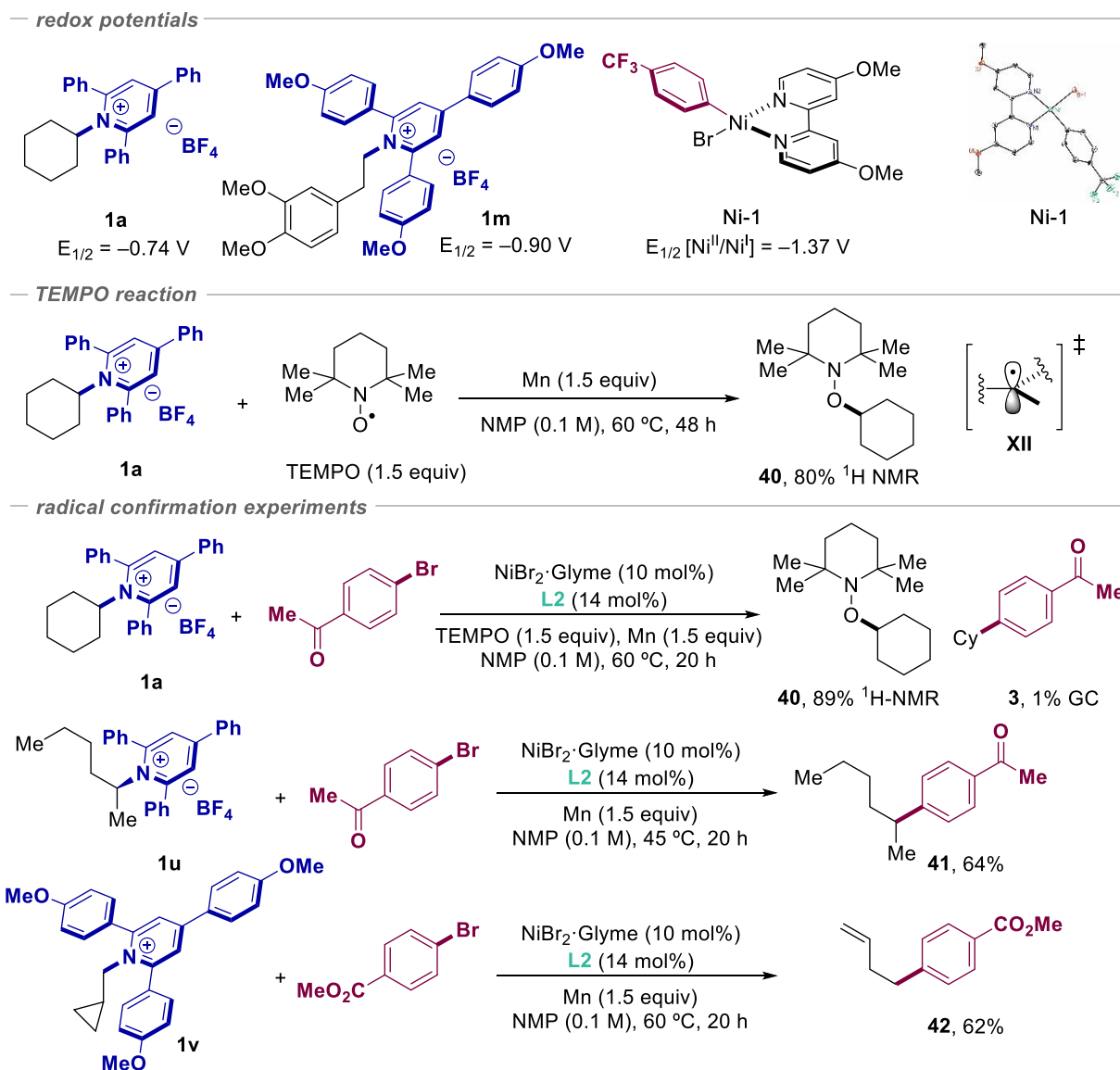
A priori, the reaction might be explained by either (a) the activation of the alkyl amine derivative *via* oxidative addition to $Ni(0)L_n$ or (b) the formation of alkyl radicals by SET from either $Ni(0)L_n$ or $Ni(I)L_n$. To this end, we turned our attention to conduct stoichiometric studies of **1** with $Ni(COD)_2/L2$ and **Ni-1**, hoping that it will reveal the mode of action by which this reaction operates at the molecular level (Scheme 3.3.6). In both cases, negligible conversion to product were observed, obtaining instead traces of homodimerization and absence of alkene formation, suggesting that the reaction might occur *via* other mechanistic manifolds.



Scheme 3.3.6. Stoichiometric mechanistic experiments.

Prompted by these results, we decided to check the redox potential of all reaction components. After some experimentation, we managed to do so and obtained the following data: **Ni-1** ($E_{1/2} [Ni^{II}/Ni^I] = -1.37$ V vs Ag/AgCl), **1a** ($E_{1/2} = -0.74$ vs Ag/AgCl), **1m** ($E_{1/2} = -0.90$ vs Ag/AgCl) and Mn ($E^0 [Mn^{II}/Mn^0] = -1.39$ V vs Ag/AgCl). A close look at this information indicates that both **Ni-1** and Mn might *a priori* be able to reduce either primary or secondary alkyl pyridinium salts (Scheme 3.3.7, *top*). Therefore, the lack of reactivity found in Scheme 3.3.6 might be explained by the inability of Ni(II) species or Ni(0) to promote C–N scission. Such uncertainty prompted us to study the reaction of Mn with **1a** in the presence of TEMPO, as Mn might be suited for triggering a SET to the alkyl pyridinium salt. Importantly, 80% yield of **40** was obtained, strongly advocating the notion that a SET process into **1a** takes place, generating an alkyl radical that is trapped in the presence of TEMPO. To gather evidences about the radical formation and to determine whether or not an oxidative addition pathway takes place, we performed three control reactions (Scheme 3.3.7, *bottom*). Interestingly, (1) the addition of TEMPO resulted in a significant inhibition, (2) racemic product was observed (**41**) upon subjecting our optimized conditions to enantiopure alkyl pyridinium salts and (3) ring-opening was observed with alkylpyridinium salts containing adjacent cyclopropyl rings (**42**).

Chapter 3



Scheme 3.3.7. Redox potentials, TEMPO and radical experiments.

These results argued against Ni being involved in C(sp³)-N scission but rather revealing that Mn might be triggering a downhill SET to **1a** or **1m**. This hypothesis was confirmed by a bulk electrolysis experiment (Figure 3.3.2, *top*), as **9** was obtained in 18% at r.t and 48% at 60 °C from **1a** and **Ni-1** at -0.8 V of constant potential (SI for more information). These results strongly suggest a catalytic regime in which C(sp³)-C(sp²) bond formation occurred by intercepting alkyl radicals of type **II** with **Ni-1** followed by reductive elimination (Figure 3.3.2, *bottom*).

Chapter 3

pyridinium salts, quaternary ammonium salts^{54,55} or via enantioconvergent scenarios with racemic pyridinium salts and chiral ligands.

3.4 Conclusions

In summary, we have developed a mild, robust and tolerant nickel-catalyzed deaminative arylation strategy with aryl halide counterparts. The potential of the methodology is illustrated by the wide functional group compatibility and by the possibility of applying this technology within the context of late-stage functionalization of advanced synthetic intermediates, thus opening a gateway to structural diversity in lead generation approaches. Although our procedure required the utilization of Mn, the stoichiometric metal reductant can be replaced by Hantzsch esters in combination with a photocatalyst under light irradiation, allowing to extend the scope of substrates that were difficult to couple otherwise. It is worth noting that while our paper was being revised, two publications from Han group⁵⁶ and Rueping group⁵⁷ reported similar transformations. In addition, the groups of Watson⁵⁸ and Molander⁵⁹ described an otherwise identical manifold, ending up in back-to-back-to-back publications in the same journal.

3.5 Experimental procedures

3.5.1 General considerations

Reagents. Commercially available materials were used as received without further purification. NiBr₂·glyme (97% purity) were purchased from Aldrich. 4-4'-Dimethoxy-2-2'-bipyridine (97% purity) was purchased from Aldrich. Manganese powder (≥ 99.9 trace metal base) was purchased from Aldrich. Anhydrous 1-methyl-2-pyrrolidinone (NMP, 99.5% purity) and *N,N*-Dimethylacetamide (DMA, 99.5% purity) were purchased from Across.

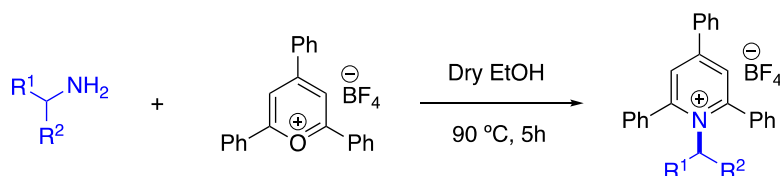
Analytical methods. ¹H and ¹³C NMR spectra were recorded on Bruker 300 MHz, Bruker 400 MHz and Bruker 500 MHz at 20 °C. All ¹H NMR spectra are reported in parts per million (ppm) downfield of TMS and were calibrated using the residual solvent peak of CHCl₃ (7.26 ppm), unless otherwise indicated. All ¹³C NMR spectra are reported in ppm relative to TMS, were calibrated using the signal of residual CHCl₃ (77.16 ppm), ¹¹B NMR and ¹⁹F NMR were obtained with ¹H decoupling unless otherwise indicated. Coupling constants, *J*, are reported in Hertz. Melting points were measured using open glass capillaries in a Büchi B540 apparatus. Gas chromatographic analyses were performed on Hewlett-Packard 6890 gas chromatography instrument with a FID detector. Flash chromatography was performed with EM Science silica gel 60 (230-400 mesh). Thin layer chromatography was used to monitor reaction progress and analysed fractions from column chromatography. To this purpose TLC Silica gel 60 F₂₅₄ aluminium sheets from Merck were used and visualization was achieved using UV irradiation and/or staining with Potassium Permanganate or Cerium Molybdate solution. The yields reported in Scheme 3.3.3, 4 and 5 refer to isolated yields and represent an average of at least two independent runs. The procedures described in this section are

representative. Thus, the yields may differ slightly from those given in the Schemes of the manuscript. In the cases the High-Resolution Mass Spectra of the molecular ion could not be obtained using ESI and APCI ionization modes the GC-MS of the compound was given. UltraPerformance Convergence Chromatography (UPC2) analysis was performed on Acquity UPC2 Waters instrument equipped with a Chiralpack IG column eluting ACN/CO₂ at ambient temperature and monitored by Photodiode Array Detector (PDA).

3.5.2 Reaction conditions

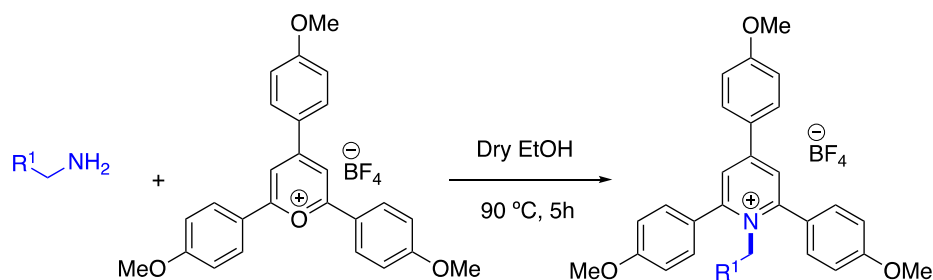
General procedure: An oven-dried 8 mL screw-cap test tube containing a stirring bar was charged with methyl 4-bromobenzoate (**2a**, 21.5 mg, 0.10 mmol) and 1-cyclohexyl-2,4,6-triphenylpyridin-1-ium tetrafluoroborate (**1a**, 66.9 mg, 0.14 mmol). The test tube was introduced in an argon-filled glovebox where manganese (8.2 mg, 0.15 mmol), NiBr₂-glyme (3.05 mg, 10 % mol) and 4,4'-dimethoxy-2,2'-bipyridine (**L2**, 3.0 mg, 14 mol %) in NMP were subsequently added followed by addition of NMP (0.8 mL, 0.1 M). The tube was taken out of the glovebox and stirred at r.t for 20 h. After diluting with EtOAc (10 mL) the yields were determined by GC FID analysis using 1-decane as internal standard. The sample was then extracted with water (10 mL) and brine (10 mL) and the organic layers were collected, dried with MgSO₄, concentrated under vacuum and the product was purified by column chromatography on silica gel (Hexane/ EtOAc 9.5/0.5).

3.5.3 Synthesis of Pyridinium salts



General Procedure A (secondary alkyl pyridinium salts): 2,4,6-triphenylpyrylium tetrafluoroborate (1.0 equiv) and a secondary amine (1.2 equiv) were added to a Schlenk containing a stirring bar. This was followed by addition of dry EtOH (1.0 M), resulting in a colour change from yellow to black orange. The mixture was then stirred and heated at reflux in an oil bath at 90 °C for 5h. At that time, the mixture was allowed to cool to room temperature. Et₂O was then added (15 mL) and shaken vigorously, forming a solid precipitate. The solid thus obtained was filtered, washed with Et₂O (2x15 mL) and dried under high vacuum. If the pyridinium salt failed to precipitate, it was subjected to flash column chromatography, eluting with DCM/Acetone mixtures.

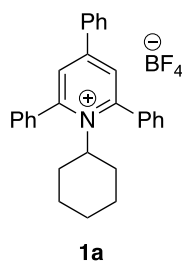
Chapter 3



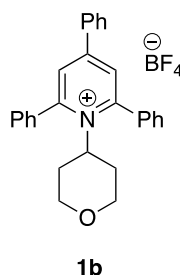
General Procedure B (primary alkyl pyridinium salts): 2,4,6-tris(4-methoxyphenyl)pyridinium tetrafluoroborate¹ (1.0 equiv) and the corresponding primary amine (1.2 equiv) were added to a Schlenk containing a stirring bar. This was followed by addition of dry EtOH (0.5-1.0 M), resulting in a colour change from yellow to black orange. The mixture was then stirred and heated at reflux in an oil bath at 90 °C for 5h. At that time, the mixture was allowed to cool to room temperature. Et₂O was then added (15 mL) and shaken vigorously, forming a solid precipitate. The solid thus obtained was filtered, washed with Et₂O (2x15 mL) and dried under high vacuum. The crude was purified by flash column chromatography, eluting with DCM/Acetone mixtures.

If the pyridinium salt failed to precipitate with the addition of Et₂O, the mixture was subjected to flash column chromatography.

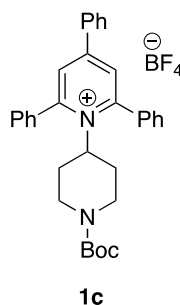
The corresponding amine hydrochloride salts or phosphoric salts can also be used by adding Et₃N (1.2 eq.) to the initial mixture. Flash column chromatography must be done in DCM/Acetone.



1-cyclohexyl-2,4,6-triphenylpyridin-1-ium tetrafluoroborate (1a). Following the General Procedure A, cyclohexylamine (275.5 mg, 2.78 mmol) and 2,4,6-triphenylpyridinium tetrafluoroborate (922.3 mg, 2.32 mmol) in 2.5 mL of EtOH were used, affording the product as a pale yellow powder (1.0 g, 90% yield). **Mp:** 183 – 182 °C. **¹H NMR** (400 MHz, CDCl₃) δ = 7.95 – 7.40 (m, 17H), 4.67 – 4.55 (m, 1H), 2.13 (d, J = 12.0 Hz, 2H), 1.65 – 1.14 (m, 5H), 0.75 (q, J = 13.0 Hz, 2H), 0.62 (t, J = 13.0 Hz, 1H) ppm. **¹³C NMR** (101 MHz, CDCl₃) δ = 157.1, 155.0, 134.2, 134.1, 131.9, 130.9, 129.6, 129.4, 128.9, 128.3, 128.2, 72.0, 33.6, 26.6, 24.7 ppm. **¹⁹F NMR** (376 MHz, CDCl₃) δ = -153.0 (minor, ¹⁰BF₄), -153.1 (major, ¹¹BF₄) ppm. Spectroscopic data for **1a** match those previously reported in the literature.¹¹

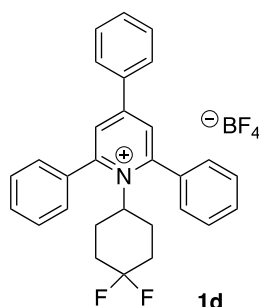


2,4,6-triphenyl-1-(tetrahydro-2H-pyran-4-yl)pyridin-1-ium tetrafluoroborate (1b). Following the General Procedure A, 4-aminotetrahydropyran (302.8 mg, 2.8 mmol) and 2,4,6-triphenylpyrylium tetrafluoroborate (1.0 g, 2.5 mmol) in 2.5 mL of EtOH were used, affording the product as a pale yellow powder (970 mg, 80% yield). **Mp:** 195 - 197 °C. **¹H NMR** (400 MHz, CDCl₃) δ = 7.79 – 7.68 (m, 6H), 7.68 – 7.61 (m, 2H), 7.57 – 7.48 (m, 6H), 7.48 – 7.46 (m, 1H), 7.40 – 7.35 (m, 2H), 4.85 (tt, J = 12.3, 3.2 Hz, 1H), 3.69 (dd, J = 11.7, 4.0 Hz, 2H), 2.78 (td, J = 11.7, 1.8 Hz, 2H), 2.05 (dt, J = 12.6, 2.4 Hz, 2H), 1.86 (tt, J = 12.2, 4.4 Hz, 2H) ppm. **¹³C NMR** (101 MHz, CDCl₃) δ = 157.1, 155.2, 133.9, 133.7, 131.9, 131.0, 129.5, 129.3, 128.9, 128.2, 128.1, 69.0, 67.7, 33.7 ppm. **¹⁹F NMR** (376 MHz, CDCl₃) δ = -152.7 (s), -152.8 (d, J = 2.3 Hz). Spectroscopic data for **1b** match those previously reported in the literature.¹¹

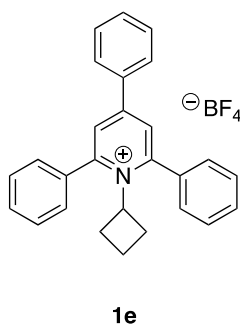


1-(1-(tert-butoxycarbonyl)piperidin-4-yl)-2,4,6-triphenylpyridin-1-ium tetrafluoroborate (1c). Following the General Procedure A, *tert*-butyl 4-aminopiperidine-1-carboxylate (630 mg, 3 mmol) and 2,4,6-triphenylpyrylium tetrafluoroborate (1.0 g, 2.5 mmol) in 2.5 mL of EtOH were used, affording the product as a white powder (1.1 g, 76% yield). **Mp:** 175 - 177 °C. **¹H NMR** (400 MHz, CDCl₃) δ = 7.75 – 7.71 (m, 5H), 7.70 – 7.64 (m, 2H), 7.62 – 7.52 (m, 6H), 7.49 (d, J = 7.4 Hz, 1H), 7.42 (t, J = 7.5 Hz, 2H), 4.75 (t, J = 12.6 Hz, 1H), 3.90 (brs, 2H), 2.11 (brs, 4H), 1.68 (brs, 2H), 1.30 (s, 9H) ppm. **¹³C NMR** (101 MHz, CDCl₃) δ = 157.1, 155.3, 154.1, 133.9, 133.7, 131.9, 131.0, 129.5, 129.3, 128.9, 128.2, 128.2, 80.0, 69.9, 44.7, 32.6, 28.2 ppm. **¹⁹F NMR** (376 MHz, CDCl₃) δ = -152.9 (s), -153.0 (d, J = 2.9 Hz). Spectroscopic data for **1c** match those previously reported in the literature.¹¹

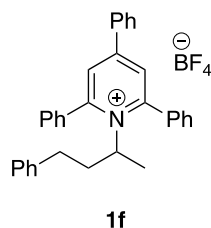
Chapter 3



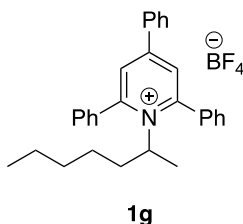
1-(4,4-difluorocyclohexyl)-2,4,6-triphenylpyridin-1-ium tetrafluoroborate (1d). Following the General Procedure A, 4,4-difluorocyclohexan-1-amine HCl salt (308.9 mg, 1.80 mmol), triethylamine (251 μ L, 1.80 mmol) and 2,4,6-triphenylpyrylium tetrafluoroborate (594.3 mg, 1.50 mmol) in 1.5 mL of EtOH were used. The title compound was obtained as a white powder (497 mg, 65% yield). **Mp:** 207 – 206 $^{\circ}$ C. **1 H NMR** (400 MHz, CDCl_3) δ = 7.84 (s, 2H), 7.75 (t, J = 7.2 Hz, 6H), 7.66 – 7.38 (m, 9H), 4.72 (t, J = 12.2 Hz, 1H), 2.22 (d, J = 12.4 Hz, 2H), 2.05 – 1.74 (m, 4H), 1.32 – 1.07 (m, 2H) ppm. **13 C NMR** (101 MHz, CDCl_3) δ = 157.3, 155.8, 134.0, 133.8, 132.3, 131.4, 129.8, 129.3, 129.2, 128.5, 128.4, 120.7 (dd, J = 328.1, 318.8 Hz), 68.7, 33.7 (t, J = 25.4 Hz), 28.7 (d, J = 10.2 Hz) ppm. **19 F NMR** (376 MHz, CDCl_3) δ = -94.3 (d, J = 241.6 Hz), -102.9 (d, J = 241.3 Hz), 152.7 (s), -152.8 (d, J = 2.2 Hz) ppm. Spectroscopic data for **1d** match those previously reported in the literature.ⁱⁱⁱ



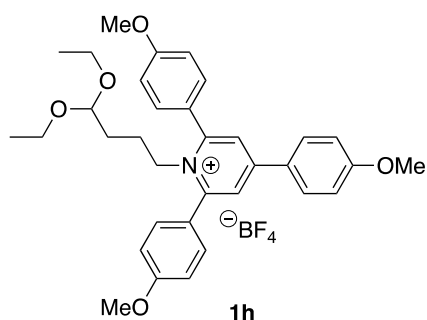
1-cyclobutyl-2,4,6-triphenylpyridin-1-ium tetrafluoroborate (1e). Following the General Procedure A, cyclobutanamine (154.7 μ L, 1.80 mmol) and 2,4,6-triphenylpyrylium tetrafluoroborate (594.3 mg, 1.50 mmol) in 1.5 mL of EtOH were used. The title compound was obtained as a pale yellow powder (577 mg, 86% yield). **Mp:** 191 – 192 $^{\circ}$ C. **1 H NMR** (400 MHz, CDCl_3) δ = 8.01 – 7.73 (m, 8H), 7.60 – 7.57 (m, 9H), 5.74 – 5.31 (m, 1H), 1.83 (s, 2H), 1.30 – 1.19 (m, 4H) ppm. **13 C NMR** (101 MHz, CDCl_3) δ = 157.5, 155.6, 134.2, 134.1, 132.2, 131.6, 129.9, 129.7, 129.5, 128.2, 126.2, 64.4, 33.2, 14.3 ppm. **19 F NMR** (376 MHz, CDCl_3) δ = -152.7 (s), -152.9 (d, J = 2.4 Hz) ppm. IR (neat, cm^{-1}): 3005, 1615, 1551, 1456, 1404, 1324, 1150, 1044, 880, 826. **HRMS** calcd. for $(\text{C}_{27}\text{H}_{24}\text{N}) [\text{M}-\text{BF}_4]^+$: 362.1903, found 362.1906.



2,4,6-triphenyl-1-(4-phenylbutan-2-yl)pyridin-1-ium tetrafluoroborate (1f). Following the General Procedure A, 4-phenylbutan-2-amine (223.2 mg, 1.5 mmol) and 2,4,6-triphenylpyrylium tetrafluoroborate (500 mg, 1.3 mmol) in 1.5 mL of EtOH were used, affording the product as a pale yellow solid (507 mg, 76% yield). **Mp:** 87 – 86 °C. **¹H NMR** (400 MHz, CDCl₃) δ = 7.78 (s, 2H), 7.72 – 7.63 (m, 4H), 7.61 – 7.31 (m, 10H), 7.16 – 7.05 (m, 4H), 6.92 – 6.81 (m, 2H), 4.95 – 4.87 (m, 1H), 2.44 – 2.32 (m, 1H), 2.23 – 2.10 (m, 2H), 1.86 – 1.70 (m, 1H), 1.45 (d, J = 7.0 Hz, 3H) ppm. **¹³C NMR** (101 MHz, CDCl₃). δ = 155.3, 138.9, 133.9, 133.7, 132.0, 130.8, 129.6, 128.7, 128.5, 128.4, 128.3, 128.0, 126.5, 66.0, 37.9, 32.5, 21.6 ppm. (1 aromatic carbon signal is not observed due to signal broadening) **¹⁹F NMR** (376 MHz, CDCl₃) δ = -152.4 (s), -152.4 (s). Spectroscopic data for **1f** match those previously reported in the literature.^{IV}



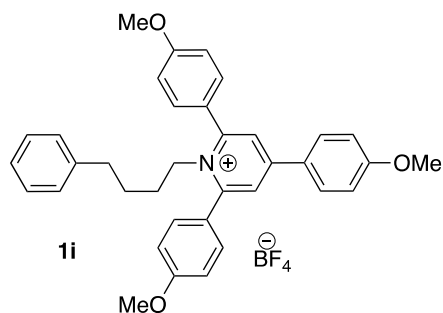
1-(heptan-2-yl)-2,4,6-triphenylpyridin-1-ium tetrafluoroborate (1g). Following the General Procedure A, heptan-2-amine (214 mg, 1.5 mmol) and 2,4,6-triphenylpyrylium tetrafluoroborate (500 mg, 1.3 mmol) in 1.5 mL of EtOH were used, affording the product as a white solid (320 mg, 51% yield). **Mp:** 162 - 164 °C. **¹H NMR** (400 MHz, CDCl₃) δ = 7.99 – 7.65 (m, 7H), 7.64 – 7.53 (m, 6H), 7.53-7.42 (m, 3H), 4.90 (dq, J = 13.4, 7.0 Hz, 1H), 1.86 – 1.70 (m, 1H), 1.47 – 1.34 (m, 4H), 1.19 – 1.08 (m, 2H), 1.05 – 0.92 (m, 3H), 0.87 – 0.80 (m, 1H), 0.78 (t, J = 7.3 Hz, 3H) ppm (1 aromatic proton signal is not observed due to signal broadening). **¹³C NMR** (101 MHz, CDCl₃). δ = 155.2, 134.0, 133.9, 131.9, 130.8, 129.6, 129.3, 128.8, 128.3, 67.0, 36.8, 30.8, 26.3, 22.2, 21.6, 13.8. ppm (5 aromatic carbon signals are not observed due to signal broadening). **¹⁹F NMR** (376 MHz, CDCl₃) δ = -153.4 (s), -153.5 (d, J = 2.2 Hz). Spectroscopic data for **1g** match those previously reported in the literature.^{IV}



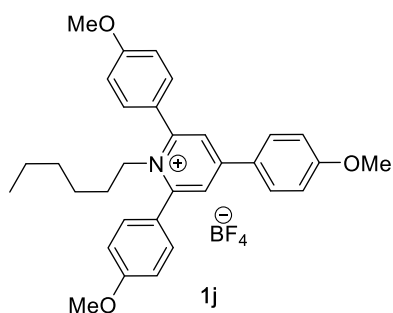
Chapter 3

1-(4,4-diethoxybutyl)-2,4,6-tris(4-methoxyphenyl)pyridin-1-ium tetrafluoroborate (1h).

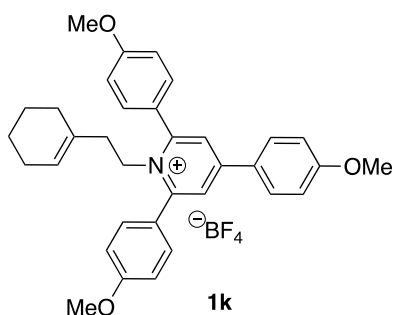
Following the General Procedure B, 4,4-diethoxybutan-1-amine (401.2 mg, 2.5 mmol) and 2,4,6-tris(4-methoxyphenyl)pyrylium tetrafluoroborate (1.0 g, 2.05 mmol) in 2.5 mL of EtOH were used. Purification by flash column chromatography (DCM/Acetone 8/2) gave the desired product as a sticky yellow solid (1.1 g, 85% yield). **Mp:** 54 - 56 °C. **¹H NMR** (400 MHz, CDCl₃) δ = 7.74 – 7.70 (m, 4H), 7.69 – 7.65 (m, 4H), 7.10 – 7.04 (m, 4H), 6.99 (d, *J* = 8.9 Hz, 2H), 4.48 (t, *J* = 8 Hz, 2H), 4.02 (t, *J* = 5.2 Hz, 1H), 3.85 (s, 6H), 3.84 (s, 3H), 3.36 (dq, *J* = 9.3, 7.0 Hz, 2H), 3.18 (dq, *J* = 9.3, 7.0 Hz, 2H), 1.41 (dq, *J* = 6.9, 3.9, 2.7 Hz, 2H), 1.09 – 1.05 (m, 2H), 1.03 (t, *J* = 7.0 Hz, 6H) ppm. **¹³C NMR** (101 MHz, CDCl₃). δ = 163.2, 161.4, 156.4, 154.3, 130.6, 129.7, 125.5, 125.0, 115.2, 114.7, 101.5, 61.5, 55.6, 55.4, 54.4, 30.4, 24.8, 15.1 ppm. **¹⁹F NMR** (376 MHz, CDCl₃) δ = -153.2 (s), -153.2 (d, *J* = 2.6 Hz). **IR** (neat, cm⁻¹): 2970, 2932, 1593, 1508, 1439, 1294, 1178, 1015, 820. **HRMS** calcd. for (C₃₄H₄₀NO₅) [M-BF₄]⁺: 542.2901, found 542.2891.



2,4,6-tris(4-methoxyphenyl)-1-(4-phenylbutyl)pyridin-1-ium tetrafluoroborate (1i). Following the General Procedure B, 4-phenylbutan-1-amine (178.9 mg, 1.20 mmol) and 2,4,6-tris(4-methoxyphenyl)pyrylium tetrafluoroborate (486.2 mg, 1.0 mmol) in 1.5 mL of EtOH were used, affording the title compound as a yellow powder (524 mg, 85% yield) by using (DCM/Acetone 5/1) as eluent. **Mp:** 82 – 83 °C. **¹H NMR** (400 MHz, CDCl₃) δ = 7.71 (d, *J* = 9.2 Hz, 4H), 7.61 (d, *J* = 8.4 Hz, 4H), 7.17 (dd, *J* = 10.7, 8.7 Hz, 3H), 7.03 (d, *J* = 8.7 Hz, 4H), 7.00 (d, *J* = 8.9 Hz, 2H), 6.85 (d, *J* = 6.8 Hz, 2H), 4.47 (t, *J* = 8.0 Hz, 2H), 3.86 (s, 6H), 3.85 (s, 3H), 2.20 (t, *J* = 7.2 Hz, 2H), 1.33 (quint, *J* = 7.8 Hz, 2H), 1.08 (quint, *J* = 7.1 Hz, 2H) ppm. **¹³C NMR** (101 MHz, CDCl₃) δ = 163.3, 161.5, 156.6, 154.4, 140.9, 130.8, 129.9, 128.4, 128.3, 126.0, 125.7, 125.2, 115.4, 114.9, 55.8, 55.6, 54.6, 34.3, 29.0, 27.6 ppm (*1 aromatic carbon signal is not observed due to signal broadening*). **¹⁹F NMR** (376 MHz, CDCl₃) δ = -153.1 (s), -153.2 (d, *J* = 2.4 Hz) ppm. **IR** (neat, cm⁻¹): 3062, 2934, 2835, 1593, 1507, 1447, 1440, 1294, 1249, 1177, 1049, 1016, 889, 831. **HRMS** calcd. for (C₃₆H₃₆NO₃) [M-BF₄]⁺: 530.2690, found 530.2683.

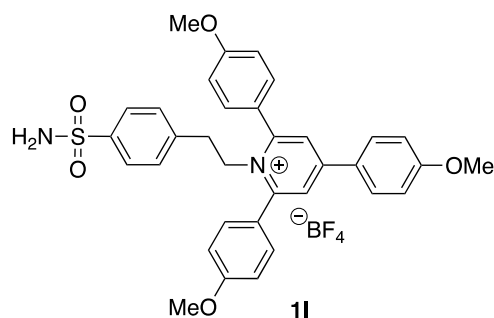


1-hexyl-2,4,6-tris(4-methoxyphenyl)pyridin-1-ium tetrafluoroborate (1j). Following the General Procedure B, 1-hexylamine (121.2 mg, 1.20 mmol) and 2,4,6-tris(4-methoxyphenyl)pyrylium tetrafluoroborate (486.2 mg, 1.0 mmol) in 1.5 mL of EtOH were used, affording the title compound as a yellow powder (500 mg, 88% yield) by using (DCM/acetone 10/1) as eluent **Mp:** 70 – 71 °C. **^1H NMR** (400 MHz, CDCl_3) δ = 8.02 – 7.58 (m, 8H), 7.07 (d, J = 8.8 Hz, 4H), 6.99 (d, J = 8.9 Hz, 2H), 4.58 – 4.37 (m, 2H), 3.85 (s, 6H), 3.83 (s, 3H), 1.29 (quint, J = 8.9 Hz, 2H), 0.93 (q, J = 7.0 Hz, 2H), 0.75 (quint, J = 3.6 Hz, 4H), 0.65 (t, J = 7.3 Hz, 3H) ppm. **^{13}C NMR** (101 MHz, CDCl_3) δ = 163.3, 161.6, 156.5, 154.4, 130.8, 129.9, 125.8, 125.3, 125.2, 115.4, 114.8, 55.7, 55.6, 54.6, 30.3, 29.5, 25.7, 21.9, 13.8 ppm. **^{19}F NMR** (376 MHz, CDCl_3) δ = -153.2 (s), -153.3 (d, J = 2.3 Hz) ppm. IR (neat, cm^{-1}): 2931, 2840, 1594, 1508, 1455, 1294, 1241, 1179, 1049, 1019, 889, 832. **HRMS** calcd. for ($\text{C}_{32}\text{H}_{36}\text{NO}_3$) [M-BF_4] $^+$: 482.2690, found 482.2672.

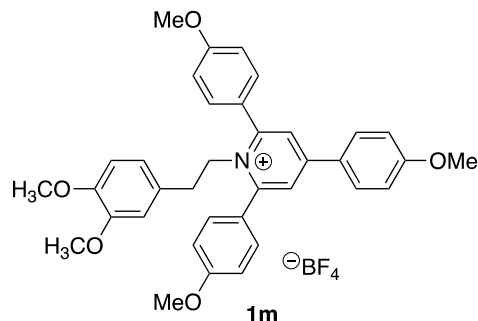


1-(2-(cyclohex-1-en-1-yl)ethyl)-2,4,6-tris(4-methoxyphenyl)pyridin-1-ium tetrafluoroborate (1k). Following the General Procedure B, 2-(cyclohex-1-en-1-yl)ethan-1-amine (233.4 mg, 1.85 mmol) and 2,4,6-tris(4-methoxyphenyl)pyrylium tetrafluoroborate (750.0 mg, 1.54 mmol) in 2.0 mL of EtOH were used. Purification by flash column chromatography (DCM/Acetone 9/1) gave the desired product as a brown solid (800 mg, 87% yield). **Mp:** 103 - 105 °C. **^1H NMR** (400 MHz, CDCl_3) δ = 7.88 – 7.61 (m, 8H), 7.17 – 7.07 (m, 4H), 7.03 (d, J = 8.9 Hz, 2H), 4.88 (s, 1H), 4.54 (m, J = 8 Hz, 2H), 3.89 (s, 6H), 3.87 (s, 3H), 1.93 (t, J = 8.1 Hz, 2H), 1.74 (s, 2H), 1.35 (dq, J = 6.3, 3.0 Hz, 4H), 1.20 (s, 2H) ppm. **^{13}C NMR** (101 MHz, CDCl_3) δ = 163.2, 161.6, 156.6, 154.3, 131.8, 130.8, 129.7, 125.8, 125.3, 125.2, 125.1, 115.3, 114.8, 55.6, 55.6, 53.8, 38.0, 27.3, 25.0, 22.4, 21.6 ppm. **^{19}F NMR** (376 MHz, CDCl_3) δ = -153.0 (s), -153.0 (d, J = 2.2 Hz). IR (neat, cm^{-1}): 2930, 2835, 1593, 1506, 1456, 1436, 1240, 1177, 1017, 832. **HRMS** calcd. for ($\text{C}_{34}\text{H}_{36}\text{NO}_3$) [M-BF_4] $^+$: 506.2690, found 506.2675.

Chapter 3

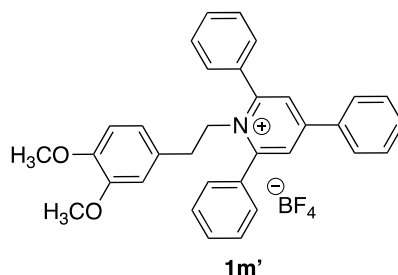


2,4,6-tris(4-methoxyphenyl)-1-(4-sulfamoylphenethyl)pyridin-1-ium tetrafluoroborate (1l). Following the General Procedure B, 4-(2-aminoethyl)benzenesulfonamide (146.2 mg, 0.73 mmol) and 2,4,6-tris(4-methoxyphenyl)pyrylium tetrafluoroborate (300 mg, 0.61 mmol) in 1.0 mL of EtOH were used. Purification by flash column chromatography (DCM/Acetone 8/2) gave the desired product as a brown solid (340 mg, 83% yield). **Mp:** 144 - 146 °C. **¹H NMR** (400 MHz, (CD₃)₂CO) δ = 8.28 (s, 2H), 8.24-8.22 (m, 2H), 7.79 - 7.69 (m, 4H), 7.65 - 7.63 (m, 2H), 7.28 - 7.21 (m, 4H), 7.20 - 7.17 (m, 2H), 6.80 - 6.78 (m, 2H), 6.55 (brs, 2H, NH₂), 4.97 (t, J = 7.3 Hz, 2H), 3.96 (s, 6H), 3.94 (s, 3H), 2.88 (t, J = 7.3 Hz, 2H), 2.09 (s, 2H) ppm. **¹³C NMR** (101 MHz, CD₃)₂CO). δ = 164.5, 162.7, 157.7, 155.5, 144.1, 141.2, 131.9, 131.3, 129.9, 127.4, 126.5, 126.4, 125.9, 116.1, 115.6, 56.5, 56.2, 56.1, 35.8 ppm. **¹⁹F NMR** (376 MHz, CD₃)₂CO) δ = 151.8 (s), -151.9 (s). **IR** (neat, cm⁻¹): 2929, 2836, 1593, 1507, 1456, 1436, 1241, 1178, 1017, 832. **HRMS** calcd. for (C₃₄H₃₃N₂O₅S) [M-BF₄]⁺: 581.2105, found 581.2102.

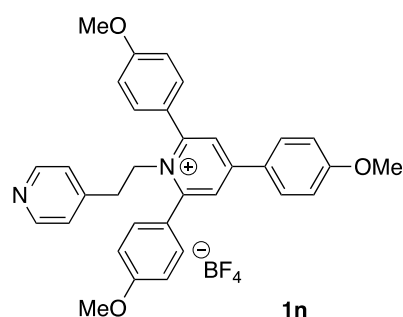


1-(3,4-dimethoxyphenethyl)-2,4,6-tris(4-methoxyphenyl)pyridin-1-ium tetrafluoroborate (1m). Following the General Procedure B, 2-(3,4-dimethoxyphenyl)ethan-1-amine (217.3 mg, 1.20 mmol) and 2,4,6-tris(4-methoxyphenyl)pyrylium tetrafluoroborate (486.2 mg, 1.0 mmol) in 1.5 mL of EtOH were used, affording the title compound as a yellow powder (730 mg, 91% yield) by using (DCM/Acetone 5/1) as eluent. **Mp:** 96 - 97 °C. **¹H NMR** (400 MHz, CDCl₃) δ = 7.75 (d, J = 8.8 Hz, 2H), 7.73 (s, 2H), 7.63 (d, J = 8.5 Hz, 4H), 7.09 (d, J = 8.5 Hz, 4H), 7.03 (d, J = 8.8 Hz, 2H), 6.55 (d, J = 8.1 Hz, 1H), 6.00 (dd, J = 8.1, 1.7 Hz, 1H), 5.80 (d, J = 1.7 Hz, 1H), 4.76 (t, J = 7.3 Hz, 2H), 3.88 (s, 9H), 3.78 (s, 3H), 3.56 (s, 3H), 2.52 (t, J = 7.3 Hz, 2H) ppm. **¹³C NMR** (101 MHz, CDCl₃) δ = 163.4, 161.7, 156.8, 154.6, 149.3, 148.4, 131.1, 130.0, 127.9, 125.8, 125.3, 125.1, 120.5, 115.5, 114.9, 111.3, 56.1, 56.1, 55.8, 55.7, 55.7, 35.3 ppm (1 aromatic carbon signal is not observed due to signal broadening). **¹⁹F NMR** (376 MHz, CDCl₃) δ = -152.6 (s), -152.7 (d, J = 2.2 Hz) ppm. **IR** (neat, cm⁻¹): 3067, 2935, 2837, 1592, 1507, 1439, 1240, 1177, 1049, 1015, 852, 760. **HRMS** calcd. for (C₃₆H₃₆NO₅) [M-BF₄]⁺: 562.2588, found

562.2587.

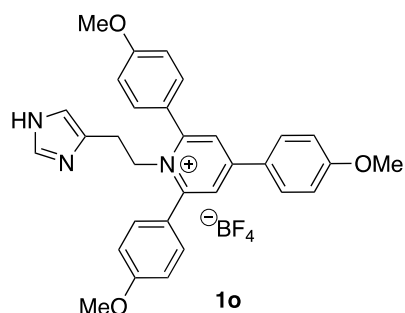


1-(3,4-dimethoxyphenethyl)-2,4,6-triphenylpyridin-1-ium tetrafluoroborate (1m'). Following the General Procedure A, 2-(3,4-dimethoxyphenyl)ethan-1-amine (217.3 mg, 1.20 mmol) and 2,4,6-triphenylpyrylium tetrafluoroborate (396.1 mg, 1.0 mmol) in 1.5 mL of EtOH were used, affording the product as a pale yellow solid (458.6 mg, 82% yield). **Mp**: 174 - 176 °C. **$^1\text{H NMR}$** (400 MHz, CDCl_3) δ = 7.77 – 7.74 (m, 6H), 7.72 – 7.63 (m, 2H), 7.62 – 7.52 (m, 6H), 7.52 – 7.34 (m, 3H), 6.51 (d, J = 8.1 Hz, 1H), 5.87 (dd, J = 8.2, 2.0 Hz, 1H), 5.68 (d, J = 2.0 Hz, 1H), 4.66 – 4.46 (m, 2H), 3.72 (s, 3H), 3.52 (s, 3H), 2.69 – 2.45 (m, 2H) ppm. **$^{13}\text{C NMR}$** (101 MHz, CDCl_3). δ = 156.3, 155.7, 148.9, 148.0, 133.9, 132.7, 131.9, 130.8, 129.5, 129.1, 129.1, 128.0, 127.6, 126.5, 120.2, 111.2, 111.0, 55.9, 55.8, 55.6, 35.1 ppm **$^{19}\text{F NMR}$** (376 MHz, CDCl_3) δ = -152.90, -152.96 (d, J = 2.3 Hz) ppm. Spectroscopic data for **1m'** match those previously reported in the literature.^{xxiii}



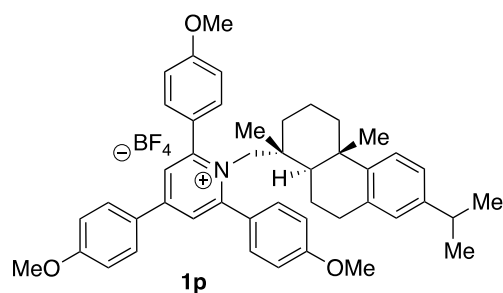
2,4,6-tris(4-methoxyphenyl)-1-(2-(pyridin-4-yl)ethyl)pyridin-1-ium tetrafluoroborate (1n). Following the General Procedure B, 2-(pyridin-4-yl)ethan-1-amine (73.2 mg, 0.60 mmol) and 2,4,6-tris(4-methoxyphenyl)pyrylium tetrafluoroborate (243.1 mg, 0.50 mmol) in 0.5 mL of EtOH were used, affording the title compound as a yellow powder (250 mg, 85% yield) by using (DCM/Acetone 1/1) as eluent. **Mp**: 94 – 95 °C. **$^1\text{H NMR}$** (300 MHz, CDCl_3) δ = 8.40 – 8.17 (m, 2H), 7.83 – 7.72 (m, 4H), 7.66 (d, J = 8.8 Hz, 4H), 7.10 (d, J = 8.9 Hz, 4H), 7.02 (d, J = 8.9 Hz, 2H), 6.37 (d, J = 6.0 Hz, 2H), 4.78 (t, J = 7.7 Hz, 2H), 3.89 (s, 6H), 3.87 (s, 3H), 2.63 (t, J = 7.7 Hz, 2H) ppm. **$^{13}\text{C NMR}$** (75 MHz, CDCl_3) δ = 163.5, 161.8, 156.7, 155.0, 150.2, 144.6, 130.9, 130.0, 125.7, 125.3, 125.0, 123.7, 115.4, 115.0, 55.8, 55.7, 54.6, 34.6 ppm. **$^{19}\text{F NMR}$** (376 MHz, CDCl_3) δ = -152.9 (s), -153.0 (d, J = 2.2 Hz) ppm. IR (neat, cm^{-1}): 2838, 1593, 1506, 1456, 1417, 1295, 1242, 1178, 1051, 1018, 833. **HRMS** calcd. for $(\text{C}_{33}\text{H}_{31}\text{N}_2\text{O}_3)$ $[\text{M}-\text{BF}_4]^+$: 503.2329, found 503.2326.

Chapter 3



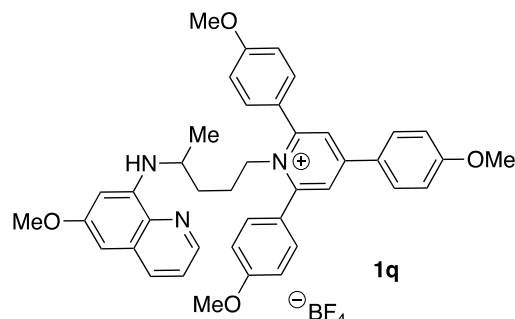
1-(2-(1H-imidazol-4-yl)ethyl)-2,4,6-tris(4-methoxyphenyl)pyridin-1-ium tetrafluoroborate (1o).

Following the General Procedure B, 2-(2-Methyl-1H-imidazol-4-yl)ethanamine dihydrochloride (300 mg, 1.63 mmol) and 2,4,6-tris(4-methoxyphenyl)pyrylium tetrafluoroborate (665 mg, 1.36 mmol), triethylamine (0.54 mL, 3.9 mmol) in 2.0 mL of EtOH were used. Extraction was done using H₂O (2 x 15) and brine (2 x 15) and the purification by flash column chromatography (DCM/Acetone 6/4) gave the desired product as a yellow solid (330 mg, 42% yield) without the anion BF₄⁻. **Mp:** 100 - 102 °C. **¹H NMR** (400 MHz, CDCl₃) δ = 7.84 – 7.75 (m, 2H), 7.71 (s, 2H), 7.59 – 7.47 (m, 4H), 7.39 (s, 1H), 7.07 – 7.02 (m, 6H), 6.33 (s, 1H), 4.89 (t, *J* = 6.2 Hz, 2H), 3.88 (s, 3H), 3.87 (s, 6H), 2.60 (t, *J* = 6.2 Hz, 2H) ppm. **¹³C NMR** (101 MHz, CDCl₃). δ = 163.5, 161.8, 157.1, 154.4, 135.3, 130.6, 129.9, 125.4, 125.1, 124.9, 115.4, 115.0, 55.9, 55.7, 55.6, 26.7 ppm. **IR** (neat, cm⁻¹): 2928, 2838, 1592, 1507, 1456, 1240, 1177, 1017, 832. **HRMS** calcd. for (C₃₁H₃₀N₃O₃) [M]⁺: 492.2282, found 492.2291.

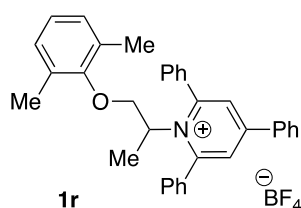


1-(((1R,4aS,10aR)-7-isopropyl-1,4a-dimethyl-1,2,3,4,4a,9,10,10a-octahydrophenanthren-1-yl)methyl)-2,4,6-tris(4-methoxyphenyl)pyridin-1-ium tetrafluoroborate (1p). Following the General Procedure B, *Leelamine* (500 mg, 1.75 mmol) and 2,4,6-tris(4-methoxyphenyl)pyrylium tetrafluoroborate (714.5 mg, 1.46 mmol) in 2.0 mL of EtOH were used. Purification by flash column chromatography (DCM/Acetone 9/1) gave the desired product as a red solid (310 mg, 28% yield). **Mp:** 175 - 177 °C. **¹H NMR** (400 MHz, CDCl₃) δ = 8.05 – 7.86 (m, 2H), 7.86 – 7.81 (m, 2H), 7.76 – 7.71 (m, 2H), 7.68 – 7.31 (m, 2H), 7.18 – 7.10 (m, 2H), 7.09 – 7.02 (m, 3H), 6.97 – 6.86 (m, 3H), 6.77 (d, *J* = 1.9 Hz, 1H), 5.19 (d, *J* = 14.7 Hz, 1H), 4.87 (d, *J* = 14.7 Hz, 1H), 3.89 (s, 3H), 3.87 (s, 3H), 3.71 (s, 3H), 2.77 (quint, *J* = 6.9 Hz, 1H), 2.66 (dd, *J* = 17.6, 6.8 Hz, 1H), 2.49 (ddd, *J* = 17.9, 11.0, 7.8 Hz, 1H), 2.10 – 2.00 (m, 1H), 1.65 (brs, 1H), 1.38 – 1.34 (m, 2H), 1.25 (s, 1H), 1.19 (d, *J* = 6.9 Hz, 6H), 1.10 – 0.96 (m, 2H), 0.94 (s, 3H), 0.75 (dd, *J* = 12.4, 2.0 Hz, 1H), 0.59 – 0.48 (m, 1H), 0.41 (s, 3H) ppm. **¹³C NMR** (101 MHz, CDCl₃). δ = 163.5, 161.7, 161.7, 159.0, 153.9, 146.4, 145.7, 134.2, 132.0, 129.9, 127.0, 126.9, 126.7, 125.1, 124.0, 124.0, 123.6, 123.4, 115.4, 114.9, 65.4, 55.7, 55.6, 55.4, 47.6, 41.7, 37.6, 37.5, 37.1,

33.4, 29.3, 25.2, 23.9, 19.5, 19.0, 18.0 ppm. (3 aromatic carbon signals are not observed due to signal broadening) ^{19}F NMR (376 MHz, CDCl_3) $\delta = -152.7, -152.7$ (d, $J = 2.8$ Hz). IR (neat, cm^{-1}): 2930, 1592, 1507, 1456, 1240, 1177, 832, 785. HRMS calcd. for $(\text{C}_{46}\text{H}_{52}\text{NO}_3)$ $[\text{M-BF}_4]^+$: 666.3942, found 666.3935.



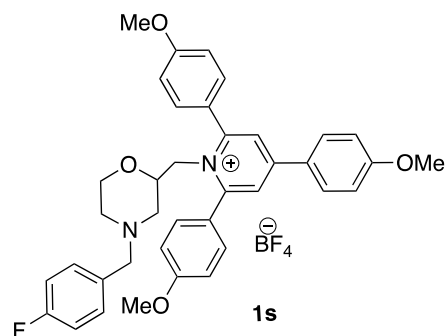
2,4,6-tris(4-methoxyphenyl)-1-((6-methoxyquinolin-8-yl)amino)pentylpyridin-1-ium tetrafluoroborate (1q). Following the General Procedure B, 2-(pyridin-4-yl)ethan-1-amine (455.3 mg, 1.10 mmol), triethylamine (307 μL , 2.20 mmol) and 2,4,6-tris(4-methoxyphenyl)pyrylium tetrafluoroborate (486.2 mg, 1.0 mmol) in 1.0 mL of EtOH were used, affording the title compound as a yellow powder (330 mg, 45% yield) by using (DCM/Acetone 5/1) as eluent. **Mp:** 109 – 110 $^\circ\text{C}$. ^1H NMR (400 MHz, CDCl_3) $\delta = 8.54$ (dd, $J = 4.2, 1.6$ Hz, 1H), 7.93 (dd, $J = 8.3, 1.7$ Hz, 1H), 7.76 – 7.61 (m, 7H), 7.33 (dd, $J = 8.2, 4.3$ Hz, 1H), 7.15 – 6.97 (m, 6H), 6.31 (d, $J = 2.5$ Hz, 1H), 6.02 (d, $J = 2.5$ Hz, 1H), 5.70 (d, $J = 8.4$ Hz, 1H), 4.54 (t, $J = 7.8$ Hz, 2H), 3.85 (s, 6H), 3.84 (s, 3H), 1.23 – 1.14 (m, 4H), 1.05 (d, $J = 6.4$ Hz, 3H) ppm. ^{13}C NMR (101 MHz, CDCl_3) $\delta = 163.3, 161.6, 159.4, 156.7, 154.4, 144.6, 144.4, 135.3, 135.0, 130.8, 129.9, 125.8, 125.1, 125.0, 122.1, 115.4, 114.9, 97.0, 92.1, 55.8, 55.6, 55.3, 54.7, 47.0, 32.5, 26.2, 20.4$ ppm (1 aromatic carbon signal is not observed due to signal broadening). ^{19}F NMR (376 MHz, CDCl_3) $\delta = -153.4$ (s), -153.4 (d, $J = 2.2$ Hz) ppm. IR (neat, cm^{-1}): 2934, 2837, 1594, 1506, 1456, 1440, 1386, 1294, 1241, 1178, 1049, 1020, 892, 831, 791. HRMS calcd. for $(\text{C}_{41}\text{H}_{42}\text{N}_3\text{O}_4)$ $[\text{M-BF}_4]^+$: 640.3170, found 640.3186.



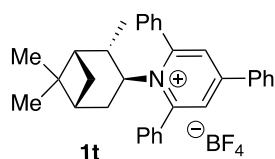
1-(1-(2,6-dimethylphenoxy)propan-2-yl)-2,4,6-triphenylpyridin-1-ium tetrafluoroborate (1r). Following the General Procedure A, Mexiletine-HCl (215.7 mg, 1.65 mmol), triethylamine (230 μL , 1.65 mmol) and 2,4,6-triphenylpyrylium tetrafluoroborate (594.3 mg, 1.50 mmol) in 1.5 mL of EtOH were used. The title compound was obtained as yellow powder (340 mg, 42% yield) by extraction with dichloromethane and water. **Mp:** 122 – 123 $^\circ\text{C}$. ^1H NMR (400 MHz, CDCl_3) $\delta = 8.02 - 7.72$ (m, 7H), 7.62 – 7.47 (m, 10H), 7.02 – 6.72 (m, 3H), 5.49 (sext, $J = 7.0$ Hz, 1H), 4.12 (dd, $J = 9.9, 6.7$ Hz, 1H), 3.53 (dd, $J = 9.9, 6.9$ Hz, 1H), 1.92 (s, 6H), 1.54 (d, $J = 7.2$ Hz, 3H) ppm. ^{13}C NMR (101 MHz, CDCl_3) $\delta =$

Chapter 3

155.9, 154.4, 134.1, 133.7, 132.2, 131.2, 130.1, 129.8, 129.4, 129.3, 129.0, 128.5, 124.6, 73.6, 65.4, 19.4, 16.4 ppm (2 aromatic carbon signals are not observed due to signal broadening). ^{19}F NMR (376 MHz, CDCl_3) δ = -153.1 (s), -153.2 (d, J = 2.2 Hz) ppm. IR (neat, cm^{-1}): 2309, 1616, 1558, 1196, 1047, 1020, 888. HRMS calcd. for $(\text{C}_{34}\text{H}_{32}\text{NO})$ $[\text{M}-\text{BF}_4]^+$: 470.2478, found 470.2469.

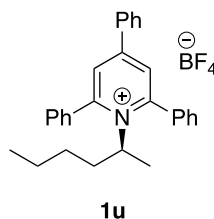


1-((4-(4-fluorobenzyl)morpholin-2-yl)methyl)-2,4,6-tris(4-methoxyphenyl)pyridin-1-ium tetrafluoroborate (1s). Following the General Procedure B, (4-(4-fluorobenzyl)morpholin-2-yl)methanamine (268.9 mg, 1.20 mmol) and 2,4,6-tris(4-methoxyphenyl)pyrylium tetrafluoroborate (486.2 mg, 1.0 mmol) in 1.5 mL of EtOH were used, affording the title compound as a yellow powder (484 mg, 70% yield) by using (DCM/Acetone 10/1) as eluent. **Mp:** 120 – 121 °C. ^1H NMR (400 MHz, CDCl_3) δ = 7.89 – 7.53 (m, 8H), 7.05 (dd, J = 16.5, 7.1 Hz, 8H), 6.93 (t, J = 7.4 Hz, 2H), 4.72 (d, J = 14.9 Hz, 1H), 4.59 (dt, J = 14.6, 7.0 Hz, 1H), 3.87 (s, 6H), 3.85 (s, 3H), 3.56 (brs, 1H), 3.24 (brs, 4H), 2.40 (d, J = 9.0 Hz, 1H), 2.09 (t, J = 7.9 Hz, 1H), 1.91 (d, J = 7.2 Hz, 1H), 1.37 (d, J = 5.6 Hz, 1H) ppm. ^{13}C NMR (101 MHz, CDCl_3) δ = 163.5, 161.6, 157.6 (d, J = 7.2 Hz), 131.2, 130.6 (d, J = 6.6 Hz), 130.6, 129.9, 125.6 (br), 124.6 (br), 115.4, 115.2 (d, J = 21.2 Hz), 114.8, 72.7, 66.4, 61.8, 56.3, 55.8, 55.6, 55.4, 52.2 ppm (2 aromatic carbon signals are not observed due to signal broadening). ^{19}F NMR (376 MHz, CDCl_3) δ = -115.5 (s), -152.9 (s), -152.9 (d, J = 2.4 Hz) ppm. IR (neat, cm^{-1}): 1593, 1506, 1455, 1294, 1241, 1178, 1016, 892, 831. HRMS calcd. for $(\text{C}_{38}\text{H}_{38}\text{FN}_2\text{O}_4)$ $[\text{M}-\text{BF}_4]^+$: 605.2810, found 605.2808.

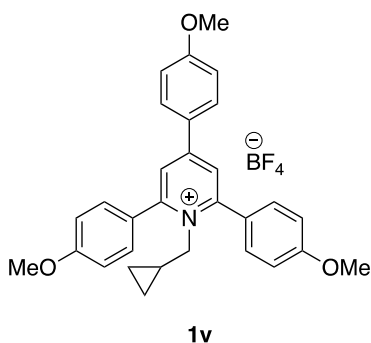


2,4,6-triphenyl-1-((1S,2S,5R)-2,6,6-trimethylbicyclo[3.1.1]heptan-3-yl)pyridin-1-ium tetrafluoroborate (1t). To a solution of triphenylpyrylium tetrafluoroborate (978 mg, 2.47 mmol) and commercially available Pinanamine (454.5 mg, 2.96 mmol) in anhydrous DCM (10 mL), it was added acetic acid (3 drops). The solution was stirred at room temperature for 3 h, then concentrated in vacuo and purified by flash column chromatography (DCM/acetone = 99:1 to 88:12) to give the desired product **1t** (570 mg, 43% yield) as a pink solid. **Mp:** 132 - 134 °C. ^1H NMR (400 MHz, CDCl_3) δ = 8.03 – 7.83 (m, 3H), 7.78 – 7.68 (m, 3H), 7.67 – 7.48 (m, 9H), 7.47 – 7.37 (m, 2H), 5.32 (q, J = 9.7 Hz, 1H), 2.94 – 2.65 (m, 2H), 2.41 (dddd, J = 14.1, 10.2, 4.0, 1.8 Hz, 1H), 1.88 – 1.64 (m, 2H), 1.51 (td, J =

5.9, 1.6 Hz, 1H), 0.99 (s, 3H), 0.79 (d, $J = 6.9$ Hz, 3H), 0.22 (s, 3H), -0.80 (d, $J = 10.1$ Hz, 1H) ppm. ^{13}C NMR (101 MHz, CDCl_3) $\delta = 159.1, 157.6, 155.1, 134.3, 133.7, 133.4, 131.9, 131.5, 130.8, 130.3, 130.2, 129.5, 129.3, 128.6, 128.4, 128.3, 128.3, 126.4, 70.1, 48.0, 42.0, 41.7, 40.1, 35.2, 30.9, 28.3, 21.8, 19.2$ ppm. ^{19}F NMR (376 MHz, CDCl_3) $\delta = -153.3, -153.3$ (d, $J = 2.2$ Hz). Spectroscopic data for **1t** match those previously reported in the literature.^{IV}



1-(hexan-2-yl)-2,4,6-triphenylpyridin-1-ium tetrafluoroborate (1u). Following the General Procedure A, hexan-2-amine (200 mg, 1.5 mmol) and 2,4,6-triphenylpyrylium tetrafluoroborate (500 mg, 1.3 mmol) in 1.5 mL of EtOH were used, affording the product as a white solid (358 mg, 59% yield). **Mp:** 153 - 155 °C. ^1H NMR (400 MHz, CDCl_3) $\delta = 7.95 - 7.64$ (m, 7H), 7.65 - 7.53 (m, 6H), 7.53 - 7.42 (m, 3H), 4.89 (dq, $J = 13.6, 7.0$ Hz, 1H), 1.78 (ddt, $J = 13.8, 11.3, 5.9$ Hz, 1H), 1.49 - 1.33 (m, 4H), 1.15 - 1.01 (m, 2H), 1.01 - 0.88 (m, 1H), 0.87 - 0.78 (m, 1H), 0.75 (t, $J = 7.3$ Hz, 3H) ppm (*1 aromatic proton signal is not observed due to signal broadening*). ^{13}C NMR (101 MHz, CDCl_3) $\delta = 155.2, 134.0, 133.9, 131.9, 130.8, 129.6, 129.3, 128.8, 128.3, 67.1, 36.4, 28.7, 21.8, 21.7, 13.7$ ppm. (*5 aromatic carbon signals are not observed due to signal broadening*) ^{19}F NMR (376 MHz, CDCl_3) $\delta = -153.4$ (s), -153.5 (d, $J = 2.1$ Hz). IR (neat, cm^{-1}): 2928, 1595, 1507, 1456, 1241, 1178, 1024, 865. HRMS calcd. for $(\text{C}_{29}\text{H}_{30}\text{N}) [\text{M}-\text{BF}_4]^+$: 392.2373, found 392.2382.

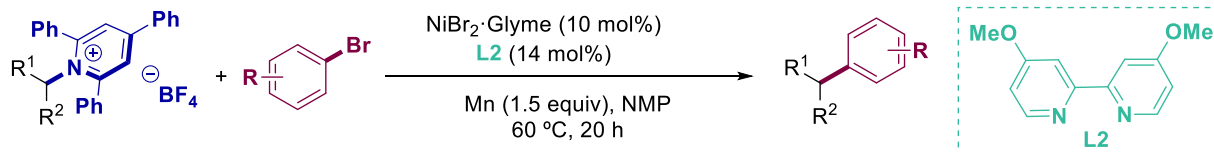


1-(cyclopropylmethyl)-2,4,6-tris(4-methoxyphenyl)pyridin-1-ium tetrafluoroborate (1v). Following the General Procedure B, cyclopropylmethanamine (85.3 mg, 1.20 mmol) and 2,4,6-tris(4-methoxyphenyl)pyrylium tetrafluoroborate (486.2 mg, 1.0 mmol) in 1.5 mL of EtOH were used, affording the title compound as a yellow powder (420.6 mg, 78% yield) by using (DCM/Acetone 10/1) as eluent. **Mp:** 96 - 98 °C. ^1H NMR (400 MHz, CDCl_3) $\delta = 7.85 - 7.68$ (m, 8H), 7.17 - 7.07 (m, 4H), 7.06 - 6.94 (m, 2H), 4.56 (d, $J = 7.1$ Hz, 2H), 3.89 (s, 9H), 0.67 - 0.52 (m, 1H), 0.31 - 0.21 (m, 2H), -0.29 - -0.31 (m, 2H) ppm. ^{13}C NMR (101 MHz, CDCl_3) $\delta = 163.2, 161.6, 156.8, 154.3, 131.1, 129.8, 125.6, 124.9, 115.3, 114.8, 59.4, 55.6, 55.5, 10.8, 4.8$ ppm (*1 aromatic carbon signals is not observed*)

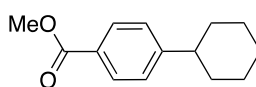
Chapter 3

due to signal broadening). **¹⁹F NMR** (376 MHz, CDCl₃) δ = -153.2 (d, J = 6.5 Hz), -153.3 (d, J = 5.7 Hz) ppm. IR (neat, cm⁻¹): 2931, 1601, 1507, 1454, 1242, 1177, 1024, 832. HRMS calcd. for (C₃₀H₃₀NO₃) [M-BF₄]⁺: 452.2220, found 452.2215.

3.5.4 Ni-catalyzed reductive deaminative arylation with aryl halides

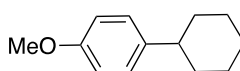


General procedure C: An oven-dried 8 mL screw-cap test tube containing a stirring bar was charged with the aryl bromide (0.20 mmol) and the corresponding pyridinium tetrafluoroborate salt (0.28 mmol, 1.40 equiv). The test tube was introduced in an argon-filled glovebox where manganese (16.5 mg, 0.30 mmol), and a mixture of NiBr₂·glyme (6.2 mg, 10 mol%) and 4,4'-dimethoxy-2,2'-bipyridine (**L2**, 6.0 mg, 14 mol%) in NMP (2 mL) was subsequently added by syringe from a stock solution. The tube was taken out of the glovebox and stirred at 60 °C for 20 h. After the reaction was finished, the reaction mixture was extracted with ethyl acetate and water/brine (3 times). Then, the organic layers were combined, dried over MgSO₄ and concentrated under vacuum. The product was purified by flash chromatography column on silica gel.



3

methyl 4-cyclohexylbenzoate (3). Following **General Procedure C** at r.t, methyl 4-bromobenzoate (43.0 mg, 0.20 mmol) and 1-cyclohexyl-2,4,6-triphenylpyridin-1-ium tetrafluoroborate (**1a**) (133.6 mg, 0.28 mmol) were used, affording the title compound as a colourless liquid (40.1 mg, 92% yield) by using toluene as eluent. In an independent experiment, 38.0 mg (87% yield) were obtained, giving an average of 90% yield. In an independent experiment, a one pot experiment was performed, starting from the amine by precipitation of the pyridinium salt (**1a**) and removing the solvent by filtration: methyl 4-bromobenzoate (137.6 mg, 0.64 mmol) and 1-cyclohexyl-2,4,6-triphenylpyridin-1-ium tetrafluoroborate (**1a**) (427.5 mg, 0.90 mmol) were used at r.t, affording the title compound in 125.6 mg (90%). ¹H NMR (400 MHz, CDCl₃) δ = 7.96 (d, *J* = 8.4 Hz, 2H), 7.27 (d, *J* = 8.4 Hz, 2H), 3.90 (s, 3H), 2.56 (tt, *J* = 11.5, 3.6 Hz, 1H), 1.92 – 1.82 (m, 4H), 1.76 (ddd, *J* = 12.5, 3.1, 1.6 Hz, 1H), 1.50 – 1.18 (m, 5H) ppm. ¹³C NMR (101 MHz, CDCl₃) δ = 167.3, 153.6, 129.8, 127.9, 127.0, 52.1, 44.8, 34.3, 26.9, 26.2 ppm. Spectroscopic data for **3** match those previously reported in the literature.^v

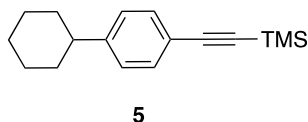


4

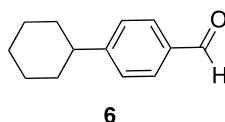
1-cyclohexyl-4-methoxybenzene (4). Following the **General Procedure C** at r.t, methyl 4-iodoanisole (37.4 mg, 0.20 mmol) and 1-cyclohexyl-2,4,6-triphenylpyridin-1-ium tetrafluoroborate

Chapter 3

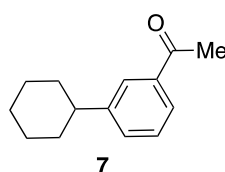
(**1a**) (133.6 mg, 0.28 mmol) were used at room temperature, affording the title compound as a white solid (31.2 mg, 82% yield) by using Hexane/EtOAc (95/5) as eluent. In an independent experiment, 31.0 mg (81%) were obtained, giving an average of 82% yield. **Mp**: 81 - 83 °C. **¹H NMR** (400 MHz, CDCl₃) δ = 7.20 – 7.07 (m, 2H), 6.91 – 6.79 (m, 2H), 3.79 (s, 3H), 2.45 (td, J = 8.0, 4.0 Hz, 1H), 1.93 – 1.79 (m, 4H), 1.75 (dtt, J = 12.8, 3.1, 1.5 Hz, 1H), 1.39 (ddt, J = 11.1, 9.6, 1.7 Hz, 4H), 1.31 – 1.18 (m, 1H) ppm. **¹³C NMR** (101 MHz, CDCl₃) δ = 157.6, 140.4, 127.6, 113.6, 55.2, 43.7, 34.7, 26.9, 26.2 ppm. Spectroscopic data for **4** match those previously reported in the literature.^{vi}



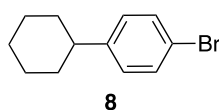
((4-cyclohexylphenyl)ethynyl)trimethylsilane (5). Following **General Procedure C** at r.t, ((4-iodophenyl)ethynyl)trimethylsilane (60 mg, 0.20 mmol) and 1-cyclohexyl-2,4,6-triphenylpyridin-1-ium tetrafluoroborate (**1a**) (133.6 mg, 0.28 mmol) were used, affording the title compound at room temperature as a colourless liquid (32.0 mg, 62% yield) by using pentane as eluent. In an independent experiment, 30.0 mg (59% yield) were obtained, giving an average of 61% yield. **¹H NMR** (300 MHz, CDCl₃) δ = 7.38 (d, J = 8.3 Hz, 2H), 7.13 (d, J = 8.3 Hz, 2H), 2.64 – 2.28 (m, 1H), 1.85 – 1.73 (m, 5H), 1.46 – 1.00 (m, 5H), 0.24 (s, 9H) ppm. **¹³C NMR** (75 MHz, CDCl₃) δ = 148.9, 132.1, 126.9, 120.5, 105.6, 93.3, 44.7, 34.4, 26.9, 26.2, 0.2 ppm. Spectroscopic data for **5** match those previously reported in the literature.^{vii}



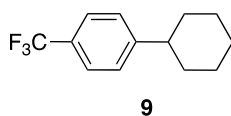
4-cyclohexylbenzaldehyde (6). Following **General Procedure C** at 45 °C, 4-bromobenzaldehyde (39.8 mg, 0.20 mmol) and 1-cyclohexyl-2,4,6-triphenylpyridin-1-ium tetrafluoroborate (**1a**) (133.6 mg, 0.28 mmol) were used at 45 °C, affording the title compound as a white solid (23.7 mg, 63% yield) by using Hexane/*tert*-butyl-methyl ether (98/2) as eluent. In an independent experiment, 23.0 mg (61%) were obtained, giving an average of 62% yield. **Mp**: 116 - 118 °C. **¹H NMR** (400 MHz, CDCl₃) δ = 9.97 (s, 1H), 7.81 – 7.80 (m, 2H), 7.38 – 7.36 (m, 2H), 2.63 – 2.54 (m, 1H), 1.92 – 1.85 (m, 4H), 1.80 – 1.75 (m, 1H), 1.48 – 1.37 (m, 4H), 1.19 (s, 1H) ppm. **¹³C NMR** (101 MHz, CDCl₃) δ = 192.0, 155.4, 134.5, 130.0, 127.5, 44.9, 34.1, 26.7, 26.0 ppm. Spectroscopic data for **6** match those previously reported in the literature.^{viii}



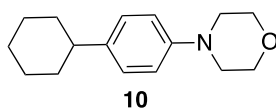
1-(3-cyclohexylphenyl)ethan-1-one (7). Following **General Procedure C** at 45 °C, 1-(3-bromophenyl)ethan-1-one (39.8 mg, 0.20 mmol) and 1-cyclohexyl-2,4,6-triphenylpyridin-1-ium tetrafluoroborate (**1a**) (133.6 mg, 0.28 mmol) were used, affording the title compound as a white solid (26 mg, 64% yield) by using Hexane/ *tert*-butyl-methyl ether (95/5) as eluent. In an independent experiment, 24.6 mg (61%) were obtained, giving an average of 63% yield. **Mp:** 110 - 112 °C. **$^1\text{H NMR}$** (400 MHz, CDCl_3) δ = 7.85 – 7.80 (m, 2H), 7.77 (dt, J = 7.3, 1.7 Hz, 2H), 7.43 (dt, J = 7.3, 1.7 Hz, 2H), 7.40 – 7.36 (m, 1H), 2.60 (s, 3H), 2.59 – 2.50 (m, 1H), 1.96 – 1.81 (m, 4H), 1.81 – 1.73 (m, 1H), 1.50 – 1.34 (m, 4H), 1.31 – 1.26 (m, 1H) ppm. **$^{13}\text{C NMR}$** (101 MHz, CDCl_3) δ = 198.5, 148.6, 137.2, 131.8, 128.5, 126.6, 126.1, 44.5, 34.3, 26.8, 26.7, 26.0 ppm. **IR** (neat, cm^{-1}): 3029, 2921, 2848, 1682, 1591, 1544, 1490, 1394, 1260, 1072. **HRMS** calcd. for ($\text{C}_{14}\text{H}_{19}\text{O}$) [$\text{M}+\text{H}$] $^+$: 203.1430, found 203.1422.



1-bromo-4-cyclohexylbenzene (8). Following **General Procedure C** in DMA at 15 °C, 1-bromo-4-iodobenzene (56.6 mg, 0.20 mmol) and 1-cyclohexyl-2,4,6-triphenylpyridin-1-ium tetrafluoroborate (**1a**) (133.6 mg, 0.28 mmol) were used in DMA at 15 °C, affording the title compound as a colourless oil (42.3 mg, 89% yield) by using Hexane (100) as eluent. In an independent experiment, 41.4 mg (87%) were obtained, giving an average of 88% yield. **$^1\text{H NMR}$** (400 MHz, CDCl_3) δ = 7.44 – 7.29 (m, 2H), 7.16 – 7.02 (m, 2H), 2.46 (td, J = 8.7, 4.2 Hz, 1H), 1.91 – 1.79 (m, 4H), 1.79 – 1.69 (m, 1H), 1.38 (td, J = 9.0, 3.0 Hz, 4H), 1.29 – 1.21 (m, 1H) ppm. **$^{13}\text{C NMR}$** (101 MHz, CDCl_3) δ = 147.0, 131.3, 128.6, 119.3, 44.0, 34.3, 26.8, 26.0 ppm. Spectroscopic data for **8** match those previously reported in the literature.^{ix}

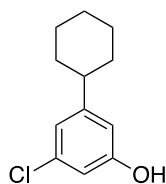


1-cyclohexyl-4-(trifluoromethyl)benzene (9). Following **General Procedure C**, 1-bromo-4-(trifluoromethyl)benzene (45.0 mg, 0.20 mmol) and 1-cyclohexyl-2,4,6-triphenylpyridin-1-ium tetrafluoroborate (**1a**) (133.6 mg, 0.28 mmol) were used, affording the title compound as a colourless oil (30.6 mg, 67% yield) by using Hexane (100) as eluent. In an independent experiment, 30.4 mg (67%) were obtained, giving an average of 67% yield. *Compound volatile under high vacuum.* **$^1\text{H NMR}$** (400 MHz, CDCl_3) δ = 7.55 – 7.53 (m, 2H), 7.32 – 7.30 (m, 2H), 2.60 – 2.53 (m, 1H), 1.91 – 1.83 (m, 4H), 1.80 – 1.73 (m, 1H), 1.49 – 1.35 (m, 4H), 1.32 – 1.24 (m, 1H) ppm. **$^{13}\text{C NMR}$** (101 MHz, CDCl_3) δ = 152.4, 128.6, 127.5, 125.6, 125.6, 125.6, 125.5, 44.9, 34.6, 27.1, 26.4 ppm. **$^{19}\text{F NMR}$** (376 MHz, CDCl_3) δ = -62.3 ppm. Spectroscopic data for **9** match those previously reported in the literature.^x



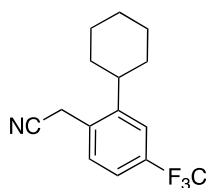
Chapter 3

4-(4-cyclohexylphenyl)morpholine (10). Following **General Procedure C**, 4-(4-bromophenyl)morpholine (48.2 mg, 0.20 mmol) and 1-cyclohexyl-2,4,6-triphenylpyridin-1-ium tetrafluoroborate (**1a**) (105 mg, 0.20 mmol) were used, affording the title compound as a white solid (27.0 mg, 55% yield) by using Hexane/EtOAc (90/10) as eluent. In an independent experiment, 26.0 mg (53%) were obtained, giving an average of 54% yield. $^1\text{H NMR}$ (400 MHz, CDCl_3) δ = 7.14 – 7.12 (m, 2H), 6.87 – 6.85 (m, 2H), 3.94 – 3.80 (m, 4H), 3.20 – 3.07 (m, 4H), 2.50 – 2.37 (m, 1H), 1.92 – 1.78 (m, 4H), 1.73 (ddd, J = 13.9, 3.0, 1.5 Hz, 1H), 1.47 – 1.32 (m, 4H), 1.31 – 1.18 (m, 1H) ppm. $^{13}\text{C NMR}$ (101 MHz, CDCl_3) δ = 149.3, 139.9, 127.4, 115.8, 67.0, 49.7, 43.6, 34.6, 26.9, 26.2 ppm. Spectroscopic data for **10** match those previously reported in the literature.^x



11

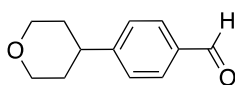
3-chloro-5-cyclohexylphenol (11). Following **General Procedure C**, 3-bromo-5-chlorophenol (36.8 mg, 0.20 mmol) and 1-cyclohexyl-2,4,6-triphenylpyridin-1-ium tetrafluoroborate (**1a**) (133.6 mg, 0.28 mmol) were used, affording the title compound as a colourless oil (21.4 mg, 51% yield) by using Hexane/ Et_2O (90/10) as eluent. In an independent experiment, 20.7 mg (49%) were obtained, giving an average of 50% yield. $^1\text{H NMR}$ (400 MHz, CDCl_3) δ = 6.82 – 6.74 (m, 1H), 6.71 – 6.59 (m, 1H), 6.57 – 6.56 (m, 1H), 4.75 (s, 1H), 2.48 – 2.36 (m, 1H), 1.85 – 1.82 (m, 4H), 1.74 (dd, J = 12.5, 1.8 Hz, 1H), 1.40 – 1.31 (m, 4H), 1.28 – 1.18 (m, 1H) ppm. $^{13}\text{C NMR}$ (101 MHz, CDCl_3) δ = 156.1, 151.4, 134.5, 119.7, 113.2, 112.3, 44.4, 34.1, 26.7, 26.0 ppm **HRMS** calcd. for ($\text{C}_{12}\text{H}_{14}\text{ClO}$) [$\text{M}-\text{H}$] $^-$: 209.0739, found 209.0749



12

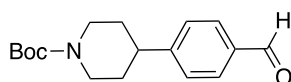
2-(2-cyclohexyl-4-(trifluoromethyl)phenyl)acetonitrile (12). Following **General Procedure C** at 45 °C, 2-(2-bromo-4-(trifluoromethyl)phenyl)acetonitrile (52.6 mg, 0.20 mmol) was used and 1-cyclohexyl-2,4,6-triphenylpyridin-1-ium tetrafluoroborate (**1a**) (133.6 mg, 0.28 mmol) were used, affording the title compound as a colourless liquid (45.4 mg, 85% yield) by using Pentane/EtOAc (30/1) as eluent. In an independent experiment, 41.6 mg (78% yield) were obtained (average of 82% yield). $^1\text{H NMR}$ (400 MHz, CDCl_3) δ = 7.55 (s, 1H), 7.52 – 7.40 (m, 2H), 3.80 (s, 2H), 2.65 (ddd, J = 11.5, 8.3, 3.1 Hz, 1H), 1.95 – 1.79 (m, 5H), 1.60 – 1.25 (m, 5H) ppm. $^{13}\text{C NMR}$ (101 MHz, CDCl_3) δ = 146.7, 131.4 – 130.9 (m), 129.7, 124.0 (q, J = 272.3 Hz), 123.7 (q, J = 3.7 Hz), 123.4 (q, J = 3.7 Hz), 117.4, 40.4, 33.9, 26.9, 26.0, 21.6 ppm. $^{19}\text{F NMR}$ (376 MHz, CDCl_3) δ = -62.8 ppm. IR (neat, cm^{-1}): 2926, 2854, 2247,

1617, 1419, 1328, 1276, 1097, 1004, 910, 817. **HRMS** calcd. for ($C_{15}H_{16}F_3N$) $[M+H]^+$: 268.1308, found 268.1310.



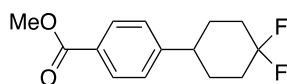
13

4-(tetrahydro-2H-pyran-4-yl)benzaldehyde (13). Following **General Procedure C** at 45 °C, 4-bromobenzaldehyde (36.8 mg, 0.20 mmol) and 2,4,6-triphenyl-1-(tetrahydro-2H-pyran-4-yl)pyridin-1-ium tetrafluoroborate (**1b**) (134 mg, 0.28 mmol) were used at 45 °C, affording the title compound as a pale yellow solid (34 mg, 89% yield) by using Hexane/EtOAc (90/10) as eluent. In an independent experiment, a gram scale was performed: 4-bromobenzaldehyde (1.0 g, 5.44 mmol) and 2,4,6-triphenyl-1-(tetrahydro-2H-pyran-4-yl)pyridin-1-ium tetrafluoroborate (**1b**) (3.6 g, 7.6 mmol) were used at 45 °C during 48h, affording the title compound in 807 mg (78%). **Mp**: 54 - 55 °C. **1H NMR** (400 MHz, $CDCl_3$) δ = 9.99 (s, 1H), 7.89 – 7.80 (m, 2H), 7.40 – 7.38 (m, 2H), 4.18 – 4.03 (m, 2H), 3.55 (td, J = 11.5, 2.5 Hz, 2H), 2.86 (tt, J = 11.6, 4.4 Hz, 1H), 1.93 – 1.74 (m, 4H) ppm. **^{13}C NMR** (101 MHz, $CDCl_3$) δ = 191.9, 152.9, 134.9, 130.1, 127.5, 68.1, 41.9, 33.5 ppm. **IR** (neat, cm^{-1}): 3044, 2947, 2839, 2752, 1690, 1602, 1572, 1312, 1166, 1120. **HRMS** calcd. for ($C_{12}H_{15}O_2$) $[M+H]^+$: 191.1067, found 191.1072.



14

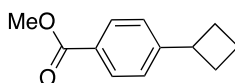
tert-butyl 4-(4-formylphenyl)piperidine-1-carboxylate (14). Following **General Procedure C** at 45 °C, 4-bromobenzaldehyde (36.8 mg, 0.20 mmol) and 1-(1-(tert-butoxycarbonyl)piperidin-4-yl)-2,4,6-triphenylpyridin-1-ium tetrafluoroborate (**1c**) (168 mg, 0.28 mmol) were used at 45 °C, affording the title compound as a white solid (40.0 mg, 69% yield) by using Hexane/EtOAc (90/10) as eluent. In an independent experiment, 38 mg (65%) were obtained, giving an average of 67% yield. **Mp**: 120 - 122 °C. **1H NMR** (400 MHz, $CDCl_3$) δ = 9.98 (s, 1H), 7.89 – 7.77 (m, 2H), 7.43 – 7.31 (m, 2H), 4.27 (d, J = 13.4 Hz, 1H), 2.82 (t, J = 12.8 Hz, 2H), 2.72 (dt, J = 12.2, 3.6 Hz, 1H), 1.84 (d, J = 13.4 Hz, 2H), 1.65 (dq, J = 12.6, 4.4 Hz, 2H), 1.49 (s, 9H) ppm. **^{13}C NMR** (101 MHz, $CDCl_3$) δ = 191.9, 154.8, 152.9, 134.9, 130.1, 127.5, 79.6, 43.0, 32.8, 28.5 ppm. Spectroscopic data for **14** match those previously reported in the literature.^{XI}



15

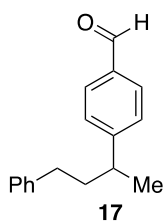
Chapter 3

methyl 4-(4,4-difluorocyclohexyl)benzoate (15). Following **General Procedure C**, methyl 4-bromobenzoate (43 mg, 0.20 mmol) and 1-(4,4-difluorocyclohexyl)-2,4,6-triphenylpyridin-1-ium tetrafluoroborate (**1d**) (143.6 mg, 0.28 mmol) were used, affording the title compound (30.0 mg, 59% yield) as a colourless oil by using toluene as eluent. In an independent experiment, 29.6 mg (58% yield) were obtained, giving an average of 59% yield. $^1\text{H NMR}$ (400 MHz, CDCl_3) δ = 7.98 (d, J = 8.4 Hz, 2H), 7.29 (d, J = 8.2 Hz, 2H), 3.91 (s, 3H), 2.67 (t, J = 11.4 Hz, 1H), 2.30 – 2.16 (m, 2H), 2.00 – 1.75 (m, 6H) ppm. $^{13}\text{C NMR}$ (101 MHz, CDCl_3) δ = 167.1, 150.6 (d, J = 2.4 Hz), 130.1, 128.7, 127.0, 121.9 (dd, J = 242.9, 238.1 Hz), 52.2, 42.8 (d, J = 1.8 Hz), 34.1 (dd, J = 25.7, 22.8 Hz), 30.2 (d, J = 10.0 Hz) ppm. $^{19}\text{F NMR}$ (376 MHz, CDCl_3) δ = -91.9 (d, J = 236.4 Hz), -102.5 (dt, J = 235.9, 34.6 Hz) ppm. IR (neat, cm^{-1}): 2940, 1717, 1608, 1434, 1275, 1096, 957, 761. HRMS calcd. for ($\text{C}_{14}\text{H}_{17}\text{F}_2\text{O}_2$) [$\text{M}+\text{H}$] $^+$: 255.1191, found 255.1181



16

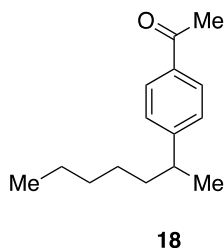
methyl 4-cyclobutylbenzoate (16). Following **General Procedure C**, methyl 4-bromobenzoate (43 mg, 0.20 mmol) and 1-cyclobutyl-2,4,6-triphenylpyridin-1-ium tetrafluoroborate (**1e**) (125.7 mg, 0.28 mmol) were used, affording the title compound (25.0 mg, 65% yield) as a colourless oil by using Pentane/EtOAc (50/50) as eluent. In an independent experiment, 26.2 mg (69% yield) were obtained, giving an average of 67% yield. $^1\text{H NMR}$ (400 MHz, CDCl_3) δ = 7.96 (d, J = 8.3 Hz, 2H), 7.27 (d, J = 8.0 Hz, 2H), 3.90 (s, 3H), 3.60 (quint, J = 8.6 Hz, 1H), 2.38 (dt, J = 10.4, 8.0 Hz, 2H), 2.23 – 2.10 (m, 2H), 2.09 – 1.97 (m, 1H), 1.93 – 1.82 (m, 1H) ppm. $^{13}\text{C NMR}$ (101 MHz, CDCl_3) δ = 167.3, 151.8, 129.7, 127.7, 126.4, 52.1, 40.4, 29.7, 18.4 ppm. Spectroscopic data for **16** match those previously reported in the literature.^{XII}



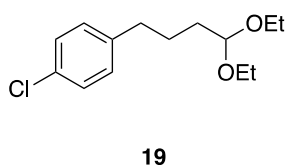
17

4-(4-phenylbutan-2-yl)benzaldehyde (17). Following **General Procedure C** at 45 °C, 4-bromobenzaldehyde (37.0 mg, 0.20 mmol) and 1-(4-phenylbutan-2-yl) triphenylpyridin-1-ium tetrafluoroborate (**1f**) (147.6 mg, 0.28 mmol) were used, affording the title compound as a colourless liquid (36.7 mg, 77% yield) at 45 °C by using toluene as eluent. In an independent experiment, 36.0 mg (76% yield) were obtained, giving an average of 77% yield. $^1\text{H NMR}$ (400 MHz, CDCl_3) δ = 9.99 (s, 1H), 7.84 (d, J = 8.3 Hz, 2H), 7.37 (d, J = 8.3 Hz, 2H), 7.30 – 6.93 (m, 5H), 2.82 (h, J = 7.0 Hz, 1H), 2.59 – 2.42 (m, 2H), 2.01 – 1.86 (m, 2H), 1.31 (d, J = 7.0 Hz, 3H) ppm. $^{13}\text{C NMR}$ (101 MHz, CDCl_3) δ = 192.2, 154.9, 142.1, 134.9, 130.2, 128.5, 128.5, 127.9, 126.0, 39.9, 39.8, 33.9, 22.3 ppm. IR (neat, cm^{-1}): 3024, 2958, 2924, 2854, 1684, 1603, 1574, 1454, 1418, 1210, 1167, 828, 720. HRMS calcd. for

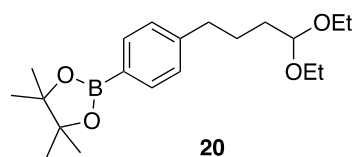
($C_{17}H_{18}O$) [$M+H$] $^+$: 239.1430, found 239.1431.



1-(4-(heptan-2-yl)phenyl)ethan-1-one (18). Following **General Procedure C** at 45 °C, 1-(4-bromophenyl)ethan-1-one (39.8 mg, 0.20 mmol) and 1-(heptan-2-yl)-2,4,6-triphenylpyridin-1-ium tetrafluoroborate (**1g**) (147.6 mg, 0.28 mmol) were used at 45 °C, affording the title compound as a colourless oil (28.3 mg, 65% yield) by using Hexane/ *tert*-butyl-methyl ether (95/5) as eluent. In an independent experiment, 26.6 mg (61%) were obtained, giving an average of 63% yield. 1H NMR (400 MHz, $CDCl_3$) δ = 7.90 – 7.88 (m, 2H), 7.31 – 7.25 (m, 2H), 2.75 (sext, J = 7.0 Hz, 1H), 2.58 (s, 3H), 1.60 – 1.54 (m, 3H), 1.27 – 1.22 (m, 7H), 1.15 – 1.13 (m, 1H), 0.8 (t, J = 7.0 Hz, 3H) ppm. ^{13}C NMR (101 MHz, $CDCl_3$) δ = 197.9, 153.8, 135.1, 128.5, 127.2, 40.1, 38.1, 31.8, 27.3, 26.5, 22.5, 22.0, 14.0 ppm. IR (neat, cm^{-1}): 2955, 2924, 2853, 1682, 1604, 1507, 1456, 4263, 1180. HRMS calcd. for ($C_{15}H_{23}O$) [$M+H$] $^+$: 219.1743, found 219.1749.



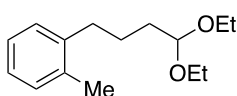
1-chloro-4-(4,4-diethoxybutyl)benzene (19). Following **General Procedure C**, 1-bromo-4-chlorobenzene (39.1 mg, 0.20 mmol) and 1-(4,4-diethoxybutyl)-2,4,6-tris(4-methoxyphenyl)pyridin-1-ium tetrafluoroborate (**1h**) (176 mg, 0.28 mmol) were used, affording the title compound as a white solid (31.7 mg, 62% yield) by using Hexane/EtOAc (95/5) as eluent. In an independent experiment, 31.2 mg (61%) were obtained, giving an average of 62% yield. **Mp**: 117 - 119 °C. 1H NMR (400 MHz, $CDCl_3$) δ = 7.50 – 7.48 (m, 2H), 7.29 – 7.17 (m, 2H), 4.51 (t, J = 5.4 Hz, 1H), 3.63 (dq, J = 9.4, 7.0 Hz, 2H), 3.48 (dq, J = 9.4, 7.1 Hz, 2H), 2.67 (t, J = 7.3 Hz, 2H), 1.80 – 1.63 (m, 4H), 1.20 (t, J = 7.0 Hz, 6H) ppm. ^{13}C NMR (101 MHz, $CDCl_3$) δ = 141.2, 138.6, 128.8, 126.9, 102.8, 261.0, 35.3, 33.3, 26.6, 215.3 ppm. IR (neat, cm^{-1}): 3029, 1685, 1490, 109, 1310, 1200, 1014, 802. GC-MS calcd. for ($C_{14}H_{21}ClO_2$) [M] $^+$: 256.1, found m/z 256.1.



2-(4-(4,4-diethoxybutyl)phenyl)-4,4,5,5-tetramethyl-1,3,2-dioxaborolane (20). Following **General Procedure C**, 2-(4-bromophenyl)-4,4,5,5-tetramethyl-1,3,2-dioxaborolane (56.4 mg, 0.20

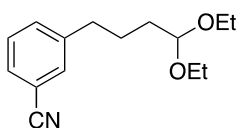
Chapter 3

mmol) and 1-(4,4-diethoxybutyl)-2,4,6-tris(4-methoxyphenyl)pyridin-1-ium tetrafluoroborate (**1h**) (176 mg, 0.28 mmol) were used, affording the title compound as a yellow oil (52.2 mg, 75% yield) by using Hexane/EtOAc (90/10) as eluent. In an independent experiment, 45.4 mg (71%) were obtained, giving an average of 73% yield. $^1\text{H NMR}$ (400 MHz, CDCl_3) δ = 7.73 – 7.73 (m, 2H), 7.23 – 7.14 (m, 2H), 4.48 (t, J = 5.4 Hz, 1H), 3.61 (dq, J = 9.4, 7.0 Hz, 2H), 3.46 (dq, J = 9.4, 7.1 Hz, 2H), 2.64 (t, J = 7.3 Hz, 2H), 1.73 – 1.61 (m, 4H), 1.34 (s, 12H), 1.19 (t, J = 7.1 Hz, 6H) ppm. $^{13}\text{C NMR}$ (101 MHz, CDCl_3) δ = 145.8, 134.9, 127.9, 102.8, 83.6, 60.9, 35.9, 33.2, 26.4, 24.8, 15.3 ppm. (*the signal for the aromatic carbon attached to boron is not observed due to quadrupolar relaxation*). $^{11}\text{B NMR}$ (128 MHz, CDCl_3) δ = 32.1 ppm. IR (neat, cm^{-1}): 2974, 2928, 1724, 1610, 1356, 1318, 1141, 1087, 858. HRMS calcd. for ($\text{C}_{22}\text{H}_{32}\text{O}_4^{10}\text{B}$) $[\text{M}+\text{Na}]^+$: 370.2424, found 370.2413.



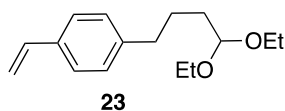
21

1-(4,4-diethoxybutyl)-2-methylbenzene (21). Following **General Procedure C**, 1-bromo-2-methylbenzene (56.4 mg, 0.20 mmol) and 1-(4,4-diethoxybutyl)-2,4,6-tris(4-methoxyphenyl)pyridin-1-ium tetrafluoroborate (**1h**) (176 mg, 0.28 mmol) were used, affording the title compound as a yellow oil (36.4 mg, 77% yield) by using Hexane/EtOAc (95/5) as eluent. In an independent experiment, 36.3 mg (77%) were obtained, giving an average of 77% yield. $^1\text{H NMR}$ (400 MHz, CDCl_3) δ = 7.18 – 7.02 (m, 4H), 4.51 (t, J = 5.5 Hz, 1H), 3.64 (dq, J = 9.4, 7.0 Hz, 2H), 3.49 (dq, J = 9.4, 7.1 Hz, 2H), 2.62 (t, J = 7.1 Hz, 2H), 2.31 (s, 3H), 1.76 – 1.62 (m, 4H), 1.20 (t, J = 7.1 Hz, 6H) ppm. $^{13}\text{C NMR}$ (101 MHz, CDCl_3) δ = 140.5, 135.8, 130.1, 128.8, 125.9, 102.8, 77.0, 60.9, 33.5, 33.0, 25.4, 19.3, 15.3 ppm. IR (neat, cm^{-1}): 2971, 2927, 1570, 1456, 1122, 1058, 976. HRMS calcd. for ($\text{C}_{11}\text{H}_{13}$) $[\text{M}-(\text{CH}_2)_3(\text{OEt})_2]^+$: 145.1012, found 145.1013.

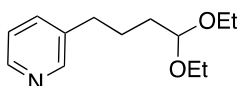


22

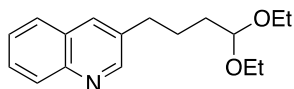
3-(4,4-diethoxybutyl)benzonitrile (22). Following **General Procedure C**, 3-bromobenzonitrile (36.4 mg, 0.20 mmol) and 1-(4,4-diethoxybutyl)-2,4,6-tris(4-methoxyphenyl)pyridin-1-ium tetrafluoroborate (**1h**) (176 mg, 0.28 mmol) were used, affording the title compound as a yellow oil (42.0 mg, 85% yield) by using Hexane/EtOAc (95/5) as eluent. In an independent experiment, 40.0 mg (81%) were obtained, giving an average of 83% yield. $^1\text{H NMR}$ (400 MHz, CDCl_3) δ = 7.52 – 7.46 (m, 2H), 7.45 – 7.32 (m, 2H), 4.49 (t, J = 5.3 Hz, 1H), 3.63 (dq, J = 9.4, 7.0 Hz, 2H), 3.48 (dq, J = 9.4, 7.0 Hz, 2H), 2.67 (t, J = 7.4 Hz, 2H), 1.77 – 1.57 (m, 4H), 1.20 (t, J = 7.0 Hz, 6H) ppm. $^{13}\text{C NMR}$ (101 MHz, CDCl_3) δ = 143.7, 133.0, 132.0, 129.6, 129.1, 119.0, 112.3, 102.6, 61.2, 35.2, 33.0, 26.1, 15.3 ppm. IR (neat, cm^{-1}): 2956, 2925, 2855, 1720, 1604, 1508, 1387, 1269, 1144, 1112, 1089, 966, 853, 767. HRMS calcd. for ($\text{C}_{15}\text{H}_{21}\text{NNaO}_2$) $[\text{M}+\text{Na}]^+$: 270.1464, found 270.1470.



1-(4,4-diethoxybutyl)-4-vinylbenzene (23). Following **General Procedure C**, 1-bromo-4-vinylbenzene (36.6 mg, 0.20 mmol) and 1-(4,4-diethoxybutyl)-2,4,6-tris(4-methoxyphenyl)pyridin-1-ium tetrafluoroborate (**1h**) (151.8 mg, 0.28 mmol) were used, affording the title compound (30.0 mg, 60% yield) as a colorless oil by using Pentane/EtOAc (30/1) as eluent. In an independent experiment, 28.0 mg (56% yield) were obtained, giving an average of 58% yield. $^1\text{H NMR}$ (400 MHz, CDCl_3) δ = 7.32 (d, J = 8.1 Hz, 2H), 7.14 (d, J = 8.1 Hz, 2H), 6.69 (dd, J = 17.6, 10.9 Hz, 1H), 5.70 (dd, J = 17.6, 1.1 Hz, 1H), 5.19 (dd, J = 10.9, 1.0 Hz, 1H), 4.49 (t, J = 5.3 Hz, 1H), 3.62 (dq, J = 9.4, 7.1 Hz, 2H), 3.47 (dq, J = 9.4, 7.1 Hz, 2H), 2.62 (t, J = 7.0 Hz, 2H), 1.72 – 1.60 (m, 4H), 1.19 (t, J = 7.1 Hz, 6H) ppm. $^{13}\text{C NMR}$ (101 MHz, CDCl_3) δ = 142.2, 136.8, 135.4, 128.7, 126.3, 113.1, 102.9, 61.1, 35.6, 33.3, 26.7, 15.5 ppm. $^{19}\text{F NMR}$ (376 MHz, CDCl_3) δ = -115.68 ppm. IR (neat, cm^{-1}): 2972, 2925, 2870, 1867, 1646, 1557, 1517, 1456, 1127, 1063, 988. HRMS calcd. for ($\text{C}_{16}\text{H}_{24}\text{O}_2$) [$\text{M}+\text{H}$] $^+$: 249.1849, found 249.1852.



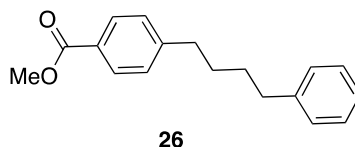
3-(4,4-diethoxybutyl)pyridine (24). Following **General Procedure C**, 3-pyridine (31.6 mg, 0.20 mmol) and 1-(4,4-diethoxybutyl)-2,4,6-tris(4-methoxyphenyl)pyridin-1-ium tetrafluoroborate (**1h**) (151.8 mg, 0.28 mmol) were used, affording the title compound (34.9 mg, 78% yield) as a colourless oil by using Pentane/EtOAc (60/30) as eluent. In an independent experiment, 35.0 mg (78% yield) were obtained, giving an average of 78% yield. $^1\text{H NMR}$ (400 MHz, CDCl_3) δ = 8.44 (brs, 2H), 7.49 (d, J = 7.8 Hz, 1H), 7.20 (dd, J = 7.6, 4.8 Hz, 1H), 4.49 (t, J = 5.3 Hz, 1H), 3.62 (dq, J = 9.4, 7.1 Hz, 2H), 3.47 (dq, J = 9.4, 7.1 Hz, 2H), 2.63 (t, J = 7.2 Hz, 2H), 1.81 – 1.53 (m, 4H), 1.19 (t, J = 7.1 Hz, 6H) ppm. $^{13}\text{C NMR}$ (101 MHz, CDCl_3) δ = 150.1, 147.5, 137.6, 136.0, 123.4, 102.8, 61.3, 33.2, 32.9, 26.4, 15.5 ppm. IR (neat, cm^{-1}): 2971, 2920, 2869, 1420, 1373, 1124, 1057, 978, 720. HRMS calcd. for ($\text{C}_{13}\text{H}_{22}\text{NO}_2$) [$\text{M}+\text{H}$] $^+$: 224.1645, found 224.1645.



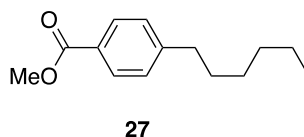
3-(4,4-diethoxybutyl)quinolone (25). Following **General Procedure C**, 3-bromoquinoline (41.6 mg, 0.20 mmol) and 1-(4,4-diethoxybutyl)-2,4,6-tris(4-methoxyphenyl)pyridin-1-ium tetrafluoroborate (**1h**) (176 mg, 0.28 mmol) were used, affording the title compound as a yellow oil (47.0 mg, 86% yield) by using Hexane/EtOAc (85/15) as eluent. In an independent experiment, 45.9 mg (84%) were obtained, giving an average of 85% yield. $^1\text{H NMR}$ (400 MHz, CDCl_3) δ = 8.79 (d, J =

Chapter 3

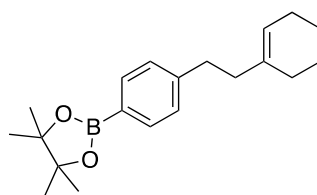
2.2 Hz, 1H), 8.17 – 8.02 (m, 1H), 7.93 (dd, $J = 2.2, 1.0$ Hz, 1H), 7.77 (dd, $J = 8.1, 1.5$ Hz, 1H), 7.66 (ddd, $J = 8.4, 6.9, 1.5$ Hz, 1H), 7.52 (ddd, $J = 8.1, 6.9, 1.2$ Hz, 1H), 4.52 (t, $J = 5.5$ Hz, 1H), 3.63 (dq, $J = 9.4, 7.1$ Hz, 2H), 3.48 (dq, $J = 9.4, 7.1$ Hz, 2H), 2.83 (t, $J = 7.5$ Hz, 2H), 1.87 – 1.75 (m, 2H), 1.74 – 1.67 (m, 2H), 1.20 (t, $J = 7.0$ Hz, 6H) ppm. $^{13}\text{C NMR}$ (101 MHz, CDCl_3) $\delta = 151.8, 146.6, 134.8, 134.4, 129.0, 128.7, 128.1, 127.3, 126.6, 102.7, 61.1, 33.1, 32.9, 26.2, 15.3$ ppm. IR (neat, cm^{-1}): 2971, 2925, 2862, 1716, 1512, 1495, 1373, 1329, 1122, 1058, 958. HRMS calcd. for ($\text{C}_{17}\text{H}_{24}\text{NO}_2$) $[\text{M}+\text{H}]^+$: 274.1802, found 274.1811.



methyl 4-(4-phenylbutyl)benzoate (26). Following **General Procedure C**, methyl 4-bromobenzoate (43 mg, 0.20 mmol) and 2,4,6-tris(4-methoxyphenyl)-1-(4-phenylbutyl)pyridin-1-ium tetrafluoroborate (**1i**) (172.0 mg, 0.28 mmol) were used, affording the title compound (40.2 mg, 75% yield) as a colorless oil by using Pentane/EtOAc (30/1) as eluent. In an independent experiment, 39.0 mg (72% yield) were obtained, giving an average of 74% yield. $^1\text{H NMR}$ (400 MHz, CDCl_3) $\delta = 7.94$ (d, $J = 8.3$ Hz, 2H), 7.28 (d, $J = 7.3$ Hz, 2H), 7.23 (d, $J = 8.4$ Hz, 2H), 7.19 – 7.14 (m, 3H), 3.90 (s, 3H), 2.69 (t, $J = 7.1$ Hz, 2H), 2.64 (t, $J = 7.1$ Hz, 2H), 1.67 (dt, $J = 6.8, 2.6$ Hz, 4H) ppm. $^{13}\text{C NMR}$ (101 MHz, CDCl_3) $\delta = 167.3, 148.2, 142.5, 129.8, 128.6, 128.5, 128.4, 125.9, 52.1, 36.0, 35.9, 31.1, 30.8$ ppm. IR (neat, cm^{-1}): 2926, 2853, 1717, 1607, 1433, 1272, 1176, 1106, 1019, 760, 719. HRMS calcd. for ($\text{C}_{18}\text{H}_{21}\text{O}_2$) $[\text{M}+\text{H}]^+$: 269.1536, found 269.1547.



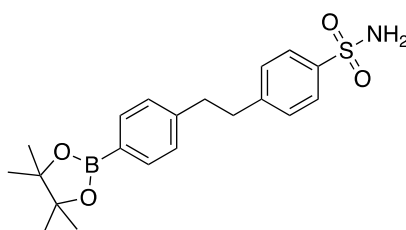
methyl 4-hexylbenzoate (27). Following **General Procedure C**, methyl 4-bromobenzoate (43 mg, 0.20 mmol) and 2,4,6-tris(4-methoxyphenyl)-1-hexylpyridin-1-ium tetrafluoroborate (**1j**) (160.0 mg, 0.28 mmol) were used, affording the title compound (28.6 mg, 65% yield) as a colorless oil by using Pentane/EtOAc (30/1) as eluent. In an independent experiment, 27.8 mg (63% yield) were obtained, giving an average of 64% yield. $^1\text{H NMR}$ (400 MHz, CDCl_3) $\delta = 7.95$ (d, $J = 8.4$ Hz, 2H), 7.23 (d, $J = 8.5$ Hz, 2H), 3.90 (s, 3H), 3.04 – 2.27 (m, 2H), 1.62 (p, $J = 7.7$ Hz, 2H), 1.41 – 1.17 (m, 6H), 1.02 – 0.74 (m, 3H) ppm. $^{13}\text{C NMR}$ (101 MHz, CDCl_3) $\delta = 167.3, 148.6, 129.7, 128.5, 127.8, 52.0, 36.1, 31.8, 31.2, 29.0, 22.7, 14.2$ ppm. Spectroscopic data for **16** match those previously reported in the literature.^{xiii}



28

2-(4-(2-(cyclohex-1-en-1-yl)ethyl)phenyl)-4,4,5,5-tetramethyl-1,3,2-dioxaborolane (28).

Following **General Procedure C**, 2-(4-bromophenyl)-4,4,5,5-tetramethyl-1,3,2-dioxaborolane (56.4 mg, 0.20 mmol) and 1-(2-(cyclohex-1-en-1-yl)ethyl)-2,4,6-tris(4-methoxyphenyl)pyridin-1-ium tetrafluoroborate (**1k**) (167 mg, 0.28 mmol) were used, affording the title compound as a white solid (37.4 mg, 60% yield) by using Hexane/EtOAc (95/5) as eluent. In an independent experiment, 36 mg (58%) were obtained, giving an average of 59% yield. **Mp**: 66 - 68 °C. **$^1\text{H NMR}$** (400 MHz, CDCl_3) δ = 7.80 – 7.67 (m, 2H), 7.22 – 7.15 (m, 2H), 5.41 (dq, J = 3.8, 1.7 Hz, 1H), 2.79 – 2.65 (m, 2H), 2.22 (t, J = 7.9 Hz, 2H), 1.99 – 1.95 (m, 4H), 1.69 – 1.48 (m, 4H), 1.34 (s, 12H) ppm. **$^{13}\text{C NMR}$** (101 MHz, CDCl_3) δ = 146.1, 137.2, 134.8, 127.9, 121.4, 83.6, 39.8, 34.7, 28.5, 25.2, 24.8, 23.0, 22.5 ppm. (*the signal for the aromatic carbon attached to boron is not observed due to quadrupolar relaxation*). **$^{11}\text{B NMR}$** (128 MHz, CDCl_3) δ = 30.2 ppm. **IR** (neat, cm^{-1}): 2977, 2922, 1610, 1396, 1357, 1319, 1261, 1087, 1140. **HRMS** calcd. for ($\text{C}_{20}\text{H}_{29}\text{NaO}_2^{10}\text{B}$) [$\text{M}+\text{Na}$] $^+$: 334.2189, found 334.2175.

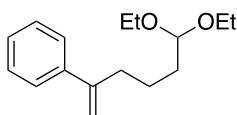


29

4-(4-(4,4,5,5-tetramethyl-1,3,2-dioxaborolan-2-yl)phenethyl)benzenesulfonamide (29).

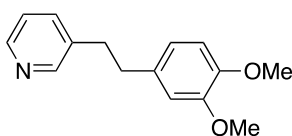
Following **General Procedure C**, 2-(4-bromophenyl)-4,4,5,5-tetramethyl-1,3,2-dioxaborolane (56.4 mg, 0.20 mmol) and 2,4,6-tris(4-methoxyphenyl)-1-(4-sulfamoylphenethyl)pyridin-1-ium tetrafluoroborate (**1l**) (188 mg, 0.28 mmol) were used, affording the title compound as a white solid (51.1 mg, 66% yield) by using Hexane/EtOAc (70/30) as eluent. In an independent experiment, 50 mg (65%) were obtained, giving an average of 66% yield. **Mp**: 138 - 140 °C. **$^1\text{H NMR}$** (400 MHz, CDCl_3) δ = 7.87 – 7.79 (m, 2H), 7.75 – 7.68 (m, 2H), 7.29 – 7.26 (m, 2H), 7.22 – 7.11 (m, 2H), 4.91 (brs, 2H, NH_2), 3.0 – 2.94 (m, 4H), 1.34 (s, 12H) ppm. **$^{13}\text{C NMR}$** (101 MHz, CDCl_3) δ = 147.0, 144.0, 139.6, 135.0, 129.2, 127.9, 126.5, 83.7, 37.5, 37.4, 24.8 ppm. (*the signal for the aromatic carbon attached to boron is not observed due to quadrupolar relaxation*). **$^{11}\text{B NMR}$** (128 MHz, CDCl_3) δ = 30.8 ppm. **IR** (neat, cm^{-1}): 3307, 3243, 2943, 2922, 2856, 1605, 1396, 1361, 1313, 1141, 1087. **HRMS** calcd. for ($\text{C}_{20}\text{H}_{26}\text{NaNO}_4\text{S}^{10}\text{B}$) [$\text{M}+\text{Na}$] $^+$: 410.1568, found 410.1578.

Chapter 3



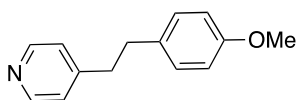
30

(6,6-diethoxyhex-1-en-2-yl)benzene (30). Following **General Conditions C**, (1-bromovinyl)benzene (36.7 mg, 0.20 mmol) and 1-(4,4-diethoxybutyl)-2,4,6-tris(4-methoxyphenyl)pyridin-1-ium tetrafluoroborate (**1h**) (176 mg, 0.28 mmol) were used, affording the title compound as a colourless oil (27.3 mg, 55% yield) by using Hexane/EtOAc (90/10) as eluent. In an independent experiment, 26.8 mg (54%) were obtained, giving an average of 55% yield. **¹H NMR** (400 MHz, CDCl₃) δ = 7.44 – 7.35 (m, 2H), 7.34 – 7.30 (m, 2H), 7.28 – 7.15 (m, 1H), 5.27 (d, J = 1.5 Hz, 1H), 5.06 (d, J = 1.4 Hz, 1H), 4.47 (t, J = 5.7 Hz, 1H), 3.60 (dq, J = 9.4, 7.0 Hz, 2H), 3.45 (dq, J = 9.4, 7.1 Hz, 2H), 2.53 (td, J = 7.5, 1.3 Hz, 2H), 1.70 – 1.59 (m, 2H), 1.58 – 1.47 (m, 2H), 1.17 (t, J = 7.1 Hz, 6H) ppm. **¹³C NMR** (101 MHz, CDCl₃) δ = 148.2, 141.2, 128.2, 127.3, 126.1, 112.5, 102.7, 60.8, 35.0, 33.1, 23.3, 15.3 ppm. **IR** (neat, cm⁻¹): 2971, 2927, 2869, 1652, 1373, 1122, 1058. **HRMS** calcd. for (C₂₀H₂₉NaO₂¹⁰B) [M]⁺: 248.1771, found 248.1775.



31

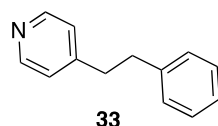
3-(3,4-dimethoxyphenethyl)pyridine (31). Following **General Procedure C**, 3-bromopyridine (31.6 mg, 0.20 mmol) and 1-(3,4-dimethoxyphenethyl)-2,4,6-tris(4-methoxyphenyl)pyridin-1-ium (1m) (181.7 mg, 0.28 mmol) were used, affording the title compound as a colourless liquid (34.0 mg, 70% yield) by using Pentane/EtOAc (60/30) as eluent. In an independent experiment, 35.6 mg (73% yield) were obtained, giving an average of 72% yield. **¹H NMR** (400 MHz, CDCl₃) δ = 8.45 – 8.42 (m, 2H), 7.41 (d, J = 7.8 Hz, 1H), 7.18 (dd, J = 7.7, 4.8 Hz, 1H), 6.77 (d, J = 8.1 Hz, 1H), 6.67 (dd, J = 8.1, 2.0 Hz, 1H), 6.61 (d, J = 1.9 Hz, 1H), 3.85 (s, 3H), 3.82 (s, 3H), 2.96 – 2.80 (m, 4H) ppm. **¹³C NMR** (101 MHz, CDCl₃) δ = 150.1, 148.9, 147.5, 137.0, 136.2, 133.5, 123.3, 120.5, 112.0, 111.4, 56.0, 55.9, 37.2, 35.3 ppm. **IR** (neat, cm⁻¹): 2931, 2831, 1589, 1512, 1456, 1418, 1257, 1233, 1145, 1025, 933, 853, 803, 720. **HRMS** calcd. for (C₁₅H₁₈NO₂) [M+H]⁺: 244.1338, found 244.1341.



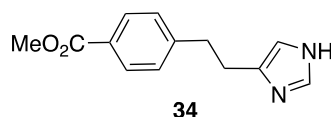
32

4-(4-methoxyphenethyl)pyridine (32). Following **General Procedure C**, 4-bromoanisole (37.2 mg, 0.20 mmol) and 2,4,6-tris(4-methoxyphenyl)-1-(2-(pyridin-4-yl)ethyl)pyridin-1-ium (**1n**) (165.2 mg, 0.28 mmol) were used, affording the title compound as a colourless liquid (28.0 mg, 66% yield) by

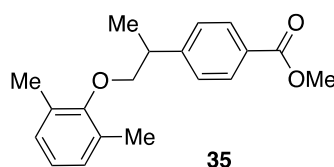
using Pentane/EtOAc (50/10) as eluent. In an independent experiment, 30.0 mg (70% yield) were obtained, giving an average of 68% yield. $^1\text{H NMR}$ (400 MHz, CDCl_3) δ = 8.47 (d, J = 5.4 Hz, 2H), 7.11 – 7.01 (m, 4H), 6.85 – 6.78 (m, 2H), 3.78 (s, 3H), 2.88 (s, 4H) ppm. $^{13}\text{C NMR}$ (101 MHz, CDCl_3) δ = 158.2, 150.7, 149.8, 132.8, 129.5, 124.1, 114.0, 55.4, 37.4, 35.8 ppm. **HRMS** calcd. for ($\text{C}_{14}\text{H}_{16}\text{NO}$) [$\text{M}+\text{H}$] $^+$: 214.1232, found 214.1229. Spectroscopic data for **16** match those previously reported in the literature.^{XIV}



4-phenethylpyridine (33). Following **General Conditions C**, bromobenzene (31.4 mg, 0.20 mmol) and 2,4,6-tris(4-methoxyphenyl)-1-(2-(pyridin-4-yl)ethyl)pyridin-1-ium (**1n**) (165.2 mg, 0.28 mmol) were used, affording the title compound as a colourless liquid (28.2 mg, 77% yield) by using Petane/EtOAc (50/10) as eluent. In an independent experiment, 27.6 mg (75% yield) were obtained, giving an average of 76% yield. $^1\text{H NMR}$ (400 MHz, CDCl_3) δ = 8.49 (d, J = 5.0 Hz, 2H), 7.31 – 7.25 (m, 2H), 7.22 (d, J = 7.3 Hz, 1H), 7.17 – 7.12 (m, 2H), 7.08 (d, J = 6.0 Hz, 2H), 2.93 (s, 4H) ppm. $^{13}\text{C NMR}$ (101 MHz, CDCl_3) δ = 150.6, 149.8, 140.8, 128.6, 128.5, 126.4, 124.1, 37.2, 36.7 ppm. **HRMS** calcd. for ($\text{C}_{13}\text{H}_{14}\text{N}$) [$\text{M}+\text{H}$] $^+$: 184.1126, found 184.1126. Spectroscopic data for **16** match those previously reported in the literature.^{XV}



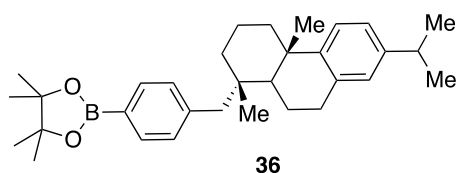
methyl 4-(2-(1H-imidazol-4-yl)ethyl)benzoate (34). Following **General Condition C** for 48 h, methyl 4-bromobenzoate (43 mg, 0.20 mmol) and 1-(2-(1H-imidazol-4-yl)ethyl)-2,4,6-tris(4-methoxyphenyl)pyridin-1-ium tetrafluoroborate (**1o**) (163 mg, 0.28 mmol) were used, affording the title compound as a yellow oil (29.9 mg, 65% yield) by using DCM/MeOH (95/5) as eluent. $^1\text{H NMR}$ (400 MHz, CDCl_3) δ = 7.96 – 7.86 (m, 2H), 7.70 (s, 1H), 7.56 (s, 1H), 7.24 – 7.17 (m, 2H), 6.72 (s, 1H), 3.89 (s, 3H), 3.03 (t, J = 7.4 Hz, 2H), 2.96 (t, J = 7.4 Hz, 2H) ppm. $^{13}\text{C NMR}$ (101 MHz, CDCl_3) δ = 167.1, 146.7, 136.3, 134.0, 129.7, 128.5, 128.1, 116.1, 52.0, 35.5, 28.1 ppm. **IR** (neat, cm^{-1}): 3125, 3074, 2845, 2614, 1708, 1607, 1507, 1434, 1276, 1178, 1018. **HRMS** calcd. for ($\text{C}_{13}\text{H}_{13}\text{N}_2\text{O}_2$) [M] $^-$: 229.0983, found 229.0979.



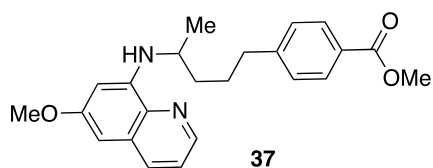
methyl 4-(1-(2,6-dimethylphenoxy)propan-2-yl)benzoate (35). Following **General Procedure C** for 48 h, methyl 4-iodobenzoate (52.2 mg, 0.20 mmol) and 1-(1-(2,6-dimethylphenoxy)propan-2-yl)-

Chapter 3

2,4,6-triphenylpyridin-1-ium tetrafluoroborate (**1r**) (156.0 mg, 0.28 mmol) were used, affording the title compound (40.0 mg, 67% yield) at room temperature as a colourless oil by using Pentane/EtOAc (100/2) as eluent. In an independent experiment, 41.5 mg (70% yield) were obtained, giving an average of 69% yield. $^1\text{H NMR}$ (400 MHz, CDCl_3) δ = 8.53 (dd, J = 4.2, 1.6 Hz, 1H), 7.92 (d, J = 8.3 Hz, 3H), 7.23 (d, J = 8.4 Hz, 2H), 6.34 (s, 1H), 6.26 (s, 1H), 6.01 (s, 1H), 3.90 (s, 3H), 3.89 (s, 3H), 3.62 (dt, J = 13.1, 6.9 Hz, 1H), 2.70 (t, J = 6.4 Hz, 2H), 1.90 – 1.61 (m, 4H), 1.29 (d, J = 6.3 Hz, 3H) ppm. $^{13}\text{C NMR}$ (101 MHz, CDCl_3) δ = 167.3, 159.6, 148.0, 145.1, 144.4, 134.9, 130.0, 129.8, 128.6, 127.9, 122.0, 96.8, 91.7, 55.3, 52.1, 48.1, 36.4, 36.0, 27.7, 20.6 ppm. IR (neat, cm^{-1}): 2950, 2917, 1717, 1609, 1472, 1434, 1274, 1193, 1108, 1006, 971, 854, 760. HRMS calcd. for ($\text{C}_{19}\text{H}_{22}\text{NaO}_3$) [$\text{M}+\text{Na}$] $^+$: 321.1461, found 321.1454.

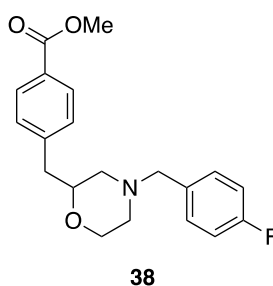


2-(4-(((1S,4aS)-7-isopropyl-1,4a-dimethyl-1,2,3,4,4a,9,10,10a-octahydrophenanthren-1-yl)methyl)phenyl)-4,4,5,5-tetramethyl-1,3,2-dioxaborolane (36). Following **General Procedure C** for 48 h, 2-(4-bromophenyl)-4,4,5,5-tetramethyl-1,3,2-dioxaborolane (56.4 mg, 0.20 mmol) and 1-(((1R,4aS,10aR)-7-isopropyl-1,4a-dimethyl-1,2,3,4,4a,9,10,10a-octahydrophenanthren-1-yl)methyl)-2,4,6-tris(4-methoxyphenyl)pyridin-1-ium tetrafluoroborate (**1p**) (212 mg, 0.28 mmol) were used, affording the title compound as a yellow solid (55.7 mg, 59% yield) by using Hexane/EtOAc (95/5) as eluent. In an independent experiment, 51.9 mg (55%) were obtained, giving an average of 57% yield. **Mp**: 133 – 135 °C. $^1\text{H NMR}$ (400 MHz, CDCl_3) δ = 7.74 – 7.62 (m, 2H), 7.15 – 7.10 (m, 3H), 6.95 (dd, J = 8.2, 2.1 Hz, 1H), 6.88 (d, J = 2.0 Hz, 1H), 2.97 – 2.88 (m, 1H), 2.81 (quint, J = 6.9 Hz, 1H), 2.69 (d, J = 13.0 Hz, 1H), 2.57 (d, J = 13.0 Hz, 1H), 2.19 (d, J = 12.9 Hz, 1H), 2.15 – 2.05 (m, 1H), 1.89 – 1.73 (m, 1H), 1.72 – 1.60 (m, 1H), 1.61 – 1.52 (m, 2H), 1.43 – 1.37 (m, 1H), 1.33 (s, 12H), 1.29 – 1.25 (m, 2H), 1.25 – 1.19 (m, 9H), 1.00 (s, 3H) ppm. $^{13}\text{C NMR}$ (101 MHz, CDCl_3) δ = 147.6, 145.4, 142.2, 134.7, 134.1, 130.5, 126.8, 124.1, 123.7, 83.6, 50.0, 46.8, 38.3, 37.8, 37.7, 37.3, 33.4, 30.1, 25.7, 24.9, 24.8, 24.0, 23.9, 20.8, 19.4, 18.8 ppm. (*the signal for the aromatic carbon attached to boron is not observed due to quadrupolar relaxation*). $^{11}\text{B NMR}$ (128 MHz, CDCl_3) δ = 30.8 ppm. IR (neat, cm^{-1}): 2926, 2156, 1770, 1739, 1652, 1517, 1395, 1267. HRMS calcd. for ($\text{C}_{32}\text{H}_{45}\text{NaNO}_2^{10}\text{B}$) [$\text{M}+\text{Na}$] $^+$: 494.3441, found 494.3440.



methyl-4-(4-(((6-methoxyquinolin-8-yl)amino)pentyl)benzoate (37). Following **General Procedure C** for 48 h, methyl 4-bromobenzoate (43.0 mg, 0.20 mmol) and 2,4,6-tris(4-

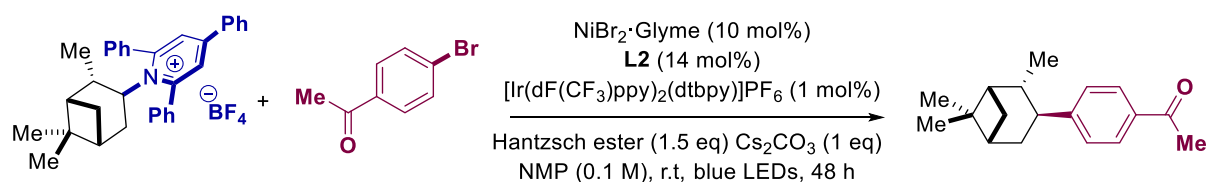
methoxyphenyl)-1-(4-((6-methoxyquinolin-8-yl)amino)pentyl)pyridin-1-ium tetrafluoroborate (**1q**) (203.6 mg, 0.28 mmol) were used, affording the title compound (45.0 mg, 60% yield) as a colourless oil by using Pentane/EtOAc (100/5) as eluent. In an independent experiment, 47.0 mg (62% yield) were obtained, giving an average of 61% yield. $^1\text{H NMR}$ (400 MHz, CDCl_3) δ = 8.03 (d, J = 8.2 Hz, 2H), 7.43 (d, J = 8.3 Hz, 2H), 6.98 (d, J = 7.3 Hz, 2H), 6.94 – 6.88 (m, 1H), 3.94 (s, 3H), 3.90 – 3.82 (m, 2H), 3.34 (h, J = 7.0 Hz, 1H), 2.16 (s, 6H), 1.50 (d, J = 7.0 Hz, 3H) ppm. $^{13}\text{C NMR}$ (101 MHz, CDCl_3) δ = 167.3, 155.6, 149.7, 131.0, 129.9, 129.0, 128.6, 127.7, 124.0, 52.2, 41.0, 18.1, 16.3 ppm. IR (neat, cm^{-1}): 3377, 2932, 2854, 1715, 1609, 1574, 1515, 1384, 1273, 1158, 1105, 1049, 966, 818, 760. HRMS calcd. for ($\text{C}_{23}\text{H}_{27}\text{NO}_3$) $[\text{M}+\text{H}]^+$: 379.2016, found 379.2025.



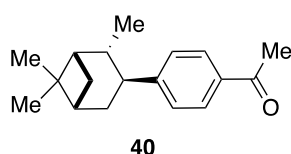
methyl 4-((4-(4-fluorobenzyl)morpholin-2-yl)methyl)benzoate (38). Following **General Procedure C** for 48 h, methyl 4-bromobenzoate (43 mg, 0.20 mmol) and 1-((4-(4-fluorobenzyl)morpholin-2-yl)methyl)-2,4,6-tris(4-methoxyphenyl)pyridin-1-ium tetrafluoroborate (**1s**) (194.0 mg, 0.28 mmol) were used, affording the title compound (50.2 mg, 73% yield) as a colorless oil by using Pentane/EtOAc (50/50) as eluent. In an independent experiment, 49.8 mg (72% yield) were obtained, giving an average of 73% yield. $^1\text{H NMR}$ (400 MHz, CDCl_3) δ = 7.97 (d, J = 8.3 Hz, 2H), 7.29 (d, J = 7.7 Hz, 4H), 7.01 (t, J = 8.7 Hz, 2H), 3.92 (s, 3H), 3.88 – 3.82 (m, 2H), 3.68 – 3.59 (m, 1H), 3.46 (q, J = 19.5 Hz, 2H), 2.88 (dd, J = 14.0, 7.6 Hz, 1H), 2.79 – 2.70 (m, 2H), 2.63 (d, J = 11.3 Hz, 1H), 2.16 (td, J = 11.3, 3.1 Hz, 1H), 1.97 (t, J = 10.5 Hz, 1H) ppm. $^{13}\text{C NMR}$ (101 MHz, CDCl_3) δ = 167.2, 163.5, 161.0, 143.8, 130.8 (d, J = 7.9 Hz), 129.8, 129.4, 128.5, 115.3 (d, J = 21.2 Hz), 76.2, 66.9, 62.5, 58.4, 52.8, 52.1, 40.3 ppm. $^{19}\text{F NMR}$ (376 MHz, CDCl_3) δ = -115.7 ppm. IR (neat, cm^{-1}): 2946, 2857, 2802, 1716, 1601, 1506, 1273, 1217, 1104, 1019, 834, 760. HRMS calcd. for ($\text{C}_{20}\text{H}_{23}\text{FNO}_2$) $[\text{M}+\text{H}]^+$: 344.1656, found 344.1663.

Chapter 3

3.5.5 Photochemical conditions

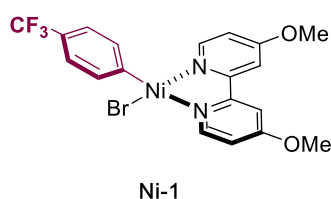


NOTE: No product was detected upon exposure of the starting precursors to our optimized conditions based on Mn. No products were detected by GC-MS and starting precursor was recovered.



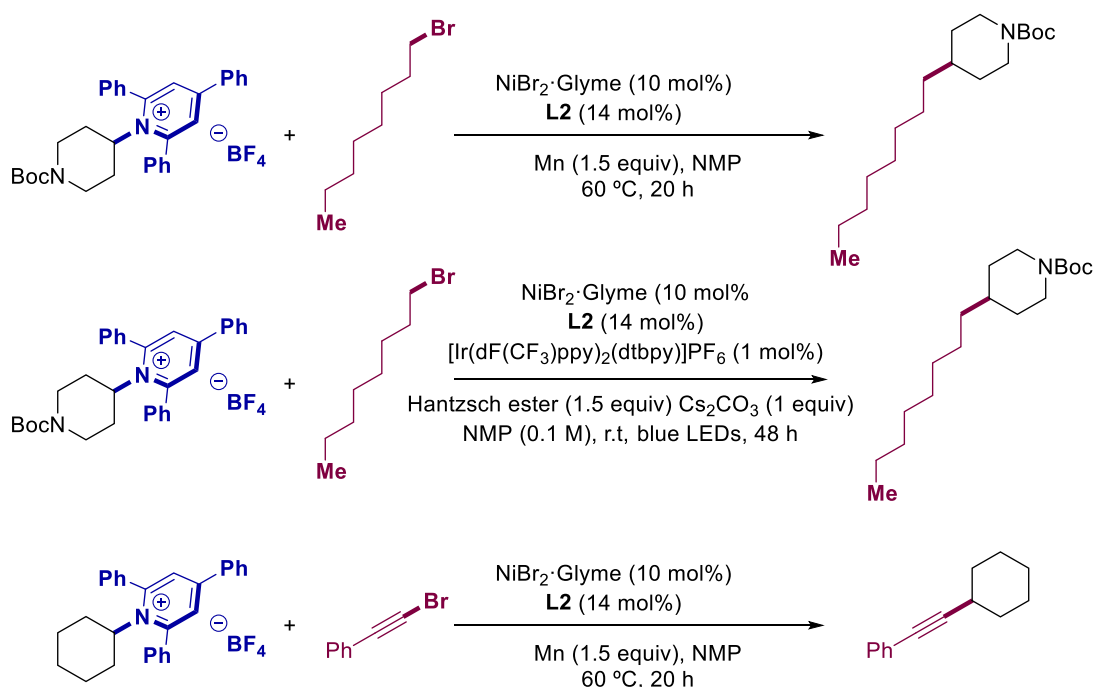
1-(4-((1S,2S,5S)-2,6,6-trimethylbicyclo[3.1.1]heptan-3-yl)phenyl)ethan-1-one (40). An oven-dried 8 mL screw-cap test tube containing a stirring bar was charged with 1-(4-bromophenyl)ethan-1-one (39.8 mg, 0.20 mmol), 2,4,6-triphenyl-1-((1S,2S,5R)-2,6,6-trimethylbicyclo[3.1.1]heptan-3-yl)pyridin-1-ium tetrafluoroborate (**2t**) (148.8 mg, 0.28 mmol, 1.4 equiv.), **[Ir{dF(CF₃)ppy}₂(dtbbpy)]PF₆** (1.1 mg, 1 mol%) and Hantzsch ester (diethyl 2,6-dimethyl-1,4-dihydropyridine-3,5-dicarboxylate). The test tube was introduced in an argon-filled glovebox where Cs₂CO₃ (32.5 mg, 0.2 mmol, 1 eq.), and 0.4 mL precatalyst mixture of NiBr₂·glyme (6.2 mg, 10 mol%) with 4,4'-dimethoxy-2,2'-bipyridine (**L2**, 6.0 mg, 14 mol%) in NMP (1.60 mL). The tube with the mixture was taken out of the glovebox and stirred at room temperature for 48 h under blue leds irradiation. After the reaction was finished, the reaction mixture was extracted with ethyl acetate and water/brine (3 times). Then the organic layers were combined, dried over MgSO₄, concentrated under vacuum and the product was purified by flash chromatography column on silica gel Hexane/*tert*-butyl-methyl ether (95/5), affording the title compound as a colourless oil (30 mg, 58% yield). ¹H NMR (400 MHz, CDCl₃) δ = 7.92 – 7.90 (m, 2H), 7.40 – 7.38 (m, 2H), 3.07 (dt, J = 10.3, 7.8 Hz, 1H), 2.59 (s, 3H), 2.52 (dtd, J = 9.7, 6.2, 2.2 Hz, 1H), 2.42 (tdd, J = 10.3, 3.7, 1.9 Hz, 1H), 2.14 – 1.99 (m, 2H), 1.96 – 1.82 (m, 2H), 1.28 (s, 3H), 1.17 (s, 3H), 0.99 (d, J = 7.1 Hz, 3H) ppm. ¹³C NMR (101 MHz, CDCl₃) δ = 197.8, 155.2, 134.9, 128.6, 128.6, 47.9, 45.7, 45.0, 41.8, 39.2, 37.2, 34.9, 28.5, 26.6, 23.0, 20.9 ppm. IR (neat, cm⁻¹): 2900, 1680, 1603, 1356, 1263, 954. HRMS calcd. for (C₁₃H₁₃N₂O₂) [M+H]⁺: 257.1900, found 257.1898.

3.5.6 Oxidative addition complex, Ni⁻¹



Following procedure described by our group,^{XVI} in a nitrogen-filled glove box, a 50 mL round bottom flask containing a stirring bar was charged with Ni(COD)₂ (138 mg, 0.5 mmol, 1.0 equiv), 4,4'-di-methoxy-2,2'-pyridine **L2** (118 mg, 0.5 mmol, 1.0 equiv) and dry THF (5 mL) giving a dark purple mixture which was stirred for 20 h hours at 25 °C. 1-bromo-4-(trifluoromethyl)benzene (0.7 mL, 5 mmol, 10.0 equiv) was added and stirred for additional 45 min. Dry pentane (30 mL) was added to the deep red coloured mixture and filtered. The resulting precipitate was washed with pentane (3 x 10 mL) and dried under vacuum to afford Ni-1 as a yellow solid (185 mg, 74% yield). The product was used without further purification. The complex was stored in a nitrogen filled glove box at -35 °C and showed to be stable in solid form. The product turned out to be highly insoluble in the vast majority of solvents used for NMR spectroscopy, obtaining in all cases broad signals. ¹H NMR (300 MHz, CD₂Cl₂) δ = 9.14 (s, 1H), 7.79 (d, *J* = 7.6 Hz, 2H), 7.35 (s, 2H), 7.19 (d, *J* = 7.8 Hz, 2H), 6.99 (s, 2H), 6.69 (s, 1H), 4.00 (s, 3H), 3.94 (s, 3H) ppm. ¹⁹F NMR (376 MHz, CD₂Cl₂) δ = -62.0 ppm. Spectroscopic data for **Ni-1** match those previously reported in the literature.^{XVI}

3.5.7 Attempted reactions with sp^3 and sp -hybridized organic halides



sp^3 hybridized organic halides: In all cases (both using Mn or Ir photoredox catalysts), no conversion to product was observed for a protocol based on Ni/**L2**, recovering substantial amounts of the starting alkyl halide and with non-negligible amounts of homodimerization being observed in the crude mixtures.

sp hybridized organic halides: Traces of the targeted alkynylation product were observed in the crude mixtures, recovering the majority of the starting alkynyl bromide.

Chapter 3

3.5.8 Mechanistic studies

3.5.8.1 Electrochemical studies

A) Experimental details

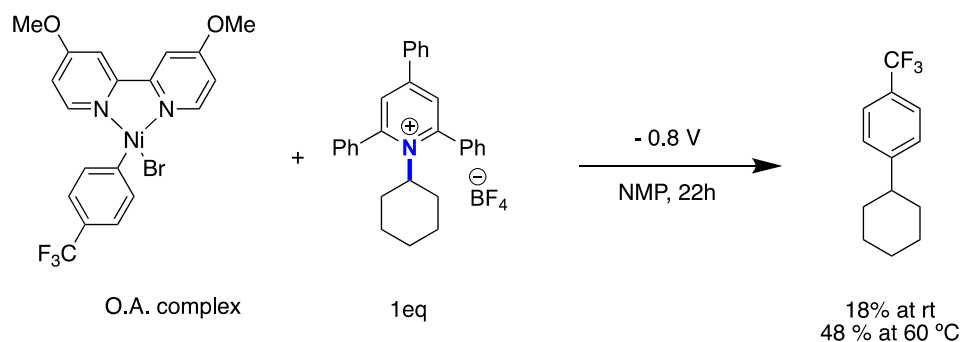
A.1 Cyclic Voltammetry

Cyclic voltammetry was conducted on a PARSTAT 2273 potentiometer (Princeton Applied Research) using a 3-electrode cell configuration. A glassy carbon working electrode was employed alongside a platinum flag counter electrode and a Ag/AgCl (KCl sat.) reference electrode. The distance between the working and reference electrode was 1 cm. A ferrocene solution was used as an internal standard to determine the precise potential scale.^{xx} The pyridiniums (**1a**, **1m** and **1m'**) were made up as 5 mM solutions in NMP (dry) along with 0.1 M supporting electrolyte (tetrabutylammonium hexafluorophosphate). The solution of Ni-complex (**Ni-1**) (10 mM) in NMP along with 0.1 M supporting electrolyte (tetrabutylammonium hexafluorophosphate) was made up in the glovebox to avoid exposure to air or moisture. Argon was passed through the samples for 10 minutes before taking any measurements and an Ar atmosphere was maintained for the duration to avoid the deleterious influence of oxygen reduction. Samples were examined at scan rates from 10 to 1000 mV s⁻¹ depending on the substrate. For quasi-reversible species, a wide range of scan rates were tested to investigate the proposed fragmentation in more detail. In the situations where there is no apparent return oxidation (or reduction) peak, we have stated the E_p (the potential corresponding to the maximum reductive or oxidative current). For reversible or quasi-reversible cyclic voltammograms, we have determined the ratio between the (baseline corrected) peak currents (i_p) to provide a quantitative measure of the degree of reversibility.

A.2 Bulk electrolysis

Bulk electrolysis was conducted on a PARSTAT 2273 potentiometer using a 3-electrode cell configuration at room temperature and at 60 °C (see scheme 1). The same electrodes were used as for CV experiments, namely a glassy carbon working electrode, platinum flag counter electrode and Ag/AgCl (KCl sat.) reference electrode. The solution of Ni-complex (**Ni-1**) (15 mg, 1.0 eq.) in NMP (10 mM) along with 0.1 M supporting electrolyte (tetrabutylammonium hexafluorophosphate) was made up in the glovebox to avoid exposure to air or moisture. After recording a CV of Ni-complex (**Ni-1**), cyclohexyl-2,4,6-triphenylpyridin-1-ium tetrafluoroborate (**1a**) (14 mg, 1.0 eq.) was added and stirred for 5 minutes. Decane was also added as an internal standard to allow quantification of the product. Another CV was taken of the **Ni-1/1a** mixture before starting the bulk electrolysis. A potential of -0.8 V vs Ag/AgCl was then applied for 22 h. Aliquots were analyzed by GC to determine the yield of **9**.

Deaminative Arylation at sp^3 Carbon Centers



Bulk electrolysis at rt



Bulk electrolysis at 60 °C

Scheme A.1.

B) Discussion

B.1 Cyclic Voltammetry of Pyridinium Precursors

The reduction profile of the pyridinium precursors investigated were reversible or quasi-reversible on the time scale of the CV experiments (Schemes 2-10). The secondary alkyl pyridinium precursor **1a** was the least reversible (illustrated by the ratio of the peak heights, $i_{pc}/i_{pa} \gg 1$) which was expected from the generation of a more stable secondary carbon-radical upon fragmentation. We expected to observe a difference in the reversibility of primary alkyl pyridiniums (**1m** and **1m'**²³) considering that **1m** performs significantly better than **1m'** in the deaminative arylation reaction. Both, however, showed highly reversible CVs ($i_{pc}/i_{pa} \approx 1$) over all scan rates tested. The reduction potential of **1m** is higher than unsubstituted **1m'** ($E_{1/2} = -0.90$ V and -0.77 V respectively) as expected from the electron donating substituents increasing the level of the LUMO. Interestingly, if the CVs are pushed to higher potentials, a second reduction profile is observed suggesting the formation of a radical dianion (Schemes 3, 6 and 9). Considering the extended aromatic moiety over which the charge can delocalize, such a scenario is feasible. Moreover, the stability of the pyridinium to fragmentation seems to decrease upon this second reduction in a more pronounced way for **1m** than unsubstituted **1m'** ($i_{pc}/i_{pa} = 7$ and 2 at 50 mVs^{-1} respectively). However, the second reduction potential of **1m** is -1.5 V which would be an uphill electron transfer from manganese ($\text{Mn}/\text{Mn}^{2+} = -1.4$ V vs. Ag/AgCl).^{xxi} The deaminative arylation reactions with primary pyridiniums give significantly higher yields

Chapter 3

at 60°C than at rt and therefore cyclic voltammetry was also carried out at this elevated temperature (Schemes 4, 7 and 10). Even at 60°C, however, primary pyridiniums still exhibited highly reversible CVs (Table 3) with **1m** being slightly less reversible than **1m'** ($i_{pc}/i_{pa} = 1.5$ and 1.2 at 50 mVs^{-1} respectively). In contrast, secondary pyridinium **1a** proved significantly less reversible at 60°C with completely irreversible CVs observed until 200 mVs^{-1} (Scheme 10). These results indicate that the higher temperature aids the reaction by promoting fragmentation of reduced pyridiniums but this is still thought to be thermodynamically challenging in the case of primary pyridiniums **1m** and **1m'**.

B.2 Cyclic Voltammetry of Ni-complex **Ni-1**

The Ni(II)-complex (**Ni-1**) exhibited rather complex electrochemical behavior, but comparable to that displayed by related Ni-complexes^{XVII}. A first partially reversible reduction (E_{R1}) is observed at -1.0 V (vs. Ag/AgCl) which is followed by 2 more significant reductions (E_{R1} and E_{R2}) at -1.4 V and -1.5 V respectively (Scheme 11). Further peaks are observed if the CV is pushed to higher potentials, but the origin of these reductions can only be speculated and they are far out the range of reduction by manganese ($\text{Mn}/\text{Mn}^{2+} = -1.4 \text{ V}$ vs. Ag/AgCl). By using a ferrocene solution as an internal standard, these values have been standardized to permit direct comparison with the work of Klein *et. al.*^{XVII}. It has been shown by spectroscopic methods and quantum chemical calculations that the LUMO of Ni-complexes (such as **Ni-1**) bearing α -diimine ligands is localized in the α -diimine π^* levels^{XVIII}. This indicates that the reduction of these complexes is largely ligand centered and will be highly dependent on the type and substitution of the α -diimine bound. Klein observed an irreversible reduction of [(4,4'-Mebpy)Ni(Mes)Br] at -1.85 V (vs. Fc/Fc⁺ at 100 mVs^{-1}) which was followed by 2 more reductions at -2.00 V (reversible) and -2.61 V (irreversible). These latter peaks were proposed to be a result of *in situ* generated Ni-species (solvated and Ni-Ni dimers) following the initial reduction and subsequent loss of bromide. In our case, the more basic 4,4'-MeObpy should result in a higher potential, which is in better agreement with the second reduction, E_{R2} at -2.00 V (vs. Fc/Fc⁺) than the initial shoulder, E_{R1} at -1.62 V (vs. Fc/Fc⁺). Moreover, on the back scan, oxidation peaks (E_{O1} and E_{O2}) are observed only when E_{R2} has been reached but not E_{R1} . Klein observed similar peaks for [(4,4'-Mebpy)Ni(Mes)Br] and speculated that E_{O1} (-1.42 V Fc/Fc⁺) resulted from oxidation of the solvated Ni(I) species formed *in situ* after reduction and bromide loss. Notably, this suggests that [(N^N)Ni(Ar)solv] complexes are relatively weak reductants. In our case, $E_{O1} = -1.35 \text{ V}$ vs. Fc/Fc⁺ or -0.73 V vs. Ag/AgCl which is essentially the same as secondary pyridinium **1a** and out the range of primary pyridinium **1m**. In contrast, the reduction of pyridinium precursors by manganese ($\text{Mn}/\text{Mn}^{2+} = -1.4 \text{ V}$ vs. Ag/AgCl) would have a gain of $0.4\text{-}0.7 \text{ V}$ and thus seems the more likely scenario. The origin of E_{R1} is still uncertain but may result from the reduction of the electron-poor *p*-CF₃ substituted phenyl. Further irreversible oxidations (E_{O3} and E_{O4}) are observed at more positive potentials which are independent of any previous reduction and can be assigned to Ni(II)/Ni(III) couples.

B.3 Bulk electrolysis

To investigate whether the arylated product is formed by alkyl radical addition to Ni(II)-complex **Ni-1** followed by reductive elimination, a bulk electrolysis was first performed on **Ni-1** and pyridinium **1a** (1:1) at room temperature. Before starting the electrolysis, a CV was taken of Ni-complex **Ni-1** before and after addition of **1a** (Scheme 12) but no noticeable change except the expected combination of the two reduction profiles was observed. A constant potential of -0.8 V was then applied to reduce **1a** and generate the cyclohexyl radical whilst avoiding reduction of **Ni-1** and the formation of any Ni(I)-species. Aliquots were taken at 2 and 6 h intervals did not show any coupled product but after 22 h 18% of **9** was detected by GC analysis. Although the ability to form **9** was exciting from a mechanistic standpoint, we were disappointed at the very sluggish reaction. As elevated temperature is required to make the deaminative arylation go to completion in 24 h, a repeat electrolysis experiment at 60 °C was performed. Again CVs taken before starting showed no noticeable change except the expected combination of the **Ni-1** and pyridinium **1a** reduction profiles, neither at rt nor 60 °C (Scheme 13). Pleasingly, after applying a constant potential of -0.8 V for 22 h, 48% of **9** was observed by GC analysis. CVs taken after the experiment showed no sign of **1a** or seemingly **Ni-1** with new reduction peaks observed that presumably correspond to (unidentified) Ni-species.

Chapter 3

3.5.8.2. Electrochemical potentials

Table 1: First reduction of Pyridinium precursors at r.t.

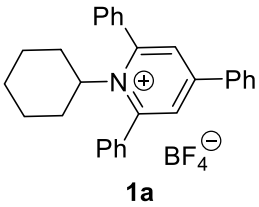
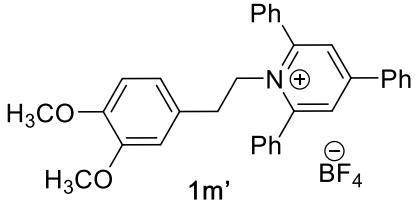
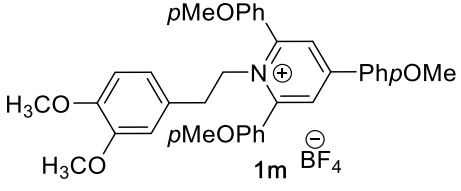
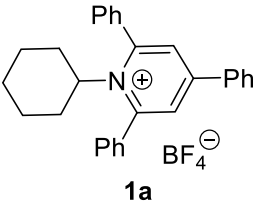
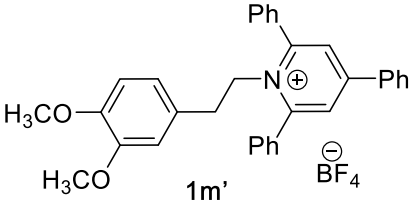
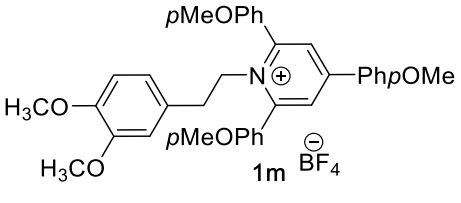
Substrate	Scan rate (mV s ⁻¹)	E _{1/2} (V) vs. Ag/ AgCl	E _{1/2} (V) vs. Fc/ Fc ⁺	Profile	i _{pc} /i _{pa}
 <p>1a</p>	10	-0.72	-1.34	Quasi-reversible	3.69
	20	-0.73	-1.35	Quasi-reversible	3.09
	50	-0.74	-1.35	Quasi-reversible	2.00
	100	-0.74	-1.35	Quasi-reversible	1.54
	500	-0.74	-1.36	Reversible	1.22
	1000	-0.74	-1.36	Reversible	1.09
 <p>1m'</p>	50	-0.77	-1.39	Reversible	1.01
	100	-0.77	-1.39	Reversible	1.02
	500	-0.77	-1.39	Reversible	1.06
	1000	-0.78	-1.40	Reversible	1.26
 <p>1m</p>	10	-0.89	-1.51	Reversible	1.24
	50	-0.89	-1.51	Reversible	1.14
	100	-0.90	-1.52	Reversible	1.07
	500	-0.91	-1.53	Reversible	1.06
	1000	-0.91	-1.52	Reversible	1.25

Table 2: First and second reductions of Pyridinium precursors at r.t.

Substrate	Scan rate (mV s ⁻¹)	First E _{1/2} (V) vs. Ag/ AgCl	Profile	i _{pc} /i _{pa}	Second E _{1/2} (V) vs. Ag/ AgCl	Profile
 1a	20	-0.72	Quasi-reversible	4.2	-1.21	Quasi-reversible
	50	-0.73	Quasi-reversible	3.7	-1.22	Quasi-reversible
	100	-0.75	Quasi-reversible	2.7	-1.24	Quasi-reversible
	500	-0.74	Quasi-reversible	1.5	-1.25	Quasi-reversible
 1m'	50	-0.77	Quasi-reversible	2.0	-1.39	Quasi-reversible
	100	-0.77	Quasi-reversible	1.8	-1.39	Quasi-reversible
	500	-0.77	Quasi-reversible	1.5	-1.39	Quasi-reversible
 1m	10	-0.89	Quasi-reversible	7.0	-1.51	Quasi-reversible
	50	-0.89	Quasi-reversible	6.3	-1.51	Quasi-reversible
	100	-0.90	Quasi-reversible	5.2	-1.52	Quasi-reversible

Chapter 3

Table 3: First reduction of Pyridinium precursors at 60 °C.

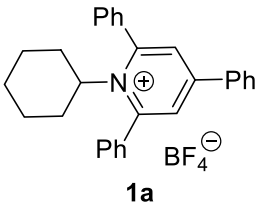
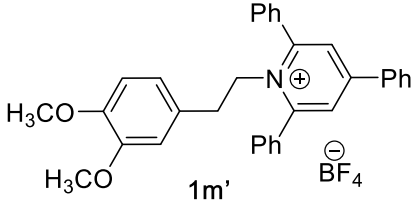
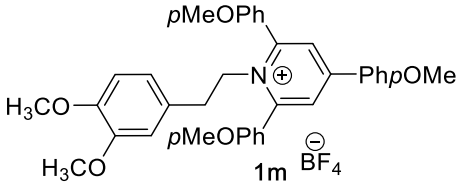
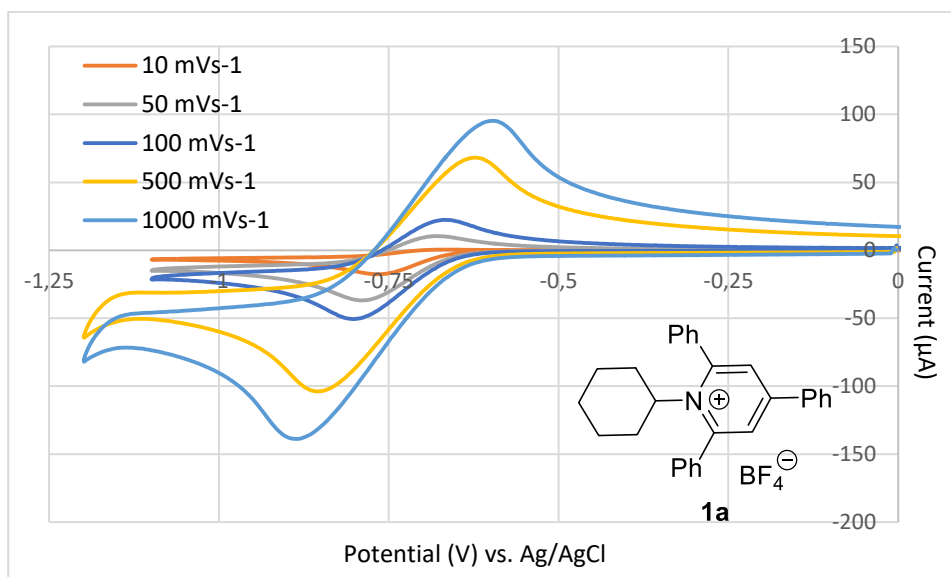
Substrate	Scan rate (mV s ⁻¹)	E _{1/2} (V) vs. Fc/ Fc ⁺	Profile	i _{pc} /i _{pa}
 <p>1a</p>	100	-1.31	Irreversible	-
	200	-1.25	Quasi-reversible	4.52
	500	-1.28	Quasi-reversible	3.81
	1000	-1.29	Quasi-reversible	2.67
	2000	-1.29	Quasi-reversible	1.85
 <p>1m'</p>	50	-1.34	Reversible	1.21
	100	-1.34	Reversible	1.19
	500	-1.34	Reversible	1.15
	1000	-1.34	Reversible	1.15
 <p>1m</p>	50	-1.44	Reversible	1.48
	100	-1.45	Reversible	1.40
	500	-1.45	Reversible	1.20
	1000	-1.45	Reversible	1.16

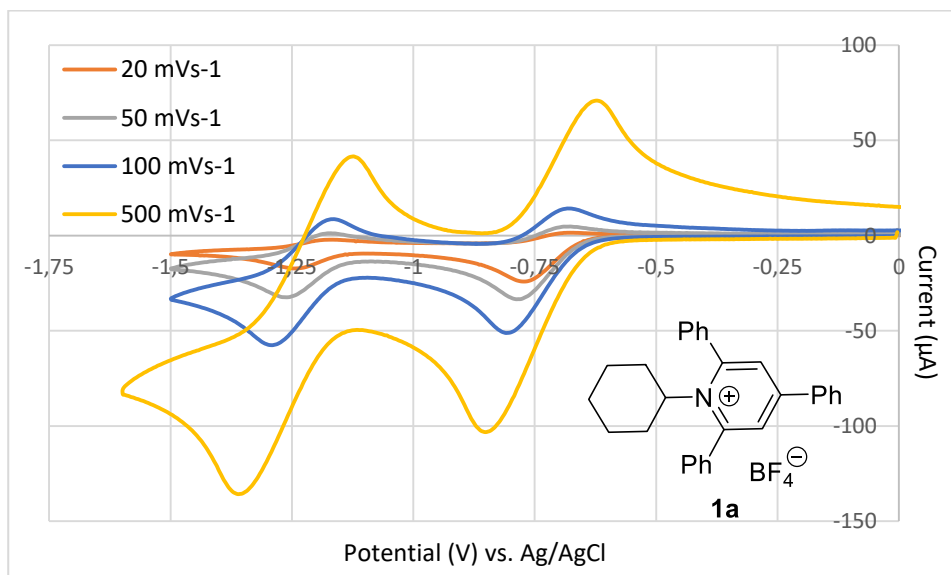
Table 4: Reduction and oxidation potentials of Ni-1

Peak	$E_{1/2}$ or E_p (V) vs. Ag/AgCl	$E_{1/2}$ or E_p (V) vs. Fc/Fc ⁺	Profile
E_{R1}	-1.0	-1.62	Quasi-reversible
E_{R2}	-1.37	-2.00	Irreversible
E_{R3}	-1.49	-2.11	Quasi-reversible
E_{R4}	-1.78	-2.40	Quasi-reversible
E_{R5}	-2.22	-2.84	Irreversible
E_{O1}	-0.73	-1.35	Irreversible
E_{O2}	-0.01	-0.63	Irreversible
E_{O3}	0.48	-0.14	Irreversible
E_{O4}	0.91	0.30	Irreversible

3.5.8.3. Cyclic voltammograms

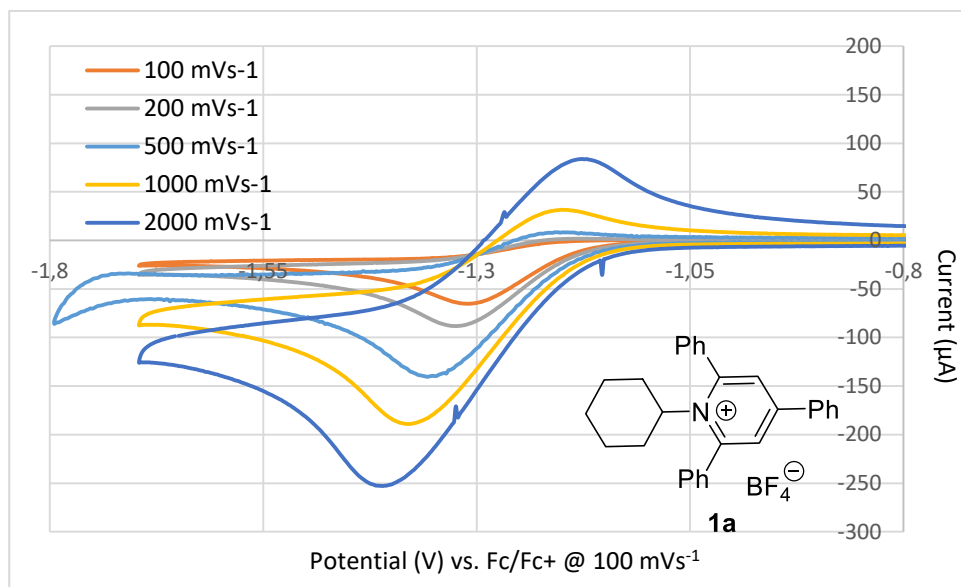


Scheme 2: Pyridinium **1a** short scan range at r.t

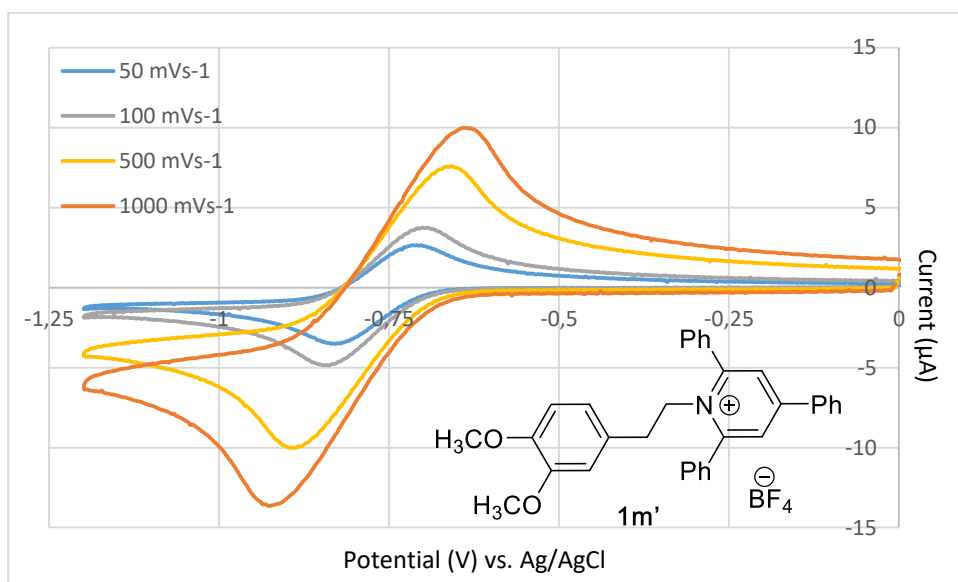


Chapter 3

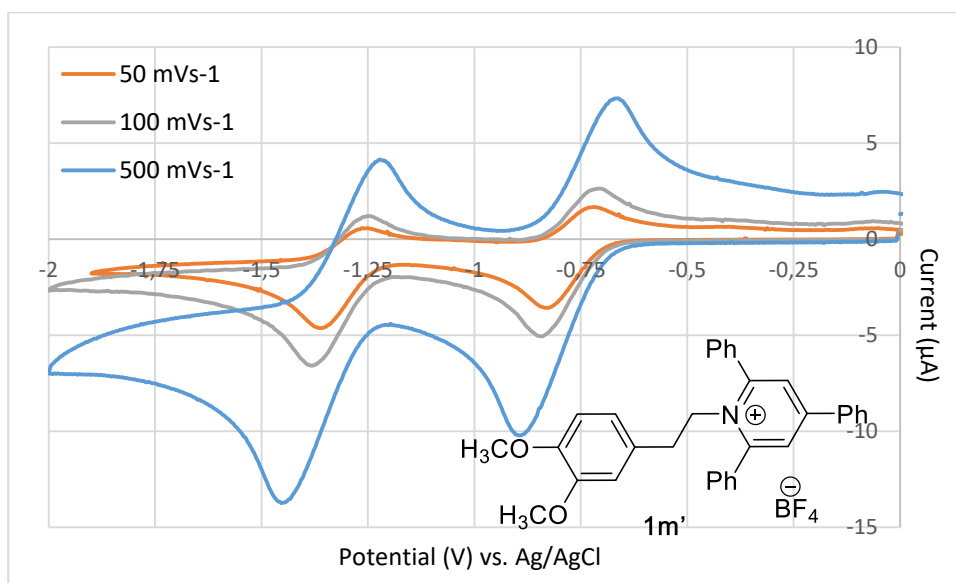
Scheme 3: Pyridinium **1a** long scan range at r.t



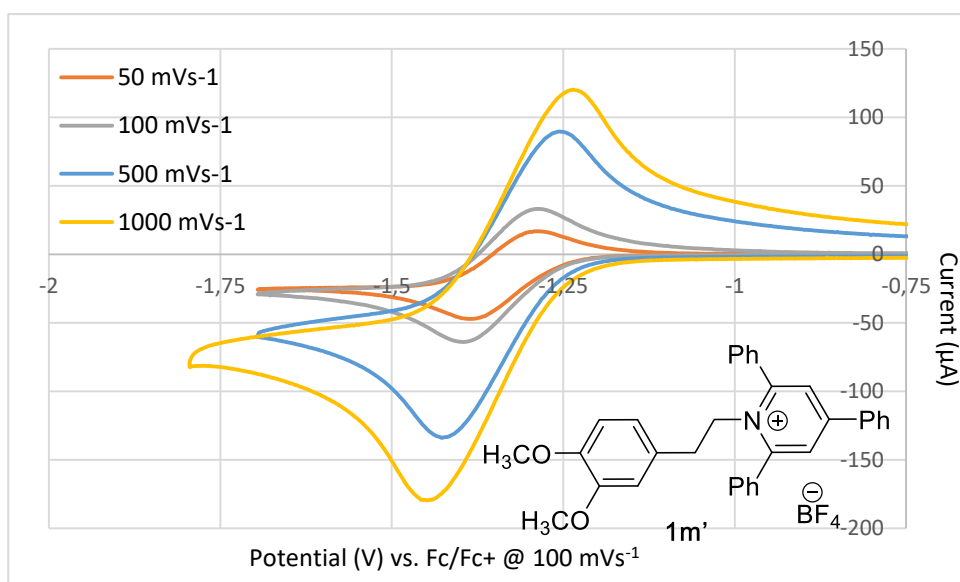
Scheme 4: Pyridinium **1a** short scan range at 60 °C



Scheme 5: Pyridinium **1m'** short scan range at r.t

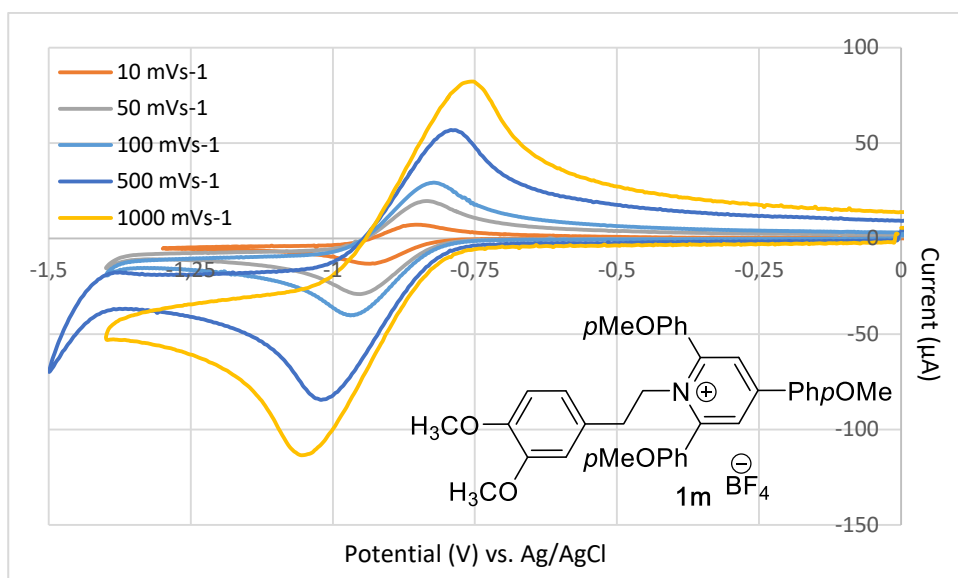


Scheme 6: Pyridinium **1m'** long scan range at r.t

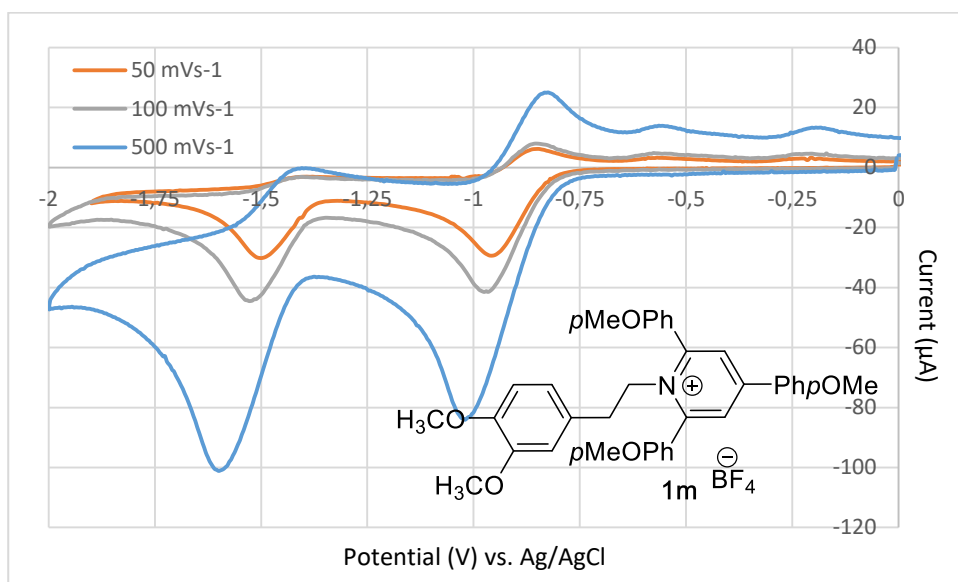


Scheme 7: Pyridinium **1m'** short scan range at 60 °C

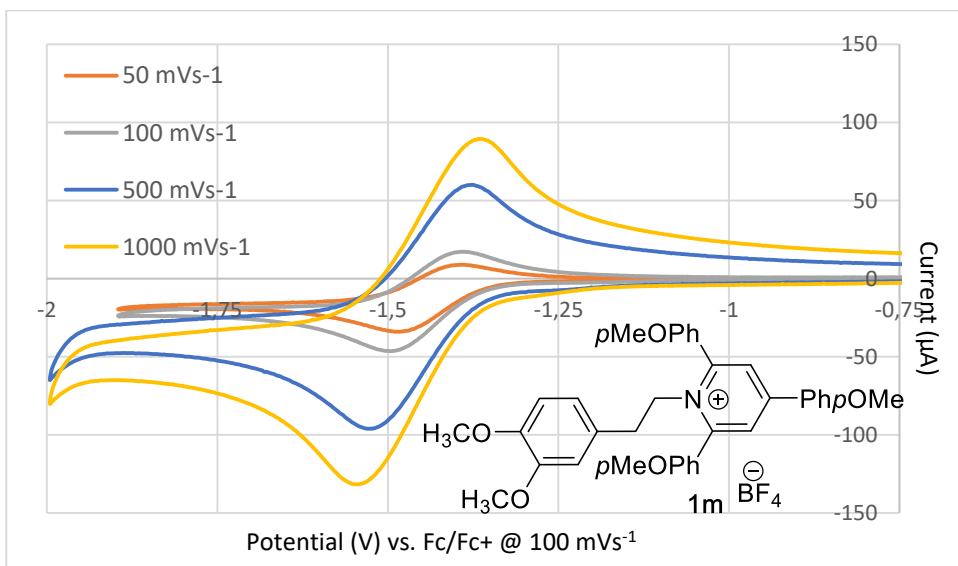
Chapter 3



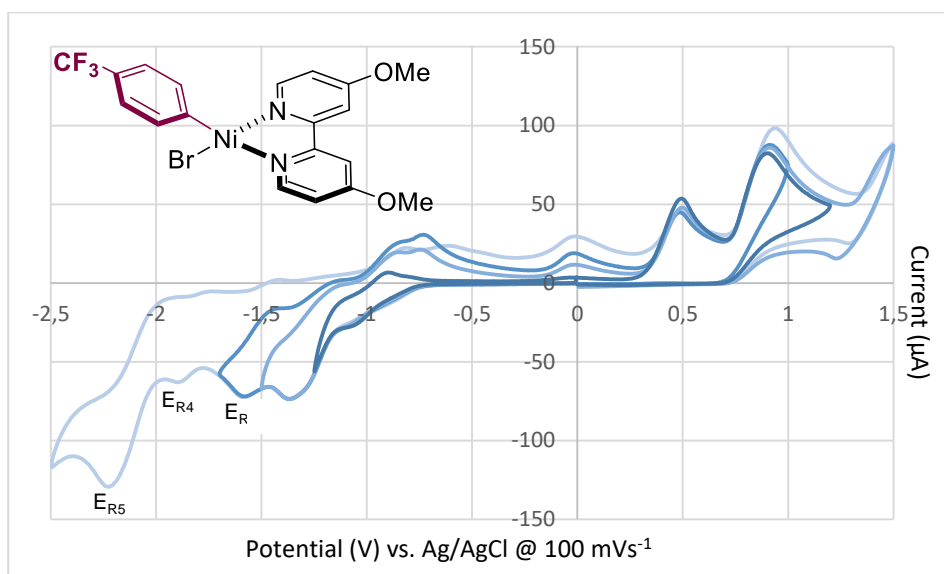
Scheme 8: Pyridinium **1m** short scan range at r.t



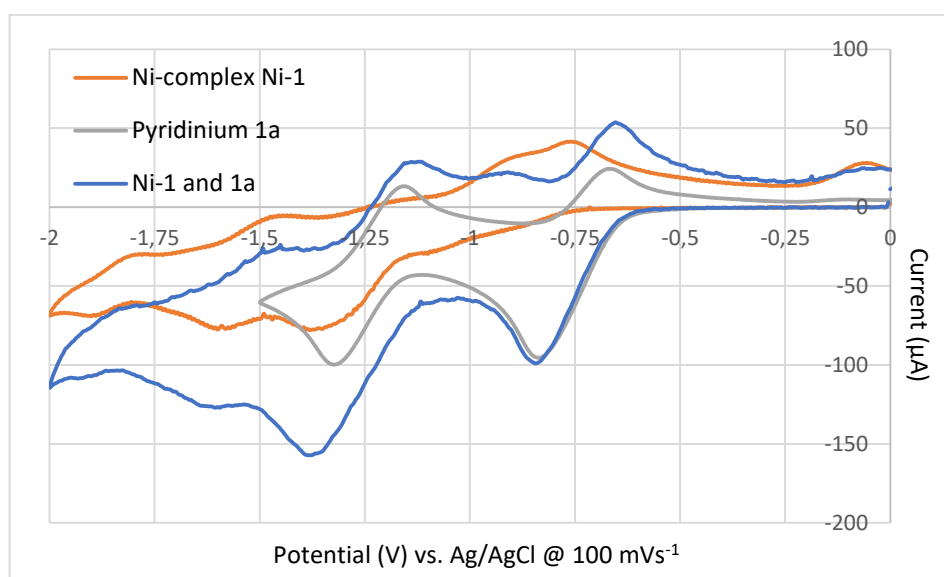
Scheme 9: Pyridinium **1m** long scan range at r.t



Scheme 10: Pyridinium **1m** short scan range at 60 °C

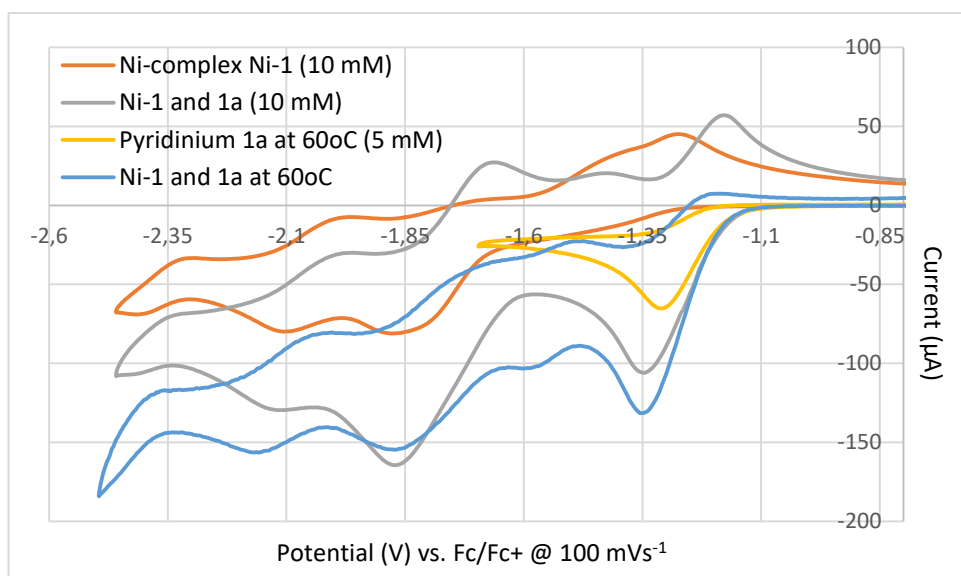


Scheme 11: Ni-complex Ni-1

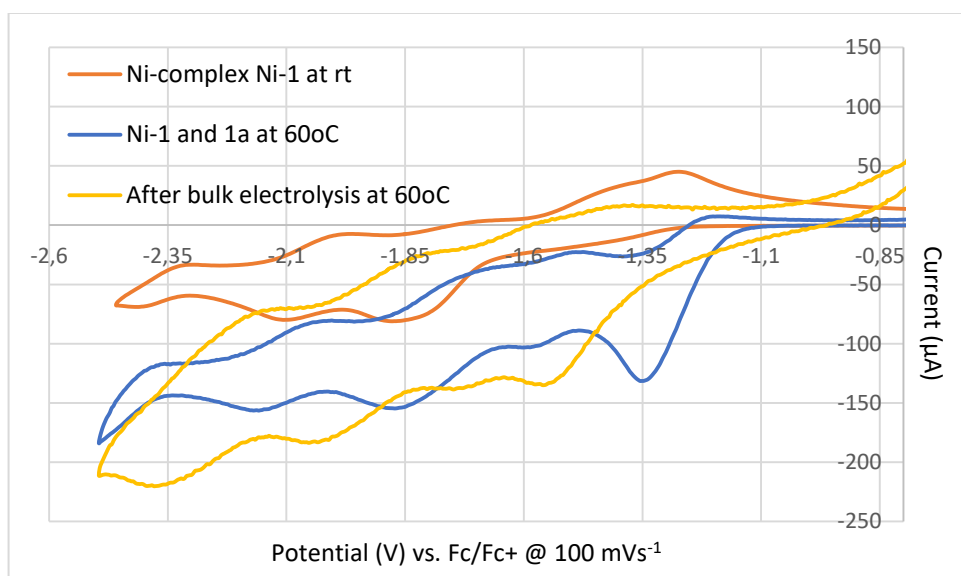


Scheme 12: CVs recorded before room temperature bulk electrolysis

Chapter 3



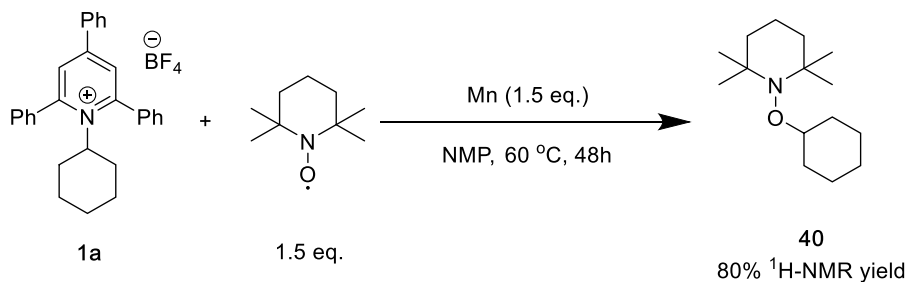
Scheme 13: CVs recorded before 60 °C bulk electrolysis



Scheme 14: Comparison of CVs before and after 60 °C bulk electrolysis

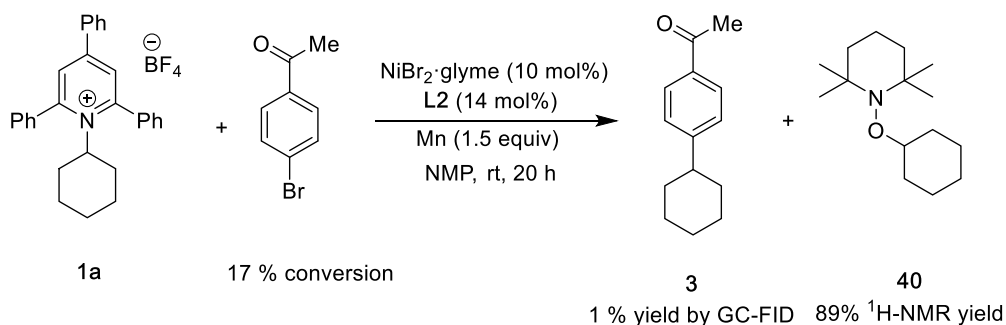
Chapter 3

3.5.8.4. Radical trap experiments with TEMPO



Entry	Mn (equiv)	Yield (%)
1	1.5	80
2	0	0

Procedure for the radical trap experiment with TEMPO: To an oven-dried 8 mL screw-cap test tube containing a stirring bar was charged with 1-cyclohexyl-2,4,6-triphenylpyridin-1-ium tetrafluoroborate (**1a**) (23.8 mg, 0.05 mmol). The test tube was introduced in an argon-filled glovebox where Mn (4.2 mg, 0.075 mmol) and TEMPO (11.7 mg, 0.075 mmol) was added, followed by the addition of NMP (0.5 mL, 0.1 M). The tube was then sealed firmly and taken out of the glovebox. The resulting reaction mixture was heated to 60 °C and stirred vigorously for 48 h. After the reaction was finished, the reaction mixture was extracted with ethyl acetate and water (3 times). Then the organic layers were combined and washed with water and brine, dried over MgSO₄, concentrated under vacuum. Mesitylene (7 μL, 0.05 mmol) was added as an internal standard and the yield of known TEMPO adduct (**40**) was determined to be 80% by analysis of the ¹H NMR spectrum of the crude reaction mixture.

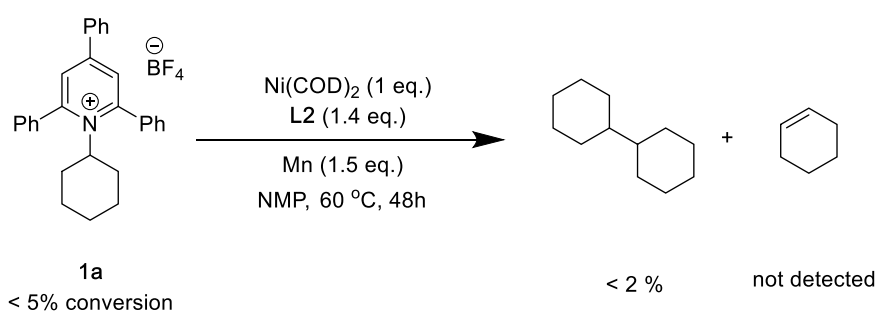


Inhibition of Ni-catalyze deaminative arylation in the presence of TEMPO: To an oven-dried 8 mL screw-cap test tube containing a stirring bar was charged with methyl 4-bromobenzoate (21.5 mg, 0.10 mmol), 1-cyclohexyl-2,4,6-triphenylpyridin-1-ium tetrafluoroborate (**1a**) (66.9 mg, 0.14 mmol). The test tube was introduced in an argon-filled glovebox where Mn (8.4 mg, 1.5 eq.), TEMPO (15.6 mg, 0.10 mmol, 1eq.), 0.2 mL precatalyst mixture of NiBr₂-glyme (3.0 mg, 10 mol%) with 4,4'-

Deaminative Arylation at sp^3 Carbon Centers

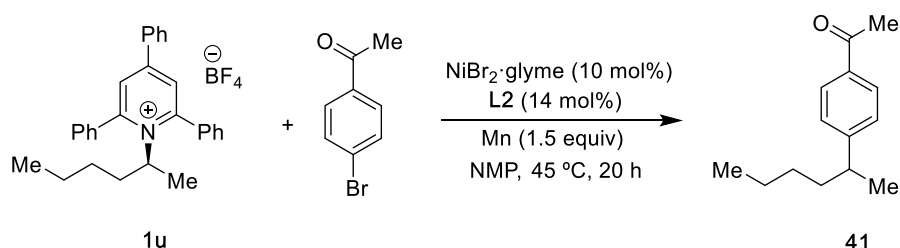
dimethoxy-2,2'-bipyridine (**L2**, 3.0 mg, 14 mol%) in NMP were added, followed by the addition of NMP (0.8 mL, 0.1 M). The tube was then sealed firmly and taken out of the glovebox. The resulting reaction mixture was stirred vigorously for 20 h. After the reaction was finished, the reaction mixture was extracted with ethyl acetate and water (3 times). Then the organic layers were combined and washed with water and brine, dried over $MgSO_4$, concentrated under vacuum. Mesitylene (14 μ L, 0.1 mmol) was added as an internal standard and the yield of known TEMPO adduct (**40**)^{XIX} was determined to be 89% by analysis of the 1H NMR spectrum of the crude reaction mixture and 1 % yield formation of **3** by GC-FID.

3.5.8.5. Stoichiometric experiment with $Ni(COD)_2$



To an oven-dried 8 mL screw-cap test tube containing a stirring bar was charged with cyclohexyl-2,4,6-triphenylpyridin-1-ium tetrafluoroborate (**1a**) (23.8 mg, 0.05 mmol), 4,4'-dimethoxy-2,2'-bipyridine (**L2**, 15.1 mg, 0.07 mmol, 1.4 equiv). The test tube was introduced in an argon-filled glovebox where Mn (4.2 mg, 1.5 equiv) and $Ni(COD)_2$ (13.8 mg, 0.05 mmol, 1 equiv) were added, followed by the addition of NMP (0.5 mL, 0.1 M). The tube was then sealed firmly and taken out of the glovebox. The resulting reaction mixture was stirred vigorously for 48 h. After that the reaction was stopped, ethyl acetate was added and measured by GC-FID obtaining less than 2% homodimerization product and not even traces of alkene.

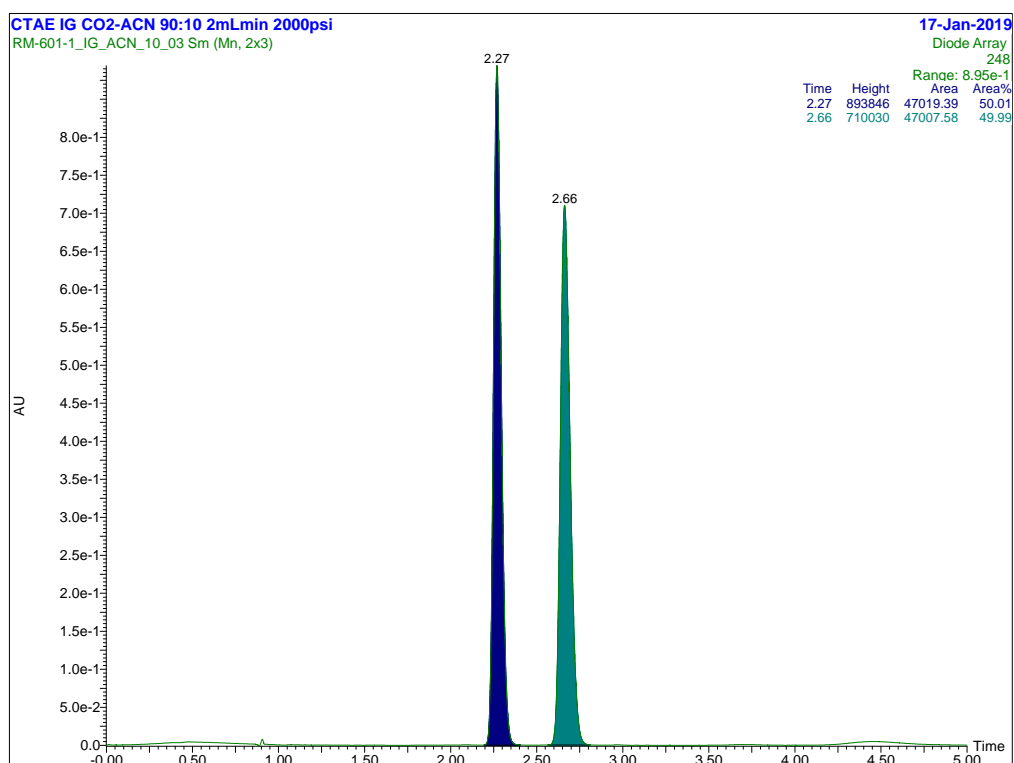
3.5.8.6. Deaminative arylation of enantiopure secondary alkyl pyridinium salts



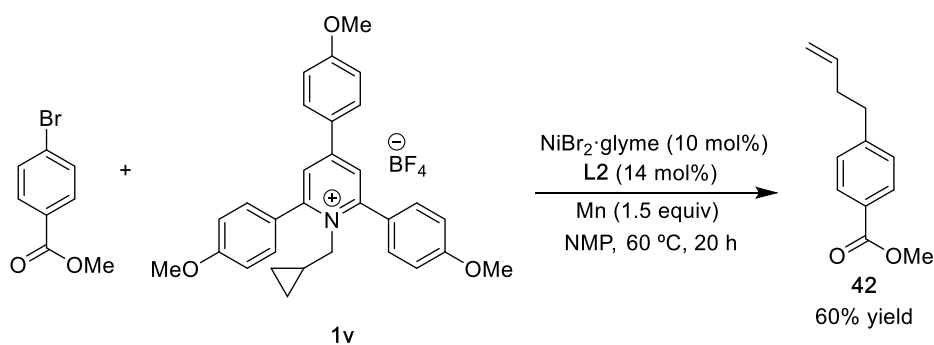
1-(4-(hexan-2-yl)phenyl)ethan-1-one (41). Following **General conditions C**, 1-(4-bromophenyl)ethan-1-one (19.9 mg, 0.10 mmol) and 1-(hexan-2-yl)-2,4,6-triphenylpyridin-1-ium tetrafluoroborate (**1u**) (73.8 mg, 0.14 mmol) were used at 45 °C, affording the title compound as a yellow oil (13 mg, 64% yield) by using Hexane/ *tert*-butyl-methyl ether (95/5) as eluent. The

Chapter 3

enantiomeric excess was determined to be racemic by chiral UPC2 analysis (CHIRALPAK IG, 2 mL/min, Isocratic CO₂/ACN 90:10, 2000 psi, λ =248 nm); t_{R1} = 2.27 min, t_{R2} = 2.66 min. ¹H NMR (400 MHz, CDCl₃) δ = 7.90 – 7.88 (m, 2H), 7.28 – 7.26 (m, 2H), 2.74 (q, J = 7.1 Hz, 1H), 2.58 (s, 3H), 1.61 – 1.52 (m, 2H), 1.34 – 1.16 (m, 6H), 1.15 – 1.06 (m, 1H), 0.85 (t, J = 7.2 Hz, 3H) ppm. ¹³C NMR (101 MHz, CDCl₃) δ = 197.9, 153.8, 135.1, 128.5, 127.2, 40.1, 37.8, 29.8, 26.5, 22.7, 22.0, 14.0 ppm. IR (neat, cm⁻¹): 2956, 2924, 2856, 1680, 1605, 1356, 1264, 954. HRMS calcd. for (C₁₄H₂₁O) [M+H]⁺: 205.1587, found 205.1579.



3.5.8.7. Radical clock experiment



1-(4-(hexan-2-yl)phenyl)ethan-1-one (41). Following **General conditions C**, methyl 4-bromobenzoate (21.5 mg, 0.10 mmol) and 1-(cyclopropylmethyl)-2,4,6-tris(4-methoxyphenyl)pyridin-1-ium tetrafluoroborate (**1v**) (75.5 mg, 0.14 mmol) were used at 60 °C,

Deaminative Arylation at sp^3 Carbon Centers

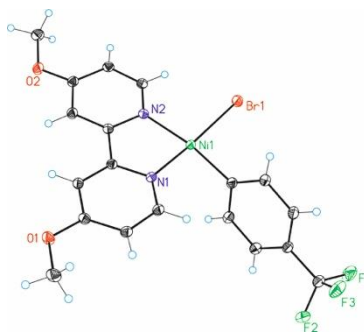
affording the title compound as a yellow oil (11.4 mg, 60% yield) by using Hexane/ *tert*-butyl-methyl ether (95/5) as eluent. $^1\text{H NMR}$ (400 MHz, CDCl_3) δ = 8.07 – 7.85 (m, 2H), 7.35 – 7.17 (m, 3H), 5.83 (ddt, J = 16.9, 10.2, 6.6 Hz, 1H), 5.11 – 4.87 (m, 2H), 3.90 (s, 3H), 2.76 (dd, J = 8.8, 6.7 Hz, 2H), 2.45 – 2.29 (m, 2H) ppm. $^{13}\text{C NMR}$ (101 MHz, CDCl_3) δ = 167.1, 147.3, 137.5, 129.6, 128.5, 127.8, 115.3, 77.0, 52.0, 35.3, 35.0 ppm. Spectroscopic data for **42** match those previously reported in the literature.^{xxii}

Chapter 3

3.5.9 References of experimental procedures.

- I) Ortgies, S.; Depken, C.; Breder, A. *Org. Lett.* **2016**, *18*, 2856.
- II) Basch, C. H.; Liao, J.; Xu, J.-Y.; Plane, J.J.; Watson, M.P. *J. Am. Chem. Soc.* **2017**, *139*, 5313.
- III) Klauk, F.J.R.; James, M.; Glorius, F. *Angew. Chem. Int. Ed.* **2017**, *56*, 12336.
- IV) Wu, J.; He, J.; Noble, A.; Aggarwal, V.K. *J. Am. Chem. Soc.* **2018**, *140*, 10700.
- V) Wang, S.; Qian, Q.; Gong, H. *Org. Lett.* **2012**, *14*, 3352.
- VI) Too, P. C.; Chan, G.H.; Tnay, Y.L.; Hirao, H.; Chiba, S. *Angew. Chem. Int. Ed.* **2016**, *55*, 3719.
- VII) Ganesh, V.; Odachowski, M.; Aggarwal, V. K. *Angew. Chem. Int. Ed.* **2017**, *56*, 9752.
- VIII) Öhberg, L.; Westman, J. *Synlett.* **2001**, *12*, 1893.
- IX) Ueda, K.; Umihara, H.; Yokoshima, S.; Fukuyama, T. *Org. Lett.* **2015**, *17*, 3191.
- X) Zhang, X.; Yang, C. *Adv. Synth. Catal.* **2015**, *357*, 2721.
- XI) Pompeo, M.; Froese, D.J.; Hadei, N.; Organ, M.G. *Angew. Chem. Int. Ed.* **2012**, *51*, 11354.
- XII) Zhang, P.; Le, C. C.; MacMillan, D. W. C. *J. Am. Chem. Soc.* **2016**, *138*, 8084.
- XIII) Liu, D.; Li, Y.-X.; Qi, X.-T.; Liu, C.; Lan, Y.; Lei, A.-W. *Org. Lett.* **2015**, *17*, 998.
- XIV) Blank, B.; Kempe, R. *J. Am. Chem. Soc.* **2010**, *132*, 924.
- XV) Panda, S.; Coffin, A.; Nguyen, Q.N.; Tantillo, D.J.; Ready, J. M. *Angew. Chem. Int. Ed.* **2016**, *55*, 2205.
- XVI) Sun, S.-Z.; Martin, R. *Angew. Chem. Int. Ed.* **2018**, *57*, 3622.
- XVII) Klein, A.; Kaiser, A.; Sarkar, B.; Wanner, M.; Fiedler, J. *Eur. J. Inorg. Chem.* **2007**, 965.
- XVIII) Klein, A.; Feth, M. P.; Bertagnolli, H.; Zális, S.; J. *Eur. J. Inorg. Chem.* **2004**, 2784.
- XIX) Sumino, S.; Ryu, I. *Org. Lett.* **2016**, *18*, 52.
- XX) An oxidation potential of 0.62 V was measured for ferrocene solution in NMP (2mM). This provided a conversion factor of -0.62 V to convert between Ag/AgCl and Fc/Fc⁺ reference electrodes.
- XXI) A conversion factor of -0.2 V was used to convert the value from that vs. NHE to Ag/AgCl reference electrode. A. J. Bard and L. R. Faulkner, *Electrochemical methods: fundamentals and applications*, Wiley, New York, **1980**.
- XXII) Greenhalgh, M.; Thomas, S.P. *Chem. Commun.* **2013**, *49*, 11230.
- XXIII) H, J.; Wang, G.; L, S.; Shi, Z. *Angew. Chem. Int. Ed.* **2018**, *57*, 15227.

3.5.10 X-Ray Crystallography data for Ni(II) Complex Ni-1



X-ray quality crystals were obtained from a saturated solution of **Ni-1** in toluene and drops of pentane were slowly added, and left it in glove box few days. A CIF file is available as a separate Supporting Information file.

Table 1. Crystal data and structure refinement for **Ni-1**.

Identification code	Ni-1	
Empirical formula	C ₁₉ H ₁₆ Br F ₃ N ₂ Ni O ₂	
Formula weight	499.96	
Temperature	100(2) K	
Wavelength	0.71073 Å	
Crystal system	Monoclinic	
Space group	P2(1)/n	
Unit cell dimensions	a = 10.4282(2)Å	a = 90°.
	b = 11.9745(2)Å	b = 96.161(2)°.
	c = 14.7268(3)Å	g = 90°.
Volume	1828.35(6) Å ³	
Z	4	
Density (calculated)	1.816 Mg/m ³	
Absorption coefficient	3.294 mm ⁻¹	
F(000)	1000	
Crystal size	? x ? x ? mm ³	

Chapter 3

Theta range for data collection	2.197 to 37.420°.
Index ranges	-16<=h<=17,-20<=k<=19,-25<=l<=19
Reflections collected	26930
Independent reflections	9139[R(int) = 0.0241]
Completeness to theta =37.420°	95.4%
Absorption correction	Multi-scan
Max. and min. transmission	0.880 and 0.677
Refinement method	Full-matrix least-squares on F ²
Data / restraints / parameters	9139/ 0/ 317
Goodness-of-fit on F ²	1.008
Final R indices [I>2sigma(I)]	R1 = 0.0291, wR2 = 0.0639
R indices (all data)	R1 = 0.0474, wR2 = 0.0688
Largest diff. peak and hole	0.777 and -0.503 e.Å ⁻³

Table 2. Bond lengths [Å] and angles [°] for **Ni-1**.

Bond lengths----

Br1-Ni1	2.30613(19)
N1-C1	1.3437(15)
N1-C5	1.3614(15)
N1-Ni1	1.9142(10)
Ni1-C13	1.8808(12)
Ni1-N2	1.9805(10)
O1-C3	1.3450(14)
O1-C11	1.4430(15)
C1-C2	1.3834(16)
C1-H1	0.945(15)
F1-C19	1.3517(16)

Deaminative Arylation at sp^3 Carbon Centers

O2-C8	1.3407(14)
O2-C12	1.4384(15)
N2-C10	1.3414(14)
N2-C6	1.3563(15)
C2-C3	1.3918(17)
C2-H2	0.898(18)
F2-C19	1.3408(15)
F3-C19	1.3413(17)
C3-C4	1.4001(16)
C6-C7	1.3806(16)
C6-C5	1.4767(15)
C5-C4	1.3795(16)
C4-H4	0.901(18)
C7-C8	1.3962(16)
C7-H7	0.920(19)
C8-C9	1.3942(17)
C9-C10	1.3901(17)
C9-H9	0.902(17)
C10-H10	0.888(18)
C11-H111	0.950(16)
C11-H112	0.973(17)
C11-H113	0.91(2)
C12-H121	0.99(2)
C12-H122	1.026(19)
C12-H123	0.972(18)
C13-C18	1.3984(17)
C13-C14	1.4025(17)

Chapter 3

C14-C15	1.3896(17)
C14-H14	0.942(18)
C15-C16	1.3865(18)
C15-H15	0.956(16)
C16-C17	1.3915(17)
C16-C19	1.4904(17)
C17-C18	1.3926(17)
C17-H17	0.957(18)
C18-H18	0.928(18)

Angles-----

C1-N1-C5	117.02(10)
C1-N1-Ni1	126.86(8)
C5-N1-Ni1	115.75(7)
C13-Ni1-N1	92.67(5)
C13-Ni1-N2	168.48(5)
N1-Ni1-N2	82.74(4)
C13-Ni1-Br1	88.93(4)
N1-Ni1-Br1	169.12(3)
N2-Ni1-Br1	97.57(3)
C3-O1-C11	117.16(10)
N1-C1-C2	124.00(11)
N1-C1-H1	117.6(11)
C2-C1-H1	118.4(11)
C8-O2-C12	117.78(10)
C10-N2-C6	117.37(10)
C10-N2-Ni1	128.69(8)
C6-N2-Ni1	113.76(7)

Deaminative Arylation at sp^3 Carbon Centers

C1-C2-C3	118.42(11)
C1-C2-H2	121.4(11)
C3-C2-H2	120.2(11)
O1-C3-C2	125.05(10)
O1-C3-C4	116.41(10)
C2-C3-C4	118.54(10)
N2-C6-C7	122.85(10)
N2-C6-C5	113.71(10)
C7-C6-C5	123.43(10)
N1-C5-C4	122.79(10)
N1-C5-C6	113.82(10)
C4-C5-C6	123.38(10)
C5-C4-C3	119.13(11)
C5-C4-H4	120.9(11)
C3-C4-H4	120.0(11)
C6-C7-C8	119.02(11)
C6-C7-H7	119.8(12)
C8-C7-H7	121.1(12)
O2-C8-C9	125.57(11)
O2-C8-C7	115.53(10)
C9-C8-C7	118.90(11)
C10-C9-C8	118.02(10)
C10-C9-H9	118.6(11)
C8-C9-H9	123.3(11)
N2-C10-C9	123.85(11)
N2-C10-H10	115.3(12)
C9-C10-H10	120.8(12)

Chapter 3

O1-C11-H111	110.8(10)
O1-C11-H112	111.5(10)
H111-C11-H112	111.2(14)
O1-C11-H113	107.1(12)
H111-C11-H113	109.2(16)
H112-C11-H113	106.8(16)
O2-C12-H121	108.8(12)
O2-C12-H122	112.2(10)
H121-C12-H122	109.8(15)
O2-C12-H123	110.6(11)
H121-C12-H123	106.9(15)
H122-C12-H123	108.4(15)
C18-C13-C14	117.96(11)
C18-C13-Ni1	125.00(9)
C14-C13-Ni1	116.93(9)
C15-C14-C13	121.26(12)
C15-C14-H14	118.5(11)
C13-C14-H14	120.2(11)
C16-C15-C14	119.59(11)
C16-C15-H15	121.1(10)
C14-C15-H15	119.3(10)
C15-C16-C17	120.47(11)
C15-C16-C19	119.97(11)
C17-C16-C19	119.51(11)
C16-C17-C18	119.46(11)
C16-C17-H17	120.7(11)
C18-C17-H17	119.7(11)

Deaminative Arylation at sp^3 Carbon Centers

C17-C18-C13	121.21(11)
C17-C18-H18	117.1(11)
C13-C18-H18	121.7(11)
F2-C19-F3	106.60(11)
F2-C19-F1	105.77(11)
F3-C19-F1	105.21(11)
F2-C19-C16	113.21(11)
F3-C19-C16	113.09(11)
F1-C19-C16	112.32(10)

Table 3. Torsion angles [°] for **Ni-1**.

C5-N1-C1-C2	0.74(17)
Ni1-N1-C1-C2	173.44(9)
N1-C1-C2-C3	1.93(19)
C11-O1-C3-C2	5.24(17)
C11-O1-C3-C4	-174.58(10)
C1-C2-C3-O1	177.31(11)
C1-C2-C3-C4	-2.88(17)
C10-N2-C6-C7	-0.37(17)
Ni1-N2-C6-C7	-175.94(9)
C10-N2-C6-C5	-179.61(10)
Ni1-N2-C6-C5	4.81(12)
C1-N1-C5-C4	-2.47(16)
Ni1-N1-C5-C4	-175.99(9)
C1-N1-C5-C6	176.63(10)
Ni1-N1-C5-C6	3.12(12)

Chapter 3

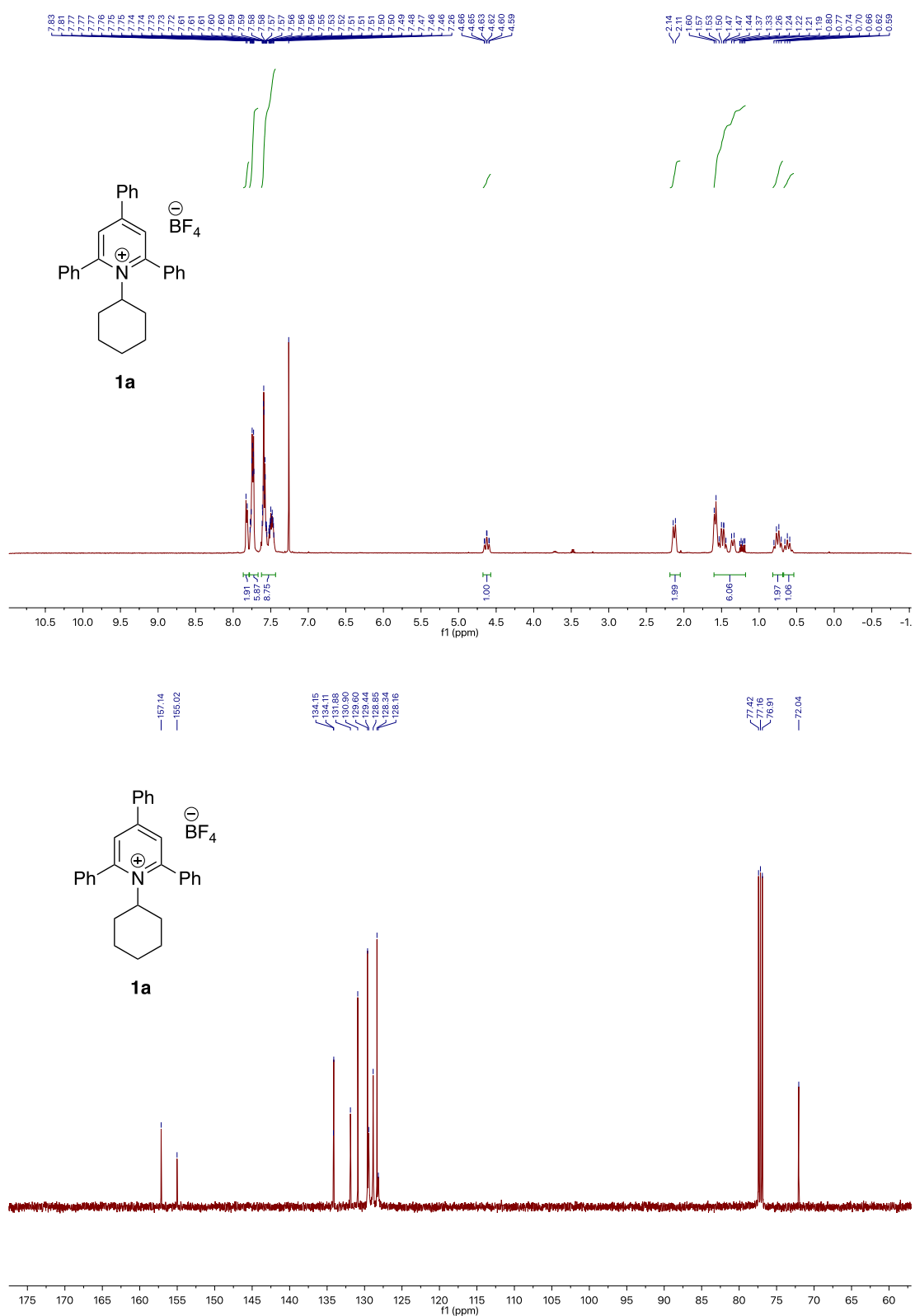
N2-C6-C5-N1	-5.21(14)
C7-C6-C5-N1	175.55(11)
N2-C6-C5-C4	173.89(11)
C7-C6-C5-C4	-5.35(18)
N1-C5-C4-C3	1.47(17)
C6-C5-C4-C3	-177.55(11)
O1-C3-C4-C5	-178.88(11)
C2-C3-C4-C5	1.29(17)
N2-C6-C7-C8	0.20(18)
C5-C6-C7-C8	179.37(11)
C12-O2-C8-C9	-7.09(18)
C12-O2-C8-C7	172.63(11)
C6-C7-C8-O2	-179.53(11)
C6-C7-C8-C9	0.21(17)
O2-C8-C9-C10	179.28(11)
C7-C8-C9-C10	-0.43(17)
C6-N2-C10-C9	0.13(17)
Ni1-N2-C10-C9	174.94(9)
C8-C9-C10-N2	0.27(18)
N1-Ni1-C13-C18	-103.44(11)
N2-Ni1-C13-C18	-169.57(19)
Br1-Ni1-C13-C18	65.79(10)
N1-Ni1-C13-C14	72.69(10)
N2-Ni1-C13-C14	6.6(3)
Br1-Ni1-C13-C14	-118.08(9)
C18-C13-C14-C15	1.27(18)
Ni1-C13-C14-C15	-175.15(10)

Deaminative Arylation at sp^3 Carbon Centers

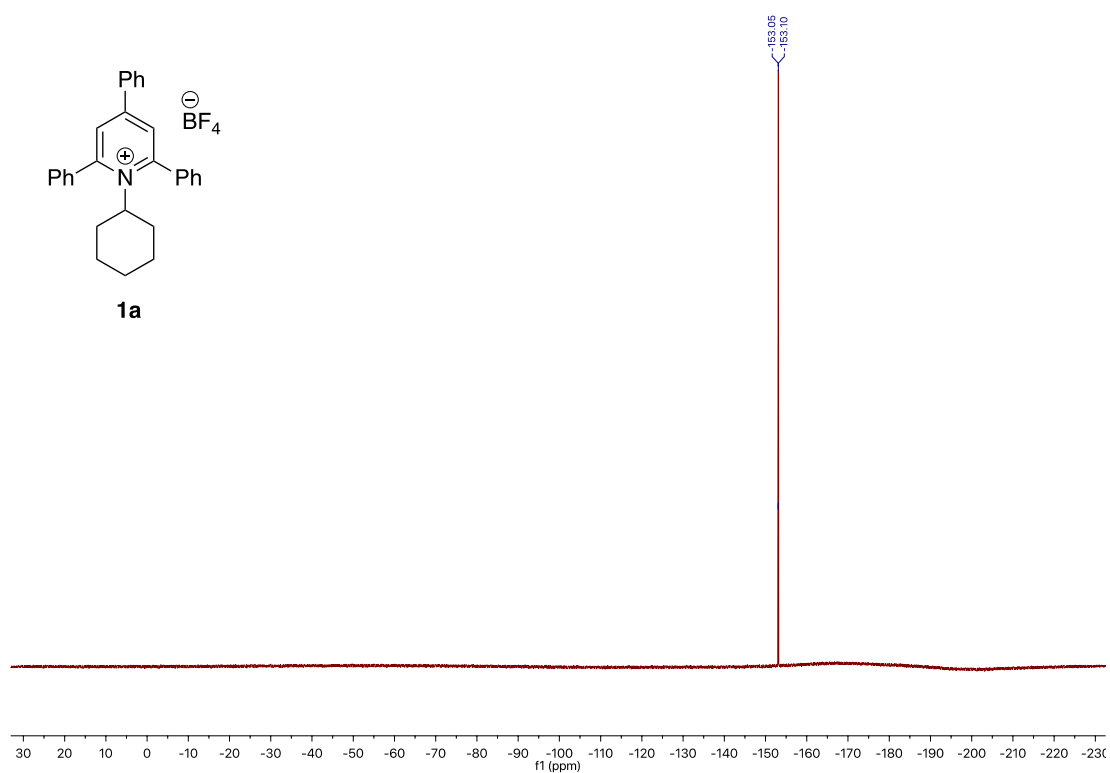
C13-C14-C15-C16	0.53(19)
C14-C15-C16-C17	-1.25(19)
C14-C15-C16-C19	-178.60(12)
C15-C16-C17-C18	0.14(18)
C19-C16-C17-C18	177.50(11)
C16-C17-C18-C13	1.73(18)
C14-C13-C18-C17	-2.40(18)
Ni1-C13-C18-C17	173.69(9)
C15-C16-C19-F2	-27.72(17)
C17-C16-C19-F2	154.90(12)
C15-C16-C19-F3	-149.10(12)
C17-C16-C19-F3	33.52(16)
C15-C16-C19-F1	91.99(15)
C17-C16-C19-F1	-85.38(15)

Chapter 3

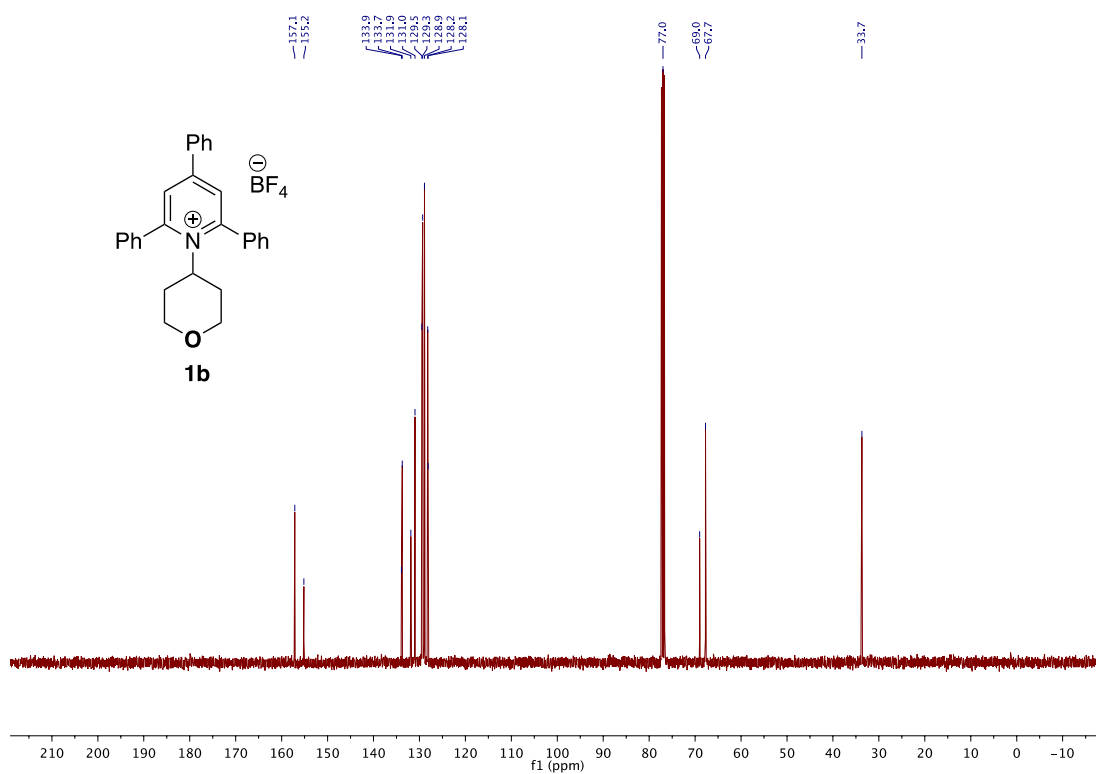
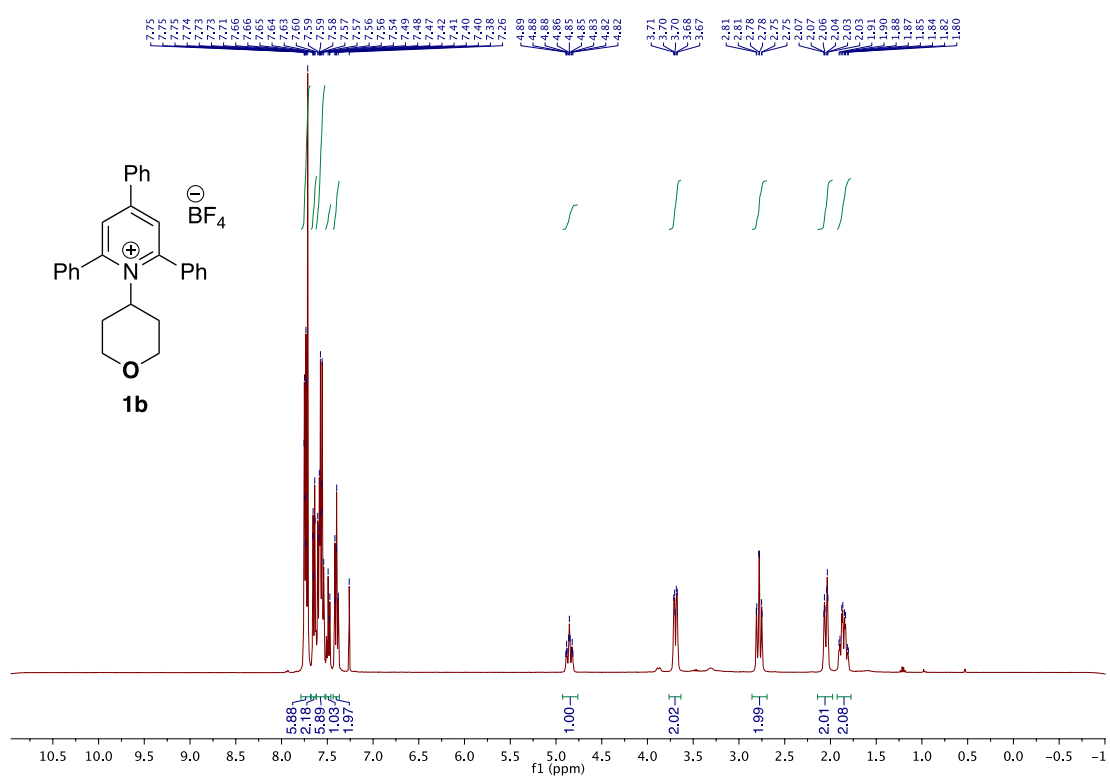
3.5.11 ^1H NMR, ^{13}C NMR & ^{19}F NMR spectra



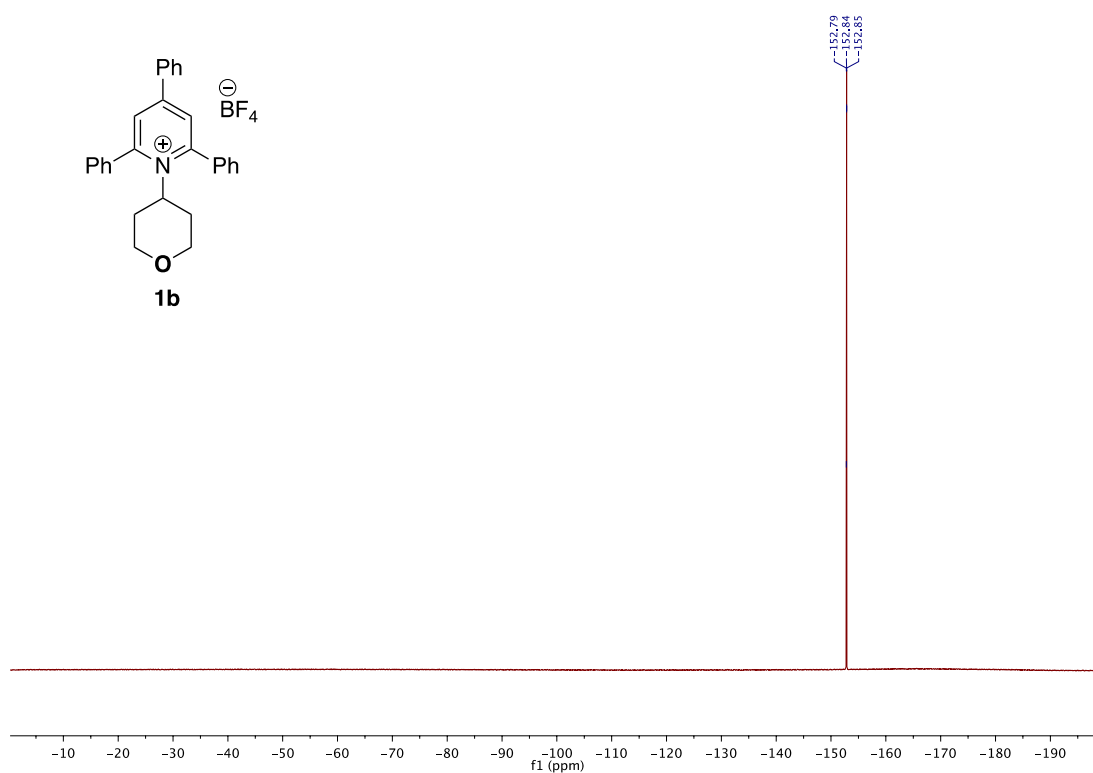
Deaminative Arylation at sp^3 Carbon Centers



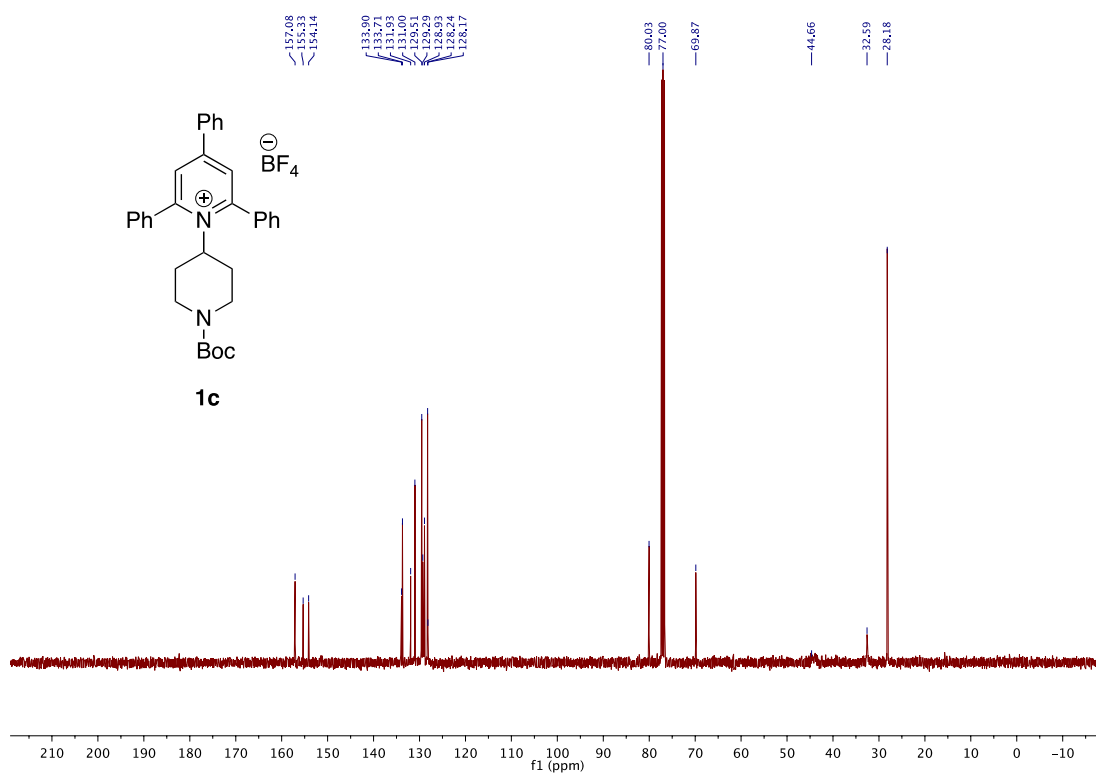
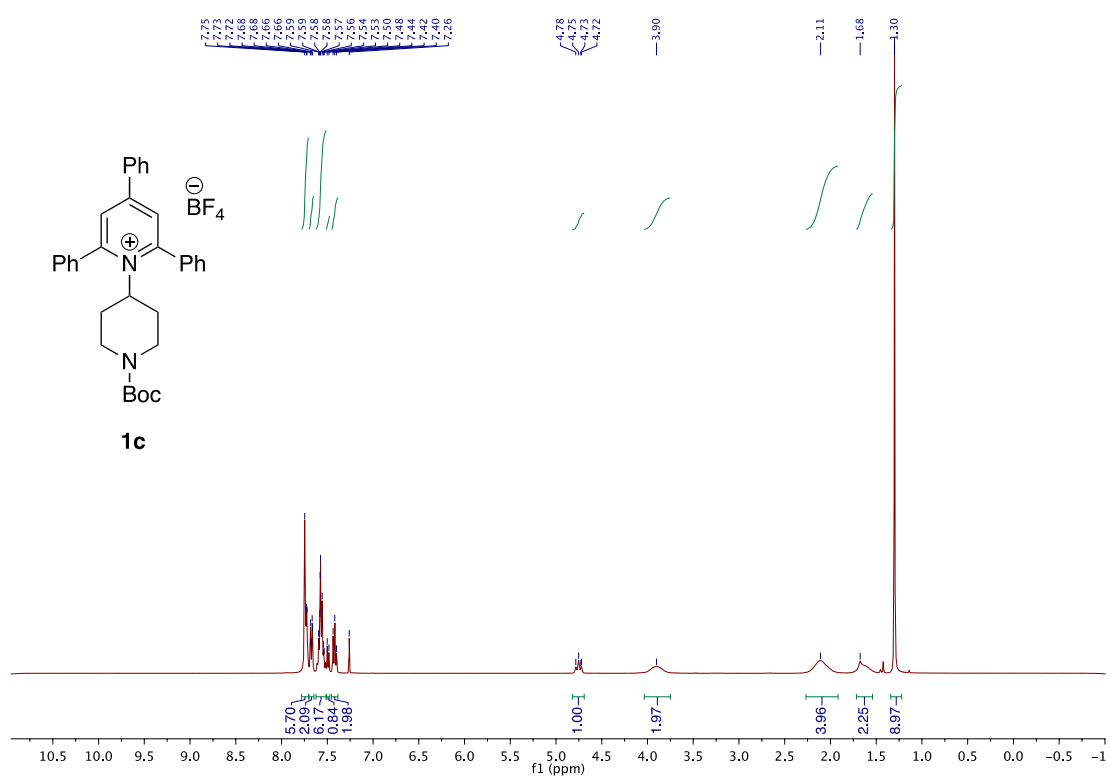
Chapter 3



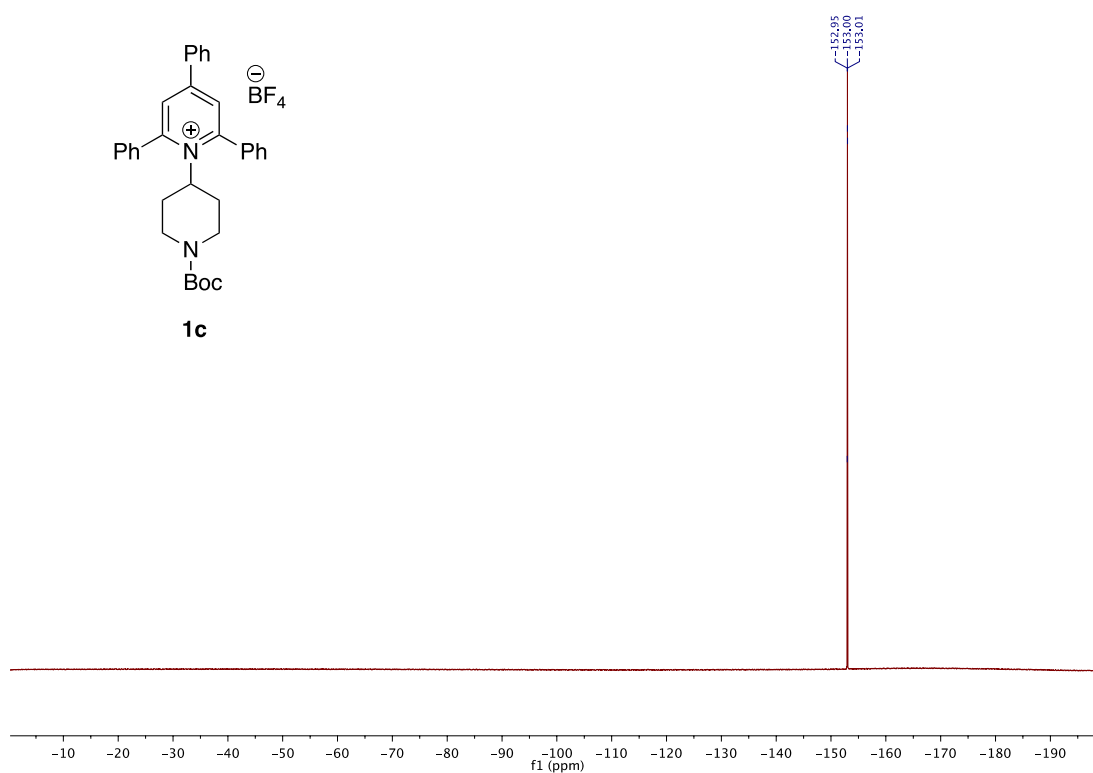
Deaminative Arylation at sp^3 Carbon Centers



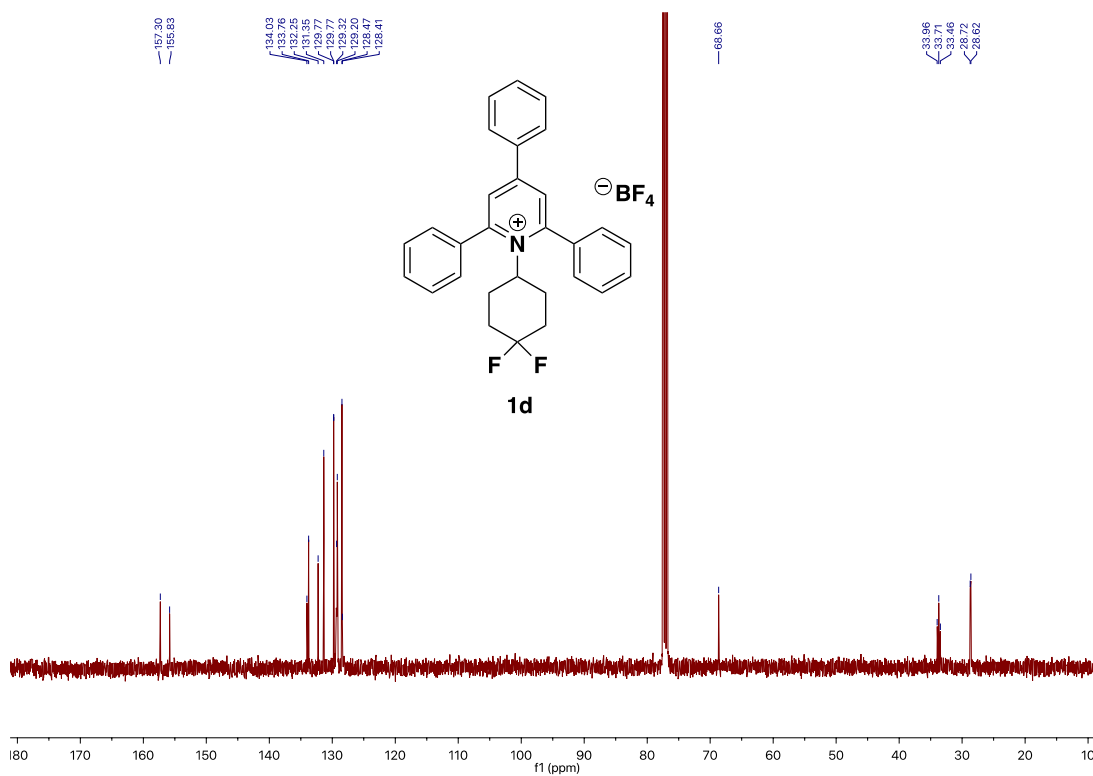
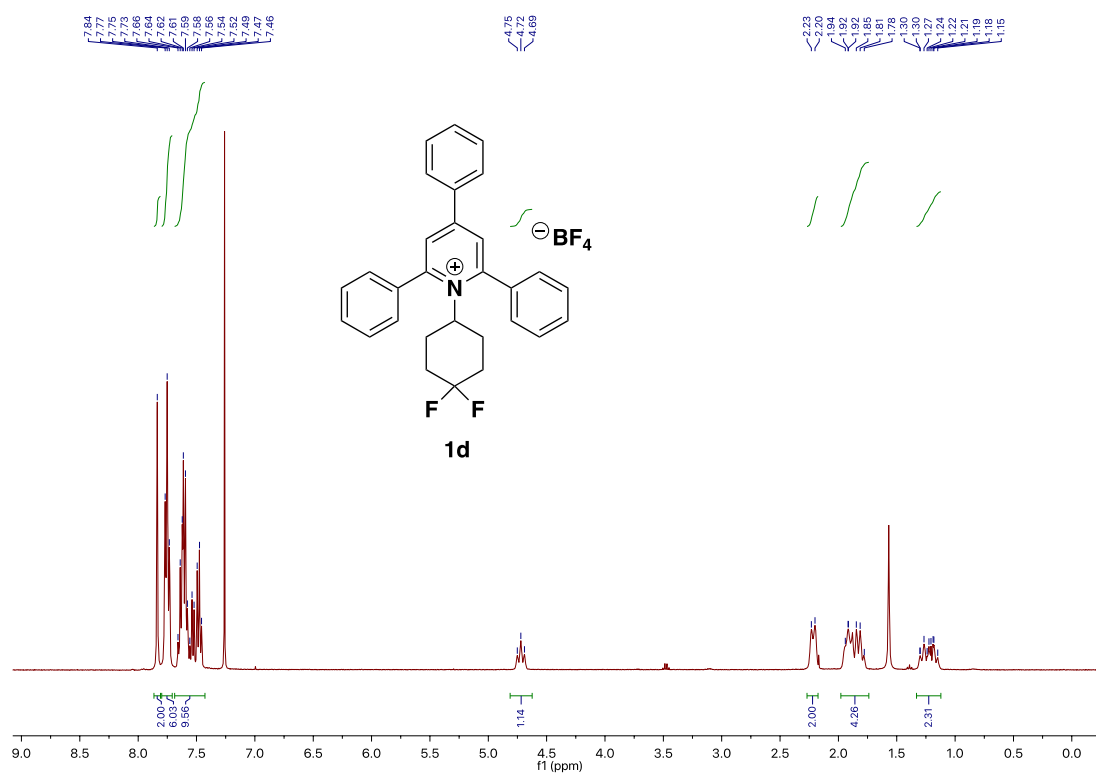
Chapter 3



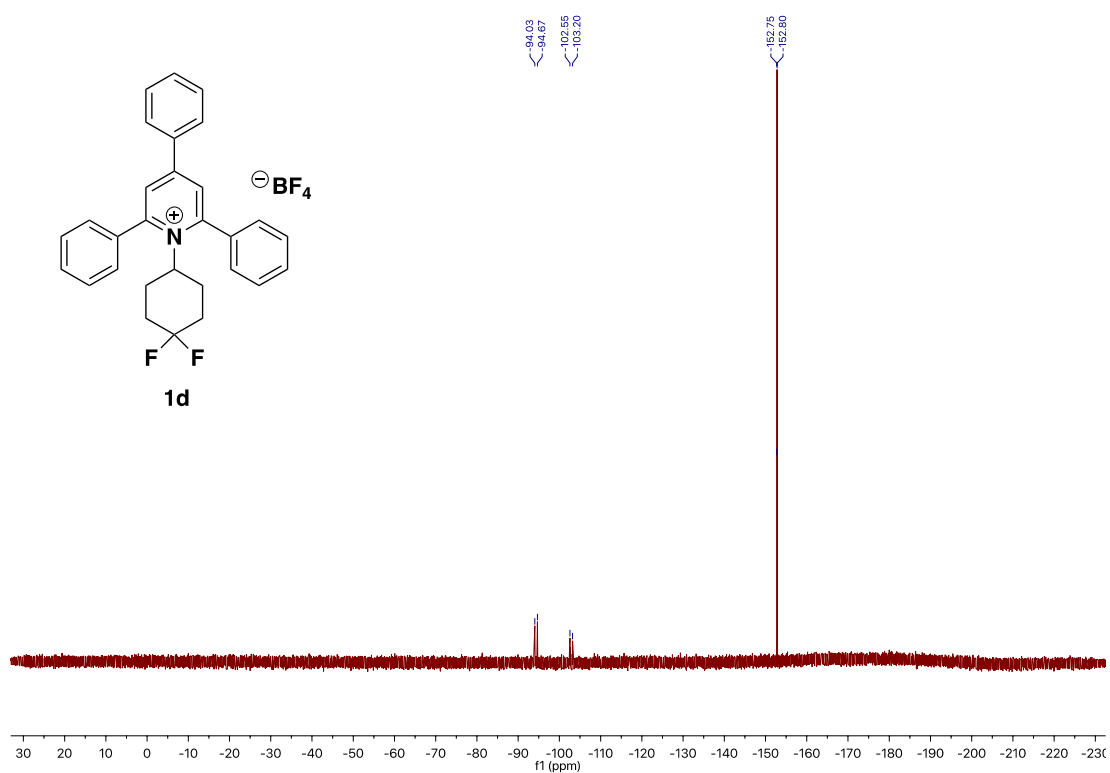
Deaminative Arylation at sp^3 Carbon Centers



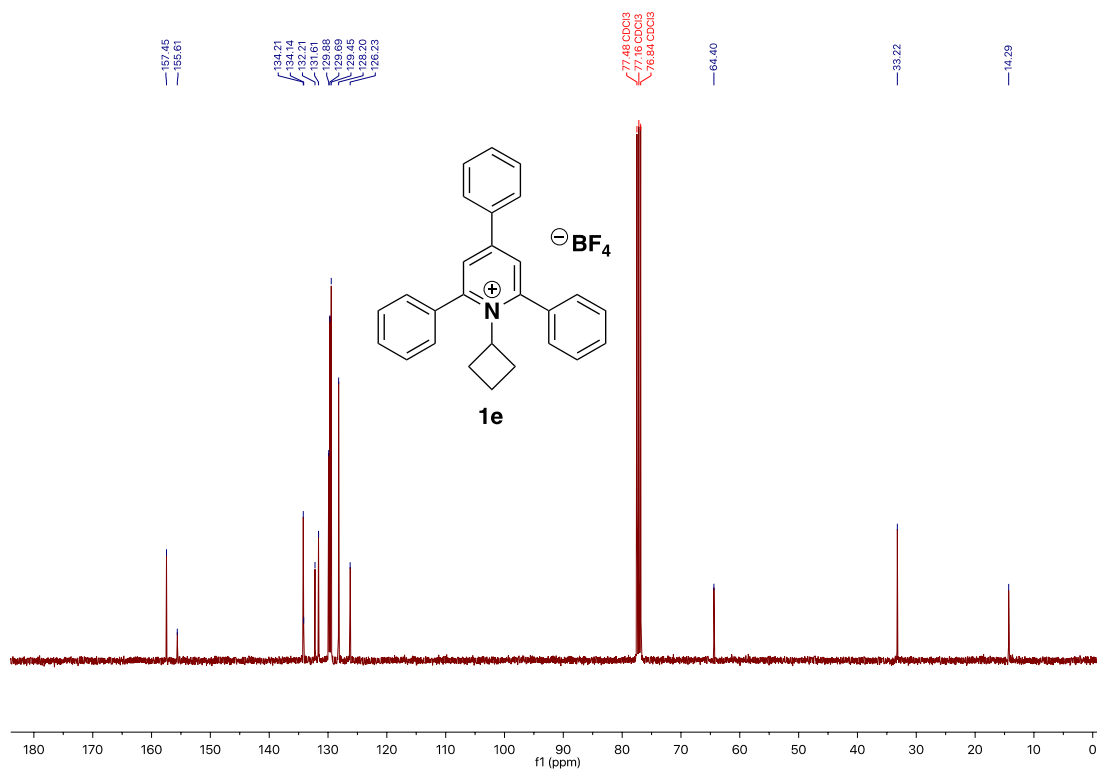
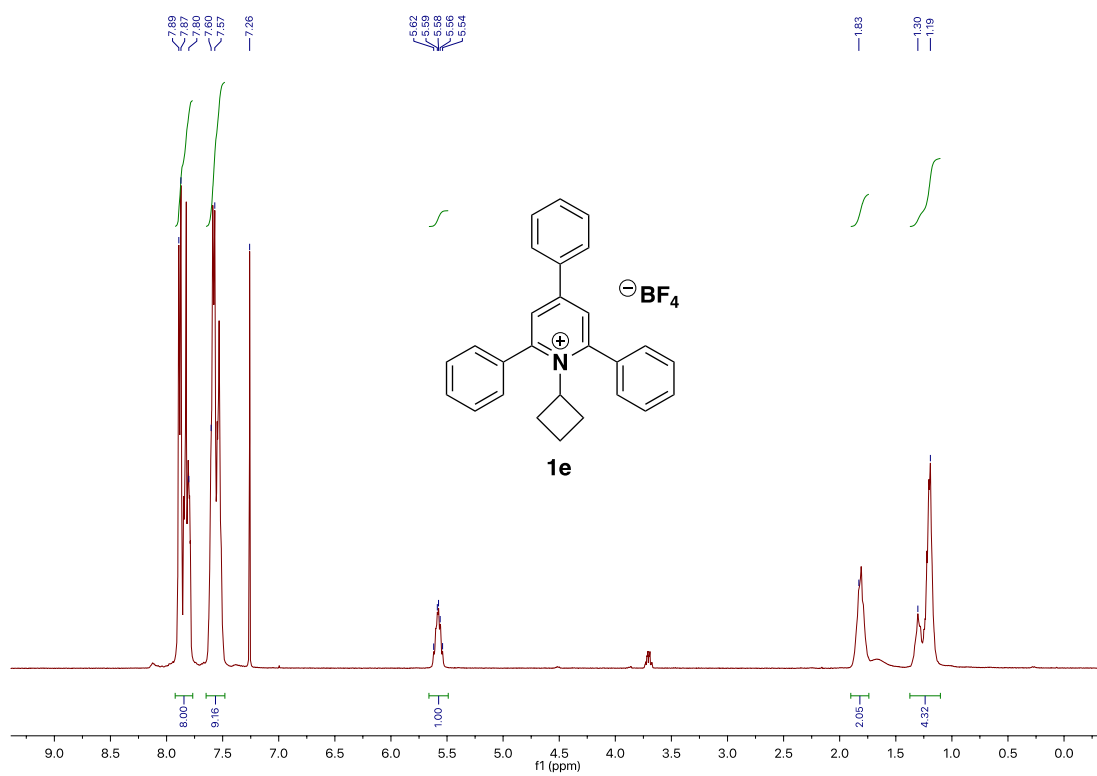
Chapter 3



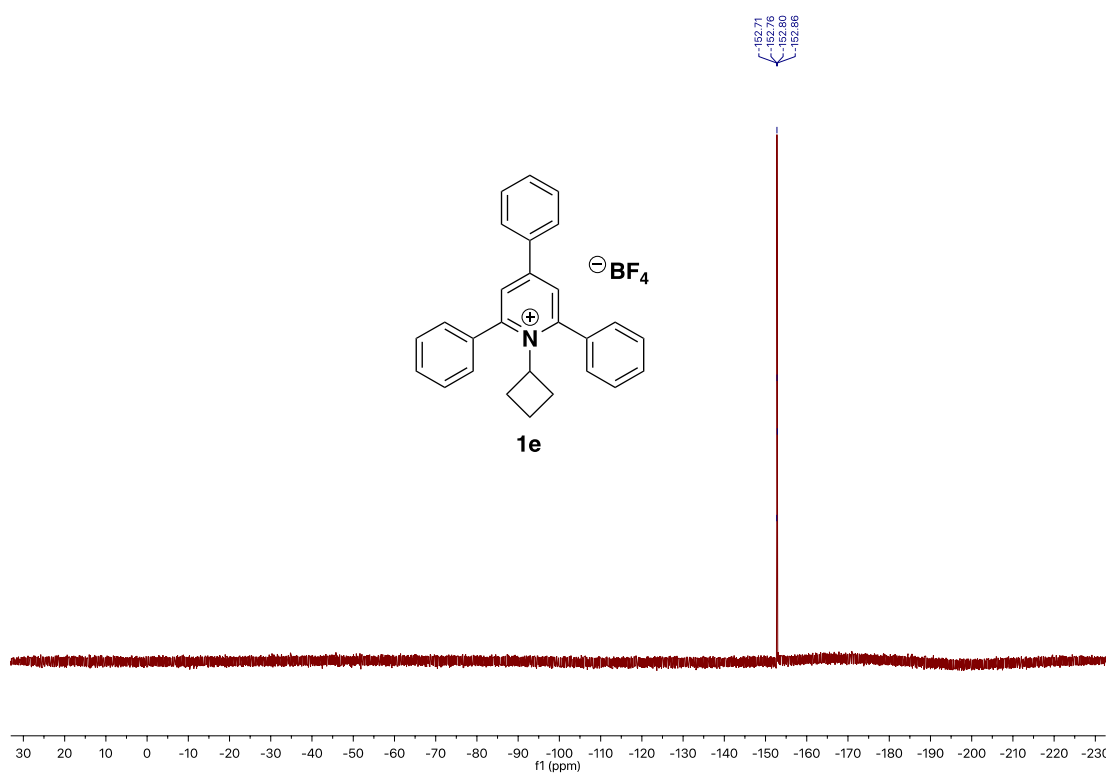
Deaminative Arylation at sp^3 Carbon Centers



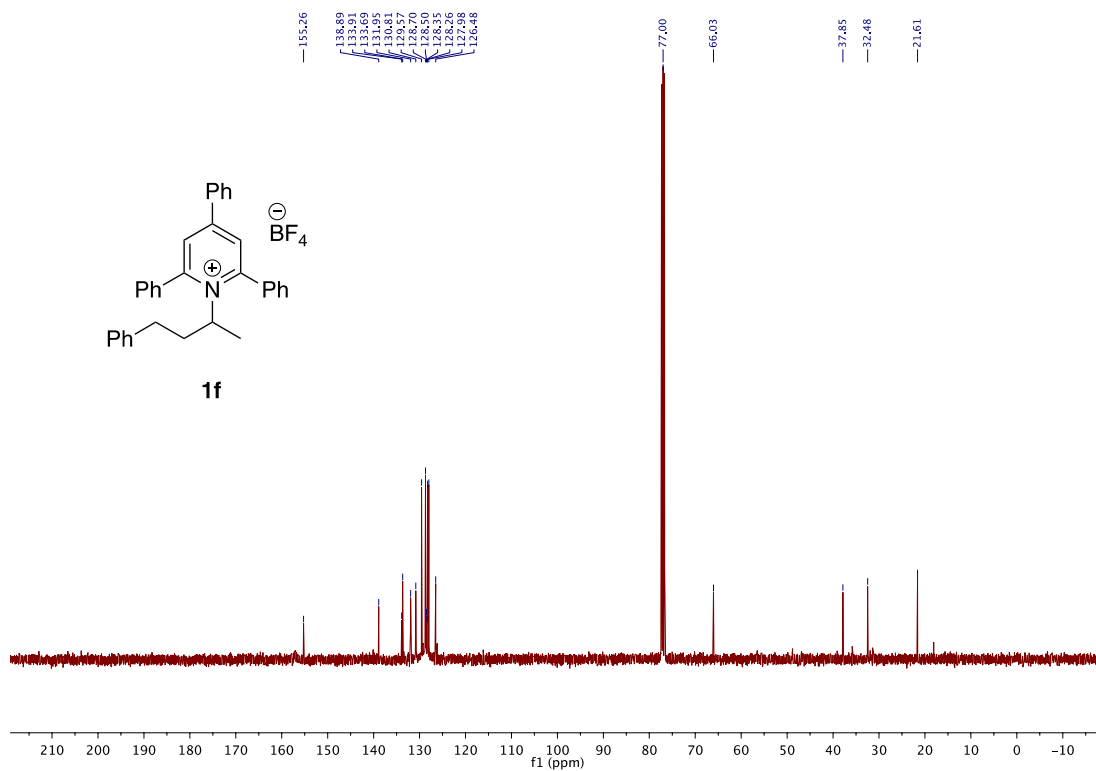
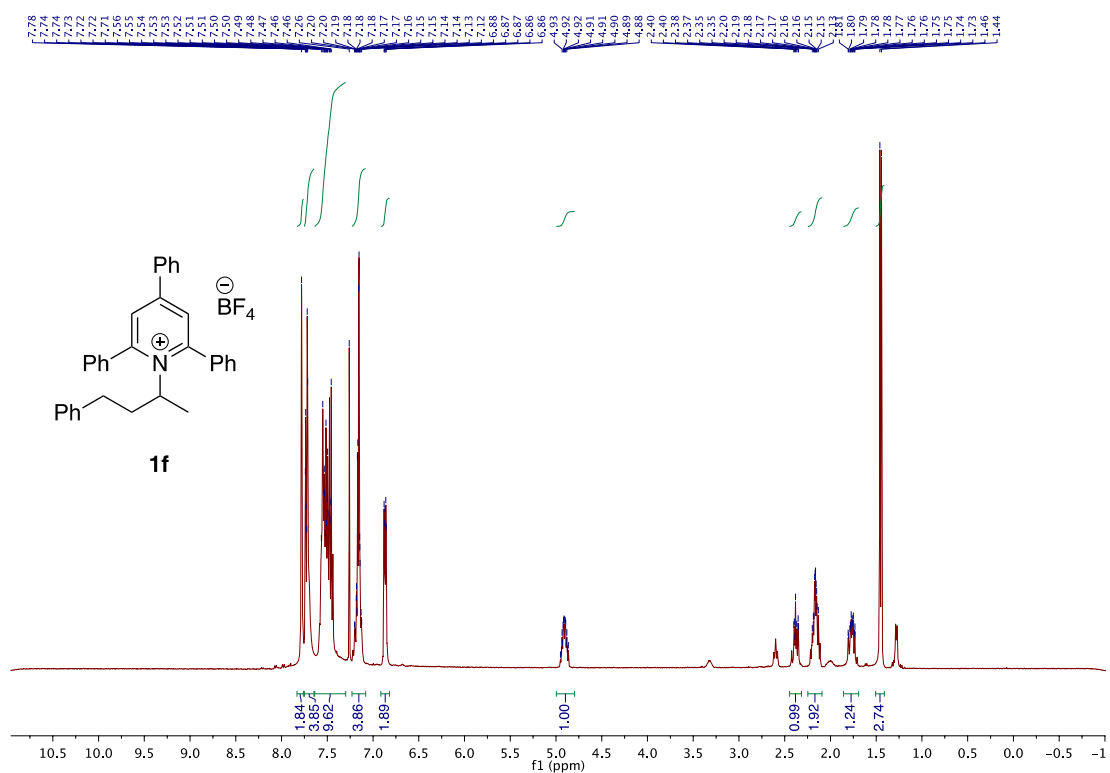
Chapter 3



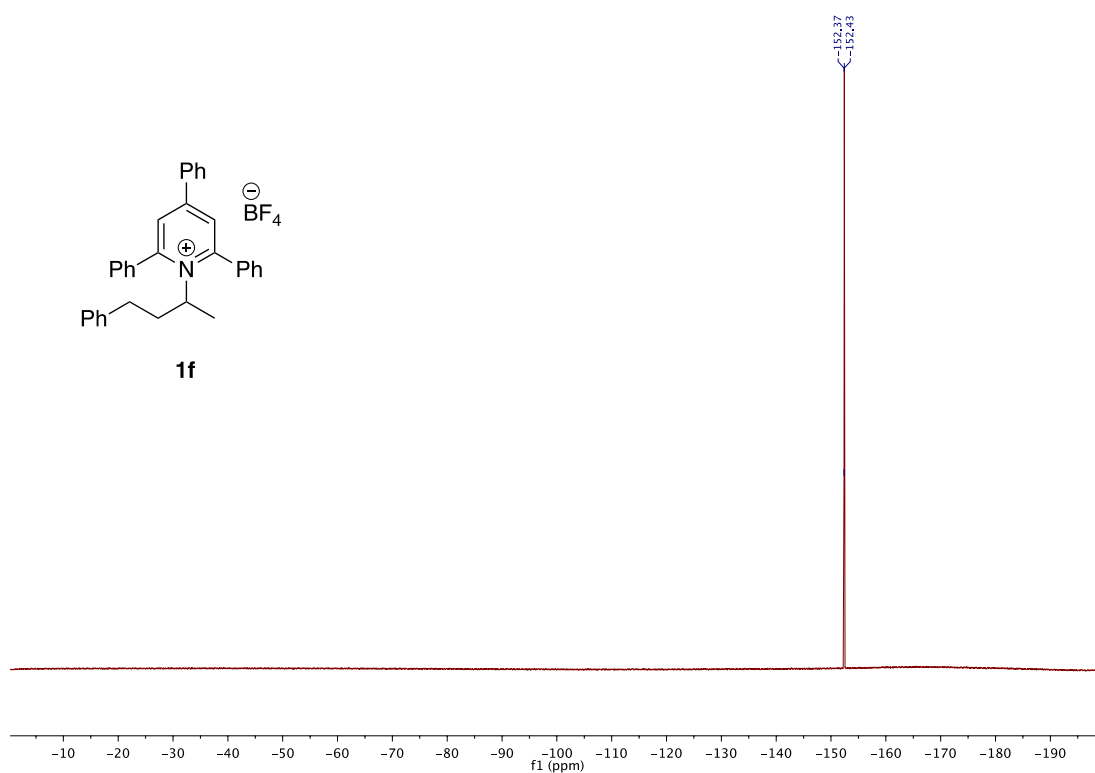
Deaminative Arylation at sp^3 Carbon Centers



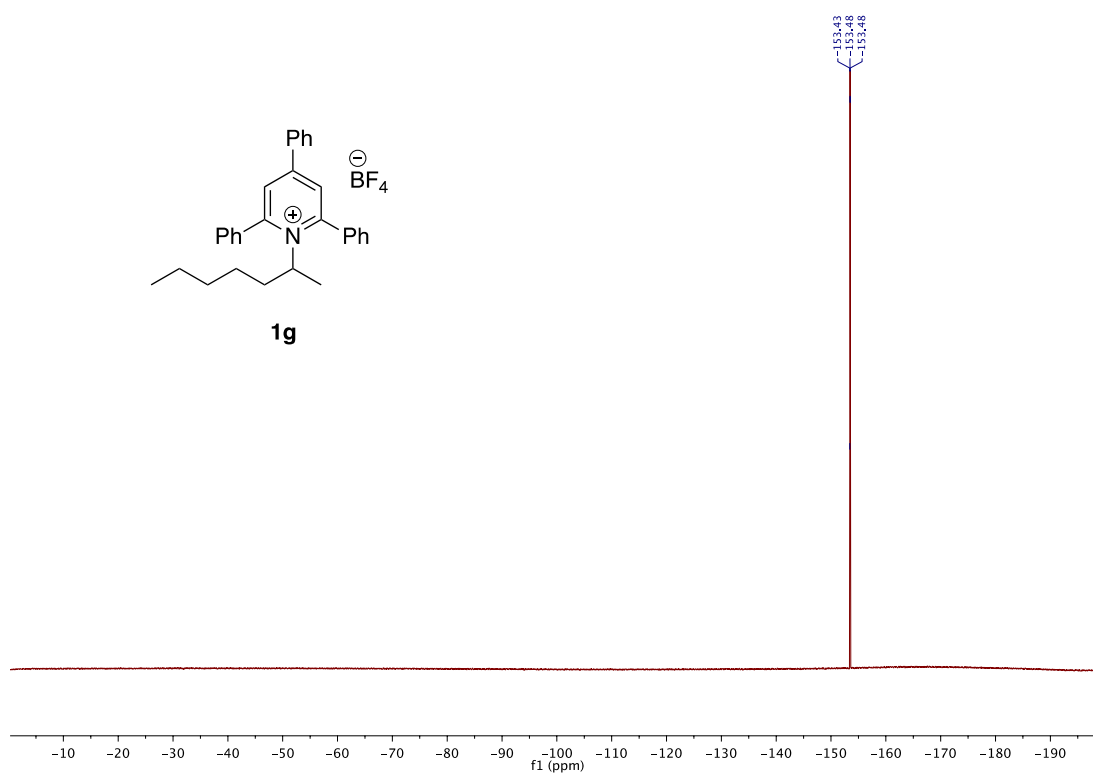
Chapter 3



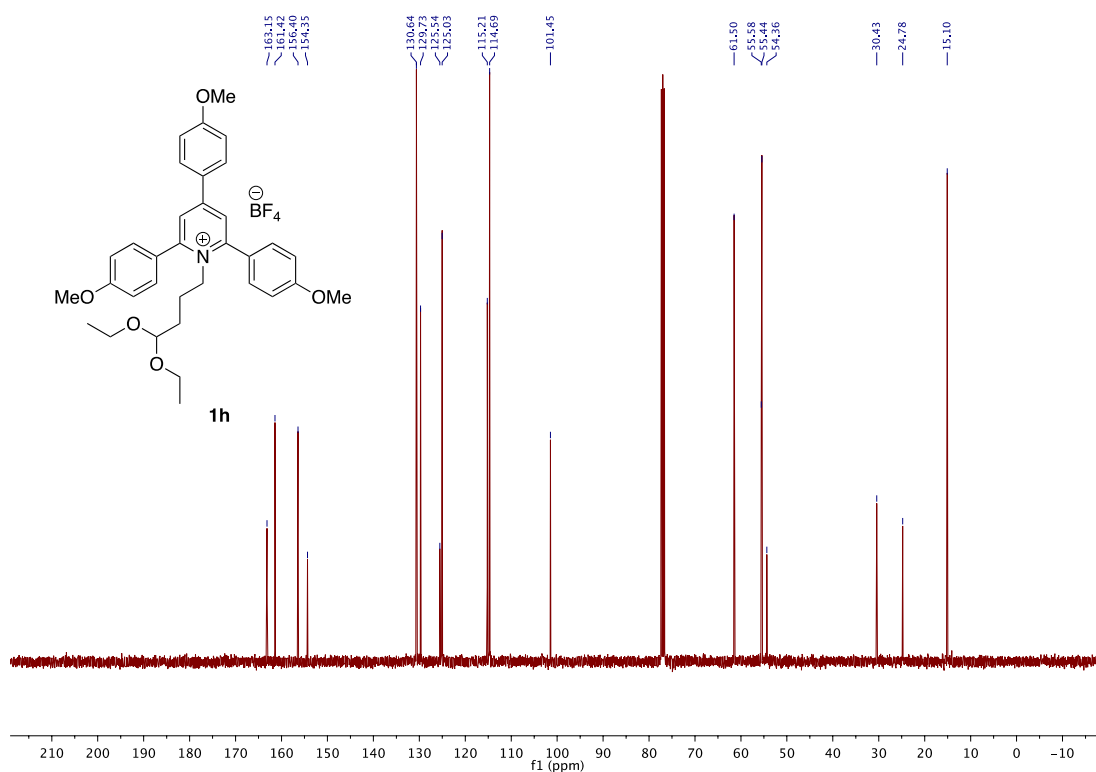
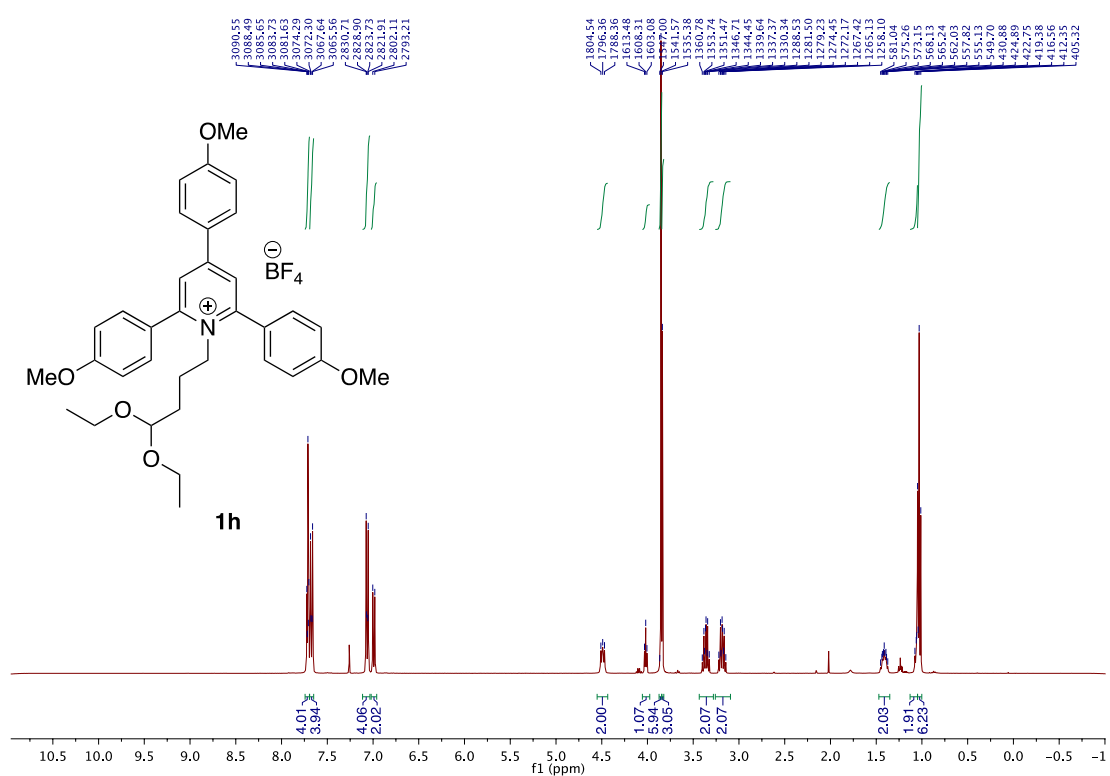
Deaminative Arylation at sp^3 Carbon Centers



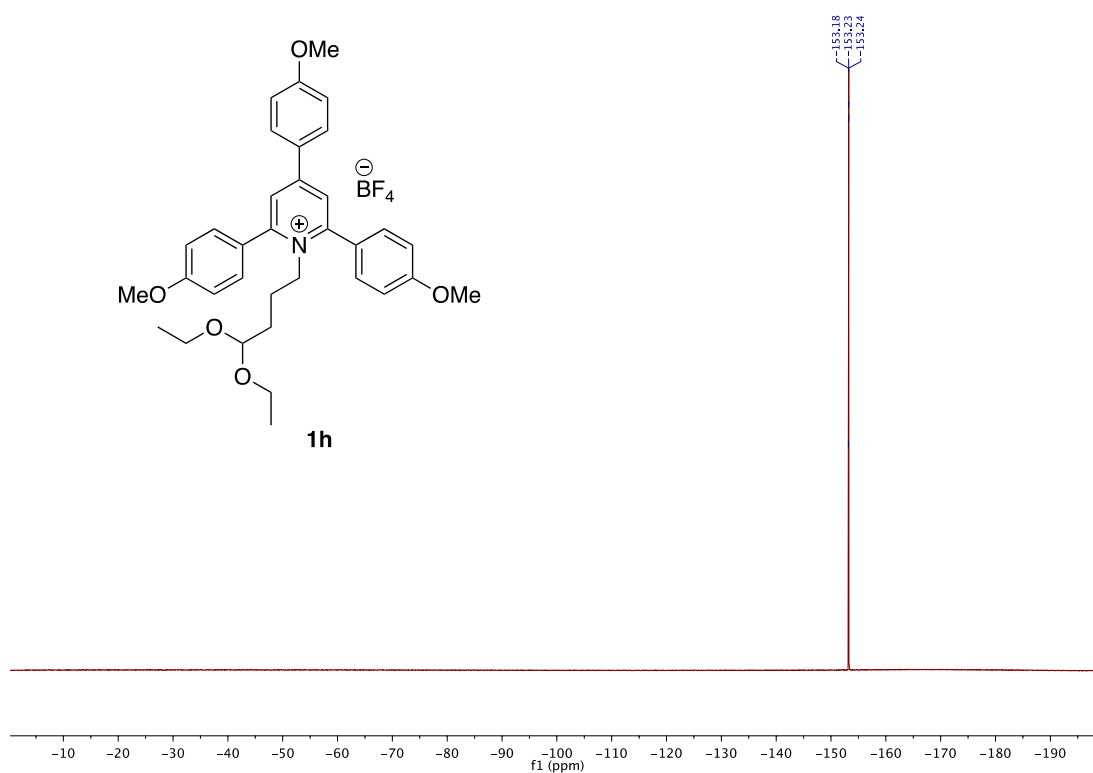
Deaminative Arylation at sp^3 Carbon Centers



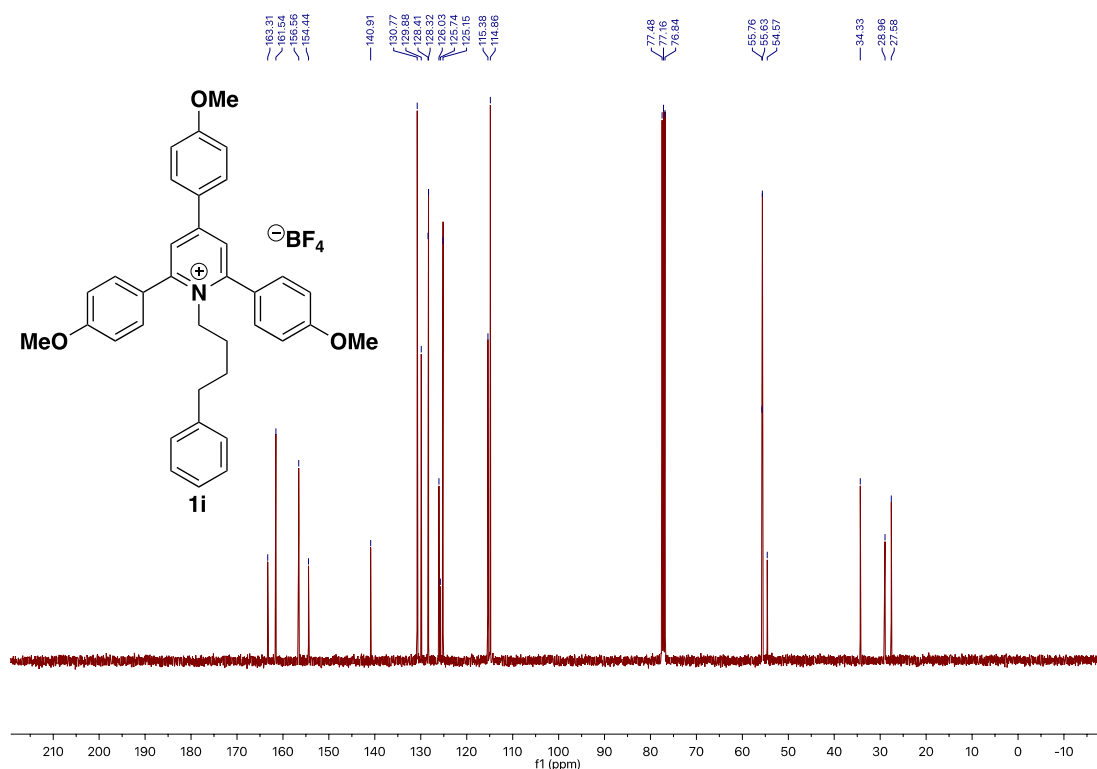
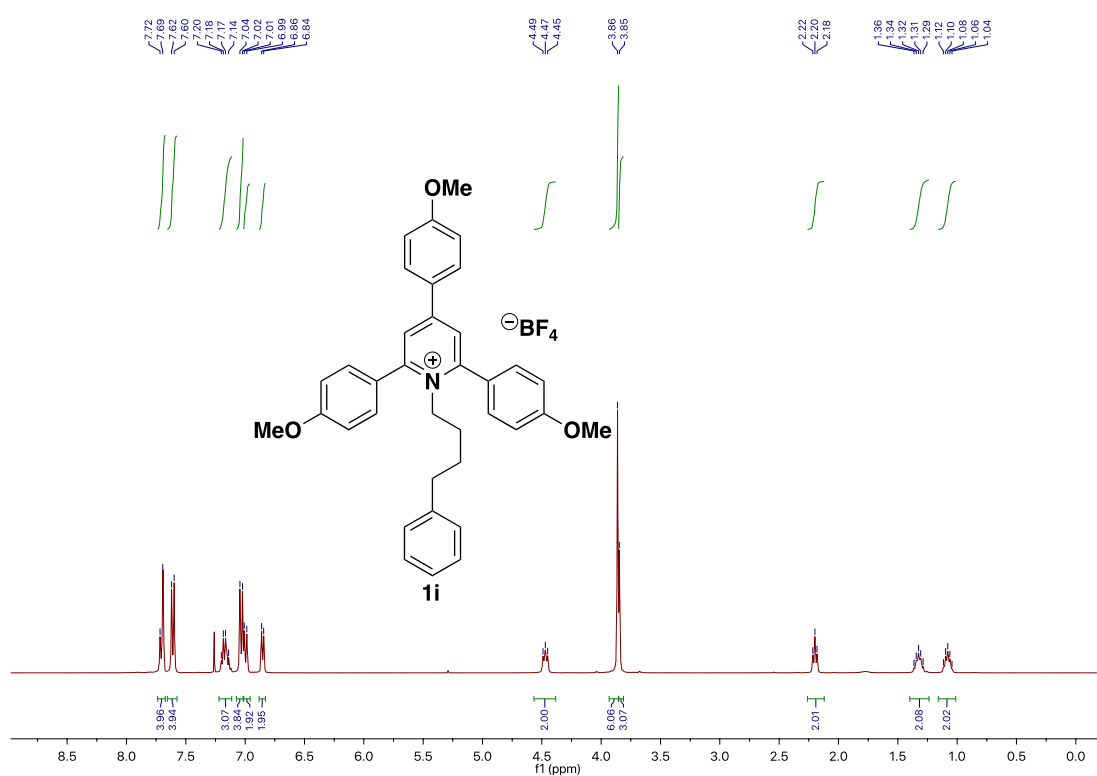
Chapter 3



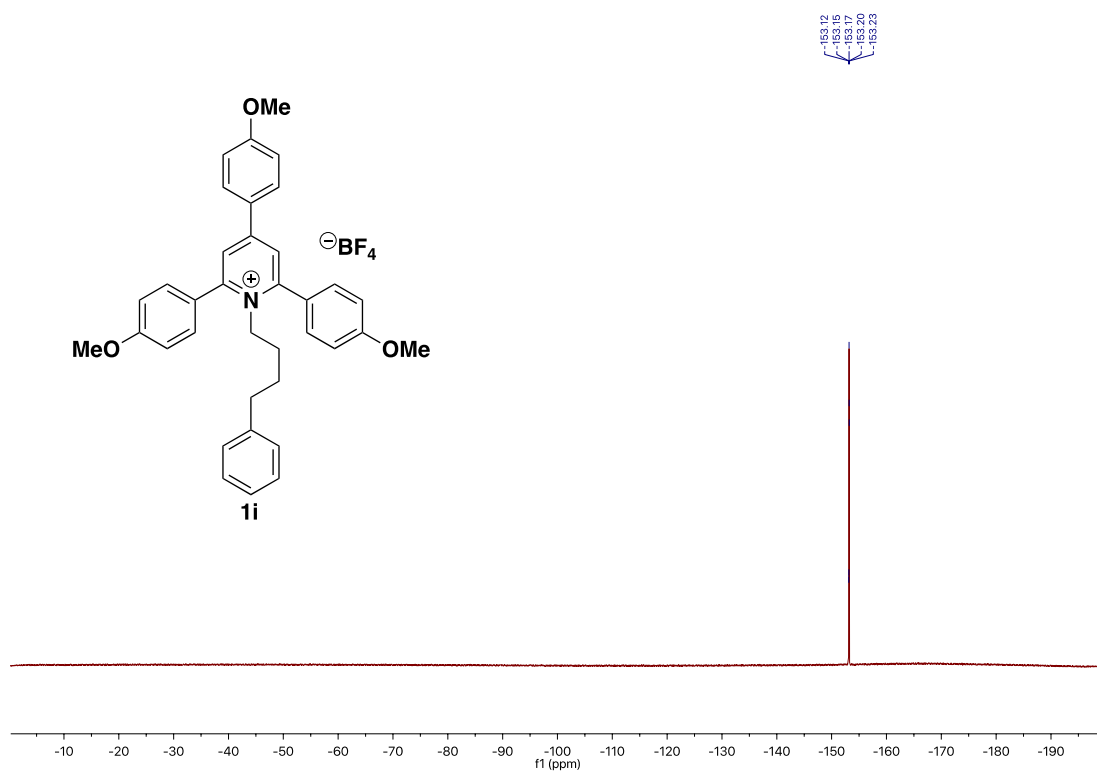
Deaminative Arylation at sp^3 Carbon Centers



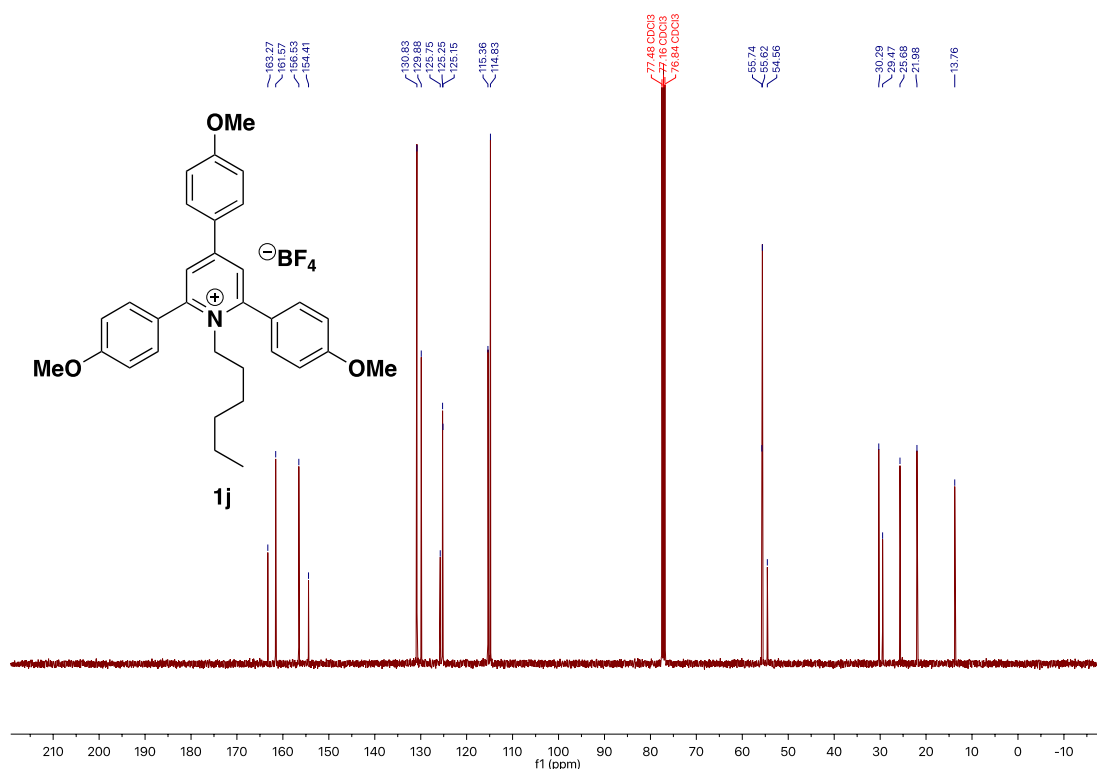
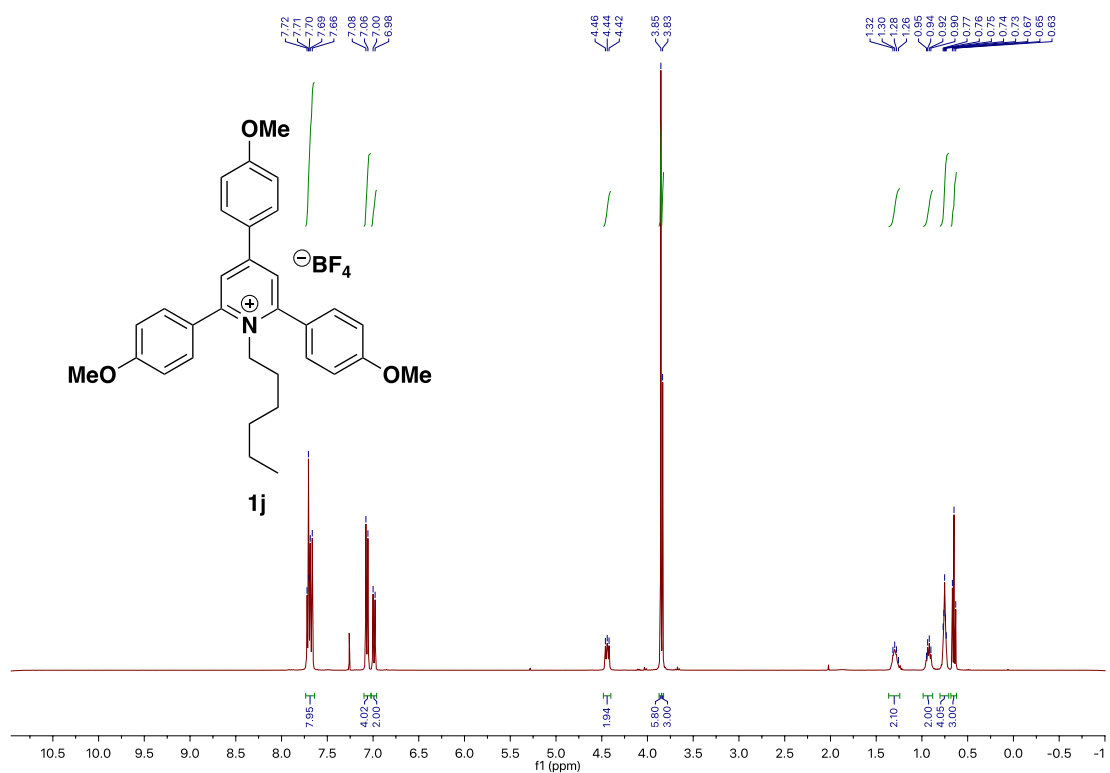
Chapter 3



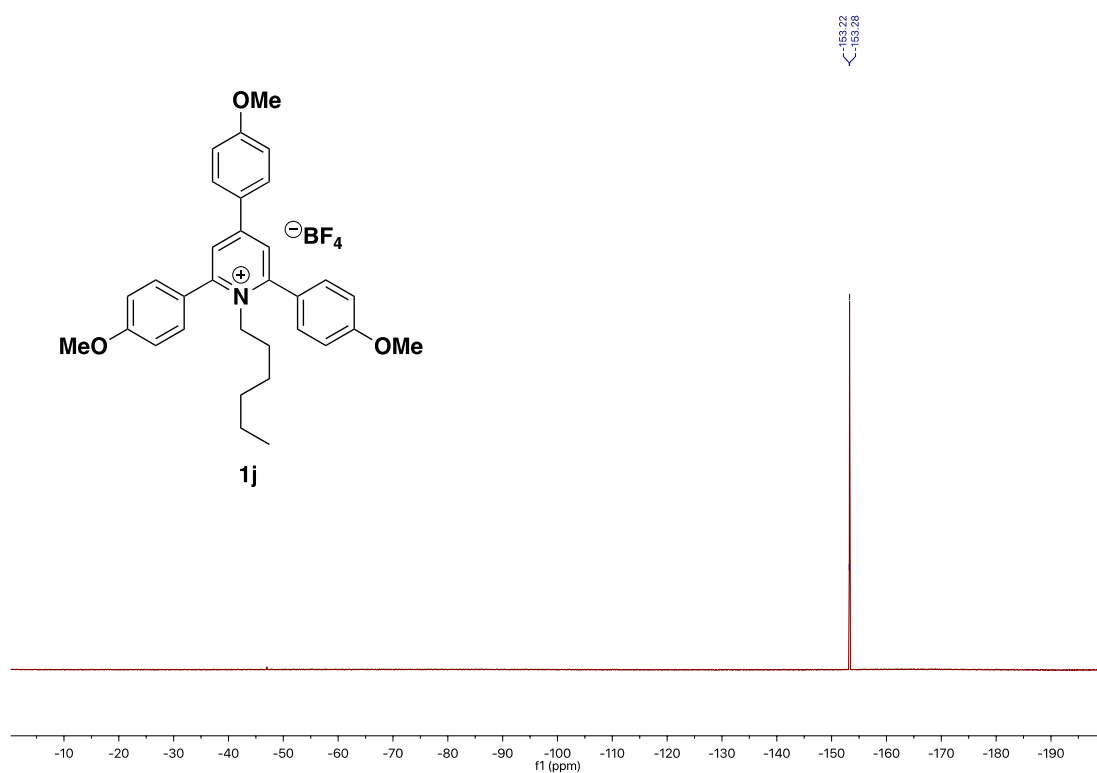
Deaminative Arylation at sp^3 Carbon Centers



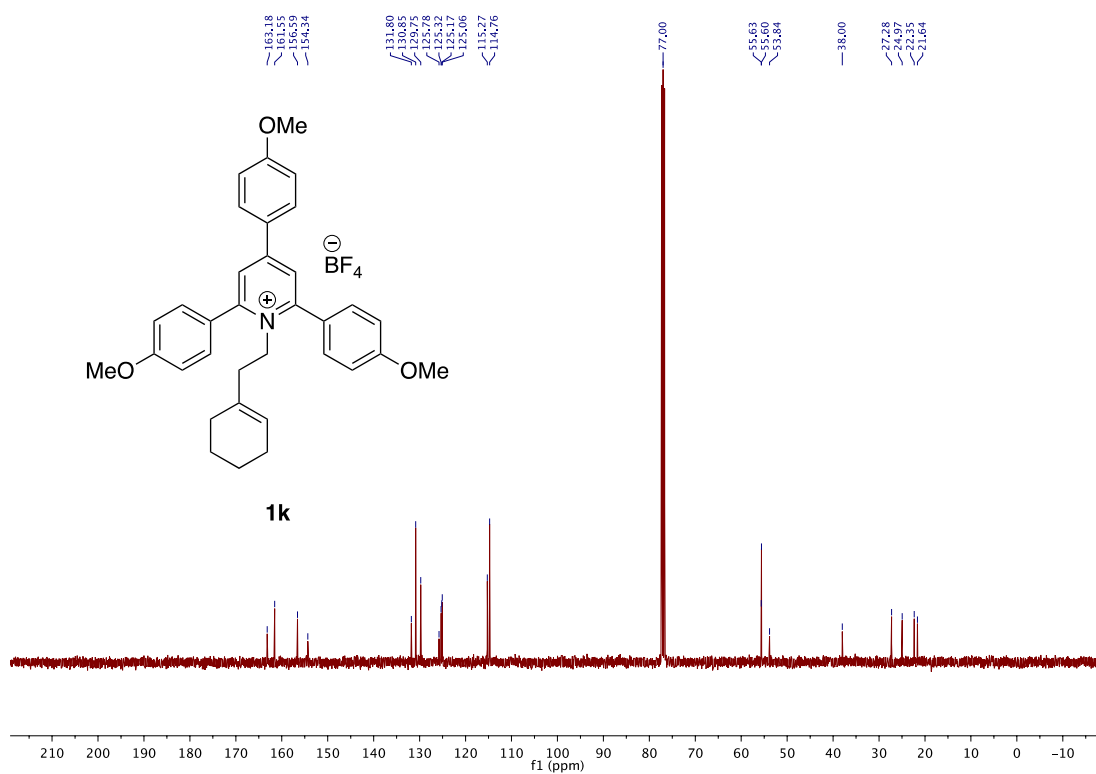
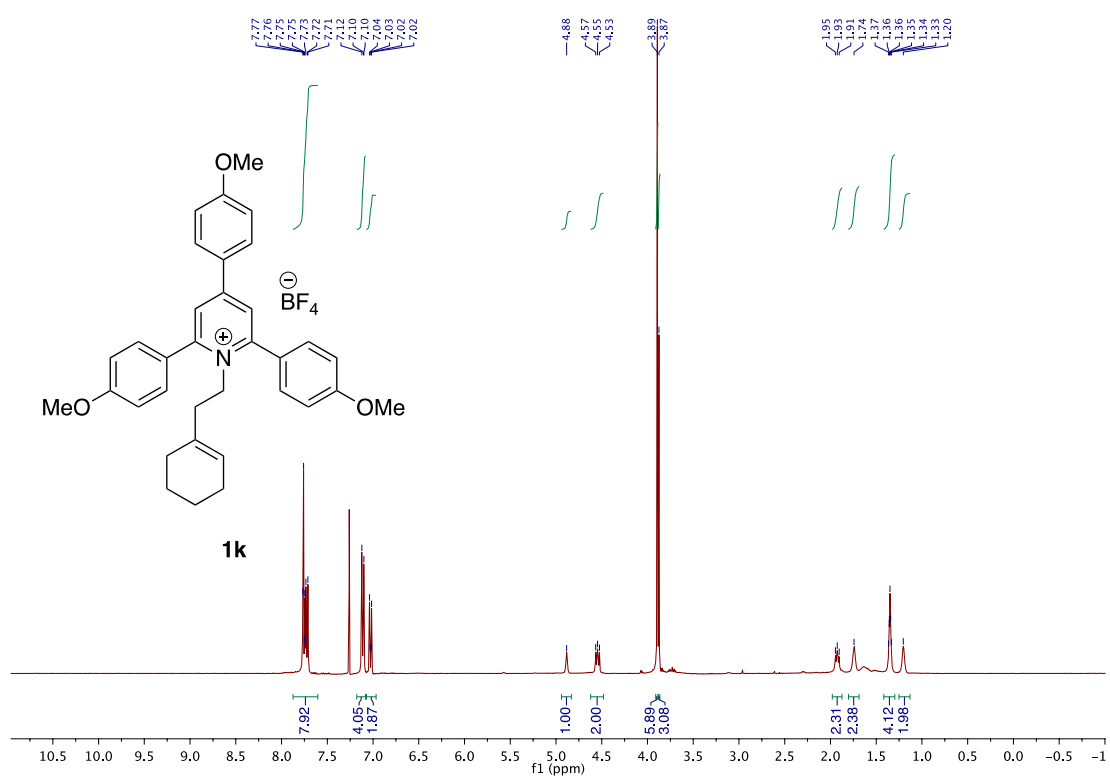
Chapter 3



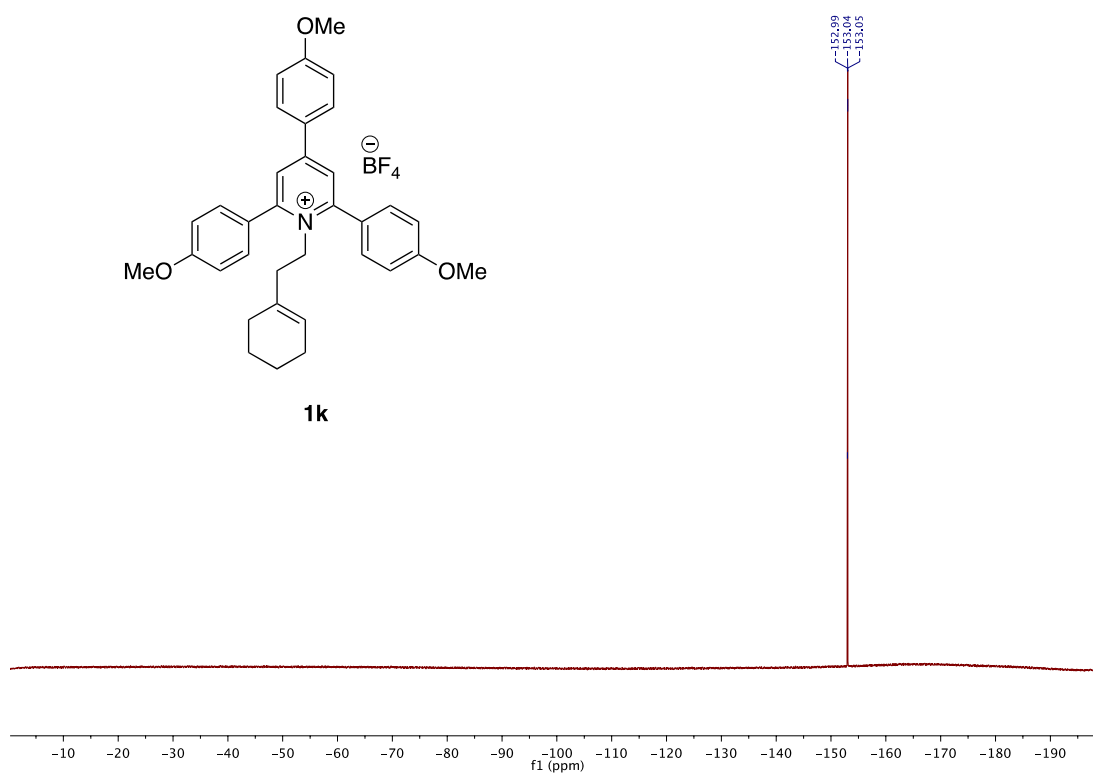
Deaminative Arylation at sp^3 Carbon Centers



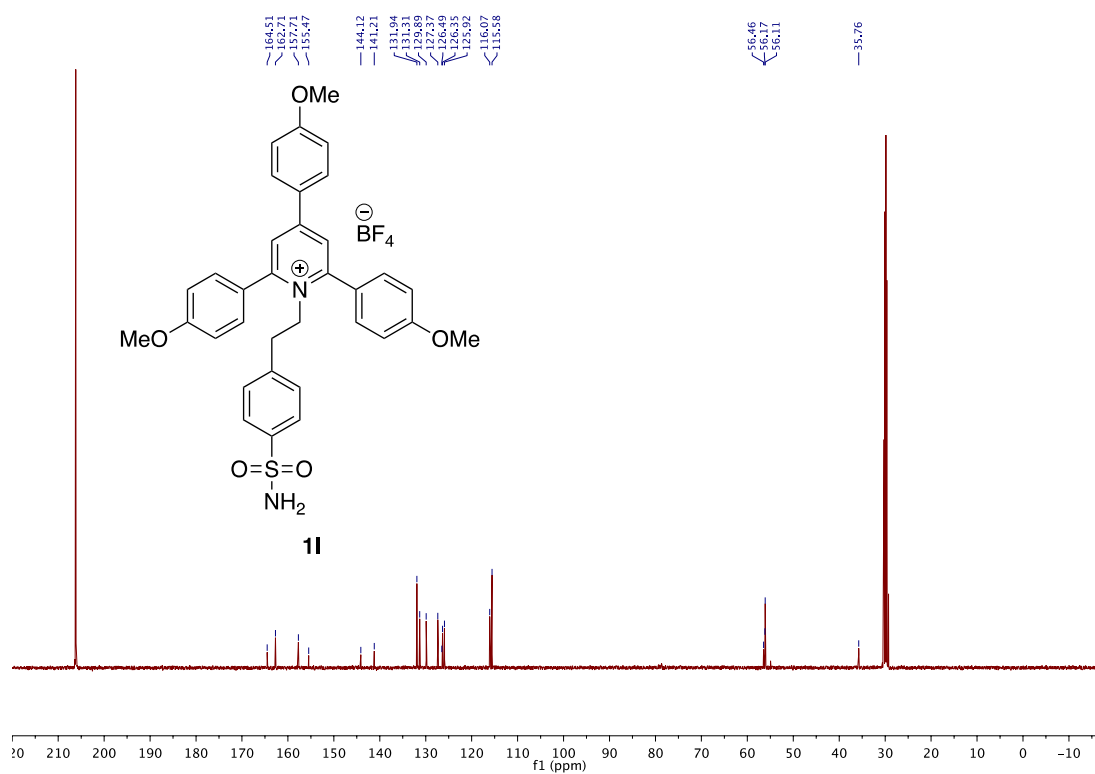
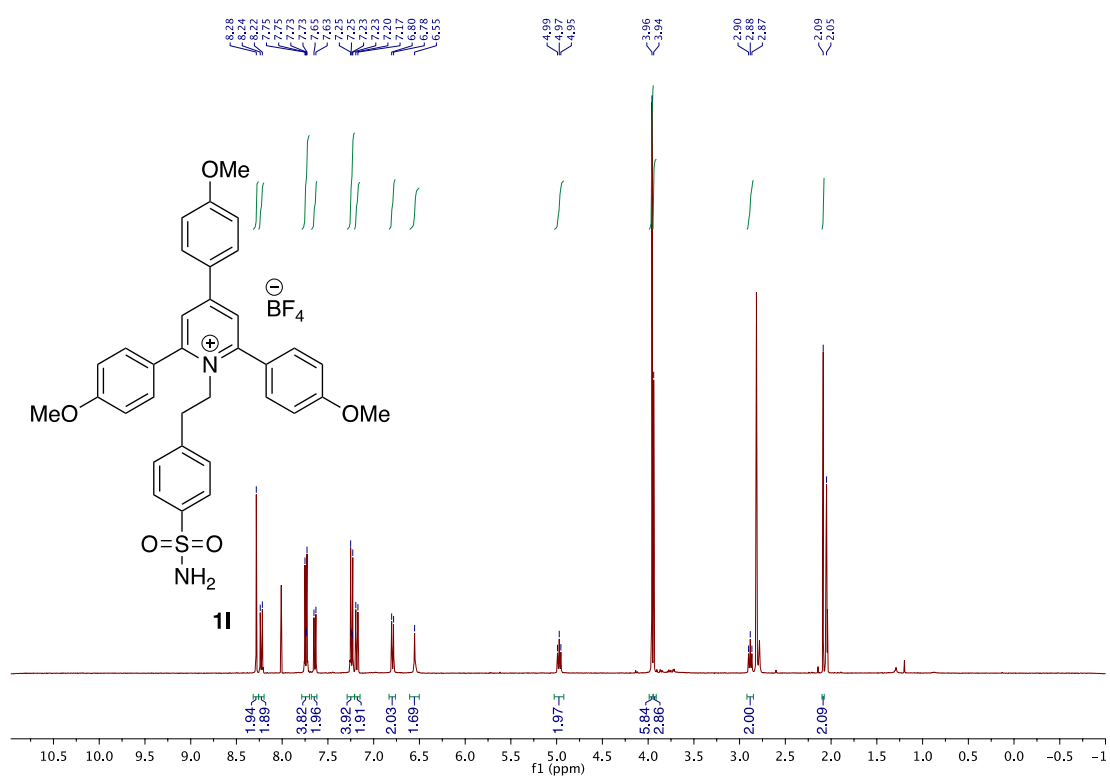
Chapter 3



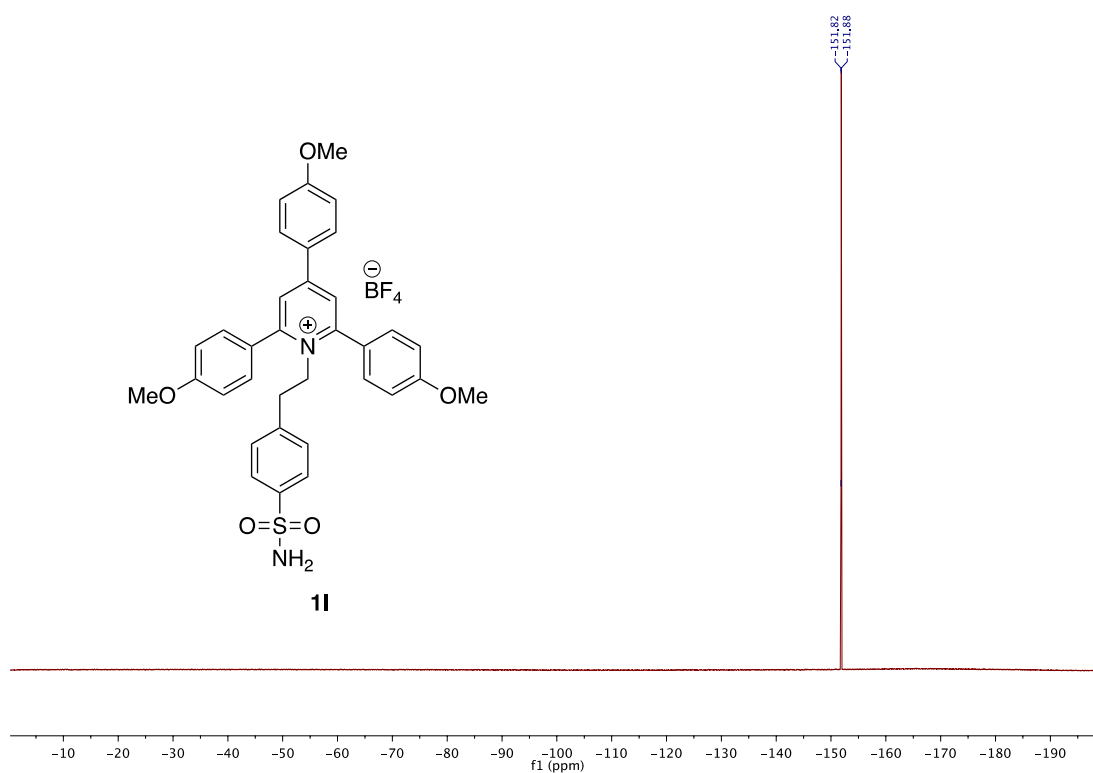
Deaminative Arylation at sp^3 Carbon Centers



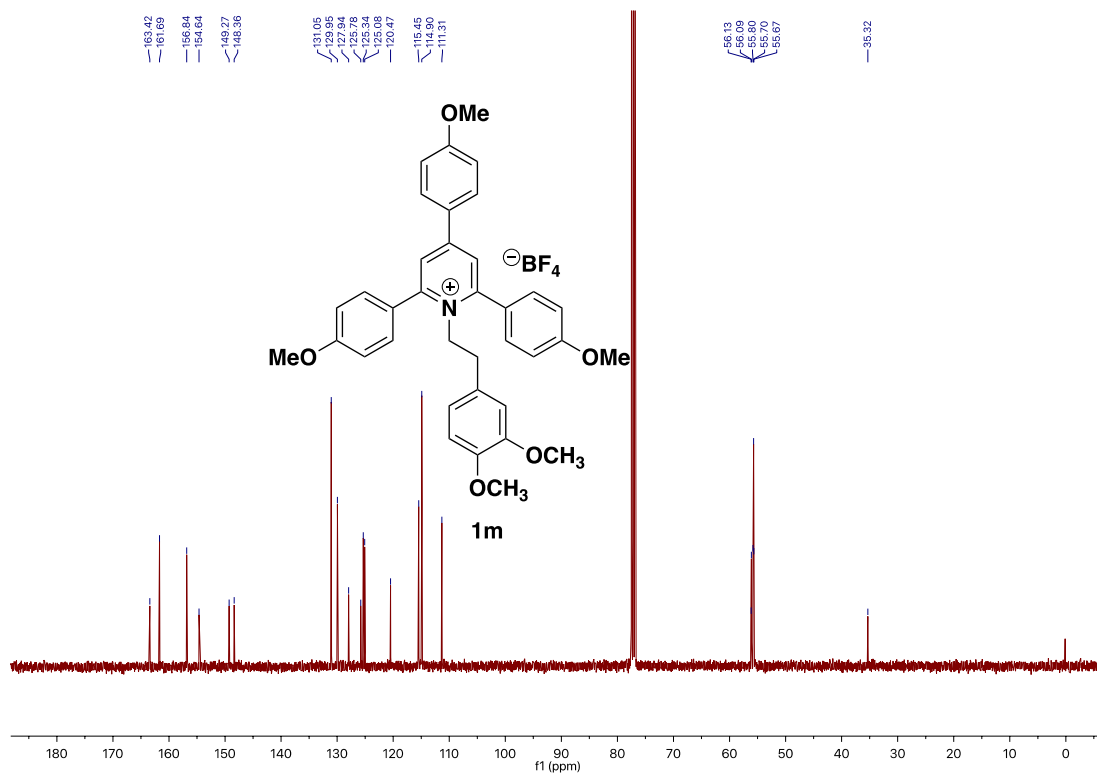
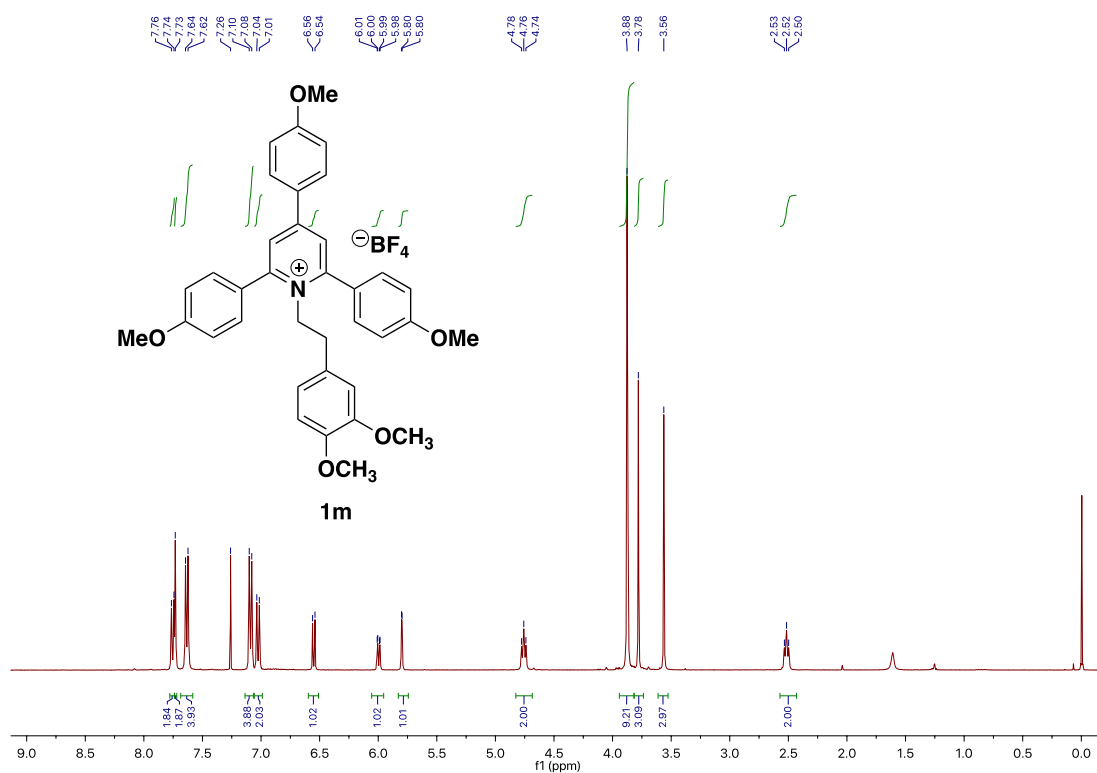
Chapter 3



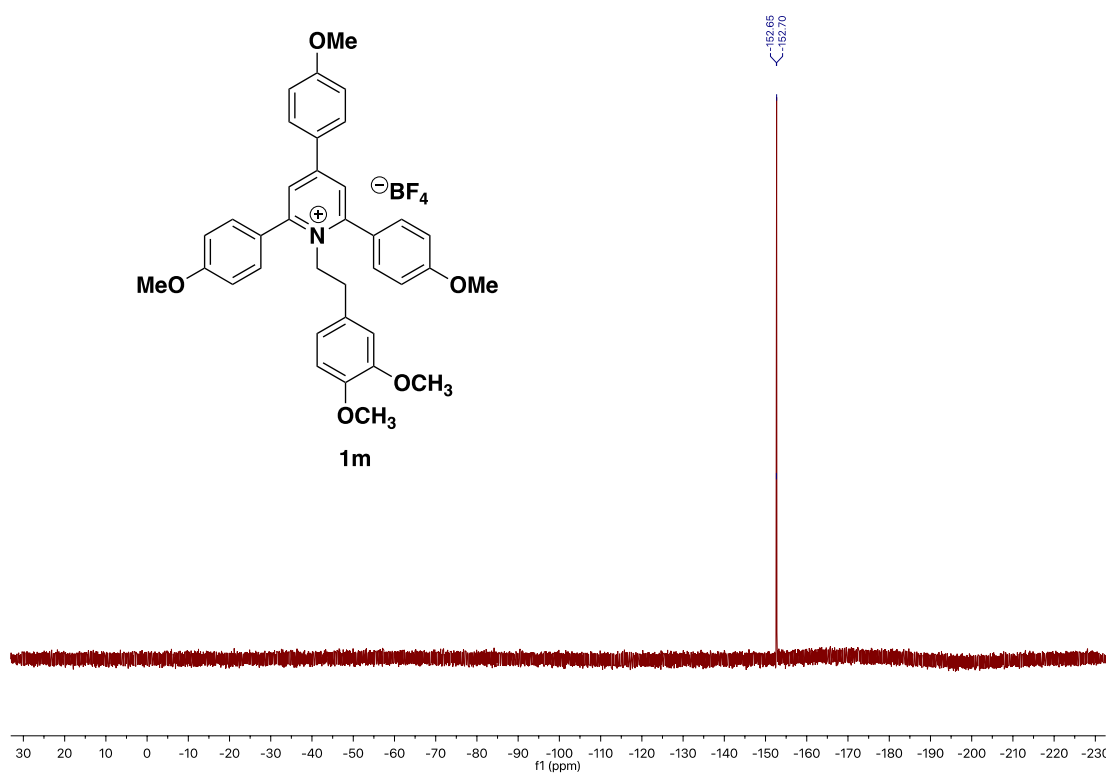
Deaminative Arylation at sp^3 Carbon Centers



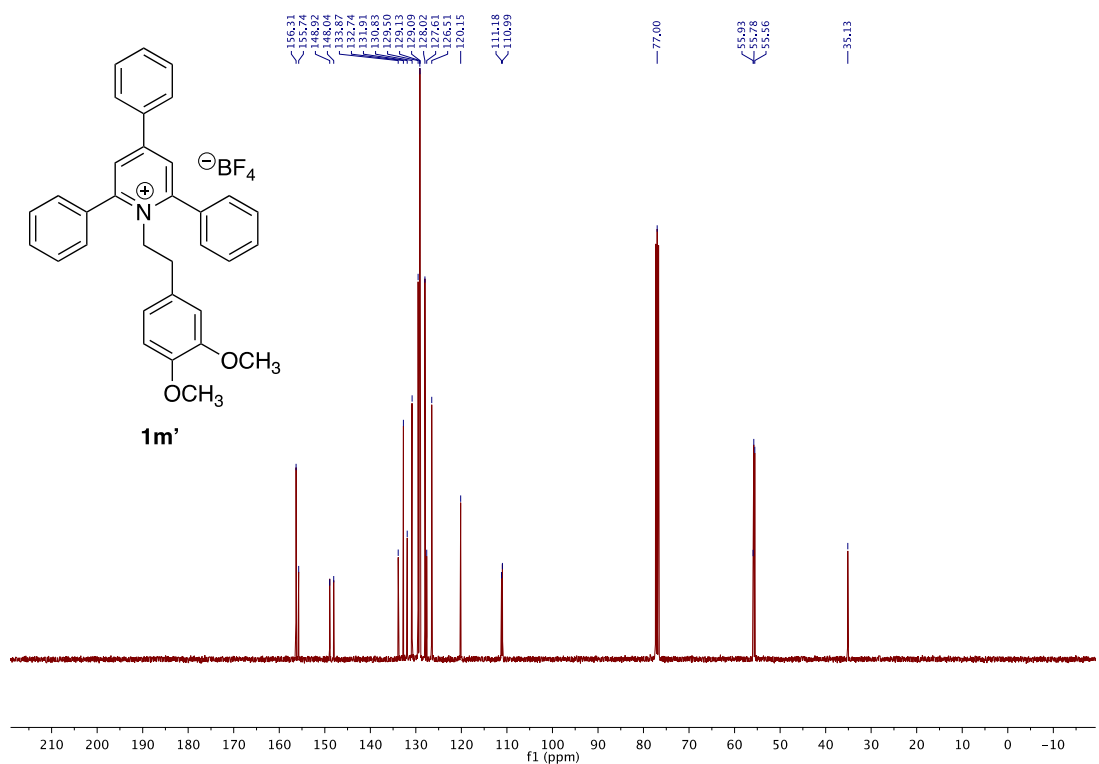
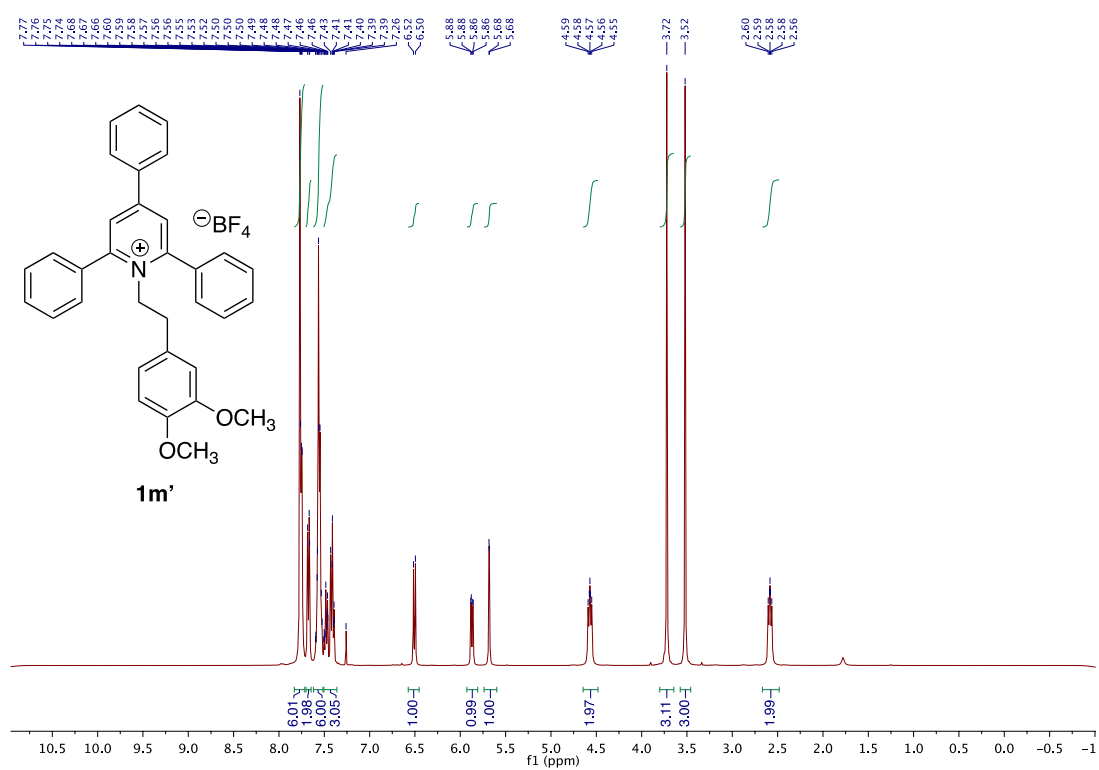
Chapter 3



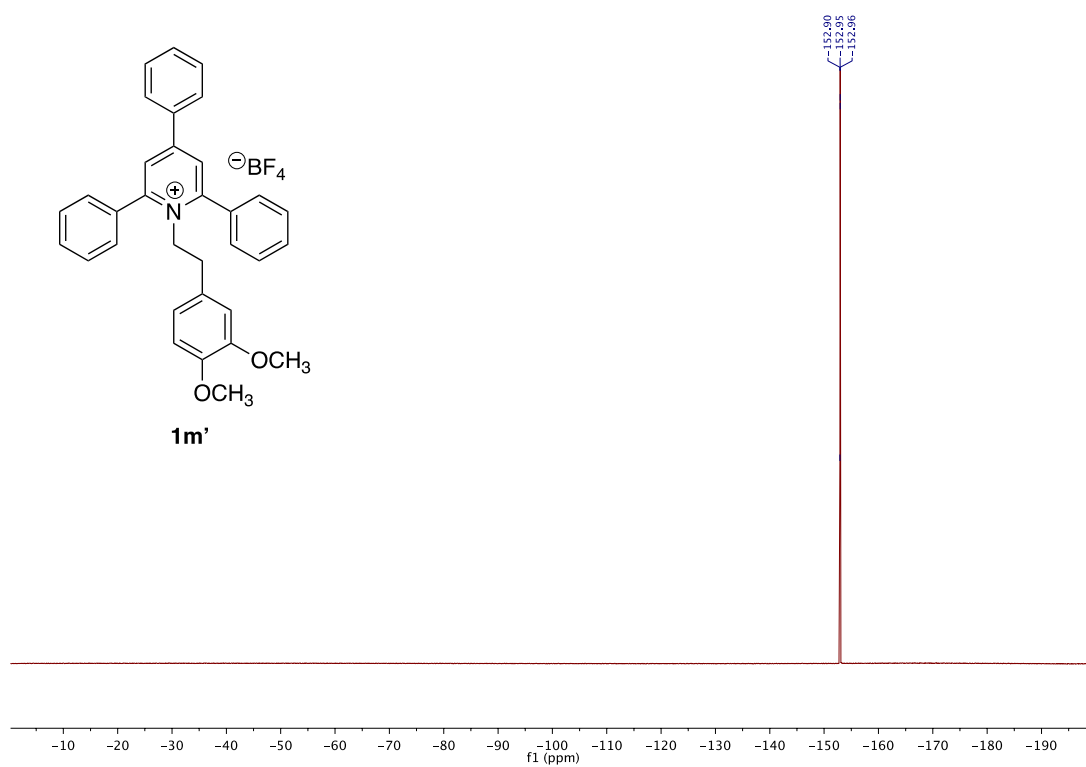
Deaminative Arylation at sp^3 Carbon Centers



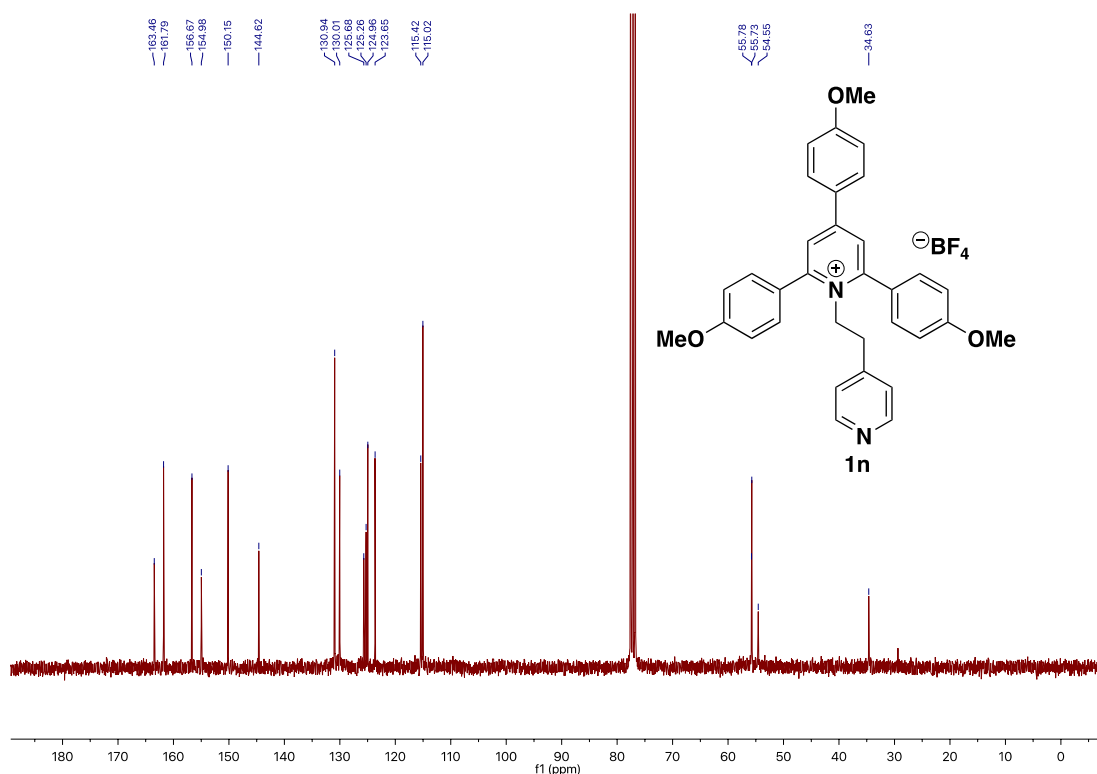
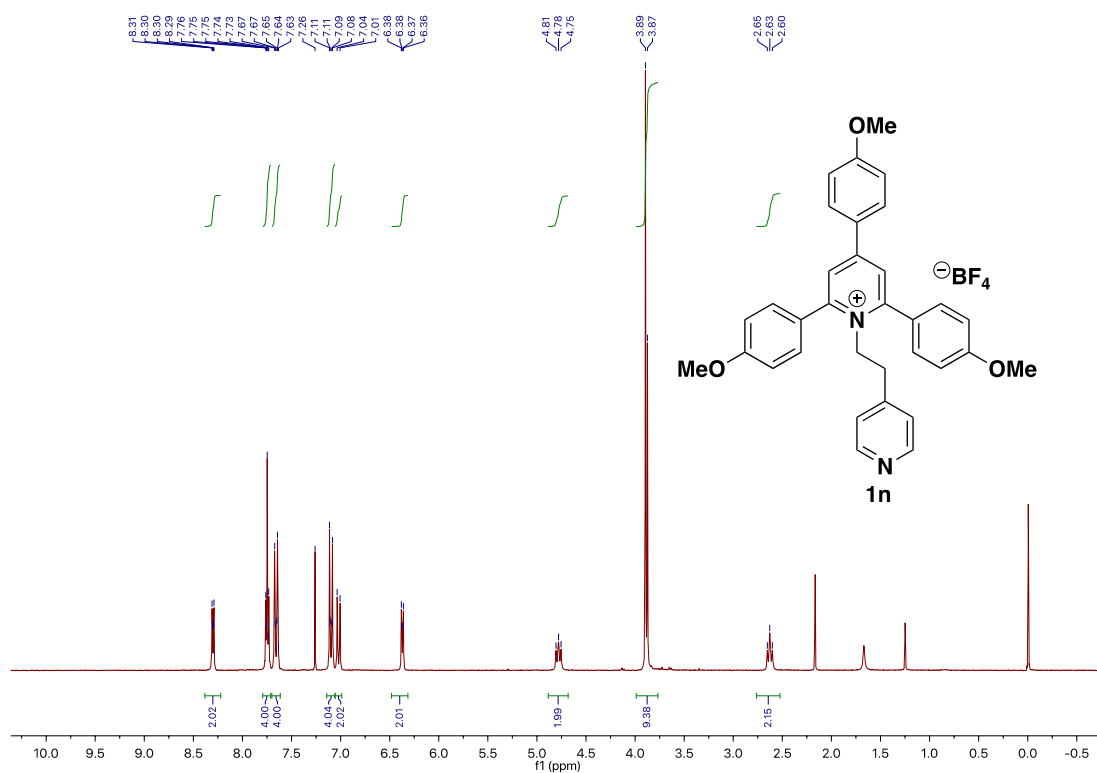
Chapter 3



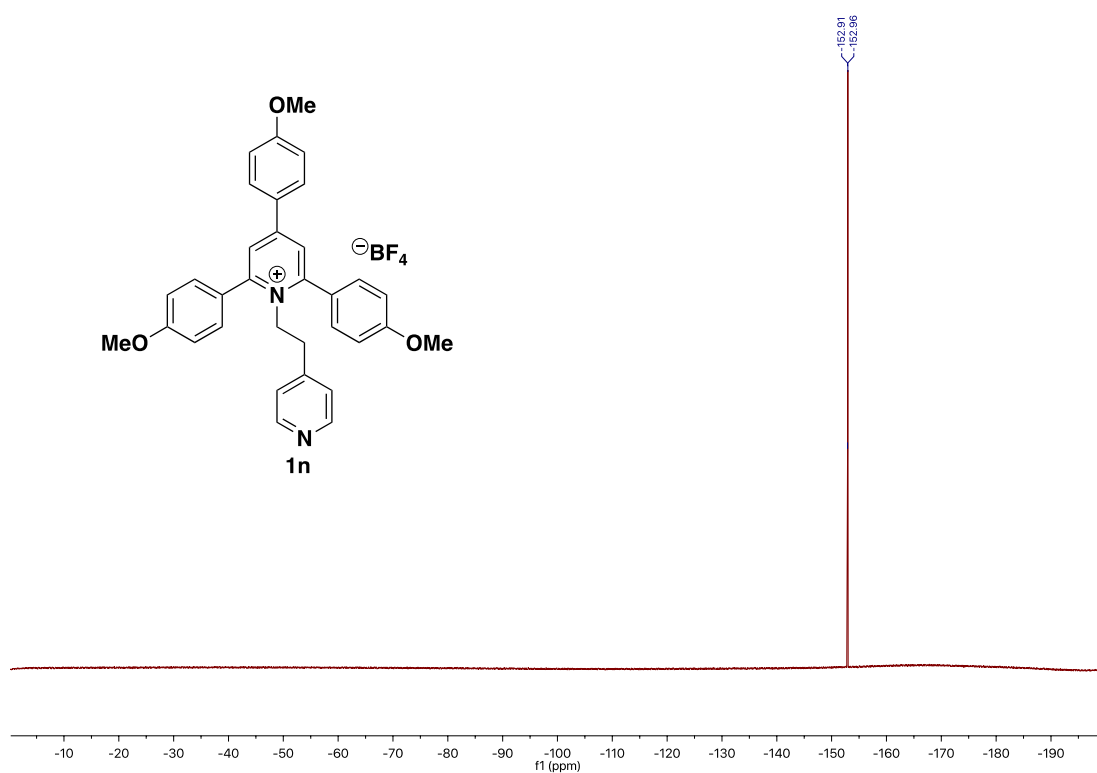
Deaminative Arylation at sp^3 Carbon Centers



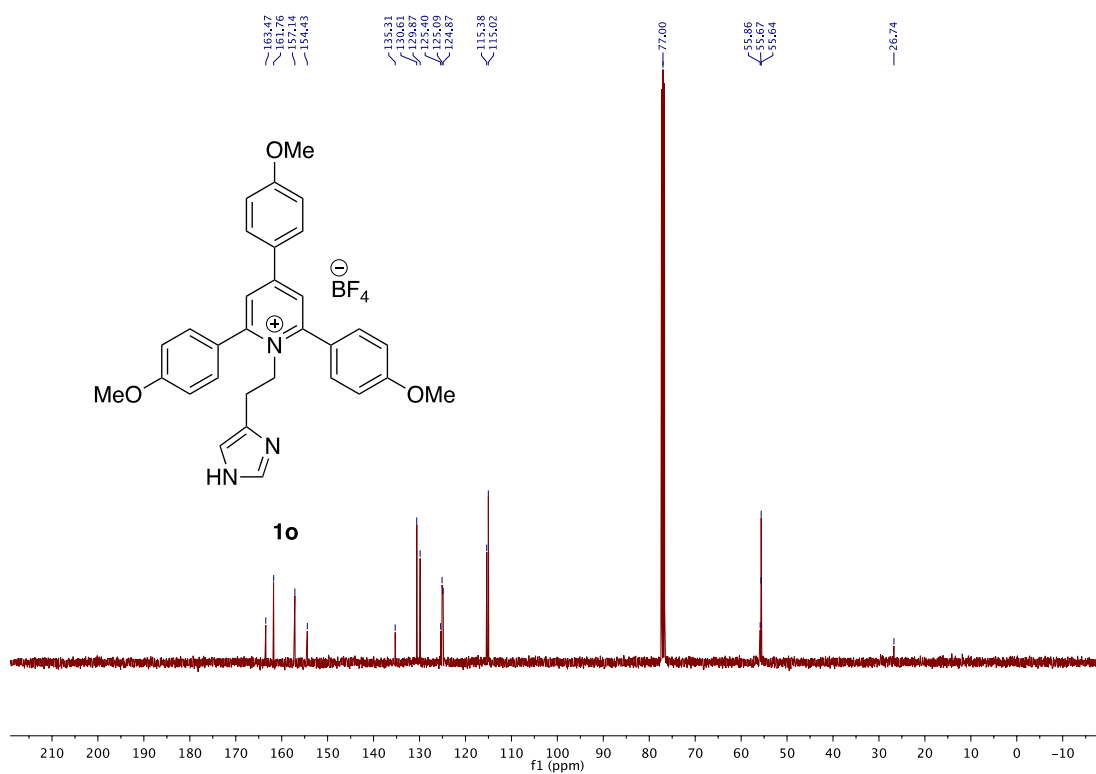
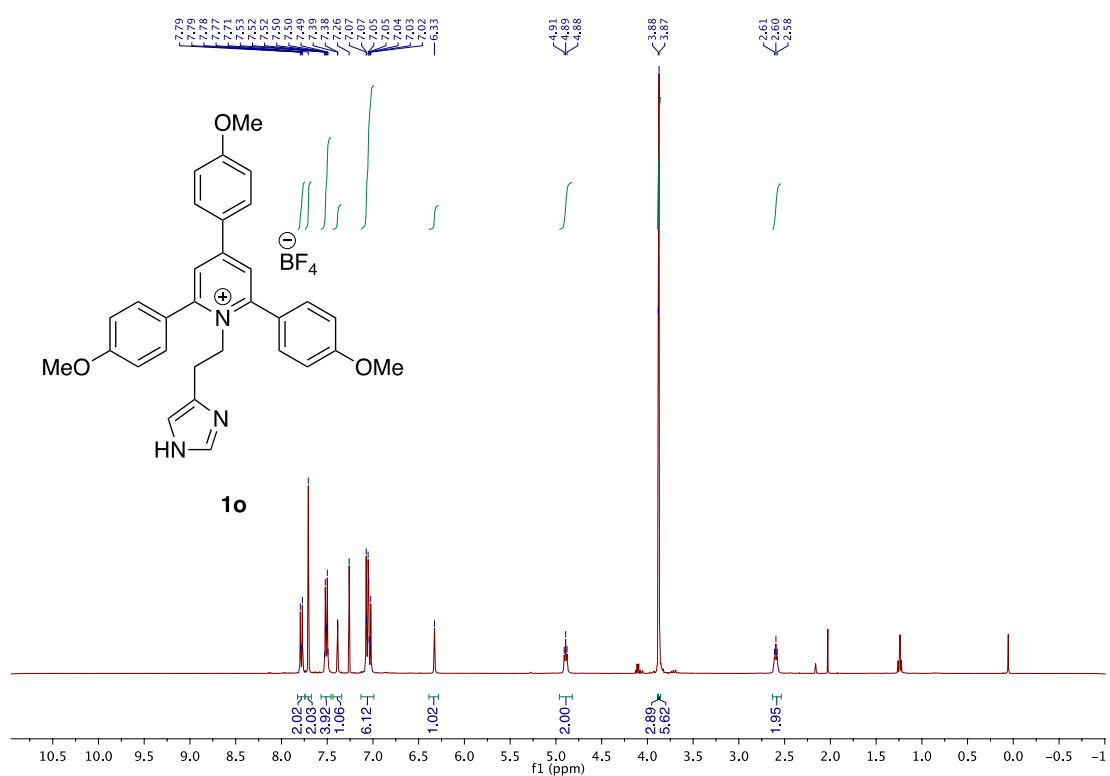
Chapter 3



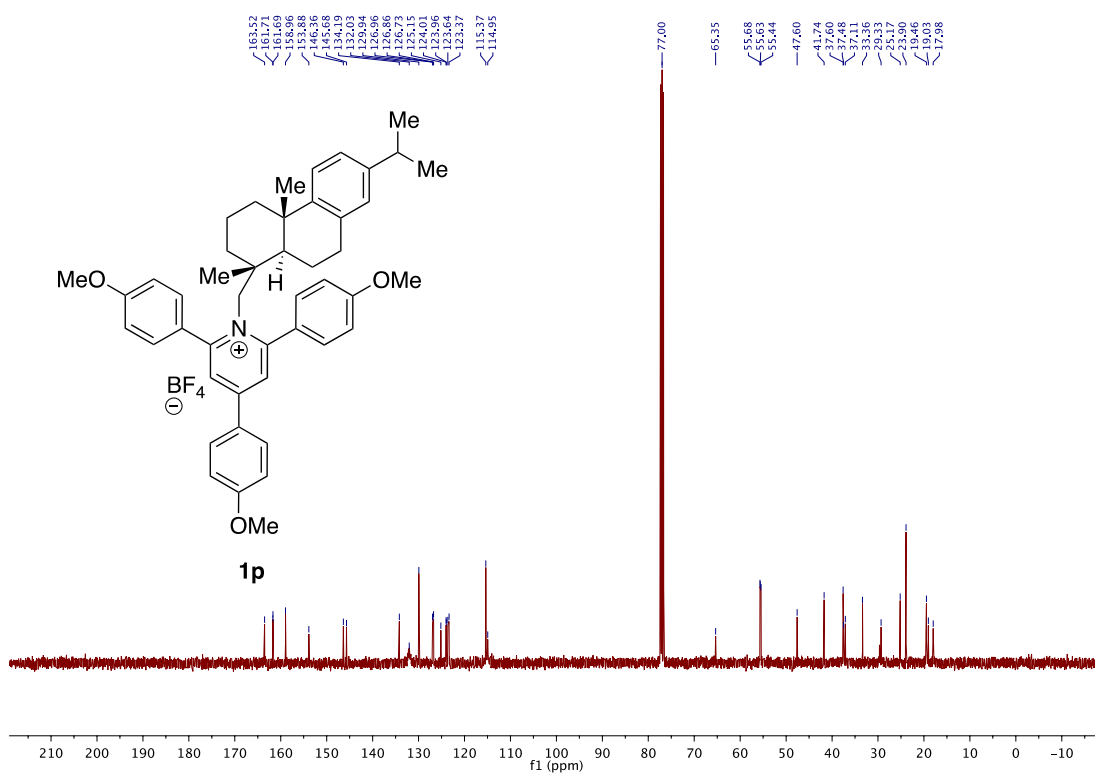
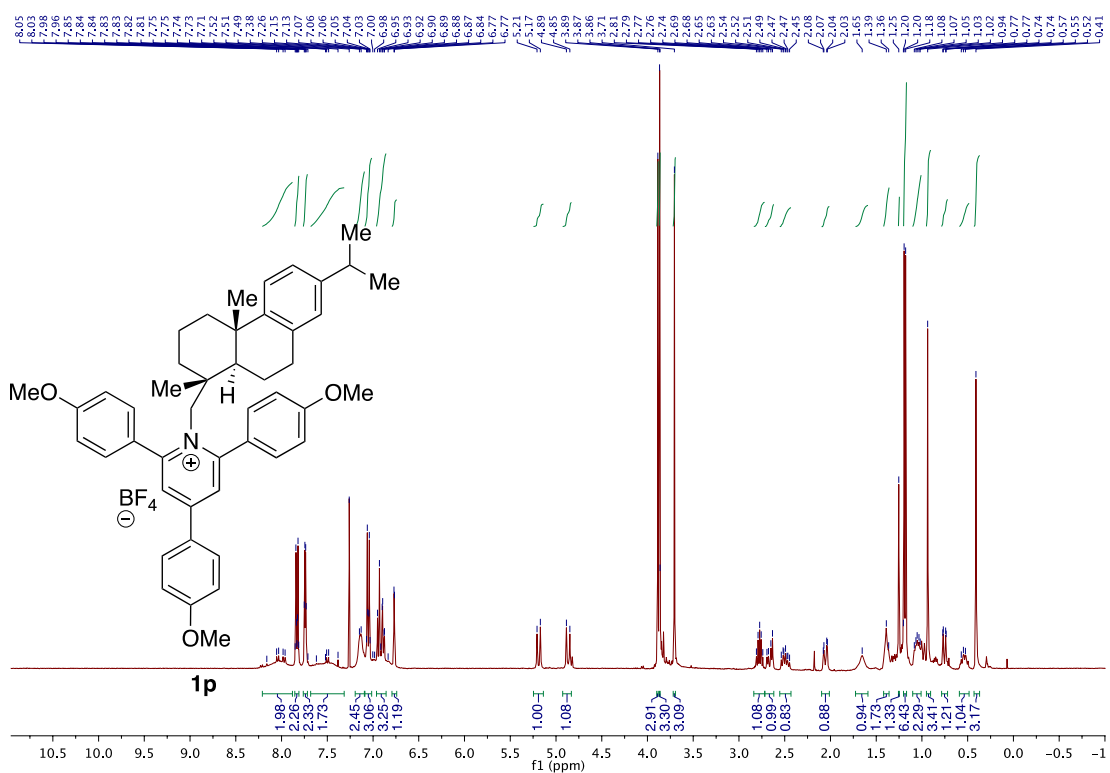
Deaminative Arylation at sp^3 Carbon Centers



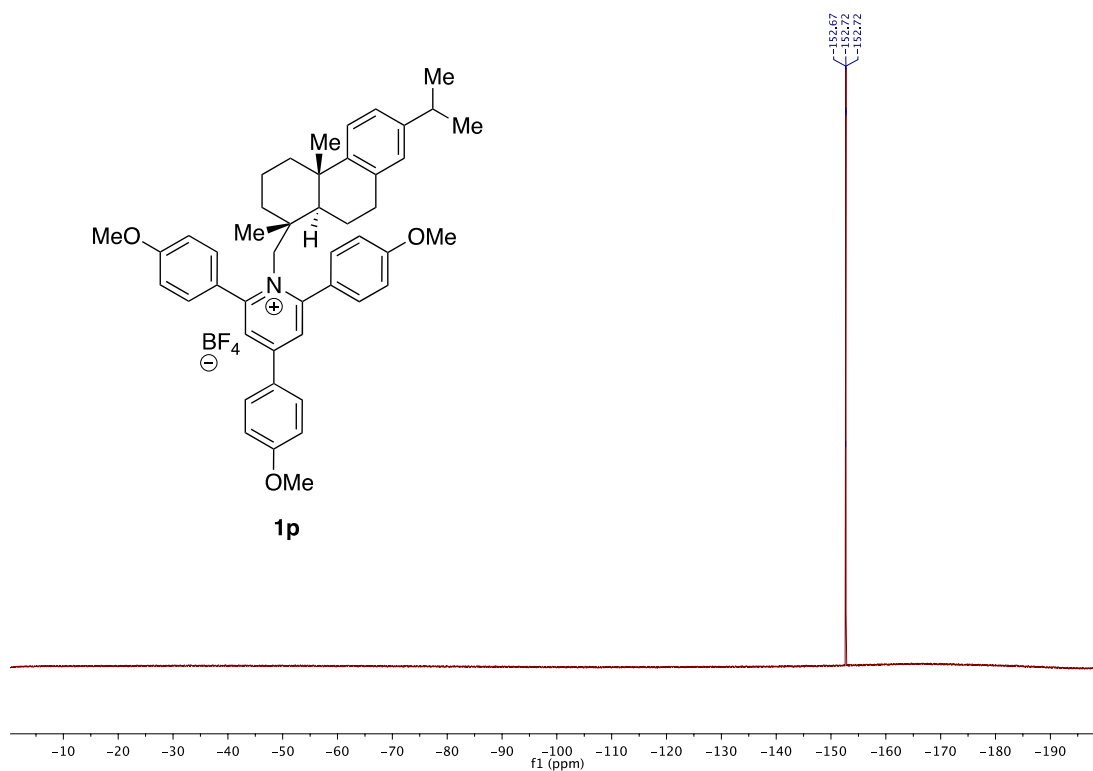
Chapter 3



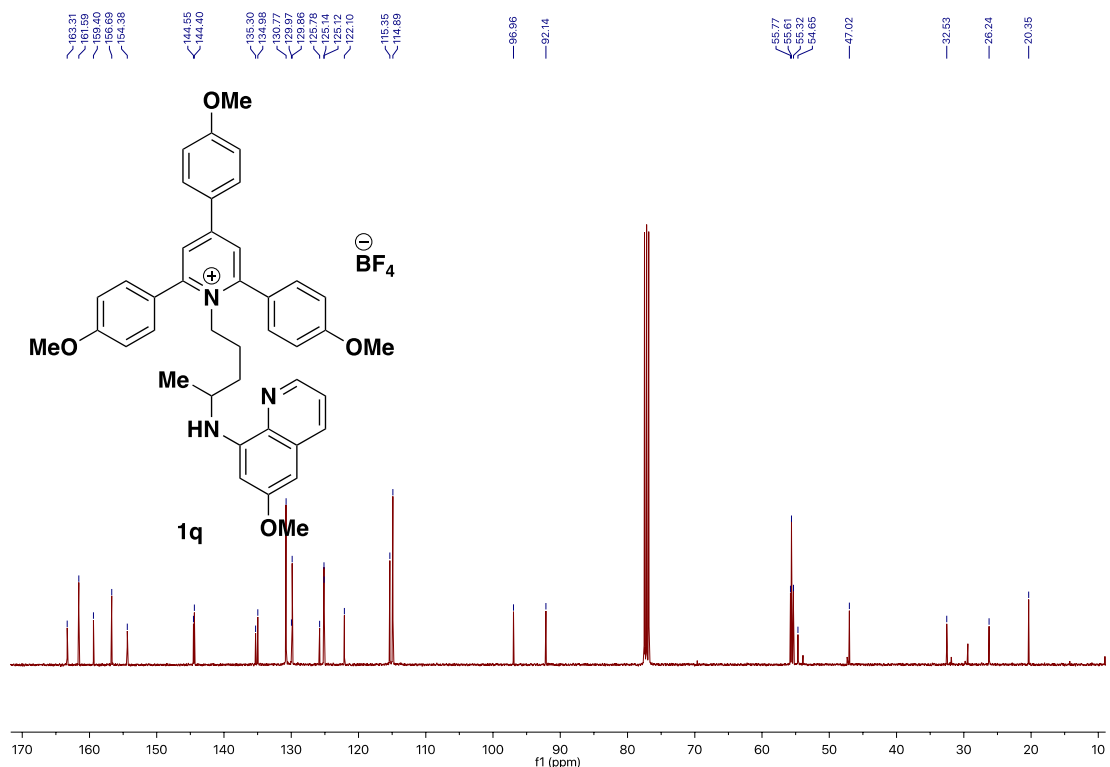
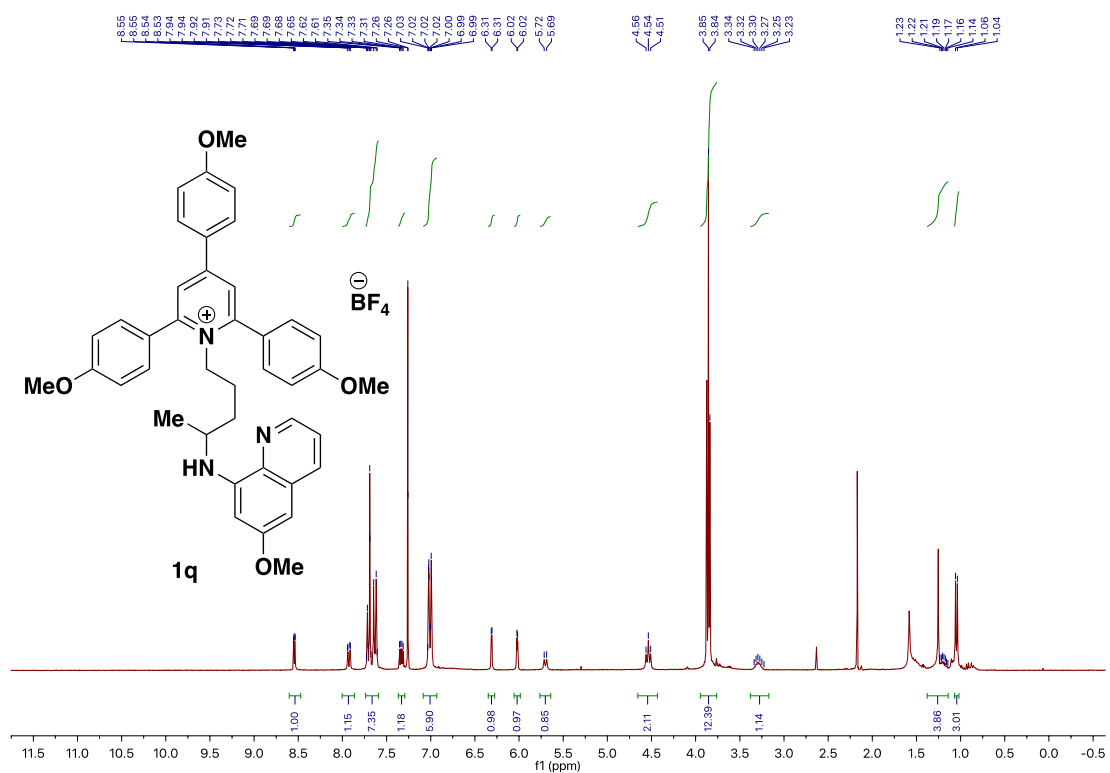
Deaminative Arylation at sp^3 Carbon Centers



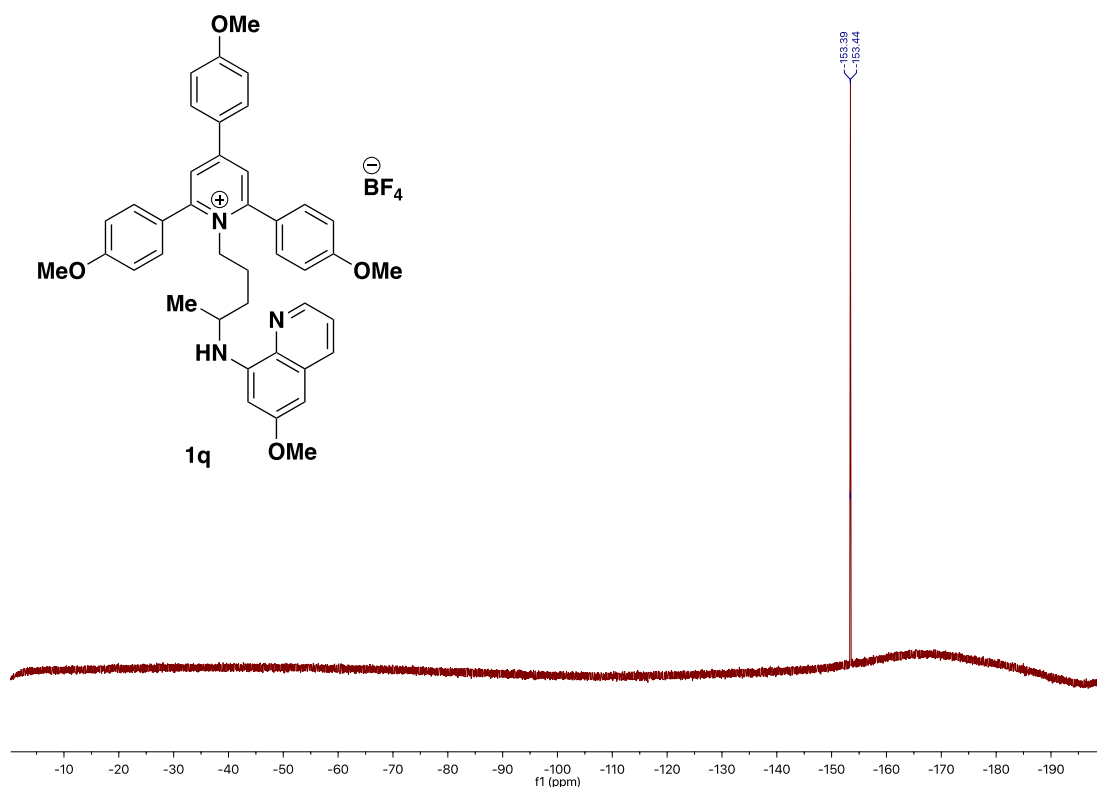
Chapter 3



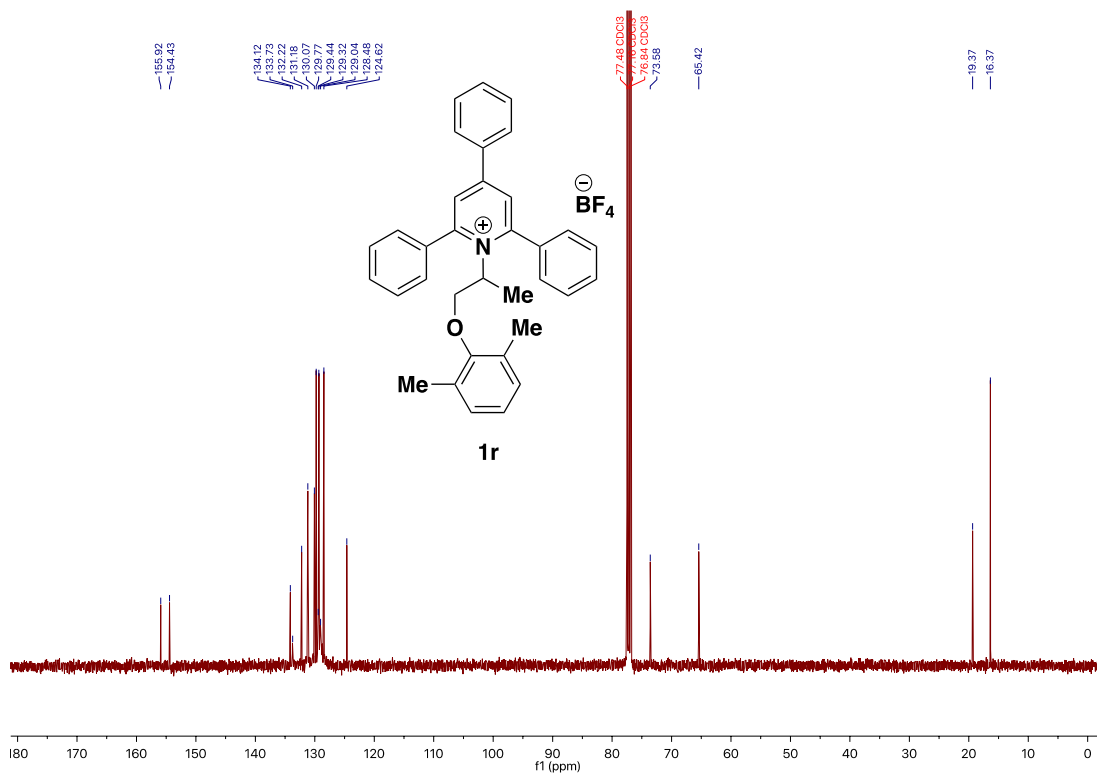
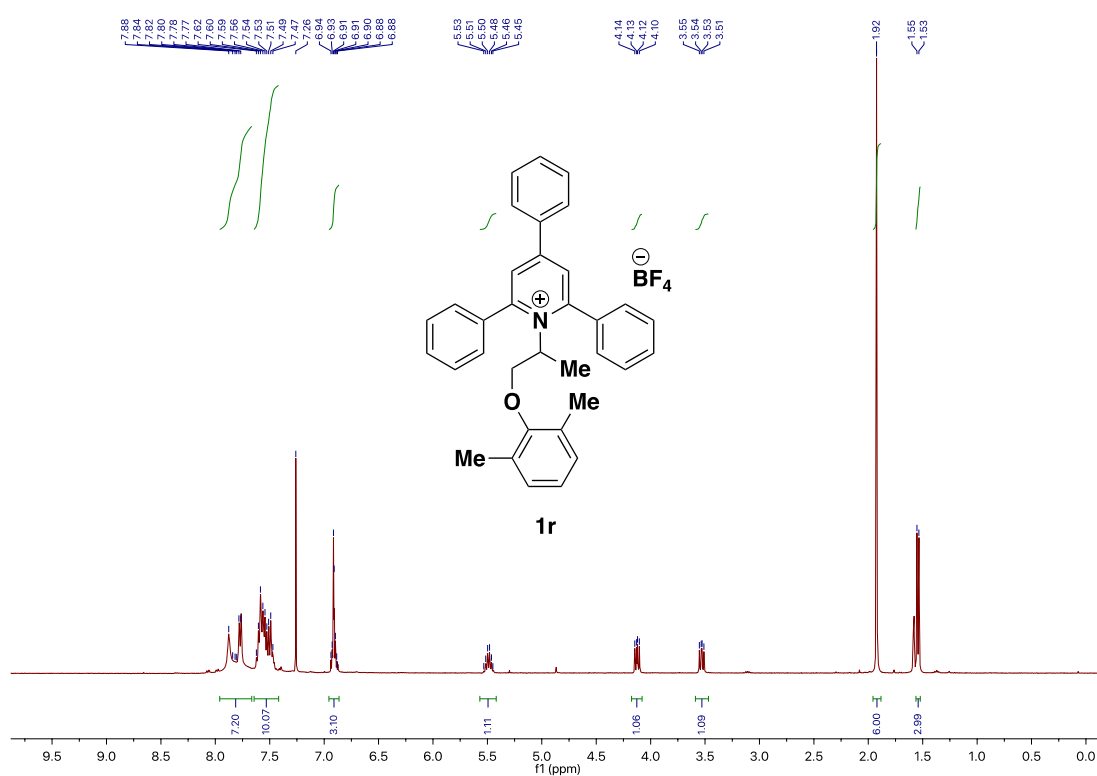
Deaminative Arylation at sp^3 Carbon Centers



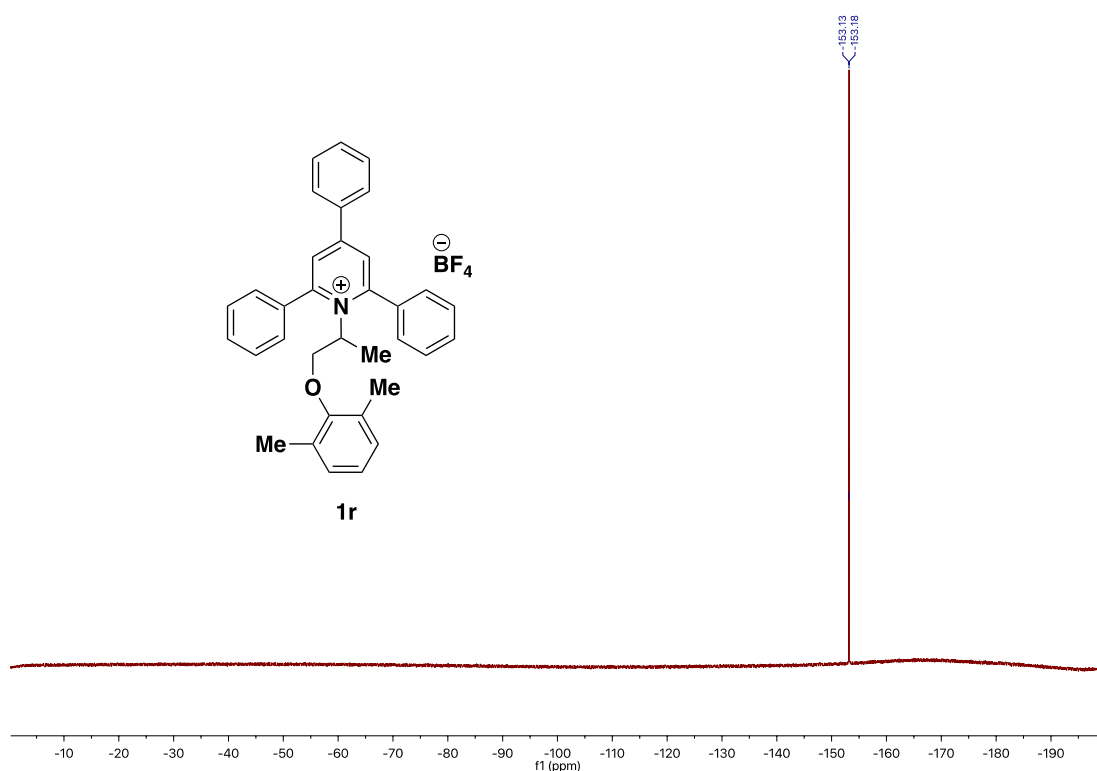
Chapter 3



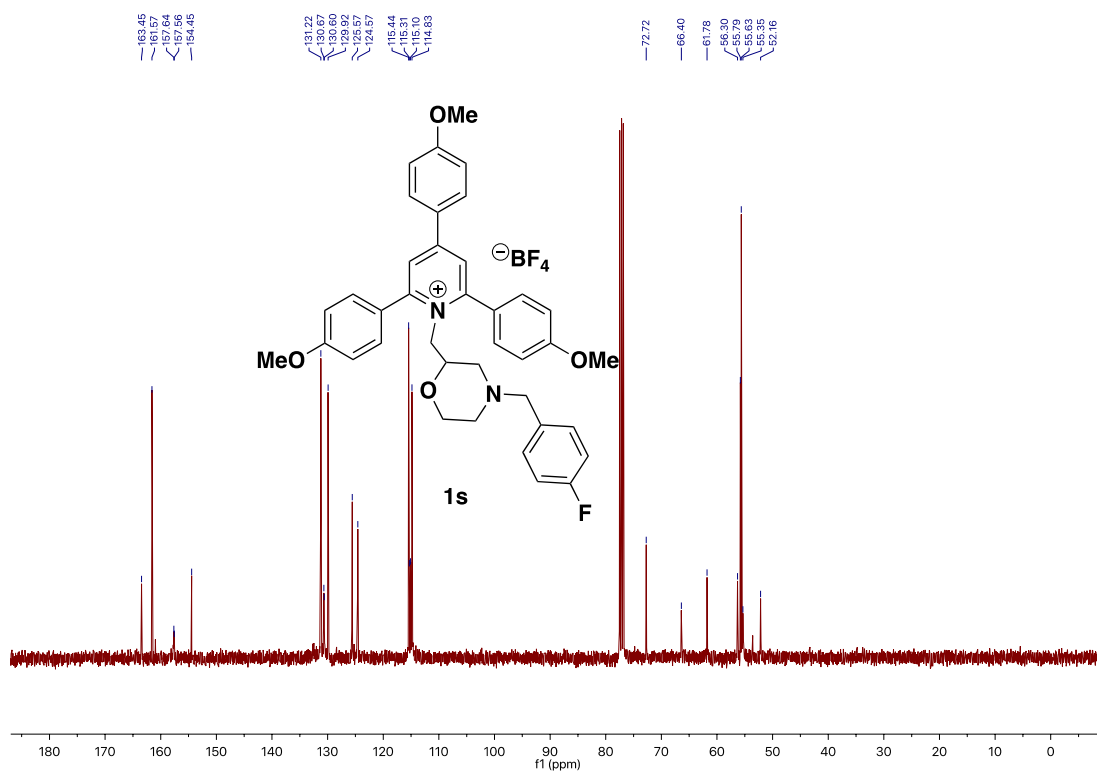
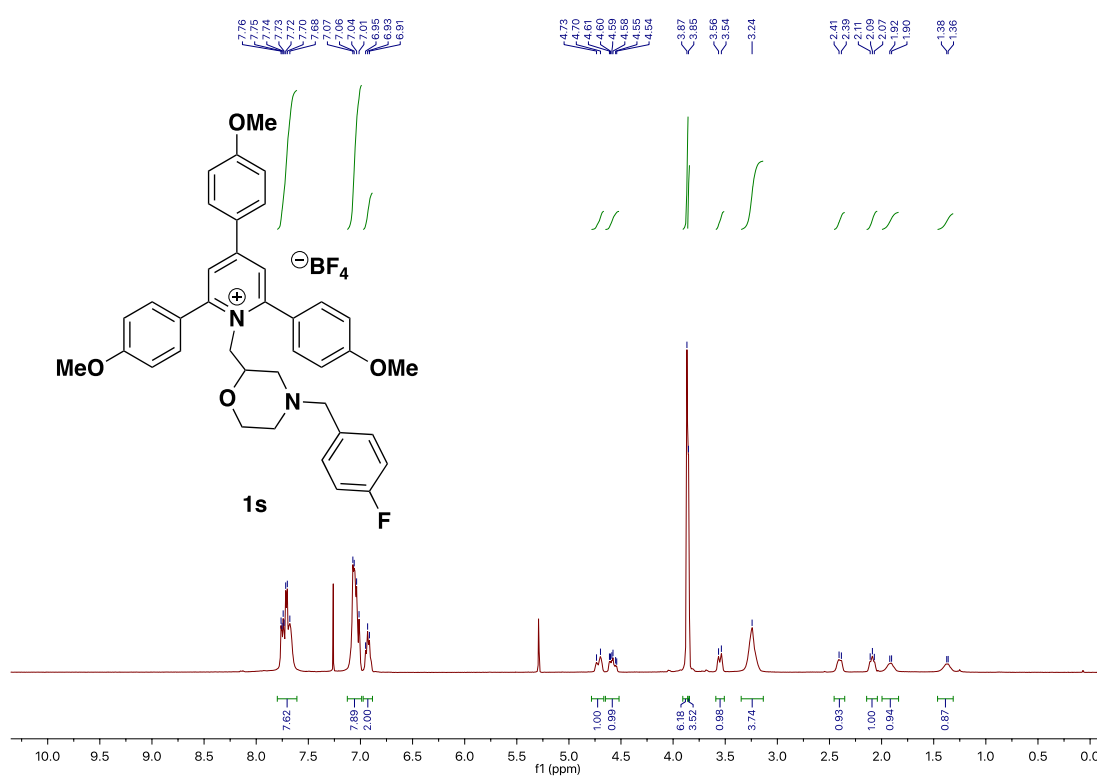
Deaminative Arylation at sp^3 Carbon Centers



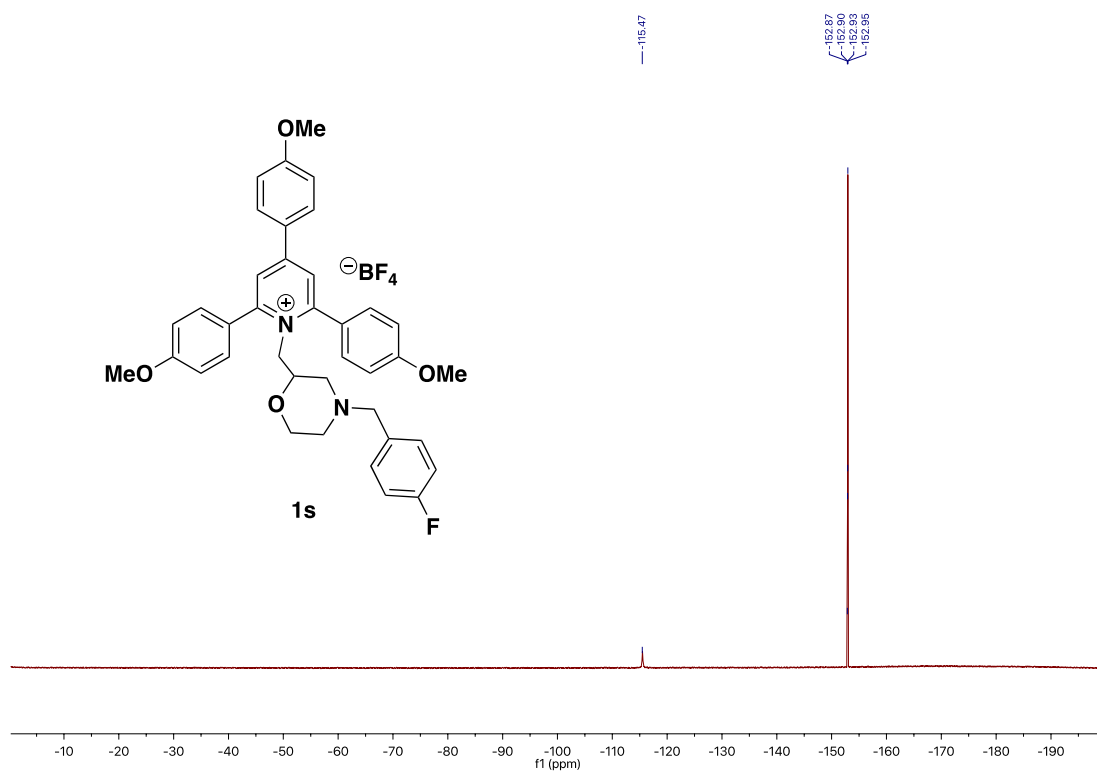
Chapter 3



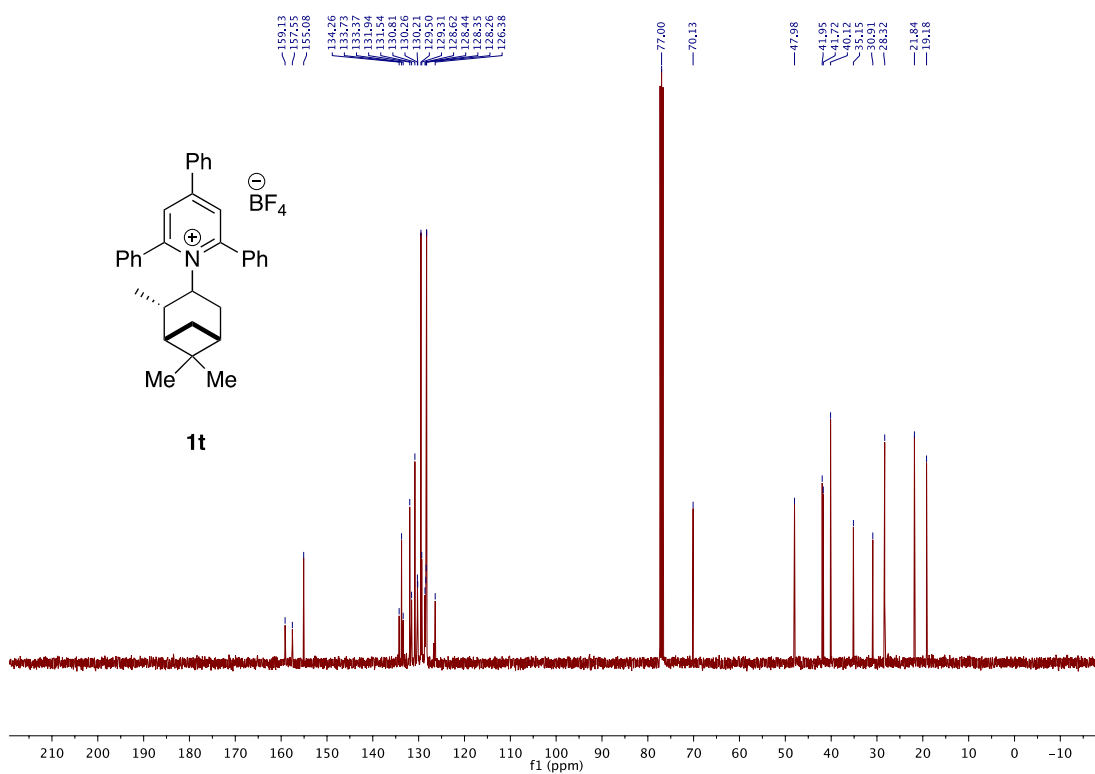
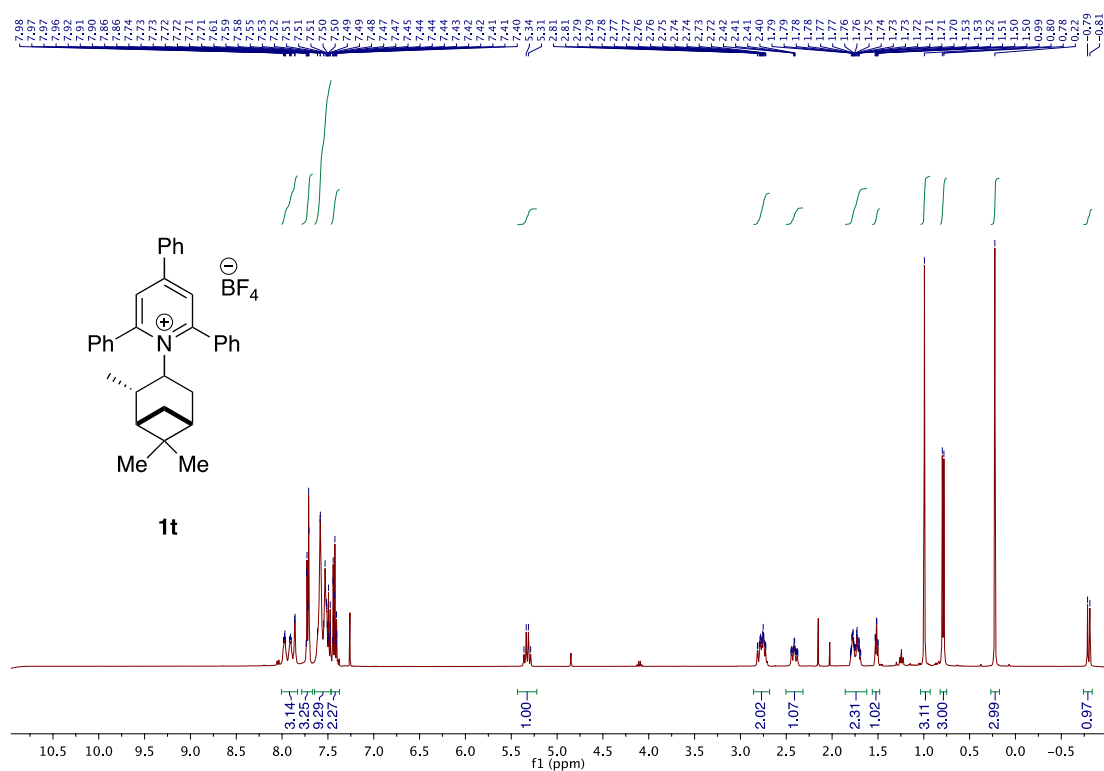
Deaminative Arylation at sp^3 Carbon Centers



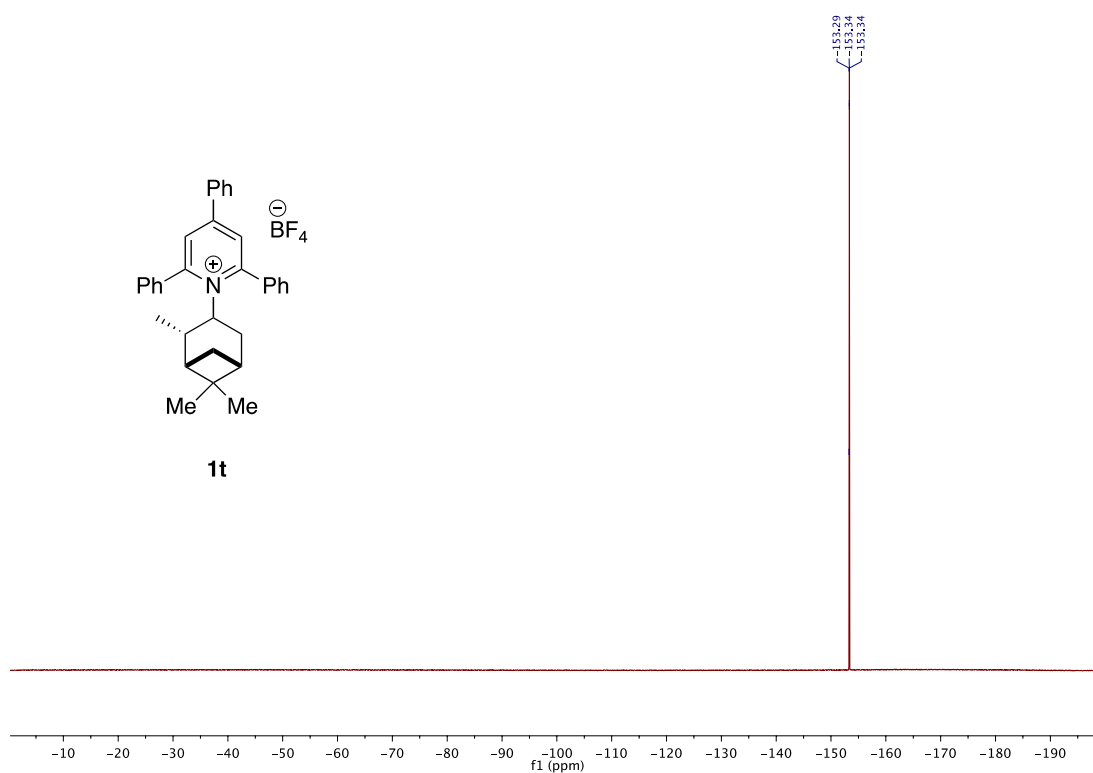
Chapter 3



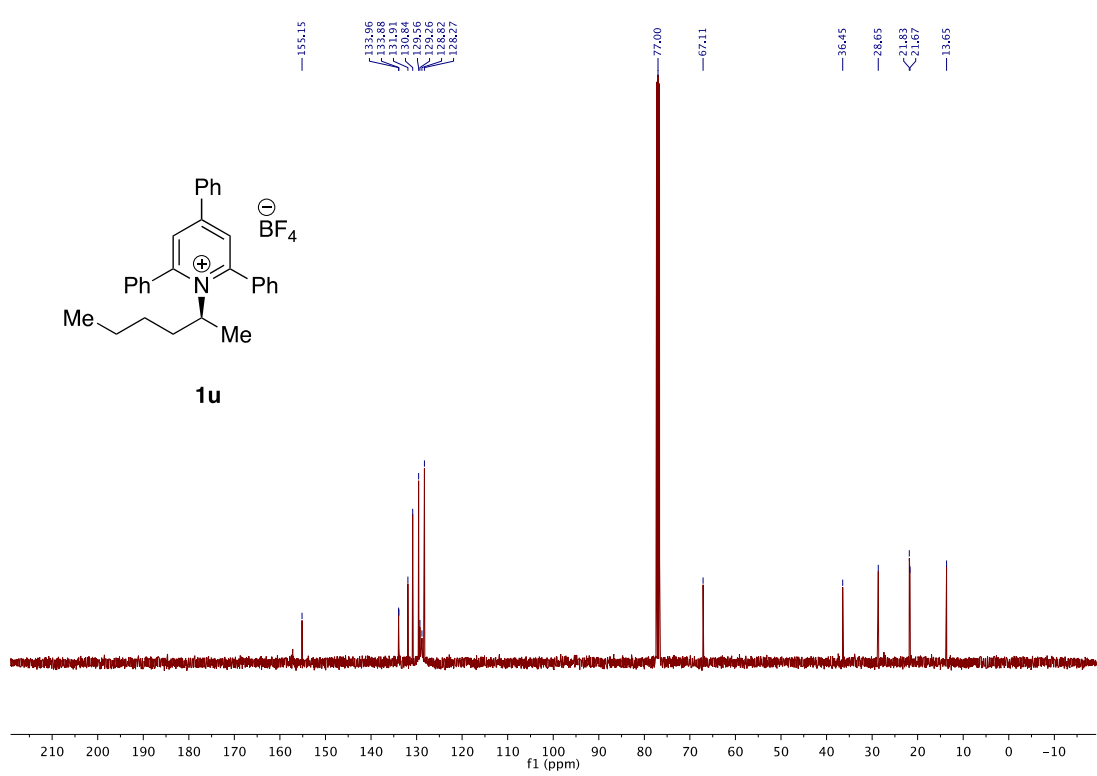
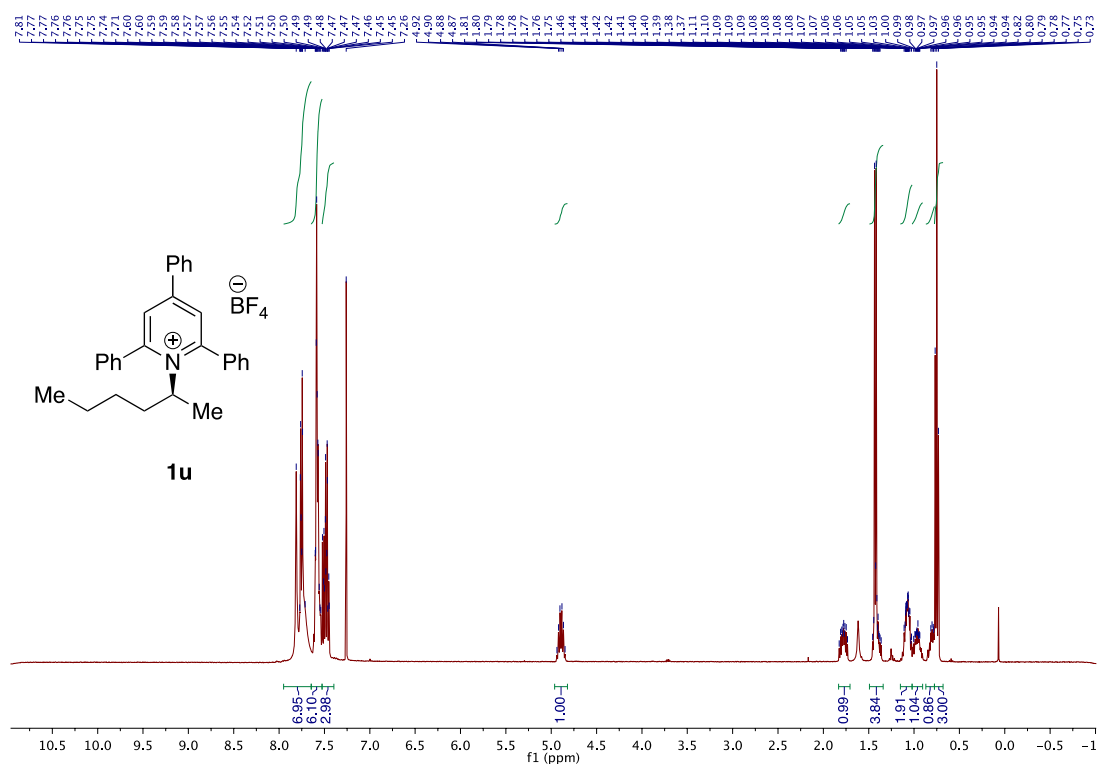
Deaminative Arylation at sp^3 Carbon Centers



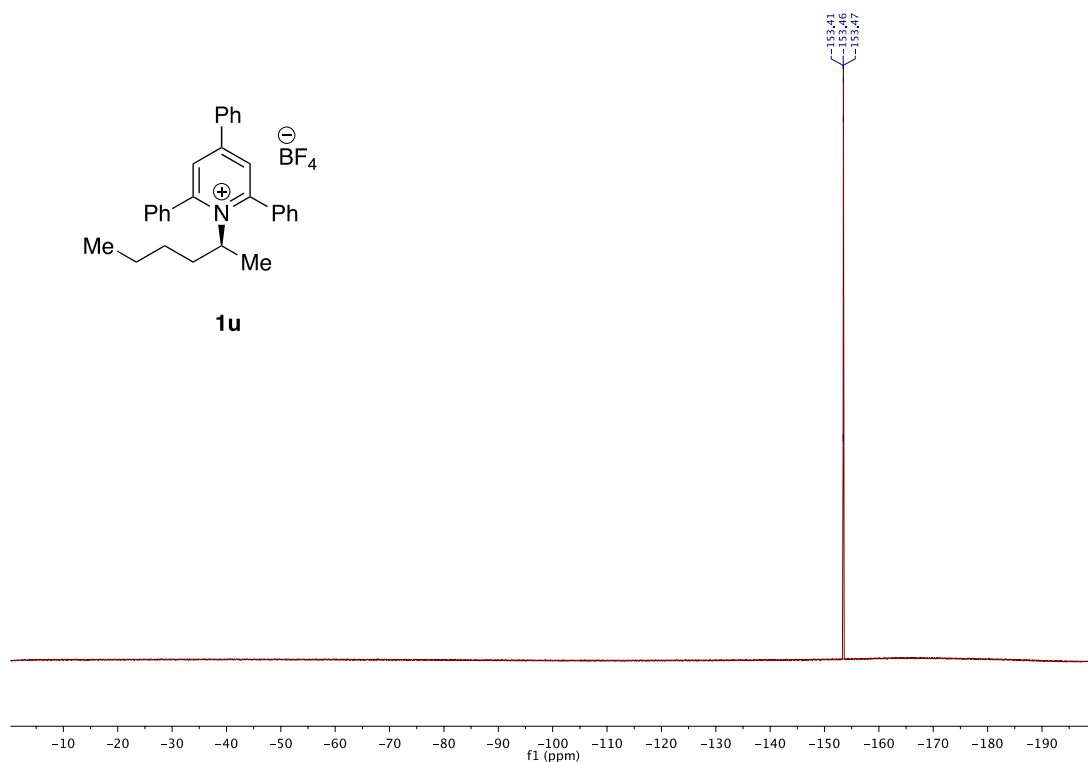
Chapter 3



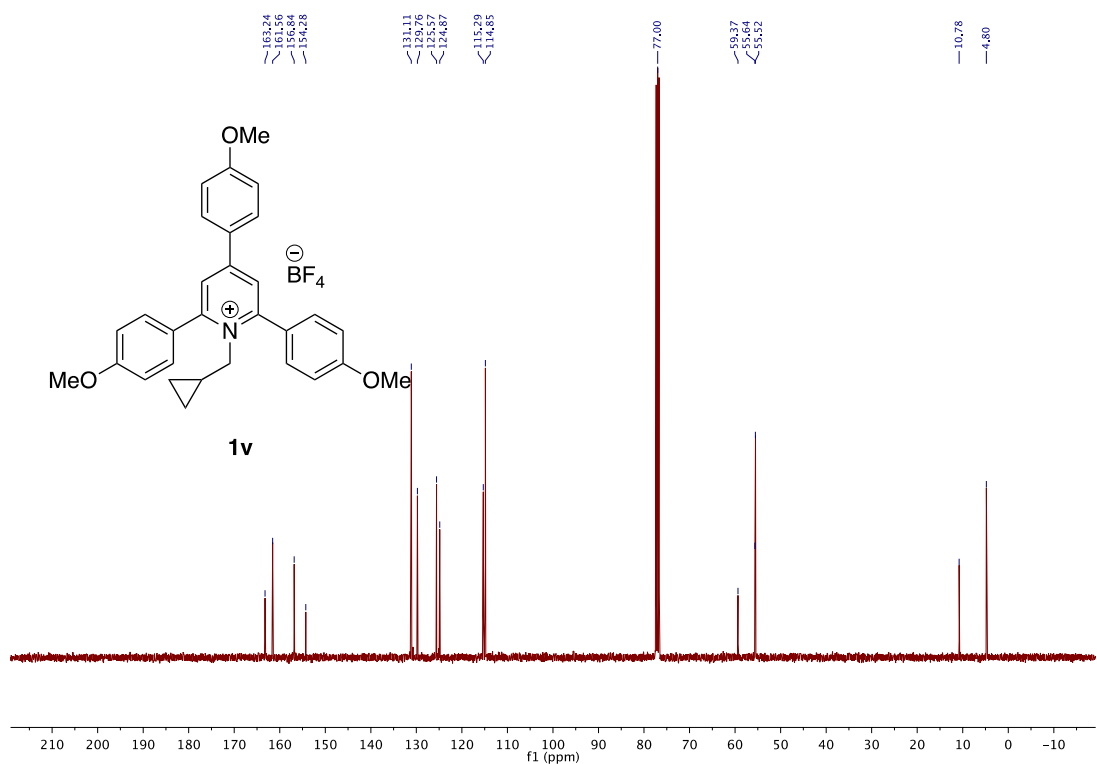
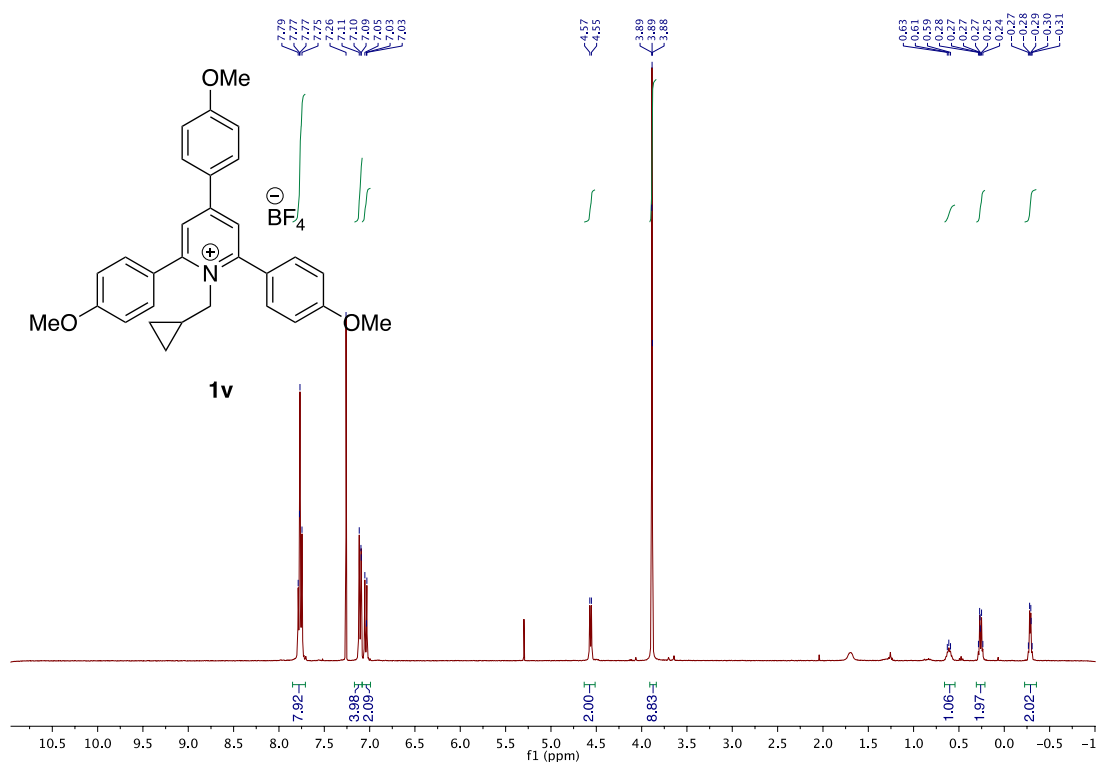
Deaminative Arylation at sp^3 Carbon Centers



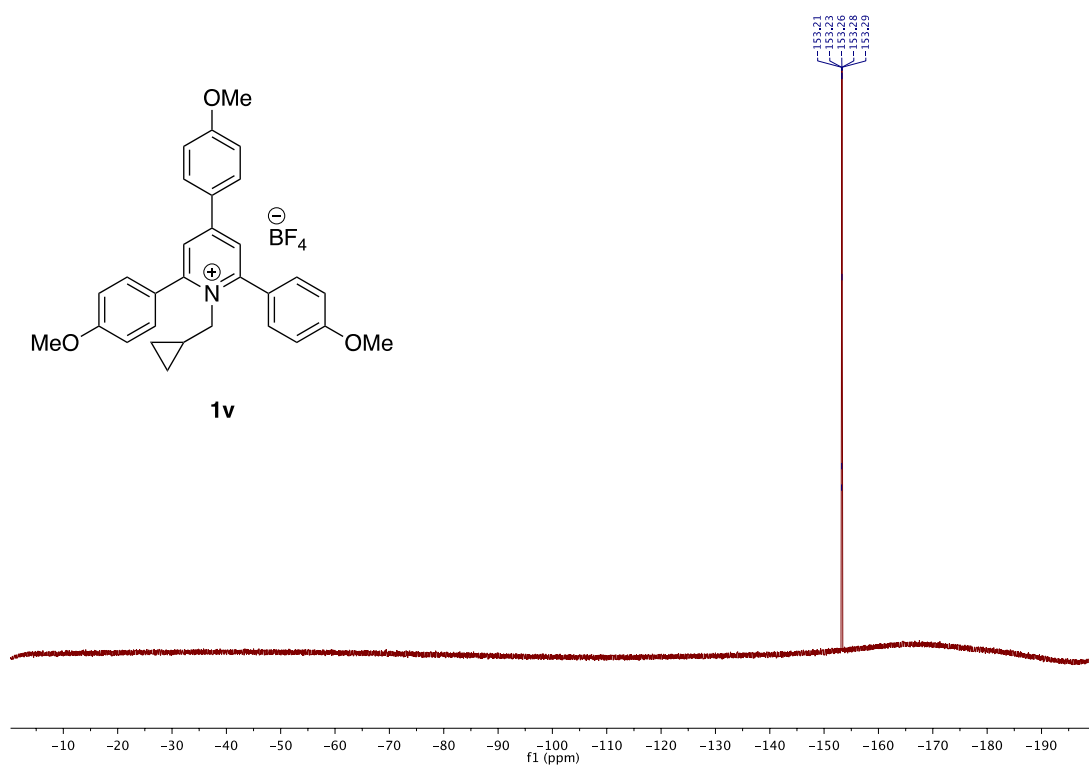
Chapter 3



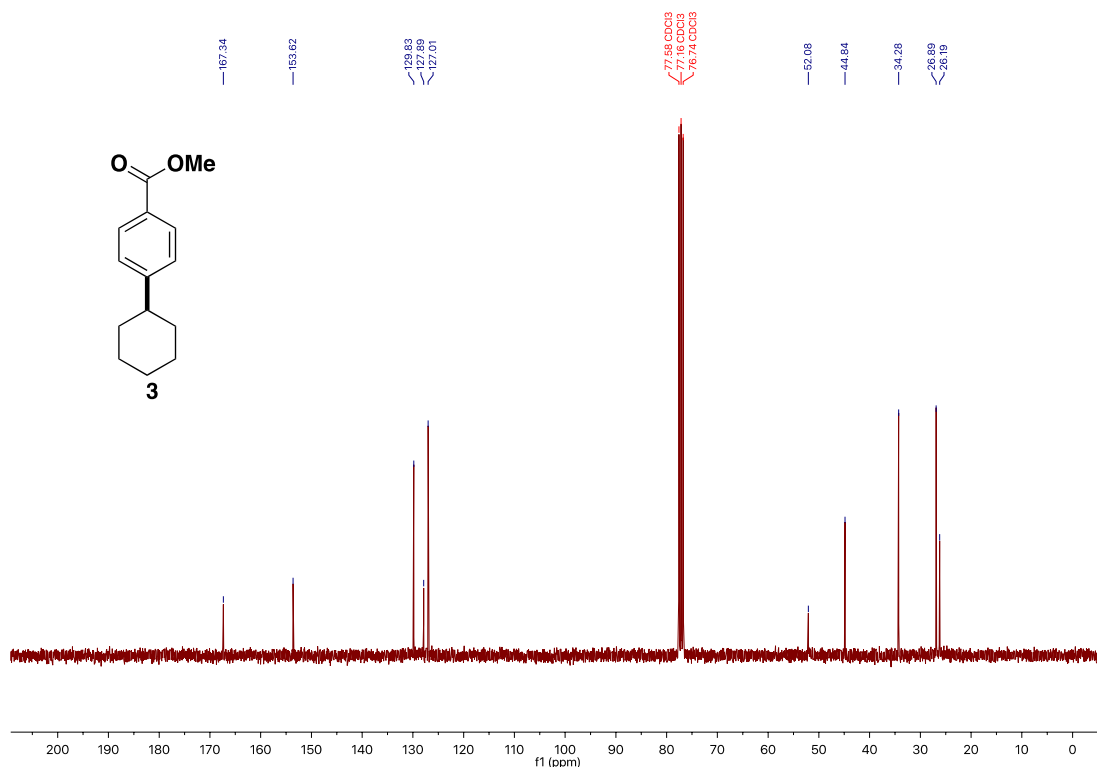
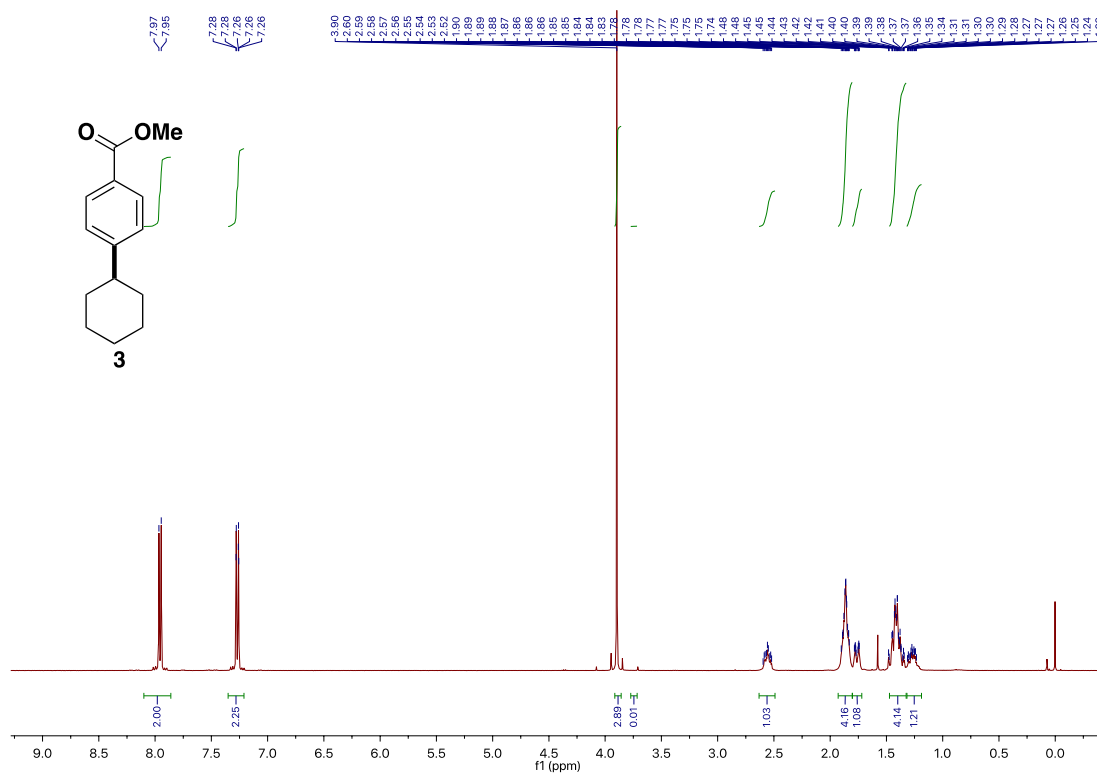
Deaminative Arylation at sp^3 Carbon Centers



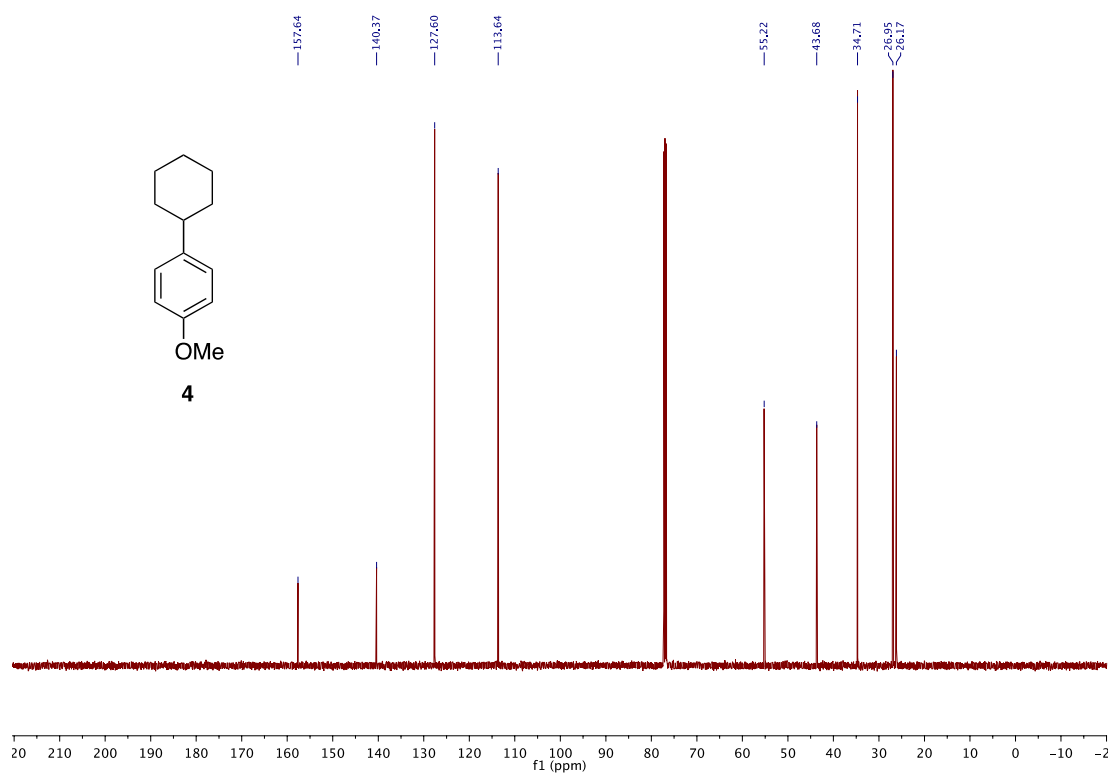
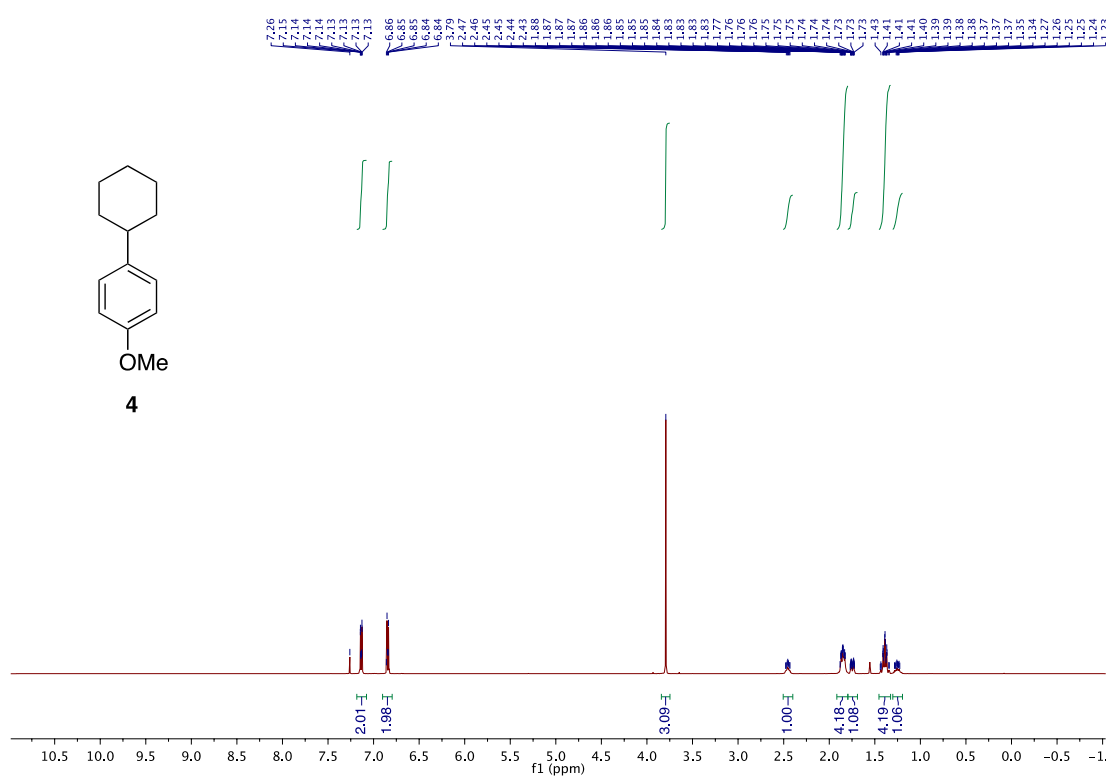
Chapter 3



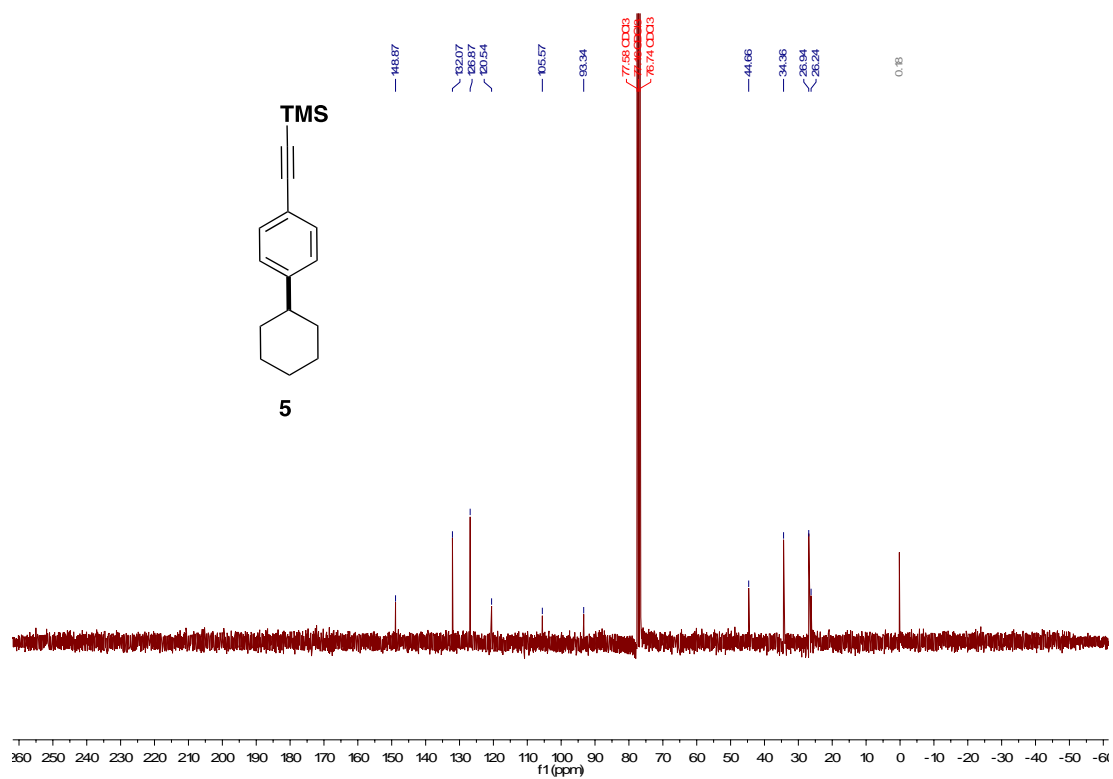
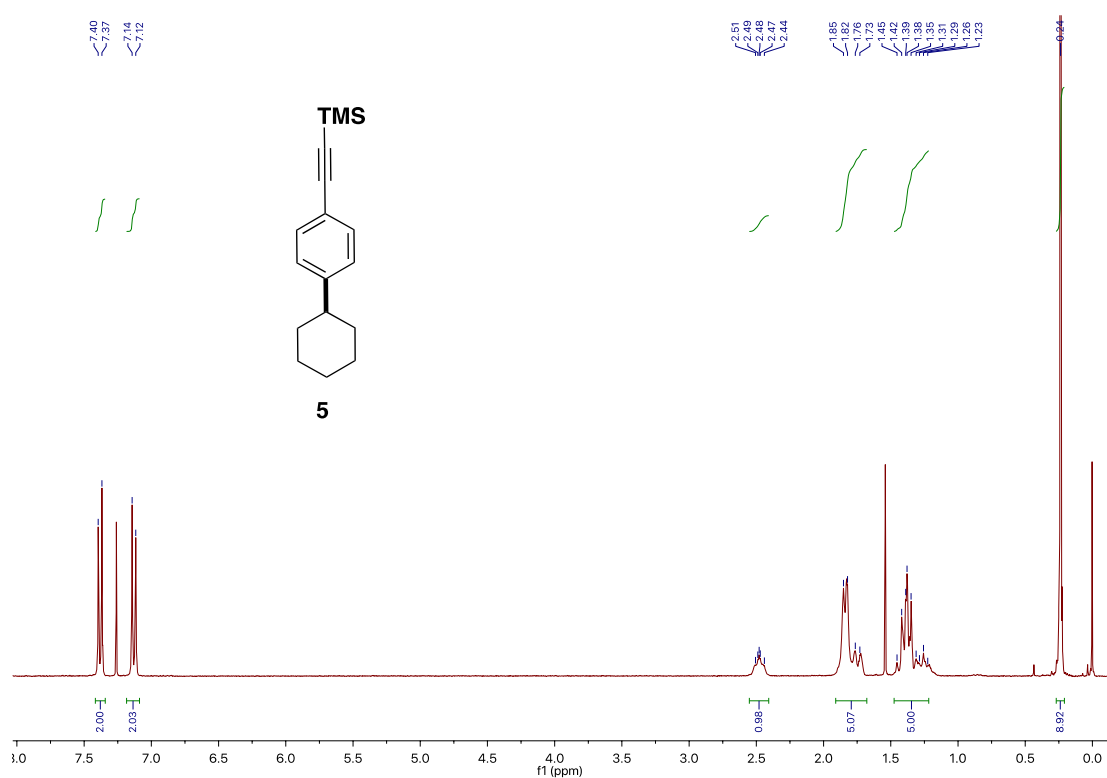
Deaminative Arylation at sp^3 Carbon Centers



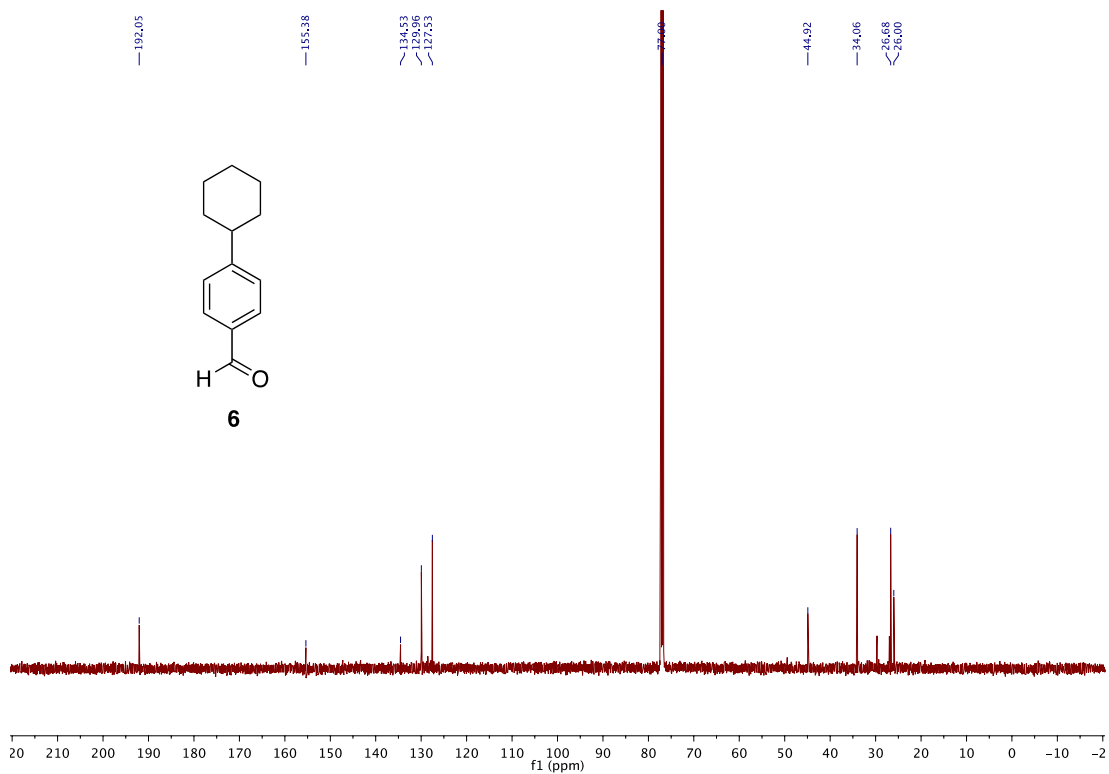
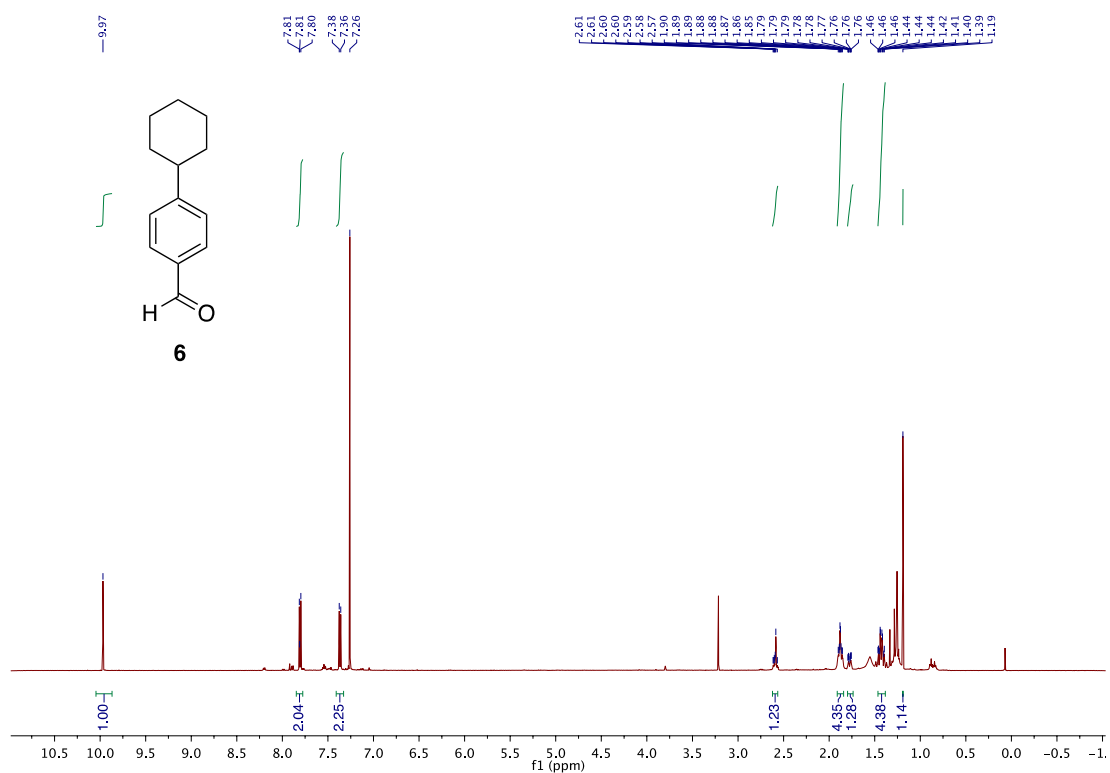
Chapter 3



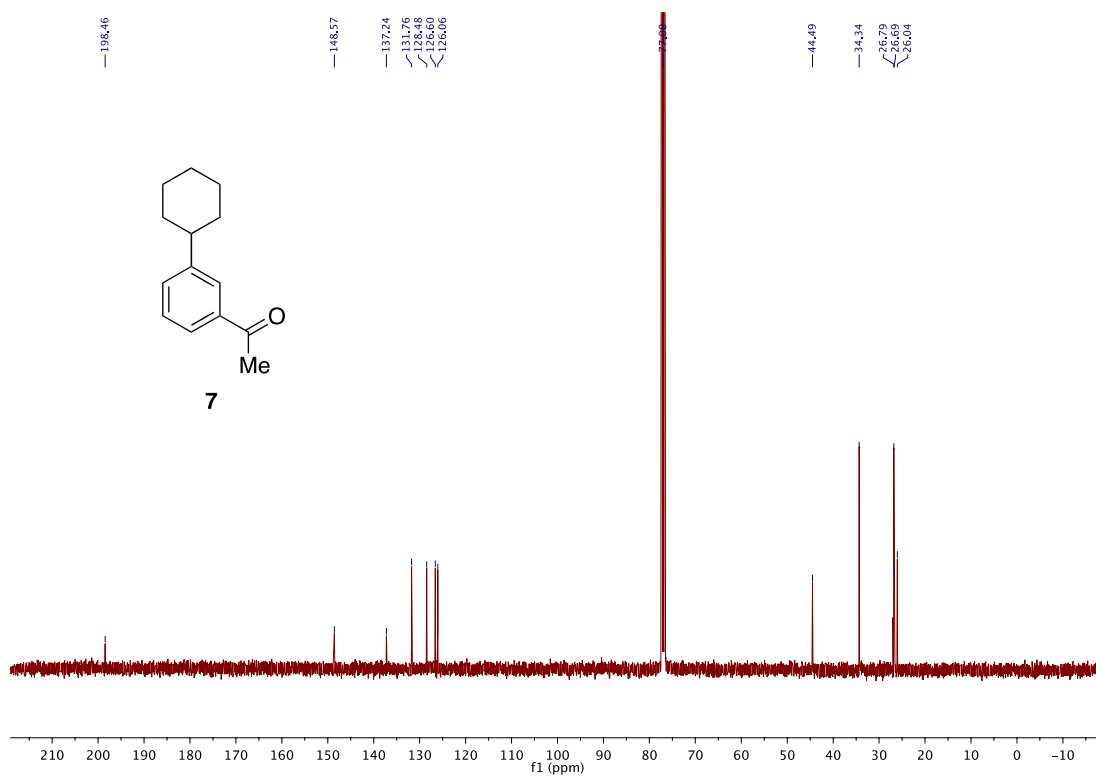
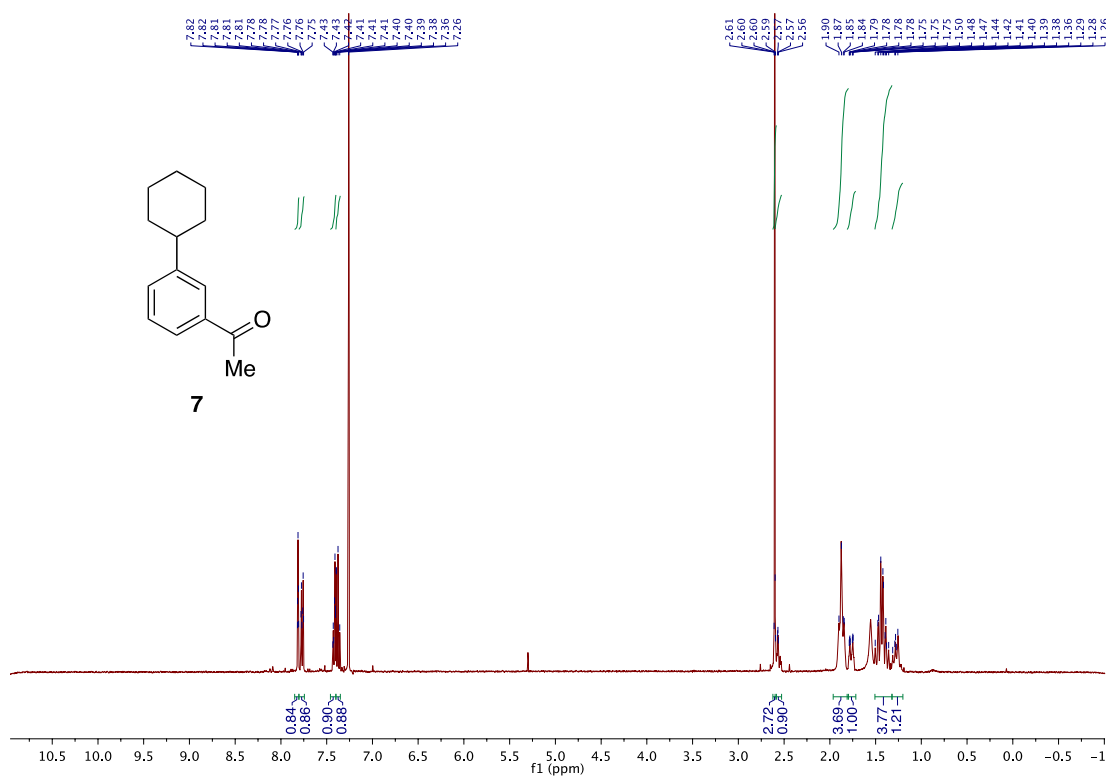
Deaminative Arylation at sp^3 Carbon Centers



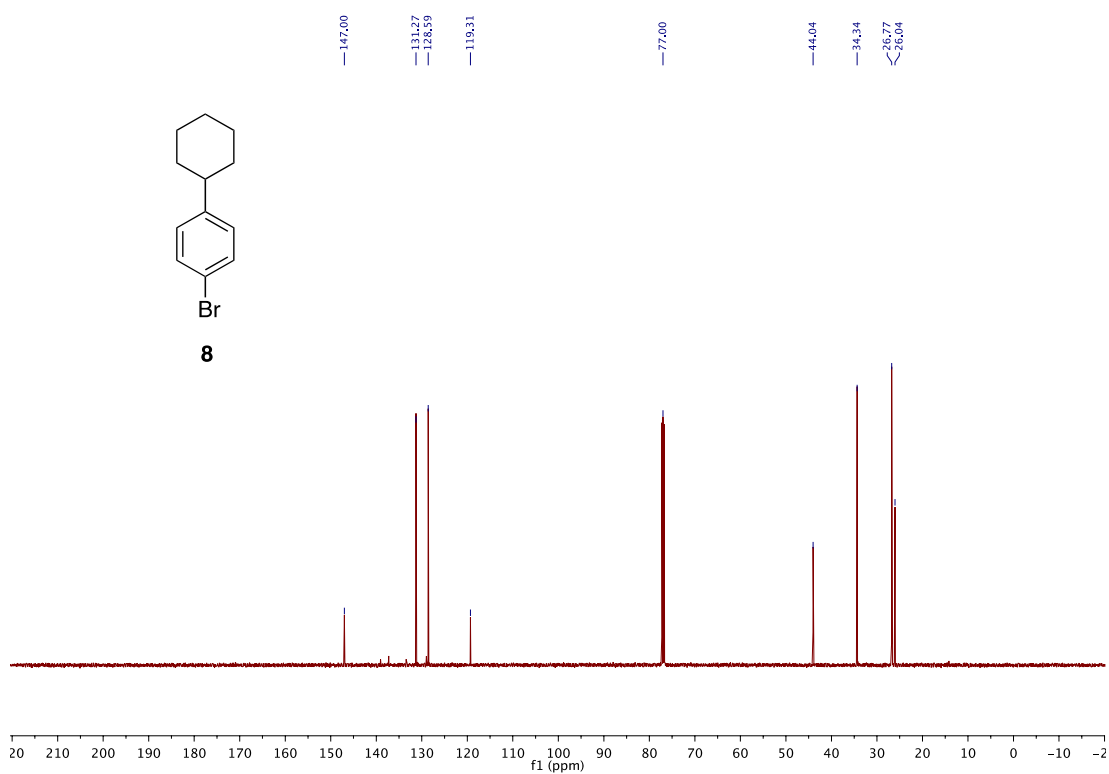
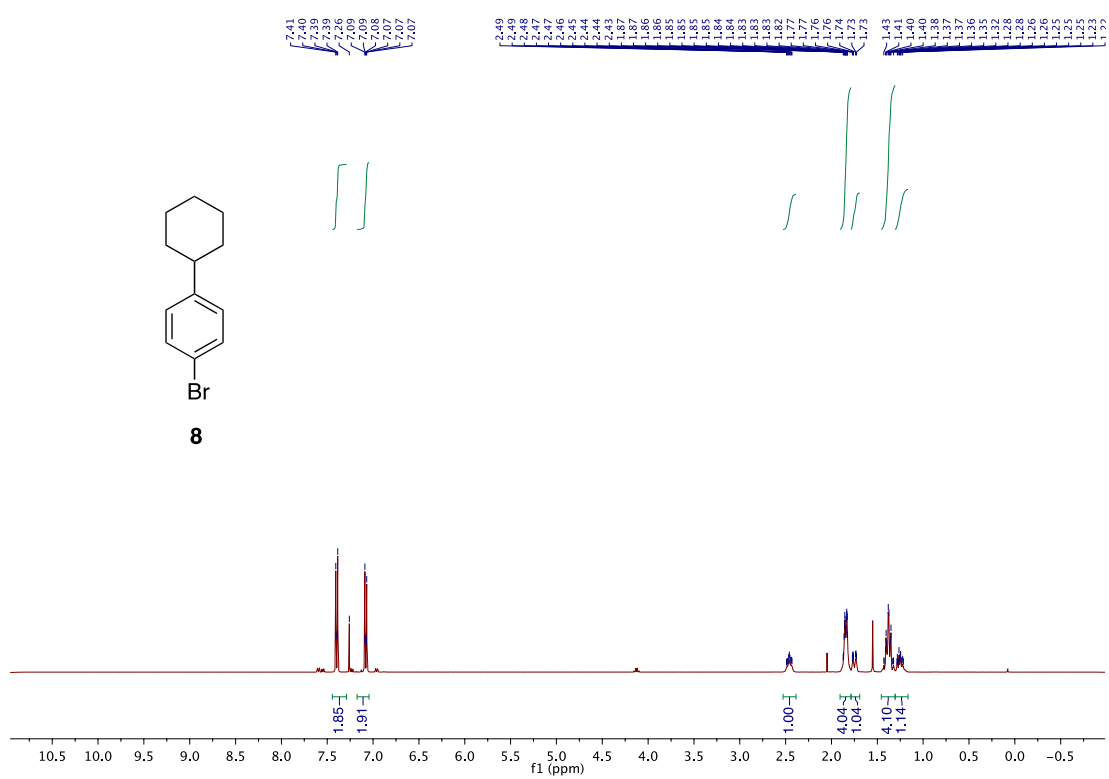
Chapter 3



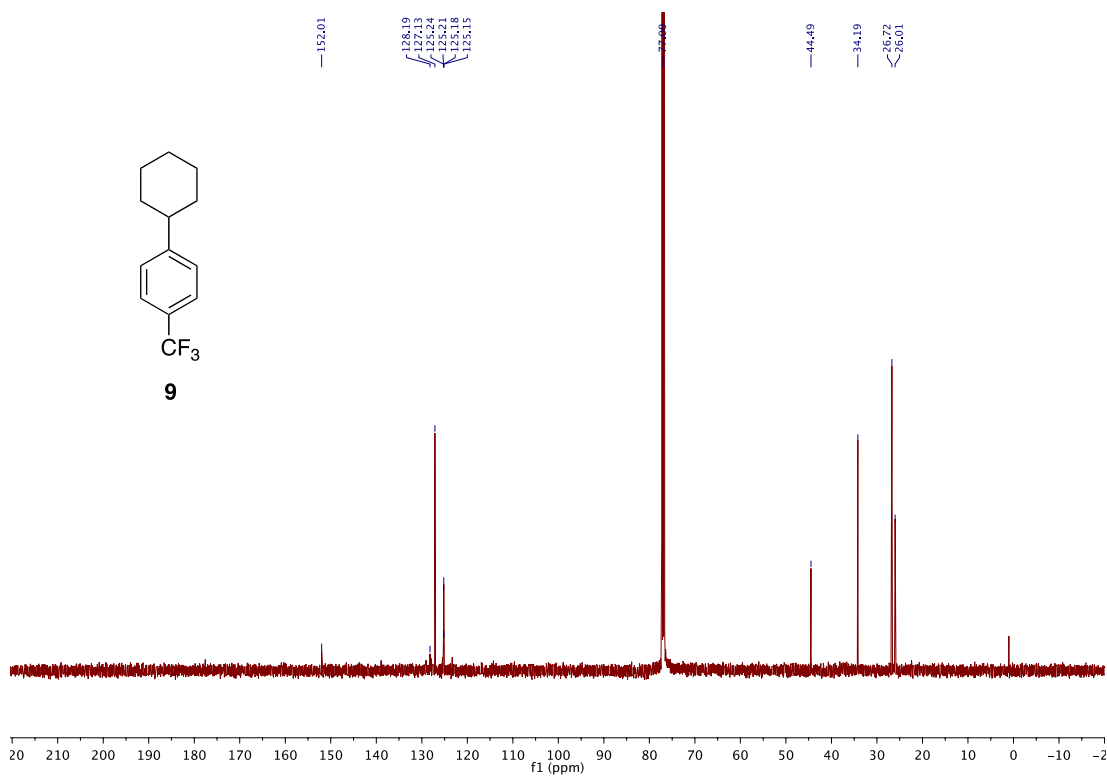
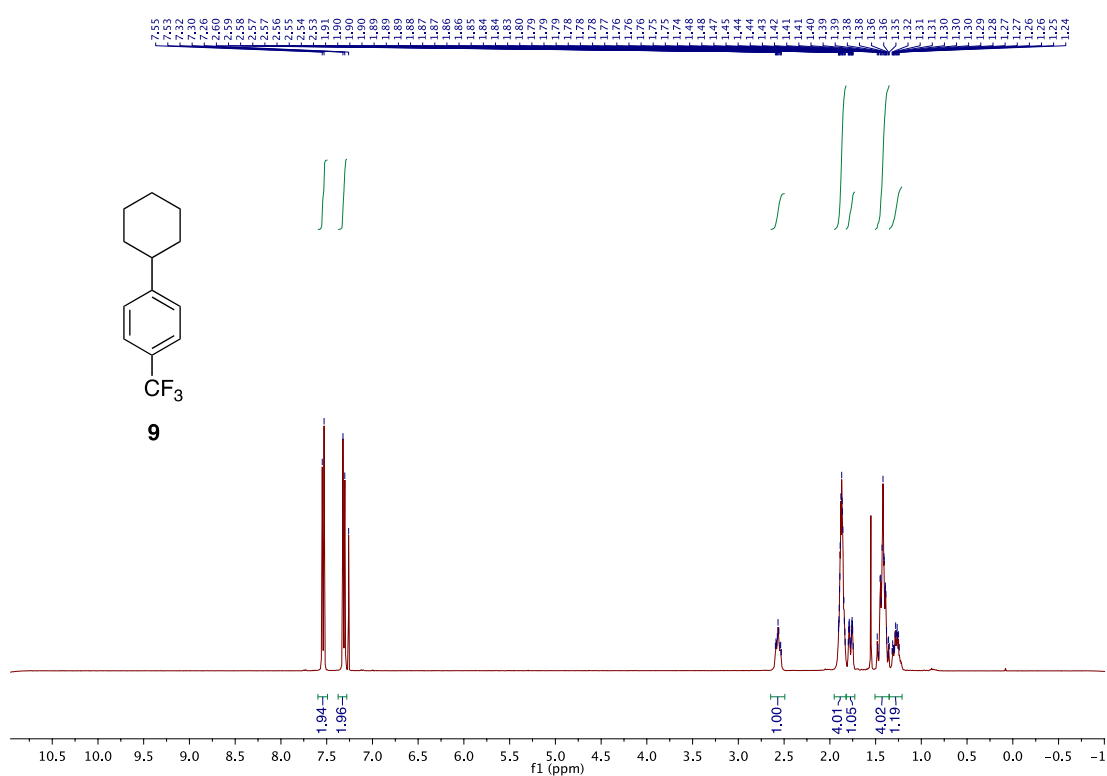
Deaminative Arylation at sp^3 Carbon Centers



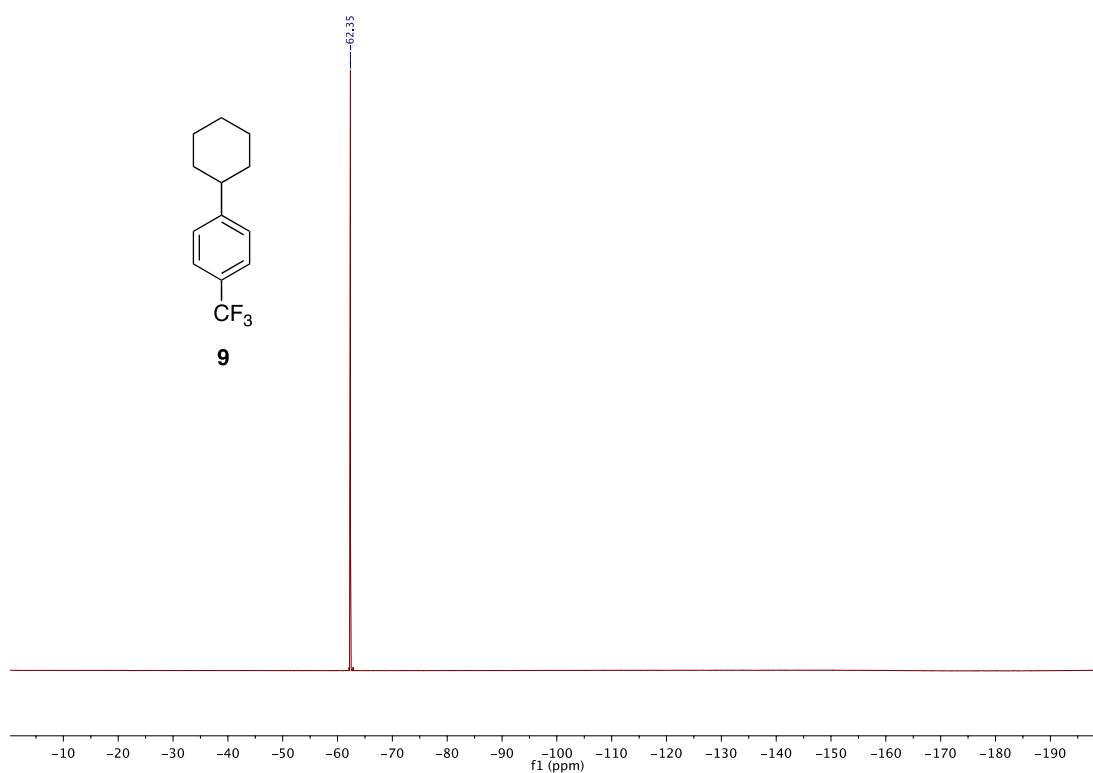
Chapter 3



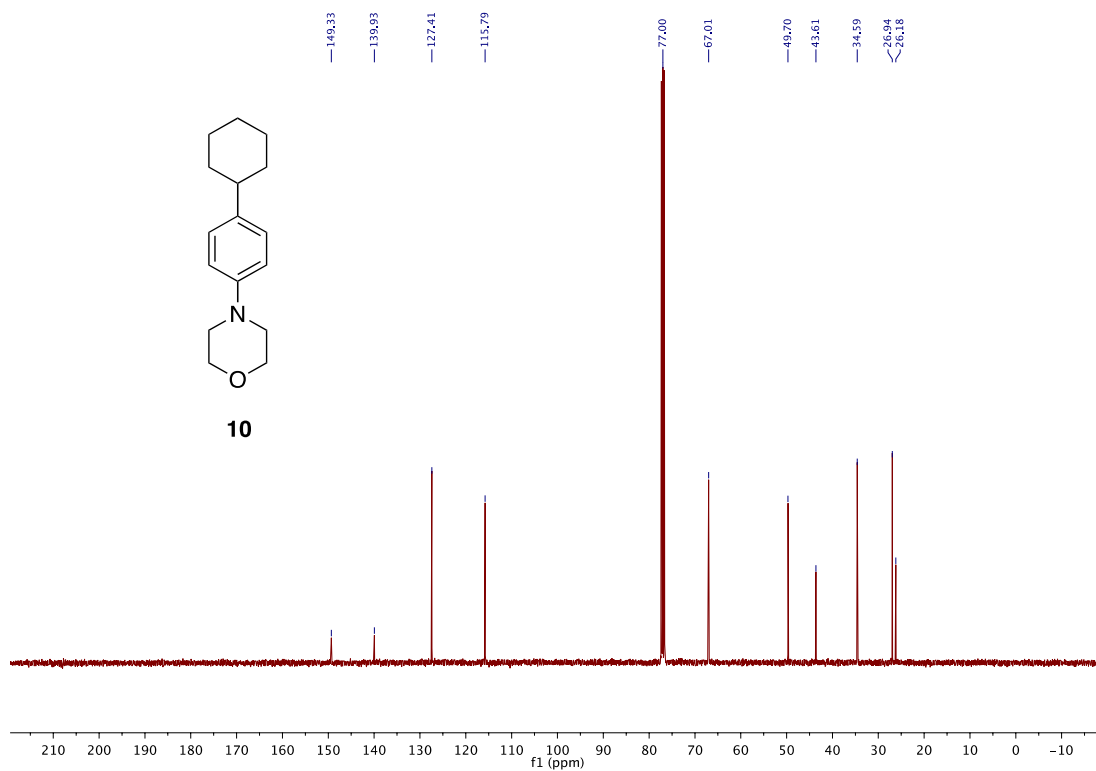
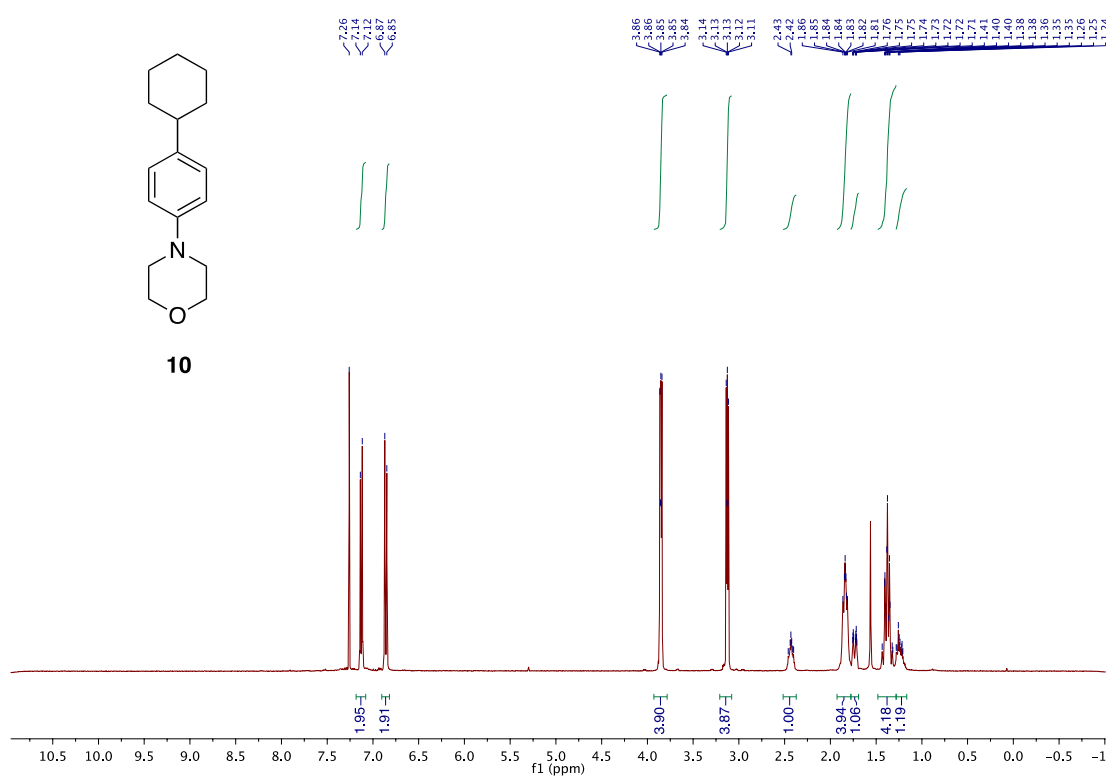
Deaminative Arylation at sp^3 Carbon Centers



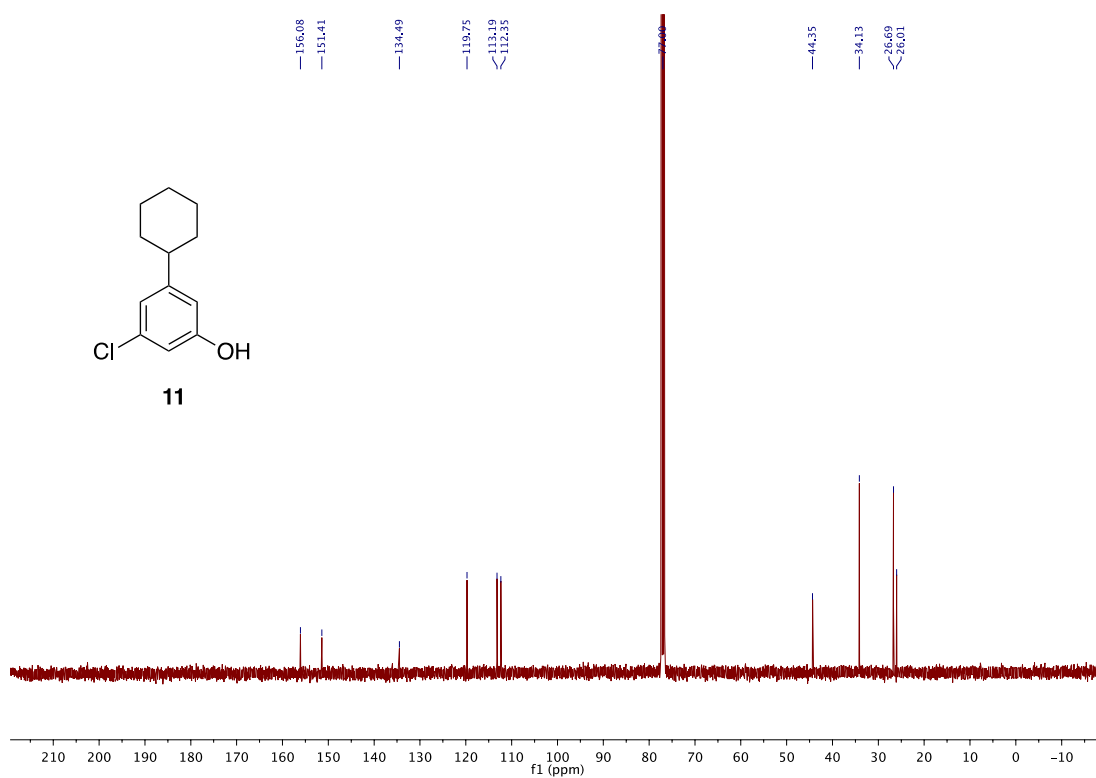
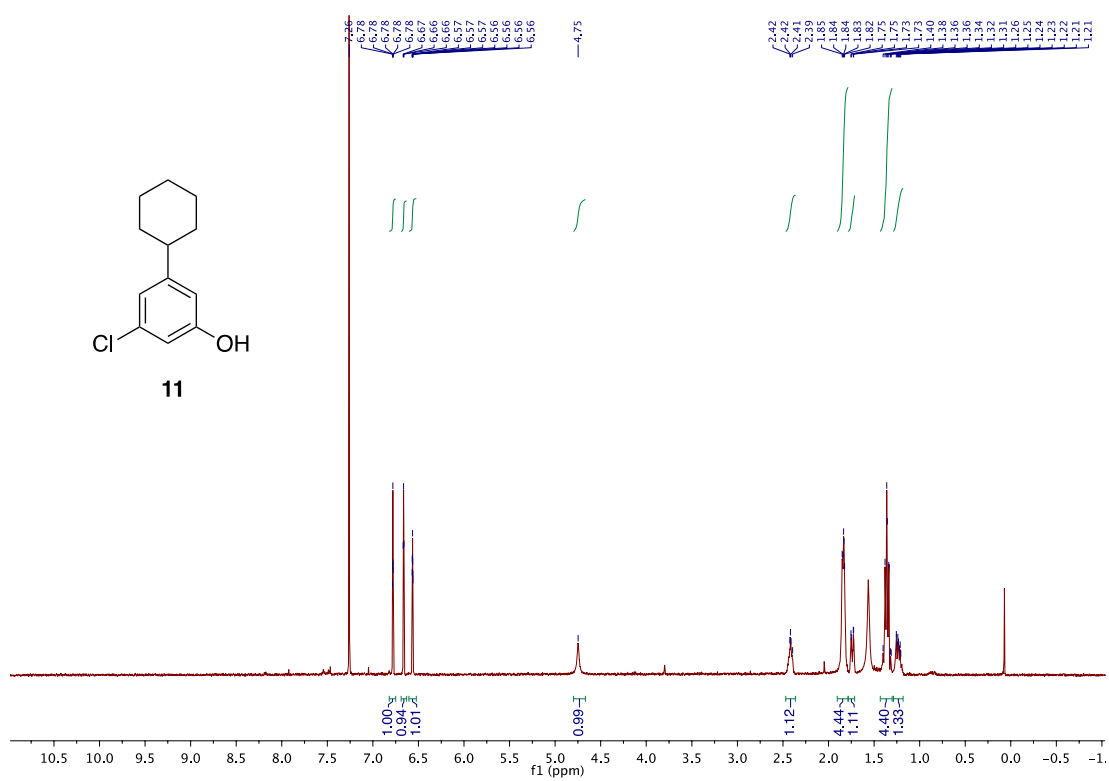
Chapter 3



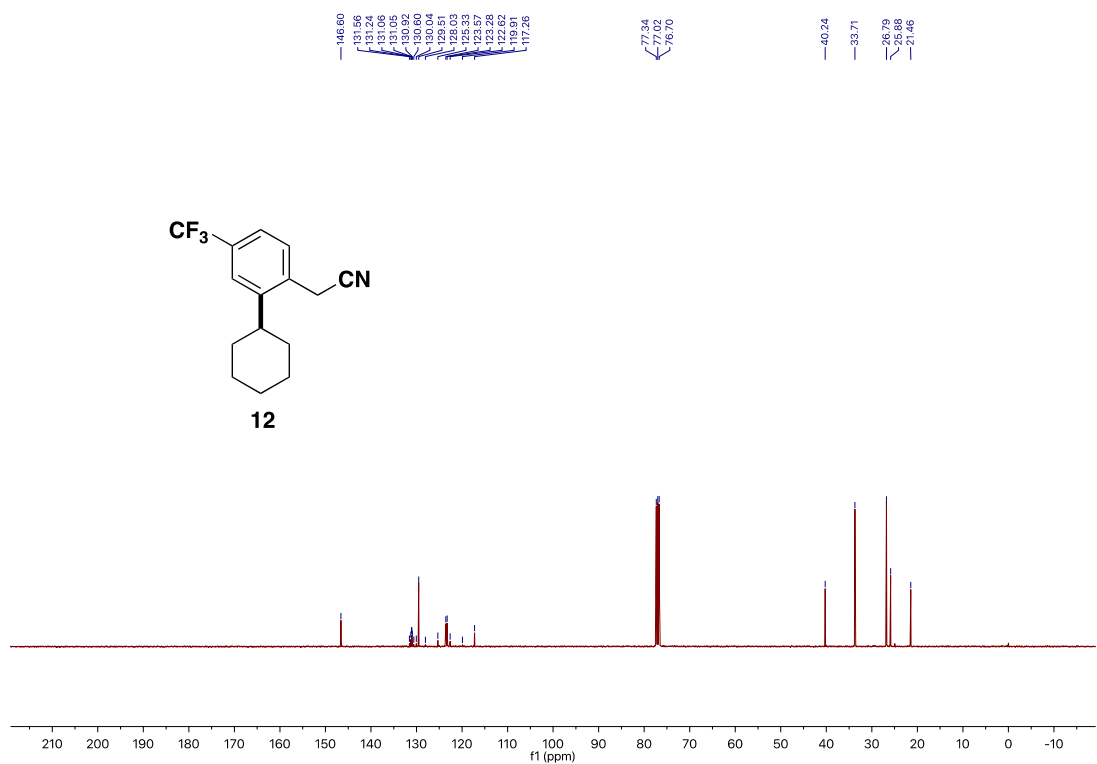
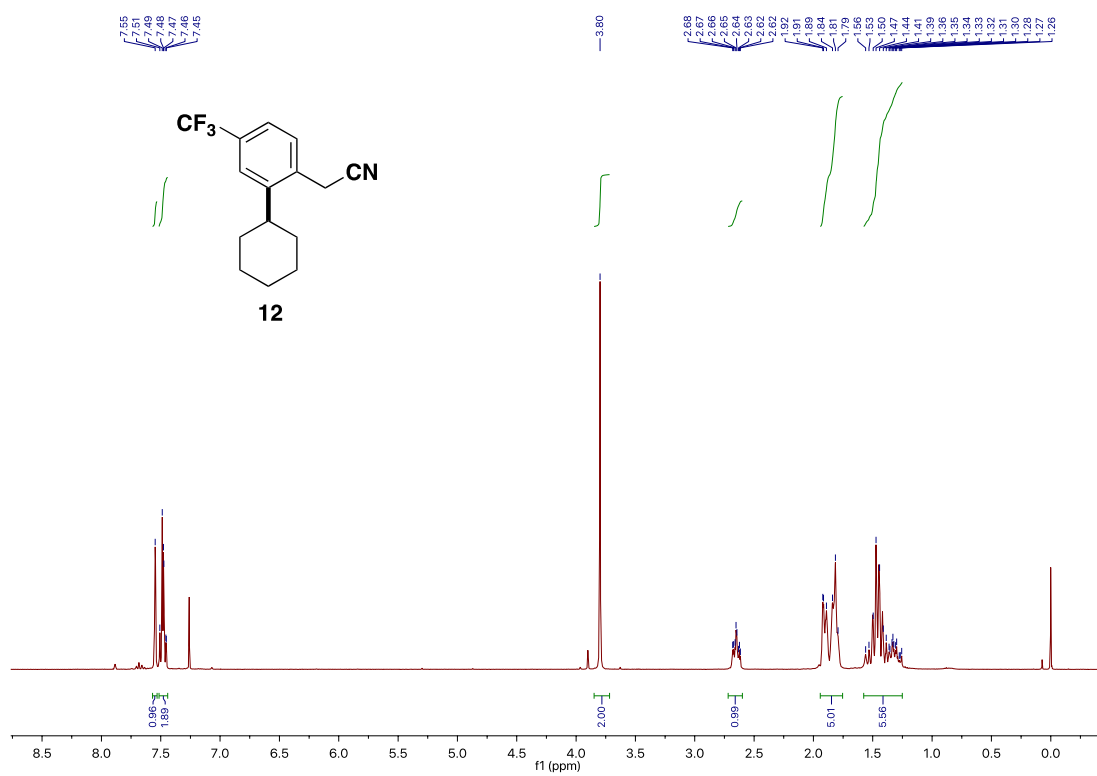
Deaminative Arylation at sp^3 Carbon Centers



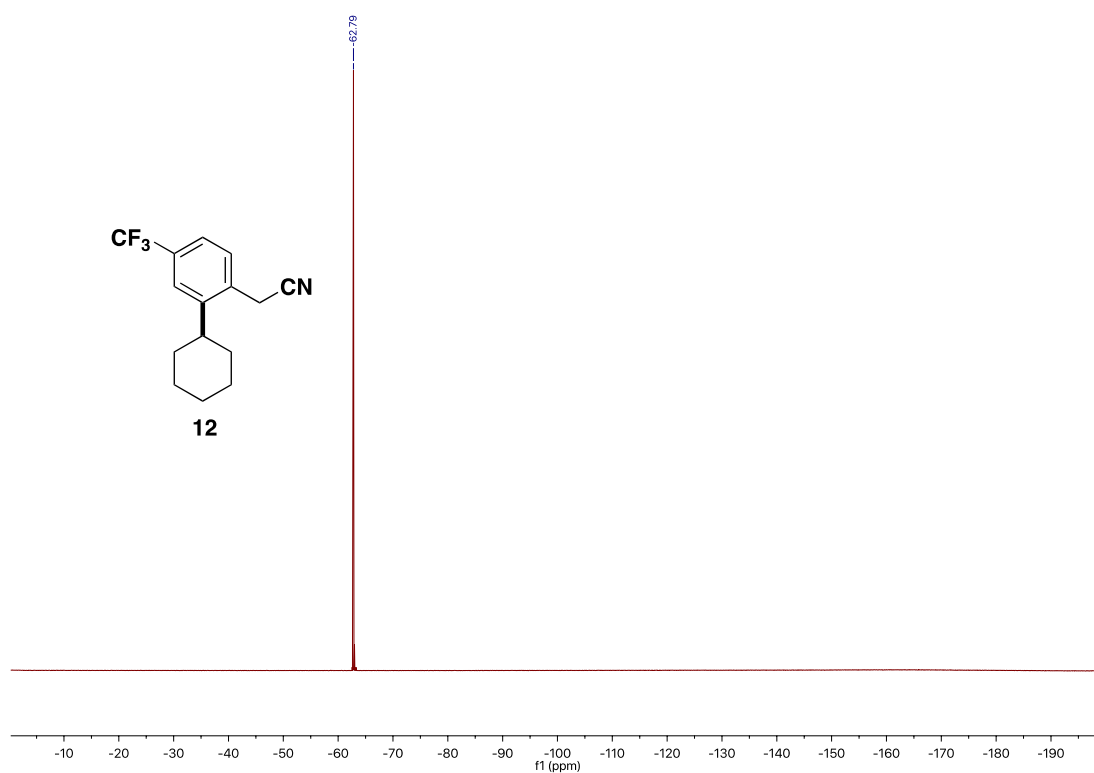
Chapter 3



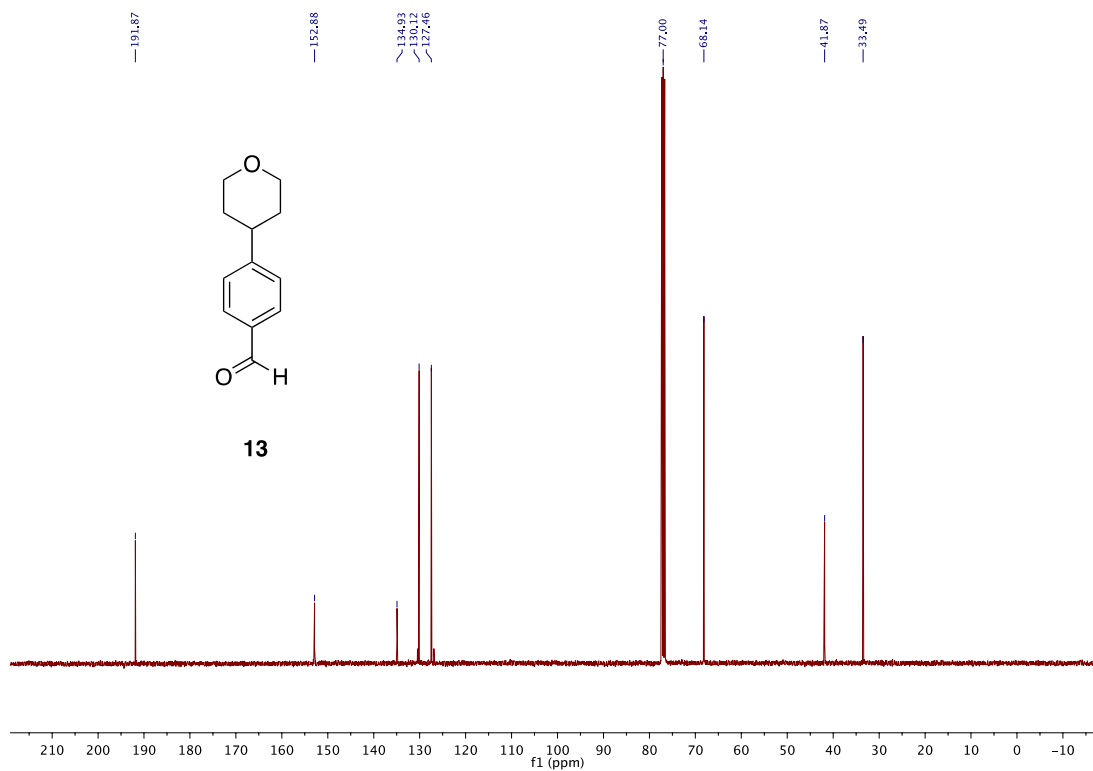
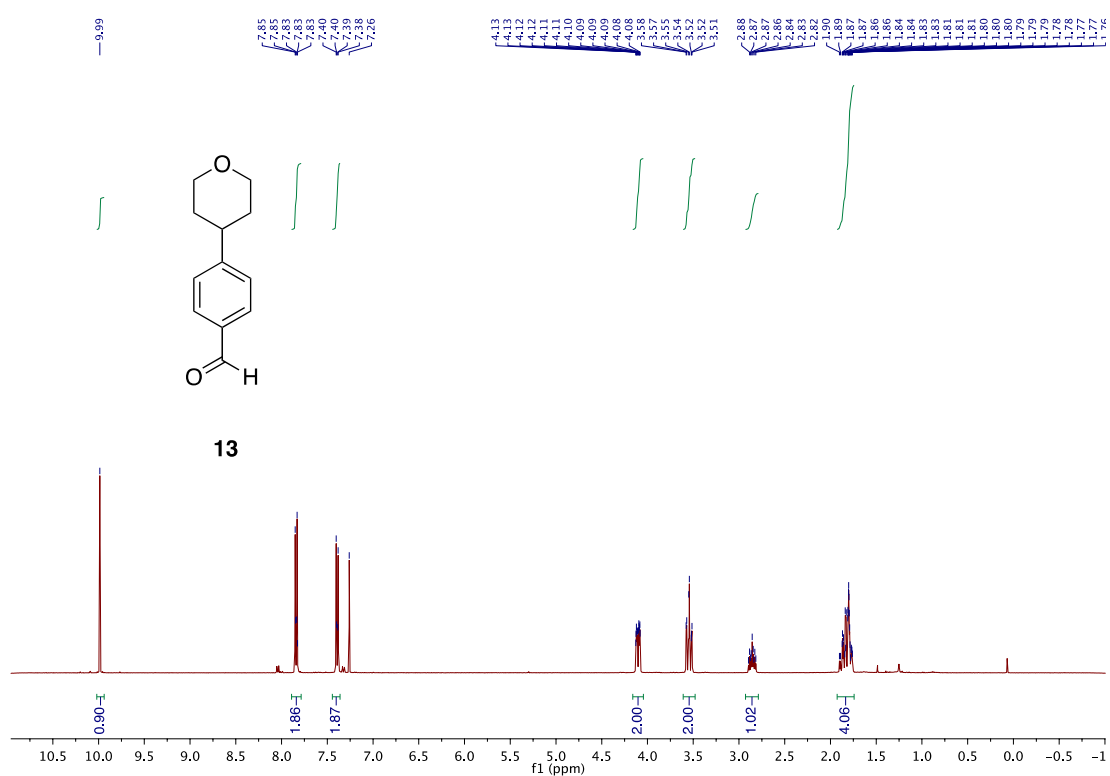
Deaminative Arylation at sp^3 Carbon Centers



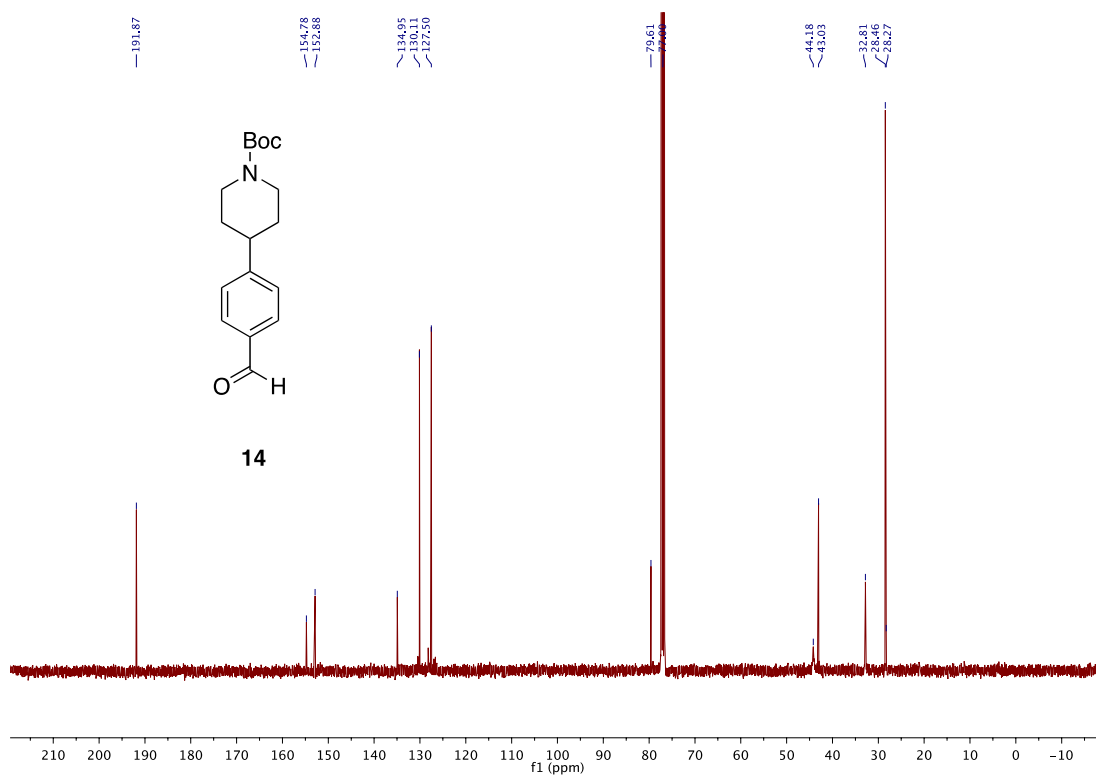
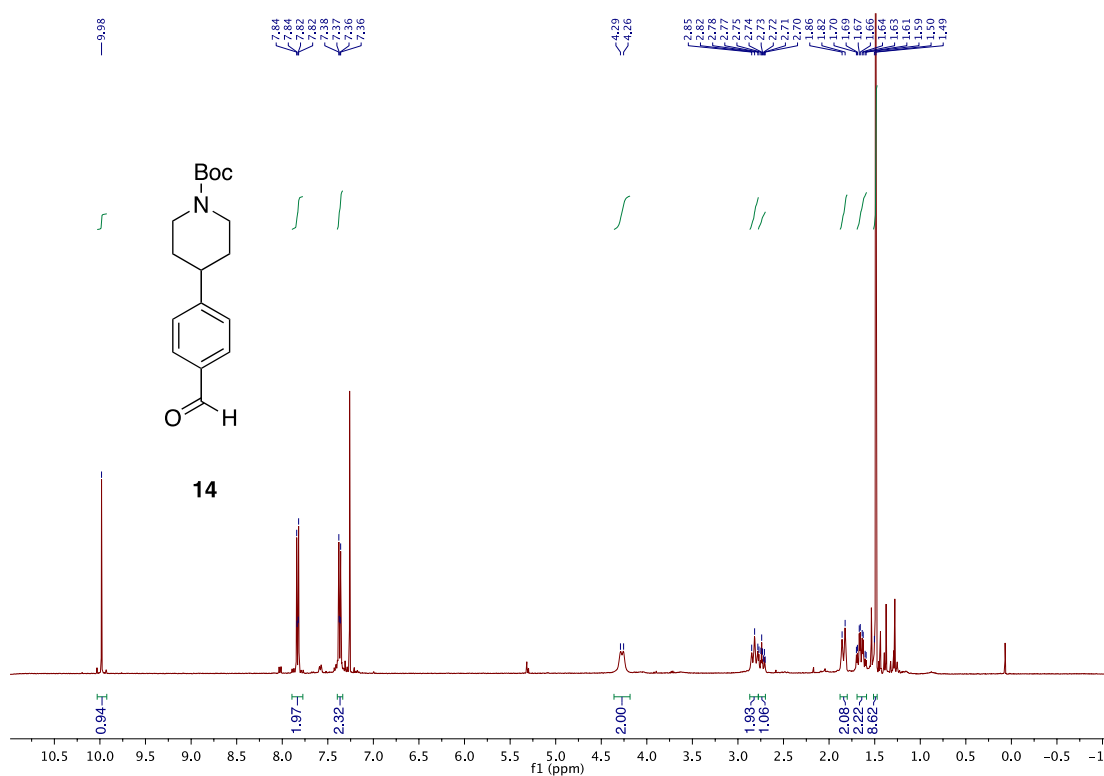
Chapter 3



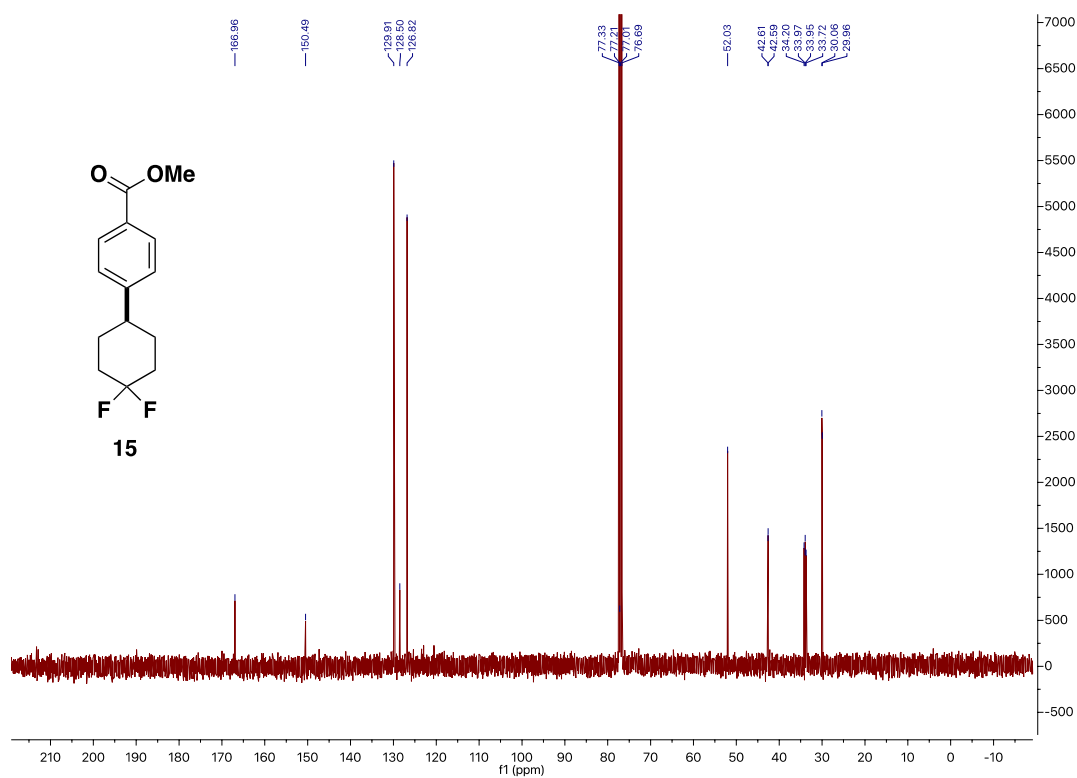
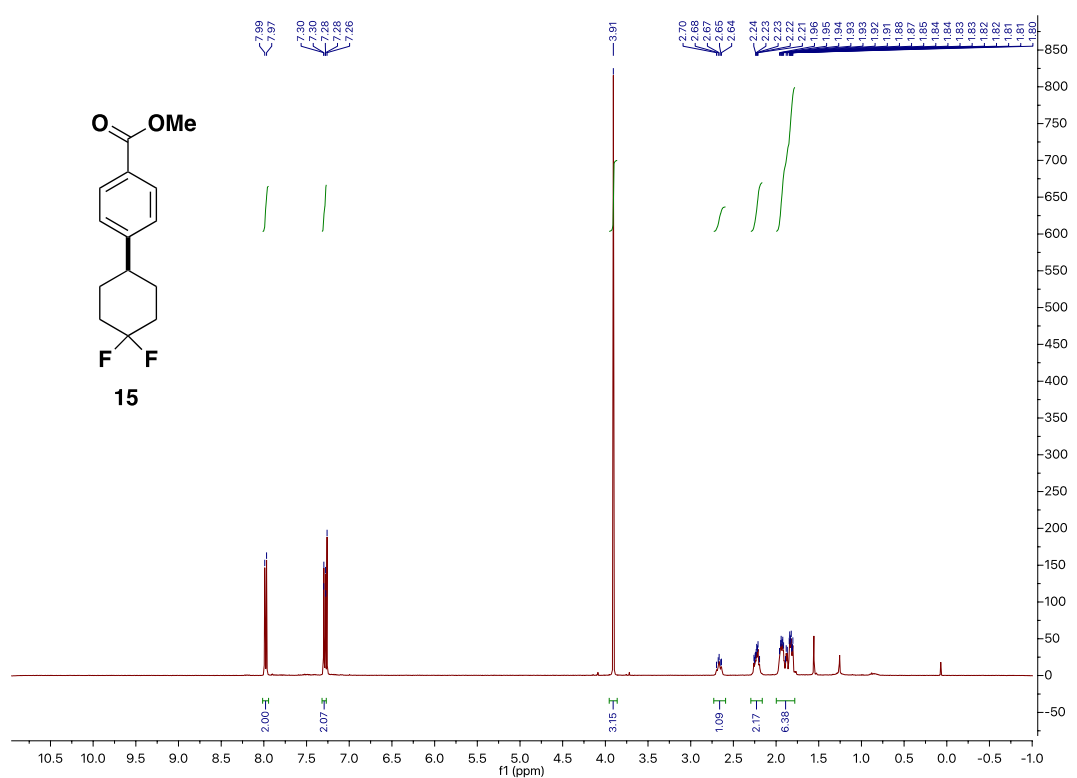
Deaminative Arylation at sp^3 Carbon Centers



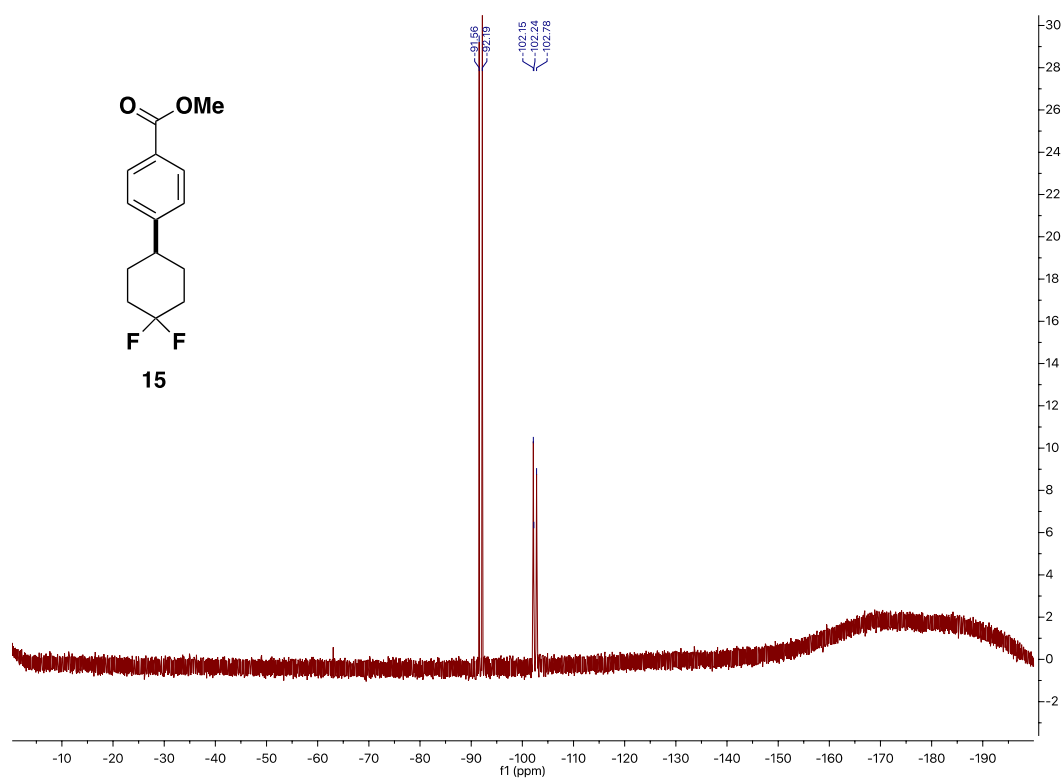
Chapter 3



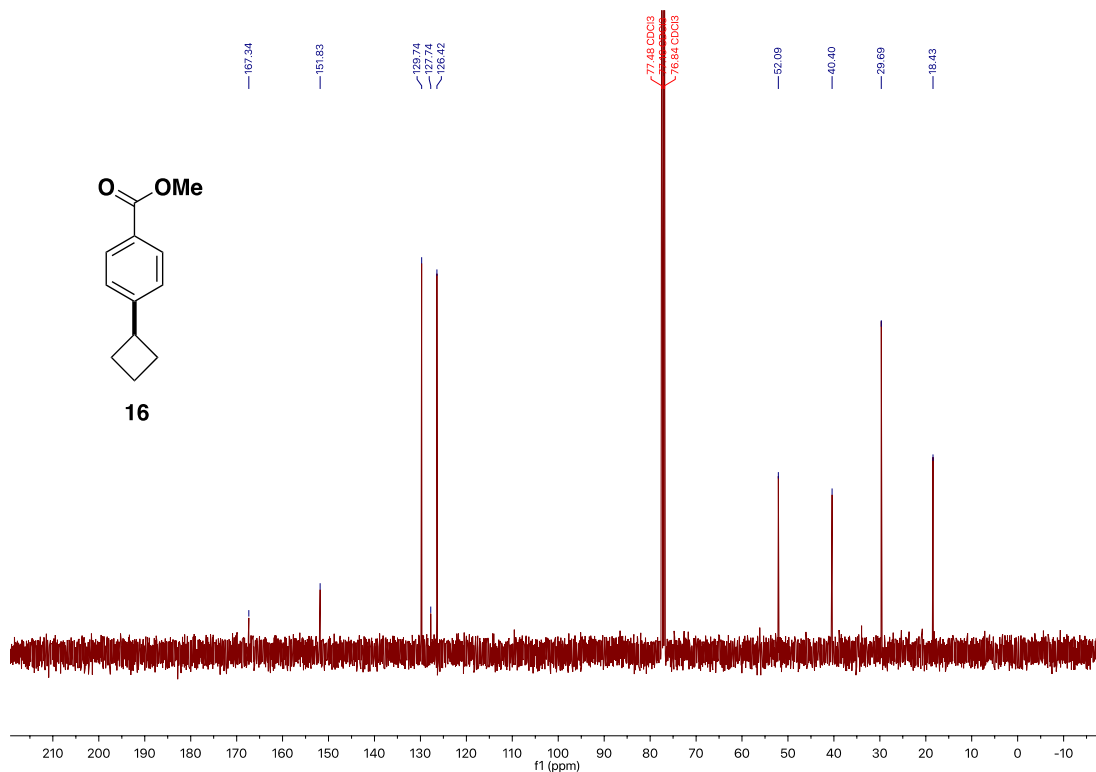
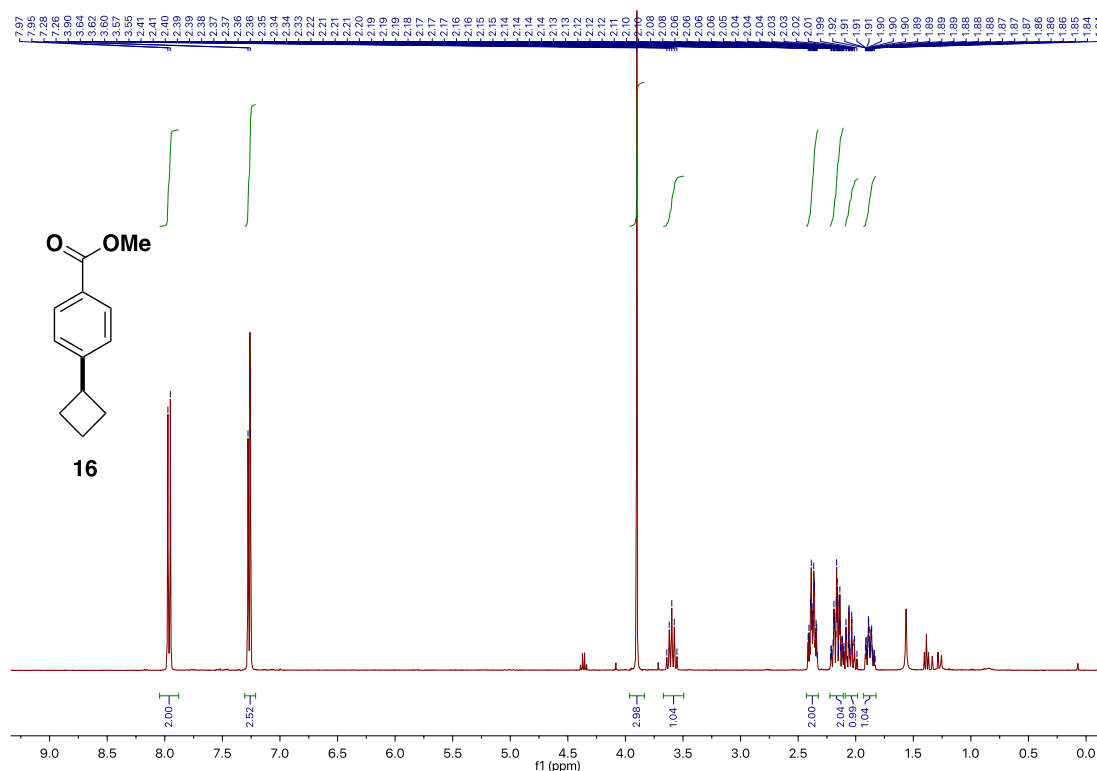
Deaminative Arylation at sp^3 Carbon Centers



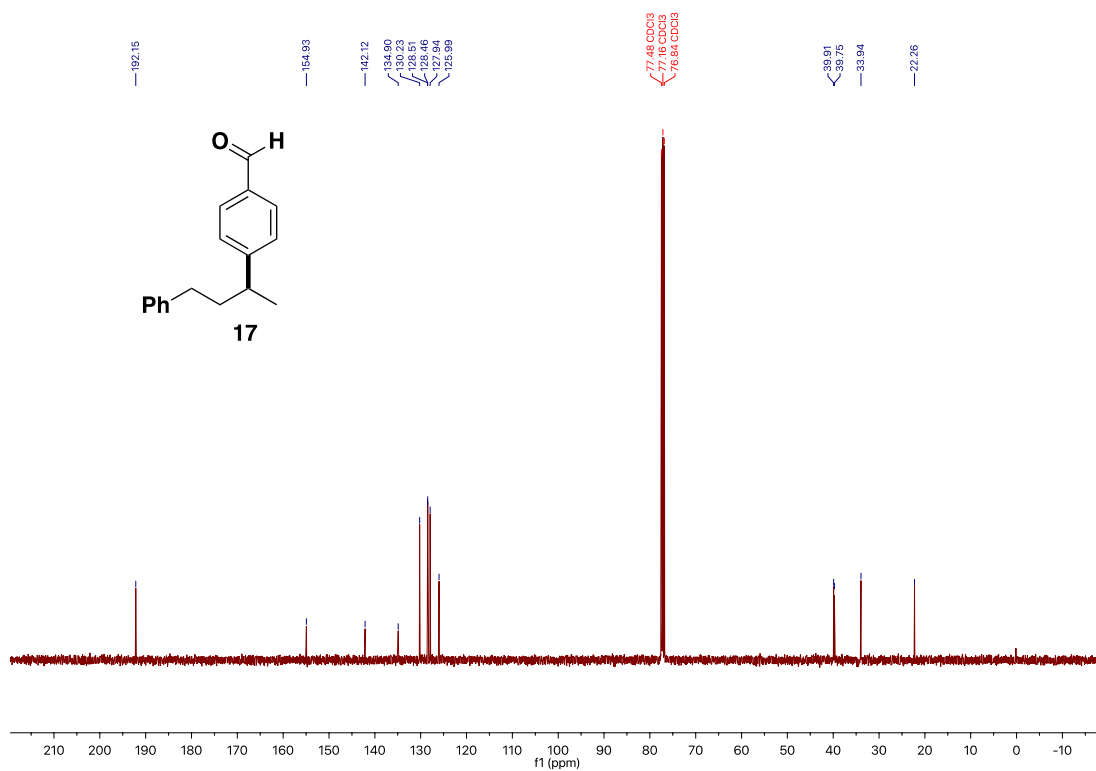
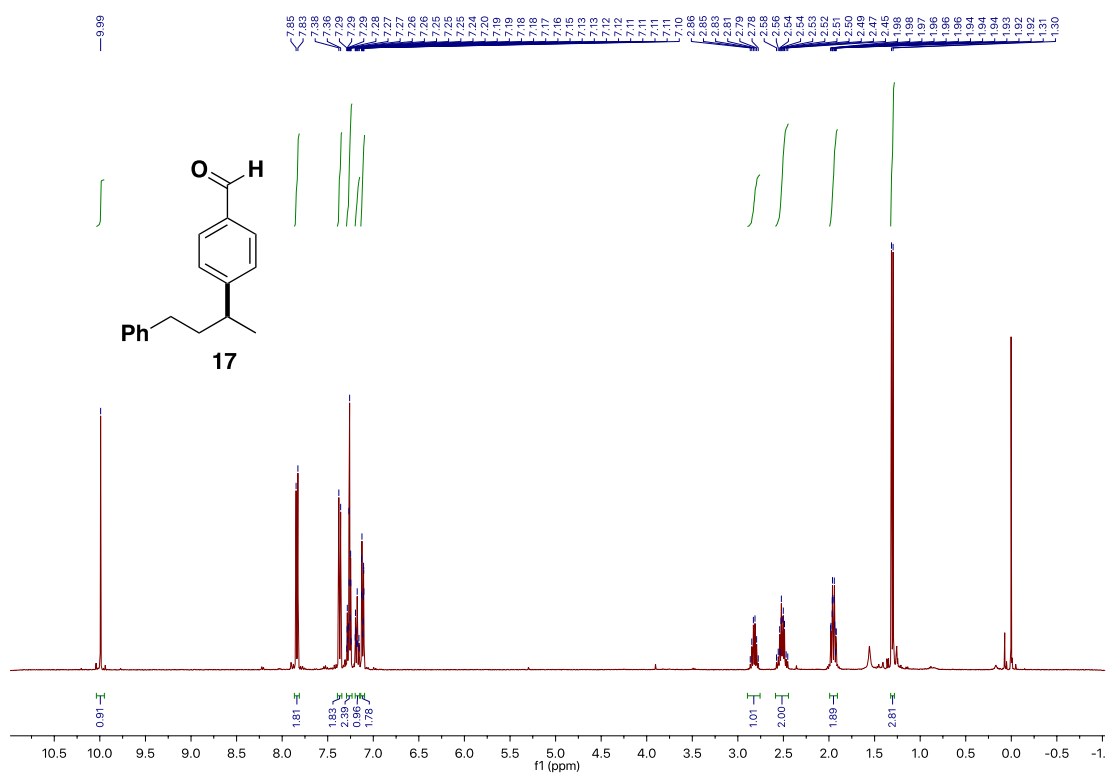
Chapter 3



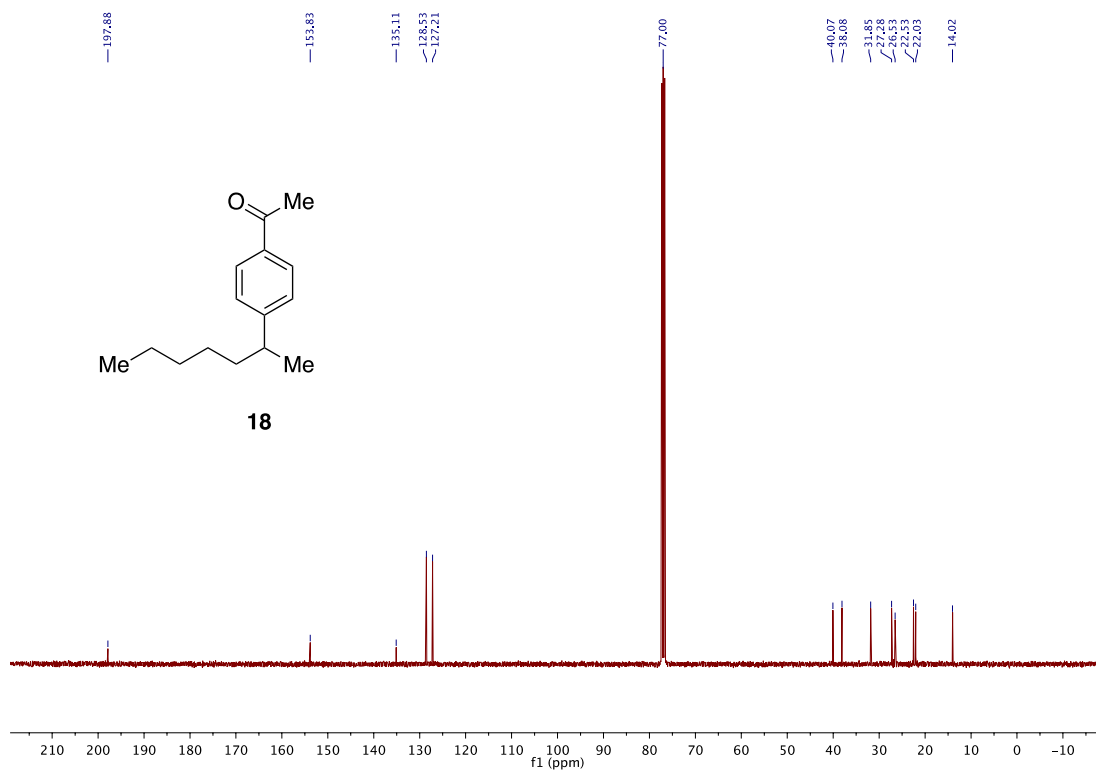
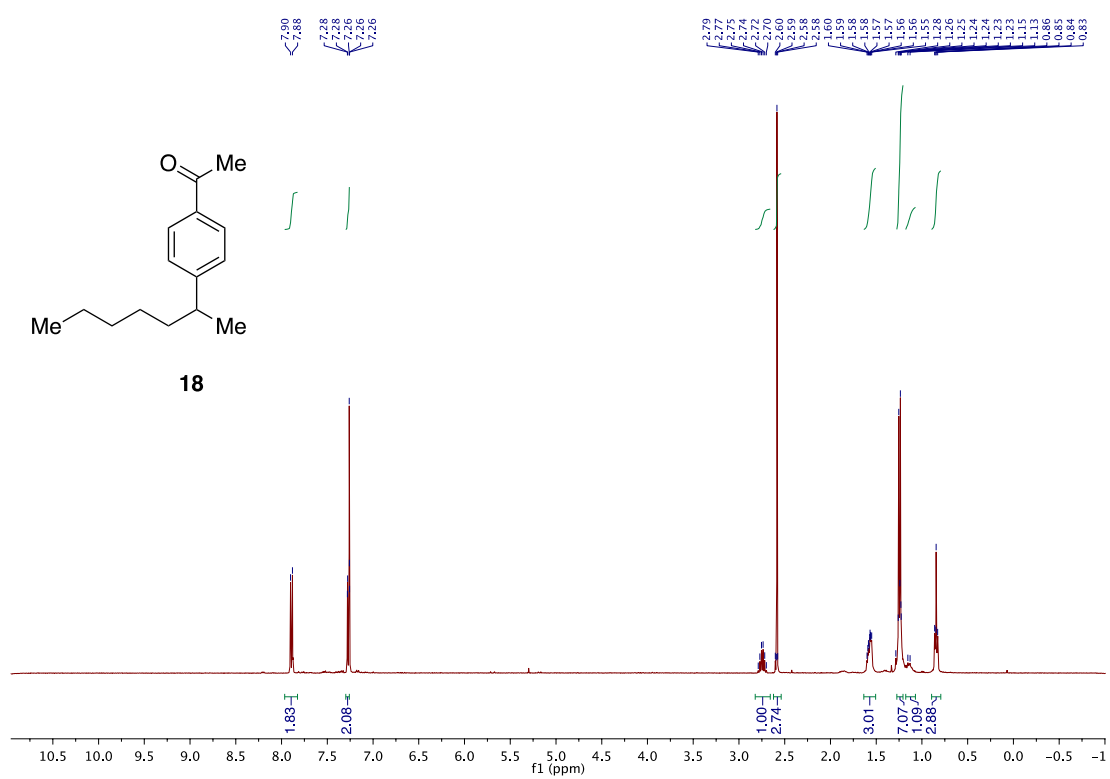
Deaminative Arylation at sp^3 Carbon Centers



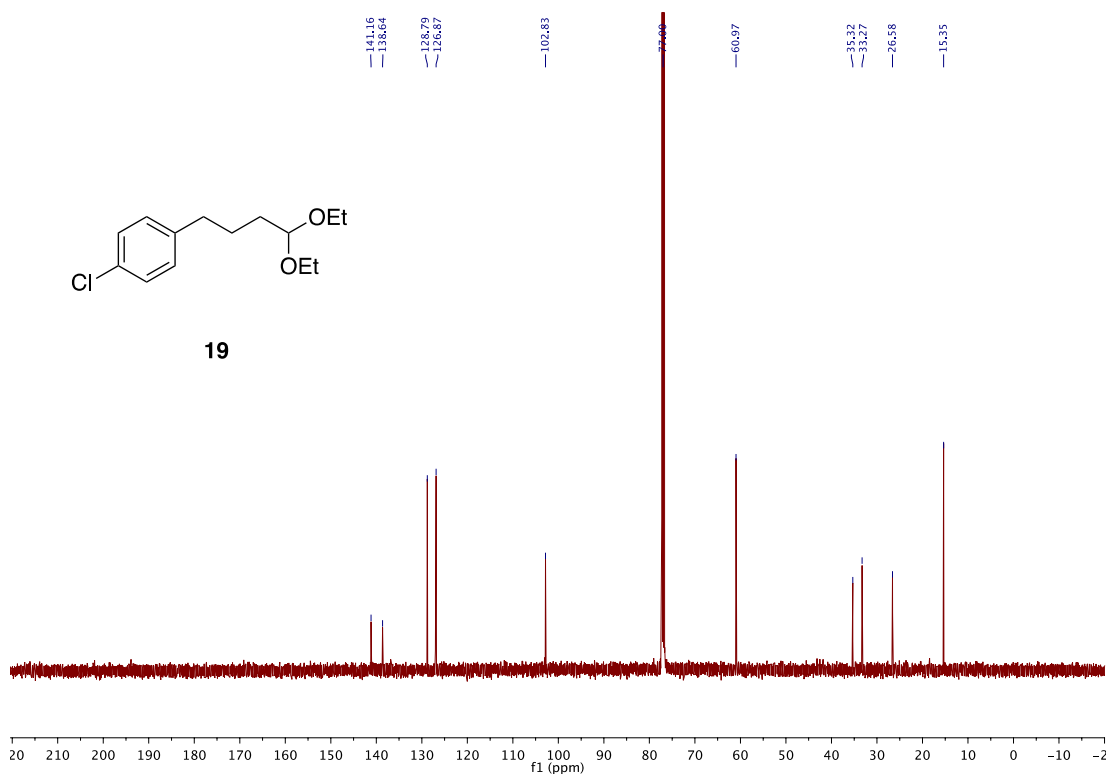
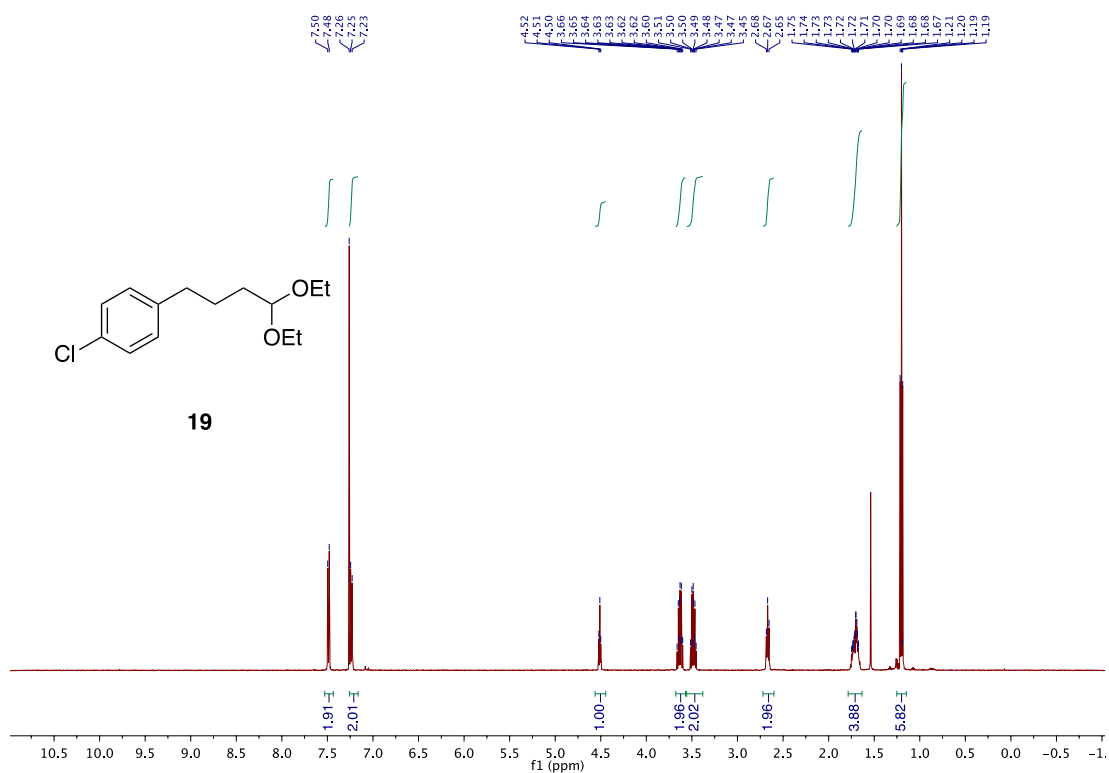
Chapter 3



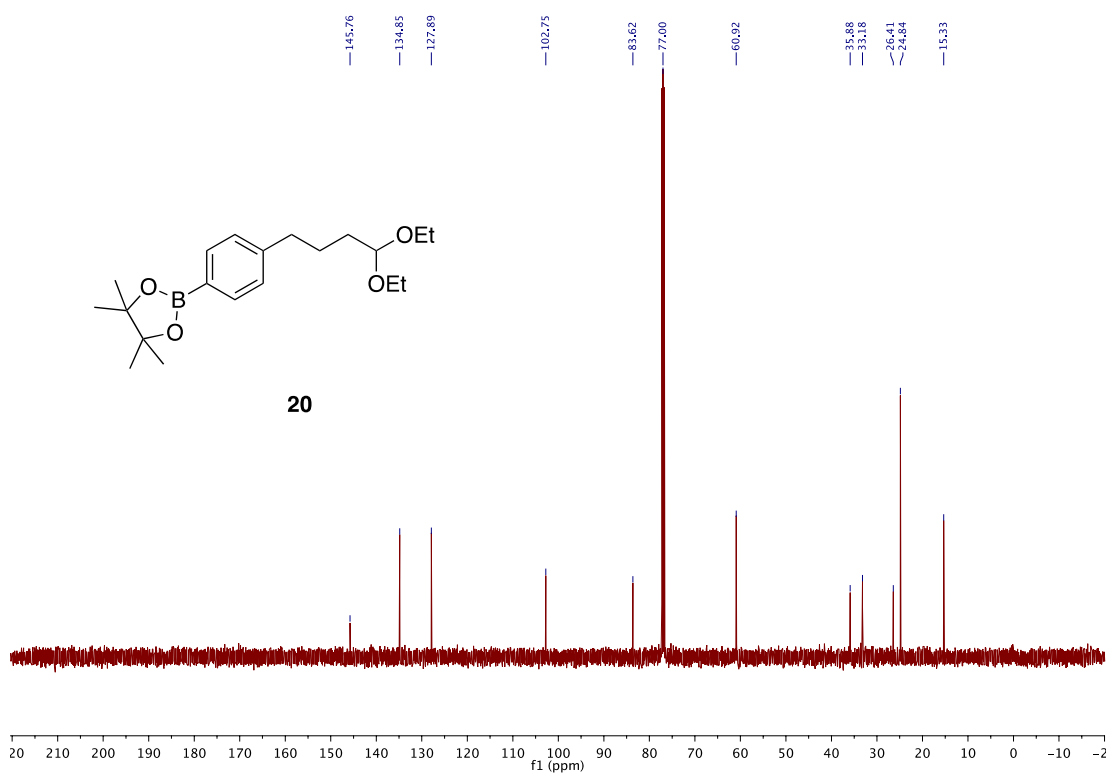
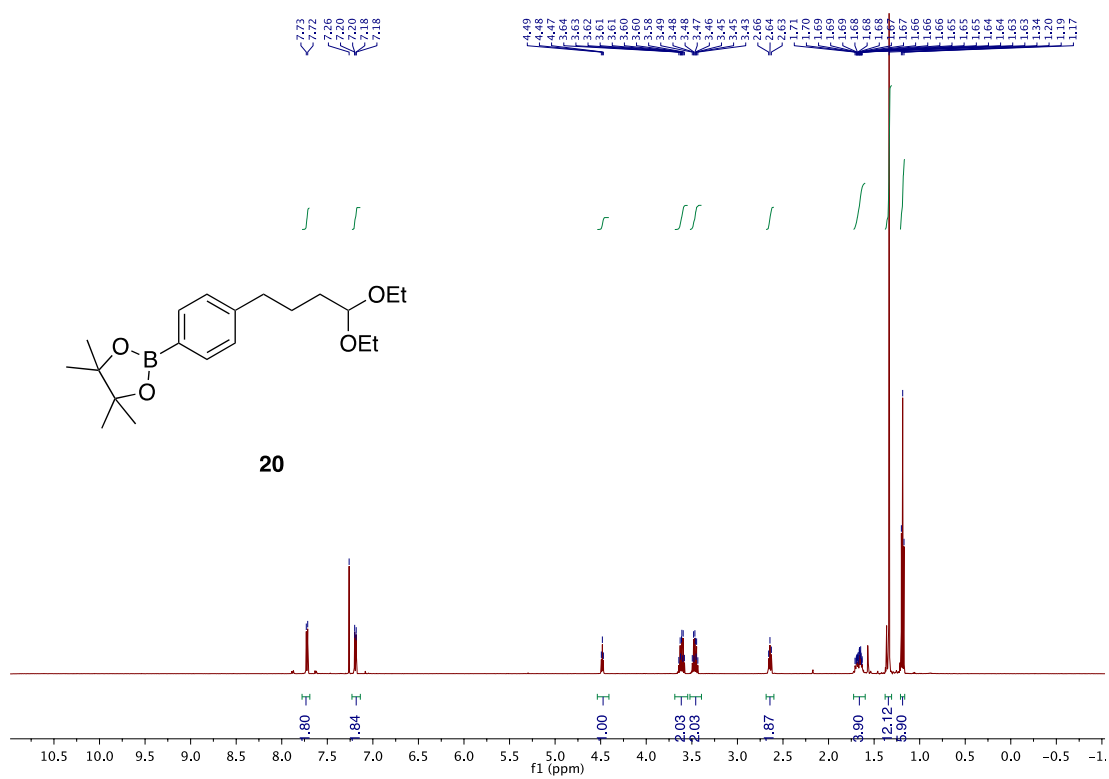
Deaminative Arylation at sp^3 Carbon Centers



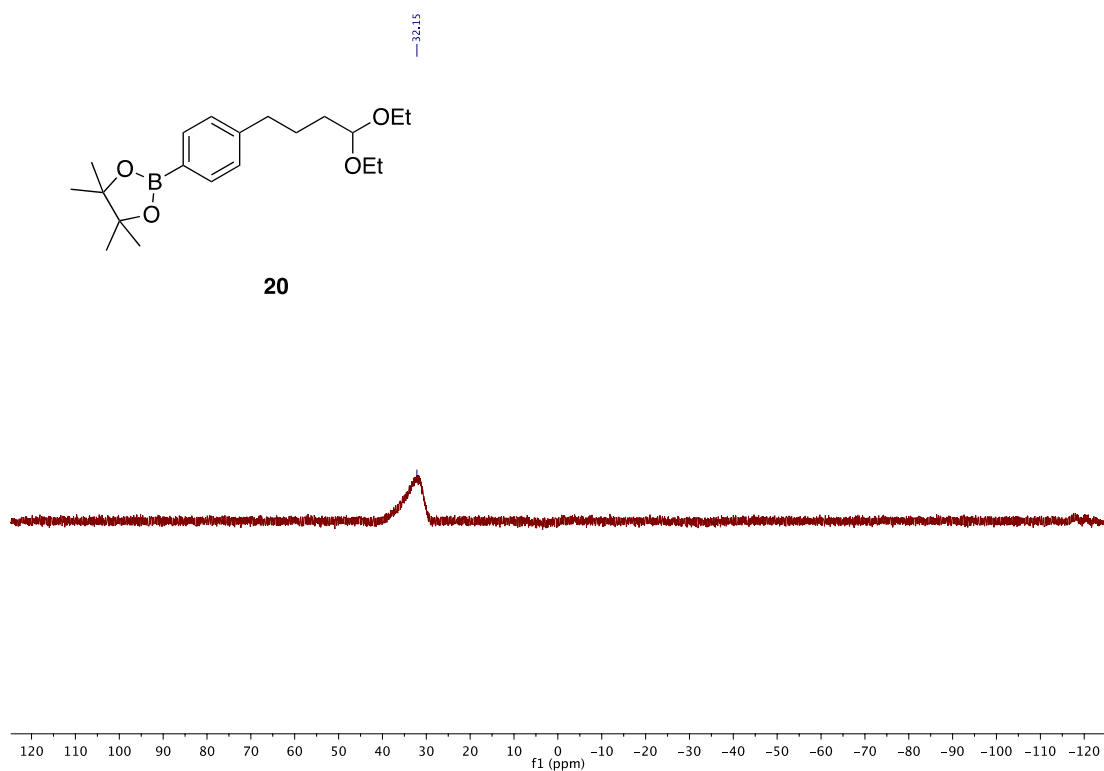
Chapter 3



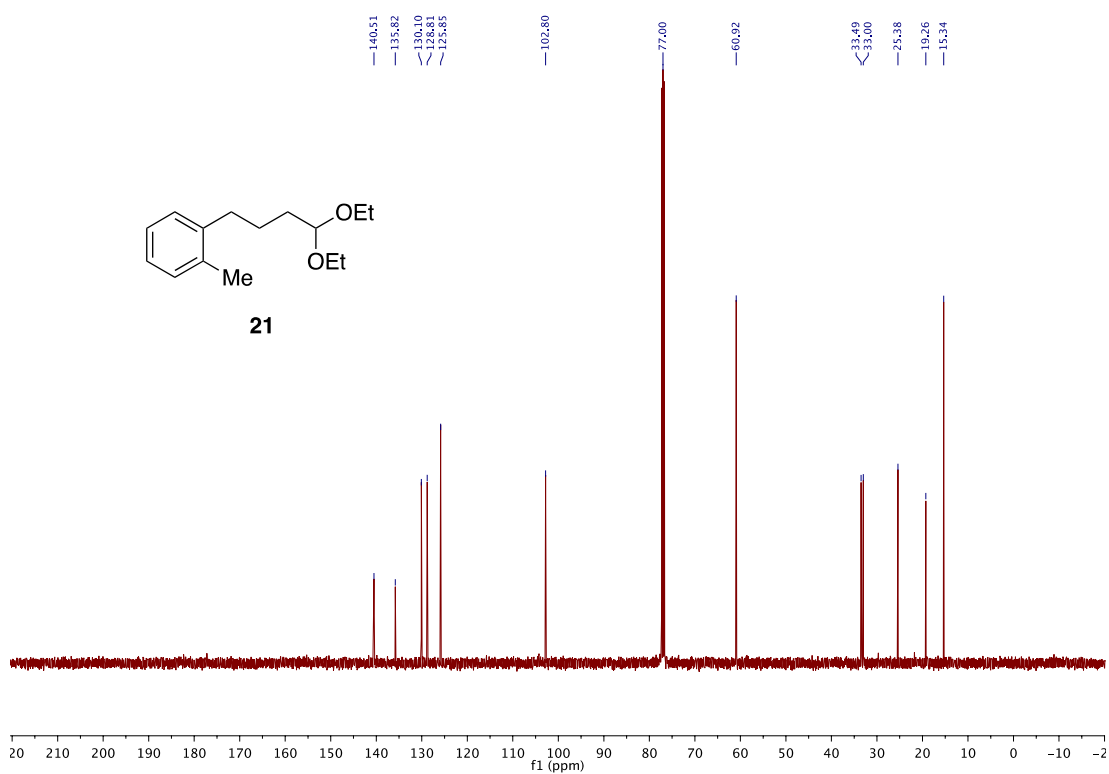
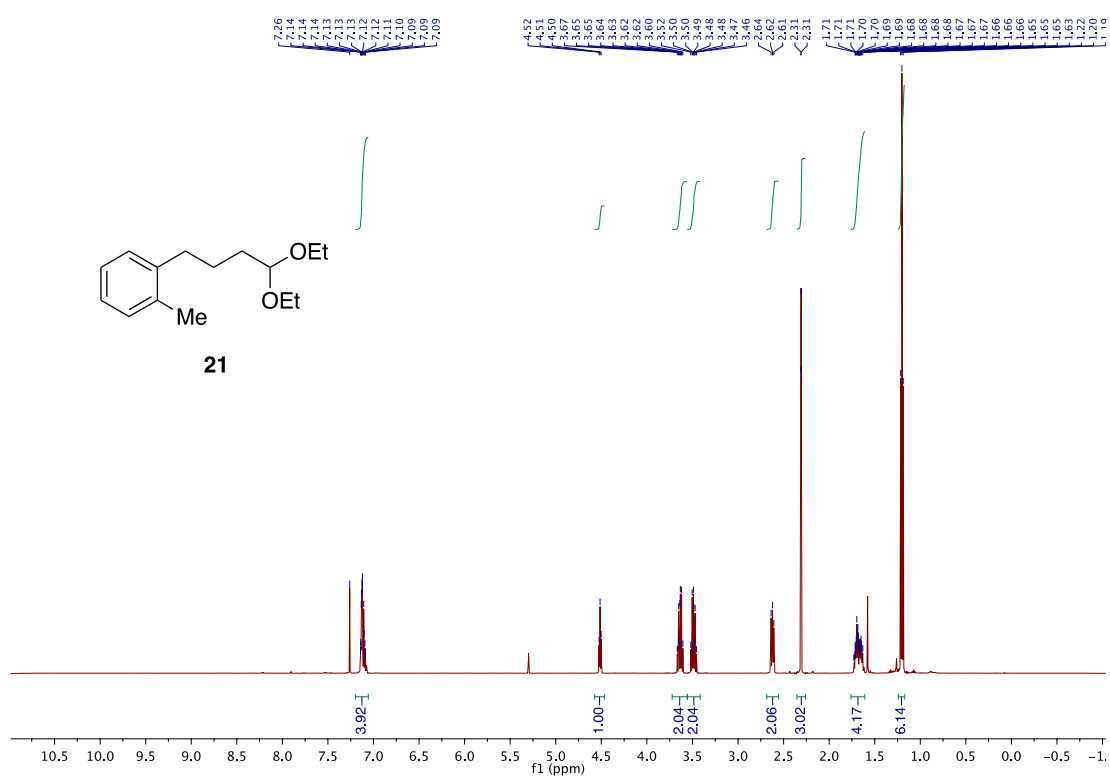
Deaminative Arylation at sp^3 Carbon Centers



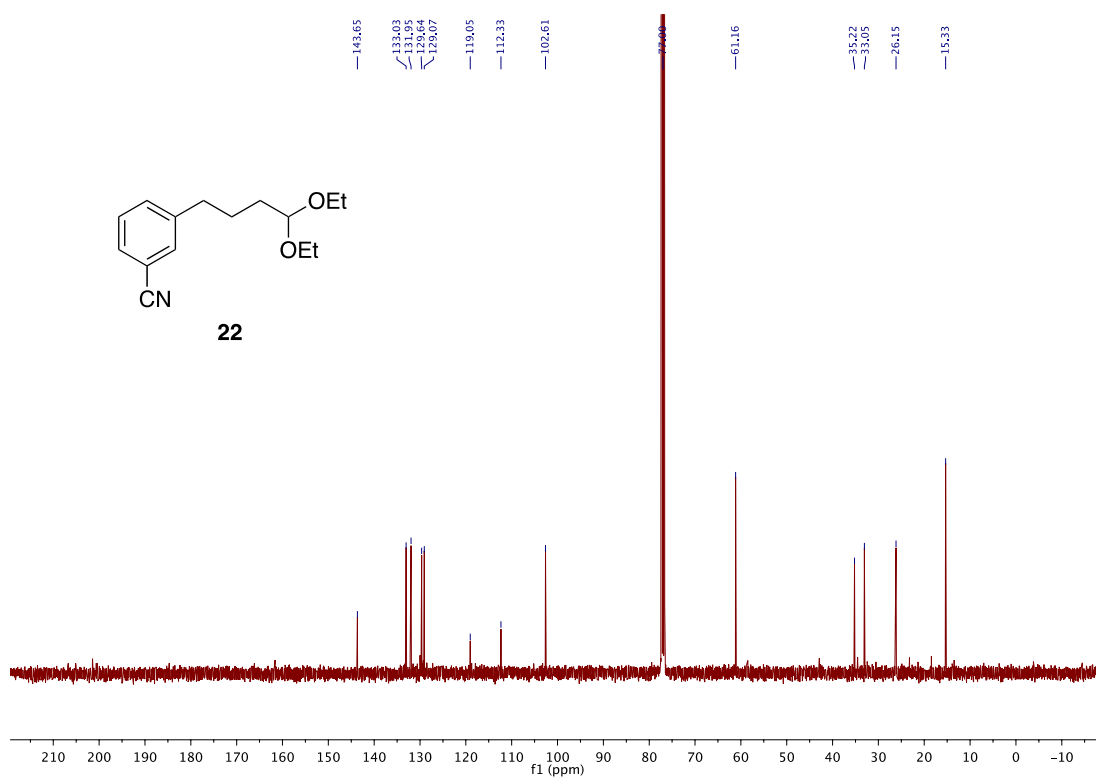
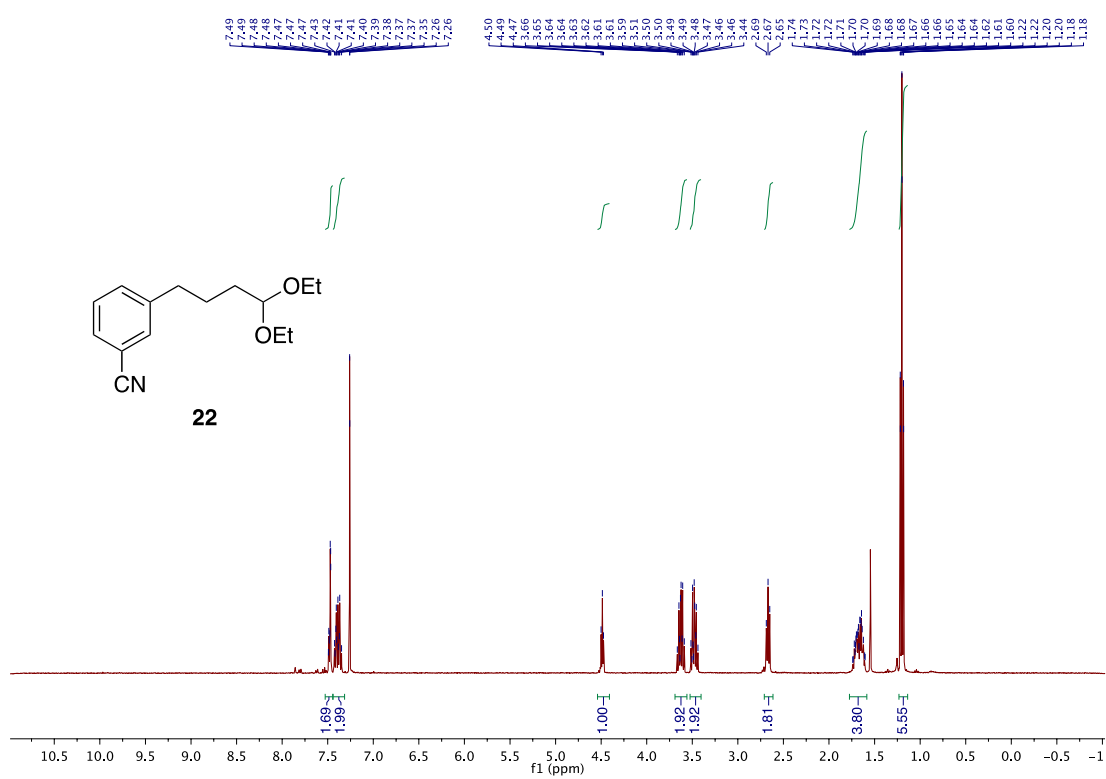
Chapter 3



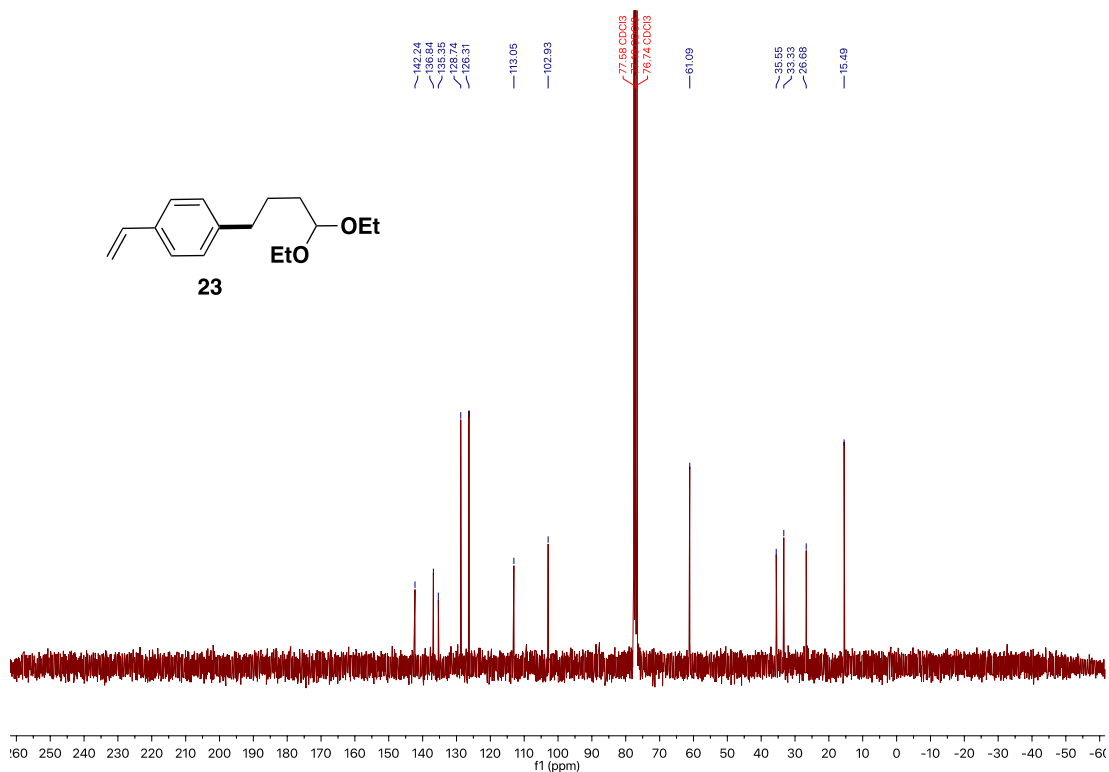
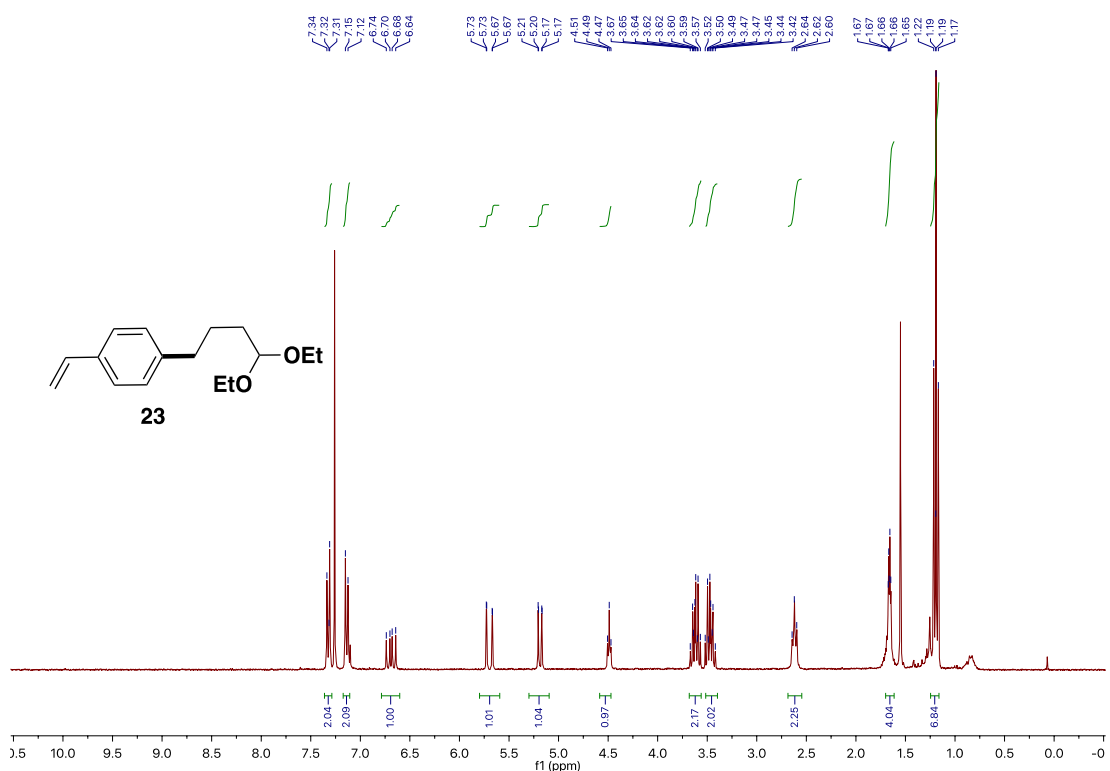
Deaminative Arylation at sp^3 Carbon Centers



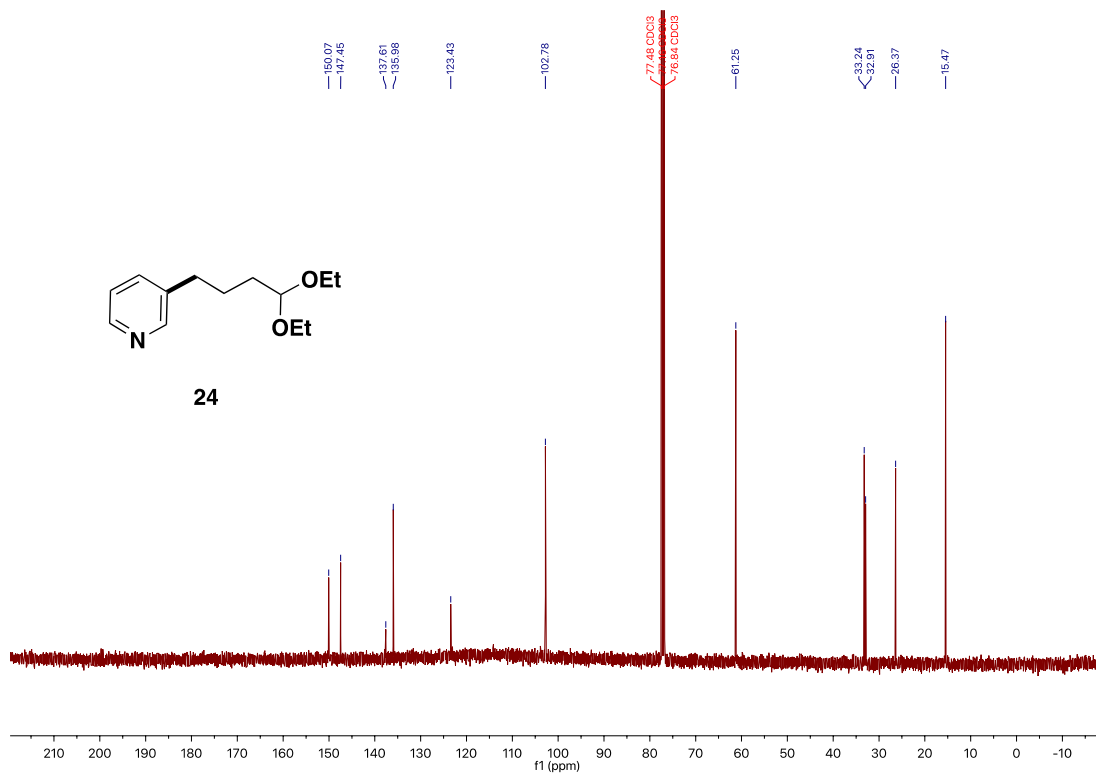
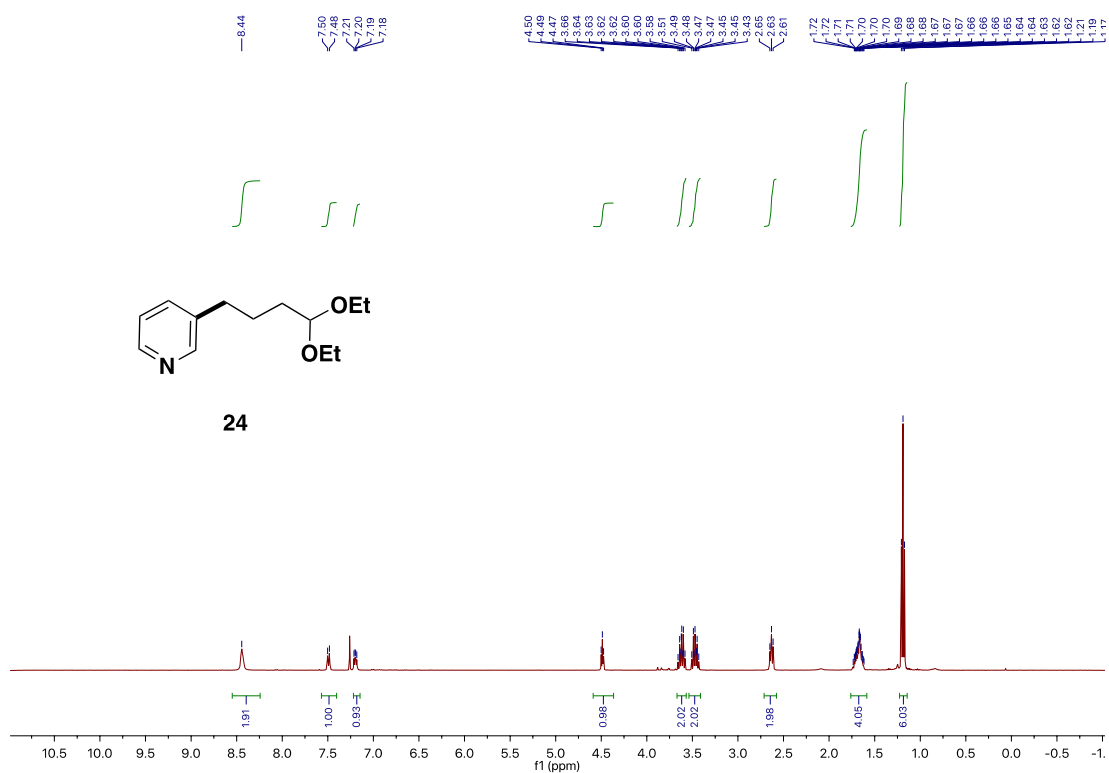
Chapter 3



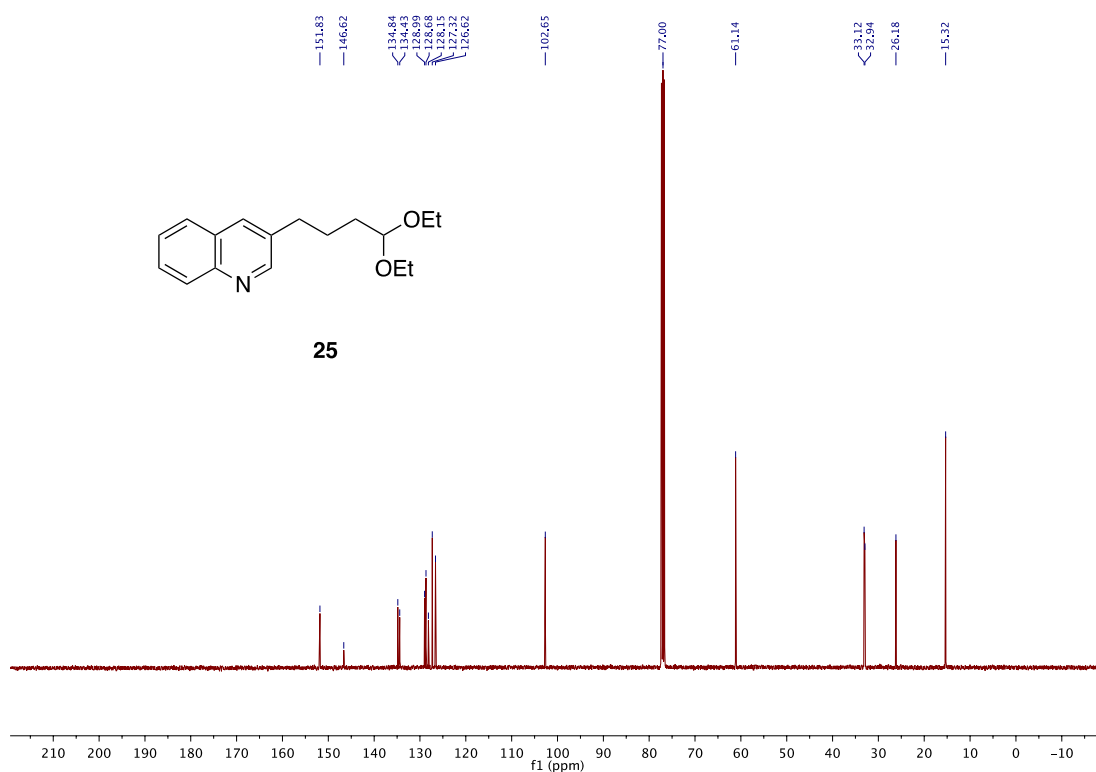
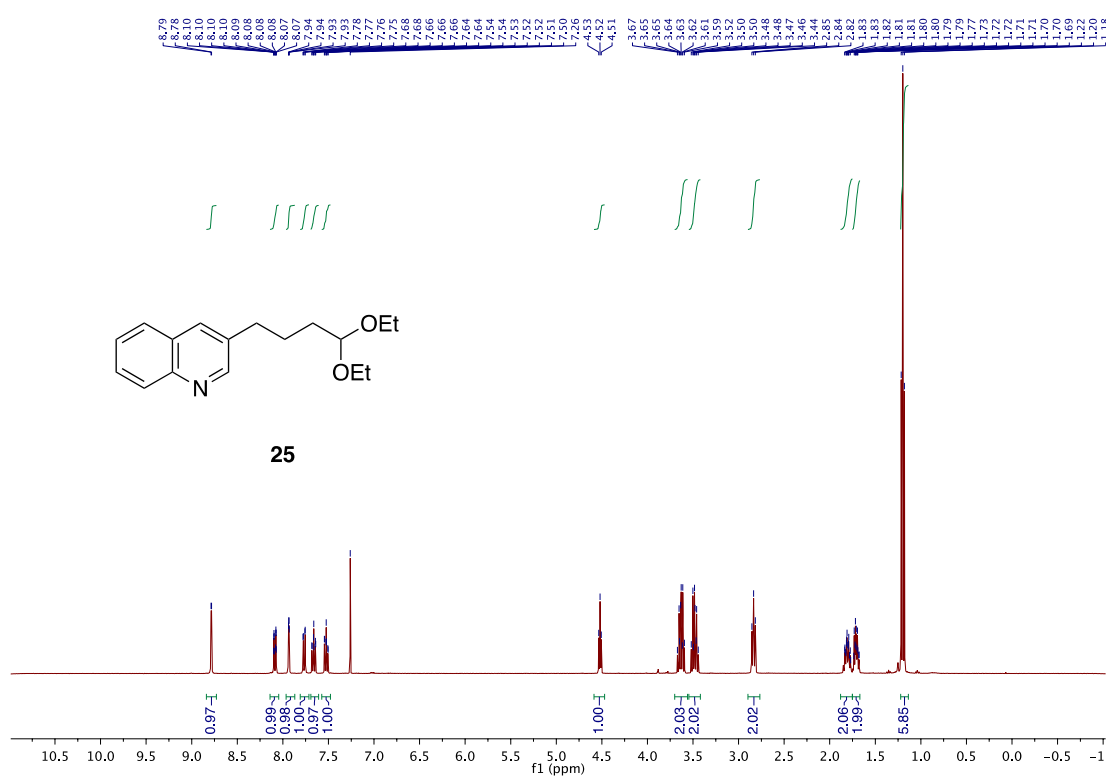
Deaminative Arylation at sp^3 Carbon Centers



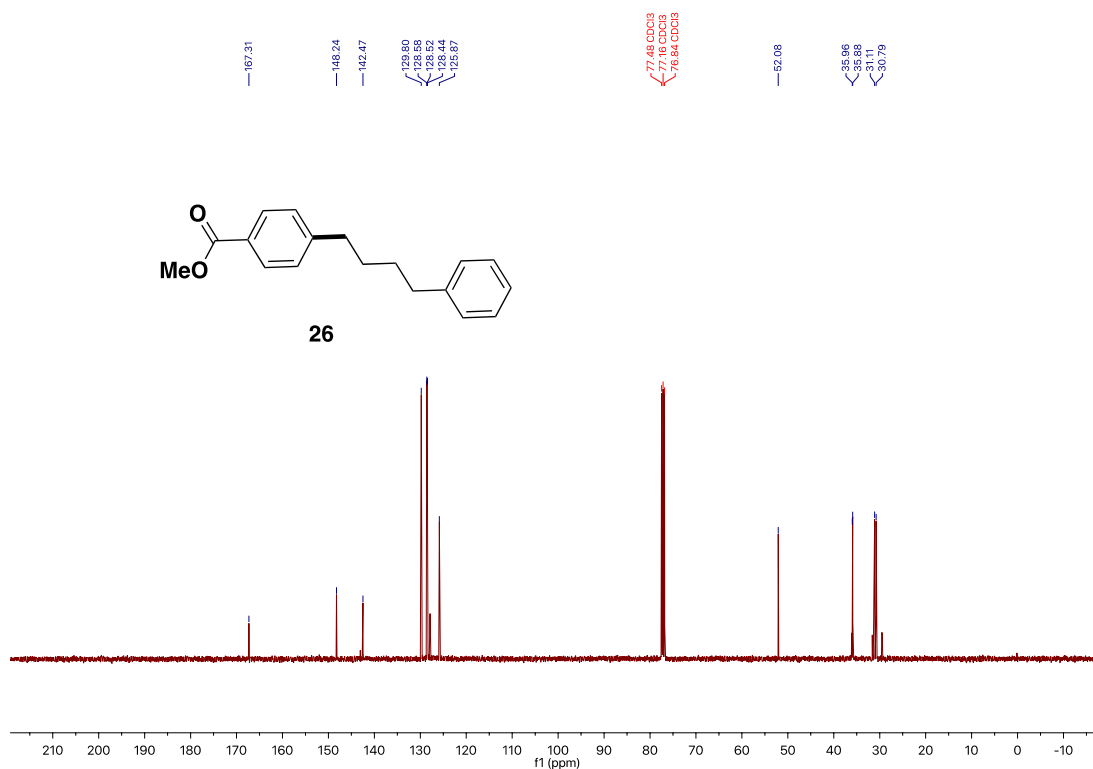
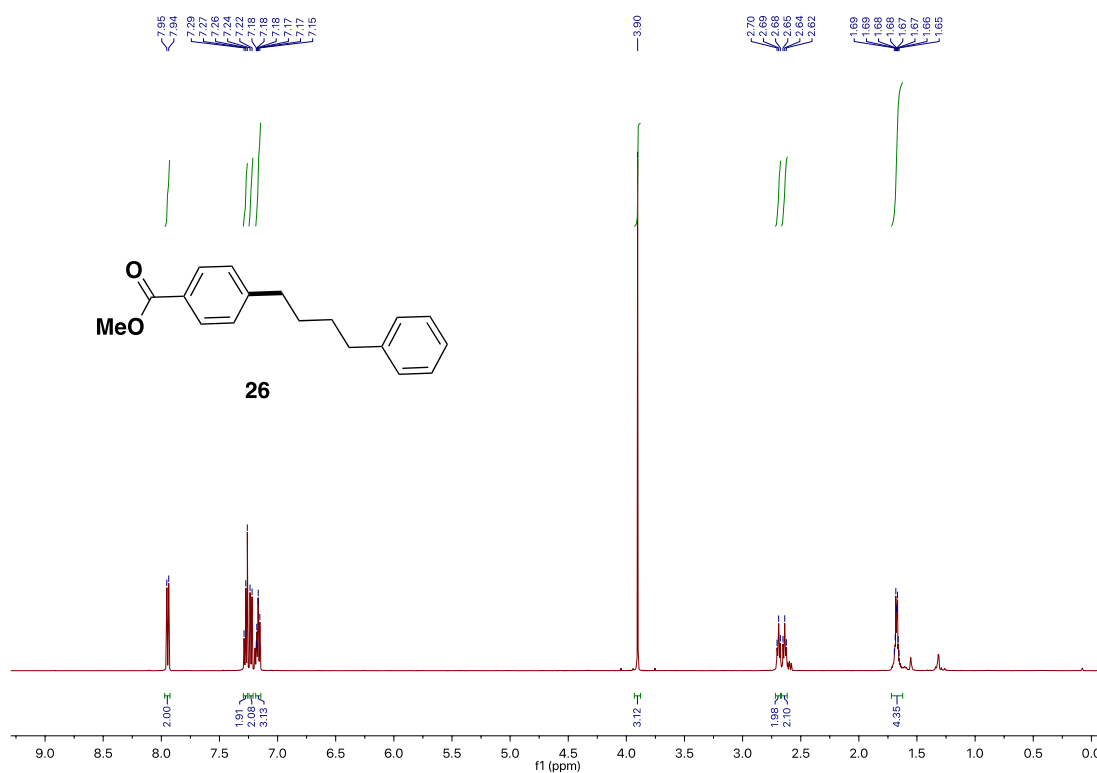
Chapter 3



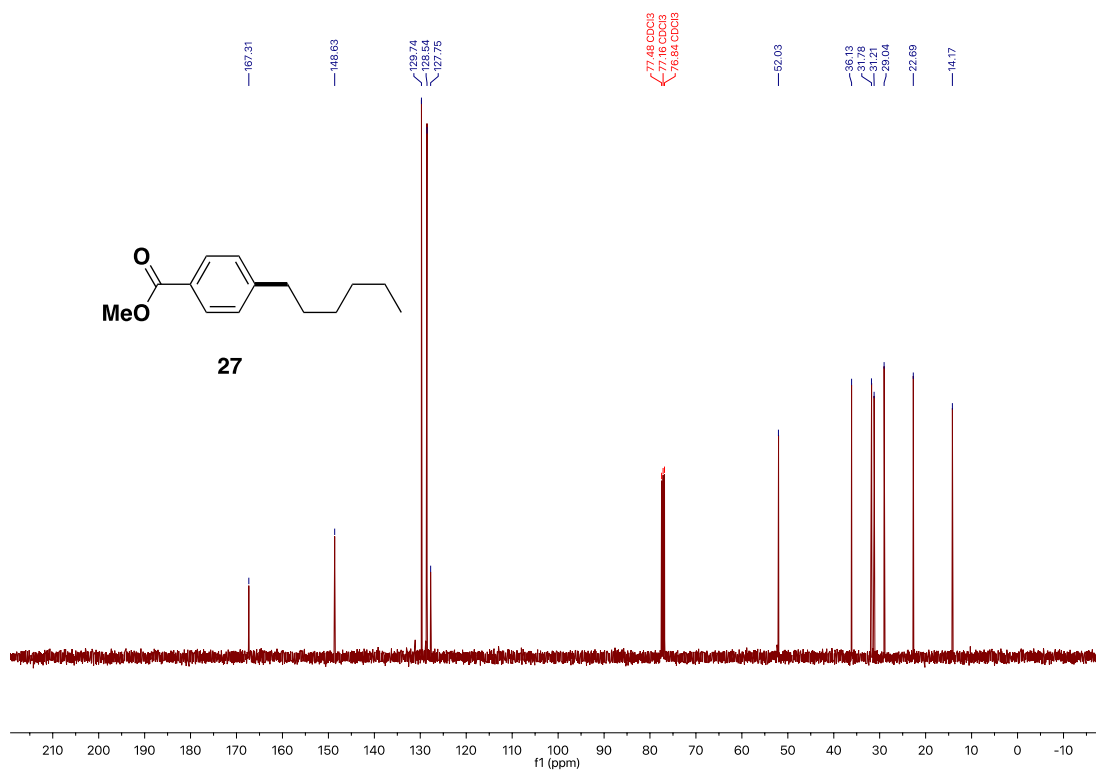
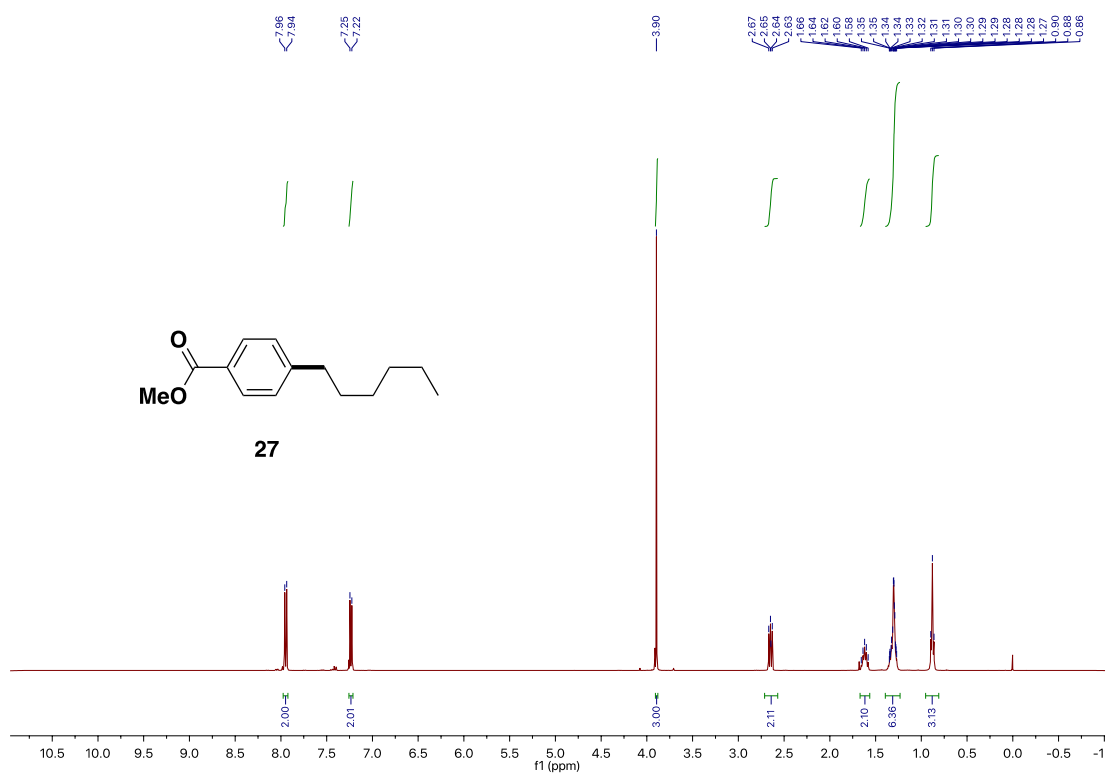
Deaminative Arylation at sp^3 Carbon Centers



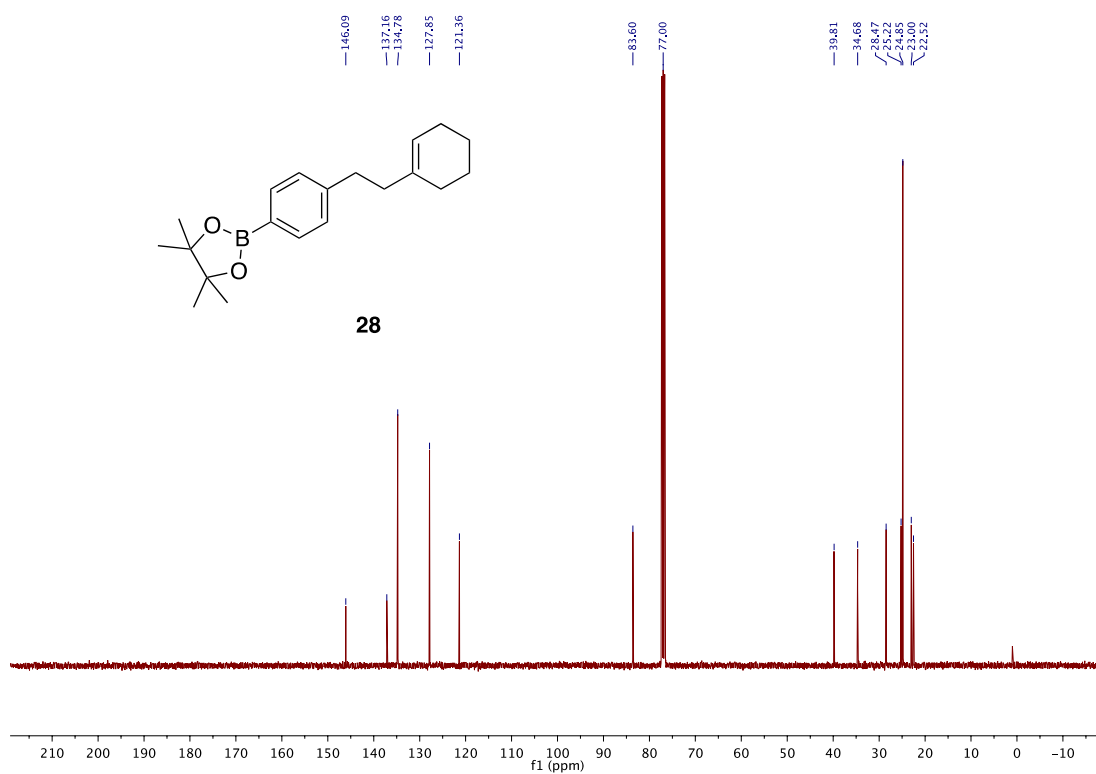
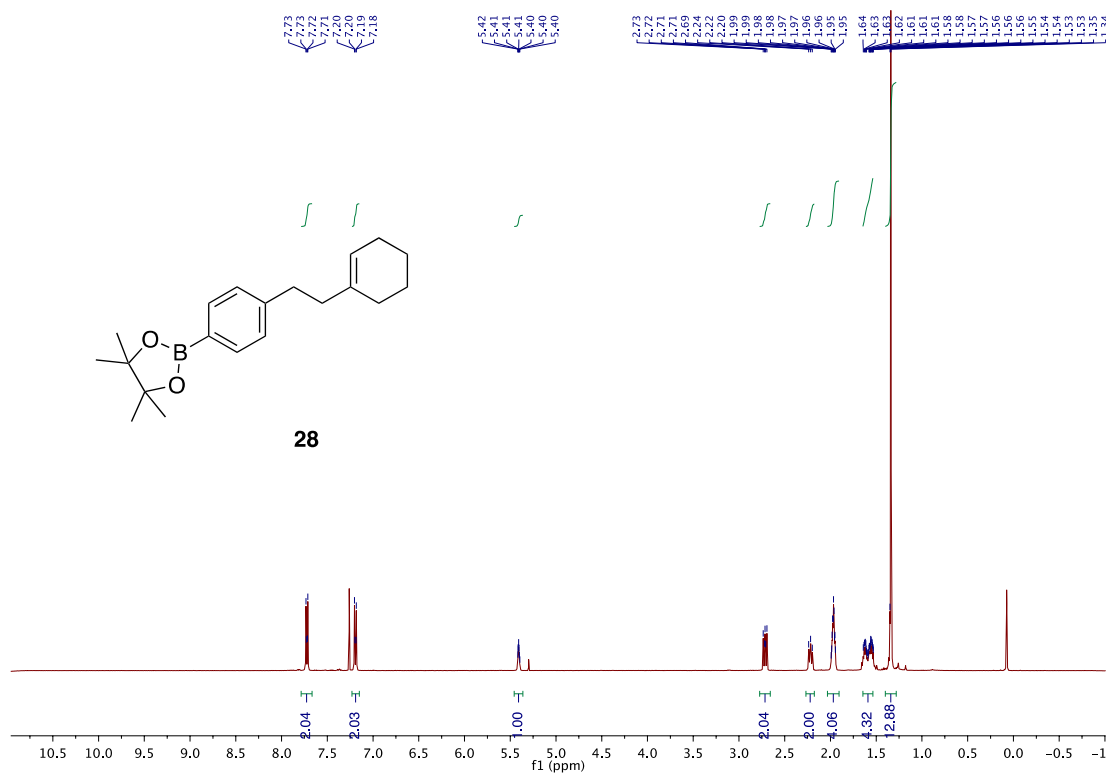
Chapter 3



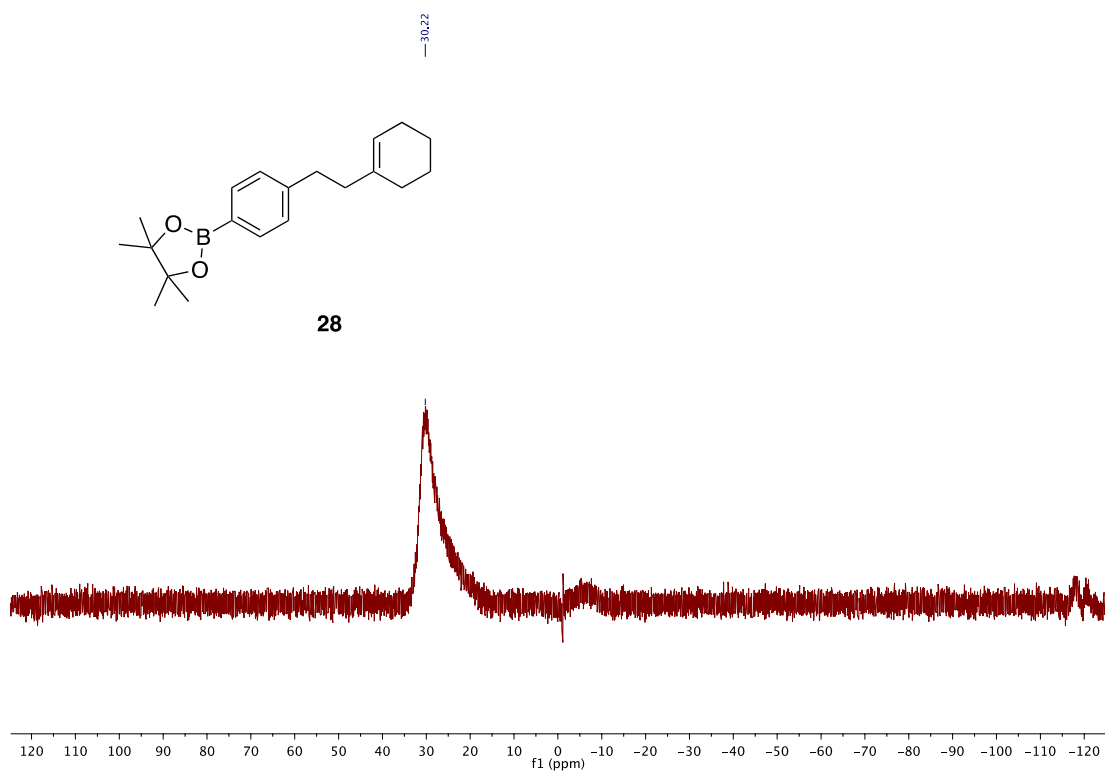
Deaminative Arylation at sp^3 Carbon Centers



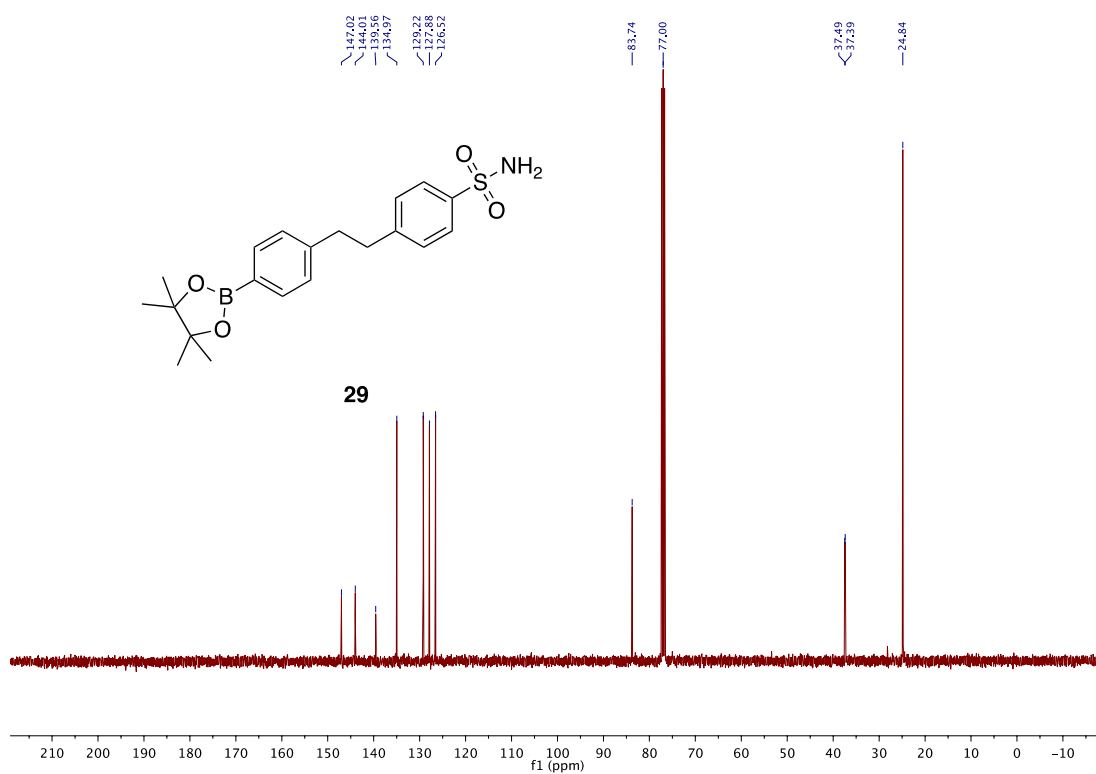
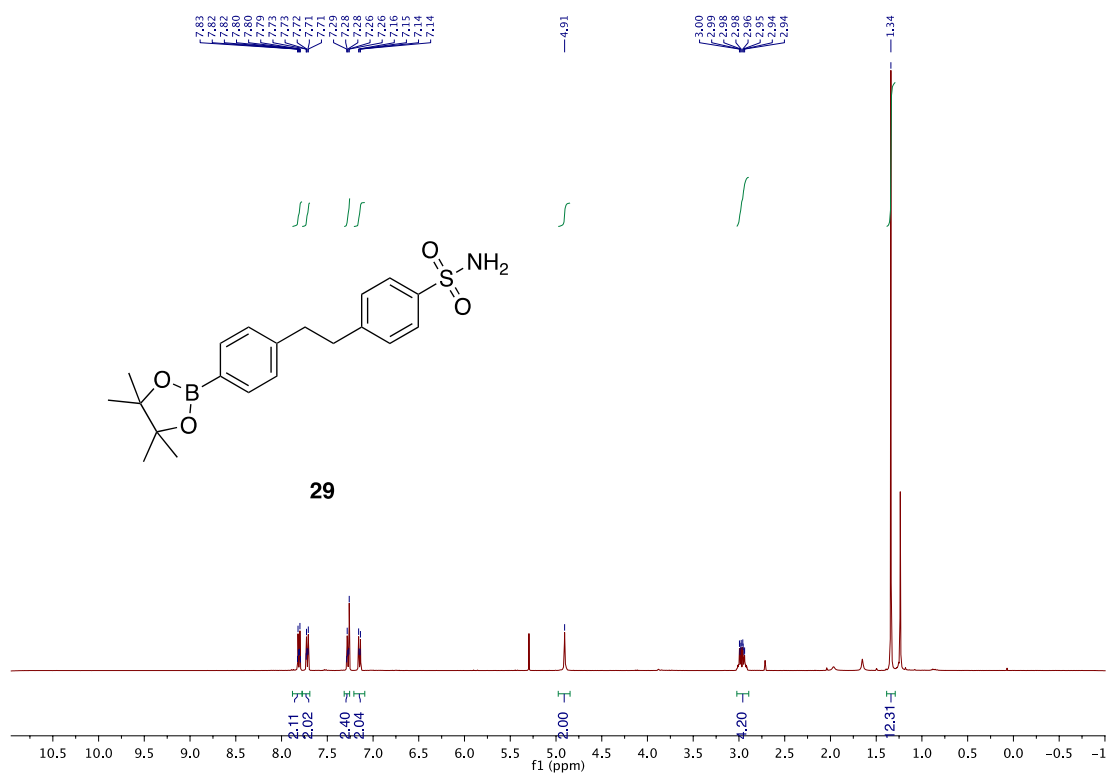
Chapter 3



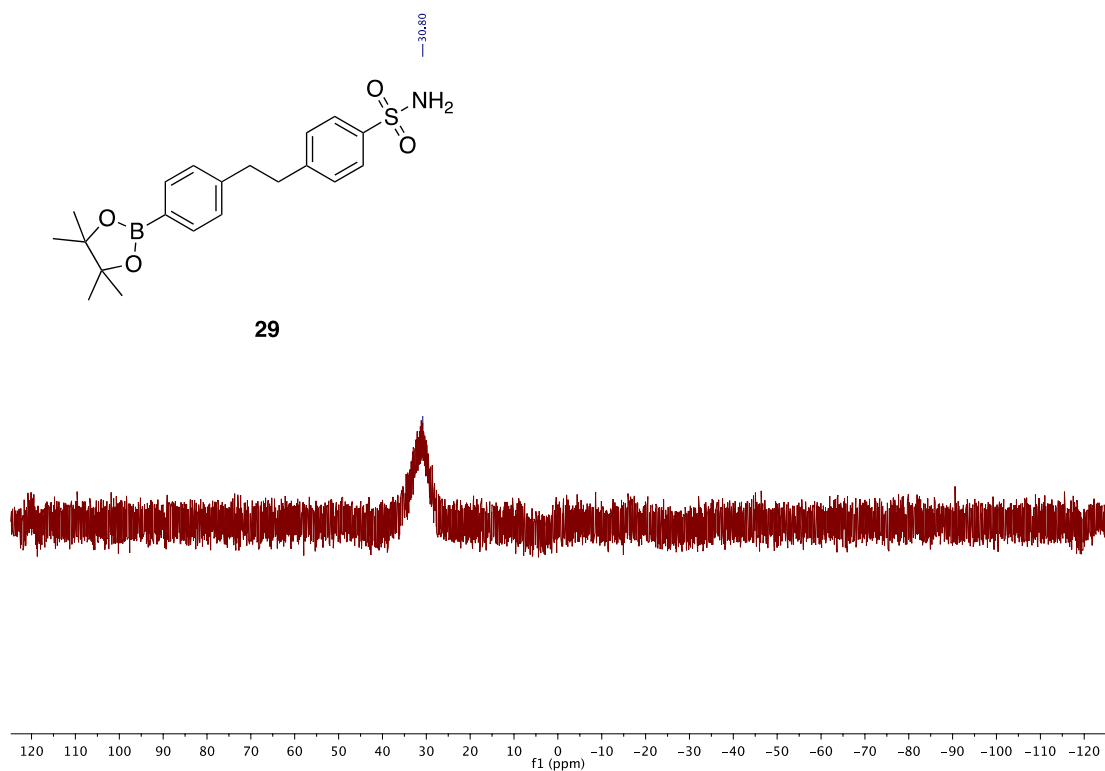
Deaminative Arylation at sp^3 Carbon Centers



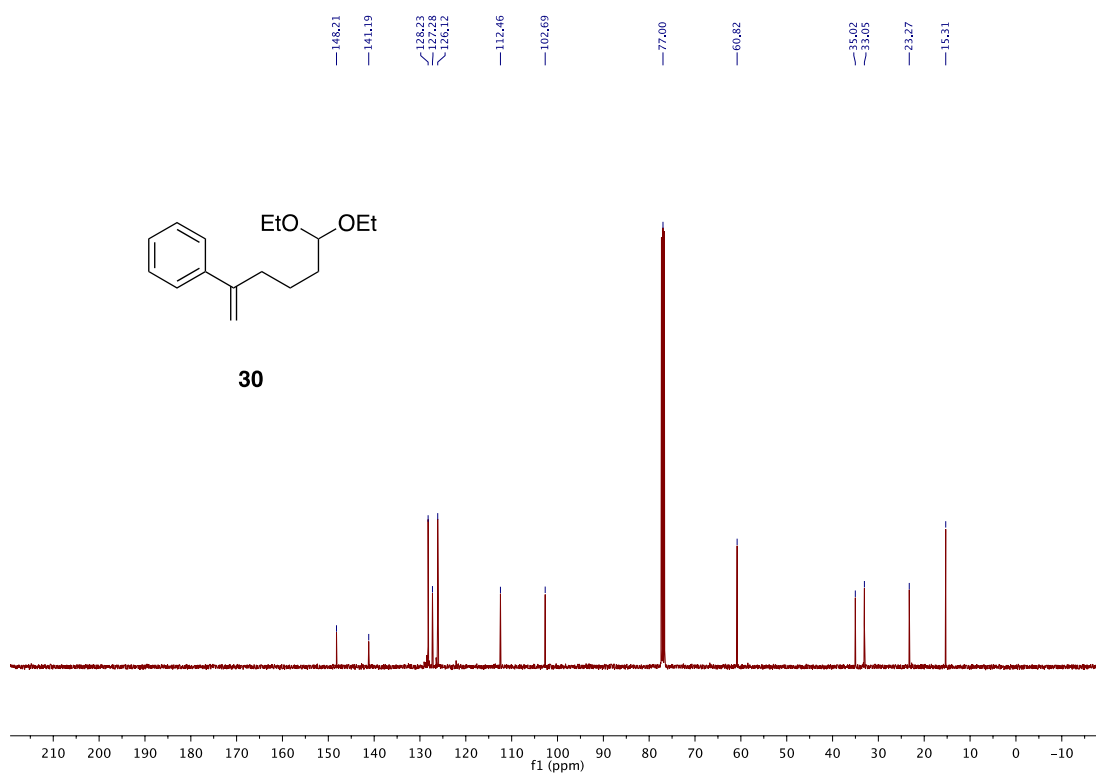
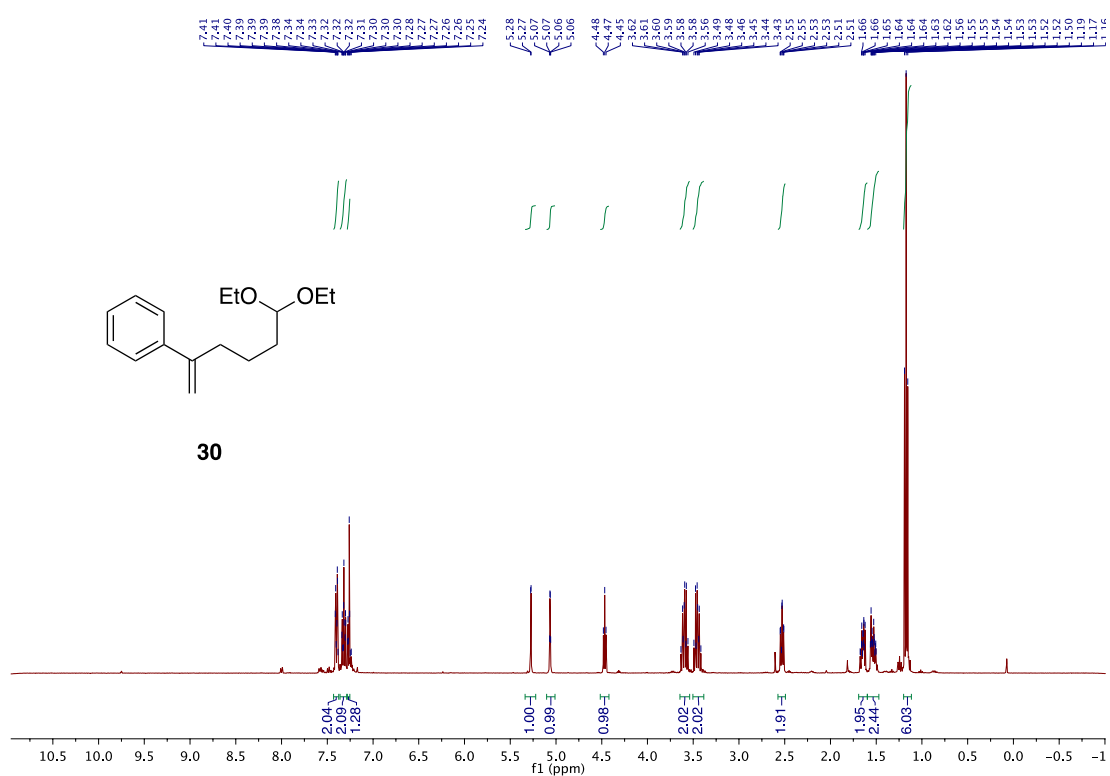
Chapter 3



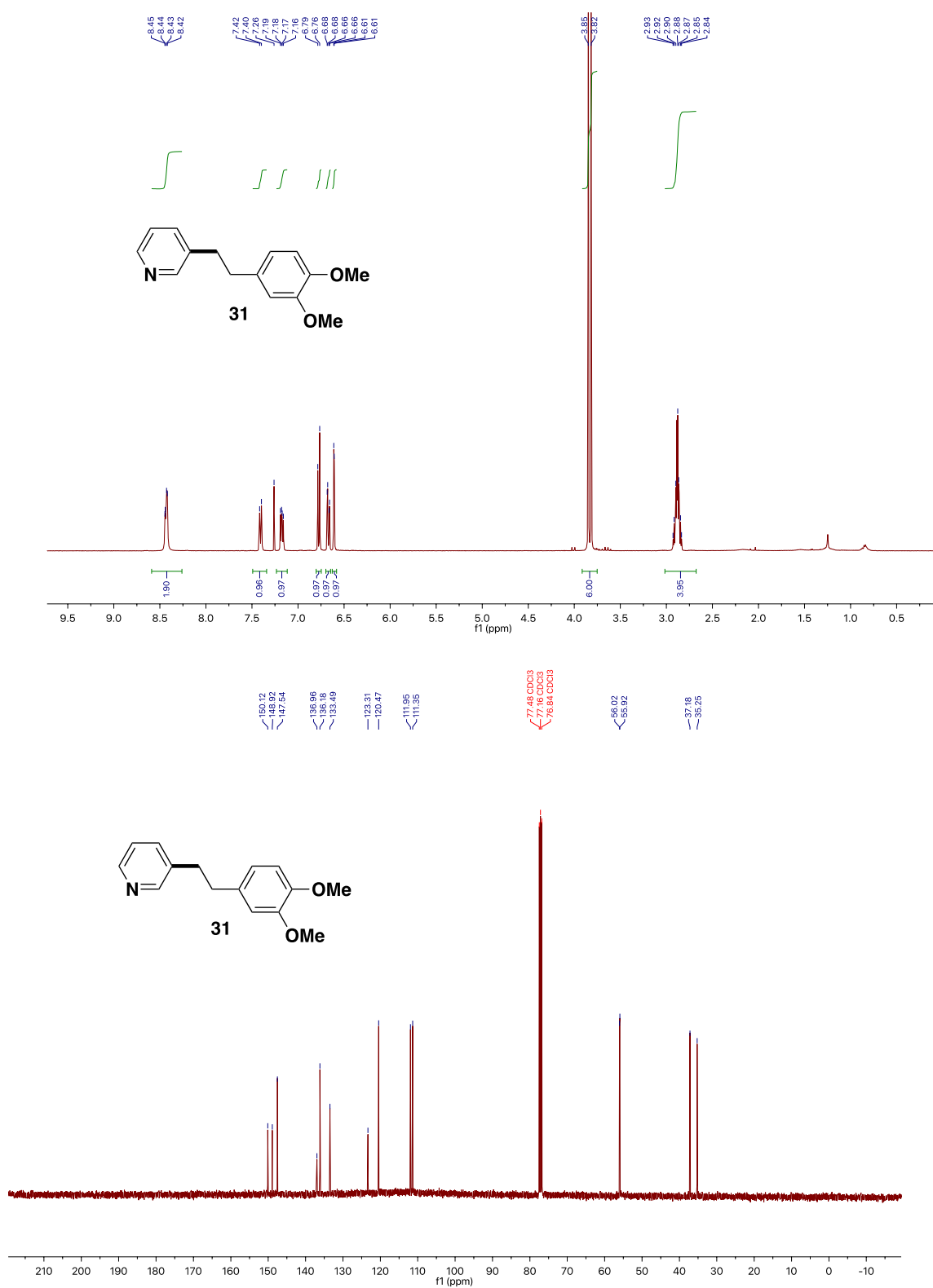
Deaminative Arylation at sp^3 Carbon Centers



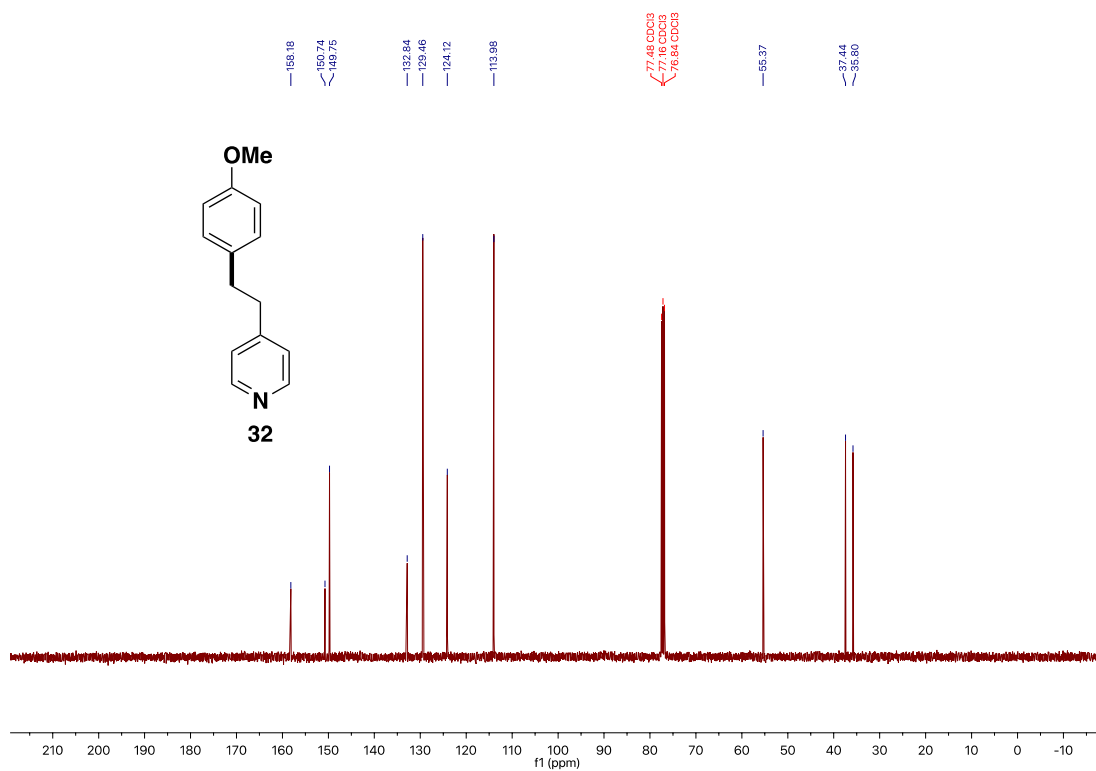
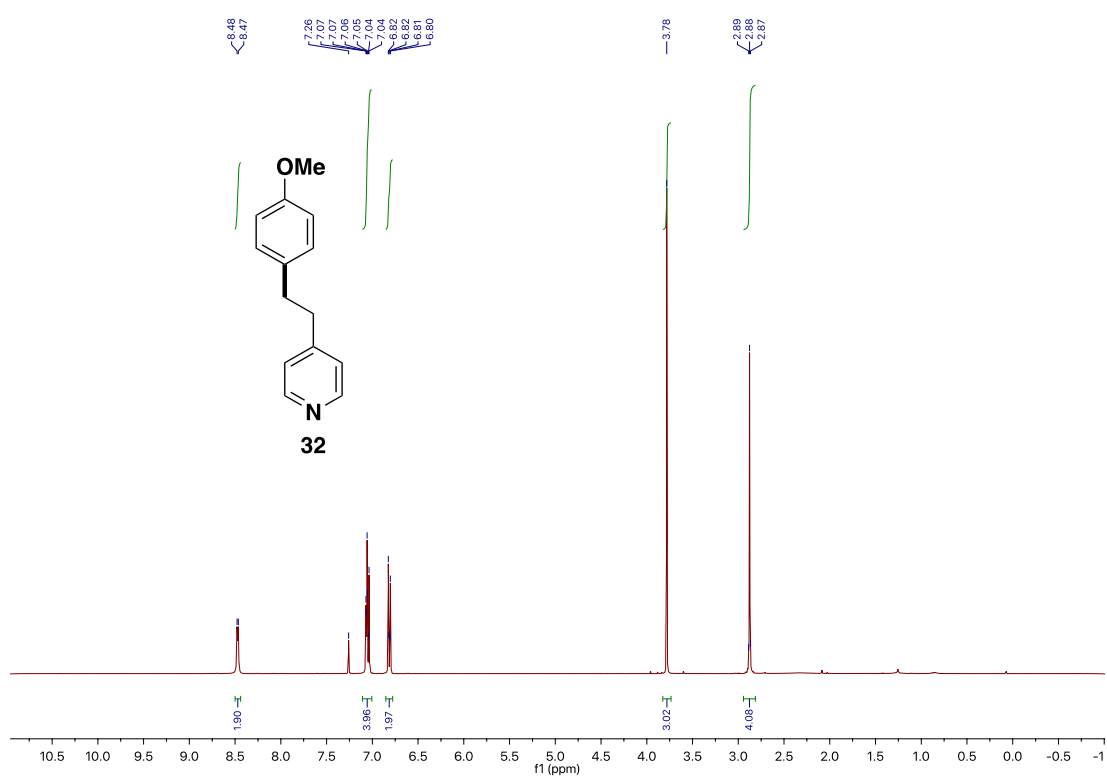
Chapter 3



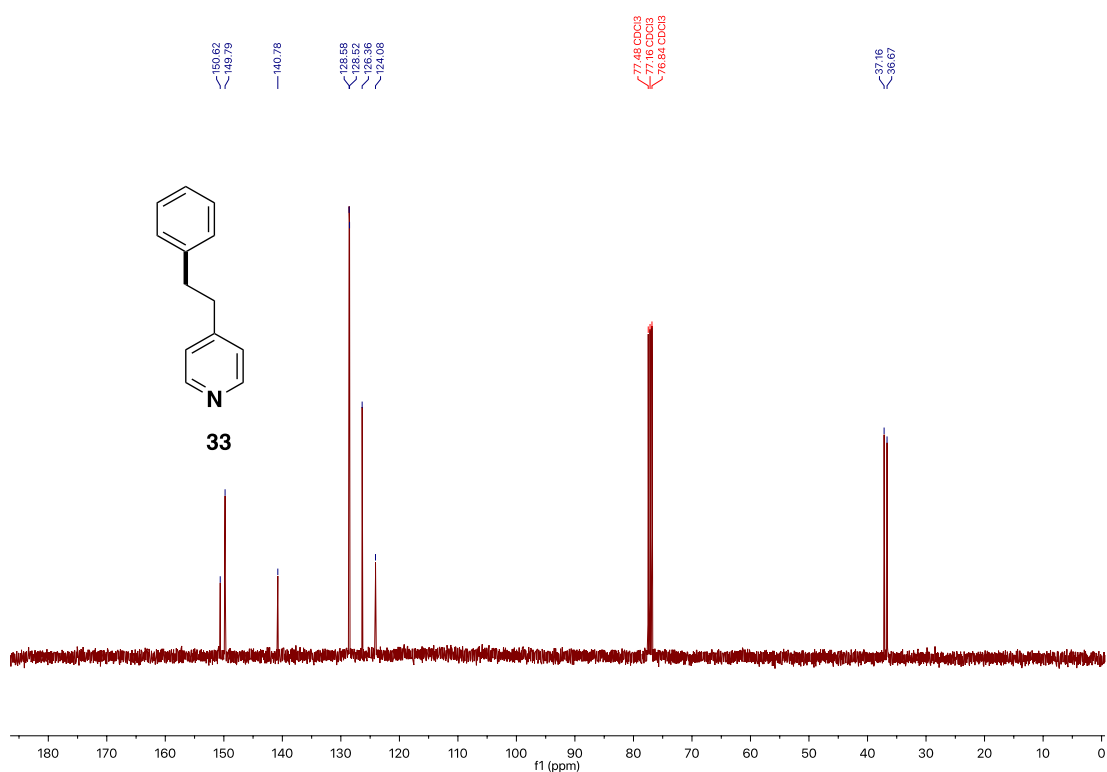
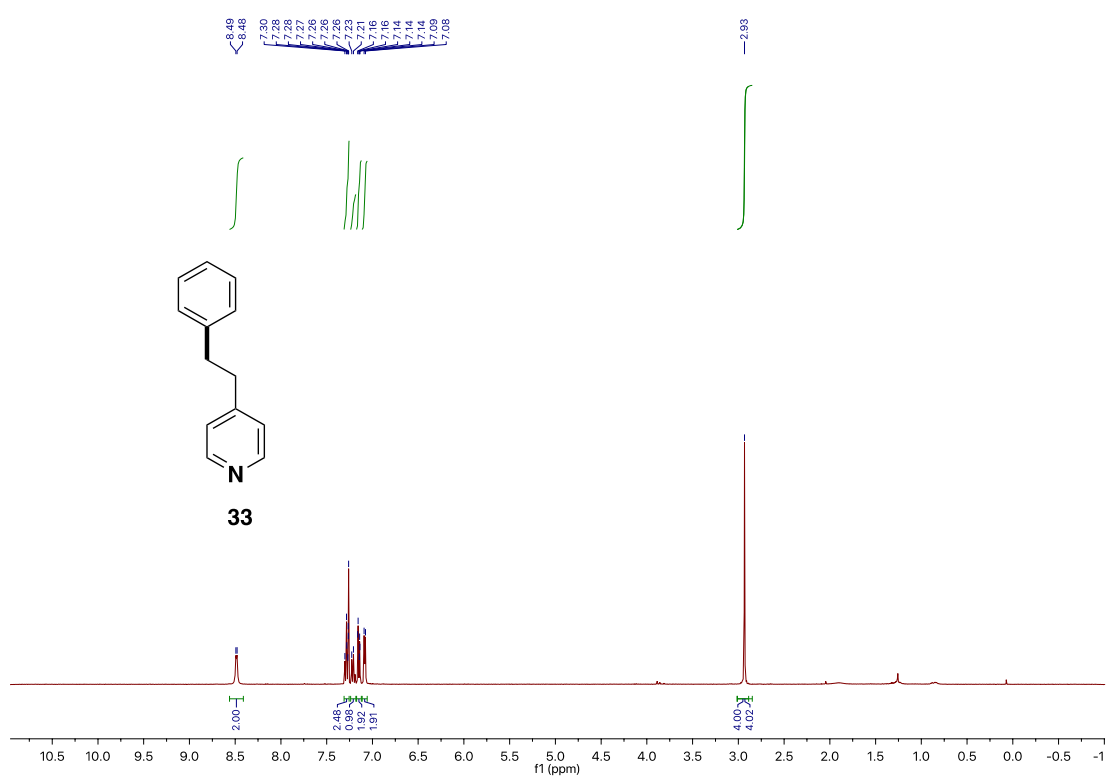
Deaminative Arylation at sp^3 Carbon Centers



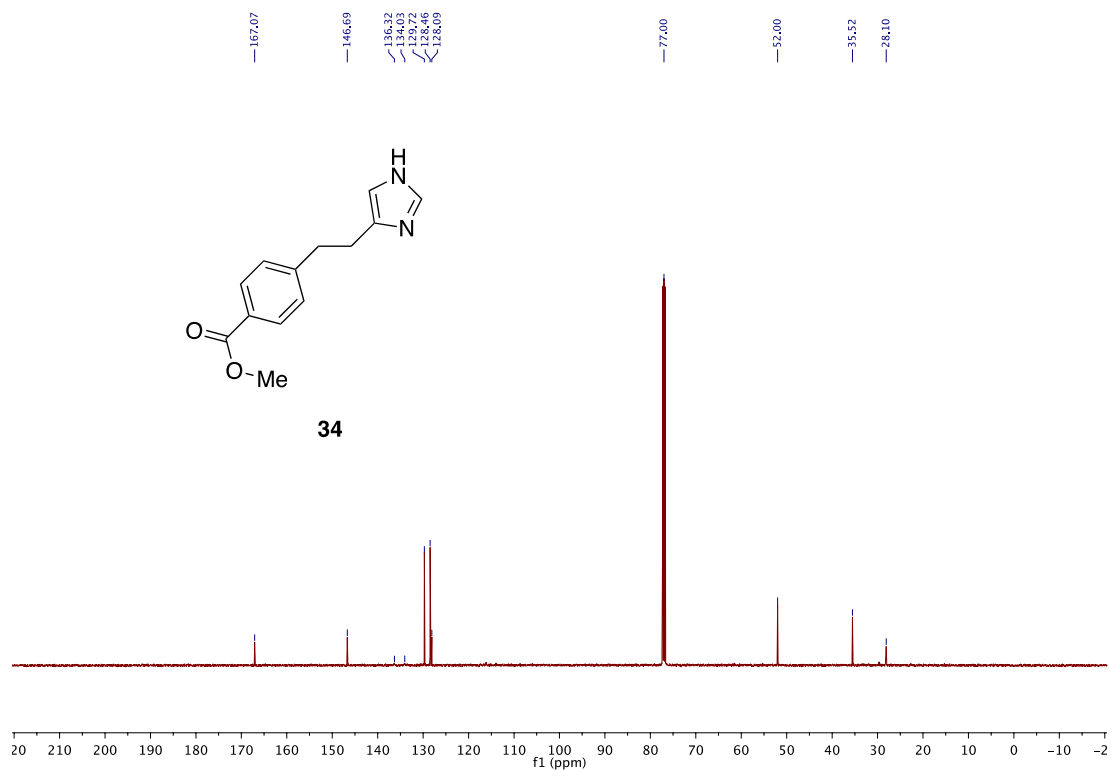
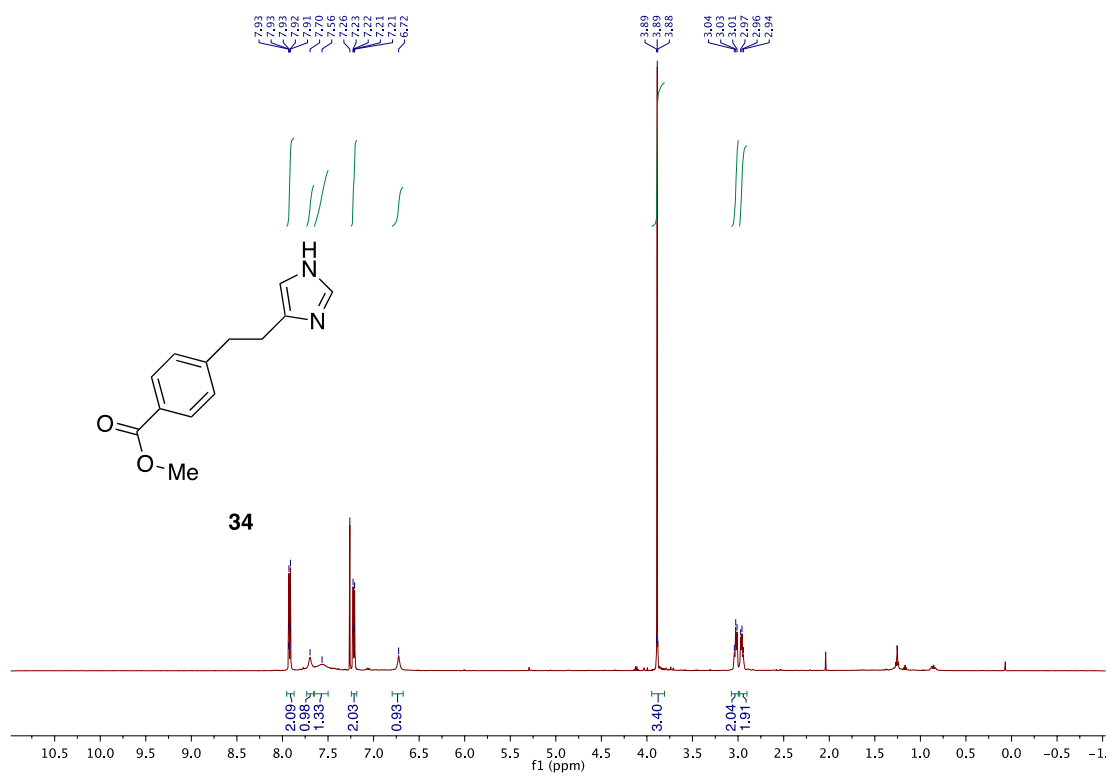
Chapter 3



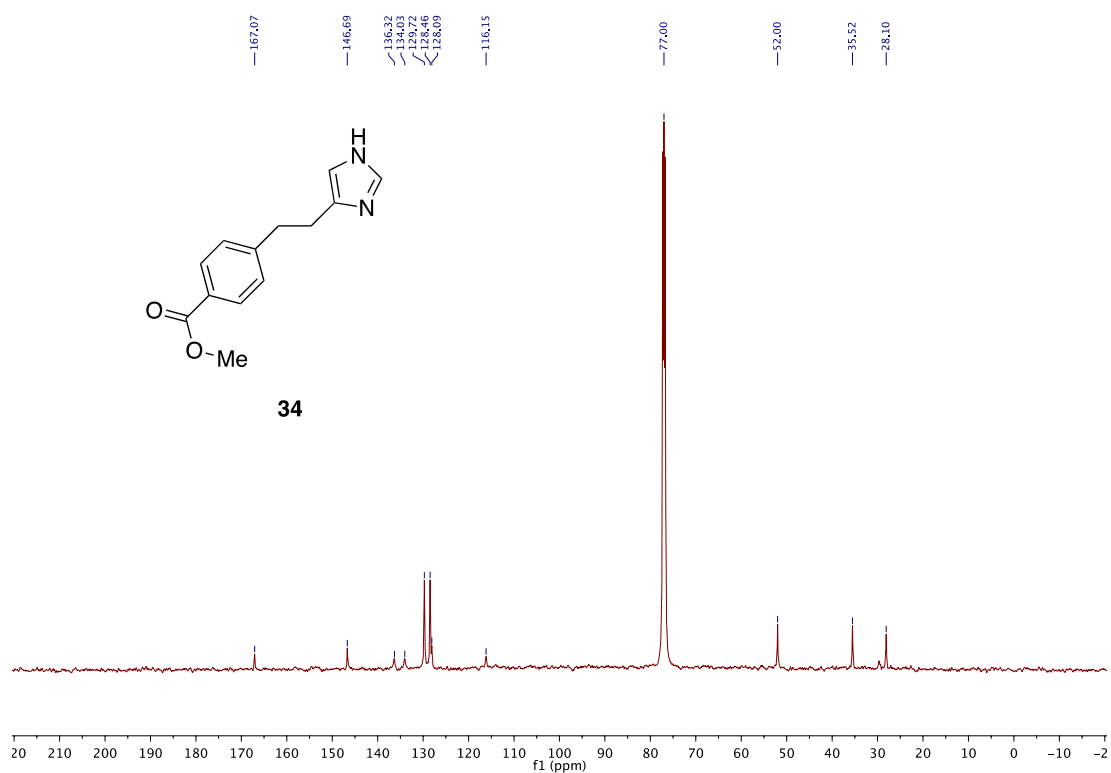
Deaminative Arylation at sp^3 Carbon Centers



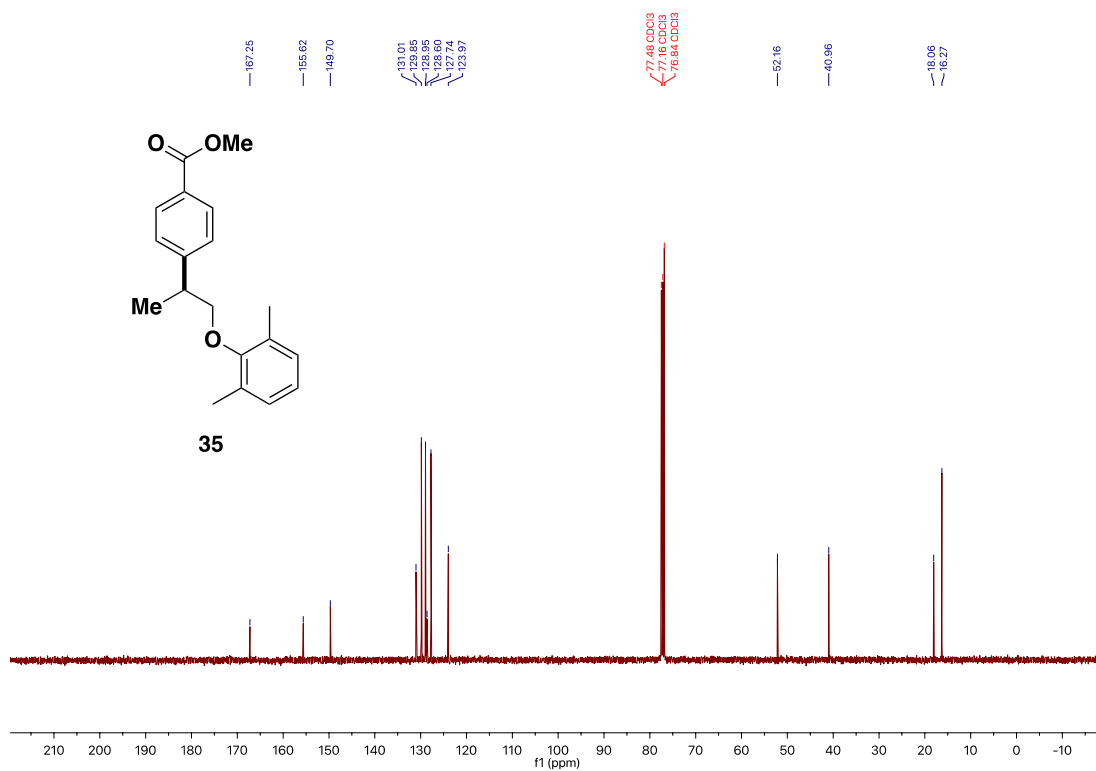
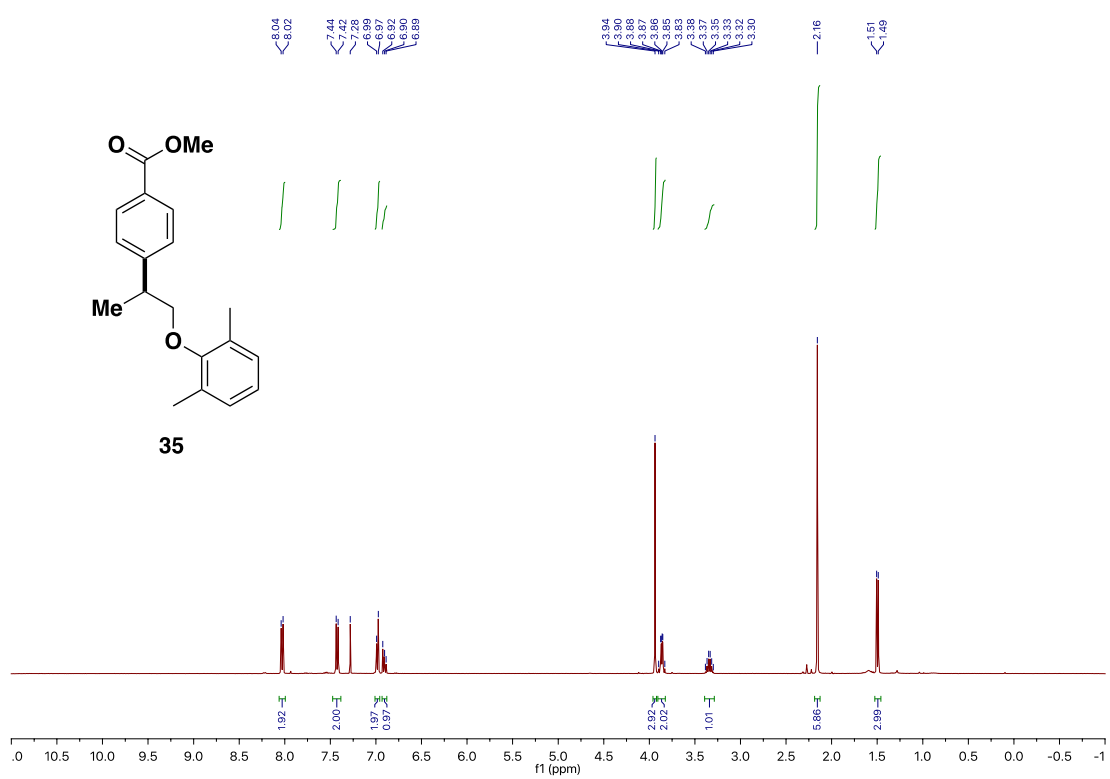
Chapter 3



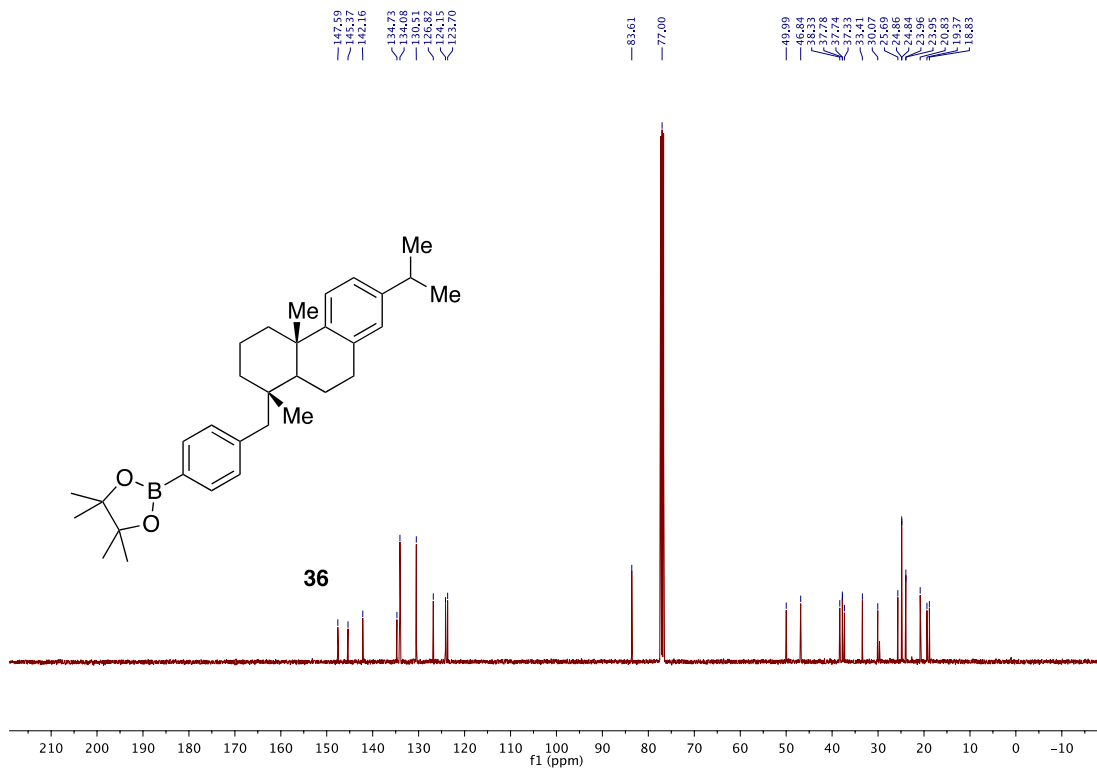
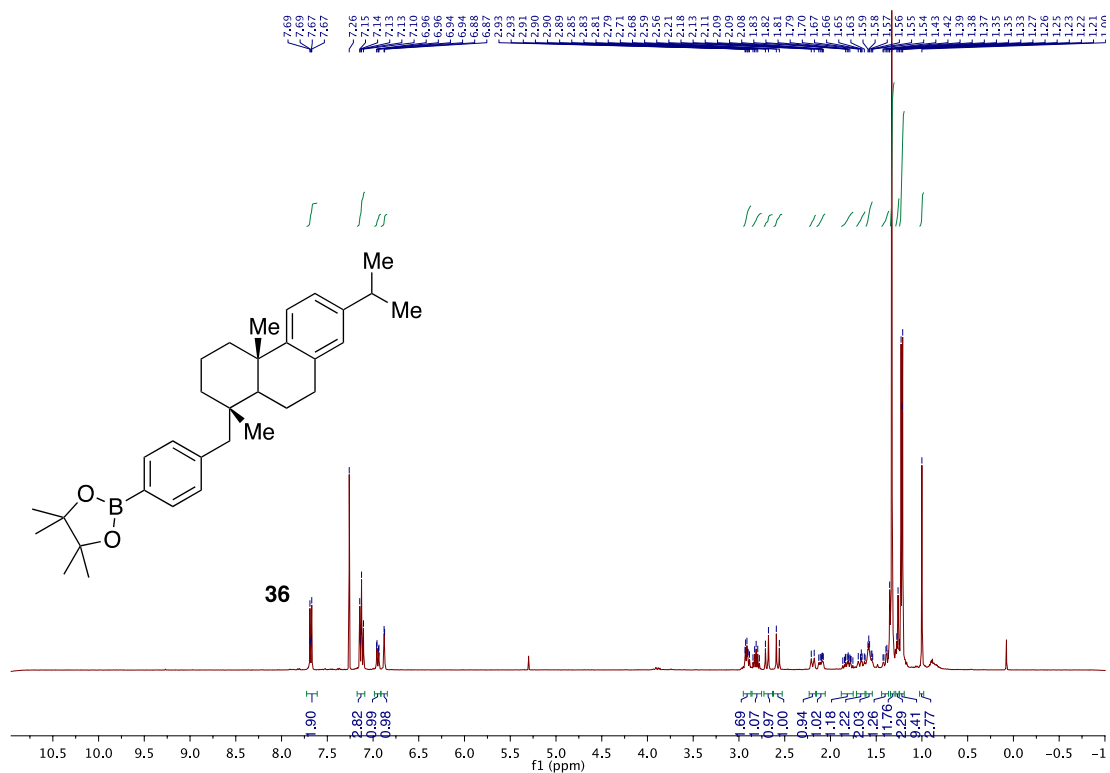
Deaminative Arylation at sp^3 Carbon Centers



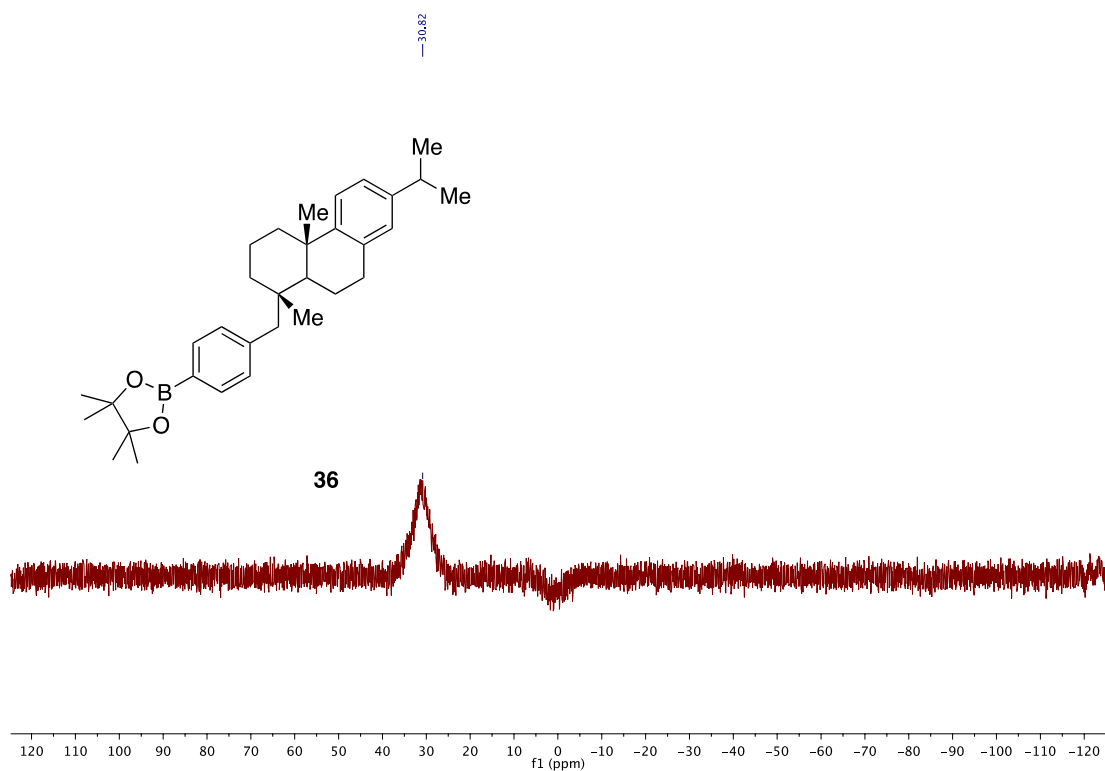
Chapter 3



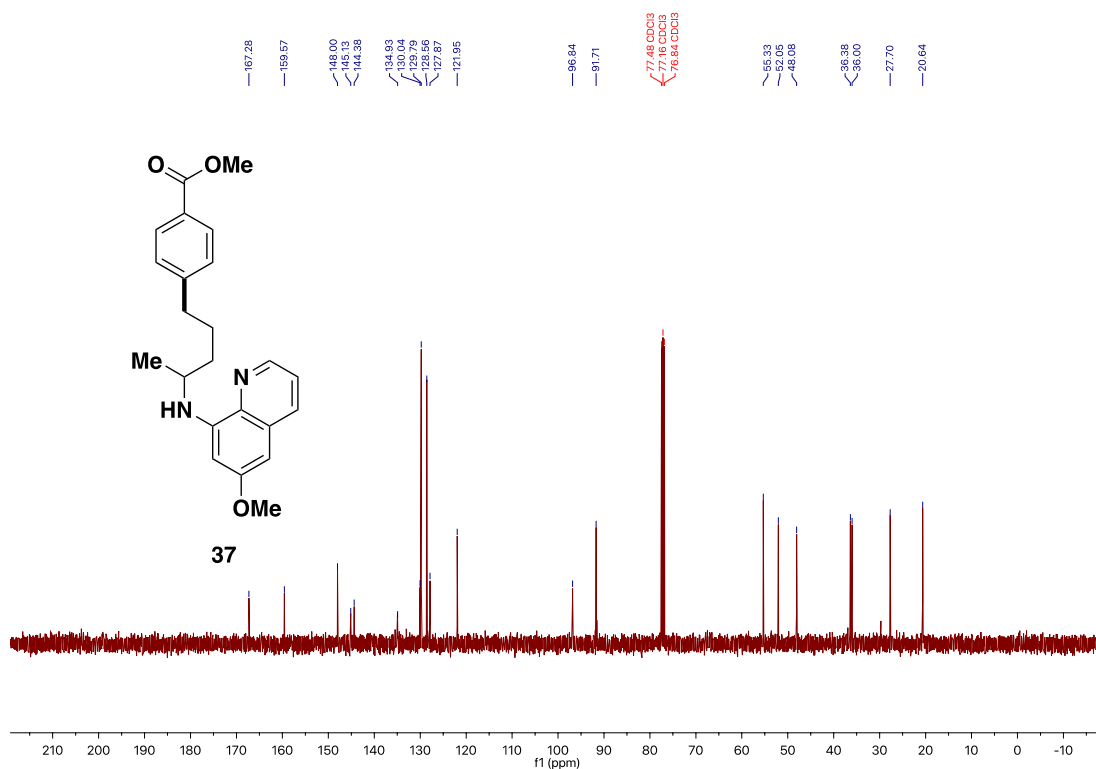
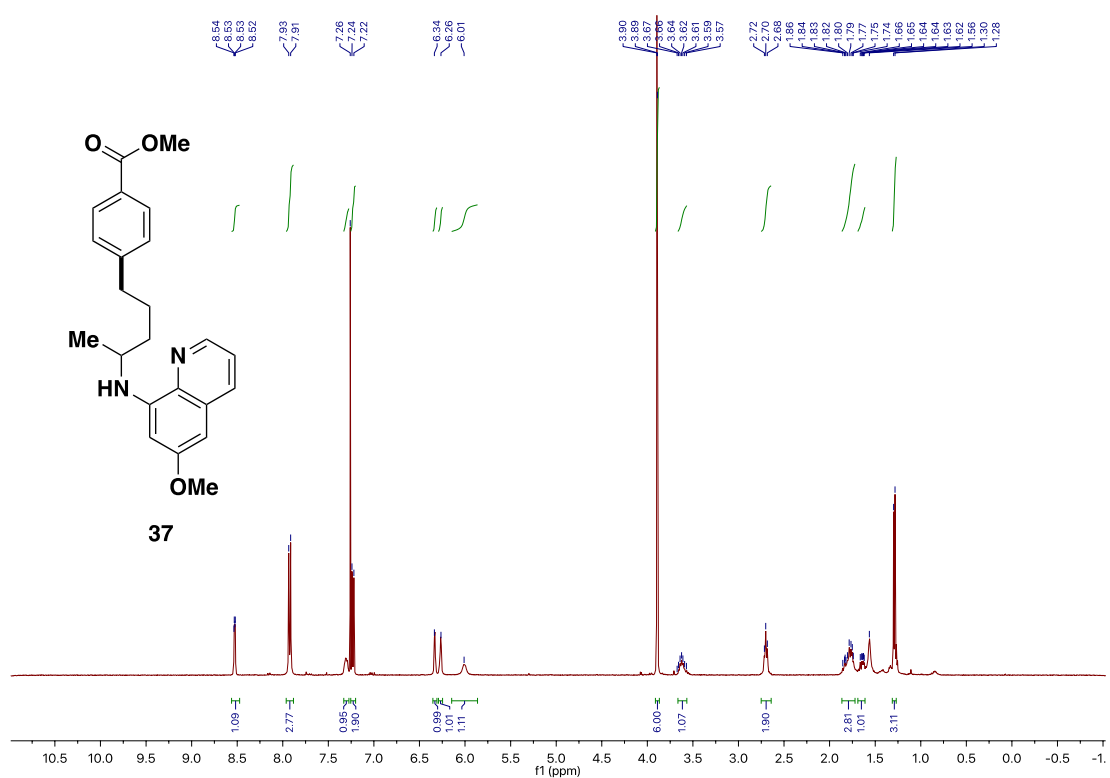
Deaminative Arylation at sp^3 Carbon Centers



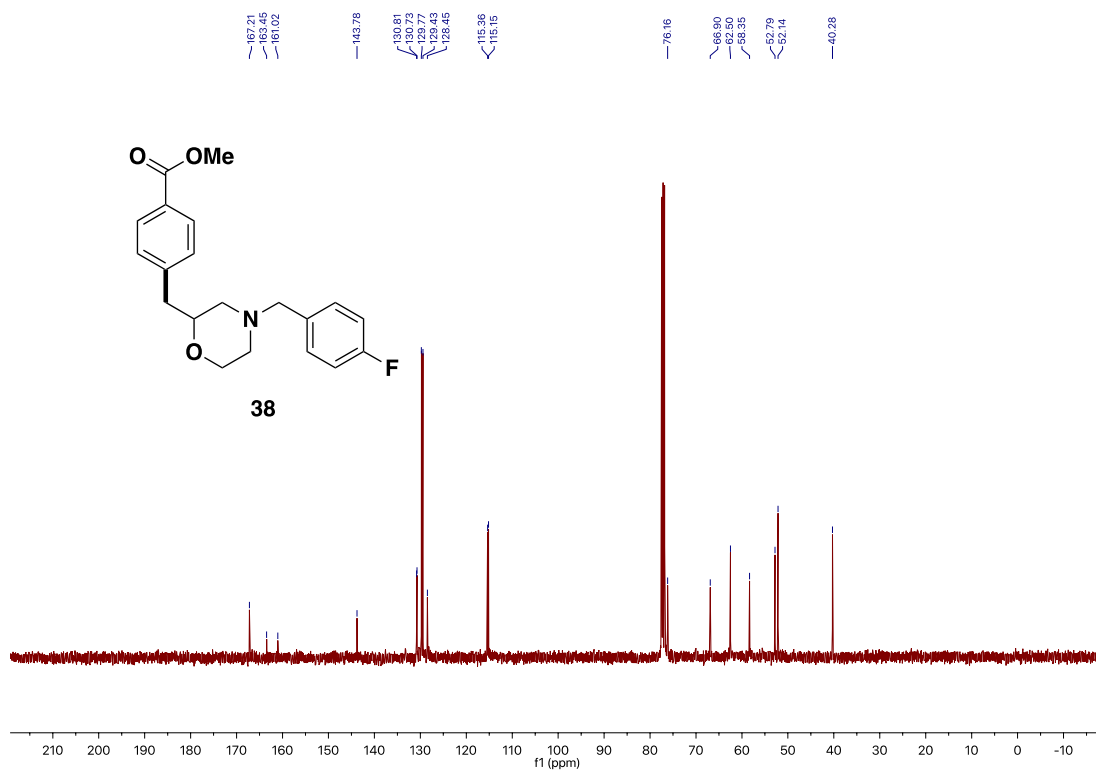
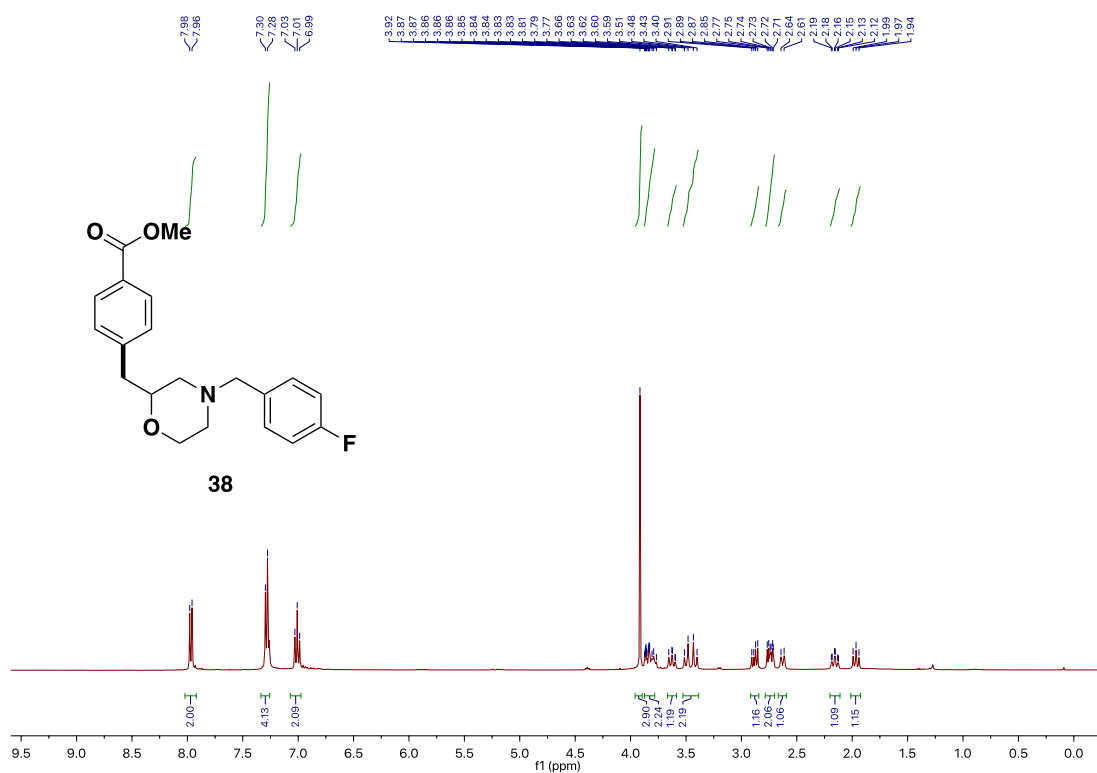
Chapter 3



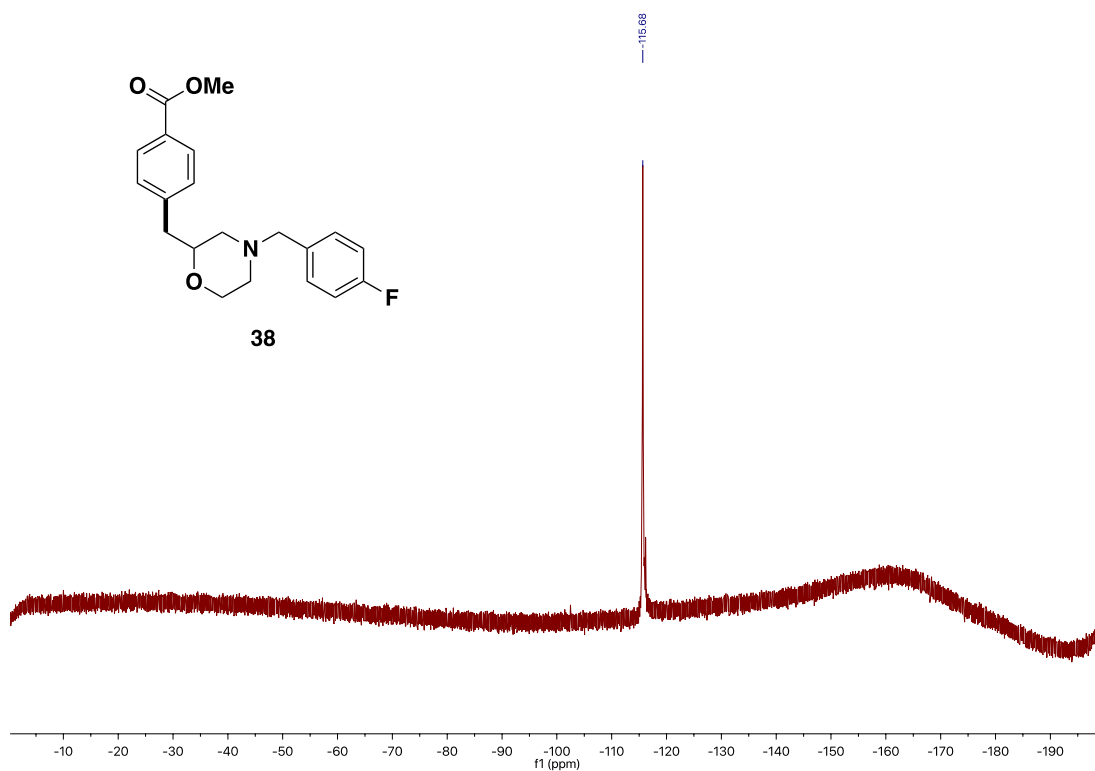
Deaminative Arylation at sp^3 Carbon Centers



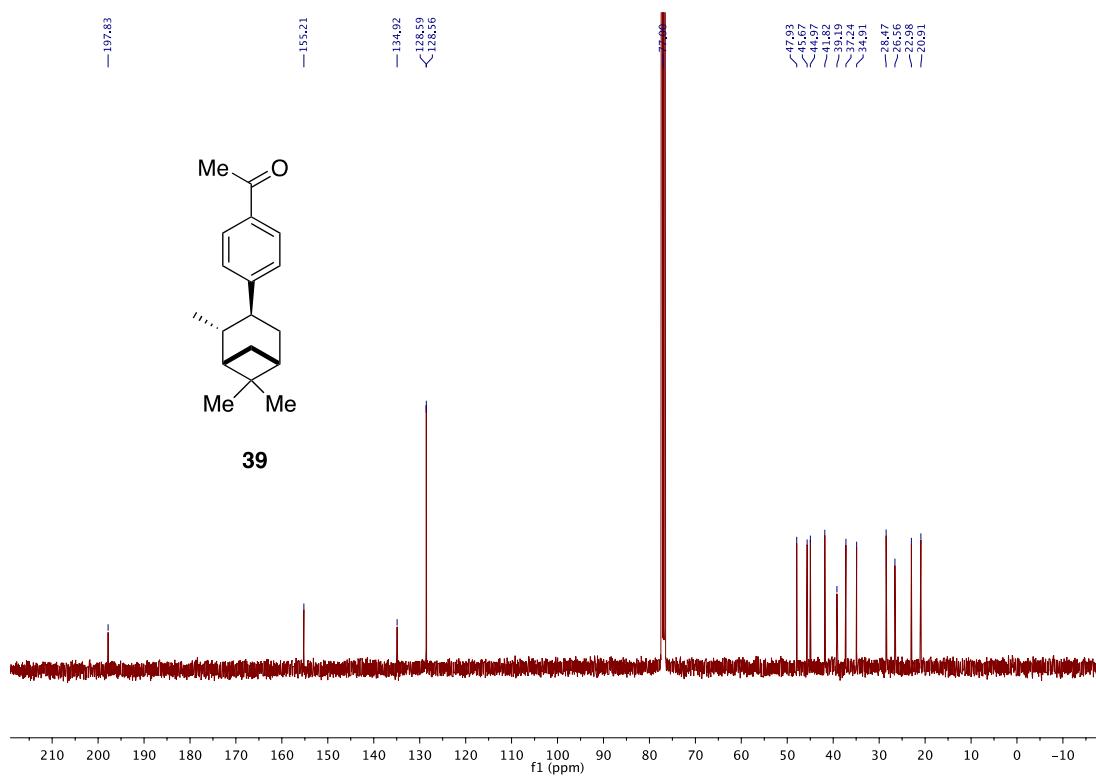
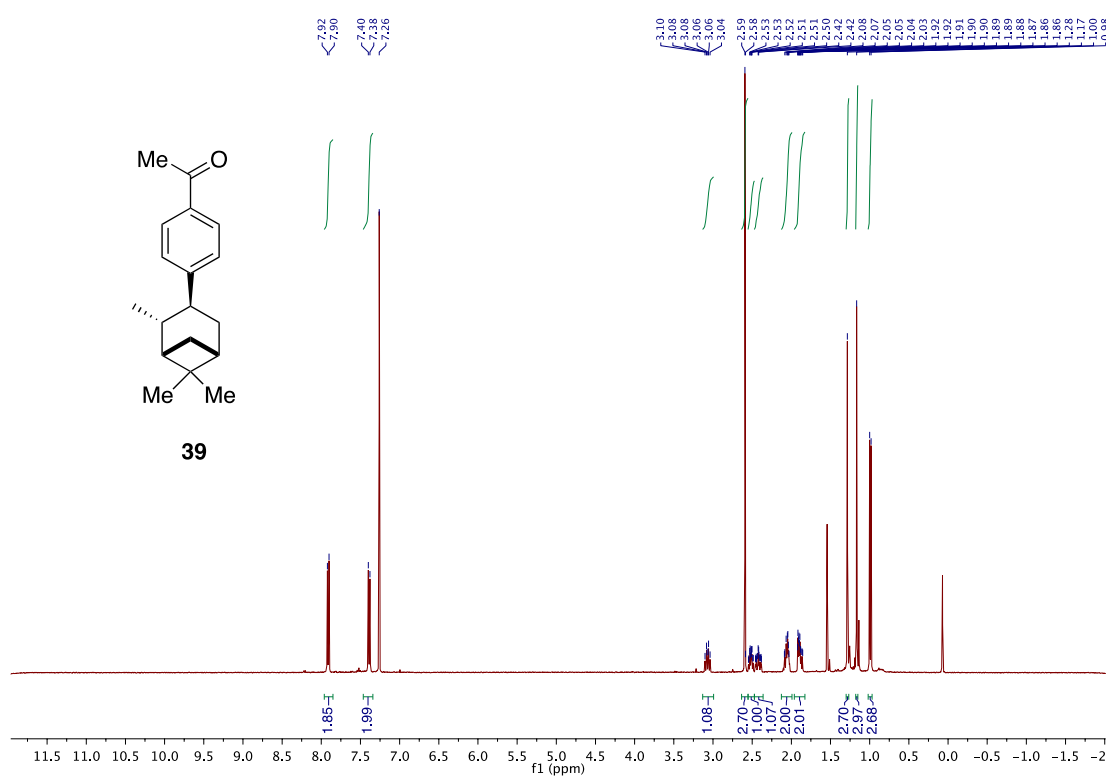
Chapter 3



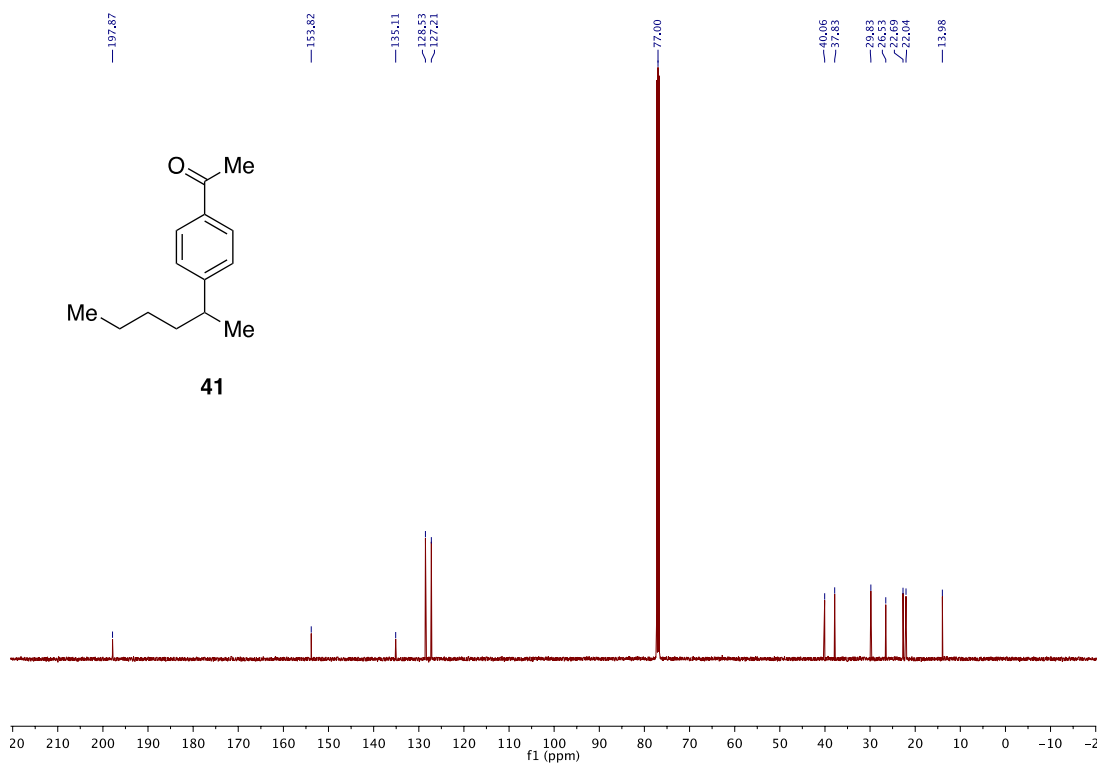
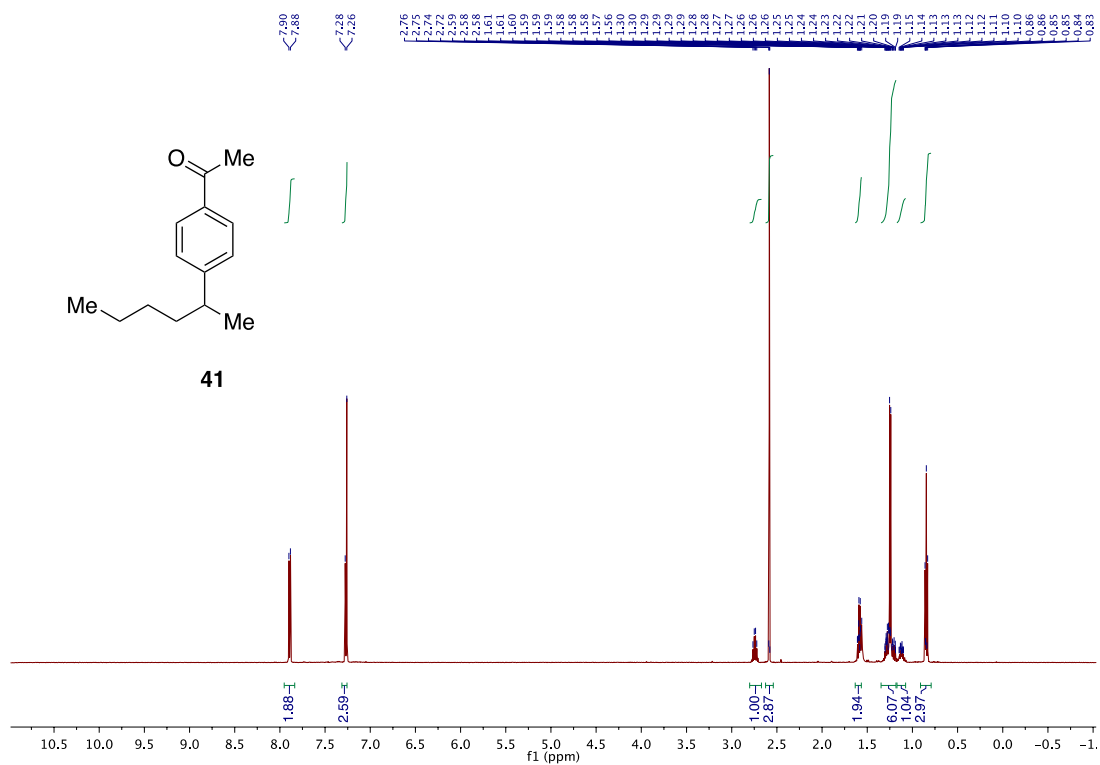
Deaminative Arylation at sp^3 Carbon Centers



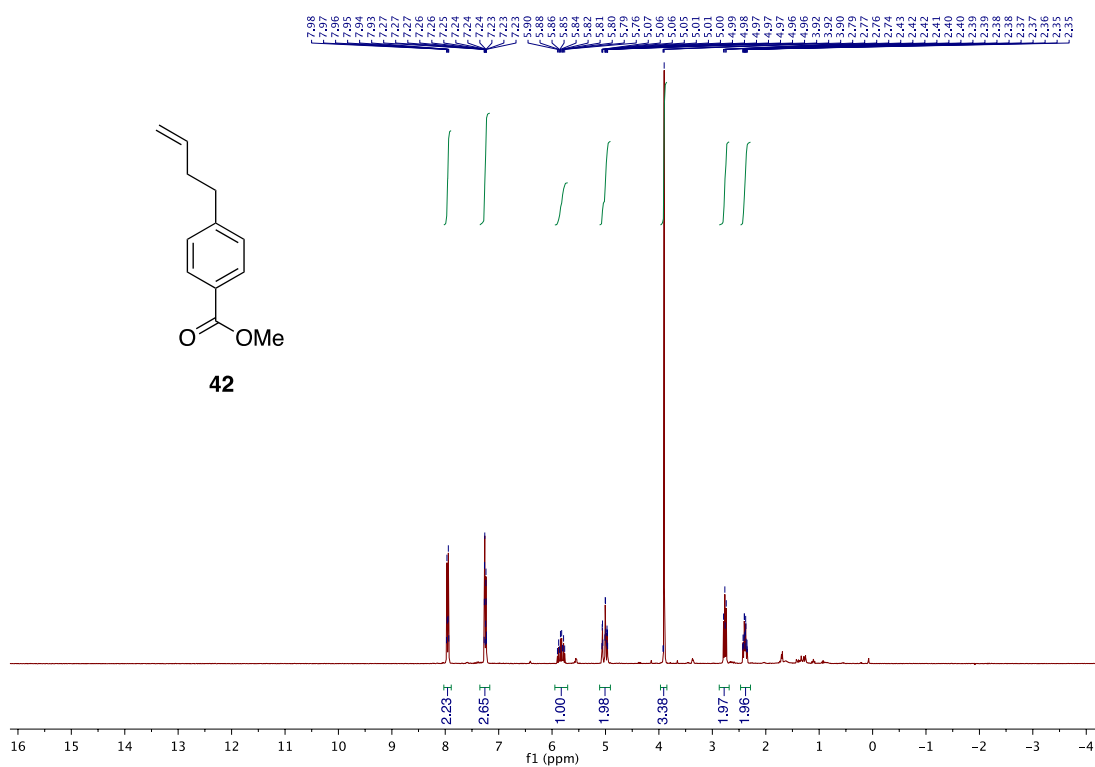
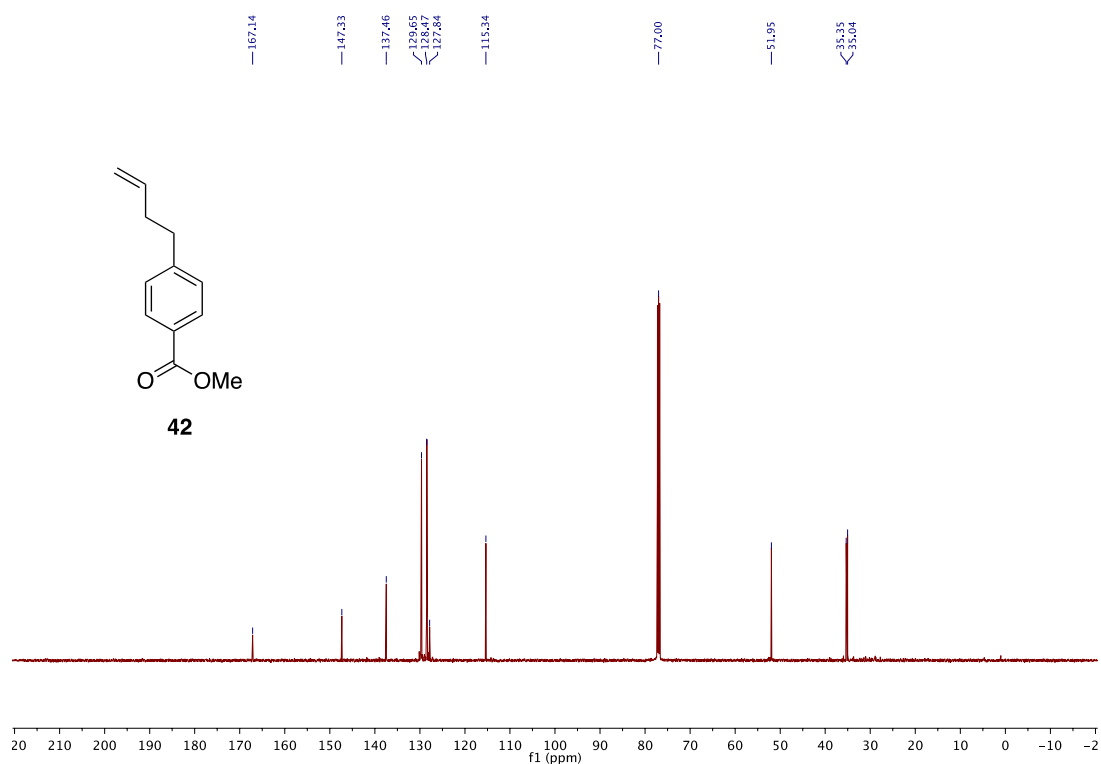
Chapter 3



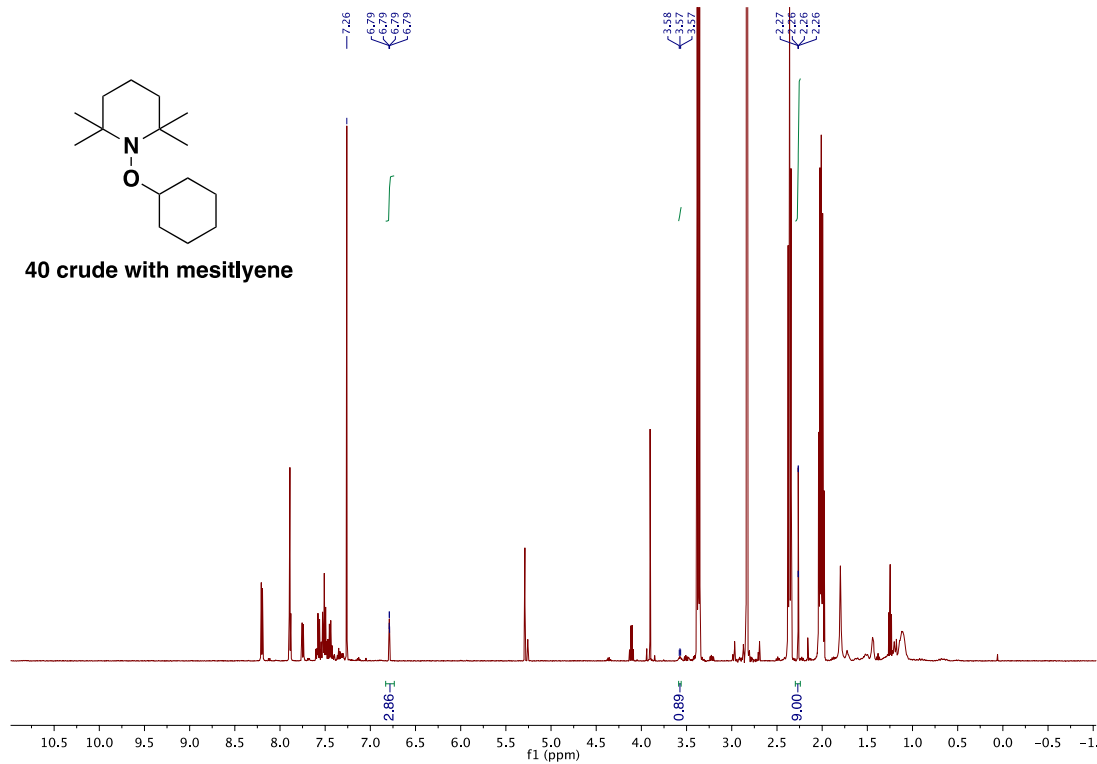
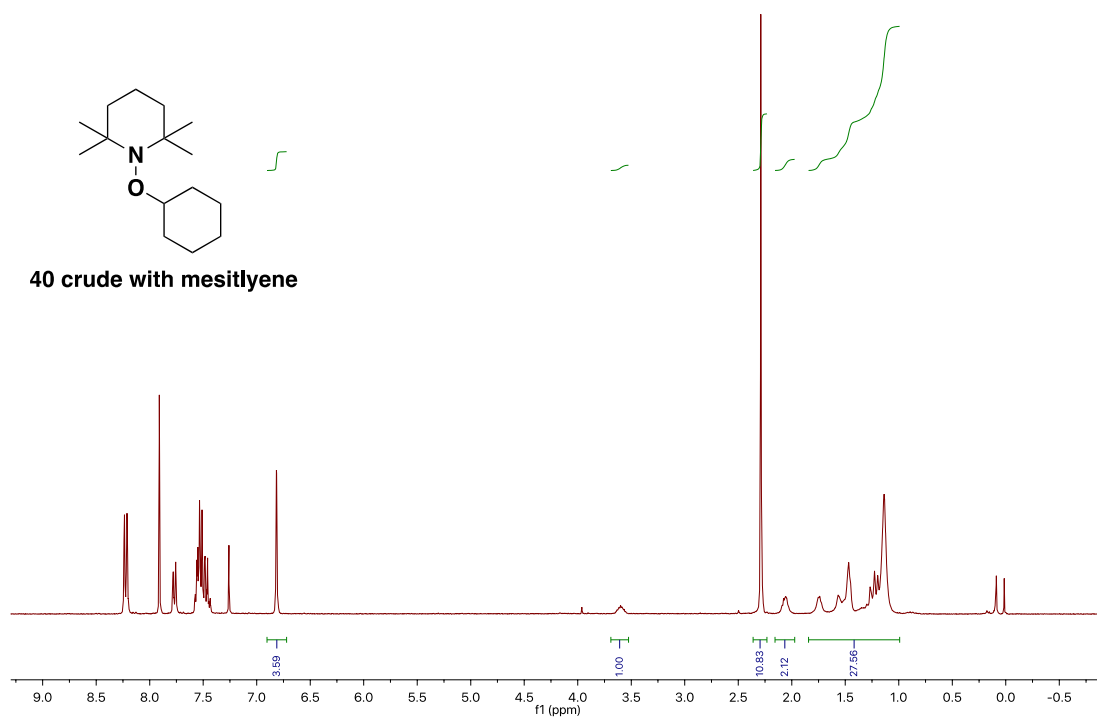
Deaminative Arylation at sp^3 Carbon Centers



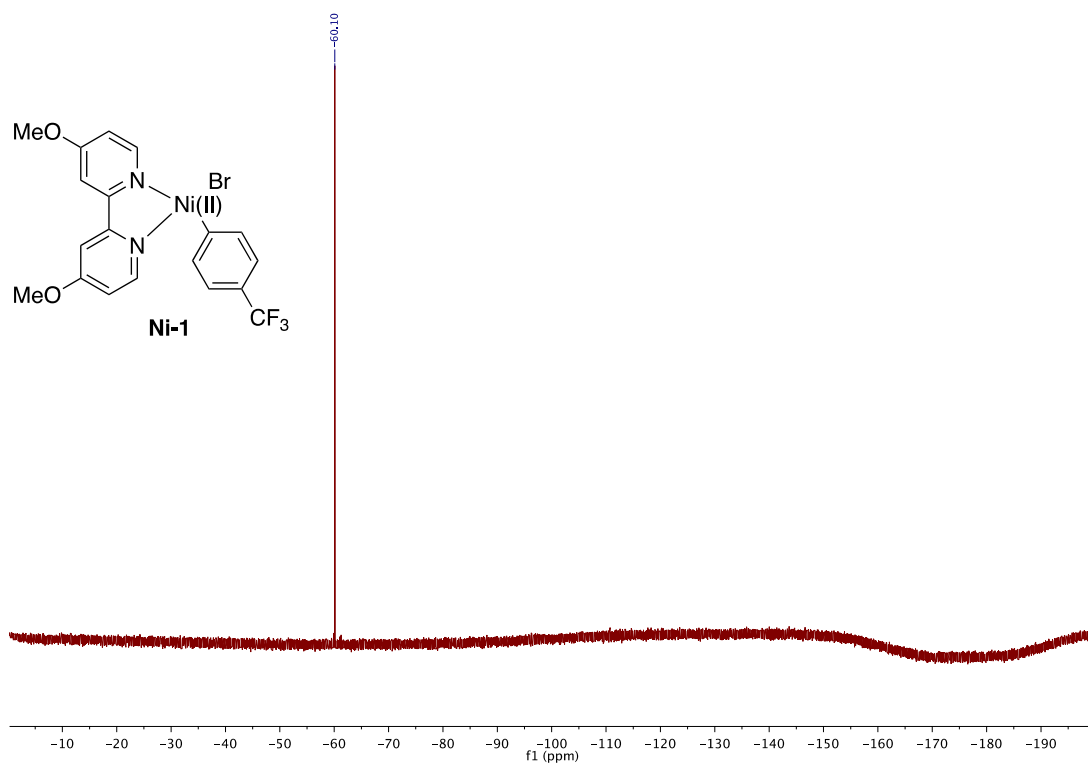
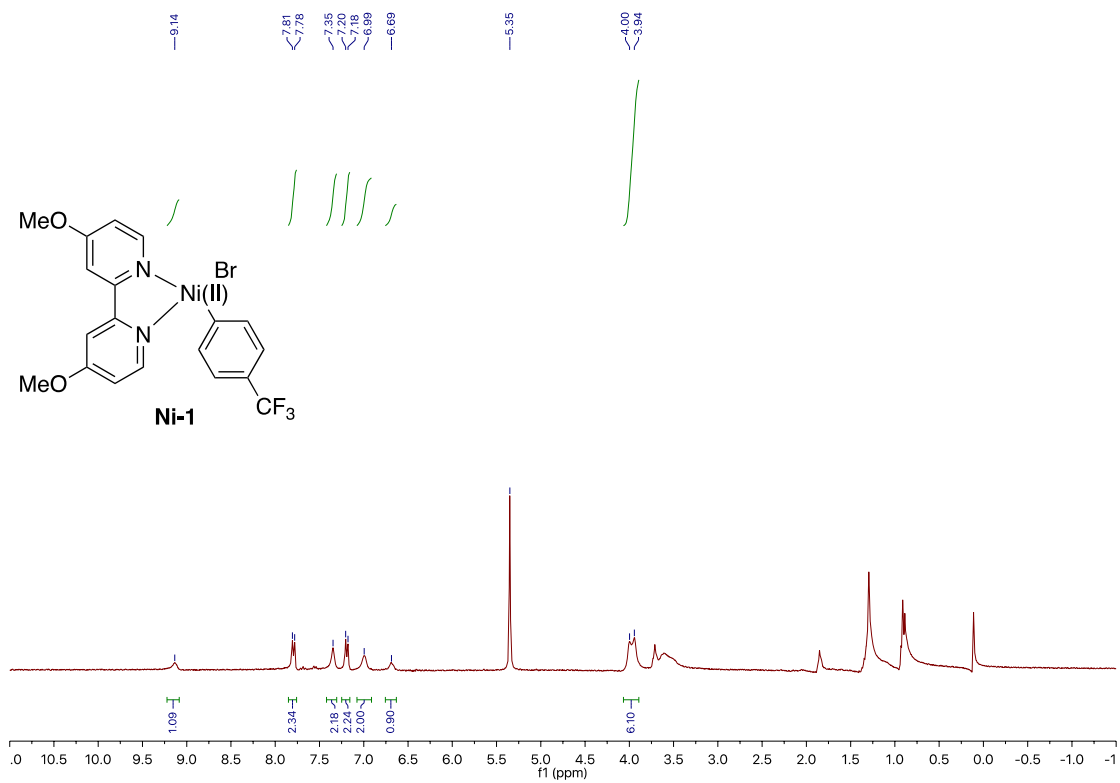
Chapter 3



Deaminative Arylation at sp^3 Carbon Centers



Chapter 3



3.6 References

- (1) Lovering, F.; Bikker, J.; Humblet, C. Escape from Flatland: Increasing Saturation as an Approach to Improving Clinical Success. *J. Med. Chem.* **2009**, *52* (21), 6752–6756. <https://doi.org/10.1021/jm901241e>.
- (2) Kaga, A.; Chiba, S. Engaging Radicals in Transition Metal-Catalyzed Cross-Coupling with Alkyl Electrophiles: Recent Advances. *ACS Catal.* **2017**, *7* (7), 4697–4706. <https://doi.org/10.1021/acscatal.7b01405>.
- (3) Choi, J.; Fu, G. C. Transition Metal-Catalyzed Alkyl-Alkyl Bond Formation: Another Dimension in Cross-Coupling Chemistry. *Science (80-.)* **2017**, *356* (6334). <https://doi.org/10.1126/science.aaf7230>.
- (4) Campeau, L. C.; Hazari, N. Cross-Coupling and Related Reactions: Connecting Past Success to the Development of New Reactions for the Future. *Organometallics* **2019**, *38* (1), 3–35. <https://doi.org/10.1021/acs.organomet.8b00720>.
- (5) Kambe, N.; Iwasaki, T.; Terao, J. Pd-Catalyzed Cross-Coupling Reactions of Alkyl Halides. *Chem. Soc. Rev.* **2011**, *40* (10), 4937–4947. <https://doi.org/10.1039/c1cs15129k>.
- (6) Ruiz-Castillo, P.; Buchwald, S. L. Applications of Palladium-Catalyzed C-N Cross-Coupling Reactions. *Chem. Rev.* **2016**, *116* (19), 12564–12649. <https://doi.org/10.1021/acs.chemrev.6b00512>.
- (7) Mayol-Llinàs, J.; Nelson, A.; Farnaby, W.; Ayscough, A. Assessing Molecular Scaffolds for CNS Drug Discovery. *Drug Discov. Today* **2017**, *22* (7), 965–969. <https://doi.org/10.1016/j.drudis.2017.01.008>.
- (8) Ouyang, K.; Hao, W.; Zhang, W. X.; Xi, Z. Transition-Metal-Catalyzed Cleavage of C-N Single Bonds. *Chem. Rev.* **2015**, *115* (21), 12045–12090. <https://doi.org/10.1021/acs.chemrev.5b00386>.
- (9) Blakemore, D. C.; Castro, L.; Churcher, I.; Rees, D. C.; Thomas, A. W.; Wilson, D. M.; Wood, A. Organic Synthesis Provides Opportunities to Transform Drug Discovery. *Nat. Chem.* **2018**, *10* (4), 383–394. <https://doi.org/10.1038/s41557-018-0021-z>.
- (10) Plunkett, S.; Basch, C. H.; Santana, S. O.; Watson, M. P. Harnessing Alkylpyridinium Salts as Electrophiles in Deaminative Alkyl-Alkyl Cross-Couplings. *J. Am. Chem. Soc.* **2019**, *141* (6), 2257–2262. <https://doi.org/10.1021/jacs.9b00111>.
- (11) Roughley, S. D.; Jordan, A. M. The Medicinal Chemist's Toolbox: An Analysis of Reactions Used in the Pursuit of Drug Candidates. *J. Med. Chem.* **2011**, *54* (10), 3451–3479. <https://doi.org/10.1021/jm200187y>.
- (12) Bleicher, K. H.; Böhm, H. J.; Müller, K.; Alanine, A. I. Hit and Lead Generation: Beyond High-Throughput Screening. *Nat. Rev. Drug Discov.* **2003**, *2* (5), 369–378. <https://doi.org/10.1038/nrd1086>.
- (13) Hie, L.; Baker, E. L.; Anthony, S. M.; Desrosiers, J. N.; Senanayake, C.; Garg, N. K. Nickel-Catalyzed Esterification of Aliphatic Amides. *Angew. Chem. Int. Ed.* **2016**, *55* (48), 15129–15132. <https://doi.org/10.1002/anie.201607856>.
- (14) Buszek, K. R.; Brown, N. N-Vinylpyridinium and -Ammonium Tetrafluoroborate Salts: New Electrophilic Coupling Partners for Pd(0)-Catalyzed Suzuki Cross-Coupling Reactions. *Org. Lett.* **2007**, *9* (4), 707–710. <https://doi.org/10.1021/olo63027h>.
- (15) Peng, C.; Wang, Y.; Wang, J. Palladium-Catalyzed Cross-Coupling of α -Diazocarbonyl Compounds with Arylboronic Acids. *J. Am. Chem. Soc.* **2008**, *130* (5), 1566–1567. <https://doi.org/10.1021/jao782293>.
- (16) Blakey, S. B.; MacMillan, D. W. C. The First Suzuki Cross-Couplings of Aryltrimethylammonium Salts. *J. Am. Chem. Soc.* **2003**, *125* (20), 6046–6047. <https://doi.org/10.1021/jao34908b>.
- (17) Zhang, P.; Le, C. C.; MacMillan, D. W. C. Silyl Radical Activation of Alkyl Halides in Metallaphotoredox Catalysis: A Unique Pathway for Cross-Electrophile Coupling. *J. Am. Chem. Soc.* **2016**, *138* (26), 8084–8087. <https://doi.org/10.1021/jacs.6b04818>.
- (18) González-Bobes, F.; Fu, G. C. Amino Alcohols as Ligands for Nickel-Catalyzed Suzuki Reactions of Unactivated Alkyl Halides, Including Secondary Alkyl Chlorides, with Arylboronic Acids. *J. Am. Chem. Soc.* **2006**, *128* (16), 5360–5361. <https://doi.org/10.1021/jao613761>.
- (19) Zhou, J.; Fu, G. C. Cross-Couplings of Unactivated Secondary Alkyl Halides: Room-Temperature Nickel-Catalyzed Negishi Reactions of Alkyl Bromides and Iodides. *J. Am. Chem. Soc.* **2003**, *125* (48), 14726–14727. <https://doi.org/10.1021/jao389366>.
- (20) Tsuji, T.; Yorimitsu, H.; Oshima, K. Cobalt-Catalyzed Coupling Reaction of Alkyl Halides with Allylic Grignard Reagents. *Angew. Chemie - Int.*

Chapter 3

- Ed.* **2002**, 41 (21), 4137–4139. [https://doi.org/10.1002/1521-3773\(20021104\)41:21<4137::AID-ANIE4137>3.0.CO;2-O](https://doi.org/10.1002/1521-3773(20021104)41:21<4137::AID-ANIE4137>3.0.CO;2-O).
- (21) Zhang, X.; MacMillan, D. W. C. Alcohols as Latent Coupling Fragments for Metallaphotoredox Catalysis: Sp₃-Sp₂ Cross-Coupling of Oxalates with Aryl Halides. *J. Am. Chem. Soc.* **2016**, 138 (42), 13862–13865. <https://doi.org/10.1021/jacs.6b09533>.
- (22) Nawrat, C. C.; Jamison, C. R.; Slutsky, Y.; MacMillan, D. W. C.; Overman, L. E. Oxalates as Activating Groups for Alcohols in Visible Light Photoredox Catalysis: Formation of Quaternary Centers by Redox-Neutral Fragment Coupling. *J. Am. Chem. Soc.* **2015**, 137 (35), 11270–11273. <https://doi.org/10.1021/jacs.5b07678>.
- (23) Johnston, G. ; Smith, R. T.; Allmendinger, S.; MacMillan, D. W. C. Metallaphotoredox-Catalysed Sp₃-Sp₃ Cross-Coupling of Carboxylic Acids with Alkyl Halides. *Nature* **2016**, 536, 322–325. <https://doi.org/10.1038/nature19056>.
- (24) Zuo, Z.; Ahneman, D. T.; Chu, L.; Terrett, J. A.; Doyle, A. G.; MacMillan, D. W. C. Merging Photoredox with Nickel Catalysis: Coupling of α -Carboxyl Sp₃-Carbons with Aryl Halides. *Science (80-.)*. **2014**, 345 (6195), 437–440. <https://doi.org/10.1126/science.1255525>.
- (25) Tellis, J. C.; Primer, D. N.; Molander, G. A. Single-Electron Transmetalation in Organoboron Cross-Coupling by Photoredox/Nickel Dual Catalysis. *Science (80-.)*. **2014**, 345 (6195), 433–436. <https://doi.org/10.1126/science.1253647>.
- (26) Tellis, J. C.; Kelly, C. B.; Primer, D. N.; Jouffroy, M.; Patel, N. R.; Molander, G. A. Single-Electron Transmetalation via Photoredox/Nickel Dual Catalysis: Unlocking a New Paradigm for Sp₃-Sp₂ Cross-Coupling. *Acc. Chem. Res.* **2016**, 49 (7), 1429–1439. <https://doi.org/10.1021/acs.accounts.6b00214>.
- (27) Qin, T.; Cornella, J.; Li, C.; Malins, L. R.; Edwards, J. T.; Kawamura, S.; Maxwell, B. D.; Eastgate, M. D.; Baran, P. S. Organic Chemistry: A General Alkyl-Alkyl Cross-Coupling Enabled by Redox-Active Esters and Alkylzinc Reagents. *Science (80-.)*. **2016**, 352 (6287), 801–805. <https://doi.org/10.1126/science.aaf6123>.
- (28) Cornella, J.; Edwards, J. T.; Qin, T.; Kawamura, S.; Wang, J.; Pan, C. M.; Gianatassio, R.; Schmidt, M.; Eastgate, M. D.; Baran, P. S. Practical Ni-Catalyzed Aryl-Alkyl Cross-Coupling of Secondary Redox-Active Esters. *J. Am. Chem. Soc.* **2016**, 138 (7), 2174–2177. <https://doi.org/10.1021/jacs.6b00250>.
- (29) Pyridiniums, B. Y. N.; Katritzky, A. R.; Ville, G. D. E.; Patel, R. C. Carbon-Alkylation of Simple Nitronate Anions by N-Substituted Pyridiniums. *Tetrahedron* **1981**, 37 (1), 25–30. [https://doi.org/10.1016/0040-4020\(81\)85037-5](https://doi.org/10.1016/0040-4020(81)85037-5).
- (30) Bapat, B.; Blade, R. J.; Boulton, A. J.; Epsstajn, J.; Katritzky, A. R.; Lewis, J.; Molina-Buendia, I.; Nie, P.-L. Pyridines as Leaving Groups in Synthetic Transformations: Nucleophilic Displacements of amino Groups, and Novel Preparations of Nitriles and Isocyanates. *Tetrahedron* **1976**, 31, 2691–2694. [https://doi.org/10.1016/S0040-4039\(00\)77797-5](https://doi.org/10.1016/S0040-4039(00)77797-5).
- (31) Buszek, K. R.; Brown, N. N-Vinylpyridinium and -Ammonium Tetrafluoroborate Salts : New Electrophilic Coupling Partners for Pd (0) -Catalyzed Suzuki Cross-Coupling Reactions. *Org. Lett.* **2007**, 2, 707–710. <https://doi.org/10.1021/ol063027h>.
- (32) Said, S. A.; Fiksdahl, A. Stereoselective Transformation of Amines via Chiral 2, 4, 6-Triphenylpyridinium Intermediates. *tetrahedron: Asymmetry* **2001**, 12, 1947–1951.
- (33) Basch, C. H.; Liao, J.; Xu, J.; Piane, J. J.; Watson, M. P. Harnessing Alkyl Amines as Electrophiles for Nickel-Catalyzed Cross Couplings via C-N Bond Activation. *J. Am. Chem. Soc.* **2017**, 139 (15), 5313–5316. <https://doi.org/10.1021/jacs.7b02389>.
- (34) Zarate, C.; van Gemmeren, M.; Somerville, R. J.; Martin, R. Phenol Derivatives: Modern Electrophiles in Cross-Coupling Reactions. *Adv. Organomet. Chem.* **2016**, 66, 143–222. <https://doi.org/10.1016/bs.adomc.2016.07.001>.
- (35) Grimshaw, J.; Moore, S.; Trocha-Grimshaw, J. Electrochemical Reactions. Part 26. Radicals Derived by Reduction of N-Alkylpyridinium Salts and Homologous N,N'-Polymethylenebispyridinium Salts. Cleavage of the C-N Bond. *Acta Chem. Scand.* **1983**, 37, 485–489.
- (36) Klauk, F. J. R.; James, M. J.; Glorius, F. Deaminative Strategy for the Visible-Light-Mediated Generation of Alkyl Radicals. *Angew. Chem. Int. Ed.* **2017**, 56 (40), 12336–12339. <https://doi.org/10.1002/anie.201706896>.
- (37) Jiang, X.; Zhang, M. M.; Xiong, W.; Lu, L. Q.; Xiao, W. J. Deaminative (Carbonylative) Alkyl-Heck-Type Reactions Enabled by Photocatalytic C-N Bond Activation. *Angew. Chem. Int. Ed.* **2019**, 58 (8), 2402–2406. <https://doi.org/10.1002/anie.201813689>.
- (38) Ociepa, M.; Turkowska, J.; Gryko, D. Redox-Activated Amines in C(Sp₃)-C(Sp) and C(Sp₃)-C(Sp₂) Bond Formation Enabled by Metal-Free

Deaminative Arylation at sp^3 Carbon Centers

- Photoredox Catalysis. *ACS Catal.* **2018**, *8* (12), 11362–11367. <https://doi.org/10.1021/acscatal.8b03437>.
- (39) Zhang, J. S.; Liu, L.; Chen, T.; Han, L. B. Transition-Metal-Catalyzed Three-Component Difunctionalizations of Alkenes. *Chem. - An Asian J.* **2018**, *13* (17), 2277–2291. <https://doi.org/10.1002/asia.201800647>.
- (40) Klauck, F. J. R.; Yoon, H.; James, M. J.; Lautens, M.; Glorius, F. Visible-Light-Mediated Deaminative Three-Component Dicarbofunctionalization of Styrenes with Benzylic Radicals. *ACS Catal.* **2019**, *9* (1), 236–241. <https://doi.org/10.1021/acscatal.8b04191>.
- (41) Zhang, M. M.; Liu, F. Visible-Light-Mediated Allylation of Alkyl Radicals with Allylic Sulfones: Via a Deaminative Strategy. *Org. Chem. Front.* **2018**, *5* (23), 3443–3446. <https://doi.org/10.1039/c8qo01046c>.
- (42) Moser, D.; Duan, Y.; Wang, F.; Ma, Y.; O'Neill, M. J.; Cornella, J. Selective Functionalization of Aminoheterocycles by a Pyrylium Salt. *Angew. Chem. Int. Ed.* **2018**, *57* (34), 11035–11039. <https://doi.org/10.1002/anie.201806271>.
- (43) Wu, J.; He, L.; Noble, A.; Aggarwal, V. K. Photoinduced Deaminative Borylation of Alkylamines. *J. Am. Chem. Soc.* **2018**, *140* (34), 10700–10704. <https://doi.org/10.1021/jacs.8b07103>.
- (44) Sandfort, F.; Strieth-Kalthoff, F.; Klauck, F. J. R.; James, M. J.; Glorius, F. Deaminative Borylation of Aliphatic Amines Enabled by Visible Light Excitation of an Electron Donor–Acceptor Complex. *Chem. - A Eur. J.* **2018**, *24* (65), 17210–17214. <https://doi.org/10.1002/chem.201804246>.
- (45) Hu, J.; Wang, G.; Li, S.; Shi, Z. Selective C–N Borylation of Alkyl Amines Promoted by Lewis Base. *Angew. Chemie - Int. Ed.* **2018**, *57* (46), 15227–15231. <https://doi.org/10.1002/anie.201809608>.
- (46) Moir, M.; Danon, J. J.; Reekie, T. A.; Kassiou, M. An Overview of Late-Stage Functionalization in Today's Drug Discovery. *Expert Opin. Drug Discov.* **2019**, *14* (11), 1137–1149. <https://doi.org/10.1080/17460441.2019.1653850>.
- (47) Tortajada, A.; Ninokata, R.; Martín, R. Ni-Catalyzed Site-Selective Dicarboxylation of 1,3-Dienes with CO₂. *J. Am. Chem. Soc.* **2018**, *140*, 2050–2053. <https://doi.org/10.1021/jacs.7b13220>.
- (48) Sun, S.; Bo, M.; Martín-montero, R.; Martín, R. Site-Selective Ni-Catalyzed Reductive Coupling of A-Haloboranes with Unactivated Olefins. *J. Am. Chem. Soc.* **2018**, *140*, 12765–12769. <https://doi.org/10.1021/jacs.8b09425>.
- (49) Juliá-Hernández, F.; Moragas, T.; Cornella, J.; Martín, R. Remote Carboxylation of Halogenated Aliphatic Hydrocarbons with Carbon Dioxide. *Nature* **2017**, *545* (7652), 84–88. <https://doi.org/10.1038/nature22316>.
- (50) Krasovskiy, A.; Malakhov, V.; Gavryushin, A.; Knochel, P. Efficient Synthesis of Functionalized Organozinc Compounds by the Direct Insertion of Zinc into Organic Iodides and Bromides. *Angew. Chem. Int. Ed.* **2006**, *45*, 6040–6044. <https://doi.org/10.1002/anie.200601450>.
- (51) Bard, A. J.; Faulkner, L. R. *Electrochemical Methods: Fundamentals and Applications*; Wiley-VCH: New York, 1980.
- (52) Luo, Y.-R. *Comprehensive Handbook of Chemical Bond Energies*. Taylor & Francis: New York 2002, pp 1–1687. <https://doi.org/10.2214/AJR.10.5057>.
- (53) Sun, S. Z.; Romano, C.; Martín, R. Site-Selective Catalytic Deaminative Alkylation of Unactivated Olefins. *J. Am. Chem. Soc.* **2019**, *141* (41), 16197–16201. <https://doi.org/10.1021/jacs.9b07489>.
- (54) Guisán-Ceinos, M.; Martín-Heras, V.; Tortosa, M. Regio- and Stereospecific Copper-Catalyzed Substitution Reaction of Propargylic Ammonium Salts with Aryl Grignard Reagents. *J. Am. Chem. Soc.* **2017**, *139* (25), 8448–8451. <https://doi.org/10.1021/jacs.7b05273>.
- (55) Guisán-Ceinos, M.; Martín-Heras, V.; Soler-Yanes, R.; Cárdenas, D. J.; Tortosa, M. Copper-Catalysed Cross-Coupling of Alkyl Grignard Reagents and Propargylic Ammonium Salts: Stereospecific Synthesis of Allenes. *Chem. Commun.* **2018**, *54* (60), 8343–8346. <https://doi.org/10.1039/c8cc03760d>.
- (56) Ni, S.; Li, C.; Han, J.; Mao, Y.; Pan, Y. Ni-Catalyzed Deamination Cross-Electrophile Coupling of Kat-Ritzky Salts with Halides via C–N Bond Activation. *ChemRxiv* **2019**. <https://doi.org/DOI:10.26434/chemrxiv.7638164.v1>.
- (57) Yue, H.; Zhu, C.; Yuan, T.; Cavallo, L. Chemical Science Nickel-Catalyzed C – N Bond Activation : Activated Primary Amines as Alkylating Reagents in Reductive. *Chem. Sci.* **2019**, No. 10, 4430–4435. <https://doi.org/10.1039/c9sc00783k>.
- (58) Liao, J.; Basch, C. H.; Hoerner, M. E.; Talley, M. R.; Boscoe, B. P.; Tucker, J. W.; Garnsey, M. R.; Watson, M. P. Deaminative Reductive Cross-Electrophile Couplings of Alkylpyridinium Salts and Aryl Bromides. *Org. Lett.* **2019**, *21* (8), 2941–2946.

Chapter 3

<https://doi.org/10.1021/acs.orglett.9b01014>.

- (59) Yi, J.; Badir, S. O.; Kammer, L. M.; Molander, G. A. Deaminative Reductive Arylation Enabled by Nickel/Photoredox Dual Catalysis. *Org. Lett.* **2019**, No. 21, 3346–3351. <https://doi.org/10.1021/acs.orglett.9b01097>.

Chapter 4.

Remote Hydroboration of Alkenes Catalyzed by Tungsten Complexes

Research carried out in collaboration with
Tanner Jenkins, Phillippa Cooper, Prof. Keary Engle*

In Preparation

Chapter 4

4.1 Introduction

Boron-containing molecules rank amongst the most versatile synthons in organic synthesis,¹ finding immediate application in small-molecule synthesis, pharmaceuticals^{2,3} and polymer synthesis.⁴ Such versatility and applicability prompted chemists to develop new catalytic reactions to forge sp^2 and sp^3 C–B bonds.^{5–7} Beyond any reasonable doubt, one of the most attractive and atom-economical protocols to incorporate the boron atom into organic scaffolds is the catalytic hydroboration^{8,9} of olefins. Recently, we have witnessed the development of remote functionalization strategies (Chapter 1.2.3),¹⁰ allowing C–B bond-forming reactions at distal positions within an alkyl side chain. Of particular relevance is the observation that this strategy allows mixtures of olefins to be converted into a single regioisomer by means of a chain-walking processes. Despite the advances realized in these endeavours, the C–B bond-forming reaction can be enabled at (a) an electronically activated position adjacent to a directing group or at (b) a sterically less-congested position within the alkyl side-chain. However, the ability to incorporate the C–B bond at different positions still remains largely problematic, thus representing a worthwhile challenge for chemical invention.

4.2 Hydroboration of alkenes

4.2.1 Uncatalyzed and catalyzed hydroboration of alkenes

The hydroboration reaction is undoubtedly one of the most powerful methods for synthesizing organoboron compounds.^{11,12} This reaction was originally reported in 1956 by H. C. Brown,¹³ establishing new opportunities in organic synthesis for the regioselective hydrofunctionalization of alkenes and alkynes. The utilization of diborane (B_2H_6), borane-tetrahydrofuran complex ($BH_3 \cdot THF$) and commonly used 9-borabicyclo[3.3.1]nonane (9-BBN) resulted in exergonic C–B bond forming reactions without the need for a catalyst (Figure 4.2.1, *top*).¹⁴ Introduction of HBpin or HBcat as boranes offered improved stability and handling; however, these compounds resulted in a lower reactivity profile with alkenes or alkynes unless transition metals were employed (Figure 4.2.1, *bottom*).^{11,12,15,16} Indeed, the utilization of transition metals opened a gateway to impart chemoselectivity, regioselectivity and enantioselectivity, enabling a powerful tool for the synthesis of advanced organoboron intermediates, thus holding promise for the implementation of these techniques in synthetic applications.

Chapter 4

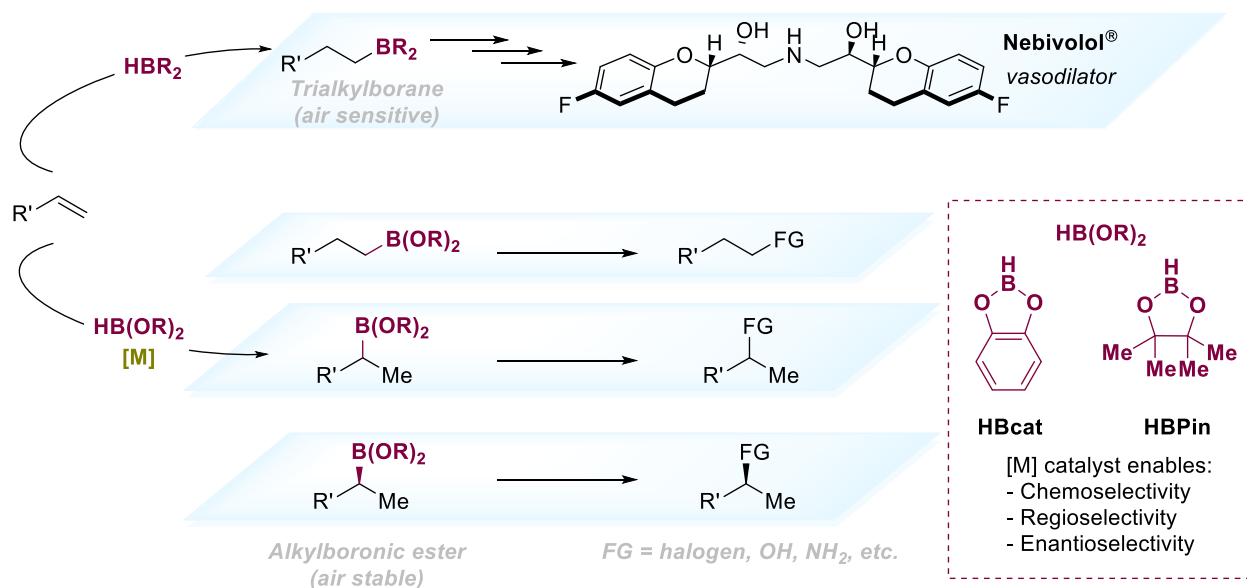


Figure 4.2.1 Uncatalyzed and catalyzed hydroboration of alkenes.

4.2.2 Overview of metal-catalyzed hydroboration of alkenes

In 1985, Nöth and co-workers described the utilization of Wilkinson's catalyst [(Ph₃P)₃RhCl] for enabling the addition of HBPin to alkenes.¹⁷ Generally, hydroboration reactions occur with terminal selectivity following an anti-Markovnikov pathway (Figure 4.2.2, I). Indeed, branched-selective hydroboration *via* Markovnikov selectivity is not particularly common, although achievable in the presence of control elements within the alkyl side-chain or by using different catalysts (Figure 4.2.2).¹⁸

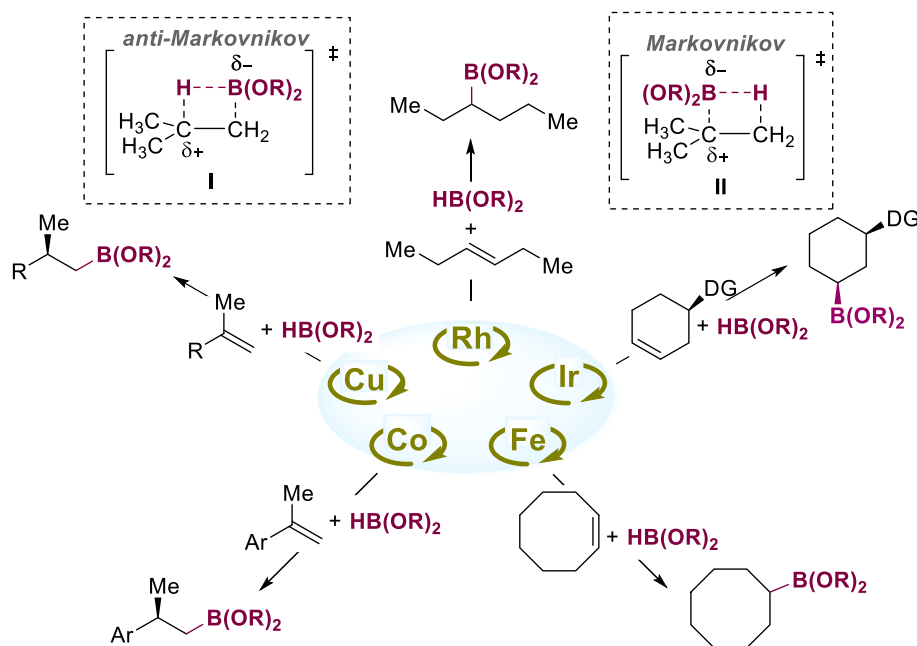


Figure 4.2.2. Metal-catalyzed hydroboration of alkenes.

4.2.3 Metal-catalyzed remote hydroboration of alkenes

In recent years, metal-catalyzed chain-walking reactions of olefins have offered a new manifold for enabling bond-formation at remote, yet previously unfunctionalized, sp^3 C–H bonds with an exquisite control of the regioselectivity profile (Chapter 1.2.3).¹⁹ In the absence of a functional group or directing group proximal to the alkene, an iterative series of β -hydride elimination/migratory insertion occurs, causing a dynamic displacement over the alkyl side-chain that locates the metal center at the terminal, primary sp^3 C–H site due to steric effects. This concept has been applied by Chirik, Stradiotto and Turculet, among others, allowing the establishment of a new rationale for triggering a remote borylation at distal sp^3 C–H bonds of an unsaturated hydrocarbon chain.^{20–23} Importantly, these authors showed that the interception of the metal secondary alkyl intermediate with HBpin, either by σ -bond metathesis or oxidative addition, is kinetically less favourable than the primary terminal metal-alkyl intermediate (Figure 4.2.3, B).

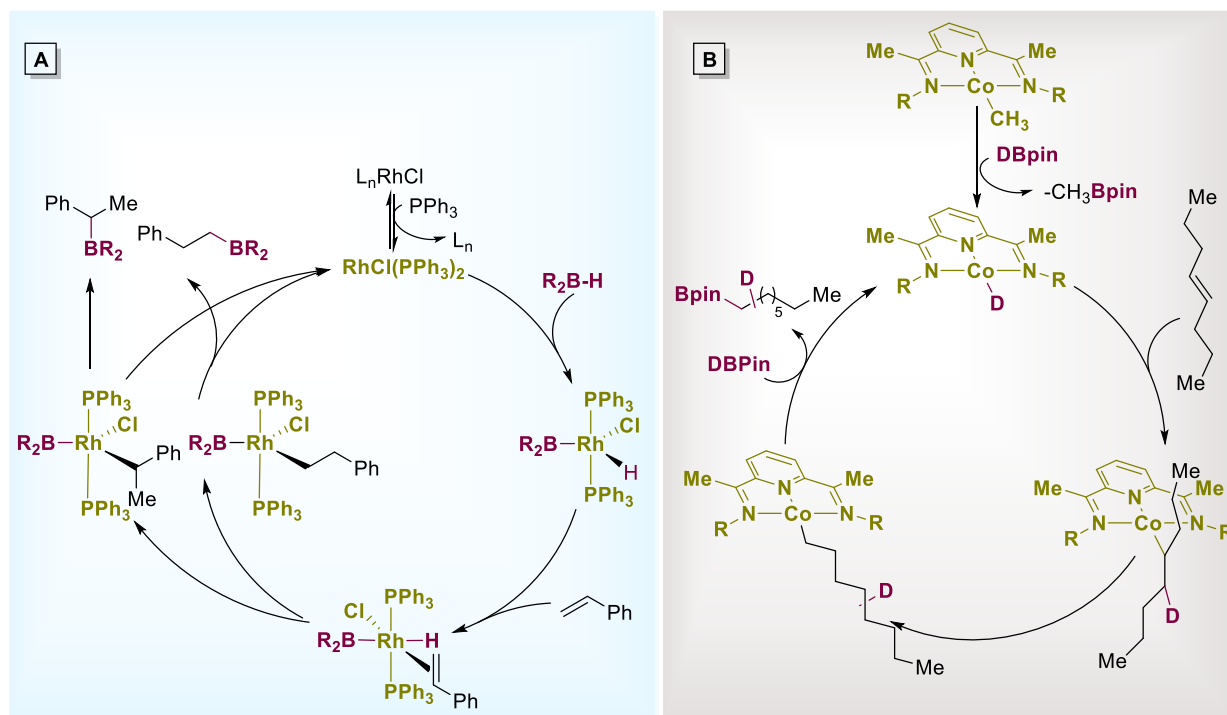


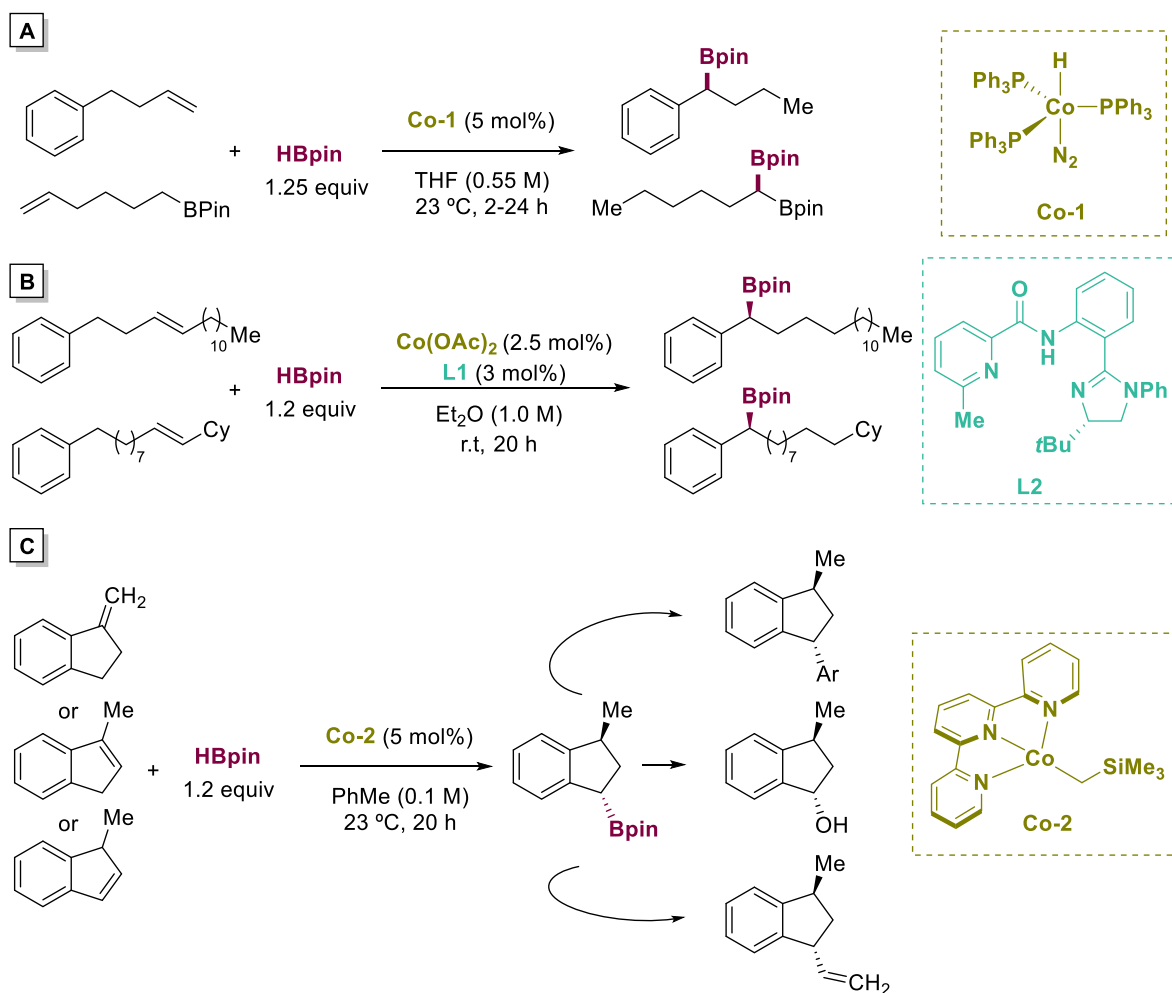
Figure 4.2.3. Formal hydroboration mechanism vs remote hydroboration mechanism.

4.2.3.1 Co-catalyzed site-selective hydroboration of alkenes

Given the intermediacy of discrete alkyl metal species in chain-walking reactions, one might argue whether these reactions could be directed in the presence of a suitable functional group within the alkyl side-chain. In line with this notion, Chirik's group described an interesting alkene isomerization-hydroboration promoted by cobalt catalysts supported by phosphine ligands (Scheme 4.2.1, A).²⁴ The authors found that the utilization of $(PPh_3)_3CoH(N_2)$ catalyst (**Co-1**) resulted in an excellent selectivity at the remote benzyl sp^3 C–H site. The selectivity of the reaction was attributed to electronic rather

Chapter 4

than steric effects, an observation that is correlated with the ability of sterically demanding redox-active α -diimine and bis(imino)pyridines to yield the borylation event at the terminal, primary sp^3 C–H bond. Notably, the methodology allowed for preparing 1,1-diboron compounds from readily available α,ω -dienes.²⁵



Scheme 4.2.1. Remote non-terminal hydroboration of internal & terminal alkenes.

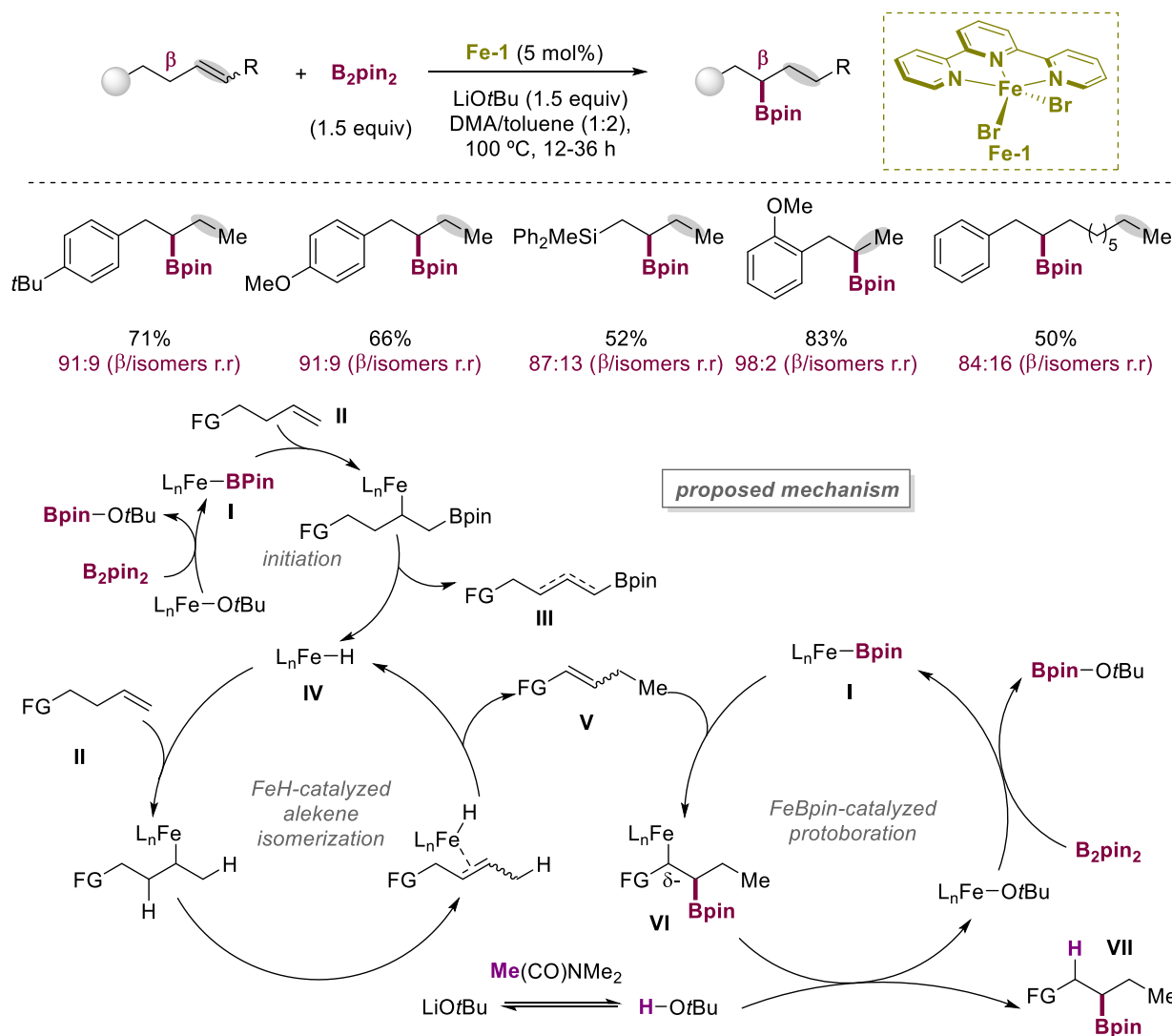
In 2018, Zhan Lu and co-workers reported an asymmetric remote C–H borylation of internal olefins *via* alkene isomerization by using simple $\text{Co}(\text{OAc})_2$ as catalyst (Scheme 4.2.1, B).²⁶ The transformation tolerated the presence of a great number of functional groups both on the phenyl ring and on the side chain, allowing isomerization of up to 8 positions along the hydrocarbon. In 2019, Chirik and co-workers reported a remote diastereoselective cobalt-catalyzed alkene isomerization-hydroboration of 2- and 3-substituted indenes (Scheme 4.2.1, C).²⁷ In this protocol, selective 1,3-*trans*-disubstituted indanyl boronic esters were obtained independently from the initial position of the alkene. The authors claimed that the regioselectivity followed a different mechanism than a classical anti-Markovnikov hydroboration due to the open coordination environment imparted to the cobalt center by the terpyridine ligand, thus lowering down the barrier for secondary C–B bond formation (Figure 4.2.3, B). While these contributions represented an interesting platform for

incorporating C–B atoms into side-chains, the means to incorporate these fragments at other unactivated positions still remains an elusive endeavour.

4.2.3.2 Fe-catalyzed site-selective hydroboration of alkenes

Similar to cobalt, other metals have been employed as catalysts for hydrofunctionalization reactions of alkenes, even at remote reaction sites. Among them, iron has attracted much attention for hydroborations of alkenes due to its low cost and abundance.¹⁰ Particularly illustrative are the contributions by Stradiotto, Sydora and Turculet on the utilization of cobalt- and iron-catalysts for the isomerization-hydroboration of branched alkenes at terminal sp^3 reaction sites.^{21,23} In 2020, Koh and co-workers developed the first catalytic regime that incorporated boryl groups at unactivated sites in olefins in the absence of strongly coordinating auxiliaries, triggering the borylation at the β -position^{28,29} (Scheme 4.2.2, *top*).³⁰ Similar to the work shown in Scheme 4.2.1, this reaction is enabled by the formation of a η^3 -benzyl intermediate. Notably, not only alkenes possessing arenes, but also silicon- and boron-containing motifs worked with similar ease. Later on, Koh's group was able to perform the reaction with olefins placed at distal positions within the side chain, achieving good yields and regioselectivities of the targeted boron compounds. Based on these empirical observations, the authors proposed a mechanism with an initiation step followed by two intertwined catalytic cycles (Scheme 4.2.2, *bottom*). The reaction begins with the addition of *in situ* generated iron-boryl species (**I**) across the alkene (**III**) followed by β -hydride elimination, furnishing iron-hydride intermediates (**IV**). This complex inserts into the olefin and, upon isomerization *via* chain-walking, the most stable olefin is released (**V**). This alkene is subsequently trapped by iron-boryl species en route to **VI**. Site-selectivity might arise from the stabilization of iron by the electron density at the α -position of the functional group (FG) and/or by steric repulsion between the Bpin and FG. Subsequently, protonolysis from the *tert*-butanol generated by the solvent leads to the final β -borylated product (**VII**), with turnover accomplished by reaction of the iron-boryl species (**I**) with the iron-*tert*-butoxide intermediate. Taking all these results into consideration, new strategies should be implemented for broadening even further the scope of the reaction, improving the functional group compatibility and to functionalize sites other than terminal positions or adjacent to functional groups.

Chapter 4



Scheme 4.2.2. Site-selective alkene borylation & proposed mechanism.

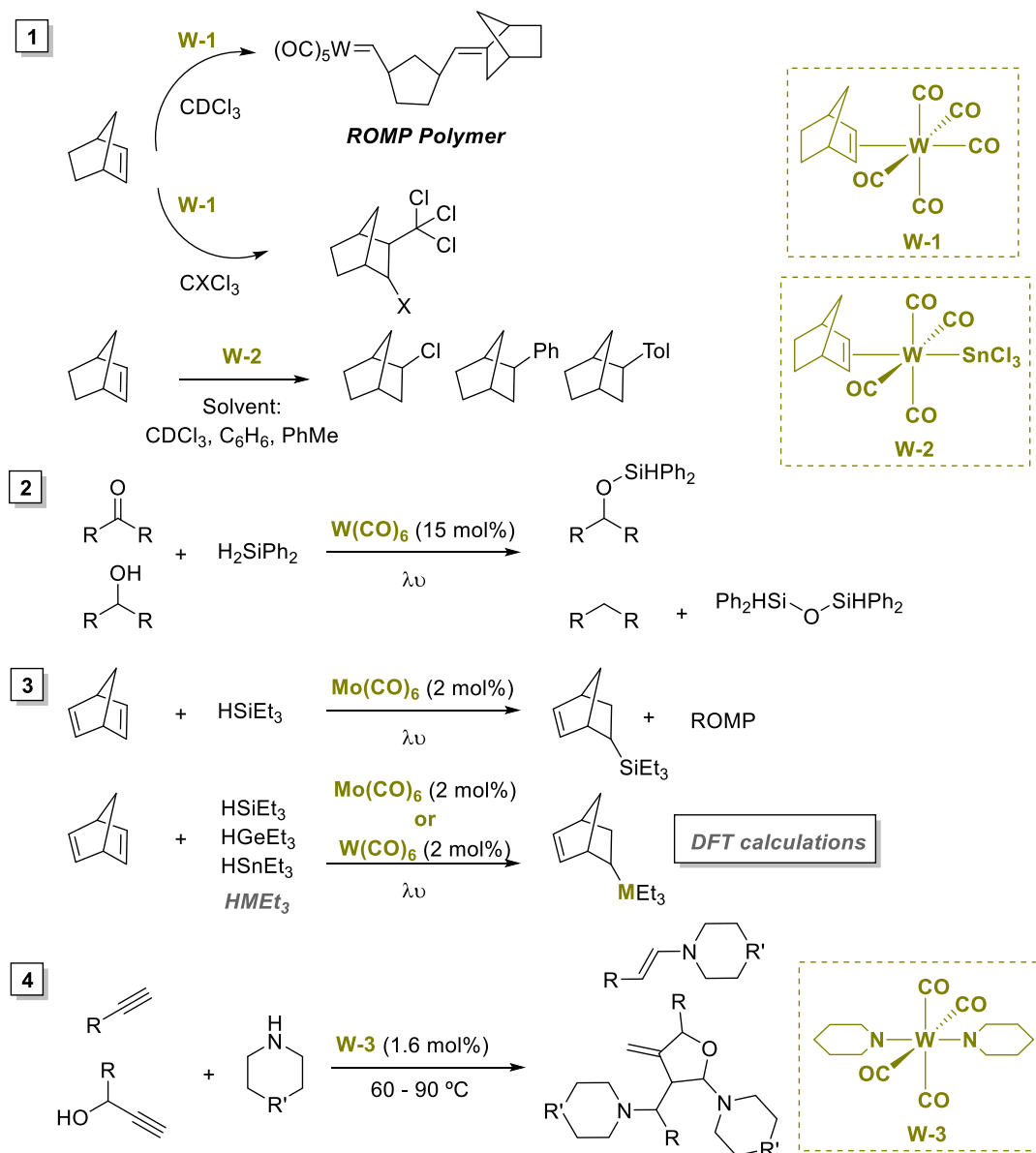
4.2.4 Tungsten as catalysts

Historically, tungsten has played an important role in the field of homogeneous catalysis, though its use has been limited to a few specific reaction types, including alkene/alkyne metathesis³¹ and polymerization of alkenes/alkynes,³² among others. These applications employ tungsten in high oxidation states (e.g., +6), where the overall reaction is redox-neutral. In these reactions, the metal center is generally Lewis acidic and oxophilic, features that make these reactions particularly sensitive to air, moisture and other Lewis basic functional groups. These limitations notwithstanding, the low cost (~10³ cheaper than Rh, Ir, or Pd), low toxicity, and ease of preparation of many tungsten catalysts make them particularly attractive as catalysts for industrial applications.

4.2.4.1 Hydrofunctionalization reactions using tungsten catalysis

Pioneering reports by Szymanska-Buzar demonstrated the ability of tungsten catalysts to trigger hydrofunctionalization of alkenes and alkynes. The authors reported an intriguing reactivity profile

of norbornene carbonyl complexes, obtaining different products depending on the reaction conditions and the reagents employed (Scheme 4.2.4, 1).³³ Ring Opening Metathesis Polymerization (ROMP) and selective addition of CHCl_3 , CDCl_3 or, CCl_4 to norbornene were found depending on the solvent and reaction conditions used in the presence of **W-1**. Interestingly, the Lewis acidic complex **W-2** catalyzed the C–H arylation of norbornene at room temperature using simple arenes such as benzene in solvent quantities, paving the way for triggering new reactivity principles within the general area of tungsten catalysis (4).



Scheme 4.2.4. Tungsten catalyzed hydrofunctionalization of alkenes & alkynes.

Tungsten has been shown to be particularly suited for triggering hydrosilylation of ketones and dehydrosilylation of alcohols with simple $\text{W}(\text{CO})_6$ catalysts (Scheme 4.2.4, 2).³⁴ This proof of concept established applications for the activation of the Si–H bond by the catalyst under photochemical conditions. Prompted by the ability of molybdenum catalysts to trigger hydrofunctionalization

Chapter 4

reactions,^{35,36} DFT studies were performed to understand the behaviour of Mo and related W in these processes (Scheme 4.2.4, 3).³⁷ These studies showed an endergonic oxidative addition to X–H bonds (X = Sn, Ge, Si) (11-13 kcal/mol), thus preventing the reaction of the resulting complexes with alkenes abandoning further investigations. Tungsten catalysts have also been employed in hydroamination of alkynes (Scheme 4.2.4, 4).^{38,39} The authors obtained an *anti*-Markovnikov selectivity, resulting in *E*-isomers for terminal alkynes using W(0) catalysts (**W-3**). However, tetrahydrofurans were obtained when using propargylic alcohols after a double rearrangement with the cyclic amine. The observed reactivity is likely attributed to the propensity of W(0) to form alkylidenes with terminal alkynes. However, the hydrofunctionalization of alkenes remained unknown with W(0) and carbene intermediates.

4.2.4.2 Tungsten possibilities

Despite the advances in low valent tungsten catalysis, its application in catalytic endeavors is still in its infancy. It is worth noting, however, that the potential to enable olefin isomerization is known since the mid 70's.⁴⁰ The attenuated reactivity of W towards the activation of X–H bonds may prove to be beneficial for allowing complementary regioselectivity profile to that shown by other transition metals in chain-walking reactions.

4.3 Remote Hydroboration of Alkenes Catalyzed by Tungsten Complexes

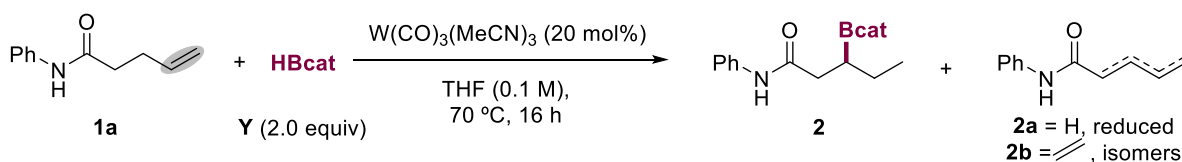
4.3.1 Aim of the project

While significant progress has been made in remote functionalization of sp^3 C–H bonds by means of chain-walking reactions, the vast majority of these processes rely on C–C bond-forming reactions at a specific location within the alkyl side-chain. Driven by the unique reactivity of tungsten and its abundance compared to other transition metals, we wondered whether we could employ simple tungsten catalysts within the context of remote functionalization of olefins, allowing us to forge C–B bonds at unconventional sp^3 C–H sites.

4.3.2 Optimization of the reaction conditions

This work was initiated during my predoctoral stage at Scripps, San Diego, under the supervision of Prof. Keary Engle in 2019. Specifically, the project was aimed at triggering a remote W-catalyzed hydroboration of terminal alkenes at the β -position of a weakly coordinating directing group, thus representing the first example of a remote functionalization of unconventional unactivated sp^3 C–H reaction sites by tungsten catalysis. We began our investigations by using **1a** as substrate and the influence of the alkene, boron source and catalyst was explored (Table 4.3.1). Based on Engle's group experience, the presence of an amide could serve as a directing group by coordination to the catalyst. Interestingly, we obtained preliminary encouraging results by using commercially available $W(CO)_3(MeCN)_3$ as catalyst (entry **1**). In order to confirm the structure of the final product, the

organoboron compound was transformed into the corresponding alcohol by conventional oxidation techniques. The formation of the reduced compound (**2a**) and the isomerization of the alkene along the side chain (**2b**) accounted for the mass balance of the reaction. Importantly, many of these results gave >50:1 regioselectivity. Interestingly, we observed a similar reactivity profile when using $\text{Mo}(\text{CO})_3(\text{MeCN})_3$ as catalyst (entry **2**), whereas the use of light irradiation had a deleterious effect on the reaction outcome, thus likely coming from decomposition of the catalyst (entries **3-6**).



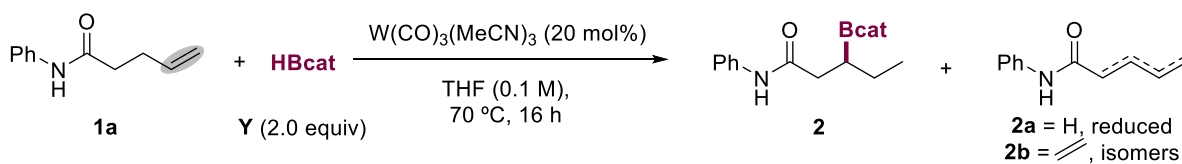
Entry	Deviation from standard conditions	Conv. (%)	2 (%)	2a (%)	2b (%)
1	None	86	42	26	14
2	$\text{Mo}(\text{CO})_3(\text{MeCN})_3$	80	38	24	16
3	$\lambda\nu$ at rt	75	12	22	19
4	$\lambda\nu$ at rt, MeCN (0.1 M)	41	6	10	10
5	$\text{Mo}(\text{CO})_3(\text{MeCN})_3$ $\lambda\nu$ at rt	52	4	13	8
6	$\text{Mo}(\text{CO})_3(\text{MeCN})_3$ $\lambda\nu$ at rt, MeCN (0.1 M)	21	3	9	6

Reaction conditions: **1a** (0.1 mmol), **Y** (2.0 equiv), $\text{W}(\text{CO})_3(\text{MeCN})_3$ (20 mol%), solvent (1.0 mL), 70 °C, 16 h. GC conversion and yields using decane as internal standard.

Table 4.3.1. First screening of a remote hydroboration reaction of alkenes.

With these conditions in hand, we next turned our attention to studying the effect of the boron source (Table 4.3.2). As shown, both HBcat and HBpin showed a similar trend (entries **1-9**). Although poor yields were obtained at room temperature, these conditions led to low amounts of isomeric products (**2b**) (entries **4** and **9**). The utilization of aminoborane reagent HBdan did not afford any traces of desired product, likely due to steric and/or electronic effects (entry **10**). Quite illustrative, a control reaction was performed in the absence of the tungsten catalyst that delivered mixtures of both **2a** and **2b** sideproducts, and *anti*-Markovnikov product with no traces of β -hydroboration (entry **11**).

Chapter 4

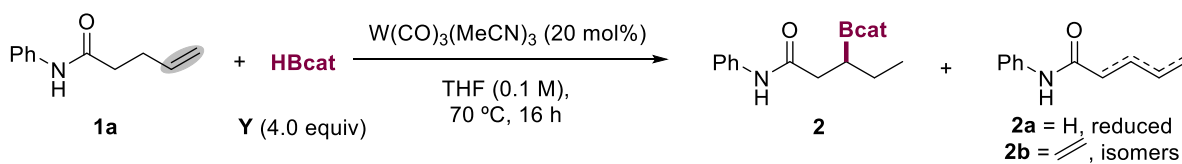


Entry	Deviation from standard conditions	Conv. (%)	2 (%)	2a (%)	2b (%)
1	HBcat (3.0 equiv)	100	65	16	16
2	HBcat (4.0 equiv)	100	74	13	13
3	HBcat (5.0 equiv)	100	75	13	12
4	HBcat (3.0 equiv), rt	52	32	16	2
5	HBpin (2.0 equiv)	40	18	22	0
6	HBpin (3.0 equiv)	49	28	21	0
7	HBpin (4.0 equiv)	82	42	40	0
8	HBpin (5.0 equiv)	100	43	46	0
9	HBpin (3.0 equiv), rt	25	10	16	0
10	HBdan (3.0 equiv)	21	0	15	5
11	No $W(CO)_3(MeCN)_3$	53	0	16	8

Reaction conditions: **1a** (0.1 mmol), **Y** (2.0 equiv), $W(CO)_3(MeCN)_3$ (20 mol%), THF (1.0 mL), 70 °C, 16 h. GC conversion and yields using decane as internal standard.

Table 4.3.2. Boron source and equivalents screening.

Next, we examined the influence of different tungsten and molybdenum catalysts at different concentrations (Table 4.3.3). However, none of the catalysts analyzed improved the reactivity of the borylation event when compared with previous conditions (entries **1-8** and **10-11**). While slightly better results were found at higher concentrations (entries **1-8**), higher yields were found by lowering the catalyst loading to 5 mol% (entry **9**).



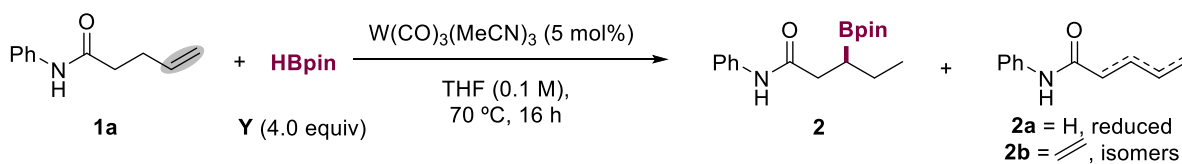
Entry	Deviation from standard conditions	Conv. (%)	2 (%)	2a (%)	2b (%)
1	$W(CO)_4(MeCN)_2$ (0.5 mL)	72	48	12	11
2	$W(CO)_4(MeCN)_2$ (1.0 mL)	100	56	13	13
3	$W(CO)_4(MeCN)_2$ (1.5 mL)	100	56	14	13
4	$W(CO)_3(MeCN)_3$ (0.5 mL)	100	76	10	10
5	$W(CO)_3(MeCN)_3$ (1.5 mL)	100	61	22	13
6	$Mo(CO)_3(MeCN)_3$ (0.5 mL)	100	65	21	11
7	$Mo(CO)_3(MeCN)_3$ (1.0 mL)	100	72	16	10
8	$Mo(CO)_3(MeCN)_3$ (1.5 mL)	100	71	16	10
9	$W(CO)_3(MeCN)_3$ (5 mol%)	100	76	10	11
10	$Mo(CO)_3(PrCN)_3$	100	46	18	9
11	$W(CO)_3(PrCN)_3$	100	51	17	11

Reaction conditions: **1a** (0.1 mmol), **Y** (4.0 equiv), $W(CO)_3(MeCN)_3$ (20 mol%), THF (1.0 mL), 70 °C, 16 h. GC conversion and yields using decane as internal standard.

Table 4.3.3. Screening of W and Mo catalyts.

Our attempts to isolate the final product revealed an inherent instability of the borylated product, a result of competing decomposition pathways during column chromatography and the need for converting the catechol borane into the more robust Bpin derivative. Therefore, we anticipated that the best-case scenario would be the employment of HBpin as the boron reagent. In this manner, we will make use of the inherent potential of the resulting alkylBPin reagents that can be further functionalized. Interestingly, we found that 5% of catalyst performed equally well (Table 4.3.4, entry **1**). After testing different solvents, equivalents of HBpin and different temperatures (entry **2-6**), we found that the concentration of the reaction was critical for success, delivering the targeted borylation in good yields (entry **3**).

Chapter 4

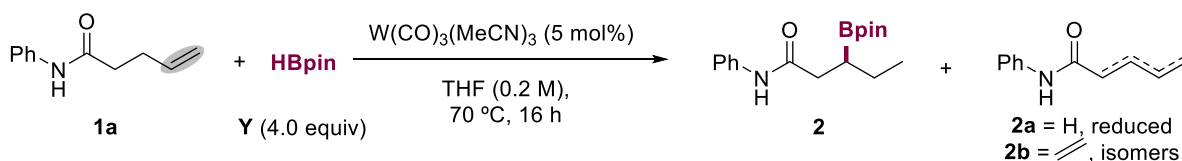


Entry	Deviation from standard conditions	Conv. (%)	2 (%)	2a (%)	2b (%)
1	None	95	41	42	3
2	THF (2.0 mL)	94	25	68	3
3	THF (0.5 mL)	100	65	32	1
4	HBpin (2 equiv) and 100 °C	50	12	30	6
5	Dioxane (1.0 ml)	30	3	25	3
6	Me-THF (1.0 ml)	20	1	0	11

Reaction conditions: **1a** (0.1 mmol), **Y** (4.0 equiv), $W(CO)_3(MeCN)_3$ (5 mol%), THF (1.0 mL), 70 °C, 16 h. GC conversion and yields using decane as internal standard.

Table 4.3.4. Screening with HBpin.

An improved **2:2a** ratio was found by conducting the reaction with just 0.20 mL of solvent (entry **1**). Remarkably, the reaction performed similarly well at 2 mol% catalyst loading (entries **2** & **3**). Gathering all the data, one might argue that the observed reactivity might be attributed to the intermediacy of an α,β -unsaturated compound prior to the C–B bond-formation step. To this end, we conducted the reaction in the absence of tungsten catalyst but using the hypothetical acrylamide intermediate. As shown in entries **4** and **5**, the reaction did not deliver the product, although trace amounts of **2a** were obtained at 40 °C whereas quantitative formation of the latter was found at 70 °C. These two entries indicate that the catalyst is needed to promote the β -hydroboration and it does not serve as a mere isomerization source for the alkene.

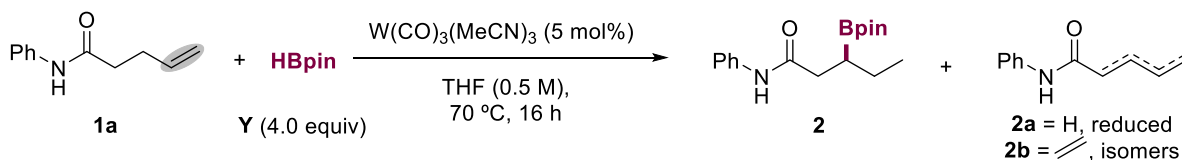


Entry	Deviation from standard conditions	Conv. (%)	2 (%)	2a (%)	2b (%)
1	THF (0.2 mL)	100	78	20	0
2	$W(CO)_3(MeCN)_3$ (2 mol%) and THF (0.2 mL)	96	66	30	1
3	$W(CO)_3(MeCN)_3$ (2 mol%)	100	52	38	2
4	No W, 40 °C	0	0	5	0
5	No W, 70 °C	100	0	96	2

Reaction conditions: **1a** (0.1 mmol), **Y** (4.0 equiv), $W(CO)_3(MeCN)_3$ (5 mol%), THF (0.5 mL), 70 °C, 16 h. GC conversion and yields using decane as internal standard.

Table 4.3.5. Screening of concentrations & control reactions.

In light of these results, we wondered if subtle modification of the reaction conditions would allow us to improve the selectivity while minimizing the formation of side-reactions (Table 4.3.6). Unfortunately, no improvement was found by the addition of the boron source in multiple batches or by its slow addition with a syringe pump. Notably, the reaction behaved equally well at low concentrations (entry **3**), whereas excellent yields were accomplished at 40 °C (entries **4-8**).



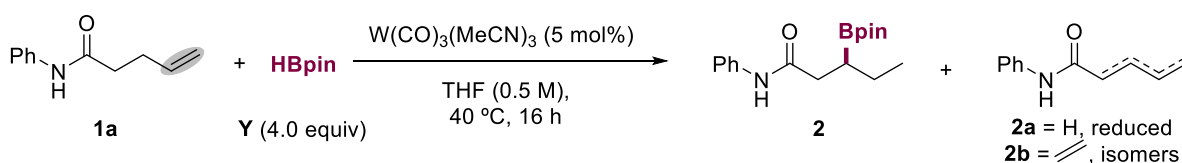
Entry	Deviation from standard conditions	Conv. (%)	2 (%)	2a (%)	2b (%)
1	HBpin (2 equiv + 2 equiv 2 h later)	71	31	20	25
2	HBpin (Syringe pump addition)	89	46	23	14
3	THF (0.1 mL)	100	79	20	0
4	50 °C	50	12	30	6
5	40 °C	94	90	4	0
6	30 °C	68	42	2	20
7	30 °C using 10% [W]	76	58	2	15
8	50 °C and 3 equiv of HBpin	98	72	9	9

Reaction conditions: **1a** (0.1 mmol), **Y** (4.0 equiv), $W(CO)_3(MeCN)_3$ (5 mol%), THF (0.2 mL), 70 °C, 16 h. GC conversion and yields using decane as internal standard.

Table 4.3.6. Further reaction optimization.

Chapter 4

Subsequently, we studied at the influence of other reaction parameters (Table 4.3.7). As shown, similar results were found by conducting the reaction for different durations (entries **1** & **2**). The reaction could not be improved at high catalyst loadings or at higher temperatures (entries **3** and **4**). However, quantitative yields were found by adjusting the concentration of the reaction (entry **5**). Importantly, no β -hydroboration was found by performing the reaction in the absence of the W catalyst, with the mass balance accounted for by the formation of small amounts of *anti*-Markovnikov and Markovnikov products (entry **6**). Although we tested the inclusion of a variety of ligands, none of these proved to be beneficial for the reaction outcome (entries **7-9**).



Entry	Deviation from standard conditions	Conv. (%)	2 (%)	2a (%)	2b (%)
1	20 h	95	90	4	0
2	24 h	95	90	4	0
3	W(CO) ₃ (MeCN) ₃ (7.5 mol%)	100	79	20	0
4	45 °C	96	76	16	0
5	1a (0.2 mmol) in THF (0.3 mL)	100	98	0	0
6	No W catalyst	20	0	5	0
7	PCy ₃ (10 mol%)	18	10	8	0
8	<i>i</i> Pr-NHC (10 mol%)	6	0	4	2
9	4,4-dtbpy (10 mol%)	13	0	7	3

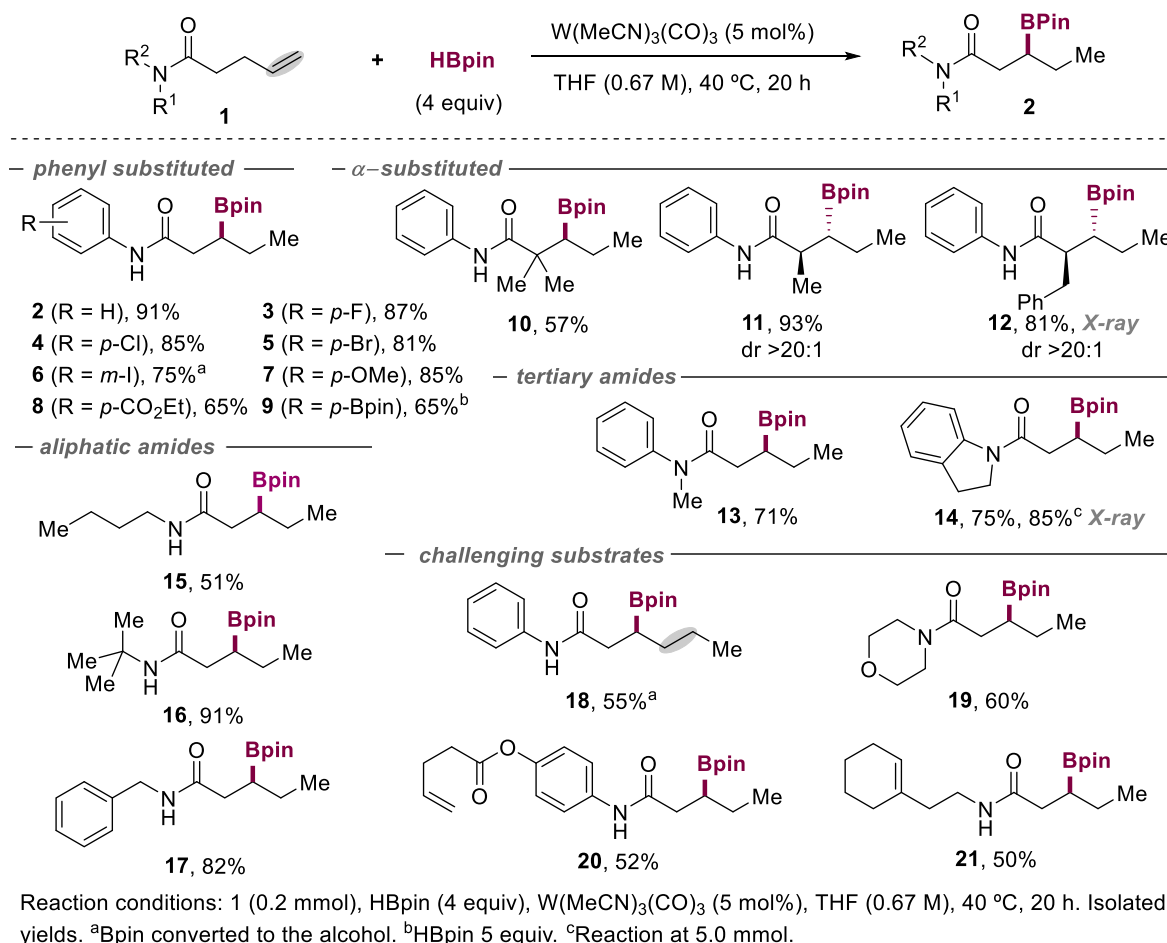
Reaction conditions: **1a** (0.1 mmol), **Y** (4.0 equiv), W(CO)₃(MeCN)₃ (5 mol%), THF (0.2 mL), 40 °C, 16 h. GC conversion and yields using decane as internal standard.

Table 4.3.7. Further optimization to achieve full conversion of the starting material.

4.3.3 Substrate scope

Encouraged by these results, we next turned our attention to studying the preparative scope of this reaction with a wide number of different alkenes (Scheme 4.3.1). As shown, electron-donor (**7**), electron-withdrawing (**8**) and organoboron functional groups (**9**) were found to be accommodated in this transformation. In addition, the presence of halogen atoms (**3-6**) did not interfere with productive C–B bond-formation. This finding is particularly important, offering not only the possibility of triggering orthogonal cross-coupling reactions in the presence of halide congeners, but also a complementary reactivity mode with Ni or Pd catalysis, as these metal species would likely enable the cleavage of the corresponding sp^3 C–halide bond.

Next, we investigated the influence of the substitution pattern adjacent to the carbonyl group. As shown in Scheme 4.3.1, α -substituted derivatives **10** and **11** could be obtained in good to excellent yields. The inclusion of a benzyl group (**12**) was perfectly tolerated, obtaining a good diastereoselectivity of the targeted product (>20:1). In this case, X-ray crystallography unequivocally identified an anti-stereochemistry pattern of the final product. Our available literature data revealed that the borylation could effectively be promoted with free N–H groups, but it left a reasonable doubt on whether this motif was critical for success. As shown by the successful preparation of **13** and **14**, this was not the case and tertiary amides could equally be employed as substrates.⁴¹ The identity of **14** was confirmed by X-ray crystallography. Moreover, a gram scale reaction was carried out to test the viability of the methodology as well as the robustness in higher catalyst and substrate amounts affording an even greater yield of **14** (85% yield).



Scheme 4.3.1. *W*-catalyzed remote C(sp³)–H hydroboration of alkenes.

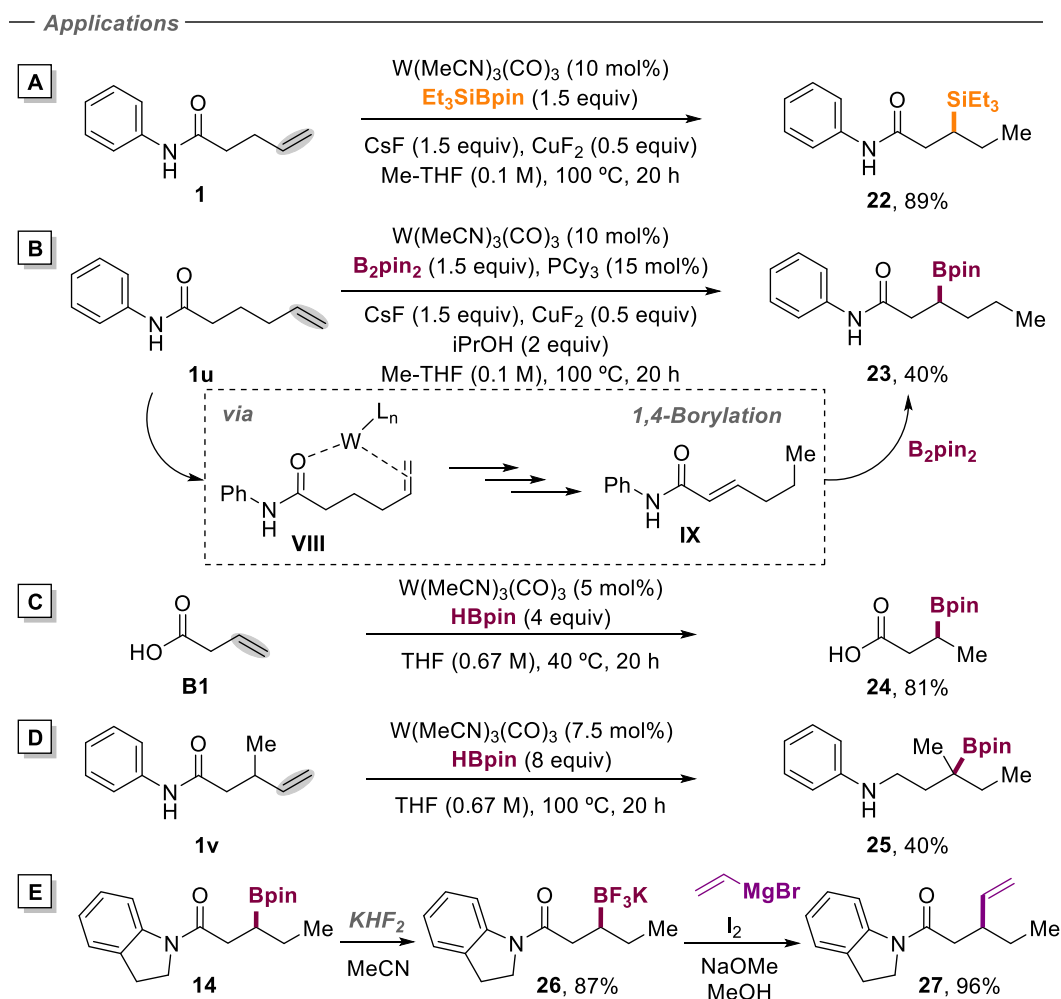
Gratifyingly, we found that the remote hydroboration is not limited to aromatic amides but it could be applied to aliphatic amides (**15–17**). Finally, we decided to test the suitability of our reaction with a series of challenging substrates to assess the selectivity, robustness and simplicity of the current protocol. Importantly, the utilization of internal alkenes afforded exclusively the corresponding β -hydroboration in moderate yields (**18**). In other hand, the utilization of bioactive

Chapter 4

morpholine derivatives allowed the formation of the borylated product in good yield (**19**). Amides possessing a pendent alkene exclusively resulted in β -hydroboration with respect to the amide group, while leaving the other alkene completely untouched (**20**, **21**). This result is particularly important, offering an opportunity that is beyond reach with other transition metals that otherwise would have resulted in competitive hydrofunctionalization of the other alkene moiety.

4.3.4 Applicability of W-catalysis

Next, we turned our attention to study the applicability of our W-catalyzed transformation. Based on our experience in catalytic silylation reactions,^{42,43} we wondered whether utilization of silylating reagent Et₃SiBpin might trigger an otherwise related silylation event at the β -position (Scheme 4.3.2, A, **22**). As shown, the reaction could be conducted with similar ease in the presence of fluoride sources, obtaining the targeted product with an exquisite regioselectivity profile. Moreover, we decided to tackle the challenge of promoting the β -borylation event with longer alkene side-chains (Scheme 4.3.2, B). Unfortunately, the reaction was not observed under the standard conditions with **1u**. After some experimentation, a cocktail similar to A was applied, finding out that the targeted borylation could be within reach (**23**), but in moderate yields, suggesting that the coordination of the catalyst to the amide backbone might be an important factor for success in the targeted borylation. In this case, an α,β -unsaturated carbonyl compound is likely formed followed by a 1,4-borylation in the presence of copper species (See SI for more information).



Scheme 4.3.2. Applications of tungsten catalysis.

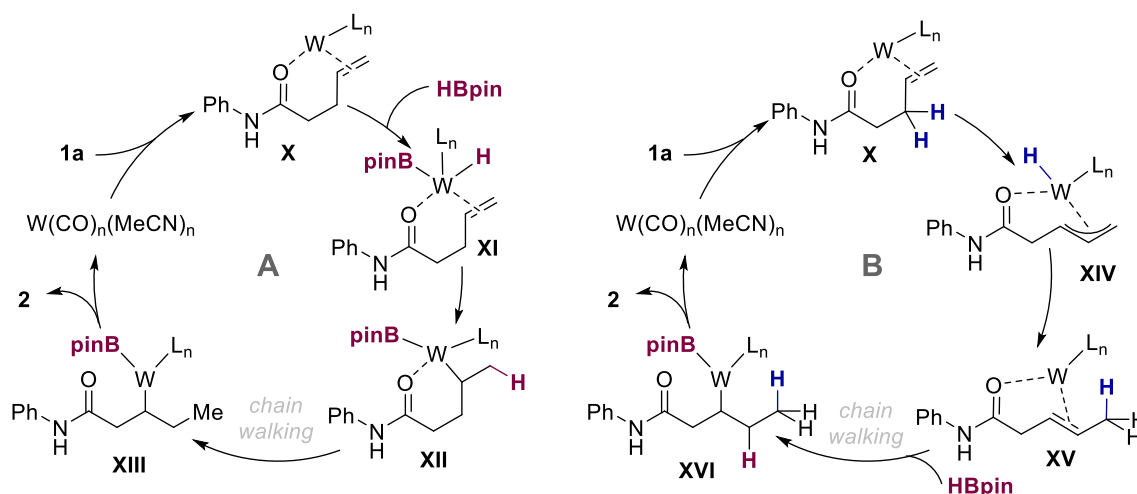
At first sight, one might argue that our reaction could be limited to alkenes containing amide-side chains. However, we found that carboxylic acids (**B1**) could be used for similar purposes, resulting in **24** in good yields (Scheme 4.3.2, C), thus suggesting that the carboxylic acid might serve as a directing group for triggering a borylation event. In addition, quaternary borylated centers could be within reach (**25**); in this case, after the borylation takes place, the high temperature and equivalents of HBpin triggered a reduction of the carbonyl group delivering the final amine bearing a fully substituted borylated center.^{44,45} Finally, we decided to test the applicability of the reaction to a downstream manipulation by synthesizing trifluoroborate salts (**26**) and reacting it with vinyl magnesium bromide in the presence of iodine and NaOMe. This sequence delivered product **27** in 96% yield.

4.3.5 Mechanistic proposal

A priori, we conceived two conceivable mechanistic pathways which account for the observed reactivity: A) coordination of the alkene (**X**) to the catalyst followed by an oxidative addition into the HBpin, thus generating tungsten-hydride species (**XI**). Upon olefin insertion/ β -hydride elimination

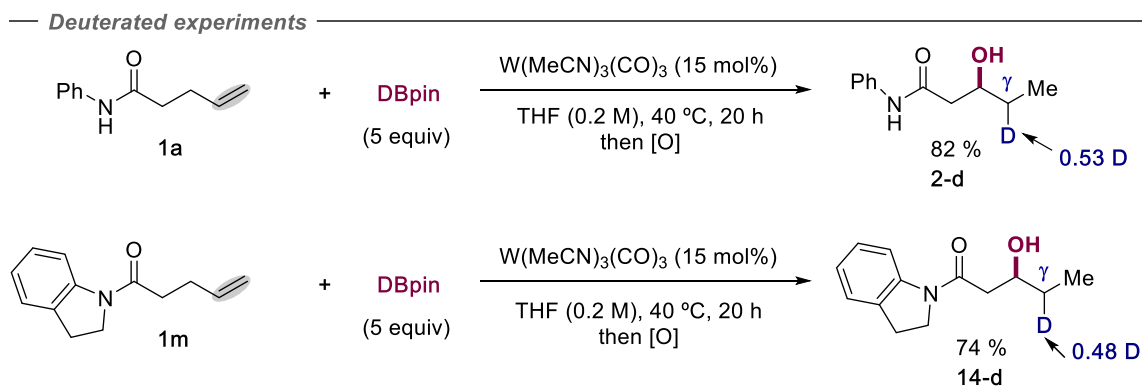
Chapter 4

sequence (**XII**), and reductive elimination (**XIII**) delivers the desired product **2** (Scheme 4.3.3, A). B) a 1,3-hydride shift mechanism might occur with the catalyst coordinating the alkene (**X**) and subsequently abstracting a hydride from the allylic position. The newly formed allyl-tungsten hydride species (**XIV**) undergoes hydride insertion at the other terminus of the allyl species, thus forming the β/γ alkene intermediate (**XV**). Next, oxidative addition into the HBpin, olefin insertion into the W–H bond (**XVI**) and reductive elimination releases the borylated product (Scheme 4.3.3, B).



Scheme 4.3.3. Possible mechanisms for the tungsten catalyzed remote hydroboration.

Although more experimental and computational studies are needed to establish the mechanism profile of this transformation, preliminary deuterium-labelling experiments have been carried out. Specifically, DBpin was synthesized and reacted with **1a** and **1m** (Scheme 4.3.4), resulting in 53% and 48% deuteration at γ position, respectively, indicating that the mechanism might follow the path **B** shown in scheme 4.3.3. This proposal is in line with the slow oxidative addition reported for $W(0)$ species.^{37,46} However, further kinetic isotope studies still need to be conducted to provide a stronger evidence for pathway **B**.



Scheme 4.3.4. Deuterium-labelling.

4.3.6 Future outlook

Although this chapter is not yet finished and subject of ongoing investigations, it is worth mentioning future objectives and scenarios that could be envisioned in this arena:

- A. *Site-selectivity at unactivated sp^3 positions.* In view of our results, one might perfectly wonder whether we could extend our β -hydroboration catalyzed by tungsten catalysts to other positions within the alkyl side-chain. This could *a priori* be executed in the presence of other directing groups and modular ligands that might prevent the reaction from occurring at the β -position.
- B. *Extension to longer alkyl chain lengths and to other substrates.* A close look at our technology reveals that the protocol is somewhat limited to amides or carboxylic acids with specific hydrocarbon alkyl side-chains. That being set, a particularly attractive endeavour would be the extension of this methodology beyond the utilization of these carbonyl groups and also the ability to trigger chain-walking scenarios with longer alkyl side-chains without a significant erosion in yield and site-selectivity.
- C. *C–C bond formation.* While we have shown the ability of tungsten catalysts to trigger a borylation at the β -position, this technology should by no means be limited to C–B bond-formation. Therefore, future efforts will be directed to the development of C–C bond-forming reactions aided by the ability of tungsten catalysts to trigger chain-walking events.

4.4 Conclusions

Overall, we have documented a catalytic strategy that enables a remote directed β -hydroboration of unactivated C–H bonds by means of tungsten catalysis. Such protocol offers a complementary reactivity mode for promoting the functionalization at unactivated sp^3 C–H sites of alkyl side-chains, thus leading to a different strategy mode than those proposed for related Pd-, Ni- or Co-catalyzed chain-walking reactions. Interestingly, this protocol can be applied across a wide range of alkenes possessing different carbonyl-type compounds, including highly substituted amide backbones. The ability to enable a β -borylation of simple carbonyl compounds possessing alkene side-chains with an exquisite site-selectivity pattern is particularly attractive, opening a new gateway for future applications of this technology. Although preliminary studies have been performed, more experiments are still required to unravel the intricacies of these processes.

Chapter 4

4.5 Experimental procedures

4.5.1 General considerations

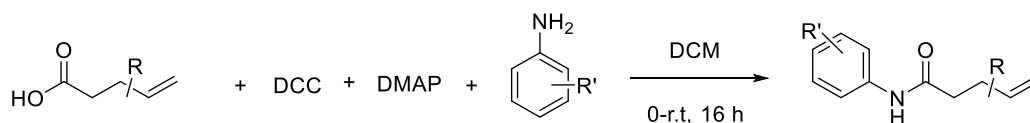
Reagents. Commercially available materials were used as received without further purification: $W(CO)_3(MeCN)_3$ (99% purity) was purchased from Aldrich. 4,4,5,5-Tetramethyl-1,3,2-dioxaborolane (97% purity) was purchased from Aldrich. Anhydrous tetrahydrofuran (THF, 99.5% purity) and anhydrous 2-methyltetrahydrofuran (2-MeTHF, 99.5% purity) were purchased from Across.

Analytical methods. 1H and ^{13}C NMR spectra were recorded on Bruker 300 MHz, Bruker 400 MHz and Bruker 500 MHz at 20 °C. All 1H NMR spectra are reported in parts per million (ppm) downfield of TMS and were calibrated using the residual solvent peak of $CHCl_3$ (7.26 ppm), unless otherwise indicated. All ^{13}C NMR spectra are reported in ppm relative to TMS, were calibrated using the signal of residual $CHCl_3$ (77.16 ppm), ^{11}B NMR and ^{19}F NMR were obtained with 1H decoupling unless otherwise indicated. Coupling constants, J , are reported in Hertz. Melting points were measured using open glass capillaries in a Büchi B540 apparatus. Gas chromatographic analyses were performed on Hewlett-Packard 6890 gas chromatography instrument with an FID detector. Flash chromatography was performed with EM Science silica gel 60 (230-400 mesh). Thin layer chromatography was used to monitor reaction progress and analysed fractions from column chromatography. To this purpose TLC Silica gel 60 F₂₅₄ aluminium sheets from Merck were used and visualization was achieved using UV irradiation and/or staining with Potassium Permanganate or Cerium Molybdate solution. The yields reported in Scheme 4.3.2.1 and 2 refer to isolated yields. The procedures described in this section are representative. In the cases the High-Resolution Mass Spectra of the molecular ion could not be obtained using ESI and APCI ionization modes the GC-MS of the compound was given.

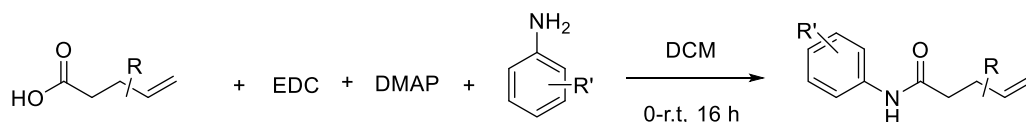
4.5.2 Optimization of the reaction conditions

General procedure: An oven-dried 8 mL screw-cap test tube containing a stirring bar was charged with the alkene (**1a**, 35 mg, 0.20 mmol). The test tube was introduced in an argon-filled glovebox where $W(CO)_3(MeCN)_3$ (3.8 mg, 5 mol%) was subsequently added followed by addition of THF (0.3 mL, 0.67 M). Then HBpin was introduced (118 μ l, 4 equiv) and the tube was taken out of the glovebox and stirred at 40 °C for 20 h. After diluting with EtOAc (10 mL) the yields were determined by GC FID analysis using decane as internal standard. The sample was purified by column chromatography on silica gel (Hexane/ EtOAc 8/2).

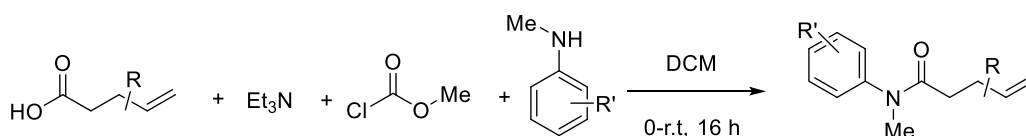
4.5.3 Synthesis of alkene amides



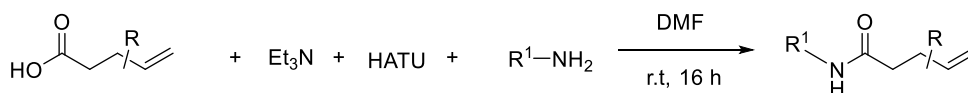
General Procedure A: a solution of the corresponding acid (1.0 equiv), primary amine (1.1 equiv) and DMAP (10 mol%) in DCM (0.33 M) was cooled to 0 °C. Subsequently, DCC (1.5 equiv) was added to the reaction and the bath was removed leaving the reaction stirring overnight. Aqueous HCl (1 M) was then added (2 times) and stirred vigorously. The organic layer was separated and then washed with sat. aq. NaHCO₃ and brine (3 times). Finally, the organic phase was dried with MgSO₄ and the solvent was evaporated with the rotavapor. Flash column chromatography, was performed eluting with Hexane/EtOAc mixtures.



General Procedure B: A round-bottomed flask was charged with DCM (25 mL, 0.4 M), EDC-HCl (1-(3-dimethylaminopropyl)-3-ethylcarbodiimide hydrochloride, 13 mmol, 1.3 equiv), and DMAP (14 mmol, 1.4 equiv). The reaction flask was cooled to 0 °C in an ice-bath and the carboxylic acid (10 mmol, 1.0 equiv) was added. After five minutes of stirring, the substituted aniline (12 mmol, 1.2 equiv) was added. The ice-bath was then removed and the reaction allowed to stir for 16 hours at r.t. Then, the reaction was quenched with 1M aq. HCl (25 mL) and the organics separated. The aqueous layer was then extracted with DCM (2 x 25 mL). The organic layers were combined and dried over MgSO₄ and concentrated. The crude product was purified by silica gel column chromatography.

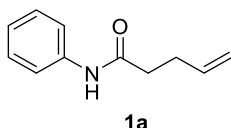


General Procedure C: a solution of the corresponding acid (1.0 equiv) and Et₃N (4.2 equiv) in THF (0.4 M) was cooled to 0 °C. Then methyl chloroformate (1 equiv) was added dropwise and stirred during 10 minutes at 0 °C. Subsequently, a solution of the secondary amine in THF (3 M) was added to the reaction mixture. The ice-bath cooled solution was stirred for 60 minutes then the precipitate formed was filtered off and the solution concentrated under vacuum. The crude was purified by flash column chromatography using Hexane/EtOAc mixtures.

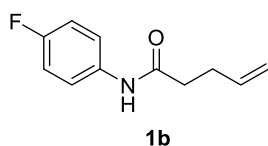


Chapter 4

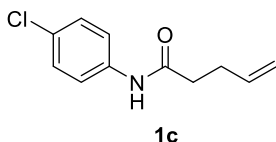
General Procedure D: HATU (1.2 equiv) was added to a solution of the appropriate carboxylic acid (1.0 equiv), primary amine (1.2 equiv) and Et₃N (2.4 equiv) in DMF (0.2 M). The reaction was left stirring overnight at r.t. Then, quenched with aq. NaOH 1M and extracted with DCM. Finally, the organic phase was dried with MgSO₄ and the solvent was evaporated with the rotavapor. Flash column chromatography, was performed eluting with Hexane/EtOAc mixtures.



N-(4-methoxyphenyl)pent-4-enamide (1a). Following the General Procedure A, 4-pentenoic acid (0.5 mL, 4.89 mmol), aniline (0.39 mL, 5.38 mmol), DMAP (61 mg, 0.48 mmol) and DCC (1.03 g, 7.34 mmol) in 15 mL of DCM were used, affording the product as a white solid (658 mg, 77% yield). ¹H NMR (500 MHz, CDCl₃) δ = 7.53 – 7.44 (m, 2H), 7.38 – 7.27 (m, 2H), 7.21 (s, 1H), 7.14 – 7.08 (m, 1H), 5.89 (ddt, J = 16.8, 10.9, 6.0 Hz, 1H), 5.27 – 4.96 (m, 2H), 2.54 – 2.40 (m, 4H) ppm. ¹³C NMR (126 MHz, CDCl₃) δ = 170.4, 137.8, 136.9, 129.0, 124.3, 119.8, 116.0, 36.9, 29.4 ppm. Spectroscopic data for **1a** match those previously reported in the literature.¹

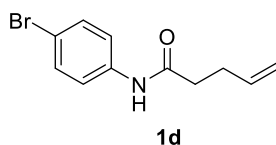


N-(4-fluorophenyl)pent-4-enamide (1b). Following the General Procedure B, 4-pentenoic acid (1.22 mL, 12.0 mmol), 4-fluoroaniline (1.33 g, 12.0 mmol), DMAP (146 mg, 1.22 mmol) and EDC (2.53 g, 13.2 mmol) in 20 mL of DCM were used, affording the product as a white solid (1.83 g, 79% yield). ¹H NMR (600 MHz, CDCl₃) δ = 7.45 (dd, J = 8.8, 4.8 Hz, 2H), 7.19 (s, 1H), 7.00 (t, J = 8.5 Hz, 2H), 5.88 (td, J = 10.5, 5.1 Hz, 1H), 5.13 (d, J = 17.1 Hz, 1H), 5.06 (d, J = 10.2 Hz, 1H), 2.46 (dq, J = 12.3, 6.7 Hz, 4H) ppm. ¹³C NMR (151 MHz, CDCl₃) δ = 170.0, 158.9 (d, J = 243.6 Hz), 136.3, 133.3, 121.2 (dd, J = 7.8, 3.5 Hz), 115.6, 115.1 (d, J = 22.6 Hz), 36.2, 28.9 ppm. ¹⁹F NMR (376 MHz, CDCl₃) δ = -118.2 ppm. Spectroscopic data for **1b** match those previously reported in the literature.¹¹

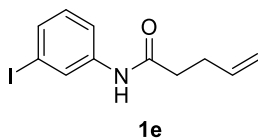


N-(4-chlorophenyl)pent-4-enamide (1c). Following the General Procedure B, 4-pentenoic acid (1.22 mL, 12.0 mmol), 4-chloroaniline (1.53 g, 12.0 mmol), DMAP (146 mg, 1.22 mmol) and EDC (2.53 g, 13.2 mmol) in 20 mL of DCM were used, affording the product as a white solid (2.21 g, 88% yield). ¹H NMR (600 MHz, CDCl₃) δ = 7.46 (d, J = 8.3 Hz, 2H), 7.30 – 7.22 (m, 2H), 7.20 (s, 1H), 5.95 – 5.76 (m, 1H), 5.18 – 4.98 (m, 2H), 2.53 – 2.43 (m, 4H) ppm. ¹³C NMR (151 MHz, CDCl₃) δ = 170.6, 136.8, 136.5,

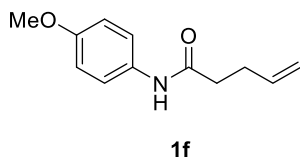
129.3, 129.1, 121.1, 116.2, 36.9, 29.4 ppm. Spectroscopic data for **1c** match those previously reported in the literature.ⁱⁱ



N-(4-bromophenyl)pent-4-enamide (1d). Following the General Procedure B, 4-pentenoic acid (1.22 mL, 12.0 mmol), 4-bromoaniline (2.064 g, 12.0 mmol), DMAP (146 mg, 1.22 mmol) and EDC (2.53 g, 13.2 mmol) in 20 mL of DCM were used, affording the product as a white solid (1.93 g, 62% yield). ¹H NMR (600 MHz, CDCl₃) δ = 7.58 – 7.31 (m, 4H), 6.05 – 5.74 (m, 1H), 5.13 (d, J = 17.2 Hz, 1H), 5.08 (d, J = 10.3 Hz, 1H), 2.48 (tt, J = 14.6, 10.5, 8.4 Hz, 4H) ppm. ¹³C NMR (151 MHz, CDCl₃) δ = 170.8, 137.0, 136.8, 132.0, 121.5, 116.9, 116.1, 36.8, 29.4 ppm. Spectroscopic data for **1d** match those previously reported in the literature.ⁱⁱⁱ

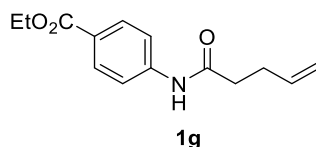


N-(3-iodophenyl)pent-4-enamide (1e) Following the General Procedure B, 4-pentenoic acid (1.22 mL, 12.0 mmol), 3-iodoaniline (2.62 g, 12.0 mmol), DMAP (146 mg, 1.22 mmol) and EDC (2.53 g, 13.2 mmol) in 20 mL of DCM were used, affording the product as a white solid (2.11 g, 58% yield). ¹H NMR (400 MHz, CDCl₃) δ = 7.92 (s, 1H), 7.45 (dd, J = 14.8, 8.0 Hz, 2H), 7.02 (dd, J = 8.9, 7.2 Hz, 1H), 5.87 (ddt, J = 16.9, 10.6, 5.9 Hz, 1H), 5.09 (dd, J = 24.1, 13.6 Hz, 2H), 2.47 (d, J = 8.8 Hz, 4H) ppm ¹³C NMR (151 MHz, CDCl₃) δ = 170.6, 139.0, 136.8, 133.4, 130.6, 128.6, 119.0, 116.2, 94.2, 36.8, 29.4 ppm. Spectroscopic data for **1e** match those previously reported in the literature.^{iv}

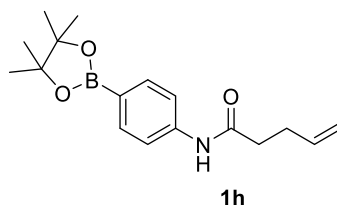


N-(4-methoxyphenyl)pent-4-enamide (1f). Following the General Procedure A, 4-pentenoic acid (0.5 mL, 4.89 mmol), p-anisidine (615 mg, 5.38 mmol), DMAP (61 mg, 0.48 mmol) and DCC (1.03 g, 7.34 mmol) in 15 mL of DCM were used, affording the product as a brown solid powder (832 mg, 83% yield). ¹H NMR (500 MHz, CDCl₃) δ = 7.50 – 7.31 (m, 2H), 7.24 (bs, 1H), 6.90 – 6.77 (m, 2H), 5.88 (ddt, J = 16.8, 10.2, 6.3 Hz, 1H), 5.09 (dd, J = 17.1, 10.2 Hz, 2H), 3.75 (s, 3H), 2.54 – 2.38 (m, 4H) ppm. ¹³C NMR (126 MHz, CDCl₃) δ = 170.4, 156.4, 136.9, 130.9, 121.8, 115.8, 114.1, 55.5, 36.6, 29.5 ppm. Spectroscopic data for **1f** match those previously reported in the literature.^v

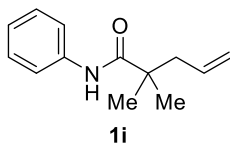
Chapter 4



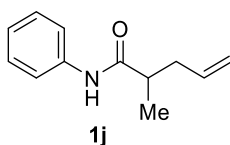
Ethyl 4-(pent-4-enamido)benzoate (1g). Following the General Procedure A, 4-pentenoic acid (0.5 mL, 4.89 mmol), p-anisidine (826 mg, 5.38 mmol), DMAP (61 mg, 0.48 mmol) and DCC (1.03 g, 7.34 mmol) in 15 mL of DCM were used, affording the product as a white solid (966 mg, 80% yield). $^1\text{H NMR}$ (500 MHz, CDCl_3) δ = 8.08 – 7.90 (m, 2H), 7.59 (d, J = 8.7 Hz, 2H), 7.53 (s, 1H), 5.96 – 5.77 (m, 1H), 5.22 – 4.97 (m, 2H), 4.35 (q, J = 7.1 Hz, 2H), 2.49 (dt, J = 3.5, 0.9 Hz, 4H), 1.38 (t, J = 7.1 Hz, 3H) ppm. $^{13}\text{C NMR}$ (126 MHz, CDCl_3) δ = 170.7, 166.1, 141.9, 136.6, 130.8, 125.9, 118.7, 116.1, 60.8, 36.9, 29.2, 14.3 ppm. Spectroscopic data for **1g** match those previously reported in the literature.^v



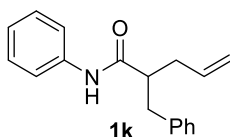
N-(4-(4,4,5,5-tetramethyl-1,3,2-dioxaborolan-2-yl)phenyl)pent-4-enamide (1h). Following the General Procedure B, 4-pentenoic acid (2.00 mL, 20.0 mmol), 4-(4,4,5,5-tetramethyl-1,3,2-dioxaborolan-2-yl)aniline (4.38 g, 20.0 mmol), DMAP (244 mg, 2.00 mmol) and EDC (4.17 g, 22.0 mmol) in 40 mL of DCM were used, affording the product as a white solid (4.49 g, 75% yield). $^1\text{H NMR}$ (600 MHz, CDCl_3) δ = 7.76 (d, J = 8.0 Hz, 2H), 7.52 (d, J = 8.0 Hz, 2H), 7.23 (s, 1H), 5.88 (ddt, J = 16.8, 10.6, 6.0 Hz, 1H), 5.12 (d, J = 17.1 Hz, 1H), 5.06 (d, J = 10.3 Hz, 1H), 2.47 (p, J = 6.6 Hz, 4H), 1.33 (s, 12H) ppm. $^{13}\text{C NMR}$ (151 MHz, CDCl_3) δ = 170.5, 140.6, 136.9, 135.9, 118.6, 116.1, 83.8, 37.1, 29.4, 25.0 ppm. (*The carbon attached to boron was not observed due to quadrupolar relaxation*). HRMS calcd. for ($\text{C}_{17}\text{H}_{25}\text{NO}_3\text{B}$) [$\text{M}+\text{H}$] $^+$: 302.1922, found 302.1920.



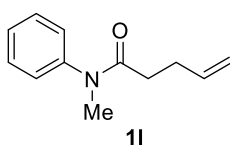
2,2-Dimethyl-N-phenylpent-4-enamide (1i). Following the General Procedure D, 2,2-dimethylpent-4-enoic acid (0.5 g, 3.9 mmol), aniline (0.42 mL, 4.68 mmol), Et_3N (1.36 mL, 9.4 mmol) and HATU (1.76 g, 4.68 mmol) in 20 mL of DMF were used, affording the product as a white solid (657 mg, 82% yield). $^1\text{H NMR}$ (500 MHz, CDCl_3) δ = 7.53 – 7.48 (m, 2H), 7.36 – 7.29 (m, 3H), 7.13 – 7.07 (m, 1H), 5.93 – 5.76 (m, 1H), 5.21 – 5.09 (m, 2H), 2.38 (d, J = 7.4 Hz, 2H), 1.30 (s, 6H) ppm. $^{13}\text{C NMR}$ (126 MHz, CDCl_3) δ = 175.6, 138.0, 134.4, 129.1, 124.4, 120.2, 118.6, 45.4, 43.0, 25.4 ppm. HRMS calcd. for ($\text{C}_{13}\text{H}_{17}\text{NO}$) [$\text{M}+\text{H}$] $^+$: 204.1388, found 204.1390.



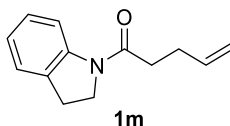
2-Methyl-N-phenylpent-4-enamide (1j). Following the General Procedure D, 2-methylpent-4-enoic acid (0.80 mL, 6.86 mmol), aniline (0.57 mL, 6.24 mmol), HATU (2.61 g, 6.86 mmol) and pyridine (0.50 mL, 6.24 mmol) in 12 mL of DCM were used, affording the product as a beige solid (980 mg, 83% yield). $^1\text{H NMR}$ (600 MHz, CDCl_3) δ = 7.56 – 7.46 (m, 2H), 7.38 (br. s, 1H), 7.36 – 7.27 (m, 2H), 7.14 – 7.00 (m, 1H), 5.89 – 5.74 (m, 1H), 5.11 (d, J = 17.1 Hz, 1H), 5.06 (d, J = 8.4 Hz, 1H), 2.55 – 2.36 (m, 2H), 2.28 – 2.16 (m, 1H), 1.24 (d, J = 6.8 Hz, 3H) ppm. $^{13}\text{C NMR}$ (151 MHz, CDCl_3) δ = 174.3, 138.0, 135.8, 129.1, 124.4, 120.1, 117.4, 42.3, 38.5, 17.6 ppm. Spectroscopic data for **1j** match those previously reported in the literature.^{vi}



2-benzyl-N-phenylpent-4-enamide (1k). Following the General Procedure B, 2-benzylpent-4-enoic acid (500 mg, 2.63 mmol), aniline (240 μL , 2.63 mmol), DMAP (32 mg, 0.26 mmol) and EDC (554 mg, 2.63 mmol) in 20 mL of DCM were used, affording the product as a white solid (390 mg, 56% yield). $^1\text{H NMR}$ (400 MHz, CDCl_3) δ = 7.37 – 7.18 (m, 10H), 7.15 – 7.05 (m, 1H), 6.85 (s, 1H), 5.87 (ddt, J = 17.1, 10.2, 6.9 Hz, 1H), 5.17 (dq, J = 17.1, 1.5 Hz, 1H), 5.11 (ddt, J = 10.1, 1.9, 1.0 Hz, 1H), 3.03 (dd, J = 13.5, 9.0 Hz, 1H), 2.88 (dd, J = 13.5, 5.1 Hz, 1H), 2.56 (ddtd, J = 22.7, 10.1, 8.5, 6.1 Hz, 2H), 2.45 – 2.28 (m, 1H) ppm. $^{13}\text{C NMR}$ (151 MHz, CDCl_3) δ 172.6, 139.7, 137.5, 135.5, 129.0, 128.7, 126.6, 124.4, 120.3, 117.6, 51.1, 38.9, 36.9 ppm. HRMS calcd. for $(\text{C}_{20}\text{H}_{16}\text{NO})$ $[\text{M}+\text{H}]^+$: 266.1539, found 266.1538.

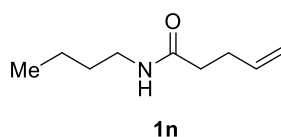


N-methyl-N-phenylpent-4-enamide (1l). Following the General Procedure C, 4-pentenoic acid (1.0 mL, 9.78 mmol), N-methylaniline (1.62 mL, 15.11 mmol), Et_3N (5.71 mL, 40.9 mmol) and methyl carbonochloridate (0.87 mL, 9.78 mmol) in 30 mL of THF were used, affording the product as yellow oil (1.40 g, 74% yield). $^1\text{H NMR}$ (500 MHz, CDCl_3) δ = 7.43-7.38 (m, 2H), 7.36-7.30 (m, 1H), 7.22 – 7.10 (m, 2H), 5.76-5.68 (m, 1H), 4.99 – 4.82 (m, 2H), 3.26 (s, 3H), 2.32 (q, J = 7.2 Hz, 2H), 2.15 (t, J = 7.6 Hz, 2H) ppm. $^{13}\text{C NMR}$ (126 MHz, CDCl_3) δ = 172.3, 144.1, 137.5, 129.7, 127.7, 127.3, 114.9, 37.3, 33.4, 29.4 ppm. Spectroscopic data for **1l** match those previously reported in the literature.^{vii}

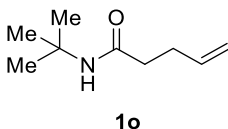


Chapter 4

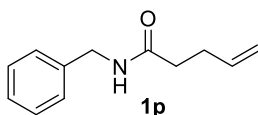
1-(indolin-1-yl)pent-4-en-1-one (1m). Following the General Procedure B, 4-pentenoic acid (2.00 mL, 20.0 mmol), indoline (2.25 mL, 20.0 mmol), DMAP (244 mg, 2.0 mmol) and EDC (4.17 g, 22.0 mmol) in 40 mL of DCM were used, affording the product as a white solid (2.04 g, 51% yield). $^1\text{H NMR}$ (600 MHz, CDCl_3) δ = 8.24 (d, J = 8.1 Hz, 1H), 7.19 (q, J = 7.0, 6.2 Hz, 2H), 7.01 (t, J = 7.4 Hz, 1H), 5.93 (ddt, J = 16.1, 11.0, 5.7 Hz, 1H), 5.15 – 5.07 (m, 1H), 5.03 (d, J = 10.1 Hz, 1H), 4.06 (t, J = 8.5 Hz, 2H), 3.20 (t, J = 8.5 Hz, 2H), 2.51 (q, J = 5.9, 5.1 Hz, 4H) ppm. $^{13}\text{C NMR}$ (151 MHz, CDCl_3) δ = 170.6, 143.1, 137.5, 131.1, 127.7, 124.6, 123.6, 117.1, 115.4, 48.0, 35.3, 28.7, 28.1 ppm. HRMS calcd. for ($\text{C}_{13}\text{H}_{16}\text{NO}$) [$\text{M}+\text{H}$] $^+$: 202.1226, found 202.1224.



N-butylpent-4-enamide (1n). Following the General Procedure D, 4-pentenoic acid (0.5 mL, 4.89 mmol), n-butylamine (0.58 mL, 5.85 mmol), Et_3N (1.7 mL, 11.75 mmol) and HATU (2.2 g, 5.85 mmol) in 25 mL of DMF were used, affording the product as pale yellow oil (623 mg, 82% yield). $^1\text{H NMR}$ (500 MHz, CDCl_3) δ = 5.81 (ddt, J = 16.8, 10.2, 6.5 Hz, 1H), 5.57 (bs, 1H), 5.19 – 4.89 (m, 2H), 3.24 (td, J = 7.2, 5.6 Hz, 2H), 2.43 – 2.35 (m, 2H), 2.29 – 2.12 (m, 2H), 1.46 (p, J = 7.4 Hz, 2H), 1.33 (dq, J = 14.3, 7.3 Hz, 2H), 0.91 (t, J = 7.3 Hz, 3H) ppm. $^{13}\text{C NMR}$ (126 MHz, CDCl_3) δ = 172.2, 137.1, 115.5, 39.2, 35.9, 31.7, 29.7, 20.0, 13.7 ppm. Spectroscopic data for **1n** match those previously reported in the literature.^{VIII}

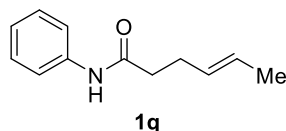


N-(tert-butyl)pent-4-enamide (1o). Following the General Procedure D, 4-pentenoic acid (0.5 mL, 4.89 mmol), t-butylamine (0.61 mL, 5.85 mmol), Et_3N (1.7 mL, 11.75 mmol) and HATU (2.2 g, 5.85 mmol) in 25 mL of DMF were used, affording the product as pale yellow oil (521 mg, 68% yield). $^1\text{H NMR}$ (500 MHz, CDCl_3) δ = 5.81 (ddt, J = 16.9, 10.2, 6.6 Hz, 1H), 5.10 – 4.83 (m, 2H), 2.35 (q, J = 7.4 Hz, 2H), 2.17 (t, J = 7.5 Hz, 2H), 1.33 (s, 9H) ppm. $^{13}\text{C NMR}$ (126 MHz, CDCl_3) δ = 171.6, 137.2, 115.4, 51.2, 36.7, 29.7, 28.8 ppm. IR (neat, cm^{-1}): 3364, 3081, 2979, 1736, 1681, 1535, 1508, 1406, 1151. HRMS calcd. for ($\text{C}_9\text{H}_{17}\text{NNaO}$) [$\text{M}+\text{Na}$] $^+$: 178.1202, found 178.1195.

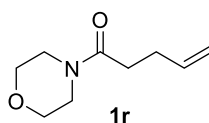


N-benzylpent-4-enamide (1p). Following the General Procedure B, 4-pentenoic acid (2.00 mL, 20.0 mmol), benzylamine (2.14 g, 20.0 mmol), DMAP (244 mg, 2.0 mmol) and EDC (4.17 g, 22.0 mmol) in 40 mL of DCM were used, affording the product as a white solid (3.36 g, 89% yield). $^1\text{H NMR}$ (600

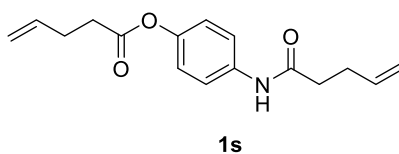
MHz, CDCl₃) δ = 7.38 – 7.31 (m, 2H), 7.31 – 7.26 (m, 3H), 5.83 (ddt, J = 16.8, 10.2, 6.5 Hz, 1H), 5.74 (s, 1H), 5.07 (dq, J = 17.1, 1.6 Hz, 1H), 5.01 (dq, J = 10.3, 1.4 Hz, 1H), 4.44 (d, J = 5.6 Hz, 2H), 2.43 (dd, J = 6.0, 1.1 Hz, 2H), 2.37 – 2.23 (m, 2H) ppm. ¹³C NMR (151 MHz, CDCl₃) δ = 172.1, 138.4, 137.1, 128.8, 127.9, 127.6, 115.8, 43.7, 36.0, 29.7 ppm. HRMS calcd. for (C₁₂H₁₆NO) [M+H]⁺: 190.1226, found 190.1226.



(E)-N-phenylhex-4-enamide (1q). Following the General Procedure A, (E)-hex-4-enoic acid (1.14 g, 10.0 mmol), aniline (0.91 mL, 11.1 mmol), DMAP (120 mg, 1.0 mmol) and DCC (2.05 g, 13.35 mmol) in 30 mL of DCM were used, affording the product as a white solid (1.2 g, 63% yield). ¹H NMR (500 MHz, CDCl₃) δ = 7.56 – 7.46 (m, 2H), 7.38 – 7.25 (m, 2H), 7.21 (bs, 1H), 7.10 (t, J = 7.4 Hz, 1H), 5.89 (ddt, J = 16.8, 10.9, 6.0 Hz, 1H), 5.35 – 4.94 (m, 2H), 2.63 – 2.37 (m, 4H), 1.66 (d, J = 6.0 Hz, 3H) ppm. ¹³C NMR (101 MHz, CDCl₃) δ = 170.4, 137.8, 136.9, 129.0, 124.3, 119.8, 116.0, 36.9, 29.4, 17.8 ppm. Spectroscopic data for **1q** match those previously reported in the literature.¹



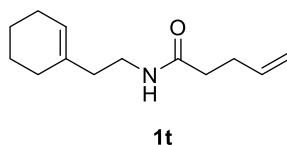
1-Morpholinopent-4-en-1-one (1r). Following the General Procedure D, pent-4-enoic acid (0.70 mL, 6.86 mmol), morpholine (0.54 mL, 6.24 mmol), HATU (2.61 g, 6.86 mmol) and pyridine (0.50 mL, 6.24 mmol) in 12 mL of DCM were used, affording the product as a colorless oil (550 mg, 52% yield). ¹H NMR (600 MHz, CDCl₃) δ = 5.91 – 5.77 (m, 1H), 5.05 (dd, J = 17.0, 1.7 Hz, 1H), 4.99 (dd, J = 10.0, 1.7 Hz, 1H), 3.70 – 3.56 (m, 6H), 3.48 – 3.42 (m, 2H), 2.42 – 2.36 (m, 4H) ppm. ¹³C NMR (151 MHz, CDCl₃) δ = 171.1, 137.4, 115.5, 67.1, 66.8, 46.1, 42.0, 32.4, 29.3 ppm. Spectroscopic data for **1r** match those previously reported in the literature.^{ix}



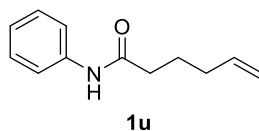
4-(pent-4-enamido)phenyl pent-4-enoate (1s). Following the General Procedure A, 4-pentenoic acid (0.5 mL, 4.89 mmol), 4-aminophenol (545 mg, 5.38 mmol), DMAP (61 mg, 0.48 mmol) and DCC (1.03 g, 7.34 mmol) in 15 mL of DCM were used, affording the product as a pale brown solid (400 mg, 59% yield). **Mp:** 111 – 109 °C. ¹H NMR (500 MHz, CDCl₃) δ = 7.55 – 7.36 (m, 2H), 7.23 (bs, 1H), 7.10 – 6.96 (m, 2H), 5.89 (m, 2H), 5.20 – 4.95 (m, 4H), 2.65 (t, J = 7.4 Hz, 2H), 2.55 – 2.39 (m, 6H) ppm. ¹³C NMR (126 MHz, CDCl₃) δ = 171.7, 170.4, 146.8, 136.8, 136.2, 135.5, 121.9, 120.8, 115.9, 36.7, 33.6,

Chapter 4

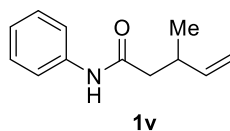
29.4, 28.8 ppm. IR (neat, cm^{-1}): 3364, 1736, 1681, 1535, 1508, 1151, 913. HRMS calcd. for ($\text{C}_{16}\text{H}_{17}\text{NO}_3$) $[\text{M}+\text{H}]^+$: 272.1292, found 272.1284.



N-(2-(cyclohex-1-en-1-yl)ethyl)pent-4-enamide (1t). Following the General Procedure D, 4-pentenoic acid (0.5 mL, 4.89 mmol), 2-(cyclohex-1-en-1-yl)ethan-1-amine (0.82 mL, 5.85 mmol), Et_3N (1.7 mL, 11.75 mmol) and HATU (2.2 g, 5.85 mmol) in 25 mL of DMF were used, affording the product as pale yellow semisolid-oil (670 mg, 66% yield). **Mp:** 30 – 32 °C. $^1\text{H NMR}$ (500 MHz, CDCl_3) δ = 5.95 – 5.68 (m, 1H), 5.45 (s, 2H), 5.10 – 4.96 (m, 2H), 3.32 (q, J = 6.2 Hz, 2H), 2.37 (q, J = 7.2 Hz, 2H), 2.25 (t, J = 7.4 Hz, 2H), 2.11 (t, J = 6.7 Hz, 2H), 1.99 (s, 2H), 1.91 (s, 2H), 1.62 (p, J = 5.8 Hz, 2H), 1.55 (p, J = 6.1 Hz, 2H) ppm. $^{13}\text{C NMR}$ (126 MHz, CDCl_3) δ = 172.1, 137.1, 134.6, 123.5, 115.5, 37.6, 37.0, 35.9, 29.6, 27.8, 25.2, 22.8, 22.3 ppm. IR (neat, cm^{-1}): 3235, 3127, 2954, 2908, 2875, 1648, 1595, 1546, 1443, 710. HRMS calcd. for ($\text{C}_{13}\text{H}_{21}\text{NO}$) $[\text{M}+\text{H}]^+$: 208.1696, found 208.1692.

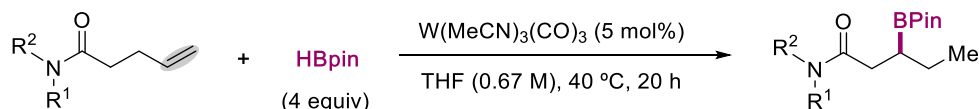


N-phenylhex-5-enamide (1u). Following the General Procedure A, 5-pentenoic acid (1.0 g, 8.76 mmol), aniline (0.8 mL, 9.63 mmol), DMAP (106 mg, 0.88 mmol) and DCC (1.80 g, 13.14 mmol) in 30 mL of DCM were used, affording the product as a white solid (1.28 g, 77% yield). $^1\text{H NMR}$ (300 MHz, CDCl_3) δ = 7.55 – 7.50 (m, 2H), 7.36 – 7.28 (m, 2H), 7.16 – 7.13 (bs, 1H), 7.14 – 7.08 (m, 1H), 5.91 – 5.69 (m, 1H), 5.18 – 4.87 (m, 2H), 2.36 (t, J = 7.5 Hz, 2H), 2.16 (q, J = 7.1 Hz, 2H), 1.84 (p, J = 7.4 Hz, 2H) ppm. $^{13}\text{C NMR}$ (101 MHz, CDCl_3) δ = 171.0, 137.8, 129.0, 124.2, 119.7, 115.5, 36.9, 33.0, 24.5 ppm. Spectroscopic data for **1u** match those previously reported in the literature.^x

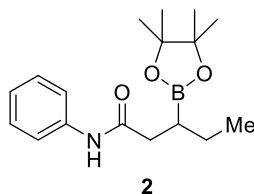


3-methyl-N-phenylpent-4-enamide (1v). Following the General Procedure A, 3-methylpent-4-enoic acid (1.0 mL, 8.76 mmol), aniline (0.8 mL, 9.6 mmol), DMAP (106 mg, 0.88 mmol) and DCC (1.80 g, 13.14 mmol) in 30 mL of DCM were used, affording the product as a white solid (1.16 g, 70% yield). $^1\text{H NMR}$ (400 MHz, CDCl_3) δ = 7.57 – 7.44 (m, 2H), 7.31 (m, 2H), 7.10 (t, J = 7.4 Hz, 1H), 5.84 (ddd, J = 17.3, 10.3, 7.0 Hz, 1H), 5.08 (dd, J = 7.0, 10.0 Hz, 2H), 2.80 (qddd, J = 17.2, 10.2, 7.0, 2.1 Hz, 1H), 2.49 – 2.24 (m, 2H), 1.12 (d, J = 6.8 Hz, 3H) ppm. $^{13}\text{C NMR}$ (101 MHz, CDCl_3) δ = 167.0, 142.6, 137.8, 129.0, 124.3, 119.9, 113.9, 44.8, 34.8, 19.7 ppm. Spectroscopic data for **1v** match those previously reported in the literature.^{vi}

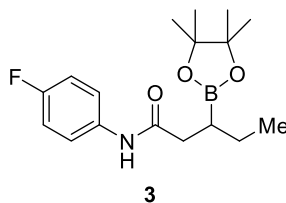
4.5.4 Remote alkene hydroboration of amides catalyzed by tungsten



General procedure E: An oven-dried 8 mL screw-cap test tube containing a stirring bar was charged with the alkene-amide (0.20 mmol). The test tube was introduced in an argon-filled glovebox where $\text{W}(\text{MeCN})_3(\text{CO})_3$ (3.8 mg, 5 mol%) was charged in THF (0.3 mL). Subsequently, HBpin (116 μL , 4 equiv) was added and the tube was taken out of the glovebox and stirred at 40 $^\circ\text{C}$ for 20 h at 800 rpm approximately. After the reaction was finished, the reaction mixture was diluted with EtOAc and transferred to a round bottom flask. After evaporation, the crude mixture was purified by flash chromatography column on silica gel eluting with Hexane/EtOAc.



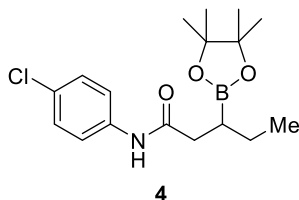
***N*-phenyl-3-(4,4,5,5-tetramethyl-1,3,2-dioxaborolan-2-yl)hexanamide (2)** Following General Procedure E, *N*-(phenyl)pent-4-enamide (**1a**) (35.0 mg, 0.20 mmol), $\text{W}(\text{CO})_3(\text{MeCN})_3$ (4 mg, 5 mol %) and HBpin (116 μL , 4 equiv) were used at 40 $^\circ\text{C}$ affording the title compound as a white solid (62 mg, 91% yield) by using DCM/MeCN (95/5) as eluent. $^1\text{H NMR}$ (600 MHz, CDCl_3) δ = 7.61 (s, 1H), 7.50 (d, J = 8.0 Hz, 2H), 7.29 (t, J = 7.7 Hz, 2H), 7.06 (t, J = 7.4 Hz, 1H), 2.51 (dd, J = 14.7, 9.4 Hz, 1H), 2.42 (dd, J = 14.7, 5.3 Hz, 1H), 1.52 (ddq, J = 39.5, 13.7, 7.0 Hz, 2H), 1.38 (dq, J = 9.9, 5.5, 3.9 Hz, 1H), 1.26 (d, J = 4.2 Hz, 1H), 0.96 (t, J = 7.4 Hz, 3H) ppm. $^{13}\text{C NMR}$ (151 MHz, CDCl_3) δ = 171.7, 138.4, 129.0, 123.9, 119.6, 83.5, 39.1, 24.9, 24.9, 24.8, 23.9, 13.4 ppm. HRMS calcd. for $(\text{C}_{18}\text{H}_{28}\text{BCINO}_3)$ $[\text{M}+\text{H}]^+$: 304.2079, found 304.2078.



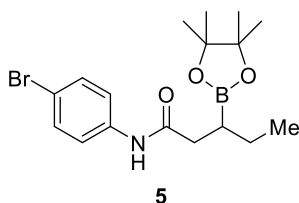
***N*-(4-fluorophenyl)-3-(4,4,5,5-tetramethyl-1,3,2-dioxaborolan-2-yl)hexanamide (3).** Following General Procedure E, *N*-(4-fluorophenyl)pent-4-enamide (**1b**) (38.6 mg, 0.20 mmol), $\text{W}(\text{CO})_3(\text{MeCN})_3$ (4 mg, 5 mol %) and HBpin (116 μL , 4 equiv) were used at 40 $^\circ\text{C}$ affording the title compound as a white solid (56 mg, 87% yield) by using DCM/MeCN (95/5) as eluent. Single crystals suitable for X-ray diffraction were grown by slow evaporation from a concentrated EtOAc solution (CCDC 2012996). $^1\text{H NMR}$ (600 MHz, CDCl_3) δ = 7.61 (s, 1H), 7.45 (dd, J = 8.7, 4.8 Hz, 2H), 6.98 (t, J = 8.5 Hz, 2H), 2.49 (dd,

Chapter 4

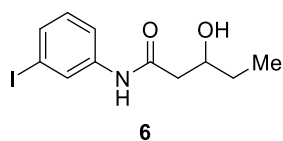
$J = 14.7, 9.5$ Hz, 1H), 2.41 (dd, $J = 14.7, 5.3$ Hz, 1H), 1.54 (dq, $J = 14.7, 7.3$ Hz, 1H), 1.46 (dq, $J = 14.2, 7.2$ Hz, 1H), 1.37 (p, $J = 6.4, 6.0$ Hz, 1H), 1.25 (d, $J = 4.8$ Hz, 12H) 0.96 (t, $J = 7.4$ Hz, 3H) ppm. ^{13}C NMR (151 MHz, CDCl_3) $\delta = 171.1, 158.6$ (d, $J = 242.7$ Hz), 133.8 (d, $J = 2.8$ Hz), 120.7 (d, $J = 7.7$ Hz), 115.0 (d, $J = 22.5$ Hz), 83.0, 38.4, 24.4, 24.3, 23.4, 21.8, 12.8 ppm. ^{19}F NMR (376 MHz, CDCl_3) $\delta = -118.9$ ppm. HRMS calcd. for $(\text{C}_{18}\text{H}_{28}\text{BFNO}_3)$ $[\text{M}+\text{H}]^+$: 322.1984, found 322.1984.



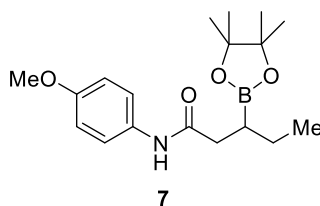
***N*-(4-chlorophenyl)-3-(4,4,5,5-tetramethyl-1,3,2-dioxaborolan-2-yl)hexanamide (4).** Following General Procedure E, *N*-(4-chlorophenyl)pent-4-enamide (**1c**) (42.0 mg, 0.20 mmol), $\text{W}(\text{CO})_3(\text{MeCN})_3$ (4 mg, 5 mol %) and HBpin (116 μL , 4 equiv) were used at 40 °C affording the title compound as a white solid (60 mg, 85% yield) by using DCM/MeCN (95/5) as eluent. ^1H NMR (600 MHz, CDCl_3) $\delta = 7.62$ (s, 1H), 7.46 (d, $J = 8.5$ Hz, 2H), 7.25 (s, 1H), 2.52 – 2.36 (m, 2H), 1.62 – 1.42 (m, 2H), 1.41 – 1.33 (m, 1H), 1.25 (d, $J = 5.3$ Hz, 12H), 0.96 (t, $J = 7.4$ Hz, 3H) ppm. ^{13}C NMR (151 MHz, CDCl_3) $\delta = 171.8, 136.9, 129.0, 128.8, 120.8, 83.6, 39.1, 25.0, 24.9, 24.0, 13.3$ ppm (The carbon attached to boron was not observed due to quadrupolar relaxation). HRMS calcd. for $(\text{C}_{18}\text{H}_{28}\text{BClNO}_3)$ $[\text{M}+\text{H}]^+$: 338.1689, found 338.1689.



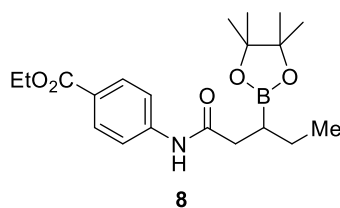
***N*-(4-bromophenyl)-3-(4,4,5,5-tetramethyl-1,3,2-dioxaborolan-2-yl)hexanamide (5).** Following General Procedure E, *N*-(4-bromophenyl)pent-4-enamide (**1d**) (50.8 mg, 0.20 mmol), $\text{W}(\text{CO})_3(\text{MeCN})_3$ (4 mg, 5 mol %) and HBpin (116 μL , 4 equiv) were used at 40 °C affording the title compound as a white solid (62 mg, 81% yield) by using DCM/MeCN (95/5) as eluent. ^1H NMR (600 MHz, CDCl_3) $\delta = 7.67$ (s, 1H), 7.45 – 7.34 (m, 4H), 2.49 (dd, $J = 14.8, 9.5$ Hz, 1H), 2.41 (dd, $J = 14.8, 5.2$ Hz, 1H), 1.60 – 1.50 (m, 1H), 1.46 (dp, $J = 14.2, 7.2$ Hz, 1H), 1.40 – 1.33 (m, 1H), 1.25 (d, $J = 5.2$ Hz, 12H), 0.95 (t, $J = 7.4$ Hz, 3H) ppm. ^{13}C NMR (151 MHz, CDCl_3) $\delta = 171.8, 137.4, 132.0, 121.1, 116.3, 83.6, 39.1, 24.9, 24.9, 23.9, 22.3, 13.3$ ppm. HRMS calcd. for $(\text{C}_{18}\text{H}_{28}\text{BBrNO}_3)$ $[\text{M}+\text{H}]^+$: 382.1184, found 382.1183.



3-hydroxy-N-(3-iodophenyl)pentanamide (6) Following General Procedure E, (**1e**) (60.2 mg, 0.20 mmol) and HBpin (116 μ L, 4 equiv) were used at 40 °C. The oxidation to the alcohol was promoted by using H₂O₂ (30 % v/v) (41 μ L, 0.400 mmol) with 1 mL aq. NaOH (3 M) and 1 mL THF affording the title compound as a white powder (48 mg, 75% yield) by using Hexane/EtOAc (70/30) as eluent. **¹H NMR** (600 MHz, CDCl₃) δ = 8.00 (s, 1H), 7.94 (t, J = 2.0 Hz, 1H), 7.51 (dd, J = 8.1, 2.1 Hz, 1H), 7.46 (d, J = 7.8 Hz, 1H), 7.06 (t, J = 8.0 Hz, 1H), 4.05 (qd, J = 7.2, 5.9, 2.5 Hz, 1H), 2.58 (dd, J = 15.5, 2.6 Hz, 1H), 2.49 (dd, J = 15.5, 8.9 Hz, 1H), 1.69 – 1.50 (m, J = 6.8 Hz, 2H), 1.02 (t, J = 7.5 Hz, 3H) ppm. **¹³C NMR** (151 MHz, CDCl₃) δ = 170.5, 138.9, 133.4, 130.6, 128.7, 119.2, 94.2, 70.3, 43.6, 30.1, 9.9 ppm. **HRMS** calcd. for (C₁₁H₁₅INO₂) [M+H]⁺: 320.0142, found 320.0141.



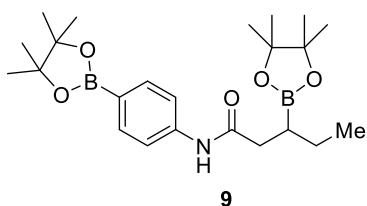
N-(4-methoxyphenyl)-3-(4,4,5,5-tetramethyl-1,3,2-dioxaborolan-2-yl)pentanamide (7). Following General Procedure E, *N*-(4-methoxyphenyl)pent-4-enamide (**1f**) (41.0 mg, 0.20 mmol) and HBpin (116 μ L, 4 equiv) were used at 40 °C, affording the title compound as a brownish solid (55 mg, 85% yield) by using Hexane/EtOAc (70/30) as eluent. **Mp**: 107 - 105 °C. **¹H NMR** (500 MHz, CDCl₃) δ = 7.51 (bs, 1H), 7.43 – 7.36 (m, 2H), 6.89 – 6.77 (m, 2H), 3.77 (s, 3H), 2.53 – 2.35 (m, 2H), 1.60 – 1.42 (m, 2H), 1.42 – 1.35 (m, 1H), 1.25 (s, 12H), 0.95 (t, J = 7.4 Hz, 3H) ppm. **¹³C NMR** (126 MHz, CDCl₃) δ = 171.4, 156.0, 131.4, 121.3, 114.0, 83.3, 55.4, 38.8, 24.8, 24.7, 23.9, 13.2 ppm. (*The carbon attached to boron was not observed due to quadrupolar relaxation*). **IR** (neat, cm⁻¹): 3365, 2961, 1677, 1508, 1408, 1299, 1218, 1142, 828. **HRMS** calcd. for (C₁₈H₂₉BNO₄) [M+H]⁺: 333.2220, found 333.2224.



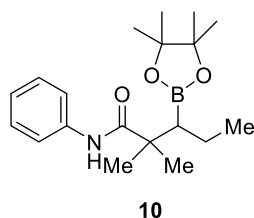
Ethyl 4-(3-(4,4,5,5-tetramethyl-1,3,2-dioxaborolan-2-yl)pentanamido)benzoate (8). Following General Procedure E, Ethyl 4-(pent-4-enamido)benzoate (**1g**) (50 mg, 0.20 mmol) and HBpin (116 μ L, 4 equiv) were used at 40 °C, affording the title compound as a white solid (51 mg, 65% yield) by using Hexane/EtOAc (75/25) as eluent. **Mp**: 119 - 117 °C. **¹H NMR** (400 MHz, CDCl₃) δ = 8.08 – 7.94 (m, 2H), 7.83 (bs, 1H), 7.66 – 7.52 (m, 2H), 4.35 (q, J = 7.1 Hz, 2H), 2.58 – 2.41 (m, 2H), 1.62 – 1.43 (m, 2H), 1.42-1.34 (m, 4H), 1.25 (d, J = 3.3 Hz, 12H), 0.96 (t, J = 7.3 Hz, 3H) ppm. **¹³C NMR** (101 MHz, CDCl₃) δ = 171.9, 166.2, 142.4, 130.7, 125.5, 118.4, 83.5, 60.8, 39.1, 24.8, 24.7, 23.8, 14.3, 13.2 ppm. (*The carbon attached to boron was not observed due to quadrupolar relaxation*). **IR** (neat, cm⁻¹): 3286,

Chapter 4

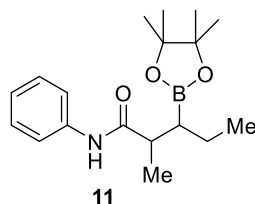
2961, 1690, 1595, 1527, 1370, 1255, 1143, 1096. **HRMS** calcd. for (C₂₀H₃₁BNO₅) [M+H]⁺: 375.2326, found 375.2324.



3-(4,4,5,5-tetramethyl-1,3,2-dioxaborolan-2-yl)-N-(4-(4,4,5,5-tetramethyl-1,3,2-dioxaborolan-2-yl)phenyl)hexanamide (9) Following a modified General Procedure E, *N*-(4-(4,4,5,5-tetramethyl-1,3,2-dioxaborolan-2-yl)phenyl)pent-4-enamide (**1h**) (60.2 mg, 0.20 mmol), W(CO)₃(MeCN)₃ (4 mg, 5 mol %) and HBpin (145 μL, 5 equiv) were used at 40 °C for 48 hr affording the title compound as a white solid (58 mg, 65% yield) by using Acetone/Hexanes (10/90) as eluent. ¹H NMR (600 MHz, CDCl₃) δ = 7.74 (d, *J* = 8.2 Hz, 2H), 7.63 (s, 1H), 7.51 (d, *J* = 7.9 Hz, 2H), 2.50 (dd, *J* = 14.7, 9.5 Hz, 1H), 2.43 (dd, *J* = 14.7, 5.3 Hz, 1H), 1.55 (dq, *J* = 14.8, 7.3 Hz, 1H), 1.47 (dp, *J* = 14.1, 7.2 Hz, 1H), 1.43 – 1.36 (m, 1H), 1.33 (s, 12H), 1.24 (d, *J* = 4.9 Hz, 12H), 0.96 (t, *J* = 7.4 Hz, 3H) ppm. ¹³C NMR (151 MHz, CDCl₃) δ = 171.8, 141.0, 135.9, 118.3, 83.8, 83.6, 39.3, 25.0, 24.8, 24.7, 24.0, 13.3 ppm. (The carbons attached to boron was not observed due to quadrupolar relaxation). **HRMS** calcd. for (C₂₄H₄₀B₂NO₅) [M+H]⁺: 430.2931, found 430.2939.

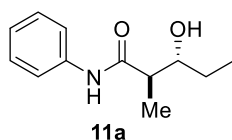


2,2-dimethyl-N-phenyl-3-(4,4,5,5-tetramethyl-1,3,2-dioxaborolan-2-yl)pentanamide (10). Following General Procedure E, 2,2-dimethyl-*N*-phenylpent-4-enamide (**1i**) (40.6 mg, 0.20 mmol) and HBpin (116 μL, 4 equiv) were used at 40 °C, affording the title compound as a white solid (38 mg, 57% yield) by using Hexane/EtOAc (80/20) as eluent. **Mp**: 162 – 164 °C. ¹H NMR (400 MHz, CDCl₃) δ = 8.37 (bs, 1H), 7.55 (d, *J* = 7.6 Hz, 2H), 7.30 (t, *J* = 8.0 Hz, 2H), 7.07 (t, *J* = 7.4 Hz, 1H), 1.53 – 1.41 (m, 2H), 1.32 (d, *J* = 1.9 Hz, 12H), 1.29 (bs, 3H), 1.30 – 1.17 (m, 3H), 0.91 (t, *J* = 7.4 Hz, 3H) ppm. ¹³C NMR (101 MHz, CDCl₃) δ = 176.2, 138.8, 128.8, 123.6, 119.5, 83.8, 44.9, 26.5, 25.7, 25.0, 24.9, 20.5, 14.5 ppm. (The carbon attached to boron was not observed due to quadrupolar relaxation). **IR** (neat, cm⁻¹): 3284, 2981, 2962, 2871, 1656, 1596, 1532, 1258, 1132, 754. **HRMS** calcd. for (C₁₉H₃₀BNO₃) [M+Na]⁺: 353.2247, found 353.2248.

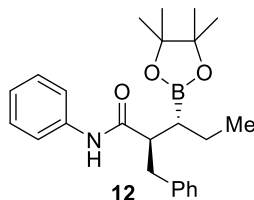


2-Methyl-N-phenyl-3-(4,4,5,5-tetramethyl-1,3,2-dioxaborolan-2-yl)pentanamide (11).

Following General Procedure E, 2-methyl-N-phenylpent-4-enamide (**1j**) (37.8 mg, 0.20 mmol) and HBpin (116 μ L, 4 equiv) were used at 40 °C, affording the title compound as a colourless solid (58.8 mg, 93% yield) by using $\text{CH}_2\text{Cl}_2/\text{MeCN}$ (97.5/2.5) as eluent. $^1\text{H NMR}$ (400 MHz, CDCl_3) δ = 7.88 (bs, 1H), 7.57 – 7.50 (m, 2H), 7.33 – 7.27 (m, 2H), 7.18 – 7.00 (m, 1H), 2.58 (m, 1H), 1.59 – 1.48 (m, 2H), 1.32 – 1.18 (m, 16H), 0.95 (t, J = 7.5 Hz, 3H) ppm. $^{13}\text{C NMR}$ (151 MHz, CDCl_3) δ = 175.2, 138.7, 129.1, 123.8, 119.5, 83.7, 44.1, 25.1, 25.0, 21.9, 17.5, 13.6 ppm (*The carbon attached to boron was not observed due to quadrupolar relaxation*). **HRMS** calcd. for ($\text{C}_{18}\text{H}_{28}\text{BNO}_3$) [$\text{M}+\text{H}$] $^+$: 317.2277, found 317.2272.



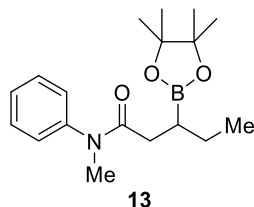
(+/-)-3-Hydroxy-2-methyl-N-phenylpentanamide (11a). To a rapidly stirred solution of **11** (22.0 mg, 0.069 mmol) in THF/Et₂O (1:1, 0.6 mL) at 0 °C, was added a solution of aq. NaOH (2M)/H₂O₂ (30%) (2:1, 0.7 mL) dropwise. The resulting solution was then warmed to ambient temperature and stirred for 2 h. Et₂O and water were added, and the organic phase was separated, washed with brine, dried over Na₂SO₄ and concentrated in vacuo. Purification of the residue by FCC hexane/EtOAc (30/70) afforded the title compound as a colourless solid (13.4 mg, 93% yield, >20:1 d.r.). $^1\text{H NMR}$ (600 MHz, CDCl_3) δ = 7.84 (br. s, 1H), 7.57 – 7.44 (m, 2H), 7.34 – 7.30 (m, 2H), 7.18 – 7.03 (m, 1H), 3.66 (br. s, 1H), 2.81 (br. s, 1H), 2.56 – 2.37 (m, 1H), 1.69 – 1.49 (m, 2H), 1.34 (d, J = 7.0 Hz, 3H), 1.01 (t, J = 7.0 Hz, 3H) ppm. $^{13}\text{C NMR}$ (151 MHz, CDCl_3) = δ 174.2, 137.9, 129.1, 124.5, 120.1, 75.4, 47.2, 28.4, 15.8, 10.2 ppm. Spectroscopic data for **11a** match those previously reported in the literature.^{xi}



2-benzyl-N-phenyl-3-(4,4,5,5-tetramethyl-1,3,2-dioxaborolan-2-yl)hexanamide (12). Following General Procedure E, 2-benzyl-N-phenylpent-4-enamide (**1k**) (53.1 mg, 0.20 mmol), $\text{W}(\text{CO})_3(\text{MeCN})_3$ (4 mg, 5 mol %) and HBpin (116 μ L, 4 equiv) were used at 40 °C affording the title compound as a white solid (66 mg, 81% yield) by using DCM/MeCN (95/5) as eluent. $^1\text{H NMR}$ (500 MHz, CDCl_3) δ =

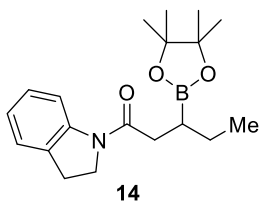
Chapter 4

7.38 – 7.18 (m, 10H), 7.06 (t, $J = 7.3$ Hz, 1H), 3.01 (d, $J = 7.5$ Hz, 2H), 2.67 (q, $J = 7.4$ Hz, 1H), 1.65 (p, $J = 7.3$ Hz, 2H), 1.31 (s, 6H), 1.31 (m, 1H), 1.30 (s, 6H), 1.02 (t, $J = 7.4$ Hz, 3H) ppm. ^{13}C NMR (126 MHz, CDCl_3) $\delta = 173.6, 140.3, 138.1, 129.1, 128.8, 128.6, 126.4, 123.8, 119.7, 83.5, 52.8, 38.4, 25.0, 25.0, 22.2, 13.5$ ppm (*The carbon attached to boron was not observed due to quadrupolar relaxation*). HRMS calcd. for $(\text{C}_{25}\text{H}_{35}\text{BNO}_3)$ $[\text{M}+\text{H}]^+$: 394.2548, found 394.2550.

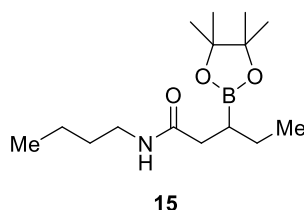


***N*-methyl-*N*-phenyl-3-(4,4,5,5-tetramethyl-1,3,2-dioxaborolan-2-yl)pentanamide (13).**

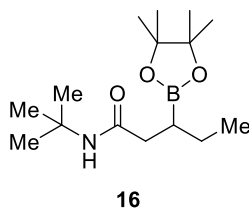
Following General Procedure E, *N*-methyl-*N*-phenylpent-4-enamide (**11**) (37.9 mg, 0.20 mmol) and HBpin (116 μL , 4 equiv) were used at 40 $^\circ\text{C}$, affording the title compound as a yellow oil (45.1 mg, 71% yield) by using Hexane/EtOAc (90/10) as eluent. ^1H NMR (500 MHz, CDCl_3) $\delta = 7.38$ (t, $J = 7.7$ Hz, 2H), 7.30 (t, $J = 7.6$ Hz, 1H), 7.17 (d, $J = 7.3$ Hz, 2H), 3.23 (s, 3H), 2.20 – 2.13 (m, 2H), 1.43 – 1.32 (m, 1H), 1.25 (d, $J = 5.5$ Hz, 12H), 1.23 – 1.09 (m, 2H), 0.80 (t, $J = 7.5$ Hz, 3H) ppm. ^{13}C NMR (126 MHz, CDCl_3) $\delta = 173.6, 144.2, 129.5, 127.5, 127.2, 82.6, 37.3, 36.1, 24.8, 24.8, 23.5, 13.4$ ppm. (*The carbon attached to boron was not observed due to quadrupolar relaxation*). IR (neat, cm^{-1}): 3286, 2976, 2930, 1748, 1686, 1655, 1596, 1372, 1134. HRMS calcd. for $(\text{C}_{18}\text{H}_{28}\text{NO}_3\text{B})$ $[\text{M}+\text{H}]^+$: 317.2271, found 317.2266.



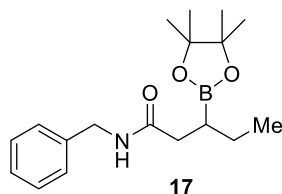
1-(indolin-1-yl)-3-(4,4,5,5-tetramethyl-1,3,2-dioxaborolan-2-yl)hexan-1-one (14) Following General Procedure E, 1-(indolin-1-yl)pent-4-en-1-one (**1m**) (40.2 mg, 0.20 mmol), $\text{W}(\text{CO})_3(\text{MeCN})_3$ (4 mg, 5 mol %) and HBpin (116 μL , 4 equiv) were used at 40 $^\circ\text{C}$ affording the title compound as a white solid (51 mg, 75% yield) by using DCM/MeCN (95/5) as eluent. Same reaction was performed at gram scale (**1m**, 5 mmol) affording the product in 1.4 g, 85% yield. Single crystals suitable for x-ray diffraction were grown by slow evaporation from acetone (CCDC 2033217). ^1H NMR (600 MHz, CDCl_3) $\delta = 8.22$ (d, $J = 8.6$ Hz, 1H), 7.16 (t, $J = 7.5$ Hz, 2H), 7.02 – 6.93 (m, 1H), 4.04 (dtd, $J = 18.4, 10.1, 8.3$ Hz, 2H), 3.17 (t, $J = 8.5$ Hz, 2H), 2.52 (h, $J = 9.7, 8.9$ Hz, 2H), 1.60 – 1.50 (m, 1H), 1.44 (dp, $J = 14.4, 7.3$ Hz, 1H), 1.37 – 1.29 (m, 1H), 1.25 (d, $J = 15.7$ Hz, 12H), 0.97 (t, $J = 7.4$ Hz, 3H) ppm. ^{13}C NMR (151 MHz, CDCl_3) $\delta = 171.7, 143.3, 131.0, 127.5, 124.5, 123.3, 117.0, 82.9, 47.8, 38.0, 28.1, 24.9, 24.8, 23.7, 13.7$ ppm (*The carbon attached to boron was not observed due to quadrupolar relaxation*). HRMS calcd. for $(\text{C}_{19}\text{H}_{29}\text{NBO}_3)$ $[\text{M}+\text{H}]^+$: 330.2235, found 330.2235.



***N*-butyl-3-(4,4,5,5-tetramethyl-1,3,2-dioxaborolan-2-yl)pentanamide (15).** Following General Procedure E, *N*-butylpent-4-enamide (**1n**) (31.0 mg, 0.20 mmol) and HBpin (116 μ L, 4 equiv) were used at 40 °C, affording the title compound as a white solid (29 mg, 51% yield) by using Hexane/EtOAc (90/10) as eluent. **Mp:** 56 - 58 °C. **$^1\text{H NMR}$** (400 MHz, CDCl_3) δ = 5.59 (s, 1H), 3.31 – 3.18 (m, 2H), 2.40 – 2.17 (m, 2H), 1.54 – 1.39 (m, 4H), 1.39 – 1.30 (m, 2H), 1.30 – 1.28 (m, 1H), 1.25 (d, J = 2.4 Hz, 12H), 0.97 – 0.89 (m, 6H) ppm. **$^{13}\text{C NMR}$** (101 MHz, CDCl_3) δ = 173.1, 83.1, 39.2, 38.0, 31.8, 24.8, 24.8, 23.8, 20.1, 13.7, 13.3 ppm. (*The carbon attached to boron was not observed due to quadrupolar relaxation*). **IR** (neat, cm^{-1}): 3285, 2974, 2928, 1655, 1597, 1541, 1368, 1145, 725. **HRMS** calcd. for ($\text{C}_{15}\text{H}_{31}\text{BNO}_3$) [$\text{M}+\text{H}$] $^+$: 283.2428, found 283.2434.



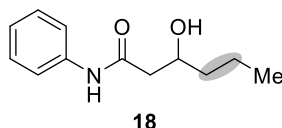
***N*-(tert-butyl)-3-(4,4,5,5-tetramethyl-1,3,2-dioxaborolan-2-yl)pentanamide (16).** Following General Procedure E, *N*-(tert-butyl)pent-4-enamide (**1o**) (31.0 mg, 0.20 mmol) and HBpin (116 μ L, 4 equiv) were used at 40 °C, affording the title compound as a white powder (51 mg, 91% yield) by using Hexane/EtOAc (90/10) as eluent. **Mp:** 41 - 43 °C. **$^1\text{H NMR}$** (400 MHz, CDCl_3) δ = 5.47 (s, 1H), 1.50 – 1.37 (m, 2H), 1.36 – 1.32 (m, 1H), 1.30 (s, 9H), 1.23 (d, J = 2.7 Hz, 12H), 0.90 (t, J = 7.4 Hz, 3H) ppm. **$^{13}\text{C NMR}$** (101 MHz, CDCl_3) δ = 172.6, 83.0, 50.9, 38.7, 28.8, 24.8, 24.7, 23.7, 13.3 ppm. (*The carbon attached to boron was not observed due to quadrupolar relaxation*). **IR** (neat, cm^{-1}): 3280, 2971, 2921, 2873, 1650, 1598, 1543, 1368, 1145, 726. **HRMS** calcd. for ($\text{C}_{15}\text{H}_{30}\text{NO}_3\text{B}$) [$\text{M}+\text{H}$] $^+$: 283.2428, found 283.2427.



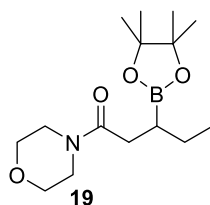
***N*-benzyl-3-(4,4,5,5-tetramethyl-1,3,2-dioxaborolan-2-yl)pentanamide (17):** Following General Procedure E, *N*-benzylbut-3-enamide (**1p**) (35 mg, 0.20 mmol), $\text{W}(\text{CO})_3(\text{MeCN})_3$ (4 mg, 5 mol %) and HBpin (116 μ L, 4 equiv) were used at 40 °C affording the title compound as a white solid (52 mg, 82% yield) by using EtOAc/Hexanes (85/15) as eluent. **$^1\text{H NMR}$** (600 MHz, CDCl_3) δ = 7.49 – 7.22 (m, 5H),

Chapter 4

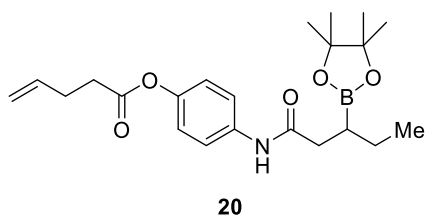
6.01 (s, 1H), 4.51 – 4.37 (m, 2H), 2.47 – 2.25 (m, 2H), 1.50 (ddq, $J = 41.4, 13.7, 7.1$ Hz, 2H), 1.38 – 1.32 (m, 1H), 1.31 – 1.15 (m, 12H), 0.96 (t, $J = 7.4$ Hz, 3H) ppm. $^{13}\text{C NMR}$ (151 MHz, CDCl_3) $\delta = 173.2, 138.64, 128.7, 128.0, 127.5, 83.3, 43.7, 37.9, 24.8, 24.8, 24.0, 13.4$ ppm (*The carbon attached to boron was not observed due to quadrupolar relaxation*). **HRMS** calcd. for ($\text{C}_{18}\text{H}_{29}\text{NBO}_3$) [$\text{M}+\text{H}$] $^+$: 318.2235, found 318.2234.



3-hydroxy-N-phenylhexanamide (18). Following General Procedure E, (E)-N-phenylhex-4-enamide (**1q**) (39.0 mg, 0.20 mmol) and HBpin (116 μL , 4 equiv) were used at 40 °C. The oxidation to the alcohol was promoted by using H_2O_2 (30 % v/v)/aq. NaOH (3 M) in THF/ H_2O and BHT affording the title compound as a white powder (21 mg, 50% yield) by using Hexane/EtOAc (70/30) as eluent. **Mp**: 82 – 84 °C. $^1\text{H NMR}$ (400 MHz, CDCl_3) $\delta = 7.77$ (s, 1H), 7.51 (d, $J = 8.6$ Hz, 2H), 7.33 (t, $J = 7.9$ Hz, 2H), 7.11 (t, $J = 7.4$ Hz, 1H), 4.12 (td, $J = 7.7, 3.2$ Hz, 1H), 2.62 – 2.37 (m, 2H), 2.03 (s, 1H), 1.63 – 1.41 (m, 4H), 0.96 (t, $J = 7.1$ Hz, 3H) ppm. $^{13}\text{C NMR}$ (101 MHz, CDCl_3) $\delta = 170.4, 137.6, 129.0, 124.4, 120.0, 68.5, 43.9, 39.1, 18.7, 13.9$ ppm. **IR** (neat, cm^{-1}): 3285, 2930, 1748, 1656, 1538, 1505, 1372, 1298, 1133. Spectroscopic data for **18** match those previously reported in the literature.^{xii}

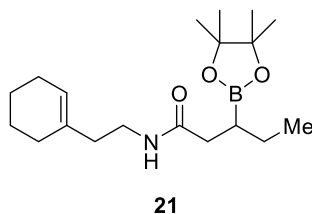


1-Morpholino-3-(4,4,5,5-tetramethyl-1,3,2-dioxaborolan-2-yl)pentan-1-one (19). Following General Procedure E, 1-morpholinopent-4-en-1-one (**1r**) (33.8 mg, 0.20 mmol) and HBpin (116 μL , 4 equiv) were used at 40 °C, affording the title compound as a colourless oil (35.6 mg, 60% yield) by using Hexane/EtOAc (10/90) as eluent. $^1\text{H NMR}$ (500 MHz, CDCl_3) $\delta = 3.69 - 3.61$ (m, 4H), 3.61 – 3.35 (m, 4H), 2.58 – 2.30 (m, 2H), 1.57 – 1.45 (m, 1H), 1.42 – 1.30 (m, 1H), 1.29 – 1.17 (m, 13H), 0.93 (t, $J = 7.4$ Hz, 3H) ppm. $^{13}\text{C NMR}$ (126 MHz, CDCl_3) $\delta = 172.5, 82.7, 67.1, 66.7, 45.9, 42.3, 35.0, 25.0, 24.9, 23.8, 13.7$ ppm (*The carbon attached to boron was not observed due to quadrupolar relaxation*). **HRMS** calcd. for ($\text{C}_{15}\text{H}_{28}\text{BNO}_4$) [$\text{M}+\text{OH}$] $^-$: 313.2175, found 313.2177.



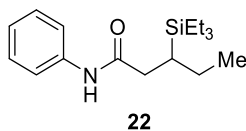
4-(3-(4,4,5,5-tetramethyl-1,3,2-dioxaborolan-2-yl)pentanamido)phenyl pent-4-enoate (20).

Following General Procedure E, 4-(pent-4-enamido)phenyl pent-4-enoate (**1s**) (54.6 mg, 0.20 mmol) and HBpin (116 μ L, 4 equiv) were used at 40 °C, affording the title compound as a white solid (42 mg, 52% yield) by using Hexane/EtOAc (75/25) as eluent. **Mp**: 79 - 81 °C. **$^1\text{H NMR}$** (400 MHz, CDCl_3) δ = 7.64 (bs, 1H), 7.57 – 7.39 (m, 2H), 7.08 – 6.85 (m, 2H), 5.98 – 5.81 (m, 1H), 5.21 – 5.01 (m, 2H), 2.64 (td, J = 7.3, 0.9 Hz, 2H), 2.55 – 2.41 (m, 4H), 1.68–1.35 (m, 2H), 1.41 – 1.31 (m, 1H), 1.25 (d, J = 3.1 Hz, 12H), 0.96 (t, J = 7.3 Hz, 3H) ppm. **$^{13}\text{C NMR}$** (101 MHz, CDCl_3) δ = 171.7, 171.5, 146.5, 136.3, 135.9, 121.8, 120.3, 115.9, 83.4, 38.9, 33.6, 28.8, 24.8, 24.7, 23.8, 13.2 ppm (*The carbon attached to boron was not observed due to quadrupolar relaxation*). **IR** (neat, cm^{-1}): 3368, 1686, 1545, 1510, 1251, 913. **HRMS** calcd. for ($\text{C}_{22}\text{H}_{33}\text{BNO}_5$) [$\text{M}+\text{H}$] $^+$: 401.2483, found 401.2483.



N-(2-(cyclohex-1-en-1-yl)ethyl)-3-(4,4,5,5-tetramethyl-1,3,2-dioxaborolan-2-yl)pentanamide

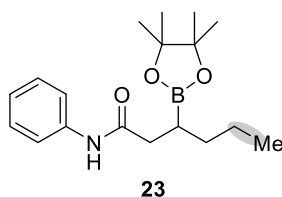
(21). Following General Procedure E, *N*-(2-(cyclohex-1-en-1-yl)ethyl)pent-4-enamide (**1t**) (41.4 mg, 0.20 mmol) and HBpin (116 μ L, 4 equiv) were used at 40 °C, affording the title compound as a colorless oil (34 mg, 50% yield) by using Hexane/EtOAc (90/10) as eluent. **$^1\text{H NMR}$** (400 MHz, CDCl_3) δ = 5.51 (bs, 1H), 5.45 (bs, 1H), 3.30 (p, J = 6.5 Hz, 2H), 2.35 – 2.16 (m, 2H), 2.10 (t, J = 6.8 Hz, 2H), 2.02 – 1.95 (m, 2H), 1.93 – 1.88 (m, J = 5.7 Hz, 2H), 1.65 – 1.59 (m, 2H), 1.58 – 1.50 (m, 2H), 1.50 – 1.35 (m, 2H), 1.24 (s, 6H), 1.23 (m, 1H), 1.22 (s, 6H), 0.91 (t, J = 7.4 Hz, 3H) ppm. **$^{13}\text{C NMR}$** (101 MHz, CDCl_3) δ = 173.0, 134.7, 123.3, 83.1, 37.9, 37.7, 37.1, 27.9, 25.2, 24.8, 24.8, 23.7, 22.8, 22.3, 13.3 ppm. (*The carbon attached to boron was not observed due to quadrupolar relaxation*). **IR** (neat, cm^{-1}): 3226, 2950, 2901, 2875, 1756, 1649, 1595, 1545, 1448, 1263. **HRMS** calcd. for ($\text{C}_{19}\text{H}_{33}\text{BNO}_3$) [$\text{M}+\text{H}$] $^+$: 333.2595, found 333.2604.



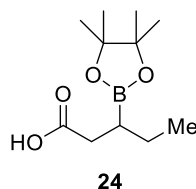
N-phenyl-3-(triethylsilyl)pentanamide (22). Following a modified General Procedure E, *N*-phenylpent-4-enamide (**1a**) (35.0 mg, 0.20 mmol), B_2Pin_2 (76 mg, 1.5 equiv), CsF (30.4 mg, 1 equiv) and CuF_2 (11.2 mg, 0.5 equiv) were used at 100 °C in Me-THF (1.0 mL) affording the title compound as a white powder (52 mg, 89% yield) by using Hexane/EtOAc (80/20) as eluent. **Mp**: 86 - 84 °C. **$^1\text{H NMR}$** (400 MHz, CDCl_3) δ = 7.52 (d, J = 7.8 Hz, 2H), 7.34 – 7.24 (m, 3H), 7.09 (t, J = 7.4 Hz, 1H), 2.44 (dd, J = 15.0, 3.8 Hz, 1H), 2.28 – 2.14 (m, 1H), 1.64 – 1.54 (m, 1H), 1.47 – 1.37 (m, 2H), 0.97 (t, J = 7.9 Hz, 12H), 0.59 (q, J = 7.9 Hz, 6H) ppm. **$^{13}\text{C NMR}$** (101 MHz, CDCl_3) δ = 172.0, 138.1, 128.9, 124.1, 119.7,

Chapter 4

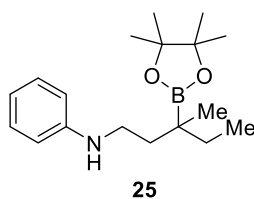
38.4, 23.5, 21.6, 14.0, 7.7, 2.7 ppm. **IR** (neat, cm^{-1}): 3234, 2954, 2908, 2874, 1649, 1595, 1545, 1443, 1261, 709. **HRMS** calcd. for $(\text{C}_{17}\text{H}_{29}\text{NO}_2\text{Si})$ $[\text{M}-\text{H}]^-$: 290.1946, found 290.1942.



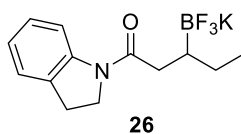
N-(4-bromophenyl)-3-(4,4,5,5-tetramethyl-1,3,2-dioxaborolan-2-yl)hexanamide (23). Following a modified General Procedure E, N-(phenyl)hex-5-enamide (**1u**) (37.8 mg, 0.20 mmol), $\text{W}(\text{CO})_3(\text{MeCN})_3$ (7.8 mg, 10 mol %), CuF_2 (15 mg, 50 mol%), cesium fluoride (30.4 mg, 0.15 mmol), PCy_3 (8.4 mg, 15 mol%), B_2Bpin_2 (76 mg, 3.0 mmol) were added followed by 2-methyl tetrahydrofuran (1 mL) and isopropyl alcohol (30 μL , 0.40 mmol) and heated to 100 °C affording the title compound as a white solid (25.5 mg, 40% yield) by using acetone/hex (15/85) as eluent. **^1H NMR** (600 MHz, CDCl_3) δ = 7.52 (bs, 1H), 7.50 (d, J = 8.1 Hz, 2H), 7.30 (t, J = 7.7 Hz, 2H), 7.07 (t, J = 7.5 Hz, 1H), 2.53 – 2.39 (m, 2H), 1.52 – 1.43 (m, 2H), 1.42 – 1.34 (m, 3H), 1.26 (d, J = 4.4 Hz, 12H), 0.91 (t, J = 7.0 Hz, 3H) ppm. **^{13}C NMR** (151 MHz, CDCl_3) δ = 171.65, 138.48, 129.09, 123.95, 119.59, 83.56, 39.44, 33.17, 25.01, 24.92, 22.06, 14.42 ppm. (*The carbon attached to boron was not observed due to quadrupolar relaxation*). **HRMS** calcd. for $(\text{C}_{18}\text{H}_{29}\text{BNO}_3)$ $[\text{M}+\text{H}]^+$: 318.2235, found 318.2235.



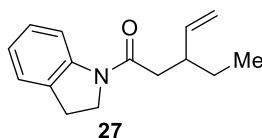
3-(4,4,5,5-tetramethyl-1,3,2-dioxaborolan-2-yl)butanoic acid (24) Following General Procedure E, vinyl acetic acid (**B1**) (17 μL , 0.20 mmol), $\text{W}(\text{CO})_3(\text{MeCN})_3$ (4 mg, 5 mol %) and HBpin (116 μL , 4 equiv) were used at 40 °C affording the title compound as a white solid (52 mg, 82% yield) by using EtOAc/Hexanes (65/35) with 1% acetic acid as eluent. The reduced starting material could not be separated from the product. Both the desired product and butanoic acid are known compounds which have previously been characterized. **^1H NMR** (600 MHz, CDCl_3) δ = 2.43 (qd, J = 16.8, 7.1 Hz, 2H), 1.40 – 1.31 (m, 1H), 1.25 – 1.18 (m, 12H), 1.00 (d, J = 7.5 Hz, 3H) ppm. **^{13}C NMR** (151 MHz, CDCl_3) δ = 178.4, 83.4, 37.3, 34.3, 24.8, 15.8, 15.1 ppm.



N-(3-methyl-3-(4,4,5,5-tetramethyl-1,3,2-dioxaborolan-2-yl)pentyl)aniline (25). Following General Procedure E, 3-methyl-N-phenylpent-4-enamide (**1v**) (39.0 mg, 0.20 mmol), $W(CO)_3(MeCN)_3$ (6 mg, 7.5 mol %) and HBpin (230 μ L, 8 equiv) were used at 100 °C affording the title compound as a brown oil (24 mg, 40% yield) by using Hexane/EtOAc (80/20) as eluent. 1H NMR (400 MHz, $CDCl_3$) δ = 7.22 – 7.12 (m, 2H), 6.69 (t, J = 7.3 Hz, 1H), 6.63 (d, J = 7.6 Hz, 2H), 3.10 (ddd, J = 8.7, 6.4, 2.1 Hz, 2H), 1.77 (ddd, J = 13.2, 8.9, 6.9 Hz, 1H), 1.54 – 1.41 (m, 2H), 1.31 (dd, J = 13.6, 7.5 Hz, 1H), 1.24 (d, J = 3.4 Hz, 12H), 0.96 (s, 3H), 0.87 (t, J = 7.5 Hz, 3H) ppm. ^{13}C NMR (101 MHz, $CDCl_3$) δ = 129.2, 117.3, 113.1, 41.5, 38.1, 31.8, 24.9, 24.8, 24.6, 21.0, 9.8 ppm (*The carbon attached to boron was not observed due to quadrupolar relaxation*). IR (neat, cm^{-1}): 3364, 2970, 2927, 1602, 1453, 1326, 1143. HRMS calcd. for $(C_{18}H_{30}NBO_2)$ $[M+H]^+$: 303.2479, found 303.2474.



(Indolin-1-yl)-3-(trifluoro-1,4-boraneyl)pentan-1-one, potassium salt (26). The title compound was prepared following a modified literature procedure.^{xiii} To a solution of 1-(indolin-1-yl)-3-(4,4,5,5-tetramethyl-1,3,2-dioxaborolan-2-yl)pentan-1-one **14** (150 mg, 0.46 mmol) in MeCN (2 mL) under nitrogen, was added saturated aq. KHF_2 (142 mg, 1.82 mmol, 0.4 mL). The resulting solution was stirred at ambient temperature for 2 h, before being concentrated *in vacuo* and azeotroped with MeOH. The crude product was placed under high vacuum overnight and then extracted with hot MeCN (3 \times 10 mL), filtered and concentrated *in vacuo*. The resulting residue was rinsed with in Et_2O (2 mL) and sonicated for 30 minutes, before being filtered to afford the title compound as a colourless solid (123 mg, 87% yield). 1H NMR (600 MHz, DMSO) δ = 8.08 (d, J = 8.1 Hz, 1H), 7.18 (d, J = 7.4 Hz, 1H), 7.15 – 7.00 (m, 1H), 6.98 – 6.86 (m, 1H), 4.24 – 3.94 (m, 2H), 3.25 – 2.96 (m, 2H), 2.43 – 2.28 (m, 1H), 2.10 – 1.75 (m, 1H), 1.39 – 1.01 (m, 2H), 0.80 (t, J = 7.5 Hz, 3H), 0.63 – 0.49 (m, 1H) ppm. ^{13}C NMR (151 MHz, DMSO) δ = 174.6, 143.7, 131.6, 126.7, 124.5, 122.3, 115.9, 47.7, 38.0, 27.5, 23.9, 13.8 ppm. (*The carbon attached to boron was not observed due to quadrupolar relaxation*). HRMS calcd. for $(C_{13}H_{16}BF_3KNO)$ $[M-K]^-$: 269.1317, found 269.1308.

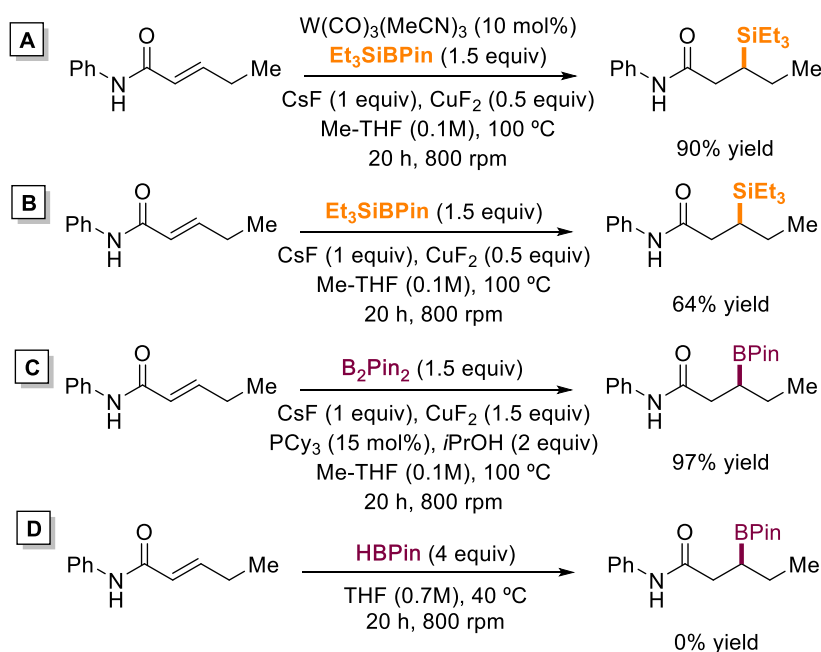


3-Ethyl-1-(indolin-1-yl)pent-4-en-1-one (27). The title compound was prepared following a modified literature procedure.^{xiv} To a solution of (Indolin-1-yl)-3-(trifluoro-1,4-boraneyl)pentan-1-one, potassium salt **26** (50.0 mg, 0.15 mmol) in THF (1.5 mL), was added vinylmagnesium bromide (0.87 mL, 0.7 M, 0.61 mmol) dropwise and the reaction was stirred at ambient temperature for 30 minutes. The reaction mixture was then cooled to –78 °C, before a solution of iodine (155 mg, 0.61 mmol) in MeOH (2.0 mL) was added dropwise. The mixture was stirred at –78 °C for a further 30

Chapter 4

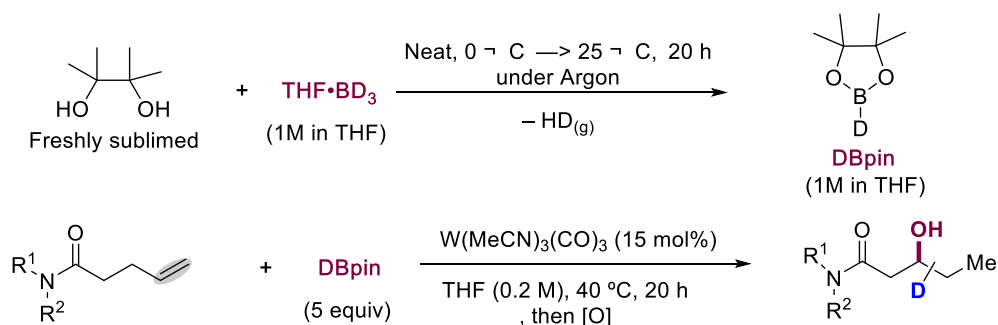
minutes, before a solution of NaOMe (64.8 mg, 1.2 mmol) in MeOH (2.5 mL) was added dropwise. The solution was warmed to ambient temperature and stirred for another 1.5 h, before being diluted with pentane (10 mL) and washed with saturated aq. Na₂S₂O₃ (5 mL) and brine (5 mL). The organic extracts were combined, dried over Na₂SO₄ and concentrated in *vacuo*. Purification of the crude residue by FCC (hexane/EtOAc 90/10) afforded the title compound as an orange oil (33.5 mg, 96%). ¹H NMR (600 MHz, CDCl₃) δ = 8.25 (d, *J* = 8.1 Hz, 1H), 7.21 – 7.10 (m, 2H), 7.07 – 6.93 (m, 1H), 5.81 – 5.63 (m, 1H), 5.15 – 4.95 (m, 2H), 4.16 – 3.95 (m, 2H), 3.26 – 3.07 (m, 2H), 2.78 – 2.33 (m, 3H), 1.71 – 1.32 (m, 2H), 0.95 – 0.85 (m, 3H) ppm. ¹³C NMR (151 MHz, CDCl₃) δ = 170.4, 143.2, 141.4, 131.2, 127.6, 124.6, 123.6, 117.3, 115.2, 48.3, 41.6, 41.2, 28.1, 27.5, 11.7 ppm. HRMS calcd. for (C₁₅H₁₉NO) [M+H]⁺: 230.1545, found 230.1541.

4.5.5 Control reactions with α,β-unsaturated amides



The control reactions for *B* showed that the reaction worked in good yield without the need of the *W* catalyst. This might point out to a mechanism similar to reaction *C*, where the tungsten promotes the isomerization of the double bond until the formation of the α,β-unsaturated amide allowing a 1,4-hydroboration or 1,4-hydroboration likely catalyzed by copper. As depicted, reaction *D* did not yield the product, leading to the conclusion that tungsten is involved in the borylative event or that intermediate is not involved through the catalytic cycle.

4.5.6 Deuterium labeling experiments with DBpin

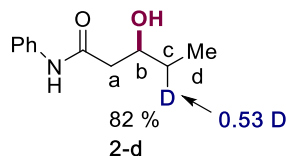


General Procedure F: freshly sublimed pinacol (118 mg, 1.00 mmol) was added to a solution of d_3 -borane-THF complex 1M (1 mL, 1.00 mmol) (commercial from Alpha Aesar) in a flame dried 6 mL screw top vial, under argon at 0 °C. The reaction mixture stirred in the glovebox and was allowed to warm up to room temperature overnight. The solution of deuterated pinacol borane was used as such, without further purification. Each experiment used freshly prepared DBpin.

To a freshly prepared DBpin solution (1M in THF) was added $W(CO)_3(MeCN)_3$ (11.4 mg, 15 mol%) followed by alkene (0.20 mmol). The vial was sealed inside the glovebox, then brought out and heated at 40 °C for 18 hours. The reaction was then allowed to cool to room temperature and 1 mL of 2M aq. K_2CO_3 was added to the reaction mixture followed by 30% H_2O_2 v/v (82 μ L, 0.800 mmol). The reaction was stirred for 1 hour then diluted with diethyl ether and the organic layer separated, and evaporated to dryness. The crude material was purified by flash chromatography on silica gel using ethyl acetate/hexane (30/70) as eluent.

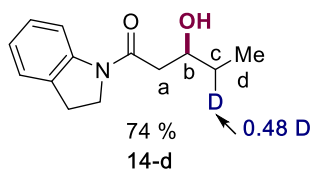
Quantitative 1H NMR were conducted according to standard procedure outlined by Bruker. The integrations are given as they appear. For ^{13}C NMR or non-deuterated data see above.

Note: the boronic ester cannot accurately be integrated due to some overlapping signal. For this same reason d_6 -dmsO was the solvent of choice to prevent inaccurate integration by residual water.



According to General Procedure F, $W(CO)_3(MeCN)_3$ (11.4 mg, 15 mol%) was added followed by alkene **1a** (35 mg, 0.20 mmol) and stirred at 40 °C for 18 hours. The oxidation to the alcohol was promoted by using H_2O_2 (30 % v/v) (82 μ L, 0.80 mmol) with 1 mL aq. K_2CO_3 (2 M) affording the title compound as a white powder (32 mg, 82% yield) by using Hexane/EtOAc (70/30) as eluent. 1H NMR (600 MHz, DMSO) δ = 9.83 (s, 1.00H), 7.60 (d, J = 8.0 Hz, 2.03H), 7.28 (t, J = 7.8 Hz, 2.02H), 7.01 (t, J = 7.4 Hz, 1.05H), 4.68 (dd, J = 5.2, 3.0 Hz, 1.00H, **b**), 3.85 (p, J = 5.9 Hz, 1.00H), 2.37 (d, J = 6.5 Hz, 2.00H, **a**), 1.41 (dddd, J = 34.5, 19.7, 13.2, 7.2 Hz, 1.47H, **c**), 0.88 (d, J = 7.8 Hz, 3.02H, **d**) ppm.

Chapter 4



According to General Procedure F, $W(CO)_3(MeCN)_3$ (11.4 mg, 15 mol%) was added followed by alkene **1m** (40.2 mg, 0.20 mmol) and stirred at 40 °C for 18 hours. The oxidation to the alcohol was promoted by using H_2O_2 (30 % v/v) (82 μ L, 0.80 mmol) with 1 mL aq. K_2CO_3 (2 M) affording the title compound as a white powder (32 mg, 74% yield) by using Hexane/EtOAc (70/30) as eluent. 1H NMR (600 MHz, DMSO) δ = 8.09 (d, J = 8.0 Hz, 0.98H), 7.33 – 7.04 (m, 2.13H), 6.97 (t, J = 7.4 Hz, 1.09H), 4.63 (dd, J = 5.1, 3.1 Hz, 1.00H, **b**), 4.11 (dq, J = 30.8, 9.5 Hz, 2.00H), 3.95 – 3.81 (m, 1.00H), 3.11 (t, J = 8.6 Hz, 2.00H), 2.59 – 2.37 (m, 2.49H, **a**), 1.54 – 1.32 (m, 1.52H, **c**), 0.90 (dd, J = 8.8, 7.3 Hz, 3.08H, **d**) ppm.

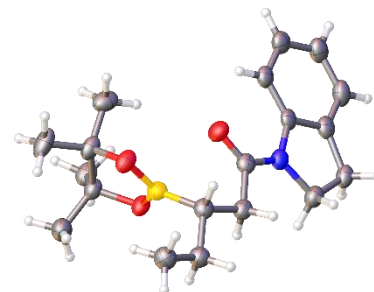
4.5.7 References of experimental procedures

- I) Miller, D.; Choi, G.; Orbe, H.; Knowles, R*. *J. Am. Chem. Soc.* **2015**, *137*, 13492–13495.
- II) Neukom, J.; Perch, N.; Wolfe, J*. *Organometallics* **2011**, *30*, 1269–1277.
- III) Jia, H.; Ho, Y.; Bülow, R.; Rueping, M. *Chemistry - A European Journal* **2018**, *24*, 14054–14058.
- IV) Nicolaou, K.; Baran, P.; Zhong, Y.; Barluenga, S.; Hunt, K.; Kranich, R.; Vega, J*. *J. Am. Chem. Soc.* **2002**, *124*, 2233–2244.
- V) Li, Z.; Song, L.; Li, C*. *J. Am. Chem. Soc.* **2013**, *135*, 4640–4643.
- VI) Metz, P*; Mues, C. *Tetrahedron*, **1988**, *44*, 6841–6853.
- VII) Briggs, M.; Zard, S*. *Synlett*, **2005**, *2*, 334–336.
- VIII) Xiao, K.; Wang, A.; Huang, Y.; Huang, P*. *Asian J. Org. Chem.* **2012**, *1*, 130 – 132.
- IX) Chen, Y.; Ellwart, M.; Toupalas, G. Ebe, Y.; Knochel, P*. *Angew. Chem. Int. Ed.* **2017**, *56*, 4612–4616.
- X) Cooke, M.; Pollock, C*. *J. Org. Chem.* **1992**, *58*, 7474–7481.
- XI) Gao, T.; Zhang, W.; Sun, Z.; Lu, H.; Li, Bi*. *J. Am. Chem. Soc.* **2019**, *141*, 4670–4677.
- XII) Smith, S.; Thacker, N.; Tackas, J*. *J. Am. Chem. Soc.* **2008**, *130*, 3734–3735.
- XIII) Perlstein, D.; Wang, T.; Doud, E.; Kahne, D.; Walker, S. *J. Am. Chem. Soc.* **2010**, *132*, 48, 17108–17110.
- XIV) Hoang, G.; Takacs, J. *Chem. Sci.* **2017**, *8*, 4511–4516.

4.5.8 X-Ray of compound 14

Table 1. Crystal data and structure refinement for **14**.

Report date	2020-09-21	
Identification code	engle265	
Empirical formula	C ₁₉ H ₂₈ B N O ₃	
Molecular formula	C ₁₉ H ₂₈ B N O ₃	
Formula weight	329.23	
Temperature	100.0 K	
Wavelength	1.54178 Å	
Crystal system	Monoclinic	
Space group	P 1 21/c 1	
Unit cell dimensions	a = 10.5238(3) Å	$\alpha = 90^\circ$.
	b = 14.0554(3) Å	$\beta = 96.2420(10)^\circ$.
	c = 25.2685(6) Å	$\gamma = 90^\circ$.
Volume	3715.46(16) Å ³	
Z	8	
Density (calculated)	1.177 Mg/m ³	
Absorption coefficient	0.614 mm ⁻¹	
F(000)	1424	
Crystal size	0.18 x 0.15 x 0.085 mm ³	
Crystal color, habit	colorless plate	
Theta range for data collection	3.519 to 58.031°.	
Index ranges	-11 ≤ h ≤ 11, 0 ≤ k ≤ 15, 0 ≤ l ≤ 27	
Reflections collected	45664	
Independent reflections	5245 [R(int) = 0.0627]	
Completeness to theta = 58.031°	99.9 %	
Absorption correction	Semi-empirical from equivalents	
Max. and min. transmission	0.751 and 0.504	
Refinement method	Full-matrix least-squares on F ²	
Data / restraints / parameters	5245 / 0 / 444	
Goodness-of-fit on F ²	1.126	
Final R indices [I > 2σ(I)]	R1 = 0.0505, wR2 = 0.1257	
R indices (all data)	R1 = 0.0591, wR2 = 0.1308	
Largest diff. peak and hole	0.304 and -0.202 e.Å ⁻³	



Chapter 4

Anisotropic displacement parameters ($\text{\AA}^2 \times 10^3$) The anisotropic displacement factor exponent takes the form: $-2\pi^2 [h^2 a^{*2} U^{11} + \dots + 2 h k a^* b^* U^{12}]$

	U ¹¹	U ²²	U ³³	U ²³	U ¹³	U ¹²
O(1)	30(1)	46(1)	46(1)	0(1)	5(1)	-6(1)
O(1')	29(1)	44(1)	49(1)	1(1)	2(1)	1(1)
O(2')	27(1)	35(1)	47(1)	1(1)	5(1)	-3(1)
O(2)	32(1)	28(1)	57(1)	-10(1)	9(1)	-3(1)
O(3)	27(1)	29(1)	50(1)	-3(1)	6(1)	-3(1)
O(3')	30(1)	30(1)	48(1)	8(1)	2(1)	-7(1)
N(1')	28(2)	28(1)	39(2)	2(1)	2(1)	-2(1)
N(1)	30(2)	25(1)	43(2)	-1(1)	2(1)	1(1)
C(1')	49(2)	59(2)	41(2)	9(2)	5(2)	-9(2)
C(1)	48(2)	45(2)	44(2)	-3(2)	3(2)	0(2)
C(2')	46(2)	48(2)	43(2)	0(2)	4(2)	-10(2)
C(2)	40(2)	36(2)	43(2)	1(1)	5(2)	-1(2)
C(3)	35(2)	27(2)	41(2)	-2(1)	2(2)	-2(1)
C(3')	35(2)	34(2)	43(2)	2(1)	2(2)	-4(2)
C(4)	33(2)	26(2)	46(2)	-1(1)	6(2)	-1(1)
C(4')	29(2)	35(2)	46(2)	5(1)	2(1)	-6(1)
C(5')	30(2)	23(2)	44(2)	3(1)	1(2)	-6(1)
C(5)	34(2)	22(2)	44(2)	-1(1)	2(2)	0(1)
C(6)	33(2)	33(2)	49(2)	-2(2)	6(2)	1(2)
C(6')	28(2)	34(2)	46(2)	2(1)	7(2)	-2(1)
C(7')	27(2)	30(2)	45(2)	3(1)	3(1)	-3(1)
C(7)	28(2)	28(2)	56(2)	-3(1)	0(2)	1(1)
C(8')	25(2)	23(2)	42(2)	1(1)	4(1)	2(1)
C(8)	35(2)	22(2)	48(2)	-3(1)	-1(2)	5(1)
C(9')	24(2)	31(2)	47(2)	1(1)	0(2)	3(1)
C(9)	37(2)	35(2)	52(2)	-7(2)	-7(2)	8(2)
C(10')	36(2)	31(2)	42(2)	-2(1)	4(2)	4(2)
C(10)	46(2)	40(2)	45(2)	-4(2)	0(2)	13(2)
C(11')	33(2)	26(2)	44(2)	-2(1)	9(2)	-4(1)
C(11)	40(2)	30(2)	47(2)	-2(1)	7(2)	10(2)
C(12)	32(2)	24(2)	47(2)	-1(1)	1(2)	7(1)
C(12')	24(2)	22(2)	50(2)	-1(1)	3(1)	-2(1)
C(13)	31(2)	20(2)	42(2)	-1(1)	0(2)	7(1)
C(13')	29(2)	18(1)	40(2)	0(1)	1(1)	-1(1)

W-catalyzed remote β -hydroboration of alkenes

C(14')	23(2)	30(2)	47(2)	-1(1)	4(1)	-3(1)
C(14)	29(2)	31(2)	56(2)	-12(2)	9(2)	0(1)
C(15)	28(2)	31(2)	47(2)	-3(1)	5(1)	0(1)
C(15')	28(2)	25(2)	46(2)	4(1)	2(1)	-7(1)
C(16')	30(2)	32(2)	64(2)	8(2)	3(2)	0(2)
C(16)	53(2)	32(2)	64(2)	-1(2)	24(2)	-5(2)
C(17)	27(2)	48(2)	86(3)	-23(2)	6(2)	-4(2)
C(17')	41(2)	45(2)	59(2)	-12(2)	4(2)	1(2)
C(18)	35(2)	30(2)	60(2)	-7(2)	6(2)	-7(2)
C(18')	40(2)	34(2)	54(2)	1(2)	10(2)	1(2)
C(19')	28(2)	30(2)	64(2)	4(2)	-4(2)	-1(2)
C(19)	42(2)	49(2)	55(2)	6(2)	8(2)	7(2)
B(1)	34(2)	31(2)	37(2)	-1(2)	4(2)	-7(2)
B(1')	33(2)	34(2)	36(2)	2(2)	1(2)	-2(2)

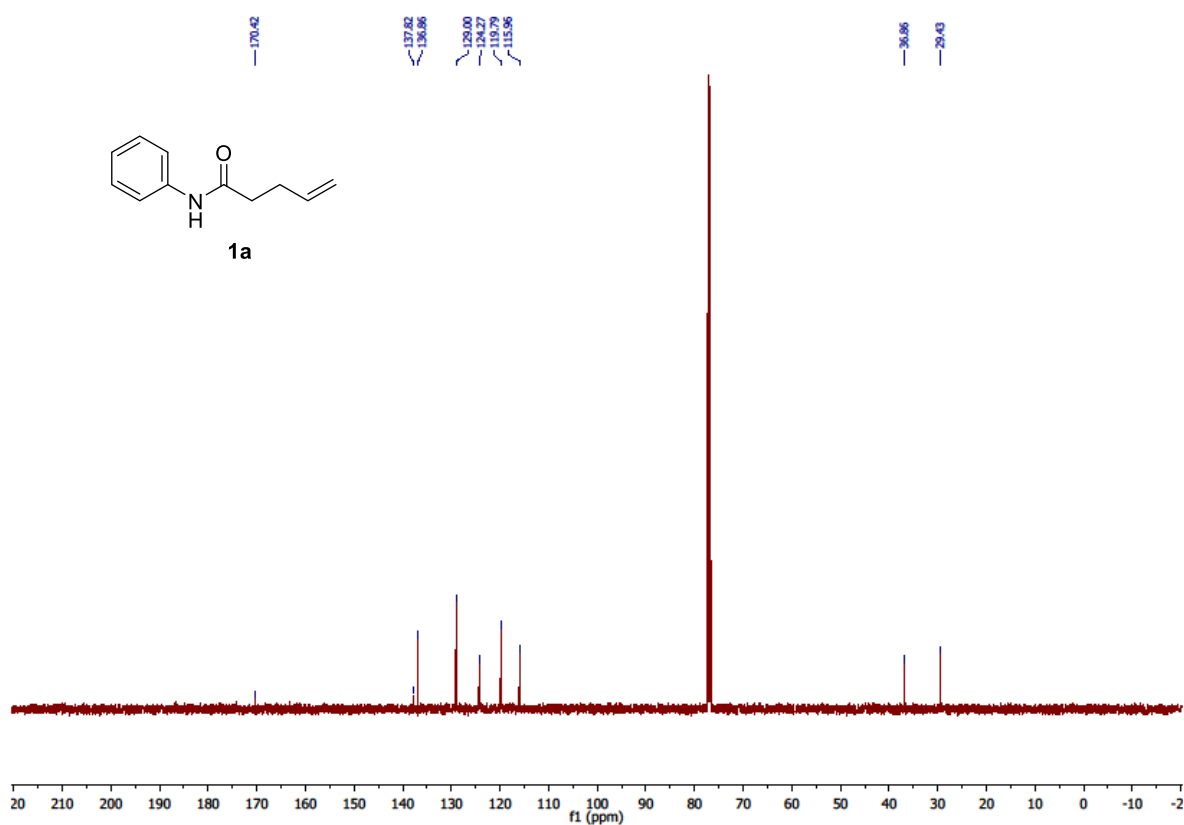
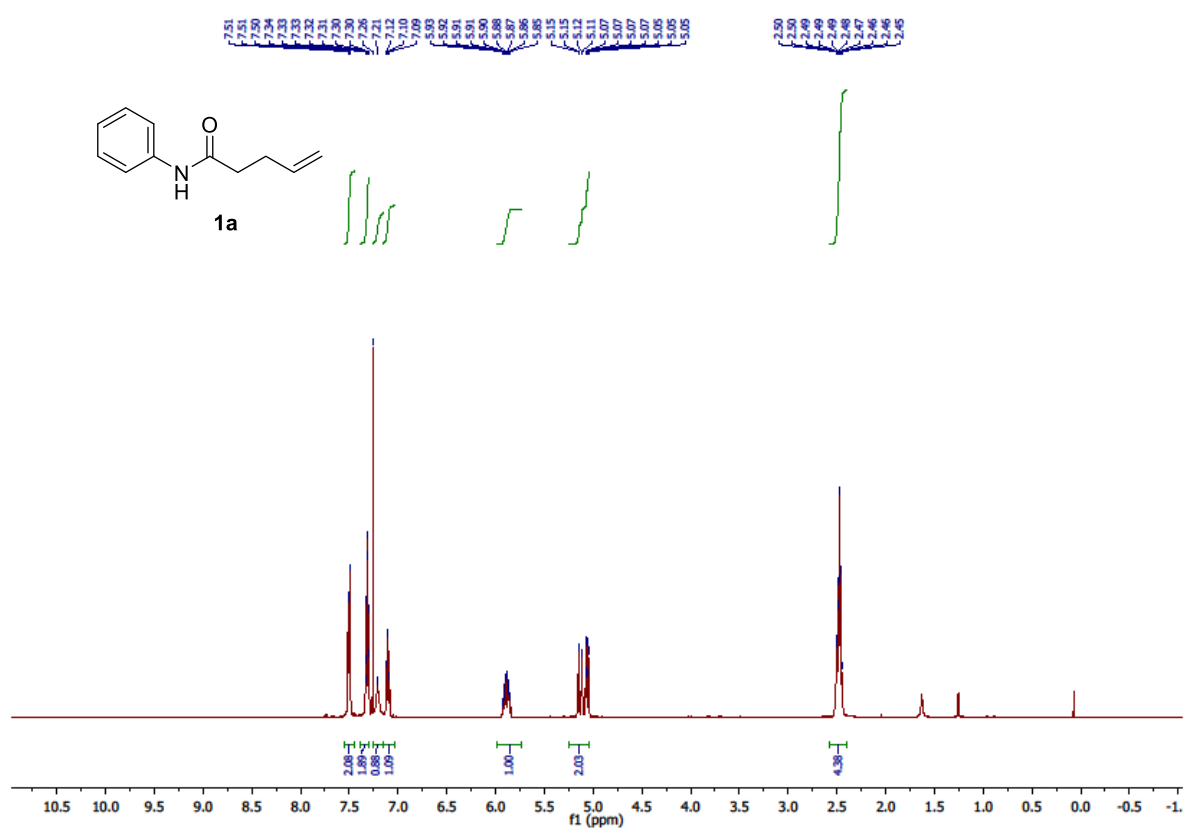
Table 5. Hydrogen coordinates ($\times 10^4$) and isotropic displacement parameters ($\text{\AA}^2 \times 10^3$) for Engle265.

	x	y	z	U(eq)
H(1'A)	5443	3291	4983	74
H(1'B)	5767	2548	4537	74
H(1'C)	6596	2554	5106	74
H(1A)	9633	3589	4634	68
H(1B)	8627	3846	5044	68
H(1C)	9219	2798	5038	68
H(2'A)	3970	1997	4919	55
H(2'B)	5129	1274	5059	55
H(2A)	10676	4464	5350	47
H(2B)	11264	3415	5346	47
H(3)	9987	2952	6026	42
H(3')	4407	2691	5779	45
H(4A)	12086	3393	6296	42
H(4B)	11715	4499	6291	42
H(4'A)	6247	1190	5983	44
H(4'B)	6559	2307	5998	44
H(6A)	13476	4747	6982	46
H(6B)	13806	3628	6999	46
H(6'A)	8351	2148	6683	43

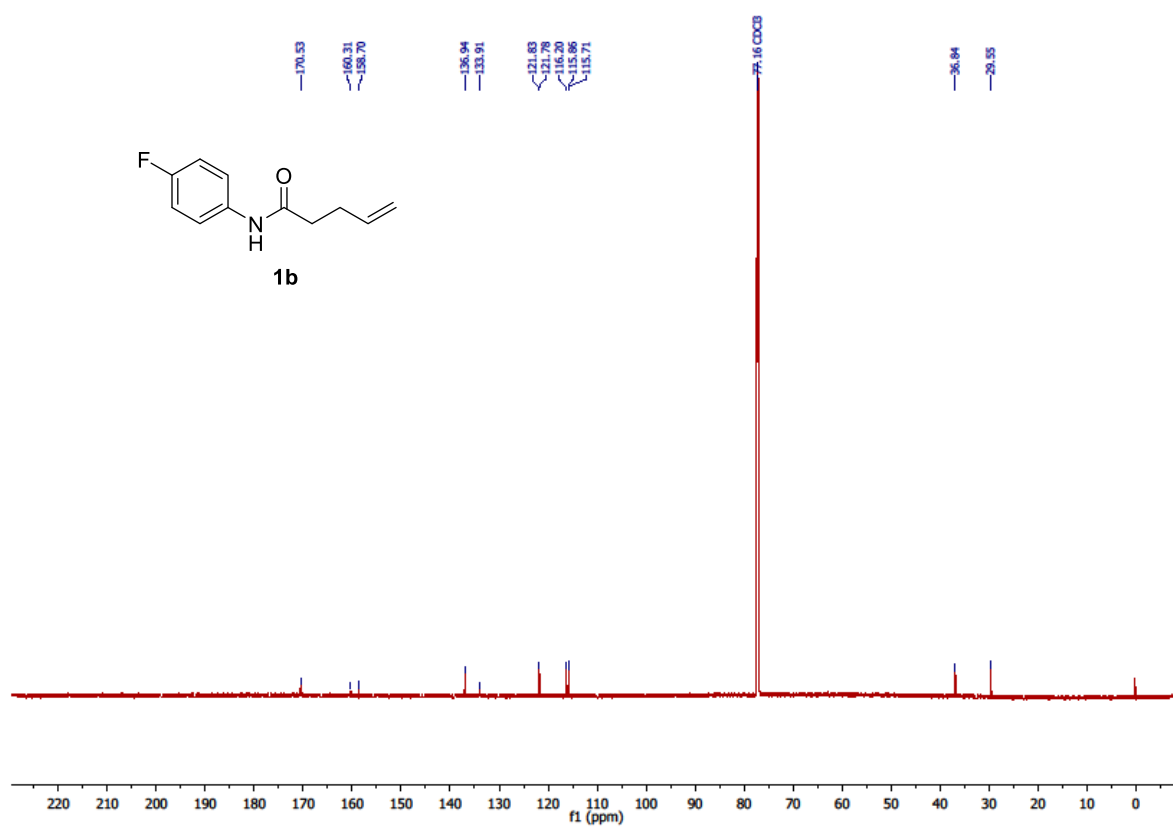
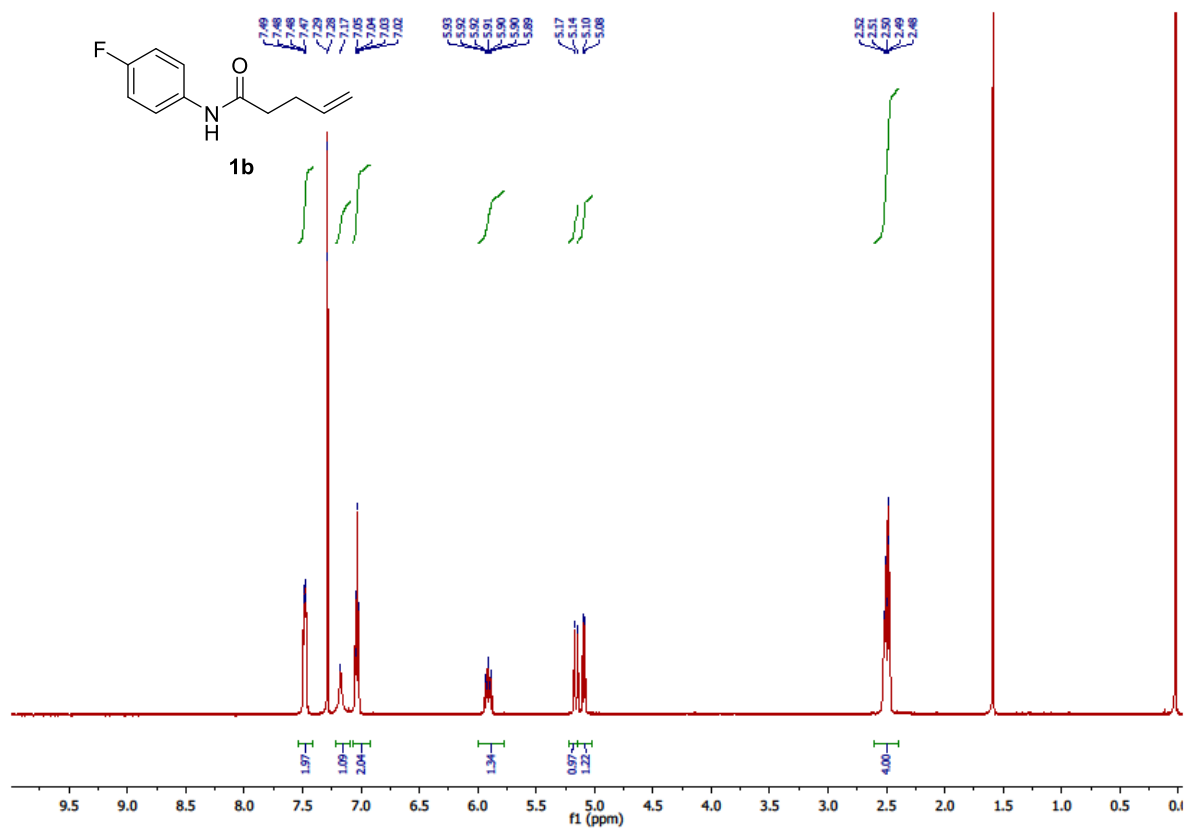
Chapter 4

H(6'B)	8097	1020	6633	43
H(7'A)	9249	777	7421	41
H(7'B)	9580	1896	7451	41
H(7A)	14950	3829	7792	45
H(7B)	14579	4942	7784	45
H(9')	9022	1389	8528	41
H(9)	14289	4237	8869	51
H(10')	7313	1617	9043	44
H(10)	12560	3899	9347	53
H(11')	5270	1915	8629	41
H(11)	10550	3581	8901	47
H(12)	10222	3588	7967	41
H(12')	4867	1976	7701	39
H(16D)	3116	-1233	6399	63
H(16E)	1672	-972	6484	63
H(16F)	2829	-381	6790	63
H(16A)	6604	3744	6962	73
H(16B)	6536	4847	7115	73
H(16C)	7893	4332	7117	73
H(17A)	5755	4686	5685	81
H(17B)	5230	5172	6191	81
H(17C)	5279	4037	6145	81
H(17D)	2181	-76	5178	73
H(17E)	1391	-871	5456	73
H(17F)	2895	-1000	5433	73
H(18A)	8224	5943	7068	63
H(18B)	7001	6477	6775	63
H(18C)	8408	6803	6668	63
H(18D)	2312	1171	6823	63
H(18E)	963	635	6786	63
H(18F)	1023	1739	6635	63
H(19D)	-185	1389	5772	62
H(19E)	-182	257	5844	62
H(19F)	408	724	5347	62
H(19A)	8107	6541	5699	73
H(19B)	6630	6345	5756	73
H(19C)	7444	5583	5465	73

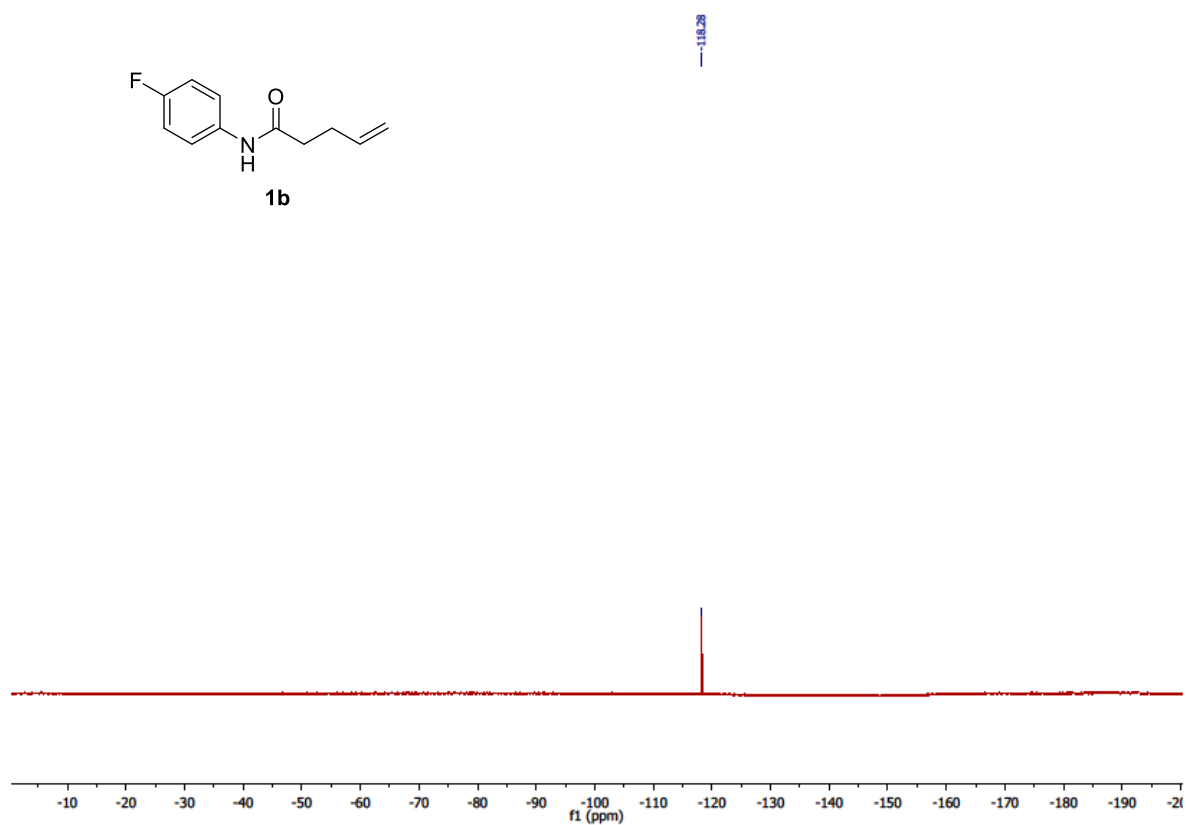
4.5.9 ^1H NMR, ^{13}C NMR & ^{19}F NMR spectra



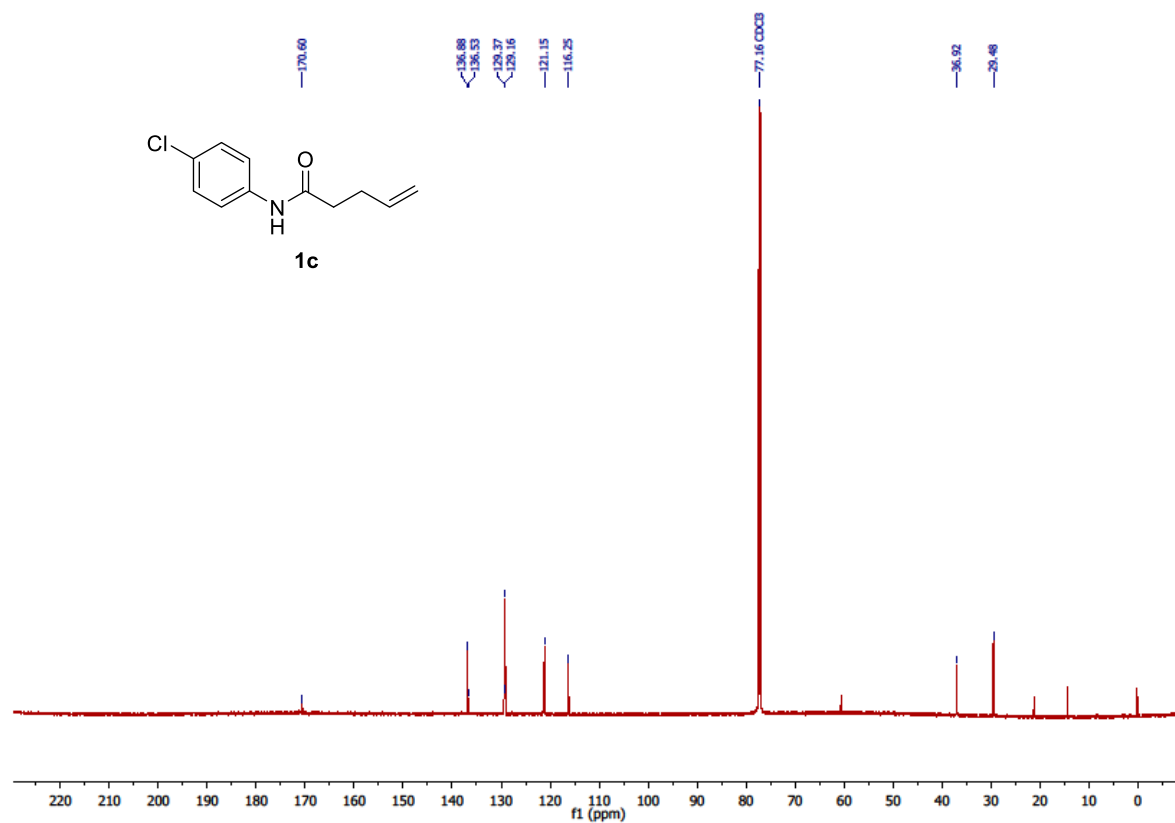
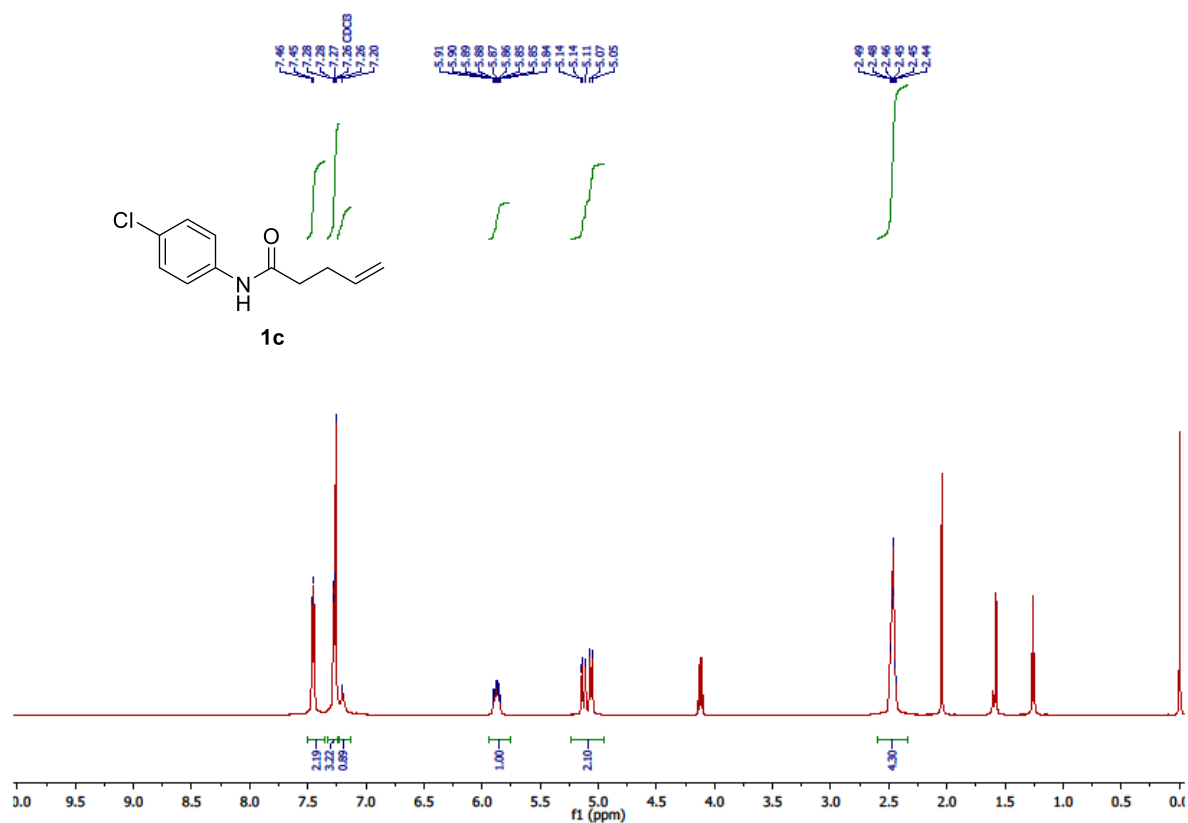
Chapter 4

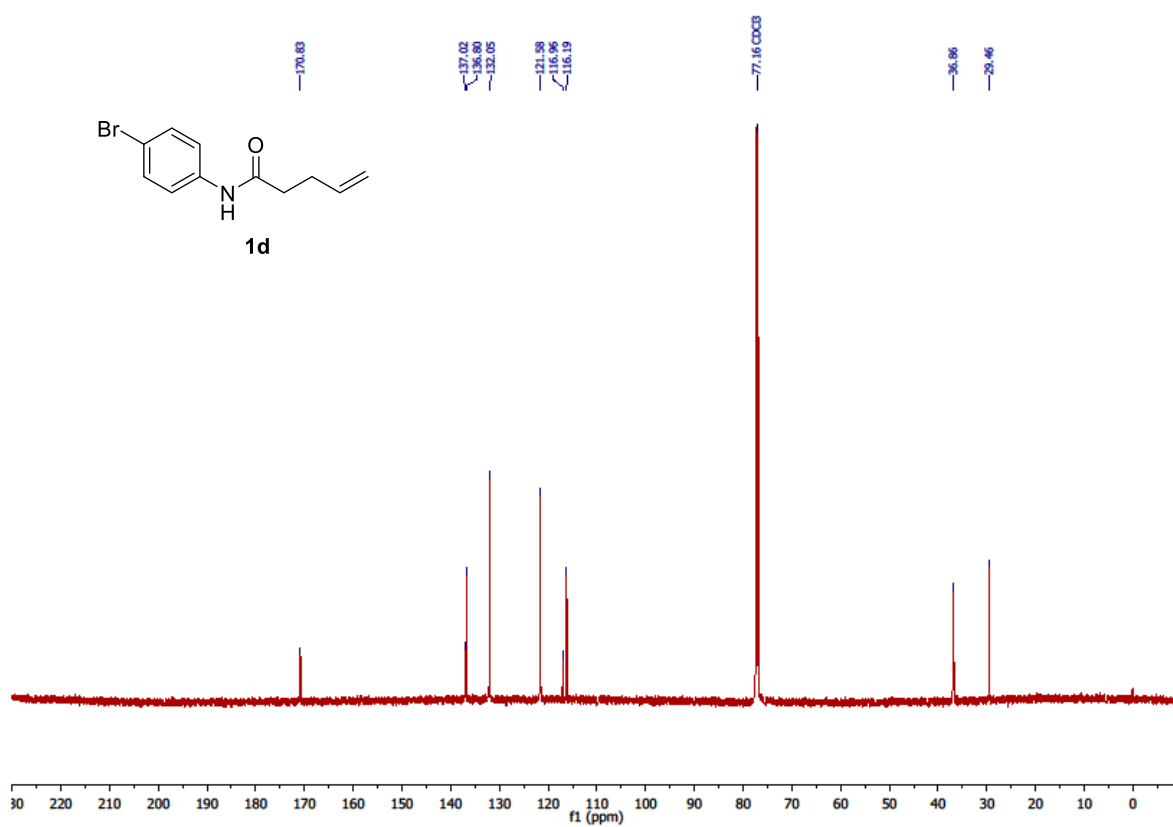
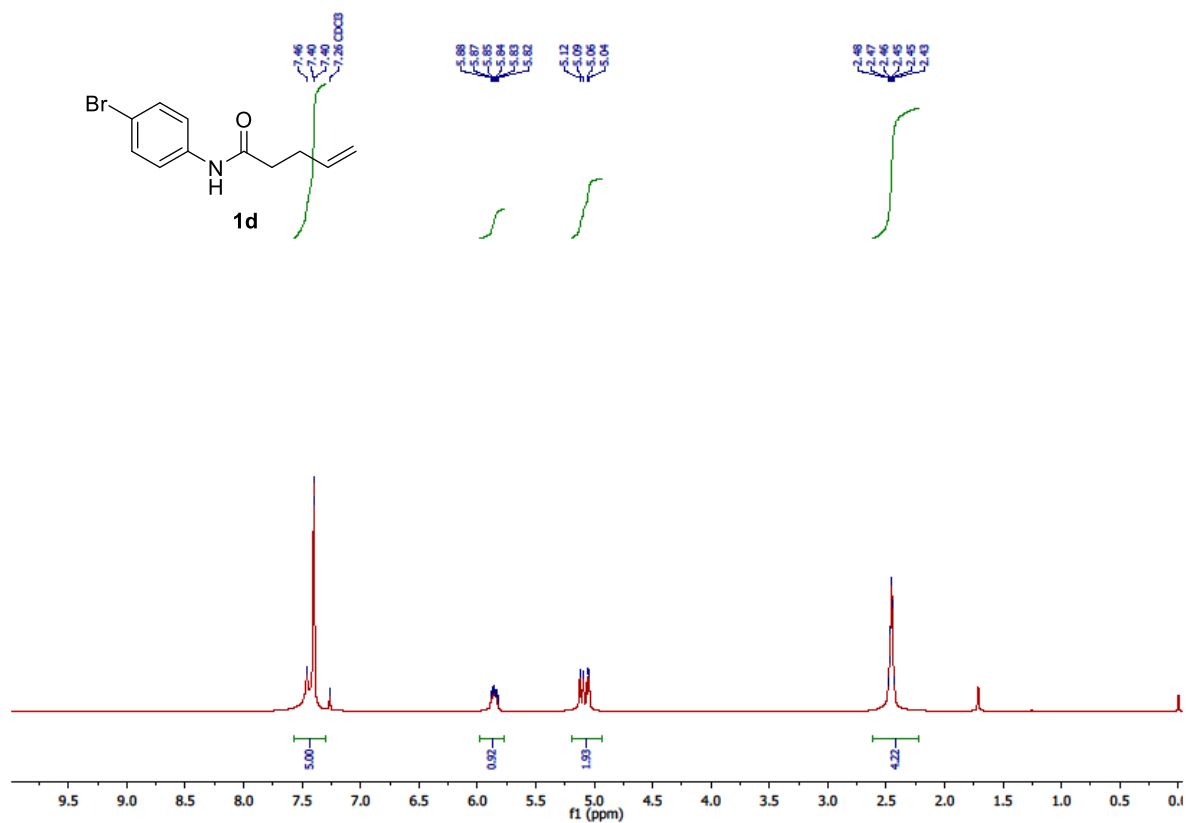


W-catalyzed remote β -hydroboration of alkenes

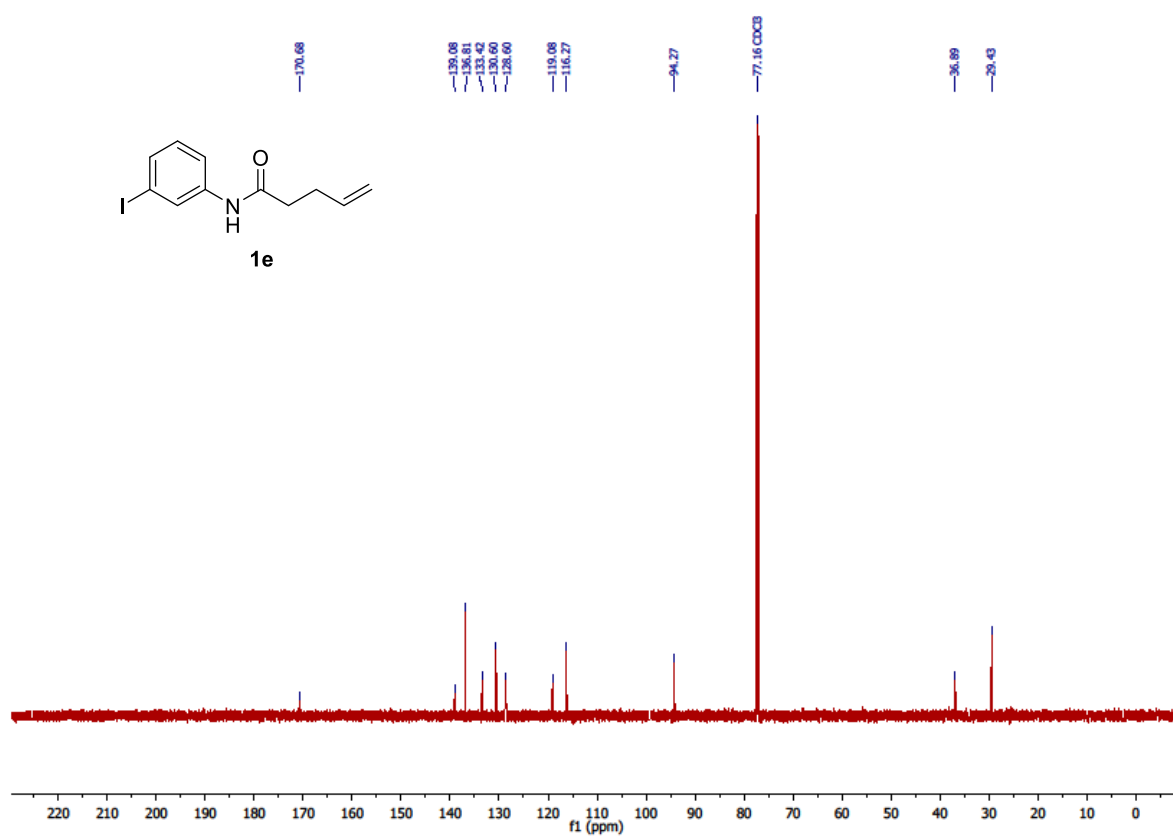
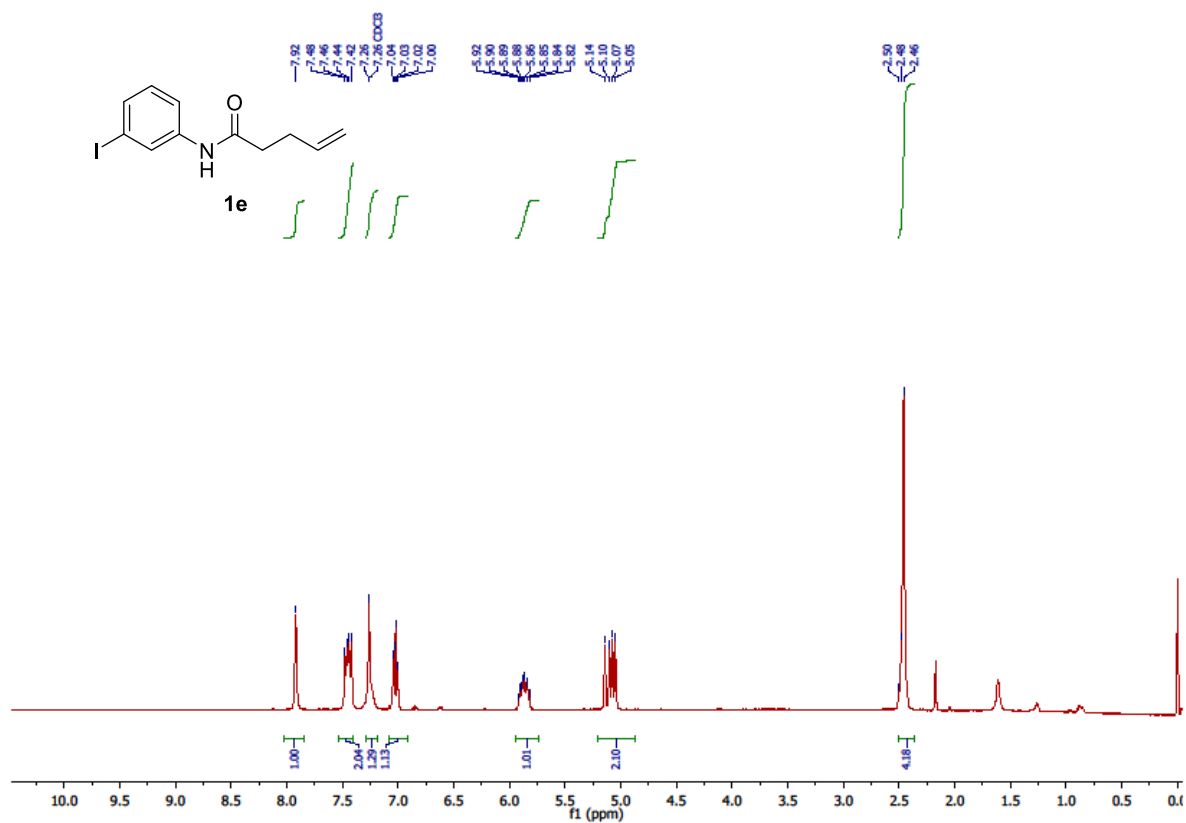


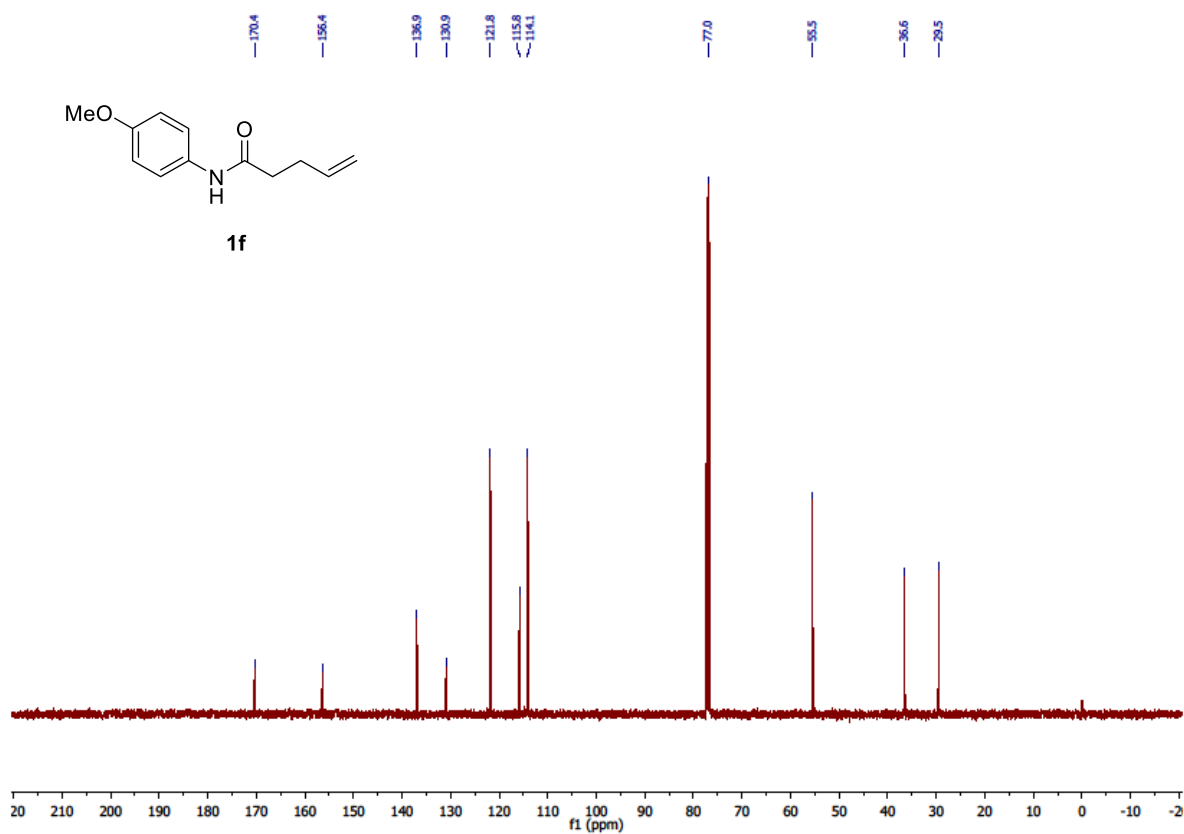
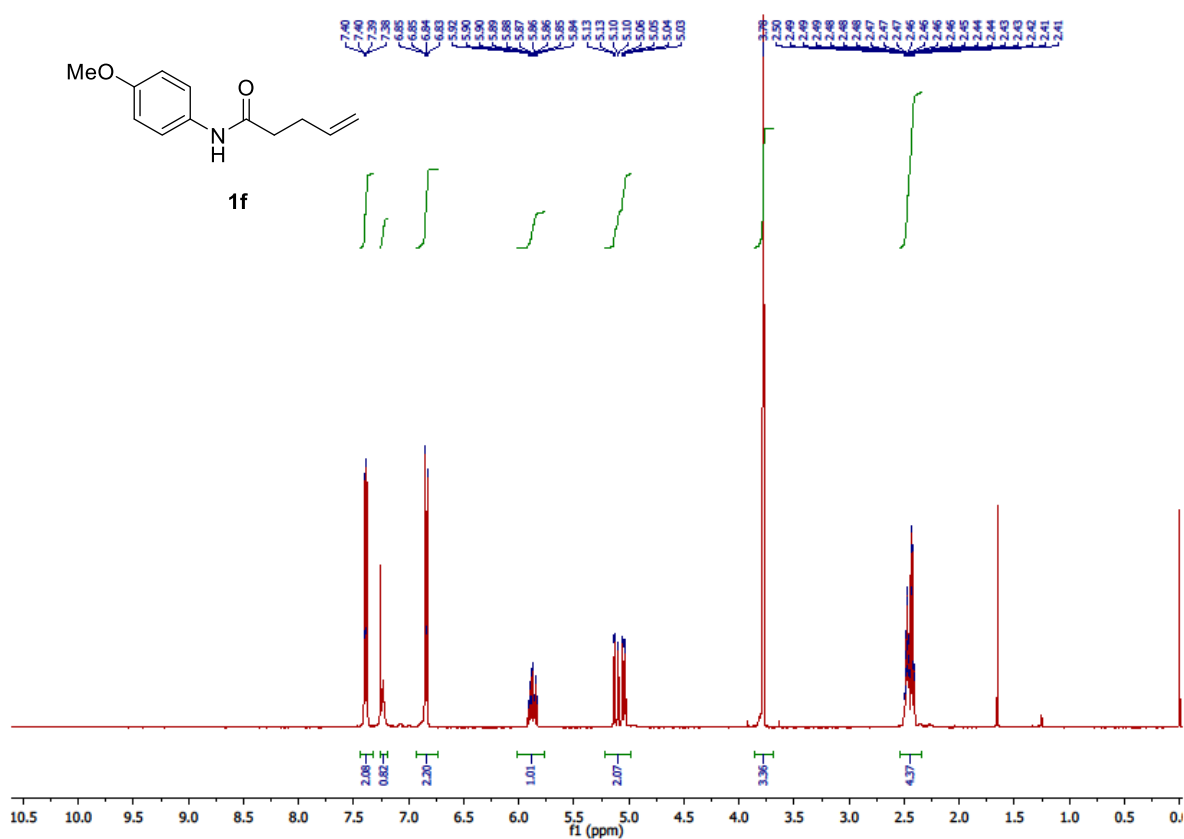
Chapter 4



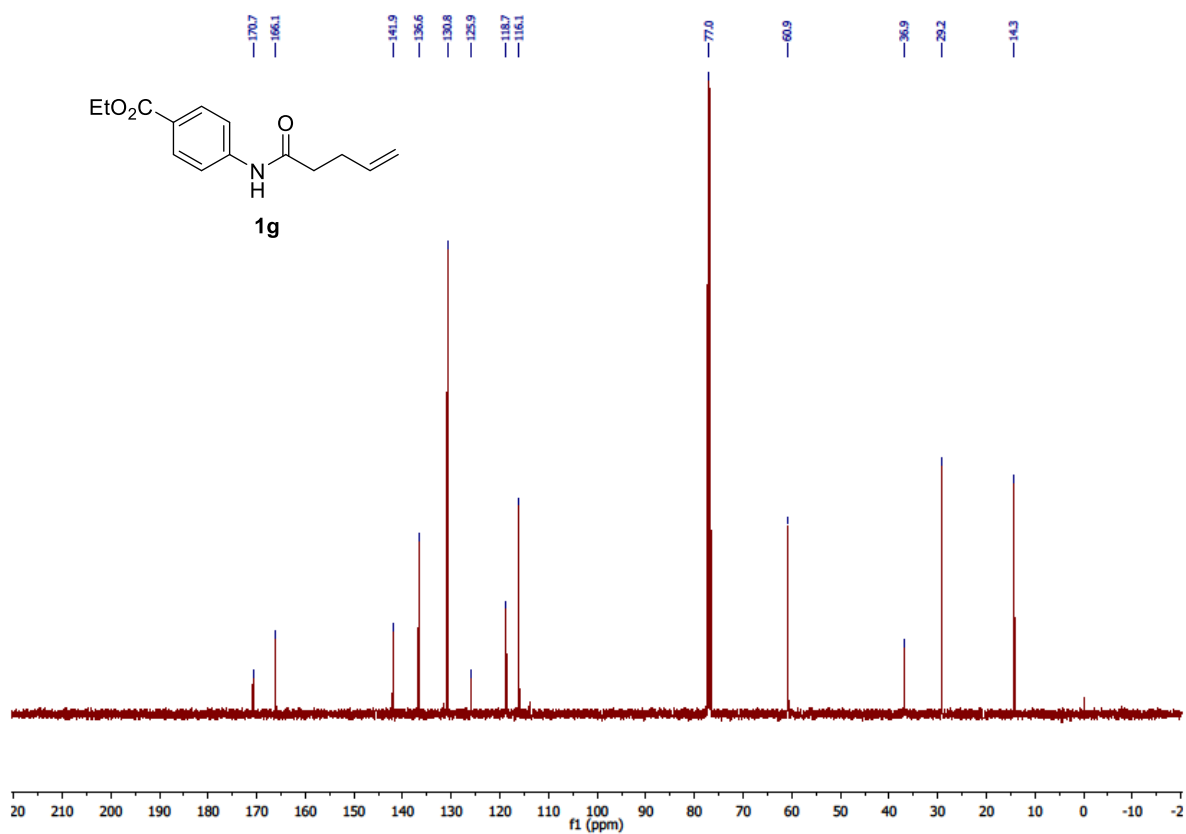
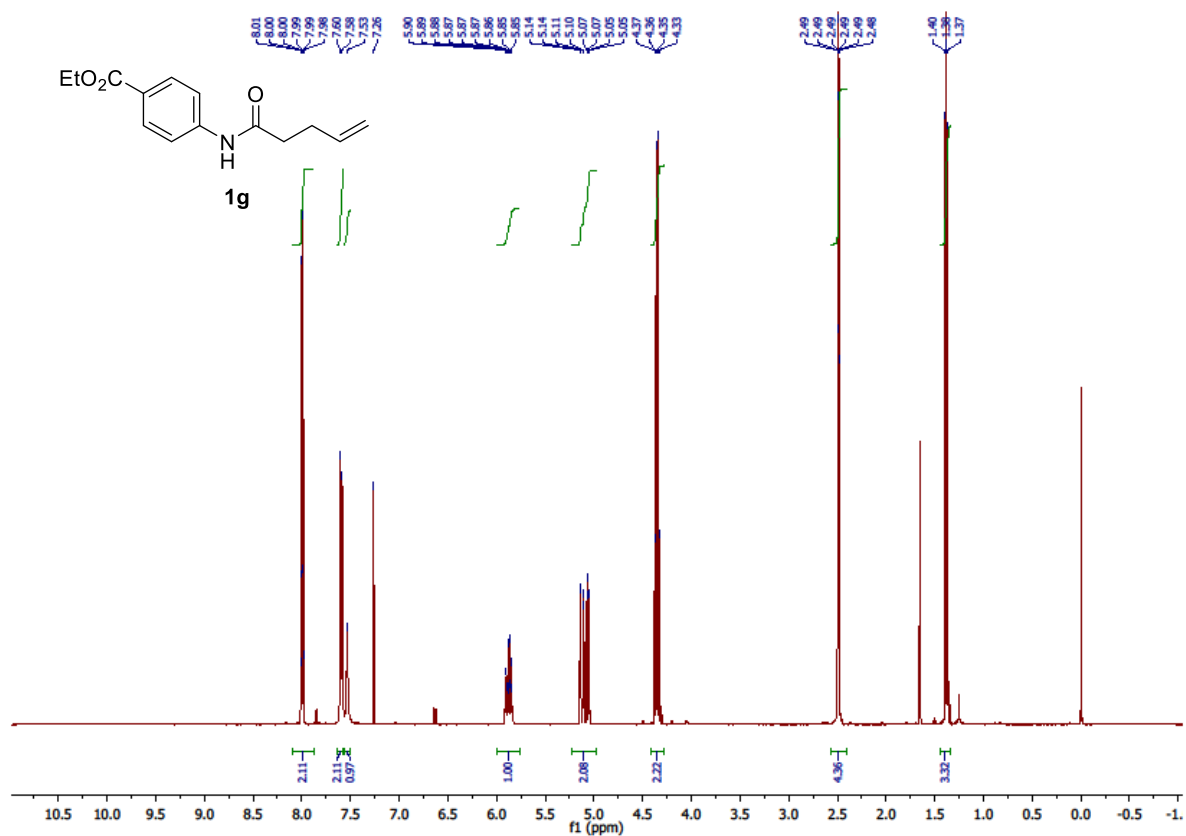


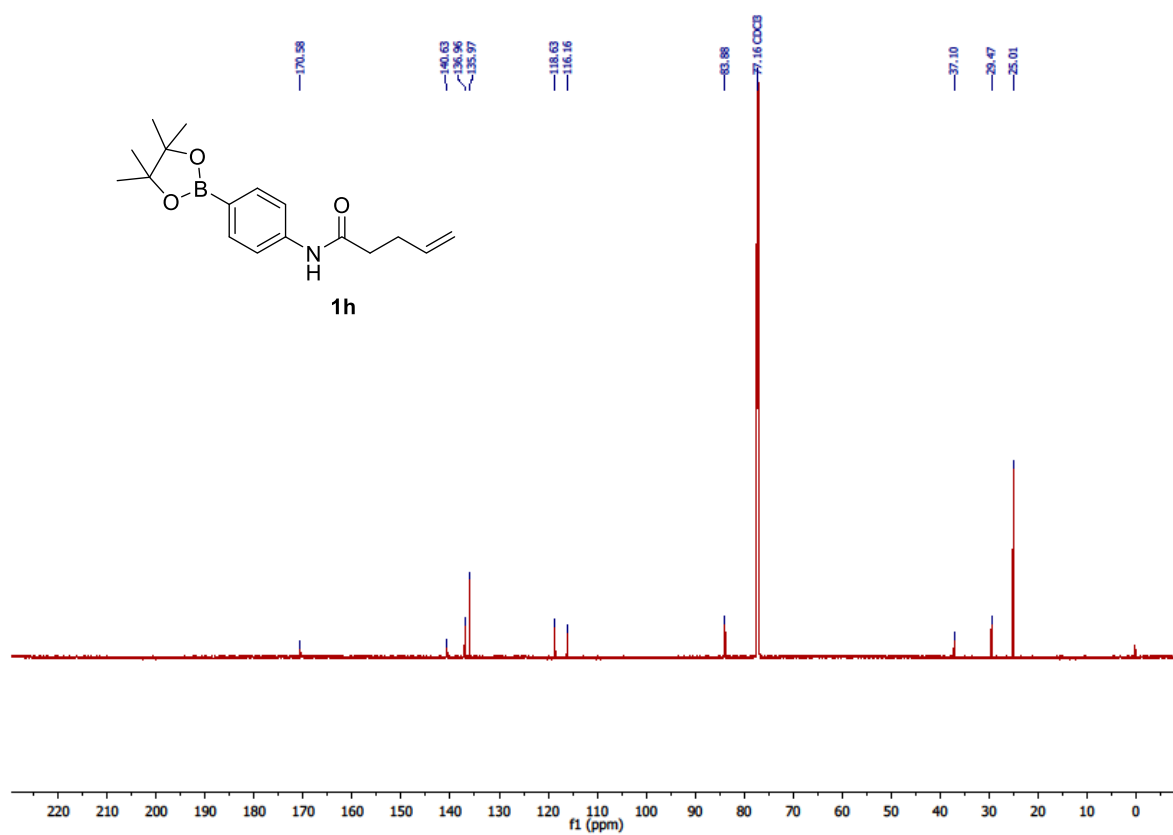
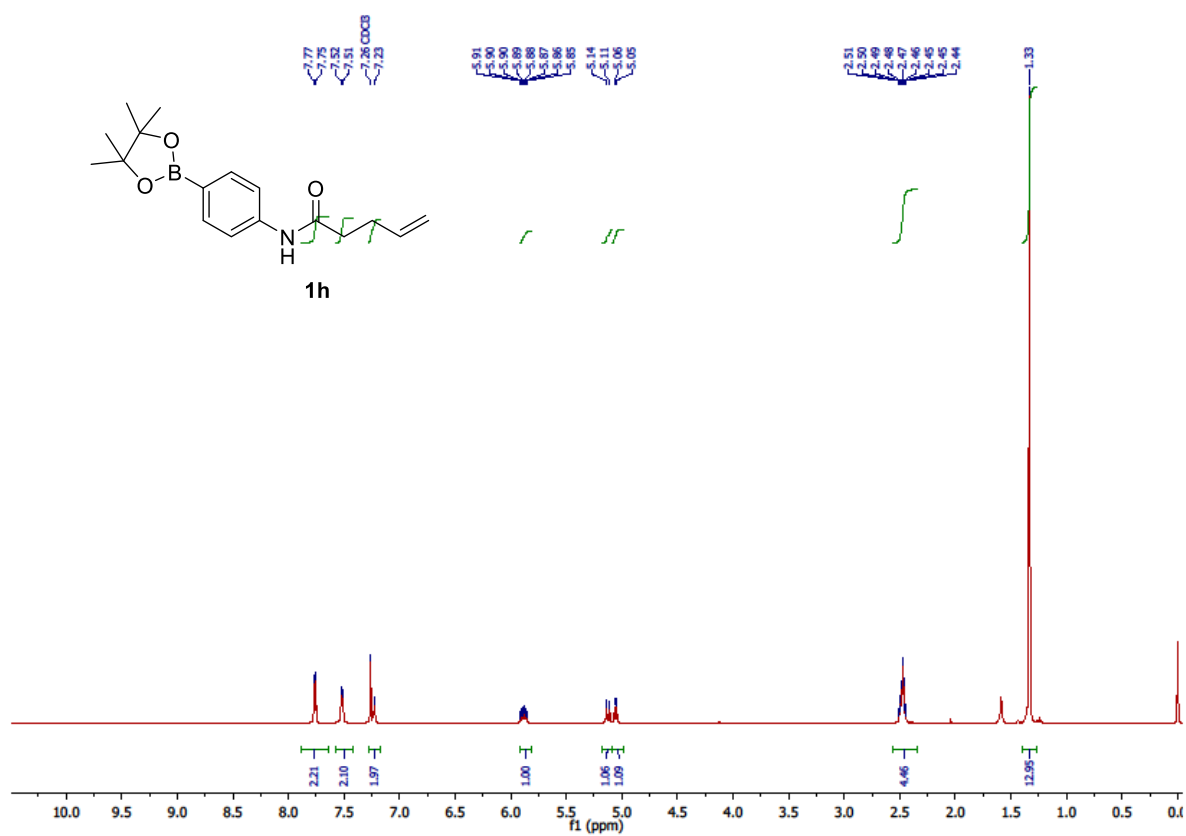
Chapter 4



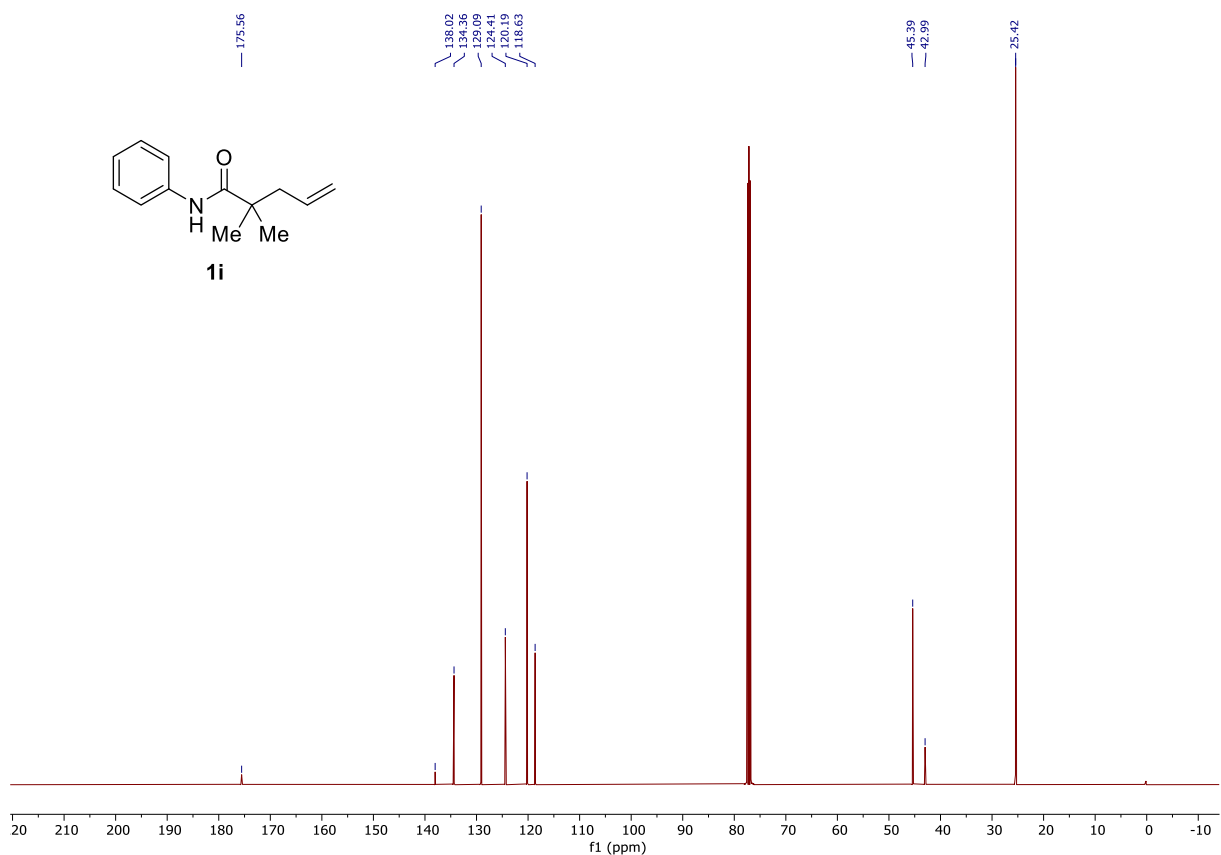
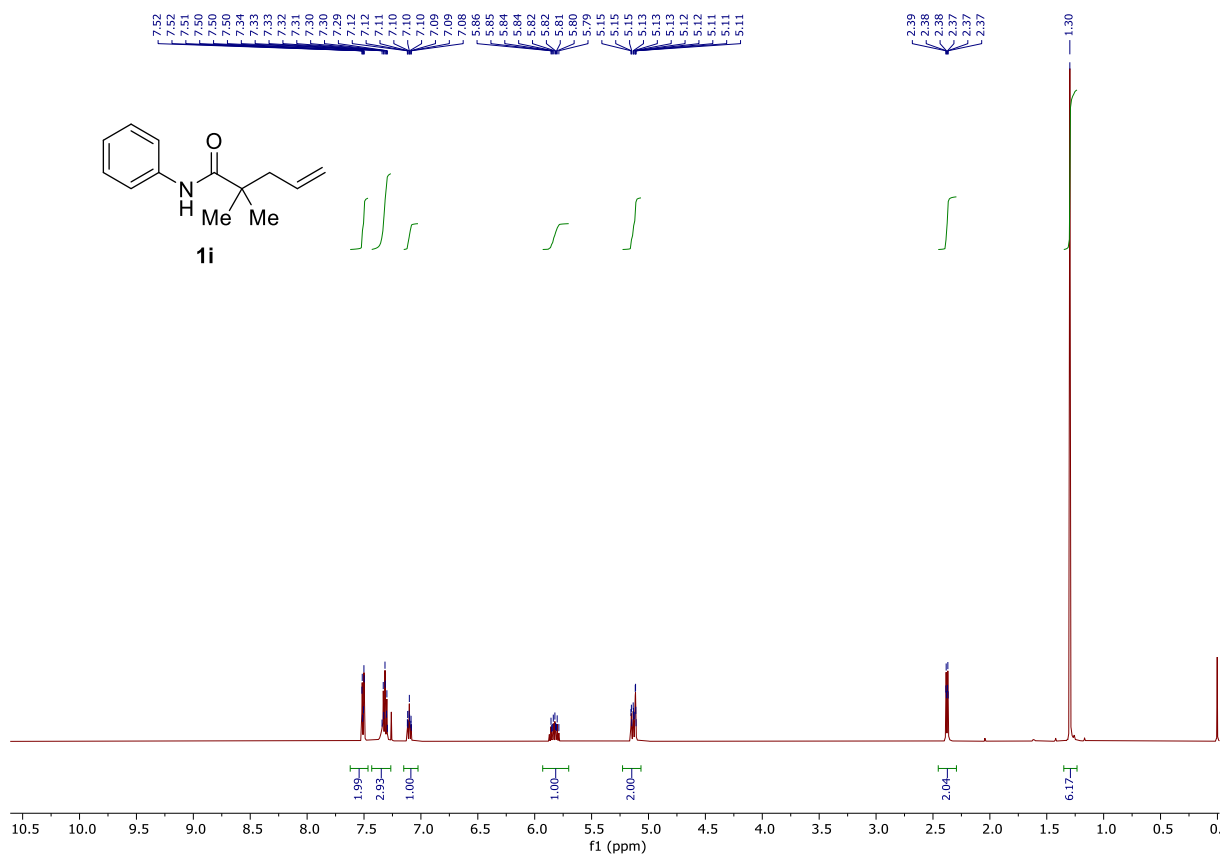


Chapter 4

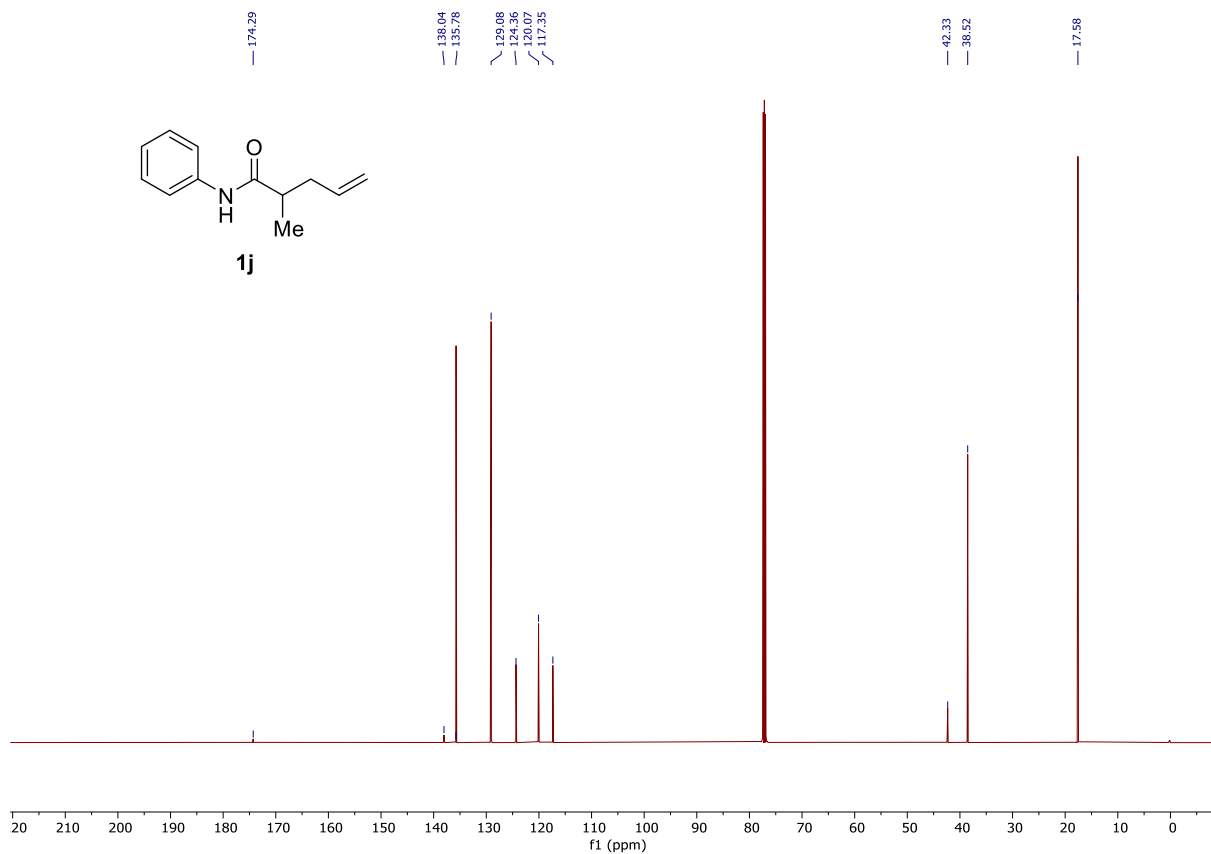
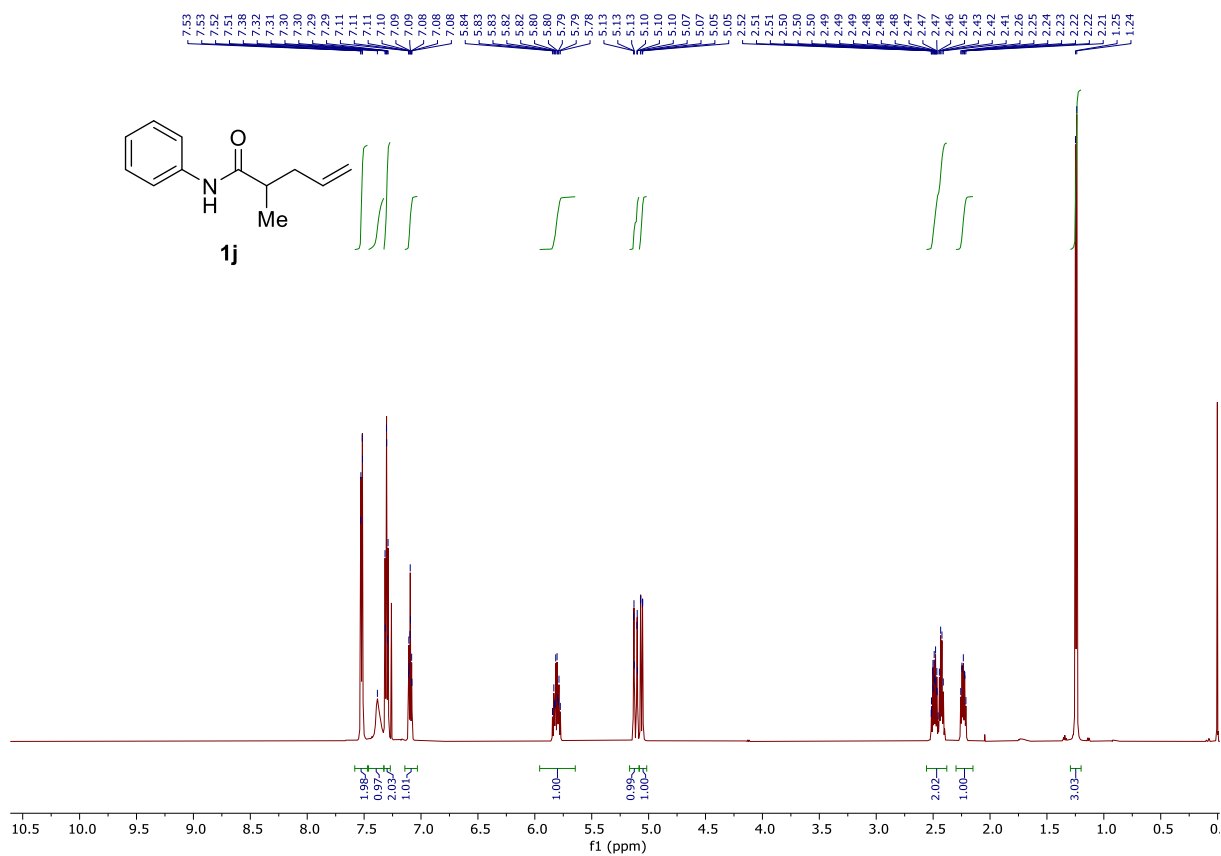




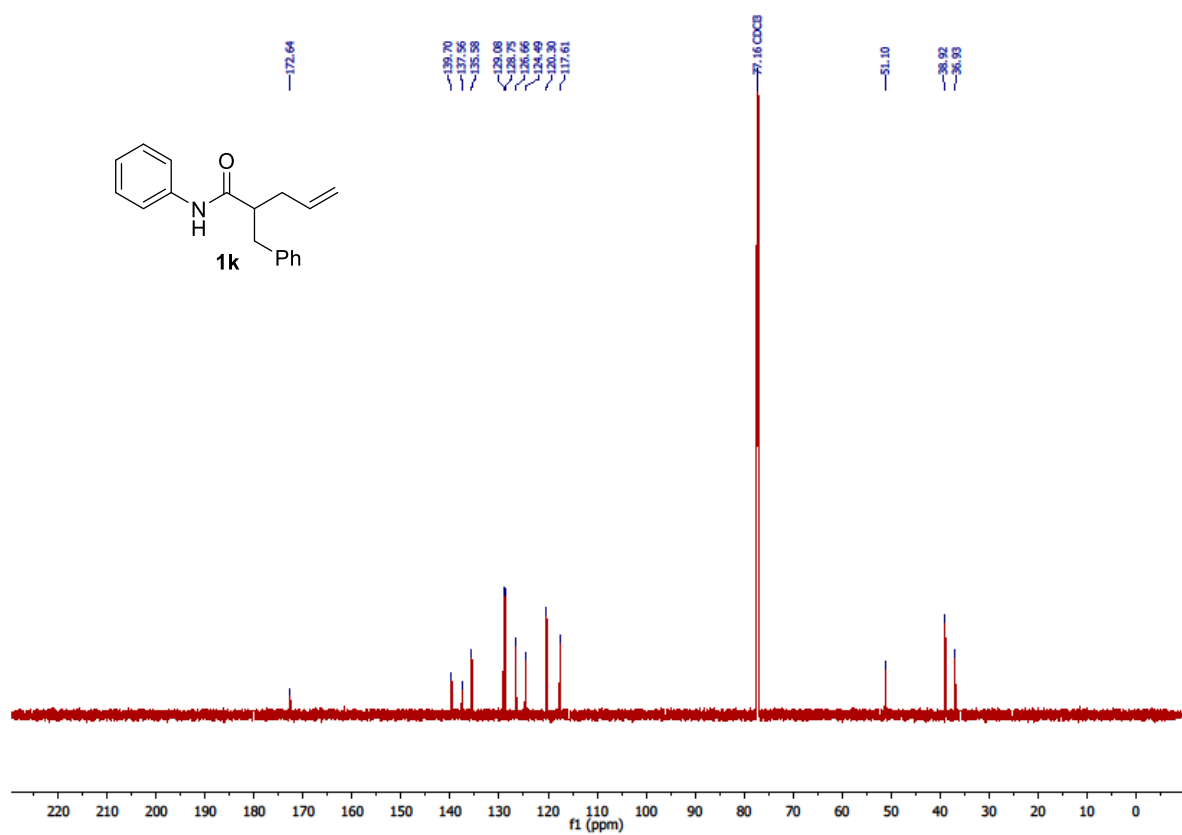
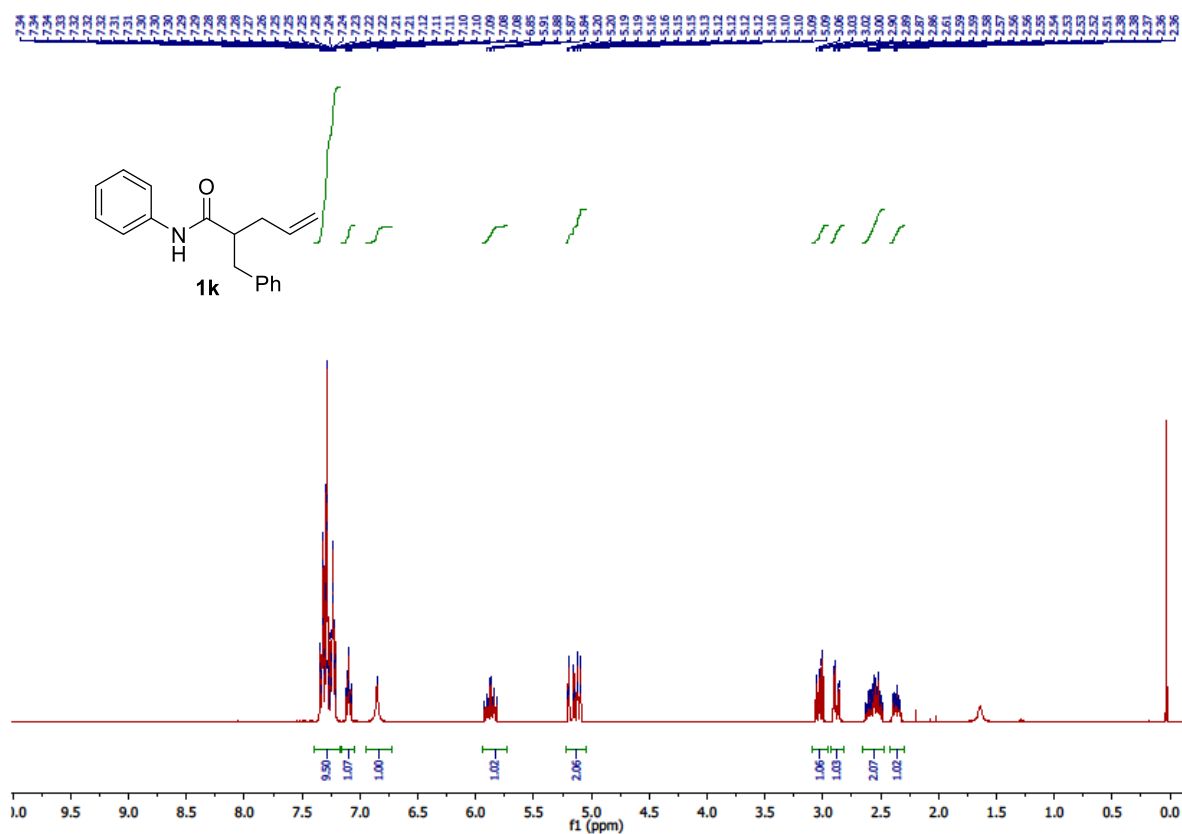
Chapter 4



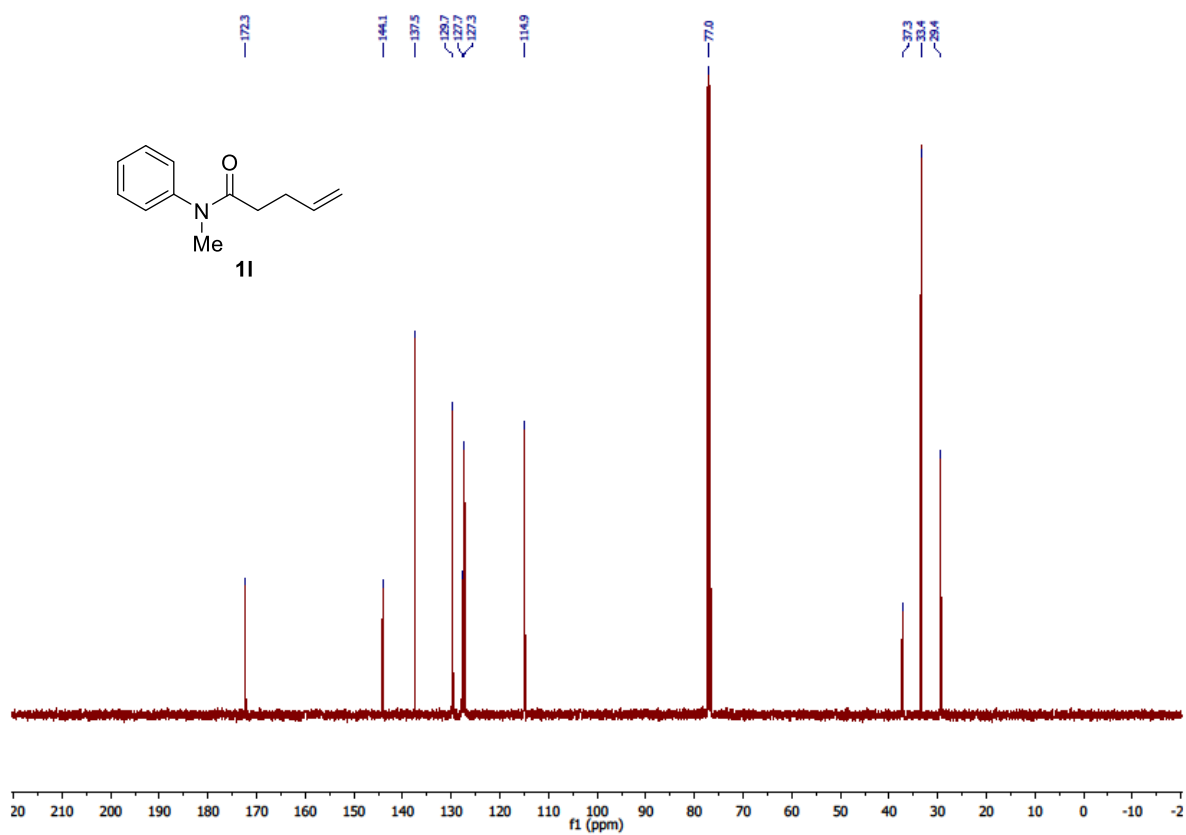
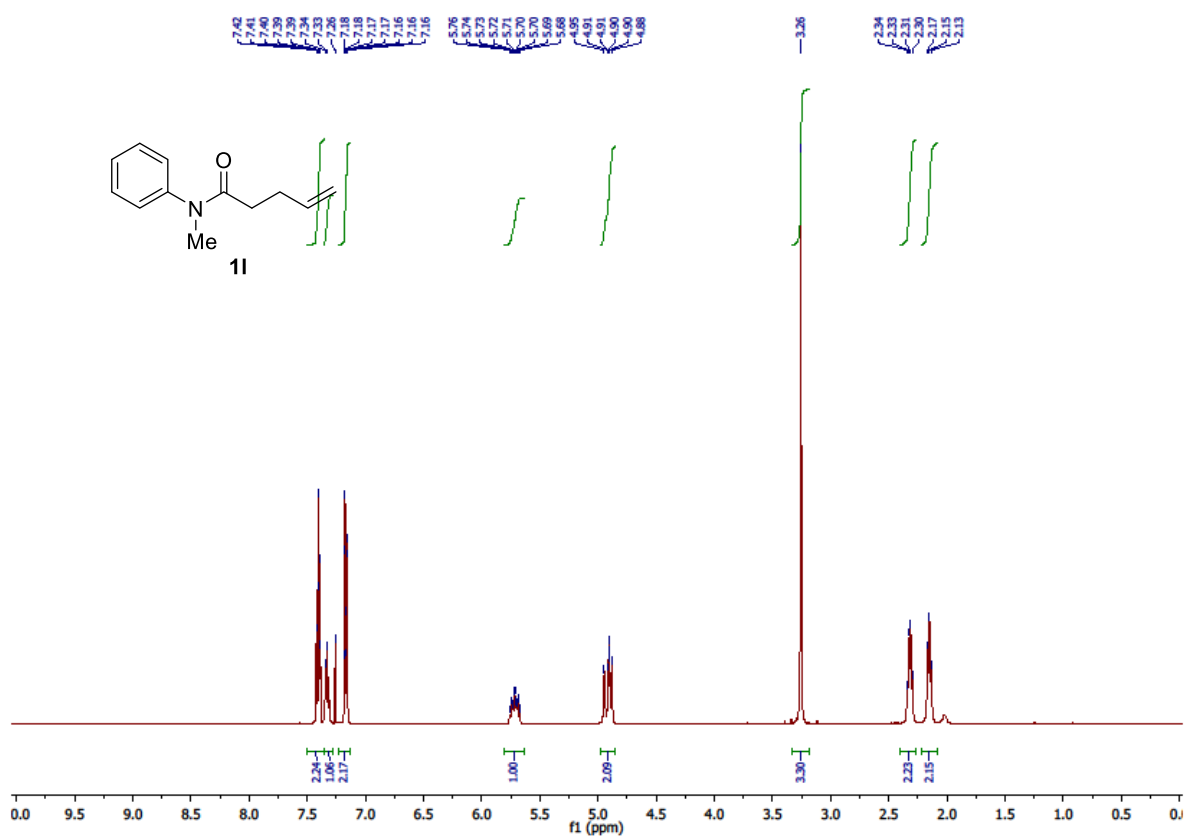
W-catalyzed remote β -hydroboration of alkenes



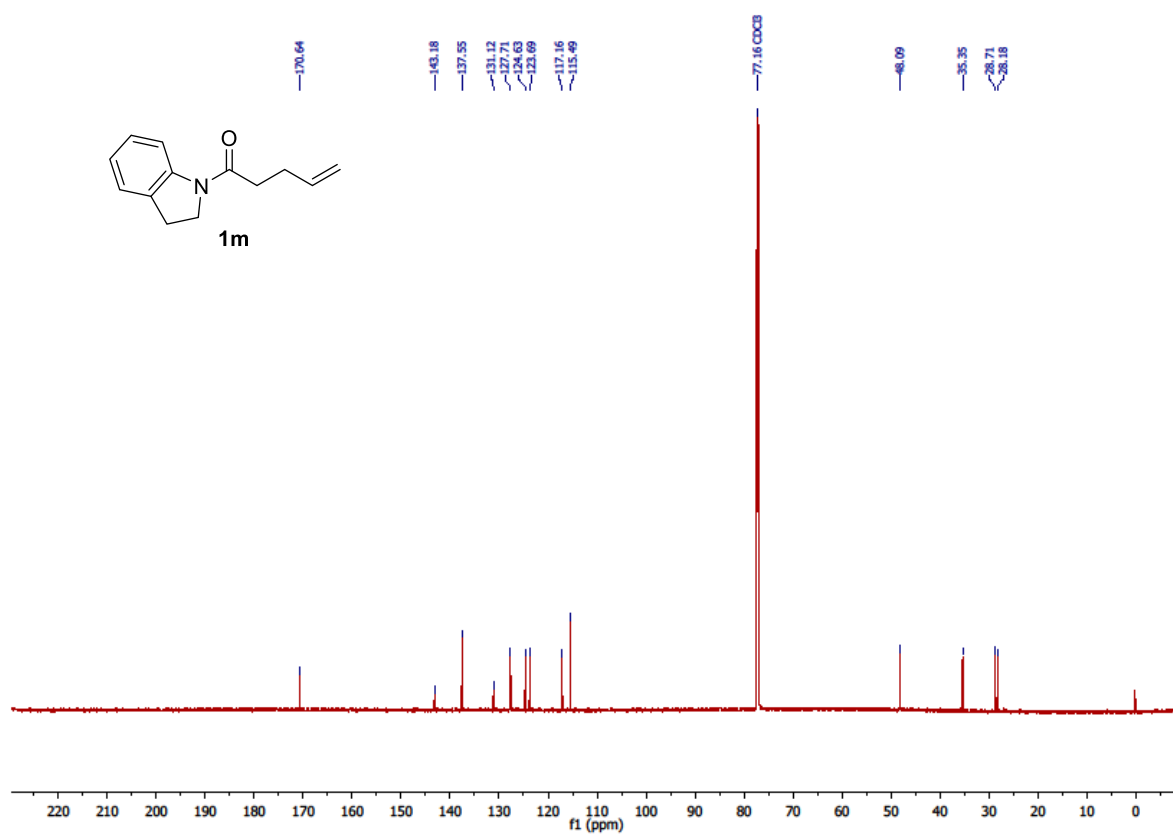
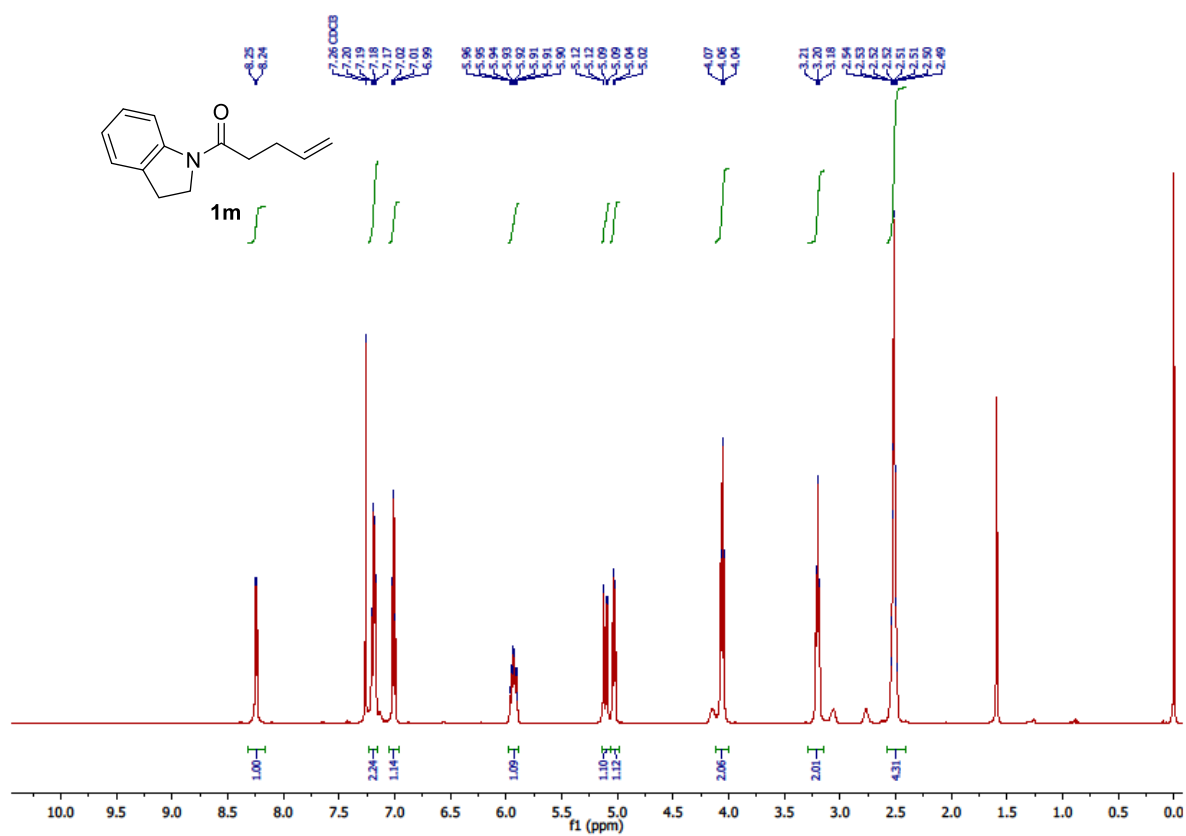
Chapter 4



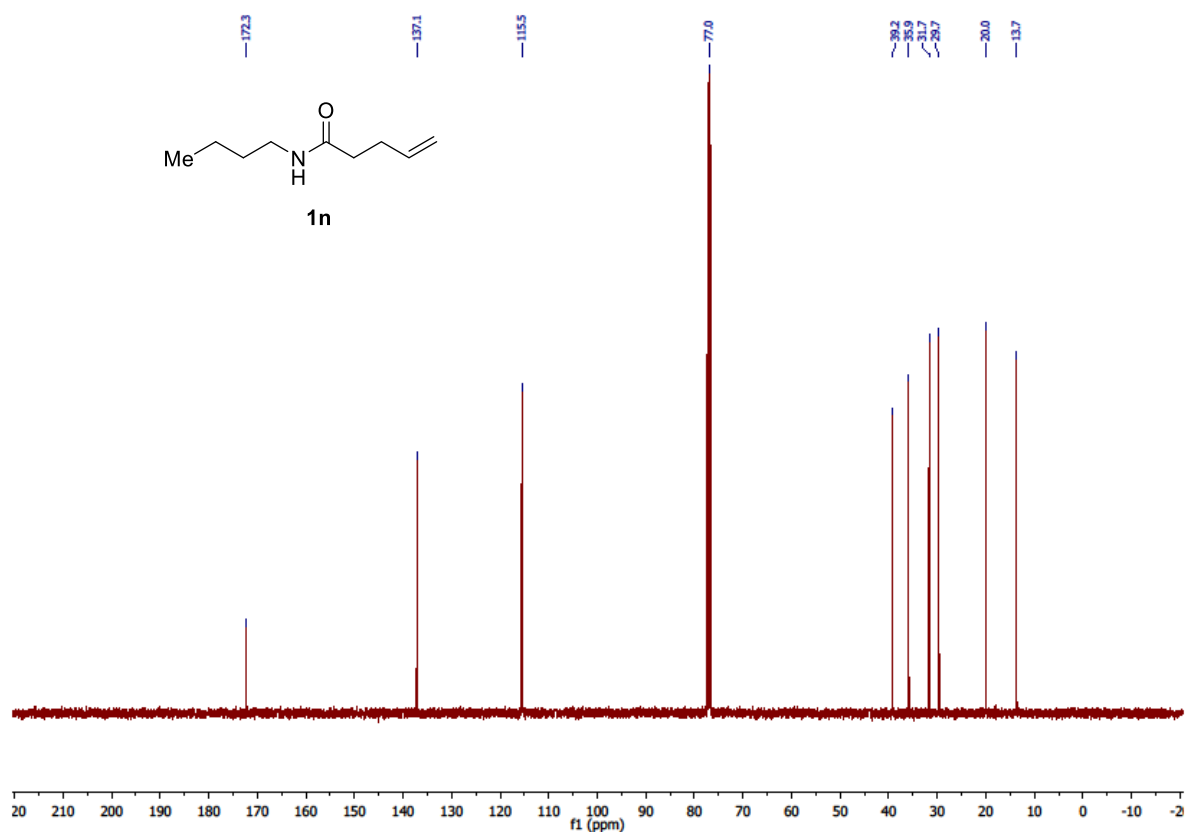
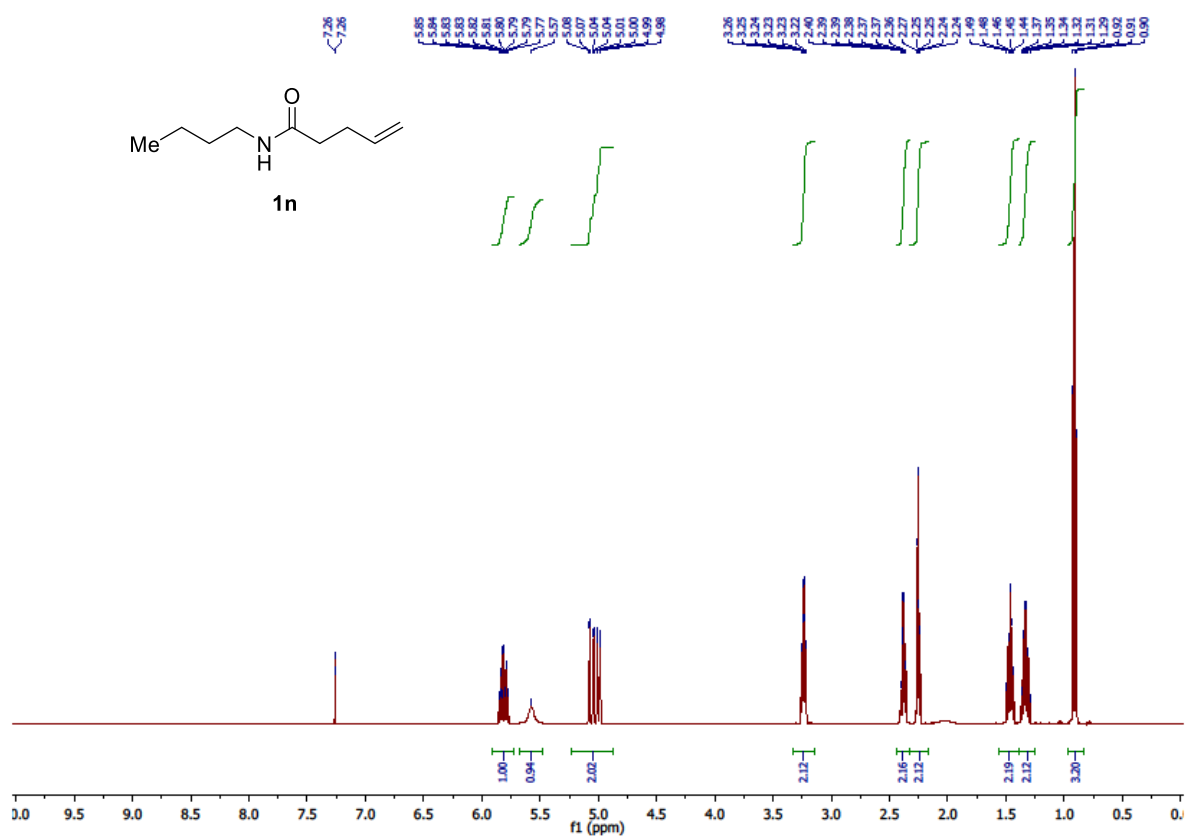
W-catalyzed remote β -hydroboration of alkenes



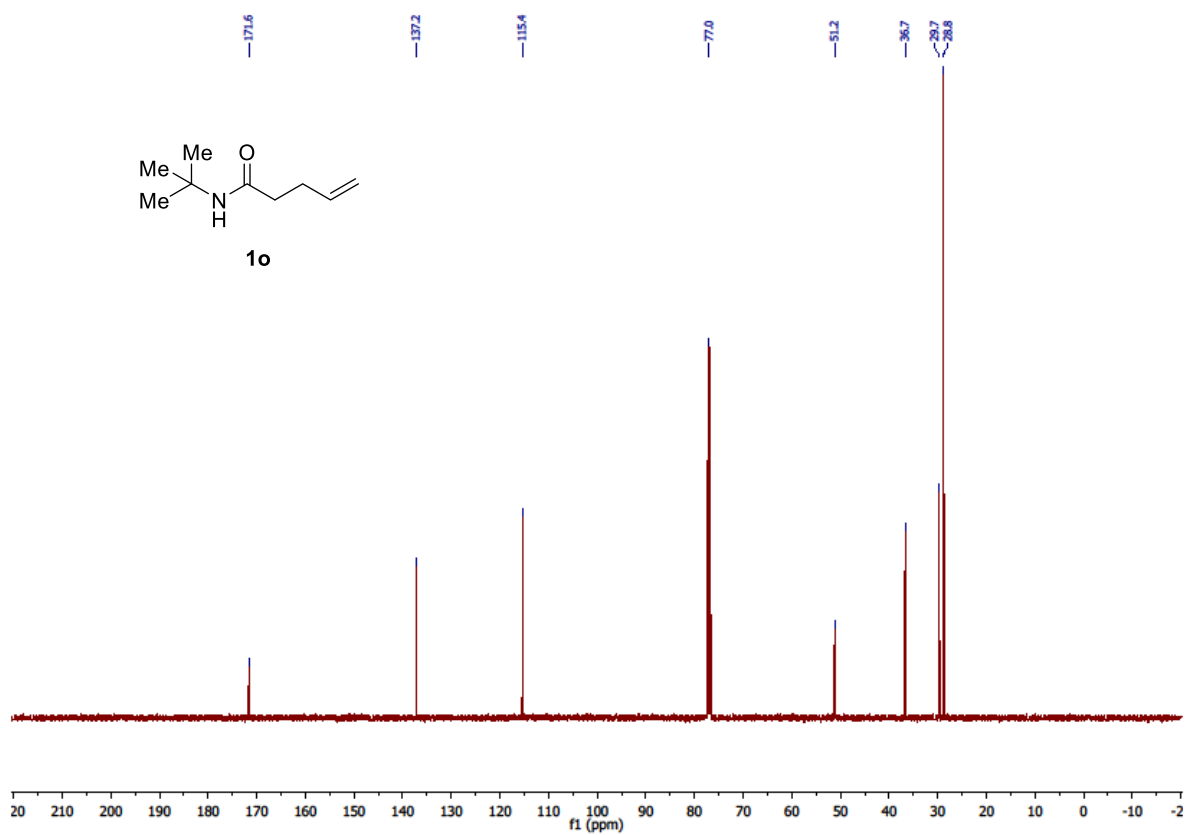
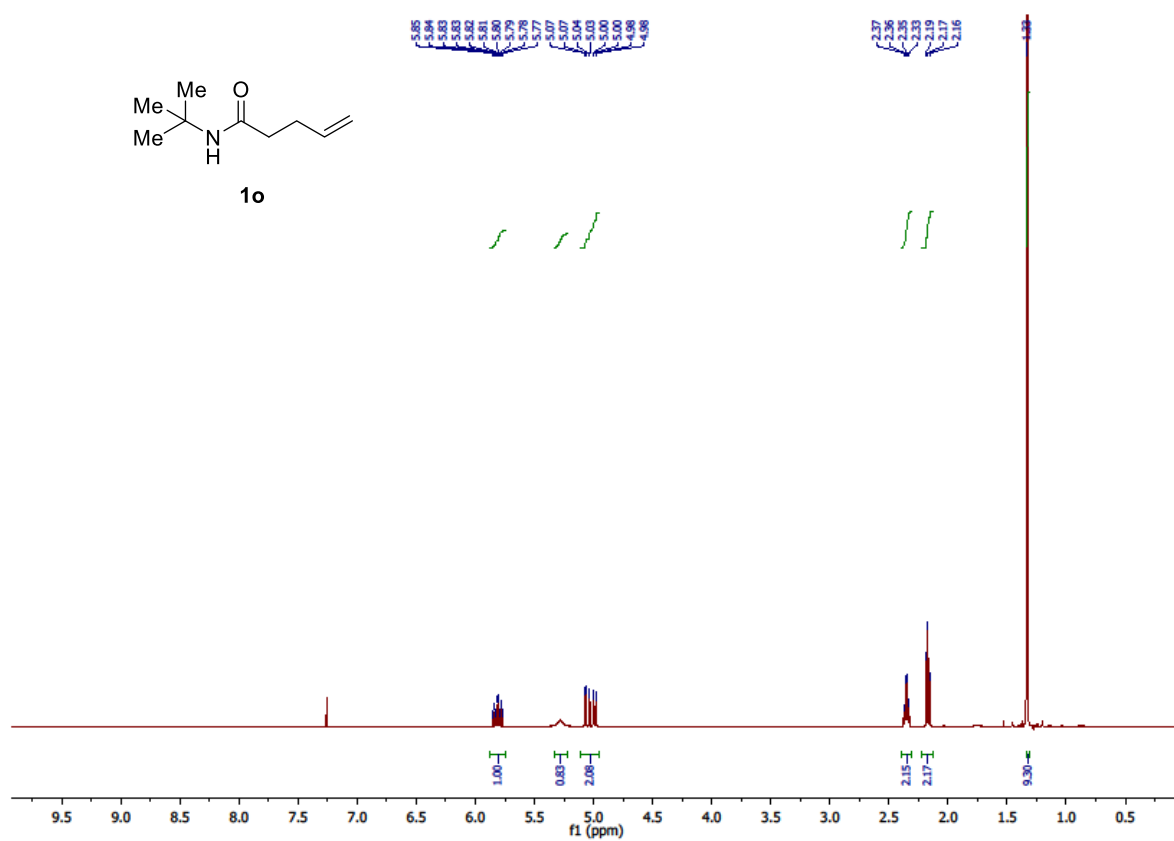
Chapter 4



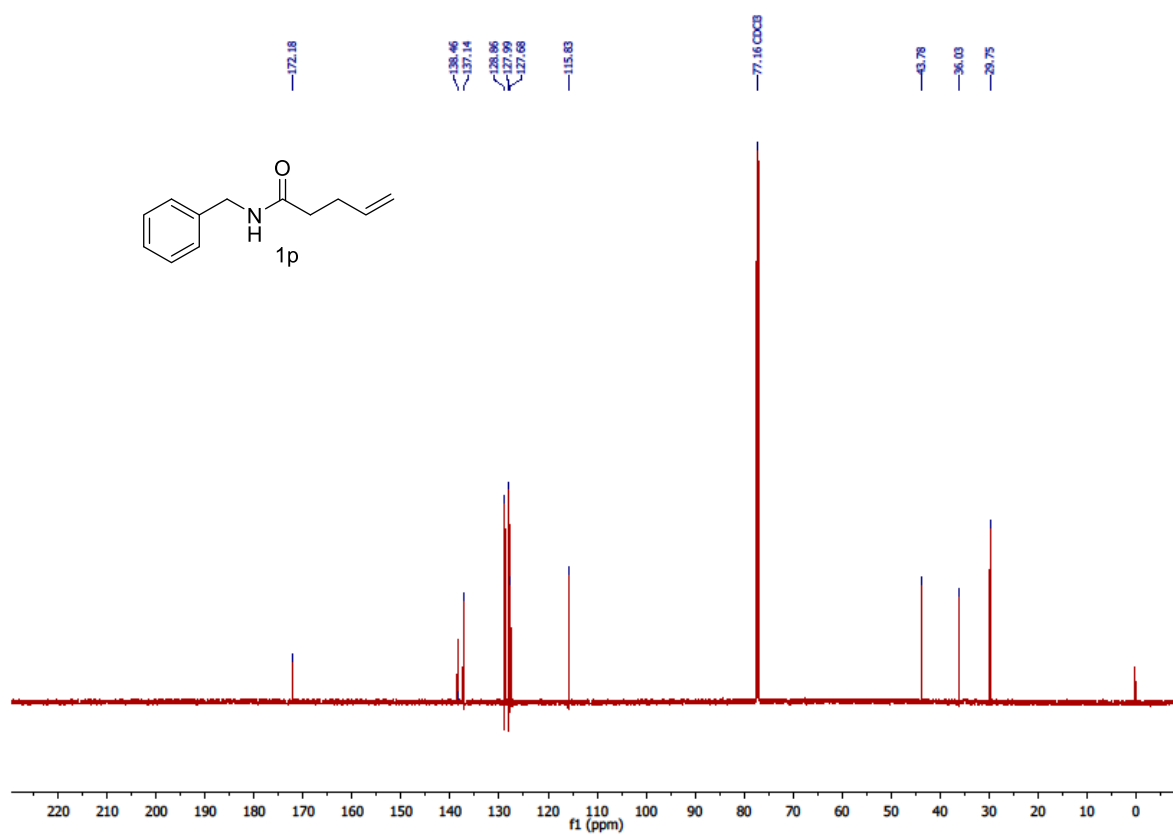
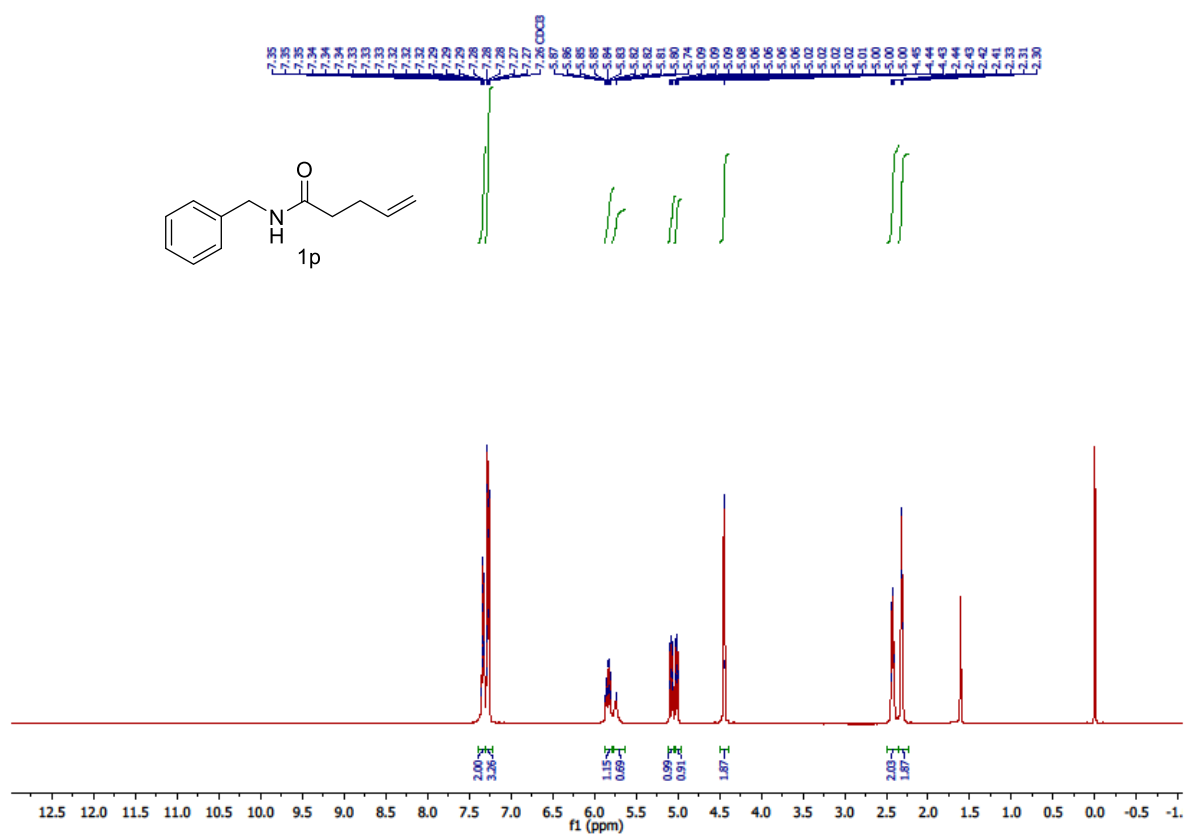
W-catalyzed remote β -hydroboration of alkenes



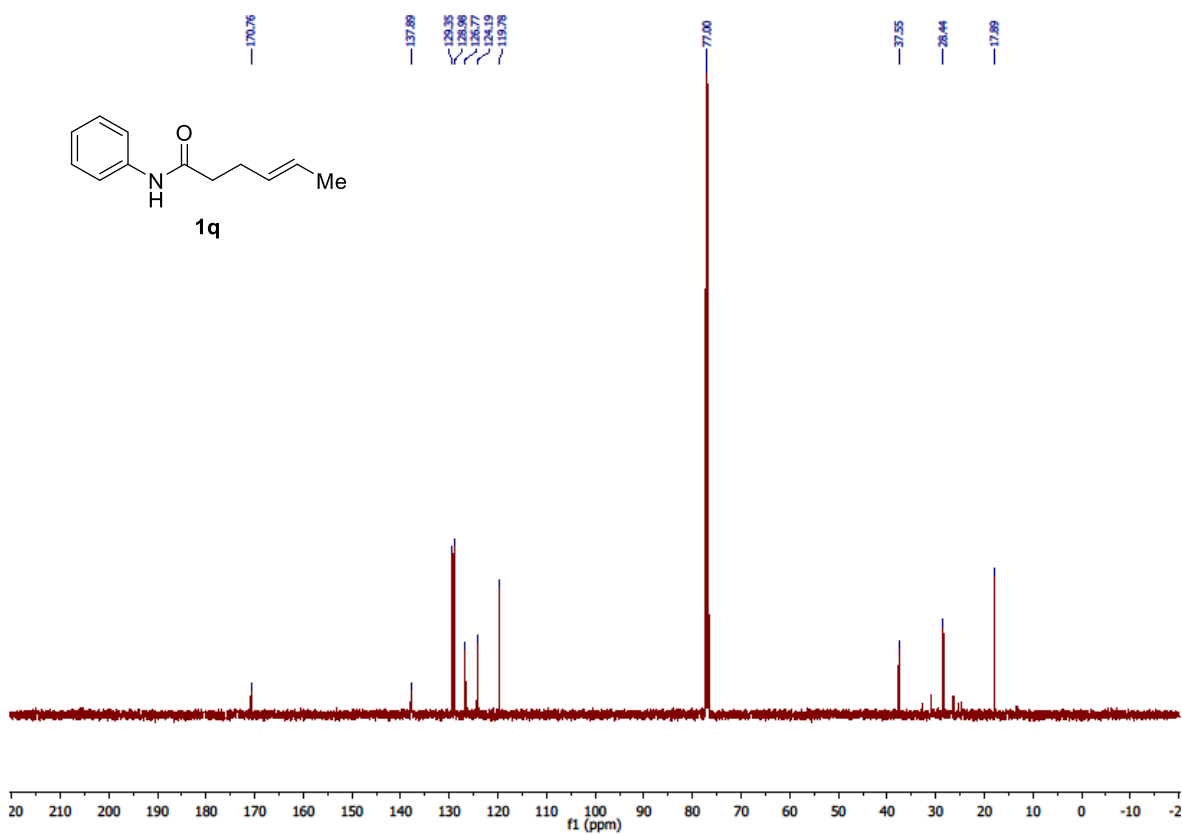
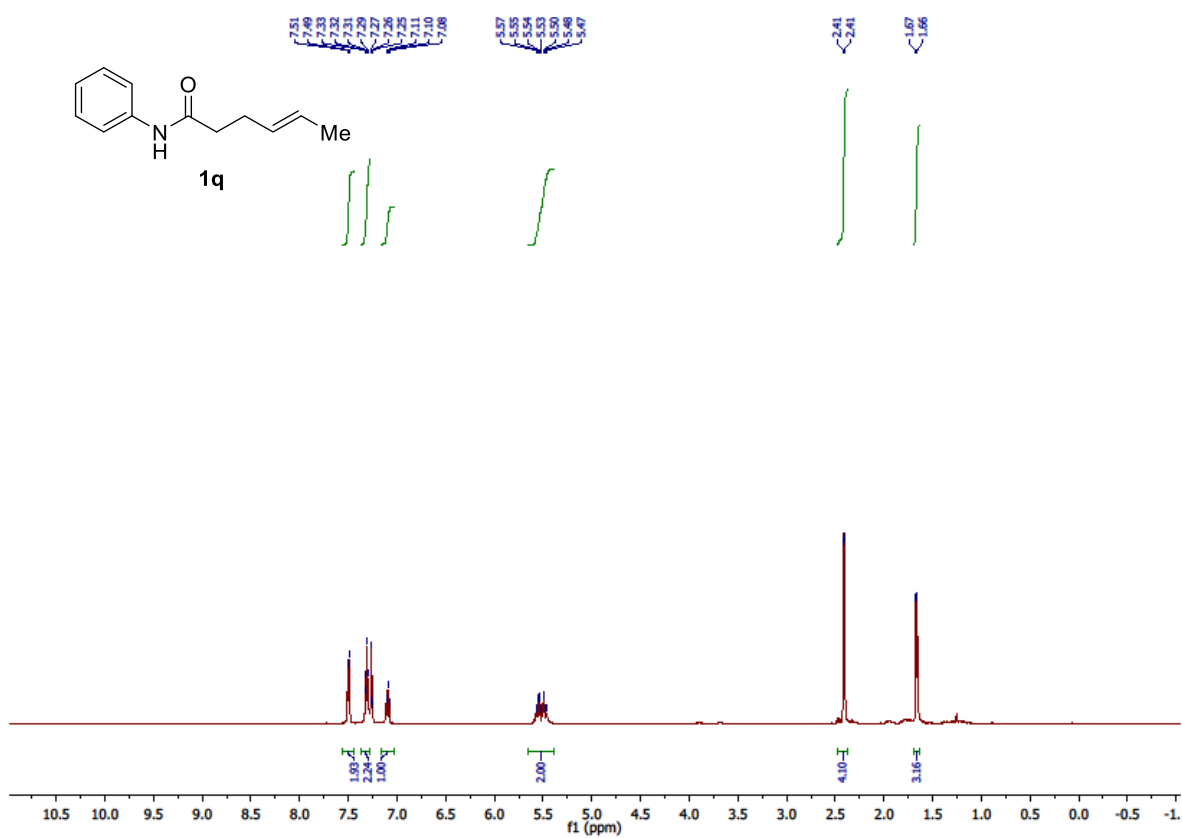
Chapter 4



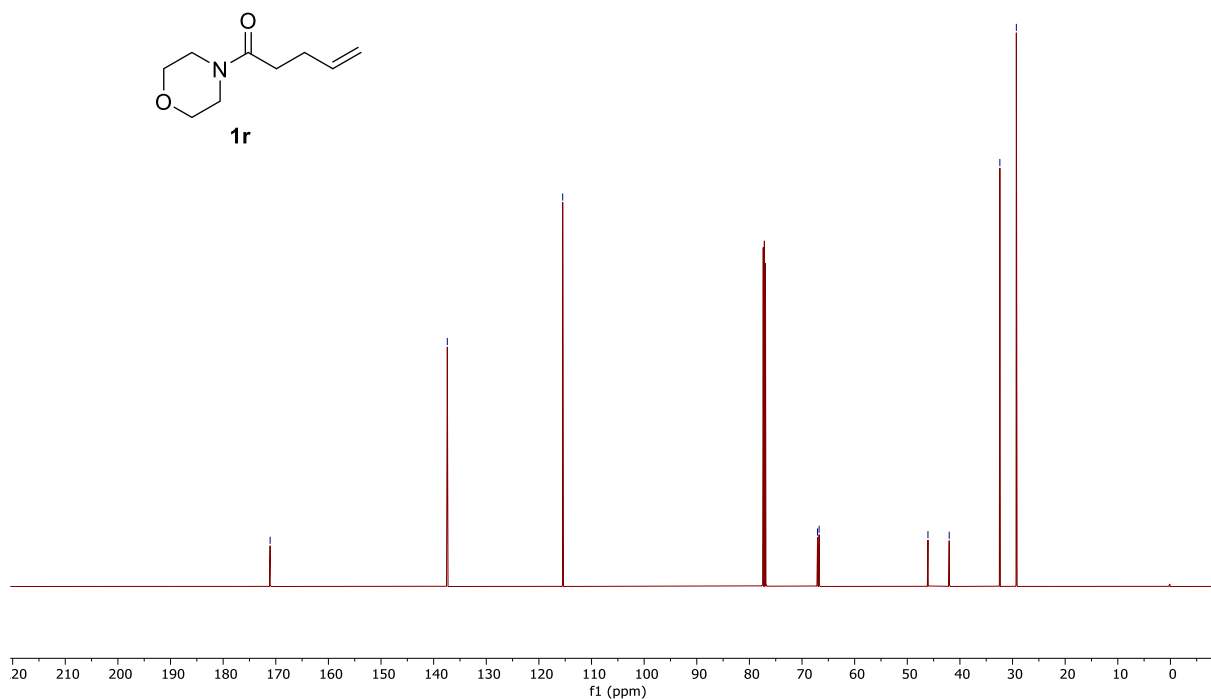
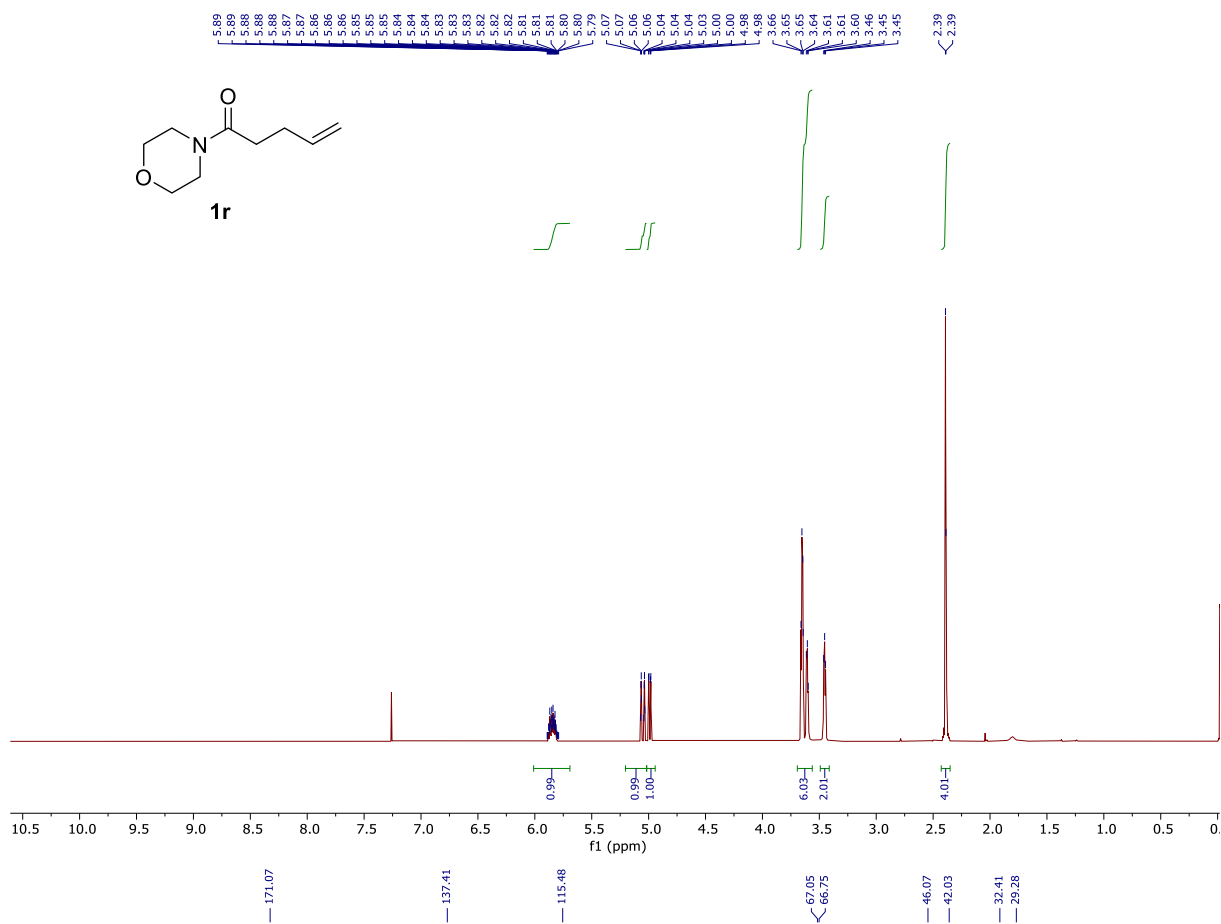
W-catalyzed remote β -hydroboration of alkenes



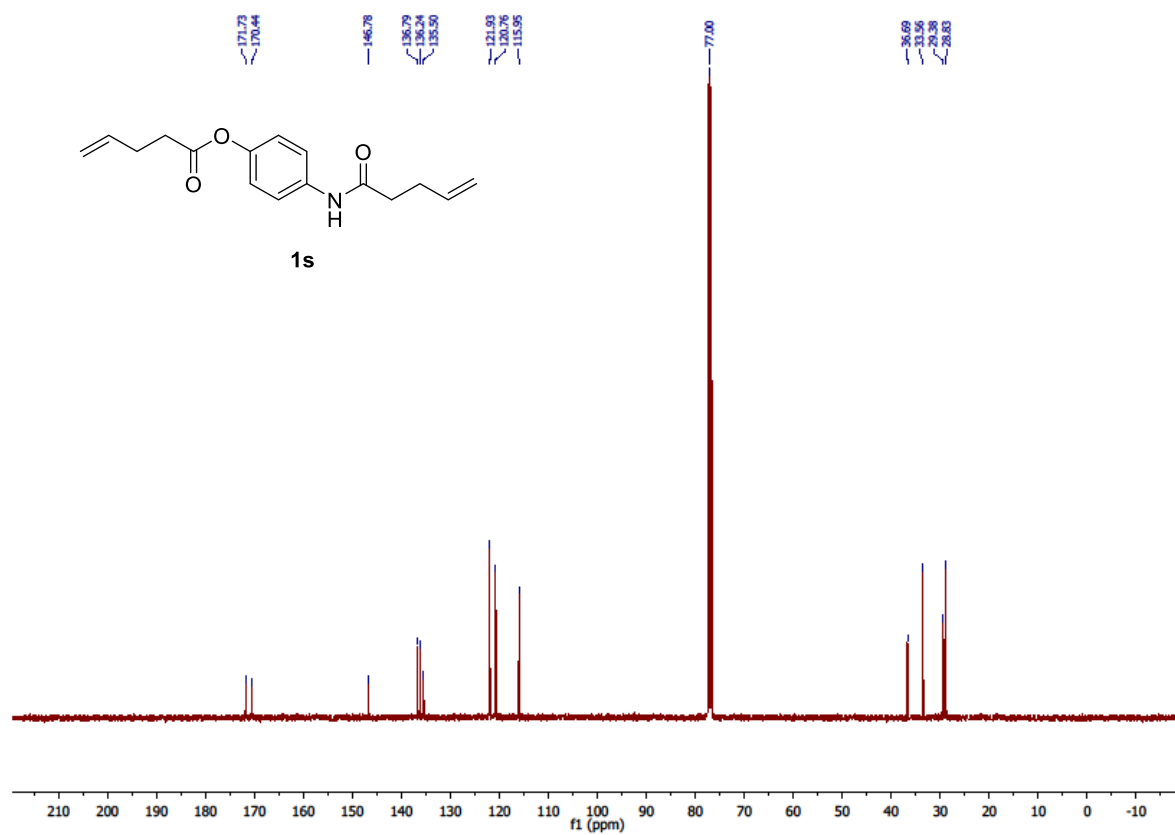
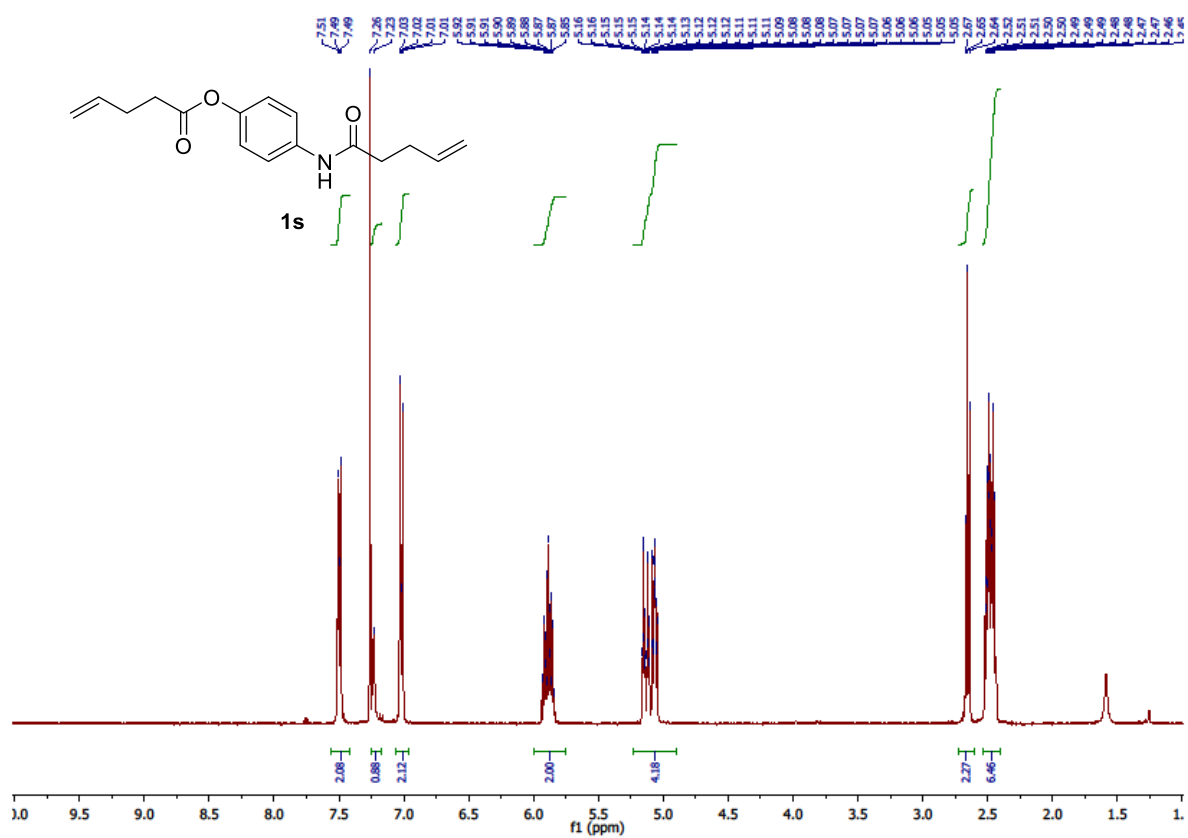
Chapter 4



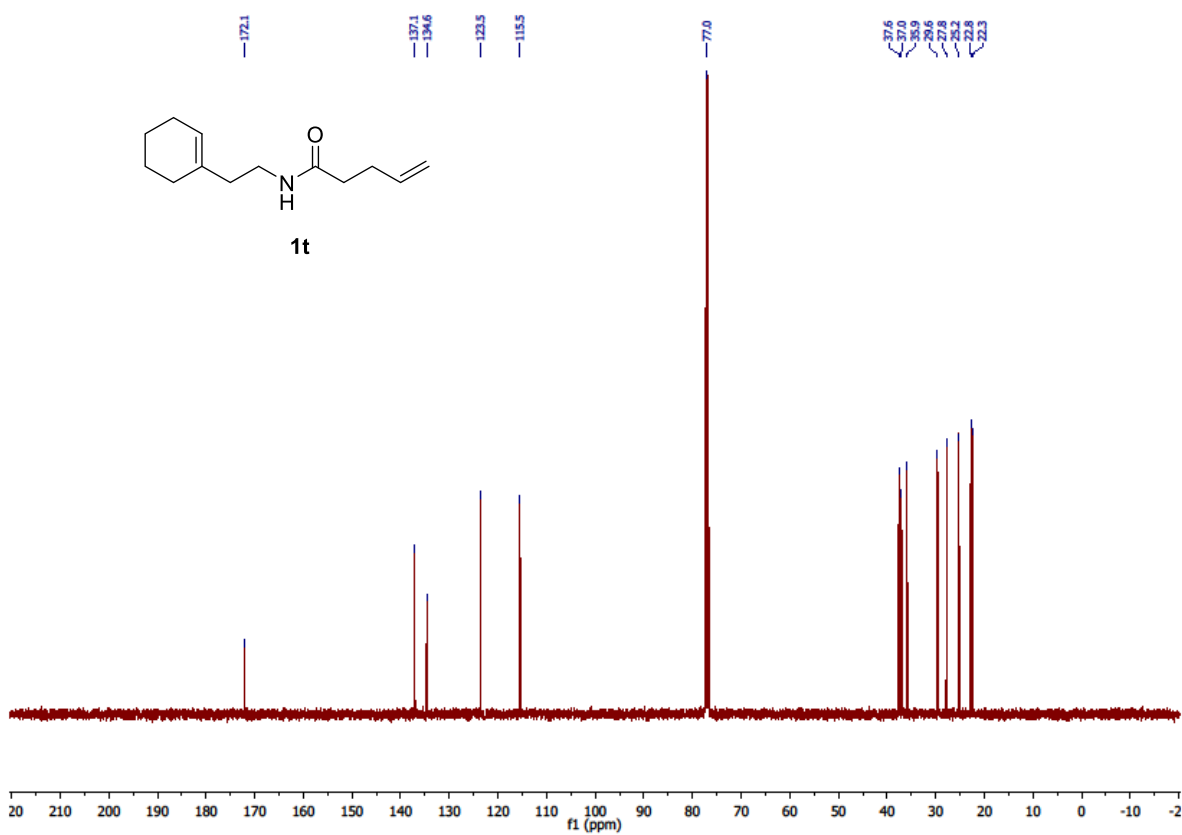
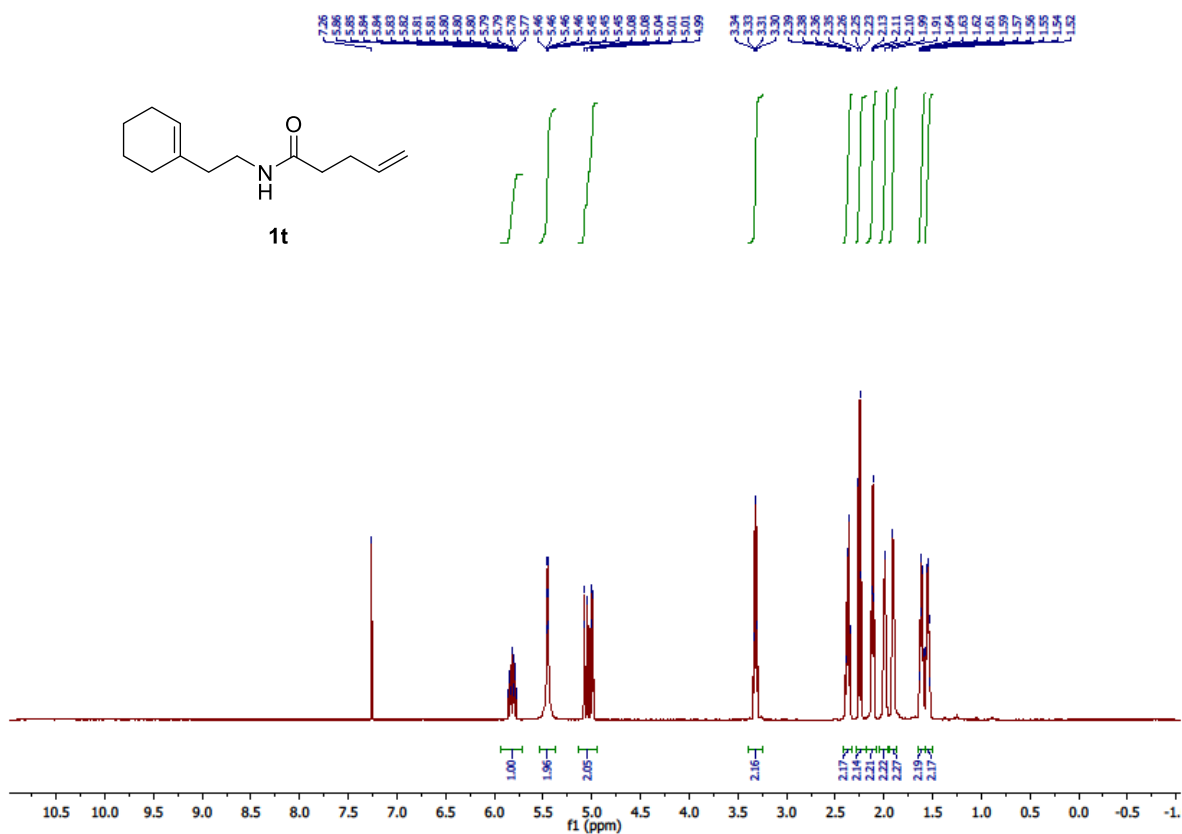
W-catalyzed remote β -hydroboration of alkenes



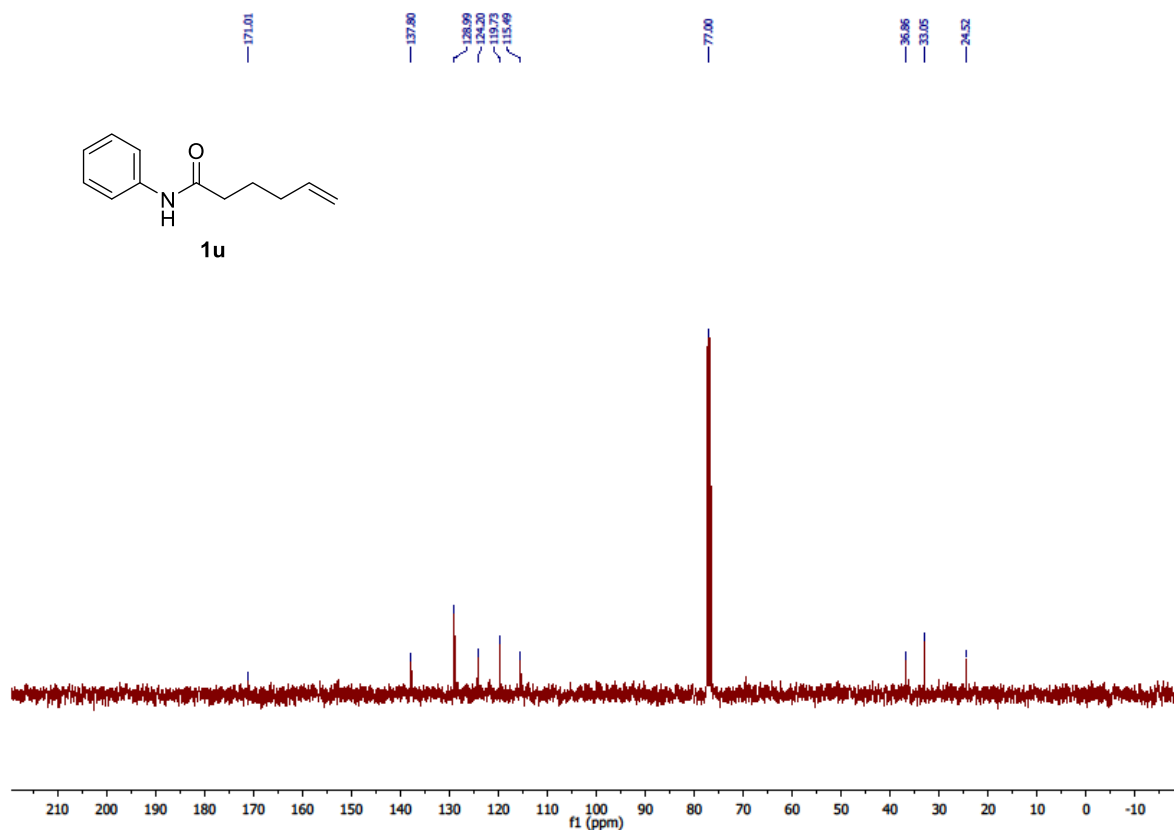
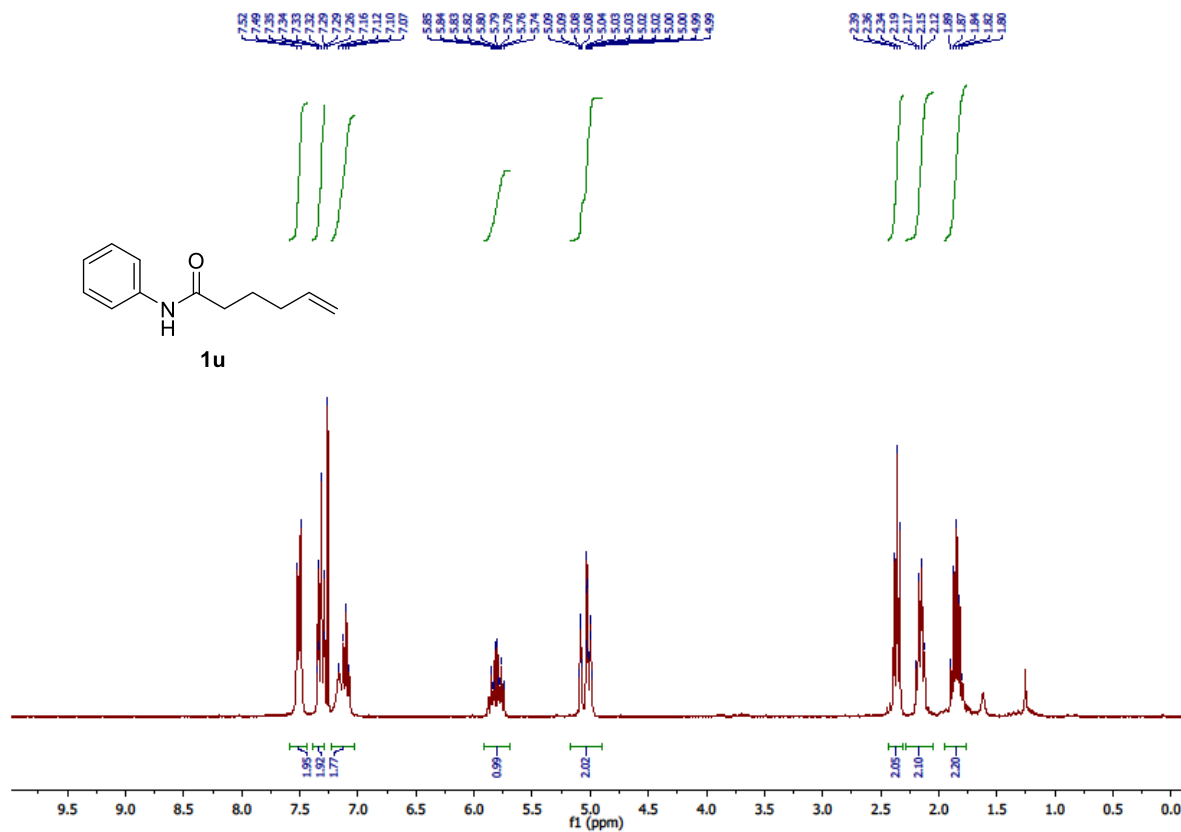
Chapter 4

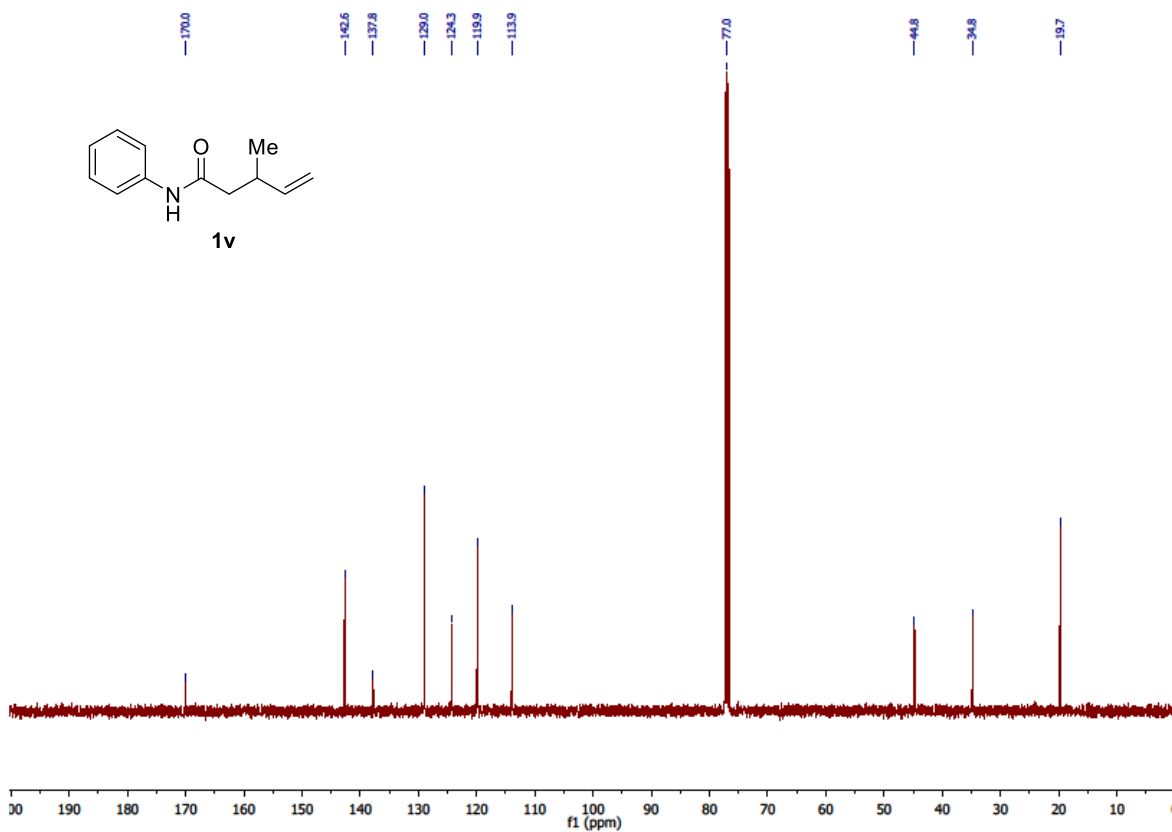
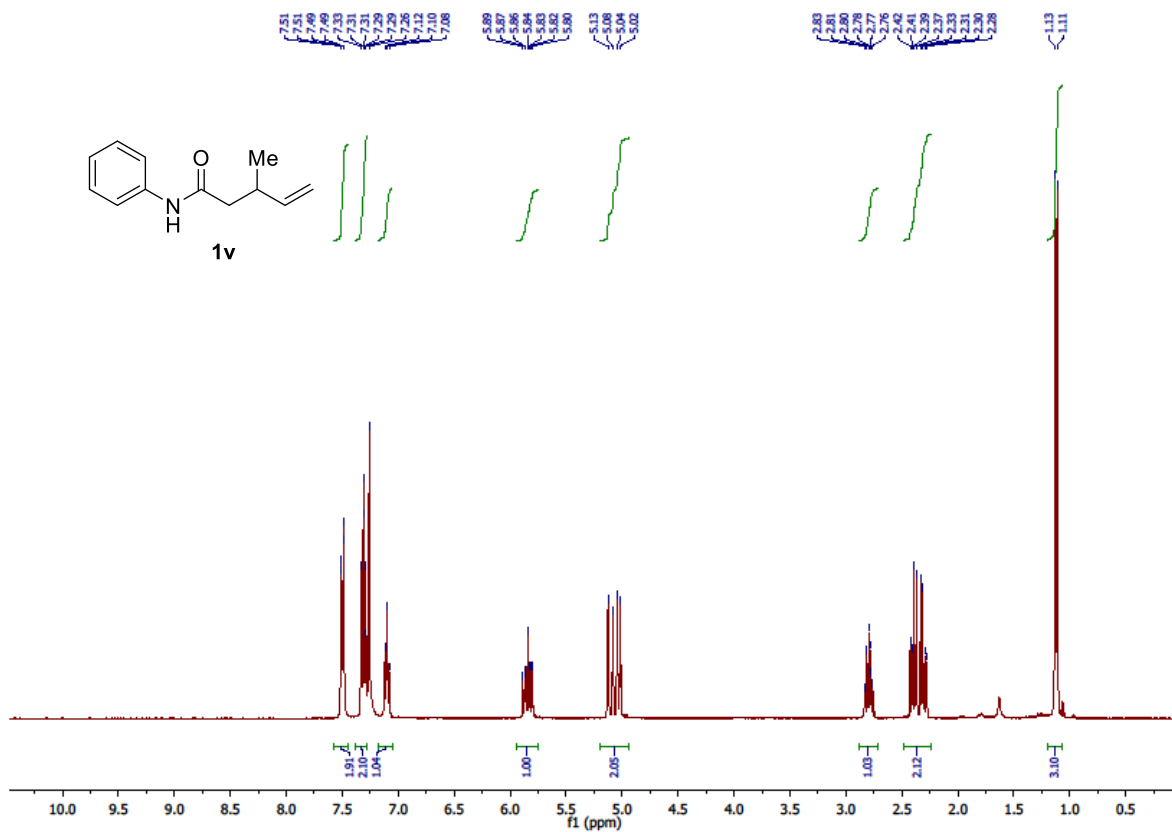


W-catalyzed remote β -hydroboration of alkenes

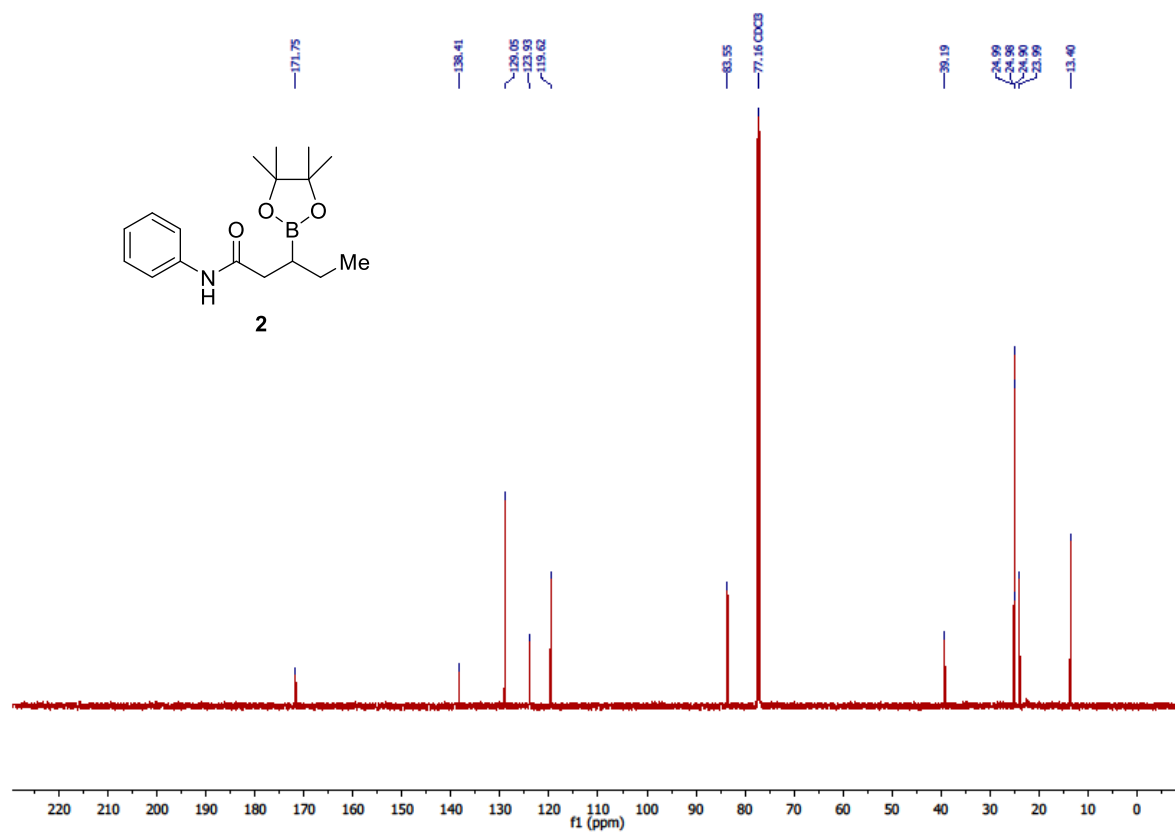
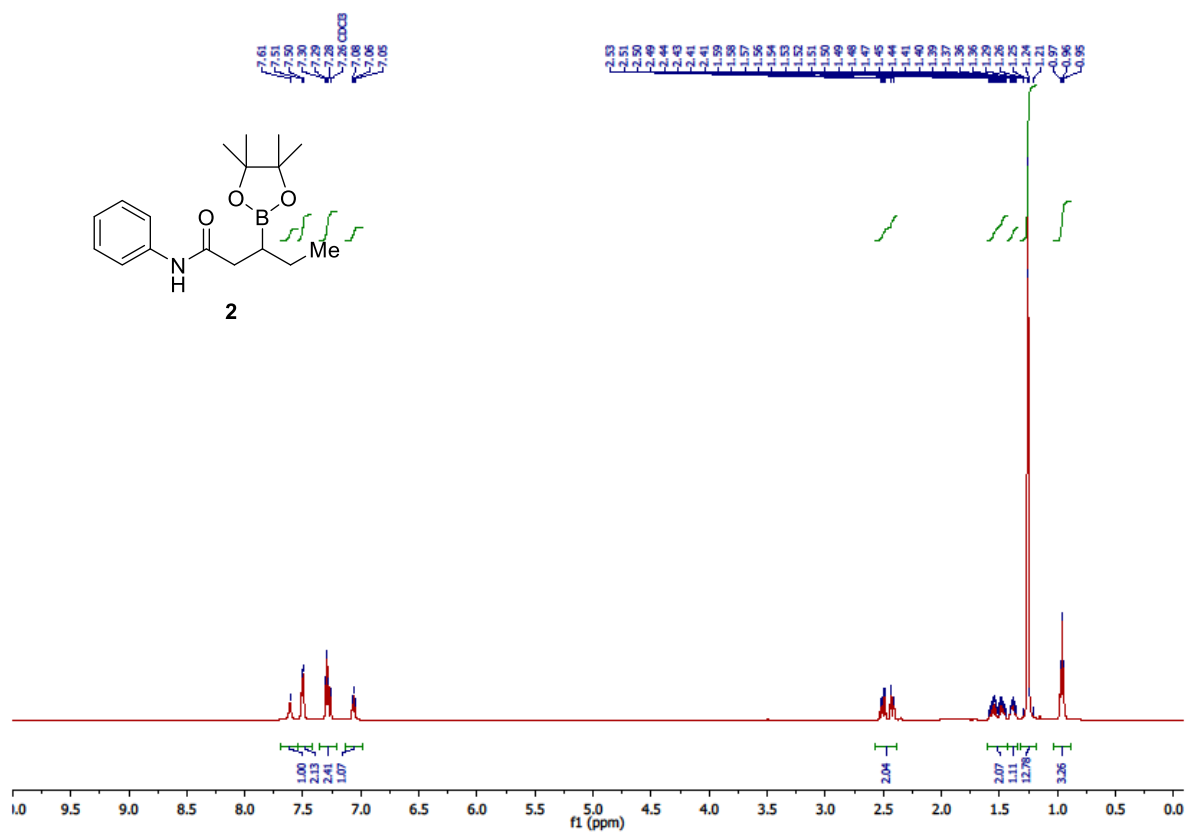


Chapter 4

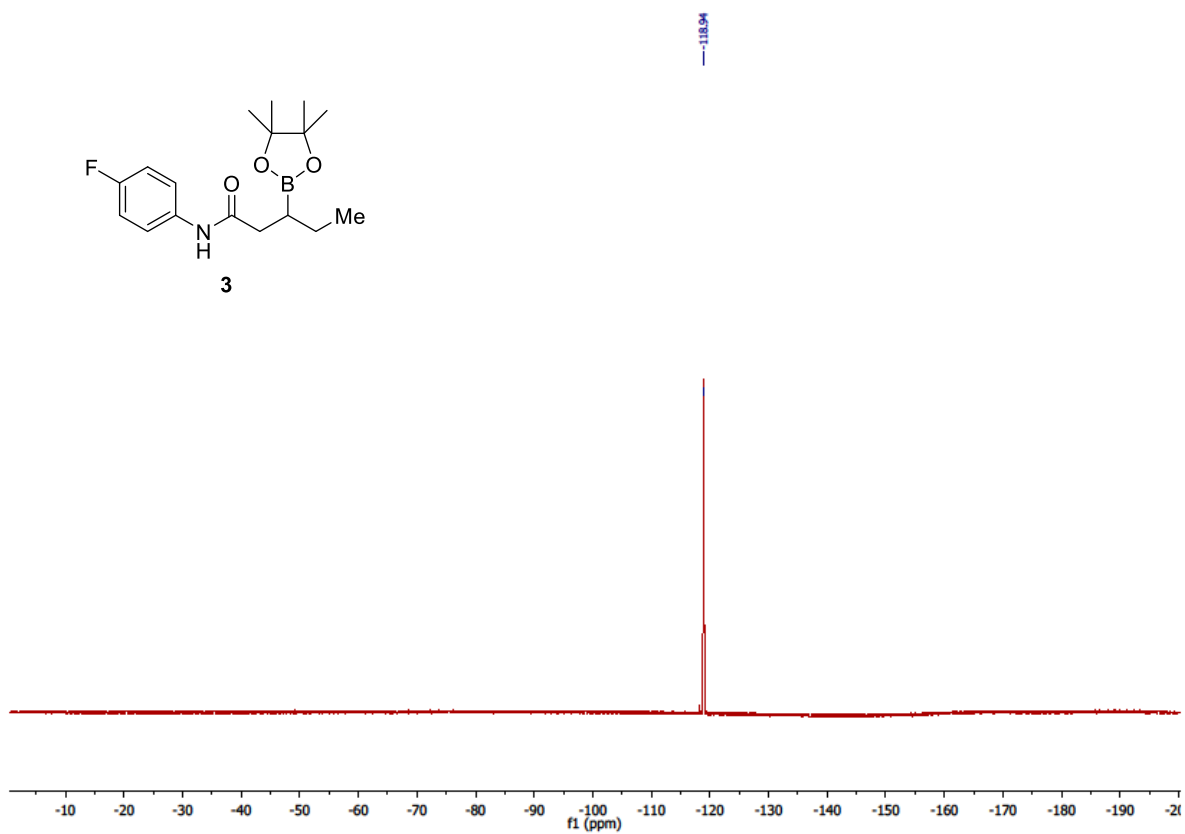




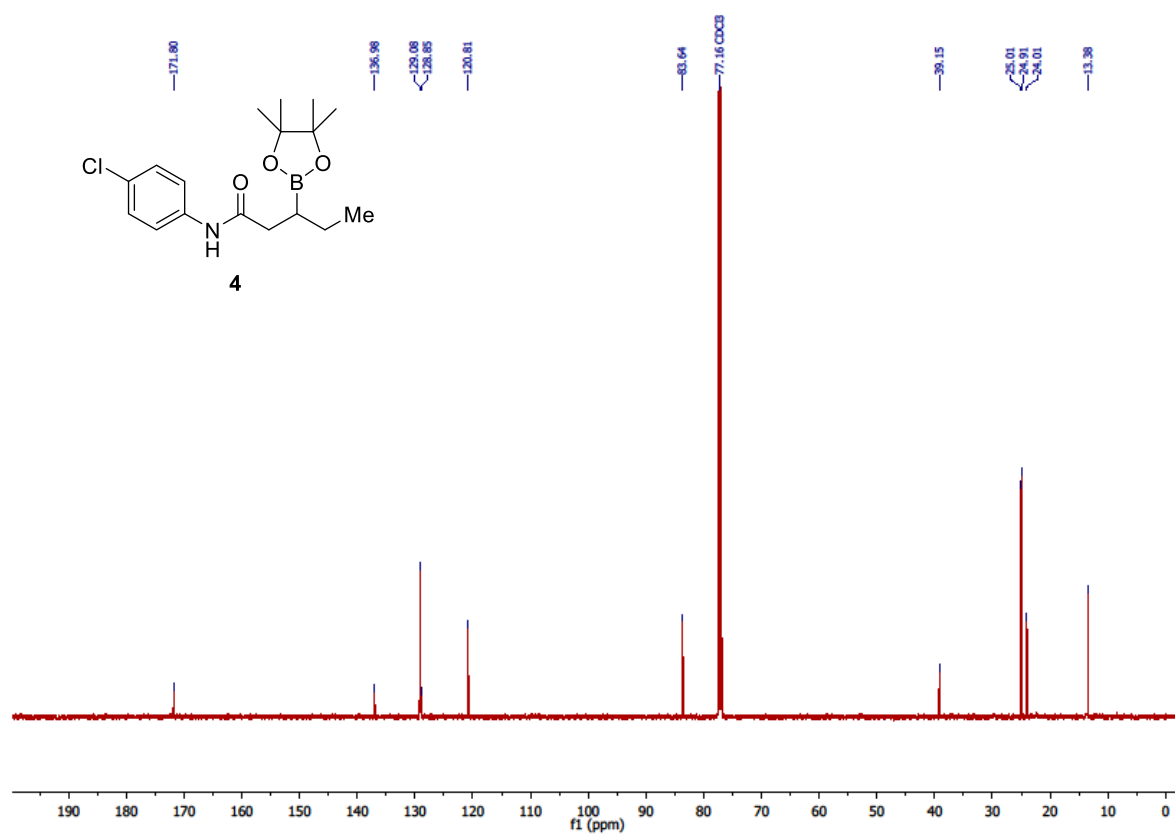
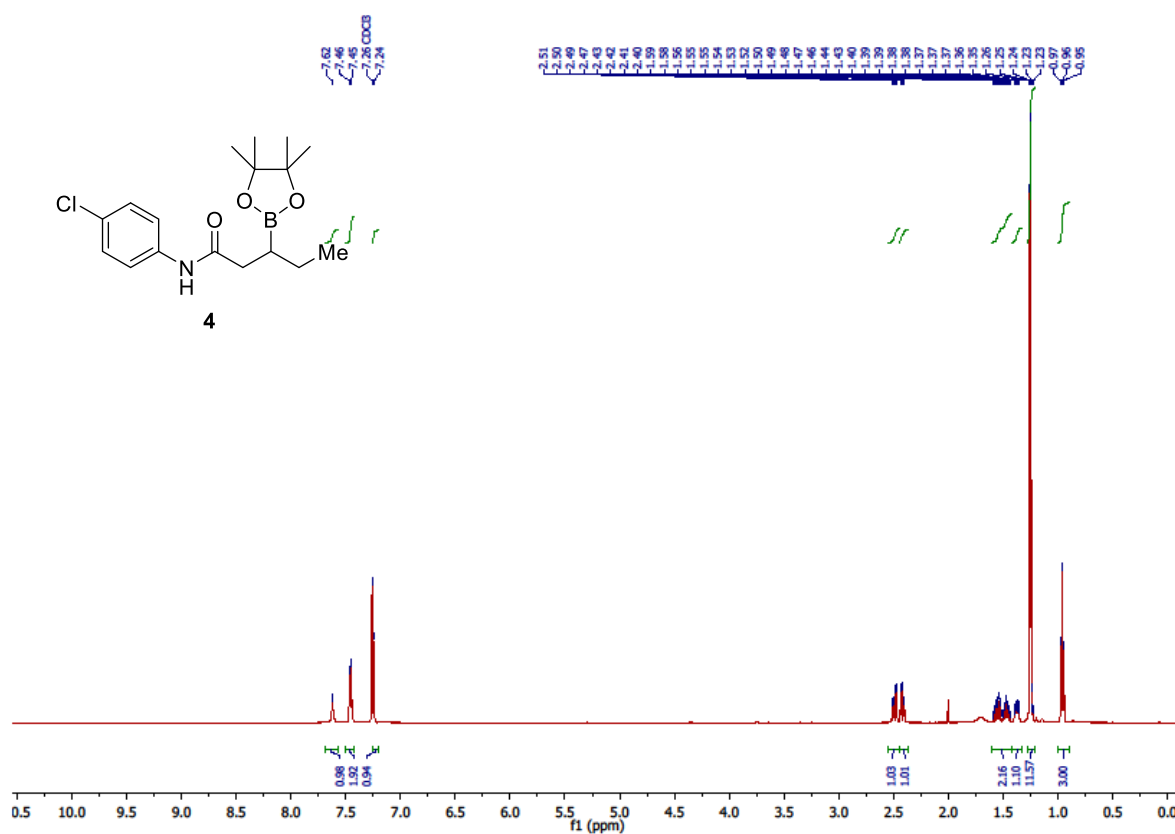
Chapter 4



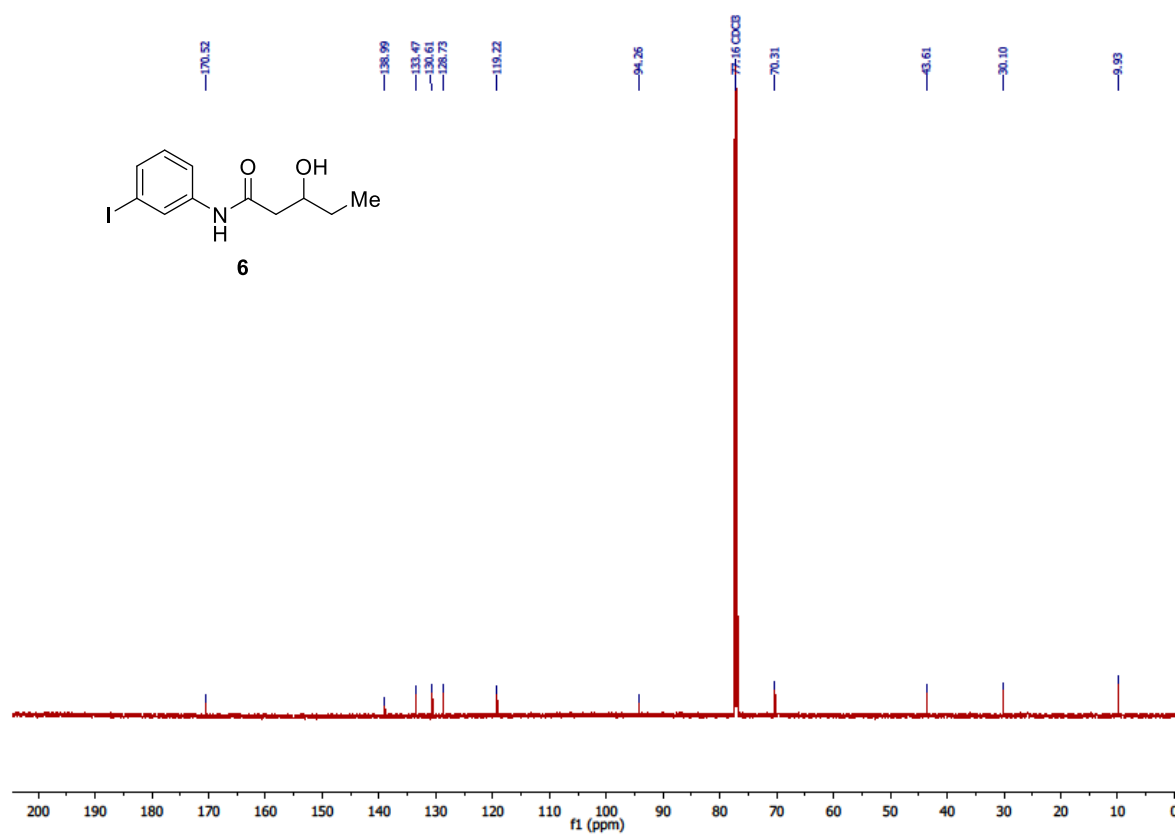
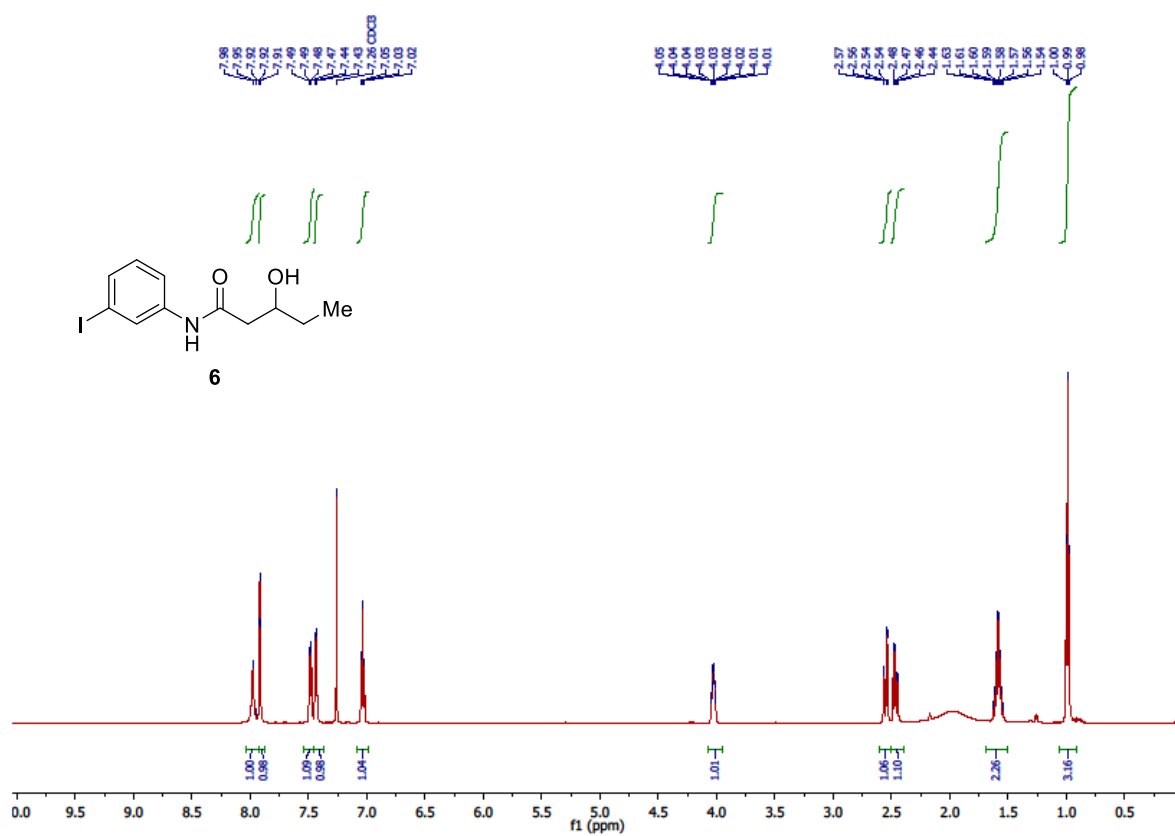
Chapter 4



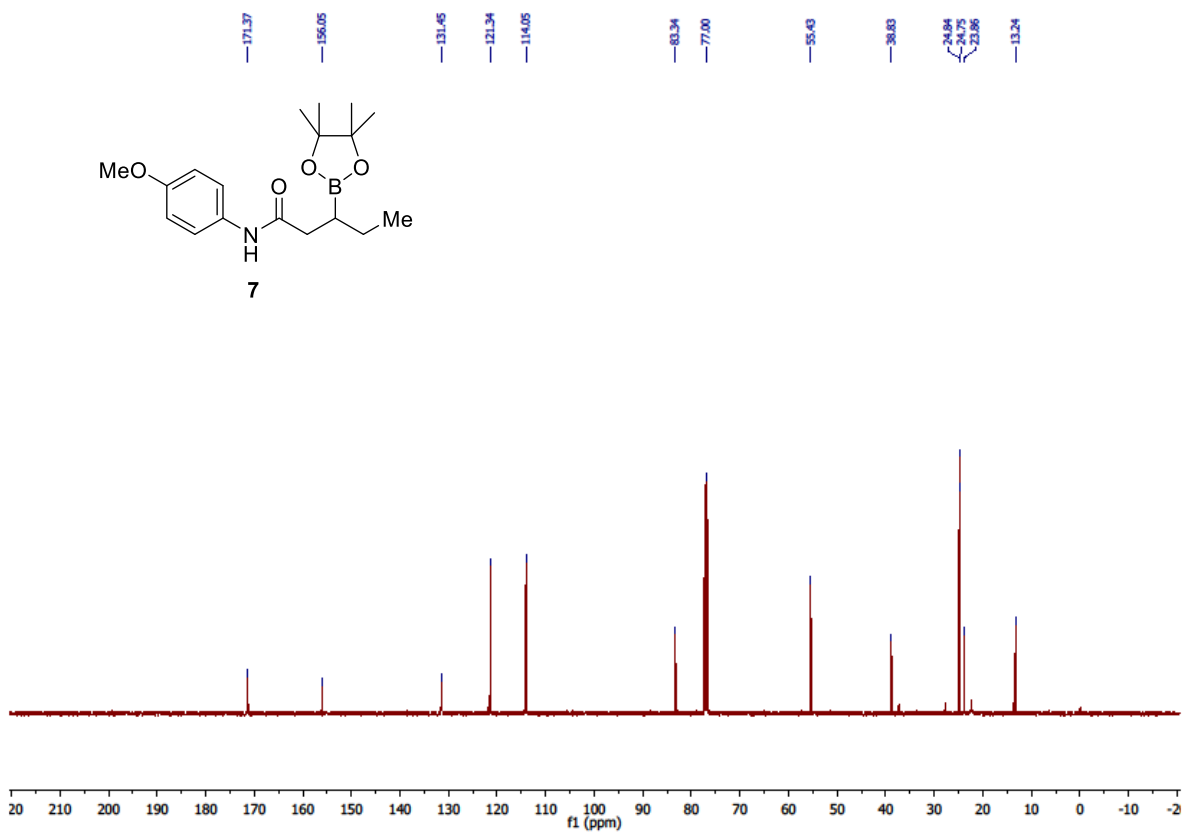
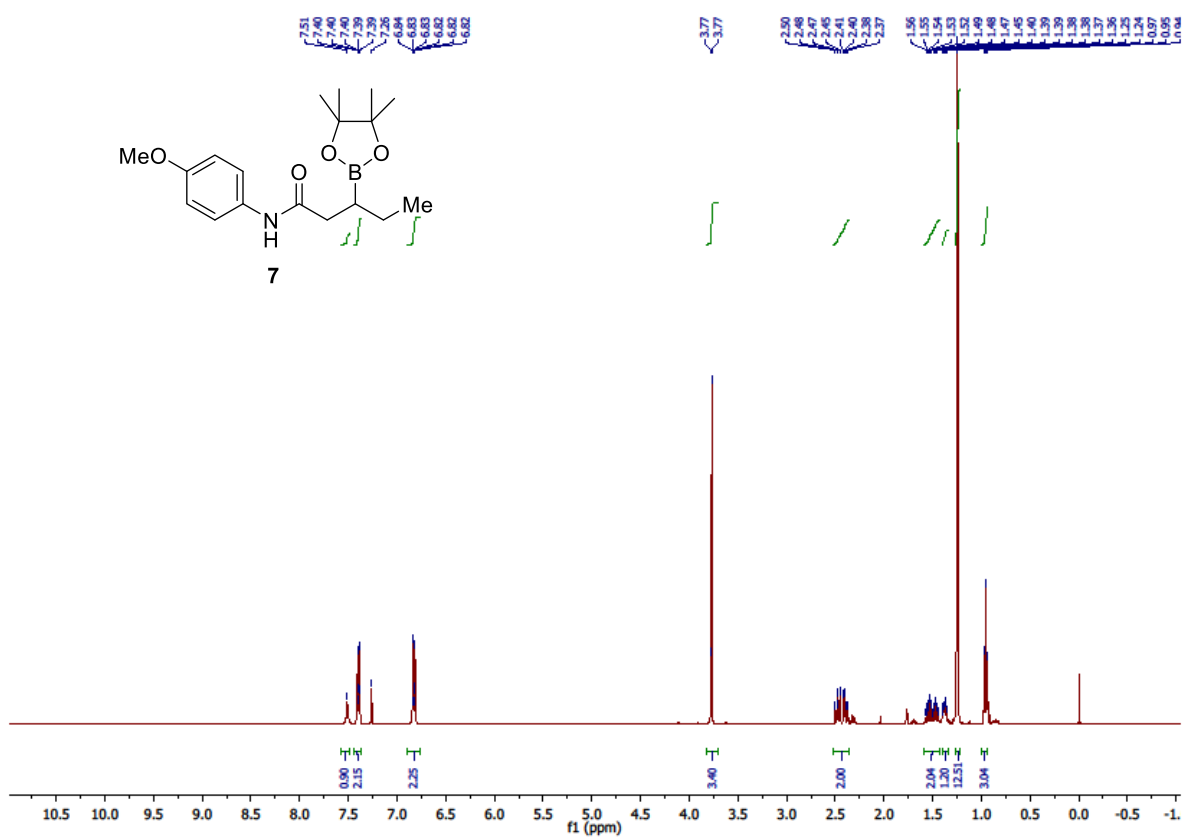
W-catalyzed remote β -hydroboration of alkenes



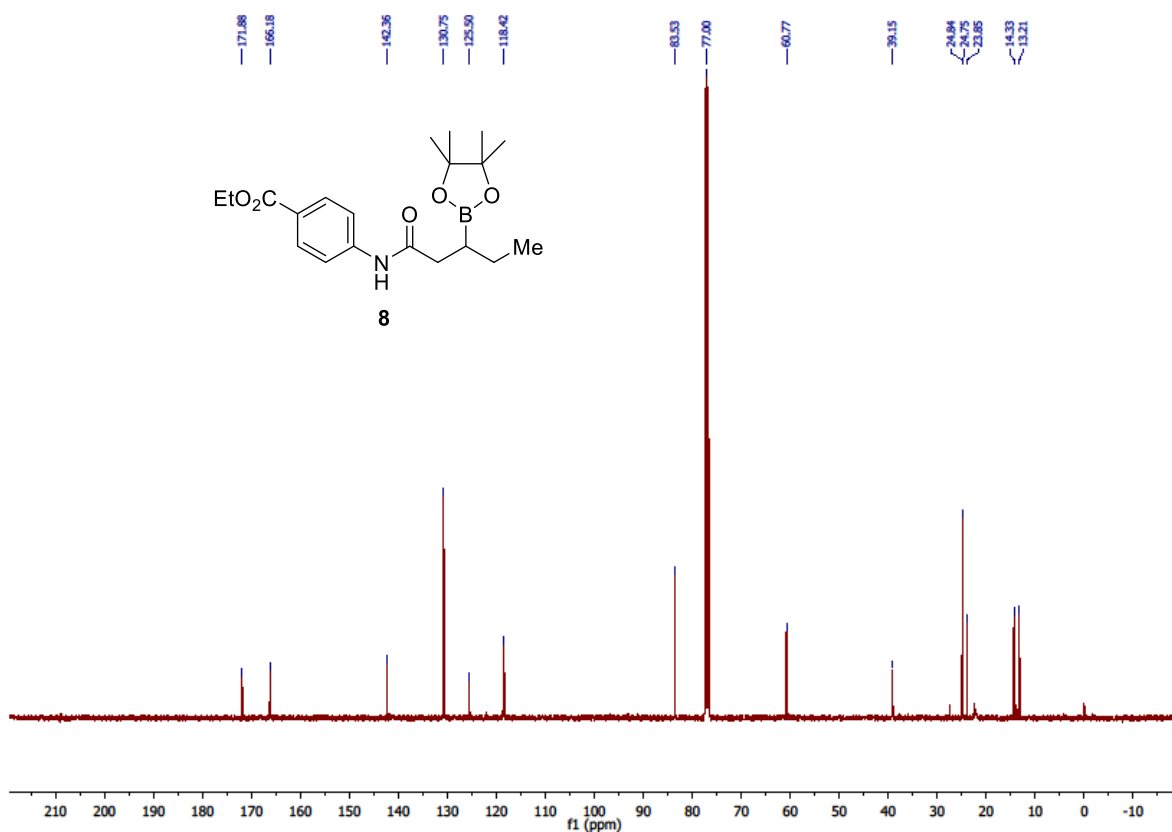
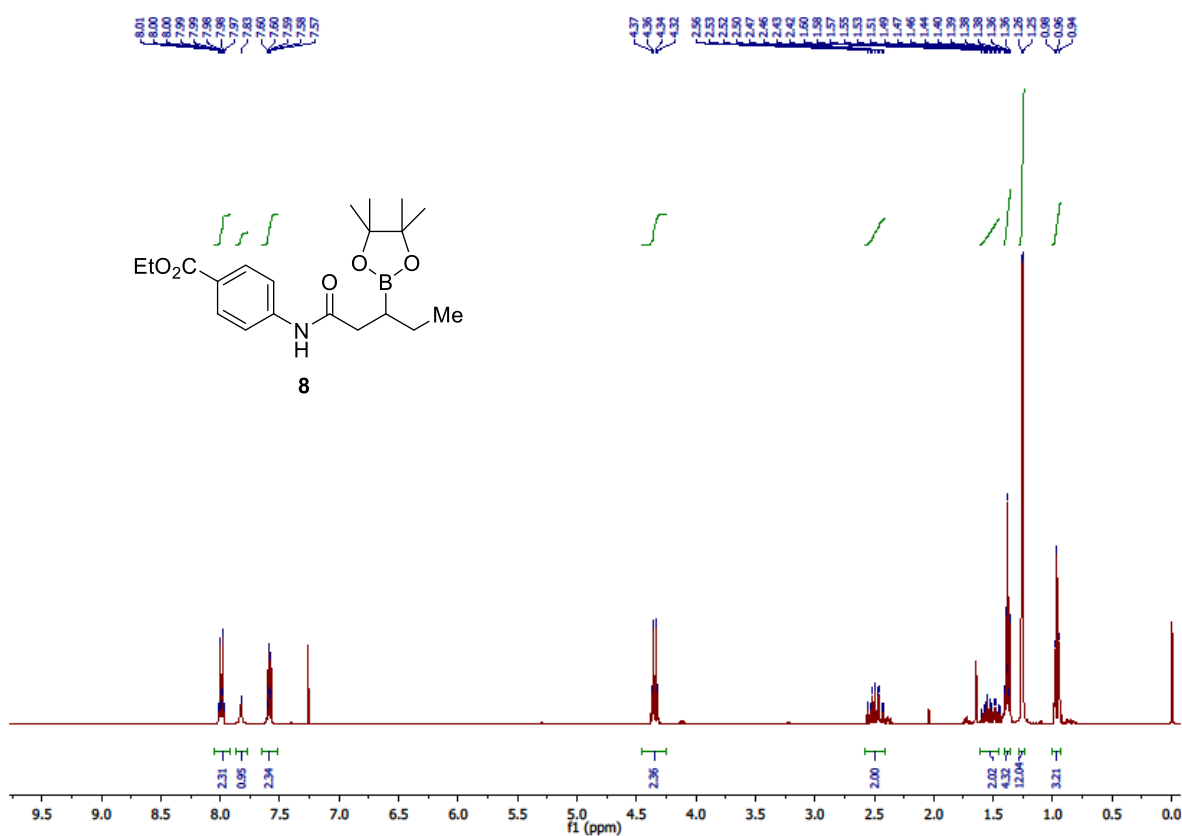
W-catalyzed remote β -hydroboration of alkenes



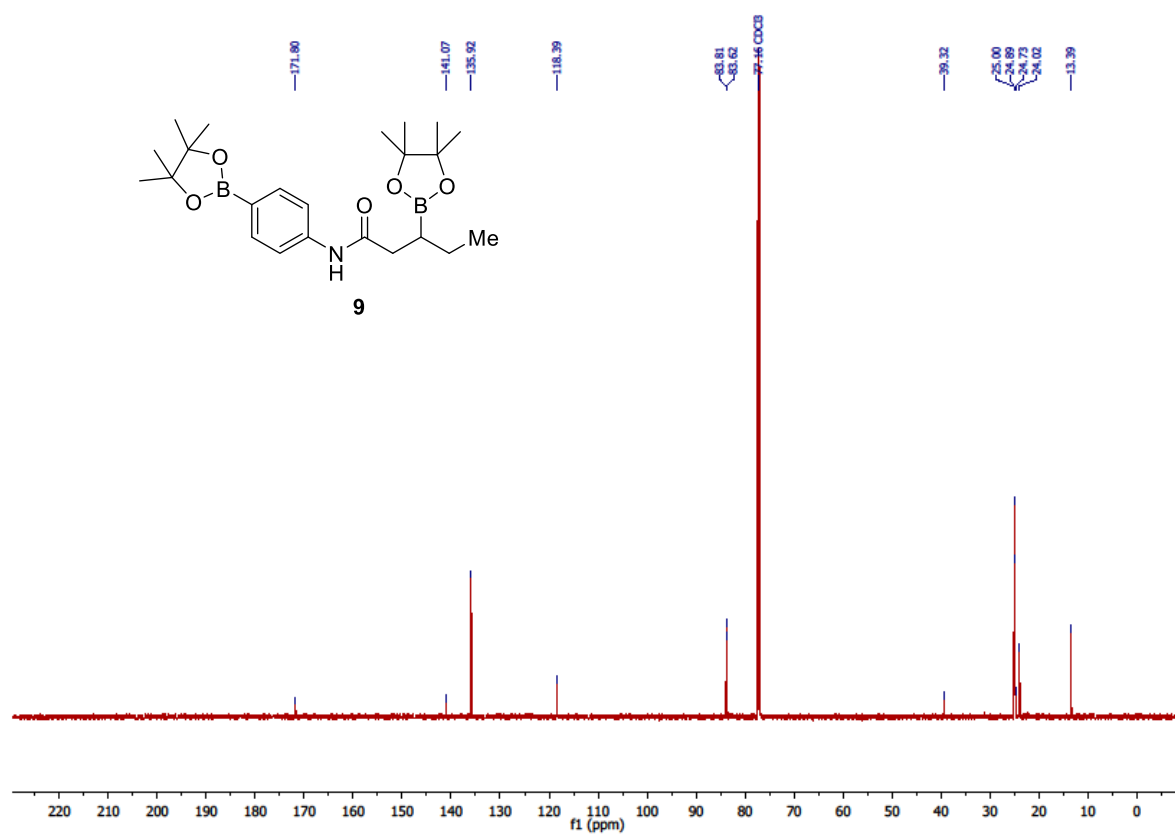
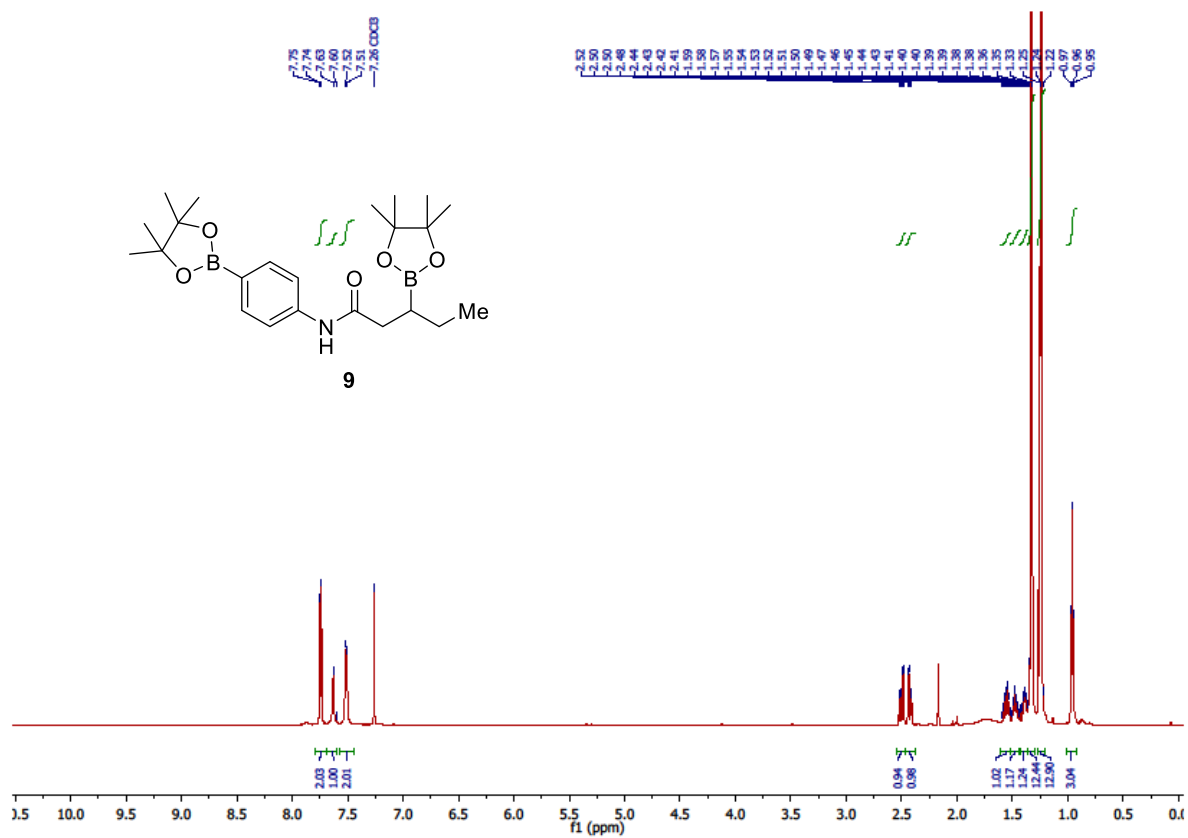
Chapter 4



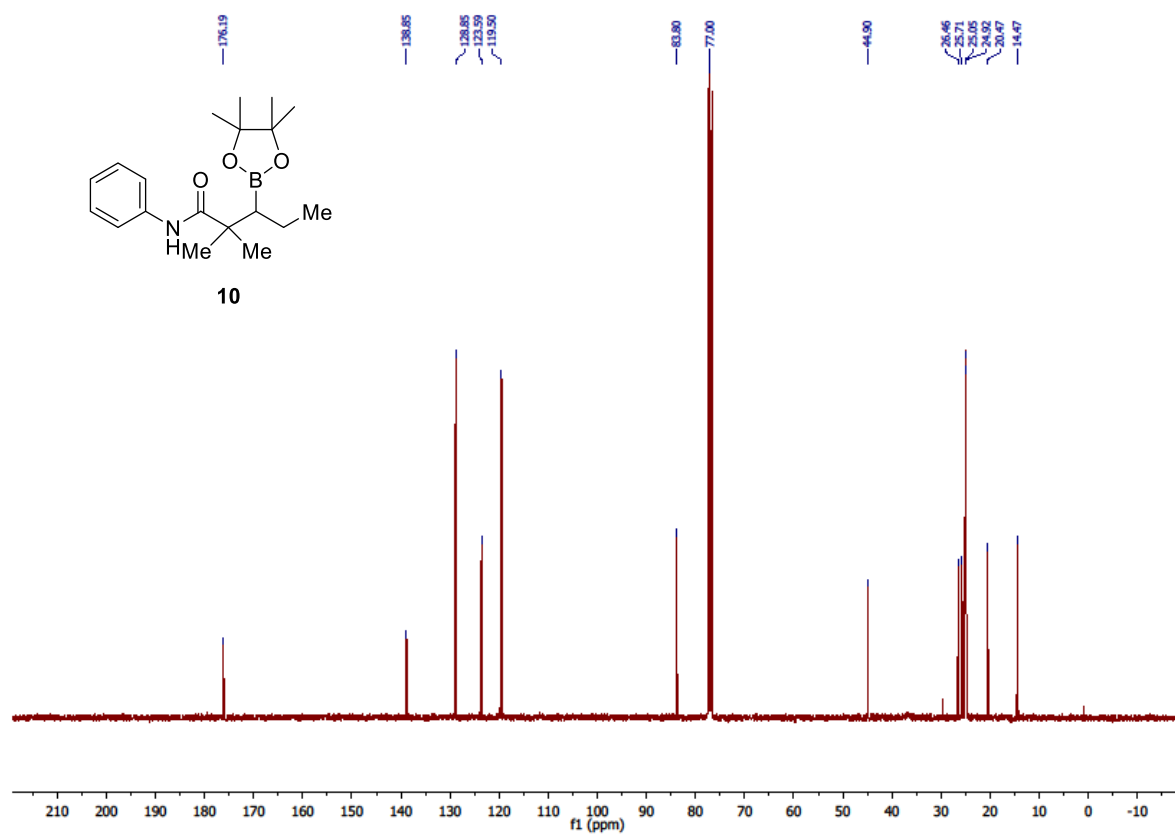
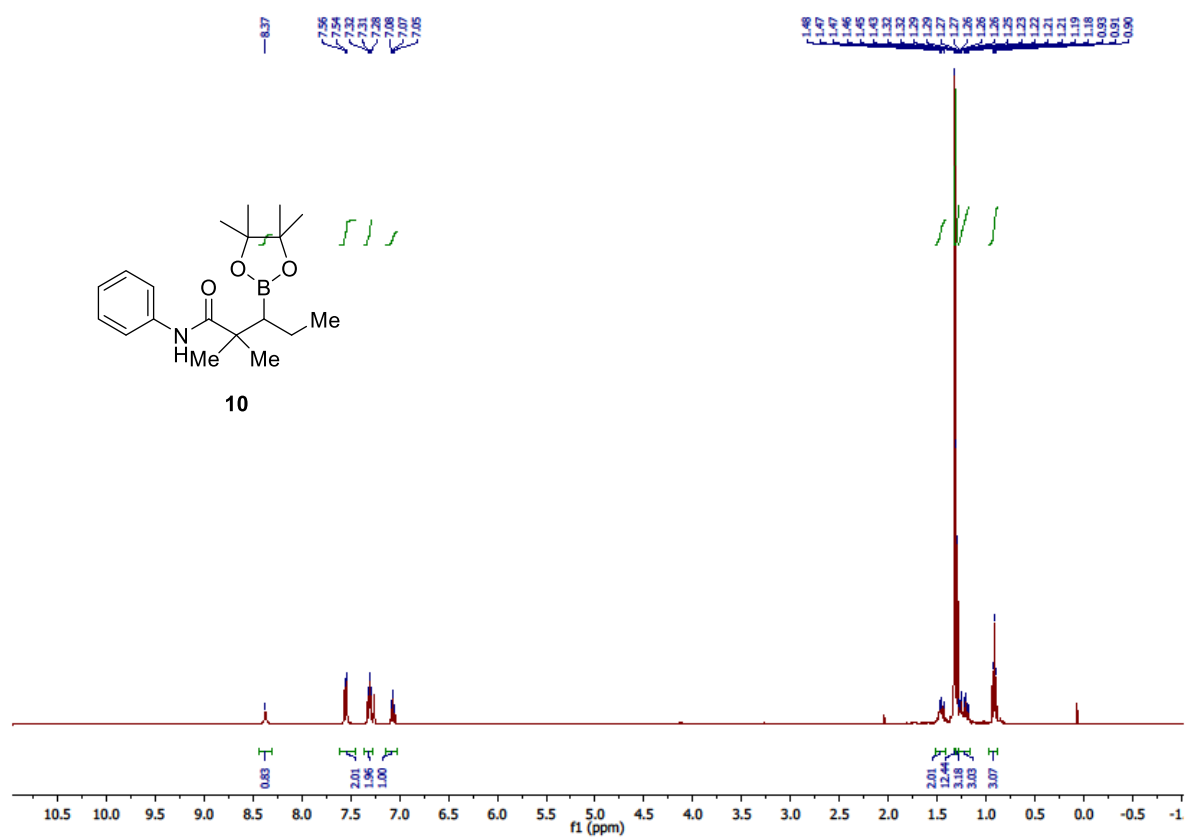
W-catalyzed remote β -hydroboration of alkenes



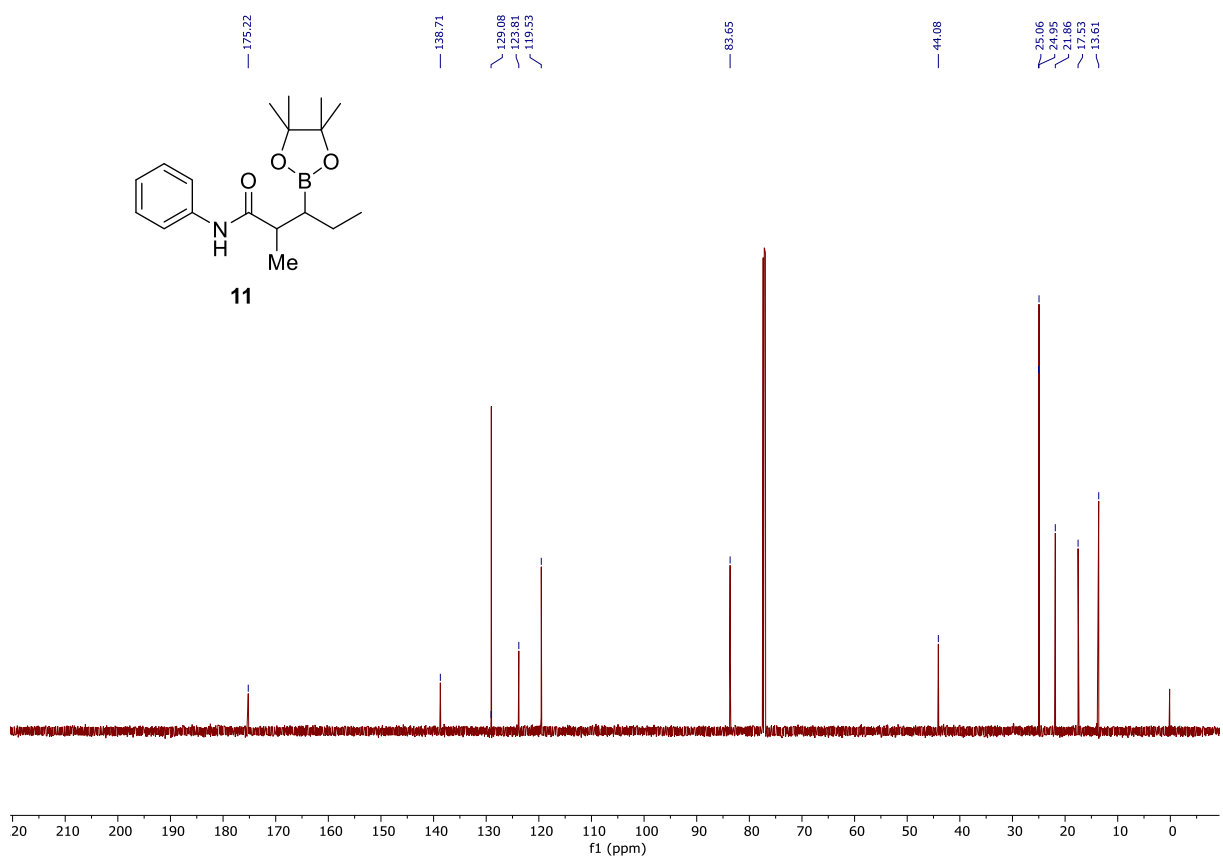
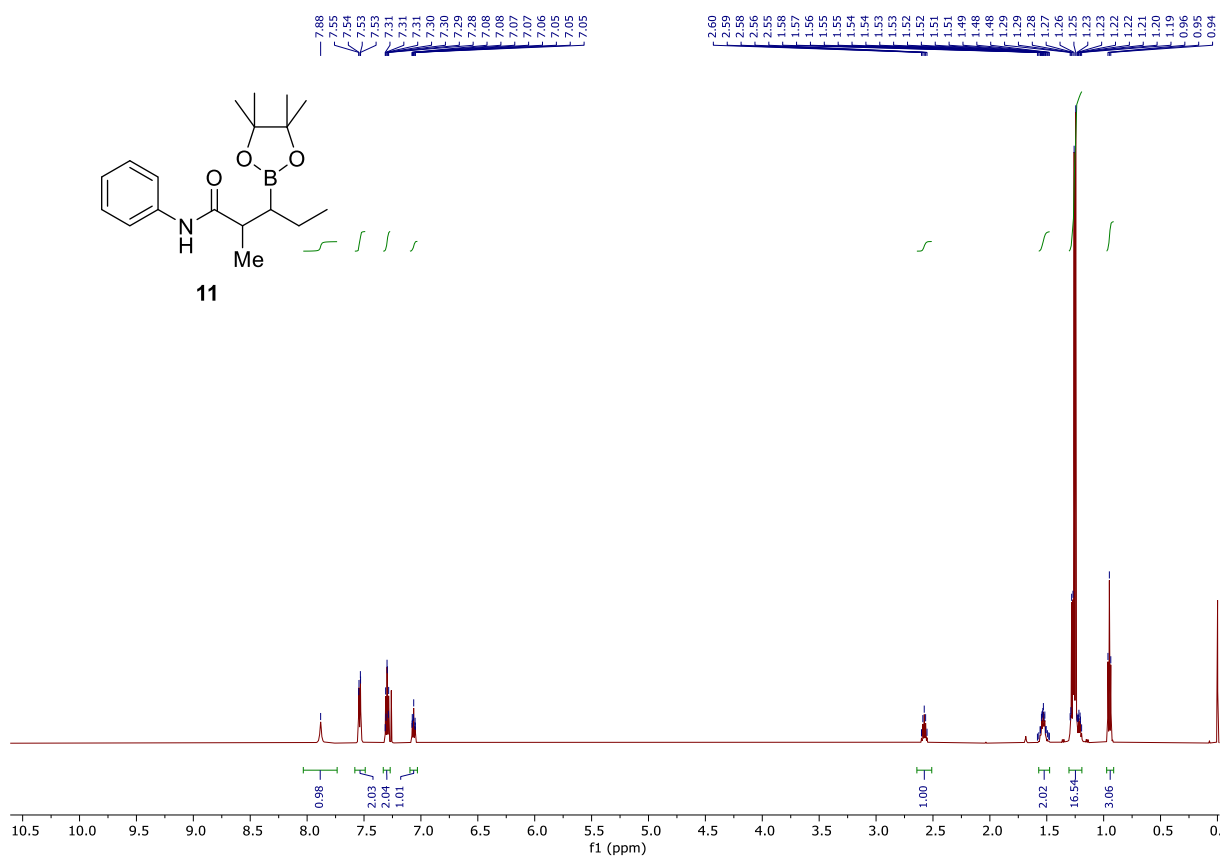
Chapter 4



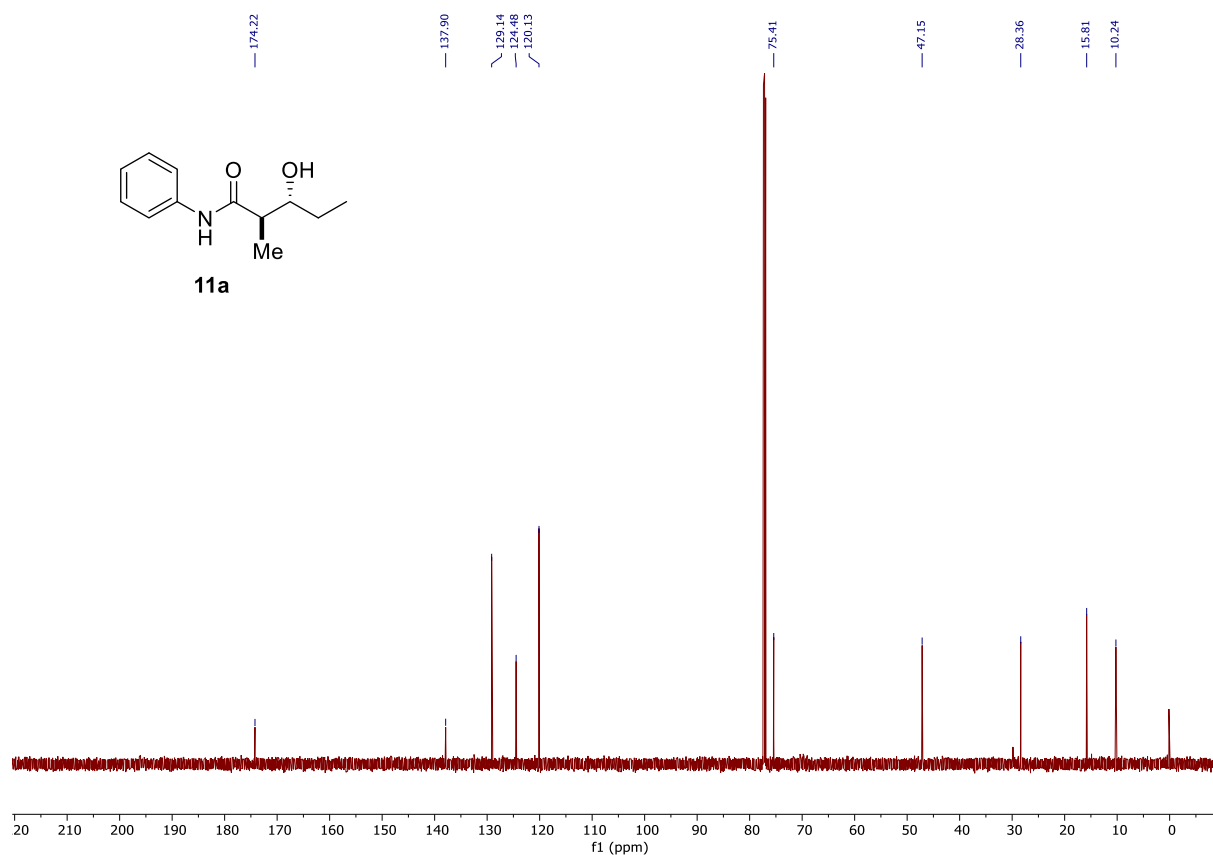
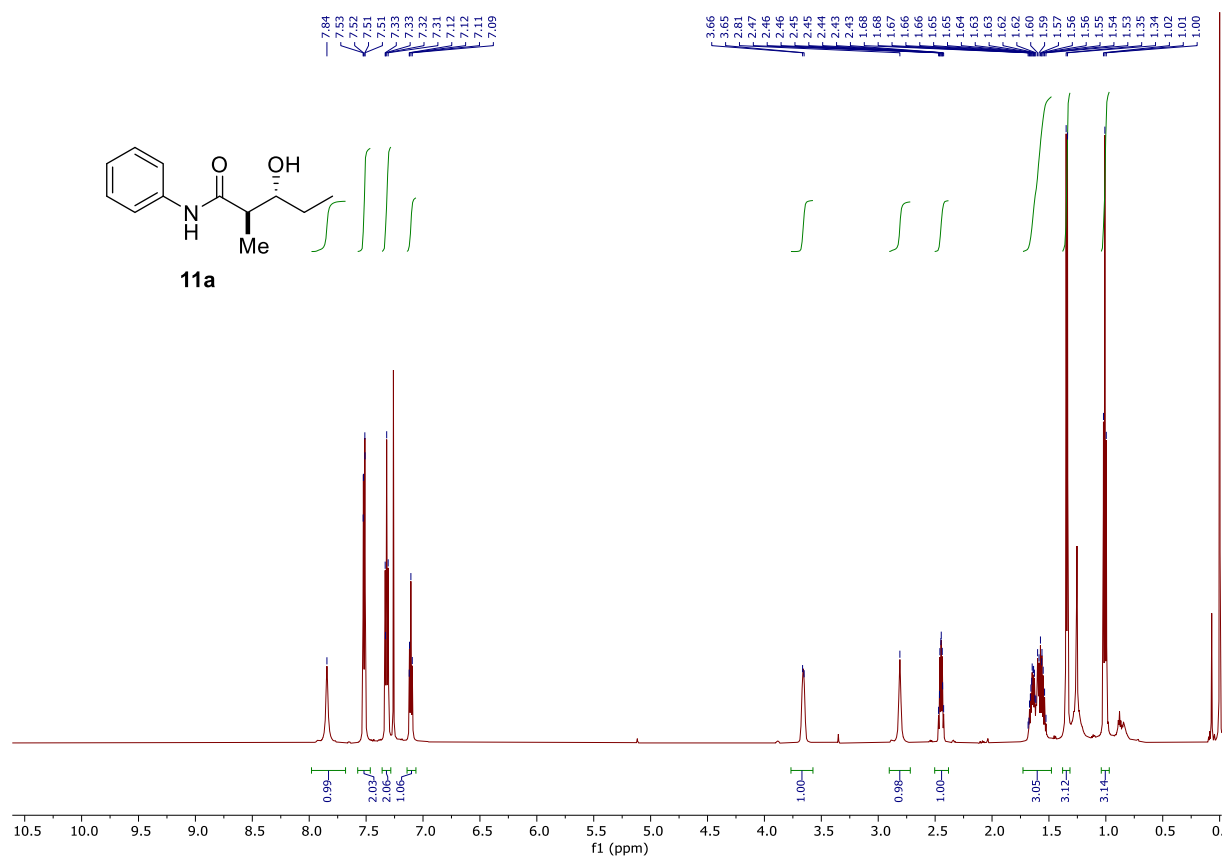
W-catalyzed remote β -hydroboration of alkenes



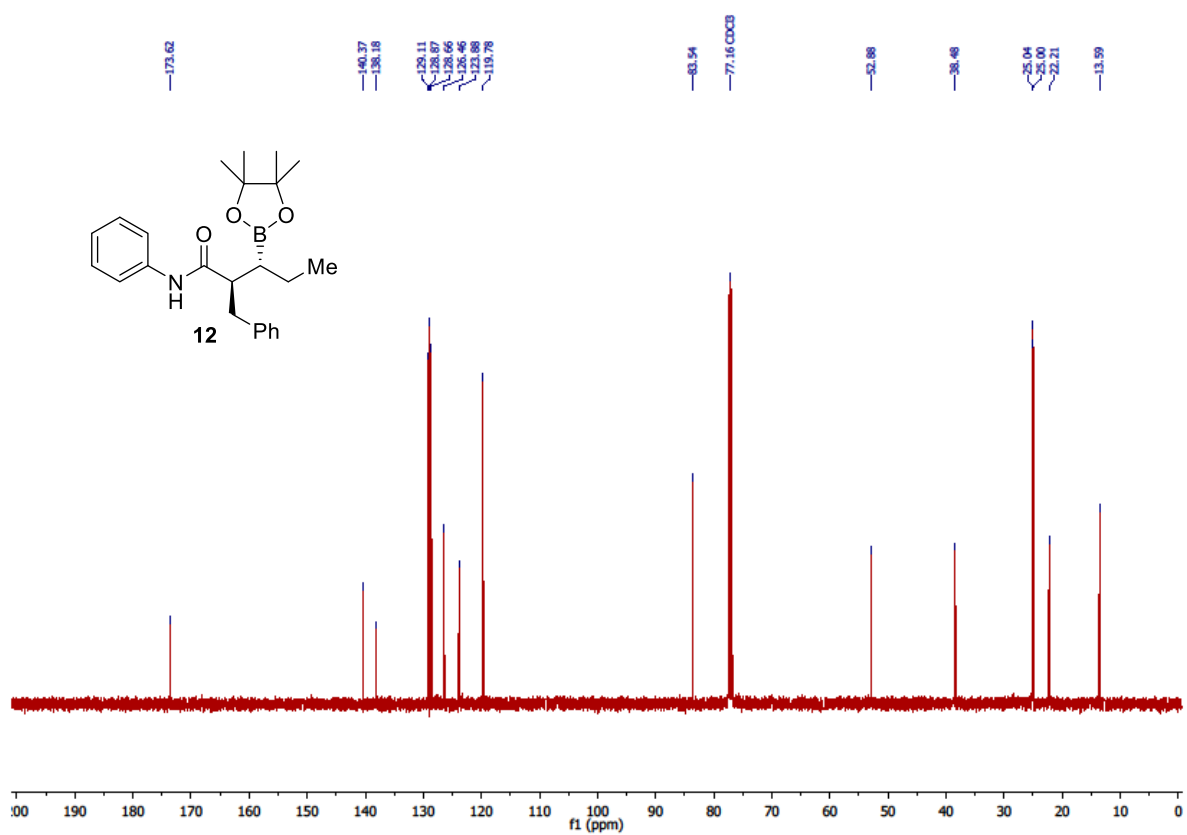
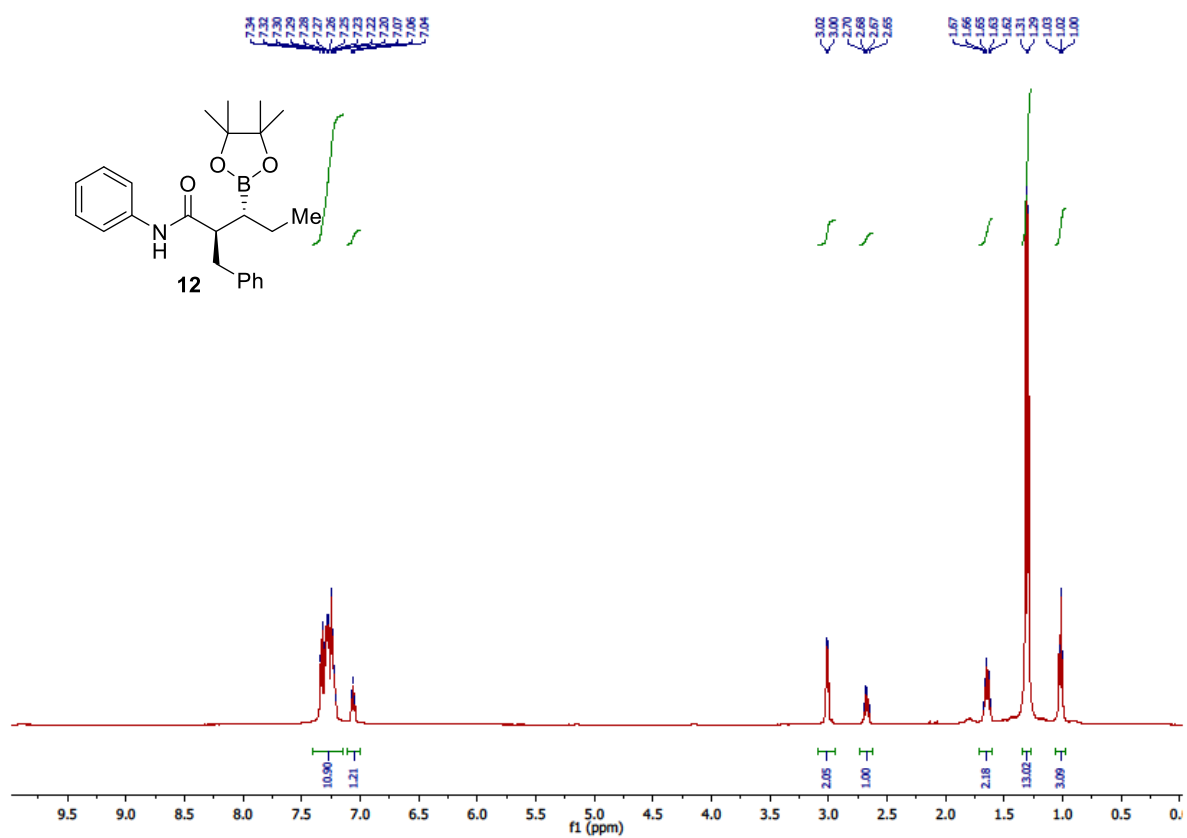
Chapter 4



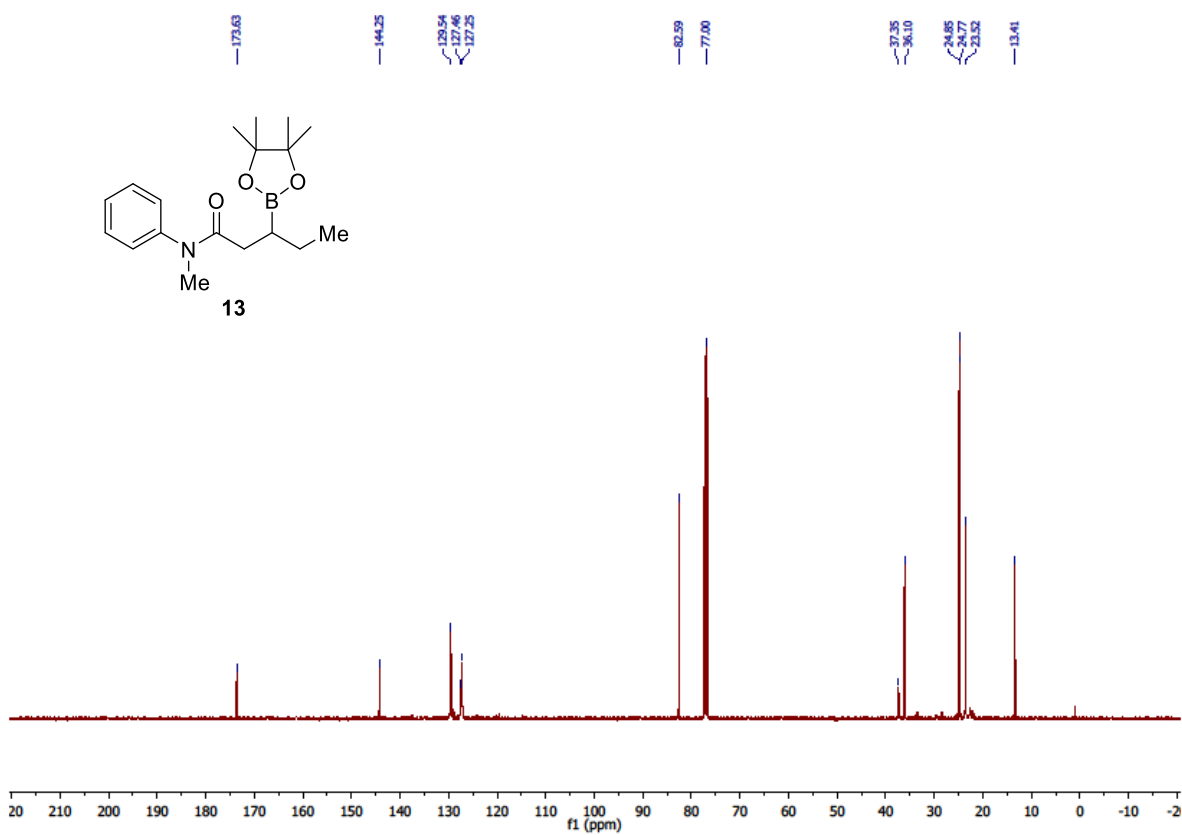
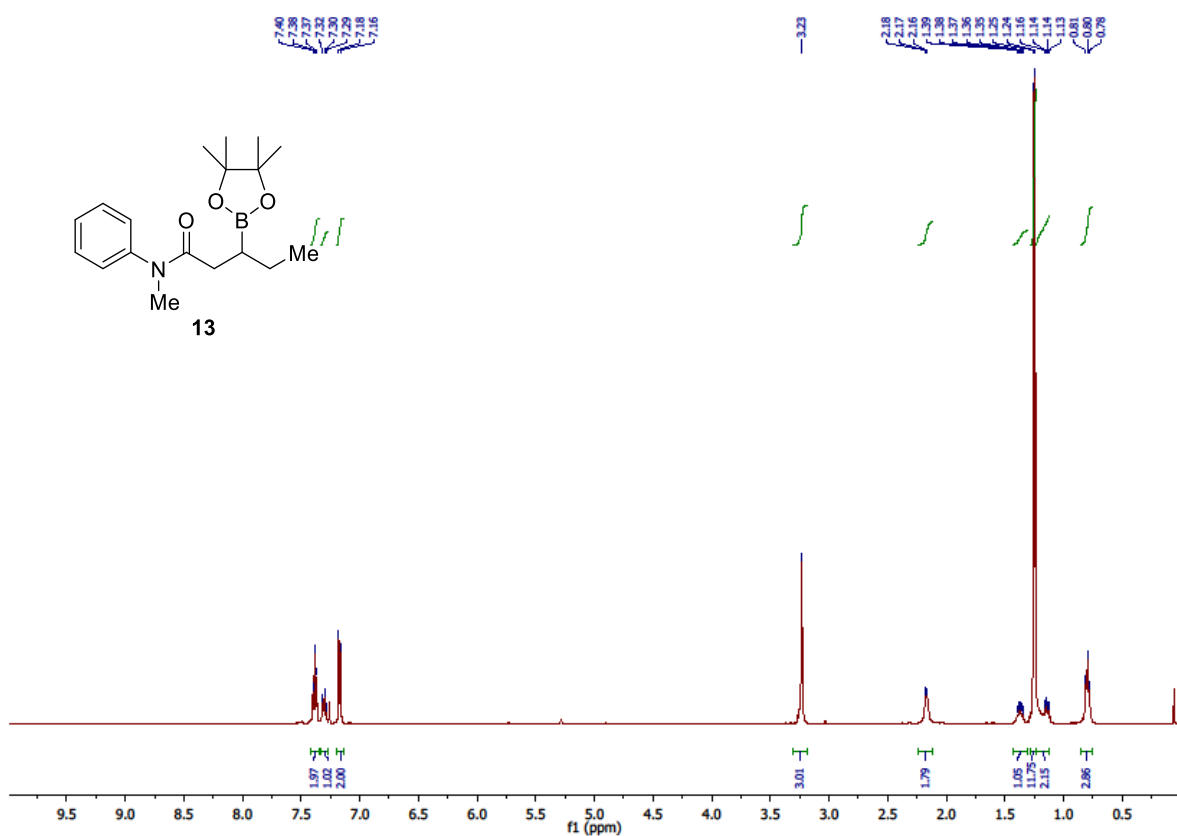
W-catalyzed remote β -hydroboration of alkenes



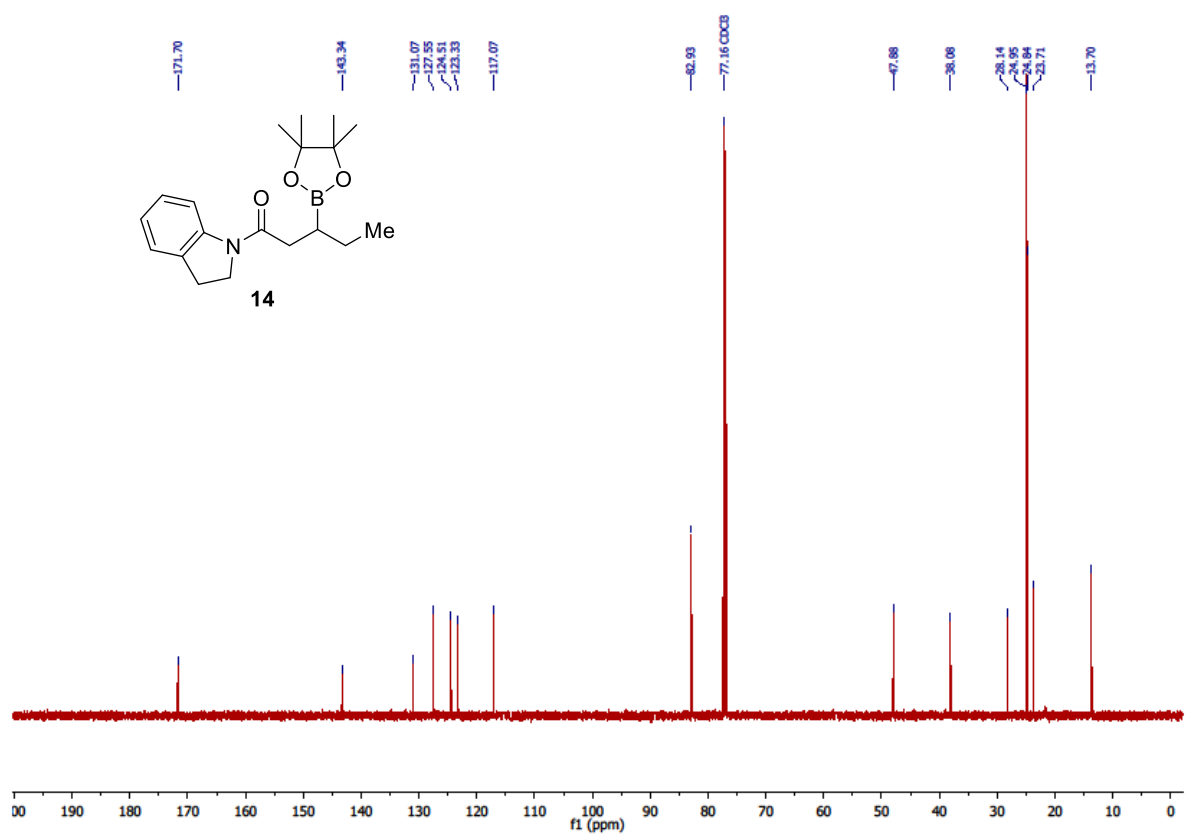
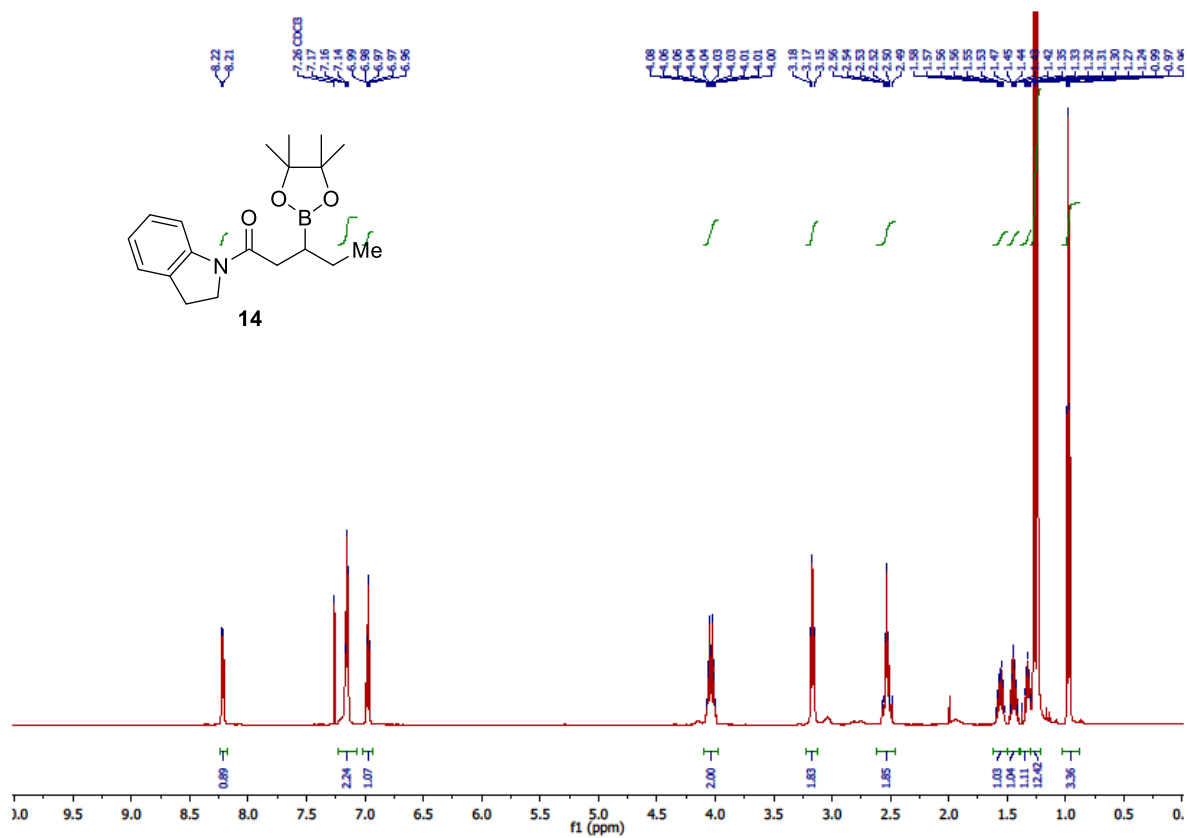
Chapter 4



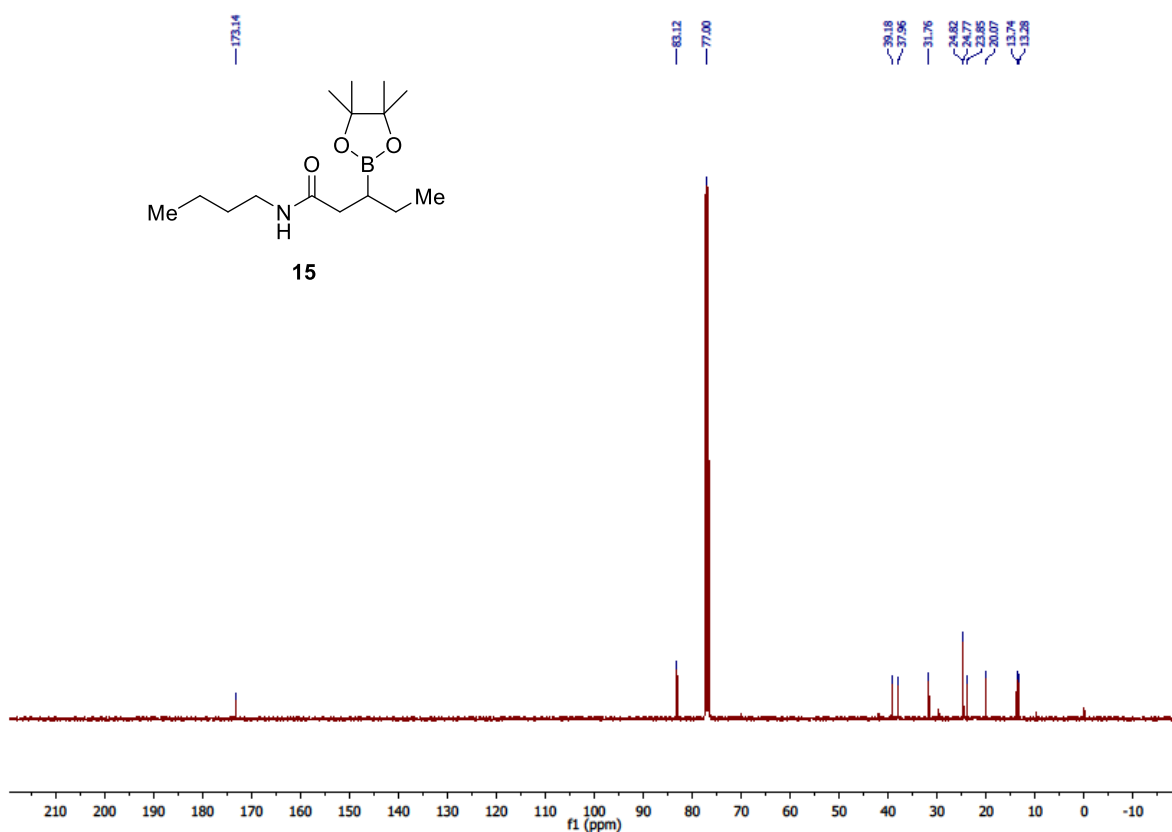
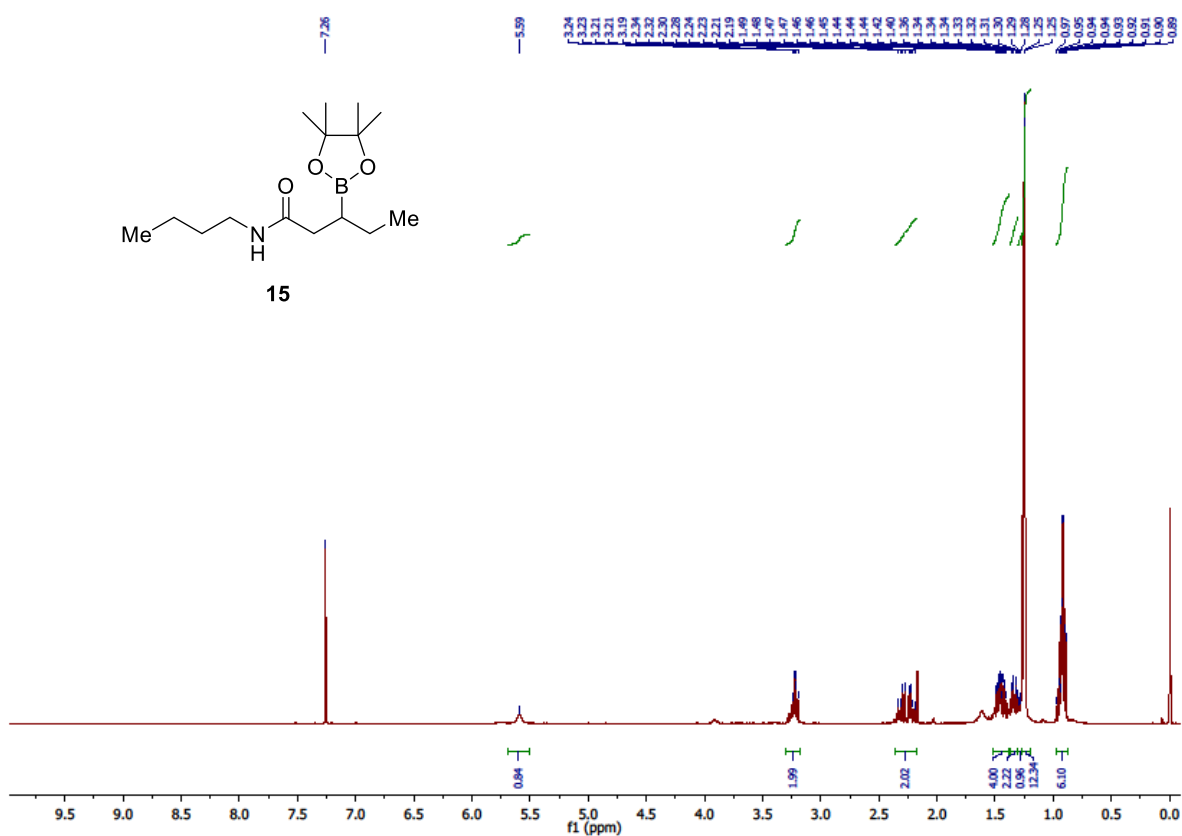
W-catalyzed remote β -hydroboration of alkenes



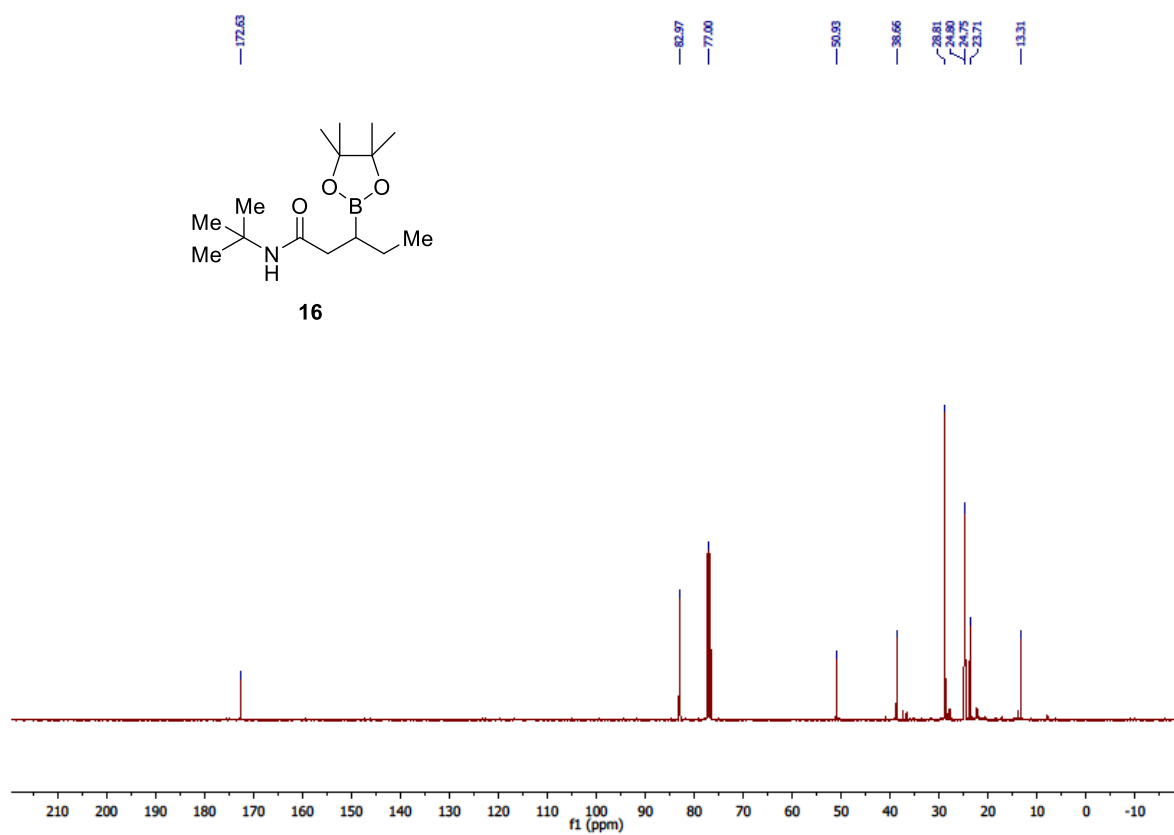
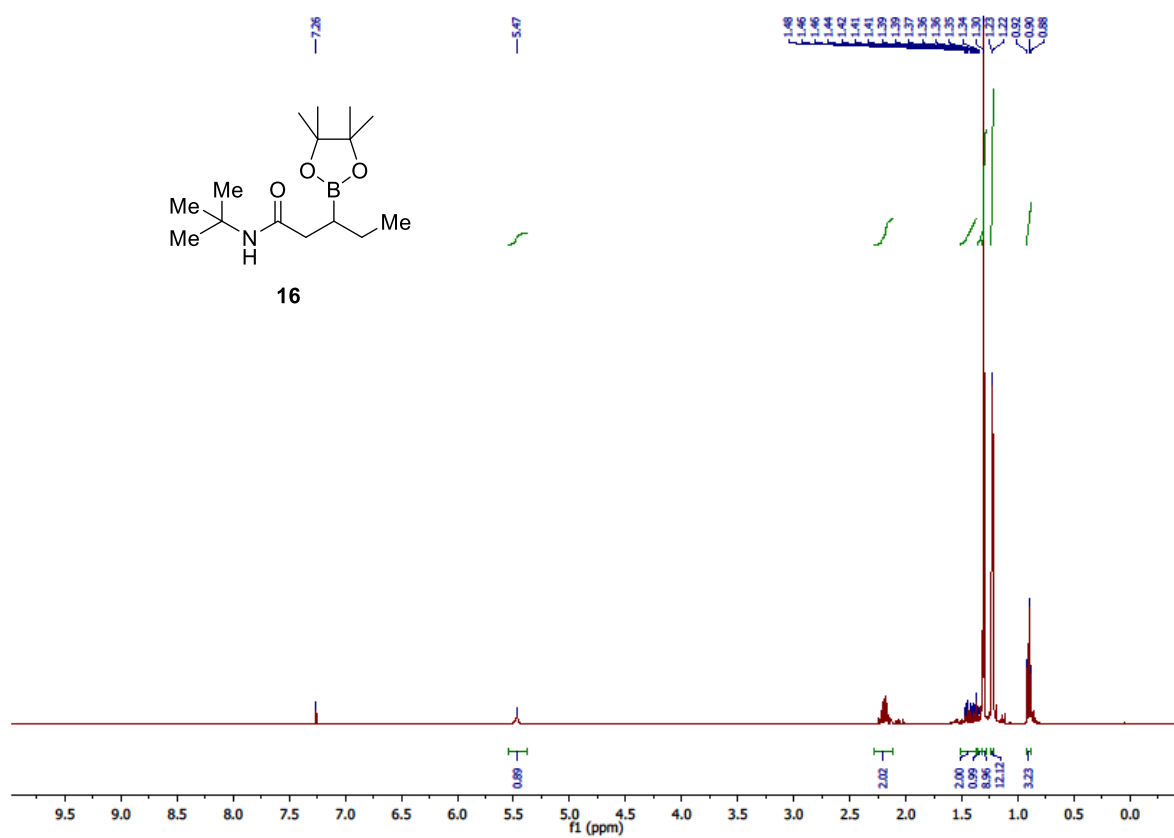
Chapter 4



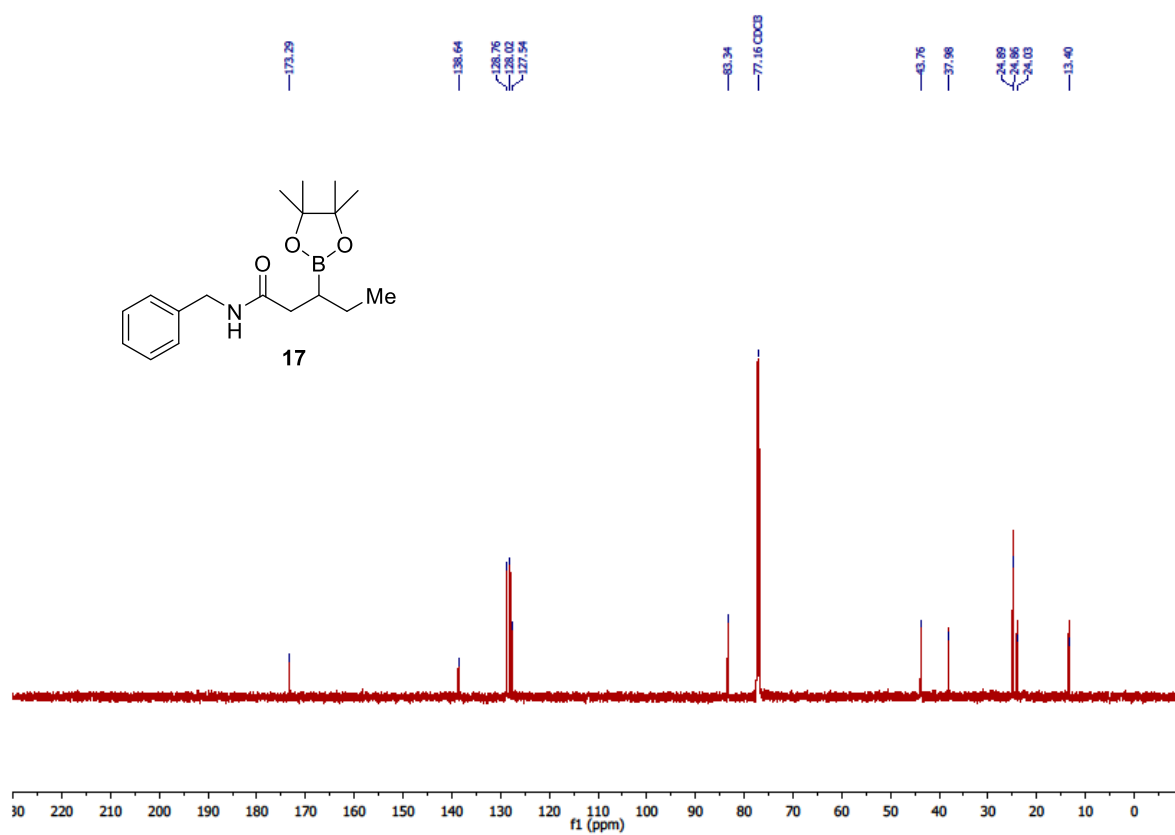
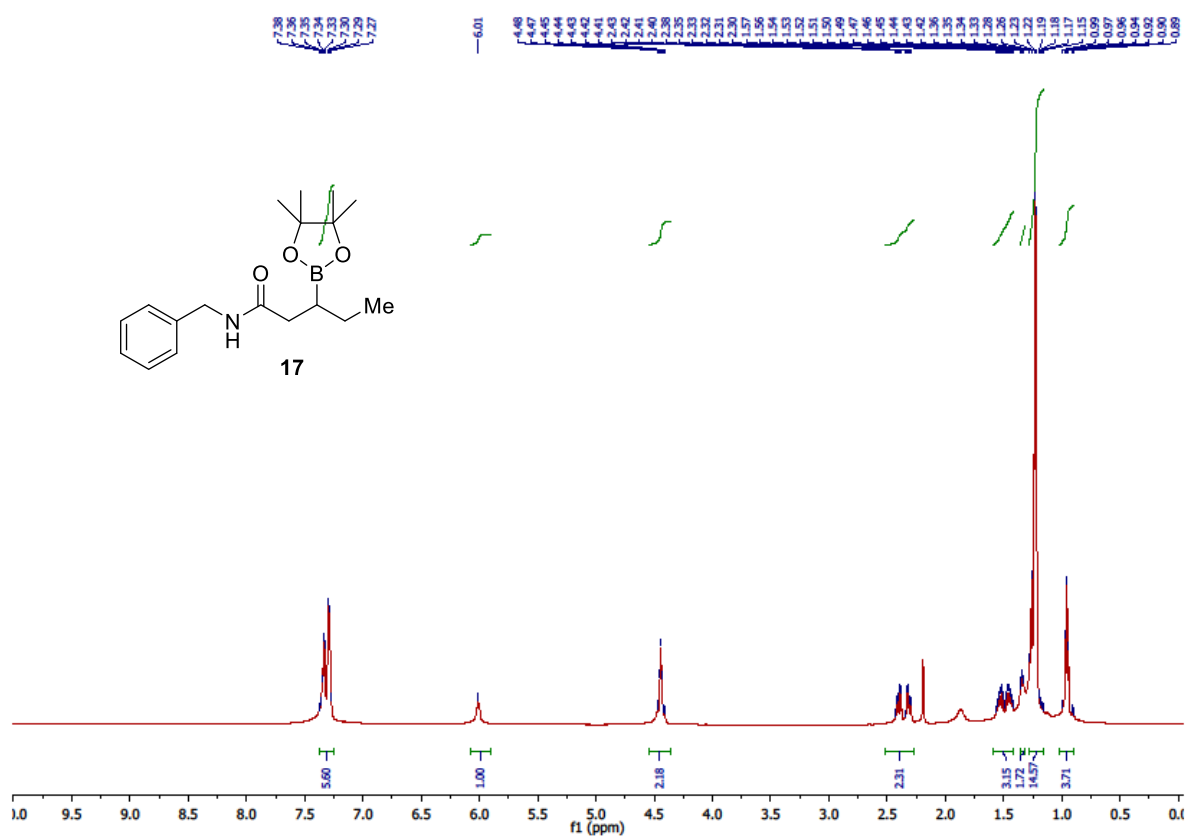
W-catalyzed remote β -hydroboration of alkenes



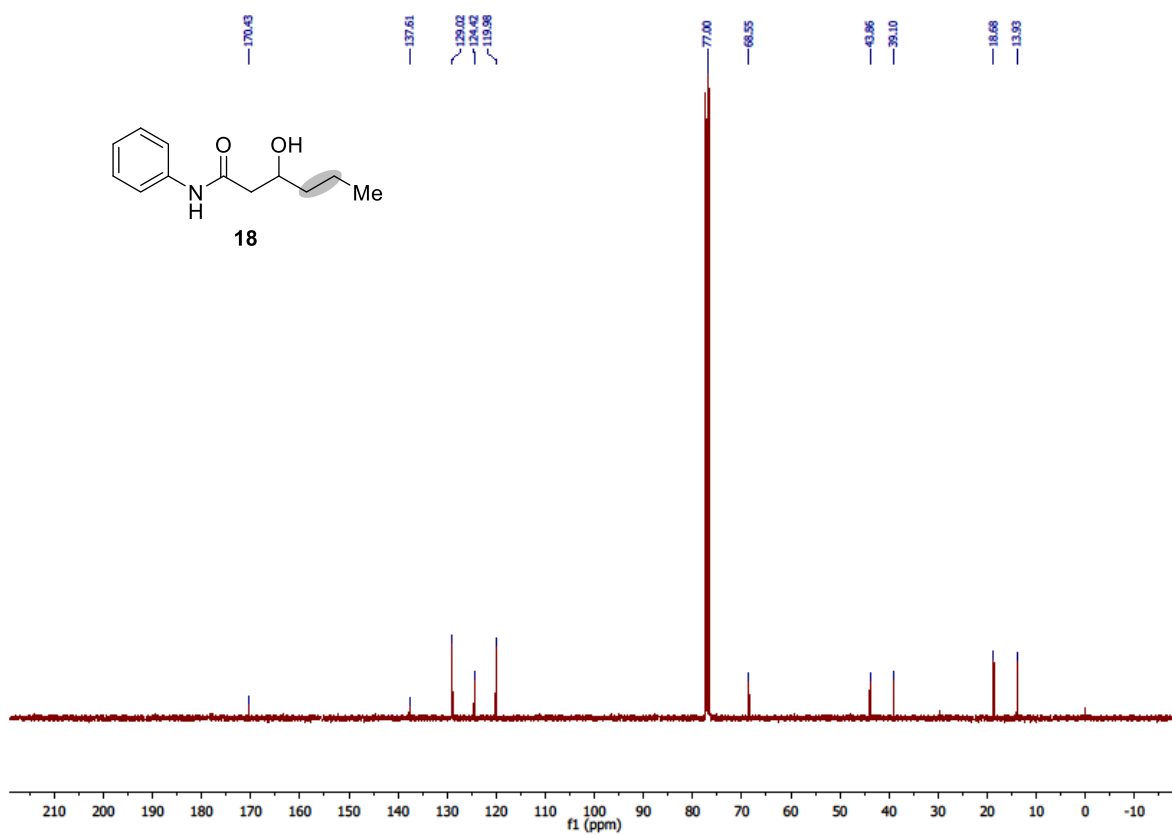
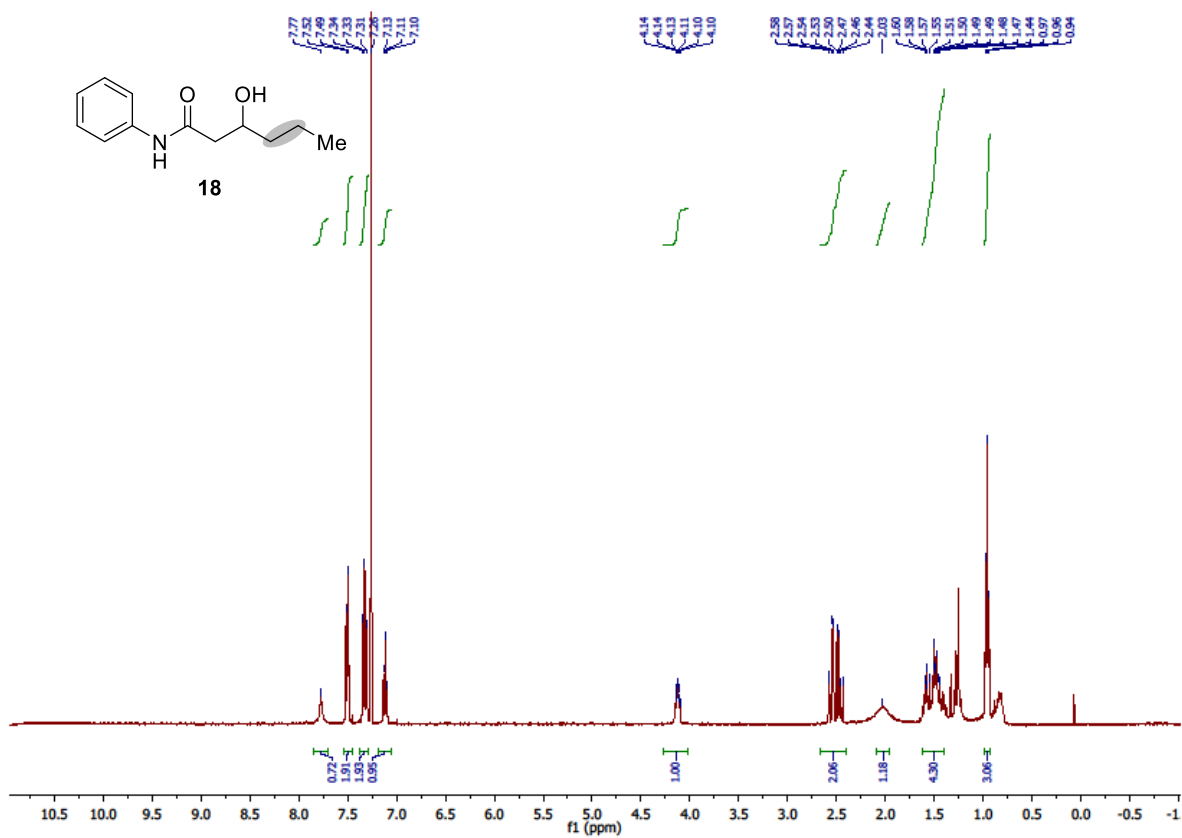
Chapter 4



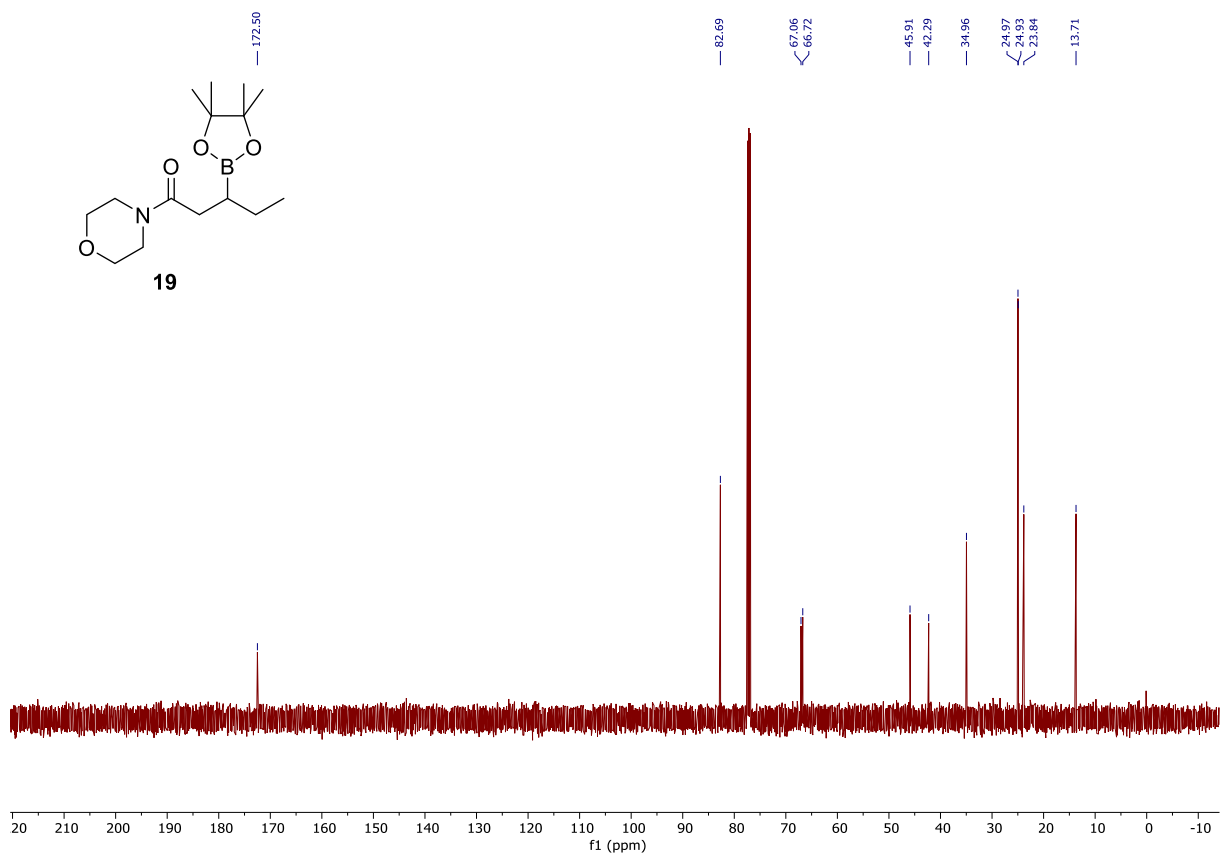
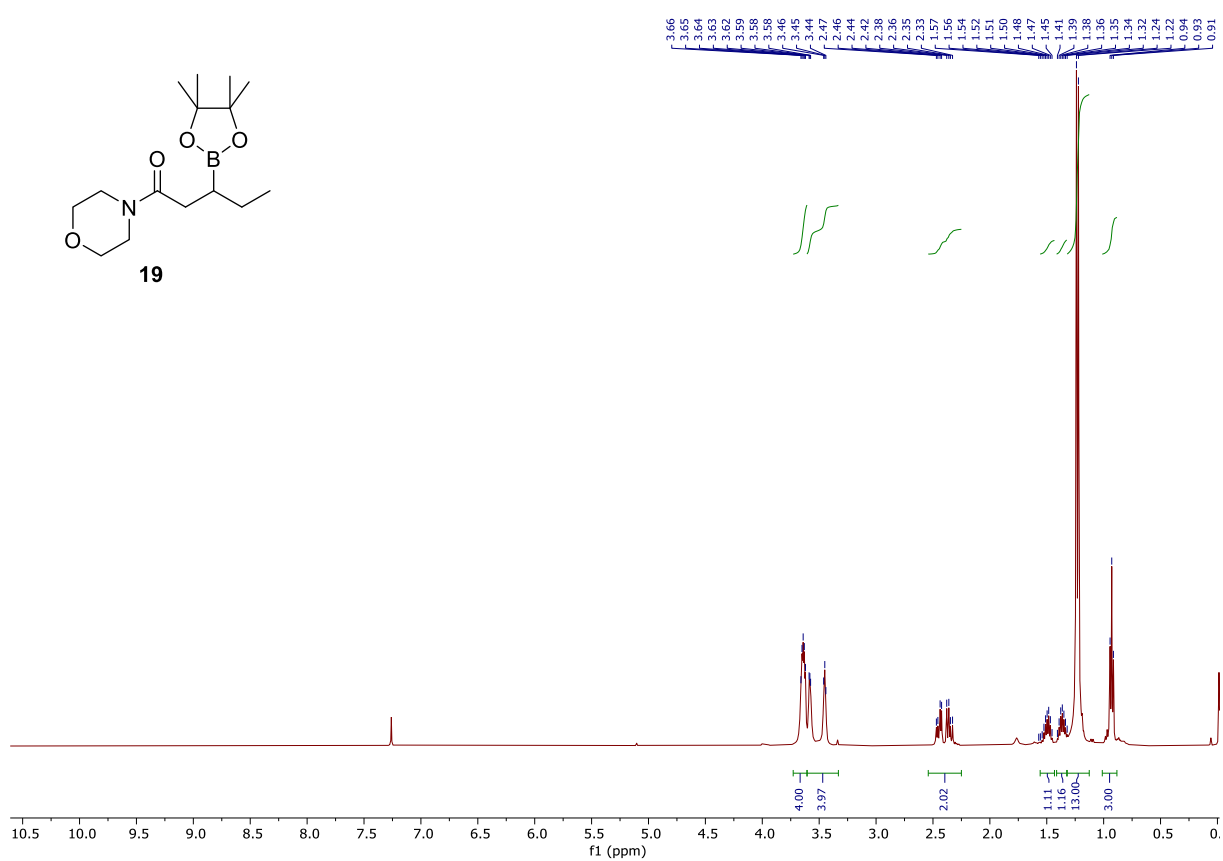
W-catalyzed remote β -hydroboration of alkenes



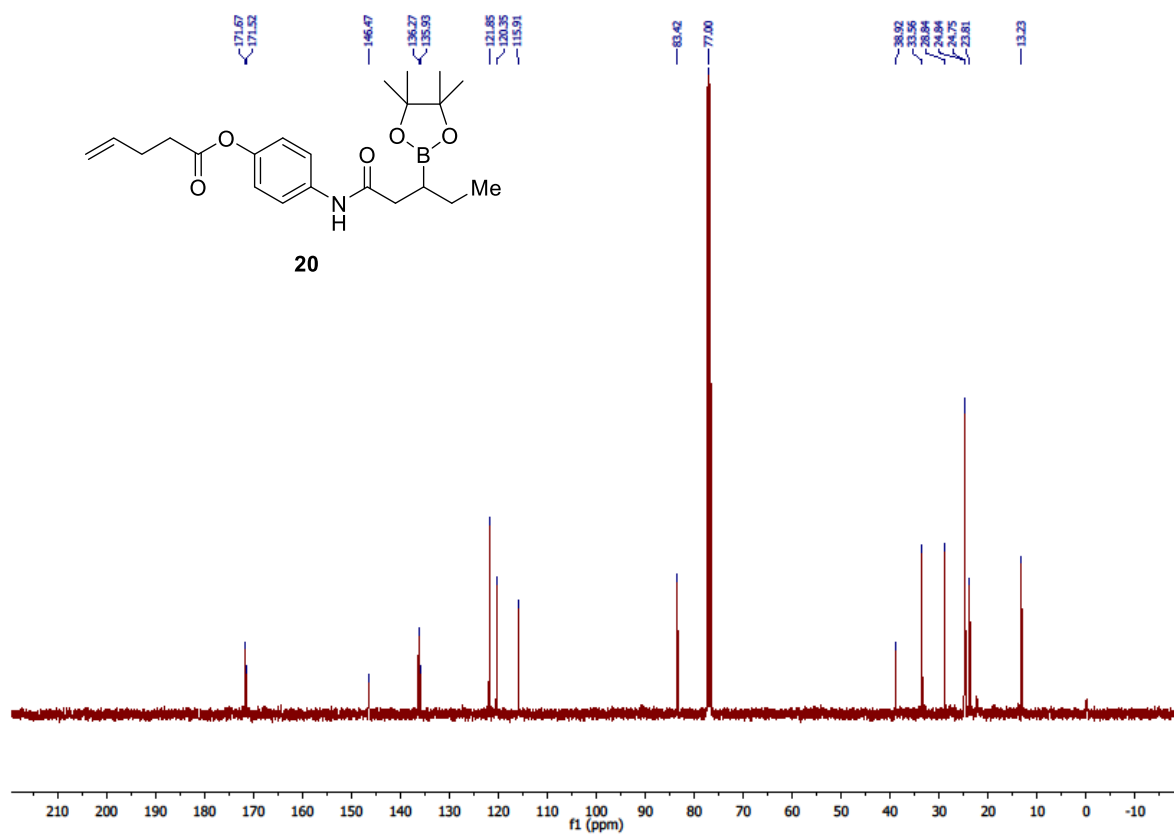
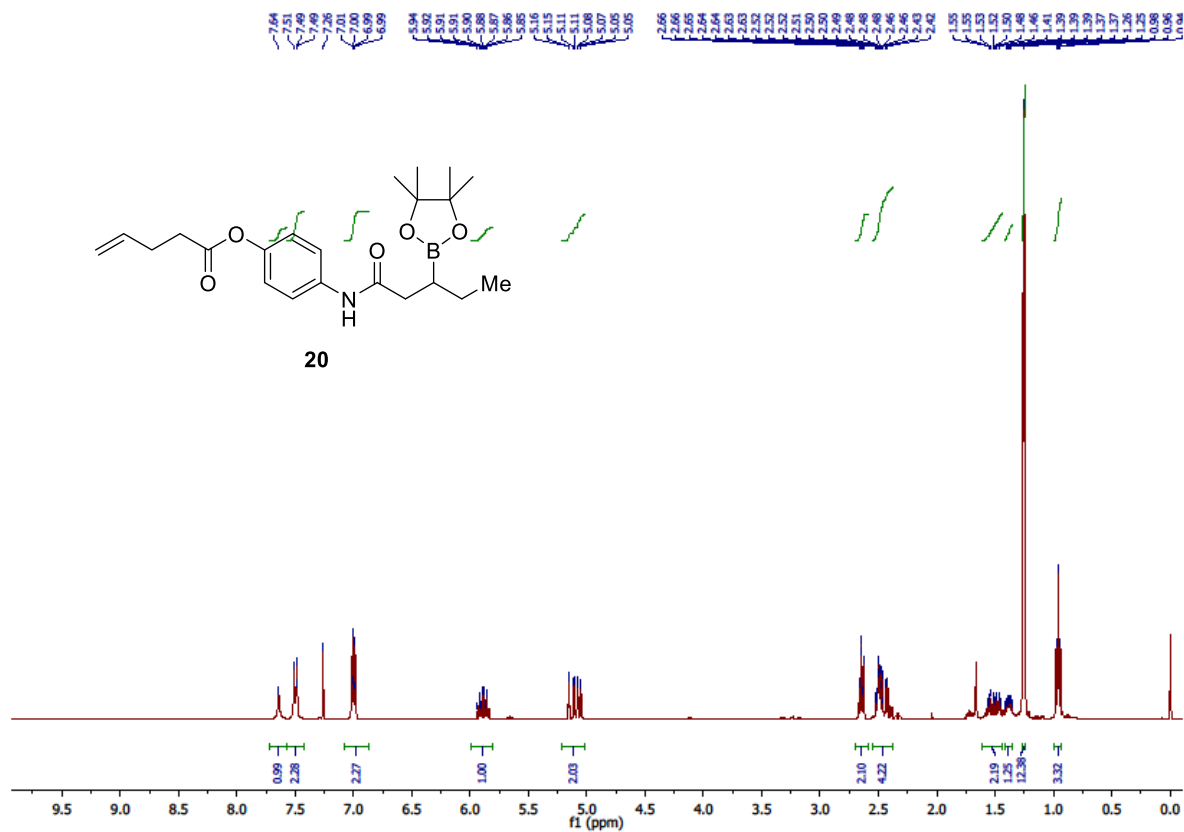
Chapter 4



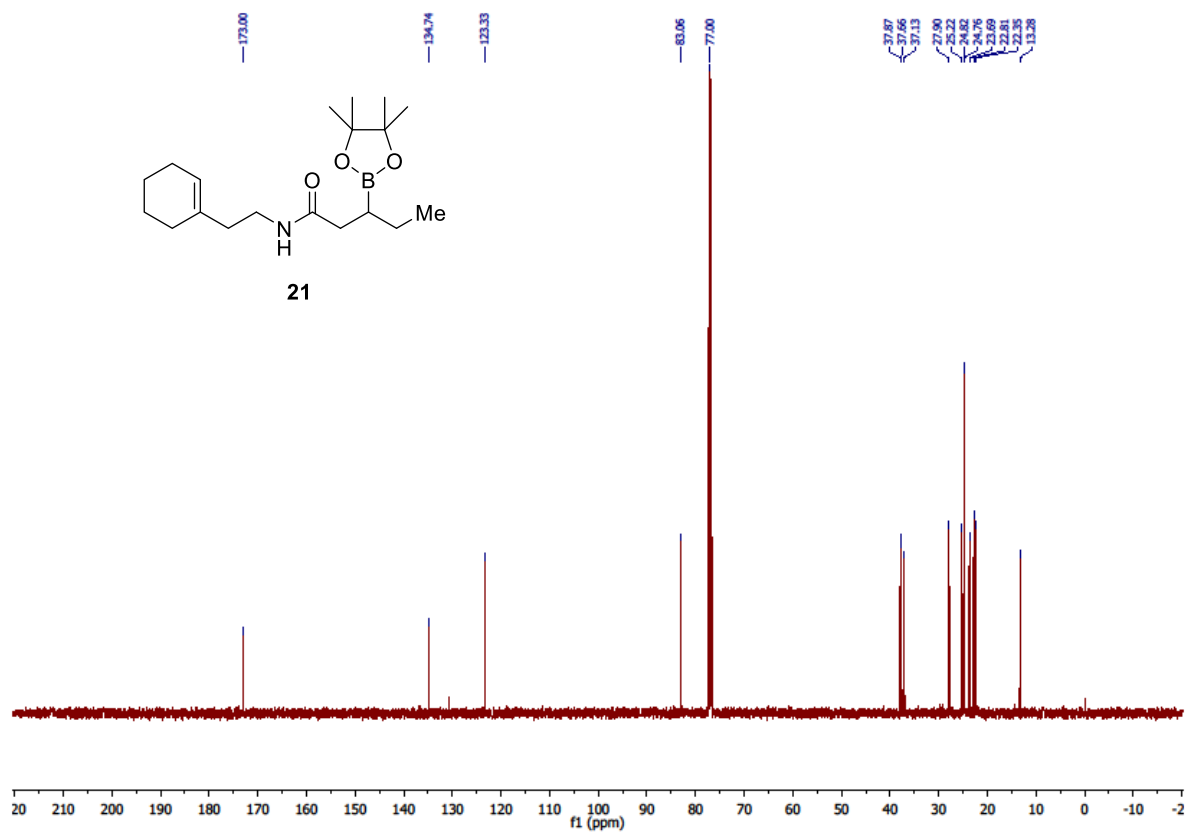
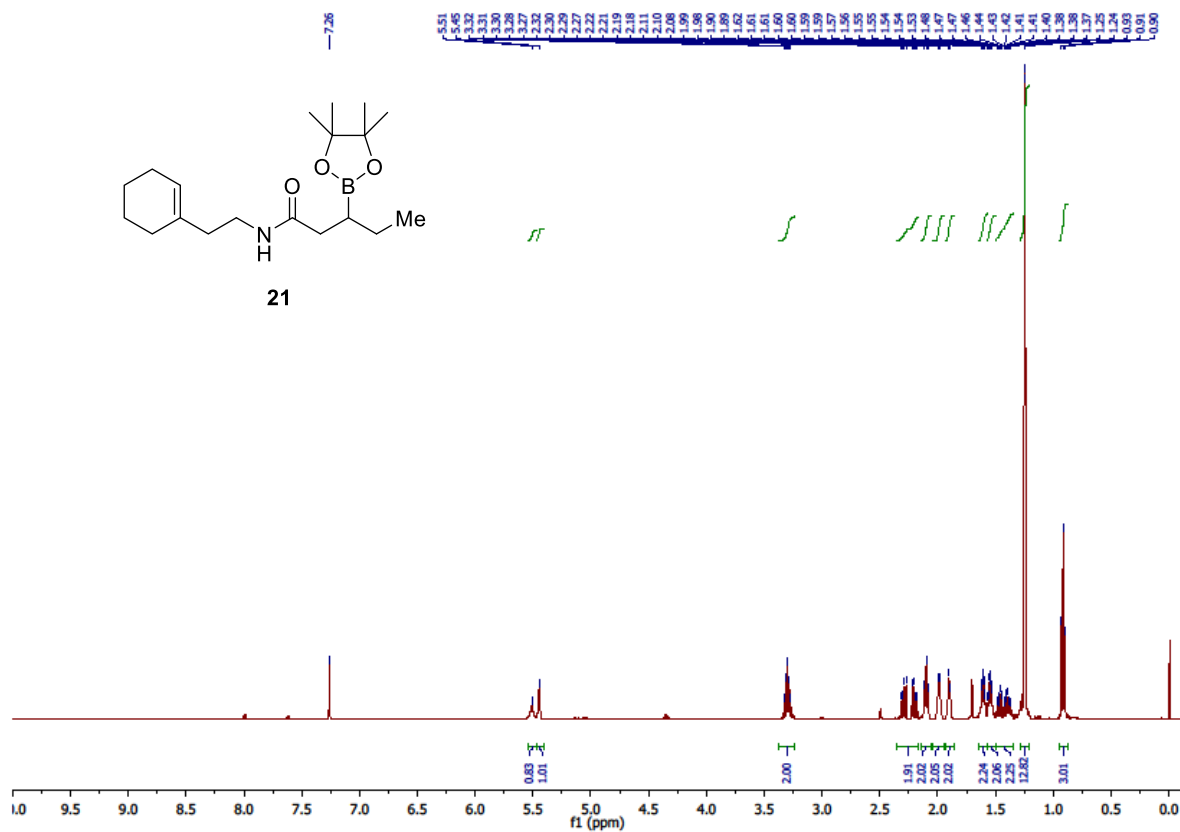
W-catalyzed remote β -hydroboration of alkenes



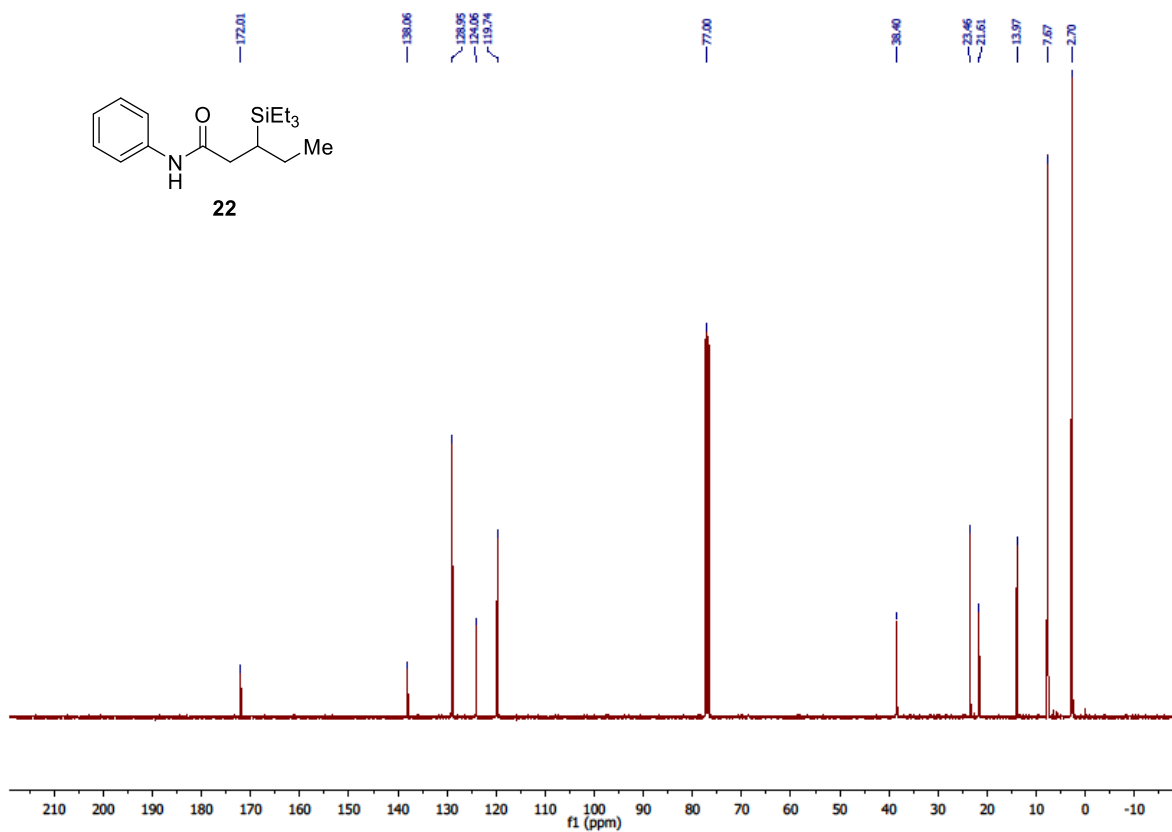
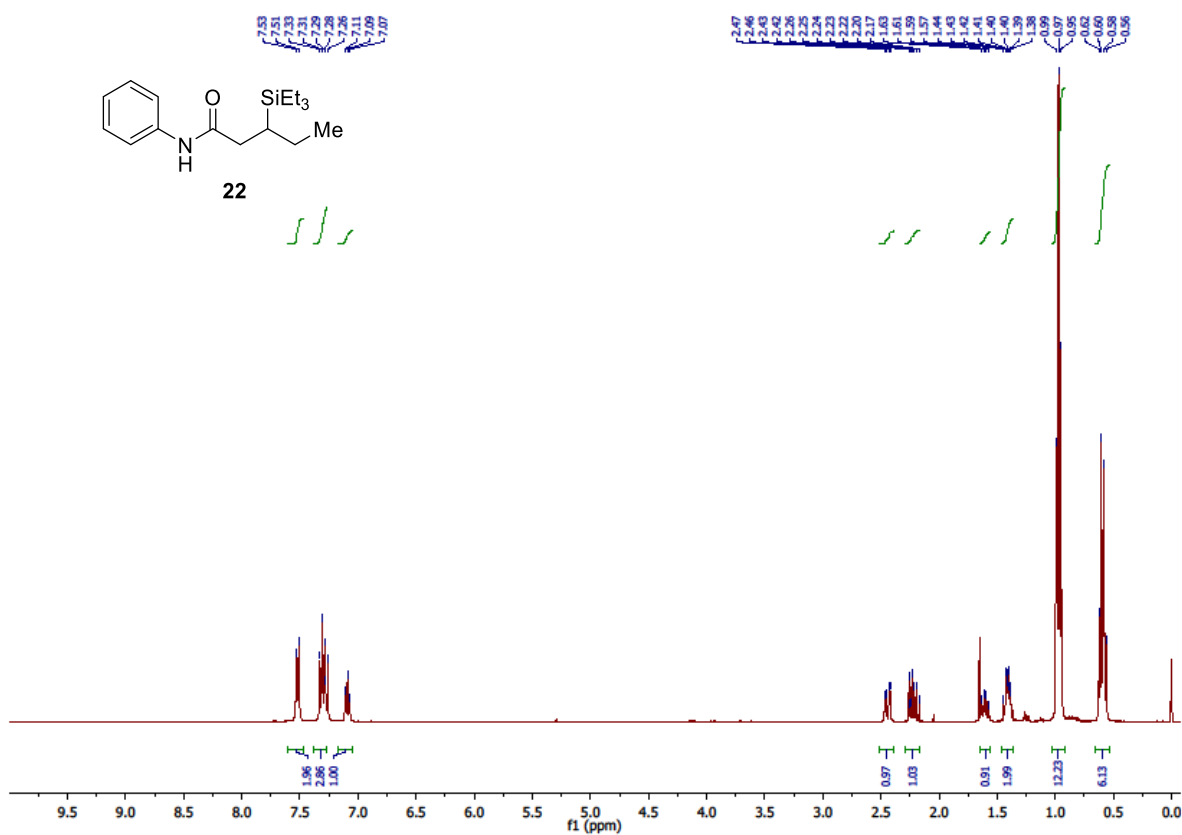
Chapter 4



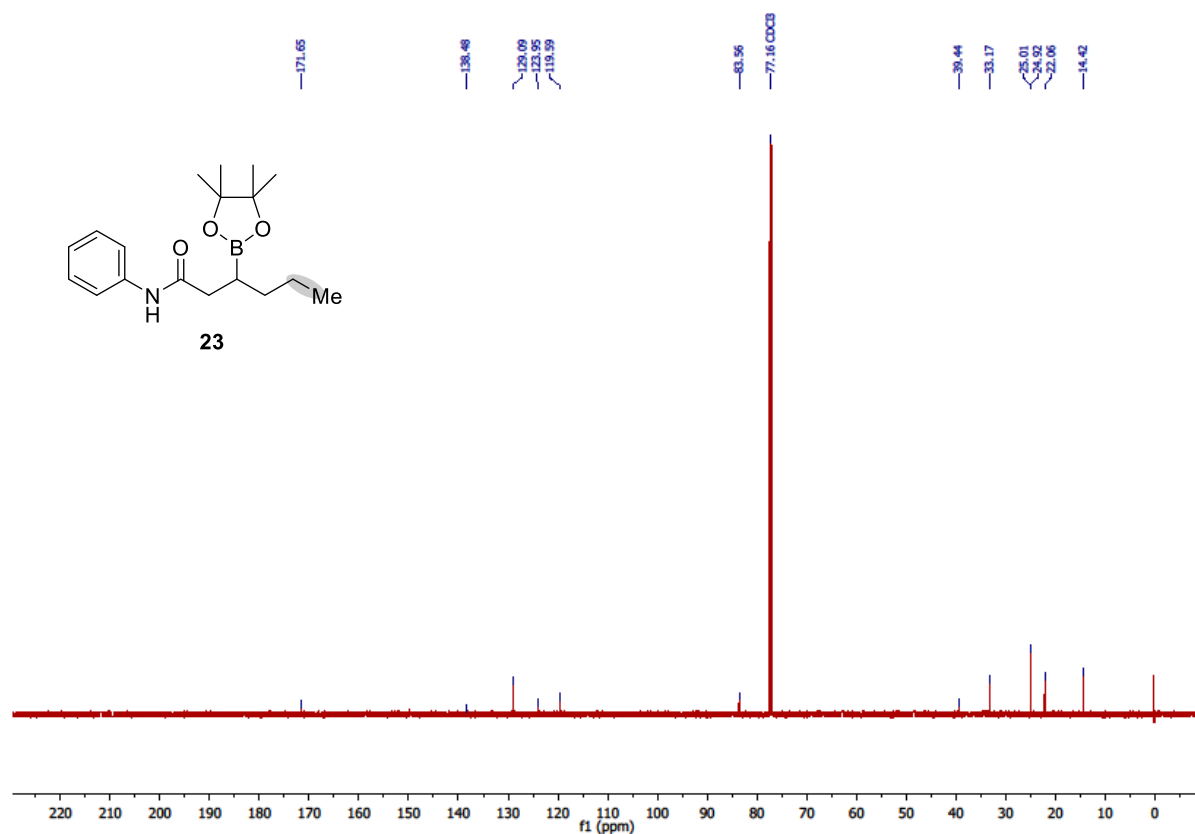
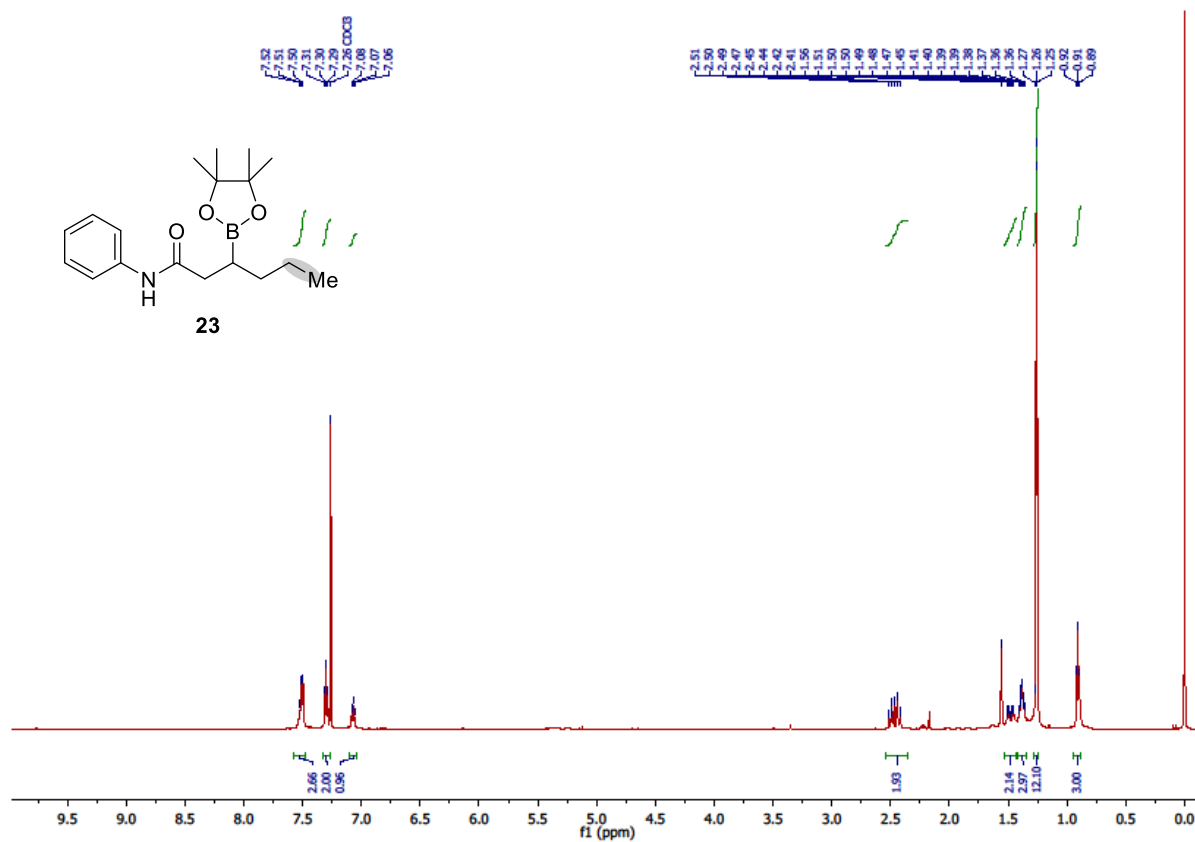
W-catalyzed remote β -hydroboration of alkenes



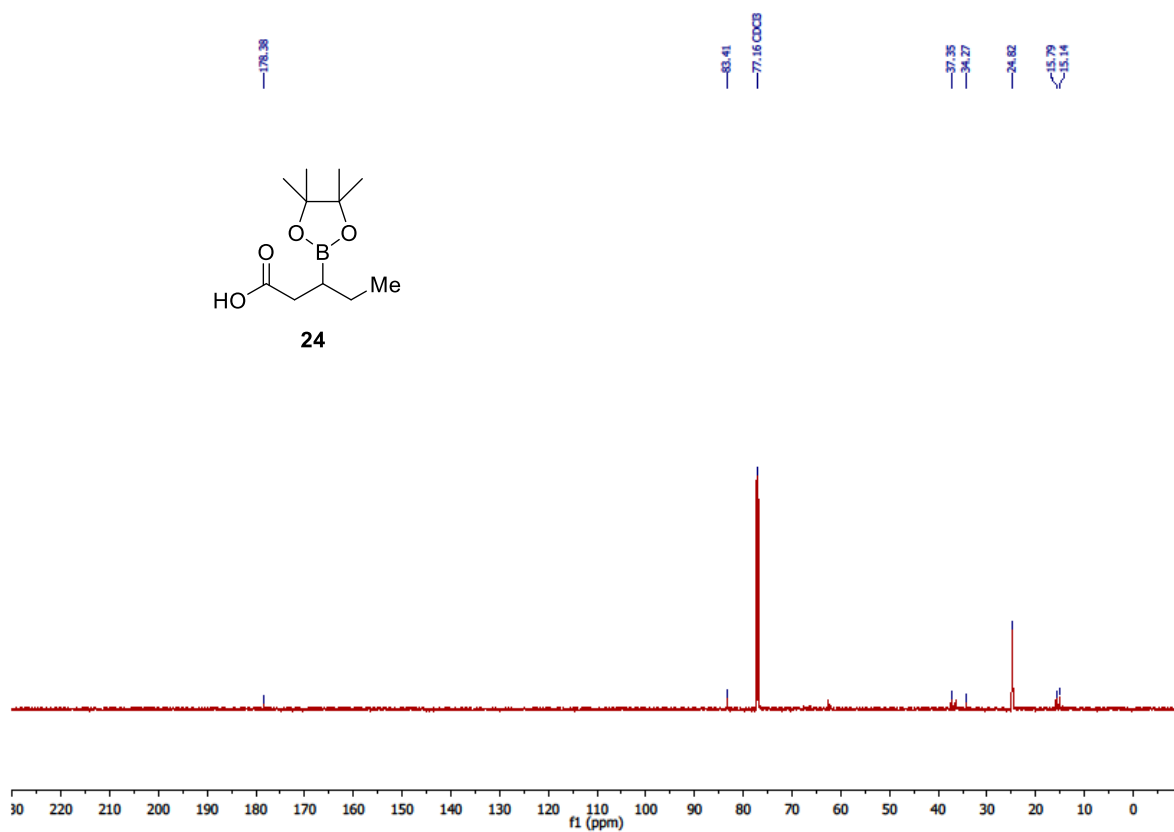
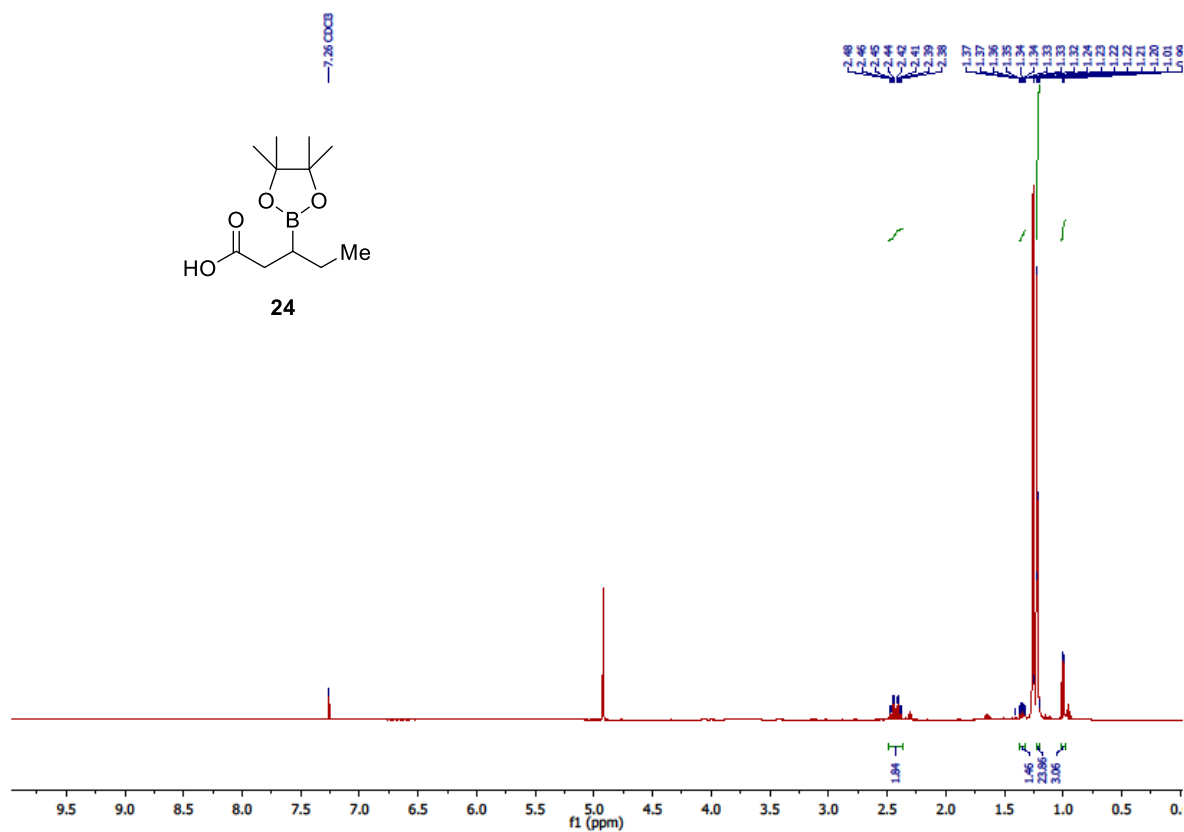
Chapter 4

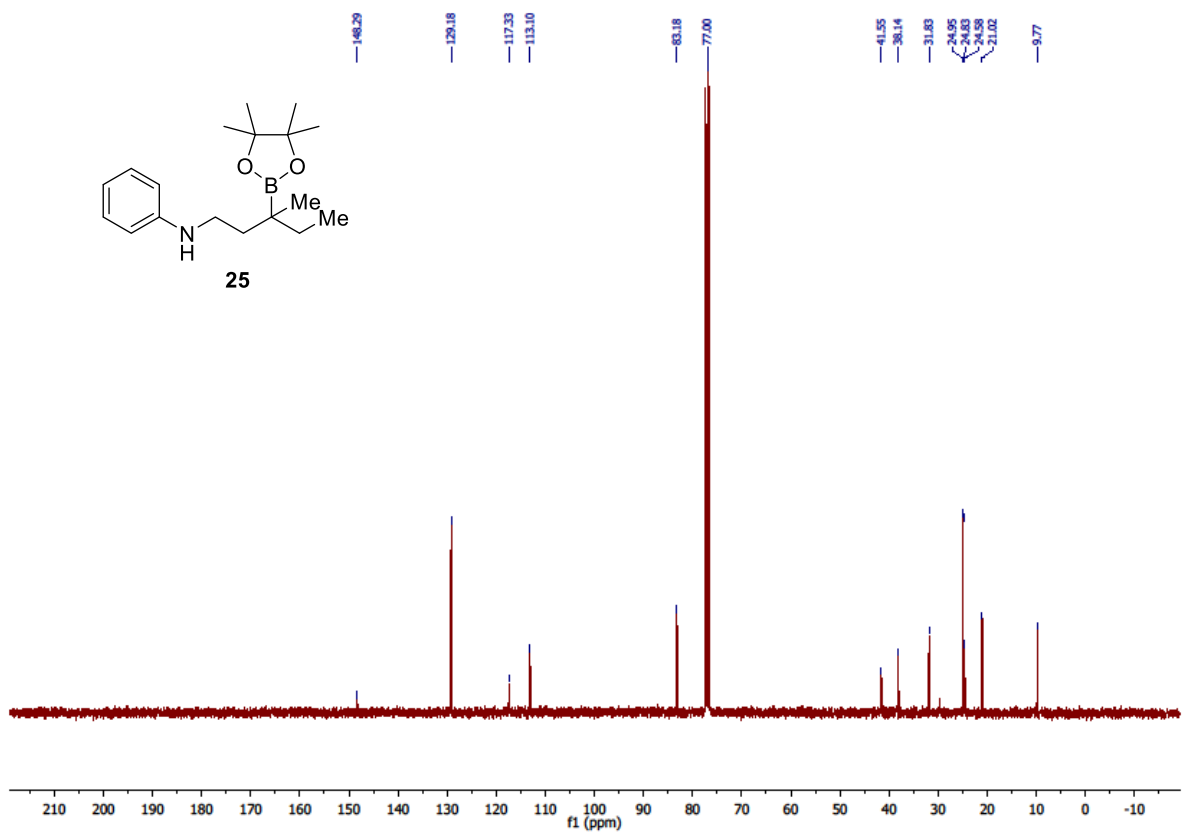
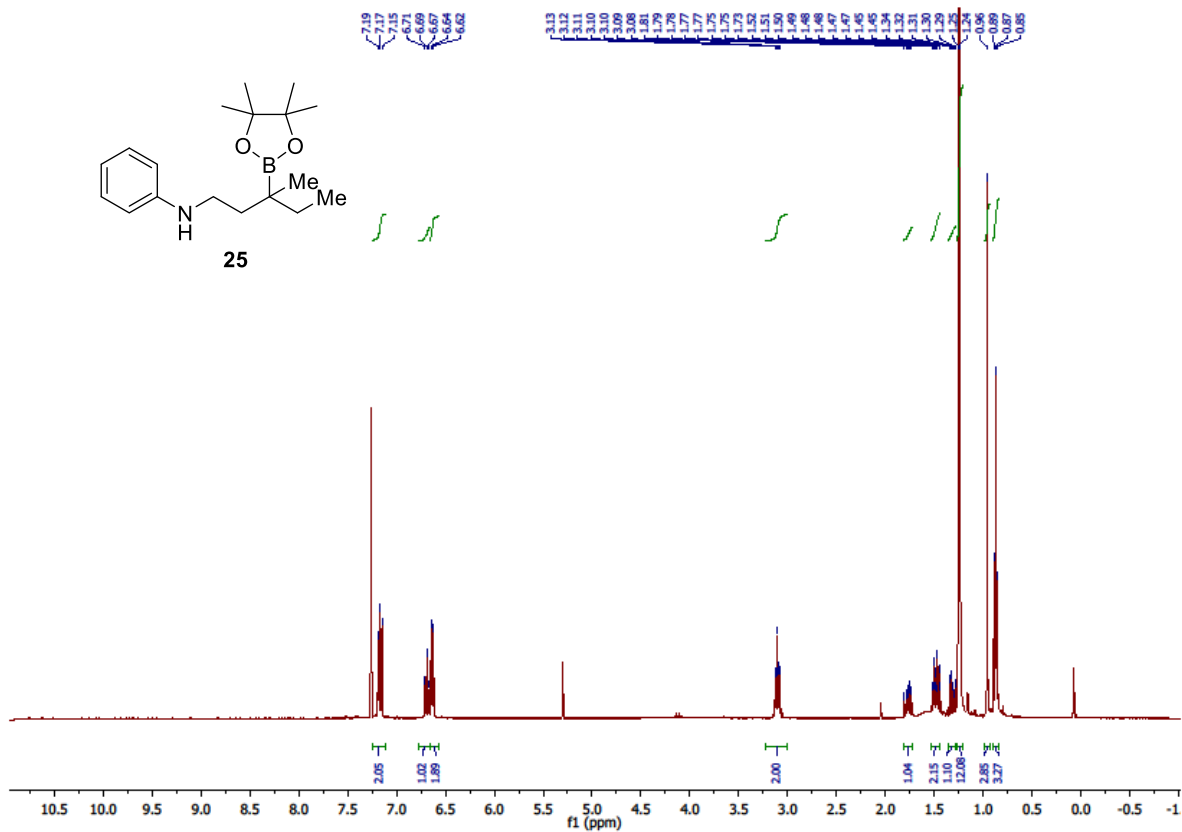


W-catalyzed remote β -hydroboration of alkenes

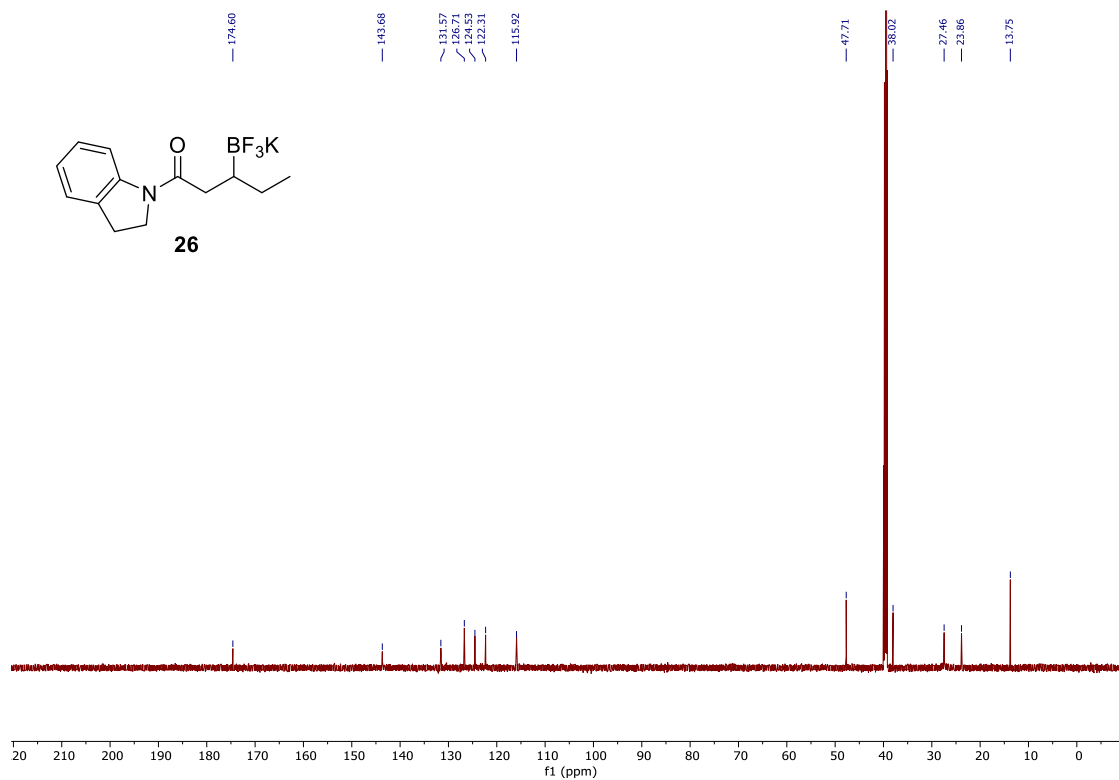
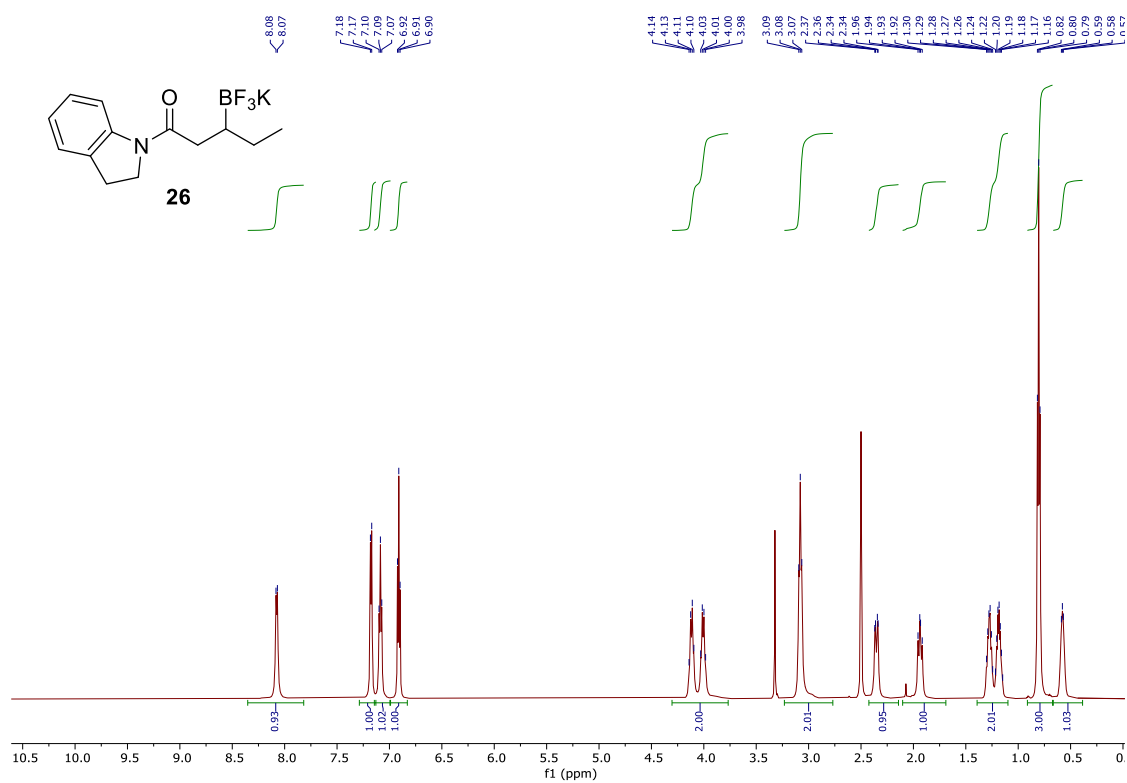


Chapter 4

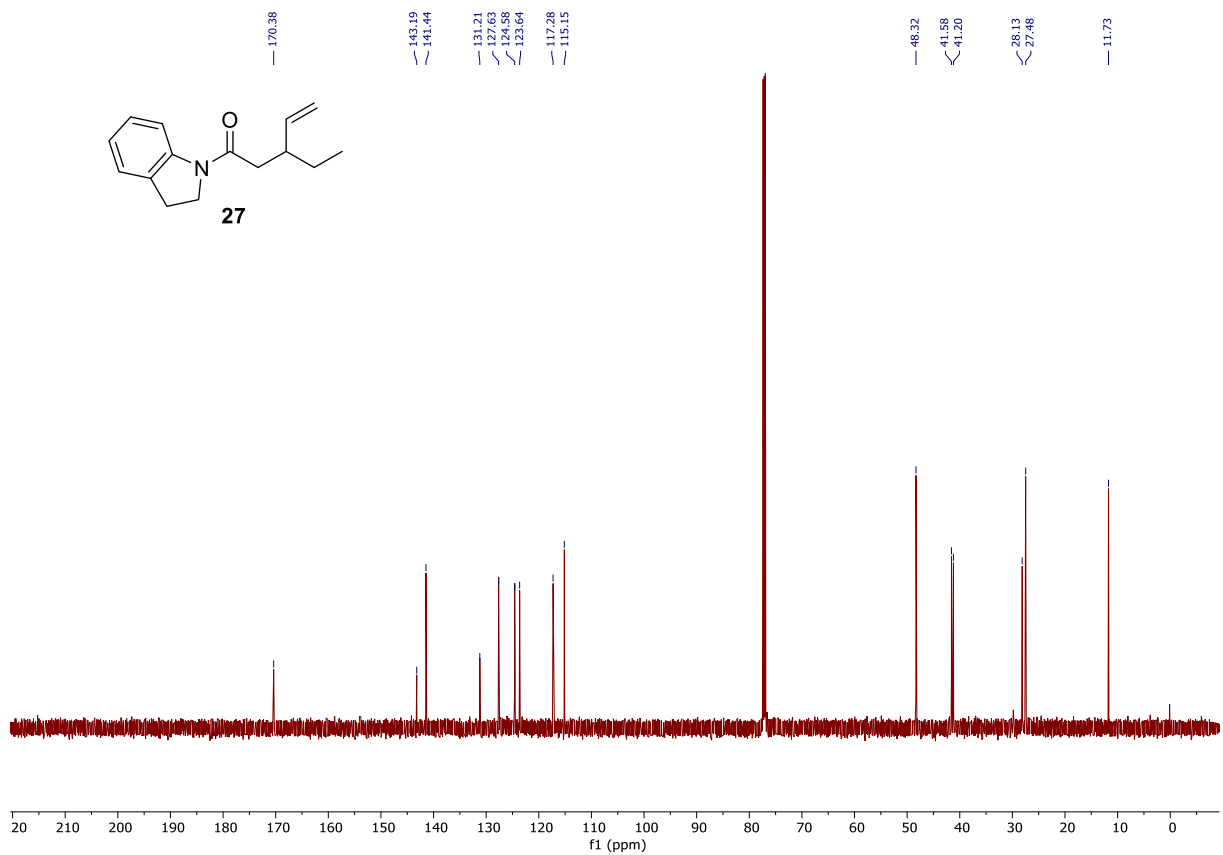
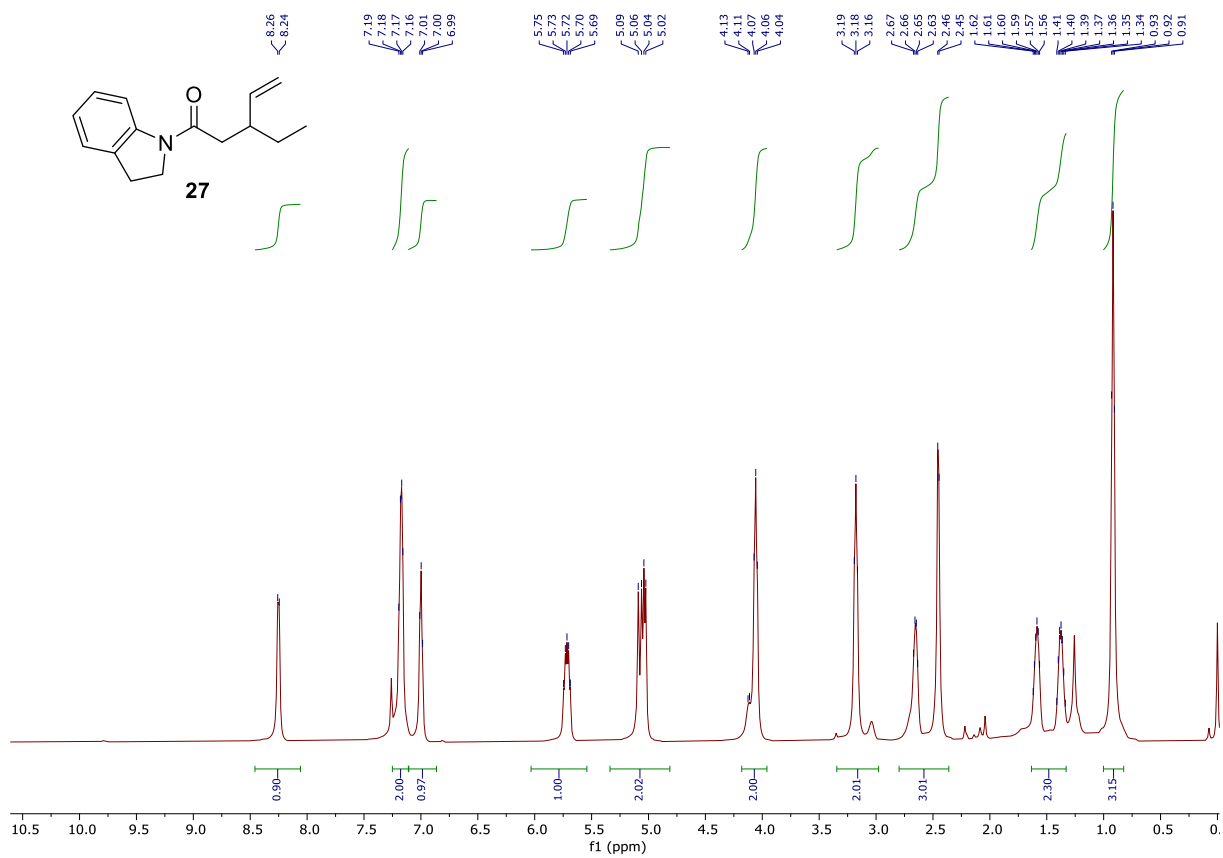




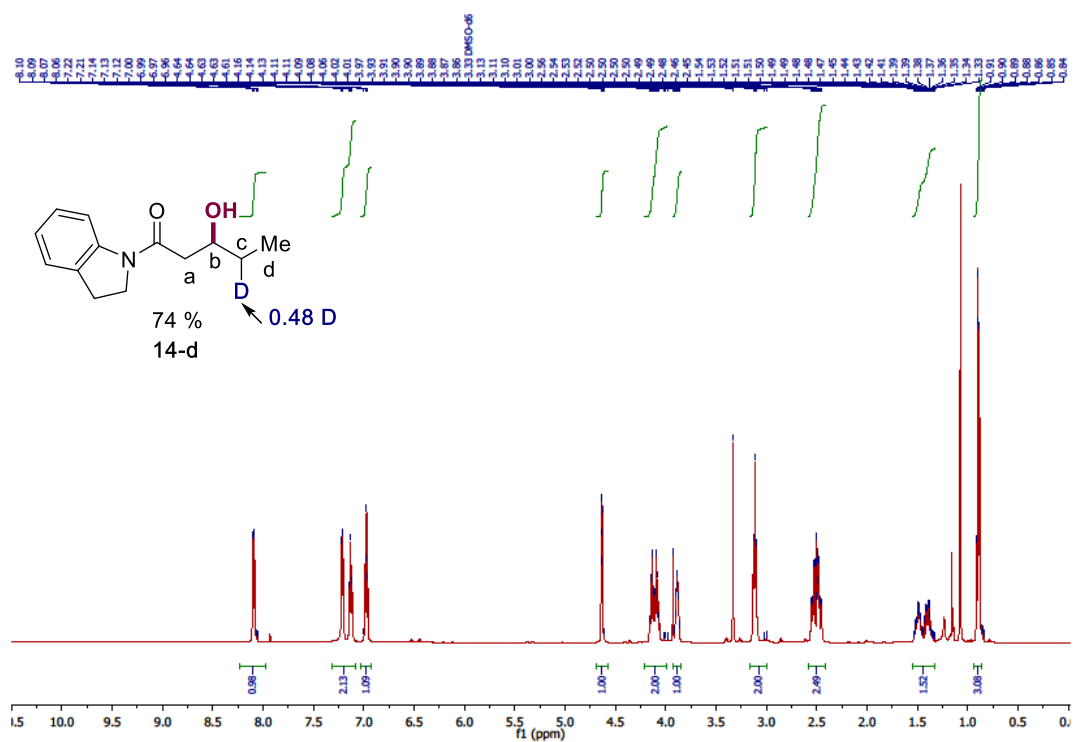
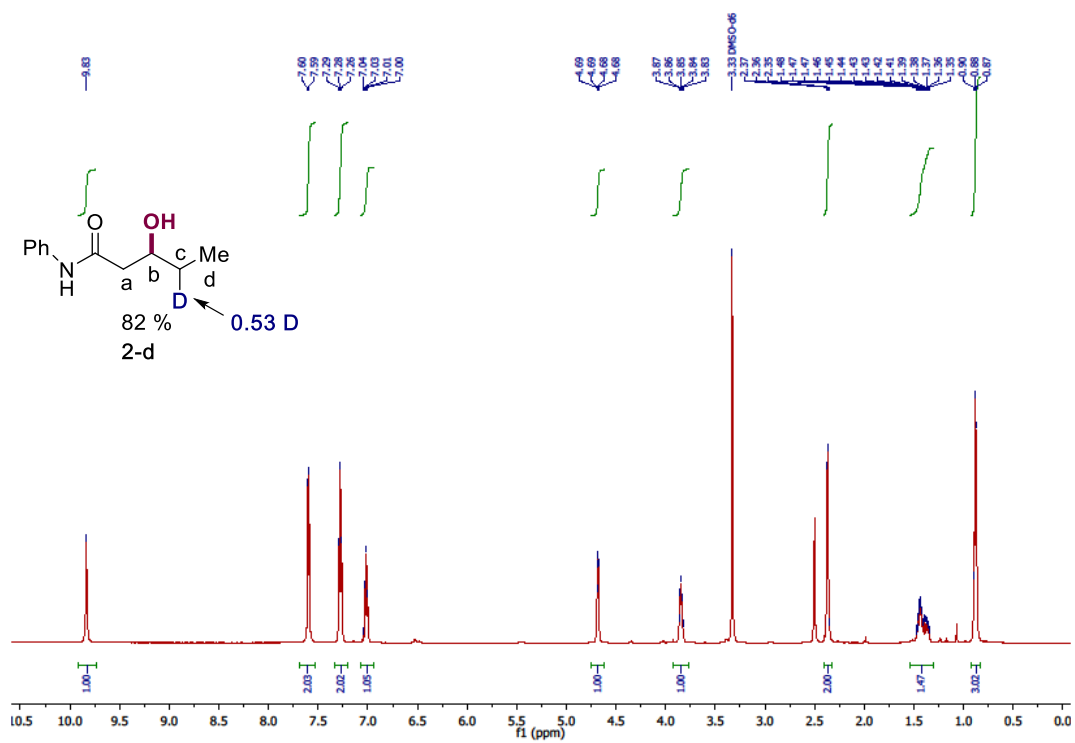
Chapter 4



W-catalyzed remote β -hydroboration of alkenes



Chapter 4



4.6 References

- (1) Hall, D. G. *Preparation and Applications in Organic Synthesis, Medicine and Materials*; Wiley-VCH Verlag GmbH & Co. KGaA: Weinheim, Germany, 2011.
- (2) Díaz, D. B.; Yudin, A. K. The Versatility of Boron in Biological Target Engagement. *Nat. Chem.* **2017**, *9*, 731–742. <https://doi.org/10.1038/nchem.2814>.
- (3) Baker, S.; Ding, C.; Akama, T.; Zhang, Y.; Hernandez, V.; Xia, Y. Therapeutic Potential of Boron-Containing Compounds. *Futur. Med. Chem.* **2009**, *3*, 1275–1288.
- (4) Qiu, F.; Zhao, W.; Han, S.; Zhuang, X.; Lin, H.; Zhang, F. Recent Advances in Boron-Containing Conjugated Porous Polymers. *Polymers (Basel)*. **2016**, *8*(5), 52–54. <https://doi.org/10.3390/polym8050191>.
- (5) Mkhaliid, I. A. I.; Barnard, J. H.; Marder, T. B.; Murphy, J. M.; Hartwig, J. F. C-H Activation for the Construction of C-B Bonds. *Chem. Rev.* **2010**, *110*(2), 890–931. <https://doi.org/10.1021/cr900206p>.
- (6) Fyfe, J. W. B.; Watson, A. J. B. Recent Developments in Organoboron Chemistry: Old Dogs, New Tricks. *Chem* **2017**, *3*(1), 31–55. <https://doi.org/10.1016/j.chempr.2017.05.008>.
- (7) Yan, G.; Huang, D.; Wu, X. Recent Advances in C–B Bond Formation through a Free Radical Pathway. *Adv. Synth. Catal.* **2018**, *360*(6), 1040–1053. <https://doi.org/10.1002/adsc.201701030>.
- (8) Chen, J.; Guo, J.; Lu, Z. Recent Advances in Hydrometallation of Alkenes and Alkynes via the First Row Transition Metal Catalysis. *Chinese J. Chem.* **2018**, *36*(11), 1075–1109. <https://doi.org/10.1002/cjoc.201800314>.
- (9) Cai, Y.; Yang, X. T.; Zhang, S. Q.; Li, F.; Li, Y. Q.; Ruan, L. X.; Hong, X.; Shi, S. L. Copper-Catalyzed Enantioselective Markovnikov Protoboration of α -Olefins Enabled by a Buttressed N-Heterocyclic Carbene Ligand. *Angew. Chemie - Int. Ed.* **2018**, *57*(5), 1376–1380. <https://doi.org/10.1002/anie.201711229>.
- (10) Obligacion, J. V.; Chirik, P. J. Earth-Abundant Transition Metal Catalysts for Alkene Hydrosilylation and Hydroboration. *Nat. Rev. Chem.* **2018**, *2*(5), 15–34. <https://doi.org/10.1038/s41570-018-0001-2>.
- (11) Burgess, K.; Ohlmeyer, M. J. Transition-Metal-Promoted Hydroborations of Alkenes, Emerging Methodology for Organic Transformations. *Chem. Rev.* **1991**, *91*(6), 1179–1191. <https://doi.org/10.1021/cr00006a003>.
- (12) Vogels, C.; Westcott, S. Recent Advances in Organic Synthesis Using Transition Metal-Catalyzed Hydroborations. *Curr. Org. Chem.* **2005**, *9*(7), 687–699. <https://doi.org/10.2174/1385272053765060>.
- (13) Brown, H. C.; Subba Rao, B. C. A New Powerful Reducing Agent—Sodium Borohydride in the Presence of Aluminum Chloride and Other Polyvalent Metal Halides. *J. Am. Chem. Soc.* **1956**, *78*(11), 2582–2588. <https://doi.org/10.1021/ja01592a070>.
- (14) Carroll, A. M.; O'Sullivan, T. P.; Guiry, P. J. The Development of Enantioselective Rhodium-Catalysed Hydroboration of Olefins. *Adv. Synth. Catal.* **2005**, *347*(5), 609–631. <https://doi.org/10.1002/adsc.200404232>.
- (15) Evans, D. A.; Fu, G. C.; Hoveyda, A. H. Rhodium(I)- and Iridium(I)-Catalyzed Hydroboration Reactions: Scope and Synthetic Applications. *J. Am. Chem. Soc.* **1992**, *114*(17), 6671–6679. <https://doi.org/10.1021/ja00043a009>.
- (16) Beletskaya, I.; Pelter, A. Hydroborations Catalysed by Transition Metal Complexes. *Tetrahedron* **1997**, *53*(14), 4957–5026. [https://doi.org/10.1016/S0040-4020\(97\)00001-X](https://doi.org/10.1016/S0040-4020(97)00001-X).
- (17) Männig, D.; Nöth, H. Catalytic Hydroboration with Rhodium Complexes. *Angew. Chemie Int. Ed. English* **1985**, *24*(10), 878–879. <https://doi.org/10.1002/anie.198508781>.
- (18) Fan, W.; Li, L.; Zhang, G. Branched-Selective Alkene Hydroboration Catalyzed by Earth-Abundant Metals. *J. Org. Chem.* **2019**, *84*(10), 5987–5996. <https://doi.org/10.1021/acs.joc.9b00550>.
- (19) Sommer, H.; Juliá-Hernández, F.; Martín, R.; Marek, I. Walking Metals for Remote Functionalization. *ACS Cent. Sci.* **2018**, *4*(2), 153–165.

Chapter 4

- <https://doi.org/10.1021/acscentsci.8b00005>.
- (20) Obligacion, J. V.; Chirik, P. J. Bis(Imino)Pyridine Cobalt-Catalyzed Alkene Isomerization-Hydroboration: A Strategy for Remote Hydrofunctionalization with Terminal Selectivity. *J. Am. Chem. Soc.* **2013**, *135* (51), 19107–19110. <https://doi.org/10.1021/ja4108148>.
- (21) Ogawa, T.; Ruddy, A. J.; Sydora, O. L.; Stradiotto, M.; Turculet, L. Cobalt- and Iron-Catalyzed Isomerization-Hydroboration of Branched Alkenes: Terminal Hydroboration with Pinacolborane and 1,3,2-Diazaborolanes. *Organometallics* **2017**, *36* (2), 417–423. <https://doi.org/10.1021/acs.organomet.6b00823>.
- (22) Palmer, W. N.; Diao, T.; Pappas, I.; Chirik, P. J. High-Activity Cobalt Catalysts for Alkene Hydroboration with Electronically Responsive Terpyridine and α -Diimine Ligands. *ACS Catal.* **2015**, *5* (2), 622–626. <https://doi.org/10.1021/cs501639r>.
- (23) Macaulay, C. M.; Gustafson, S. J.; Fuller, J. T.; Kwon, D. H.; Ogawa, T.; Ferguson, M. J.; McDonald, R.; Lumsden, M. D.; Bischof, S. M.; Sydora, O. L.; Ess, D. H.; Stradiotto, M.; Turculet, L. Alkene Isomerization-Hydroboration Catalyzed by First-Row Transition-Metal (Mn, Fe, Co, and Ni) N-Phosphinoamidinate Complexes: Origin of Reactivity and Selectivity. *ACS Catal.* **2018**, *8* (11), 9907–9925. <https://doi.org/10.1021/acscatal.8b01972>.
- (24) Scheuermann, M. L.; Johnson, E. J.; Chirik, P. J. Alkene Isomerization-Hydroboration Promoted by Phosphine-Ligated Cobalt Catalysts. *Org. Lett.* **2015**, *17* (11), 2716–2719. <https://doi.org/10.1021/acs.orglett.5b01135>.
- (25) Endo, K.; Ohkubo, T.; Hirokami, M.; Shibata, T. Chemoselective and Regiospecific Suzuki Coupling on a Multisubstituted Sp³-Carbon in 1,1-Diborylalkanes at Room Temperature. *J. Am. Chem. Soc.* **2010**, *132*, 11033–11035. <https://doi.org/10.1021/ja105176v>.
- (26) Chen, X.; Cheng, Z.; Guo, J.; Lu, Z. Asymmetric Remote C-H Borylation of Internal Alkenes via Alkene Isomerization. *Nat. Commun.* **2018**, *9* (1), 1–8. <https://doi.org/10.1038/s41467-018-06240-y>.
- (27) Léonard, N. G.; Palmer, W. N.; Friedfeld, M. R.; Bezdek, M. J.; Chirik, P. J. Remote, Diastereoselective Cobalt-Catalyzed Alkene Isomerization-Hydroboration: Access to Stereodefined 1,3-Difunctionalized Indanes. *ACS Catal.* **2019**, *9* (10), 9034–9044. <https://doi.org/10.1021/acscatal.9b03444>.
- (28) Larsen, M. A.; Cho, S. H.; Hartwig, J. Iridium-Catalyzed, Hydrosilyl-Directed Borylation of Unactivated Alkyl C–H Bonds. *J. Am. Chem. Soc.* **2016**, *138*, 762–765. <https://doi.org/10.1021/jacs.5b12153>.
- (29) Kawamorita, S.; Murakami, R.; Iwai, T.; Sawamura, M. Synthesis of Primary and Secondary Alkylboronates through Site-Selective C(Sp³)–H Activation with Silica-Supported Monophosphine–Ir Catalysts. *J. Am. Chem. Soc.* **2013**, *135*, 2947–2950. <https://doi.org/10.1021/ja3126239>.
- (30) Yu, X.; Zhao, H.; Xi, S.; Chen, Z.; Wang, X.; Wang, L.; Lin, L. Q. H.; Loh, K. P.; Koh, M. J. Site-Selective Alkene Borylation Enabled by Synergistic Hydrometallation and Borometallation. *Nat. Catal.* **2020**, *3* (7), 585–592. <https://doi.org/10.1038/s41929-020-0470-9>.
- (31) Lefebvre, F.; Bouhoute, Y.; Szeto, K. C.; Merle, N.; Mallmann, A. De; Gauvin, R.; Lefebvre, F.; Bouhoute, Y.; Szeto, K. C.; Merle, N.; Mallmann, A. De. Olefin Metathesis by Group VI (Mo, W) Metal Compounds. In *Alkenes*; IntechOpen, 2018. <https://doi.org/10.5772/intechopen.69320>.
- (32) Urzhuntsev, G. A.; Kodenev, E. G.; Echevskii, G. V. Prospects for Using Mo- and W-Containing Catalysts in Hydroisomerization: A Patent Review. II: Catalysts Based on Molybdenum and Tungsten Carbides. *Catal. Ind.* **2016**, *8* (3), 224–230. <https://doi.org/10.1134/S2070050416030120>.
- (33) Ćrski, M.; Kochel, A.; Szymańska-Buzar, T. Synthesis, Structure, and Unusual Reactivity of the First Norbornene Carbonyl Complexes of Tungsten. *Organometallics* **2004**, *23* (12), 3037–3046. <https://doi.org/10.1021/omo400043>.
- (34) Gądek, A.; Szymańska-Buzar, T. Activation of the Si–H Bond of Silanes in Photochemical Reactions with W(CO)₆: Hydrosilylation of Ketones and Dehydrosilylation of Alcohol by H₂SiPh₂. *Polyhedron* **2006**, *25* (6), 1441–1448. <https://doi.org/10.1016/j.poly.2005.10.002>.
- (35) Stosur, M.; Szymańska-Buzar, T. Facile Hydrosilylation of Norbornadiene by Silanes R₃SiH and R₂SiH₂ with Molybdenum Catalysts. *J. Mol. Catal. A Chem.* **2008**, *286* (1–2), 98–105. <https://doi.org/10.1016/j.molcata.2008.02.005>.
- (36) Zyder, M.; Szymańska-Buzar, T. Hydrostannation of Norbornadiene by NBu₃SnH and Ph₃SnH with Molybdenum Catalysts. *J. Organomet. Chem.* **2010**, *695* (12–13), 1734–1737. <https://doi.org/10.1016/j.jorganchem.2010.03.023>.
- (37) Handzlik, J.; Szymańska-Buzar, T. The Formation of a σ -Bond Complex vs. an Oxidation Addition Product in Reaction of [M(CO)₄(H₄-Nbd)]

- (M = W, Mo) and H-EEt₃ (E = Si, Ge, Sn): DFT Optimized Structures and Predicted Chemical Shifts of Hydride Ligands. *J. Organomet. Chem.* **2014**, 769, 136–143. <https://doi.org/10.1016/j.jorganchem.2014.07.017>.
- (38) Kocięcka, P.; Czeluśniak, I.; Panek, J.; Szymańska-Buzar, T. Unusual Product Formation in Tungsten(o)-Catalysed Reactions of Propargylic Alcohols and Secondary Amines: Hydroamination and the Construction of the Tetrahydrofuran Ring. *Mol. Catal.* **2018**, 455 (May), 23–31. <https://doi.org/10.1016/j.mcat.2018.05.022>.
- (39) Kocięcka, P.; Czeluśniak, I.; Szymańska-Buzar, T. Efficient and Selective Synthesis of E-Vinylamines via Tungsten(o)-Catalyzed Hydroamination of Terminal Alkynes. *Adv. Synth. Catal.* **2014**, 356 (16), 3319–3324. <https://doi.org/10.1002/adsc.201400568>.
- (40) Wrighton, M.; Hammond, G.; Gray, H. Group VI Metal Carbonyl Photoassisted Isomerization of Olefins. *J. Org. Chem.* **1974**, 70, 283–301.
- (41) Xie, L. G.; Dixon, D. J. Iridium-Catalyzed Reductive Ugi-Type Reactions of Tertiary Amides. *Nat. Commun.* **2018**, 9 (1), 1–8. <https://doi.org/10.1038/s41467-018-05192-7>.
- (42) Zarate, C.; Martin, R. A Mild Ni/Cu-Catalyzed Silylation via C–O Cleavage. *J. Am. Chem. Soc.* **2014**, 136 (6), 2236–2239. <https://doi.org/10.1021/ja412107b>.
- (43) Zarate, C.; Nakajima, M.; Martin, R. A Mild and Ligand-Free Ni-Catalyzed Silylation via C-OMe Cleavage. *J. Am. Chem. Soc.* **2017**, 139 (3), 1191–1197. <https://doi.org/10.1021/jacs.6b10998>.
- (44) Yao, W.; Wang, J.; Zhong, A.; Wang, S.; Shao, Y. Transition-Metal-Free Catalytic Hydroboration Reduction of Amides to Amines. *Org. Chem. Front.* **2020**, 7, 3515–3520. <https://doi.org/10.1039/d0qo01092h>.
- (45) Barger, C. J.; Dicken, R. D.; Weidner, V. L.; Motta, A.; Lohr, T. L.; Marks, T. J. La[N(SiMe₃)₂]₃-Catalyzed Deoxygenative Reduction of Amides with Pinacolborane. Scope and Mechanism. *J. Am. Chem. Soc.* **2020**, 142, 8019–8028. <https://doi.org/10.1021/jacs.0c02446>.
- (46) Adrjan, B.; Szymańska-Buzar, T. Photochemical Reactions of [W(CO)₄(H₄-Nbd)] with Hydrosilanes: Generation of New Hydrido Complexes of Tungsten and Their Reactivity. *J. Organomet. Chem.* **2008**, 693 (12), 2163–2170. <https://doi.org/10.1016/j.jorganchem.2008.03.017>.

Chapter 5.

General Conclusions

To conclude this doctoral dissertation, it would be useful to highlight the main features found in this PhD thesis.

In *Chapter 2*, we met the goal of establishing the first stereospecific borylation of secondary benzyl pivalates. Mild conditions and exquisite stereospecificities generated a reliable and robust method, setting the basis for future C–Heteroatom bond formations through C–O bond scission. In addition, the incorporation of an enantioenriched boryl unit afforded a series of stereospecific derivatizations that might be expanded beyond Suzuki-Miyaura cross-couplings reactions. Two mechanistic pathways have been proposed, although further studies are necessary to determine the full picture of the protocol.

In *Chapter 3*, we developed a catalytic reductive deamination of alkyl pyridinium salts with a diverse set of aryl halides. The transformation could be executed for a wide number of alkyl amines and aryl bromides bearing multiple functional groups. Particularly noteworthy was the ability to extend this technology to primary alkyl amines, counterparts that are difficult to reach otherwise, or the application to advanced bioactive compounds. Cyclic voltammetry experiments of the substrates and the nickel oxidative addition complexes allowed for unravelling an unusual mechanistic manifold that might have consequences within the general area of deaminative protocols.

In *Chapter 4*, we have described the implementation of tungsten catalysts for triggering a remote hydroboration of sp^3 C–H bonds of carbonyl compounds possessing alkenes on the side chain. The protocol could be conducted under mild conditions and tolerated a wide number of different carbonyl counterparts, including amides or carboxylic acids. The transformation showed an exquisite regio- and chemoselectivity profile at the β position of the carbonyl group.

UNIVERSITAT ROVIRA I VIRGILI

Functionalization of Strong Sigma Bonds by Nickel and Tungsten Catalysis

Raúl Martín Montero



UNIVERSITAT
ROVIRA i VIRGILI